WILEY

The Electrochemical Society Series

FUNDAMENTALS OF ELECTROCHEMISTRY

SECOND EDITION

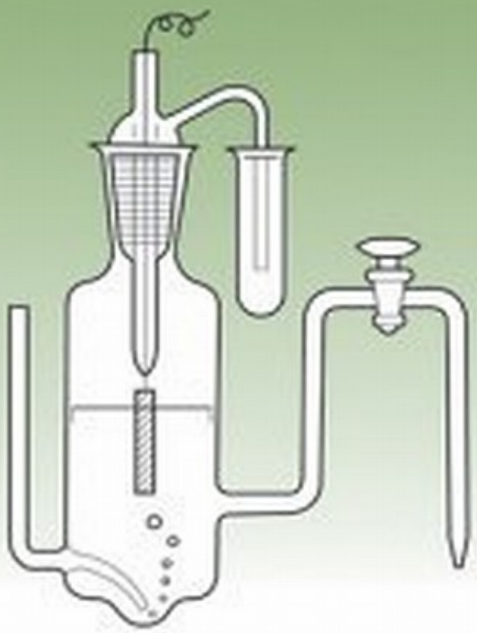

V. S. BAGOTSKY

FUNDAMENTALS OF ELECTROCHEMISTRY

Second Edition

V. S. BAGOTSKY
A. N. Frumkin Institute of Physical Chemistry and Electrochemistry
Russian Academy of Sciences
Moscow, Russia

Sponsored by

THE ELECTROCHEMICAL SOCIETY, INC. *Pennington, New Jersey*

WILEY-INTERSCIENCE

A JOHN WILEY & SONS, INC., PUBLICATION

Published by John Wiley & Sons, Inc., Hoboken, New Jersey
Published simultaneously in Canada

Library of Congress Cataloging-in-Publication Data:

Bagotsky, V. S. (Vladimir Sergeevich)
Fundamentals of electrochemistry / V. S. Bagotsky—2nd ed.
p. cm.
Includes bibliographical references and index.
ISBN-13 978-0-471-70058-6 (cloth : alk. paper)
ISBN-10 0-471-70058-4 (cloth : alk. paper)
1. Electrochemistry I. Title.
QD553.B23 2005
541′.37—dc22 2005003083

Printed in the United States of America

10 9 8 7 6 5 4 3 2 1

CONTENTS

CONTRIBUTORS

Prof. Vladimir S. Bagotsky (retired from the A. N. Frumkin Institute of Physical Chemistry and Electrochemistry, Russian Academy of Sciences, Leninskij Prospekt 31, 119071 Moscow, Russia), Mountain View, CA 94043, E-mail: vbag@mail.ru—main author

Dr. Leonid S. Kanevsky, A. N. Frumkin Institute of Physical Chemistry and Electrochemistry, Russian Academy of Sciences, Leninskij Prospekt 31, 119071 Moscow, Russia, E-mail: c/o askundin@mail.ru—Section 33.2

Prof. Alexander M. Kuznetsov, A. N. Frumkin Institute of Physical Chemistry and Electrochemistry, Russian Academy of Sciences, Leninskij Prospekt 31, 119071 Moscow, Russia, E-mail: theor@elchem.ac.ru—Chapter 34

Prof. Ezequiel P. M. Leiva, INFIQC-Facultad de Ciencias Químicas, Universidad Nacional de Córdoba, 5000 Córdoba, Argentina, E-mail: eleiva@mail.fcq.unc.edu.ar—Chapters 35 and 36

Dr. James McBreen, Brookhaven National Laboratory, Material Sciences Department, P.O. Box 5000, Upton, NY 11973-5000, E-mail: jmcbreen@bnl.gov—Chapter 27

Dr. Klaus Müller (retired from Battelle, Geneva, Switzerland), D-85560 Ebersberg, Germany, E-mail: Klaus-mueller-ebersberg@freenet.de—Chapter 25

Prof. Alvin J. Salkind, Bioengineering Division, University of Medicine and Dentistry of New Jersey, Piscataway, NJ 08854-3635, E-mail: Alvin.salkind@umdnj.edu—Section 24.5

Prof. Zdeněk Samec, J. Heyrovský Institute of Physical Chemistry, Academy of Sciences of the Czech Republik, CZ-182 23 Prague, Czech Republic, E-mail: zdenek.samec@jh-inst.cas.cz—Chapter 32

Dr. Alexander M. Skundin, A. N. Frumkin Institute of Physical Chemistry and Electrochemistry, Russian Academy of Sciences, Leninskij Prospekt 31, 119071 Moscow, Russia, E-mail: askundin@mail.ru—Sections 24.1 to 24.4

Prof. Ulrich Stimming, Physik-Department E-19, Technische Universität München, D-85748 Garching, Germany, E-mail: stimming@ph.tum.de—Chapter 26, Part A

Prof. Yurij Tolmachev, Kent State University, Kent, OH 44242-0001, E-mail: ytolmach@kent.edu—Section 33.1

Dr. Hengyong Tu, Physik-Department E-19, Technische Universität München, D-85748 Garching, Germany—Chapter 26, Part A

PREFACE TO THE SECOND EDITION

Substantial changes from the first English edition of this book (1993, Plenum Press, New York) have been introduced in this second edition. The content was rearranged such that all basic knowledge is contained in the first part of the book. This part was rewritten and to some extent simplified and can be used as a textbook for undergraduate students in electrochemistry and related branches. More advanced topics that will be of interest for people at a postgraduate level can be found in the subsequent parts. Eight new chapters have been added to these parts, most of which describe recent developments in theoretical and applied electrochemistry. Some of the new chapters were written by the author; other chapters and sections of the book were written by well-known experts in the corresponding fields. The author is very grateful to all coauthors for their cooperation in preparing this book and to Dr. Nina Osetrova and Dr. Alexander Skundin from Moscow for compiling the references for many chapters. The author is also greatly indebted to Dr. Klaus Müller from Geneva for translating from Russian the chapters or sections written by the main author and some coauthors, and for many helpful comments and remarks during preparation of the manuscript.

VLADIMIR SERGEEVICH BAGOTSKY

Moscow and Mountain View, CA
December 2004

PREFACE TO THE FIRST EDITION

> Of all electrical phenomena electrolysis appears the most likely to furnish us with a real insight into the true nature of the electric current. because we find currents of ordinary matter and currents of electricity forming essential parts of the same phenomenon.
>
> —James Clerk Maxwell
> *A Treatise on Electricity and Magnetism*,
> Vol. 1, Oxford, 1873

Two very important fields of natural science—chemistry and the science of electricity—matured and grew vigorously during the first half of the nineteenth century. Electrochemistry developed simultaneously. From the very beginning, electrochemistry was not merely a peripheral field but evolved with an important degree of independence, and it also left very significant marks on the development of chemistry and of the theory of electricity.

The first electrochemical device was the voltaic pile, built in 1800. For the first time, scientists had a sufficiently stable and reliable source of electric current. Research into the properties of this current provided the basis for progress in electrodynamics and electromagnetism. The laws of interaction between electric currents (André-Marie Ampère, 1820), of proportionality between current and voltage (Georg Simon Ohm, 1827), of electromagnetic induction (Michael Faraday, 1831), of heat evolution during current flow (James Prescott Joule, 1843), and others were discovered.

Work involving the electrolysis of aqueous solutions of salts and salt melts that was performed at the same time led to the discovery and preparation of a number of new chemical elements, such as potassium and sodium (Sir Humphry Davy, 1807). Studies of current flow in solutions (Theodor von Grotthuss, 1805) formed the starting point for the concept that the molecular structure of water and other substances is polar, and led to the electrochemical theory of the structure of matter formulated by Jons Jakob Berzelius (1820). The laws of electrolysis discovered in 1833 by Faraday had an even greater significance for knowledge concerning the structure of matter. During the second half of the nineteenth century, the development of chemical thermodynamics was greatly facilitated by the analysis of phenomena occurring in electrochemical cells at equilibrium.

Today, electrochemistry is a rigorous science concerned with the quantitative relations among the chemical, surface, and electrical properties of systems. Electrochemistry has strong links to many other fields of science. Electrochemical concepts proved particularly fruitful for studying and interpreting a number of very important biological processes.

Modern electrochemistry has vast applications. Electrochemical processes form the basis of large-scale chemical and metallurgical production of a number of materials. Electrochemical phenomena are responsible for metallic corrosion, which causes untold losses in the economy. Modern electrochemical power sources (primary and secondary batteries) are used in many fields of engineering, and their production figures are measured in billions of units. Other electrochemical processes and devices are also used widely.

A variety of definitions exist for electrochemistry as a subject. Thus, electrochemistry can be defined as the science concerned with the mutual transformation of chemical and electrical energy. According to another definition, electrochemistry deals with the structure of electrolyte solutions as well as with the phenomena occurring at the interfaces between metallic electrodes and electrolyte solutions. These and similar definitions are incomplete and do not cover all subject areas treated in electrochemistry. By the very general definition adopted today by most research workers, electrochemistry is the science concerned with the physical and chemical properties of ionic conductors as well as with phenomena occurring at the interfaces between ionic conductors, on the one hand, and electronic conductors or semiconductors, other ionic conductors, and even insulators (including gases and vacuum), on the other hand. All these properties and phenomena are studied both under equilibrium conditions, when there is no current flow, and under nonequilibrium conditions, when there is electric current flow in the system. In a certain sense, electrochemistry can be contrasted to electronics and solid-state theory, where the properties of electronic conductors and electronic or hole-type semiconductors as well as the phenomena occurring at the interfaces between these materials or between the materials and vacuum are examined.

This definition of electrochemistry disregards systems in which nonequilibrium charged species are produced by external action in insulators: for example, by electric discharge in the gas phase (electrochemistry of gases) or upon irradiation of liquid and solid dielectrics (radiation chemistry). At the same time, electrochemistry deals with certain problems often associated with other fields of science, such as the structure and properties of solid electrolytes and the kinetics of ionic reactions in solutions.

This book seeks essentially to provide a rigorous, yet lucid and comprehensible outline of the basic concepts (phenomena, processes, and laws) that form the subject matter of modern theoretical and applied electrochemistry. Particular attention is given to electrochemical problems of fundamental significance, yet those often treated in an obscure or even incorrect way in monographs and texts. Among these problems are some, that appear elementary at first glance, such as the mechanism of current flow in electrolyte solutions, the nature of electrode potentials, and the values of the transport numbers in diffusion layers.

By considering the theoretical and applied aspects of electrochemistry jointly, one can more readily comprehend their intimate correlation and gain a fuller insight into this science as a whole. The applied part of the book outlines the principles of some processes and illustrates their practical significance but does not describe technical or engineering details or the design of specific equipment, as these can be found in specialized treatises on applied electrochemistry.

As a rule, the mathematical tools used in electrochemistry are simple. However, in books on electrochemistry, one often finds equations and relations that are quite unwieldy and not transparent enough. The author's prime aim is that of elucidating the physical ideas behind the laws and relations and of presenting all equations in the simplest possible, though still rigorous and general, form.

There is a great deal of diversity in the terminology and names used for electrochemical concepts in the literature. It is the author's aim to introduce uniform terminology in accordance with valid standards and recommendations. For a profitable reading of the book and understanding of the material presented, the reader should know certain parts of physics (e.g., electrostatics), the basics of higher mathematics (differentiation and integration), and the basics of physical chemistry, particularly chemical thermodynamics.

VLADIMIR SERGEEVICH BAGOTSKY

LIST OF PHOTOGRAPHS

Some outstanding scientists who have advanced the science of electrochemistry

Italic numbers at the end are pages where the photographs appear.

ABBREVIATIONS

ac	alternating current
AFC	alkaline fuel cell
AE	auxiliary electrode
BL	γ-butyrolactone
CD	current density
dc	direct current
DME	dropping mercury electrode
DMF	dimethylformamide
DMFC	direct methanol fuel cell
DSA®	dimensionally stable anode
ECC	electrocapillary curves
EDL	electric double layer
EMF	electromotive force
EPS	electrochemical power source
ESE	excess surface energy
ETR	electron transfer reaction
eV	electron-volt
hap	high anodic potentials
ITIES	interface between two immiscible electrolyte solutions
LPD	linear potential scan
MCFC	molten carbonate fuel cell
MEA	membrane-electrode assembly
MIEC	mixed ionic-electronic conductor
OCP	open-circuit potential
OCV	open-circuit voltage
Ox, ox	oxidized form
PAFC	phosphoric acid fuel cell
PEMFC	proton exchange membrane fuel cell
PC	propylene carbonate
PD	potential difference
PTFE	polytetrafluoroethylene
PVC	poly(vinyl chloride)
PZC	point (or potential) of zero charge
RDE	rotating disk electrode

These abbreviations are used in most chapters. In some chapters other (specific) abbreviations are used. Abbreviations employed in physical experimental methods used in electrochemistry are listed in Chapter 27.

RDS	rate determining step
RE	reference electrode
Red, red	reduced form
RHE	reversible hydrogen electrode
RRDE	rotating ring disk electrode
SCE	saturated calomel electrode
SECM	scanning electrochemical microscope
THF	tetrahydrofuran
SCE	saturated calomel electrode
SOFC	solid oxide fuel cell
SHE	standard hydrogen electrode
UDP	underpotential deposition
UME	ultramicroelectrode
WE	working electrode
YSZ	yttria stabilized zirconia

SYMBOLS

Symbol	Meaning	Usual Dimensions (values)	Section References*
Roman Symbols			
a_j	thermodynamic activity	$mol \cdot dm^{-3}$	3.3.1
$a_\pm$	mean ion thermodynamic activity	$mol \cdot dm^{-3}$	3.3.2
	(2) activation energy	$kJ \cdot mol^{-1}$	8.3
	(3) adsorption	$mol \cdot cm^{-2}$	10.2
B	adsorption coefficient	$dm^3 \cdot mol^{-1}$	10.2.4
c_j	concentration	$mol \cdot dm^{-3}$	1.2
C	differential double layer capacity	$\mu F \cdot cm^{-2}$	10.1.2
D_j	diffusion coefficient	$cm^2 \cdot s^{-1}$	4.1
E	electrode potential	V	2.4
$\mathbf{E}$	electrostatic field strength	$V \cdot cm^{-1}$	1.3
$E_{1/2}$	half-wave potential	V	6.3.1
ε	voltage of a galvanic cell	V	2.3
f	(1) number of revolutions per second	s^{-1}	4.4.2
	(2) ac frequency	s^{-1}	12.5
f_j	activity coefficient	none	3.3.1
F	Faraday constant	$96485\ C \cdot mol^{-1}$	1.2
G	Gibbs energy	$kJ \cdot mol^{-1}$	3.3.2
h	Planck constant ($\hbar \equiv h/2\pi$)	$6.626 \cdot 10^{-34}\ J \cdot s$	14.1.1
h_j	generalized rate constant	$cm \cdot s^{-1}$	6.4
H	enthalpy	$kJ \cdot mol^{-1}$	3.2.1
i	current density (CD)	$mA \cdot cm^{-2}$	1.3
i^{O}	exchange current density	$mA \cdot cm^{-2}$	2.2
$\vec{i}$	partial anodic CD	$mA \cdot cm^{-2}$	2.2
$\overleftarrow{i}$	partial cathodic CD	$mA \cdot cm^{-2}$	2.2
I_c	ionic strength	$mol \cdot dm^{-3}$	7.3.2

These symbols are used in most chapters, but in some chapters other symbols are also used. Symbols similar to those listed may have different meanings in a local context.

*Sections where this symbol is used for the first time and/or where its definition is given.

J_j	flux density	$mol \cdot s^{-1} \cdot cm^{-2}$	1.3
k	(1) rate constant	$cm \cdot s^{-1}$	6.2.2
	(2) Boltzman constant	$1.381 \cdot 10^{-23}\ J \cdot K^{-1}$	14.1.1
m	molal concentration	$mol \cdot kg^{-1}$	
M	molar concentration	$mol \cdot dm^{-3}$	
n	number of electrons in the reaction's elementary act	none	1.6
N_A	Avogadro constant	$6.022 \cdot 10^{23}\ mol^{-1}$	1.2
p	(1) gas pressure	MPa	3.2.1
	(2) reaction order	none	6.2
	(3) specific power	$kW \cdot kg^{-1}$	19.2.1
P	power	W, kW	19.2.1
Q	heat of reaction	J	7.2
Q	electric charge	C, μC	1.2
Q^0	elementary electric charge	$1.602 \cdot 10^{-19}$ C	1.2
R	(1) molar gas constant	$8.314\ J \cdot mol^{-1} \cdot K^{-1}$	3.2.1
	(2) resistance	Ω	
S	(1) surface area	cm^2	
	(2) entropy	$kJ \cdot K^{-1}$	3.2.1
t_j	transport number of ions j	none	1.3
T	absolute temperature	K	
u_j	mobility of ion j	$cm^2 \cdot V^{-1} \cdot s^{-1}$	1.2
U	(1) internal energy	$kJ \cdot mol^{-1}$	3.2.1
	(2) level of electron energy	eV	29.1
v	(1) linear velocity	$cm \cdot s^{-1}$	1.3
	(2) rate of reaction (specific)	$mol \cdot cm^{-2} \cdot s^{-1}$	1.7
	(3) linear scan rate	$V \cdot s^{-1}$	23.5.3
w	(1) work	kJ	
	(2) specific energy	$kWh \cdot kg^{-1}$	19.2.1
X_j	reactant in an electrode reaction	none	
$\overline{Y}$	admittance (ac conductance)	complex	12.5
z_j	charge number of ions j	none	
$\overline{Z}$	impedance of ac circuits	complex	12.5

Greek Symbols

α	(1) transfer coefficient	none	6.2.1
	(2) enhancement factor	none	3.3.4
β	transfer coefficient	none	6.2.3
γ	formal roughness factor	none	18.4
γ_j	(1) stoichiometric activity coefficient	none	3.3.2
	(2) nonequilibrium factor	none	6.3.3
Γ	Gibbs surface excess	$mol \cdot cm^{-2}$	10.3
δ	diffusion layer thickness	cm	4.2

ε	(1) relative permittivity of a dielectric	none	2.0
	(2) coefficient of resistance rise	none	18.2.2
ε_0	permittivity of vacuum	($8.85 \cdot 10^{-14}$ F·cm^{-1})	2.0
ζ	electrokinetic potential	V	3.1.1
η	(1) cell overvoltage	V	2.5.2
	(2) viscosity coefficient	N·s/cm^2	4.4.1
θ	(1) drag coefficient	J/s	1.3
	(2) degree of surface coverage	none	10.2
κ	diffusion flux constant	cm·s^{-1}	4.2
λ	degree of partial charge transfer	none	10.1.2
λ_j	molar conductivity of ions j	S·cm^{-2} ·mol^{-1}	1.3
Λ	molar conductivity of an electrolyte solution	S·cm^{-2}·mol^{-1}	1.3
μ_j	chemical potential	kJ·mol^{-1}	3.2.1
$\overline{\mu}_j$	electrochemical potential	kJ·mol^{-1}	3.2.2
ν_j	stoichiometric coefficient	none	1.5
ν_{kin}	kinematic viscosity	m^2·s^{-1}	4.4.1
Π	(1) osmotic pressure	MPa	7.1
	(2) pore perimeter	cm	19.3
ρ	resistivity	Ω·cm	1.3
σ	conductivity	S·cm^{-2}	1.3
τ_j	number of ions *j*	none	1.2
φ_G	Galvani potential	V	2.1
φ_V	Volta potential	V	9.3
χ	surface potential	V	9.1
Ψ	electrostatic potential	V	2.0
ω	(1) angular velocity	radian·s^{-1}	4.4.2
	(2) angular ac frequency	radian·s^{-1}	12.5

Subscripts

ads	adsorbed
A	acid
B	base
e	electrical
ext	external
d	discharge
E	electrolyte
ch	(1) chemical
	(2) charge
fin	final
in	initial
j	any ion
+	cation
−	anion

d	diffusion
k	kinetic
l	limiting
m	(1) migration
	(2) maximal
	(3) any electrode reaction
M	metal
ohm	ohmic
R	reference electrode
r	reactant
p	product
red	reducer
S	per unit area
V	per unit volume
ox	oxidizer
k	solute
kv	convection
0	(1) standard
	(2) without current
σ	all particles in electrolyte

Superscripts

E	electrolyte
M	metal
or	orientational
σ	surface excess

PART I
Basic Concepts

1
Electric Currents in Ionic Conductors

1.1 VARIOUS TYPES OF CONDUCTORS

By the nature of conduction and values of conductivity, materials can be classified as conductors, semiconductors, or insulators (dielectrics). It is a special attribute of conductors that free electric charges are present in them. The migration of these free charges in an applied electric field manifests itself as electric current.

Real charge is always associated with well-defined physical carriers such as electrons and ions; this is not so for the idealized "physical" charge considered in electrostatics. Each conductor can be characterized by stating the nature and concentration of the free charges. In the present section we consider free charged particles of atomic (or molecular) size, not larger, aggregated entities, such as colloidal particles.

Conduction of electric current in conductors can be electronic or ionic, depending on the type of charge involved. Substances exist where conduction is mixed (i.e., where both ions and electrons are moving). *Electronic conduction* is found in all metals and also in certain other substances: carbon materials (graphite, carbon black), some oxides and other inorganic compounds (e.g., tungsten carbide), and a number of organic substances. *Ionic conductors* (conductors of the second kind) are also known as *electrolytes*. This term is used not only in the sense of an ionic conductor (e.g., in expressions such as "solid electrolytes," but also in a second sense, in speaking of substances that ordinarily are not conducting but produce ionic conduction after being dissolved in water or in another solvent (e.g., in terms such as "electrolyte solution" and "weak electrolyte").

The main topic of electrochemistry is investigation of the properties of ionic conductors and of electric circuits containing ionic conductors, and investigation of phenomena occurring during passage of an electric current through such circuits.

Aqueous solutions of acids, bases, and salts are the ionic conductors used most widely and studied most thoroughly. The importance of other types of ionic conductors has increased in recent times, but aqueous solutions are still preeminent. Their significance goes far beyond electrochemistry as such; they can be found in practically all spheres of human activity. They are of exceptional importance in the

Fundamentals of Electrochemistry, Second Edition, By V. S. Bagotsky

form of intracellular fluids in the biological and physiological processes of all living beings. They are of equal importance in the form of natural waters in the oceans, rivers, and underground for geomorphologic processes.

1.2 IONS IN ELECTROLYTE SOLUTIONS

Acids, bases, and salts (i.e., electrolytes in the second sense of the word) dissociate into ions when dissolved in water (or in other solvents). This dissociation can be complete or partial. The fraction of the original molecules that have dissociated is known as the *degree of dissociation*, α. Substances that exhibit a low degree of dissociation in solution are called *weak electrolytes*, whereas when the value of α comes close to unity we speak of *strong electrolytes*.

In general, we can write the dissociation equation

$$\mathrm{M}_{\tau_+}\mathrm{A}_{\tau_-} \rightleftharpoons \tau_+\mathrm{M}^{z+} + \tau_-\mathrm{A}^{z-}. \tag{1.1}$$

It is evident that $z_+\tau_+ = z_-\tau_- = z_k$, where z_k is the electrolyte's charge number (the number of elementary charges of each sign appearing on dissociation of one molecule of the electrolyte).

Let c_k be the original concentration of substance k (e.g., of the compound $\mathrm{M}_{\tau+}\mathrm{A}_{\tau-}$) without dissociation. Then the concentrations c_+ and c_- of the ions, the concentration c_n of the undissociated molecules, and the total concentration c_σ of all species dissolved in the solution can be written as

$$c_+ = \alpha\tau_+ c_k, \quad c_- = \alpha\tau_- c_k, \quad c_n = (1-\alpha)c_k, \quad c_\sigma = [1+\alpha(\tau_k - 1)]c_k, \tag{1.2}$$

where $\tau_k = \tau_+ + \tau_-$ is the total number of ions into which one original molecule dissociates. In the limit of $\alpha = 1$, we have $c_\sigma = \tau_k c_k$. Thus, electrolyte solutions contain several types of particles, but their concentrations are interrelated and only one of the concentration values is independent [e.g., that of the original compound k (which is c_k)]. A subscript k is used instead of j to point out, in the following, that this independent component is considered rather than its dissociation products. A substance such as $ZnSO_4$ where $z_+ = z_-$ ($\tau_+ = \tau_-$) is called a *symmetrical* or $z:z$ *electrolyte*; a particular case of the $z:z$ electrolytes are the $1:1$ electrolytes, of which KCl is an example.

Binary electrolyte solutions contain just one solute in addition to the solvent (i.e., two independent components in all). Multicomponent solutions contain several original solutes and the corresponding number of ions. Sometimes in multicomponent solutions the behavior of just one of the components is of interest; in this case the term *base electrolyte* is used for the set of remaining solution components. Often, a base electrolyte is actually added to the solutions to raise their conductivity.

The concentration of ions of type j in the solution can be stated in terms of the number of moles n_j of these ions per unit of the volume V: $c_j = n_j/V$. The electric charge Q_j of an ion can be described as $Q_j = Q^0 z_j$, where $Q^0 = 1.62 \times 10^{-19}$ C is the

elementary charge (charge of the proton) and z_j is the charge number (an integer; i.e., the number of elementary charges associated with one ion). The charge of 1 mol of ions is given by z_jF, where $F \equiv N_A Q^0 = 96{,}485$ C/mol (or roughly 96,500 C/mol), which is the Faraday constant, and N_A is the Avogadro constant.

The volume density of charge of a given type, $Q_{V,j}$, is defined as $Q_{V,j} = z_j F c_j$. A conductor is always electroneutral: that is, in any part of it the combined density of all ions (and other charges, free and localized) is zero and hence

$$\Sigma z_j c_j = 0 \quad \text{or} \quad \Sigma_{(+)} z_j c_j = -\Sigma_{(-)} z_j c_j, \tag{1.3}$$

where $\Sigma_{(+)}$ and $\Sigma_{(-)}$ denote summation over all species of positive and negative charge, respectively. The electroneutrality condition is disturbed only within thin layers (a few atoms in thickness) directly at the interfaces formed by the conductor with other conductors or insulators, where excess charge of a particular sign can exist in the form of monolayers or thin space-charge layers.

All forms of electrostatic (*coulombic*) interaction of charged particles with each other and with their environment are determined by the magnitude and sign of the charge and by the concentration of the charged particles. However, in contrast to physical charges, ions and other real charged particles experience interactions other than electrostatic. Without discussing these additional interaction forces in depth, we shall designate them as chemical forces. It is because of these forces that each type of real charge has its own chemical individuality. In contrast to electrostatics, electrochemistry deals with both the chemical and electrostatic properties of free charged particles.

1.3 CONDUCTIVITY OF ELECTROLYTE SOLUTIONS

Conductivity is a very important parameter for any conductor. It is intimately related to other physical properties of the conductor, such as thermal conductivity (in the case of metals) and viscosity (in the case of liquid solutions). The strength of the electric current I in conductors is measured in amperes, and depends on the conductor, on the electrostatic field strength $\mathbf{E}$ in the conductor, and on the conductor's cross section S perpendicular to the direction of current flow. As a convenient parameter that is independent of conductor dimensions, the current density i[†] is used, which is the fraction of current associated with the unit area of the conductor's cross section: $i \equiv I/S$ (units: A/cm^2).

The current density is proportional to the field strength:

$$i = \sigma \mathbf{E} \tag{1.4}$$

(a differential form of *Ohm's law*). The proportionality factor σ is the (electrical) conductivity (units: S/cm); it characterizes quantitatively the ability of a material to

[†] The Symbol i is preferred over the recommended symbol j, since I is used for currents and J is used for fluxes.

conduct electric current, and for any given material it depends on the temperature but not on the size and geometry of the sample. The reciprocal $\rho \equiv 1/\sigma$ is the resistivity (units: $\Omega \cdot$ cm); numerically, it is the resistance of a conductor sample 1 cm long and 1 cm^2 in cross section.

Electric currents in electrolyte solutions are the directed motions of ions under the influence of an applied electric field. Ions in solution are in a state of continuous kinetic molecular (thermal) motion. This motion is chaotic when an electrostatic field is not present (i.e., the ions do not move preferentially in any particular direction, and there is no current flow).

When an electrostatic field of field strength **E** is applied, each type j of ion carrying charge z_jF (per mole) finds itself under the effect of an electric driving force $f_{dr} = z_jF\mathbf{E}$, causing the ions to move in a direction given by the field. This motion under the effect of a field is called the *migration* of ions. Migration is superimposed on the thermal motion of the ions. The flux density J_j of migrating ions (the number of moles crossing in unit time a unit cross-sectional area S^0 perpendicular to the flux direction) depends on the volume concentration c_j and linear velocity of the ions υ_j. In unit time the cross-sectional area S^0 will be crossed by all ions no farther than υ_j from S^0 (i.e., all those residing in a volume equal to υ_j). Thus,

$$J_j = c_j\upsilon_j. \tag{1.5}$$

In the steady state, the total flux is constant along the entire path. This condition (i.e., that of flux continuity) is a reflection of mass balance; nowhere in a steady flux will the ions accumulate or vanish (i.e., their local concentrations are time invariant). The condition of continuity of the steady flux is disturbed in those places where ions are consumed (sinks) or produced (sources) by chemical reactions. It is necessary to preserve the balance that any excess of ions supplied correspond to the amount of ions reacting, and that any excess of ions eliminated correspond to the amount of ions formed in the reaction.

The mean velocity of migration υ_j depends on the external driving force $f_{dr} = z_jF\mathbf{E}$ and on the resistance to motion set up by the medium's viscosity. This retarding force as a rule is proportional to the velocity. Under the influence of the external force, the velocity will increase until it attains the value υ_j where the retarding force $\upsilon_j\theta$ (θ is the drag coefficient) becomes equal to the external driving force. Hence,

$$\upsilon_j = \frac{1}{\theta} f_{dr} = \frac{1}{\theta} z_jF\mathbf{E} \tag{1.6}$$

and

$$J_j = c_j\upsilon_j = c_j \frac{1}{\theta} f_{dr} = c_j \frac{1}{\theta} z_jF\mathbf{E}. \tag{1.7}$$

The velocity of migration corresponding to unit field strength (1 V/cm) is called the *mobility* of the ions u_j:

$$u_j \equiv \frac{v_j}{\mathbf{E}} = \frac{1}{\theta} z_j F. \tag{1.8}$$

The expression for the migration flux density becomes

$$J_j = c_j u_j \mathbf{E}. \tag{1.9}$$

By definition the partial current density i_j is the number of charges that in unit time cross the unit cross-sectional area due to the migration of ions j; that is,

$$i_j = z_j F J_j = z_j F c_j u_j \mathbf{E}. \tag{1.10}$$

In electrolyte solutions the positively and negatively charged ions will move in opposite directions when an electric field is applied. Therefore, outwardly the effect of motion of positive ions is exactly the same as that of the motion of negative ions, and the total current density is the sum of the partial currents due to transport of each type of ion:

$$i = \Sigma i_j = F \mathbf{E} \, \Sigma z_j c_j u_j. \tag{1.11}$$

We can see when comparing Eqs. (1.4) and (1.11) that a conductor's conductivity depends on the concentrations and the mobilities of all types of ions:

$$\sigma = F \Sigma \, z_j c_j u_j. \tag{1.12}$$

The fraction of current transported by ions of a given type is called the *transport number* t_j of these ions:

$$t_j = \frac{i_j}{i} = \frac{z_j c_j u_j}{\Sigma z_j c_j u_j}. \tag{1.13}$$

It is obvious that $0 \leq t_j \leq 1$ and $\Sigma t_j = 1$. For conductors with a single type of ion, the transport number of these ions is unity. For conductors with different types of ions, the individual transport number of a given ion depends on the concentrations and mobilities of all ions.

For the conductivity of a binary electrolyte solution with the degree of dissociation α, we have, according to Eq. (1.12),

$$\sigma = \alpha z_k c_k F (u + u_-). \tag{1.14}$$

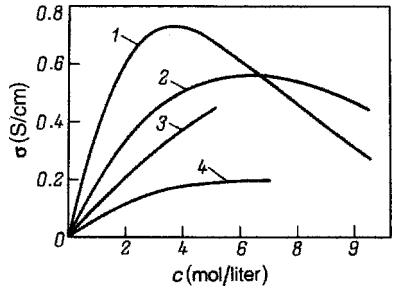

FIGURE 1.1 Conductivities (at 25°C) as functions of concentration in aqueous solutions of (1) H_2SO_4; (2) KOH; (3) NH_4Cl; (4) $NaNO_3$.

For binary electrolytes Eq. (1.13) for transport numbers becomes

$$t_j = \frac{u_j}{u_+ + u_-}. \tag{1.15}$$

The mobilities u_j of ions in solutions are concentration dependent. They are highest in dilute solutions (the limiting mobilities u_j^0) and decrease gradually with increasing concentration. Hence in dilute binary solutions of strong electrolytes ($\alpha = 1$), the conductivity is proportional to the total concentration c_k. Because of decreasing mobility, the conductivity rise becomes slower as the concentration increases. In solutions of weak electrolytes, this slowdown is more pronounced since the degree of dissociation decreases in addition to the mobilities. In certain cases the plots of conductivity against concentration go through a maximum (Fig. 1.1).

The parameters of *molar conductivity of the electrolyte*, $\Lambda \equiv \sigma/c_k$, and *molar conductivity of ions*, $\lambda_j \equiv z_j F u_j$ (units: $S \cdot cm^2/mol$), are also used to describe the properties of electrolyte solutions (Λ is used only in the case of binary solutions). With Eq. (1.14), we can write for a binary solution

$$\Lambda = \alpha\,(\tau_+\lambda_+ + \tau_-\lambda_-). \tag{1.16}$$

For the change of molar conductivity of the ions which occurs with increasing concentration, only the mobility decrease is responsible; in dilute solutions a limiting value of $\lambda_j^0 \equiv z_j F u^0 j$ is attained. A limiting value of molar conductivity Λ^0 implies limiting values λ_j^0 as well as complete dissociation:

$$\Lambda^0 = \tau_+\lambda_+^0 + \tau_-\lambda_-^0. \tag{1.17}$$

In the past the parameter $1/z_j$ moles of a given ion j had been called the ion's *chemical dissociation equivalent*, and the corresponding mass M_j/z_j (where M_j is the molar mass) was called the ion's *equivalent mass*. The ion's equivalent concentration $c_{(eq)j}$ is related to its mole concentration c_j as $c_{(eq)\,j} = z_j c_j$. However, since the

chemical equivalent of any given substance in dissociation reactions may differ from the equivalents relevant in electrochemical reactions (see Section 1.6), this term should be used with caution. These equivalent concentrations had often been used as a basis for the values of Λ and λ_j. In this case the equivalent conductance was defined as $\Lambda_{eq} \equiv \sigma/c_{eq}$, and the ionic equivalent conductance (or equivalent mobility) was defined as $\lambda_{(eq)j} \equiv Fu_j$; in this notation,

$$\Lambda_{eq} = \alpha[\lambda_{(eq)+} + \lambda_{(eq)-}] \quad \text{and} \quad \Lambda^0_{eq} = \lambda^0_{(eq)+} + = \lambda^0_{(eq)-}. \tag{1.18}$$

These terms are no longer recommended. Instead, we consider the molar conductivities of electrolytes and ions as defined above and where necessary indicate the electrolyte units to which the concentrations refer: for example, $\Lambda(MgCl_2)$ or $\Lambda(\frac{1}{2}MgCl_2)$, $\lambda(Ca^{2+})$ or $\lambda(\frac{1}{2}Ca^{2+})$. We evidently have $\Lambda(\frac{1}{2}MgCl_2) = \frac{1}{2}\Lambda(MgCl_2)$.

It is a typical feature of aqueous electrolyte solutions that one can, within wide limits, change the solute concentrations and hence the conductivities themselves. Pure water has a very low value of σ; it is about 5 μS/m at room temperature after careful purification of the water. In the most highly conducting solutions (i.e., concentrated solutions of acids and bases), values of 80 S/m can be attained at the same temperature: values seven orders of magnitude higher than those found for pure water.

1.4 CIRCUITS INVOLVING IONIC CONDUCTORS. ELECTRODES

As a rule, electric circuits consist not of a single conductor but of several conductors connected, forming a sequence of conductors. This circuit can be closed or open. An open circuit is *properly open* when terminating at both ends with the same type of conductor.

In electrical engineering and electronics, circuits are employed that consist of electronic conductors exclusively. Circuits that in addition include at least one ionic conductor are called *galvanic circuits*. The technical realization of a galvanic circuit is also called a *galvanic cell* (or *electrochemical cell* or *electrolysis cell*). Galvanic circuits have a number of characteristic features not present in purely electronic circuits. It is one of the more important tasks of electrochemistry to consider these features.

The sequence of conductors constituting a properly open galvanic circuit can be described schematically, for example, as

$$\mathrm{Cu}\,|\,\mathrm{Zn}\,|\,\mathrm{ZnCl_2},\ aq\,|\,\mathrm{graphite}\,|\,\mathrm{Cu} \tag{1.19}$$

($ZnCl_2$, *aq* denotes an aqueous solution of $ZnCl_2$). Vertical lines in the scheme denote the areas of contact (interfaces) between two adjacent conductors.

Other galvanic circuits contain two or more ionic conductors, which may be in direct contact with each other or may alternate with electronic conductors. An example of the former case is that of the circuit

$$\mathrm{Cu}\,|\,\mathrm{Zn}\,|\,\mathrm{ZnSO_4},\ aq\,\vdots\,\mathrm{CuSO_4},\ aq\,|\,\mathrm{Cu}. \tag{1.20}$$

The broken vertical line denotes an area of contact between any two ionic conductors, particularly between liquid ionic conductors (electrolyte–electrolyte interface or *liquid junction*). Ions can transfer between phases by diffusion across such a boundary; hence, circuits containing such an interface are often called *circuits* or *cells with transference*.

In a galvanic circuit, electronic conductors are in contact with ionic conductors in at least two places. An electronic conductor in contact with an ionic conductor is called an *electrode*. When an electric current is made to flow in a galvanic cell, the current will pass from electrode to electrolyte ("enter" the electrolyte) at one of the electrodes, and it will pass from electrolyte to electrode ("leave" the electrolyte) at the other electrode. The first of these electrodes has been named the *anode* (from Greek ανα, "up"), the second has been named the *cathode* (from Greek κατα, "down"). It follows from this definition that the designations "anode" and "cathode" depend on the direction of current flow in the galvanic cell. An anode becomes a cathode, and vice versa, when the direction of current flow is inverted. Within the electrolyte, the current flow is always from the anode to the cathode. Therefore, the positively charged electrolyte ions migrating toward the cathode have been named *cations*, and the negatively charged ions migrating toward the anode have been named *anions*. In the external parts of the closed circuit ("external" relative to the electrolyte), the current flow is from cathode to anode.

1.5 PASSAGE OF CURRENT THROUGH ELECTRODES. ELECTRODE REACTIONS

The area of contact between two different types of conductors is a special place in any circuit. The character of current flow in this region depends on the phases in contact. The simplest case is that of contact between two metals. In both conductors the conduction is due to the same species (i.e., electrons). When current crosses the interface, the flow of electrons is not arrested; all electrons, which come from one of the phases freely, cross over to the other phase on their arrival at the interface. No accumulation or depletion of electrons is observed. In addition, current flow at such a junction will not produce any chemical change.

More complex phenomena occur when current crosses interfaces between semiconductors. The most typical example is the rectification produced at interfaces between *p*- and *n*-type semiconductors. Electric current freely flows from the former into the latter semiconductor, but an electric field "repelling" the free carriers from the junction arises when the attempt is made to pass current in the opposite direction: Holes are sent back into the *p*-phase, and electrons are sent back into the *n*-phase. As a result, the layers adjoining the interface are depleted of free charges, their conductivities drop drastically, and current flow ceases ("blocking" the interface).

When the current is carried by different species in the two adjacent phases, the continuous flow of carriers is interrupted. Charges of one type come up to (or depart from) the area of contact on one side, and carriers of a different type come up to (or depart from) this area on the other side. To sustain steady current flow, one needs a steady sink for the particles arriving, and a steady source for those departing.

In galvanic cells the carriers are ions and electrons. In this case, chemical reactions occurring at the interface—at the electrode surface—and involving carriers

from both phases (including electrons) are the sink and source for the corresponding particles. Chemical reactions involving electrons are called *electrochemical* or *electrode reactions*. Reactions at anodes are also called *anodic*, and reactions at cathodes are called *cathodic*. At an anode, electrons go away from the junction into the metal; hence, an anodic reaction must generate electrons. Similarly, at a cathode, electrons supplied by the circuit must react (and thus are eliminated from the reaction zone).

For instance, when current flow is from the right to the left in galvanic cell (1.19), the zinc electrode will be the cathode, and its surface is the site of the cathodic reaction involving the deposition of zinc by discharge of zinc ions from the solution:

$$Zn^{2+} + 2e^- \rightarrow Zn. \tag{1.21}$$

This reaction satisfies the requirements listed above; the zinc ions and electrons arriving at the surface from different sides disappear from the reaction zone. The anodic reaction

$$2Cl^- \rightarrow Cl_2 + 2e^- \tag{1.22}$$

occurs at the surface of the graphite electrode (the anode); it generates electrons while Cl^- ions disappear.

Electron withdrawal from a material is equivalent to its oxidation, while electron addition is equivalent to its reduction. In the anodic reaction, electrons are generated and a reactant (in our example, the chloride ions) is oxidized. In the cathodic reaction the reactant (the zinc ions) is reduced. Thus, anodic reactions are always oxidation reactions, and cathodic reactions are reduction reactions for the initial reactants.

In all cases the electrode reaction secures continuity of current flow across the interface, a "relay" type of transfer of charges (current) from the carriers in one phase to the carriers in the other phase. In the reaction, the interface as a rule is crossed by species of one type: electrons [e.g., in reaction (1.22)] *or* ions [e.g., in reaction (1.21)].

In complete galvanic cells, electrochemical reactions occur simultaneously at the anode and cathode. Since the current is of equal strength at the two electrodes, the corresponding electrode reactions are interrelated, in that the number of electrons set free in unit time at the anode is equal to the number of electrons reacting during the same time at the cathode. Electrode reactions subject to such a condition are called *coupled reactions*.

Current flow in cells is attended by an overall chemical reaction, more particularly a *current-producing* (or *current-consuming*) *reaction* in which electrons do not appear explicitly. In the example reported above, decomposition of dissolved zinc chloride,

$$ZnCl_2 \ (\rightleftharpoons Zn^{2+} + 2Cl^-) \rightarrow Zn + Cl_2 \tag{1.23}$$

is the reaction that results when the cathodic and anodic reaction are combined.

In symmetrical galvanic cells, cells consisting of two identical electrodes (e.g., zinc electrodes), current flow does not produce a net chemical reaction in the cell as a whole; only a transfer of individual components occurs in the cell (in our example, metallic zinc is transferred from the anode to the cathode).

1.6 CLASSIFICATION OF ELECTRODES AND ELECTRODE REACTIONS

The type of electrode reaction that will occur depends on the electrode and electrolyte and also on external conditions: the temperature, impurities that may be present, and so on. Possible reactants and products in these reactions are (1) the electrode material, (2) components of the electrolyte, and (3) other substances (gases, liquids, or solids) which are not themselves component parts of an electrode or the electrolyte but can reach or leave the electrode surface. Therefore, when discussing the properties or behavior of any electrode, we must indicate not merely the electrode material but the full electrode system comprising electrode and electrolyte as well as additional substances that may be involved in the reaction: for example, $ZnCl_2$, $aq \mid (Cl_2)$, graphite [the right-hand electrode in (1.19)].

Among all the substances that may be involved in an electrode reaction, substances for which the oxidation state does not change (such as complexing agents) must be distinguished from the principal reactants and products, for which there is a change in oxidation state in the reaction. Using specific examples, we shall consider different types of electrodes and electrode reactions. The examples are cases involving aqueous solutions, but the features pointed out are found as well in other electrolytes. In the examples we first indicate the electrode system, then the reaction equation (cathodic reactions follow these equations from the left to the right and the corresponding anodic reactions follow the same equations in the opposite direction). Special features of anodic reactions are stated in square brackets in the text that follows.

Unfortunately, a unique terminology for the various types of electrodes and reactions has not yet been established. Electrodes can be classified according to different distinguishing features:

Reacting and Nonconsumable Electrodes

$$AgNO_3,\ aq \mid Ag \qquad Ag^+ + e^- \rightleftharpoons Ag, \tag{1.24}$$

$$FeCl_2, FeCl_3,\ aq \mid Pt \qquad Fe^{3+} + e^- \rightleftharpoons Fe^{2+}, \tag{1.25}$$

$$HClO_3, HCl,\ aq \mid Pt \qquad ClO_3^- + 6H^+ + 6e^- \rightleftharpoons Cl^- + 3H_2O, \tag{1.26}$$

$$H_2SO_4,\ aq \mid (H_2),\ Pt \qquad 2H^+ + 2e^- \rightleftharpoons H_2. \tag{1.27}$$

In the first of the four examples, the electrode material (metallic silver) is chemically involved in the electrode reaction; hence it becomes more [less] as a function of time. Such electrodes are called reacting [or consumable] electrodes.

In the other examples, the electrode materials are not involved in the reactions chemically, but constitute the source [sink] of electrons. Such electrodes are called *nonconsumable*. The term *inert electrodes* sometimes used is unfortunate insofar as the electrode itself is by no means inert; rather, it has a strong catalytic effect on the electrode reaction. For reactions occurring at such electrodes, the terms *oxidation– reduction*

reaction and *redox reaction* are widely used, but even these terms are not very fortunate, since reactions occurring at reacting electrodes are also reducing and oxidizing in character. Reactions of type (1.25), where just a single electron is transferred (or more rarely, two electrons at the same time), will in the following be called *simple redox reactions*; reactions of type (1.26), where other solution components also are involved, will be called *complex* (*demanding*) *redox reactions*.

Electrodes at which gases are evolved or consumed [e.g., by reaction (1.27)] can be called *gas electrodes*. In the conventional formulation of the electrode system, the reacting gas is indicated in parentheses.

Specific types of consumable electrode are designated in terms of the constituent material (e.g., as a "silver electrode"). Nonconsumable electrodes are designated either in terms of the electrode material or in terms of the chief component in the electrode reaction; for instance, the terms *platinum electrode* and *hydrogen electrode* are used for electrode (1.27). Neither of these names completely describes the special features of this electrode.

Reacting Electrodes with Soluble and Insoluble Reaction Products (Reactants)

$$\mathrm{KCl},\ aq\,|\,\mathrm{Ag} \qquad \mathrm{AgCl} + e^- \rightleftharpoons \mathrm{Ag} + \mathrm{Cl}^- \tag{1.28}$$

Depending on electrolyte composition, the metal will either dissolve in the anodic reaction, that is, form solution ions [reaction (1.24)], or will form insoluble or poorly soluble salts or oxides precipitating as a new solid phase next to the electrode surface [reaction (1.28)]. Reacting metal electrodes forming soluble products are also known as *electrodes of the first kind*, and those forming solid products are known as *electrodes of the second kind*.

Electrodes with Invertible and Noninvertible Electrode Reactions Most electrode reactions are invertible[‡] in the sense that they will occur in the opposite direction when the direction of current is inverted. Two types of reactions exist that are noninvertible in this sense.

1. Reactions noninvertible on principle or, more probably, reactions for which no conditions have been found so far under which they will proceed in the opposite direction. An example of such a reaction is the cathodic reduction of hydrogen peroxide:

$$\mathrm{H_2O_2} + 2\mathrm{H}^+ + 2e^- \rightarrow 2\mathrm{H_2O}. \tag{1.29}$$

   The formation of hydrogen peroxide by anodic oxidation of water has so far not been realized.

[‡] The concepts of invertibility and reversibility must be distinguished. *Invertibility* is the term proposed to be used for reactions that can be made to occur in both directions, regardless of the departure from thermodynamic equilibrium that is necessary to achieve this. *Reversibility* of a reaction means that it occurs with a minimum departure from the thermodynamic equilibrium state.

2. Reactions which under existing conditions cannot be inverted because of lack of reactants. Thus, metallic zinc readily dissolves anodically in sulfuric acid solution [reaction (1.21) from the right to the left], but when this solution contains no zinc salt, the reverse reaction in which zinc is deposited cathodically cannot occur.

Monofunctional and Polyfunctional Electrodes At monofunctional electrodes, one sole electrode reaction occurs under the conditions specified when current flows. At polyfunctional electrodes, two or more reactions occur simultaneously; an example is the zinc electrode in acidic zinc sulfate solution. When the current is cathodic, metallic zinc is deposited at the electrode [reaction (1.21)] and at the same time, hydrogen is evolved [reaction (1.27)]. The relative strengths of the partial currents corresponding to these two reactions depend on the conditions (e.g., the temperature, pH, solution purity). Conditions may change so that a monofunctional electrode becomes polyfunctional, and vice versa. In the case of polyfunctional electrodes secondary (or side) reactions are distinguished from the principal (for the given purpose) reaction (e.g., zinc deposition). In the electrolytic production of substances and in other practical applications, one usually tries to suppress all side reactions so that the principal (desired) reaction will occur with the highest possible efficiency.

Current-Carrying and Indicator Electrodes According to their functions in galvanic cells used in laboratory practice and in industry, indicator and current-carrying electrodes are distinguished. The latter are intended for productive use of an electrode reaction [i.e., for producing certain substances (in electrolyzers) or electrical energy (in batteries)]. The current-carrying electrodes in electrolyzers include the working electrodes at which the desired products are formed, and auxiliary electrodes, which serve merely to pass current through the working electrode.

Indicator electrodes are used both for analytical purposes (in determining the concentrations of different substances from values of the open-circuit potential or from characteristic features of the polarization curves) and for the detection and quantitative characterization of various phenomena and processes (as electrochemical sensors or signal transducers). One variety of indicator electrode are the reference electrodes, which have stable and reproducible values of potential and thus can be used to measure the potentials of other electrodes.

General Form of the Reaction Equations Equations for electrode reactions can generally be written as

$$\Sigma_{\text{ox}} \nu_j X_j + ne^- \rightleftharpoons \Sigma_{\text{red}} \nu_j X_j, \tag{1.30}$$

where X_j are the species involved in the reaction and ν_j are their stoichiometric coefficients. The summation index "ox" implies that the sum is taken over the oxidized form of the principal reaction component and the substances reacting together with it; the index "red" implies that the sum is taken over the reactant's reduced form and substances associated with it.

Sometimes a general conventional formulation,

$$\mathrm{Ox} + ne^- \rightleftharpoons \mathrm{Red}, \tag{1.31}$$

can be used for relatively simple redox reactions; here Ox and Red are the oxidized and reduced form of the principal reaction component.

When writing an equation for an electrode reaction we must observe the balance of the products, reactants, and electronic charges:

$$\Sigma_{\mathrm{ox}} \nu_j z_j - \Sigma_{\mathrm{red}} \nu_j z_j = n. \tag{1.32}$$

The overall current-producing reaction can be obtained by combining the cathodic reaction occurring at one electrode (index "1") with the anodic reaction occurring at the other electrode (index "2"), while the equations for these reactions must be written so that the values of n in these equations are identical (the reactions must be coupled):

$$\Sigma_{1,\mathrm{ox}}\, \nu_j \mathrm{X}_j + \Sigma_{2,\mathrm{red}}\, \nu_j \mathrm{X}_j \rightleftharpoons \Sigma_{1,\mathrm{red}}\, \nu_j \mathrm{X}_j + \Sigma_{2,\mathrm{ox}}\, \nu_j \mathrm{X}_j. \tag{1.33}$$

The parameter ν_j/n mol, which can be written for each component of the electrode reaction, is sometimes called the *chemical equivalent* of the component in the reaction named, and the value of $(\nu_j/n)M_j$ is called the *equivalent mass* (see the discussion of chemical equivalent in Section 1.3).

1.7 FARADAY'S LAWS

The number of reactant molecules involved in an electrode reaction is related stoichiometrically to the number of charges (electrons) flowing in the circuit. This is the basic argument of the laws formulated by Michael Faraday in 1832–1833.

Faraday's first law reads: In electrolysis, the quantities of substances involved in the chemical change are proportional to the quantity of electricity which passes through the electrolyte. *Faraday's second law* reads: The masses of different substances set free or dissolved by a given amount of electricity are proportional to their chemical equivalents.

In honor of the discoverer of these laws, the amount of charge, which corresponds to the conversion of one chemical equivalent of substance, has been named the *Faraday constant*. An amount of charge nF/ν_j is required to convert 1 mol of substance j. When an amount of charge Q has been consumed at the electrode, the number of moles Δn_j of substance that have formed or reacted is given by

$$\Delta n_j = \frac{\nu_j Q}{nF}. \tag{1.34}$$

This formula unites the two laws of Faraday.

Michael Faraday (1791–1867).

Since the total amount of substance being converted is proportional to the amount of charge, the specific reaction rate v_j, which is the amount of substance j converted in unit time per unit surface area of the electrode, is proportional to the current density i:

$$v_j \equiv \frac{1}{S}\frac{dn_j}{dt} = \nu_j \frac{i}{nF}. \tag{1.35}$$

For this reason the specific rates of electrode reactions are often stated in the electrical units of current density.

Faraday's laws are absolutely rigorous for steady currents. They are the basis for a highly accurate method of measuring the amount of charge: in terms of the mass or volume of substance reacting or set free (coulometry). Faraday's laws have served in the past for defining the unit of electric current: The *international ampere* was that strength of invariant current which when sent through aqueous silver nitrate solution would deposit 1.111800 mg of silver per second at the cathode (another definition is now provided for the ampere as an SI unit).

Deviations from Faraday's laws can be observed in the case of transient currents, when charge, aside from being involved in the electrode reactions, accumulates in certain parts of the circuit (near interfaces). Such transient currents are also known as *nonfaradaic*. An apparent departure from the laws of Faraday can be observed at polyfunctional electrodes when the set of reactions taking place is not fully accounted for.

1.8 EQUATIONS FOR MASS BALANCE

When a current flows in a galvanic cell, balance should exist not only with respect to the charges but also with respect to the reactants. Hence, these materials should be

brought up to (or carried away from) the electrode surface at the rates with which they are consumed (or produced) by the reaction.

Allowing for Eq. (1.35), we can write the condition for mass balance of the reacting component j as

$$J_j = \frac{\nu_j}{nF} i. \tag{1.36}$$

The value of J_j defined by this equation is the flux density of the substance j in the electrolyte stoichiometrically required when the electrode reaction proceeds under steady-state conditions.

With Eqs. (1.10) and (1.13) we can at the same time write the migration flux density as

$$J_{m,j} = \frac{t_j}{z_j F} i. \tag{1.37}$$

The values of the fluxes that can be calculated from these two equations differ substantially. Therefore, an apparent contradiction exists between the balance requirements with respect to charges and substances. This contradiction is particularly obvious in two cases:

1. According to Eq. (1.36), ions not involved in the reaction need not be transported, since $\nu_j = 0$, while according to Eq. (1.37), they are transported.
2. Reacting neutral molecules should be transported according to Eq. (1.36), but they are not, according to Eq. (1.37), since for them $t_j / z_j = 0$.

Under realistic conditions a balance is secured during current flow because of additional mechanisms of mass transport in the electrolyte: *diffusion* and *convection*. The initial inbalance between the rates of migration and reaction brings about a change in component concentrations next to the electrode surfaces, and thus gives rise to concentration gradients. As a result, a diffusion flux $J_{d,j}$ develops for each component. Moreover, in liquid electrolytes, hydrodynamic flows bringing about convective fluxes $J_{kv,j}$ of the dissolved reaction components will almost always arise.

Uncharged reaction components are transported by diffusion and convection, even though their migration fluxes are zero. The total flux density J_j of species j is the algebraic (vector) sum of densities of all flux types, and the overall equation for mass balance must be written not as Eq. (4.1) but as

$$\frac{\nu_j i}{nF} = J_j = J_{m,j} + J_{d,j} + J_{kv,j}. \tag{1.38}$$

The contradiction mentioned above is an apparent one since the overall flux density is relevant for the stoichiometrically required flux contained in Eq. (1.36),

whereas only the migrational component is contained in Eq. (1.37). In the steady state, the diffusion and convection fluxes are always set up in such a way as to secure mass balance.

These questions are considered in more detail in Chapter 4. Any description of current flow in galvanic cells is incomplete if these additional phenomena are disregarded.

1.9 SIGN CONVENTION FOR CURRENT AND FLUXES

A difficulty arises when the total flux is calculated via Eq. (1.38), since the different types of flux can have different directions. The migration flux of cations is always toward the cathode, and that of anions is always toward the anode, but the total flux of any reactant is always in the direction of the corresponding electrode, and the product fluxes are always away from the electrode surface. To allow for this situation, a particular sign system is sometimes used in electrochemistry. According to a recommendation by IUPAC, the anodic current (and current density) is regarded as positive and the cathodic current is regarded as negative (note that in the bulk of any conductor the current is always regarded as positive). This sign convention implies that if for the cathode a flux of cations toward the electrode surface is regarded as positive, that of the anions away from the surface must be regarded as negative.

However, it must be noted that using this convention, equations for similar phenomena containing current densities must always be written in two different ways: for anodic currents with the symbol i and for cathodic currents with the symbol $|\, i \,|$. For this reason, a mixed system is used in the following chapters: All current densities (anodic as well as cathodic) are regarded as positive and denoted by the same symbol, i. In this way the same equations containing current densities can be used for all types of reactions. For the ion fluxes near the surface of electrodes, the aforementioned signs are preserved (see Chapter 4).

REFERENCE

Faraday, M., *Philos. Trans*., 125, 163 (1832); *Philos. Mag.*, **3**, 161, 214, 353 (1833).

2
Electrode Potentials

Classical electrostatics deals with the interactions of idealized electric charges. Electrochemistry deals with real charged particles having both electrostatic and chemical properties. For a clearer distinction of these properties, let us briefly recall some of the principles of electrostatics.

An electrostatic field can be described with the aid of electrostatic potential ψ or field strength **E**, a vectorial parameter that is equal to the negative potential gradient: $\mathbf{E} = -\text{grad}\,\psi$. The directions of the vector at different points are often pictured as the lines of force. The potential gradient will be $d\psi/dx$ in linear fields, where the lines of force are parallel along the x-axis (the one-dimensional problem). In nonlinear fields other coordinate systems that describe a given system more conveniently can also be used: for instance, spherical or cylindrical.

The potential difference $\Delta\psi^{(\mathrm{B,A})} \equiv \psi^{(\mathrm{B})} - \psi^{(\mathrm{A})}$ between points A and B is defined *as* the work w_e performed by external forces when moving an electric test charge Q_t from A to B, divided by the magnitude of this charge:

$$\Delta\psi^{(\mathrm{B,A})} = \frac{w_e}{Q_t}. \tag{2.1}$$

It is assumed here that the test charge is small, so that it will not distort the field (or relative positions of other charges), and that the work performed in moving the charge is only that necessary to overcome electrostatic forces and not any others, such as chemical forces (i.e., the charge is ideal). The potential difference between two points is defined with the aid of Eq. (2.1). The concept of the potential of an individual (isolated) point is undefined and becomes meaningful only when this potential is referred to the potential of another point chosen as the point of reference.

Often, the concept of (two-dimensional) surface or (three-dimensional) space charge is employed. Here it is assumed that the charge is distributed in a continuous fashion (*smeared out*) over the surface S or volume V. Surface and space charge can be described in terms of surface-charge density $Q_S = dQ/dS$ or space-charge density $Q_V = dQ/dV$, which may either be constant or vary between points.

Fundamentals of Electrochemistry, Second Edition, By V. S. Bagotsky

The relation between the spatial potential distribution and the spatial distribution of space-charge density can be stated, generally, in terms of Poisson's differential equation,

$$\frac{d^2\psi}{dx^2} = \frac{Q_V}{\varepsilon_0 \varepsilon}, \tag{2.2}$$

where $\varepsilon_0 = 8.85 \times 10^{-12}$ F/m is the permittivity of vacuum and ε is the relative (dielectric) permittivity of the medium considered. To integrate this equation, boundary conditions must be supplied in addition to the functional relation between charge density and the coordinates.

2.1 INTERFACIAL POTENTIAL DIFFERENCES (GALVANI POTENTIALS)

2.1.1 Metal–Metal Contact

An arbitrary potential difference usually exists between two pieces of metal that are insulated relative to each other; its value depends on excess charges accidentally accumulated on the metal surfaces. When the two pieces are brought in contact, the charges will undergo a redistribution and the potential difference will become well defined. When identical metals are involved, the potential difference will vanish completely, but when different metals are involved, a certain potential difference will be set up across the junction (interface) which depends on the conductors. This potential difference, $\varphi_G^{(2,1)} = \psi^{(2)} - \psi^{(1)}$, between arbitrary points within the first and second metals is called the *Galvani potential* of this junction; $\psi^{(1)}$ and $\psi^{(2)}$ are the inner potentials of the two phases.[†] The sign of the Galvani potential depends on the relative positions stipulated for the phases, and $\varphi_G^{(2,1)} = -\varphi_G^{(1,2)}$.

Galvani potentials are produced by the difference in chemical forces exerted on the electrons within the surface layers by each of the two metals (Fig. 2.1). The unidirectional resultant f_{ch} of these forces causes the transition of electrons from one metal to the other. As a result, if the two metals are uncharged initially, one of them will charge up negatively, and the other (owing to its electron deficit) will charge up positively. The excess charges of opposite sign accumulate near the interface and form an *electrical double layer* (EDL). The field that arises within this layer stops a further transition of electrons. In the end an equilibrium state is established in which the electric force f_e in the EDL completely balances the effect of the chemical forces.

The chemical interaction between carriers j (here electrons) and the surrounding medium can also be described in terms of a chemical potential μ_j, which is the

[†] Instead of the symbol φ_G preferred here, IUPAC recommends $\Delta\varphi = \varphi^2 - \varphi^1$ and uses the term *Galvani potential difference*. In this book we use the symbol ψ at selected points within a phase, φ for potential differences between phases (e.g., the Galvani potential), and χ for potential differences near or across interfaces.

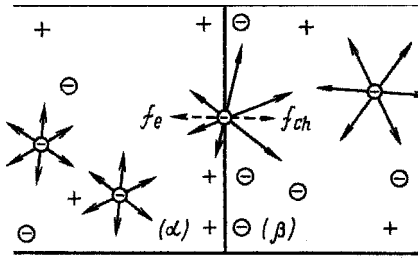

FIGURE 2.1 Forces acting on charged particles near the interface between phases (α) and (β).

potential energy of these particles due to the interaction. By analogy to the electrostatic potential difference, one can define the chemical potential difference for particles in two media as the work w_{ch} performed against chemical forces in transferring these particles, divided by the number n_j of particles transferred:

$$\Delta\mu_j = \frac{w_{ch}}{n_j}. \tag{2.3}$$

(The chemical potential refers to 1 mol of the substance; hence, the values of n_j are stated in moles. A more rigorous definition of chemical potentials is given in Chapter 3.)

The total potential energy $\bar{\mu}_j$ of the charged particles (again per mole, with charge z_jF) is the sum of a chemical and an electrostatic component:

$$\bar{\mu}_j = \mu_j + z_jF\psi; \tag{2.4}$$

it is called the *electrochemical potential* of the species involved.

The condition of equilibrium of the charged particles at the interface between two conductors can be formulated as the state where their electrochemical potentials are the same in the two phases:

$$\bar{\mu}_j^{(1)} = \bar{\mu}_j^{(2)} \tag{2.5}$$

(the combined work of transfer, $w_e + w_{ch}$, then, is zero). From this equality, and allowing for Eq. (2.4), the value of the Galvani potential established at equilibrium will be

$$\varphi_G \equiv \Delta\psi = -\frac{\Delta\mu_j}{z_jF}. \tag{2.6}$$

It follows from Eq. (2.6) that the equilibrium Galvani potential depends only on the nature of the two phases (their bulk properties, which are decisive for the values of μ_j), not on the state of the interphase (i.e., its size, any contamination present, etc.).

2.1.2 Metal–Electrolyte Contact

Galvani potentials also arise at interfaces between other types of conductors. For the interface between a metal electrode and an electrolyte, the Galvani potential can be written as $\varphi_G^{(M,E)} = \psi^{(M)} - \psi^{(E)}$, that is, as the inner potential of the electrode (metal) relative to that of the electrolyte. The statement "there is a shift of electrode potential in the positive direction" means that the potential of the electrode becomes more positive (or less negative) than that of the electrolyte.

The general way in which a Galvani potential is established is similar in all cases, but special features are observed at the metal–electrolyte interface. The transition of charged species (electrons or ions) across the interface is possible only in connection with an electrode reaction in which other species may also be involved. Therefore, equilibrium for the particles crossing the interface [Eq. (2.5)] can also be written as an equilibrium for the overall reaction involving all other reaction components. In this case the chemical potentials of all reaction components appear in Eq. (2.6) (for further details, see Chapter 3).

If, depending on the external conditions imposed, different electrode reactions can occur and different equilibria can be established at a given interface, the Galvani potentials will differ accordingly; in each case, they are determined by the nature of the equilibrium that is established. For instance, at a platinum electrode in sulfuric acid solution through which hydrogen is bubbled, the equilibrium of the hydrogen oxidation–reduction reaction [reaction (1.27)] will be established, but when Fe^{2+} and Fe^{3+} ions are added to the solution, the oxidation–reduction equilibrium of these ions [reaction (1.25)] will be established. The values of Galvani potential established between the platinum and the solution will be different in these two cases. Thus, the Galvani potential between metal and electrolyte is determined by the nature of the electrode reaction occurring at the interface between them.

2.1.3 Electric Double Layers at Interfaces

The existence of Galvani potentials between two different conducting phases is connected with the formation of an electric double layer (EDL) at the phase boundary (i.e., of two parallel layers of charges with opposite signs, each on the surface of one of the contacting phases). It is a special feature of such an EDL that the two layers forming the double layer are a very small (molecular) distance apart, between 0.1 and 0.4 nm. For this reason EDL capacitances are very high (i.e., tenths of $\mu F/cm^2$).

2.1.4 Galvani Potentials Cannot Be Determined

Galvani potentials between two conductors of different types cannot be measured by any means. Methods in which the force acting on a test charge is measured cannot actually be used here, since any values that could be measured would be distorted by the chemical forces. The same holds true for determinations of the work of transfer. At least one more interface is formed when a measuring device such as a voltmeter or potentiometer is connected, and the Galvani potential of that interface will be

contained in the quantity being measured. Galvani potentials also cannot be calculated from indirect experimental data in any rigorous thermodynamic way. Thus, potential differences can only be measured between points located within phases of the same nature.

It might be possible to attempt a theoretical calculation of Galvani potentials on the basis of certain molecular model concepts [e.g., with the aid of Eq. (2.6)]. But at the present level of scientific development, such calculations are still impossible, since the full set of chemical forces acting on charged particles and also the chemical potentials of the corresponding species cannot yet be accounted for quantitatively. In the case of metals, the chemical potential of the electrons corresponds to the value of the Fermi energy (relative to the ground state). However, theoretical calculations of this value are highly inaccurate and cannot be used as a basis for calculating Galvani potentials.

Despite the fact that Galvani potentials for individual interfaces between phases of different types cannot be determined, their existence and the physical reasons that they develop cannot be doubted. The combined values of Galvani potentials for certain sets of interfaces that can be measured or calculated are very important in electrochemistry (see Section 2.3.2).

2.2 EXCHANGE CURRENTS

Equilibria at interfaces between conducting phases are dynamic; every second a certain number of charges cross the interface in one direction, and an equal number of charges cross over in the other direction. Thus, even though the overall current is zero, partial currents constantly cross the interface in both directions, and we observe an exchange of charged particles between the two phases.

At junctions between electronic conductors and electrolytes, the exchange is associated with continuing anodic and cathodic partial reactions. It therefore follows that equilibrium can be established for an electrode reaction only when this reaction is invertible (i.e., can be made to occur in the opposite direction).

When stated in electrical units, the rate of exchange is called the *exchange current* I^0 or (when referring to unit area of the interface) *exchange current density* i^0. The partial current densities in the anodic and cathodic direction are designated as $\vec{i}$ and $\overleftarrow{i}$. The condition for equilibrium can be written as

$$\vec{i} - \overleftarrow{i} = 0 \quad \text{or} \quad \vec{i} = \overleftarrow{i} = i^0. \tag{2.7}$$

The values of exchange current density observed for different electrodes (or reactions) vary within wide limits. The higher they are (or the more readily charges cross the interface), the more readily will the equilibrium Galvani potential be established and the higher will be the stability of this potential against external effects. Electrode reactions (electrodes) for which equilibrium is readily established are called *thermodynamically reversible reactions* (electrodes). But low values of the exchange current indicate that the electrode reaction is slow (kinetically limited).

2.3 OPEN-CIRCUIT VOLTAGES

2.3.1 Metal Circuits

At zero current, when the potential within each conductor is constant, the potential difference between the terminal members of a sequence of conductors joined together as an open circuit is the algebraic sum of all Galvani potentials at the individual interfaces: for example,

$$\psi^{(3)} - \psi^{(1)} = \varphi_G^{(3,2)} + \varphi_G^{(2,1)}. \tag{2.8}$$

As in the case of an individual Galvani potential, this parameter can be neither measured nor calculated for an incomplete open circuit. But for a sequence of conductors with the same metal at either end, the obstacle pointed out in Section 2.1.4 vanishes, because potential differences between the identical terminal members can be measured. This parameter,

$$\mathscr{E} \equiv \psi^{(1')} - \psi^{(1)} = \varphi_G^{(1,3)} + \varphi_G^{(2,3)} + \varphi_G^{(2,1)}, \tag{2.9}$$

is called the *open-circuit voltage* (OCV). When equilibrium exists at all interfaces, the term EMF (from the obsolete concept of an "electromotive force") is also used. The individual components written on the right-hand side of this equation remain unmeasurable.

The OCV of any circuit consisting only of metals or other electronic conductors that are all at the same temperature and not subjected to external force fields is always zero (*Volta's law*). In fact, at any interface the Galvani potential is defined as the chemical potential difference of the electrons: $\varphi_G = \Delta\mu_j$ (for electrons, $z_j = -1$). When these expressions are put into Eq. (2.9), the values of μ_e in the intermediate phases cancel and we obtain the expression $\mathscr{E} = [\mu_e^{(1')} - \mu_e^{(1)}]/F$. Since the terminal members are identical in nature, the chemical potentials in them are the same and the OCV is zero.

It follows from Volta's law that

$$\varphi_G^{(n,1)} = -\varphi_G^{(1,n)} = \varphi_G^{(n,n-1)} + \cdots + \varphi_G^{(3,2)} + \varphi_G^{(2,1)}. \tag{2.10}$$

Therefore, the potential difference between metallic conductors 1 and n will remain unchanged when metallic conductors 2, 3, . . . , $n-1$ are interposed between them.

2.3.2 Galvanic Circuits

For galvanic circuits (cells) the OCV generally is not zero. In contrast to metal circuits, where electrons are the sole carriers, in galvanic circuits the current is transported by different carriers in the different circuit parts (i.e., by electrons and by ions). Hence when substituted into Eq. (2.9), the chemical potentials of the carriers in the intermediate circuit parts will not cancel. The concept of OCV in the case of

galvanic cells always refers to a complete open-circuit arrangement with identical electronic conductors as terminals. It follows from Volta's law that the nature of the terminal conductor has no effect on the OCV, so identical OCV values are obtained for all possible options for the terminal conductor. Hence, in the conventional written formulation of galvanic cells, one usually does not include any terminal phases not in contact with the solution; the phases omitted may normally be taken as the terminals of the measuring instrument.

In the case of cell (1.19) involving a zinc electrode, a graphite electrode, and a $ZnCl_2$ solution, the electrode potentials of the electrodes correspond to the OCV values of cells:

$$\mathrm{M}_R \,|\, \mathrm{E}_R \,\|\, \mathrm{ZnCl_2},\, aq \,|\, \text{graphite} \tag{2.11a}$$

and

$$\mathrm{M}_R \,|\, \mathrm{E}_R \,\|\, \mathrm{ZnCl_2},\, aq \,|\, \mathrm{Zn}\,|. \tag{2.11b}$$

A nonzero OCV of a galvanic cell implies that the potential of one of the electrodes is more positive than that of the other (there is a "positive" and a "negative" electrode). For the galvanic cell without transference, the OCV can be written as

$$\mathscr{E} = \varphi_{\mathrm{G}}^{(\mathrm{M_2,E})} - \varphi_{\mathrm{G}}^{(\mathrm{M_1,E})} + \varphi_{\mathrm{G}}^{(\mathrm{M_1,M_2})}. \tag{2.12}$$

When the cell is symmetrical (i.e., consists of two identical electrodes), its OCV will be zero.

In the case of the cell with transference (1.20), the OCV includes an additional *liquid-junction potential* (a potential difference between electrolytes), and

$$\mathscr{E} = \varphi_{\mathrm{G}}^{(\mathrm{M_2,E})} - \varphi_{\mathrm{G}}^{(\mathrm{M_1,E})} + \varphi_{\mathrm{G}}^{(\mathrm{M_1,M_2})} + \varphi_{\mathrm{G}}^{(\mathrm{E_2,E_1})}. \tag{2.13}$$

True equilibrium cannot be established at the interface between two different electrolytes, since ions can be transferred by diffusion. Hence, in thermodynamic calculations concerning such cells, one often uses *corrected OCV*, $\mathscr{E}^*$:

$$\mathscr{E}^* = \mathscr{E} - \varphi_{\mathrm{G}}^{(\mathrm{E_2,E_1})}. \tag{2.14}$$

which correspond to the OCV of the same cell without the liquid-junction potential. For two electrolytes with similar chemical properties (e.g., two different solutions having the same solvent), one can calculate somewhat approximately this liquid-junction potential (see Chapter 5). Experimental means are also available for reducing the value of this potential difference. Thus, an approximate value of $\mathscr{E}^*$ can be either calculated or measured directly. However, as a rule this parameter cannot be determined with high accuracy. The double broken vertical line in Eqs (2.11) denotes a contact between two electrolytes for which the liquid-junction potential is eliminated. Values of the liquid-junction potential and hence the corrected OCV can be

neither calculated nor measured when the two electrolytes in contact differ chemically (e.g., when they are solutions in different solvents).

2.4 ELECTRODE POTENTIALS

2.4.1 Defining the Concept of Electrode Potential

A galvanic cell's OCV is the algebraic sum of at least three Galvani potentials, two at the interfaces between the electrodes and the electrolyte, and one at the interface between the two electrodes. Since in the cell two arbitrary electrodes are combined, it will be desirable to state the OCV as the difference between two parameters, each of which is characteristic of only one of the electrodes. In the past, the relation $\mathscr{E} = \varphi_G^{(M_2,E)} - \varphi_G^{(M_1,E)}$, involving the individual Galvani potentials between the electrodes and the electrolyte, had been examined under this aspect. However, this relation disregards the Galvani potential between the metals; moreover, it is not useful, insofar as it contains parameters that cannot be determined.

A parameter that is convenient for said purpose is the *electrode potential E*; it must not be confused with the concept of a potential difference between the electrode and the electrolyte. By convention the term *electrode potential E* is used[‡] to denote the OCV of a galvanic cell that consists of the given electrode (the one that is studied) and a reference electrode selected arbitrarily. Thus, the potential of this electrode is compared with that of a reference electrode that is identical for all electrodes being studied. In accordance with this definition, the electrode potential of the reference electrode itself is (conventionally) regarded as zero. Any electrode system for which the equilibrium Galvani potential is established sufficiently rapidly and reproducibly can be used as a reference electrode. We shall write the electrode system to be used as the reference electrode, generally, as M_R/E_R:

$$E = \mathscr{E} = \varphi_G^{(M,E)} + \varphi_G^{(M,M_R)} + \varphi_G^{(M_R,E_R)}. \tag{2.15}$$

The same reference electrode can be used to characterize electrodes in contact with different electrolytes; therefore, the cell used to determine the electrode potential often includes a liquid junction (electrolyte–electrolyte interface). In this case the electrode potential is understood as being the corrected OCV value, $\mathscr{E}^*$, which is the value for this cell after elimination of the liquid-junction potential. For instance, for the zinc electrode (2.11*b*), the expression for the electrode potential can be written as

$$E = \varphi_G^{(Zn,E)} + [\varphi_G^{(M_X,M_R)} + \varphi_G^{(Zn,M_X)} + \varphi_G^{(Zn,M_X)}]. \tag{2.16}$$

It follows from Eqs. (2.15) and (2.16) that for a given electrode, the value of electrode potential corresponds to the Galvani potential of the electrode–electrolyte interface, up to a constant term $E = \varphi_G^{(Zn,E)} + \text{const}$. If for any reason the value of the

[‡] IUPAC uses the same symbol, *E*, for the quantities $\mathscr{E}$ and *E* as defined here.

Galvani potential changes by a certain amount, the electrode potential will change by the same amount: $\Delta E = \Delta\varphi_G^{(M,E)}$. Hence the value of electrode potential yields a rather good description of the properties of this electrode. In what follows, the term *electrode potential* will always be understood as being an electrode potential relative to a defined reference electrode.

We can readily show that for cells without transference, the OCV value is equal to the difference in electrode potentials of the two electrodes (i.e., it can be written in terms of two parameters that are measurable, and each of them refers to just one of the electrodes). In the expression for OCV, the φ_G values for the reference electrode cancel, so that the reference electrode itself has no effect on the results (provided that all potentials refer to the same reference electrode). In the case of cells with transference, the difference in electrode potentials is equal not to the total but to the corrected OCV value, $\mathscr{E}^*$.

The following sign convention applies to OCV and electrode potentials. The OCV values are conventionally regarded as positive values, but the values of electrode potentials are reported as positive or negative, depending on the polarity of this electrode relative to the reference electrode. In practice, different types of reference electrode are used, which gives rise to different scales. The values of the electrode potentials in these scales differ by amounts given by the potential differences between the reference electrodes themselves. Most common is the scale of the standard hydrogen electrode (SHE), and values of potential measured with the aid of other reference electrodes are often converted to this scale.

2.4.2 Nonequilibrium Electrode Potentials

Electrochemical equilibrium is not always established at electrode surfaces. When there is no equilibrium, the value of the Galvani potential will not be the same as the equilibrium value defined by Eq. (2.6); the value of electrode potential will also differ accordingly.

Two cases where equilibrium is lacking must be distinguished: that which is unrelated to current flow and can be observed even for a nonworking electrode, and that which is related exclusively to the passage of current through the electrode. The former is the case of nonequilibrium open-circuit potentials (nonequilibrium OCP), and the latter is that of electrode polarization.

Nonequilibrium Open-Circuit Potentials Different reasons exist for lack of equilibrium at electrode–electrolyte interfaces even in the absence of an electric current:

1. *Effectively impossible charge transfer*. If, under given conditions, not even a single electrode reaction is possible, any accidental accumulation of charge in the EDL will be stable, as it cannot be removed by charge transfer (or "leakage" of charges). One can supply charge from outside, as in the case of ordinary electrostatic capacitors, and vary the electrode potential arbitrarily. Hence, the potential has no unique equilibrium value but depends on an accidental or deliberate accumulation of charge in the EDL. An electrode having these attributes is called *ideally*

polarizable. Ideal polarizability usually is observed only within a certain interval of potentials, whereas outside this interval charge transfer across the EDL (current flow) is possible.

2. *Low exchange currents*. When an electrode reaction is possible but its exchange current is low, the equilibrium potential is readily disturbed by external effects. Such an influence is exerted in particular by foreign components (contaminants), the reactions of which are superimposed on the basic reaction.

3. *Several electrode reactions occurring simultaneously*. The following reactions can occur at an iron electrode in HCl solution containing $FeCl_2$ while a hydrogen atmosphere is maintained:

$$Fe^{2+} + 2e^- \rightleftharpoons Fe, \tag{2.17}$$

$$2H^+ + 2e^- \rightleftharpoons H_2. \tag{2.18}$$

Each of these reactions has its own exchange current density and its own equilibrium potential. The condition of overall balance at this electrode is determined not by Eq. (2.7) but by the equation

$$\vec{i}_1 + \vec{i}_2 + \overleftarrow{i}_1 + \overleftarrow{i}_2 = 0, \tag{2.19}$$

where subscripts "1" and "2" refer to reactions (2.17) and (2.18), respectively. Generally $\vec{i}_1 \neq \overleftarrow{i}_1$ [i.e., reaction (2.17) will occur in one direction and reaction (2.18) will occur in the other direction]. In our example, iron will dissolve anodically ($\vec{i}_1 > \overleftarrow{i}_1$) and hydrogen will be evolved at the cathode ($\vec{i}_2 > \overleftarrow{i}_2$). The nonequilibrium potential being established will be intermediate between the individual equilibrium potentials corresponding to reactions (2.17) and (2.18) and is called a *mixed potential* or, when it is well reproducible and almost time invariant, a steady-state or *rest potential*.

Equilibrium potentials can be calculated thermodynamically (for more details, see Chapter 3) when the corresponding electrode reaction is known precisely, even when they cannot be reached experimentally (i.e., when the electrode potential is nonequilibrium despite the fact that the current is practically zero). The open-circuit voltage of any galvanic cell where at least one of the two electrodes has an nonequilibrium open-circuit potential will also be nonequilibrium. Particularly in thermodynamic calculations, the term EMF is often used for measured or calculated equilibrium OCV values.

Electrode Potentials During Current Flow At nonzero current, the flow of charges crossing the interface in one direction is larger than that crossing it in the other direction:

$$i = \vec{i} \pm \overleftarrow{i}. \tag{2.20}$$

The partial current $\vec{i}$ is larger than the partial current $\overleftarrow{i}$ in the case of anodic currents, and vice versa in the case of cathodic currents. Thus, when there is a net current flow, the partial currents are not the same as in equilibrium [when condition (2.7) is observed]. For this change in partial currents a unidirectional force is needed [i.e., the electric force f_e should be stronger (or weaker) than the chemical force f_{ch} (see Fig. 2.1)]. The electrode potentials change accordingly. Anodic current flow is associated with a positive potential shift (easier transfer of positive charges from the electrode into the electrolyte or of negative charges in the opposite direction); cathodic current flow is associated with a negative potential shift.

The shift of electrode potential caused by current flow,

$$\Delta E \equiv E_i - E_0 \tag{2.21}$$

(where E_i and E_0 are the potentials at a current density i and at zero current, respectively), has been termed *electrode polarization*. The quantity ΔE is positive in the case of anodic currents and negative in the case of cathodic currents. For a given electrode, the absolute value of polarization or departure from equilibrium will be larger at higher currents. The exchange current density is used here as the reference quantity. When the net current is low compared to the exchange current, the departure from equilibrium will be minor and polarization low (for further details, see Chapter 6).

2.5 CELL VOLTAGE AT NONZERO CURRENT

2.5.1 Two Directions of Current Flow

Two directions of current flow in galvanic cells are possible: a spontaneous direction and an imposed direction. When the cell circuit is closed with the aid of electronic conductors, current will flow from the cell's positive electrode to its negative electrode in the external part of the circuit, and from the negative to the positive electrode within the cell (Fig. 2.2*a*). In this case the current arises from the cell's own voltage, and the cell acts as a chemical source of electric current or *battery*. But when a power source of higher voltage, connected so as to oppose the cell, is present in the external circuit, it will cause current to flow in the opposite direction (Fig. 2.2*b*), and the cell works as an *electrolyzer*.

It follows that in batteries, the negative electrode is the anode and the positive electrode is the cathode. In an electrolyzer, to the contrary, the negative electrode is the cathode and the positive electrode is the anode. Therefore, attention must be paid to the fact that the concepts of "anode" and "cathode" are related only to the direction of current flow, not to the polarity of the electrodes in galvanic cells.

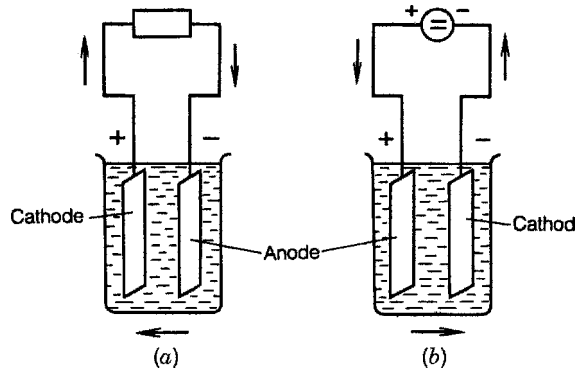

FIGURE 2.2 Directions of current flow when the galvanic cell functions as a battery (*a*) and as an electrolyzer (*b*).

2.5.2 Polarization and Ohmic Losses

The way in which the voltage of a galvanic cell changes when a current flow depends on the direction of the current. In a cell working as a battery, the positive electrode is the cathode and the negative electrode is the anode. Owing to polarization the potential of the former moves in the negative direction and that of the latter moves in the positive direction [i.e., the potentials of the two electrodes move closer together, and the voltage decreases (Fig. 2.3*a*)]. In addition, an ohmic voltage drop φ_{ohm} develops in the cell (chiefly in the electrolyte); the potential of the electrolyte will be more negative at the cathode, to which the cations migrate. This leads to an

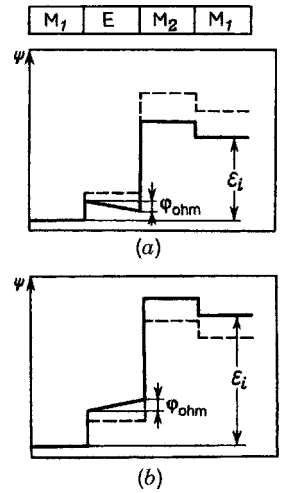

FIGURE 2.3 Potential distribution in galvanic cells functioning as a battery (*a*) and as an electrolyzer (*b*); the dashed lines are for the zero-current situation.

additional voltage decrease. Thus, in this case the voltage under current flow, $\mathscr{E}_i$, will always be lower than the OCV, $\mathscr{E}_0$:

$$\mathscr{E}_i = \mathscr{E}_0 - \Delta E_a - |\Delta E_c| - \varphi_{\text{ohm}} = \mathscr{E}_0 - \eta_{\text{cell}} \tag{2.22}$$

(the subscript a stand for the anode and c stand for the cathode).

In cells working as electrolyzers, the positive electrode is the anode and the negative electrode is the cathode. All the factors listed above (for the case of a battery) will now produce an increase in voltage relative to the OCV (Fig. 2.3*b*):

$$\mathscr{E}_i = \mathscr{E}_0 + \Delta E_a + |\Delta E_c| + \varphi_{\text{ohm}} = \mathscr{E}_0 + \eta_{\text{cell}}. \tag{2.23}$$

The modulus of the voltage change,

$$\eta_{\text{cell}} \equiv |\mathscr{E}_i - \mathscr{E}_0| = \Delta E_a + |\Delta E_c| + \varphi_{\text{ohm}}, \tag{2.24}$$

is called the *total cell overvoltage*. (Sometimes the term *overvoltage* and the symbol η are used to denote the polarization ΔE of a single electrode.)

3

Thermodynamics of Electrochemical Systems

3.1 CONVENTIONAL AND UNDEFINED PARAMETERS

Often, parameters of which the absolute values are not known are contained in physical and thermodynamic equations. Among these parameters, two types can be distinguished:

1. *Conventional parameters*, which can be defined only in terms of differences of the values in two states or points. The value of such a parameter in any given state depends on a conventional point of reference and hence can only be determined to a constant term. It is physically meaningless to define absolute values of such parameters. The electrostatic potential is an example.
2. *Experimentally undefined parameters*, which have a real physical meaning; that is, they reflect an actual physical phenomenon but cannot be determined from the experimental data (even a thought experiment to measure them cannot be conceived) or by a thermodynamic calculation. In isolated cases such parameters can be calculated on the basis of nonthermodynamic models. The equations used for calculations generally contain sums, differences, or other combinations of such parameters that are measurable. The Galvani potential at the interface between two dissimilar conducting phases is an example.

The values of all these parameters are unknown, yet it is useful to include them in physical arguments and equations in order to facilitate an understanding of correlations between different phenomena.

Fundamentals of Electrochemistry, Second Edition, By V. S. Bagotsky

3.2 THERMODYNAMIC FUNCTIONS IN ELECTROCHEMISTRY

3.2.1 Thermodynamic Functions

The well-known tools of chemical thermodynamics [e.g., the book of Guggenheim (1923)] are used in electrochemical systems to describe equilibria and processes, but some special features arising from the presence of charged particles and potential differences between the phases must be taken into account. Electrochemical systems are usually discussed under conditions of constant temperature T and pressure p. Under these conditions the most convenient thermodynamic functions are the Gibbs energy G, given by $U + pV - TS$, and the enthalpy H, given by $U + pV$ (where U is the internal energy, V is the volume, and S is the entropy).

The values of these functions change when thermodynamic processes take place. Processes in which the Gibbs energy decreases (i.e., for which $\Delta G < 0$), will take place spontaneously without specific external action. The Gibbs energy is minimal in the state of equilibrium, and the condition for equilibrium are given as

$$\Delta G = 0 \quad \text{or} \quad dG = 0. \tag{3.1}$$

In systems with different components, the values of the thermodynamic functions depend on the nature and number of these components. One distinguishes components forming independent phases of constant composition (the "pure" components) from the components that are part of mixed phases of variable composition (e.g., solutions).

The Gibbs energy is an additive function of all components. For systems consisting of pure components only,

$$G = \Sigma n_k G_k, \tag{3.2}$$

where G_k is the specific (molar) Gibbs energy of component k (in J/mol) and n_k is the number of moles of this component in the system.

In phases of variable composition, the contribution of each component to the total value of G for a given phase depends not only on the amount of this component present in this phase but also on its concentration. For small changes in composition,

$$dG = \Sigma_k \frac{dG}{dn_k} dn_k = \Sigma \mu_k dn_k. \tag{3.3}$$

The parameter

$$\mu_k \equiv \frac{dG}{dn_k} \tag{3.4}$$

is called the *chemical potential* of the component k (in J/mol). The partial derivatives in Eqs. (3.3) and (3.4) are evaluated where the values of all remaining variables beyond n_k are kept constant. The values of μ_k are not constant, in contrast to parameter G_k,

but depend on the concentration of the given substance in the phase of variable composition and hence on the presence of other components.

The chemical potential of a gas depends on its partial pressure p_k. When the gas obeys ideal gas laws, we have

$$\mu_k = \mu_k^0 + RT \ln p_k. \tag{3.5}$$

For sufficiently dilute solutions the concentration dependence of chemical potential is given similarly by

$$\mu_k = \mu_k^0 + RT \ln c_k. \tag{3.6}$$

Solutions in which the concentration dependence of chemical potential obeys Eq. (3.6), as in the case of ideal gases, have been called *ideal solutions*. In nonideal solutions (or in other systems of variable composition) the concentration dependence of chemical potential is more complicated. In phases of variable composition, the values of the Gibbs energy are determined by the equation

$$G = \Sigma n_k \mu_k \tag{3.7}$$

instead of Eq. (3.2).

3.2.2 Electrochemical Potentials

The energy of an ion in a given medium depends not only on chemical forces but also on the electrostatic field; hence the chemical potential of an ion j customarily is called its *electrochemical potential* and labeled $\overline{\mu}_j$.The electrostatic potential energy of an ion j when reckoned per mole is given by $\pm z_j F\psi$, where ψ is the electrostatic (inner) potential of the phase containing the ion; a plus sign for cations and a minus sign for anions. Hence, the electrochemical potential can be written as the sum of two terms:

$$\overline{\mu}_j = \mu_j \pm z_j F\psi, \tag{3.8}$$

where μ_j is the chemical component of the ion's electrochemical potential (it is commonly called the ion's *chemical potential*).

This formulation is somewhat conditional, since it assumes that a concentration change will affect only the value of μ_j and a potential change will affect only the second term on the right-hand side of (3.8). Actually, a potential change is associated with a change in the amount of charge in the EDL and implies some change in concentration of the ions in the bulk phase. Hence, the potential ψ cannot be varied independent of the concentration or of μ_j. However, in most cases (other than extremely dilute systems) a change in potential is associated with concentration changes so small that the concentration can for all practical purposes be regarded as constant.

The Gibbs energy of an electroneutral system is independent of the electrostatic potential. In fact, when substituting into Eq. (3.7) the electrochemical potentials of the ions contained in the system and allowing for the electroneutrality condition, we can readily see that the sum of all terms $\pm_j z_j F\psi$ is zero. The same is true for any electroneutral subsystem consisting of the two sorts of ion M^{z+} and A^{z-} (particularly when these are produced by dissociation of a molecule of the original compound k into τ_+ cations and τ_- anions), for which

$$\tau_+\overline{\mu}_+ + \tau_-\overline{\mu}_- = \tau_+\mu_+ + \tau_-\mu_- = \mu_k, \tag{3.9}$$

where μ_k is the chemical potential of compound k. (In the following, the symbol k will only be used for electroneutral compounds or ensembles of ions).

The thermodynamics of electrochemical systems has two distinctive features:

1. *The electrochemical potential of single ionic species cannot be determined.* In systems with charged components, all energy effects and all thermodynamic properties are associated not with ions of a single type but with combinations of different ions. Hence, the electrochemical potential of an individual ionic species is an experimentally undefined parameter, in contrast to the chemical potential of uncharged species. From the experimental data, only the combined values for electroneutral ensembles of ions can be found. Equally inaccessible to measurements is the electrochemical potential, $\overline{\mu}_e$, of free electrons in metals, whereas the chemical potential, μ_e, of the electrons coincides with the Fermi energy and can be calculated very approximately.

2. *The energy effects of individual electrode reactions cannot be measured.* Any given electrode reaction can occur only in parallel with a second, coupled reaction. Because of the interfering effects of this reaction (which include heat, diffusion, and other fluxes in the electrolyte), it is not possible to determine the energy effects experimentally, and hence the thermodynamic parameters, of an individual electrode reaction. Nor can these parameters be calculated, since this would require knowledge of the electrochemical potentials of individual ionic species and of the Galvani potential at the electrode–electrolyte interface. All thermodynamic calculations and measurements refer to the current-producing reaction as a whole (this also holds true for reactions involving the reference electrode).

3.3 THERMODYNAMIC ACTIVITY

3.3.1 Definition of the Concept of Activity

By virtue of the function (3.6), concentrations, which are readily determined parameters, can be used instead of chemical potentials in the thermodynamic equations for ideal systems. The simple connection between the concentrations and chemical potentials is lost in real systems. To facilitate the changeover from ideal to nonideal systems and to avoid the use of two different sets of equations in chemical thermodynamics,

Gilbert N. Lewis (1907) suggested employing another parameter, the *thermodynamic activity* a_k, which has the dimensions of concentration and is defined by the equation

$$\mu_k \equiv \mu_k^0 + RT \ln a_k, \tag{3.10}$$

where μ_k^0 is a constant that is independent of phase composition, called the *standard chemical potential.*

The changeover to thermodynamic activities is equivalent to a change of variables in mathematical equations. The relation between parameters μ_k and a_k is unambiguous only when a definite value has been selected for the constant μ_k^0. For solutes this constant is selected so that in highly dilute solutions where the system μ_k^0 approaches an ideal state, the activity will coincide with the concentration: $(\lim a_k)_{c_k \to 0} = c_k$. Hence the value of μ_k^0 in Eq. (3.10) coincides with that in Eq (3.6). For single-component liquid and solid phases of constant composition, the activity is also always taken to be unity.

A system's standard state is defined as the state in which $\mu_k = \mu_k^0$ and hence $a_k = 1$. We must bear in mind that the standard state does not coincide with the limiting state (at low concentrations) when the system becomes ideal. Hence, in the standard state the value of activity differs from the value of concentration (except for the solvent).

Using activities instead of chemical potentials has the major advantage that the equations derived for ideal systems can be retained in the same form for real systems, but with activities in the place of concentrations. For the practical application of these equations, we must know the values of activity as a function of concentration.

The degree of departure of a system from the ideal state can be described by another parameter, the *activity coefficient*, which is defined as the ratio of activity to concentration:

$$f_k \equiv \frac{a_k}{c_k}. \tag{3.11}$$

Activity coefficients are dimensionless. With standard states selected as indicated above, activity coefficients will be unity in ideal systems. The degree of departure of a system from the ideal state is described by the departure of the activity coefficients from unity.

3.3.2 Activities of Ions in Electrolyte Solutions

In electrolyte solutions, nonideality of the system is much more pronounced than in solutions with uncharged species. This can be seen in particular from the fact that electrolyte solutions start to depart from an ideal state at lower concentrations. Hence, activities are always used in the thermodynamic equations for these solutions. It is in isolated instances only, when these equations are combined with other equations involving the number of ions per unit volume (e.g., equations for the balance of charges), that concentrations must be used and some error thus is introduced.

Like its chemical potential, the activity of an individual ion cannot be determined from experimental data. For this reason the parameters of *electrolyte activity* a_k and *mean ionic activity* $a_\pm$ are used, which are defined as follows:

$$a_k \equiv a_\pm^{\tau_k} \equiv a_+^{\tau_+} a_-^{\tau_-}. \tag{3.12}$$

Values of a_k and of $a_\pm$ can be found experimentally.

In binary electrolyte solutions with an initial concentration c_k and ionic concentrations $c_j = \alpha \tau_j c_k$ [cf. Eq. (1.2)] the ionic activities can be written as

$$a_j = f_j \alpha \tau_j c_k = \gamma_j \tau_j c_k, \tag{3.13}$$

where $\gamma_j \equiv f_j \alpha$ is the *stoichiometric activity coefficient*, in which the degree of activation is taken into account (for solutions of strong electrolytes $\gamma_j \approx f_j$).

Substituting into Eq. (3.12) the (expanded) expression (3.13) for the activities of the individual ions, we obtain

$$a_\pm = \alpha f_\pm \lambda c_k. \tag{3.14}$$

Here $f_\pm$ is the mean ionic activity coefficient defined, by analogy with the mean ionic activity, as

$$f_\pm^{\tau_k} \equiv f_+^{\tau_+} f_-^{\tau_-}, \tag{3.15}$$

and λ is the numerical factor

$$\lambda \equiv (\tau_+^{\tau_+} \tau_-^{\tau_-})^{1/\tau_k}. \tag{3.16}$$

For symmetric electrolytes $\lambda = 1$; for 1:2 electrolytes (e.g., Na_2SO_4), 1:3 electrolytes ($AlCl_3$), and 2:3 electrolytes ($[Al_2(SO_4)_3]$, the corresponding values of λ are 1.587, 2.280, and 2.551. Mean ionic activity coefficients of many salts, acids, and bases in binary aqueous solutions are reported for wide concentration ranges in special handbooks.

In saturated solutions of electrolytes (particularly those having low solubility), the overall chemical potential, μ_k, of the substance in the solution is equal to the specific Gibbs energy, G_k, of the solid phase in equilibrium with the solution. Hence, the values of α_k and μ_k are constant in the solution, and according to Eq. (3.12),

$$a_+^{\tau_+} a_-^{\tau_-} = L(k), \tag{3.17}$$

where the constant $L(k)$ is called the *solubility product* or *ionic product* of the substance k.

In aqueous solutions, H^+ and OH^- ions are present, owing to the dissociation of water molecules. In dilute solutions, the activity of water is constant. Hence, for the activities of these ions an equation of the type (3.17) is obeyed, too. The ionic product

of water is written as K_w. This parameter is given by $K_w = a_{H^+} a_{OH^-}$ and at 25°C has a value of 1.27×10^{-14} mol^2/L^2.

3.4 EQUATIONS FOR THE EMF OF GALVANIC CELLS

Let us write ΔG_m for the Gibbs energy change occurring during a chemical reaction m involving the conversion of ν_j moles of reactants (index "react") and products ("prod"). We find that

$$\Delta G_m = \Sigma_{\text{prod}} \nu_j \mu_j - \Sigma_{\text{react}} \nu_j \mu_j \tag{3.18}$$

when the concentrations and hence the chemical potentials of the components do not change markedly during the reaction (when the degree of conversion is low). For electrode reactions of the type (1.30) involving n electrons, Eq. (3.18) can be written as

$$\pm \Delta G_m = \Sigma_{\text{ox}} \nu_j \overline{\mu}_j - \Sigma_{\text{red}} \nu_j \overline{\mu}_j + n\overline{\mu}_e, \tag{3.19}$$

where the plus sign is used for the anodic and the minus sign for the cathodic direction of the reaction. The electrons that are involved in the reaction are at a potential $\psi^{(M)}$ inside the metal, and all ions are at a potential $\psi^{(E)}$ inside the electrolyte. Using the expanded form (3.8) for the electrochemical potential of these components and allowing for Eq. (1.32) as well as for the definition of the Galvani potential, we can transform Eq. (3.18) to

$$\pm \Delta G_m = \Sigma_{\text{ox}} \nu_j \mu_j - \Sigma_{\text{red}} \nu_j \mu_j + n\mu_e - nF\varphi_G. \tag{3.20}$$

It follows from this equation that the Galvani potential in the point of equilibrium of the electrode reaction ($\Delta G_m = 0$) is given by

$$\varphi_G = \frac{1}{nF} (\Sigma_{\text{ox}} \nu_j \mu_j - \Sigma_{\text{red}} \nu_j \mu_j + n\mu_e). \tag{3.21}$$

None of the terms of this equation can be determined experimentally. The equation represents a generalization of Eq. (2.6) for the case where charge transfer between phases is attended by an electrochemical reaction.

For a galvanic cell with two electrodes where the overall current-producing reaction (1.33) takes place, allowing for charge balance we can write for the Gibbs energy change of this reaction [when using Eq. (3.19) for electrodes 1 and 2]:

$$\Delta G_m = \Sigma_1 \nu_j \mu_j - \Sigma_2 \nu_j \mu_j. \tag{3.22}$$

The reaction will occur spontaneously (without an external supply of energy) and the value of ΔG_m will be negative when the cell is operated as a battery [i.e., when electrode (1) is the anode (the negative electrode)].

The OCV of this cell is the algebraic sum of the Galvani potentials at three interfaces. When each of them is in equilibrium, we find for the overall potential difference (which in this case we can call an electromotive force or EMF; see Section 2.4.2.1), by putting functions (2.06) and (3.21) into an equation of type (2.17):

$$\mathscr{E} = \Sigma_2 \nu_j \frac{\mu_j}{nF} + \frac{\mu_e^{(M_2)}}{F} - \Sigma_1 \frac{\nu_j \mu_j}{nF} - \frac{\mu_e^{(M_1)}}{F} + \left[\frac{\mu_e^{(M_2)}}{F} - \frac{\mu_e^{(M_1)}}{F} \right], \tag{3.23}$$

or, after simplification and allowing for Eq. (3.22),

$$\mathscr{E} = \frac{\Sigma_2 \nu_j \mu_j - \Sigma_1 \nu_j \mu_j}{nF} = -\frac{\Delta G_m}{nF}. \tag{3.24}$$

This equation links the EMF of a galvanic cell to the Gibbs energy change of the overall current-producing reaction. It is one of the most important equations in the thermodynamics of electrochemical systems. It follows directly from the first law of thermodynamics, since $nF\mathscr{E}$ is the maximum value of useful (electrical) work of the system in which the reaction considered takes place. According to the basic laws of thermodynamics, this work is equal to $-\Delta G_m$.

The open cell discussed was considered as an equilibrium cell since equilibrium was established across each individual interface. However, the cell as a whole is not in equilibrium; the overall Gibbs energy of the full reaction is not zero, and when the circuit is closed, an electric current flows that is attended by chemical changes (i.e., a spontaneous process sets in).

It is typical that in Eq. (3.23) for the EMF, all terms containing the chemical potential of electrons in the electrodes cancel in pairs, since they are contained in the expressions for the Galvani potentials, both at the interface with the electrolyte and at the interface with the other electrode. This is due to the fact that the overall current-producing reaction comprises the transfer of electrons across the interface between two metals in addition to the electrode reactions.

This gives rise to an important conclusion. For nonconsumable electrodes that are not involved in the current-producing reaction, and for which the chemical potential of the electrode material is not contained in the equation for electrode potential, the latter (in contrast to a Galvani potential) depends only on the type of reaction taking place; it does not depend on the nature of the electrode itself.

For instance, in the galvanic cell

$$\mathrm{Pt(H_2)\,|\,H_2SO_4\,|\,(H_2)Pd\,|\,Pt}, \tag{3.25}$$

which contains two hydrogen electrodes, one made of platinum and the other of palladium, the Galvani potentials at the two interfaces involving the solution will be different. However, in a thermodynamic sense the cell is symmetric, and current flow does not lead to an overall chemical reaction (hydrogen is evolved at one of the electrodes but ionized at the other). For this reason the Gibbs energy change and the

EMF are zero and the electrode potentials of the two electrodes are identical. When reporting electrode potentials and EMF, one indicates, when necessary, the reactions to which they refer [e.g., $E(Zn^{2+} + 2e^- \rightleftharpoons Zn)$ or simply $E(Zn^{2+}, Zn)$ and $E(Cu^{2+} + Zn \rightleftharpoons Cu + Zn^{2+})$, etc.].

3.5 CONCENTRATION DEPENDENCE OF ELECTRODE POTENTIALS

3.5.1 Nernst Equation for Ideal Systems

Electrode potentials (as well as values of the EMF of galvanic cells) depend on the composition of the electrolyte and other phases of variable composition. The electrode potential corresponds to the Galvani potential of the electrode–electrolyte interface, up to a constant term $E = \varphi_G + \text{const}$. Introducing the concentration dependence of the chemical potential μ into Eq. (3.21), we find that

$$E = E_c^0 + \frac{RT}{nF}\left(\Sigma_{ox}\nu_j \ln c_j - \Sigma_{red}\nu_j \ln c_j\right). \tag{3.26}$$

The partial pressures p_j will appear here for gaseous substances instead of concentrations c_j [see Eq. (3.5)].

In Eq. (3.39), E_c^0 is a constant that depends on the nature of the electrode reaction; it is equal to the electrode potentials for values $c_j = 1$. The value of the electrode potential E depends primarily on the value of this constant, since the second term of this equation, which is the correction term for concentrations, is relatively small, although in certain cases it becomes the major term. The components that are involved in the electrode reaction and therefore influence the value of the electrode potential are called *potential-determining substances.* It follows from this equation that the potential will shift in the positive direction when the concentration of the oxidizing agent or of components entering the reaction together with it is raised, but it will shift in the negative direction when the concentration of the reducing agent or of components entering the reaction together with it is raised.

The combination of constants RT/F often appears in electrochemical equations; it has the dimensions of voltage. At 25°C (298.15 K) it has a value of 0.02569 V (or roughly 25 mV). When including the conversion factor for changing natural to common logarithms, we find a value of 0.05916 V (about 59 or 60 mV) for 2.303 (RT/F) at 25°C. Values for other temperatures can be found by simple conversion, since this parameter is proportional to the absolute temperature.

For metal electrodes of the first type at which the reaction $M^{z+} + z_+ e^- \rightleftharpoons M$ takes place, Eq. (3.26) becomes

$$E = E_c^0 = \frac{RT}{z_+ F} \ln c_{M^{z+}}. \tag{3.27}$$

Walther Nernst (1864–1941; Nobel prize, 1920).

An equation of this form had been suggested by Walther Nernst in 1869. In the case of amalgam electrodes (e.g., sodium amalgam in NaOH solution), the potential depends on the concentrations of the oxidizing agent (the cations in the electrolyte) as well as of the reducing agent (the metal in the amalgam, $c_{\mathrm{Na}}^{(\mathrm{Hg})}$):

$$E = E_c^0 + \frac{RT}{F} \ln \frac{c_{\mathrm{Na}^+}^{(\mathrm{E})}}{c_{\mathrm{Na}}^{(\mathrm{Hg})}}. \tag{3.28}$$

An equation for the very simple redox reaction $\mathrm{Fe}^{3+} + e^- \rightleftharpoons \mathrm{Fe}^{2+}$,

$$E = E_c^0 \frac{RT}{F} \ln \frac{c_{\mathrm{Fe}}^{3+}}{c_{\mathrm{Fe}}^{2+}}, \tag{3.29}$$

had been suggested by Franz C. A. Peters in 1898. At present, all equations of this type are known as *Nernst equations*.

3.5.2 Equations for Real Systems

Equations describing the relation between electrode potential and composition of the system in the case of real systems can be written, by analogy with Eq. (3.26), as functions of the component activities

$$E = E_a^0 + \frac{RT}{nF} (\Sigma_{\mathrm{ox}} \nu_j \ln a_j - \Sigma_{\mathrm{red}} \nu_j \ln a_j). \tag{3.30}$$

For the particular case of electrodes of the first type, we have, instead of Eq. (3.27),

$$E = E_a^0 = \frac{RT}{z_+ F} \ln a_{\mathrm{M}^{z+}}. \tag{3.31}$$

There is a major difficulty that arises when such equations are used in practice, in that the activities of individual ions are unknown unless the solutions are highly dilute and the ionic components involved in the electrode reaction do not form electroneutral groups. Hence, for practical calculations we must employ values of mean ionic activity $a_{\pm}$:

$$E = E_a^0 + \frac{RT}{nF} (\Sigma_{\text{ox}} \nu_j \ln a_{\pm} - \Sigma_{\text{red}} \nu_j \ln a_{\pm}), \tag{3.32}$$

which makes the results somewhat provisional. But this can be tolerated insofar as the experimental values of electrode potentials are also slightly distorted and depend on the activities of other ions, because reference electrodes with other potential-determining ions or liquid-junction potentials are present. In cases where data for the activity coefficients are altogether unavailable (particularly in multicomponent solutions), concentrations must be used instead of activities [Eq. (3.26)]. This leads to appreciable errors and is admissible only for the purposes of approximate calculations.

Parameter E_a^0 in Eqs. (3.30) and (3.32) is called the *standard electrode potential*; it corresponds to the value of electrode potential that is found when the activities of the components are unity. Values E_a^0 differ somewhat from values E_c^0. For a more distinct differentiation between these parameters, E_c^0 is called the *formal electrode potential*.

The values of E_a^0 for electrode reactions (or of E_c^0, when sufficiently reliable activity data are not available) are listed in special tables; some values of this type are shown in Table 3.1. When using such tables we must bear in mind that the values of E^0 for reactions involving gases have been calculated for partial pressures of 1 atm, which in SI units corresponds to 101, 325 Pa (about 0.1 MPa). Hence, in the Nernst equation we must use gas pressures in the now-obsolete unit atmospheres.

The overall current-producing reaction in a cell involves only electroneutral sets of species; hence, in the equation for the EMF $\mathscr{E}$ of such cells,

$$\mathscr{E} = E_+ - E_-, \tag{3.33}$$

it is entirely legitimate to replace the true activities of individual ions by mean ionic activities.

Subscripts a and c for the parameter E^0 are dropped in the following.

3.5.3 Electrodes of the Second Kind

A silver electrode in aqueous KCl solution is the example of an electrode of the second type. Here the reaction

$$\text{Ag} + \text{C1}^- \rightleftharpoons \text{AgC1} + e^- \tag{3.34}$$

takes place. Owing to the low solubility of AgCl, the product of the anodic process precipitates as a solid and the electrolyte is almost always saturated with it. The solubility

TABLE 3.1 Standard Electrode Potentials (25°C)

Reaction	E^0 (V) (SHE)	Reaction	E^0 (V) (SHE)
$Li^+ + e^- \rightleftharpoons Li$	−3.045	$HgO + H_2O + 2e^- \rightleftharpoons Hg + 2OH^-$	0.098
$K^+ + e^- \rightleftharpoons K$	−2.935	$Sn^{4+} + 2e^- \rightleftharpoons Sn^{2+}$	0.154
$Ca^{2+} + 2e^- \rightleftharpoons Ca$	−2.866	$Cu^{2+} + e^- \rightleftharpoons Cu^+$	0.153
$Na^+ + e^- \rightleftharpoons Na$	−2.714	$AgCl + e^- \rightleftharpoons Ag + Cl^-$	0.2224
$Mg^{2+} + 2e^- \rightleftharpoons Mg$	−2.363	$HgCl_2 + 2e^- \rightleftharpoons 2Hg + 2Cl^-$	0.2676
$Al^{3+} + 3e^- \rightleftharpoons Al$	−1.662	$Cu^{2+} + 2e^- \rightleftharpoons Cu$	0.337
$Ti^{2+} + e^- \rightleftharpoons 2e^- \rightleftharpoons Ti$	−1.628	$Fe(CN)_6^{3-} + e^- \rightleftharpoons Fe(CN)_6^{4-}$	0.36
$Zn(OH)_2 + 2e^- \rightleftharpoons Zn + 2OH^-$	−1.245	$Cu^{2-} + e^- \rightleftharpoons Cu$	0.521
$Mn^{2+} + 2e^- \rightleftharpoons Mn$	−1.180	$I_2 + 2e^- \rightleftharpoons 2I^-$	0.536
$2H_2O + 2e^- \rightleftharpoons H_2 + 2OH^{2-}$	−0.822	$O_2 + 2H^+ + 2e^- \rightleftharpoons H_2O_2$	0.682
$Zn^{2+} + 2e^- \rightleftharpoons Zn$	−0.764	$Fe^{3+} + e^- \rightleftharpoons e^- \rightleftharpoons Fe^{2+}$	0.771
$S + 2e^- \rightleftharpoons S^{2-}$	−0.48	$Br_2 + 2e^- \rightleftharpoons 2Br^-$	1.065
$Fe^{2+} + 2e^- \rightleftharpoons Fe$	−0.441	$O_2 + 4H^+ + 4e^- \rightleftharpoons 2H_2O$	1.229
$Cd^{2+} + 2e^- \rightleftharpoons Cd$	−0.403	$Cl_2 + 2e^- \rightleftharpoons 2Cl^-$	1.358
$Ni^{2-} + 2e^- \rightleftharpoons Ni$	−0.250	$PbO_2 + 4H^+ + e^- \rightleftharpoons Pb^{2+} + 2H_2O$	1.455
$Sn^{2+} + 2e^- \rightleftharpoons Sn$	−0.136	$Ce^{4+} + e^- \rightleftharpoons Ce^{3+}$	1.61
$2H^+ + 2e^- \rightleftharpoons H_2$	0.0000	$F_2 + 2e^- \rightleftharpoons 2F^-$	1.87

product $L(\text{AgCl}) = a_{Ag^+}a_{Cl^-} = 1.56 \times 10^{-10}$ mol^2/L^2; that is, the 1 *M* KCl solution is saturated with AgCl at an Ag^+ ion concentration as low as about 10^{-10} mol/L.

Since in a saturated solution of a silver salt the activity of the Ag^+ ions depends on the activity of the anions, the potential of this electrode will depend on the activity of the anions:

$$E = E^0 - \frac{RT}{F} \ln a_{Cl^-}. \tag{3.35}$$

Here the value of E^0(Ag, AgCl) differs from that of a silver electrode of the first type, E^0(Ag, Ag^+):

$$E^0(\text{Ag, AgCl}) = E^0(\text{Ag, Ag}^+) - \frac{RT}{F} \ln L(\text{AgCl}). \tag{3.36}$$

It is sometimes said that this electrode is reversible with respect to the anion. This claim must be examined in more detail. An electrode potential that depends on anion activity still constitutes no evidence that the anions are direct reactants. Two reaction mechanisms are possible at this electrode, a direct transfer of chloride ions across the interface in accordance with Eq. (3.34) or the combination of the electrode reaction

$Ag \rightleftharpoons Ag^+ + e^-$ (transfer of the Ag^+ ions) with the ionic reaction in the bulk solution: $Ag^+ + Cl^- \rightleftharpoons AgCl$. The overall reaction is the same; hence, in both cases Eq. (3.50) is legitimate, yet in the second case the chloride ions are additional, not primary reactants. Thus, thermodynamic data do not suffice if we want to unravel the true mechanism of an electrode process.

Electrodes of the second type can formally be regarded as a special case of electrodes of the first type where the standard state (when $E = E^0$) corresponds not to $a_{Ag^+} = 1$ but to a value of $a_{Ag^+} \approx 10^{-10}$ mol/L, which is established in a KCl solution of unit activity. In this case, the concentration of the potential-determining cation can be varied by varying the concentration of an anion, which might be called the *controlling ion*. The oxides and hydroxides of most metals (other than the alkali metals) are poorly soluble in alkaline solutions; hence, almost all metal electrodes in alkaline solutions are electrodes of the second type.

A picture similar to that just described is seen for metal electrodes when the solution contains a complexing agent (e.g., for the silver electrode when KCN has been added to a $AgNO_3$ solution). Then the complex formation equilibrium

$$Ag^+ + 3CN^- \rightleftharpoons [Ag(CN_3]^{2-} \tag{3.37}$$

will be established in the solution, and as a result the concentration of free Ag^+ ions decreases drastically. By suitable selection of complexing agents, one can alter the equilibrium potentials of metal electrodes within wide limits.

3.5.4 Nernst Equation at Very Low Concentrations

At zero concentration of the potential-determining substances, the values of electrode potential calculated with Eq. (3.26) or (3.30) tend toward $\pm\infty$, which is physically meaningless. This implies that these equations cannot be used below a certain concentration.

Two types of notion exist with respect to the term *low concentrations* [i.e., a low absolute concentration (highly dilute solutions) and a low equilibrium concentration (as in the formation of complexes or compounds of low solubility)]. In the latter case, when potential-determining substances start to be withdrawn from the solution, they re-form because of the shift in equilibrium (i.e., their potential supply is large).

The Nernst equation is of limited use at low absolute concentrations of the ions. At concentrations of 10^{-7} to 10^{-9} mol/L and the customary ratios between electrode surface area and electrolyte volume ($S/V \approx 10^{-2}$ cm^{-1}), the number of ions present in the electric double layer is comparable with that in the bulk electrolyte. Hence, EDL formation is associated with a change in bulk concentration, and the potential will no longer be the equilibrium potential with respect to the original concentration. Moreover, at these concentrations the exchange current densities are greatly reduced, and the potential is readily altered under the influence of extraneous effects. An absolute concentration of the potential-determining substances of 10^{-5} to 10^{-7} mol/L can be regarded as the limit of application of the Nernst equation. Such a limitation does not exist for low-equilibrium concentrations.

3.6 SPECIAL THERMODYNAMIC FEATURES OF ELECTRODE POTENTIALS

3.6.1 Table of Standard Potentials

The value of electrode potential is a quantitative measure of the redox properties of substances involved in the electrode reaction. When undergoing reduction, an oxidizing agent takes up electrons from the cathode. The stronger its oxidizing power, the more positive will be the electrode potential. To the contrary, a reducing agent undergoing oxidation gives off electrons to the anode, and the potential will be more negative the higher its reducing power.

The series of metals arranged in the order of decreasing reducing, and increasing oxidizing, power (or increasingly positive potential values) used to be called the *electromotive series*. An example is the series

$$\text{Li, Al, Zn, Cd, Pb, Cu, Hg, Au.} \tag{3.38}$$

When a metal is immersed into the solution of salt of another metal farther to the right in the electromotive series, the first metal dissolves (is oxidized) while the second metal is deposited (its ions are reduced). Thus, the first metal "displaces" the second from its solution.

Nowadays, tables of standard electrode potentials are used instead of the electromotive series. They include electrode reactions not only of metals but also of other substances [Table 3.1; for detailed tables, see the books of Lewis and Rendall (1923) and Bard et al. (1985)].

3.6.2 pH Dependence of Potentials; Pourbaix Diagrams

Often, H^+ or OH^- ions are involved in the electrode reactions, and the electrode potential then depends on the concentration of these ions (or solution pH). Because of the dissociation equilibrium of water, the activities of these ions are interrelated as $a_{H^+}a_{OH^-} = K_w = 1.27 \times 10^{-14}$ mol^2/L^2. For this reason these reactions can be formulated in two ways: for example, for the hydrogen electrode,

$$2H^+ + 2e^- \rightleftharpoons H_2 \tag{3.39a}$$

and

$$2H_2O + 2e^- \rightleftharpoons H_2 + 2OH^-. \tag{3.39b}$$

The former way is used predominantly for acidic, the latter for alkaline solutions, but thermodynamically, the two ways are equivalent (provided, of course, that the change in pH does not produce a change in direction of the reaction or in the form of individual reactants, as by dissociation). The equations for electrode potential can also be written in two ways, with H^+ ions or with OH^- ions, which again is

thermodynamically equivalent. However, the values of E^0 will, of course, differ, since in one case they refer to $a_{H^+} = 1$ and in the other to $a_{OH^-} = 1$ In the former case the standard potential is written as E^0_A, and in the latter as E^0_B (from the words *acid* and *base*). Usually, E^0_A is implied when a subscript is not written (as in Table 3.1).

The expressions for potential of the hydrogen electrode are

$$E = \begin{cases} E^0_A + \dfrac{RT}{2F} \ln \dfrac{a^2_{H^+}}{p_{H_2}} & (3.40a) \\ E^0_B + \dfrac{RT}{2F} \ln \left(\dfrac{a^2_{H_2O}}{p_{H_2}} a^2_{OH^-} \right). & (3.40b) \end{cases}$$

On the scale of the standard hydrogen electrode (SHE), we have $E^0_A = 0$ for reaction (3.39*a*), by definition. Since $a_{OH^-} = K_w/a_{H^+}$ and $a_{OH^-} \approx 1$, we have for reaction (3.39*b*) at 25°C, when allowing for the value of K_w,

$$E^0_B = \frac{RT}{2F} \ln K_w^{-2} = -0.822 \text{ V}. \tag{3.41}$$

For many electrodes it is found that one H^+ or OH^- ion is involved in the reaction per electron; hence, the electrode potential becomes 0.059 V more negative when the pH is raised by 1 unit; this is the same potential shift as found for the hydrogen electrode. For such electrodes a special scale of electrode potentials is occasionally employed: These potentials, designated as E_r, refer to the potential of a reversible hydrogen electrode (RHE) in the same solution (i.e., at the given pH). For the electrodes of the type considered, potentials in this scale are independent of solution pH.

When there are changes in the form of reactants and (or) products with solution pH, the values of E^0 and the pH dependence of electrode potential will change accordingly. These changes are clearly illustrated by phase diagrams constructed in the coordinates of E and pH. Diagrams of this kind were suggested in 1963 by Marcel Pourbaix and became known as *Pourbaix diagrams*.

A simplified Pourbaix diagram for the zinc electrode at pH between 0 and 14 is shown as an example in Fig. 3.1. The vertical axis is that of the values of electrode potential on the SHE scale for activities of the Zn^{2+} and $HZnO_2^-$ ions of 1 mol/kg. The segments of solid lines correspond to the equilibrium potentials of the following electrode reactions:

$$1: Zn \rightleftharpoons Zn^{2+} + 2e^- \qquad \text{pH} < 5.8$$

$$2: Zn + 2OH^- \rightleftharpoons Zn(OH)_2 + 2e^- \qquad 5.8 < \text{pH} < 10.4$$

$$3: Zn + 3OH^- \rightleftharpoons HZnO^- + 2e^- \qquad \text{pH} > 10.4$$

Segments 4 and 5 reflect the chemical equilibria of acid and base dissociation of $Zn(OH)_2$, yielding Zn^{2+} and $HZnO_2^-$ ions, respectively.

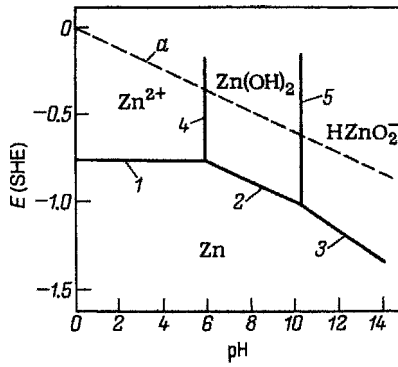

FIGURE 3.1 Pourbaix diagram for the zinc electrode in aqueous solutions.

The areas bounded by solid lines correspond to regions of thermodynamic stability of certain substances that are named in the diagram. This stability is relative. The dashed line *a* in the diagram corresponds to the equilibrium potential of the hydrogen electrode. Metallic zinc, for which the reaction lines are below the line for the hydrogen electrode, can be oxidized while hydrogen is evolved (see Section 2.4.1).

3.6.3 Electrode Potentials in Nonaqueous Electrolytes

For any type of nonaqueous electrolyte (nonaqueous solutions, melts, solid electrolytes) we can select suitable reference electrodes, measure the potentials of other electrodes, and set up tables of electrode potentials. The order of the reactions (electrodes) as a rule does not strongly differ between the different media. A strong reducing agent such as lithium will have a more negative potential than a weaker reducing agent such as copper, both in water and in other media.

However, the electrode potentials measured for different types of electrolytes cannot quantitatively be compared with each other, even when the same reference electrode has been used throughout. This is due to the fact that the potential differences at interfaces between dissimilar electrolytes cannot be determined experimentally. For this reason the electrode potentials are measured separately for each type of electrolyte medium.

For a qualitative comparison of the electrode potentials measured in different media, models and assumptions are sometimes employed. Thus, it can be assumed according to a suggestion of Viktor A. Pleskov (1947) that the interaction of the relatively large rubidium (or cesium) ion with water and with different nonaqueous solvents is very slight. The same is true for the even larger ferrocene ions. Hence, the chemical potentials of these ions and the Galvani potentials at the corresponding electrode–solution interface will be approximately the same for all media. When such an electrode is used as a reference electrode, an almost universal potential scale is obtained. According to a recommendation by IUPAC, the potentials of all other electrodes in each medium must be referred to a ferrocene reference electrode.

3.6.4 Temperature Coefficients of Electrode Potentials

The EMF values of galvanic cells and the electrode potentials are usually determined isothermally, when all parts of the cell, particularly the two electrode–electrolyte interfaces, are at the same temperature. The EMF values will change when this temperature is varied. According to the well-known thermodynamic *Gibbs–Helmholtz equation*, which for electrochemical systems can be written as

$$\frac{-d\,\Delta G_m}{dT} \equiv nF\frac{d\mathscr{E}}{dT} = \frac{\Delta H_m - \Delta G_m}{T} = \Delta S_m, \tag{3.42}$$

the temperature coefficient of the EMF of isothermal cells is related to the entropy change for the current-producing reaction.

As the temperature is varied, the Galvani potentials of all interfaces will change, and we cannot relate the measured value of $d\mathscr{E}/dT$ to the temperature coefficient of Galvani potential for an individual electrode. The temperature coefficient of electrode potential probably depends on the temperature coefficient of Galvani potential for the reference electrode and hence is not a property of the test electrode alone.

The Gibbs–Helmholtz equation also links the temperature coefficient of Galvani potential for individual electrodes to energy effects or entropy changes of the electrode reactions occurring at these electrodes. However, since these parameters cannot be determined experimentally for an isolated electrode reaction (this is possible only for the full current-producing reaction), this equation cannot be used to calculate this temperature coefficient.

We might try to measure the temperature coefficient of the Galvani potential for an individual electrode under nonisothermal conditions; then only the temperature T_2 of the test electrode would be varied, while the reference electrode remains at a constant temperature T_1 and retains a constant value of Galvani potential (Fig. 3.2).

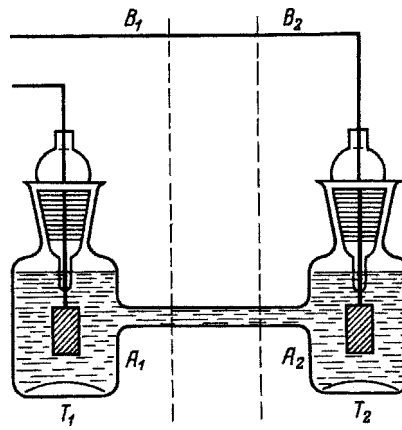

FIGURE 3.2 Nonisothermal galvanic cell.

However, in this case the EMF measured will be distorted by another effect [i.e., the variation of electrostatic potential within a given conductor, which is caused by a temperature gradient in the conductor (the *Thomson effect*, 1856)]. Potential gradients will arise even at zero current, in both the electrolyte (between points A_1 and A_2) and the metallic conductors (between points B_1 and B_2), but cannot be determined.

Thus, the temperature coefficient of Galvanic potential of an individual electrode can be neither measured nor calculated. Measured values of the temperature coefficients of electrode potentials depend on the reference electrode employed. For this reason a special scale is used for the temperature coefficients of electrode potential: It is assumed as a convention that the temperature coefficient of potential of the standard hydrogen electrode is zero; in other words, it is assumed that the value of $E^0_A(H^+, H_2)$ is zero at all temperatures. By measuring the EMF under isothermal conditions we actually compare the temperature coefficient of potential of other electrodes with that of the standard hydrogen electrode.

REFERENCES

Lewis, G. N., *Proc. Am. Acad.*, **43**, 259 (1907).

Nernst, W., *Z. Phys. Chem.*, **4**, 129 (1869).

Peters, R., *Z. Phys. Chem.*, **26**, 193 (1898).

Pleskov, V., *Usp. Khim.*, **16**, 254 (1947).

MONOGRAPHS AND REFERENCE BOOKS

Bard, A., R. Parsons, and J. Jordan, *Standard Potentials in Aqueous Solutions*, Marcel Dekker, New York, 1985.

Guggenheim, E. A., *Thermodynamics by the Methods of Willard Gibbs*, Methuen & Co, London, 1933.

Lewis, G. N. and M. Randall, *Thermodynamics and the Free Energy of Substances*, 1923.

Pourbaix, M., *Atlas d'équilibres électrochimiques*, Gauthier-Villars, Paris, 1963; English translation: *Atlas of Electrochemical Equilibria in Aqueous Solutions*, Pergamon Press, Oxford, 1966.

4

Mass Transfer in Electrolytes

It was shown in Section 1.8 that in addition to ion migration, diffusion and convection fluxes are a substantial part of mass transport during current flow through electrolyte solutions, securing a mass balance in the system. In the present chapter these processes are discussed in more detail.

4.1 BASIC LAWS OF IONIC DIFFUSION IN SOLUTIONS

In multicomponent systems such as solutions, diffusion will arise when at least one of the components is nonuniformly distributed, and its direction will be such as to level the concentration gradients. The diffusion flux (in the direction of decreasing concentrations) is proportional to the concentration gradient of the diffusing substance:

$$J_{d,j} = D_j \operatorname{grad} c_j \tag{4.1}$$

(*Fick's first law*, 1855). The proportionality factor D_j is called the *diffusion coefficient* of the substance concerned (units: cm^2/s). In the diffusion of ions in solutions, Eq. (4.1) is obeyed only at low concentrations of these ions. At higher concentrations the proportionality between flux and concentration gradient is lost (i.e., coefficient D_j ceases to be constant).

A possible reason for the departures from Fick's first law is the fact that the diffusion process tends to level chemical potentials (thermodynamic activities) rather than concentrations of the substances involved. Hence, the equation sometimes is written as

$$J_{d,j} = D_{a,j} \operatorname{grad} a_j. \tag{4.2}$$

However, even in this form the equation does not provide a sufficiently accurate description of the experimental results in solutions unless these are highly dilute, and again coefficient $D_{a,j}$ is not constant when the concentration is varied. This is due to

Fundamentals of Electrochemistry, Second Edition, By V. S. Bagotsky

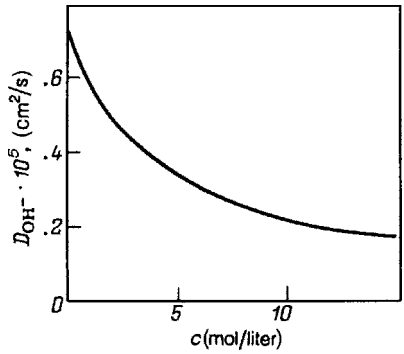

FIGURE 4.1 Diffusion coefficients of the OH^- ions in KOH solutions as a function of KOH concentration at 25°C.

the complexities of diffusion processes, particularly to the fact that the diffusing ions transport solvent molecules which are present in their solvation sheaths, and that these molecules are then transported back. Since Eq. (4.2) has no conspicuous advantages over Eq. (4.1), the latter is used more often when discussing diffusion processes. It is simpler to use in practice, since a knowledge of activity coefficients is not required. All departures from proportionality between the diffusion flux and the concentration gradients are taken into account by assuming that in real systems, the diffusion coefficients D_j are a parameter that depends on concentration.

In dilute aqueous solutions the diffusion coefficients of most ions and of many neutral substances are similar and have values that at room temperature are within the limits of 0.6×10^{-5} and 2×10^{-5} cm²/s. The values generally exhibit a marked decrease with increasing solution concentration (Fig. 4.1).

The ionic mobilities u_j depend on the retarding factor θ_j valid for a particular medium [Eq. (1.8)]. It is evident that this factor also influences the diffusion coefficients. To find the connection, we shall assume that the driving force of diffusion f_d is the chemical potential gradient; that is, in an ideal solution,

$$f_d = \operatorname{grad} \mu_j = RT \operatorname{grad}(\ln c_j) = \frac{RT}{c_j} \operatorname{grad} c_j. \tag{4.3}$$

Therefore [see Eq. (1.7)],

$$J_{d,j} = \frac{RT}{\theta_j} \operatorname{grad} c_j. \tag{4.4}$$

We see when comparing Eqs. (1.7) and (4.1) that

$$D_j = \frac{RT}{\theta_j}. \tag{4.5}$$

It follows from relations (1.8) and (4.5), finally, that

$$D_j = u_j \frac{RT}{z_j F} \tag{4.6}$$

(Nernst, 1888). This equation is valid in dilute solutions. An analogous equation including activity coefficients can be derived, but for the reasons outlined above, it again is not sufficiently accurate in describing the experimental data in concentrated solutions. Equation (4.6) is of great value because it can be used to evaluate ionic diffusion coefficients from values of u_j which are more readily measured.

4.2 LIMITING DIFFUSION CURRENTS IN ELECTROLYTES

In the present section we consider diffusion processes in electrochemical systems that are not complicated by migration and convection. To exclude migration, we consider the behavior of uncharged reaction components. The condition of a complete absence of convections of the liquid can be realized, for example, when the electrode is provided with a porous lining of thickness δ filled with the electrolyte (Fig. 4.2). In the small pores of the lining, convection of the liquid is almost impossible. By vigorous stirring of the solution a concentration of the reactant that is sufficiently close to the starting concentration can be maintained at the outer surface of the lining. The influence of convection is examined in Section 4.4.

When current flows in an electrolyte solution, the concentration, $c_{S,j}$, of a reactant and/or product close to the electrode surface will change relative to its bulk concentration $c_{V,j}$ as a result of the electrode reaction. For reactants, $c_{S,j} < c_{V,j}$, and for products, $c_{S,j} > c_{V,j}$.

Diffusion fluxes develop as a result of these concentration gradients. The layer of electrolyte where the concentration changes occur and within which the substances are transported by diffusion is called the *diffusion layer*. Its thickness, δ (the diffusion path length), depends on cell design features and on the intensity of convective

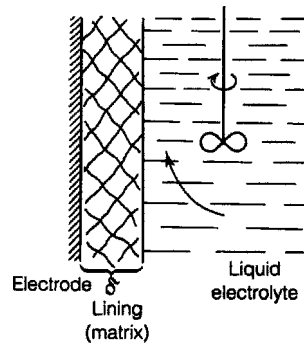

FIGURE 4.2 Diffusion layer of constant thickness.

fluxes (for further details, see Section 4.4). In the following we assume that the diffusion-layer thickness δ is constant.

The concept of surface concentration $c_{S,j}$ requires closer definition. At the surface itself the ionic concentrations will change not only as a result of the reaction but also because of the electric double layer present at the surface. Surface concentration is understood to be the concentration at a distance from the surface small compared to diffusion-layer thickness, yet so large that the effects of the EDL are no longer felt. This condition usually is met at points about 1 nm from the surface.

The changes in surface concentrations of the components caused by current flow have two important effects: They produce a change in electrode potential, and they imply that there is an upper limit to the cell currents when the diffusion flux attains its limiting value. The first of these effects is considered in Section 6.3; the second, in the present section.

In electrochemical systems with flat electrodes, all fluxes within the diffusion layers are always linear (one-dimensional) and the concentration gradient grad c_j can be written as dc_i/dx. For electrodes of different shape (e.g., cylindrical), linearity will be retained when thickness δ is markedly smaller than the radius of surface curvature. When the flux is linear, the flux density under steady-state conditions must be constant along the entire path (throughout the layer of thickness δ). In this the concentration gradient is also constant within the limits of the layer diffusion layer δ and can be described in terms of finite differences as $dc_j/dx = \Delta c_j/\delta$, where for reactants, $\Delta c_j = c_{V,j} - c_{S,j}$ (diffusion from the bulk of the solution toward the electrode's surface), and for reaction products, $\Delta c_j = c_{S,j} - c_{V,j}$ (diffusion in the opposite direction). Thus, the equation for the diffusion flux becomes

$$J_{d,j} = D_j \frac{\Delta c_j}{\delta} = \kappa_j \Delta c_j, \tag{4.7}$$

where $\kappa_j \equiv D_j/\delta$ is the diffusion-flux constant (units: cm/s).

For the case considered here, the balance equation for reactants is given by

$$i = \frac{n}{\nu_j} F \kappa_j \Delta c_j \tag{4.8}$$

(i.e., the current density is proportional to the concentration difference between bulk and surface). For a given current density i and known values of the remaining parameters, this equation yields the surface concentration

$$c_{S,j} = c_{V,j} - \frac{\nu_j i}{nF\kappa_j}. \tag{4.9}$$

The surface concentration decreases with increasing current density. When the current density has attained a certain critical value,

$$i_{l,j} = \frac{n}{\nu_j} \kappa_j c_V, \tag{4.10}$$

the surface concentration of the reactant has fallen to zero. This current density corresponds to the highest possible value of the concentration gradient, $c_{V,j}/\delta$; further increase in the diffusion flux is impossible. The parameter $i_{l,j}$, sometimes written as $i_{d,j}$, is the *limiting diffusion current density* for a given reactant.

Using the expression for the limiting diffusion current density, we can rewrite the surface concentration as

$$c_{S,j} = c_{V,j}\left(1 - \frac{i}{i_{l,j}}\right). \tag{4.11}$$

The limiting currents are a typical feature found in galvanic circuits but not in circuits consisting entirely of electronic conductors.

During current flow, the concentration of reaction products near the surface of the electrode will increase, and a limiting condition may also arise, but for different reasons, which are related to attainment of the solubility limits by given substances. The material precipitating will screen the electrode surface and interfere with a further increase in current. The value of the limiting current will depend on the nature of the deposit formed and is less reproducible than in the previous case; specifically, it may depend on time.

In analogy to Eq. (4.11), we can write the surface concentration of reaction products as

$$c_{S,j} = c_{V,j}\left(1 + \frac{i}{i_l}\right), \tag{4.12}$$

but here the limiting current does not refer to the given reaction; it refers to the back reaction in which the given species are consumed.

Key Components Most electrochemical reactions involve several reactants and/or products. The surface concentrations of all of them change. As the current density is raised, the limiting concentration for one of them will be attained before it is attained for the others. This substance can be called the *key component* for this reaction. The actual limiting current attained in the system corresponds to the limiting current of this key component (i.e., is determined by its parameters, in particular by its concentration).

4.3 IONIC TRANSPORT BY MIGRATION AND DIFFUSION

4.3.1 Equations for the Total Flux

The equation for the total flux of ions under the simultaneous effects of an electrostatic field **E** [see Eq. (1.9)] and a concentration gradient [see Eq. (4.1)] is

$$J_j = J_{m,j} \pm J_{d,j} = c_j u_j \mathbf{E} \pm D_j \frac{dc_j}{dx} \tag{4.13}$$

(the *Nernst–Planck equation*, 1890). In this equation a minus sign should be used when the direction of the diffusion flux is opposite that of the migration flux.

Equation (4.13) is fulfilled for all the ions in the electrolyte, as well as for those involved in the reaction and for those not involved in the reaction, which do not move from or toward the electrode's surface ($J_j = 0$) and for which therefore $J_{d,j} = -J_{m,j} \neq 0$. For uncharged reaction components ($z_j = 0$, but $\nu_j \neq 0$), Eq. (4.13) changes into Eq. (4.1). Allowing for equality (4.6), which links the parameters u_j and D_j, we can write the equation for the total flux as

$$J_j = D_j\left(\frac{F}{RT} z_j c_j \mathbf{E} \pm \frac{dc_j}{dx}\right). \tag{4.14}$$

The total number of such equations corresponds to the number N of all these components in the electrolyte. The unknowns in these equations are the steady values of field strength $\mathbf{E}$ and the concentration gradients dc_j/dx. The ionic concentrations are interrelated by the electroneutrality condition (1.3); therefore, between the gradients the constraint

$$\Sigma_N z_j \frac{dc_j}{dx} = 0 \tag{4.15}$$

exists (i.e., the gradients of $N - 1$ components are independent). We thus obtain a system of N equations with N unknowns which in principle can be solved (although in the general case this is a very complex task and requires computer use). This implies that in the system a steady state actually can be realized, where there is a complete balance with respect to charges and substances and where the parameters (voltage, concentration distribution) have unique values.

Often, the electrolyte contains only one reacting ion, which has a low concentration, while other ions not involved in the reaction are present in excess concentrations. As the concentration of such foreign ions is raised, the conductivity σ increases, and in accordance with Eq. (1.4), at a given current density the field strength E decreases. In the limit, the first term on the right-hand side of Eq. (4.13) becomes small and the reacting ion will be transported mainly by diffusion. In this case the expression for current density will be the same as Eq. (4.8) for the transport of uncharged particles, and the equation for the limiting current also remains unchanged.

4.3.2 Total Fluxes in Binary Electrolytes

In a binary electrolyte the solution of the set of equations (4.13) for the total flux of ions is considerably simplified. For a binary solution of an electrolyte $M_{\tau_+}A_{\tau_-}$ with a concentration c_k, the migration direction of the anion A^{z-} is opposite that of the cation M^{z+}. Taking into account that $c_+ = \tau_+ c_k$, $c_- = \tau_- c_k$, and $z_+\tau_+ = z_-\tau_- = \tau_k$, we can write the equations for the total flux of the two ions as

$$J_+ = D_+\left(\frac{F}{RT}\tau_k c_k \mathbf{E} + \tau_+ \frac{dc_k}{dx}\right), \tag{4.16}$$

$$J_- = D_-\left(\frac{F}{RT}\tau_k c_k \mathbf{E} - \tau_- \frac{dc_k}{dx}\right). \tag{4.17}$$

Diffusion in Binary Electrolytes at Zero Current Consider diffusional transport at zero current in binary electrolytes in which initially a concentration gradient dc_k/dx has developed through the action of external forces. Diffusional transport of ions in the direction of lower concentrations will start in the system. Generally, the diffusion coefficient of the cation differs from that of the anion; therefore, the diffusional fluxes of these ions will also be different. This gives rise to a partial charge separation and development of an electric field with a strength $\mathbf{E}_d$ that holds back the fast-moving ions but accelerates the slower ones. In the end a steady state is attained in which equivalent amounts of the two ions are transported by a combination of migration and diffusion, as if an electroneutral compond was transported. Solving Eq. (4.16) for field strength $\mathbf{E}_d$ and taking into account that $J_- = J_+$, we find that

$$\mathbf{E}_d = \frac{RT}{F}\frac{z_-D_- - z_+D_+}{D_+ + D_-}c_k\frac{dc_k}{dx}. \tag{4.18}$$

The parameter $\mathbf{E}_d$, which is called the *diffusional field strength*, arises only when the D_j values of the cation and anion differ appreciably; when they are identical, $\mathbf{E}_d$ is zero. As a result of this field strength in the electrolyte, a diffusional potential difference φ_d arises along the diffusion path from $x = 0$ to $= \delta$:

$$\varphi_d = \psi_\delta - \psi_0 = \int_0^\delta \mathbf{E}_d\,dx = \frac{z_-D_- - z_+D_+}{D_+ + D_-}\ln\frac{c_\delta}{c_0} \tag{4.19}$$

where ψ_δ, ψ_0, c_δ, and c_0 are the values of the potential and of the concentration at the points $x = \delta$ and $x = 0$.

Diffusion in Binary Electrolytes at Nonzero Currents Consider a reaction in which one of the ions of the binary solution is involved. For the sake of definition, we shall assume that its cation is reduced to metal at the cathode. The cation concentration at the surface will decrease when current flows. Because of the electroneutrality condition, the concentration of anions should also decrease under these conditions (i.e., the total electrolyte concentration c_k should decrease).

The anions, which are not involved in the reaction $\nu_- = 0$, should not move in the steady state [i.e., in Eq. (4.17), $J_- = 0$]. This implies that the diffusional component of their flux to the surface should be fully compensated by a migration component away from the surface (Fig. 4.3).

For the cations, both flux components move toward the surface (i.e., their combined flux is higher in absolute value than the pure diffusion flux). It follows from Eq. (4.17), with $J_- = 0$, that

$$\frac{dc_k}{dx} = \frac{F}{RT}c_k\mathbf{E}\frac{\tau_k}{\tau_-}. \tag{4.20}$$

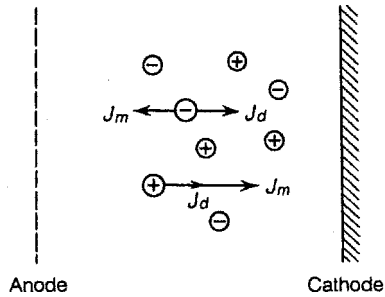

FIGURE 4.3 Migration (J_m) and diffusion (J_d) fluxes of anions and cations in cathodic metal deposition from a symmetric binary solution.

Substituting this value of dc_k/dx into Eq. (4.16) and taking into account that $z_+/z_- = \tau_-/\tau_+$, we find for the flux of the cations that

$$J_+ = \tau_+\left(1 + \frac{\tau_-}{\tau_+}\right)D_+\frac{dc_k}{dx}. \tag{4.21}$$

We see that in binary electrolytes, the flux of the reacting cation increases by a factor of $1 + (\tau_-/\tau_+)$ relative to the pure diffusion current that would be observed (at a given concentration gradient) in the presence of an excess of foreign electrolyte. We shall call

$$\alpha = 1 + \frac{\tau_-}{\tau_+} \tag{4.22}$$

the enhancement factor of the total current above the diffusion current. For symmetric electrolytes ($\tau_+ = \tau_-$) we have $\alpha = 2$. For electrolytes of the type of $ZnCl_2$ and Ag_2SO_4, the values of α are 3 and 1.5, respectively.

From Eq. (1.36) and taking into account that in our case obviously $n/\nu_+ = z_+$, we find for the current density,

$$i = z_+FJ_+ = z_+\alpha F\tau_+D_+\frac{dc_k}{dx}. \tag{4.23}$$

It follows that for ionic reactants in binary solutions, the limiting current is given not by Eq. (4.10) but by the equation

$$i_{l,j} = \frac{n}{\nu_j}F\alpha\kappa_j\,\Delta c_j. \tag{4.24}$$

Equations (4.11) and (4.12) remain valid for the calculation of surface concentrations when this value of the limiting current is used in them.

It must be pointed out that in a diffusion layer where the ions are transported not only by migration but also by diffusion, the effective transport numbers t_j^* of the ions (the ratios between partial currents i_j and total current i) will differ from the parameter t_j [defined by Eq. (1.13)], which is the transport number of ion j in the bulk electrolyte, where concentration gradients and diffusional transport of substances are absent. In fact, in our case the effective transport number of the reacting ions in the diffusion layer is unity and that of the nonreacting ions is zero.

Influence of the Diffusional Potential Drop In the case being considered, a potential difference φ_σ is established across the diffusion layer whose value can be found by integrating Eq. (4.20) from $x = 0$ to $x = \delta$:

$$\varphi_\sigma = \int_0^\delta \mathbf{E}\, dx = \frac{1}{z_-}\frac{RT}{F}\ln\frac{c_\delta}{c_0} \tag{4.25}$$

(we must remember that $\tau_-/\tau_k = z_-$). This potential difference is partly the result of ohmic losses in the electrolyte. To calculate these losses, we must take into consideration that due to the change in concentration the conductivity of the electrolyte is not constant along the diffusion path. If we assume a linear change of the concentration

$$c_x = c_0 + \gamma x, \qquad \text{where} \quad \gamma = \frac{c_\delta - c_0}{\delta}, \tag{4.26}$$

the conductivity of the electrolyte at point x has the value

$$\sigma_x = F(c_0 + \gamma x)(\tau_+ z_+ u_+ + \tau_- z_- u_-) = F(c_0 + \gamma x)\tau_k(u_+ + u_-), \tag{4.27}$$

or, taking Eq. (4.6) into account,

$$\sigma_x = \frac{F}{RT}F(c_0 + \gamma x)\tau_k(z_+ D_+ + z_- D_-). \tag{4.28}$$

According to Eqs. (4.23) and (4.28), the ohmic component of the field strength $\mathbf{E}_{\text{ohm},x} = i/\sigma_x$ will be

$$\mathbf{E}_{\text{ohm},x} = \int_0^\delta \frac{i}{\sigma_x}\, dx = \frac{RT/F}{c_0 + \gamma x}(z_+ D_+ + z_- D_-), \tag{4.29}$$

and for the overall ohmic potential drop we have

$$\varphi_{\text{ohm}} = \int_0^\delta \mathbf{E}_{\text{ohm},x}\, dx = \frac{RT/F}{z_+ D_+ + z_- D_-}\ln\frac{c_\delta}{c_0}. \tag{4.30}$$

It can be seen that the ohmic potential drop φ_{ohm} differs from the overall potential drop φ_σ in the electrolyte as given by Eq. (4.25). The difference between these two values corresponds exactly to the diffusional potential drop φ_d for the given concentration ratio that was given in Eq. (4.19).

Thus, the potential difference in electrolytes during current flow is determined by two components: an ohmic component φ_{ohm} proportional to current density and a diffusional component φ_d, which depends on the concentration gradients. The latter arises only when the D_j values of the individual ions differ appreciably; when they are all identical, φ_d is zero. The existence of the second component is a typical feature of electrochemical systems with ionic concentration gradients. This component can exist even at zero current when concentration gradients are maintained artificially. When a current flows in the electrolyte, this component may produce an apparent departure from Ohm's law.

As the diffusional field strength $\mathbf{E}_d$ depends on the coordinate x in the diffusion layer, the diffusion flux density (in contrast to the total flux density) is no longer constant and the concentration gradients dc_j/dx will also change with the coordinate x.

4.3.3 The General Case

Generally, an electrolyte may contain several ionic reactant species but no obvious excess of a foreign electrolyte. Then, as already mentioned, a calculation of the migration currents [or coefficients α in equations of the type (4.22)] is very complex and requires computer use.

Often, we need only a qualitative estimate; that is, we want to know whether the limiting current is raised or lowered by migration relative to the purely diffusion-limited current, or whether α_j is larger or smaller than unity. It is evident that α_j will be larger than unity when migration and diffusion are in the same direction. This is found in four cases: for cations that are reactants in a cathodic reaction (as in the example above) or products in an anodic reaction, and for anions that are reactants in an anodic reaction or products in a cathodic reaction. In the other four cases (for cations that are reactants in an anodic or products in a cathodic reaction, and for anions that are reactants in a cathodic or products in an anodic reaction), we have $\alpha_j < 1$, a typical example being the cathodic deposition of metals from complex anions.

4.4 CONVECTIVE TRANSPORT

Convective transport is the transport of substances with a moving medium (e.g., the transport of a solute in a liquid flow). The convective flux is given by

$$J_{kv,j} = \upsilon c_j, \tag{4.31}$$

where υ is the linear velocity of the medium and c_j is the concentration of the substance. In electrolyte solutions, the convective flux is always electroneutral because of the medium's electroneutrality.

In electrochemical cells we often find convective transport of reaction components toward (or away from) the electrode surface. In this case the balance equation describing the supply and escape of the components should be written in the general form (1.38). However, this equation needs further explanation. At any current density during current flow, the migration and diffusion fluxes (or field strength and concentration gradients) will spontaneously settle at values such that condition (4.14) is satisfied. The convective flux, on the other hand, depends on the arbitrary values selected for the flow velocity v and for the component concentrations (i.e., is determined by factors independent of the values selected for the current density). Hence, in the balance equation (1.38), it is not the total convective flux that should appear, only the part that corresponds to the true consumption of reactants from the flux or true product release into the flux. This fraction is defined as the difference between the fluxes away from and to the electrode:

$$\Delta J_{kv,j} = nF\upsilon(c_j - c_j'), \tag{4.32}$$

where c_j' is the concentration of substance j in the flow leaving the electrode.

For the present argument and in what follows, we assume that the migrational transport is absent (that we have uncharged reaction components or an excess of foreign electrolyte).

Let us estimate the ratios of diffusion and maximum convective fluxes, $J_{d,j}/J_{kv,j} = D_j \times \text{grad}\, c_j/c_j\upsilon$. The order of magnitude of the concentration gradient is c_j/δ. Therefore,

$$\frac{J_{d,j}}{J_{kv,j}} \approx \frac{D_j}{\delta\upsilon}. \tag{4.33}$$

In aqueous solutions $D_j \approx 10^{-5}\,\text{cm}^2/\text{s}$; a typical value of δ is $10^{-2}\,\text{cm}$. It follows that the convective and diffusional transport are comparable even at the negligible linear velocity of $10^{-3}\,\text{cm/s}$ of the liquid flow. At larger velocities, convection will be predominant.

4.4.1 Flow-by Electrodes

Flow of the liquid past the electrode is found in electrochemical cells where a liquid electrolyte is agitated with a stirrer or by pumping. The character of liquid flow near a solid wall depends on the flow velocity υ, on the characteristic length L of the solid, and on the kinematic viscosity ν_{kin} (which is the ratio of the usual rheological viscosity η and the liquid's density ρ). A convenient criterion is the dimensionless parameter $\text{Re} \equiv \upsilon L/\nu_{\text{kin}}$, called the *Reynolds number*. The flow is laminar when this number is smaller than some critical value (which is about 10^3 for rough surfaces and about 10^5 for smooth surfaces); in this case the liquid moves in the form of layers parallel to the surface. At high Reynolds numbers (high flow velocities) the motion becomes turbulent and eddies develop at random in the flow. We shall only be concerned with laminar flow of the liquid.

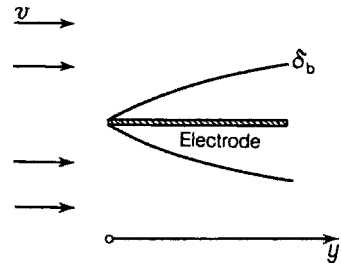

FIGURE 4.4 Schematic of a flow-by electrode.

In the flow, the thin layer of liquid that is directly adjacent to the solid is retained by molecular forces and does not move. The liquid's velocity relative to the solid increases from zero at the very surface to the bulk value v which is attained some distance away from the surface. The zone within which the velocity changes is called the *Prandtl* or *hydrodynamic boundary layer*.

Hydrodynamic theory shows that the thickness, δ_b, of the boundary layer is not constant but increases with increasing distance y from the flow's stagnation point at the surface (Fig. 4.4); it also depends on the flow velocity:

$$\delta_b \approx \nu_{\text{kin}}^{1/2} y^{1/2} v^{-1/2}. \tag{4.34}$$

It is important to note that even in a strongly stirred solution, a thin layer of stagnant liquid is present directly at the electrode surface, within which convection is absent so that substances involved in the reaction are transported in it only by diffusion and migration. Here the concentration gradient $(\text{grad } c_j)_{x=0}$ is steepest and (in the absence of convection) determined by the balance equation

$$i\frac{\nu_j}{nF} = -D_j(\text{grad}\, c_j)_{x=0}. \tag{4.35}$$

In the bulk, to the contrary, concentration gradients are leveled only as a result of convection, and diffusion has practically no effect. In the transition region we find both diffusional and convective transport. The concentration gradient gradually falls to zero with increasing distance from the surface.

Diffusion in a convective flow is called *convective diffusion*. The layer within which diffusional transport is effective (the diffusion layer) does not coincide with the hydrodynamic boundary layer. It is an important theoretical problem to calculate the diffusion-layer thickness δ. Since the transition from convection to diffusion is gradual, the concept of diffusion-layer thickness is somewhat vague. In practice, this thickness is defined so that $\Delta c_j/\delta = (dc_{j/dx})_{x=0}$. This calculated distance δ (or the value of κ_j) can then be used to find the relation between current density and concentration difference.

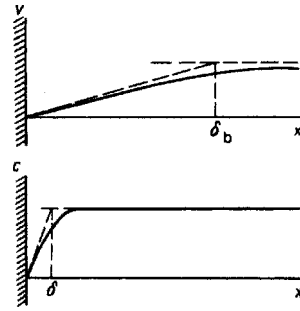

FIGURE 4.5 Distributions of flow velocities and concentrations close to the surface of a flow-by electrode.

An analogy exists between mass transfer (which depends on the diffusion coefficient) and momentum transfer between the sliding liquid layers (which depends on the kinematic viscosity). Calculations show that the ratio of thicknesses of the diffusion and boundary layer can be written as

$$\frac{\delta}{\delta_b} \approx \left(\frac{D_j}{\nu_{\text{kin}}}\right)^{1/3} = \text{Pr}^{-1/3}. \tag{4.36}$$

The dimensionless ratio ν_{kin}/D_j is called the *Prandtl number*, Pr. In aqueous solutions $D_j \approx 10^{-5}\,\text{cm}^2/\text{s}$ and $\nu_{\text{kin}} \approx 10^{-2}\,\text{cm}^2/\text{s}$ (i.e., $\text{Pr} \approx 10^{-3}$). Thus, the diffusion layer is approximately 10 times thinner than the boundary layer. This means that in the major part of the boundary layer, motion of the liquid completely levels the concentration gradients and suppresses diffusion (Fig. 4.5).

Allowing for Eqs. (4.34) and (4.36), we obtain

$$\delta \approx D_j^{1/3} \nu_{\text{kin}}^{1/6} y^{1/2} \upsilon^{-1/2}. \tag{4.37}$$

The gradual increase in thickness δ that occurs with increasing distance y leads to a decreasing diffusion flux. It follows that the current density is nonuniform along the electrode surface.

It is important to note that the diffusion-layer thickness depends not only on hydrodynamic factors but also (through the diffusion coefficient) on the nature of the diffusing species. This dependence is minor, of course, since the values of D_j differ little among the various substances, and in addition are raised to the power one-third in Eq. (4.37).

It follows that convection of the liquid has a twofold influence: It levels the concentrations in the bulk liquid, and it influences the diffusional transport by governing the diffusion-layer thickness. Slight convection is sufficient for the first effect, but the second effect is related in a quantitative way to the convective flow velocity: The higher this velocity is, the thinner will be the diffusion layer and the larger the concentration gradients and diffusional fluxes.

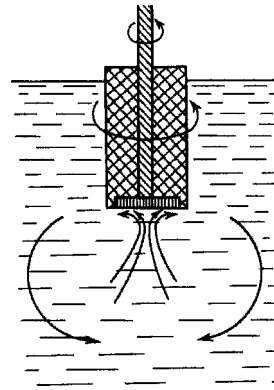

FIGURE 4.6 Rotating-disk electrode (arrows in the space below the electrode indicate the directions of liquid flow).

4.4.2 Rotating-Disk Electrode

At the rotating-disk electrode (RDE; Fig. 4.6), it is the solid electrode and not the liquid that is driven; but from a hydrodynamic point of view this difference is unimportant. Liquid flows, which in the figure are shown by arrows, are generated in the solution when the electrode is rotated around its vertical axis. The liquid flow impinges on the electrode in the center of the rotating disk, then is diverted by centrifugal forces to the periphery.

Let ω be the angular velocity of rotation; this is equal to $2\pi f$, where f is the disk frequency or number of revolutions per second. The distance r of any point from the center of the disk is identical with the distance from the flow stagnation point. The linear velocity of any point on the electrode is ωr. We see when substituting these quantities into Eq. (4.34) that the effects of the changes in distance and linear velocity mutually cancel, so that the resulting diffusion-layer thickness is independent of distance.

The constancy of the diffusion layer over the entire surface and thus the uniform current-density distribution are important features of rotating-disk electrodes. Electrodes of this kind are called *electrodes with uniformly accessible surface*. It is seen from the quantitative solution of the hydrodynamic problem (Levich, 1944) that for RDE to a first approximation

$$\delta = 1.616\, D_j^{1/3} \nu_{\text{kin}}^{1/6} \omega^{-1/2}, \tag{4.38}$$

and hence,

$$i = 0.62 \frac{n}{\nu_j} F D_j^{2/3} \nu_{\text{kin}}^{-1/6} \omega^{-1/2} \tag{4.39}$$

(the *Levich equation*). A more exact calculation leads to complex expressions with a number of correction terms; however, some of these corrections mutually cancel, so

Veniamin G. Levich (1917–1987).

that the accuracy of the equation reported is quite adequate. Equation (4.39) can be used for a quantitative analysis of the experimental data as well as for calculating diffusion coefficients from experimental limiting-current values. Equally exact calculations of convective diffusion are not possible for any other electrode type. The derivation of Eqs. (4.37) to (4.39) marked the first step in the development of a new branch in electrochemistry called *physicochemical hydrodynamics* (see Levich, 1962).

In practice, RDEs with disk speeds between 1 and 170 rps (or 60 to 10,000 rpm) are used. According to Eq. (4.38), in aqueous solutions this speed range corresponds to thicknesses δ between approximately 60 and 4.5 µm. Whirling liquid flow and wobble of the rapidly spinning electrode cause considerable complications at higher speeds.

4.4.3 Rotating Ring–Disk Electrode

In 1959, Frumkin et al. suggested a new electrode type, the rotating ring–disk electrode (RRDE). Here a thin ring used as a second electrode is arranged concentrically around the disk electrode (Fig. 4.7). The gap r_2–r_1 between disk and ring is narrow (less than 1 mm). The primary electrochemical reaction occurs at the disk electrode. The ring electrode is used for the quantitative, and sometimes for a qualitative, determination of reaction products (intermediate and final) which are formed at the disk and dissolve. To this end the potential set at the ring is such that these products will react electrochemically (i.e., will be reduced or oxidized). Using the hydrodynamic theory of convective diffusion, we can calculate exactly which fraction N of the particles released at the disk electrode will reach the surface of the ring electrode and react there. This fraction depends on the ratio of radii of disk and ring and usually is about 40%. Thus, by measuring the limiting current, I_R, at the ring electrode, we can estimate the rate of formation of the products at the disk electrode. The RRDE is useful when studying chemical aspects of electrode reactions or the quantitative aspects of electrode reactions with several parallel pathways.

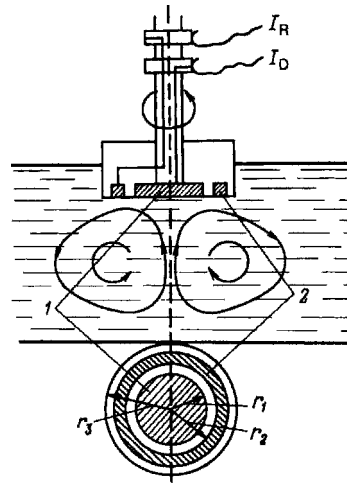

FIGURE 4.7 Rotating ring–disk electrode: (1) disk electrode (current I_D); (2) ring electrode (current I_R).

4.4.4 Cells with Natural Convection of the Electrolyte

It follows from Eqs. (4.37) and (4.38) that the diffusion-layer thickness will increase without limits and the diffusion flux will decrease to zero when the electrolyte is not stirred ($v = 0$) or the electrode not rotated ($\omega = 0$). This implies that a steady electric current cannot flow in such cells. But this conclusion is at variance with the experimental data.

This discrepancy arises primarily from the fact that spontaneous liquid flows will always develop in any liquid even without artificial stirring (e.g., under the action of density gradients caused by local temperature or concentration fluctuations). This phenomenon has been termed *natural convection*. Electrochemical reactions reinforce natural convection, since the concentrations of substances involved in the reaction will change near the electrode surfaces, and also since heat is evolved. Gas evolution attending the reactions has a particularly strong effect on natural convection.

Natural convection depends strongly on cell geometry. No convection can arise in capillaries or in the thin liquid layers found in narrow gaps between electrodes. The rates of natural convective flows and the associated diffusion-layer thicknesses depend on numerous factors and cannot be calculated in a general form. Very rough estimates show that the diffusion-layer thickness under a variety of conditions may be between 100 and 500 μm.

Natural convection can be eliminated entirely when electrolytes held in a matrix or porous support are used instead of free liquids. Natural convection will not develop in a pore space when the individual pores are sufficiently narrow. When such electrolytes are used, the diffusion layer propagates across the entire matrix (i.e., across the full electrode gap).

REFERENCES

Frumkin, A. N., L. Nekrasov, V. G. Levich, and Yu. Ivanov, *J. Electroanal. Chem*., **1**, 84 (1959).

Levich, V. G., *Zh. Phys. Khim*., **18**, 335 (1944).

Levich, V. G., *Physicochemical Hydrodynamics*, Prentice-Hall, Englewood Cliffs, N.J., 1962.

Nernst, W., Z. *Phys. Chem*., **2**, 613 (1888).

5

Phase Boundaries (Interfaces) Between Miscible Electrolytes

5.1 TYPES OF INTERFACES BETWEEN ELECTROLYTES

In practical galvanic cells with more than one electrolyte, pairs of different electrolytes are in mutual contact, forming electrolyte–electrolyte interfaces. Such an interface will be mechanically stable when at least one of the two paired electrolytes is solid. The interface will also be stable when two immiscible liquid electrolytes are brought together in the form of horizontal layers, and the liquid with the lower density is above the one with the higher density. But when miscible liquids are paired, they will start to mix under the effect of hydrodynamic flows, and the interface rapidly disappears. Such interfaces can be stabilized by separating the two electrolytes with a porous diaphragm, which hinders or completely prevents liquid flows, but at the same time does not interfere with conduction (ionic migration) between the electrolytes. In laboratory practice the liquids are often separated by glass stopcocks wetted with the solution. We shall be concerned only with stable interfaces between electrolytes.

For interfaces between liquid electrolytes, we can distinguish three cases: (1) interfaces between similar electrolytes, (2) interfaces between dissimilar but miscible electrolytes, and (3) interfaces between immiscible electrolytes. In the first case the two electrolytes have the same solvent (medium), but they differ in the nature and/or concentration of solutes. In the second case the interface separates dissimilar media (e.g., solutions in water and ethanol). An example for the third case is a system consisting of salt solutions in water and nitrobenzene. The interface between immiscible dissimilar liquid electrolytes is discussed in more detail in Chapter 32.

The interfaces between similar electrolytes are often called liquid junctions even though this concept includes interfaces between electrolytes that are not liquid (e.g., between gelled aqueous solutions and despite the fact that the cases 2 and 3 are also connected with liquid electrolytes).

Fundamentals of Electrochemistry, Second Edition, By V. S. Bagotsky

All ions that can exist in both phases can diffuse across the electrolyte–electrolyte interface. The diffusion leads to leveling of their electrochemical potentials and eventually brings about an equilibrium distribution between the phases. In a homogeneous system, equilibrium signifies the complete leveling of composition and concentrations in the two phases: disappearance of the interface as such. For interfaces of type 2 one must distinguish between the processes of equilibration of the solute and of mixing of the solvents by their mutual diffusion, which can proceed at a different rate. Complete equilibration by diffusion processes as a rule is a long process. In systems of types 1 and 2, therefore, only phenomena occurring in a predetermined original state prior to equilibration are considered (Section 5.2). In an inhomogeneous system with immiscible electrolytes, the interface is preserved even after equilibration. In this case the conditions under which equilibria exist are of interest as well (Chapter 32).

Systems with dissimilar media (cases 2 and 3) as a rule are selective; because of differences in the chemical driving forces, the equilibrium distributions of the components between the two phases are dissimilar. When the selectivity is perfect, some components may exist in only one of the phases and will not transfer to the other.

One of the features found at interfaces between two electrolytes (α) and (β) is the development of a Galvani potential, $\varphi_G^{(\beta,\alpha)}$, between the phases. This potential difference is a component of the total OCV of the galvanic cell [see Eq. (2.13)]. In the case of similar electrolytes, it is called the *diffusion potential* φ_d and can be determined, in contrast to potential differences across interfaces between dissimilar electrolytes.

A special case of interfaces between electrolytes are those involving *membranes*. A membrane is a thin, ion-conducting interlayer (most often solid but sometimes also a solution in an immiscible electrolyte) separating two similar liquid phases and exhibiting selectivity (Fig. 5.1). Nonselective interlayers, interlayers uniformly permeable for all components, are called *diaphragms*. Completely selective membranes (i.e., membranes that are permeable for some and impermeable for other substances) are called *permselective membranes*.

When the original compositions of the outer phases are different, the permselective membrane will prevent the complete leveling of these compositions. Some equilibrium component distribution between phases (α) and (β) will be established, and between points *A* and *B* a potential difference called the *membrane potential* (or transmembrane potential) φ_m will develop. This potential difference is determined by

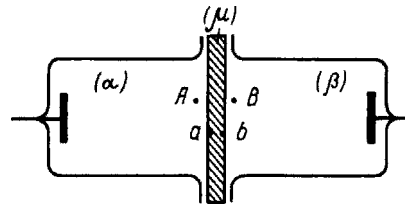

FIGURE 5.1 Schematic of an electrochemical cell with membrane μ.

the Galvani potentials across the two interfaces between the membrane and the outer phases. Moreover, while the system is not yet in equilibrium, a diffusion potential or intramembrane potential φ_d exists inside the membrane (between points *a* and *b*). Thus, generally,

$$\varphi_m \equiv \psi^{(\beta)} - \psi^{(\alpha)} = \varphi_G^{(\mu,\alpha)} - \varphi_G^{(\mu,\beta)} + \varphi_d. \tag{5.1}$$

Since the outer phases are similar, membrane potentials can be measured.

5.2 POTENTIALS BETWEEN SIMILAR ELECTROLYTES (DIFFUSION POTENTIALS)

At the interface between two similar solutions (α) and (β) merely differing in their composition, a transition layer will develop within which the concentrations of each component *j* exhibit a smooth change from their values $c_j^{(\alpha)}$ in phase (α) to the values $c_j^{(\beta)}$ in phase (β). The thickness of this transition layer depends on how this boundary has been realized and stabilized. When a porous diaphragm is used, it corresponds to the thickness of this diaphragm, since within each of the phases outside the diaphragm, the concentrations are practically constant, owing to the liquid flows.

The ionic concentration gradients in the transition layer constitute the reason for development of the diffusion component $\mathbf{E}_d$ of electric field strength (the component arising from the difference in diffusion or mobilities between the individual ions). The diffusion potential between the solutions, $\varphi_d^{(\beta,\alpha)} \equiv \psi^{(\beta)} - \psi^{(\alpha)}$, can be calculated by integrating $\mathbf{E}_d$ over the full diffusion-layer thickness from phase (α) to phase (β).

When both solutions are binary and identical in nature and differ only by their concentration and the component $\mathbf{E}_d$ of the field strength is given by Eq. (4.18), the diffusion potential φ_d can be expressed by Eq. (4.19). An equation of this type was derived by Walther Nernst in 1888. Like other equations resting on Fick's law (4.1), this equation, is approximate and becomes less exact with increasing concentration. For the more general case of multicomponent solutions, the *Henderson equation* (1907),

$$\varphi_d = \frac{RT}{F} \frac{\sum u_j (c_j^{(\beta)} - c_j^{(\alpha)})}{\sum u_j z_j (c_j^{(\beta)} - c_j^{(\alpha)})} \ln \frac{\sum z_j u_j c_j^{(\beta)}}{\sum z_j u_j c_j^{(\alpha)}}, \tag{5.2}$$

is generally used. Another equation for multicomponent solutions was proposed in 1890 by Max Planck.

For binary solutions of symmetric $z:z$ electrolytes having a common ion and the same concentration $c_{KA} = c_{MA}$, the general Henderson equation changes to

$$\varphi_d = \frac{RT}{zF} \ln \frac{u_{K^+} + u_{A^-}}{u_{M^+} + u_{A^-}} \tag{5.3}$$

(the *Lewis–Sargent equation*, 1909).

TABLE 5.1 Diffusion Potentials Calculated for Interfaces Between Aqueous Solutions of Different Composition from Eq. (5.2) or (5.3), and Similar Potentials Determined Experimentally ($\varphi_d = \psi^{(\beta)} - \psi^{(\alpha)}$)

Composition of Phases		φ_d (mV)	
(α)	(β)	Calculation	Experiment
0.005 *M* HCl	0.04 *M* HCl	−33.3	
0.005 *M* KCl	0.04 *M* KCl	1.0	
0.01 *M* NaCl	0.01 *M* LiCl	1.3	1.1
0.01 *M* HCl	0.01 *M* KCl	27.5	25.7
0.1 *M* KCl	0.01 *M* NaCl	4.9	6.4
0.1 *M* HCl	0.1 *M* KCl	28.5	26.8
0.1 *M* HCl	4.2 *M* KCl	3.2	
4.2 *M* KCl	0.1 KCl	−1.9	
0.1 *M* HCl ¦ 4.2 *M* KCl	0.1 *M* KCl	1.3	1.1

5.2.1 Values of Diffusion Potentials for Different Interfaces

Table 5.1 lists values of φ_d for interfaces between aqueous solutions of different composition calculated from Eq. (4.19), (5.2), or (5.3) as well as values determined experimentally (in cases where this could be done with sufficient accuracy). A minus sign indicates that the potential of phase (β) is more negative than that of phase (α). We can see from the table that the calculated values agree quite well with those measured. The values of φ_d are small; their absolute values are not over 10 mV when the ions have similar diffusion coefficients. But the diffusion potentials attain several tens of millivolts when the solutions contain H^+ or OH^- ions, which have diffusion coefficients several times higher than those of other ions. In this case the phase containing the higher concentration of H^+ ions is negatively charged relative to the other phase. For systems involving OH^- ions, the diffusion potentials have the opposite sign.

5.2.2 Ways of Reducing Diffusion Potentials

Aqueous solutions of the salts KCl and NH_4NO_3 are of interest inasmuch as here the mobilities (and also the diffusion coefficients) of the anion and cation are very similar. The higher the concentration of these salts, the larger is the contribution of their ions to transition-layer composition and, as can be seen from Table 5.1, the lower the diffusion potentials will be at interfaces with other solutions. This situation is often used for a drastic reduction of diffusion potentials in cells with transference. To this end one interposes between the two solutions a third solution, usually saturated KCl solution (which is about 4.2 mol/L):

$$\mathrm{M}\,|\,(\alpha)\,\vdots\,\mathrm{KCl},\ aq(\varepsilon)\,\vdots\,(\beta)\,|\,\mathrm{M}. \tag{5.4}$$

In laboratory practice *salt bridges* are often used to connect the vessels holding the two solutions. The reduction of the overall diffusion potential is particularly marked

when solutions (α) and (β) are either both acids or both bases. In this case the residual diffusion potentials at interfaces (β)/(ε) and (α)/(ε) compensate each other to an appreciable degree.

The diffusion-potential reduction thus attained is entirely satisfactory for many measurements not demanding high accuracy. However, this approach is not feasible for the determination of the accurate corrected OCV values of cells with transference that are required for thermodynamic calculations.

5.3 DISTRIBUTION OF THE IONS BETWEEN DISSIMILAR BUT MISCIBLE ELECTROLYTES

Two dissimilar electrolytes (α) and (γ) that are in contact may contain ions existing in both phases and transferring freely across the interface (the permeating ions, in the following provisionally labeled K^{z+}, M^{z+}, A^{z-}, etc.) as well as ions existing in only one of the phases (e.g., anions Q^{z-} and R^{z-}). For the permeating ions the equilibrium condition can be written, in accordance with Eq. (2.6), as

$$\Delta\varphi_{\mathrm{G}}^{(\gamma,\alpha)} = \frac{-\Delta\mu_j^0}{z_j F} + \frac{RT}{z_j F} \ln \frac{a_j^{(\alpha)}}{a_j^{(\gamma)}}. \tag{5.5}$$

When several types of permeating ion are present in the system, condition (5.5) must be fulfilled for each of them. But since the potential difference $\varphi_{\mathrm{G}}^{(\gamma,\alpha)}$ between the phases can have just one unique value, the sum of terms on the right-hand side of this equation must also be the same for all permeating ions. It follows that

$$\kappa_j^{1/zj}\left[\frac{a_j^{(\alpha)}}{a_j^{(\gamma)}}\right]^{1/zj} = \kappa_j^{1/zk}\left[\frac{a_k^{(\alpha)}}{a_k^{(\gamma)}}\right]^{1/zk} = \cdots = \lambda, \tag{5.6}$$

where $\kappa_j \equiv \exp(-\Delta\mu_j^0/RT)$ is a constant that is typical for each type of ion, and $\lambda \equiv \exp[\varphi_{\mathrm{G}}^{(\gamma,\alpha)}/RT]$ is a constant independent of the ion, which is often called the *distribution coefficient*.

This thermodynamic equation defines the equilibrium distribution of all permeating ions between the two phases. For quantitative calculations, the conditions of electroneutrality of the phases must be taken into account in addition to this equation.

Consider a few examples where the equilibrium concentrations of components of one of the phases [e.g., (γ)] are calculated when their concentrations in the other phase (α) are given. Assumptions will be made that simplify the notation; we assume that the activities of the ions appearing in the thermodynamic equations are equal to their concentrations, and we consider systems where the ions have like valencies z.

Under these assumptions, Eq. (5.6) becomes

$$\kappa\frac{c_j^{(\alpha)}}{c_j^{(\gamma)}} = \kappa\frac{c_k^{(\alpha)}}{c_k^{(\gamma)}} = \cdots = \lambda^z. \tag{5.7}$$

For the particular case where two ions of like sign are involved in the transfer (e.g., the two ions K^{z+} and M^{z+}), this equation becomes

$$\frac{c_M^{(\gamma)} c_K^{(\alpha)}}{c_K^{(\gamma)} c_M^{(\alpha)}} = \sigma_{M/K}, \tag{5.8}$$

while for transfer of a cation M^{z+} and an anion A^{z-} it becomes

$$\frac{c_M^{(\gamma)} c_A^{(\gamma)}}{c_M^{(\gamma)} c_A^{(\alpha)}} = \sigma_{MA}, \tag{5.9}$$

where $\sigma_{M/K} \equiv \kappa_M/\kappa_K$ and $\sigma_{MA} \equiv \kappa_M \kappa_A$ are the *selectivity coefficients* (which are a quantitative measure for the degree of selectivity in a given system).

Unlike constants κ_j, the values of $\sigma_{M/K}$ and σ_{MA} can be determined from experimental data [e.g., with the aid of Eqs. (5.8) and (5.9) using the analytical values for the ionic concentrations in the two phases].

The equation for the potential difference between the phases becomes

$$\varphi_G^{(\gamma,\alpha)} = \frac{RT}{zF} \ln \kappa_j \frac{c_j^{(\alpha)}}{c_j^{(\gamma)}}, \tag{5.10}$$

where j is any of the permeating ions.

Using this equation we can calculate the concentration-dependent changes in φ_G (absolute values of φ_G and κ_j cannot be determined experimentally).

Example Consider the system

$$KQ(\alpha) + MQ \,\vdots\, KR + MR(\gamma). \tag{5.11}$$

In this system two types of cation are exchanged between the phases. The electroneutrality conditions are $c_K^{(\alpha)} + c_M^{(\alpha)} = c_Q$ and $c_K^{(\gamma)} + c_M^{(\gamma)} = c_R$. Solving Eq (5.7) jointly with these electroneutrality equations, we find for the concentration of cations M^{z+},

$$c_M^{(\gamma)} = c_R c_M^{(\alpha)} [c_M^{\alpha} + \sigma_{K/M} c_K^{(\alpha)}], \tag{5.12}$$

and an analogous equation for the cations K^{z+}. The expression for the potential difference becomes

$$\varphi_G^{(\gamma,\alpha)} = \frac{RT}{F} \ln \frac{\kappa_M}{c_M^{(\alpha)}} [c_M^{(\alpha)} + \sigma_{K/M} c_K^{(\alpha)}], \tag{5.13}$$

5.4 DISTRIBUTION OF IONS IN CELLS WITH MEMBRANE

Consider the system that consists of two similar solutions (α) and (β) which are separated by a membrane unpermeable for at least one of the solution components Y. We write $\mu[Y]$ for such a membrane.

5.4.1 Equilibrium Systems

For any initial composition of the two solutions, an equilibrium distribution of the species between the membrane, any initial composition of the two solutions, an equilibrium distribution of the species between the membrane, and hence also between the two solutions is attained after some time.

The condition of complete equilibrium for any permeating ion in phases (α) and (β) can be written in a form similar to that of Eq. (5.7). Since the phases were assumed to be similar, the standard chemical potentials of the ions will be the same in the two phases: $\Delta\mu_j^0 = 0$, and hence $\kappa_j = 1$. On this basis we find that

$$\frac{c_j^{(\alpha)}}{c_j^{(\beta)}} = \cdots = \frac{c_k^{(\alpha)}}{c_k^{(\beta)}} = \cdots = \lambda^z, \tag{5.14}$$

$$\varphi_m = \frac{RT}{F} \ln \frac{c_j^{(\alpha)}}{c_j^{(\beta)}}, \tag{5.15}$$

where φ_m is the membrane potential (by definition).

The equilibrium conditions for homogeneous systems with membranes were first formulated in this form by Frederick G. Donnan in 1911. Hence, such equilibria are often called *Donnan equilibria*, and the membrane potentials associated with them are called *Donnan potentials*. Sometimes these terms are used as well for the equilibria arising at junctions between dissimilar solutions (Section 5.3).

5.4.2 Quasiequilibrium Systems

Complete equilibration of two solutions separated by a membrane is a very slow process. Often quasiequilibrium systems are used, where there is no equilibrium between the outer solutions (their composition is that arbitrarily given at the outset), although each of these solutions is in equilibrium with an adjacent thin membrane surface layer; there is no equilibrium within the membrane between these surface layers.

We shall write (μ) and (η) for the membrane surface layers adjacent to solutions (α) and (β), respectively. Using the equations reported in Section 5.3, we can calculate the ionic concentrations in these layers as well as the potential differences $\varphi_G^{(\mu,\alpha)}$ and $\varphi_G^{(\eta,\beta)}$ between the phases. According to Eq. (5.1), the expression for the total membrane potential additionally contains the diffusion potential φ_d within the membrane itself, where equilibrium is lacking. Its value can be found with the equations of Section 5.2 when the values of $c_j^{(\mu)}$ and $c_j^{(\eta)}$ have first been calculated.

Example Consider the system

$$\mathrm{MA}(\alpha)\,\vdots\,\mu[\mathrm{A}^{z-}]\,\vdots\,\mathrm{MA} + \mathrm{KA}(\beta). \tag{5.16}$$

Since the membrane is permeable for cations but not for the anions A^{z-}, it should intrinsically contain anions R^{z-}. When these are fixed, their concentration, c_R, will remain the same everywhere. Hence in layers (μ) and (η) the overall cation concentration should also be the same, and the diffusion potential (which is caused by a possible difference in cation mobilities) is extremely small. In the left-hand part of the membrane system, the concentration of cations M^{z+} in each of the phases is equal to the given (invariant) concentration of anions A^{z-} or R^{z-}, respectively; the potential difference between the phases is determined, according to Eq. (5.10), by the cation concentration ratio. The right-hand part of the membrane system corresponds to the system (5.22), where phase (β) now takes the place of phase (α), and phase (η) takes that of phase (γ). As a result, we obtain for the membrane potential,

$$\varphi_m = \frac{RT}{F} \ln \frac{c_{\mathrm{M}}^{(\beta)} + \sigma_{\mathrm{K/M}} c_{\mathrm{K}}^{(\beta)}}{c_{\mathrm{M}}^{(\alpha)} + \varphi_d}. \tag{5.17}$$

5.5 GALVANIC CELLS WITH TRANSFERENCE

Galvanic cells that include at least one electrolyte–electrolyte interface (which may be an interface with a membrane) across which ions can be transported by diffusion are called *cells with transference*. For the electrolyte–electrolyte interfaces considered in earlier sections, cells with transference can be formulated, for example, as

$$\mathrm{M}\,|\,(\alpha)\,\vdots\,(\beta)\,|\,\mathrm{M}, \tag{5.18}$$

$$\mathrm{M}\,|\,(\alpha)\,\vdots\,(\gamma)\,|\,\mathrm{M}, \tag{5.19}$$

$$\mathrm{M}\,|\,(\alpha)\,\vdots\,(\mu)(\beta)\,|\,\mathrm{M}, \tag{5.20}$$

where (α) and (β) are similar, (α) and (γ) are dissimilar phases, (μ) is the membrane, and M is an electrode reversible with respect to the ions M^{z+} present in all electrolyte phases considered.

The OCV values of these cells can be measured experimentally. We shall write them as

$$\mathscr{E} = \mathscr{E}^* + \varphi^{(\mathrm{E})}, \tag{5.21}$$

where $\varphi^{(\mathrm{E})}$ is the potential difference between the electrolytes or membrane potential, and $\mathscr{E}^*$ is the potential difference between the two electrodes, that is, the corrected OCV value [see Eq. (2.14)]. It is only when one of the two terms on the right-hand side can be calculated independently that the other term can be determined from experimental data of $\mathscr{E}$.

After attainment of the ionic equilibrium distribution, cell (5.18) has become a symmetric cell (the electrolyte–electrolyte interface disappears) for which the OCV is zero. It is important to note that even for cell (5.19) the OCV becomes zero after equilibration, but the electrolyte–electrolyte interface does not disappear here. This implies that at equilibrium the value of $\varphi^{(E)}$ is compensated exactly by the potential difference $\mathscr{E}^*$. In fact, the current flowing in such a cell is not associated with any chemical or concentration changes, or changes in Gibbs energy of the system. The values of $\varphi^{(E)}$ and $\mathscr{E}^*$ cannot be determined individually for this inhomogeneous cell. For all types of nonequilibrium cells and also for cell (5.20) in the quasiequilibrium state, nonzero OCV values are measured. For the homogeneous cells (5.18) and (5.20), values of $\varphi^{(E)}$ can be calculated with the aid of the equations reported in Sections 5.2 and 5.4, but the results are approximate, owing to the assumptions made in deriving these equations. Therefore, the individual components of the right-hand part of Eq. (5.20) can be determined for homogeneous cells, but the accuracy is limited.

REFERENCES

Donnan, F., *Z. Elektrochem*., **17**, 572 (1911).

Henderson, P., *Z. Phys. Chem*., **59**, 118 (1907).

Lewis, G., and S. Sargent, *J. Am. Chem. Soc.*, **31**, 363 (1909).

Planck, M., *Wied. Ann. Phys*., **40**, 561 (1890).

6
Polarization of Electrodes

6.1 BASIC CONCEPTS

6.1.1 Electrochemical Reaction Rates

For thermodynamic reasons, an electrochemical reaction can occur only within a definite region of potentials: a cathodic reaction at electrode potentials more negative, an anodic reaction at potentials more positive than the equilibrium potential of that reaction. This condition only implies a possibility that the electrode reaction will occur in the corresponding region of potentials; it provides no indication of whether the reaction will actually occur, and if so, what its rate will be. The answers are provided not by thermodynamics but by electrochemical kinetics.

The concept of *electrochemical reaction rate* needs explanation. The reaction rate (i.e., the amount of reactant converted in unit time) is proportional to the current. But the current does not depend on intrinsic properties of the galvanic cell; it is impressed and can be varied arbitrarily between zero and the limiting value that is typical for a given system. Therefore, the effective rate is not an indicative figure for the electrode reaction. However, current flow gives rise to electrode polarization, which means a shift of potential away from the equilibrium value. The magnitude of polarization depends on both current density (CD) and the nature of the reaction. For a given value of current density, some reactions exhibit high polarization and others exhibit low polarization. The term *slow reaction* is used for reactions associated with high polarization; for them, low ("normal") values of polarization can only be attained at very low current densities. Low values of polarization are typical for *fast reactions*. Thus, the value of current density at a particular value of polarization, or the value of polarization at a particular value of current density, quantitatively characterize the relative rate of an electrochemical reaction.

In the case of redox reactions, polarization also depends on the nature of the nonconsumable electrode at which a given reaction occurs (for the equilibrium potential, to the contrary, no such dependence exists). Hence, the term *reaction* will be understood as "reaction occurring at a specified electrode."

Fundamentals of Electrochemistry, Second Edition, By V. S. Bagotsky

6.1.2 Electrode Polarization

In the electrochemical literature, the concept of *electrode polarization* has three meanings:

1. The phenomenon of change in electrode potential under current flow
2. An operation performed by the experimenter aiming at obtaining a potential change by passing current of a suitable strength and direction
3. The quantitative measure, ΔE, of the shift of electrode potential E relative to the equilibrium value E_0 that occurs under current flow [cf. Eq. (2.21)]

In the case of anodic currents, the potential shifts in a positive direction, and ΔE has positive values; in the case of cathodic currents, ΔE has negative values. In expressions such as "high polarization" and "the polarization increases," the absolute value of polarization denoted simply as ΔE is implied in the case of cathodes.

The value of polarization defined by Eq. (2.21) is referred to a calculated value of equilibrium potential of the reaction, rather than to the electrode's effective open-circuit potential, when the latter is not the equilibrium potential. Sometimes a thermodynamic calculation of the equilibrium potential is not possible: for instance, when several electrode reactions occur simultaneously. In this case one either uses, conditionally, the concept of a polarization which via Eq. (2.21) refers to the effective open-circuit potential, or (since the latter is often irreproducible) one simply discusses electrode potentials at specified current densities rather than the potential shift away from some original value.

When currents flow in galvanic cells, the polarization phenomena that arise at any one of the two electrodes are independent of the properties of the second electrode and of the processes occurring there. Therefore, when studying these phenomena, one considers the behavior of each electrode individually.

6.1.3 Overall and Partial Reaction Currents

It had been shown in Section 2.2 that at the equilibrium potential, the net (external) current density i is zero, but partial current densities $\vec{i}$ and $\overleftarrow{i}$ of the anodic and cathodic reaction exist for which the relation $\vec{i} = \overleftarrow{i} = i^0$ holds where i^0 is the exchange current density. The value of $\vec{i}$ increases, that of $\overleftarrow{i}$ decreases, when the potential is made more positive; but $\vec{i}$ decreases and $\overleftarrow{i}$ increases when the potential is made more negative. The net current density i is the difference of the partial current densities:

$$i = \vec{i} - \overleftarrow{i} \cdot \tag{6.1}$$

When anodic polarization is appreciable, the reverse (cathodic) partial CD becomes exceedingly low and practically, we can assume that $i \approx \vec{i}$; when cathodic polarization is appreciable, we can assume that $i \approx \overleftarrow{i}$. Thus, the total range of potential can be divided into three regions: one region at low values of polarization (to both sides of the equilibrium potential), where the two partial reactions occur at comparable rates,

and two regions at high values of anodic and cathodic polarization, where the reverse partial reactions can be neglected.

6.1.4 Various Types of Polarization

Electrode reactions are heterogeneous since they occur at interfaces between dissimilar phases. During current flow the surface concentrations $c_{S,j}$ of the substances involved in the reaction change relative to the initial (bulk) concentrations $c_{V,j}$. Hence, the value of the equilibrium potential is defined by the Nernst equation changes, and a special type of polarization arises where the shift of electrode potential is due to a change in equilibrium potential of the electrode. The surface concentrations that are established are determined by the balance between electrode reaction rates and the supply or elimination of each substance by diffusion [Eq. (4.9)]. Hence, this type of polarization, ΔE_d, is called *diffusional concentration polarization* or simply concentration polarization. (Here we must take into account that another type of concentration polarization exists which is not tied to diffusion processes; see Section 13.5.)

Other types of polarization are caused by specific features in the various steps of the electrochemical reaction that produce a potential shift relative to the effective equilibrium potential (i.e., that which already accounts for the prevailing values of surface concentrations). These types of polarization, which may differ in character, are jointly termed *activation polarization*. The value of activation polarization is sometimes called the *overvoltage* (this term should be reserved for the complete cell; see Section 2.5.2).

When concentration changes affect the operation of an electrode while activation polarization is not present (Section 6.3), the electrode is said to operate in the *diffusion mode* (under diffusion control), and the current is called a *diffusion current* i_d. When activation polarization is operative while marked concentration changes are absent (Section 6.2), the electrode is said to operate in the *kinetic mode* (under kinetic control), and the current is called a *reaction* or *kinetic current* i_k. When both types of polarization are operative (Section 6.4), the electrode is said to operate in the *mixed mode* (under mixed control).

The polarization equation describes polarization as a function of current density. In the case of concentration polarization, the form of the polarization equation is unrelated to the nature of reaction or electrode. In the case of activation polarization, the parameters of the polarization equations depend decisively on the nature of the reaction. At identical values of current density and otherwise identical conditions, the values of polarization for different reactions will vary within wide limits, from less than 1 mV to more than 2 or 3 V. However, these equations still have common features. A relatively simple set of equations is obtained for simple redox reactions of the type

$$\text{Red} \rightleftharpoons \text{Ox} + ne^- \tag{6.2}$$

[e.g., reaction (1.25) between Fe^{2+} and Fe^{3+} ions], for which it is typical that (1) the reaction involves only the transfer of electrons (one or several) and substances other

than the principal components are not involved, (2) the stoichiometric numbers of the components are unity, (3) the reaction rate is proportional to the reactant concentration, (4) the reaction occurs in a single step without the formation of intermediates, and (5) solid or gaseous phases are not produced or consumed in the reaction. Simple polarization functions are observed for some of the more complicated reactions, but in most of them the equations are highly complex.

Here we consider the polarization equations for simple redox reactions and for reactions that are similar to them. The special features of more complex reactions are discussed in Part II of this book.

6.2 LAWS OF ACTIVATION POLARIZATION

6.2.1 Polarization Equations

At high values of polarization (the exact limits of the corresponding region are indicated below), the relation between activation polarization and current density can often be written in the form

$$\Delta E = a + b \ln i = a + b' \log i, \tag{6.3}$$

where a and b are constants (in volts) and $b' = 2.303b$. Such a "semilogarithmic" relation was first established by Julius Tafel in 1904–1905 for cathodic hydrogen evolution at a number of metal electrodes and is known in the electrochemical literature as the *Tafel equation.*

Because of the logarithmic relation, polarization depends more strongly on parameter a than on parameter b. The parameter a, which is the value of polarization at the unit current density (1 mA/cm^2), assumes values which for different electrodes and reactions range from 0.03 to 2–3 V. Parameter b, which is called the *Tafel slope*, changes within much narrower limits; in many cases, at room temperature $b \approx 0.05$ V and $b' \approx 0.115$ V (or roughly 0.12 V).

Julius Tafel (1862–1918).

For reasons that will become clear later, the slopes are often written in the form

$$b \equiv \frac{RT}{\alpha F} \qquad \left(or\ b' \equiv 2.303\ \frac{RT}{\alpha F} \right), \tag{6.4}$$

where α is a dimensionless coefficient termed the *transfer coefficient*. For the particular value of $b = 0.05$ V mentioned above, this coefficient has a value of $\alpha = 0.5$.

Equation (6.3) can also be written in a form where the current density is a function of polarization:

$$i = nFk \exp\left(\pm \alpha F\ \frac{\Delta E}{RT} \right), \tag{6.5}$$

where k is the reaction rate constant [$k = (1/nF) \exp(-\alpha F/RT)/a$]. In this and all subsequent equations of this type, a plus sign refers to anodic reactions and a minus sign to cathodic reactions. Equations of the type (6.5) can be interpreted by the theory of slow discharge (Erdey-Grúz and Volmer, 1930; see Chap. 15).

The polarization relations found in the region of high polarization are usually plotted semilogarithmically as ΔE vs. log i (Fig. 6.1). These plots are straight lines, called *Tafel lines* (curve 1 in Fig. 6.1), when relation (6.3) holds. More complicated polarization functions are found at many real electrodes in the region of high polarization. Sometimes several Tafel sections can be distinguished in an actual polarization curve (curve 2 of Fig. 6.1); each of these sections has its own characteristic values of parameters a and b).

In the region of low polarization the values of activation polarization are usually proportional to current density:

$$\Delta E = \rho i. \tag{6.6}$$

The proportionality factor ρ (units: $\Omega \cdot \text{cm}^2$) formally has the same function as the electric resistance (per unit cross-sectional area) in Ohm's law, hence is sometimes called the *reaction resistance*. However, this "resistance" is not ohmic.

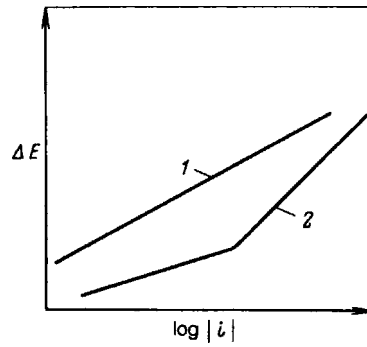

FIGURE 6.1 Polarization curves in the region of high polarization: (1) Tafel; (2) complex.

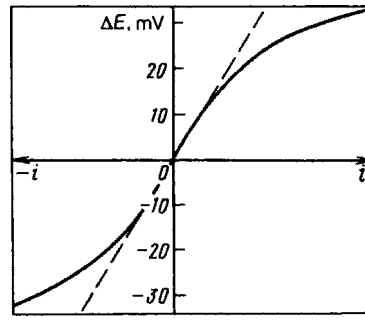

FIGURE 6.2 Polarization curves in the region of low polarization.

Equation (6.6) applies to anodic and cathodic currents. At low values of polarization the parameter ρ usually has the same value for anodic and cathodic currents, and the slope of the ΔE vs. i straight-line plots does not change at the coordinate origin (Fig. 6.2).

6.2.2 Influence of Reactant Concentrations

The specific rate of an electrode reaction depends not only on electrode polarization but also on the reactant concentrations. Changes in reactant concentrations affect not only reaction rates but also the values of equilibrium potentials. To differentiate both these influences, kinetic equations are generally used (especially at high values of polarization), relating the current density not with the value of polarization ΔE but with the potential of the electrode E:

$$E = a + b \ln i \quad \text{or} \quad i = nFk \exp\left(\pm\frac{\alpha FE}{RT}\right) \tag{6.7}$$

In this case, in contrast to the earlier relations, the values of constants a and k depend not only on the reaction being considered but also on the reference electrode against which the potential is measured; only the value of constant b remains unchanged.

For many electrochemical reactions the reaction rate is proportional to the concentration of the reacting species (first-order reaction):

$$i = nFkc_j \exp\left(\pm\frac{\alpha FE}{RT}\right). \tag{6.8}$$

In this equation the rate constant k has the units of cm/s.

In some cases more complex concentration dependencies are observed where the reaction rate is proportional to c_j^p (where p can be larger or smaller than unity) or to $c_1^p c_2^q$, where $j = 2$ represent other substances influencing the reaction rate (including substances decreasing the rate, e.g., reaction products, in which case q has negative values).

Thus, all electrochemical reactions can be characterized by the form of kinetic relation and by the set of coefficients k, α (and, if necessary p), and the values of the concentrations c_j. Particular values of the coefficients always hold for specific reactions; hence, the corresponding indices should be appended to the coefficients. In the following, when considering the relatively simple redox reaction (6.2), we use the notations k_{red}, α, and c_{red} for the coefficients and concentration of the anodic reaction (from left to right) and k_{ox}, β, and c_{ox} for those of the cathodic reaction occurring in the opposite direction.

6.2.3 General Kinetic and Polarization Equations

In the region of high polarization the kinetic equations for partial current densities $\vec{i}$ and $\overleftarrow{i}$ coincide with the equation for the net anodic i_a or cathodic i_c current density, respectively:

$$\vec{i} = i_a = nFk_{red}c_{red}\exp\left(\frac{\alpha FE}{RT}\right), \tag{6.9a}$$

$$\overleftarrow{i} = i_c = nFk_{ox}c_{ox}\exp\left(-\frac{\beta FE}{RT}\right). \tag{6.9b}$$

When the laws of the partial reactions are preserved throughout the entire range of potentials (Butler, 1924), a general kinetic equation that is valid for both the anodic and cathodic currents can be written

$$i = \vec{i} - \overleftarrow{i} = nF\left[k_{red}c_{red}\exp\left(\frac{\alpha FE}{RT}\right) - k_{ox}c_{ox}\exp\left(\frac{-\beta FE}{RT}\right)\right]. \tag{6.10}$$

The expression for the exchange current density $i^0 = \vec{i} = \overleftarrow{i}$ at the equilibrium potential E_0 becomes

$$i^0 = nFkc_{red}c_{red}\exp\left(\frac{\alpha FE_0}{RT}\right) = nFkc_{ox}c_{ox}\exp\left(\frac{-\beta FE_0}{RT}\right). \tag{6.11}$$

The kinetic equations (6.9*a*) and (6.9*b*), which are valid for the partial CD at all values of polarization and for the net CD at high anodic and cathodic polarization, can be written, with expression (6.11) for the exchange CD, as

$$i_a = \vec{i} = i^0\exp\left(\frac{\alpha\Delta E}{RT}\right), \tag{6.12a}$$

$$i_c = \overleftarrow{i} = i^0\exp\left(-\frac{\beta\Delta E}{RT}\right), \tag{6.12b}$$

while

$$i = i^0\left[\exp\left(\frac{\alpha\,\Delta E}{RT}\right) - \exp\left(\frac{-\beta\,\Delta E}{RT}\right)\right] \tag{6.13}$$

is an equation that holds for the net CD over the entire potential range. Equations of this type are often called *Volmer–Butler equations*.

It follows when Eqs. (6.5) and (6.12) are compared that the value of the empirical constant a in the Tafel equation is given by

$$a = -\frac{RT}{\alpha F}\ln i^0. \tag{6.14}$$

Equations (6.9) and (6.10), which contain the rate constants, the electrode potential, and the concentrations, are equivalent to Eqs. (6.12) and (6.13), which contain the exchange CD and the electrode's polarization. But in the second set of equations the concentrations do not appear explicitly; they enter the equations through the values of exchange CD and equilibrium potential. By convention, equations of the former type will be called *kinetic equations*, and those of the latter type will be called *polarization equations*.

Polarization equations are convenient when (1) the measurements are made in solutions of a particular constant composition, and (2) the equilibrium potential is established at the electrode, and the polarization curve can be measured both at high and low values of polarization. The kinetic equations are more appropriate in other cases, when the equilibrium potential is not established (e.g., for noninvertible reactions, or when the concentration of one of the components is zero), and also when the influence of component concentrations on reaction kinetics is of interest.

6.2.4 Relations Between the Parameters of the Forward and Reverse Process

Different electrode reactions will occur independently, and their kinetic coefficients are unrelated. But for the forward and reverse process of a given reaction, such a correlation should exist, since at the equilibrium potential the corresponding partial current densities assume equal values.

Solving Eq. (6.11) for E_0, we find that

$$E = E_0 + \frac{RT}{(\alpha+\beta)F}\left(\ln\frac{k_{ox}}{k_{red}} + \ln\frac{c_{ox}}{c_{red}}\right). \tag{6.15}$$

This equation can be compared with the thermodynamic Nernst equation for the equilibrium potential of the system concerned, which when written in terms of the component concentrations is

$$E_0 = E^0 + \frac{RT}{nF}\ln\frac{c_{ox}}{c_{red}}. \tag{6.16}$$

This comparison yields the following important relations between the kinetic coefficients of the forward and reverse process:

$$\alpha + \beta = n, \tag{6.17a}$$

$$\frac{k_{ox}}{k_{red}} = \exp\left(\frac{FE^0}{RT}\right). \tag{6.17b}$$

These equations show that whereas the kinetic coefficients of an individual reaction can assume any value, the coefficients of its forward and reverse process are always interrelated. The relation between the standard equilibrium potential E^0 and the rate constants k_{ox} and k_{red} is analogous to the well-known physicochemical relation between equilibrium constant K and the rate constants of the forward and reverse process.

In one-electron reactions ($n = 1$), coefficients often assume values $\alpha = \beta = 0.5$, even though Eq. (6.17*a*) is consistent with any value of these coefficients that is in the interval $n \geq \alpha \geq 0$.

6.2.5 Relation Between the Kinetic Parameters in Regions of Low and High Polarization

In the region of low polarization where $\Delta E < RT/F$, the exponential terms of Eq. (6.13) can be expanded into a series, and it will suffice to retain the first two terms of each series: $\exp(y) \approx 1 + y$. As a result, when allowing for Eq. (6.17*a*), we obtain

$$i = i^0 \frac{nF}{RT} \Delta E. \tag{6.18}$$

Thus, while the relation between the partial current densities and potential is exponential, in the region of low polarization a linear relation is obtained between polarization and the net CD, owing to a superposition of the currents of forward and reverse process. At $\Delta E = 10$ mV, the error introduced by the approximation above will be between 1 and 20%, depending on the relative values of α and β; it becomes even smaller with decreasing polarization. Hence we can by convention consider the interval of polarization values between -10 and 10 mV as that of low polarization where the linear relation (6.6) is valid.

It is clear from Eq. (6.18) that the kinetic parameter ρ of Eq. (6.6) is related to the exchange CD as

$$\rho \equiv \left(\frac{d\,\Delta E}{di}\right)_{\Delta E = 0} = \frac{RT}{nF}\frac{1}{i^0}. \tag{6.19}$$

In the regions of high anodic and cathodic polarization we can use the approximations $i \approx \vec{i}$ and $i \approx \overleftarrow{i}$, respectively. The error introduced when the reverse process is neglected is 5% for a polarization of 80 mV (for $n = 1$), and it decreases as the polarization increases further. The value of 80 mV can be regarded as the lower limit of the region of high polarization. For reactions with $n = 2$, this limit drops to 40 mV.

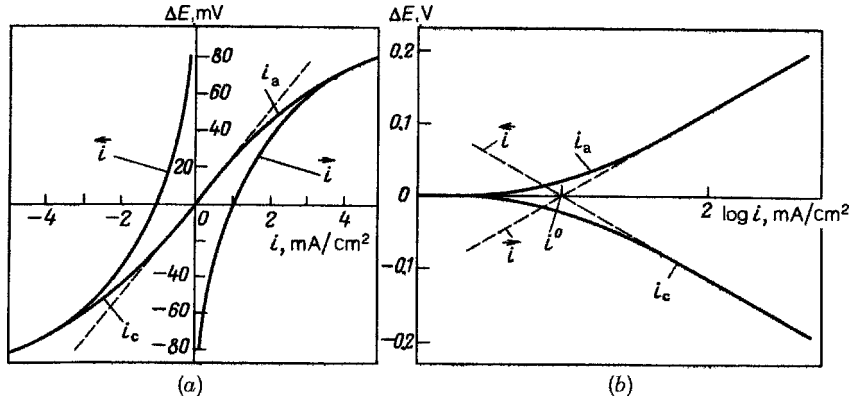

FIGURE 6.3 Potential dependence of the anodic ($\vec{i}$) and cathodic ($\overleftarrow{i}$) partial current densities as well as of the anodic (i_a) and cathodic (i_c) net current densities.

In the intermediate region of moderate polarization (between 10 and 80 mV) we must use the polarization equation (6.13) in its general form.

An analysis of Eq. (6.13) show that for $n = 1$ and $\beta = 0.5$ and for current densities less than 4% of i^0, the polarization is very low (less than 1 mV) and can practically be neglected. The linear section of the polarization curve extends up to current densities which are 40% of i^0. At current densities higher than $4i^0$, the semilogarithmic polarization relation is observed.

Figure 6.3*a* shows curves where the partial current densities $\vec{i}$ and $\overleftarrow{i}$ and the net current densities i_a or i_c are plotted against polarization. Figure 6.3*b* shows the same curves plotted semilogarithmically. We clearly see the region of low polarization values where ΔE is a linear function of i, the regions of high polarization values where the relation is semilogarithmic, and also the corresponding intermediate regions of moderate polarization values.

The straight lines for the partial CD $\vec{i}$ and $\overleftarrow{i}$ in Fig. 6.3*b* intersect at the equilibrium potential $\Delta E = 0$. The value of CD corresponding to the point of intersection is that of the exchange CD i^0, according to Eq. (6.11). It follows that the exchange CD can be determined when the linear sections of the anodic or cathodic polarization curve, which have been measured experimentally and plotted as log i vs. ΔE, are extrapolated to the equilibrium potential. Moreover, according to Eq. (6.19) the exchange CD can be determined from the slope of the polarization curve near the equilibrium potential when the curve is plotted as i vs. ΔE.

6.2.6 Concentration Dependence of the Exchange Current Density

Substituting into Eq. (6.11) the relation (6.16) between equilibrium potential and component concentrations, we obtain

$$i^0 = nFk^0 \exp\left(\frac{\alpha FE^0}{RT}\right) c_{\text{ox}}^{\alpha/n} c_{\text{red}}^{\beta/n}, \tag{6.20}$$

where $k^0 \equiv k_{\text{red}}^{\beta/n} k_{\text{ox}}^{\alpha/n}$. We can see from this equation that the exchange CD of the reaction increases with increasing concentrations of all reaction components.

The standard rate constant k^0 characterizes the rates of both the forward and reverse processes. Its value is independent of the reference electrode selected, in contrast to what holds true for the values of k_{red} and k_{ox}, and it is also independent of the component concentrations, in contrast to what holds true for the exchange CD. Therefore, this constant is an unambiguous characteristic of the kinetic properties exhibited by a given electrode reaction.

6.3 DIFFUSIONAL CONCENTRATION POLARIZATION

6.3.1 Solutions with Excess Foreign Electrolyte

Under the effect of pure concentration polarization, when activation polarization is absent, the electrode potential retains an equilibrium value, but this is a value tied to the variable nonequilibrium values of surface concentrations $c_{S,j}$:

$$E = E^0 + \frac{RT}{nF} \ln c_{S,j}. \tag{6.21}$$

It follows that concentration polarization is defined by the expression

$$\Delta E_d \equiv E - E_0 + \frac{RT}{nF} \ln \frac{c_{S,j}}{c_{V,j}}. \tag{6.22}$$

(Equations for concentration polarization are often used in conjunction with the diffusion and kinetic equations; hence, it will be more convenient here to use concentrations rather than activities.)

The surface concentrations that are attained as a result of balance between the electrode reaction rates and the rates of supply or escape of components by diffusion and migration are given by Eqs. (4.11) and (4.12). Hence, the overall expression for concentration polarization becomes

$$\Delta E_d = \frac{RT}{nF} \ln \frac{1+(i/i_{l,\text{red}})}{1-(i/i_{l,\text{ox}})}. \tag{6.23}$$

In the region of low polarization (low current densities), where two terms in the series expansion of the logarithms are sufficient, it follows from this equation that

$$\Delta E_d = i \frac{RT}{nF} \left(\frac{1}{i_{l,\text{red}}} + \frac{1}{i_{1,\text{ox}}} \right); \tag{6.24}$$

that is, we obtain a linear relation between current density and polarization. Comparison with Eq. (6.6) reveals that in the case of pure concentration polarization, parameter ρ is related to the limiting current density:

$$\rho = \frac{RT}{nF}\left(\frac{1}{i_{l,\text{red}}} + \frac{1}{i_{l,\text{ox}}}\right). \tag{6.25}$$

Curve 1 of Fig. 6.4*a* shows a plot of CD against ΔE which corresponds to Eq. (6.42) with $n = 2$. At zero polarization the current is zero. Under anodic polarization the current tends toward its limiting value $i_{l,\text{red}}$. We can see from Fig. 6.4*b* that the surface concentration $c_{S,\text{red}}$ then falls to zero, while the value of $c_{S,\text{ox}}$ increases to $c_{V,\text{ox}} + (\kappa_{\text{red}}/\kappa_{\text{ox}})c_{V,\text{red}}$ [cf. Eq. (4.15)]. Under cathodic polarization, similarly, the current tends toward a limiting value of $i_{l,\text{red}}$, the surface concentration of Ox falls to zero, and the surface concentration of Red increases to $c_{V,\text{red}} + (\kappa_{\text{ox}}/\kappa_{\text{red}})c_{V,\text{ox}}$.

Curve 1 in Fig. 6.4*a* is symmetric relative to the inflection point *A*. In this point $i = \frac{1}{2}(i_{l,\text{red}} - i_{l,\text{ox}})$; hence, this point has been termed the *half-wave point*. According to Eqs. (4.11) and (4.12), the values of surface concentrations $c_{S,\text{red}}$ and $c_{S,\text{ox}}$ in this point

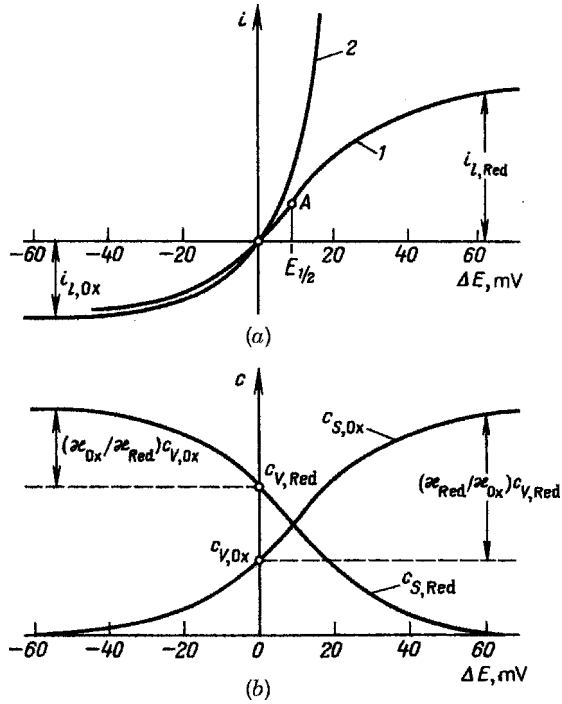

FIGURE 6.4 (*a*) Curves of concentration polarization [(1) $c_{V,\text{red}} \approx c_{V,\text{ox}}$; (2) $c_{V,\text{red}} \gg c_{V,\text{ox}}$] and (*b*) plots of surface concentrations against polarization for polarization curve 1.

are half the limiting values listed above. Substituting these values into the Nernst equation, we obtain for the potential, $E_{1/2}$, of this point (the *half-wave potential*):

$$E_{1/2} = E^0 + \frac{RT}{nF} \ln \frac{\kappa_{red}}{\kappa_{ox}}. \tag{6.26}$$

The half-wave potential is independent of component concentrations. But because of the change in equilibrium potential, the value of polarization in this point depends on the component concentrations. The half-wave potential is usually close to E^0, since κ_{red} and κ_{ox} differ little in most cases.

Using the parameter $E_{1/2}$ (and allowing for the Nernst equation), we can rewrite Eq. (6.28) in the rather convenient form

$$\Delta E_d = E_{1/2} + \frac{RT}{nF} \ln \frac{i_{l,red} + i}{i_{l,ox} - i}. \tag{6.27}$$

Curves showing the concentration polarization for various concentration ratios are presented in Fig. 6.5.

Let us consider a few particular cases.

1. The concentration of one of the components, and hence its limiting current density, is zero. In this case the Nernst equation is not applicable for the equilibrium potential; therefore, we must use a kinetic equation that is written in terms of potential rather than polarization. When an oxidizing agent is not present in the solution $c_{V,ox} = 0$, only anodic currents are possible in the system, and these produce an oxidizing agent. It then follows from Eq. (6.32) that

$$\Delta E_d = E_{1/2} + \frac{RT}{nF} \ln \frac{i}{i_{l,red} - i} \tag{6.28}$$

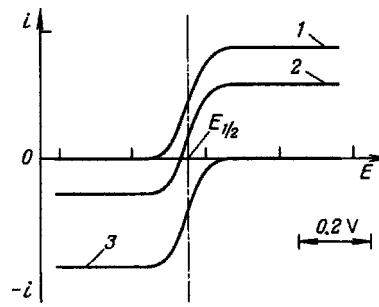

FIGURE 6.5 Curves of concentration polarization (i vs. E): (1) $c_{V,ox} \approx 0$; (2) $c_{V,ox} < c_{V,red}$; (3) $c_{V,red} = 0$.

(Fig. 6.5, curve 1). Similarly, when a reducing agent is not present in the system, $c_{V,\mathrm{red}} = 0$, only cathodic currents are possible (curve 3), and

$$\Delta E_d = E_{1/2} - \frac{RT}{nF} \ln \frac{i}{i_{l,\mathrm{ox}} - i}. \tag{6.29}$$

2. The concentration of one of the components (e.g., the reducing agent), and its limiting current density are large, so that practically $c_{S,\mathrm{red}} = \mathrm{const}$, or a solid component with constant concentration (such as metallic zinc in the reaction $Zn^{2+} + 2e^- \rightarrow Zn$) is involved in the reaction. In this case, Eq. (6.41) becomes

$$\Delta E_d = \frac{RT}{nF} \ln \left(1 + \frac{i}{i_{l,\mathrm{ox}}}\right) \tag{6.30}$$

(Fig. 6.4*a*, curve 2), and the polarization curve is of unusual shape in the region of high anodic CD where $i \gg i_{l,\mathrm{ox}}$ (the oxidizing agent is the anodic reaction product, hence this relation is possible). In this region

$$\Delta E_d = \frac{RT}{nF} \ln i_{l,\mathrm{ox}} + \frac{RT}{nF} \ln i; \tag{6.31}$$

that is, in contrast to other cases of concentration polarization, we obtain a linear relation between polarization and the logarithm of current density. This function is the analog of Eq. (6.3) with a coefficient b that has the value RT/nF. A similar expression is obtained when a component that has constant concentration is the oxidizing agent.

6.3.2 Binary Electrolyte Solutions

The trends of behavior described above are found in solutions containing an excess of foreign electrolyte, which by definition is not involved in the electrode reaction. Without this excess of foreign electrolyte, additional effects arise that are most distinct in binary solutions. An appreciable diffusion potential φ_d arises in the diffusion layer because of the gradient of overall electrolyte concentration that is present there. Moreover, the conductivity of the solution will decrease and an additional ohmic potential drop φ_{ohm} will arise when an electrolyte ion is the reactant and the overall concentration decreases. Both of these potential differences are associated with the diffusion layer in the solution, and strictly speaking, are not a part of electrode polarization. But in polarization measurements, the potential of the electrode usually is defined relative to a point in the solution which, although not far from the electrode, is outside the diffusion layer. Hence, in addition to the true polarization ΔE_d, the overall potential drop across the diffusion layer, $\varphi = \varphi_d + \varphi_{\mathrm{ohm}}$, is included in the measured value of polarization, ΔE_{meas}.

Consider as an example the cathodic deposition of metal from a binary solution of the electrolyte MA of concentration c_k. The concentration changes from $c_{V,k}$ to $c_{S,k}$

within the diffusion layer. The anion is not discharged, and its distribution in the diffusion layer is determined by the equilibrium condition of $\overline{\mu}_{S,A} = \overline{\mu}_{V,A}$. Substituting into this expression the electrochemical potential as a function of electrode potential and of anion concentration $c_A = \tau_- c_k$, we find that

$$\Delta E_{meas} = 2\frac{RT}{nF} \ln \frac{c_{S,k}}{c_{V,k}}. \tag{6.32}$$

Comparing this expression with the value of concentration polarization according to Eq. (6.27), we readily notice that in binary solutions the measured value of polarization is two times higher than that found for the same concentration gradient of the reactant ion when there is an excess of foreign electrolyte (we recall that according to the results of Section 4.3, the limiting CD in binary solutions is also higher by the same factor).

We can also calculate the individual values of φ_d (with the equations reported in Section 5.2) and of φ_{ohm} by determining the concentration distribution in the diffusion layer, and from this, the distribution of solution conductivity. The resulting combined value of φ coincides with the value determined from Eq. (6.32).

6.4 SUPERPOSITION OF CONCENTRATION AND ACTIVATION POLARIZATION

The kinetic and polarization equations described in Sections 6.1 and 6.2 have been derived under the assumption that the component concentrations do not change during the reaction. Therefore, the current density appearing in these equations is the kinetic current density i_k. Similarly, the current density appearing in the equations of Section 6.3 is the diffusion current density i_d. When the two types of polarization are effective simultaneously, the real current density i (Fig. 6.6, curve 3) will be smaller than current densities i_k and i_d (Fig. 6.6, curves 1 and 2) for a given value of polarization.

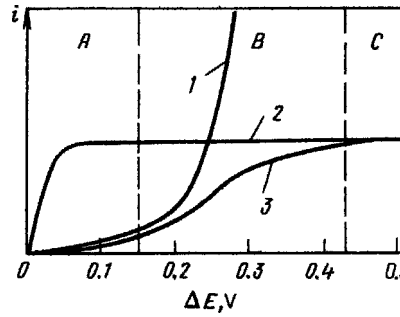

FIGURE 6.6 Plots of i vs. ΔE for activation (1), concentration (2), and combined (3) polarization.

The kinetic equations describing the joint effects of activation and concentration polarization are very complex and we shall consider only the the case of a simple first-order reaction of the type (6.2) proceeding in the presence in the solution of an excess of a foreign electrolyte. To simplify the appearance of these equations (which even in this case are very cumbersome), in this section we use a more compact notation that contains two new kinetic parameters:

1. A generalized rate constant that includes the potential dependence of the reaction rate:

$$h_j = k_j \exp\left(\pm\frac{\alpha FE}{RT}\right) \tag{6.33}$$

(here j stands for Ox and Red). This parameter does not depend on the reference electrode selected, in contrast to the rate constants k_j. The particular value of parameter h_j at the equilibrium potential E_0 will be designated as h_i^0.

2. The systems nonequilibrium factor:

$$\gamma_j \equiv \frac{h_j}{h_j^0} = \exp\left(\pm\frac{\alpha F\,\Delta E}{RT}\right) \tag{6.34}$$

(at the equilibrium potential $\gamma_j = 1$). Using parameter h_j, we can write the general kinetic equation (6.10) as

$$i = nF(h_{\text{red}}c_{\text{red}} - h_{\text{ox}}c_{\text{red}}), \tag{6.35}$$

and the expression for the exchange CD as

$$i^0 = nFh_j^0 c_j. \tag{6.36}$$

Using parameter γ_j, we can write the polarization equation (6.13) as

$$i = i^0\,(\gamma_{\text{red}} - \gamma_{\text{ox}}). \tag{6.37}$$

In the case considered in this section of a joint action of concentration and activation polarization, in the polarization equation (6.10) we must take into account the concentration changes of the rectants near the electrode surface:

$$i = i^0\left(\gamma_{\text{red}}\frac{c_{S,\text{red}}}{c_{V,\text{red}}} - \gamma_{\text{ox}}\frac{c_{S,\text{ox}}}{c_{V,\text{ox}}}\right). \tag{6.38}$$

Replacing the surface concentrations in accordance with Eq. (4.11), we obtain

$$i = i^0\left[\gamma_{\text{red}}\left(\frac{1-i}{i_{l,\text{red}}}\right) - \gamma_{\text{ox}}\left(\frac{1+i}{i_{l,\text{ox}}}\right)\right], \tag{6.39}$$

or, solving for i, we have

$$i = i^0(\gamma_{\text{red}} - \gamma_{\text{ox}}) \left(1 + \gamma_{\text{red}} \frac{i^0}{i_{l,\text{red}}} + \gamma_{\text{ox}} \frac{i^0}{i_{l,\text{ox}}}\right)^{-1}. \tag{6.40}$$

In the region of low polarization where $\gamma_{\text{red}} \approx 1 + \alpha F\,\Delta E/RT$ and $\gamma_{\text{ox}} \approx 1 - \alpha F \times \Delta E/RT$, this equation becomes

$$\Delta E = \frac{RT}{nF} \left(\frac{1}{i^0} + \frac{1}{i_{l,\text{red}}} + \frac{1}{i_{1,\text{ox}}}\right) i, \tag{6.41}$$

which for the kinetic parameter ρ yields the expression

$$\rho = \frac{RT}{nF} \left(\frac{1}{i^0} + \frac{1}{i_{1,\text{red}}} + \frac{1}{i_{1,\text{ox}}}\right). \tag{6.42}$$

Equation (6.42) is a generalization of Eqs. (6.25) and (6.30); it shows that the formal resistance is the sum of reaction resistance (the first term in parentheses) and diffusion resistance (the second and third terms). Equation (6.40) yields directly the important relation

$$\frac{1}{i} = \frac{1}{i_k} + \frac{1}{i_d}. \tag{6.43}$$

In those cases where $i_d \gg i_k$ (region A in Fig. 6.6), the real current density i essentially coincides with the kinetic current density: $i \approx i_k$, and the electrode reaction is controlled kinetically. When $i_d \ll i_k$ (region C), we practically have $i \approx i_d$, and the reaction is diffusion controlled. When i_d and i_k have comparable values, the electrode operates under mixed control (region B). The relative values of these current densities depend on the kinetic parameters and on the potential.

Often, it is claimed that at a given current density, the total polarization ΔE is the sum of pure concentration polarization ΔE_d and pure activation polarization ΔE_{act}. This is true only in the region of low polarization, where the values of polarization are proportional to current density. In other regions it is not true. In fact, the total polarization defined by Eq. (6.39) (Fig. 6.6, curve 3) is larger than the sum of the individual types of polarization, which for the same current density are defined by Eqs. (6.13) and (6.28) (curves 1 and 2). This is due to the fact that concentration changes affect activation and concentration polarization in different ways.

Figures 6.7 and 6.8 show polarization curves that correspond to the equations obtained in the particular case where $\alpha = \beta = 0.5$ ($n = 1$) and $i_{d,\text{red}} \approx i_{d,\text{ox}}$ (since κ_{red} and κ_{ox} have similar values, this implies that $c_{V,\text{red}} \approx c_{V,\text{ox}}$). Curve 1 of Fig. 6.7 shows the case of pure concentration polarization (i^0 has a very large value); the other curves show the influence of decreasing exchange CD (decreasing reaction rate constants), which is revealed at constant values of the limiting-current densities.

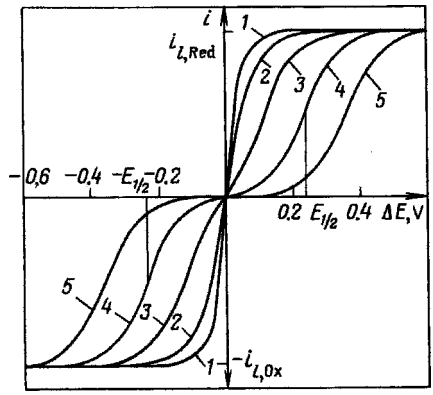

FIGURE 6.7 Plots of i vs. ΔE for combined polarization with $i_{l,\text{red}} = i_{l,\text{ox}}$ and different ratios i^0/i_l: (1) ∞, (2) 1, (3) 0.1, (4) 0.01, (5) 0.001 (the values of $E_{1/2}$ are indicated in the case of curve 4).

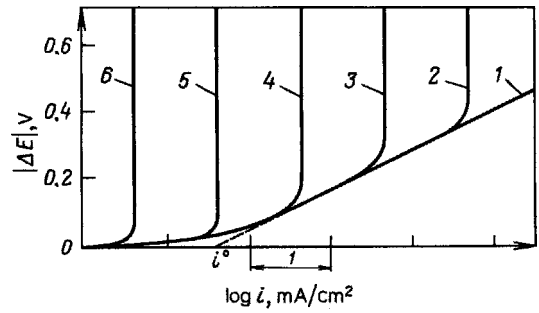

FIGURE 6.8 Plots of ΔE vs. $\log i$ for combined polarization at $i^0 = \text{const}$ and different ratios i^0/i_l: (1) 0, (2) 0.001, (3) 0.01, (4) 0.1, (5) 1, (6) 10.

Curve 1 of Fig. 6.8 corresponds to pure kinetic control (i_d is very large), while the other curves for which the exchange CD has the same value show the influence of a gradual decrease in limiting diffusion CD caused by decreasing diffusional transport constants κ_j (e.g., when the electrode is rotated more and more slowly, but not when the concentration is reduced, since this would alter the exchange CD).

It follows from the figures and also from an analysis of Eq. (6.40) that in the particular case being discussed, electrode operation is almost purely diffusion controlled at all potentials when $i^0/i_d > 5$. By convention, reactions of this type are called *reversible* (reactions thermodynamically in equilibrium). When this ratio is decreased, a region of mixed control arises at low current densities. When the ratio falls below 0.05, we are in a region of almost purely kinetic control. In the case of reactions for which the ratio has values of less than 0.02, the kinetic region is not restricted to low values of polarization but extends partly to high values of polarization. By convention, such reactions are called *irreversible*. We must remember

that even highly irreversible reactions (with very low values of i^0/i_d) remain controlled kinetically only up to current densities that are about 10% of the limiting current density. At higher CD the influence of diffusion processes always becomes evident as we approach the limiting diffusion CD, and electrode operation then is under mixed control.

It will be more convenient sometimes to describe the boundaries of the various regions in terms of the overall reaction rate constant k^0 and the diffusional transport constant κ_j. In our example, we can replace the ratio i^0/i_d by the ratio k^0/κ_j.

The values of κ_j that can be realized experimentally vary between 5×10^{-4} cm/s (natural convection) and 2×10^{-2} cm/s (rotating-disk electrode at $f = 10{,}000$ rpm). Therefore, reactions for which $k^0 \geq 10^{-1}$ cm/s will remain reversible whatever the stirring intensity. Such reactions are called *completely reversible* ("very fast"). Reactions with $k^0 \leq 10^{-5}$ cm/s will always be irreversible and are called *completely irreversible* ("very slow"). In the region of intermediate values of the constant, the character of the reaction will depend on stirring conditions. With other values of α and of ratios $i_{d,\mathrm{red}}/i_{d,\mathrm{ox}}$, the boundaries between the various regions of electrode operation will shift slightly, but the overall picture of the phenomena remains the same.

Figure 6.7 shows a typical special feature of the polarization curves. In the case of reversible reactions (curve 1), the anodic and cathodic branches of the curve form a single step or *wave*. In the case of irreversible reactions, independent, anodic and cathodic, waves develop, each having its own inflection or *half-wave point*. The differences between the half-wave potentials of the anodic and cathodic waves will be larger the lower the ratio i^0/i_d.

Curve 1 in Fig. 6.9 shows the influence of constant κ_j (or of parameters $\omega^{1/2}$ or $f^{1/2}$, which are proportional to it) on the current density at constant potential for a reaction with an intermediate value of k^0. Under diffusion control (low values of f) the current density increases in proportion to $f^{1/2}$. Later, its growth slows down, and at a certain disk speed kinetic control is attained where the current density no longer depends on disk speed. The figure also shows curves for the kinetic current density i_k and the diffusion current density i_d.

All the equations reported above were derived for first-order reactions with respect to the reactant. The laws change when different reaction orders are involved. In particular, plots of i vs. $f^{1/2}$ will be different in shape. At zero reaction order (Fig. 6.9,

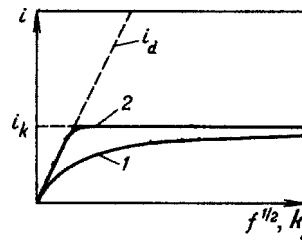

FIGURE 6.9 Plots of the total current density vs. $f^{1/2}$ (or κ_j) for (1) first-order and (2) zeroth-order reactions.

curve 2), since concentration changes can have no effect on reaction rate, the real current will either be a pure diffusion current (at low values of f) or a pure kinetic current, and the curve has a sharp break at $i_d = i_k$.

REFERENCES

Butler, J. A. V., *Trans. Faraday Soc.*, **19**, 659 (1924).

Erdey-Grúz, T., and M. Volmer, *Z. Phys. Chem.,* **150A**, 203 (1930).

Tafel, J., *Z. Phys. Chem.*, **34**, 641(1905).

7
Aqueous Electrolyte Solutions

Aqueous solutions of acids, bases, and salts are the ionic conductors used most widely and studied most thoroughly. The importance of other types of ionic conductors has increased in recent times, but aqueous solutions are still preeminent. Their significance goes far beyond electrochemistry as such; they can be found in practically all spheres of human activity. They are of exceptional importance in the form of intracellular fluids in the biological and physiological processes of all living beings. They are of equally great importance in the form of natural waters in the oceans, rivers, and underground for geomorphological processes.

Aqueous electrolyte solutions have been a subject of determined studies for over a century. Numerous attempts were made to construct theories that could link the general properties of solutions to their internal structure and predict properties as yet unknown. Modern theories of electrolyte solutions are most intimately related to many branches of physics and chemistry. The electrochemistry of electrolyte solutions is a large branch of electrochemistry sometimes regarded as an independent science.

7.1 ELECTROLYTIC DISSOCIATION

7.1.1 Early Ideas

Of great importance for the development of solution theory were the studies of *colligative solution properties*, detected in the 1870s and 1880s by F. M. Raoult, J. H. van't Hoff, and others. These are properties that depend not on the chemical nature of solutes but on their concentration. Three such colligative properties exist:

1. *Osmotic pressure of the solvent*. In dilute ideal solutions the osmotic pressure Π of the solution obeys the equation

$$\Pi = RTc_k. \qquad \text{(van't Hoff's law)}, \tag{7.1}$$

where c_k is the concentration of the solute (in mol/L).

Fundamentals of Electrochemistry, Second Edition, By V. S. Bagotsky

2. *Relative lowering of the solvent's vapor pressure*. The equilibrium vapor pressure of the solvent over a dilute ideal solution p obeys the equation

$$\frac{p^0 - p}{p^0} = M_0 c_k \qquad \text{(Raoult's law)}, \tag{7.2}$$

where p^0 is the vapor pressure of the pure solvent and M_0 is the molar mass of the solvent (for aqueous solutions, $M_0 = 18$ kg/mol).

3. *Elevation of boiling point and depression of freezing point of the solution*. Within certain limits, the change in temperature of these phase transitions obeys the equation

$$\pm\Delta T = (RT^2 q_{\text{ph}}) M_0 c_k, \tag{7.3}$$

where q_{ph} is the (molar) heat of the corresponding phase transition.

It follows from these equations that in dilute ideal solutions, said effects depend only on the concentration, not on the nature of the solute. These relations hold highly accurately in dilute solutions of nonelectrolytes (up to about $10^{-2} M$). It is remarkable that Eq. (7.1) coincides, in both its form and the numerical value of constant R, with the equation of state for an ideal gas. It was because of this coincidence that the concept of ideality of a system was transferred from gases to solutions. As in an ideal gas, there are no chemical and other interactions between solute particles in an ideal solution.

In contrast to nonelectrolyte solutions, in the case of electrolyte solutions the colligative properties depart appreciably from the values following from the equations above, even in highly dilute electrolyte solutions that otherwise by all means can be regarded as ideal (anomalous colligative properties).

At the beginning of the nineteenth century, the first theories were advanced to explain the two major features of electrolyte solutions known at the time: conduction, and the fact that chemical reactions could occur at electrodes during current flow.

The first theory was that of Th. Grotthuss, a Lithuanian physicist, who in 1806 introduced the concept that water molecules are dipolar. According to his hypothesis, in an electric field the water molecules will align in chainlike fashion. The molecules forming the terminal chain links in contact with the electrodes will decompose, evolving hydrogen and oxygen, respectively. The remnants of the broken molecules will combine with fragments of neighboring molecules. After rotating through an angle of 180°, the new molecules are again aligned in the field, and the cycle is repeated. Hence, a relay-type transfer of particles is accomplished; the H or O atoms which eventually are discharged are transferred from the bulk solution to the electrode surfaces through chains of water molecules.

A clear idea about independent charged particles (atoms or atom groups) existing in solutions was formulated in 1834 by M. Faraday. He introduced the new, now current terms *ion* (from the Greek word for "wanderer"), *anion*, *cation*, and others. Faraday first pointed out that the moving ions at once secure the transport

of electricity (charges) and the transport of the substance reacting at the electrode. He assumed, however, that the ions are formed from uncharged molecules only upon application of the electric field, which gave rise to the term *electrolyte* (i.e., "one untied or dissolved by electricity").

The first ideas that ions might form spontaneously (without an electric field effect) were formulated in the 1850s. In 1857, R. Clausius thought that ions could form spontaneously during collisions of the solute molecules, but gave them a very short lifetime and assumed their fraction among the total number of molecules to be insignificant.

7.1.2 Arrhenius's Theory of Electrolytic Dissociation

A theory close to modern concepts was developed by a Swede, Svante Arrhenius. The first version of the theory was outlined in his doctoral dissertation of 1883, the final version in a classical paper published at the end of 1887. This theory took up van't Hoff's suggestions, published some years earlier, that ideal gas laws could be used for the osmotic pressure in solutions. It had been found that anomalously high values of osmotic pressure which cannot be ascribed to nonideality sometimes occur even in highly dilute solutions. To explain the anomaly, van't Hoff had introduced an empirical correction factor i larger than unity, called the *isotonic coefficient* or *van't Hoff factor,*

$$\Pi = iRTc_k, \tag{7.4}$$

into the equation for the osmotic pressure of such solutions. Values of factor i determined experimentally depend on the nature and concentration of the solute. In dilute solutions they sometimes approach integers between 2 and 4.

Arrhenius was the first to point out that conductivity and a departure of colligative properties from the normal values always occur together. He concluded from this observation that the two effects have the same origin.

Jacobus Hendricus van't Hoff (1852–1911; Nobel prize, 1901).

Svante August Arrhenius (1859–1927; Nobel prize, 1903).

The chief points of Arrhenius's theory are as follows:

1. In electrolyte solutions the molecules dissociate into ions spontaneously, so that the solution becomes conductive. Different electrolytes exhibit different degrees of dissociation, α, which will influence the actual values of molar conductivity Λ; the two parameters are interrelated as

$$\alpha = \frac{\Lambda}{\Lambda^0}, \tag{7.5}$$

where Λ^0 is the limiting value of Λ at complete dissociation.

2. Because of dissociation and the resulting increase in the total number of particles in solution, the parameters of the colligative properties assume higher values. These values are proportional to the total concentration, c_σ, of particles (ions and undissociated molecules) in the solution, which for a binary electrolyte is given by $[1 + \alpha(\tau_k - 1)]c_k$. The isotonic coefficient i is the ratio of c_σ and the concentration c_k that would be observed in the absence of dissociation:

$$i = 1 + \alpha(\tau_k - 1) \quad \text{or} \quad \alpha = \frac{i-1}{\tau_k - 1}. \tag{7.6}$$

In the case of complete dissociation, $\alpha = 1$ and $i = \tau_k$ (i.e., the isotonic coefficient assumes integer values).

3. For any given electrolyte that is dissolved, the degree of dissociation increases as the solution is made more dilute.

Thus, quantitative criteria that could be tested experimentally had now been formulated for the first time in the theory of electrolytic dissociation, in contrast to earlier theories. The good agreement between degrees of dissociation calculated from independent measurements of two different properties with Eqs. (7.5) and

(7.6) was a fundamental and rather convincing argument for this theory and contributed to its success (in 1903 Arrhenius was awarded the Nobel Prize in Chemistry for its development).

The third point of Arrhenius's theory was amplified in 1888 by Wilhelm Ostwald. He introduced the idea of an equilibrium between the ions and the undissociated molecules:

$$M_{\tau_+} A_{\tau_-} \rightleftharpoons \tau_+ M^{z+} + \tau_- A^{z-}, \tag{7.7}$$

which obeys the laws of chemical equilibria:

$$\frac{[M^{z+}]^{\tau+}[A^{z-}]^{\tau-}}{[M_{\tau_+}A_{\tau_-}]} = K_{\text{diss}}, \tag{7.8}$$

where K_{diss} is the dissociation constant, which for a given system (of solute and solvent) is solely a function of temperature.

Using the expressions for the concentrations of ions and undissociated molecules, we can write this equation as well in the form

$$\frac{\alpha^2 \tau_+ \tau_- c_k}{1-\alpha} = K_{\text{diss}}. \tag{7.9}$$

It follows for the degree of dissociation, as a function of solute concentration, that

$$\alpha = \frac{K_{\text{diss}}}{2\tau_+\tau_- c_k}\left[1 + \left(\frac{4\tau_+\tau_- c_k}{K_{\text{diss}}}\right)^{1/2} - 1\right] \tag{7.10}$$

(i.e., the higher the concentration, the lower will be the value of α) (Fig. 7.1). Substituting the value of α into Eq. (7.5), we obtain the relation between Λ and concentration:

$$\Lambda = \frac{K_{\text{diss}}\Lambda^0}{2\tau_+\tau_- c_k}\left[1 + \left(\frac{4\tau_+\tau_- c_k}{K_{\text{diss}}}\right)^{1/2} - 1\right]. \tag{7.11}$$

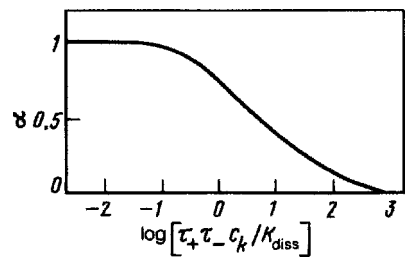

FIGURE 7.1 Degrees of dissociation of a 1 : 1 electrolyte as a function of solution concentration.

At low concentrations when $c_k \ll K_{\text{diss}}/4\tau_+\tau_-$ and the value of α approaches unity, relation (7.11) becomes (after series expansion of the square root)

$$\Lambda = \Lambda^0 - \frac{4\tau_+\tau_-}{K_{\text{diss}}} c_k. \tag{7.12}$$

At higher concentrations when $c_k \gg K_{\text{diss}}/4\tau_+\tau_-$ and the value of α is very low, we obtain, accordingly,

$$\Lambda = \Lambda^0 \left(\frac{K_{\text{diss}}}{\tau_+\tau_- c_k} \right)^{1/2}. \tag{7.13}$$

The relations described by Eqs. (7.9) to (7.13) became known as *Ostwald's dilution law*. They reflect the dependence of conductivity on the dissociation degree α, which changes with increasing concentration c_k.

It must be noted here that a decrease of the value of α is not the sole reason for a decrease in conductivity with increasing concentration. In 1900, Friedrich Kohlrausch found that in binary solutions of strong electrolytes for which $\alpha = 1$ (i.e., does not change with the concentration), the conductivity is a linearly function of the value of $c_k^{1/2}$ (*Kohlrausch's square-root law*):

$$\Lambda = \Lambda^0 - k c_k^{1/2}, \tag{7.14}$$

where k is a constant that depends on the charge but not on the nature of the ions. This relation could not be explained in terms of the Arrhenius concepts. It was only in 1926 that an interpretation could be offered in terms of the theory of ion–ion interaction (Section 7.4), and a method for calculating constant k was proposed.

Soon after inception of the theory of electrolytic dissociation, it was shown that two types of compounds exist that can dissociate upon dissolution in water (or other solvents):

1. Compounds forming ionic crystals (e.g., NaCl). In them the ions exist even prior to dissolution, but are held in lattice sites, owing to electrostatic interaction. In ionic lattices covalent bonds between the ions are practically nonexistent. These lattices disintegrate during dissolution and the ions become mobile (free). Such substances are called *ionophors*.
2. Compounds consisting of molecules with covalent bonding (e.g., HCl). They form ions only upon dissolution as a result of interaction with the solvent. They are called *ionogens*.

The concept of degree of dissociation made it possible to distinguish strong electrolytes (where the values of α in the solution are close to unity) and weak electrolytes (where the values of α are low). This distinction is somewhat arbitrary, since according to Eq. (7.10) the degree of dissociation depends on solution concentration.

Experimental data show that at the usual concentrations (10^{-3} to $10\,M$), most salts and also the hydroxides of alkali metals are strong electrolytes. This is true also for some inorganic acids: HCl, $HClO_4$, and others. Weak electrolytes are the organic acids and the hydroxides of metals other than alkali. Few electrolytes of the intermediate type (with moderate values of α) exist; in particular, certain transition-metal halides such as $ZnCl_2$, ZnI_2, and $CdCl_2$ are in this category.

The theory of electrolytic dissociation also provided the possibility for a transparent definition of the concept of acids and bases. According to the concepts of Arrhenius, an acid is a substance which upon dissociation forms hydrogen ions, and a base is a substance that forms hydroxyl ions. Later, these concepts were extended.

7.1.3 Further Development of the Theory of Electrolytic Dissociation

The theory of electrolytic dissociation was not immediately recognized universally, despite the fact that it could qualitatively and quantitatively explain certain fundamental properties of electrolyte solutions. For many scientists the reasons for spontaneous dissociation of stable compounds were obscure. Thus, an energy of about 770 kJ/mol is required to break up the bonds in the lattice of NaCl, and about 430 kJ/mol is required to split H–Cl bonds during the formation of hydrochloric acid solution. Yet the energy of thermal motions in these compounds is not above 10 kJ/mol. It was the weak point of Arrhenius's theory that this mismatch could not be explained.

Between 1865 and 1887, Dmitri I. Mendeleev developed the *chemical theory of solutions*. According to this theory, the dissolution process is the chemical interaction between the solutes and the solvent. Upon dissolution of salts, dissolved hydrates are formed in the aqueous solution which are analogous to the solid crystal hydrates. In 1889, Mendeleev criticized Arrhenius's theory of electrolytic dissociation. Arrhenius, in turn, did not accept the idea that hydrates exist in solutions.

It was found in later work that it is precisely the idea of ionic hydration that is able to explain the physical nature of electrolytic dissociation. The energy of interaction between the solvent molecules and the ions that are formed is high enough to break up the lattices of ionophors or the chemical bonds in ionogens (for more details, see Section 7.2). The significance of ionic hydration for the dissociation of electrolytes had first been pointed out by Ivan A. Kablukov in 1891.

According to modern views, the basic points of the theory of electrolytic dissociation are correct and were of exceptional importance for the development of solution theory. However, there are a number of defects. The quantitative relations of the theory are applicable only to dilute solutions of weak electrolytes (up to 10^{-3} to $10^{-2}\,M$). Deviations are observed at higher concentrations; the values of α calculated with Eqs. (7.5) and (7.6) do not coincide; the dissociation constant calculated with Eq. (7.9) varies with concentration; and so on. For strong electrolytes the quantitative relations of the theory are altogether inapplicable, even in extremely dilute solutions.

Arrhenius's theory contains the idea that the effects of ions on colligative properties are additive (i.e., that interactions between the ions are absent). However, a simple calculation shows that at distances of less than 10 to 20 nm between ions, marked

electrostatic interaction will arise. These are the distances between ions in solutions having concentrations of 10^{-3} to $10^{-4}\,M$. The fact that electrostatic forces must be taken into account was pointed out in 1895 by Johannes Jacobus van Laar.

At the beginning of the twentieth century the idea was put forward that in solutions of strong electrolytes the degree of dissociation is not simply high but dissociation of the solute is complete (i.e., equilibrium between ions and undissociated molecules does not exist). This point is particularly evident for ionophors, which in the solid state do not possess individual molecules and for which it is unlikely that undissociated molecules should appear in a solution.

Hence, the theory of electrolyte solutions subsequently developed in two directions: (1) studies of weak electrolyte solutions in which a dissociation equilibrium exists and where because of the low degree of dissociation the concentration of ions and the electrostatic interaction between the ions are minor; and (2) studies of strong electrolyte solutions, in which electrostatic interaction between the ions is observed.

Of great importance for the development of solution theory was the work of Gilbert N. Lewis, who introduced the concept of activity in thermodynamics (1907) and in this way greatly eased the analysis of phenomena in nonideal solutions. Substantial information on solution structure was also gathered when the conductivity and activity coefficients (Section 7.3) were analyzed as functions of solution concentration.

7.2 IONIC SOLVATION (HYDRATION) IN SOLUTIONS

Ionic solvation is interaction between ions and solvent molecules that leads to the formation of relatively strong aggregates, the solvated ions. In aqueous solutions the terms *ionic hydration* and *hydrated ions* are used as well.

Ions not solvated are unstable in solutions; between them and the polar solvent molecules, electrostatic ion–dipole forces, sometimes chemical forces of interaction also arise which produce solvation. That it occurs can be felt from a number of effects: the evolution of heat upon dilution of concentrated solutions of certain electrolytes (e.g., sulfuric acid), the precipitation of crystal hydrates upon evaporation of solutions of many salts, the transfer of water during the electrolysis of aqueous solutions), and others. Solvation gives rise to larger effective radii of the ions and thus influences their mobilities.

Solvated ions have a complicated structure. The solvent molecules nearest to the ion form the *primary*, or *nearest*, *solvation sheath* (Fig. 7.2). Owing to the small distances, ion–dipole interaction in this sheath is strong and the sheath is stable. It is unaffected by thermal motion of the ion or solvent molecules, and when an ion moves it carries along its entire primary shell. In the *secondary*, or farther *shells*, interactions are weaker; one notices an orientation of the solvent molecules under the effect of the ion. The disturbance among the solvent molecules caused by the ions becomes weaker with increasing distance and with increasing temperature.

Thus, ionic solvation is associated with a substantial rearrangement of solvent structure; its primary structure is broken where the ion is located, and its molecules undergo reorganization (reorientation) within a certain volume around the ion.

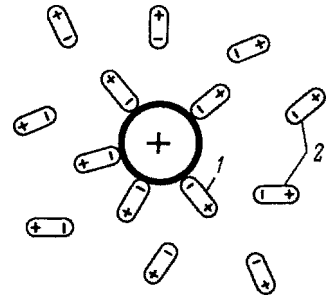

FIGURE 7.2 Solvation of an ion: (1) nearest; (2) farther.

An ion's solvated state can be described in two ways: (1) in terms of the energy effects: the heat, $q^{(s)} = -\Delta H^{(s)}$, work, $w^{(s)} = -\Delta G^{(s)}$, and entropy, $\Delta S^{(s)}$, of solvation (index$^{(s)}$), and (2) in terms of physical parameters: the solvation number h_j (the number of solvent molecules associated with ion j) and the radius $r^{(s)}$ of the solvated ion. These parameters refer to the primary sheath.

7.2.1 Solvation Energies of Electrolytes

Energy effects associated with the dissolution of a given substance (which in the following is distinguished with the index$^{(d)}$) can be determined experimentally. They depend on the system's initial and final state, but not on the path taken by the process. Hence, for calculations, the device of thermodynamic cycles is often used, where the true path of the process is replaced by another path (which may even be a path that actually cannot be realized) for which the energy effects of the individual intermediate steps can be determined.

The dissolution process can be performed mentally in two steps: (1) from the original substance, ions are formed in the gas phase (or in vacuum) where they are sufficiently far apart so that their electrostatic interaction can be excluded; and (2) transfer of these ions from the gas phase into the solvent. The first step is independent of the solvent. For ionophors, it implies breakdown of the lattice, and for ionogens, it implies breaking the chemical bonds in the original molecule and ionizing the resulting atoms or atom groups. Provisionally, this step will be called *breakup* (index$^{(b)}$). The energy effects of the second step are related to ionic solvation. The total heat of solution of a compound is the sum of the heats of the two steps:

$$q^{(d)} = q^{(b)} + q^{(s)}. \tag{7.15}$$

This equation is used in calculating heats of solvation of electrolytes. The heat of solution can be determined highly accurately by calorimetry (with an error of $<0.1\%$). This heat is relatively small, and the values are between -100 and $+40$ kJ/mol. Different methods exist to calculate the breakup energies approximately on the basis of indirect experimental data or models. Unfortunately, the accuracy of these calculations is much lower (i.e., not better than $\pm 5\%$).

Determination of Lattice Breakup Energies from Experimental Data The process of lattice breakup can be split into individual steps for which the energies can be measured. Thus, breaking up the NaCl lattice to form free ions in the gas phase can be described (with a *Born–Haber cycle*) as

$$\mathrm{NaCl\,(s)} \begin{cases} \xrightarrow{(1)} \mathrm{Na\,(s)} \xrightarrow{(2)} \mathrm{Na\,(g)} \xrightarrow{(4)} \mathrm{Na^+\,(g)} \\ \longrightarrow \tfrac{1}{2}\mathrm{Cl_2\,(g)} \xrightarrow[(3)]{} \mathrm{Cl\,(g)} \xrightarrow[(5)]{} \mathrm{Cl^-\,(g)} \end{cases} \tag{7.16}$$

Calorimetrically or otherwise, heats can be determined for the following steps: (1) decomposition of NaCl into the elements, $q^{(1)} = -411\,\mathrm{kJ/mol}$; (2) evaporation of sodium, $q^{(2)} = -409\,\mathrm{kJ/mol}$; and (3) dissociation of the chlorine molecules, $q^{(3)} = -121\,\mathrm{kJ/mol}$. From spectroscopic data one can determine the work required in the following steps: (4) ionization of the sodium atoms, $w^{(4)} = -496\,\mathrm{kJ/mol}$; and (5) ionization of the chlorine atoms, $w^{(5)} = +364\,\mathrm{kJ/mol}$. Neglecting the difference between heats and work in individual steps (the error thus introduced is within $\pm 5\%$ in the present case), we obtain for the total heat of crystal NaCl breakup: $q^{(\mathrm{b})} = \Sigma q^{(\mathrm{i})} = -722\mathrm{kJ/mol}$.

Calculation of the Electrostatic Energy of Lattice Breakup In 1919, Max Born proposed a method for calculating the energy necessary to draw apart a pair of ions from a crystal lattice to infinite distance against electrostatic attraction forces. The equation derived by Born gives for the lattice energy of a NaCl crystal the value $-762\,\mathrm{kJ/mol}$ (i.e., a value close to the experimental value of the heat of breakup that we had mentioned).

Determination of the Breakup Energies of Ionogens Through the analysis of molecular spectra one can determine the bond energies [i.e., the energies required to break a given molecule into atoms (or atom groups)]. Through the analysis of atomic spectra, on the other hand, one can calculate the energy of ion formation from atoms. The energy of breaking an HCl molecule into free ions H^+ and Cl^- thus determined is $-432\,\mathrm{kJ/mol}$.

Table 7.1 lists values for the breakup energies and first heats of solution in water for various compounds as well as values for the hydration energies of these compounds calculated from Eq. (7.15). In view of what we had said, we can estimate that values of $q^{(\mathrm{s})}$ are accurate to $\pm 5\%$. We see that the ionic solvation energies are high (several hundred kJ/mol); hence, they can compensate for the rather high breakup energies of ionophors and ionogens.

7.2.2 Solvation Energies of Individual Ions

If in an electrolyte solution, the solvation energy of each ion is independent of the second ion's identity, the solvation energy of the electrolyte k can be written as

$$q_k^{(\mathrm{s})} = \tau_+ q_+^{(\mathrm{s})} + \tau_- q_-^{(\mathrm{s})}. \tag{7.17}$$

TABLE 7.1 Heats of Breakup $q^{(b)}$, First Heats of Dissolution $q^{(d)}$, and Heats of Solvation $q^{(s)}$ for Various Ionophors in Water (kJ/mol)

Ionophor	$q^{(d)}$	$q^{(b)}$	$q^{(s)}$	Ionophor	$q^{(d)}$	$q^{(b)}$	$q^{(s)}$
LiF	−4.6	1031.0	1026.4	KI	−20.5	637.9	617.4
NaF	−0.4	912.1	911.7	RbF	+26.4	780.2	806.6
NaCl	−3.8	773.1	769.3	RbBr	−21.8	658.8	637.1
NaBr	+0.8	741.3	742.1	RbI	−26	622.0	596.1
KF	+17.6	810.4	828.0	CsF	+37.7	744.7	782.3
KCl	−17.2	702.8	685.6	CsI	−33.1	604.8	571.8
KBr	−20.1	678.5	658.4				

Above, the solvation energy had been defined as the energy set free upon transfer of ions of a given type from the gas phase into the solution. During this transfer the ions cross the phase boundary between gas and solution where the solution's surface potential $\chi \equiv \psi^{(sol)} - \psi^{(g)}$ is effective. During the crossing an additional energy $q^{(\psi)} = -zF\chi$ is evolved (per mole of the ions). Hence, two types of ionic solvation energy are distinguished: chemical, $q^{(w,chem.)}$, which only characterizes the ion–solvent interaction, and real, $q^{(s,real)}$, which in addition includes crossing the surface layer by the ions. These two parameters are interrelated as follows:

$$q^{(s,real)} = q^{(s,chem.)} - zF\chi. \tag{7.18}$$

For the electrolyte as a whole, the effects associated with cations and anions crossing the surface layer cancel, and Eq. (7.17) is valid, with both the chemical and the real ionic solvation energies. Next, we describe ways of theoretically calculating the solvation energies of individual ions or of calculating them from indirect experimental data.

Theoretical Calculation of Ionic Solvation Energies The first method for such calculations was suggested by M. Born in 1920. In this method the solution is regarded as a homogeneous continuum with the relative permittivity ε. The ion's transfer from vacuum into the solution is split mentally into three steps: (1) removal of the electric charge from the ion in vacuum, (2) transfer of the uncharged particle from vacuum into the solution, and (3) restitution of charge to the particle in solution. Since only electrostatic forces, not the chemical forces, are considered, the work performed in the second step is zero. So to find the energy of an ion's solvation, it is necessary to calculate the work of discharge of the ion in vacuum (first step) and the work of charging the ion in solution. In calculating the work of discharging and charging, the assumption is made that the particle is a sphere of radius r_j.

For the total (real) work required to transfer an ion from vacuum into solution, Born's theory gives the expression

$$w^{(s)} = \frac{(zQ^0)^2}{8\pi\varepsilon_0\varepsilon r_j}. \tag{7.19}$$

Comparison with experimental data shows that Born's equation yields high values of $w^{(s)}$ (or $q^{(s)}$). It is a defect of Born's model that the solvent is regarded as a continuum with the unchanged bulk value of the parameter ε, even at short distances from the ion. However, the solvent molecules in the first solvation sheath are strongly oriented, and one cannot disregard the real structure of this sheath. In the model developed by John D. Bernall and Ralph H. Fowler in 1933 and in models of other workers, the solvent around the ion is split conditionally into two regions, a first shell containing h_j solvent molecules, and the remainder which, as in Born's model, is regarded as a continuum.

Let μ_0 be the dipole moment of a solvent molecule and r_0 its radius. The electrostatic energy of interaction between the ion and h_j solvent molecules in the primary shell when computed per mole of ions can be written as

$$w^{\text{prim}} = \frac{N_A h_j \mu_0 z Q^0}{4\pi\varepsilon_0 \varepsilon (r_j + r_0)^2}. \tag{7.20}$$

The interaction with the remainder of the solvent is determined by Born's equation, but taking into account that the molecules of this part of the solvent are found at distances greater than $r_j + 2r_0$.

In addition to these interactions, one must take into account that reorganization of the solvent molecules requires the expenditure of some energy w^{reorg}. Calculations show that this energy for water has values of -60 to -120 kJ/mol.

Calculation of the Solvation Energy from Experimental Data The solvation energies of individual ions can be calculated from experimental data for the solvation energies of electrolytes when certain assumptions are made. If it is assumed that an ion's solvation energy depends only on its crystal radius (as assumed in Born's model), these energies should be the same for ions K^+ and F^-, which have similar values of these radii (0.133 ± 0.002 nm). It follows that in aqueous solutions, $q^{(s)}_{K^+} = q^{(s)}_{F^-} = \frac{1}{2} q^{(s)}_{KF} = 414.0$ kJ/mol. With the aid of these values we can now determine the values for other ions. According to another hypothesis, it is the ions Cs^+ and I^- that have identical solvation energies: $q^{(s)}_{Cs^+} = q^{(s)}_{I^-} = \frac{1}{2} q^{(s)}_{CsI} = -285.9$ kJ/mol. Here the smaller radius of the cesium ion (0.169 nm, compared to 0.215 nm for the iodide ion) compensates for the asymmetry of the water molecules.

Values for the heats of hydration of a number of ions that were calculated by the aforementioned methods on the basis of theoretical models and experimental data are reported in Table 7.2. We see that there is a certain general agreement, but in individual cases the discrepancies are large, due to inadequacies of the theoretical concepts used in the calculations.

7.2.3 Solvation Numbers

Various methods are available for determining the solvation number h_j and (or) the radius of the primary solvation sheath: (1) by comparing the values of the true and apparent ionic transport numbers, (2) by determining the Stokes radii of the ions, or (3) by measuring the compressibility of the solution [the compressibility decreases

TABLE 7.2 Heats of Hydration of Individual Ions (kJ/mol) and Hydration Numbers h_j

		Calculation		Experimental Data		
Ion	r_{cryst} (nm)	Eq. (7.19)	Improved	From KF	From CaI	h_j
Li^+	0.060	1162.4	670.1	612.4	529.9	5–6
Na^+	0.095	734.6	498.9	497.7	415.2	6–7
K^+	0.133	524.5	378.8	414.0	331.5	4
Rb^+	0.148	473.4	342.8	392.6	310.1	3
Cs^+	0.169	412.7	300.5	368.4	285.9	1–2
F^-	0.136	513.2	329.0	414.0	496.5	2–5
Cl^-	0.184	385.5	237.8	271.6	354.1	0–3
Br^-	0.195	357.9	216.0	244.4	326.9	0–1
I^-	0.216	323.1	187.1	203.4	285.9	0–1

in the presence of ions, owing to the decrease in specific volume of the water (electrostriction of water)]. These methods are not highly accurate.

The values of h_j for different ions are between 0 and 15 (see Table 7.2). As a rule it is found that the solvation number will be larger the smaller the true (crystal) radius of the ion. Hence, the overall (effective) sizes of different hydrated ions tend to become similar. This is why different ions in solution have similar values of mobilities or diffusion coefficients. The solvation numbers of cations (which are relatively small) are usually higher than those of anions. Yet for large cations, of the type of $N(C_4H_9)_4^+$, the hydration number is zero.

7.2.4 Hydration of Protons

The behavior of protons in aqueous solutions differs widely from that of other ions and from that of protons themselves in organic solvents. The proton's hydration energy (about 1100 kJ/mol) and its mobility in aqueous solutions are two to four times higher than the corresponding parameters of other ions.

These special features are explained by an interaction between the proton and one of the water molecules, which is not merely electrostatic but also covalent. This yields a new chemical species, the hydroxonium ion, H_3O^+. The existence of such ions was demonstrated in the gas phase by mass spectrometry and in the solid phase by X-ray diffraction and nuclear magnetic resonance. The H^+–H_2O bond has an energy of 712 kJ/mol, which is almost two-thirds of the total proton hydration energy.

The species H_3O^+ is subject to further hydration in the usual manner. Its primary sheath contains three water molecules linked through electrostatic forces, and in part through hydrogen bonds (i.e., the ion with its primary solvation sheath can be formulated as $H_9O_4^+$).

The H^+–H_2O bond has the special feature that although the bond energy is high, the proton will readily hop from one water molecule in the hydration complex to a neighboring water molecule. This hop is a quantum motion and will occur only when the water molecules have a favorable mutual orientation. It will occur predominantly

in the direction of an electric field that may be present in the solution. Therefore, in solutions with hydroxonium ions, two transport mechanisms exist: (1) transport of hydrated hydroxonium ions (which is analogous to the transport of other types of ion), and (2) transport of nonhydrated protons along the relatively immobile framework of oriented water molecules. The second mechanism resembles that of charge transport suggested by Grotthuss early in the nineteenth century. As a result of the joint operation of these two mechanisms, protons have a higher mobility than other ions in aqueous solutions. The elevated mobility of hydroxyl ions is explained in analogous fashion.

7.3 ACTIVITY OF REAL ELECTROLYTE SOLUTIONS

7.3.1 Ways to Determine the Activity of Electrolyte Solutions

The thermodynamic properties of real electrolyte solutions can be described by various parameters: the solvent's activity a_0, the solute's activity a_k, the mean ion activities $a_{\pm}$, as well as the corresponding activity coefficients. Two approaches exist for determining the activity of an electrolyte in solution: (1) by measuring the solvent's activity and subsequently converting it to electrolyte activity via the thermodynamic Gibbs–Duhem equation, which for binary solutions can be written as

$$n_0 \, d \ln a_0 + n_k \, d \ln a_k; \tag{7.21}$$

and (2) by measuring the solute's activity directly.

The solvent's activity can be determined by measuring the saturation vapor pressure above the solution. Such measurements are rather tedious and their accuracy at concentrations below 0.1 to 0.5 M is not high enough to produce reliable data; therefore, this method is used only for concentrated solutions. The activity can also be determined from the freezing-point depression or boiling-point elevation of the solution. These temperature changes must be ascertained with an accuracy of about 0.0001 K, which is quite feasible. This method is used primarily for solutions with concentrations not higher than 1 M.

Direct measurements of solute activity are based on studies of the equilibria in which a given substance is involved. The parameters of these equilibria (the distribution coefficients, equilibrium constants, and EMF of galvanic cells) are determined at different concentrations. Then these data are extrapolated to very low concentrations, where the activity coincides with concentration and the activity coefficient becomes unity.

Electrochemical Cell Without Transference Assume that we want to determine the activities of HCl solutions of various concentrations. We assemble a galvanic cell with hydrogen and calomel electrode:

$$\mathrm{Pt,\ (H_2)\ |\ HCl}(c_1)\ |\ (\mathrm{Hg_2H_2Cl_2}),\ \mathrm{Pt}. \tag{7.22}$$

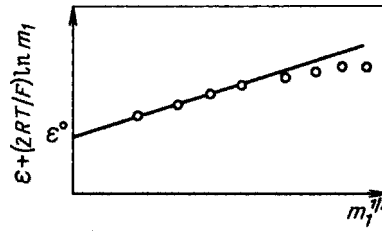

FIGURE 7.3 Extrapolation of experimental data for the determination of activity coefficients.

The EMF of this cell is defined by the equation

$$\mathscr{E} = \mathscr{E}^0 - \frac{RT}{F} \ln a_1. \tag{7.23}$$

Taking into account that in this case $a_k = f_{\pm}^2 c_1^2$, we can also write this equation as

$$\mathscr{E} + \frac{2RT}{F} \ln c_1 = \mathscr{E}^0 - \frac{2RT}{F} \ln f_{\pm}. \tag{7.24}$$

Experimentally we can determine the values of $\mathscr{E}$ at various values of c_1. Then we construct a plot of the left-hand side of Eq. (7.24) vs. concentration and extrapolate it to zero concentration [i.e., into the region of ideal solutions where $\ln f_{\pm} = 0$ (Fig. 7.3)]. We thus determine the value of $\mathscr{E}^0$. Knowing this, we can readily find the values of $f_{\pm}$ for any solution concentration investigated when using Eq. (7.24).

The accuracy of this method depends on correct extrapolation of the experimental data. The error associated with the extrapolation can be reduced by plotting the experimental data not as a function of concentration but as a function of the square root of concentration. It will be shown below that in this case the experimental data for dilute solutions fall onto a straight line that can be extrapolated more accurately than a curve to zero concentration.

7.3.2 Concentration Dependence of the Activity Coefficient

The activities have by now been determined for binary solutions of most electrolytes. As a rule, the values determined by different methods are in good mutual agreement (the scatter is not over 0.5%). These data are reported in special tables listing coefficients $f_{\pm}$ as functions of concentrations [in the tables the concentrations are usually quoted in molalities (m), i.e., the number of moles of the given substance in 1 kg of the solvent].

Figure 7.4 shows such functions for binary solutions of a number of strong electrolytes and for the purposes of comparison, for solutions of certain nonelectrolytes (f_k). We can see that in electrolyte solutions the values of the activity coefficients vary within much wider limits than in solutions of nonelectrolytes. In dilute electrolyte solutions the values of $f_{\pm}$ always decrease with increasing concentration. For

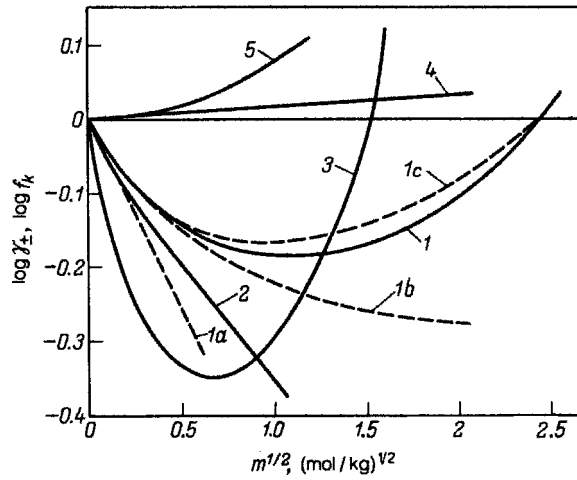

FIGURE 7.4 Mean ionic activity coefficients as functions of molality for solutions of (1) NaCl, (2) KNO_3, (3) $CaCl_2$; activity coefficients as functions of molality for solutions of (4) glycerol, (5) glycine. The dashed lines: curves for solutions of 1 : 1 electrolytes calculated (1a) via Eq. (7.39), (1b) via Eq. (7.43), and (1c) via Eq. (7.44).

many (but not all) electrolytes they go through a minimum and then increase with increasing concentration. In a number of cases, very high values of $f_\pm$ are attained in concentrated solutions. In other cases these values vary relatively little or decrease monotonically. The highest value, $f_\pm = 1457$, was obtained for a $5.5\,m$ $UO_2(ClO_4)$ solution, and the lowest (among strong electrolytes) value, $f_\pm = 0.0168$, for a $2.5\,m$ $CdCl_2$ solution.

The individual differences between electrolytes appear mainly in concentrated solutions; in dilute solutions distinct common traits are exhibited. When the experimental data are plotted as $\log f_\pm$ vs. $f_\pm^{1/2}$, a linear relation is observed in very dilute solutions, as can be seen from Fig. 7.4:

$$-\log f_\pm = k c_k^{1/2}. \tag{7.25}$$

It is typical that in this region the curves of electrolytes of the same valence type almost coincide (i.e., at a given concentration the activity coefficients depend only on the electrolyte's valence type, not on its identity).

In activity studies in multicomponent systems, G. N. Lewis and M. Randall found in 1923 that in the case of dilute solutions, when a foreign electrolyte is added, the activity change of the substance studied depends only on the concentration and valence type of the substance added, not on its identity. For a quantitative characterization of solutions, they introduced the concept of *ionic strength* I_c of a solution (units: mol/L),

$$I_c \equiv \tfrac{1}{2} \Sigma c_j z_j^2, \tag{7.26}$$

where the c_j are the real concentrations of the ions (not counting the undissociated molecules).

They formulated the *ionic-strength principle* according to which "in dilute solutions, the activity coefficient of a given strong electrolyte is the same in all solutions of the same ionic strength."

In 1922, Johannes Nicolaus Brønsted established an empirical relation for the activity coefficients in dilute electrolyte solutions:

$$-\log f_{\pm} = z_+ z_{-\tau} h I_c^{1/2}, \tag{7.27}$$

where h is a constant that does not depend on the identity or valence type of the electrolyte and has the approximate value 0.50 $(\text{L/mol})^{1/2}$.

Equation (7.25) can be regarded as a particular case of the more general Eq. (7.27), since for binary solutions of strong electrolytes, $I_c = \frac{1}{2}(\tau_+ z_+^2 + \tau_- z_-^2)$. For binary 1:1, 1:2, and 2:2 electrolytes the values of I_c are c_k, $3c_k$, and $4c_k$, respectively. It follows that the coefficients k in Eq. (7.25) have values of h, $3.46h$, and $8h$ for the same electrolytes.

7.3.3 Physical Meaning of Activity Coefficients

The departure of a system from the ideal state is due to interaction forces between the individual particles contained in the system. The dependence of chemical potential of a species on its concentration can be written as

$$\mu_j = \mu_j^0 + RT \ln c_j + RT \ln f_j. \tag{7.28}$$

The last term on the right-hand side,

$$w_{\text{int},j} \equiv RT \ln f_j \tag{7.29}$$

(in kJ/mol), represents the energy contributed by this interaction; it is zero for ideal solutions.

When repulsion forces exist between the particles, the chemical potential of the corresponding species will increase (an additional energy $w_{\text{int},j} > 0$ must be expended to place a particle into a given volume), and hence, the activity coefficient will be larger than unity. When attraction forces are present, the activity coefficient will be smaller than unity.

The ions in solution are subject to two types of forces: those of interaction with the solvent (solvation) and those of electrostatic interaction with other ions. The interionic forces decrease as the solution is made more dilute and the mean distance between the ions increases; in highly dilute solutions their contribution is small. However, solvation occurs even in highly dilute solutions, since each ion is always surrounded by solvent molecules. This implies that the solvation energy, which to a first approximation is independent of concentration, is included in the standard chemical potential μ_j^0 and has no influence on the activity.

Therefore, the activity coefficients in solutions are determined primarily by the energy of electrostatic interaction $w_{e,j}$ between the ions. It is only in concentrated solutions when solvation conditions may change, that changes in (but not the existence of) solvation energy must be included, and that nonelectrostatic interactions between ions must be accounted for.

7.4 PHYSICAL THEORIES OF ION–ION INTERACTIONS

It is the aim of physical solution theories to calculate ion–ion interactions quantitatively (i.e., to theoretically calculate the activity coefficients). In an ionic lattice the energy of electrostatic interaction between the ions is high compared to the thermal energy RT; hence, the ions are rigidly fixed in space and arranged in orderly fashion. In dilute solutions of nonelectrolytes, there are practically no interaction forces between dissolved particles, and at any given time the relative positions of the particles are random and disordered, owing to thermal motion. In electrolyte solutions the situation is intermediate: Relatively weak electrostatic forces having an energy comparable with that of thermal motion exist between the ions. A certain degree of short-range order is observed in them; at short distances from a given ion, ions of opposite sign are more likely to be found. As a result, attraction forces are predominant between the ions at short distances, and hence $w_{e,j} < 0$.

The first attempt at statistical calculation of the distribution of ions in a solution while allowing for electrostatic interaction and thermal motion was made by S. Roslington Milner in 1913. The mathematical procedures used by him were very complicated.

In 1918, Jnanendra Chandra Ghosh proposed to calculate the energy of electrostatic interaction of the ions while assuming the ions in the solution to have a rigid arrangement resembling that in crystals, although allowing for the actual interionic distances. The function obtained by him is close to the experimental function (7.25),

Peter Debye (1884–1966; Nobel prize, 1936).

Erich Hückel (1896–1980).

although with a different exponent of concentration. However, the model used is physically unsound, since the distorting influence of thermal motion of the ions on their distribution in the solution is not taken into account.

An appreciable advance in the theory of electrostatic interaction between ions in solution was made in 1923 by Peter Debye and Erich Hückel, who introduced the concept of *ionic atmosphere* to characterize the averaged distribution of the ions. In its initial form the theory was applied to fully dissociated electrolytes; hence, it was named the *theory of strong electrolytes*.

7.4.1 Ionic Atmosphere

In Debye–Hückel (DH) theory, the interaction of a particular central ion m with all other ions in the solution, including other ions of the same sort, is analyzed. Because of electrostatic forces in the immediate vicinity of the central ion, an excess of ions of the opposite sign is found, which gives rise to a certain space charge compensating for the charge of the central ion. This space charge surrounding the central ion (Fig. 7.5) is called an *ionic atmosphere* or *ionic cloud*.

The ionic atmosphere has a blurred (diffuse) structure. Because of thermal motion, one cannot attribute precise locations to its ions relative to the central ion; one can only define a probability to find them at a certain point or define a time-average ionic concentration at that point (the charge of the ionic atmosphere is "smeared out" around the central ion). In DH theory, the interaction of the central ion with specific (discrete) neighboring ions is replaced by its interaction with the ionic atmosphere (i.e., with a continuum).

The most important parameters of the ionic atmosphere are the charge density $Q_V(r)$ and the electrostatic potential $\psi(r)$ at the various points. Each of these parameters is understood as the time-average value. These values depend only on distance r from the central ion, not on a direction in space. For such a system it is convenient to use a polar (spherical) coordinate system having its origin at the point where the central ion is located; then each point can be described by a single and unique coordinate, r.

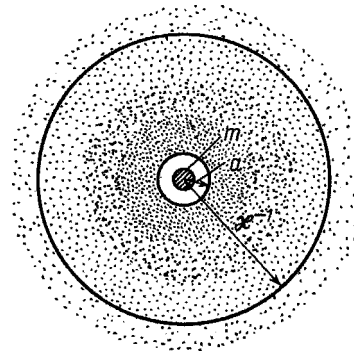

FIGURE 7.5 Ionic atmosphere.

Because of the thermal motion of the central ion, the coordinate system considered is in continuous three-dimensional motion. Thus, when a cation moves, a certain average density of negative charge will always exist at points at a distance r from it. However, at any stationary point of the solution that has been defined (e.g., relative to the vessel walls), positive and negative charges are equally likely to materialize. Therefore, at stationary points the time-average charge density is zero and the average potential is constant and independent of the coordinate, while at points in the moving coordinate system the charge densities and potential are not zero and the potential depends on the coordinate. It follows that an ionic atmosphere exists only in the moving coordinate system of the central ion.

The total charge, Q_{atm}, of the ionic atmosphere can be calculated by integrating the charge density over its total volume. Since the system is electroneutral, the total charge of the ionic atmosphere must be equal in absolute value and opposite in sign to the central ion's charge Q_m. The charge density is constant in an elementary volume $dV = 4\pi r^2\, dr$ enclosed between two concentric spherical surfaces with radii r and $r + dr$. Therefore,

$$Q_{\text{atm}} = -z_m Q^0 = \int_V Q_V\, dV = 4\pi \int_0^\infty Q_V(r) r^2 dr. \tag{7.30}$$

The electrostatic potential $\psi(r)$ at each point is reckoned relative to the solution's constant average potential; the latter is assumed to be zero. The total value of potential $\psi_0(r)$ can be written as the sum of two components, one due to the central ion; $\psi_m(r)$, and one due to the ionic atmosphere; $\psi_{\text{atm}}(r)$:

$$\psi_0(r) = \psi_m(r) + \psi_{\text{atm}}(r). \tag{7.31}$$

According to the laws of electrostatics, the potential set up by the central ion (a point charge) is determined by

$$\psi_m(r) = \psi^0 + \frac{Q_m}{4\pi\varepsilon_0 \rho r} \qquad (\text{here } \psi^0 = 0). \tag{7.32}$$

The energy of interaction of the central ion with its ionic atmosphere depends on the potential of this atmosphere $\psi_{\text{atm}}(0)$ at a point where the central ion is located ($r = 0$). Therefore, it is the main task of the physical theory of ion–ion interaction to calculate the potential of the ionic atmosphere, ψ_{atm}.

7.4.2 Debye–Hückel Limiting Law

In the first version of DH theory it was shown that the potential of the ionic atmosphere can be represented by the equation

$$\psi_{\text{atm}}(r) = \frac{z_m Q^0}{4\pi\varepsilon_0 \varepsilon r} [\exp(-\kappa r) - 1], \tag{7.33}$$

where κ is a constant (units: cm^{-1}) containing parameters independent of coordinates and is defined by

$$\kappa \equiv Q^0 \left(\frac{2I_c}{kT\varepsilon_0\varepsilon} \right)^{1/2} \tag{7.34}$$

The derivation of this equation is given in Appendix A.)

It follows for the potential at the point where the central ion in located ($r = 0$) that

$$\psi_0(0) = -\gamma\, Q_m, \qquad \text{where} \quad \gamma \equiv \frac{\kappa}{4\pi\varepsilon_0\varepsilon} = \frac{-z_m Q^0 (2I_c)^{1/2}}{4\pi (kT)^{1/2} (\varepsilon_0\varepsilon)^{3/2}}. \tag{7.35}$$

We can see from this equation that the potential ψ_{atm} at the point $r = 0$ has the value that would exist if there were at distance $1/\kappa$ a point charge $-z_m Q^0$ or, if we take into account the spherical symmetry of the system, if the entire ionic atmosphere having this charge were concentrated on a spherical surface with radius $1/\kappa$ around the central ion. Therefore, the parameter $r_D \equiv 1/\kappa$ with the dimensions of length is called the *effective thickness* of the ionic atmosphere or *Debye radius* (*Debye length*). This is one of the most important parameters describing the ionic atmosphere under given conditions.

According to Eq. (7.34), the values of the Debye radius depend on the ionic strength I_c of the solution and increase with decreasing ionic strength; they are 0.3, 3, and 30 nm for values of I_c of 1, 10^{-2}, and $10^{-4}\,M$ (note that here I_c is given in the units mol/L).

An equation for quantitatively determining the interaction energy $w_{e,m}$ between the central ion and the ionic atmosphere can be derived with the aid of the following thought experiment. We assume that in the initial state the central ion is deprived of its charge ($Q_m = 0$), and hence, neither an ionic atmosphere nor the potential of this atmosphere exist. We now charge the ion gradually. According to Eq. (7.35), at all times the value of $\psi_{atm}(0)$ is proportional to the momentary value of $Q_m \psi_m(0) = -\gamma Q_m$. For each consecutive charge increment dQ_m, an energy $dw_{e,m} = \psi_{atm}(0) \times dQ_m = -\gamma Q_m\, dQ_m$ must be expended. The energy corresponding to complete charging of the ion from $Q_m = 0$ to $Q_m = z_m Q^0$ is determined by the expression

$$w_{e,m} = \int_0^{Q_m} \psi_{atm}(0)\, dQ_m = \gamma \int_0^{Q_m} Q_m\, dQ_m = Q_m^2; \tag{7.36}$$

it is evidently equal to the interaction energy sought.

With Eqs. (7.29) and (7.35) the expression for the activity coefficient of ion m becomes finally

$$\log f_m = D Q_m^2 I_c^{1/2}, \qquad \text{where} \quad D = \frac{w_{e,m}}{2.303kT} = \frac{4.0489}{(kT\varepsilon_0\varepsilon)^{3/2}}. \tag{7.37}$$

For aqueous solutions at 25°C, the constant $D = 0.51$ (L/mol)$^{1/2}$.

This is an equation for calculating the activity coefficient of an individual ion m (i.e., a parameter inaccessible to experimental determination). Let us, therefore, change to the values of mean ionic activity. By definition [see Eq. (3.27)],

$$\tau_k \log f_\pm = \tau_+ \log f_+ + \tau_- \log f_-. \tag{7.38}$$

Substituting into (7.38) the values of f_+ and f_- according to Eq. (7.37) and taking into account that the electroneutrality condition of $\tau_+ z_+ = \tau_- z_- = \tau_k$ yields the equality $\tau_+ z_+^2 + \tau_- z_-^2 = \tau_k z_+ z_-$, we finally obtain

$$\log f_\pm = -D z_+ z_- I_c^{1/2}. \tag{7.39}$$

We can see from Fig. 7.4, curve 1a, that this equation describes the experimental data in very dilute solutions of strong electrolytes (i.e., for 1 : 1 electrolytes approximately up to $10^{-2} M$); for other electrolytes the concentration limit is even lower. It correctly conveys the functional dependence on the charge of the ions and the ionic strength of the solution (as well as the lack of dependence on individual properties of the ions); it can, moreover, be used to calculate the value of empirical constant h in Eq. (7.27).

The behavior expressed by Eq. (7.39) became known as the *Debye–Hückel limiting law*. Its derivation was one of the first instances in physical chemistry where with the aid of models built at the molecular level, it was possible to formulate an equation of state of a real system with which the properties of this system could be calculated without the use of empirical ("fitting") constants. This was the basis for the triumph of this theory, which had great significance for the general development of electrolyte solution theory even though its range of application was limited to very low concentrations. Subsequent theoretical work focused on interpreting the departures of concentrated solutions from the properties predicted by the limiting law. The DH theory is always one of the criteria for other, more general theories, which in the limit of low concentrations should lead to the equations of the DH limiting law.

7.4.3 Second and Third Approximation of the Theory

The great success of DH theory provoked numerous attempts at improvement and extension to more concentrated solutions. In the equations reported in Section 7.4.2, known as the *first approximation*, ion size was disregarded; all ions were treated as point charges. This is reflected in Eq. (7.30), where the integration was started from $r = 0$ (i.e., it was assumed that other ions can, however, closely approach the central ion and that all these ions have zero radius).

In the *second approximation*, Debye and Hückel introduced the idea that the centers of the ions cannot come closer than a certain minimum distance a, which depends on ion size; the ions were now treated as entities with a finite radius. The mathematical result of this assumption are charge densities Q_V, which are zero for $r < a$, and Eq. (7.30) is integrated from $r = a$ to $r = \infty$. This produces a change in

the value of integration constant C_2 (see Appendix A). Instead of Eq. (A.8), we obtain

$$C_2 = \frac{z_m Q^0 \exp(a\kappa)}{4\pi\varepsilon_0\varepsilon(1+a\kappa)}. \tag{7.40}$$

The expression for the distribution of potential of the ionic atmosphere becomes

$$\frac{\psi_{\text{atm}}(r) z_m Q^0}{4\pi\varepsilon_0\varepsilon r} \frac{\exp\ \kappa(a-r)}{(1+a\kappa)-1} \tag{7.41}$$

Within a spherical space of radius a, by definition $Q_V = 0$, so that the value of potential of the ionic atmosphere here is constant and equal to that at point $r = a$:

$$\psi_{\text{atm}}(0) = \psi_{\text{atm}}(a) = \frac{-z_m Q^0 \kappa}{4\pi\varepsilon_0\varepsilon(1+a\kappa)}. \tag{7.42}$$

As a result, we obtain for the mean ionic activity coefficient,

$$\log f_{\pm} = \frac{-Dz_+z_-I_c^{1/2}}{1+aBI_c^{1/2}}, \tag{7.43}$$

where $B = 2^{1/2}/\text{k}T\varepsilon_0\varepsilon$.

For highly dilute solutions the value of $aBI_c^{1/2}$ is small compared to unity, and the solution of Eq. (7.43) coincides with the limiting law. In more concentrated solutions, in agreement with experiment, the values of $f_{\pm}$ calculated by Eq. (7.43) are larger than the values obtained from the limiting law.

In practical applications of this equation, one must pick values for constant a. To a first approximation it can be regarded as equal to the sum of the radii of two solvated ions. It is not clear, however, whether the solvation sheaths of approaching ions would not be deformed. Moreover, in deriving Eq. (7.43) it was assumed without sufficient reasoning that the constant a for a given central ion will be the same for different ions present in the ionic atmosphere.

Therefore, the constant a is regarded not as a physical parameter that can be determined in independent ways but as a fitting factor which in each case is picked so that Eq. (7.43) will give the best agreement with the experimental data. The equation is thus converted from one theoretically founded to a semiempirical one. In a number of cases good agreement with experiment can be attained up to concentrations of 0.1 M with values of $a = 0.3$ to 0.4 nm (Fig. 7.4, curve 1b).

At higher concentrations, this equation is no longer suitable for calculating $f_{\pm}$. In particular, it cannot explain why $f_{\pm}$ goes through a minimum and increases so strongly at high concentrations.

In solutions of nonelectrolytes where the particles do not interact electrostatically, the value of $\log f_k$ often increases linearly with increasing concentration: $\log f_k = b'c$

(Fig. 7.4, curve 4). By analogy with this behavior, it has been proposed as a way of accounting for nonelectrostatic interaction forces between ions, to supplement Eq. (7.43) with an additional term $b'c$ or bI_c:

$$\log f_{\pm} = \frac{-Dz_+z_-I_c^{1/2}}{1+aBI_c^{1/2}} + bI_c, \tag{7.44}$$

where b is an empirical constant.

Values of b are usually small (e.g., $b \approx 0.1 z_+z_-$ L/mol). This expression provides a good description for the increase in $f_{\pm}$ values at higher concentrations. Thus, for aqueous NaCl solutions, Eq. (7.44) describes the experimental data up to 4 M [Fig. 7.4, curve 1b, with values of $a = 0.4$ nm and $b = 0.055$ L/mol].

Equation (7.44) is known as the *third approximation* of the Debye–Hückel theory. Numerous attempts have been made to interpret it theoretically. In these attempts, either individual simplifying assumptions that had been made in deriving the equations are dropped or additional factors are included. The inclusion of ionic solvation proved to be the most important point. In concentrated solutions, solvation leads to binding of a significant fraction of the solvent molecules. Hence, certain parameters may change when solvation is taken into account since solvation diminishes the number of free solvent molecules (not bonded to the ions). The influence of these and some other factors was analyzed in 1948 by Robert A. Robinson and Robert H. Stokes.

7.4.4 Ion–Ion Interaction and Conductivity

In the classical theory of conductivity of electrolyte solutions, independent ionic migration is assumed. However, in real solutions the mobilities u_j and molar conductivities λ_j of the individual ions depend on the total solution concentration, a situation which, for instance, is reflected in Kohlrausch's square-root law. The values of said quantities also depend on the identities of the other ions. All these observations point to an influence of ion–ion interaction on the migration of the ions in solution.

Ideas concerning the ionic atmosphere can be used for a theoretical interpretation of these phenomena. There are at least two effects associated with the ionic atmosphere, the electrophoretic effect and the relaxation effect, both lowering the ionic mobilities. Formally, this can be written as

$$\lambda = \lambda^0 - \Delta\lambda_{\text{eph}} - \Delta\lambda_{\text{rel}}, \tag{7.45}$$

where λ^0 is the limiting value of molar conductivity of an ion in the absence of ion–ion interaction (highly dilute solutions), and λ_{eph} and λ_{rel} are the changes produced in this parameter by the electrophoretic and relaxation effect, respectively.

The *electrophoretic (cataphoretic) effect* arises because the central ion and its ionic atmosphere, which differ in the sign of the charge, will move in opposite directions in an electric field (Fig. 7.6). The countermovement of the ionic atmosphere (as the surrounding medium) slows down the motion of the central ion. Usually, the value of the ionic atmosphere's own "conductivity," λ_{atm} is adopted as the value of

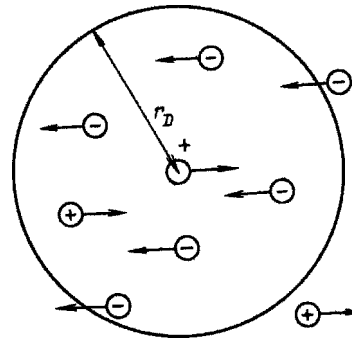

FIGURE 7.6 Electrophoretic effect.

$\Delta\lambda_{\text{eph}}$. Conditionally, the ionic atmosphere is regarded as a sphere with radius r_D. The values of r_D approach the size of colloidal particles, for which Stokes's law applies (i.e., the drag coefficient $\theta = 6\pi\eta r_{\text{D}}$, where η is the liquid's viscosity) when they move in an electric field (electrophoresis or cataphoresis). We then have

$$\Delta\lambda_{\text{eph}} = k_{\text{eph}} z 2 I_c^{1/2}, \qquad \text{where} \quad k_{\text{eph}} \equiv \frac{F^2 B}{N_A 6\pi\eta}. \tag{7.46}$$

The *relaxation effect* arises because a certain time, t_{rel}, is required for the formation or collapse of an ionic atmosphere around the central ion. When an ion moves in an electric field, its ionic atmosphere lags somewhat behind, as it were; its center (Fig. 7.7, point *B*) is at a point where the central ion had been a little earlier. The configuration of the ionic atmosphere around the central ion (point *A*) will no longer be spherical but elongated (ovoid). Because of this displacement of the charges, the ionic atmosphere has an electrostatic effect on the central ion which acts in a direction opposite to the ion's motion. A rigorous calculation of this effect was made in 1927 by Lars Onsager. His solution was

$$\Delta\lambda_{\text{rel}} = k_{\text{rel}} \lambda^0 I_c^{1/2}, \qquad \text{where} \quad k_{\text{rel}} \equiv \frac{\omega F^2 B}{N_A RT 8\pi\varepsilon_0\varepsilon} \tag{7.47}$$

(ω is a numerical factor; its value is 0.1953 for symmetric electrolytes).

Thus,

$$\lambda = \lambda^0 - (k_{\text{eph}} z^2 + k_{\text{rel}} \lambda^0) I_c^{1/2}. \tag{7.48}$$

It follows (when taking into account that $\tau_+ z_+ = \tau_- z_- = z_k$) that the molar conductivity of binary electrolyte solutions is given by

$$\Lambda = \Lambda^0 - [k_{\text{eph}} z_k (z_+ + z_-) + k_{\text{rel}} \Lambda^0] I_c^{1/2}. \tag{7.49}$$

These equations are known as the *Debye–Hückel–Onsager equations*.

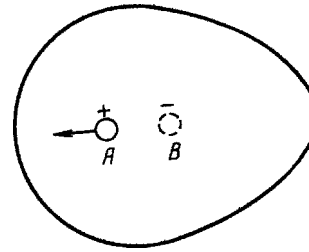

FIGURE 7.7 Relaxation effect.

In the case of binary solutions, Eq. (7.49) coincides with the empirical Eq. (7.14), both in form and in the value of the numerical constant k. Therefore, the empirical square-root law can be explained quantitatively on the basis of the theory of ion–ion interaction.

An analysis of Eq. (7.49) shows that the electrophoretic effect accounts for about 60 to 70% of the decrease in solution conductivity, and the relaxation effect for the remaining 40 to 30%.

The ideas outlined also provide an explanation for anomalous conductivity effects that occur under certain extreme conditions. Thus, in electrostatic fields having very high field strength $\mathbf{E}$ ($>10^6$ to 10^7 V/m) the conductivities σ of electrolyte solutions (and also the values of Λ) were found to become higher (the *Wien effect*), whereas according to Ohm's law [Eq. (1.3)], these parameters should not depend on $\mathbf{E}$. At high values of $\mathbf{E}$ the distance between the central ion and the center of the ionic atmosphere becomes larger than r_D (i.e., the central ion "pulls out," as it were, from its ionic atmosphere). Then the electrophoretic and relaxation effects disappear and the value of Λ will approach Λ^0. The values of σ and Λ also increase when very high frequencies (above 1 MHz) are used for the measurements (the *Debye–Falkenhagen effect* or frequency dispersion of conductivity). When the period between sign changes of the ac field is shorter than the relaxation time t_{rel}, the central ion is practically not displaced relative to the center of the ionic atmosphere. But electrophoretic phenomena persist. Therefore, at high field frequencies the value of Λ increases somewhat but does not reach the value of Λ^0.

7.4.5 Further Development of Electrolyte Solution Theory

The first ideas concerning a role of pairwise electrostatic interaction between ions were advanced in 1924 by Vladimir K. Semenchenko. A quantitative theory of the formation of *ion pairs* was formulated in 1926 by Niels Bjerrum.

According to the basic ideas concerning ionic atmospheres, the ions contained in them are in random thermal motion, uncoordinated with the displacements of the central ion. But at short distances between the central ion m and an oppositely charged ion j of the ionic atmosphere, electrostatic attraction forces will develop which are so strong that these two ions are no longer independent but start to move together in space like one particle (i.e., the ion pair). The total charge of the ion pair

is $(z_m - z_j)Q^0$; when the two ions carry identical numbers of charges, the ion pair will be electrically neutral but constitute a dipole.

Ion-pair formation lowers the concentrations of free ions in solution, and hence the conductivity of the solution. It must be pointed out that ion-pair formation is not equivalent to the formation of undissociated molecules or complexes from the ions. In contrast to such species, ions in an ion pair are linked only by electrostatic and not by chemical forces. During ion-pair formation a common solvation sheath is set up, but between the ions thin solvation interlayers are preserved. The ion pair will break up during strong collisions with other particles (i.e., not in all collisions). Therefore, ion pairs have a finite lifetime, which is longer than the mean time between individual collisions.

For ion-pair formation the electrostatic attraction energy $w_e = N_{Ai}z_m z_j(Q^0)^2/4\pi\varepsilon_0\varepsilon r$ (per mole of ion pairs) should be larger than the ion pair's mean thermal energy (i.e., at least $2RT$). This condition yields for the critical distance of ion pair formation in aqueous solutions at 25°C:

$$r_{cr} = \frac{N_A z_m z_j (Q^0)^2}{8\pi\varepsilon_0\varepsilon RT} - z_m z_j (0.357\,\text{nm}) \tag{7.50}$$

Ion pairs can form only when the distance of closest approach, a, of the two ions is less than r_{cr}. For 1 : 1 electrolytes for which $r_{cr} = 0.357$ nm, this condition is not always fulfilled, but for others it is. The fractions of paired ions increase with increasing concentration of solutions. In nonaqueous solutions which have lower values of permittivity ε than water, the values of r_{cr} and the fractions of paired ions are higher. In some cases the values of r_{cr} coincide with the statistical mean distance between the ions (i.e., the association of the ions is complete).

Bjerrum's theory of ion pairs qualitatively correctly explains a number of experimental data, but cannot be used to the full extent in quantitative calculations, particularly because of the provisional character of quantities a and r_{cr} (the integration limits).

Ion-pair formation (or the formation of triplets, etc.) is a very simple kind of interaction between ions of opposite charge. As the electrolyte concentration increases and the mean distance between ions decreases, electrostatic forces are no longer the only interaction forces. Aggregates within which the ions are held together by chemical forces have certain special features (i.e., shorter interatomic distances and a higher degree of desolvation than found in ion pairs) and can form a common solvation sheath instead of the individual sheaths. These aggregates are seen distinctly in spectra, and in a number of cases their concentrations can be measured spectroscopically.

A more general theory of solutions would require detailed notions of solution structure and of all types of interactions between the particles (ions and solvent molecules) in the solution. Numerous experimental and theoretical studies have been carried out, and some progress has been made, but a sufficiently universal theory that could describe all properties in not very dilute electrolyte solutions has not yet been developed.

REFERENCES

Arrhenius, S., *Z. Phys. Chem.*, **1**, 631 (1887).

Bernall, J. D., and R. H. Fowler, *J. Chem. Phys.*, **1**, 515 (1933).

Bjerrum, N., *Det. Kgl. Dan. Videnkabernes Selskab Math-Fys. Meddeleser*, **7**(9) (1926).

Born, M., *Verh. Dtsch. Phys. Ges.*, **21**, 13, 679 (1919).

Clausius, R., *Ann. Phys. (Poggendorff's)*, **101**, 338 (1857).

Debye, P., and E. Hückel, *Phys. Z.*, **47**, 206, 305 (1923).

Faraday, M., *Philos. Mag.*, Ser. VII (1834).

Ghosh, J. Ch., *J. Chem. Soc.*, **113–114**, 449, 627, 707 (1918).

Grothus, Th., *Ann. Chim.*, **58**, 54 (1806).

Kablukov, I. A., *Contemporary Theories of Solutions* [in Russian], M. Schepkin, Moscow, 1891.

Kohlrausch, F., and L. Holborn, *Das Leitvermögen der Elektrolyte*, Teubner, Leipzig, 1898.

Lewis, G. N., *Proc. Am. Acad.*, **43**, 259 (1907).

Mendeleev, D. I., *Solutions* [in Russian], Academic Publishing, Moscow, 1959.

Milner, S. R., *Philos. Mag.*, Ser. 6, **25**, 742 (1913).

Onsager, L., *Phys. Z.*, **28**, 277 (1927).

Ostwald, W., *Z. Phys. Chem.*, **2**, 270 (1888).

Semenchenko, W. K., *Z. Phys. Chem.*, **112**, 128 (1924).

van Laar, J. J., *Z. Phys. Chem.*, **18**, 245 (1895).

van't Hoff, J. Y., *Études de dynamique chimique*, Frederick, Müller, Amsterdam, 1884.

MONOGRAPHS

Hirata, Fumio, *Molecular Theory of Solvation*, Kluwer, New York, 2003.

Lewis, G., and M. Randall, *Thermodynamics and the Free Energy of Substances*, 1923.

Robinson, R., and R. Stokes, *Electrolyte Solutions*, Butterworth, London, 1959.

8

Nonaqueous Electrolytes

8.1 DIFFERENT TYPES OF ELECTROLYTES AND THEIR PRACTICAL UTILIZATION

Electrolytes are highly important components of all galvanic cells and electrochemical devices. In most electrochemical devices, such as electrolyzers, batteries, and the like, aqueous solutions of acids and salts are used as electrolytes. Aqueous solutions are easy to prepare, convenient to handle, and as a rule are made from readily available, relatively inexpensive materials. By changing the composition and concentration of the components, it is relatively easy to adjust the specific conductance and other physicochemical properties of these aqueous solutions.

Cases exist, however, where for fundamental reasons aqueous solutions cannot be used. One such case is that of devices in which electrochemical processes take place at elevated temperatures (above 180 to 200°C): for example, the electrowinning of aluminum performed at temperatures close to 1000°C. Another case is that of devices in which electrodes consisting of alkali metals are used, which are unstable in aqueous solutions, such as batteries with a lithium negative electrode.

For this reason, other types of electrolytes are used in addition to aqueous solutions (i.e., nonaqueous solutions of salts (Section 8.1), salt melts (Section 8.2), and a variety of solid electrolytes (Section 8.3). More recently, a new type of solid electrolyte is being employed more often (i.e., water-impregnated ionically conducting polymer films; more about them in Chapter 26).

The problems of electrolyte selection have become particularly acute in connection with the miniaturization and sealing of a variety of electrochemical devices, such as batteries, sensors, and the like. Apart from all their advantages, aqueous electrolyte solutions here exhibit certain defects, insofar as sealing of a device containing them often is difficult and leaking of the liquid occurs readily (particularly when alkaline solutions are used). From devices that are not sealed, the electrolyte solvent can evaporate, which leads to changes in electrolyte concentration. In certain cases when gas evolution is strong, solutions may tend to become dispersed as an ultrafine spray, constituting a health hazard. Nonaqueous solutions must be carefully isolated from the open atmosphere so that they will not absorb traces of water from it.

Fundamentals of Electrochemistry, Second Edition, By V. S. Bagotsky

The problems of sealing and miniaturization of various devices are greatly alleviated when solid electrolytes are used. Certain solid electrolytes have another important advantage over liquid electrolytes (i.e., unipolar conduction). In fact, liquid electrolytes (aqueous and nonaqueous solutions, salt melts) always exhibit bipolar conduction; that is, the current is transported at the same time by positive and negative ions. This leads to concentration changes in the electrolyte layers close to the electrode that have been described in Chapter 4. These concentration changes induce specific volume changes, causing additional sealing problems.

In many solid electrolytes, to the contrary, conduction is strictly monopolar; that is, conduction involves transfer of ions of just one sign (and most often, of ions of just one type). When the ion carrying the current is that involved in the electrochemical reactions, both at the anode and at the cathode, current flow does not lead to any concentration changes in the electrolyte. This is the case, for instance, in the sodium–sulfur storage battery. Here sodium β-aluminate is used as the electrolyte, which at a temperature of 300°C exhibits good conductivity due to Na^+ ion transport. During discharge, metallic sodium is ionized at the negative electrode of this battery ($Na \rightarrow Na^+ + e^-$), while at the positive electrode sulfur is reduced, forming sodium sulfide ($S + 2\,Na^+ + 2e^- \rightarrow Na_2S$).

An imperative condition for materials being used as an electrolyte is the complete (or practically complete) absence of electronic conduction. Such conduction would amount to internal short-circuiting, leading to unproductive power consumption and/or waste of electrode materials.

8.2 NONAQUEOUS ELECTROLYTE SOLUTIONS

Nonaqueous electrolyte solutions are analogous to aqueous solutions; they, too, are systems with a liquid solvent and a solute or solutes dissociating and forming solvated ions. The special features of water as a solvent are its high polarity, $\varepsilon = 78.5$, which promotes dissocation of dissolved electrolytes and hydration of the ions, and its protolytic reactivity. When considering these features, we can group the nonaqueous solvents as follows:

1. Protic, which are analogous to water, have polar character, and are involved in protolytic reactions
2. Aprotic polar (with values of $\varepsilon > 15$)
3. Aprotic with low or zero polarity (values $\varepsilon < 15$)

The third group of solvents comprises the hydrocarbons and their halogen derivatives. They are not of interest for electrochemistry, since the solubilities and dissociation of salts, acids, and bases in them are low. Systems with protic or aprotic polar solvents are used in practice and have been investigated widely.

In the following, we write the protic solvents conventionally as SH, where H is the proton and S is the solvent "residue." They include many compounds with −OH and >NH groups, also some others (Table 8.1). All these solvents are polar, have

TABLE 8.1 Physical Properties of Certain Solvents at 25°C

Solvent	Formula	ε	η (Mpa·s)	d (g/cm^3)	t_f (°C)	t_b (°C)
Protic						
Water	H_2O	78.5	0.89	0.997	0	100
Ammonia (−20°C, 0.2 MPa)	NH_3	20	0.26	0.67	−78	−33
Acetic acid	CH_3COOH	6.2	1.13	1.05	16.7	−118.1
Methanol	CH_3OH	32.6	0.547	0.792	−97.9	64.5
Aprotic						
Acetonitrile	CH_3CN	36	0.345	0.786	−45.7	81.6
Dimethylformamide	$(CH_3)_2NCHO$	37	0.796	0.944	−61	153
Propylene carbonate	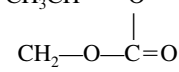	66.1	2.53	1.198	−49.2	242
γ-Butyrolactone	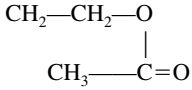	30.1	1.75	1.125	−43.5	204
Tetrahydrofuran	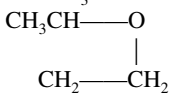	7.4	0.46	0.880	−65	64

high values of ε (larger than 20 as a rule), and high solvating power, and many electrolytes have high degrees of dissociation when dissolved in them. The protic solvents distinctly tend to form hydrogen bonds, and all of them are involved in protolytic reactions. They may, like water, undergo autoprotolysis:

$$2SH \Leftrightarrow SH_2^+ + S^-, \tag{8.1}$$

which yields lyonium and lyate ions, SH_2^+ and S^-, as the analogs of hydroxonium and hydroxyl ions, H_3O^+ and OH^- (solvent "dissociation").

Of greatest interest among the protic solvents are liquid ammonia (where solutions with a very low freezing point can be prepared) and anhydrous (glacial) acetic acid (which has a high proton-donating power).

Aprotic polar solvents such as those listed in Table 8.1 are widely used in electrochemistry. In solutions with such solvents the alkali metals are stable and will not dissolve under hydrogen evolution (by discharge of the proton donors) as they do in water or other protic solvents. These solvents find use in new types of electrochemical power sources (batteries), with lithium electrodes having high energy density.

Compounds with the >CO group, particularly esters and ketones, are the most important aprotic polar solvents. The solubilities of most simple salts in these solvents are low, but salts with large (even complex) anions such as $LiClO_4$, $LiAlCl_4$, or $LiAsF_6$ have solubilities as high as 1 to 2 M.

The solubilities of electrolytes and their degrees of dissociation in various solvents depend on the polarity of the solvent molecules, which also is the factor influencing the relative permittivity ε and the solvating power. The common tendency that the degree of dissociation and the conductivity of the solutions are higher in solvents with higher values of ε had been noticed in the 1890s. However, this tendency is not unambiguous in all cases. Thus, the dipole moment of HCN molecules is 1.5 times that of water molecules, but the solubilities of most salts are lower in hydrocyanic acid than in water, which is due to the higher solvent reorganization energy required for solvation of the ions in HCN.

In some cases the degree of dissociation of a dissolved electrolyte depends not only on the solvent's polarity or ε value but on other properties as well. Thus, when dissolved in ethanol, hydrogen chloride dissociates practically completely and behaves as a strong electrolyte. This is possible because of protolytic reactions yielding solvated protons $C_2H_5)OH_2^+$. In nitrobenzene, although it has practically the same ε value as ethanol, the degree of dissociation of HCl is low, owing to the low proton-accepting power.

The ionic mobilities also depend on the solvent. In 1905–1906, Paul Walden, Lev Pisarzhevsky, and others established the rule according to which the product of limiting mobility of an ion and viscosity η of the solution is approximately constant:

$$u_j^0 \eta \approx \text{const.} \tag{8.2}$$

This rule follows immediately from Stokes's law for the motion of spherical bodies in viscous fluids when assuming constant radii. It is applicable in particular for the change in ionic mobility that occurs in a particular solvent when the temperature is varied. Between solvents it remains valid when the electrolytes have poorly solvated ions, such as $N(C_2H_5)_4I$. For other electrolytes we find rather significant departures from this rule. These are due in particular to the different degrees of solvation found for the ions in different solvents, and hence their different effective radii.

In aqueous electrolyte solutions the molar conductivities of the electrolyte, Λ, and of individual ions, λ_j, always increase with decreasing solute concentration [cf. Eq. (7.11) for solutions of weak electrolytes, and Eq. (7.14) for solutions of strong electrolytes]. In nonaqueous solutions even this rule fails, and in some cases maxima and minima appear in the plots of Λ vs. c (Fig. 8.1). This tendency becomes stronger in solvents with low permittivity. This anomalous behavior of the nonaqueous solutions can be explained in terms of the various equilibria for ionic association (ion pairs or triplets) and complex formation. It is for the same reason that concentration changes often cause a drastic change in transport numbers of individual ions, which in some cases even assume values less than zero or more than unity.

In aqueous solutions we see enhanced mobility and conductivity of the hydrogen ions, which is caused by additional proton transfer along chains of water molecules linked by hydrogen bonds (see Section 7.2.4). Solutions with nonaqueous, proton-containing solvents (e.g., in ammonia) sometimes also exhibit enhanced hydrogen

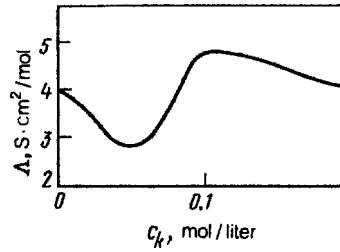

FIGURE 8.1 Molar conductivities of $AgNO_3$ in pyridine as a function of solution concentration.

ion mobility. In solutions with aprotic solvents that contain H^+ ions (e.g., after HCl addition), the mobility of these ions does not differ from that of other ions (i.e., the solvated protons present in the solution follow the usual migration mechanism).

8.3 IONICALLY CONDUCTING MELTS

Many electrochemical devices and plants (chemical power sources, electrolyzers, and others) contain electrolytes which are melts of various metal halides (particularly chlorides), also nitrates, carbonates, and certain other salts with melting points between 150 and 1500°C. The salt melts can be single- (neat) or multicomponent (i.e., consist of mixtures of several salts, for their lower melting points in the eutectic region). Melts are highly valuable as electrolytes, since processes can be realized in them at high temperatures that would be too slow at ordinary temperatures or which yield products that are unstable in aqueous solutions (e.g., electrolytic production of the alkali metals).

A special class of ionically conducting melts are the oxide-based systems (usually, mixtures of a metal oxide and a nonmetal oxide, e.g., CaO and SiO_2) with melting points between 1200 and 2500°C. Such melts are often formed in the high-temperature processes of metallurgy.

The ionic conductivities of most solid crystalline salts and oxides are extremely low (an exception are the solid electrolytes, which are discussed in Section 8.4). The ions are rigidly held in the crystal lattices of these compounds and cannot move under the effect of applied electric fields. When melting, the ionic crystals break down, forming free ions; the conductivities rise drastically and discontinuously, in some cases up to values of over 100 S/m (i.e., values higher than those of the most highly conducting electrolyte solutions).

When crystals with covalent bonds (e.g., $AlCl_3$ or $TiCl_4$) melt, the melt conductivity remains low (e.g., below 0.1 S/m), which implies that the degree of dissociation of the covalent bonds after melting is low. The covalent crystals also differ from the ionic crystals by their much lower melting points. The differences between these two types of crystal are rather pronounced, whereas there are few crystalline solids with intermediate properties.

A typical special feature of the melts of ionic crystals (ionic liquids) are their high concentrations of free ions, of about 25 *M*. Because of the short interionic distances, considerable electrostatic forces act between the ions, so that melts exhibit pronounced tendencies for the formation of different ionic aggregates: ion pairs, triplets, complex ions, and so on.

Another special feature of ionic liquids is the lack of a foreign ("inert") molecular medium, particularly a solvent, between the ions. Hence, they lack ion–molecule and the many types of nonelectrostatic interactions.

The results of X-ray studies show that upon melting, the ionic crystals retain some short-range order; an anion is more likely to be found in the immediate vicinity of a cation, and vice versa. The interionic distances do not increase upon melting; rather, they decrease somewhat. Yet the volume of a salt markedly increases upon melting, usually by 10 to 20%. This indicates that melts contain a rather large number of voids (holes). These holes form and perish constantly, owing to fluctuation phenomena attending the kinetic–molecular motion of the ions. Their mean size is between one and two interionic distances; they are distributed uniformly throughout the entire liquid volume.

Table 8.2 lists the conductivities, transport numbers t_+, and molar conductivities of the electrolyte $\Lambda = \sigma/c_k$ and ions $\lambda_j = t_+\Lambda$ for a number of melts as well as for 0.1 *M* KCl solution. Melt conductivities are high, but the ionic mobilities are much lower in ionic liquids than in aqueous solutions; the high concentrations of the ions evidently give rise to difficulties in their mutual displacement.

It is now thought that the holes present in the melts are decisive for the conduction in melts. When an electric field is applied, the ion nearest a hole (in the direction of migration) will jump into the hole and leave a hole in its own former place, and thus the next ion can jump into this hole, and so on. Ionic migration thus is not a smooth motion in a viscous medium but, rather, a sequence of ion–hole transitions.

TABLE 8.2 Conductivities, σ, Cationic Transport Numbers, t_+, Molar Conductivities of the Electrolyte (Λ) and Cation (λ_+), and Activation Energies of Conduction, A_σ, for a Number of Melts and Aqueous KCl Solution

Compound	T (°C) Melt.	T (°C) Meas.	$\sigma \cdot 10^2$ (S/cm)	$t+$	Λ (S·cm²/mol)	λ_+ (S·cm²/mol)	A_σ (kJ/mol)
LiCl	614	620	587	0.75	183	137.2	5.2
NaCl	800	850	375	0.62	113.5	82.8	9.2
KCl	790	800	219	0.62	103.5	64.2	15
RbCl	715	715	117	0.58	94	54.2	16.7
CsCl	646	660	114	0.64	66.7	42.7	15
$MgCl_2$	712	730	105	0.48	28.8	13.8	15.9
$CaCl_2$	772	800	200	0.48	64	30.7	19.1
$SrCl_2$	873	900	198	0.26	55.7	14.5	18.1
$PbCl_2$	501	550	169	0.24	53	12.7	7.2
0.1 *M* KCl(*aq*)	—	18	1.12	0.494	112	55.3	11.3

For the jump of an ion into a hole, a certain energy barrier must be overcome with the activation energy A_σ. The rate of this process (or value of conductivity) is subject to temperature dependence, according to the well-known Arrhenius equation (see Section 14.1):

$$\sigma = B \exp\left(-\frac{A_\sigma}{RT}\right). \tag{8.3}$$

Values of A_σ for a number of melts are listed in Table 8.2.

The conductivities of melts, in contrast to those of aqueous solutions, increase with decreasing crystal radius of the anions and cations, since the leveling effect of the solvation sheaths is absent and ion jumps are easier when the radius is small. In melts constituting mixtures of two salts, positive or negative deviations from additivity are often observed for the values of conductivity (and also for many other properties). These deviations arise for two reasons: a change in hole size and the formation of new types of mixed ionic aggregates.

In a number of general properties, such as viscosity and thermal conductivity, melts differ little from solutions. Their surface tensions are two to three times higher than those of aqueous solutions. This leads to poorer wetting of many solids, including important electrode materials such as carbon and graphite, by the ionic liquids.

Diffusion of ions can be observed in multicomponent systems where concentration gradients can arise. In individual melts, self-diffusion of ions can be studied with the aid of radiotracers. Whereas the mobilities of ions are lower in melts, the diffusion coefficients are of the same order of magnitude as in aqueous solutions (i.e., about $10^{-5}\,cm^2/s$). Thus, for melts the Nernst relation (4.6) is not applicable. This can be explained in terms of an appreciable contribution of ion pairs to diffusional transport; since these pairs are uncharged, they do not carry current, so that values of ionic mobility calculated from diffusion coefficients will be high.

Equilibrium electrode potentials are readily established when metal electrodes are in contact with melts. However, two difficulties arise in attempts to measure them: suitable, sufficiently corrosion-resistant reference electrodes must be selected, and marked diffusion potentials develop at interfaces between different melts.

Experience shows that the potentials of metal electrodes in melts of their own salts (i.e., the activities of the cations) depend on the nature of the anions. However, the variation in the values of activity in melts is not very pronounced. This is due to the relatively small spread of interionic distances found in different melts (their entire volume is filled up with ions of similar size) compared to the spread found in aqueous solutions. For this reason the electrostatic forces between the ions (which are very significant) do not differ greatly between different melts.

During electrolysis there is no change in composition of an individual melt close to the electrode surfaces; only its quantity (volume) will change. The resulting void space is filled again by flow of the entire liquid melt mass. This flow replaces the diffusional transport of ions customarily associated with aqueous solutions. This has particular consequences for the method used to measure ionic transport numbers;

rather than determining the concentration changes in the melt layers near the electrodes by Hittorf's method, the volume changes occurring in these regions must be studied in the case of melts.

As a rule, because of the high temperatures, electrochemical reactions in melts are fast and involve little polarization. For such reactions the exchange current densities are as high as 10^3 to 10^4 mA/cm^2. Therefore, reactivities in melts (and also in high-temperature systems with solid electrolytes) are usually determined not by kinetic but by thermodynamic features of the system.

Electrochemical processes in melts are often attended by side reactions and phenomena complicating the primary process. This is true, in particular, for the technically very important class of reactions in which a number of metals (calcium, barium, and others) are obtained electrometallurgically from molten salts. In many of these processes the metal that is deposited (sometimes in a highly disperse state) is found to interact with the corrosive melt: for example, in a reaction such as

$$Ca + CaCl_2 \rightarrow 2CaCl \quad (= Ca{\cdot}CaCl_2), \tag{8.4}$$

producing valence-unsaturated (often colored) compounds. When forming at the cathode, these compounds will dissolve in the melt and can be reoxidized when reaching the anode (in our example, to $CaCl_2$). These processes markedly depress the current yields of metal. They are equivalent to the transport of metal (calcium) atoms or electrons through the melt from the cathode to the anode. Their intensity depends on melt composition, and can be lowered by the addition of salts, which can form various ionic aggregates or complexes with the primary salt.

As a rule, the melts have a strong corrosive effect, not only on the reaction products but also on the various metallic and nonmetallic structural materials used to build the cells and reactors. At high current densities, sometimes the *anode effect* occurs in melts during electrolysis: A gas skin is formed at the electrode surface, and there is intense sparking and a drastic increase in voltage. This effect depends on the anode material and on the melt anions, but its reasons are not fully understood. An important reason is insufficient wetting of the electrode surface by the melt, which causes "sticking" of gas bubbles to the surface.

8.4 INORGANIC SOLID ELECTROLYTES

8.4.1 Ionic Semiconductors

The conductivity of solid salts and oxides was first investigated by M. Faraday in 1833. It was not yet known at that time that the nature of conduction in solid salts is different from that in metals. A number of fundamental studies were performed between 1914 and 1927 by Carl Tubandt in Germany and from 1923 onward by Abram Ioffe and co-workers in Russia. These studies demonstrated that a mechanism of ionic migration in the lattice over macroscopic distances is involved. It was shown that during current flow in such a solid electrolyte, electrochemical changes obeying Faraday's laws occur at the metal–electrolyte interface.

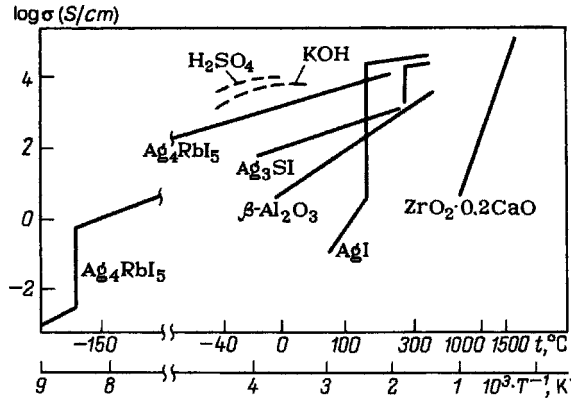

FIGURE 8.2 Conductivities of a number of solid electrolytes as functions of temperature (dashed lines: the conductivities of 4 *M* H_2SO_4 and 8 *M* KOH solution).

In some cases (particularly at elevated temperatures) mixed electronic and ionic conduction is observed in solid salts. Typical materials with purely ionic conduction are the halides and sulfides of a number of metals (i.e., AgBr, Ag_2S, $PbCl_2$, $CuCl_2$, and many others). The conductivity, σ, of such materials is usually low at room temperature. The values of σ increase strongly with temperature (Fig. 8.2). The temperature dependence of conductivity can be described by Eq. (8.3). The appreciable temperature dependence is matched by the corresponding, high values of the activation energy of conduction, A_σ. The conductivities of ionic crystals depend strongly on their purity. Impurities in the crystals raise the values of σ markedly, particularly at lower temperatures, when the intrinsic conductivity of the pure material is still low.

All these features—low values of σ, a strong temperature dependence, and the effect of impurities—are reminiscent of the behavior of *p*- and *n*-type semiconductors. By analogy, we can consider these compounds as ionic semiconductors with intrinsic or impurity-type conduction. As a rule (although not always), ionic semiconductors have unipolar conduction, due to ions of one sign. Thus, in compounds AgBr, $PbCl_2$, and others, the cation transport number t_+ is close to unity. In the mixed oxide $ZrO_2 \cdot nY_2O_3$, pure O^- anion conduction $t_- = 1$) is observed.

In an ideal ionic crystal, all ions are held rigidly in the lattice sites, where they perform only thermal vibratory motion. Transfer of an ion between sites under the effect of electrostatic fields (migration) or concentration gradients (diffusion) is not possible in such a crystal. Initially, therefore, the phenomenon of ionic conduction in solid ionic crystals was not understood.

Yakov Frenkel showed in 1926 that ideal crystals could not exist at temperatures above the absolute zero. Part of the ions leave their sites under the effect of thermal vibrations and are accommodated in the interstitial space, leaving vacancies at the sites formerly taken up. Such point defects have been named *Frenkel defects*. These ideas were developed further by Walter Schottky in 1929, who pointed out that defects will also arise when individual ions or ion pairs are removed from the bulk

lattice and brought (e.g., to the crystal surface); such defects have been named *Schottky defects*. Both types of point defect are in thermal equilibrium with the remainder of the crystal and have the character of fluctuations; they appear and disappear spontaneously. Their concentrations increase drastically with temperature (i.e., their formation is associated with a high activation energy). The defect concentrations can be calculated statistically. For NaCl crystals close to the melting point, it is about $10^{-3}\,M$.

The point defects are decisive for conduction in solid ionic crystals. Ionic migration occurs in the form of relay-type jumps of the ions into the nearest vacancies (along the field). The relation between conductivity σ and the vacancy concentration is unambiguous, so that this concentration can also be determined from conductivity data.

In addition to the thermal vacancies, impurity-related vacancies will develop in ionic crystals. When impurity ions have a charge different from ions of like charge which are the crystal's main constituents, part of the lattice sites must remain vacant in order to preserve electroneutrality. Such impurity-type defects depend little on temperature, and their major effects are apparent at low temperatures when few thermal vacancies exist.

Because of the low concentration of thermal vacancies, pure ionic semiconductors have low conductivities, between 10^{-12} and 10^{-4} S/cm. In impurity-type ionic semiconductors the conductivities are sometimes higher; the best known examples are solid electrolytes on the basis of zirconium dioxide: $ZrO_2 \cdot nMO_x$, where $MO_x = CaO$, Y_2O_3, and others. The number of negative ions O^- must decrease when a certain number of di- or trivalent cations are incorporated into the ZrO_2 lattice instead of the Zr^+ ions. For this reason, oxygen vacancies are formed and oxygen ion conduction arises. This conduction is of practical importance only at high temperatures. Solid electrolytes $ZrO_2 \cdot 0.11Y_2O_3$ have a conductivity of about 0.012 S/cm at 1000°C.

8.4.2 Ionic Conductors

It had been discovered long ago that the character of conduction in AgI changes drastically at temperatures above 147°C, when β- and λ-AgI change into α-AgI. At the phase transition temperature the conductivity, σ, increases discontinuously by almost four orders of magnitude (from 10^{-4} to 1 S/cm). At temperatures above 147°C, the activation energy is very low and the conductivity increases little with temperature, in contrast to its behavior at lower temperatures (see Fig. 8.2).

Starting in the 1960s, many compounds with such properties were discovered (i.e., with high conductivities and low-temperature coefficients of conductivity). Some of them are double salts with silver iodide (nAgI·mMX) or other silver halides where MX has either the cation or the anion in common with the silver halide. The best-known example is $RbAg_4I_5$ (= 4AgI·RbI), where this sort of conduction arises at −155°C and is preserved up to temperatures above 200°C. At 25°C this compound has a conductivity of 26 S/m (i.e., the same value as found for a 7% KOH solution). Another example is Ag_3SI, which above 235°C forms an α-phase with a conductivity of 100 S/m.

The same conduction type is found for another class of compounds, the sodium polyaluminates or β-aluminas $Na_2O \cdot nAl_2O_3$, where n has values between 3 and 8.

Polycrystalline samples of these materials have a room-temperature conductivity of about 0.5 S/m, but at 300°C the conductivity is about 10 S/m.

Because of the high values of conductivity which in individual cases are found at room temperature, such compounds are often called *superionic conductors* or *ionic superconductors*; but these designations are unfounded, and a more correct designation is *solid ionic conductors*. Strictly unipolar conduction is typical for all solid ionic conductors; in the silver double salts, conduction is due to silver ion migration, whereas in the sodium polyaluminates, conduction is due to sodium ion migration.

The discovery of the various ionic conductors has elicited strong interest, since they can be used in chemical power sources and other devices. It could be shown after numerous studies that the high ionic mobilities in these compounds are the result of particular lattice structures. In such lattices, immobile ions of one type (most often, the anions) are fixed at their lattice sites and form a rather rigid, nondeformable sublattice. The sublattice of the other ions (most often the cations), to the contrary, is disordered: The cations are not bound to particular sites but can occupy any of a large number of equally probable sites. Since at any particular time, an ion physically occupies just one site, the other available sites function as the vacancies for the ion's motion. The differences between sites and interstitials are obliterated here, and a peculiar, highly mobile cation fluid is formed. The conductivity in the crystal will be anisotropic (i.e., depend on the direction in space) when the vacancies have a particular spatial configuration relative to the rigid anionic sublattice. As in the case of ionic semiconductors, this state is characteristic for certain structures and can exist only within the temperature range where the particular crystal structure is stable.

More details about solid electrolytes are discussed in Chapter 25.

REFERENCES

Frenkel, Ya., *Z. Phys.*, **35**, 652 (1926).

Ioffe, A., *Ann. Phys.*, Ser. 4, **72**, 461 (1923).

Pisarzhevsky, L., and H. Lemke, *Zh. Russ. Fiz. Khim.Ova.*, **37**, 492 (1905).

Schottky, W., *Thermodynamik*, Springer-Verlag, Berlin, 1929.

Tubandt, C., and E. Lorenz, *Z. Phys. Chem.*, **87**, 513 (1914).

Walden, P., *Z. Phys. Chem.*, **55**, 207 (1906).

MONOGRAPHS AND REVIEWS

Aurbach, D., ed., *Non-aqueous Electrochemistry*, Marcel Dekker, New York, 1999.

Izutsu, Kosuke, *Electrochemistry in Nonaqueous Solutions*, Wiley, Chichester, West Sussex, England, 2002.

Mamontov, G., and A. I. Popov, Eds., *Chemistry of Nonaqueous Solutions: Current Progress*, Wiley, Chichester, West Sussex, England, 1994.

9

Electron Work Functions and Volta Potentials

9.1 SURFACE POTENTIAL OF A PHASE

Consider a conductor α in contact with an insulator (or vacuum) not containing charges (Fig. 9.1). Let x be the distance of a point inside the insulator measured from the interface. The potential will be referred to the conventional point of reference at $x \to \infty$ within the insulator.

When the conductor as a whole is charged (i.e., has excess charge of one sign in its surface layer), an electrostatic field and a potential gradient will develop in the insulator region adjacent to it. The name of the outer potential, $\psi_{ex}^{(\alpha)}$, of the conductor is used for the potential at a point a located in the insulator just outside the conductor. Since point a and the point of reference are located in the same phase, this potential can be measured.

The concept of "just outside" must be defined more closely. When the test charge is moved from the point of reference toward the surface, work is performed due to the (primary) electrostatic field being discussed. However, very close to the surface, image forces start to act on the test charge; they give rise to an additional

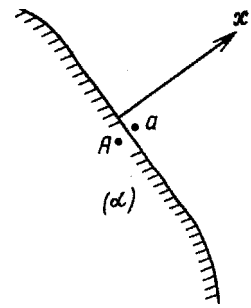

FIGURE 9.1 Conductor–insulator interface.

Fundamentals of Electrochemistry, Second Edition, By V. S. Bagotsky

work term and distort the primary field. Hence, the distance of point *a* from the surface is selected large enough so that the contribution of the image forces will be small; at the same time, this distance should be short enough so that we can neglect the change in primary field between point *a* and the surface. Calculations show that these conditions are fulfilled at distances of about 1 μm from the surface.

No potential gradient exists within the conductor; hence the conductor's inner potential $\psi_{in}^{(\alpha)}$ is the potential at any point *A* inside the conductor. The potential difference between points *A* and *a*, defined as

$$\chi^{(\alpha)} \equiv \psi_{in}^{(\alpha)} - \psi_{ex}^{(\alpha)}, \tag{9.1}$$

is called the conductor's *surface* potential[†]. The electric field producing this potential is wholly concentrated in the conductor's surface layer, where an EDL is formed as a result of the nonuniform charge distribution. The value of the surface potential depends on the structure and chemical properties of the conductor surface. In contrast to the outer potential, the values of surface and inner potential defined as indicated cannot be measured, since they refer to points in different phases.

9.2 WORK FUNCTIONS

9.2.1 Work Function for the Metal–Vacuum Interface

Conductor–insulator and conductor–vacuum interfaces lack a continuous exchange of free charges, and there is no electrochemical equilibrium. For this reason the work that is performed in transferring charged particles from one phase to the other is not zero. The total work, λ, which must be performed by the external forces in transferring (extracting) an electron from a metal (M) into vacuum (0) is called the *electron work function* (or simply the *work function*). The work function for all metals is always positive, since otherwise the electrons would leave the conductor spontaneously.

Because of the influence of potential gradients, the work function depends on the position of the point to which the electron is transferred. As in the definition of surface potential, a point (*a*) situated in the vacuum just outside the metal is regarded as the terminal point of transfer. It is assumed, moreover, that when the transfer has been completed, the velocity of the electron is close to zero (i.e., no kinetic energy is imparted on it).

The work function thus defined is equal to the difference in electrochemical potentials of the electron at point *a* in vacuum, $\overline{\mu}^{(0)}$, and any point in the metal $\overline{\mu}^{(M)}$.

[†] For χ, which like φ_G and φ_V is a potential difference, IUPAC and the present book agree in using the same symbol and the same name, *surface potential*.

In the vacuum where there is no chemical interaction between the electron and the medium, we have $\mu_e^{(0)} = 0$; hence (since for electrons $z_e = -1$), $\bar{\mu}_e^{(0)} = -Q^0\psi_{ex}^{(\alpha)}$. Using this quantity as well as Eq. (9.1), we find that

$$\lambda = \bar{\mu}_e^{(0)} - \bar{\mu}_e^{(M)} = -Q^0\psi_{ex} - (\mu_e^{(M)} - Q^0\psi_{in}) = -\mu_e^{(M)} + Q^0\chi^{(M)}. \tag{9.2}$$

Work functions refer traditionally not to one mole of electrons (with the charge $-F$) but to one electron with the charge $-Q^0$, and usually are stated in electrical units of electron volts (1 eV = 1.62×10^{-19} J). In equations of the type of (2.32), therefore, the value of μ_e also refers to one electron.

It follows from Eq. (9.2) that the work function has a chemical and an electrostatic component. Its overall value can be measured, whereas an exact determination of its individual components is not possible. The chemical component depends on the interaction between the charge and the surrounding medium; moreover, it includes the work performed in overcoming the image forces.

The work function of charged particles found for a particular conductor depends not only on its bulk properties (its chemical nature), which govern parameter $\mu_e^{(\alpha)}$, but also on the state of its surface layer, which influences the parameter $\chi^{(\alpha)}$. This has the particular effect that for different single-crystal faces of any given metal, the electron work functions have different values. This experimental fact is one of the pieces of evidence for the existence of surface potentials. The work function also depends on the adsorption of foreign species, since this influences the value of $\chi^{(\alpha)}$.

Several methods exist for measuring the electron work functions of metals. In all these methods one determines the level of an external stimulus (light, heat, etc.) required to extract electrons from the metal.

In the method of electron photoemission one determines the lowest frequency of light (ν_0, the "red" limit in the spectrum) at which electrons can be knocked from the metal. The quantum energy $h\nu_0$ of this light gives directly the work of extraction of one electron. When light quanta of higher energies are employed, the electrons acquire additional kinetic energy.

The saturation current I_{sat} observed in thermionic electron emission is related to temperature by the famous *Richardson–Fowler law*,

$$\ln\frac{I_{sat}}{T^2} = \text{const} - \frac{\lambda}{kT}, \tag{9.3}$$

($k \equiv R/N_A$ is the Boltzmann constant). The work function can be determined from the slope of straight lines obtained when plotting $\ln(I_{sat}/T^2)$ vs. T^{-1}.

9.2.2 Work Function for Metals Contacting Electrolytes

In electrochemical reactions the electron is not extracted into the vacuum. For cathodic reactions it is extracted from the electrode into the electrolyte, and for

anodic reactions it is transferred in the opposite direction. During both of these transfers the electron must overcome the full Galvani potential at the metal–electrolyte interphase. The work function λ^{E} found at such an interface differs from the work function λ found in vacuum. It depends on the value of the Galvani potential. The work function is the difference of the electrochemical potentials of the electrons in the two phases. Therefore, we have, when taking into account the definition of Galvani potential,

$$\lambda^{E} = \overline{\mu}_e^{(E)} - \overline{\mu}_e^{(M)} = [\mu_e^{(E)} - \mu_e^{(M)}] + Q^0 \varphi_G^{(M,E)}, \tag{9.4}$$

where $\mu_e^{(E)}$ is the chemical potential of solvated electrons in the electrolyte solution (for further details concerning solvated electrons, see Section 29.2). In electrochemistry, electrode potentials E measured against a certain reference electrode M_R are mostly used rather than the Galvani potentials, which cannot be measured experimentally. Replacing in Eq. (9.4) the parameter $\varphi_G^{(M,E)}$ by E $(= \varphi_G^{(M,E)} - \varphi_G^{(M_R,E)} + \varphi_G^{(M_R,M)})$ and taking into account that $(Q^0 \varphi_G^{M,E)} = \mu_e^{(M)} - \mu_e^{(E)})$, we find after transformation that

$$\lambda^{E} = A + Q^0 E, \tag{9.5}$$

where A is a constant that depends on the reference electrode and not on the nature of the metal electrode M. It is readily seen, in fact, that when the transition to electrode potentials E has been made, the term $\mu_e^{(M)}$ enters Eq. (9.4) both explicitly and as component part of the term $Q^0 \varphi_G^{(M,M_R)}$, and hence cancels.

We thus reach the important conclusion *that a metal's electron work function in solutions is independent of the nature of the metal when determined at the same value of electrode potential* (i.e., it has identical values for all electrodes).

Electron work functions of metals in solution can be determined by measurements of the current of electron photoemission into the solution. In an electrochemical system involving a given electrode, the photoemission current (I_{ph}) depends not only on the light's frequency ν (or quantum energy $h\nu$) but also on the potential E. According to the quantum-mechanical theory of photoemission, this dependence is given by

$$I_{ph} = C(h\nu - \lambda^{E})^{5/2} = C(h\nu - A - Q^0 E)^{5/2} \tag{9.6}$$

(the "law of five halves"). Here C is a constant that depends on light intensity and on the experimental conditions. In the measurements, light of a certain frequency ν is used and the photoemission currents are determined at different values of potential. Plots of $I_{ph}^{0.4}$ vs. E are straight lines which are readily extrapolated to $I_{ph} = 0$. At this point, $h\nu = \lambda^{E} = A + Q^0 E_{thr}$ (the threshold potential is denoted as E_{thr}). The value of the constant A in Eq. (9.5) calculated from photoemission data is 3.10 ± 0.005 eV when the standard hydrogen electrode is used as the reference electrode.

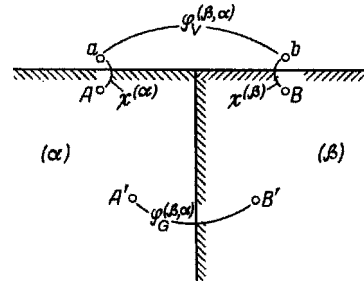

FIGURE 9.2 Volta potential, Galvani potential, and surface potentials.

9.3 VOLTA POTENTIALS

Consider two conductors, α and β, in mutual contact in a vacuum (Fig. 9.2). Each of them has a certain surface potential; these potentials are $\chi^{(\alpha)}$ and $\chi^{(\beta)}$, respectively. Between the conductors the Galvani potential $\varphi_G^{(\beta,\alpha)}$ is established. The potential difference between points *a* and *b* located in the vacuum just outside conductors α and β, respectively, is called the *Volta potential* $\varphi_V^{(\beta,\alpha)}$, or the *outer* or *contact potential difference*, of this pair of conductors.‡ Taking into account that the potential difference between two points is independent of the path taken between these points, we have

$$\varphi_V^{(\beta,\alpha)} = \chi^{(\alpha)} - \chi^{(\beta)} + \varphi_G^{(\beta,\alpha)}. \tag{9.7}$$

Points *a* and *b* are located in the same phase (vacuum); therefore, the Volta potential can be measured, in contrast to what is found for the Galvani potential (between points A' and B') and for the surface potentials (between points *a* and *A*, and between points *b* and *B*).

For measurements of the Volta potentials, one uses a special feature of the electrostatic capacitor. In fact, when the two sides of a capacitor do not (as usual) consist of identical conductors but of different ones, the charge on the capacitor plates, according to the capacitor relation, is not related to the difference between the inner potentials of the two conductors but to their Volta potential (to the difference between the outer potentials). Knowing the value of capacitance of the capacitor and measuring the charge that flows when the plates are made part of a suitable circuit, one can thus determine the Volta potential.

The Volta potential between two metals is related directly to the electron work functions of these metals. Taking into account that for two metals in contact at equilibrium we have $\mu_e^{(\alpha)} = \mu_e^{(\beta)}$ and that $z_e = -1$, we obtain from Eq. (9.2):

$$\lambda^{(\alpha)} - \lambda^{(\beta)} = -Q^0[\psi_{ex}^{(\beta)} - \psi_{ex}^{(\alpha)}] = -Q^0\varphi_V^{(\beta,\alpha)}. \tag{9.8}$$

‡ Instead of φ_V, IUPAC recommends $\Delta\psi \equiv \psi^2 - \psi^1$ and uses the term *Volta potential difference*.

With the aid of this equation and the results of Volta potential measurements we can determine the electron work function of a second metal when that of the first metal is known.

The fact that there is a potential difference between points close to the surfaces of two conductors in contact implies that the excess charge densities on their exposed surfaces are different. This also implies that when two conductors come in contact, there will be a redistribution of free electrons not only at the actual inner contact surface (which gives rise to the Galvani potential) but also at their exposed surfaces.

9.4 TWO PROBLEMS IN ELECTROCHEMISTRY

9.4.1 Volta Problem

During the nineteenth century, opinions were divided as to where in galvanic cells of the type

$$M_1 \,|\, E \,|\, M_2 \,|\, M_1 \tag{9.9}$$

the interfacial potential differences responsible for the OCV value exhibited by the cell were located. Alessandro Volta thought that the potential difference resided wholly at the metal–metal junction and that Galvani potentials did not exist at metal–electrolyte interfaces (*physical EMF theory*). According to Walther Nernst, to the contrary, the potential difference resided at the two metal–electrolyte interfaces where electrochemical reactions take place (*chemical EMF theory*). The dependence of OCV on solution composition and its connection with the Gibbs reaction energy were arguments weighing heavily in favor of Nernst's ideas. However, experimental evidence exists that is in favor of the views of Volta: The Volta potentials measured between any two metals in vacuum correlate with the OCV values observed when the same metals are immersed in an electrolyte solution; the metal that is more negative in vacuum as a rule is that which is more negative in the solution, and metal pairs with higher Volta potentials exhibit higher OCV values. The conflict which thus arises between these two viewpoints became known as the *Volta problem* in electrochemistry.

A solution to this problem was suggested in 1928 by A. Frumkin and A. Gorodetzkaya, as follows. In galvanic cells, interfacial potential differences develop across all interfaces. According to Eq. (9.1), each Galvani potential $\varphi_G^{(\beta,\alpha)}$ can be written as the algebraic sum of three components: the interfacial potential $\Phi^{(\beta,\alpha)}$ and two surface potentials. Let the surface potential of phase (α) at its interface with vacuum be $\chi^{(\alpha,0)}$. At its interface with another condensed phase (γ), a somewhat different surface potential $\chi^{(\alpha,\gamma)}$ exists because of surface-layer interaction. Let the difference be $\delta\chi^{(\alpha/\gamma)}$ [$\equiv \chi^{(\alpha,\gamma)} - \chi^{(\alpha,0)}$]. Using this partition of Galvani potentials into their components in Eq. (2.12) for the OCV, Frumkin obtained, after transformations,

$$\begin{aligned} E^{(1,2)} = {} & \Phi^{(1,2)} + \Phi^{(2,E)} - \Phi^{(1,E)} + [\delta\chi^{(1/2)} - \delta\chi^{(2/1)}] \\ & + [\delta\chi^{(2/E)} - \delta\chi^{(1/E)}] - [\delta\chi^{(E/2)} - \delta\chi^{(E/1)}]. \end{aligned} \tag{9.10}$$

According to Eqs (9.7) and (9.1), the expression for the Volta potential can be written as

$$\varphi_V^{(1,2)} = \Phi^{(1,2)} + [\delta\chi^{(1/2)} - \delta\chi^{(2/1)}]. \tag{9.11}$$

It will be assumed that the interactions between each of metals (1) and (2) and the corresponding surface layers of the electrolyte solution are approximately identical, and also that specific adsorption of ions does not occur in the system being considered. In this case the values of the expressions in the last two sets of brackets in Eq. (9.10) become zero, and from (9.10) and (9.11) an important relation is obtained which links the OCV of galvanic cells with the Volta potential:

$$E^{(1,2)} \approx \varphi_V^{(1,2)} + \Phi^{(2,E)} - \Phi^{(1,E)}. \tag{9.12}$$

This expression explains the qualitative agreement found to exist between the OCV values of galvanic cells and the Volta potentials of the corresponding metal pairs. But through terms $\Phi^{(1,E)}$ and $\Phi^{(2,E)}$, it also explains why OCV values depend on solution composition. All parameters of this equation can be measured experimentally.

Equation (9.12) yields another important result: When both electrodes are at the potential of their respective PZC (and the values of $\Phi^{(M,E)}$ are zero), the cell voltage (which is the PZC potential difference between the two electrodes) will be equal to the Volta potential between the corresponding metals:

$$\Delta E_{zc}^{(1,2)} \approx \varphi_V^{(1,2)}. \tag{9.13}$$

In a number of cases, Eqs. (9.12) and (9.13) are in good agreement with experimental data. However, sometimes the quantitative agreement is not as good, and this can be attributed to the approximations made in connection with Eq. (9.12). Therefore, when comparing the calculations with experiment, one can reach certain conclusions as to the way in which the surface potentials vary (i.e., as to the way a metal interacts with the electrolyte).

9.4.2 Problem of Absolute Potential

Many attempts have been made by experiment or calculation to determine the absolute values of Galvani potentials at interfaces, particularly across the electrode–electrolyte interface. Basically, if one knew the Galvani potential between one metal and the associated electrolyte and that at the interface between the metal and another metal, one could then find the Galvani potentials for all other interfaces from the data of OCV measurements with other galvanic cells.

It had already been pointed out that there is not a single interface for which the Galvani potential can be either measured experimentally or calculated thermodynamically from indirect experimental data. The only way of determining it is through theoretical calculations based on nonthermodynamic models.

A frequent starting point for such calculations are the values of Volta potentials, $\varphi_V^{(M,E)}$, between electrodes and electrolytes (which can be measured by the same methods as Volta potentials between metals). According to Eq. (9.7),

$$\varphi_V^{(M,E)} = \varphi_G^{(M,E)} + \chi^{(E,0)} - \chi^{(M,0)}. \tag{9.14}$$

The problem of calculating Galvani potentials now reduces to that of calculating the surface potentials of the metal and solution.

Equation (9.2) can be used to calculate the metal's surface potential. The value of the electron work function λ can be determined experimentally. The chemical potential of the electrons in the metal $\mu_e^{(M)}$ can be calculated approximately from equations based on the models in modern theories of metals. The accuracy of such calculations is not very high. The surface potential of mercury determined in this way is roughly $+2.2$ V.

The surface potential of a solution can be calculated, according to Eq. (10.18), from the difference between the experimental real energy of solvation of one of the ions and the chemical energy of solvation of the same ion calculated from the theory of ion–dipole interaction. Such calculations lead to a value of $+0.13$ V for the surface potential of water. The positive sign indicates that in the surface layer, the water molecules are oriented with their negative ends away from the bulk.

It follows from these values that at the potential of the standard hydrogen electrode, the Galvani potential between a mercury electrode and the solution is about 1.6 V. The accuracy of all such calculations is low.

REFERENCE

Frumkin, A. and A. Gorodetzkaya, *Z. Phys. Chem.*, **136**, 215, 451 (1928).

10

Structure and Properties of Surface Layers

Macroscopically, the region of contact between an electrode and an electrolyte is a two-dimensional surface (an interface) separating the two phases. Microscopically, the same region is structured in a complex way. When two condensed phases are brought in contact, the surface-layer properties of each phase will change under the effect of the other phase. Close to the boundary in both phases, surface layers of a certain thickness develop which differ from the principal phases in their properties. In a surface layer, particles are surrounded by other particles in an asymmetric fashion, and the forces acting on them do not balance. This gives rise to concentration changes relative to the values found in the bulk phase; it also leads to changes in the energy state of the individual particles and of the layer as a whole. The set of two surface layers existing at the junction of two condensed phases is called the *interphase* (in contrast to the macroscopic interface).

The interphase between an electrode and an electrolyte solution has a very complex electrical structure (Section 10.1). In this interphase various adsorption processes take place:

1. *Adsorption of ions from the solution.* There are two types of ionic adsorption from solutions onto electrode surfaces: an electrostatic (physical) adsorption under the effect of the charge on the metal surface, and a specific adsorption (chemisorption) under the effect of chemical (nonelectrostatic) forces. Specifically adsorbing ions are called *surface active*. Specific adsorption is more pronounced with anions.
2. *Solvent adsorption*. The adsorption of solvent molecules is manifested in their orientation and ordered arrangement at the interface.
3. *Adsorption of other components of the system*. This includes components taking part in the electrode reaction as well as "inert" components not taking part (see Section 10.2 about adsorption processes).

Fundamentals of Electrochemistry, Second Edition, By V. S. Bagotsky

Both the electrical structure of the interphase and the occurrence of adsorption processes have a great influence on electrochemical reactions on an electrode's surface and on various electrochemical phenomena.

10.1 ELECTRICAL STRUCTURE OF INTERPHASES

When an electrode is in contact with an electrolyte, the interphase as a whole is electroneutral. However, *electric double layers* (EDLs) with a characteristic potential distribution are formed in the interphase because of a nonuniform distribution of the charged particles.

Two types of EDL are distinguished: superficial and interfacial. *Superficial EDLs* are located wholly within the surface layer of a single phase (e.g., an EDL caused by a nonuniform distribution of electrons in the metal, an EDL caused by orientation of the bipolar solvent molecules in the electrolyte solution, an EDL caused by specific adsorption of ions). The potential drops developing in these cases (the potential inside the phase relative to a point just outside) is called the *surface potential* $\chi^{(k)}$ of the given phase k. *Interfacial EDLs* have their two parts in different phases: the "inner" layer with the charge density $Q_{S,\mathrm{M}}$ in the metal (because of an excess or deficit of electrons in the surface layer), and the "outer" layer of counterions with the charge density $Q_{S,\mathrm{E}} = -Q_{S,\mathrm{M}}$ in the solution (an excess of cations or anions); the potential drop caused by this double layer is called the *interfacial potential* $\Phi^{(\mathrm{M,E})}$.

Hermann von Helmholtz put the concept of EDL formation at electrode surfaces forward in 1853. For a long time only the interfacial EDLs were taken into account. The considerable importance of various kinds of superficial EDLs was pointed out by Alexander N. Frumkin in 1919.

The formation of any kind of EDL implies the development of strong electrostatic fields in the interphase. The distance between the two sides of an EDL as a rule is

Hermann von Helmholtz (1821–1894).

less than 1 nm, and the potential differences can attain several volts. Hence the field strength **E** within EDLs can be higher than 10^7 V/cm.

Each type of EDL and the potential drop produced by it contribute to the total Galvani potential, φ_G, at the interface considered:

$$\varphi_G^{(M,E)} = \Phi^{(M,E)} + \chi^{(M)} - \chi^{(E)} \tag{10.1}$$

(here the surface potential $\chi^{(E)}$ of the electrolyte solution can be the sum of several components: those due to adsorption of ions, $\chi_{ads}^{(E)}$; to the orientation of solvent molecules, $\chi_{or}^{(E)}$; etc.).

Adsorption and orientation in surface layers are phenomena evolving by their own specific laws, whereas the equilibrium value of the Galvani potential depends only on the bulk properties of the phases, according to Eq. (2.6). A question arises, then, as to how the sum of all independent components on the right-hand side of Eq. (10.1) can always be constant and equal to the given value of $\varphi_G^{(M,E)}$. The explanation must be sought in the regulating function assumed by the interfacial EDL in the process of equilibration: Between the phases (the electrode and the solution), charges will be transferred in one direction until the interfacial potential $\Phi^{(M,E)}$ has assumed a value satisfying Eq. (10.1). The interfacial potential will change in appropriate fashion when there has been, for whatever reason, a change in the adsorption, orientation, or other components of the surface potentials.

At a definite value of the electrode potential E, the charge of the electrode's surface $Q_{S,M}$ and hence the value of $\Phi^{(M,E)}$, drop to zero. This potential E_{zc} is called the *point of zero charge* (PZC). The metal surface is positively charged at potentials more positive than the PZC and is negatively charged at potentials more negative than the PZC. The point of zero charge is a characteristic parameter for any electrode–electrolyte interface. The concept of PZC is of exceptional importance in electrochemistry.

Some of the components of the EDL, such as a nonuniform electron distribution in the metal's surface layer and the layer of oriented dipolar solvent molecules in the solution surface layer adjacent to the electrode, depend on external parameters (potential, electrolyte concentration, etc.) to only a minor extent. Usually, the contribution of these layers is regarded as constant, and it is only in individual cases that we must take into account any change in these surface potentials, $\delta_\chi^{(M)}$ and $\delta_{\chi_{or}}^{(E)}$, which occurs as a result of changes in the experimental conditions.

Changes in the parameters listed above influence primarily the interfacial EDL: that is, the excess charge densities $Q_{S,M} = -Q_{S,E}$ and the distribution of electrostatically adsorbed ions in the solution region next to the electrode, as well as that part of the solution's superficial EDL which is associated with specific adsorption of solution ions. These two kinds of EDL together are called the *ionic EDL*. Many electrochemical properties of electrodes are determined precisely by the structure of the ionic EDL and its changes during an experiment.

Because of mutual repulsion forces and of attraction forces arising on the other side of the EDL, the excess charges in the metal are always tightly "packed" against the interface. The excess charges in the solution (i.e., the ions) are subject to thermal

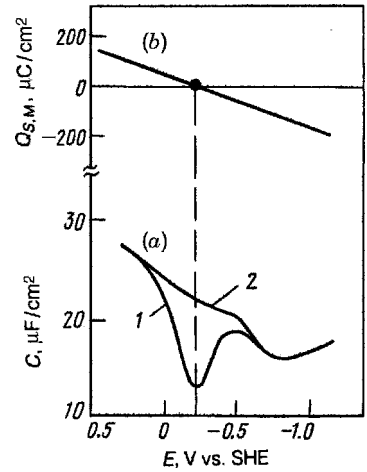

FIGURE 10.1 (*a*) Differential capacitance of a mercury electrode as a function of potential in NaF solutions: (1) 0.01 *M*, (2) 0.1 *M*; (*b*) plot of surface charge density vs. potential calculated from curve 2.

motion, and despite the electrostatic attraction, can roam some small distance away from the surface.

A convenient parameter characterizing the charge distribution in the solution side of the edl is the electrode's differential capacitance, $C \equiv dQ_{S,\mathrm{M}}/dE$ (units: μF/cm²). Evidently, the value of capacitance will be lower the larger the (mean) distance of the excess ions from the surface (i.e., the thicker the EDL). The value of differential capacitance can be found by direct ac measurements at high frequencies (Section 12.5.1). A typical value of EDL capacitance referred to true surface area is about 20 μF/cm². The value of the differential capacitance depends on potential and, in dilute solutions, on electrolyte concentration (Fig. 10.1*a*). At low electrolyte concentrations a capacitance minimum is seen near the point of zero charge. The capacitance increases with increasing distance from the PZC, and at appreciable positive and negative potentials it tends toward certain limiting values. The capacitance in the region of the minimum increases with increasing concentration, and the minimum disappears when certain values of concentration are attained.

By integrating the C vs. E curves from the PZC to a given potential E, the surface charge density $Q_{S,\mathrm{M}}$ can be calculated (Fig. 10.1*b*).

Different structural models of the ionic EDL have been suggested in order to describe the electrical properties of interfaces. Consider the distribution of electrostatic potential ψ at the solution side of the ionic EDL as a function of distance x from the surface. By convention we locate the point of reference in the solution interior (i.e., we shall assume that $\psi = 0$ when $x \to \infty$). The potential at $x = 0$ will be designated as ψ_0. The sign of parameter ψ_0 corresponds to that of $Q_{S,\mathrm{M}}$.

10.1.1 Helmholtz Model

Following the concepts of H. Helmholtz (1853), the EDL has a rigid structure, and all excess charges on the solution side are packed against the interface. Thus, the EDL is likened to a capacitor with plates separated by a distance δ, which is that of the closest approach of an ion's center to the surface. The EDL capacitance depends on δ and on the value of the dielectric constant ε for the medium between the plates. Adopting a value of δ of 10 to 20 nm and a value of $\varepsilon = 4.5$ (the water molecules in the layer between the plates are oriented, and the value of ε is much lower than that in the bulk solution), we obtain $C = 20$ to $40\,\mu F/cm^2$, which corresponds to the values observed. However, this model has a defect, in that the values of capacitance calculated depend neither on concentration nor on potential, which is at variance with experience (the model disregards thermal motion of the ions).

10.1.2 Gouy–Chapman Model

Thermal motion of the ions in the EDL was included in the theories developed independently by Georges Gouy in France (1910) and David L. Chapman in England (1913). The combined effects of the electrostatic forces and of the thermal motion in the solution near the electrode surface give rise to a diffuse distribution of the excess ions, and a diffuse EDL part or *diffuse ionic layer* with a space charge $Q_V(x)$ (depending on the distance x from the electrode's surface) is formed. The total excess charge in the solution per unit surface area is determined by the expression

$$Q_{S,E} = \int_0^\infty Q_V(x)dx. \tag{10.2}$$

When taking into account both the electrostatic forces and the thermal motions of the ions, these theories lead to the following equation connecting the very important

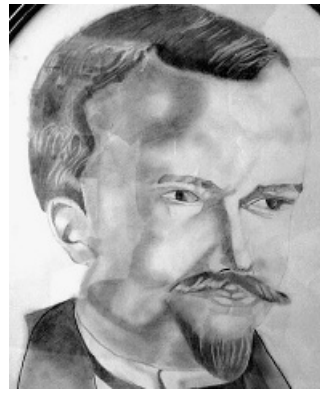

Georges Gouy (1854–1926).

David L. Chapman (1867–1958).

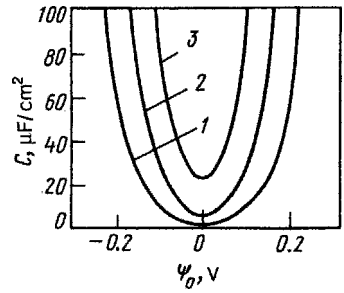

FIGURE 10.2 Potential dependence of differential capacitance calculated from Gouy–Chapman theory for $z_+ = z_- = 1$ and various concentrations: (1) 10^{-4}, (2) 10^{-3}, (3) 10^{-2} *M*.

parameter characterizing the degree of diffuseness of the EDL: the (specific) differential capacitance of the EDL C, with the potential ψ_0:

$$C = 2A \cosh \frac{zF\psi_0}{RT}, \quad \text{where} \quad A \equiv \left(\frac{2RTc_V}{\varepsilon_0 \varepsilon}\right)^{1/2}. \tag{10.3}$$

(A full mathematical treatment of the Gouy–Chapman theory and the derivation of these equations is given in Appendix B.)

Figure 10.2 shows plots of differential capacitance against the potential ψ_0 calculated for different concentrations c_V with Eq. (10.3), while assuming that $z = 1$ and that in the diffuse layer $\varepsilon = 78$. Unlike the Helmholtz model, the Gouy–Chapman model provides a qualitatively correct description of the capacitance minimum near the PZC and of the capacitance rise that occurs with increasing values of concentration and $|\psi_0|$. However, for concentrations higher than 10^{-2} *M* and for potentials $|\psi_0| > 0.05$ V, the capacitance values calculated are much higher than the experimental values. The discrepancies can be explained by the fact that the Gouy–Chapman model, unlike that of Helmholtz, disregards the ions' own size and allows the centers of the ions to come close to the physical surface.

10.1.3 Models of Stern and Grahame

In 1924, Otto Stern (Germany) suggested a new version of EDL theory where the true size of the ions and the possibility of specific (nonelectrostatic) adsorption of the ions are taken into account. In 1947, David C. Grahame considerably improved this theory by eliminating a number of defects that had been present in earlier versions. By combining the ideas of Helmholtz and those of Gouy and Chapman, Stern introduced the notion of a plane of closest approach of the ions to the surface, called the *Helmholtz plane* with coordinate x_H (which depends on the ionic radius) and the potential ψ_H. The charges on the solution side of the EDL can be divided into two parts. One part ($Q_{S,H}$) is located at this plane and constitutes the compact or Helmholtz part of the EDL. The other part ($Q_{S,d}$), which is under the effect of thermal motion, constitutes the diffuse part of the edl. Specifically adsorbed ions are located at the Helmholtz plane and determine the value of $Q_{S,H}$. However, according to the equations of Stern's

Otto Stern (1888–1969; Nobel prize, 1943).

theory, some nonzero value of $Q_{S,\mathrm{H}}$ is retained even in the absence of chemical forces, which is physically difficult to explain.

Grahame introduced the idea that electrostatic and chemical adsorption of ions are different in character. In the former, the adsorption forces are weak, and the ions are not deformed during adsorption and continue to participate in thermal motion. Their distance of closest approach to the electrode surface is called the *outer Helmholtz plane* (coordinate x_2, potential ψ_2, charge of the diffuse EDL part $Q_{S,2}$). When the more intense (and localized) chemical forces are operative, the ions are deformed, undergo partial dehydration, and lose mobility. The centers of the specifically adsorbed ions constituting the charge $Q_{S,1}$ are at the *inner Helmholtz plane* with the potential ψ_1 and coordinate $x_1 < x_2$.

Since the EDL as a whole is electroneutral, we have

$$Q_{S,\mathrm{M}} = -(Q_{S1} + Q_{S,2}). \tag{10.4}$$

David C. Grahame (1912–1958).

Consider first the situation when specific adsorption of ions is absent. In this case the ions cannot penetrate to the inner Helmholtz plane, the charge density $Q_{S,1}$ is zero, and hence $Q_{S,M} = -Q_{S,2}$. Since no charges exist in the compact EDL part, $x_2 \geq x \geq 0$, the value of $d\psi/dx$ will be constant and the potential will vary linearly from ψ_0 to ψ_2. For the Helmholtz layer we can write

$$Q_{S,M} = C_H(\psi_0 - \psi_2), \tag{10.5}$$

where $C_H \equiv \varepsilon_0\varepsilon/x_2$ is the Helmholtz layer capacitance.

This capacitance depends on the nature of the ions on the solution side of the EDL but not on their concentration. When the metal is negatively charged, the solution side is formed by cations, and $C_H \approx 20\,\mu F/cm^2$. But when the metal is positively charged, the solution side is formed by anions (for which the distances x_2 are smaller than for the cations), and the values of C_H can be as high as $40\,\mu F/cm^2$. Thus, in passing through the PZC the value of C_H changes discontinuously; but in each of the regions on the two sides of the PZC it is only weakly potential dependent.

The charge of the diffuse EDL part ($x > x_2$) can be described by the equations of Gouy–Chapman theory, but with the value ψ_2 rather than ψ_0:

$$-Q_{S,2}[= Q_{S,M}] = 2A \sinh \frac{zF\psi_2}{2RT}. \tag{10.6}$$

Combining the last two equations, we finally obtain

$$Q_{S,M} = C_H(\psi_0 - \psi_2) = 2A \sinh \frac{zF\psi_2}{2RT}. \tag{10.7}$$

An important parameter of this combined EDL is the potential ψ_2. Its dependence on concentration c_V and on the total potential ψ_0 (or total charge $Q_{S,M}$) can be found with the aid of Eq. (10.7) At sufficiently large values of $|\psi_0|$, this dependence can be written as

$$|\psi_2| = \text{const} + \frac{2RT}{F} \ln|\psi_0| - \frac{RT}{F} \ln c_V. \tag{10.8}$$

By definition, the total differential capacitance, C, of the EDL is given by $C \equiv dQ_{,M}/d\psi_0$. We shall introduce the notion of a capacitance of the diffuse EDL part, $C_d \equiv dQ_{S,2}/d\psi_2$. It can be calculated via Eq. (10.3), except that ψ_2 must be used instead of ψ_0.

To establish the connection between the three types of capacitance, C, C_H, and C_d, let us differentiate Eq. (10.4) with respect to $Q_{S,M}$. It follows from the result obtained that in the case being discussed, when $Q_{S,2}$ can be replaced by $Q_{S,M}$,

$$\frac{1}{C} = \frac{1}{C_H} + \frac{1}{C_d}. \tag{10.9}$$

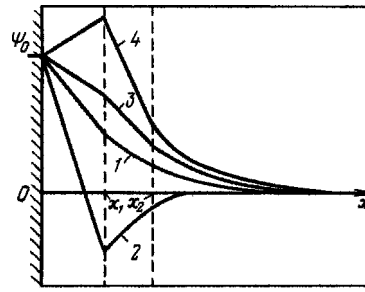

FIGURE 10.3 Potential–distance plots in EDL with specific adsorption of ions.

Therefore, electrically the EDL can be likened to a network of two capacitances, C_{H} and C_d, connected in series. The total capacitance is lower than that of the smaller component. Considering that C_{H} depends little on potential while C_d varies as shown in Fig. 10.2, the relations between total capacitance C and potential obtained at different concentrations are in good agreement with the experimental data shown in Fig. 10.1*a*. At very high concentrations and high $|\psi_0|$, the diffuse EDL part is compressed, the capacitance C_d increases, and the total capacitance C tends toward the limiting value of C_{H}.

Specific adsorption of ions from the solution occurs at the inner Helmholtz plane. Depending on the sign of charge of the specifically adsorbing ions and on adsorption strength, different types of potential distribution in the EDL are possible (Fig. 10.3). When ions become adsorbed which carry charge opposite in sign to $Q_{S,\mathrm{M}}$, the potential gradient in the inner Helmholtz layer between $x = 0$ and $x = x_1$ will increase in absolute value (curve 1). When specific adsorption is appreciable, a change in the sign of surface charge is possible; this occurs when the charge density of opposite sign at the inner Helmholtz plane is larger than the charge density of the metal surface (curve 2). In this case the sign of ψ_1 is opposite to that of ψ_0, and the diffuse EDL part must compensate for this surplus charge $|Q_{S,1} - Q_{S,\mathrm{M}}|$. When the specifically adsorbed ions have charge of the same sign, the potential gradient in the Helmholtz layer decreases (curve 3), and it may even change sign (curve 4).

Specific adsorption of ions changes the value of E_{zc}; hence, one distinguishes the notion of a point of zero charge, E_{zc}, in solutions of surface-inactive electrolytes, which depends on the metal, from that of a point of zero charge, $E_{\mathrm{zc,ads}}$, in solutions of surface-active ions, which in addition depends on the nature and concentration of these ions. The difference between these quantities,

$$E_{\mathrm{zc,ads}} - E_{\mathrm{zc}} = -\chi^{(E)}_{\mathrm{ads}}, \tag{10.10}$$

is the adsorption potential drop of the ions at the uncharged surface (this potential drop is opposite in sign to the change in E_{zc} value).

Quantitative calculations are beset by a number of difficulties when specific adsorption occurs. Since the ions at the inner Helmholtz plane are localized (contrary to those at the outer Helmholtz plane, which are "smeared out"), it is not correct to

define a unique potential ψ_1 for all points in this plane. Instead, one must allow for a discrete distribution of charges and potential along the surface. As a rule, the micropotential $\psi_{1(0)}$ at a point of the inner Helmholtz plane that is not occupied, and to which an ion can be transferred from the solution, is lower (in absolute value) than the averaged macropotential ψ_1 that would be observed for delocalized charge. The effect of discreteness can be characterized quantitatively by the factor $\lambda \equiv \psi_{1(0)}/\psi_1$; this is unity for delocalized charge, and decreases with increasing discreteness-of-charge effect. An important result of discreteness is weaker repulsive interaction between adsorbed ions of like charge. This leads to higher values of the adsorption coefficients and to a stronger dependence of adsorption on bulk concentration.

10.2 ADSORPTION PHENOMENA

10.2.1 Types of Adsorption

Many electrochemical phenomena and processes are to a great extent influenced by different adsorption processes. Of prime importance is the adsorption on the electrode's surface of components of the electrolyte solution, as well of those participating in the electrode reaction, as those "inert" components that do not participate.

The amount of species of the adsorbed substance j (adsorbate) per unit area of the true surface area of the electrode or of any other adsorbent will be labeled A_j and will be called *real adsorption* (in contrast to the notion of Gibbs adsorption Γ_j; see Section 10.4.1). In the limiting case, all adsorbed particles are packed right again the adsorbent's surface. This limiting case is called *monolayer adsorption*. In other cases, several layers of the adsorbate can form on the adsorbent's surface (*multilayer adsorption*).

When the component j can exist in both phases (e.g., the electrolyte and the electrode) it will undergo redistribution after the phases have come into contact, and in particular, some of it will be transferred into the interior of the phase, where none of it had existed previously. In this case the term *absorption* (or bulk uptake) is used for the component.

When the two phases in contact are condensed phases and the entire volume is taken up by incompressible substances, positive adsorption of one component must be attended by negative adsorption (desorption) of other components. This phenomenon is called *adsorptive displacement*.

In the case of monolayer adsorption, a limiting adsorption value exists that is attained when the surface is covered completely by particles of a given substance (i.e., at full monolayer coverage). The limiting adsorption value A_j^0 depends on the effective surface area S_j taken up by one particle: $1/S$. This parameter characterizes the number of sites that can be occupied by adsorbed particles on a given surface.

A convenient parameter for quantitative estimates of adsorption which is of the monolayer type is the degree of surface coverage defined by the relation

$$\theta \equiv \frac{A_j}{A_j^0} \qquad (1 \geq \theta \geq 0). \tag{10.11}$$

In any particular case, the adsorption value depends on the properties of both the adsorbate (its *adsorbability*) and the adsorbent (its *adsorptive power*). Substances with enhanced adsorbability are called *surface active*. By convention, adsorption is regarded as insignificant when $\theta < 0.1$, and as significant when $\theta > 0.5$.

10.2.2 Adsorption energy

Adsorption of any component in the interphase is attended by a change in Gibbs energy and in enthalpy of the system (i.e., work $w_{\text{ads},j}$ is performed and heat $q_{\text{ads},j}$ is evolved). The adsorption energy is the algebraic sum of all energy effects associated with (1) the formation of adsorbent–adsorbate bonds, (2) the desorption of other components, (3) bond breaking (e.g., in the dissociation or dehydration of adsorbate molecules), and (4) other types of system reorganization.

The (unbalanced) forces acting in surface layers are diverse in their intensities and character. Physical (van der Waals) forces between molecules are weak and give rise to slight energy effects (up to 20 kJ/mol). These forces decrease slowly with increasing distance (i.e., they operate within a relatively wide region) and are responsible for weak physical (often multiplayer) adsorption.

Unlike the van der Waals forces, chemical forces decay rapidly with increasing distance and are highly localized; they represent the chemical interaction between surface atoms (or ions) of the adsorbent and the adsorbate particles. These forces are strong; the energies of the bonds formed can be as high as 400 to 500 kJ/mol. Hence, in these cases adsorption is mostly of the monolayer type, and it is often attended by chemical changes such as adsorbate dissociation. Thus, when adsorbed on a bare platinum surface, molecular hydrogen will dissociate into atoms, and each atom adsorbed is covalently bonded to one surface atom of the platinum lattice:

$$2\text{Pt}^{(s)} + \text{H}_2 \rightarrow 2\text{Pt}^{(s)} - \text{H}_{\text{ads}}. \tag{10.12}$$

Adsorption due to the operation of chemical forces is called *chemisorption*. A typical example of chemisorption is also the adsorption of methanol on platinum electrodes, which is accompanied by a deep destruction of the methanol molecule.

10.2.3 Reversible and Irreversible Adsorption

Depending on the nature of the system, the adsorption process can be either reversible or irreversible. In the first case an adsorption equilibrium exists between the particles adsorbed on the adsorbent's surface and the particles in the electrolyte (or in any other phase contacting with the adsorbent). After removing the substance from the electrolyte, adsorbed particles leave the surface and reenter into the electrolyte. In the case of an irreversible adsorption, the adsorbed particles remain at the surface even if their concentration in the bulk phase drops to zero. In this case the adsorbed particles can be removed from the surface only by means of a chemical reaction

(e.g., their oxidation by oxygen) or by a displacement process during the adsorption of other substances. Processes of physical adsorption are often reversible, wheras processes of chemisorption are mostly irreversible.

10.2.4 Adsorption Isotherms

The adsorption of a component j in a given system depends on temperature T and on the component's concentration, $c_{V,j}$, in the bulk phase. The overall adsorption equation can be written as $A_j = f(T, c_{V,j})$. The relation between adsorption and the adsorbate's bulk concentration (or pressure, in the case of gases) at constant temperature is called the *adsorption isotherm*; the relation between adsorption and temperature at constant concentration is called the *adsorption isobar*. From the shape of the adsorption isotherms, the adsorption behavior can be interpreted. In the case of monolayer adsorption, the isotherms are usually written in the form $\theta_j = f(c_{V,j})$. (The subscript j is dropped in what follows.)

Henry Isotherm In the simplest case, the degree of surface coverage is proportional to the bulk concentration:

$$\theta = Bc_V. \tag{10.13}$$

An analogous law was established in 1803 by W. Henry for the solubilities of gases in water; hence, this expression is called the *Henry isotherm*. The adsorption coefficient B (units: dm^3/mol) depends on the heat of adsorption: $B = B^0 \exp(q_{ads}/RT)$. The Henry isotherm is valid for low surface coverages (e.g., at $\theta < 0.1$).

Langmuir Isotherm At higher values of θ, when the number of free sites on the surface diminishes, one often observes relations of the form

$$\theta = Bc_V(1 + Bc_V) \quad \text{or} \quad \theta(1 - \theta) = Bc_V. \tag{10.14}$$

At low values of the bulk concentration ($Bc_V \ll 1$), the degree of surface coverage is proportional to this concentration, but at high values it tends toward a limit of unity. This equation was derived by Irving Langmuir in 1918 with four basic assumptions: (1) the adsorption is reversible; (2) the number of adsorption sites is limited, and the value of adsorption cannot exceed A^0; (3) the surface is homogeneous: all adsorption sites have the same heat of adsorption and hence, the same coefficient B; and (4) no interaction forces exist between the adsorbed particles. The rate of adsorption is proportional to the bulk concentration and to the fraction $1 - \theta$ of vacant sites on the surface: $v_a = k_a(1 - \theta)$, while the rate of desorption is proportional to the fraction of sites occupied: $v_d = k_d\theta$. In the steady state these two rates are equal. With the notation $k_a/k_d = B$, we obtain Eq. (10.14).

Temkin Isotherm Numerous departures of the experimental data from the Langmuir isotherm can be explained in terms of insufficient arguments for the third

Irving Langmuir (1881–1957; Nobel prize, 1932).

and fourth assumptions. In 1939, Mikhail I. Temkin[+] examined the case of *uniform surface inhomogeneity*, where the heats of adsorption associated with different sites are different and range from a maximum value q_0 to a minimum value q_1 (B varies between the values B_0 and B_1), while the various values for the heat of adsorption are equally probable in this interval. The surface can be characterized by a dimensionless inhomogeneity factor $f \equiv q_0 - q_1$. It follows from the solution obtained by Temkin that for $f \geq 5$ in the range of intermediate degrees of coverage $0.8 \geq \theta \geq 0.2$,

$$\theta = g + \frac{1}{f} \ln c_V \quad \text{or} \quad \exp(f\theta) = B_0 c_V, \tag{10.15}$$

where $g \equiv (1/f)B_0$. This equation is called the *logarithmic Temkin isotherm*.

Michail I. Temkin (1908–1991).

[+] Pronounced as "Tyomkin."

Frumkin Isotherm In 1928, Frumkin derived an equation for interaction between the adsorbed particles. Mutual attraction leads to an increase in the heat of adsorption, whereas repulsion leads to a decrease. Quantitatively, these effects depend on the degree of surface coverage and can be written as $q_\theta = q_0 - f_{\text{int}} RT\theta$, where f_{int} is an interaction factor that has positive values when there is repulsion, and negative values when there is attraction between the particles (often, the attraction constant $\alpha \equiv -f_{\text{int}}/2$ is used instead of the factor f_{int}). As a result, an isotherm of the form

$$\frac{\theta}{1-\theta}\exp(f_{\text{int}}\theta) = B_0 c_V \tag{10.16}$$

is obtained. At values of $f_{\text{int}} \geq 5$ and intermediate degrees of coverage ($0.8 \geq \theta \geq 0.2$), this equation practically coincides with the equation of the Temkin isotherm. This implies that strong repulsive forces have the same effect as uniform surface inhomogeneity. Hence, from the shape of an experimental adsorption isotherm, one cannot deduce the reasons for departure from the Langmuir isotherm.

10.2.5 Adsorption in Electrochemical Systems

Adsorption phenomena at electrode–electrolyte interfaces have a number of characteristic special features.

Adsorption of Reaction Components In many cases, adsorption of a reactant is one of the first steps in the electrochemical reaction, and precedes charge transfer and/or other steps of the reaction. In many cases, intermediate reaction products are also adsorbed on the electrode's surface. Equally, the adsorption of reaction products is possible. The example of the adsorption of molecular hydrogen on platinum had been given earlier. Hydrogen adsorption is possible on the platinum electrode in aqueous solutions even when there is no molecular hydrogen in the initial system; at potentials more negative than 0.3 V (RHE), the electrochemical reaction

$$\text{Pt}^{(s)} + \text{H}^+ + e^- \rightleftharpoons \text{Pt}^{(s)} - \text{H}_{\text{ads}} \tag{10.17}$$

proceeds, which yields hydrogen atoms adsorbed on the surface. This is a transient process ending when a certain (potential-dependent) value of θ_{H} is attained. In exactly the same way, at more positive potentials electrochemical oxygen adsorption

$$\text{Pt}^{(s)}\text{H}_2\text{O} \rightleftharpoons \text{Pt}^{(s)} - \text{OH}_{\text{ads}} + \text{H}^+ + e^- \rightarrow \text{PtO}_{\text{ads}} + \text{H}^+ + e^- \tag{10.18}$$

proceeds on platinum and many other metals.

The adsorption of reaction components can be strongly influenced by the electrode potential. Ions, neutral molecules, and various radicals can be adsorbed in one potential region and displaced from the surface in another region.

Inasmuch as the electrode's surface is covered completely by adsorbed solvent molecules (see Section 10.2.5.3), the adsorption of other components is possible only upon desorption of part of the solvent molecules.

Partial Charge Transfer Specific adsorption of ions is often attended by a partial transfer of their charge to the metal surface: for instance, in the specific adsorption of cations M^{z+} on platinum

$$M^{z+} + \lambda e^- + Pt \rightarrow Pt-M^{(z-\lambda)}, \tag{10.19}$$

where λ is the degree of charge transfer. Complete charge transfer $\lambda = z$ corresponds to the ion's complete discharge yielding an atom M adsorbed on the surface (i.e., an adatom). Partial charge transfer is possible, too, in the adsorption of neutral species when a (partly charged) adsorbed ion (i.e., an adion) is formed. The formation of hydrogen atoms adsorbed on platinum, which occurs as a result of hydrogen ion discharge, can be regarded as an example for almost complete charge transfer. The resulting Pt–H bonds are slightly polar, hence the degree of charge transfer is still somewhat different from unity. The degree of charge transfer, λ, cannot be calculated thermodynamically directly from experimental data, and therefore difficulties arise in defining the concept of surface charge $Q_{S,M}$.

Interaction of Metals with Solvents (Solvent Adsorption) Up to the 1950s, it was believed that in solutions of completely inactive electrolytes, the influence of solvents on the properties of the metal–solution interface was determined exclusively by the solvent's dielectric constant, the diameter of its molecules, and the energy of solvation of the ions by it. If this was true, then in solutions of indifferent electrolytes in a given solvent, electric double-layer structure should not depend on the metal. This means that all conditions listed in Section 9.4.1 are fulfilled and that the difference between the potentials of zero charge between two given metals (or between their potentials at a given surface charge density Q_S) would in all solvents be given by their work function difference, according to Eq. (9.13). It was seen in studies of *d*-metals in aqueous solutions as well as in solutions prepared with other solvents, however, that the solvent cannot a priori be regarded as an inert solution component.

When an electrode comes in contact with an electrolyte solution, then apart from a possible adsorption of different solution components, another phenomenon occurs (i.e., a certain orientation of all dipolar solvent molecules that are close to the surface, with respect to this surface). Sometimes this is discussed as solvent adsorption including the formation of a monolayer of solvent molecules at the surface.

The reason for such an orientation of the solvent molecules is a chemical interaction between the metal surface and the functional groups of these molecules. This interaction is more pronounced the higher the solvent's donor number and (for *d*-metals) the higher the metal's work function. This is an experimental finding pointing to donor–acceptor interactions. Here the solvent molecules function as the electron donor and the electrode functions as the electron acceptor. Metals exhibiting strong interaction with the solvent molecules have been named *lyophilic* or, with water as the solvent, *hydrophilic*. Metals exhibiting weak interaction accordingly are known as *lyophobic* and *hydrophobic*, respectively.

As a result of interaction between the metal and the OH^- groups of water molecules (or the negative functional groups of other solvent molecules), these molecules take up an orientation with the negative ends of their dipoles toward the metal and the positive ends toward the bulk solution. Thus, an additional electric double layer is formed on the surface, giving rise to a negative surface potential $\chi^{(or)}$ that becomes one of the components of the potential difference between the metal and the solution.

The interactions depend on the sign and density of the metal's surface charge Q_S. They increase with increasing positive charge of the metal surface, and decrease (or vanish altogether) with increasing negative charge. A change in orientation of the solvent molecules with respect to the surface is possible when, as the potential changes, the metal's surface charge changes sign.

It is not possible to measure the orientation potential $\chi^{(or)}$ directly. Hence the following approach is taken to arrive at a relative quantitative characterization of the degree of interaction between different metals and solvents. For two metals (the test metal and a standard or reference metal), the relation between surface charge density Q_S and the potential is determined in a given solvent (e.g., by integrating curves representing plots of differential capacitance vs. potential). A relatively hydrophobic (lyophobic) metal is selected as the standard. Then potential differences $(\Delta E)_Q$ between the two metals at given values of surface charge Q_S are determined for a number of values of Q_S. At strongly negative values of Q_S ($Q_S \ll 0$), the interactions between metals and solvents vanish. The relative degree of hydrophilicity (lyophilicity) of a given metal relative to the standard at different values of Q_S is reflected in the differences $(\Delta E_Q - \Delta E_{Q \ll 0})$. This is a rather rough estimate of the degree of interaction, yet it is quite instructive. The most lyophobic *d*-metals are mercury and thallium; among the most lyophilic we find gallium, indium, cadmium, and the (111) face of silver single crystals. Among the solvents studied, dimethyl sulfoxide and water belong to the most active, and acetonitrile and propylene carbonate are among the most highly indifferent.

The interactions between electrode metals and solvents are reflected in the adsorption and catalytic properties. The adsorption of other solution components (ions and neutral molecules other than the solvent) is attended by a displacement of adsorbed solvent molecules or their reorientation. Therefore, a metal's adsorptive power is low under conditions where its energy of interaction with the solvent is high.

The interaction of metals with the OH^- groups in water molecules is attended by a stretching of the H–OH bonds, which raises the donor properties of these water molecules and serves to accelerate electrochemical reactions with a slow step that involves hydrogen. This was confirmed in the electroreduction of anions NO_3^-, BrO_3^-, and the like on metals exhibiting varying degrees of hydrophilicity.

10.3 THERMODYNAMICS OF SURFACE PHENOMENA

This section is based on concepts developed by Josiah Willard Gibbs in 1874–1878 [see also Guggenheim (1933) and Delahay (1965)].

Josiah W. Gibbs (1839–1903).

10.3.1 Surface Excesses of Substances

The thickness of the surface layer is usually measured in nanometers or fractions of a nanometer. There is a smooth change in properties as one moves from the surface into the interior of a phase; hence, one cannot exactly define the limits of the surface layer or its thickness. This gives rise to difficulties in the layer's quantitative characterization. For this reason in thermodynamic discussions of surface phenomena, another parameter is often used to characterize adsorption processes. To circumvent the difficulty, the outer limits of the interphase (Fig. 10.4, the planes with coordinates x_α and x_β) are deliberately positioned beyond the region affected by the superficial perturbations. In the interphase itself a conditional dividing plane, called the *Gibbs surface* (with the coordinate x_γ), is selected. The state of the real layer [with superscript $^{(s)}$] is compared with that of an idealized layer having the same thickness but properties which, in each of the phases, remain unchanged right up to the Gibbs surface [i.e., a layer without changes; superscript $^{(id)}$]. The concept of *surface excesses* [with superscript $^{(\sigma)}$] of substances in the real layer relative to the ideal layer is introduced:

$$n^{(\sigma)} \equiv n^{(s)} - n^{(id)}. \tag{10.20}$$

Surface excesses are usually referred to the unit surface area of the dividing plane S (surface excess densities).

The number of moles n_j of component j in the real interphase is given by $n_j = S\int_{x\alpha}^{x\beta} c_j^{(s)} dx$, and that in the ideal layer is given by $n_j^{(id)} = S[c_j^{(\alpha)}(x_{(\gamma)} - x_{(\alpha)}) + c_J^{(\beta)}(x_\beta - x_\gamma)]$. We thus obtain an equation for the surface excess, $\Gamma_j \equiv n_j^{(\sigma)}/S$ (units: mol/cm^2), of a substance per unit surface area:

$$\Gamma_j = \int_{x\alpha}^{x\beta} c_j^{(s)} dx - [c_j^{(\alpha)}\,(x_{(\gamma)} - x_{(\alpha)}) + c_J^{(\beta)}(x_\beta - x_\gamma)]. \tag{10.21}$$

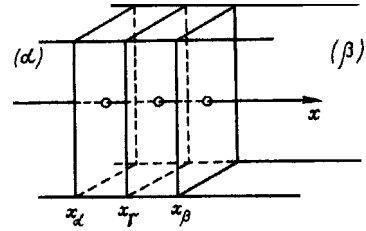

FIGURE 10.4 Coordinates of interphase boundaries and Gibbs surface.

The parameter $n_j^{(s)}$ always has positive values, whereas the parameters $n_j^{(\sigma)}$ and Γ_j can have positive or negative values. Parameter Γ_j is called the *Gibbs adsorption* or *Gibbs surface excess*.

The adsorption value given by Γ_j is independent of the position selected for the outer limits of the interphase; even when the limits are pushed too far into a phase, in the corresponding regions $c_j^{(s)}$ is equal to $c_j^{(\alpha)}$ (or $c_j^{(\beta)}$), and the value of Γ_j remains unchanged.

However, the value of Γ_j depends on the position of the Gibbs surface. By common convention, this position is selected so that for one of the components (with the index $j = 0$), the value of Γ_j defined by Eq. (10.21) will become zero. The solvent is chosen in this capacity when one of the phases in contact is a solution. Once the position of the Gibbs surface has been fixed, one can unambiguously determine the Gibbs surface excesses of the other components. The adsorption of a component j is thus defined relative to the component $j = 0$ (*relative Gibbs surface excess* $\Gamma_{j(0)}$).

More commonly used is another definition of Gibbs surface excesses, according to which Γ_j is equal to the amount of substance j that must be added to the system (with a constant amount of the substance $j = 0$) so that the composition of the bulk phases will remain unchanged when the interface area is increased by unity. This definition can also be used when chemical reactions take place in the surface layer. In the case discussed here, the two definitions coincide. The set of surface excesses of all components is sometimes called the *surface phase* (in contrast to the *real surface layer* or *interphase*).

10.3.2 Excess Surface Energy

By analogy to Gibbs surface excesses of substances, we can define the excess Gibbs energy of the surface layer of phase (α) at an interface with another phase (β), which, when referred to unit surface area of the phase, is called the *excess surface energy* (ESE) of this phase (units: J/cm^2) and designated as σ (or, if necessary, as $\sigma^{(\alpha,\beta)}$). When calculating the surface excesses of the Gibbs energy, the position of the Gibbs surface is maintained as described above.

By definition, ESE is the work that must be performed to form a unit area of new surface while preserving all other parameters (e.g., the amount n of all components):

$$\sigma \equiv \left(\frac{\partial G^{(\sigma)}}{\partial S}\right)_n. \tag{10.22}$$

For stable interfaces, the values of σ are always positive.

Because of ESE, and because of the real forces acting on the particles in the surface layer, there is a tendency for spontaneous contraction of the interfacial area. In practice, such a contraction can be realized only in the case of liquid phases, where the particles can move freely relative to each other. Hence, liquids tend to assume spherical shape with a minimum ratio of surface area to volume (liquid drops), at least when the volume is small and gravitation does not interfere, and when they are not in contact with solid surfaces.

The tendencies of liquid surfaces to contract had in the past been regarded as the result of forces acting along the surface and causing it to contract (like an elastic film enveloping the liquid). This was the origin of the term *surface tension* still used today. The surface tension is stated as a force acting over unit length (units: N/m); for liquids, it coincides numerically with the value of ESE stated in the units of J/m^2 ($1\ J = 1\ N{\cdot}m$). The concept of surface tension is convenient for visualization of certain phenomena. However, it can merely convey the essence of the phenomena conditionally, since the real forces act in a direction perpendicular to the surface and not along the surface.

10.3.3 Gibbs Adsorption Equation

At constant temperature and pressure the excess Gibbs energy of the surface layer depends on surface area S and on the composition of the layer (i.e., on the excess amounts $n_j^{(\sigma)}$ of the components). When there are changes in surface area and composition (which are sufficiently small so that accompanying changes in parameters σ and $\mu_j^{(\sigma)}$ can be disregarded), we have

$$dG^{(\sigma)} = \left[\frac{\partial G^{(\sigma)}}{\partial S}\right]_{n_j} dS + \Sigma\left[\frac{\partial G^{(\sigma)}}{\partial n_j^{(\sigma)}}\right]_S dn_j^{(\sigma)}$$

$$= \sigma S + \Sigma\, \mu_j^{(\sigma)}\, dn_j^{(\sigma)}. \tag{10.23}$$

Parameter $G^{(\sigma)}$ is an additive function of surface area and of the amount of components:

$$G^{(\sigma)} = \sigma S + \Sigma\, n_j^{(\sigma)} \mu_j^{(\sigma)}. \tag{10.24}$$

Subtracting Eq. (10.23) from the exact differential of Eq. (10.24), we find that

$$S\, d\sigma + \Sigma\, n_j^{(\sigma)}\, d\mu_j^{(\sigma)} = 0. \tag{10.25}$$

This equation for the surface excesses is the analog of the Gibbs–Duhem equation for bulk phases.

Thermodynamic discussions of surface-layer properties rely on the assumption of adsorption equilibrium (i.e., on the assumption that for each component the chemical potential in the surface layer is equal to that in the bulk phase, $\mu_j^{(\sigma)} = \mu_j^{(V)}$). When

substituting into Eq. (10.25) the bulk value of chemical potential and dividing all terms into S, we obtain the *Gibbs adsorption equation*, which is a very important equation of surface-layer thermodynamics:

$$-d\sigma = \Sigma\, \Gamma_j\, d\mu_j^{(V)} = \Sigma\, RT\Gamma_j\, d\ln a_j, \tag{10.26}$$

or when the system is ideal and adsorption is possible for only one component,

$$-d\sigma = -\sigma\Gamma\, RT\, d\ln c. \tag{10.27}$$

10.3.4 Electrocapillary Curves

When the Gibbs equation is used for an electrode–electrolyte interface, the charged species (electrons, ions) are characterized by their electrochemical potentials, while the interface is regarded as electroneutral; that is, the surface density, $Q_{S,\mathrm{M}}$, of excess charges in the metal caused by positive or negative adsorption of electrons $Q_{S,\mathrm{M}} = F\Gamma_e$ (in what follows called *surface charge* for the sake of brevity) is regarded as equal in size but opposite in sign to the charge, $Q_{S,\mathrm{E}} = F\Sigma z_j\Gamma_j$, in the solution's surface layer:

$$Q_{S,\mathrm{M}} = -Q_{S,\mathrm{E}} = -F\Sigma\, z_j\Gamma_j. \tag{10.28}$$

The Gibbs equation for metal–electrolyte interfaces is of the form

$$-d\sigma = \Gamma_e\, d\bar{\mu}_e + \Sigma\ \Gamma_j\, d\bar{\mu}_j \tag{10.29}$$

For charged species we have $d\bar{\mu}_j = d\mu_j + z_jF\psi$ when taking into account Eq. (3.17). For the electrons in the metal (which have a constant concentration), $d\mu_e = 0$. The Galvani potential at the interface considered is given by $\varphi_{\mathrm{G}} = \psi^{(\mathrm{M})} - \psi^{(\mathrm{E})}$. Using these relations as well as equality (10.28), we can transform Eq. (10.29) to

$$-d\sigma = Q_{S,\mathrm{M}}\, d\varphi_{\mathrm{G}} + \Sigma\,\Gamma_j\, d\mu_j. \tag{10.30}$$

The equation obtained can be used when the electrode potential can be varied independent of solution composition (i.e., when the electrode is ideally polarizable). For practical calculations we must change from the Galvani potentials, which cannot be determined experimentally, to the values of electrode potential that can be measured: $E = \varphi_{\mathrm{G}} + \mathrm{const}$ (where the constant depends on the reference electrode chosen and on the diffusion potential between the working solution and the solution of the reference electrode). When a constant reference electrode is used and the working solutions are sufficiently dilute so that the diffusion potential will remain practically constant when their concentration is varied, $dE \approx d\varphi_{\mathrm{G}}$ and

$$-d\sigma = Q_{S,\mathrm{M}}\, dE + \Sigma\,\Gamma_j\, d\mu_j. \tag{10.31}$$

When measurements are performed in solutions of a particular constant composition (where evidently, $\mu_j = \text{const}$ and $d\mu_j = 0$), we have

$$Q_{S,\text{M}} = -\left(\frac{\partial\sigma}{\partial E}\right)_{\mu}. \tag{10.32}$$

This equation was first obtained by Gabriel Lippmann in 1875. The *Lippmann equation* is of basic importance for electrochemistry. It shows that surface charge $Q_{S,\text{M}}$ can be calculated thermodynamically from data obtained when measuring ESE. The values of ESE can be measured with high accuracy on liquid metals [e.g., on mercury ($t_f = -39°\text{C}$)] and on certain alloys of mercury, gallium, and other metals that are liquid at room temperature.

The simplest device for measuring ECC at mercury is Gouy's capillary electrometer (Fig. 10.5). Under the effect of a mercury column of height h, mercury is forced into the slightly conical capillary K. In the capillary, the mercury meniscus is in contact with electrolyte solution E. The radius of the mercury meniscus is practically equal to the capillary radius r_{K} at that point. The meniscus exerts a capillary pressure $p_{\text{K}} = 2\sigma^{(\text{Hg,E})}/r_{\text{K}}$ directed upward which is balanced by the pressure $p_{\text{Hg}} = h\rho_{\text{Hg}}g$ of the mercury column (g is the acceleration of gravity); hence,

$$\sigma^{(\text{Hg,E})} = \frac{h\rho_{\text{Hg}}r_{\text{K}}g}{2}. \tag{10.33}$$

When potential is applied, the meniscus moves, owing to the resulting change in surface tension. By varying the height of the mercury column during the measurements

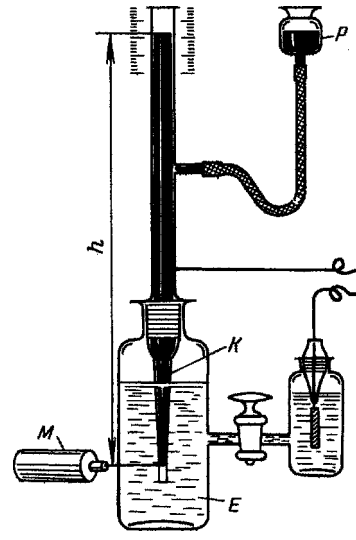

FIGURE 10.5 Gouy's capillary electrometer.

(which is done by raising or lowering the reservoir R), one returns the meniscus to its original position, which is checked with the aid of a horizontal microscope M. Thus, the meniscus radius remains constant and the value of $\sigma^{(Hg,E)}$ measured is proportional to mercury column height. For calibration of the instrument it will suffice to make a single measurement under conditions where $\sigma^{(Hg,E)}$ is known (in solutions of surface-inactive electrolytes at the PZC at 18°C, it has the value 42.67 μJ/cm^2).

Several methods exist that can be used to measure changes of ESE for solid electrodes as a function of potential or other factors, but the accuracy of such measurements is much lower than that for liquid electrodes. A plot of ESE vs. potential is called the *electrocapillary curve* (ECC). Typical ECCs measured at a mercury electrode in NaF solutions of different concentration are shown in Fig. 10.6. Also shown in this figure is a plot of $Q_{S,M}$ values vs. potential calculated via Eq. (10.27). This plot almost coincides with that obtained from capacitance measurements (Fig. 10.1*b*). This is evidence for the mutual compatibility of results obtained by these two methods of measurement.

Electrocapillary curves have a maximum. At this point, according to Eq. (10.32), the surface charge $Q_{S,M} = 0$. The potential, E_{zc}, of the maximum is called the *point of zero charge* (PZC). Knowing the charge density $Q_{S,M}$, one can calculate the interfacial potential $\Phi^{(M,E)}$ contained in Eq. (10.1). This is insufficient, however, for a calculation of the total Galvani potential, since other terms in this equation cannot be determined experimentally.

It is a typical special feature of electrochemical systems that the ESE values of interfaces between two conducting phases depend on the potential difference between them. The excess charge densities in the surface layer of each of the phases change with potential. The coulombic repulsion forces acting between excess charges of like sign along the surface counteract the tendency of the surface to contract and reduce the ESE. Therefore, the ESE will be lower the higher the charge density is in the interphase.

Let us consider the case when measurements are made in a binary solution containing only two types of ion (with the charge numbers z_+ and z_-) and when a

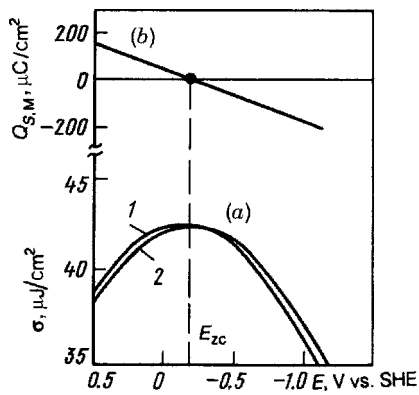

FIGURE 10.6 (*a*) Electrocapillary curve of mercury in NaF solutions: (1) 0.01 *M*, (2) 0.1 *M*; (*b*) plot of surface charge density vs. potential calculated from curve 2.

reference electrode reversible in respect to the anion and containing the same solution is used. In this case there is no diffusion potential. For the reference electrode it follows from Eq. (2.11) that $d\varphi_{RE} = \mu_-/z_-F$. The differential of electrode potential (here designated as E_-) is given by $dE_- = d\varphi_G - d\varphi_{RE}$, and the surface charge density of the metal by $Q_{S,M} - F[z_+\Gamma_+ + z_-\Gamma_-]$. Substituting these expressions into Eq. (10.25) and allowing for the fact that $z_+/z_- = \tau_-/\tau_+$ and [according to Eq. (3.24)] $\tau_+ d\mu_+ + \tau_- d\mu_- = RT(\tau_+ + \tau_-)\, d \ln a_\pm$, we obtain, after simple transformations,

$$-d\sigma = Q_{S,M}\, dE + \left(1 + \frac{\tau_-}{\tau_+}\right) RT\Gamma_+\, d \ln a_\pm). \tag{10.34}$$

Cation adsorption in binary solutions can be determined according to Eq. (10.34) from the relation between ESE and $a_\pm$ at a constant value of E_-:

$$\Gamma_+ = -\frac{1}{RT}\frac{\tau_+}{\tau_+ + \tau_-}\left(\frac{\partial\sigma}{\partial \ln a_\pm}\right)_{E_-}, \tag{10.35}$$

while anion adsorption can be determined from an analoguous expression for the parameter Γ_- (from measurements where a reference electrode was used that is reversible with respect to the cation).

Equations (10.34) and (10.35) are different forms of the *general equation of electrocapillarity*. The parameters contained in them can be determined experimentally. These equations can be used to calculate one set of parameters when experimental values for another set of parameters are available.

10.4 MERCURY ELECTRODE SURFACE

In the first half of the twentieth century, mercury electrodes were widely used for investigation of adsorption and other phenomena in electrochemical systems. This was due to the following features of these electrodes, connected with their liquid nature: (1) the true working surface area coincides with the geometric surface of the electrode, in contrast to solid electrodes, which always have a well-pronounced surface roughness; (2) the surface can be easily renewed (e.g., in dropping electrodes) and cleaned from impurities; (3) the ESE (surface tension) and its dependence from potential and solution composition can easily be determined. Measurements of ECC and of the differential capacitance C by ac techniques are used mostly for investigation of the mercury surface. Both methods lead to identical results: The values of $Q_{S,M}$ derived from ECC and those calculated by integrating C,E curves essentially coincide.

10.4.1 Ion Adsorption

An important aspect is that of studying the effects of composition of the electrolyte solution on the electrocapillary and capacitance curves. Identical curves are obtained for solutions of fluorides, sulfates, and certain other alkali metal salts having identical

concentrations. The PZC in such solutions is found at a potential of -0.193 V (SHE). A constant potential of the electrocapillary maximum for different solution concentrations of a salt usually implies that at the PZC, ionic adsorption is minor. At other potentials, ions are adsorbed only as a result of electrostatic interaction. Thus, no other specific (nonelectrostatic) forces of interaction exist between these ions and the mercury surface; they are surface inactive. Experience shows that surface activity is absent (or at least very low) in the case of ions F^-, OH^-, SO_4^{2-}, HCO_3^-, and most inorganic cations. The halide ions Cl^-, Br^-, I^-, and a number of additional anions, as well as cations Tl^+ and NH_4^+, are surface active; they interact chemically with the mercury surface.

Specific adsorption of ions influences the shape of ECC and capacitance curves. Figure 10.7 shows the ECC for halide solutions. Anion adsorption depresses the ascending branch of the curves, which corresponds to positive surface charge. At negative potentials (starting from a potential about 0.2 V more negative than the PZC), the ECC for other halides practically coincide with the curve for fluoride, which implies that in this region the electrostatic repulsion forces prevail over the chemical attraction forces, and the anions are desorbed from the surface. The maximum value of ESE decreases, and the PZC shifts to potentials more negative than the PZC of NaF solution. For 0.9 *M* NaI solution, the value of $E_{zc,ads}$ is about -0.6 V (i.e., the PZC has shifted by more than 0.4 V). This shift is due to formation of an additional adsorptive EDL consisting of specifically adsorbed anions at the inner Helmholtz plane and an equivalent number of cations distributed diffusely in the solution. Ionic adsorption at the PZC amounts to 1.4×10^{-5} mol/m^2, which corresponds to a charge density of 14 μC/cm^2. As a result, an additional component of the solution's surface potential arises: the adsorption potential χ_{ads}. In NaI solutions, the mercury surface is positively charged at potentials between -0.2 and -0.6 V (in contrast to NaF solutions).

The effects of the anions (i.e., their specific adsorbabilities) increase in the order $F^- < Cl^- < Br^- < I^-$. This trend is due to the fact that the solvation energy decreases with increasing crystal radius as one goes from F^- to I^-, and the transfer of the ions to the inner Helmholtz plane is facilitated accordingly. The opposite picture is seen for surface-active cations (e.g., $[N(C_4H_9)_4]^+$); the descending branch of the ECC is depressed, and the PZC shifts in the positive direction.

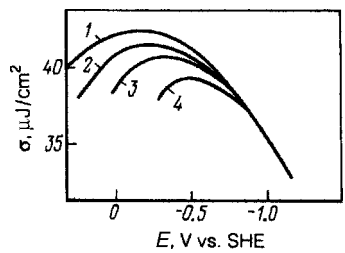

FIGURE 10.7 Electrocapillary curves for a mercury electrode in 0.9 *M* solutions: (1) NaF; (2) NaCl; (3) NaBr; (4) NaI.

Anion adsorption also influences the shape of the capacitance curves. In the region of the PZC and at positive surface charge, the capacitance increases to values of 60 to 80 μF/cm^2 as EDL thickness drops to a value of x_1. The capacitance minimum in dilute solutions is distorted, and its position no longer coincides with that of the PZC.

10.4.2 Adsorption of Organic Substances

Many neutral organic substances containing functional groups (e.g., the alcohols) are surface active and adsorb on the mercury electrode. Figure 10.8*a* and *b* show how the ECC and capacitance curves change when *n*-butyl alcohol is added to the solution. It follows from these curves that adsorption of the alcohol molecules (which lowers the ESE) occurs in a region around the PZC. The organic particles become desorbed when the potential is made much more positive or negative, and then the curves coincide with those of the base–electrolyte solution. The potential of the PZC is shifted in the positive direction. It appears that the alcohol molecules, which are dipolar, have an orientation at the metal surface that is with the negative ends (the −OH groups) away from the surface. In other cases (e.g., in phenol adsorption),

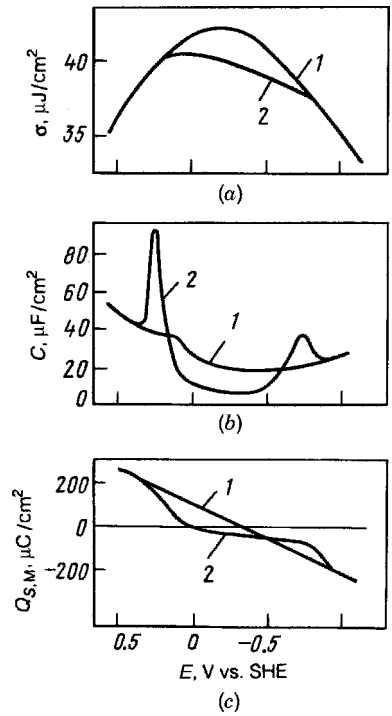

FIGURE 10.8 Influence of the adsorption of organic substances (*a*) on the electrocapillary curve, (*b*) on the capacitance curve, and (*c*) on the plot of surface charge against potential: (1) 0.1 *M* H_2SO_4 solution; (2) the same, with 0.1 *M* C_4H_9OH.

the PZC shifts in the negative direction, which indicates that the adsorbing molecules have the opposite orientation.

The values of EDL capacitance are strongly depressed in the region where the organic substances are adsorbed, which indicates that their molecules are wedged in between the metal surface and the solution side of the EDL. On the one hand, this leads to larger distances x_2; on the other hand, the value of ε in the compact EDL part decreases.

A typical feature is that of the sharp capacitance peaks appearing at the limits of the adsorption region of organic molecules: the adsorption or desorption peaks. They facilitate an accurate determination of the adsorption region. They arise because of the drastic change in distance x_2 that occurs over a very narrow potential interval during the adsorption or desorption of the organic substance (i.e., when the metal surface changes from covered to free, or vice versa). In this narrow region, therefore, there is a drastic change in EDL charge density, which is equivalent to a high capacitance value (Fig. 10.8*b* and *c*).

Desorption of the organic molecules at potentials where $Q_{S,\mathrm{M}}$ is large is due to a phenomenon known in electrostatics: In any charged electrostatic capacitor, forces are operative that tend (when this is possible) to replace a medium with a low ε value with a medium with a higher ε value. Therefore, regardless of any chemical interaction of the organic molecules with the surface, they are expelled electrostatically from the EDL at a certain value of $Q_{S,\mathrm{M}}$, and replaced by water molecules.

10.5 PLATINUM ELECTRODE SURFACE

The platinum electrode is also very convenient for investigating various adsorption phenomena in electrochemical systems. The surface of platinum is very stable and reproducible. As will be shown in what follows, the true working area can be determined with high accuracy for platinum surfaces with appreciable roughness and even for electrodes with highly dispersed platinum deposits. It is comparatively easy to clean the surface of adsorbed impurities and to control the state of the surface.

The surface of the platinum electrode can be studied conveniently in the potential range between 0 and 1.7 V (RHE), where in inert solutions (not containing substances able to be oxidized or reduced), the surface is ideally polarizable. At a more negative potential, cathodic hydrogen evolution starts, whereas at more positive potentials, oxygen is evolved anodically.

10.5.1 Electrochemical Methods for Investigating the Surface of Platinum Electrodes

When an electrode is ideally polarizable, all of the current through it is nonfaradaic (charging current) and depends on the properties of the electrode surface:

$$i = i_{\mathrm{ch}} \equiv \frac{dQ_{S,\mathrm{M}}}{dt} = C\,\frac{dE}{dt}. \tag{10.36}$$

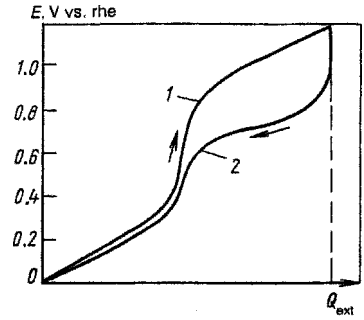

FIGURE 10.9 Galvanostatic charging curve for a platinized platinum electrode in 0.1 *M* H_2SO_4 solution: (1) anodic scan, (2) cathodic scan.

The method of galvanostatic charging curves was developed by A. Frumkin and A. I. Shlygin in 1935 for studies of platinized platinum electrodes. First, hydrogen is passed through a cell with the test electrode and an inert solution; under these conditions a layer of adsorbed hydrogen atoms is formed on the surface [reaction (10.12)] and the equilibrium hydrogen potential is established. Then nitrogen or argon are passed through the cell in order to eliminate excess molecular hydrogen, which produces a minor shift (20 to 30 mV) of electrode potential in the positive direction, but the major quantity of the adsorbed atomic hydrogen remains on the surface. Next, an anodic current of constant strength is made to pass the electrode ($i = i_{ch} = \text{const}$). The dependence of potential on time t or on the amount of charge $Q_{ext} = i_{ch}t$ that has passed the external circuit (the values of Q_{ext} are always referred to the unit surface area of the electrode) is shown in Fig. 10.9. From the slope of the curve one can determine the electrode's capacitance C. In this method there is no need for complex equipment; it is very convenient for samples with large true surface areas (highly disperse deposits, powders, etc.).

Toward the end of the 1950s, a number of workers developed methods to record potentiodynamic charging curves which proved to be convenient for electrodes with smooth surfaces but require complex equipment. Figure 10.10 shows a typical voltammogram measured at a smooth platinum electrode. Such i_{ch} vs. E curves are the

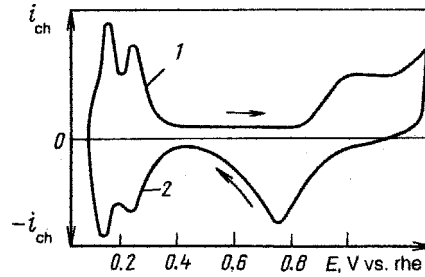

FIGURE 10.10 Potentiodynamic charging curve for a smooth platinum electrode in 0.1 *M* H_2SO_4 solution: (1) anodic scan, (2) cathodic scan.

differential forms of the galvanostatic Q_{ext} vs. E curves. They reveal certain details that are less noticeable in the integral curves.

When the solution is not quite inert, ac techniques are widely used to investigate the capacitance and other surface properties of platinum electrodes as well as of various other electrodes. Their chief advantage is the possibility to apply them in the case of electrodes passing some faradaic current. It is shown in Section 12.5.1 that in this case the electrode's capacitance can be determined by extrapolating results obtained at different ac frequencies to the region of high frequencies. This extrapolation can be used for electrodes where electrode reactions occur that have standard rate constants, k^0, of up to 1 cm/s.

10.5.2 Hydrogen Adsorption on Platinum

The galvanostatic and potentiodynamic charging curves of platinum electrodes shift approximately 60 mV in the negative direction when the solution pH is raised by 1 unit. This implies that when potentials E_r which refer to the equilibrium potential of a hydrogen electrode in the same solution (RHE) are used, these curves remain practically at the same place within a wide range of solution pH. Hence, we shall use this scale while analyzing these curves.

The galvanostatic charging curves distinctly reveal three linear sections with different slopes; in the first and third sections the slopes correspond to capacitances of 400 to 700 μF/cm^2; in the second section the slope corresponds to a capacitance of 40 to 70 μF/cm^2. The capacitance of the second section is of the same order of magnitude as that for the ideally polarizable mercury electrode. This section is called the *double-layer region*. The anodic current that passes through the electrode when its potential is at points within the other two sections is consumed not only for EDL charging but also for the electrochemical oxidation and desorption of adsorbed atomic hydrogen [reaction (10.14)] or for electrochemical oxygen adsorption [reaction (10.15)]. In the case of cathodic currents the same processes occur in the opposite directions. Because of these processes, the total electrode capacitance (the *pseudocapacitance*) is much higher than the EDL capacitance. These sections with high capacitance values correspond to sections with high currents in the potentiodynamic charging curves (see Figs. 10.9 and 10.10).

The region of atomic hydrogen adsorption stretches from 0 to 0.30–0.35 V. Hydrogen adsorption on platinum is a reversible or equilibrium process. The charging curves measured with low current densities in the hydrogen adsorption region, either in the cathodic (hydrogen deposition) or in the anodic directions, coincide. Because of its equilibrium character, hydrogen adsorption can be analyzed thermodynamically.

For absolute calculations it is necessary to refer the value of Q_{ext} to the unit area of the true surface. This area can be determined by independent methods (e.g., by the BET method). Experience shows that $Q_{ext} \approx 220$ μC/cm^2 (of true surface area) is required to shift the potential from 0 to 0.35 V. A small part of this charge (about 10 μC/cm^2) accounts for the charging of the EDL (i.e., for changes in the value of $Q_{S,M}$). It follows that the charge for adsorption (or desorption of hydrogen atoms (reaction 10.14) is about 210 μC/cm^2. Assuming that at the potential 0.35 V, hydrogen is fully desorbed

from the surface, this indicates that at 0 V the value of hydrogen adsorption A_H is about 2.5×10^{-9} mol/cm^2 = 1.3×10^{15} cm^{-2}. This number actually coincides with the mean number of platinum atoms exposed on faces of the platinum lattice (the number varies slightly depending on the face index). Thus, at $E_r = 0$ V, practically every platinum surface atom is bonded to an adsorbed hydrogen atom (i.e., the limiting surface coverage of $\theta_H = 1$ is attained). As the potential is made more positive, θ decreases until it attains a value of zero at 0.35 V. To a first approximation it varies linearly with potential:

$$\theta_H = 1 - \frac{1}{0.35} E_r \tag{10.37}$$

(here E_r is stated in volts).

By using the value $Q_{ext} = 220\,\mu$C/cm^2, one can readily determine the true surface area of any compact or disperse sample of platinum without adducing any other methods, simply by measuring the total amount of charge required to accomplish the potential shift.

10.5.3 Surface Inhomogeneity of Platinum

It is not a trivial point that θ_H vs. E_r curves are practically linear. In a reversible system the electrode potential can be linked to the activities (concentrations) of the potential-determining substances. In the system being discussed, this substance is atomic hydrogen. According to the Nernst equation we have $E_r = \text{const} - (RT/F) \times \ln c_H$. It follows that the degree of coverage, θ_H, is linearly related to the logarithm of concentration c_H in the solution:

$$\theta_H = g + \frac{1}{f} \ln c_H \tag{10.38}$$

(i.e., by a logarithmic adsorption isotherm). This equation was derived in 1941 by Temkin, just for interpreting results obtained when measuring charging curves at platinum electrodes. When comparing Eqs. (10.37) and (10.38), we find that the inhomogeneity factor f has a value of $0.35(F/RT) \approx 14$.

The shape of the isotherm arises because the heat of adsorption, q_θ, decreases with increasing degree of coverage of the electrode. Hydrogen ion discharge producing molecular hydrogen (gas) is possible, for thermodynamic reasons, only at values of potential more negative than 0 V. But since the intermediates (hydrogen atoms) are adsorbed, a discharge of hydrogen ions producing these atoms is possible even at more positive potentials because of the adsorption energy gained. When the electrode potential is moved from a value of +0.4 V (where the surface is known to be free of adsorbed hydrogen) in the negative direction, adsorption of the first numbers of hydrogen atoms will start at 0.35 V on the sites with the highest heat of adsorption, q_0 (strongly bound hydrogen). As the potential is moved further to the negative side and θ_H increases, the heat of adsorption gradually decreases, and its

minimum value of q_1 is attained near the potential of 0 V when $\theta_H \approx 1$. Thus, the total change in heat of adsorption is about 0.35 eV or, roughly, 34 kJ/mol.

The reasons for the change in hydrogen adsorption energy on platinum, or for inhomogeneity of the platinum surface, have not yet been established in an unambiguous way. The inhomogeneity may arise from different geometries of the adsorption sites (e.g., the exposed face of a metal crystallite) or by the influence of the hydrogen atoms adsorbed earlier. Accordingly, *geographic* or *biographic* and *induced inhomogeneity* are discussed for metal surfaces.

10.5.4 Adsorption of Other Substances on Platinum

The adsorbabilities of different anions on platinum increase in approximately the same order as on mercury. Anions as a rule become desorbed with increasing oxygen adsorption. This special ability of the adsorbed oxygen to displace other adsorbed substances from the surface is of great value for experimental work. The platinum electrode is held for a few seconds or minutes at potentials of 1.1 to 1.4 V (RHE) to rid the surface of impurities. Following this, if the potential is moved to a value of 0.4 V, the oxygen will desorb and a clean surface is obtained. A highly sensitive indication for the degree of cleanliness attained by the surface is the shape of the potentiodynamic charging curves (see Fig. 10.14), which will be distorted by minute amounts of impurities.

When charging curves are measured while the potential is shifted in the anodic direction, oxygen adsorption will start at a potential of about 0.75 V, long before the thermodynamic potential for the evolution of free oxygen (1.23 V) is attained. This indicates that the bond energy between platinum and adsorbed oxygen is high. The first amounts of oxygen evidently are adsorbed in the form of hydroxyl groups:

$$\mathrm{Pt} + \mathrm{H_2O} \rightleftharpoons \mathrm{Pt} - \mathrm{OH} + \mathrm{H^+} + e^- . \tag{10.39}$$

At more positive potentials, bonds of the type Pt=O or of more complex types can be formed. It follows from the amount of charge that is consumed when recording the charging curve that formation of a monolayer of oxygen in the form of $(OH)_{ads}$ is complete at a potential of about 1.15 V, and formation of a monolayer of oxygen in the form of O_{ads} is complete at a potential of about 1.5 V. Oxygen adsorption continues at more positive potentials, and at a potential of about 2.2 V, a limiting value is attained that corresponds formally to degrees of coverage of 2.0 to 2.2 [for platinum, the region of high anodic potentials (HAPs)].

10.5.5 Aging of Adsorbed Particles

Oxygen adsorption that occurs at platinum at potentials more positive than 0.9 to 1.0 V is irreversible, in contrast to hydrogen adsorption. Oxygen can be removed from the surface by cathodic current, but the curves obtained in the anodic and cathodic scan do not coincide; cathodic oxygen desorption occurs within a narrower region of potentials, and these potentials are more negative than the region where the

major amount of oxygen becomes adsorbed (see Fig. 10.10). Thus, immediately after adsorption there is a drastic increase in the bond energy of the oxygen on the surface. The initial fast rise is followed by a further slow increase in bond energy, or "aging" of the adsorbed oxygen.

The adsorption of organic substances from solutions on platinum surfaces can be measured by various techniques. A platinum surface atom bonded to an organic particle loses its ability to adsorb hydrogen; hence, the fraction of surface taken up by organic species can be estimated from the decrease in hydrogen adsorption noticed when recording cathodic charging curves. Sometimes a horizontal section of constant potential, which is due to anodic oxidation of adsorbed organic particles, appears in anodic charging curves at potentials of 0.6 to 0.8 V. The amount of particles adsorbed can be estimated from the length of this section.

Many organic species are adsorbed on platinum at potentials ranging from approximately 0.1 to 0.7 V (RHE). At more positive potentials they desorb because of oxidation or of displacement from the surface by adsorbing oxygen. The extent of adsorption of the organic substances can be considerable, and they can take up as many as 70% of the surface sites.

The relation between platinum with adsorbed organic species θ_j and the bulk solution concentration of these substances often obeys the logarithmic Temkin isotherm with values of the factor f of 10 to 14 (i.e., practically the same value as found in hydrogen adsorption). Such behavior is not trivial. The Temkin isotherm (like the Langmuir isotherm) was derived for the case of a reversible adsorption. The adsorption of organic substances from solutions as a rule is irreversible; material already adsorbed will not desorb when the solution concentration is reduced (not even when it is reduced to zero). In these cases the existence of a distinct isotherm is probably due to the fact that in a first stage, the adsorption of the substance on the platinum surface is reversible. After being adsorbed the adsorbed species undergo some kind of aging processes with an increase in the bond energy (the development of chemical bonds with the surface) and in some cases with destruction of the initial molecule but without a change in the amount of species sorbed. For instance, in methanol adsorption on a platinum electrode, three hydrogen atoms are split off from the CH_3OH molecule and become adsorbed on the surface, and chemisorbed species of the type $\equiv$CHO are formed which are bonded to three platinum surface atoms:

$$CH_3OH \rightarrow \equiv CHO + 3H_{ads}. \tag{10.40}$$

In a further aging process the $\equiv$CHO species can be transformed by oxidation with adsorbed $-$OH groups to species of the type $=$CO. For this reason after these processes are completed, infrared spectroscopy shows the presence on the platinum surface of mainly the latter species.

Types of aging processes such as those described for the adsorption of oxygen and methanol on platinum are also characteristic of the adsorption of other substances and of adsorption on other electrodes. In some cases these changes manifest themselves as a change (mostly an increase) in the adsorption energy with time. In

some cases these changes are accompanied by changes in the stoichiometry of the adsorbed particle and/or by a change in their attachment to the electrode.

10.5.6 Ideally and Perfectly Polarizable Electrodes

We have seen that there are substantial differences in the surface properties of platinum and mercury electrodes. The latter are ideally polarizable; all of the charge supplied from outside accumulates in the EDL and merely produces a change in the value of surface charge $Q_{S,M}$ characterizing the condition of the system. Platinum electrodes (except for the double-layer region) are not ideally polarizable; electrochemical reactions (10.17) or (10.18) occur at their surfaces. It is true that these reactions are transient and will cease when the adsorption of hydrogen or oxygen atoms has attained a certain level. Thus, even here any charge supplied from outside will merely produce a change in surface condition but will not be consumed for the formation of reaction products escaping from the electrode surface. By convention, the transient electric current crossing the electrode is regarded as nonfaradaic in this case, even though it is associated in part with an electrochemical reaction.

The concept of ideal polarizability implying the total absence of charge transfer between the two EDL sides was formulated in 1934 by F. O. Koenig. But as early as 1891, Max Planck had made the suggestion that the term *perfectly polarizable electrode* should be used when the surface condition of the electrode is uniquely defined by the amount of charge consumed. This concept is broader than that of ideal polarizability. It covers not only ideally polarizable electrodes of the mercury type but also electrodes of the platinum type in the region of hydrogen adsorption. A platinum electrode in the region of oxygen adsorption is already outside this definition, since here the electrochemical reaction is irreversible, and owing to aging of the adsorbed oxygen, the surface condition is not defined uniquely by the amount of charge consumed. For exactly the same reasons, the concept does not cover electrodes where phase layers of reaction products are formed on the surface because of a reaction.

10.6 SURFACES OF OTHER ELECTRODES

In their electrochemical surface properties, a number of metals (lead, tin, cadmium, and others) resemble mercury, whereas other metals of the platinum group resemble platinum itself. Within each of these groups, trends in the behavior observed coincide qualitatively, sometimes even semiquantitatively. Some of the differences between mercury and other *s*- or *p*-metals are due to their solid state. Among the platinum group metals, palladium is exceptional, since strong bulk absorption of hydrogen is observed here in addition to surface adsorption, an effect that makes it difficult to study the surface itself.

Surface studies are difficult in the case of many metal electrodes since their regions of ideal or perfect polarizability are very narrow; that is, the potentials of anodic dissolution (or oxidation) of the metal and of cathodic hydrogen evolution are close

TABLE 10.1 Potentials of Zero Charge of Certain Metals in Aqueous Solutions

Metal	Solution Composition	E_{zc} (V) (SHE)
Bismuth	0.002 *M* KF	−0.39
Gallium (liquid)	0.008 *M* $HClO_4$	−0.69
Iron	0.0006 *M* Na_2SO_4	−0.70
Gold	0.02 *M* NaF	+0.19
Indium	0.03 *M* NaF	−0.65
Cadmium	0.001 *M* KF	−0.75
Tin	0.001 *M* K_2SO_4	−0.38
Mercury	0.001 *M* NaF	−0.193
Lead	0.01 *M* NaF	−0.60
Silver (polycryst.)	0.002 *M* Na_2SO_4	−0.70
Silver [the (111) face]	0.001 *M* KF	−0.46
Silver [the (100) face]	0.002 *M* NaF	−0.61
Silver [the (110) face]	0.005 *M* NaF	−0.77
Antimony	0.002 *M* $KClO_4$	−0.15
Thallium	0.001 *M* NaF	−0.71

together. In a number of cases such a region is not found at all. Often, the qualitative results obtained when studying other electrodes are extended to such electrodes.

A very important characteristic of surface constitution for any metal is the position of its PZC. Table 10.1 reports values for the PZC for a number of metals. We can see that these values vary within rather wide limits. An important difference between platinum group metals and most other metals is the ability of the latter upon anodic polarization to form relatively thick superficial oxide or salt layers. Owing to their great practical value, these layers are considered in more detail in Section 16.3. For investigations of the structure and of properties of platinum and other electrodes, many nonelectrochemical methods are also widely applied, which is discussed in more detail in Chapter 27.

In addition to metals, semiconductors with *n*- or *p*-type conduction are used as electrodes. The surface layers of semiconductors differ strongly from those of metals in their electrical constitution. The concentrations of free carriers are much lower in semiconductors (e.g., $10^{14}\,cm^{-3}$ or 2×10^{-7} mol/L) than in metals ($10^{22}\,cm^{-3}$ or 20 mol/L, in order of magnitude); therefore, the excess electric charge in semiconductors (the electrode side of the EDL) is not tightly packed against the surface but is distributed diffusely within a surface layer 0.01 to 1 μm thick (i.e., extending over 10^2 to 10^4 atom layers). In this region a potential drop is generated by the resulting space charge. An appreciable part of the Galvani potential across the semiconductor–electrolyte interface is located in a relatively thick surface layer inside the semiconductor rather than on its surface. The charge and potential distribution in this layer are analogous to the same distributions in the diffuse EDL part in very dilute electrolyte solutions, and can be described by the same equations (see Section 10.2.2).

The diffuse charge distribution in the semiconductor's surface layer leads to a drastically lower cell capacitance at the semiconductor–electrolyte interface. Typical

values for metal electrodes are 20 to 40 μF/cm^2, but for semiconductor electrodes, these values are three to three orders of magnitude lower.

REFERENCES

Chapman, D. L., *Philos. Mag*., Ser. 6, **25**, 475 (1913).

Frumkin, A. N., *Electrocapillary Phenomena and Electrode Potentials* [in Russian], dissertation, Commercial Publishing, Odessa, Ukraine, 1919.

Frumkin, A., *Philos. Mag*., **40**, 363 (1921).

Frumkin, A., *Z. Phys. Chem*., **103**, 43 (1923).

Frumkin, A., *Ergeb. Exakten Naturwiss*., **7**, S235 (1928).

Frumkin, A. N., and A. I. Shlygin, *Acta Phys.-Chim. URSS*, **3**, 791 (1935).

Frumkin, A., P. Dolin, and B. Ershler, *Acta Phys.-Chim. URSS*, **12**, 747, 779, 793 (1940).

Gibbs, J. W., *Trans. Conn. Acad. Arts Sci*., **3**, 108, 343 (1874–1878).

Gouy, G., *Compt. Rend*., **9**, 133 (1906); **149**, 654 (1910).

Grahame, D. C., *Chem. Rev*., **41**, 441 (1947).

Koenig, F. O., *J. Phys. Chem*., **38**, 111, 338 (1934).

Langmuir, I., *J. Am. Chem. Soc*., **40**, 1361 (1918).

Lippmann, G., *Ann. Phys. (Poggendorff's)*, **29**, 546 (1873).

Planck, M., *Vorträge über die Kinetische Theorie und der Elektrizität*, 1914.

Stern, O., *Z. Elektrochem*., **30**, 508 (1924).

Temkin, M., *Zh. Phys. Khim*., **15**, 296 (1941).

von Helmholtz, H., *Ann. Phys. (Poggendorff's)*, **89**, 221 (1853).

MONOGRAPHS

Delahay, P., *Double Layer and Electrode Kinetics*, Interscience, New York, 1965.

Frumkin, A. N., *Potentials of Zero Charge*, 2nd ed. [in Russian], Nauka Publishers, Moscow, 1982.

Guggenheim, E. A., *Thermodynamics by the Method of Willard Gibbs*, Methuen, London, 1933.

Henderson, M. A., The interaction of water with solid surfaces: fundamental aspects revisited, *Surf. Sci. Rep*., **46**, 1–308 (2002).

11
Transient Processes

11.1 EVIDENCE FOR TRANSIENT CONDITIONS

In electrochemical systems, a steady state during current flow implies that a time-invariant distribution of the concentrations of ions and neutral species, of potential, and of other parameters is maintained in any section of the cell. The distribution may be nonequilibrium, and it may be a function of current, but at a given current it is time invariant.

The steady state is disturbed and the system exhibits transient behavior when at least one of its parameters is altered under an external stimulus (*perturbation*). Transitory processes that adjust the other parameters set in (*response*) and at the end produce a new steady state. The time of adjustment (transition time, relaxation time) is an important characteristic of the system.

In electrochemical systems, transient processes are of major practical significance because they are an efficient route for studying electrode reactions and phenomena (see Chapter 12). In addition, transient measurements are useful for analytical purposes (see Chapter 23).

The polarization functions described in Chapter 6 are valid in the steady state. These laws are not obeyed initially, when the current has just been turned on. Let us look more closely at the notion that "the current is turned on." In the steady state the current (or current density) and electrode polarization are inseparably linked; polarization can be the result of current flow, or vice versa. Things are different in the transient state. Here we can initially set either the current or the electrode potential. When "the current is turned on," that is, when the current is set to a certain value (*galvanostatic conditions*) from the very beginning, during a transition time the electrode potential will change from its initial value at zero current to its final steady-state value. If, to the contrary, a certain value of electrode potential is set (*potentiostatic conditions*), the current will change during the transition time by certain laws. Electrochemical systems can be perturbed in other ways, too [e.g., by applying a potential that varies with time according to a particular law (*potentiodynamic conditions*) or by applying an alternating

Fundamentals of Electrochemistry, Second Edition, By V. S. Bagotsky

current]. The different possibilities for perturbation are considered in more detail in Chapter 12.

During the transition time, a variety of processes of adjustment take place: development or change of an ohmic potential gradient, a change in EDL charge density, the development of concentration gradients in the electrolyte, and so on. Each of these processes has its own rate and its own characteristic time of adjustment.

Ohmic potential gradients are established practically instantaneously across conductors, certainly within times shorter than the response time of the fastest measuring devices, which is about 1 ns. They are caused by formation of a double layer, the charge of which is located on the opposite faces of the conductor in question.

Electrode polarization is associated with a change in EDL charge density at the electrode surface. Other changes in surface state of the electrode are possible, too (e.g., the adsorption or desorption of different components, which also involve a consumption of electric charge). By convention, we describe this set of nonfaradaic processes as charging of the electrode surface.

The net current crossing the electrode at any time is the algebraic sum of the faradaic and various nonfaradaic currents. During the transition time, part of the net current is consumed for surface-layer charging and is not available for the primary electrode reaction. This part of the current is called the *charging current* (I_{ch}). It is highest at the start of the transition period, but toward the end of this period it falls to zero. The transition time of charging, t_{ch}, depends on the value of current and on the system, and may vary within wide limits (between 0.1 ms and 1 s).

Concentration gradients in the electrolyte layer next to the electrode surface will develop or change as a result of the primary electrode reaction. Therefore, the current associated with these changes is faradaic, although it is also transient and falls to zero when adjustment of the concentration profile is complete. Unlike other transient processes, these processes, can be described in a quantitative way (Sections 11.2 and 11.3). The transition times of such processes as a rule are longer than 1 s.

The various processes of adjustment have different values of the transition time; therefore, which of them become evident will depend on the method used in the measurements, in particular on the time interval between perturbation and measurement of the response. It thus becomes possible to study the different transitory processes individually.

11.2 TRANSIENT DIFFUSION TO ELECTRODES OF LARGE SIZE

Under transient conditions the concentration distribution depends not only on the coordinate but also on time. The relevant functions can be found by considering the linear diffusion occurring along the x-axis in a volume element dV bounded by the two planes S which are a distance dx apart (Fig. 11.1); it is obvious that $dV = S\,dx$. The rate of concentration change $\partial c_j/\partial t$ in this volume is given by the ratio of $-S\,dJ_j$ (the

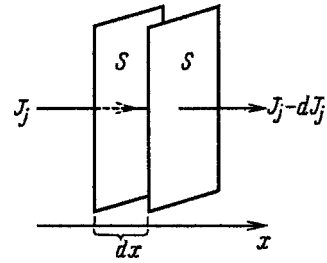

FIGURE 11.1 Concerning the derivation of Eq. (11.1).

decrease in total flux seen when advancing through the volume) to dV. Using Eq. (4.1), we thus have

$$\frac{\partial c_j}{\partial t} = \frac{\partial J_j}{\partial /x} = Dj\left(\frac{\partial^2 c_j}{\partial /x^2}\right) \tag{11.1}$$

(*Fick's second law*). To solve this differential equation, we additionally must know the boundary conditions, which depend on the conditions used in the measurements.

Solutions for a number of typical cases are reported below. To simplify our task we use the assumption that reactant migration is not observed (a large excess of foreign electrolyte), that the diffusion coefficients D_j do not depend on concentration, and that for the reactant $\nu = 1$. (The subscript j is dropped in what follows.)

11.2.1 Galvanostatic Conditions

At time $t = 0$ an electric current of constant strength begins to flow in the system. At this time the uniform initial concentration distribution is still not disturbed, and everywhere in the solution, even close to the electrode surface, the concentration is the same as the bulk concentration $c_{V,j}$. Hence, the first boundary condition (for any value of x) is given by

$$c = c_V \qquad \text{for} \quad i = 0. \tag{11.2}$$

According to Eq. (4.47), the current density is related to the concentration gradient at the surface. Since the current density is constant, the gradient will be also constant and at all times t,

$$\frac{\partial c}{\partial x} = -\frac{i}{nFD} \qquad \text{for} \quad x = 0. \tag{11.3}$$

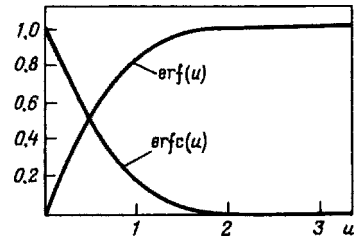

FIGURE 11.2 Plots of functions erf(u) and erfc(u).

The solution of differential equation (11.1) with boundary conditions (11.2) and (11.3) is

$$c(x,t) = c_V + \frac{i}{nFD}\left[2\left(\frac{Dt}{\pi}\right)^{1/2}\exp\left(-\frac{x^2}{4Dt}\right) - \operatorname{erfc}\left(\frac{x}{2\sqrt{Dt}}\right)\right]. \tag{11.4}$$

Here erfc(u) is the error function complement, a mathematical function of the argument u given by $1 - \operatorname{erf}(u)$, where erf($u$) is the error or Euler–Laplace integral. This integral in turn is defined by the expression

$$\operatorname{erf}(u) = \frac{2}{\pi^{-1/2}}\int_0^u \exp(-y^2). \tag{11.5}$$

The variable y in the expression under the integral sign is an auxiliary variable; the value of the integral depends only on the limits of integration (i.e., on the value of u). The numerical values of the error function vary from zero for $u = 0$ to an upper limit of unity for $u \to \infty$ (this value is practically attained already for $u \approx 2$). Plots of functions erf(u) and erfc(u) are shown in Fig. 11.2.

It follows from Eq.(11.4) that at the electrode surface ($x = 0$) the concentration varies with time according to the function

$$c_S = c_V + \frac{2i}{nF}\left(\frac{t}{\pi D}\right)^{1/2}. \tag{11.6}$$

The concentration change near the electrode surface gradually reaches solution layers farther away from the electrode. In these layer the rate of concentration change is the same as at the electrode, but there is a time lag. The concentration distributions found at different times are shown in Fig. 11.3. The diffusion-layer thickness δ_{tr} gradually increases with time; it follows from Eqs. (11.3) and (11.6) that

$$\delta_{tr} = 2\left(\frac{Dt}{\pi}\right)^{1/2}. \tag{11.7}$$

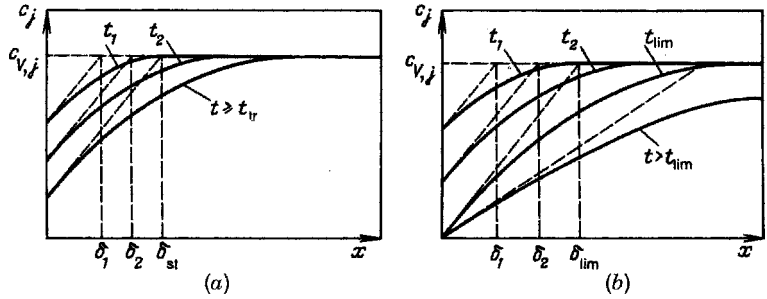

FIGURE 11.3 Distributions of reactant concentration near the electrode after different times of galvanostatic operation: (*a*) $t_{tr} < t_{lim}$; (*b*) $t_{tr} > t_{lim}$.

This equation holds only at short times when thickness δ_{tr} is small compared to the steady-state diffusion-layer thickness δ_{st}, which will be attained under given experimental conditions, particularly when the solution is stirred. As soon as δ_{tr} attains the value of δ_{st}, the transitory processes end and a steady state is attained; there is no further change in concentration distribution with time (Fig. 11.3*a*). It follows from Eq. (11.7) that the transition time of the transient process

$$t_{tr} = \frac{\pi \delta_{st}^2}{4D}. \tag{11.8}$$

In cases where the values of δ_{st}, and thus of t_{tr}, are large enough (without significant convection in the electrolyte solution), another limiting state is attained which is typical for galvanostatic conditions and where the reactant concentration at the surface falls to zero (Fig. 11.3*b*). For the time t_{lim} required to attain this state, Eq. (11.6) yields

$$t_{lim} = \pi D \left(\frac{nFc_V}{2i} \right)^2. \tag{11.9}$$

When the surface concentration has fallen to zero, further current flow and the associated increase in δ_{tr} lead to a decrease in concentration gradient and in current (Fig. 11.3*b*, the curve for $t > t_{lim}$). Therefore, at $t > t_{lim}$ the original, constant current density can no longer be sustained. It follows that a steady state can only exist under the condition $t_{tr} < t_{lim}$.

When, after the attainment of zero surface concentration, a constant current density is maintained artificially from outside, the electrode potential will shift to a value such that a new electrochemical reaction involving other solution components can start (e.g., in aqueous solution, the evolution of hydrogen or oxygen). It follows from Eq. (11.9) that at a given concentration c_V the product $i^2 t_{lim}$ is constant and is

independent of the set current density. Using the value found for time t_{lim}, we can write the expression for the surface concentration of reactants replacing Eq. (11.6) as

$$c_S = c_V\left[1 - \left(\frac{t}{t_{\text{lim}}}\right)^{1/2}\right]. \tag{11.10}$$

11.2.2 Potentiostatic conditions

Equation (11.2) remains valid as the first boundary condition in this case. The surface concentrations, c_S, of the reactants will remain constant, in accordance with the Nernst equation, when the electrode potential is held constant during current flow (and activation polarization is absent). Hence, the second boundary condition can be formulated as

$$c_S = \text{const} \qquad \text{for} \quad x = 0. \tag{11.11}$$

With these boundary conditions, the differential equation (11.1) has the solution

$$c(x,t) = c_S + \frac{2\Delta c}{\pi^{1/2}}\,\text{erf}\left(\frac{x}{2Dt}\right), \tag{11.12}$$

where $\Delta c \equiv c_V - c_S$. Differentiating this equation with respect to x and setting $x = 0$, we find that

$$\left(\frac{\partial c}{\partial x}\right)_{x=0} = \frac{\Delta c}{(\pi D t)^{1/2}}, \tag{11.13}$$

and for the current density

$$i = nFD\left(\frac{\partial c}{\partial x}\right)_{x=0} = nF\Delta c\left(\frac{D}{\pi t}\right)^{1/2}. \tag{11.14}$$

We see from these equations that the current density decreases with the inverse square root of time.

From Eq. (11.13) we obtain an expression for the effective transient diffusion-layer thickness:

$$\delta_{\text{tr}} = (\pi D t)^{1/2}. \tag{11.15}$$

The concentration distributions found at different times after the start of current flow are shown in Fig. 11.4. It is a typical feature of the solution obtained that the variable parameters x and t do not appear independently but always as the ratio $x/t^{1/2}$. Like Eq. 11.15), this indicates that the diffusion front advances in proportion to the square root of time. This behavior arises because as the diffusion front advances toward the bulk solution, the concentration gradients become flatter and thus diffusion slows down.

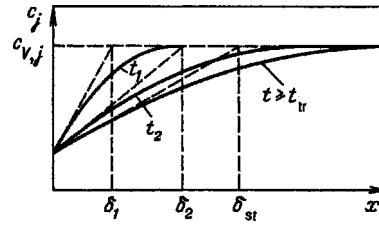

FIGURE 11.4 Distributions of reactant concentration near the electrode after different times of potentiostatic operation; $t_1 < t_2 < t_{lim}$.

The transient process continues until thickness δ_{tr} has attained the value of diffusion-layer thickness δ_{st} corresponding to the applicable experimental conditions. Hence, we obtain for the duration of this transitory process,

$$t_{tr} = \frac{\delta_{st}^2}{\pi D}. \tag{11.16}$$

11.2.3 Use of Alternating Currents

In electrochemical measurements, a method often employed is that of applying an alternating current of low amplitude to the electrode. For sinusoidal ac $i = i_m \sin \omega t$ (i_m is the amplitude and ω the angular frequency), the concentration gradient at the surface varies according to the law

$$\left(\frac{\partial c}{\partial x}\right)_{x=0} = \frac{i}{nFD} \sin \omega t \qquad \text{for} \quad x = 0. \tag{11.17}$$

With the boundary conditions (11.2) and (11.17), the differential equation (11.1) has the solution

$$c(x,t) = c_V + nFi_m(\omega D)^{-1/2} \left\{ \exp\left[-x\left(\frac{2D}{\omega}\right)^{-1/2} \right] \right\} \sin\left[\omega t - x\left(\frac{2D}{\omega}\right)^{-1/2} - \frac{\pi}{4} \right]. \tag{11.18}$$

It follows from this equation that ac passing through the solution gives rise to periodic concentration variations having the same frequency and reaching out from the electrode into the bulk solution with an amplitude decreasing in proportion to $\exp(-2D/\omega)^{1/2}$ (i.e., faster the higher the ac frequency).

For the surface concentration (at $x = 0$) we find that

$$c_S = c_V + nFi_m(\omega D)^{-1/2} \sin\left(\omega t - \frac{\pi}{4}\right). \tag{11.19}$$

It follows from this equation that the effective diffusion-layer thickness can be described as

$$\delta \approx \left(\frac{D}{\omega}\right)^{1/2}. \tag{11.20}$$

Diffusion is transient in each of the half-periods, but the effects produced in one half-period (e.g., an increase in concentration) are compensated by the effects produced in the following half-period (in this example, a decrease in concentration). Therefore, the time-average thickness of the diffusion layer remains unchanged and the state of the system as a whole is quasisteady.

11.3 TRANSIENT DIFFUSION TO ELECTRODES OF FINITE SIZE

In Chapter 4 and in the preceding section, cases of linear diffusion to a flat electrode were considered where the particles advance toward the entire surface along parallel lines normal to the surface. This implies that the electrode considered was large enough for edge effects ("lateral" diffusion to peripheral sections of the electrode) to be practically negligible. "Large enough" means, in this case, that the linear dimensions of the electrode (its width, height, and radius of curvature) were large compared to the diffusion-layer thickness. When this condition is not met and substances diffuse toward the surface along pathways converging on the surface, the total diffusion flux evidently will be larger.

Consider the specific example of a spherical electrode having the radius a. We shall assume that diffusion to the spherical surface occurs uniformly from all sides (spherical symmetry). Under these conditions it will be convenient to use a spherical coordinate system having its origin in the center of the sphere. Because of this symmetry, then, all parameters have distributions that are independent of the angle in space and can be described in terms of the single coordinate r (i.e., the distance from the center of the sphere). In this coordinate system, Fick's second diffusion law becomes

$$\frac{\partial c}{\partial t} = D\left(\frac{2}{r}\frac{\partial c}{\partial r} + \frac{\partial^2 c}{\partial r^2}\right) \tag{11.21}$$

[this equation can be derived in exactly the same way as Eq. (11.1)].

Consider the case of transient diffusion at constant potential (constant surface concentration). The first boundary condition, (11.2), is preserved and the second boundary condition can be written (for any time t) as

$$c_S = \text{const} \qquad \text{for} \quad r = a. \tag{11.22}$$

With these boundary conditions, the differential equation (11.1) has the solution (for $r > a$)

Differentiating this expression with respect to r and setting $r = a$, we find for the concentration gradient at the surface that

$$c(r,t) = \Delta c \frac{2a}{r\pi^{1/2}} \operatorname{erf}\left[\frac{1}{2}(r-a)(Dt)^{-1/2}\right] + \Delta c\left(1 - \frac{a}{r}\right). \tag{11.23}$$

Differentiating this expression with respect to r and setting $r = a$, we find for the concentration gradient at the surface,

$$\left(\frac{\partial c}{\partial r}\right)_{r=a} = \Delta c\left[(\pi Dt)^{-1/2} + \frac{1}{a}\right]. \tag{11.24}$$

and for the current density,

$$i = nFD\ \Delta c\left[(\pi Dt)^{-1/2} + \frac{1}{a}\right], \tag{11.25}$$

We see that the expression for the current consists of two terms. The first term depends on time and coincides completely with Eq. (11.14) for transient diffusion to a flat electrode. The second term is time invariant. The first term is predominant initially, at short times t, where diffusion follows the same laws as for a flat electrode. During this period the diffusion-layer thickness is still small compared to radius a. At longer times t the first term decreases and the relative importance of the current given by the second term increases. At very long times t, the current tends not to zero as in the case of linear diffusion without stirring (when δ_{st} is large) but to a constant value. For the characteristic time required to attain this steady state (i.e., the time when the second term becomes equal to the first), we can write

$$t_{tr} \approx \frac{a^2}{\pi D}. \tag{11.26}$$

At this time δ_{tr} has the approximate value of $a/2$.

It is a typical feature of the diffusion processes at electrodes of small size, which are reached by converging diffusion fluxes, that a steady state can be attained even without convection (e.g., in gelled solutions). Such electrodes, which have dimensions comparable to typical values of δ, are called *microelectrodes*.

12

Electrochemical Research Techniques

Experimental studies in electrochemistry deal with the bulk properties of electrolytes (conductivity, etc.); equilibrium and nonequilibrium electrode potentials; the structure, properties, and condition of interfaces between different phases (electrolytes and electronic conductors, other electrolytes, or insulators); and the nature, kinetics, and mechanism of electrochemical reactions.

Electrochemical as well as nonelectrochemical techniques are used when studying these aspects. Electrochemical techniques are commonly used, too, in chemical analysis, in determining the properties of various substances and for other purposes. The nonelectrochemical techniques include chemical (determining the identity and quantity of reaction products), radiotracer, optical, spectral, and many other physical methods. Sometimes these methods are combined with electrochemical methods: for instance, when studying the optical properties of an electrode surface while this is polarized. Nonelectrochemical techniques are described in more detail in Chapter 27.

In the present chapter we consider the electrochemical methods used to measure OCV and electrode potentials and to study the kinetics of electrode reactions. These methods are also described in great detail in the book by Bard and Faulkner (2001).

Electrochemical measurements usually concern not a galvanic cell as a whole but one of the electrodes, the working electrode (WE). However, a complete cell including at least one other electrode is needed to measure the WE potential or allow current to flow. In the simplest case a two-electrode cell (Fig.12.1*a*) is used for electrochemical studies. The second electrode is used either as the reference electrode (RE) or as an auxiliary electrode (AE) to allow current to flow. In some cases these two functions can be combined; for example, when the surface area of the auxiliary electrode is much larger than that of the working electrode so that the current densities at the AE are low, it is essentially not polarized and thus can be used as RE.

For measurements involving current flow, three-electrode cells (Fig. 12.1*b*) are more common; they contain both an AE and a RE. No current flows in the circuit of the reference electrode, which therefore is not polarized. However, the OCV value that is measured includes the ohmic potential drop in the electrolyte section between the working and reference electrode. To reduce this undesired contribution from ohmic

Fundamentals of Electrochemistry, Second Edition, By V. S. Bagotsky

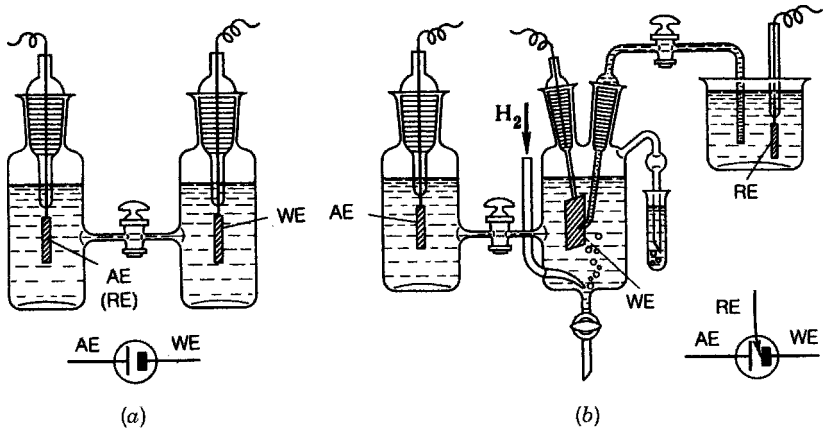

FIGURE 12.1 (*a*) Two- and (*b*) three-electrode cell for electrochemical studies.

losses, one brings the connecting tube with the electrolyte of the reference electrode right up to the surface of the working electrode. To reduce screening of this surface, the end of the tube is drawn out to a fine capillary, the *Luggin capillary*. The design and emplacement of this capillary are very important for measuring accuracy. It is necessary to bring the tip of the capillary as close as possible to the electrode, yet the capillary should not screen the segment of electrode surface being measured or disturb the uniform current distribution. During the experiments the electrochemical cell is usually placed in a thermostat. When required, the liquid electrolyte is agitated with a stirrer or a rotating WE is used.

Impurities can have an important influence on the properties of electrode–electrolyte electrochemical systems; even minor quantities of foreign material (both organic and inorganic) readily adsorb at the interface and strongly affect its properties. Therefore, the purity requirements for the chemicals used in electrochemical studies are very high. The chances for the electrode surface to become contaminated by impurities before and during the experiments must be reduced to the maximum possible extent.

In many cases the system being studied must not come in contact with air oxygen; hence, the measurements are conducted in an atmosphere of hydrogen or inert gas (argon, helium, etc.), and one must monitor the complete exclusion of air (or other undesirable gases) from the system.

12.1 REFERENCE ELECTRODES

An important step in measurements of electrode potentials is that of selecting a suitable reference electrode (RE). Reference electrodes with electrolytes of the same nature and same (or similar) composition as that at the working electrode are used

to reduce the liquid-junction potentials. During the measurements both electrodes must be at the same temperature.

One distinguishes practical and standard reference electrodes. A standard RE is an electrode system of particular configuration, the potential of which, under specified conditions, is conventionally taken as zero in the corresponding scale of potentials (i.e., as the point of reference used in finding the potentials of other electrodes). Practical REs are electrode systems having a sufficiently stable and reproducible value of potential which are used in the laboratory to measure the potentials of other electrodes. The potential of a practical reference electrode may differ from the conventional zero potential of the standard electrode, in which case the potential of the test electrode is converted to this scale by calculation.

The standard RE universally adopted is the standard hydrogen electrode (SHE). At this electrode the equilibrium of the hydrogen evolution and ionization reaction (1.33) is established, and the electrode is under standard-state conditions for this reaction; that is, it is in contact with a gas atmosphere containing hydrogen at a partial pressure of 1 atm and with a binary electrolyte solution that contains hydrogen ions and has a mean ionic activity $a_{\pm}$ of 1 mol/kg. The potential E of this electrode according to Eq. (3.61a) is identical to the value of the standard potential E^0, which, on the hydrogen scale, is adopted as zero. It is important to point out that this definition applies at any temperature: It is assumed as a convention that for the standard hydrogen electrode, not only the potential but even the temperature coefficient of potential is zero (see Section 3.7.5).

Hydrogen electrodes and different versions of electrodes of the second kind are in use as practical reference electrodes. They are designed as half-cells. A version with hydrogen RE is shown in Fig. 12.2. Here a piece of platinum foil on which a layer of highly disperse (spongy) platinum has been deposited electrolytically serves as the electrode. Part of it is in contact with the gas phase; the other part dips into the electrolyte solution. Hydrogen is passed through the cell and solution for 20 to 30 min prior to measurements to remove all air, including that dissolved in the

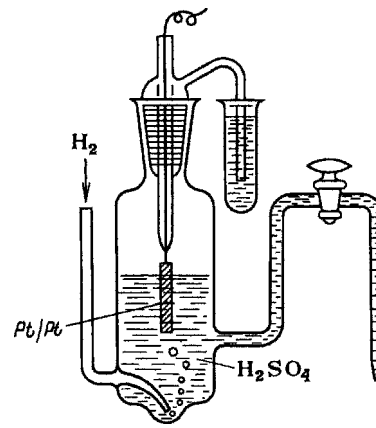

FIGURE 12.2 Half-cell with hydrogen reference electrode.

solution. Gas and solution should both be carefully purified. The value of potential that is established under these conditions is highly reproducible (to $\pm 1 \times 10^{-5}$ V) and time invariant. The slightest contamination with mercury or arsenic compounds, hydrogen sulfide, and certain other compounds strongly reduces the stability (they "poison" the electrode).

The potential of the hydrogen RE depends on the hydrogen partial pressure and on the hydrogen ion activity [Eq. (3.61*a*)]. The gas phase always contains water vapor in addition to hydrogen; its equilibrium pressure, p_{0H_2O}, depends on temperature. Therefore, the hydrogen partial pressure p_{H_2} is given by the difference $p_0 - p_{H_2O}$, where p_0 is the total pressure of the gas mixture (usually equal to the ambient pressure). The electrolytes most often used are 0.1 to 1 *M* sulfuric acid solutions. The 3.4 *m* solution where $a_\pm \approx 1$ and the hydrogen electrode is the standard electrode has no advantages over solutions with other concentrations. When a reduction of diffusion potentials is required, one can use sulfuric acid solutions with concentrations between 0.01 and 15 *M* and even alkaline solutions (e.g., 0.01 to 5 *M* KOH solutions). But since in alkaline solutions the ionic activity arises from OH^- rather than H^+ ions, it will be more convenient here to use the value $E_B^0(H_2,OH^-)$ as the standard electrode potential [see Eq. (3.61*b*)], which at 25°C is -0.822 V, and which in contrast to the value $E_A^0(H^+,H_2)$ depends on temperature. Hydrogen REs are not used in unbuffered neutral solutions, since here the hydrogen ion concentration (and activity) changes readily, so that the potential is much less stable.

The potential of an electrode of the second kind is determined by the activity (concentration) of anions, or more correctly, by the mean ionic activity of the corresponding electrolyte [see Eq. (3.50)]. The most common among electrodes of this type are the calomel REs. In them, a volume of mercury is in contact with KCl solution which has a well-defined concentration and is saturated with calomel Hg_2Cl_2, a poorly soluble mercury salt. The E^0 value of such an electrode is 0.2676 V (all numerical values refer to 25°C, and potentials are reported on the SHE scale). Three types of calomel electrode are in practical use; they differ in KCl concentration and, accordingly, in the values of ionic activity and potential:

1. Decimolar(decinormal), $c_{KCl} = 0.1\ M$, $E = 0.3337$ V
2. Molar(normal), $c_{KCl} = 1\ M$, $E = 0.2801$ V
3. Saturated (SCE), $c_{KCl} \approx 4.2\ M$, $E = 0.2412$ V

Because of solubility changes, the saturated calomel RE has a large temperature coefficient (0.65 mV/K). Its main advantages are ease of preparation (an excess of KCl is added to the solution) and low values of diffusion potential at interfaces with other solutions (see Section 5.2). The potentials of calomel REs can be reproduced to ± 0.1 mV. These electrodes are very convenient for measurements in neutral solutions (particularly chloride solutions).

In a half-cell with a calomel RE, mercury purified by distillation and mixed with solid calomel is placed on the bottom of the cell. A length of platinum wire fused into glass tubing is fully immersed into the mercury in order to make electrical contact.

The cell and connecting tubes are filled with a KCl solution of the chosen concentration.

Similar designs are used for other REs on the basis of poorly soluble mercury compounds: (1) the mercury–mercurous sulfate RE with H_2SO_4 or K_2SO_4 solutions saturated with Hg_2SO_4, for which $E^0 = 0.6151\,V$; and (2) the mercury–mercuric oxide RE, for measuring electrode potentials in alkaline solutions, with KOH solution saturated with HgO, for which $E_A^0 = 0.098\,V$ and $E_B^0 = 0.920\,V$.

The silver–silver chloride RE consists of a small length of silver wire or piece of silver sheet coated with a thin layer of silver chloride (this layer can be deposited by anodic polarization of the silver in chloride-containing solution) and dipping into HCl or KCl solutions of defined concentration; its $E^0 = 0.2224\,V$.

In alkaline solutions, sometimes the cadmium–cadmium oxide RE is used; its design is the same as that of the silver–silver chloride RE (a thin layer of cadmium oxide is formed on the surface of metallic cadmium). This electrode is quite simple to make and manipulate, but its potential is not very stable; $E_B^0 = +0.013\,V$.

In selecting reference electrodes for practical use, one should apply two criteria: that of reducing the diffusion potentials and that of a lack of interference of RE components with the system being studied. Thus, mercury-containing REs (calomel or mercury–mercuric oxide) are inappropriate for measurements in conjunction with platinum electrodes, since the mercury ions readily poison platinum surfaces. Calomel REs are also inappropriate for systems sensitive to chloride ions.

12.2 VOLTAGE AND ELECTRODE POTENTIAL MEASUREMENTS (POTENTIOMETRY)

An accuracy of 0.1 to 1 mV is needed ordinarily in measurements of the OCV of galvanic cells and of electrode potentials. An accuracy of $10\,\mu V$ is needed when determining thermodynamic parameters. The device used to measure the OCV should not cause any current flow in a galvanic cell. Currents of 10^{-3} to 10^{-4} A would arise when connecting an ordinary permanent-magnet moving-coil voltmeter to the cell; with a circuit resistance of $100\,\Omega$, the ohmic voltage drop would cause the results to be off by several tens of millivolts even without counting the error due to polarization. Therefore, electronic voltmeters with digital readout and very low current drain (10^{-8} to 10^{-14} A) are used for such measurements at present. In the past, compensating potentiometers based on the Wheatstone bridge principle were used for these purposes.

12.3 STEADY-STATE POLARIZATION MEASUREMENTS

12.3.1 Special Technical Features

Steady-state measurements of polarization characteristics can be made when all transitory processes associated with changes in current or potential have ended. Here

one does not count the relatively slow changes in a system's condition, such as a gradual decrease in reactant concentration. The currents measured in the steady state are purely faradaic.

Steady-state measurements can be made over a wide range of current densities (e.g., between 10^{-5} and 10^{4} mA/cm^2), provided that the system being studied will sustain such current densities. The measurements become difficult at lower current densities because of longer transitory processes. For instance, when the electrode's EDL capacitance is 20 μF/cm^2, approximately 10 min would be required at a nonfaradaic current density of 10^{-6} mA/cm^2 to shift the potential by 30 mV (where the charge to be supplied is 6×10^{-4} mC/cm^2). The distorting effects caused by low-level impurities in the system increase strongly during longer measurements. Ohmic factors (in the gap between the electrode and the tip of the Luggin capillary) and local temperature rise affect measurements at high current densities.

In steady-state measurements at current densities such as to cause surface-concentration changes, the measuring time should be longer than the time needed to set up steady concentration gradients. Microelectrodes or cells with strong convection of the electrolyte are used to accelerate these processes. In 1937, B. V. Ershler used for this purpose a "thin-layer electrode," a smooth platinum electrode in a narrow cell, contacting a thin electrolyte layer.

Steady-state measurements can be made *pointwise* or continuously. In the first case the level of perturbation (current or potential) is varied discontinuously, and at some time after the end of transitory processes the response is measured. In the second case the perturbation level is varied continuously, but slowly so as not to disturb the system's steady state.

It is basically irrelevant in steady-state measurements in which direction the polarization curves are recorded: that is, whether the potential is moved in the direction of more positive (anodic scan) or more negative (cathodic scan) values. But sometimes the shape of the curves is seen to depend on scan direction; that is, the curve recorded in the anodic direction does not coincide with that recorded in the cathodic direction (Fig. 12.3). This is due to changes occurring during the measurements in the properties of the electrode surface (e.g., surface oxidation at anodic potentials) and producing changes in the kinetic parameters.

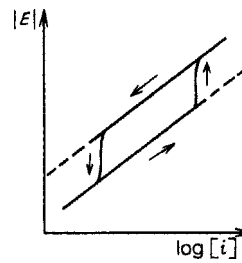

FIGURE 12.3 Schematic shape of polarization curves during an anodic and a cathodic potential scan.

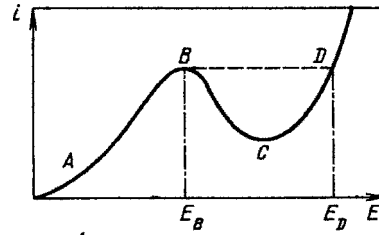

FIGURE 12.4 Polarization (i vs. E) curve with falling section.

12.3.2 Galvanostatic and Potentiostatic Circuits

Steady-state measurements can be made under both galvanostatic and potentiostatic conditions. It is irrelevant for the results of the measurements whether the current or the potential was set first. But in certain cases in which the polarization (i vs. E) curve is nonmonotonic and includes a "falling" section (BC in Fig. 12.4), the potentiostatic method has important advantages, since it allows the potential to be set to any point along the curve and the corresponding current measured. But when the galvanostatic method is used, an increase in current beyond point B causes a jump in potential to point D (i.e., the potential changes discontinuously from the value E_B to the value E_D) and the entire intermediate part of the curve is inaccessible.

Galvanostatic conditions can be realized very simply by connecting in series with the cell an external power source having a much higher voltage ($\mathscr{E}_{\text{ext}}$) than the cell's OCV ($\mathscr{E}_{\text{cell}}$). The current I in the circuit is adjusted with the aid of a high-resistance rheostat R, whereupon its value will be $(\mathscr{E}_{\text{ext}} - \mathscr{E}_{\text{cell}})$. Small fluctuations in cell voltage $\mathscr{E}_{\text{cell}}$ under transitory conditions have little effect in view of the large value of $\mathscr{E}_{\text{ext}}$, so that there is little change in current during the transition period. In practice, various special electronic instruments are used (i.e., galvanostats maintaining the current highly accurately constant whatever the changes in cell voltage).

Potentiostatic conditions are realized with electronic potentiostats. The potential of the working electrode is monitored continuously with the aid of a reference electrode. When the potential departs from a set value, the potentiostat will adjust the current flow in the cell automatically so as to restore the original value of potential. Important characteristics of potentiostats are their rise time and the maximum currents which they can deliver to the cell. Modern high-quality potentiostats have rise times of 10^{-5} to 10^{-6} s.

12.3.3 Calculation of the Kinetic Parameters

Measurements must be made under kinetic control or at least under mixed control of electrode operation if we want to determine the kinetic parameters of electrochemical reactions. When the measurements are made under purely kinetic control (i.e., when the kinetic currents i_k are measured directly), the accuracy with which the kinetic parameters can be determined will depend only on the accuracy with which

the polarization relation is measured. Measurements under mixed control require quantitative estimates of the diffusion currents i_d (e.g., through use of a rotating-disk electrode). The overall accuracy here depends on the ratio of i_k to i_d and on the accuracy with which i_k was determined. For instance, with a ratio of $i_k/i_d = 3$, an error of $\pm 5\%$ in the determination of i_d according to Eq. (6.57) will produce an additional error of $\pm 15\%$ in the calculation of the kinetic current. Hence, this ratio should be regarded as the highest admissible limit.

For a reliable calculation of coefficient α from the potential dependence of kinetic currents, experimental data are needed in which the kinetic currents are varied by at least an order of magnitude. It follows that in at least one point the ratio i_k/i_d should not be higher than 3. In the case considered in Section 6.4, where $i_{d,\text{red}} = i_{d,\text{ox}}$, this corresponds to values of i^0/i_d or k^0/κ_j which are not higher than 0.15. The highest value of κ_j typically found in aqueous solutions is about 2×10^{-2} cm/s. It follows that steady-state methods can yield reliable kinetic parameters only for reactions in which $k^0 \leq 3 \times 10^{-3}$ cm/s. At a component concentration of $10^{-2} M$, this corresponds to exchange current densities $i^0 \leq 3$ mA/cm^2. The possibilities for a determination of kinetic parameters for very slow reactions (e.g., with $k^0 < 10^{-10}$ cm/s) are also limited, this time because of the difficulties encountered in measurements at very low current densities.

In the region of mixed kinetics, graphical methods are often used in determining the kinetic current and corresponding parameters. In measurements with the rotating-disk electrode, the experimental data are plotted as i^{-1} vs. $\omega^{-1/2}$ (Fig. 12.5). According to Eq. (4.52), the values of $\omega^{-1/2}$ are proportional to $1/\omega^{-1/2}$, $1/\kappa_j$, or $1/i_{d,j}$; hence experimental points when thus plotted will adhere to a straight line [see Eq. (6.43)]. The e point of intersection of the straight line with the vertical axis $\omega \to \infty$ immediately yields $1/i_k$ (i.e., the value of the kinetic current).

In measurements under mixed control in the region of high polarization, it will be convenient to plot the experimental data as E vs. $\log i/(i_{d,j} - i)$. From the slope of the resulting straight line we can find the coefficient α, from the ordinate of the half-wave point (where $i = i_{d,j}/2$ and the logarithmic term becomes zero) we can find the values of i^0 or h.

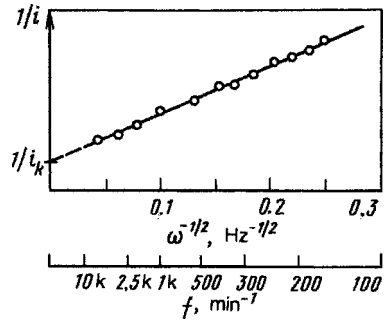

FIGURE 12.5 Calculation of the kinetic current from experimental data obtained with a rotating-disk electrode.

Boris V. Ershler (1908–1978).

12.4 TRANSIENT (PULSE) MEASUREMENTS

Transient measurements (relaxation measurements) are made before transitory processes have ended, hence the current in the system consists of faradaic and nonfaradaic components. Such measurements are made to determine the kinetic parameters of fast electrochemical reactions (by measuring the kinetic currents under conditions when the contribution of concentration polarization still is small) and also to determine the properties of electrode surfaces, in particular the EDL capacitance (by measuring the nonfaradaic current). In 1940, A. N. Frumkin, B. V. Ershler, and P. I. Dolin were the first to use a relaxation method for the study of fast kinetics when they used impedance measurements to study the kinetics of the hydrogen discharge on a platinum electrode.

It is the essence of transient measurements that a certain perturbation is applied to the electrode and then the response is recorded as a function of time. Usually, the transition times are short (fractions of a second), and the transient measurements are performed very rapidly with automated data acquisition.

The transient techniques can be grouped according to various criteria (Fig. 12.6), as follows:

1. *According to the shape of the perturbation*. A step (static perturbation: curve a) when the perturbing parameter is raised discontinuously to a new level, then remains constant; or a continuous (dynamic) variation of the same parameter occurring with a rate sufficiently high to upset the system's steady state; when the rate of variation is constant (curve b), the variation of the perturbation level is called linear (linear scan).
2. *According to the number of perturbations*. Single perturbations (curves a and b); pulses (perturbation in the form of an excursion): square or rectangular (curve c) or triangular (curve d); cyclic perturbations (repetitive excursions: curves e and f); and complex pulses resulting from the combination of several

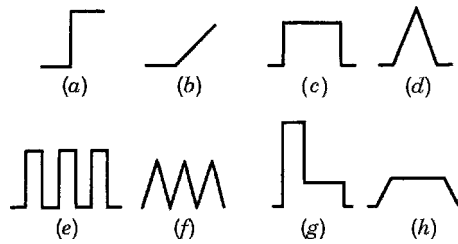

FIGURE 12.6 Various types of perturbation for transient measurements.

of the types of pulses already mentioned: double-step (curve g) and trapezoidal (curve h).

3. *According to the parameter controlled.* When this is the potential, we speak of potentiostatic and potentiodynamic methods; when it is the current, we speak of galvanostatic and galvanodynamic methods (galvanodynamic methods are rarely used); in the coulostatic method a certain amount of charge is delivered to the electrode (e.g., from a capacitor) and the potential–time variation is followed.

For a practical realization of the foregoing transient modes, special programming units or signal synthesizers are used which are integrated in the potentiostatic or galvanostatic equipment.

For the individual types of transient measuring techniques, special names exist but their terminology lacks uniformity. The potentiostatic techniques where the time-dependent current variation is determined are often called *chronoamperometric*, and the galvanostatic techniques where the potential variation is determined are called *chronopotentiometric*. For the potentiodynamic method involving linear potential scans, the term *voltammetry* is used, but this term is often used for other transient methods as well.

12.4.1 Potentiostatic Method (Chronoamperometry)

A certain potential is applied to the electrode with the potentiostatic equipment, and the variation of current is recorded as a function of time. At the very beginning a large current flows, which is due largely to charging of the electrode's EDL as required by the potential change. The maximum current and the time of EDL charging depend not only on the electrode system and size but also on the parameters of the potentiostat used. When this process has ended, mainly the faradaic component of current remains, which in particular will cause the changes in surface concentrations described in Section 11.2.

In a reversible process that occurs under diffusion control, the time-dependent drop of the faradaic current is due to the gradual increase in diffusion-layer thickness. According to Eq. (11.14), we have, for reactants,

$$i_d = nF\,\Delta c\left(\frac{D}{\pi t}\right)^{1/2}. \tag{12.1}$$

In an irreversible reaction that occurs under kinetic or mixed control, the boundary condition can be found from the requirement that the reactant diffusion flux to the electrode be equal to the rate at which the reactants are consumed in the electrochemical reaction:

$$D\left(\frac{\partial c}{\partial x}\right)_{x=0} = hc_S. \tag{12.2}$$

With these boundary conditions, the differential transient-diffusion equation (11.1) has the solution

$$i = nFh\,\Delta c\,\exp(\lambda^2)\,\mathrm{erfc}(\lambda), \tag{12.3}$$

where $\lambda \equiv h(t/D)^{1/2}$ is a dimensionless parameter. It follows from Eqs. (12.1) and (12.3) that

$$\frac{i}{i_d} = \pi^{1/2} h\,\exp(\lambda^2)\,\mathrm{erfc}\,(\lambda). \tag{12.4}$$

We can see when analyzing this equation that the right-hand side is smaller than unity and increases with increasing λ. For $\lambda > 5$ it tends toward unity (i.e., the reaction is practically reversible under the given conditions). Therefore, the kinetic reaction parameters (λ, and hence h) can be determined from the current decay curve only when $\lambda < 5$ (i.e., when $ht^{1/2} < D^{1/2}$). Parameters of reactions for which $h < 3 \times 10^{-2}$ cm/s can be determined when the minimum time at which reliable measurements of the faradaic current are possible is assumed to be a few tenths of a second.

12.4.2 Potentiodynamic Method (Voltammetry)

A linear potential scan (LPS) is applied to the electrode with the aid of the potentiodynamic equipment, that is, a potential that has a constant rate of variation $\upsilon \equiv dE/dt$:

$$E = E_{\text{in}} \pm \upsilon t, \tag{12.5}$$

where E_{in} is the initial potential (at $t = 0$); the plus sign is for the anodic direction, the minus sign for the cathodic direction.

The current is recorded as a function of time. Since the potential also varies with time, the results are usually reported as the potential dependence of current, or plots of i vs. E (Fig.12.7), hence the name *voltammetry*. Curve 1 in Fig. 12.7 shows schematically the polarization curve recorded for an electrochemical reaction under steady-state conditions, and curve 2 shows the corresponding kinetic current i_k (the current in the absence of concentration changes). Unless the potential scan rate υ is very low, there is no time for attainment of the steady state, and the reactant surface concentration will be higher than it would be in the steady state. For this reason the

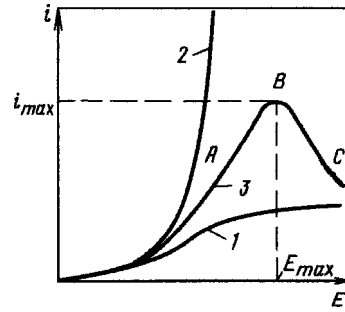

FIGURE 12.7 Polarization curves: (1) steady state, (2) without concentration polarization, (3) potentiodynamic.

current will also be higher than the steady value (section *AB* of curve 3), although it is still lower than the purely kinetic current. As the time increases, the concentration drop will become ever more important, and at some point this factor will begin to predominate over the accelerating effect of potential [i.e., the current will begin to decrease (section *BC*)]. Therefore, in the i vs. E curve, a maximum appears that is typical for this technique and has the coordinates $i_{\max}$ and $E_{\max}$.

A theoretical analysis of the functions obtained is mathematically difficult, hence a simplified analysis is given here. In reversible reactions, the reactant surface concentrations are related to potential in an unambiguous way. For reactions of the type $\mathrm{Ox} + ne^- \rightleftharpoons \mathrm{Red}$, it follows from the Nernst equation and Eq. (12.5) that

$$\frac{c_{S,\mathrm{ox}}}{c_{S,\mathrm{red}}} = \exp\left[\frac{(nF(E_{in} - E^0)}{RT}\right]\exp\left(\frac{\pm nF\upsilon t}{RT}\right). \tag{12.6}$$

A differential equation with these boundary conditions was solved independently by Augustin Ševčík and John E. B. Randles in 1948. The expression obtained for the current is

$$i = nF\left(\frac{nFD\upsilon}{RT}\right)^{1/2} c_V P(u), \tag{12.7}$$

where $u \equiv nF(E - E_{1/2})/RT$ and $E_{1/2}$ is the half-wave potential in the curve of concentration polarization [Eq. (6.26)].

The function $P(u)$ is complicated; it is dimensionless, and can be found numerically. Its shape as shown in Fig. 12.8 at once determines the shape of the i vs. E curve. The value of P in the maximum is 0.446. Hence we obtain for the current in the maximum, at 25°C (when substituting numerical values for F, R, and T),

$$i_{\max} = 2.59 \times 10^5 n^{3/2} (D\upsilon)^{1/2} c_V, \tag{12.8}$$

where the numerical factor has the units $\mathrm{C/mol \cdot V^{1/2}}$.

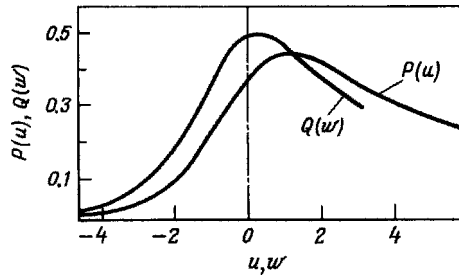

FIGURE 12.8 Functions $P(u)$ and $Q(w)$.

The potential (in volts) corresponding to the maximum of function P is shifted relative to $E_{1/2}$:

$$E_{\max} = E_{1/2} \pm \frac{0.028}{n}. \tag{12.9}$$

Like $E_{1/2}$, the value of $E_{\max}$ is independent of the initial concentrations.

In an irreversible reaction the boundary condition can be written, by analogy with Eq. (12.2),

$$D\left(\frac{\partial c}{\partial x}\right)_{x=0} = k_{\text{in}} c_S \exp\left(\frac{\alpha F v t}{RT}\right), \tag{12.10}$$

where $k_{\text{in}} \equiv k \exp(\alpha F E_{\text{in}}/RT)$.

The differential diffusion equation has the solution

$$i = \left(\frac{\alpha F D v}{RT}\right)^{1/2} c_{V,j} Q(w), \tag{12.11}$$

where $w \equiv \alpha F(E - E_a)/RT$ and $E_a \equiv E^0 - (RT/2\alpha F) \ln(\pi\alpha F D v/RTk_{\text{in}}^2)$.

The dimensionless function $Q(w)$ (see Fig. 12.8) also goes through a maximum, where its value is 0.496. Hence we obtain for the maximum current:

$$i_{\max} = 3 \times 10^5 n(\alpha D v)^{1/2} c_{V,j}. \tag{12.12}$$

The numerical factor in this equation is larger than that in Eq. (12.9), yet the current for an irreversible reaction is lower than that for a reversible reaction, since $\alpha < n$ (for $\alpha = 0.5$ it is 78% of the current for a reversible reaction).

Solutions (12.7) and (12.11) are valid when the initial scan potential, E_{in}, in an anodic scan is at least 0.1 to 0.2 V more negative (in a cathodic scan: more positive) than $E_{1/2}$ or E_a (i.e., when the current in the system is still very low). Under these conditions the current during the scan is still independent of the value selected for E_{in}.

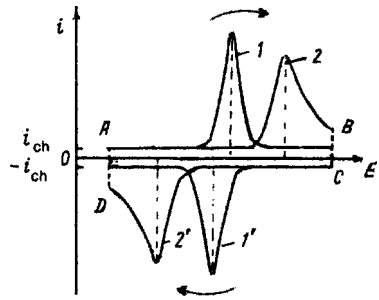

FIGURE 12.9 Anodic (1,2) and cathodic (1′,2′) potentiodynamic i vs. E curves for a reversible (1,1′) and an irreversible (2,2′) reaction (horizontal lines above and below the axis of E refer to the charging current in the absence of reactants).

In a round-trip potential scan the values of E_{max} corresponding to the anodic and cathodic direction are different. For reversible reactions the difference is minor, according to Eq. (12.9) (i.e., only $0.056/n$ V regardless of the component concentrations and of the potential scan rate υ). It is typical for irreversible reactions that the difference between these potentials is much larger (Fig. 12.9); the gap between the maxima increases with decreasing value of the reaction rate constant and increasing scan rate υ.

During the measurements, a nonfaradaic current

$$i_{ch} = \frac{dQ_S}{dt} = C\frac{dE}{dt} = \pm C\upsilon, \tag{12.13}$$

which is consumed for charging the electrode, is superimposed on the faradaic current. If in the region of potentials considered the EDL capacitance, C, is approximately constant, the charging current will also be constant. This implies that the experimental i vs. E curve is shifted vertically relative to the curve which corresponds to the equations above. The influence of charging currents is seen particularly clearly in i vs. E curves recorded with a triangular scan (Fig. 12.9).

At the instant when the scan direction is changed (point B), the charging current changes sign (point C). At this potential, therefore, a discontinuous change in current is observed which corresponds to double the charging current. In repetitive triangular scans an analogous change in current is seen between the terminal (D) and initial (A) points of the curve.

12.4.3 Galvanostatic Method (Chronopotentiometry)

A particular constant current density is applied to the electrode, and the potential variation is followed as a function of time. When there is no electrode reaction, the entire current is a nonfaradaic charging current i_{ch}. According to Eq. (12.13), the slope of the E vs. t curve (Fig. 12.10, curve 1) is determined by the EDL capacitance.

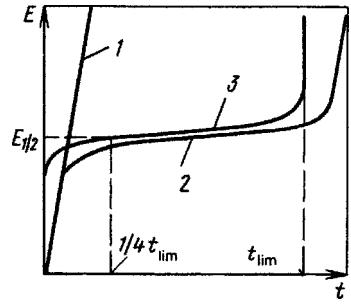

FIGURE 12.10 Galvanostatic curves: (1) without a reaction; (2) with a reaction; (3) corrected for the charging current.

When an electrode reaction takes place, the applied current is divided between the nonfaradaic components and a faradaic component. Because of the latter, there is a gradual decrease in surface concentration of the reactant [according to Eq. (11.6)]. When the time, t_{tr}, required for diffusion to change from transient to steady is large compared to the transition time t_{lim} [Eq. (11.9)], the reactant's surface concentration will fall to zero within the time t_{lim} (see Fig. 11.3).

Consider the shape of the E vs. t relation for the cathodic reaction $Ox + ne^- \rightarrow$ Red, and assume that the initial product concentration $c_{V,red} = 0$. Assume further that the share of nonfaradcaic current is small and that all the applied current can be regarded as faradaic. In reversible reactions the electrode potential is determined by the values of $c_{S,ox}$ and $c_{S,red}$. Prior to current flow the potential is highly positive since $c_{S,red} = c_{V,red} = 0$. When the current has been turned on, the changes in surface concentrations are determined by Eqs. (11.10). Substituting these values into the Nernst equation and taking into account that in our case $c_{V,red} = 0$, we obtain

$$E = E_{1/4} + \frac{RT}{nF} \ln \frac{t_{lim}^{1/2} - t^{1/2}}{t^{1/2}}, \tag{12.14}$$

where $E_{1/4} \equiv E^0 + (RT/nF) \ln(D_{ox}/D_{red})$ is the potential at $t = t_{lim}/4$ (when the logarithmic term becomes zero), which is analogous to the half-wave potential in Eq. (6.26).

The relation between E and t is S-shaped (curve 2 in Fig. 12.10). In the initial part we see the nonfaradaic charging current. The faradaic process starts when certain values of potential are attained, and a typical potential "arrest" arises in the curve. When zero reactant concentration is approached, the potential again moves strongly in the negative direction (toward potentials where a new electrode reaction will start, e.g., cathodic hydrogen evolution). It thus becomes possible to determine the transition time t_{lim} precisely. Knowing this time, we can use Eq. (11.9) to find the reactant's bulk concentration or, when the concentration is known, its diffusion coefficient.

When the nonfaradaic current is not small enough, the appropriate correction must be included when constructing the curves. At constant current, the charge consumed

is proportional to time; therefore, we can graphically correct by subtracting at each potential the time t_{ch} spent for charging of the electrode (or actually, the charge) from the current value of time t (curve 3).

Equations (11.6) or (11.10), which do not depend on the mode of electrode operation, remain valid for irreversible reactions. Substituting the value of $c_{S,ox}$ into the kinetic equation (6.10) for a cathodic process at significant values of polarization, we obtain, after transformations,

$$E = E_{t=0} + \frac{RT}{\alpha F} \ln \frac{1 - t^{1/2}}{t^{1/2}}, \tag{12.15}$$

where $E_{t=0} \equiv (RT/\alpha F) \ln(nFc_{V,ox}k/i)$.

When plotting the experimental data as E vs. $\ln[(1 - t^{1/2})/t^{1/2}]$, we obtain straight lines. The values of α can be determined from their slopes; the values of $E_{t=0}$ and hence k can be obtained by extrapolating these plots to $t = 0$. It is one of the advantages of the galvanostatic method that even if present when measuring the potential, an ohmic error will remain constant during the measurements.

A version of the galvanostatic method is that where the current is turned off (or "a current $i = 0$ is applied") and the polarization decay curve is measured. Consider an electrode which up to the time $t = 0$, when the current was turned off, had the potential E_i at the net current density i_{net}. When the current is turned off, the ohmic voltage drop in the electrolyte gap between the electrode and the tip of the Luggin capillary vanishes, so that the potential instantaneously shifts to the value E_{net} (Fig. 12.11). After that the electrode potential returns (falls) relatively slowly to its open-circuit value, for which a certain nonfaradaic charging current is required. Since $i_F + i_{ch} = i = 0$ after the current has been turned off, the charging current must be compensated by a faradaic current i_f and the electrochemical reaction will continue to the end of the transitory process rather than cease immediately.

Assume that the current i_{net} is sufficiently small and will not cause any marked concentration changes. We shall also assume that the faradaic current in major part

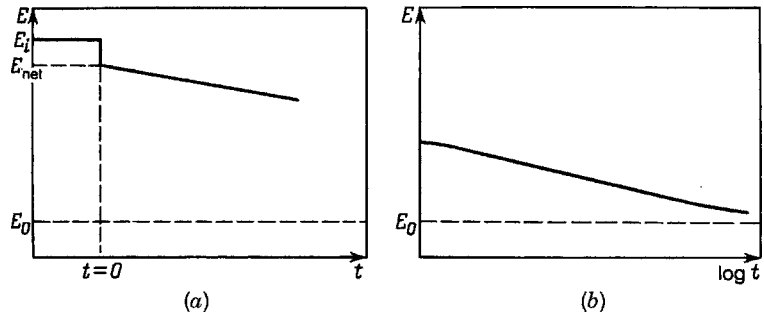

FIGURE 12.11 Potential decay curves recorded after switching off the current: (*a*) at short times; (*b*) at long times.

of the potential decay curve obeys the kinetic equation (6.6); that is, at time t and the potential E_t,

$$i_t = i_{\text{net}} \exp\left(\pm \frac{E_t - E_{\text{net}}}{b} \right) \tag{12.16}$$

(the plus sign is for an anodic reaction). Substituting the expressions for currents i_{ch} and i_t into the relation $i_{\text{ch}} = -i_t$, we find in the case of an anodic reaction that

$$C \frac{dE}{dt} = -i_{\text{net}} \exp\left(\frac{E_t - E_{\text{net}}}{b} \right). \tag{12.17}$$

Integrating this equation between the limits of $t = 0$ and t, taking into account that at $t = 0$ the potential $E = E_{\text{net}}$, and performing simple transformations, we obtain an equation for the potential decay curve:

$$E_t = E_{\text{net}} - b\left(1 + \frac{i_{\text{net}} t}{bC} \right) \tag{12.18}$$

which at short times $t < bC/i_{\text{net}}$ changes to the linear relation (Fig. 12.11*a*)

$$E_t = E_{\text{net}} - \frac{i_{\text{net}} t}{C} \tag{12.19a}$$

and at long times to the logarithmic relation

$$E_t = E_{\text{net}} - b \ln \frac{i_{\text{net}}}{bC} - b \ln t \tag{12.19b}$$

(Fig. 12.11*b*). From the slope of the latter relation we can determine the coefficient b, and from the second term on the right-hand side of Eq. (12.19*b*) or from the slope of the linear relation we can find the electrode's capacitance for the time during which the electrochemical reaction took place at it.

12.5 IMPEDANCE MEASUREMENTS

12.5.1 Electrode Impedance Measurements

When alternating current is used for the measurements, a transient state arises at the electrode during each half-period, and the state attained in any half-period changes to the opposite state during the next half-period. These changes are repeated according to the ac frequency, and the system will be quasisteady on the whole (i.e., its average state is time invariant).

For measurements, an ac component $I_{\sim} = I_m \sin \omega t$ with the amplitude I_m and angular frequency ω ($\omega = 2\pi f$, where f is the ac frequency) is passed through the electrode (alone or in addition to a direct current). Alternating potential (polarization) changes

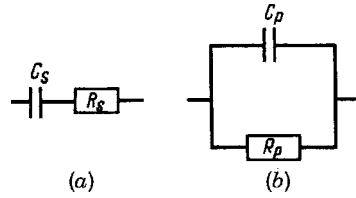

FIGURE 12.12 Equivalent circuits with resistance and capacitance in series (*a*) and in parallel (*b*).

$\Delta E_{\sim}$ having the same frequency and an amplitude ΔE_m are the response. Sometimes alternating potential components are applied, and the resulting alternating current component is measured. In all cases the potential changes are small in amplitude ($\leq$10 mV).

For an electrode behaving like a pure (ohmic) resistance R, the relation between the instantaneous values of current and the changes in potential at all times would be $\Delta E_{\sim}/I_{\sim} = \Delta E_m/I_m = R$. This is actually not found in real electrodes, but instead, a phase shift α analoguous to that observed in electric circuits containing reactive elements appears between alternating current and alternating polarization. In electrochemical systems the potential changes always lag the current changes: $\Delta E_{\sim} = \Delta E_m \times \sin(\omega t - \alpha)$, which corresponds to an electric circuit with capacitive elements. Thus, the ac behavior of an electrode cannot be described in terms of a simple polarization resistance R (even if variable) but only in terms of an impedance $\overline{Z}$ characterized by two parameters: the modulus of impedance $Z \equiv \Delta E_m/I_m$ and the phase shift α. The reciprocal of impedance, $\overline{Y} \equiv 1/\overline{Z}$, is known as *admittance* or *ac conductance*.

A model for the ac response of real electrodes is the simple electric equivalent circuit consisting of a resistance R_s and capacitance C_s connected in series (Fig. 12.12*a*). It follows from the rules for *ac* circuits that for this combination

$$Z = \left[R_s^2 + \left(\frac{1}{\omega C_s}\right)^2\right]^{1/2}, \qquad \tan\alpha = \frac{1}{\omega C_s R_s}. \tag{12.20}$$

We can also use a circuit with a resistance R_p and capacitance C_p connected in parallel (Fig. 12.12*b*). For this circuit

$$Z = \left[\left(\frac{1}{R_p}\right)^2 + \omega C_p\right]^{1/2}, \qquad \tan\alpha = \omega C_p R_p. \tag{12.21}$$

The elements of these two circuit versions are interrelated as

$$\begin{aligned} R_s &= R_p[1 + (\omega C_p R_p)^2]^{-1}, \qquad C_s = C_p[1 + (\omega C_p R_p)^{-2}]; \\ R_p &= R_s[1 + (\omega C_s R_s)^{-2}], \qquad C_p = C_s[1 + (\omega C_s R_s)^2]^{-1}. \end{aligned} \tag{12.22}$$

For the calculations, the capacitive (reactive) impedances $X_s \equiv 1/\omega C_s$ and $X_p \equiv 1/\omega C_p$ are often used instead of capacitances C_s and C_p. The impedance (admittance) of an ac circuit can be stated in terms of a complex number where the

real and imaginary part are the resistive and reactive part of impedance (admittance), respectively. All calculations concerning these circuits can be performed following the rules for manipulation of complex numbers. The impedance of the series network (Fig. 12.12*a*) can be written as

$$\overline{Z} = R_s - jX_s \tag{12.23a}$$

(here j is an imaginary unit). An analogous expression can be written for the admittance of the parallel network (Fig. 12.12*b*):

$$\overline{Y} = \frac{1}{R_p} + j\left(\frac{1}{X_p}\right) = K_p + j\omega C_p \tag{12.23b}$$

(K_p is the conductance, which is equal to $1/R_p$). Thus, the behavior of an electrode at any particular frequency ω can be described by any of the following pairs of parameters: Z and α, R_s and C_s (or X_s), R_p and C_p (or X_p).

But when considered over a wide range of frequencies, the properties of a real electrode do not match those of the equivalent circuits shown in Fig. 12.12; the actual frequency dependence of Z and α does not obey Eq. (12.21) or (12.22). In other words, the actual values of R_s and C_s or R_p and C_p are not constant but depend on frequency. In this sense the equivalent circuits described are simplified. In practice they are used only for recording the original experimental data. The values of R_s and C_s (or R_p and C_p) found experimentally for each frequency are displayed as functions of frequency. In a subsequent analysis of these data, more complex equivalent circuits are explored which might describe the experimental frequency dependence and where the parameters of the individual elements remain constant. It is the task of theory to interpret the circuits obtained and find the physical significance of the individual elements.

In the measurements, one commonly determines the impedance of the entire cell, not that of an individual (working) electrode. The cell impedance $\overline{Z}_{\text{cell}}$ (Fig. 12.13) is the series combination of impedances of the working electrode ($\overline{Z}_{\text{WE}}$), auxiliary electrode ($\overline{Z}_{\text{AE}}$), and electrolyte ($\overline{Z}_e$), practically equal to the electrolyte's resistance (R_e). Moreover, between parallel electrodes a capacitive coupling develops that represents an impedance $\overline{Z}_C$ parallel to the other impedance elements. The experimental conditions are selected so that $\overline{Z}_C \gg \overline{Z}_{\text{WE}} \gg \overline{Z}_{\text{AE}}$. To this end the surface area of the auxiliary electrode should be much larger than that of the working electrode, and these electrodes should be sufficiently far apart. Then the measured cell impedance $\overline{Z}_{\text{cell}}$ is practically given by $\overline{Z}_{\text{WE}} + \overline{Z}_e$.

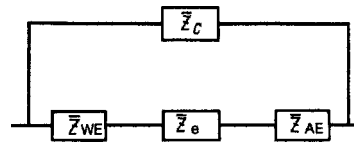

FIGURE 12.13 Equivalent circuit for the impedance of a galvanic cell.

Bridge schemes are used to measure impedance (the Wheatstone bridge, Fig. 12.14). The test cell with its impedance $\overline{Z}_{\text{cell}}$ is connected as one arm of the bridge; the other arm contains sets of precision capacitors and resistors connected in series ($R_{s,2}$ and $C_{s,2}$) [or parallel ($R_{p,2}$ and $C_{p,2}$)], which allow any value of impedance $\overline{Z}_2$ to be selected for this arm. The third and fourth arm have constant, precisely known values of impedance $\overline{Z}_3$ and $\overline{Z}_4$ (usually, standard resistors are used). Potentiometer P is used to compensate the cell's (dc) OCV. An ac of preselected frequency is made to flow across the bridge with the aid of signal generator G. During measurements the impedance of the second arm is adjusted until the ac detected in null detector ND has dropped to zero. The condition of complete bridge balance (equal instantaneous values of potential in points *A* and *B* at any phase of the current) is

$$\overline{Z}_{\text{cell}} : \overline{Z}_2 = \overline{Z}_3 : \overline{Z}_4. \tag{12.24}$$

Knowing the values of all other parameters, we thus can find the cell's impedance. When a symmetric bridge is used (where the values of impedance in the third and fourth arms are identical), the unknown cell impedance components will be equal to the values of $R_{s,2}$ and $C_{s,2}$ or $R_{p,2}$ and $C_{p,2}$ in the second bridge arm.

Ordinarily, the measurements are made over a frequency range from 20 Hz to 50 kHz. Certain difficulties arise in measurements extended over wider ranges of frequency. However, methods suitable for measurements at very low frequencies, down to 1 mHz, have recently been developed that can be used to obtain additional information concerning the properties of electrochemical systems.

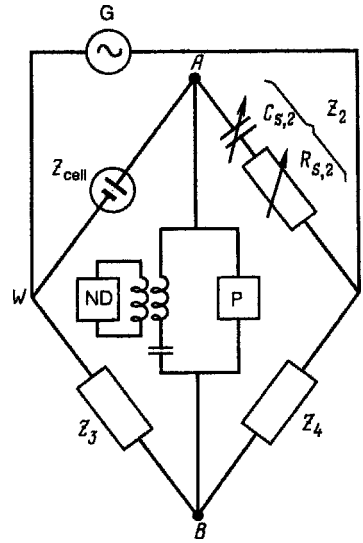

FIGURE 12.14 Bridge arrangement for impedance measurements.

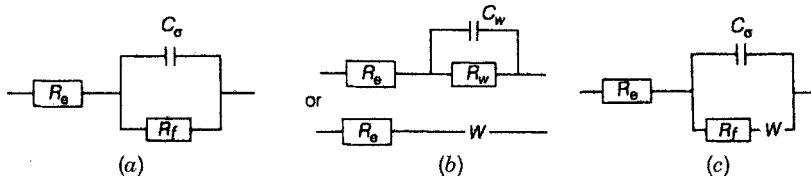

FIGURE 12.15 Electrode impedance with kinetic (*a*), diffusional (*b*), and combined (*c*) reaction control (W is the Warburg impedance).

12.5.2 Impedance in the Case of Irreversible Reactions

Consider the ac behavior of an electrode at which an electrochemical reaction occurs under kinetic control at low polarization [i.e., under conditions where the polarization equation (6.7) is obeyed]. The impedance of a cell containing such an electrode corresponds to the equivalent circuit shown in Fig. 12.15*a*. The impedance of the working electrode is in series with the electrolyte resistance R_e. The current passing through the electrode has a faradaic and a nonfaradaic component. The former gives rise to periodic potential changes as described by Eq. (6.7). The corresponding branch of the equivalent circuit can be represented as a resistance R_f given by the ratio of the (specific) polarization resistance ρ to the electrode's surface area: $R_f = \rho/S$. The nonfaradaic charging current is required for the periodic changes in the amounts of charge in the electric double layer necessitated by the potential variation. It depends on the total capacitance C_σ of the EDL, which is SC (C is the specific capacitance). The charging current in the circuit is independent of the faradaic current, since the circuit element with capacitance C_σ is in parallel with the resistance R_f.

To find the relation between the values of R_s and C_s measured experimentally in terms of the circuit of Fig. 12.11*a* and the parameter values in the circuit of Fig. 12.14*a*, we must first convert [with the aid of Eq. (12.23)] the parameters of the circuit with parallel elements R_f and C_σ into the parameters of a circuit with a resistance and capacitance in series, and to the value of resistance obtained we must add R_e. As a result, we have

$$R_s = R_e + R_f\,[1 + (\omega C\rho)^2]^{-1}; \qquad C_s = C_\sigma\,[1 + (\omega C\rho)^2] \tag{12.25}$$

(here the obvious equality of $R_f C_\sigma = \rho C$ was used).

We can see here that at very low frequencies, R_s tends toward the sum $R_e + R_f$, and C_s tends toward infinity. At very high frequencies, R_s becomes equal to R_e and C_s becomes equal to C_σ. Therefore, by extrapolating the experimental data to zero and to infinite frequency, we basically can find the kinetic reaction parameter R_f (or ρ) and the EDL capacitance as well as the electrolyte's ohmic resistance.

In many cases the extrapolation of experimental data is difficult. To make this extrapolation more accurate, we can use different ways of plotting the experimental

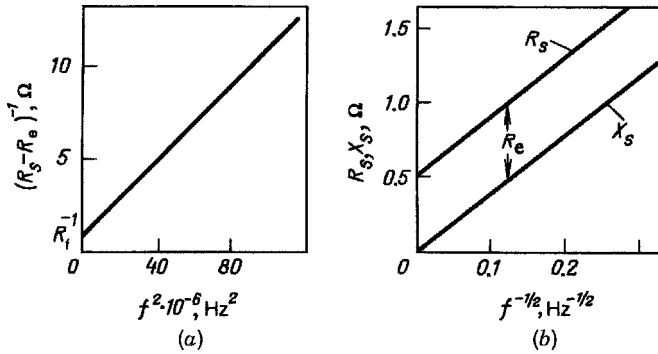

FIGURE 12.16 Examples for an extrapolation of experimental data to determine equivalent circuit parameters under kinetic (*a*) and diffusional (*b*) reaction control.

results. For instance, when R_e has first been determined at high frequencies, we can plot the experimental data as $(R_s - R_e)^{-1}$ vs. f^2. It follows from Eq. (12.25) that the experimental points will then fall onto a straight line, which is readily extrapolated to zero frequency where an intercept $1/R_f$ is produced on the vertical axis. Figure 12.16*a* shows a realistic example for this extrapolation of the experimental data. With the parameters chosen for this example ($S = 1\,\text{cm}^2$, $R_f = 1\,\Omega$, $R_e = 0.5\,\Omega$, and $C_\sigma = 60\,\mu\text{F}$), an ac frequency of at least 50 kHz is required for the prior determination of R_e.

Another coordinate system, plots of capacitive component of impedance X_s, against the resistive component R_s was proposed in 1941 by K. S. Cole and R. H. Cole for electric circuits. In 1963 this system (called *Cole–Cole plots*) was used by M. Sluyters-Rehbach and J. H. Sluyters in electrochemistry for extrapolation of the experimental data. In the case discussed, the resulting *impedance diagram* has the typical form of a semicircle with the center on the horizontal axis (Fig. 12.17*a*). This is readily understood when the term $\omega C\rho$ is eliminated from the expressions for R_s and C_s in Eq. (12.25). Then we obtain, after simple transformations,

$$X_s^2 + \left(R_s - \frac{R_f}{2}\right)^2 = \left(\frac{R_f}{2}\right)^2, \tag{12.26}$$

which is the analytical equation for a semicircle of radius $R_f/2$ having its center in the point of $X_s = 0$ and $R_s = R_e + R_f/2$ when the coordinates of X_s and R_s are used (and these parameters have positive values). Experimental data falling on a semicircle are readily extrapolated to the semicircle's intersections with the horizontal axis. Point *A* corresponds to zero frequency, and point *B* corresponds to infinite frequency. The abscissas of these points are $R_e + R_f$ and R_e, respectively. The frequency is not explicitly apparent in this coordinate system. The corresponding values of the frequencies are stated at the individual points when required.

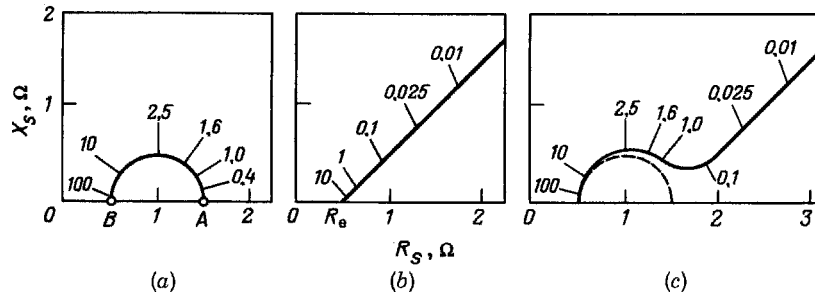

FIGURE 12.17 Impedance diagrams for electrodes under kinetic (*a*), diffusional (*b*), and combined (*c*; very simple case) control of electrode operation (numbers indicate the frequencies f in kHz).

12.5.3 Impedance in the Case of Reversible Reactions

As an example, consider a simple reaction of the type (6.2) taking place under pure diffusion control. At all times the electrode potential, according to the Nernst equation, is determined by the reactant concentrations at the electrode surface. It was shown in Section 11.2.3 that periodic changes in the surface concentrations which can be described by Eq. (11.19) are produced by ac flow. We shall assume that the amplitude of these changes is small (i.e., that $\Delta c_j \ll c_{V,j}$). In this case we can replace $\ln(c_{S,j}/c_{V,j})$ by $\Delta c_j/c_{V,j}$ in Eq. (6.39) for electrode polarization. With this substitution and using Eq. (11.19), we obtain

$$\Delta E = \frac{RT}{nF}\left(\frac{\Delta c_{\text{ox}}}{c_{\text{ox}}} - \frac{\Delta c_{\text{red}}}{c_{\text{red}}}\right)$$

$$= \frac{RT}{n^2F^2} i_m \omega^{-1/2}\left(\frac{1}{c_{V,\text{ox}} D_{\text{ox}}^{1/2}} + \frac{1}{c_{V,\text{red}} D_{\text{red}}^{1/2}}\right) \sin\left(\omega t - \frac{\pi}{4}\right). \tag{12.27}$$

We see that in this case the phase shift is $\pi/4$ (45°). This phase shift corresponds to the circuit shown in Fig. 12.15*b*, which includes the resistance R_w and a capacitance C_w for which $X_w = R_w$; hence, $\tan\alpha = 1$ and $Z_w = 2^{1/2}R_w$ (it does not matter in this case whether the capacitance and resistance are connected in parallel or in series). It follows from Eq. (12.27) that

$$R_w = X_w = A_w \omega^{1/2} \quad \text{and} \quad C_w = \frac{1}{A_w \omega^{1/2}}, \tag{12.28}$$

where $A_w \equiv (RT/n^2F^2)\{[1/(c_{V,\text{ox}} D_{\text{ox}}^{1/2})][1/(c_{V,\text{red}} D_{\text{red}}^{1/2})]\}$ (units: $\Omega \cdot \text{m}^2/\text{s}^{1/2}$).

The impedance Z_w with its components R_w and C_w is known as the *Warburg diffusion impedance*, and constant A_w as the *Warburg constant*. In the equivalent circuits for electrochemical reactions, a Warburg impedance is represented by the symbol −W− as shown in the lower part of Fig. 12.15*b*.

In the Warburg impedance, parameters R_w and C_w are not constant but depend on frequency according to Eq. (12.28). Figure 12.16*b* shows plots of the values of R_s and X_s vs. $f^{-1/2}$ as an example ($A_w/S = 10\ \Omega/s^{1/2}$, $i_f = 0$; the other parameters have the same values as in the example above). The plots are parallel straight lines in these coordinates, according to Eq. (12.28). The line for X_s goes through the coordinate origin; that for R_s is shifted upward since the measured values of R_s in addition to R_w contain the frequency-independent electrolyte resistance.

When the data are plotted in the coordinates of X_s and R_s, the diagram for the present example is a straight line rising at an angle of 45° and producing an intercept corresponding to resistance R_e on the horizontal axis (Fig. 12.16*b*).

12.5.4 Impedance in the Case of More Complex Reactions

In the case of reactions that are not completely irreversible (or not completely reversible), we must account for both the kinetic factors (e.g., the polarization resistance R_f) and the concentration changes (the Warburg impedance). The simplest equivalent circuit for this case is shown in Fig. 12.15*c*, while Fig. 12.17*c* shows the impedance diagram for this circuit ($A_w/S = 10\ \Omega/s^{1/2}$, $R_f = 1\ \Omega$; the other parameters have the same values as in the earlier examples). We see that the character of the plot changes with frequency. At high frequencies (short half-periods) the relative concentration changes are insignificant, and the behavior of the electrodes is determined mainly by the reaction kinetics; plots of X_s against R_s contain the semicircular segment that is typical for this case. The contribution of the concentration changes increases with decreasing ac frequency, and below a certain frequency a linear segment arises that corresponds to the Warburg impedance and constitutes evidence for slow diffusion processes.

In many cases the plots are even more complex, and a theoretical interpretation is difficult. Often, the plots of vs. R_s are evaluated only in a qualitative way, and segments with kinetic semicircles or diffusional straight lines are considered separately.

REFERENCES

Cole, K. S., and R. H. Cole, *J. Chem. Phys.*, **9**, 341 (1941).

Ershler, B. V., *Acta Physicochim. URSS*, **7**, 327 (1937). Ershler, B. V., and A. N. Frumkin, *Trans. Faraday Soc.*, **35**, 464 (1939).

Frumkin, A. N., B. V. Ershler, and P. I. Dolin, *Acta Physicochim. URSS*, **12**, 793, 795 (1940).

Randles, J. E. B., *Trans. Faraday Soc.*, **44**, 327 (1948); **48**, 828 (1952).

Ševčík, A., *Coll. Czech. Chem. Commun.*, **13**, 349 (1948).

Sluyters, J. H., *Recl. Trav. Chim.*, **79**, 1092 (1960); **82**, 100 (1963).

Sluyters-Rehbach, M., and J. H. Sluyters, *Recl. Trav. Chim.*, **82**, 535 (1963).

REVIEWS AND MONOGRAPHS

Bard, A., and L. Faulkner, *Electrochemical Methods: Fundamentals and Applications*, Wiley, New York, 2001.

Gosser, D. K., Jr., *Cyclic Voltammetry: Simulation and Analysis of Reaction Mechanisms*, Wiley, Chichester, West Sussey, England, 1994.

Stojnov, S. B., B. M. Grafov, B. Savova-Stojnova, and V. V. Yelkin, *Electrochemical Impedance* [in Russian], Nauka Publishers, Moscow, 1991.

Varma, R., and J. R. Selman, Eds., *Techniques of Characterization of Electrodes and Electrochemical Processes*, Wiley, New York, 1991, Chap. 2.

PART II
Kinetics of Electrochemical Reactions

13
Multistep Electrode Reactions

13.1 INTERMEDIATE REACTION STEPS

In Chapter 6 we considered the basic rules obeyed by simple electrode reactions occurring without the formation of intermediates. However, electrochemical reactions in which two or more electrons are transferred more often than not follow a path involving a number of consecutive, simpler steps producing stable or unstable intermediates (i.e., they are multistep reactions).

The set of all intermediate steps is called the *reaction pathway*. A given reaction (involving the same reactants and products) may occur by a single pathway or by several parallel pathways. In the case of invertible reactions, the pathway followed in the reverse direction (e.g., the cathodic) may or may not coincide with that of the forward direction (in this example, the anodic). For instance, the relatively simple anodic oxidation of divalent manganese ions which in acidic solutions yields tetravalent manganese ions: $Mn^{2+} \rightarrow Mn^{4+} + 2e^-$, can follow these two pathways:

$$Mn^{2+} \xrightarrow{-e^-} Mn^{3+} \xrightarrow{-e^-} Mn^{4+}, \qquad \text{(I)}$$

$$2[Mn^{2+} \xrightarrow{-e^-} Mn^{3+}]\,; Mn^{3+} \longrightarrow Mn^{2+} + Mn^{4+}. \qquad \text{(II)}$$

The second pathway includes a step in which the trivalent manganese ions formed as intermediates disproportionate.

It is convenient to represent multistep electrode reactions involving one or more pathways in the form of tables such as this:

k	Step	l_k	μ_k(I)	μ_k(II)
1	$Mn^{2+} \rightarrow Mn^{3+} + e^-$	1	1	2
2	$Mn^{3+} \rightarrow Mn^{4+} + e^-$	1	1	
3	$Mn^{3+} \rightarrow Mn^{2+} + Mn^{4+}$	0		1

where l_k is the number of electrons in a step, and μ_k is the *stoichiometric number of a step* in pathways I and II, which indicates how many times this step is repeated in an

Fundamentals of Electrochemistry, Second Edition, By V. S. Bagotsky

elementary reaction act (i.e., during the loss of two electrons from one Mn^{2+} ion). For instance, in a reaction following the second pathway, the first step occurs twice ($\mu_1 = 2$), but one of the Mn^{2+} ions that had reacted is regenerated in the step that follows.

For electrochemical steps as a rule, $l_k = 1$, although for the sake of generality we shall retain the symbol l_k in the equations. Purely chemical steps are also possible, in which electrons are not involved and $l_k = 0$ (e.g., the third step in the example above). Obviously, $\Sigma\mu_k l_k = n$, where n is the total number of electrons involved in one elementary reaction act (here $n = 2$).

Electrochemical steps are often denoted by the letter E (or *e*), and chemical steps by the letter C (or *c*). Thus, the first pathway in the example above can be said to follow an EE scheme, and the second an EC scheme. Except for Section 13.7, the reactions considered below will occur by only a single pathway (in both the forward and reverse directions), and there will be no parallel path.

In multistep reactions, the number of particles of any intermediate B_k produced in unit time in one of the steps is equal to the number of particles reacting in the next step (in the steady state the concentrations of the intermediates remain unchanged). Hence, the rates of all intermediate steps are interrelated. Writing the rate v_k of an individual step as the number of elementary acts of this step that occur in unit time, and the rate v of the overall reaction as the number of elementary acts of the overall reaction that occur within the same time, we evidently have

$$v = \frac{v_1}{\mu_1} = \frac{v_2}{\mu_2} = \cdots = \frac{v_k}{\mu_k} = \cdots = \frac{v_z}{\mu_z}. \tag{13.1}$$

Therefore, in the steady state the reduced rates v_k/μ_k are identical for all steps and equal to the rate of the overall reaction.

Each of the intermediate electrochemical or chemical steps is a reaction of its own (i.e., it has its own kinetic peculiarities and rules. Despite the fact that all steps occur with the same rate in the steady state, it is true that some steps occur readily, without kinetic limitations, and others, to the contrary, occur with limitations. Kinetic limitations that are present in electrochemical steps show up in the form of appreciable electrode polarization. It is a very important task of electrochemical kinetics to establish the nature and kinetic parameters of the intermediate steps as well as the way in which the kinetic parameters of the individual steps correlate with those of the overall reaction.

13.2 RATE-DETERMINING STEP

Consider the correlation between the kinetic parameters of the overall reaction and those of its individual steps in the instance of a very simple, invertible two-step chemical reaction:

$$A \underset{(-1)}{\overset{(1)}{\rightleftharpoons}} B \underset{(-2)}{\overset{(2)}{\rightleftharpoons}} D, \tag{13.2}$$

where B is the reaction intermediate and $\mu_1 = \mu_2 = 1$. We shall assume that both steps are first order in the reactants, that is,

$$v_1 = k_1 c_A - k_{-1} c_B; \qquad v_2 = k_2 c_B - k_{-2} c_D. \tag{13.3}$$

In the steady state, $v_1 = v_2 = v$. With the values of v_1 and v_2 from Eq. (13.3), we find that

$$c_B = \frac{k_1 c_A + k_{-2} c_D}{k_{-1} + k_2} \tag{13.4}$$

for the steady concentration of intermediate B and

$$v = \frac{k_1 k_2 c_A - k_{-1} k_{-2} c_D}{k_{-1} + k_2} \tag{13.5}$$

for the rate of the overall reaction.

The direction of the reaction will depend on the relative concentrations of reactants and products; the reaction will go from left to right when $k_1 k_2 c_A > k_{-1} k_{-2} c_D$, and in the opposite direction, $v < 0$, when the opposite inequality holds.

When we consider the overall reaction while disregarding the formation of intermediates, we can write its rate as

$$v = k_0 c_A - k_{-0} c_D. \tag{13.6}$$

By comparing Eqs. (13.5) and (13.6), we find the connection between the kinetic parameters of the overall reaction and those of the individual steps:

$$k_0 = \frac{k_1 k_2}{k_{-1} + k_2}; \qquad k_{-0} = \frac{k_{-1} k_{-2}}{k_{-1} + k_2} \tag{13.7}$$

A quantity of great importance in these equations is the ratio of parameters k_{-1} and k_2 (i.e., of the constants in the expressions for the rate of reconversion of the intermediates to original reactants and for the rate of conversion of the intermediates to final products). In the particular case of $k_{-1} \ll k_2$, it follows from Eq. (13.5) that

$$v = k_1 c_A - \frac{k_{-1} k_{-2}}{k_2} c_D = k_1 c_A - k_{-1} c^0_{B(D)}. \tag{13.8}$$

Here $k_{-1} c^0_{B(D)}$ is the concentration of intermediate B that would be found under conditions of complete equilibrium between it and the reaction products (i.e., $k_2 c^0_{B(D)} = k_{-2} c_D$):

$$c^0_{B(D)} = \frac{k_{-2}}{k_2} c_D. \tag{13.9}$$

It is a very important conclusion following from Eq. (13.8) that in the case considered, the rate of the overall reaction is determined wholly by the kinetic parameters of the first step (k_1 and k_{-1}), while the second step influences this rate only through the equilibrium concentration of the intermediate B. We say, therefore, that the first step (with its low value of parameter k_{-2}) is the *rate-determining step* (RDS) of this reaction. Sometimes the term *slow step* is used, but this term is not very fortunate, inasmuch as the *effective* rates, υ_1 and υ_2, of the two steps actually are identical. Analogously, when $k_{-1} \gg k_2$, we have

$$\upsilon = \frac{k_1 k_2}{k_{-1}} c_A - k_{-2} c_D = k_2 c^0_{B(A)} - k_{-2} c_D, \tag{13.10}$$

where

$$c^0_{B(A)} = \frac{k_1}{k_{-1}} c_A. \tag{13.11}$$

In this case, the overall reaction rate is determined by the parameters of the second step (i.e., this step is now rate determining, and the concentration of the intermediate B is determined by the equilibrium of the first step).

Generally, reactant A and product D will not be in chemical equilibrium since their concentrations, c_A and c_D, are defined arbitrarily. Hence, $c^0_{B(A)}$ and $c^0_{B(D)}$ will have different values; they will coincide only in the particular case of overall equilibrium between substances A and D, which will be established at concentration ratios $c_D/c_A = k\, k_2/k_{-1}k_{-2}$.

It is important to note that it is precisely the ratio of k_{-1} and k_2 that decides which step is rate determining, not the ratios of the parameters of both steps in the forward reaction (k_1 and k_2) or in the reverse reaction (k_{-1} and k_{-2}).

In chemical reactions, the kinetic parameters k_k and k_{-k} are constant for given conditions (of temperature, etc.). Hence, the same step will be rate determining in the forward and reverse directions of the reaction (provided that the reaction pathways are the same in both directions).

The assumption had been made in deriving Eq. (13.4) that the concentration of the intermediate B is determined solely by the balance of rates of individual steps of the process. It is implied here that this intermediate cannot escape from the reaction zone by processes such as diffusion and evaporation.

13.3 TWO-STEP ELECTROCHEMICAL REACTIONS

13.3.1 Equilibrium Conditions

All the relations reported above are valid for simple two-step electrochemical reactions, when instead of rate constants k_k of the individual steps or of the reaction as a whole, we use the corresponding kinetic parameters h_k. We shall assume for the sake

of definition that in the electrochemical reaction substance A is the reducing agent and substance D is the oxidizing agent [i.e., that in Eq. (13.2) the anodic reaction is that going from left to right].

Electrochemical reactions differ fundamentally from chemical reactions in that the kinetic parameters h_k are not constant (i.e., they are not rate "constants") but depend on the electrode potential. In the typical case this dependence is described by Eq. (6.33). This dependence has an important consequence: At given arbitrary values of the concentrations c_A and c_D, an equilibrium potential E_0 exists in the case of electrochemical reactions which is the potential at which substances A and D are in equilibrium with each other. At this point (E_0) the intermediate B is in common equilibrium with substances A and D. For this equilibrium concentration we obtain from Eqs. (13.9) and (13.11),

$$c_B^0 = \frac{h_1^0}{h_{-1}^0} c_A = \frac{h_{-2}^0}{h_2^0} c_D. \tag{13.12}$$

At the point of equilibrium, the exchange rate of the reaction as a whole is given by

$$\upsilon_1^0 = h_0^0 c_A = h_{-0}^0 c_B^0; \qquad \upsilon_2^0 = h_2^0 c_B^0 = h_{0-2}^0 c_D. \tag{13.13}$$

and the exchange rates of the individual steps are given by

$$\upsilon_1^0 = h_1^0 c_A = h_{-0}^0 c_D; \qquad \upsilon_2^0 = h_2^0 c_B^0 = h_{-2}^0 c_D. \tag{13.14}$$

With Eq. (13.7), this yields the following relation between the exchange rates:

$$\frac{1}{\upsilon^0} = \frac{1}{\upsilon_1^0} + \frac{1}{\upsilon_2^0}, \tag{13.15}$$

which is valid for electrochemical reactions at the equilibrium potential.

When the rate of the overall reaction is stated in electrical units [i.e., in terms of the current density (CD) $i \equiv nF\upsilon$], it will be convenient to use the concept of partial current densities of the first and second steps, which are defined as $i_1 \equiv l_1 F \upsilon_1$ and $i_2 \equiv l_2 F \upsilon_2$. In the steady state, $\upsilon = \upsilon_1 = \upsilon_2$ and $i = i_1 + i_2$. With these parameters, Eq. (13.15) becomes

$$\frac{n}{i^0} = \frac{l_1}{i_1^0} + \frac{l_2}{i_2^0}. \tag{13.16}$$

13.3.2 General Kinetic Equation

The rates of an electrochemical reaction at potentials away from the equilibrium value are given by Eq. (13.5), which in this case can be written as

$$i = nF\left(h_2 c_A - \frac{h_{-1} h_{-2} c_D}{h_{-2} + h_2}\right). \tag{13.17}$$

Since parameters h_k depend on potential, the RDS may not be the same in different regions of potential. Consider the two pairs of inequalities

$$\begin{aligned} &\text{(1a) } h_1 h_2 c_A > h_{-1} h_{-2} c_D \quad \text{and} \quad \text{(1b) } h_1 h_2 c_A < h_{-1} h_{-2} c_D; \\ &\text{(2a) } h_2 > h_{-1} \quad \text{and} \quad \text{(2b) } h_2 > h_{-1}. \end{aligned} \tag{13.18}$$

Inequality (1a) is valid for anodic polarization, inequality (1b) for cathodic polarization $i < 0$. In this case, the point of changeover is evidently the equilibrium potential E_0. However, the changeover from inequality (2a) to inequality (2b) generally occurs at another value of potential, that of the change in mechanism, E_{cm}. At potentials more positive than E_{cm} inequality (2a) holds, and step 1 is the RDS at potentials more negative than E_{cm}, step 2 is the RDS.

At high anodic potentials when the electrode potential is more positive than both E_0 and E_{cm}, inequalities (1a) and (2a) hold and step 1 is the RDS. The kinetic equation then is

$$i = nFh_1 c_A = nFk_1 c_A \exp\left(\frac{\beta_1 FE}{RT}\right) \tag{13.19}$$

(the reverse reaction can be disregarded). In exactly the same way, at high values of cathodic polarization when the electrode potential is more negative than both E_0 and E_{cm}, step 2 is the RDS; it is the first step in the cathodic direction [i.e., of reaction (13.2) occurring from right to left]. The kinetic equation now is

$$i = nFh_{-2} c_D = nFk_{-2} c_D \exp\left(-\frac{\beta_2 FE}{RT}\right). \tag{13.20}$$

The behavior in the regions of moderate anodic or cathodic polarization depends on the relative positions of potentials E_{cm} and E_0, which in turn depend on the relative values of constants k_1 and k_{-2}. For E_{cm} which are more positive than E_0 (Fig. 13.1*a*), relation (13.20) for the cathodic CD remains valid at all values of cathodic polarization (except for the region of low values where the reverse reaction must be taken into account). At moderate values of anodic polarization, inequalities (1a) and (2b) are found to be valid at potentials more negative than E_{cm}, while step 2 becomes rate determining, which is the second step along the reaction path. In this case [see Eq. (13.10)], we have

$$i = nF\frac{h_1}{h_{-1}} h_2 c_A \tag{13.21}$$

or when we decode the parameters h_k [Eq. (6.33)] and take into account that according to Eq. (6.20), $\beta_m + \beta_{-m} = l_m$,

$$i = nF\frac{k_1}{k_{-1}} k_2 c_A \exp\left[\frac{(l_1 + \beta_2)FE}{RT}\right]. \tag{13.22}$$

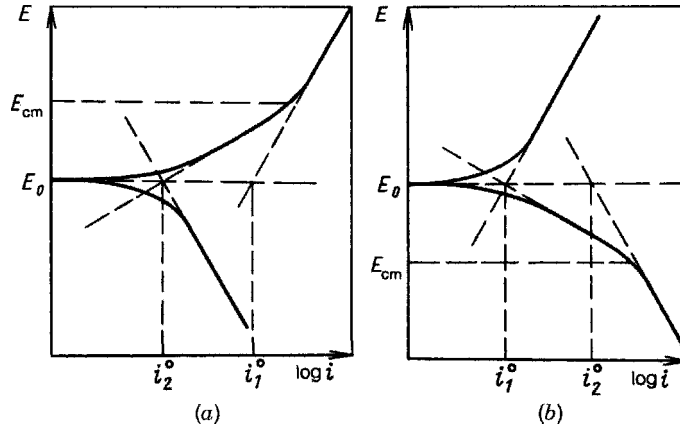

FIGURE 13.1 Polarization curves for a two-step reaction.

However, for E_{cm} which are more negative than E_0 (Fig. 13.1*b*), relation (13.19) remains valid at all values of anodic polarization. At moderate values of cathodic polarization or potentials more positive than E_{cm}, step 1 will be rate determining, which is the second step along the reaction path, and we find for the kinetic equation

$$i = nF\frac{h_{-2}}{h_2}h_{-1}c_D = nF\frac{k_{-2}}{k_2}k_{-1}c_D \exp\left[\frac{(l_2+\beta_{-2})FE}{RT}\right]. \tag{13.23}$$

We can see here that a formal change occurs in the polarization equation at potential E_{cm}; in particular, transfer coefficient β_0 changes. When the two steps are one-electron steps $l_k = 1$ and all transfer coefficients of the individual steps are close to 0.5, the value of β_0 will change from 0.5 in the region of very large polarization to 1.5 at lower values of polarization, on the other side of E_{cm}. Slope b' in the Tafel equation changes accordingly from 0.12 to 0.04 V, and the polarization curve exhibits two logarithmic sections (two Tafel slopes). Such breaks in the polarization curve (when plotted semilogarithmically) are a typical indication for multistep electrochemical reactions involving a change in the RDS.

It follows from these kinetic equations that in reactions where the RDS occurs after another step, which is an equilibrium step, the kinetic coefficients k_0 and β_0 of the overall reaction are different from the corresponding coefficients of the RDS; in fact, in the first case, $k_0 \equiv (k_1/k_{-1})k_2$ and $\beta_0 \equiv l_1 + \beta_2$, and in the second case, $k_{-0} \equiv (k_{-2}/k_2)k_{-1}$ and $\beta_0 \equiv l_2 + \beta_{-1}$. It is important to note that if the preceding equilibrium step is an electrochemical step ($l_1 \geq 1$), the transfer coefficient β_0 of the overall reaction will always be larger than unity. The sum of transfer coefficients in the forward and reverse directions of the overall reaction is given by

$$\beta_0 + \beta_{-0} = l_1 + \beta_2 + \beta_{-2} = l_1 + l_2 = n \tag{13.24}$$

[i.e., relation (6.17*a*) remains valid]. However, when different steps are rate determining under cathodic and anodic polarization, the sum of transfer coefficients of these steps, $\beta_1 + \beta_{-2}$ or $\beta_2 + \beta_{-1}$, generally will be different from n, l_1, or l_2.

When the logarithmic sections of the polarization curves are extrapolated to the equilibrium potential E_0, they yield intercepts on the horizontal axis which represent the logarithms of exchange CD of the individual steps (up to factors n/l). By extrapolation of the section at high anodic potentials, we obtain, according to Eq. (13.20), the exchange CD $(n/l_1)i_1^0$ of step 1, but by extrapolation of the section at high cathodic potentials we obtain, again according to Eq. (13.20), the exchange CD $(n/l_2)i_2^0$ of step 2. It follows that in both cases we obtain the exchange CD of the step that comes first in the reaction path. Analogously, when extrapolating the section in the region of less important polarization (between potentials E_{cm} and E_0), we obtain, according to Eqs. (13.22) or (13.24), the exchange CD of the step that comes second in the reaction path (see Fig. 13.1).

Thus, in the region of very high anodic or cathodic polarization, the RDS is always the first step in the reaction path. The transfer coefficient of the full reaction which is equal to that of this step is always smaller than unity (for a one-electron RDS), while slope i' in the Tafel equation is always larger than 0.06 V. When the potential E_{cm} is outside the region of low polarization, a section will appear in the polarization curve at intermediate values of anodic *or* cathodic polarization where the transfer coefficient is larger than unity and b' is smaller than 0.06 V. This indicates that in this region the step that is second in the reaction path is rate determining.

A break in the polarization curve will not be observed when the kinetic parameters of the two steps (h_1 and E_{cm-2}, i_1^0 and i_2^0) are drastically different, and hence, potential E_{cm} is in the region of excessive anodic or cathodic polarization where measurements become impossible or where the behavior observed is distorted by other phenomena (e.g., concentration polarization). For this reason two-step reactions often follow the behavior outlined in Chapter 6 for simple one-step reactions throughout the range where measurements can be made and have the same rate-determining step in the forward and reverse directions (quasi-one-step reactions).

13.3.3 Region of Low Polarization

For an analysis of the polarization curves at low values of polarization (low overpotentials), we shall use the general polarization equation

$$i = \frac{n i_1^0 i_2^0 (\gamma_1\gamma_2 - \gamma_{-1}\gamma_{-2})}{l_2\gamma_{-1} i_1^0 + l_1\gamma_2 i_2^0}, \tag{13.25}$$

which follows from the kinetic equation (13.17) when h_k is replaced by $\gamma_k h_k^0$ and we take into account that $i_1^0 = l_1 F h_1^0 c_A = l_1 F h_{-1}^0 c_B$ and $i_2^0 = l_2 F h_2^0 c_A = l_2 F h_{-2} c_D$.

At low values of polarization it will suffice to retain the first two terms of series expansions of the exponentials (i.e., to assume that $\gamma_k \equiv 1 + \beta_k F\,\Delta E/RT$ and $\gamma_{-k} \equiv 1 - \beta_{-k} F\,\Delta E/RT$). When substituting these values into Eq. (13.25) and taking into account that $\beta_1 + \beta_{-1}\beta_2 + \beta_{-2} = l_1 + l_2 = n$, we find that

$$i = \frac{i_1^0 i_2^0 (nF\,\Delta E/RT)}{l_2 i_1^0 + l_1 i_2^0 + (l_1\beta_2 i_2^0 - l_2\beta_{-1} i_1^0)(nF\,\Delta E/RT)} \tag{13.26}$$

This equation is of the general form $i = K\Delta E/(M + N\Delta E)$, where K, M, and N are constants. Derivative $di/d\,\Delta E$ of this function has the value $KM/(M + N\Delta E)^2$; and in the particular case where $\Delta E = 0$ the derivative has the value K/M. Thus, when allowing for Eq. (13.17) we find for polarization resistance ρ, which for $\Delta E = 0$ is equal to dE/di:

$$\rho = \frac{RT}{nF}\,\frac{l_2 i_1^0 + l_1 i_2^0}{n\, i_1^0 i_2^0} = \frac{RT}{nF}\,\frac{1}{i_0^0}. \tag{13.27}$$

It follows that from the slope of the linear section in the polarization curve close to the equilibrium potential, we can determine the exchange CD i_0^0 of the overall reaction.

Thus, in the case of two-step reactions, different methods of determining the exchange CD generally yield different results (in contrast to the case of simple reactions discussed earlier): Extrapolation of the limiting anodic and cathodic sections of the semilogarithmic plots yields values i_1^0 and i_2^0, respectively, while the slope of the linear section in an ordinary plot of the polarization curve yields the value of i_0^0. It is typical for multistep reactions that the exchange CD determined by these methods differ.

The exchange CD determined by different methods will coincide only in the case of quasi-one-step reactions mentioned above. Thus, when the value of i_1^0 is so much higher than i_2^0 that the extreme anodic section cannot be measured and there is no break in the polarization curve, all three methods of determination lead to the same value of i_2^0. This implies that step 1 has no effect at all on the kinetics of the overall reaction and that its (high) exchange CD cannot be determined. The same conclusion holds in the opposite case of $i_1^0 \ll i_2^0$.

13.4 COMPLEX ELECTROCHEMICAL REACTIONS

In many electrochemical reactions the individual steps differ in their stoichiometric numbers, in contrast to what was found for reactions of the type of (13.2). A two-step reaction can generally be formulated as

$$\text{(step 1)} \qquad \nu_A A \rightleftharpoons \nu_B B + l_1 e^-, \tag{13.28}$$

$$\text{(step 2)} \qquad \nu'_B B \rightleftharpoons \nu_D D + l_2 e^-. \tag{13.29}$$

It follows from the steady-state condition for the numbers of particles B generated and consumed in the reaction that

$$\mu_1 \nu_B = \mu_2 \nu'_B, \tag{13.30}$$

where μ_1 and μ_2 are the stoichiometric numbers of steps 1 and 2. For the number of electrons, the relation

$$\mu_1 l_1 + \mu_2 l_2 = n \tag{13.31}$$

is valid.

Consider the case of a quasi-one-step reaction for which step 1 is rate determining at all potentials, while step 2 is in equilibrium. When using the Nernst equation (3.40) for this equilibrium, we find that

$$c_B^{\nu'_B} = K_2 c_D^{\nu_D} \exp\left(\frac{-l_2 FE}{RT}\right). \tag{13.32}$$

When a current flows, the kinetic laws are determined by step 1. For the region where anodic polarization is sufficiently high, we obtain

$$i = nFk_{-1} c_A^{\nu_A} \exp\left(\frac{\beta_1 FE}{RT}\right) = i_1^0 \exp\left(\frac{\beta_1 F\Delta E}{RT}\right) \tag{13.33}$$

(here the factor n/l_1 has conditionally been included into the value of i_1^0). For the region of cathodic polarization, and allowing for Eqs. (13.32) and (13.30), we find that

$$\begin{aligned} i &= nFk_{-1} c_B^{\nu_B} \exp\left(-\frac{\beta_{-1} FE}{RT}\right) \\ &= i_1^0 \exp\left[\left(-\beta_{-1} + \frac{\mu_2 l_2}{\mu_1}\right)\frac{F\Delta E}{RT}\right]. \end{aligned} \tag{13.34}$$

In the region of low polarization, when retaining only two terms in the series expansions of the exponentials, we obtain

$$i = i_1^0 \left(\beta_1 + \beta_{-1} + \frac{\mu_2 l_2}{\mu_2}\right) \frac{F\Delta E}{RT} \tag{13.35}$$

and when allowing for Eq. (13.31) and the relation $l_1 = \beta_1 + \beta_{-1}$ [see Eq. (6.24)], we obtain

$$i = i_1^0 \frac{1}{\mu_1} \frac{nF\Delta E}{RT}. \tag{13.36}$$

This equation is of interest since it contains the stoichiometric number, μ_1, of the rate-determining step. This number did not appear in the analogous Eq. (6.18), since in the example considered when deriving this equation, it was unity. Using the exchange CD i_1^0 determined by extrapolation of the Tafel sections with Eq. (13.33) or (13.34), we can determine μ_1 from the slope of the linear section of the polarization curve and Eq. (13.36). In a number of cases this method can be used to find out which of the intermediate steps is rate determining. An analogous expression is obtained when step 2 is rate determining. The stoichiometric number of the RDS is often simply called the stoichiometric number of the reaction itself.

The general kinetic equations for electrode reactions with more than two steps are extremely complex and practically never used. The kinetic features of such reactions are usually examined separately in different regions of potential each having a particular step as the RDS. When the exchange CD of one of the steps is much lower than the exchange CD of all other steps, the polarization characteristics of the multistep reaction will coincide with those of a simple one-step electrochemical reaction, practically throughout the region of measurements (as in the analogous case of two-step reactions).

13.5 REACTIONS WITH HOMOGENEOUS CHEMICAL STEPS

Consider an electrochemical reaction of the type $\mathrm{Red} \rightleftharpoons \mathrm{Ox} + e^-$, which occurs under conditions when the chemical reaction (and equilibrium)

$$\nu_A A + \nu_{red}\mathrm{Red} \rightleftharpoons \nu_j X_j + \nu_l X_l \tag{13.37}$$

is possible between the component Red and a substance A in the bulk electrolyte; here X_j and X_l are other possible reaction components.

When the current is anodic, component Red is consumed and the equilibrium in the electrolyte close to the surface is disturbed; reaction (13.37) will start to proceed from left to right, producing additional amounts of species Red. In this case the chemical precedes the electrochemical reaction. However, when the current is cathodic, substance Red is produced and the chemical reaction (13.37), now as a subsequent reaction, will occur from right to left. When component Ox rather than component Red is involved in the chemical reaction, this reaction will be the preceding reaction for cathodic currents, but otherwise all the results to be reported below remain valid.

Preceding and subsequent homogeneous chemical reactions that occur in the bulk solution are very common. Examples include dehydration (when only a nonhydrated form of the substance is involved in the electrochemical reaction), protonation (e.g., of the anions of organic acids), and decay of complexes (in metal deposition from solutions of complex salts).

Equilibrium between substances A and Red will be preserved during current flow not only in the bulk solution but even near the electrode surface when the chemical reaction has a high exchange rate. Therefore, a change in surface concentration of the substance Red which occurs as a result of the electrochemical reaction will give

rise to the corresponding change in equilibrium concentration of the substance A and to the development of concentration gradients with respect to both substances. When the current is anodic, reactant Red will be supplied from the bulk solution both as such and in the form of particles of substance A which near the surface are converted to particles Red. The diffusion fluxes of the two substances have a common effect, and the total limiting diffusion CD i_l is the sum of two components, $i_{l,\mathrm{red}}$ and $i_{l,\mathrm{A}}$. When calculating the surface concentration of substance Red in Eq. (4.11), we must use the combined limiting CD of both substances.

The situation is different when the chemical reaction is not very fast. In this case the equilibrium between substances Red and A in the solution layers near the electrode will be disturbed, and the rate at which reactant Red is replenished on account of reaction (13.37) decreases. When the chemical reaction is very slow, the limiting CD will approach the value $i_{l,\mathrm{red}}$.

Consider the case when the equilibrium concentration of substance Red, and hence its limiting CD due to diffusion from the bulk solution, is low. In this case the reactant species Red can be supplied to the reaction zone only as a result of the chemical step. When the electrochemical step is sufficiently fast and activation polarization is low, the overall behavior of the reaction will be determined precisely by the special features of the chemical step; concentration polarization will be observed for the reaction at the electrode, not because of slow diffusion of the substance but because of a slow chemical step. We shall assume that the concentrations of substance A and of the reaction components are high enough so that they will remain practically unchanged when the chemical reaction proceeds. We shall assume, moreover, that reaction (13.37) follows first-order kinetics with respect to Red and A. We shall write c_0 for the equilibrium (bulk) concentration of substance Red, and we shall write c_S and c for the surface concentration and the instantaneous concentration (to simplify the equations, we shall not use the subscript "red").

Under the assumptions made, the rate of the chemical step can be written as

$$v_{\mathrm{ch}} = k_{\mathrm{ch}} c_{\mathrm{A}} - k_{-\mathrm{ch}} c \tag{13.38}$$

or, when we use the parameter of exchange rate, $v^0 = k_{\mathrm{ch}} c_{\mathrm{A}} = k_{-\mathrm{ch}} c_0$, as

$$v_{\mathrm{ch}} = v^0 \left(1 - \frac{c}{c_0}\right) = k_{-\mathrm{ch}}(c_0 - c). \tag{13.39}$$

Each of the particles of Red produced in the chemical reaction will, after some (mean) time t, have been reconverted to A. Hence, when the current is anodic, only those particles of Red will be involved in the electrochemical reaction which within their own lifetime can reach the electrode surface by diffusion. This is possible only for particles produced close to the surface, within a thin layer of electrolyte called the *reaction layer*. Let this layer have a thickness δ_r. As a result of the electrochemical reaction, the concentration of substance Red in the reaction layer will vary from a value c_0 at the outer boundary to the value c_S right next to the electrode; within the layer a concentration gradient and a diffusion flux toward the surface are set up.

It is a special feature of this diffusion situation that substance Red is produced by the chemical reaction, all along the diffusion path (i.e., sources of the substance are spatially distributed). For this reason the diffusion flux and the concentration gradient are not constant but increase (in absolute values) in the direction toward the surface. The incremental diffusion flux in a layer of thickness dx [$(dJ_d/dx)dx$ or $-D(d^2c/dx^2)\,dx$] should be equal to the rate, $v_{ch}\,dx$, of the chemical reaction in this layer. Hence, we have

$$\frac{d^2c}{dx^2} = \frac{v_{ch}}{D} = \frac{k_{-ch}}{D}(c - c_0). \tag{13.40}$$

When the sign convention adopted for rate v_{ch} is taken into account, this equation holds for both anodic and cathodic currents.

The method used for integrating Eq. (B.5) in Appendix B will be used to integrate the differential equation (13.40) over the variable x. Then we obtain

$$\left(\frac{dc}{dx}\right)^2 = \frac{k_{-ch}}{D}(c - c_0). \tag{13.41}$$

Far from the surface ($x \to \infty$), the value of c tends toward c_0, while the value of (dc/dx) tends toward zero. Hence, we can determine the integration constant, $K = (k_{-ch}/D)c_0^2$. We finally have

$$\frac{dc}{dx} = \sqrt{\frac{k_{-ch}}{D}}(c_0 - c) \tag{13.42}$$

[the sign of the root of Eq. (13.41) is selected so that for $c < c_0$ we have $dc/dx > 0$, and vice versa].

The current density is determined by the diffusion flux directly at the surface ($x = 0$), where substance Red has the concentration c_S:

$$i = nFD\left(\frac{dc}{dx}\right)_{x=0} = \pm\left(1 - \frac{c_S}{c_0}\right), \tag{13.43}$$

where

$$i_r = nFc_0\sqrt{\frac{k_{-ch}}{D}}. \tag{13.44}$$

This equation links the current density to surface concentration. In the case discussed (where there is no activation polarization), the Nernst equation unequivocally links the electrode's polarization to the difference between surface and bulk concentration:

$$\frac{c_S}{c_0} = \exp\left(-\frac{nF\,\Delta E}{RT}\right). \tag{13.45}$$

For the polarization function we obtain, as a result,

$$i = i_r\left[1 - \exp\left(-\frac{nF\,\Delta E}{RT}\right)\right]. \tag{13.46}$$

When anodic polarization is appreciable ($\Delta E \gg 0$), the CD will tend toward the value i_r and then remain unchanged when polarization increases further. Therefore, parameter i_r, as defined by Eq. (13.44), is a limiting CD arising from the limited rate of a homogeneous chemical reaction when c_S drops to a value of zero; it is the *kinetic limiting current density*.

At low values of $|\Delta E|$, the exponential term in Eq. (13.46) can be replaced by the first two terms of the series expansion, and hence

$$i = i_r\frac{nF\,\Delta E}{RT} = \frac{n^2F^2}{RT}c_0\sqrt{k_{-\mathrm{ch}}D}\,\Delta E. \tag{13.47}$$

Thus, at low values of polarization we again find proportionality between current density and polarization.

When cathodic polarization is appreciable ($\Delta E \ll 0$), Eq. (13.46) changes into

$$i = i_r\exp\left(-\frac{nF\,\Delta E}{RT}\right). \tag{13.48}$$

In this case the usual exponential dependence analogous to Eq. (6.12) is obtained.

All these equations differ from the corresponding equations for diffusion polarization, only in that the equilibrium concentration c_0 appears in them instead of bulk concentration c_V. Formally, diffusion can be regarded as a first-order reaction, the limiting diffusion flux being proportional to the first power of concentration.

The concentration distribution in the reaction layer can be found by integrating Eq. (13.42):

$$c(x) = c_0 - (c_0 - c_S)\exp\left(-\sqrt{\frac{k_{-\mathrm{ch}}}{D}}x\right). \tag{13.49}$$

The concentration asymptotically approaches the value c_0 with increasing distance x (i.e., the reaction zone has no distinct boundary). Conventionally, thickness δ_r is defined just like the diffusion-layer thickness δ [i.e., by the condition that $c_0/\delta_r = (dc/dx)_{x=0}$ for zero surface concentration. Using Eq. (13.41), we find that

$$\delta_r = \sqrt{\frac{D}{k_{-\mathrm{ch}}}}. \tag{13.50}$$

It can be seen here that the larger the value of k_{-ch}, the thinner will be the reaction layer and the more readily will the particles avoid getting involved in the electrochemical reaction and instead, participate in the reverse chemical reaction. However, because of the increase in concentration gradient, the flux to the surface and the current density will still increase.

The development of a kinetic limiting current is a characteristic of electrochemical reactions with a preceding chemical step. However, in contrast to limiting diffusion currents, these limiting currents do not depend on the intensity of electrolyte stirring. Thus, by examining the effect of stirring, one can clearly determine the nature of the limiting current arising in the electrochemical system.

13.6 REACTIONS WITH MEDIATORS

One of the types of multistep electrochemical reactions with chemical steps are those involving mediators (transfer agents). Often, a dissolved oxidizing agent is electrochemically inactive, and at platinum or other nonconsumable electrodes, the equilibrium redox potential is not set up; even at appreciable cathodic polarization of the electrode, the reduction reaction will either not occur at all or it will, but very slowly. Yet the same substance is reduced readily in a chemical way when reacting with other substances having reducing properties. This implies inhibition of the electrochemical step involving electron transfer from the electrode to the reacting species, but lack of inhibition of the chemical steps involving electron or hydrogen-atom transfer from other species.

The same situation is found in the oxidation of certain dissolved reducing agents; in many cases these reactions occur only by reaction with oxidizing agents, not on anodic polarization of an electrode. Such behavior is observed primarily in systems with organic reactants, more rarely in systems with inorganic reactants.

In systems of this type, the electrochemical reactions can be realized or greatly accelerated when small amounts of the components of another redox system are added to the solution. These components function as the auxiliary oxidizing or reducing intermediates of the primary reactants (i.e., as electron or hydrogen-atom transfer agents). When consumed they are regenerated at the electrode.

The oxidation of an anthracene suspension in sulfuric acid conducted in the presence of cerium salts can serve as an example of mediated oxidation. In the bulk solution the Ce^{4+} ions chemically oxidize anthracene to anthraquinone. The resulting Ce^{3+} ions are then reoxided at the anode to Ce^{4+}. Thus, the net result of the electrochemical reaction is the oxidation of anthracene, even though the electrochemical steps themselves involve only cerium ions, not anthracene. Since the cerium ions are regenerated continuously, a small amount will suffice to oxidize large amounts of anthracene.

In a similar fashion, chromium ions Cr^{2+} will reduce dissolved acetylene to ethylene and then are regenerated at the cathode from the Cr^{3+} ions that were formed in the reaction. Or, at a platinum electrode in a solution of AsO_4^{3-} and AsO_3^{3-} ions, the equilibrium potential of this redox system is not established. After the addition

of small amounts of iodine and odide ions, an ionic reaction leads to equilibrium between the two redox systems, while the concentration ratio of the AsO_4^{3-} and AsO_4^{3-} ions which are present in excess remains practically unchanged. It is because of the iodine–iodide system that an overall equilibrium potential can be set up at the electrode; it practically coincides with the thermodynamic potential of the original arsenate–arsenite system.

Inorganic systems such as Br_2/Br^-, AsO_4^{3-}, Ce^{4+}/Ce^{3+}, and Sn^{4+}/Sn^{2+} which have high electrochemical activity most often are used as the mediating redox systems. In a few cases, organic redox systems are used (e.g., the quinone–hydroquinone system).

Mediating redox systems can be formed even without the addition of special reactants. In the electrochemical reduction of ethylene at platinum, a layer of adsorbed hydrogen atoms is formed in the first place on the electrode surface by the cathodic electrochemical reaction (10.17). These atoms chemically reduce the ethylene molecules. Hydrogen atoms consumed are continuously regenerated cathodically, and the reaction can continue. Similarly, the anodic oxidation of methanol at platinum occurs by chemical reaction of adsorbed methanol particles with –OH groups generated electrochemically on the electrode surface by reaction (10.18). In these two examples, the chemical reaction occurs not in the bulk solution, as in the earlier examples, but on the electrode surface. All these reactions have in common that the actual reducing or oxidizing agent is generated or regenerated during the reaction.

In the past it had been a popular belief that the electrochemical reduction of any inorganic or organic substance involves the primary electrochemical formation of a special, active form of hydrogen in the nascent state (*in statu nascendi*) and subsequent chemical reaction of this hydrogen with the substrate. However, for many reduction reactions a mechanism of direct electron transfer from the electrode to the substrate could be demonstrated. It is only in individual cases involving electrodes with superior hydrogen adsorption that the mechanism above with an intermediate formation of adsorbed atomic hydrogen is possible.

In other cases, to the contrary, certain substances may act as proton transfer agents in cathodic hydrogen evolution. Thus, in the presence of organic compounds containing –SH groups, hydrogen evolution at the mercury electrode is strongly accelerated, and we have *catalytic hydrogen evolution* at mercury. This acceleration arises from the cathodic reduction of –SH groups and simultaneous hydrogen evolution:

$$\text{R–SH} + e^- \rightarrow \text{RS}^- + \text{H}_{\text{ads}} (\rightarrow \tfrac{1}{2}\text{H}_2). \tag{13.51}$$

The reactant R–SH consumed in this step is regenerated from the ions RS^- by their chemical reaction with the principal proton donors, which are H_2O molecules or H_3O^+ ions:

$$\text{RS}^- + \text{H}_2\text{O} \rightarrow \text{R–SH} + \text{OH}^-. \tag{13.52}$$

The system R–SH/RS–RS^- thus acts as a hydrogen transfer agent.

13.7 PARALLEL ELECTRODE REACTIONS

Current flow at electrode surfaces often involves several simultaneous electrochemical reactions, which differ in character. For instance, upon cathodic polarization of an electrode in a mixed solution of lead and tin salt, lead and tin ions are discharged simultaneously, and from an acidic solution of zinc salt, zinc is deposited, and at the same time hydrogen is evolved. Upon anodic polarization of a nonconsumable electrode in chloride solution, oxygen and chlorine are evolved in parallel reactions.

Different reactions (anodic and cathodic) can occur simultaneously at an electrode, even when there is no net current flow. In Section 2.5.1 we mentioned the example of an iron electrode in $HCl + FeCl_2$ solution where anodic iron dissolution (2.24) and cathodic hydrogen evolution (2.25) occur simultaneously; these are the reactions of *spontaneous dissolution* of iron not requiring a net current.

The net (external or overall) current density at an electrode is the algebraic sum of the partial current densities of all reactions:

$$i = \Sigma i_m \tag{13.53}$$

(here i_m denotes current densities of both forward $\vec{i}$ and back $\overleftarrow{i}$ reactions). In the particular case where the total current is zero, we have $\Sigma i_m = 0$.

The *current yield* g_n is a useful parameter for the quantitative characterization of parallel reactions. This is the ratio of the partial CD, i_n, consumed in a given reaction n, to the total CD:

$$g_n = \frac{i_n}{i} = \frac{i_n}{\Sigma i_m}; \tag{13.54}$$

most often this parameter is used in connection with the desired (useful) reaction.

The *principle of independent electrochemical reactions* applies when several reactions occur simultaneously. It says that each reaction follows its own quantitative laws, irrespective of other reactions. At a given potential, the rates of the different reactions are not at all interrelated, and at a given CD they are merely tied together by relation (13.53). This does not mean that the reactions have no influence on each other at all. One of the reactions may produce changes in the external conditions for other reactions (e.g., in the temperature or solution pH, the amount of impurities adsorbed on the electrode). However, the form of the kinetic equation of each reaction is not affected by these changes. The principle of independent electrochemical reactions is quite general, and rarely violated (we discuss an instance of such a departure in Section 22.2).

All of the remarks above also apply to the case where a given reaction occurs along several parallel pathways. As a result of the principle of independence, the concept of a rate-determining step of the overall reaction becomes meaningless for such a reaction.

Consider in more detail the example mentioned, where a metal electrode dissolves anodically while hydrogen is evolved. This process is feasible when the equilibrium

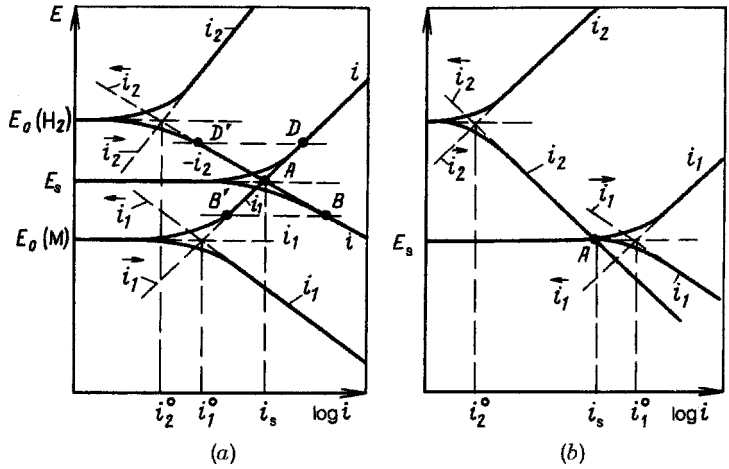

FIGURE 13.2 Polarization curves for the partial current densities of reactions involving the metal and hydrogen, and the polarization curves for the overall current density.

potential of metal dissolution and deposition (index 1) is more negative than the potential of the hydrogen reaction (index 2). In general, when the values of these equilibrium potentials are similar, both the partial anodic forward ($\vec{i}_1$) and the partial cathodic reverse ($\overleftarrow{i}_1$) reactions must be taken into account. The effective rate of metal dissolution, i_1, is given by $\vec{i}_1 - \overleftarrow{i}_1$, while the effective rate of cathodic hydrogen evolution, i_2, is given by $\overleftarrow{i}_2 - \vec{i}_2$. At zero current the rates of these two reactions are identical, according to Eq. (13.53) (i.e., the anodic conversion in one reaction is compensated, with respect to charge consumed, by cathodic conversion in the other reaction). Reactions of this type that are forced to proceed at identical rates are called *coupled reactions*. In the present example, the rate of the coupled reactions, $i_s = i_1 = i_2$, is called the *rate* (or *current density*) of spontaneous metal dissolution.

Figure 13.2 shows anodic and cathodic polarization curves for the partial CD of dissolution $\vec{i}_1$ and deposition $\overleftarrow{i}_1$ of the metal and for the partial CD of ionization $\vec{i}_2$ and evolution $\overleftarrow{i}_2$ of hydrogen, as well as curves for the overall reaction current densities involving the metal (i_1) and the hydrogen (i_2). The spontaneous dissolution current density i_s evidently is determined by the point of intersection, A, of these combined curves.

The electrode's open-circuit potential (steady potential) E_s depends on the relative values of the exchange CD of both reactions and also on the slopes of the polarization curves. When the exchange CD and slopes are similar, the open-circuit potential will have a value, the mixed (or "compromise") potential, which is intermediate between the two equilibrium potentials (Fig. 13.2*a*). However, when the exchange CD for one of the reactions is much higher than that for the other, the open-circuit potential will practically coincide with the equilibrium potential of this reaction (Fig. 13.2*b*).

A relatively simple analytical expression linking the current density i_s and potential E_s to the kinetic parameters of the reactions can be obtained when the exchange CD of the reactions are comparable, whereas their equilibrium potentials diverge strongly. In this case the currents of metal deposition ($\overleftarrow{i_1}$) and hydrogen ionization ($\overleftarrow{i_2}$) can be neglected in the region of the open-circuit potential. It follows that at $E = E_s$ we have $i_s = i_1 = i_2$. Substituting kinetic equations of the type (6.10) into these relations, we obtain

$$i_s = 2Fk_1 \exp\left(\frac{\beta_1 FE_s}{RT}\right) = 2Fk_{-1}c_{H^+} \exp\left(-\frac{\beta_{-2}FE_s}{RT}\right). \tag{13.55}$$

Solving this equation, we find the expression for the steady (or rest) potential E_s:

$$E_s = \frac{RT}{(\beta_1 + \beta_{-2})F} \ln\frac{k_{-2}c_{H^+}}{k_1}. \tag{13.56}$$

To find the final expression for i_s, we must substitute this value of E_s into Eq. (13.55):

$$i_s = 2Fk_1^{\beta_{-2}/(\beta_{-2} + \beta_1)}(k_{-2}c_{H^+})^{\beta_1/(\beta_{-2} + \beta_1)}. \tag{13.57}$$

When more complex polarization functions are involved, particularly when concentration polarization is superimposed, the values of E_s and i_s are preferably determined by graphical rather than analytical means.

When such a polyfunctional electrode is polarized, the net current, i, will be given by $i_1 - i_2$. When the potential is made more negative, the rate of cathodic hydrogen evolution will increase (Fig. 13.2*b*, point *B*), and the rate of anodic metal dissolution will decrease (point *B′*). This effect is known as *cathodic protection* of the metal. At potentials more negative than the metal's equilibrium potential, its dissolution ceases completely. When the potential is made more positive, the rate of anodic dissolution will increase (point *D*). However, at the same time the rate of cathodic hydrogen evolution will decrease (point *D′*), and the rate of spontaneous metal dissolution (the share of anodic dissolution not associated with the net current but with hydrogen evolution) will also decrease. This phenomenon is known as the *difference effect*.

14

Some Aspects of Electrochemical Kinetics

14.1 ENERGY OF ACTIVATION

14.1.1 Chemical Reactions

The rate constants, k_m, of most reactions increase with increasing temperature. This function is described quantitatively by the *Arrhenius equation* (Arrhenius, 1889),

$$k_m = B_m \exp\left(-\frac{A_m}{RT}\right), \tag{14.1}$$

where B_m (the preexponential factor) and A_m (the activation energy) are empirical parameters valid for a reaction m.

When the experimental data are plotted as $\ln k_m$ vs. T^{-1}, they will fall onto a straight line. From its slope the value of A_m, and hence that of B_m, can be obtained. The value of A_m can also be determined from the derivative of Eq. (14.1),

$$A_m = RT^2 \frac{d \ln k_m}{RT}. \tag{14.2}$$

For an interpretation of activation energies, one often uses potential energy–distance curves (Fig. 14.1). For a reaction $X \rightarrow Y$, the potential energy (enthalpy) of the system of reacting particles is plotted on the vertical axis, and the conditional reaction pathway (the set of all intermediate states) is plotted as a distance λ (the reaction coordinate, which is not a true geometric distance) on the horizontal axis. In the initial state (point P_X) the system is stable and enthalpy H_X has a minimum value. The first stage of the reaction involves some change (activation) of the system (e.g., the stretching of chemical bonds, which needs additional energy input). The system's potential energy increases accordingly. The interaction between the activated particles forming new chemical bonds is attended by liberation of energy. Hence the

Fundamentals of Electrochemistry, Second Edition, By V. S. Bagotsky

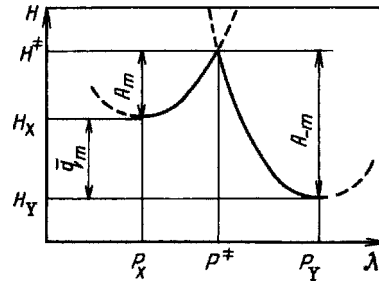

FIGURE 14.1 Potential energy–distance curves for reactants and products in a chemical reaction.

potential energy after going through a maximum falls to a new minimum equilibrium value for the reaction products (point P_Y). The maximum of the curve (point $P^{\ddagger}$) can be regarded as the point of intersection of two partial curves (the dashed lines) for reactants X and products Y, respectively. The system's state in the maximum is called the *transition state* or *activated state* (*activated complex*), and the enthalpy value in this point is written as $H^{\ddagger}$. The difference $\Delta H_m^{\ddagger} \equiv H^{\ddagger} - H_X$, which is the height of the potential-energy barrier, constitutes the activation energy (enthalpy) A_m of the forward reaction. For the reverse reaction $Y \rightarrow X$, the activation energy A_{-m} is given by $\Delta H_{-m}^{\ddagger} \equiv H^{\ddagger} - H_Y$.

The total energy effect of the reaction is given by $q_m = -\Delta H_m \equiv H_X - H_Y$. When it is assumed that the forward and reverse reactions pass through the same transition state, then, evidently,

$$q_m = -q_{-m} = A_{-m} - A_m \tag{14.3}$$

(i.e., the activation energies of the forward and reverse reactions are interrelated through the thermodynamic parameter q_m).

Using Gibbs free energies rather than the enthalpies in constructing the potential energy–distance curves, we will, accordingly, obtain the Gibbs free energy of activation $\Delta G^{\ddagger}$. The difference in values of this parameter between the forward and reverse reactions is the maximum work of reaction, $w_m^0 \equiv -\Delta G_m$. Data for the enthalpies are more readily accessible than data for the Gibbs free energies; hence, the potential energy–distance curves are usually constructed with enthalpies.

According to the theory of rate processes (Eyring et al., 1941), reaction rate constants are determined by the expression

$$k_m = \kappa_m \frac{kT}{h} \exp\left(-\frac{-\Delta G_m^{\ddagger}}{RT}\right), \tag{14.4}$$

where $k \equiv R/N_A$ is the Boltzmann constant, h is the Planck constant, and κ_m is the dimensionless transmission coefficient $\kappa_m < 1$.

This expression corresponds to the Arrhenius equation (14.1) and basically provides the possibility of calculating the preexponential factor k_m (a calculation of κ_m is, in fact, not easy). It also shows that in the Arrhenius equation it will be more correct to use the parameter $\Delta G_m^{\ddagger}$ rather than $\Delta H_m^{\ddagger}$. However, since $\Delta G_m^{\ddagger} = \Delta H_m^{\ddagger} - T\Delta S_m^{\ddagger}$, it follows that the preexponential factor of Eq. (14.4) will contain an additional factor $\exp(\Delta S_m^{\ddagger}/R)$ reflecting the entropy of formation of the transition state when the enthalpy is used in this equation.

An important experimental rule for protolytic reactions was established by Johannes Nicolaus Brønsted in 1918 (it was later extended to other reactions). He showed that for a series of reactions of the same type, the rate constants k_m and the equilibrium constants K_m are related simply as

$$k_m = \gamma_n K_{m,n}^{\alpha}, \tag{14.5}$$

where γ_n and α_n are constants and $0 < \alpha_n < 1$ (here the subscript n refers to the reaction type rather than to any specific reaction; i.e., the values of γ_n and α_n are constant for an entire series of reactions m of the same type n).

If two reactions differ in maximum work by a certain amount δw_m^0 ($\equiv -\delta \Delta G_m^0$), it follows from the Brønsted relation [when taking into account the Arrhenius equation and the known relation between the equilibrium constant and the Gibbs standard free energy of reaction, $K_m = \exp(-\Delta G_m^0/RT)$] that their activation energies will differ by a fraction of this work, with the opposite sign:

$$\delta A_m = -\alpha_n \delta w_m^0. \tag{14.6}$$

According to Eq. (14.3), the activation energies of the reverse reactions will also differ by a fraction of this work (but this time with the same sign):

$$\delta A_{-m} = \alpha_{-n} \delta w_m^0, \tag{14.7}$$

where between transfer coefficients α_n and α_{-n} the relation

$$\alpha_n + \alpha_{-n} = 1 \tag{14.8}$$

exists.

These relations can also be interpreted with the aid of potential energy–distance curves (Fig. 14.2). For reactions of a given type, the conditional reaction pathways and shapes of potential energy–distance curves are approximately identical in these diagrams. Here an increase in maximum work corresponds to a relative displacement of the curves along the vertical: to an upward displacement of curve 1 for the reactants by an amount δw_m^0 to the position of curve 2. We see that in this case the height of the energy barrier of the forward reaction actually decreases by a certain fraction α_n of the total displacement of the curve. The activation energy for the reverse reaction, in accordance with Eqs. (14.7) and (14.8), increases by a fraction $\alpha_{-n} = 1 - \alpha_n$. The values of these factors are related to the slopes ($\tan\gamma_j$) of the potential

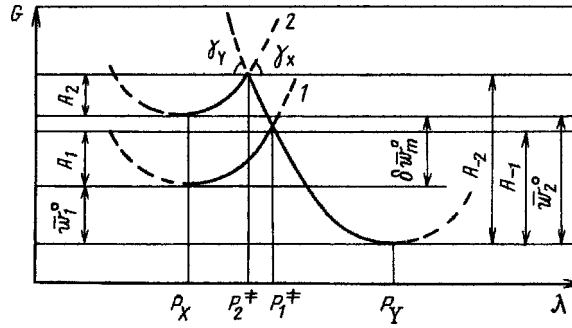

FIGURE 14.2 Potential energy–distance curves for two reactions of the same type.

energy–distance curves of reactants X and products Y close to their point of intersection, as

$$\alpha_n = \frac{\tan\gamma_X}{\tan\gamma_X + \tan\gamma_Y}. \tag{14.9}$$

When the potential energy–distance curves for the reactants and products are symmetric and have the same slope, we have $\alpha_n = \alpha_{-n} = 0.5$.

14.1.2 Electrochemical Reactions

According to Eq. (14.2), the activation energy can be determined from the temperature dependence of the reaction rate constant. Since the overall rate constant h_m of an electrochemical reaction also depends on potential, it must bemeasured at constant values of the electrode's Galvani potential. However, as shown in Section 3.6, the temperature coefficients of Galvani potentials cannot be determined. Hence, the conditions under which such a potential can be kept constant while the temperature is varied are not known, and the true activation energies of electrochemical reactions, and also the true values of factor B_m, cannot be measured.

For this reason and following a suggestion of M. I. Temkin (1948), another conventional parameter is used in electrochemistry [i.e., the real activation energy W_m described by Eq. (14.2)], not at constant potential but at constant polarization of the electrode. These conditions are readily realized in the measurements (an electrode at zero current and the working electrode can be kept at the same temperature), and the real activation energy can be measured.

A more detailed analysis shows that the ideal and real activation energy are interrelated as

$$W_m = A_m \pm \alpha_m T\,\Delta S_m = A_m - (\pm\,\alpha_m q_{\mathrm{lat},m}), \tag{14.10}$$

where ΔS_m, the entropy change, and $q_{\text{lat},m}$, the latent heat of the electrode reaction, are parameters that cannot be measured (the plus sign is valid for anodic, the minus sign for cathodic reactions).

In the Arrhenius equation, the real activation energy is combined with a real (measurable) preexponential factor. According to Eqs. (14.1) and (14.10), this factor differs from the true factor by the multiplicative entropy term $\exp(\pm\alpha_m \Delta S_m/R)$.

During the elementary act of an electrochemical reaction, charged particles cross the electrode/electrolyte interface, and the net charge on particles in the electrolyte changes by $\pm nF$ [see Eq. (1.32)]. Hence, a term describing the change in electrostatic energy, $\pm nF\varphi_G$ or (to a constant term) $\pm nFE$, appears in the expression for the total Gibbs free energy of the reaction:

$$w_m^0 \equiv -\Delta G_m^0 = -(\Delta G_0^0)_m \pm nFE, \tag{14.11}$$

where $(\Delta G_0^0)_m$ is independent of potential and the plus sign holds for anodic reactions.

Alexander N. Frumkin pointed out in 1932 that an electrochemical reaction occurring at different potentials can be regarded as an ideal set of chemical reactions of the same type, and suggested that the Brønsted relation be used to explain the potential dependence of electrochemical reaction rates. On the basis of Eqs. (14.6) and (14.11), the relation for the activation energy becomes

$$A_m = A_m^0 - (\pm\alpha_n nFE), \tag{14.12}$$

where A_m^0 is the activation energy at the potential of the reference electrode ($E = 0$). Substituting (14.12) into the Arrhenius equation and using the notation $\beta_m \equiv n\alpha_n$ for the electrochemical reaction n, we obtain the well-known relation between the rate constant of an electrochemical reaction, h_m, and potential:

$$h_m = k_m \exp\left(\pm\frac{\beta_m FE}{RT}\right), \tag{14.13}$$

where the constant k_m, which does not depend on potential (but depends on the reference electrode), includes the factor $\exp(-A_m^0/RT)$ in addition to the preexponential factor B_m.

In a diagram of the potential energy–distance curves for an anodic reaction, a potential change δE in the positive direction corresponds to an upward shift $nF\,\delta E$ of the curve for reactants relative to that for the products (or the equivalent downward shift of the curve for the products). The analogous shifts occur for a cathodic reaction when the potential is made more negative. In both cases the activation energies of these reactions decrease and the reactions themselves are accelerated. Such diagrams of potential energy–distance curves were first used for an electrochemical reaction (cathodic hydrogen evolution) by Juro Horiuti and Michael Polanyi in 1935.

It had been assumed in the past that the main reason for development of an activated transition state with enhanced energy is a stretching of chemical bonds. Thus, in the model of Horiuti and Polanyi it was assumed that stretching of H^+–H_2O bonds

(i.e., the "tearing away" of a proton from an hydroxonium ion and its approach to the electrode surface) is the initial stage in cathodic hydrogen evolution; the system's potential energy increases under these conditions. Some distance from the surface the proton is discharged (i.e., an electron is transferred to it and it is converted to a hydrogen atom). Under the effect of the new chemical bond between it and the electrode material, this atom then moves closer still to the surface (until reaching the equilibrium distance), and the potential energy decreases again.

So the popular polarization equations of the type (6.5) for electrochemical reactions thus acquire some physical basis. However, according to current concepts the nature of the activated state is different, and quantum-mechanical approaches must be used for a theoretical calculation of the values A_m^0 and B_m. These concepts are discussed in more detail in Chapter 34.

14.1.3 Activationless and Barrierless Reactions

Relation (14.12) cannot remain valid at all potentials. In an anodic reaction where the potential is highly positive (or in a cathodic reaction where it is highly negative), a potential E_{al} should be attained where A_m becomes zero. In the diagram of potential energy–distance curves (Fig. 14.3), curve 3 corresponds to the potential E_{al}; in the transition from the minimum in curve 3 to curve 4 no energy barrier must be overcome. Now the activation energy (which cannot be negative) ceases to depend on potential, which implies that $\beta_m = 0$; rate constant h_m in this range of currents will not depend on potential, and the current will attain some limiting value (section *CD* in Fig. 14.4). Reactions occurring under such conditions are called *activationless* (hence the subscript "al").

It was shown by Lev I. Krishtalik in 1968 that another limiting case is possible in the opposite region of potentials (curves 2 and 4 in Fig. 14.3), when at potential E_{bl}

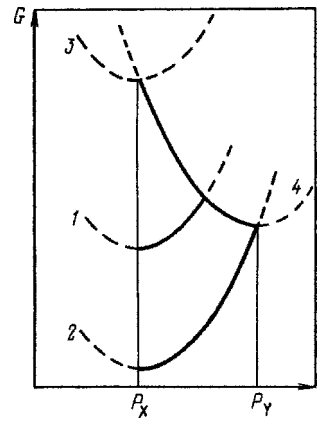

FIGURE 14.3 Schematic potential energy–distance curves of reactants in (1) a normal, (2) a barrierless, (3) an activationless reaction, and (4) potential energy–distance curve for the products.

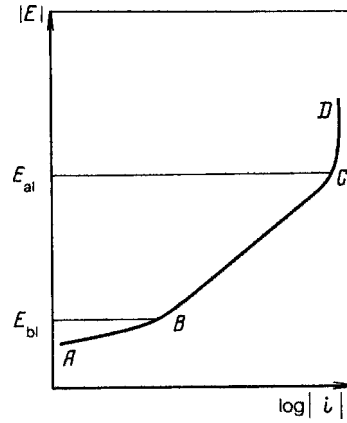

FIGURE 14.4 Schematic polarization curve with barrierless (section *AB*) and activationless (section *CD*) regions.

the descending part of the plot of potential energy against the reaction coordinate vanishes. Starting from this potential the activation energy will be equal to the total energy change occurring during the reaction (i.e., a value of $\beta_m = 1$ is attained). For polarization curves plotted as E vs. ln i, the slope changes from $RT/\beta_m F$ to RT/F (i.e., the Tafel coefficient b' decreases from 0.12 to 0.06 V; section *AB* in Fig. 14.4). Such reactions are called *barrierless* (hence the suffix "bl"). We can see from Fig. 14.3 that the activationless region of the forward reaction corresponds to the barrierless region of the reverse reaction, and vice versa.

Activationless and barrierless regions cannot be realized in all reactions. Often E_{al} or E_{bl} are in regions of potentials where measurements are impossible or extremely difficult (e.g., because of parallel reactions). The crossover to the barrierless region has been demonstrated experimentally for cathodic hydrogen and anodic chlorine evolution at certain electrodes. Clear-cut experimental evidence has not yet been obtained for limiting currents appearing as a result of an activationless reaction.

14.2 KINETIC INFLUENCE OF THE ELECTRIC DOUBLE LAYER

Reactant concentrations $c_{V,j}$ in the bulk solution, as well as the Galvani potential between the electrode and the bulk solution (which is a constituent term in electrode potential E), appear in kinetic equations such as (6.8). However, the reacting particles are not those in the bulk solution but those close to the electrode surface, near the outer Helmholtz plane when there is no specific adsorption, and near the inner Helmholtz plane when there is specific adsorption. Both the particle concentrations and the potential differ between these regions and the bulk solution. It was first pointed out by Alexander N. Frumkin in 1933 that for this reason, the kinetics of electrochemical reactions should strongly depend on EDL structure at the electrode surface.

Alexander N. Frumkin (1895–1976).

Let ψ' be the potential at the point where the reacting particle had been prior to the reaction, or where a product particle just generated by the reaction would be. This potential (which is referred to the potential in the bulk solution) has a value similar to potentials ψ_2 or ψ_1, respectively, and gives rise to two effects important for the electrochemical reaction rates.

The first effect is that of a concentration change of the charged reactant particles in the reaction zone; this change is determined by Boltzmann's distribution law:

$$c_{S,j} = c_{V,j} \exp\left(-\frac{z_j F \psi'}{RT}\right). \tag{14.14}$$

Depending on the signs of parameters z_j and ψ', the concentration in the reaction zone can be higher or lower than the bulk concentration. There is no change in the concentration of uncharged particles.

The second effect is that of a change in the potential difference effectively influencing the reaction rate. By its physical meaning, the activation energy should not be influenced by the full Galvani potential φ_G across the interface but only by the potential difference $(\varphi_G - \psi')$ between the electrode and the reaction zone. Since the Galvani potential is one of the constituent parts of electrode potential E, the difference $E - \psi'$ should be contained instead of E in Eq. (14.13):

$$h_m = k_m \exp\left[-\frac{(\pm \beta_m F(E - \psi')}{RT}\right]. \tag{14.15}$$

When substituting the new values of $c_{S,j}$ and h_m into the kinetic equation (6.10) for a simple first-order reaction, we find that

$$i = nFk_m c_{V,j} \exp\left(\frac{-(z_j \pm \beta_m) F \psi'}{RT}\right) \exp\left(\pm \frac{\beta_m FE}{RT}\right) \tag{14.16}$$

(the plus sign for anodic reactions). The first exponential factor describes the influence of edl structure on reaction rate (the ψ'-*effect*).

Consider two examples. In the first example, hydrogen is evolved cathodically by H_3O^+ ion discharge at metals where this reaction occurs with high polarization (e.g., at mercury, $z_j = 1$, $\beta_m \approx 0.5$). In this case the reaction occurs at potentials much more negative than the PZC, and the value of ψ' is negative. It follows from Eq. (14.16) that when ψ' is made still more negative (or $|\psi'|$ is raised), the absolute value of current will increase, and vice versa. Therefore, when an excess of foreign electrolyte is added to a dilute solution of pure acid, the reaction rate will decrease, at constant potential E, owing to the decrease in $|\psi'|$. In dilute solutions where $|\psi'|$ can attain values of more than 0.15 V, the reaction rate will decrease by one to two orders of magnitude.

In the second example, $S_2O_8^{2-}$ ions ($z_j = -2$) are reduced cathodically in dilute $Na_2S_2O_8$ solution at a mercury electrode:

$$S_2O_8^{2-} + 2e^- \rightarrow 2SO_4^{2-}. \tag{14.17}$$

In the initial section of the curve, the current increases as usual with increasing polarization and in the end attains the limiting (diffusion) value. In this region the mercury surface is positively charged. Then the potential moves through the PZC and attains the region where the surface charge and the values of ψ' are negative. The value of $|\psi'|$ increases more slowly with increasing polarization than the potential ψ_0 contained in E. However, since in Eq. (14.16) the factor $z_j - \beta_m$ in front of $\psi' F/RT$ has a value of about -2.5, the inhibiting effect of the ψ'-potential (the first exponential factor) prevails over the accelerating effect of the electric field (the second exponential factor). As a result, when the polarization increases, the reaction rate decreases because of increasing repulsion of the anions by the negatively charged surface, and a distinct current drop appears in the curve (Fig. 14.5, curve 1). At still more negative potentials the growth of $|\psi'|$ slows down, and the reaction rate resumes its rise. In the presence of base electrolyte the values of $|\psi'|$ are smaller, and the current drop is less pronounced (curves 2 to 4).

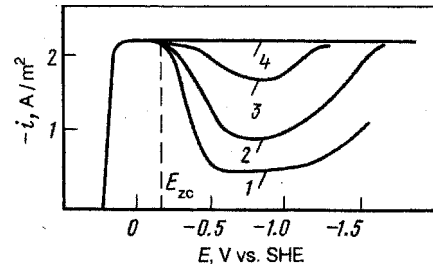

FIGURE 14.5 Polarization curves for the reduction of $S_2O_8^-$ ions at a rotating amalgamated silver electrode in 5×10^{-4} *M* $Na_2S_2O_8$ solutions with various concentrations of Na_2SO_4: (1) 0; (2) 0.004; (3) 0.05; (4) 0.5 *M*.

14.3 KINETIC INFLUENCE OF ADSORPTION

When considering how the adsorption of different substances on electrodes influences the kinetics of electrochemical reactions, we must distinguish two cases: that where components are adsorbed which are involved in the reaction, and that where incidental substances are adsorbed which are not involved in the reaction.

14.3.1 Reactant Adsorption

Often, multistep reactions are encountered where a reactant j first becomes adsorbed on the electrode, then is converted electrochemically (or chemically) to a desorbing product. We shall consider the case where the electrochemical step involving adsorbed particles is rate determining. With a homogeneous electrode surface and without interaction forces between the adsorbed particles [i.e., in conditions when the Langmuir isotherm (10.14) can be applied], the assumption can be made that the rate of this step is proportional not to the bulk concentration $c_{V,j}$ but to the surface concentration A_j or to the degree of surface coverage θ_j; hence,

$$i = nFh_m\theta_j = nFh_m \frac{B_j c_{V,j}}{1 + B_j c_{V,j}}; \tag{14.18}$$

that is, the relation between the current and the bulk concentration is formally the same as the analogous adsorption function: At low concentrations, direct proportionality, and at high concentrations, a limiting value are found.

However, with an inhomogeneous electrode surface and adsorption energies that are different at different sites, the reaction rate constant k_m and the related parameter h_m will also assume different values for different sites. In this case the idea that the reaction rate might be proportional to surface concentration is no longer correct. It was shown by M. Temkin that when the logarithmic adsorption isotherm (10.15) is obeyed, the reaction rate will be an exponential function of the degree of surface coverage by the reactant:

$$i = nFh_m \exp(\gamma f \theta_j), \tag{14.19}$$

where f is the surface inhomogeneity factor and γ is a coefficient ($0 < \gamma$); here the value of h_m will not depend on the surface segment chosen.

Substituting into this equation the expression for θ_j from the isotherm equation, we find that

$$i = nFh_m B_{0,j}^{\gamma} c_{V,j}^{\gamma}; \tag{14.20}$$

that is, the reaction rate is found to be proportional to the fractional power of reactant bulk concentration (often, $\gamma \approx 0.5$).

In a number of cases, electrochemical reactions involving adsorbed substances exhibit special kinetic features. For instance, when the reactant bulk concentration is

raised and the degree of coverage approaches unity (e.g., when $\theta_j > 0.9$), the reaction rate fails to tend toward a limiting value following a further concentration rise but instead, starts to decrease. Sometimes this decrease is quite dramatic. This effect, which became known as the *effect of high coverages*, can be seen when several reactants are involved in the reaction. When the surface is almost completely covered by one of them, the others (whether adsorbing or not) will be displaced from the surface layer and cannot take part in the reaction.

Another example are the sometimes rather complex relations existing between the potential and the reaction rate. The electrode potential influences not only the parameter h_m [see, e.g., Eq. (14.15)] but also the degree of surface coverage by reactant particles [i.e., the coefficients B_j in Eq. (14.18) or (14.20)]. When a sharp drop in adsorption occurs with increasing electrode polarization (rising values of h_m), the monotonic relation between reaction rate and potential may break down and the current actually may decrease within a certain region while polarization increases.

14.3.2 Adsorption of Foreign Substances

Electrochemical reaction rates are also influenced by substances which, although not involved in the reaction, are readily adsorbed on the electrode surface (reaction products, accidental contaminants, or special additives). Most often this influence comes about when the foreign species l by adsorbing on the electrode partly block the surface, depress the adsorption of reactant species j, and thus lower the reaction rate. On a homogeneous surface and with adsorption following the Langmuir isotherm, a factor $1 - \theta_l$ will appear in the kinetic equation which is the surface fraction free of foreign species l:

$$i = i_0(1 - \theta_l), \tag{14.21}$$

where i_0 is the reaction rate observed when species l are not present.

On inhomogeneous surfaces where adsorption obeys the Temkin isotherm, an exponential factor will appear in the kinetic equation:

$$i = i_0 \exp(-\gamma f \theta_l). \tag{14.22}$$

Adsorption of surface-active substances is attended by changes in EDL structure and in the value of the ψ'-potential. Hence, the effects described in Section 14.2 will arise in addition. When surface-active cations $[NR]_4^+$ are added to an acidic solution, the ψ'-potential of the mercury electrode will move in the positive direction and cathodic hydrogen evolution at the mercury, according to Eq. (14.16), will slow down (Fig. 14.6, curve 2). When I^- ions are added, the reaction rate, to the contrary, will increase (curve 3), owing to the negative shift of ψ'-potential. These effects disappear at potentials where the ions above become desorbed (at values of polarization of less than 0.6 V in the case of $[NR]_4{}^+$ and at values of polarization of over 0.9 V in the case of I^-).

In the adsorption of certain organic substances (α-naphthol, diphenylamine, and others) a strong inhibition of cathodic deposition is found for a number of metals.

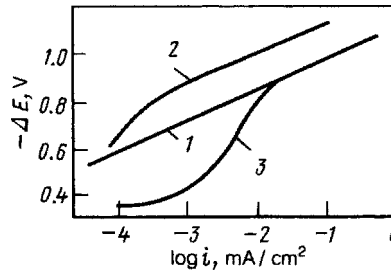

FIGURE 14.6 Influence of surface-active ions $[N(C_4H_9)_4]^+$ (curve 2) and I^- (curve 3) on the polarization curve for hydrogen evolution at a mercury electrode in acidic solutions (curve 1 is for the base electrolyte).

Under these conditions rather low limiting currents arise that are independent of potential up to the desorption potential of the organic substance. This effect can be explained in terms of the difficulties encountered by the reactant metal ions when, in penetrating from the bulk solution to the electrode surface, they cross the adsorbed layer.

In certain cases an adsorbed foreign species *l* can directly influence the rate constant for conversion of the reactant species *j*. This can occur through changes in surface-layer properties of the electrode (e.g., changes in its electronic structure), through direct interaction between the reactant and foreign particles, or through other mechanisms, and can lead to lower or higher reaction rates.

14.4 SPECIAL FEATURES OF REACTIONS AT SEMICONDUCTOR ELECTRODES

Electrochemical reactions at semiconductor electrodes have a number of special features relative to reactions at metal electrodes; these arise from the electronic structure found in the bulk and at the surface of semiconductors. The electronic structure of metals is mainly a function only of their chemical nature. That of semiconductors is also a function of other factors: acceptor- or donor-type impurities present in bulk, the character of surface states (which in turn is determined largely by surface pretreatment), the action of light, and so on. Therefore, the electronic structure of semiconductors having a particular chemical composition can vary widely. This is part of the explanation for the appreciable scatter of experimental data obtained by different workers. For reproducible results one must clearly define all factors that may influence the state of the semiconductor.

Depending on the nature of the electrode and reaction, the carriers involved in an electrochemical reaction at a semiconductor electrode can be electrons from the conduction band (in the following to be called simply *electrons*), electrons from the valence band (*holes*), or both. The concentration of the minority carriers in semiconductors (electrons in *p*-type, and holes in *n*-type semiconductors) is always much

less than that of the majority carriers, let alone the concentration of electrons in metals. Therefore, the specific features of reactions at semiconductor electrodes will be much more pronounced when the minority carriers are involved.

A typical feature of semiconductor electrodes is the space charge present in a relatively thick surface layer (see Section 10.6), which causes a potential drop across this layer (i.e., the appearance of a surface potential χ). This potential drop affects the rate of an electrochemical charge-transfer reaction in exactly the same way as the potential drop across the diffuse EDL part (the ψ'-potential): first, through a change in carrier concentration in the surface layer, and second, through a change in the effect of potential on the reaction's activation energy.

As an example, consider a simple anodic redox reaction involving electrons of the valence band (i.e., holes). The reaction equation can be written as

$$\text{Red} + nh^+ \rightarrow \text{Ox}, \tag{14.23}$$

where h^+ is the symbol for holes.

We shall assume for the sake of simplicity that the total solution concentration is high enough for the influence of the ψ'-potential to be neglected. Other conditions being the same, the reaction rate will be proportional to the surface concentration of holes, $c^+_{S,h}$. We shall assume here that the relation between surface and bulk concentration of the holes is given by the Boltzmann distribution law (14.14) (an assumption that is not always justified). The activation energy of the reaction is influenced not by the full Galvani potential φ_G of the interface, but only by the potential difference in the reaction zone between the semiconductor's outer surface and the solution (i.e., the potential difference $\Phi = \varphi_G - \chi$ between the phases). Allowing for these two factors, we obtain an expression resembling Eq. (14.16) for the reaction rate:

$$i = nFk_m c_{V,\text{red}} \exp\left[\frac{(1-\beta_m)F\chi}{RT}\right] \exp\left(\frac{\beta_m FE}{RT}\right), \tag{14.24}$$

where the bulk concentration of holes in the semiconductor, $c^+_{V,h}$, is contained in the value of rate constant k_m.

The form of the kinetic equation depends on the way in which the surface potential χ varies with electrode potential E. When the surface potential is practically constant, the first factor in Eq. (14.24) will also be constant, and the potential dependence of the reaction rate is governed by the second factor alone. The slope b of the polarization curve will be $RT/\beta_m F$ (i.e., has the same value as that found when the same reaction occurs at a metal electrode). When in another case a change in electrode potential E produces an equally large change in surface potential (i.e., $E = \chi + \text{const}$), while there is practically no change in interfacial potential. Then Eq. (14.24) changes into

$$i = nFk_m c_{V,\text{red}} \exp\left(\frac{EF}{RT}\right), \tag{14.25}$$

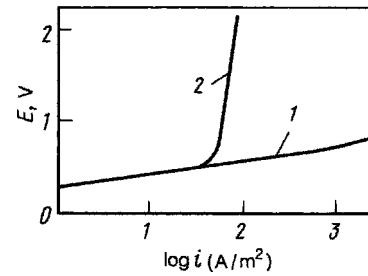

FIGURE 14.7 Polarization curves for the anodic dissolution of (1) *p*-type and (2) *n*-type germanium in 0.1 *M* HCl solution.

and the slope changes to *RT*/*F* (i.e., is about twice as small as in the first case). In general, intermediate values of the slope are possible.

A typical feature of reactions involving the minority carriers are the limiting currents developing when the surface concentration of these carriers has dropped to zero and they must be supplied by slow diffusion from the bulk of the semiconductor. A reaction of this type, which has been studied in detail, is the anodic dissolution of germanium. Holes are involved in the first step of this reaction $Ge \rightarrow Ge(II)$, and electrons in the second $Ge(II) \rightarrow Ge(IV)$. The overall reaction equation can be written as

$$Ge + 3H_2O + 2h^+ \rightarrow H_2GeO_3 + 4H^+ + 2e^-. \qquad (14.26)$$

It can be seen from Fig. 14.7 that the polarization curve for this reaction involving *p*-type germanium in 0.1 *M* HCl is the usual Tafel straight-line plot with a slope of about 0.12 V. For *n*-type germanium, where the hole concentration is low, the curve looks the same at low current densities. However, at current densities of about 50 A/m^2 we see a strong shift of potential in the positive direction, and a distinct limiting current is attained. Thus, here the first reaction step is inhibited by slow supply of holes to the reaction zone.

Under the effect of illumination, new phenomena arise at semiconductor electrodes, which are discussed in Chapter 29.

14.5 REACTIONS PRODUCING A NEW PHASE

14.5.1 Intermediate Stages in the Formation of New Phases

In applied electrochemistry, reactions are very common in which a new phase is formed (i.e., gas evolution, cathodic metal deposition, etc.). They have a number of special features relative to reactions in which a new phase is not formed and in which the products remain part of the electrolyte phase.

The first step in reactions of the type to be considered here is the usual electrochemical step, which produces the primary product that has not yet separated out to

form a new phase. In gas evolution, this is the step that produces gas molecules dissolved in the electrolyte (possibly forming a supersaturated solution). In cathodic metal deposition, this is the formation of metal atoms by discharge of the ions; these atoms are in an adsorbed state (called *adatoms*) on the substrate electrode and have not yet become part of a new metal phase. These steps follow the usual laws of electrochemical reactions described in earlier chapters and are spread out uniformly over all segments of the electrode surface.

These primary electrochemical steps may take place at values of potential below the equilibrium potential of the basic reaction. Thus, in a solution not yet saturated with dissolved hydrogen, hydrogen molecules can form even at potentials more positive than the equilibrium potential of the hydrogen electrode at 1 atm of hydrogen pressure. Because of their energy of chemical interaction with the substrate, metal adatoms can be produced cathodically even at potentials more positive than the equilibrium potential of a given metal–electrolyte system. This process is called the *underpotential deposition of metals*.

Subsequent steps are the formation of nuclei of the new phase and the growth of these nuclei. These steps have two special features.

1. The nuclei and the elements of new phase generated from them (gas bubbles, metal crystallites) are macroscopic entities; their number on the surface is limited (i.e., they emerge not at all surface sites but only at a limited number of these sites). Hence, the primary products should move (by bulk or surface diffusion) from where they had been produced to where a nucleus appears or grows.
2. The process as a whole is transient; nucleation is predominant initially, and nucleus growth is predominant subsequently. Growth of the nuclei usually continues until they have reached a certain mean size. After some time a quasi-steady state is attained, when the number of nuclei that cease to grow in unit time has become equal to the number of nuclei newly formed in unit time.

Any of the steps listed can be rate determining: formation of the primary product, its bulk or surface diffusion, nucleation, or nucleus growth. Hence, a large variety of kinetic behavior is typical for reactions producing a new phase.

Two types of reactions producing a new phase can be distinguished: (1) those producing a noncrystalline phase (gas bubbles; liquid drops as, e.g., in the electrolytic deposition of mercury on substrates not forming amalgams), and (2) those producing a crystalline phase (cathodic metal deposition, anodic deposition of oxides or salts having low solubility).

Features common to these two reaction types are the sequence of steps above, particularly the step producing nuclei of small size (e.g., in the nanometer range). The excess surface energy (ESE) contributes significantly to the energy of these highly disperse entities (with their high surface-to-volume ratio). The thermodynamic properties of highly disperse (extremely small) particles differ from those of larger ones.

When crystal structure is involved, it gives rise to special features in the reactions and makes their mechanisms more complex. Therefore, at first we consider

the common behavior of reactions producing a new phase in the instance . gas evolution reactions (Section 14.2), then we discuss the special features linked to crystal structure (Section 14.3).

14.5.2 Formation of Gas Bubbles

Nucleation Consider an idealized spherical nucleus of a gas with the radius r_{nucl} on the surface of an electrode immersed in an electrolyte solution. Because of the small size of the nucleus, the chemical potential, μ_{nucl}, of the gas in it will be higher than that (μ_0) in a sufficiently large phase volume of the same gas. Let us calculate this quantity.

At the curved surface of the sphere, a force is acting that is directed toward the center of the sphere and tends to reduce its surface area. Hence, the gas pressure p_{nucl} in the nucleus will be higher than the pressure p_0 in the surrounding medium. An infinitely small displacement dr of the surface in the direction of the sphere's center is attended by a surface-area decrease dS ($= 8\pi r\,dr$) and a volume decrease dV ($= 4\pi r^2\,dr$). The work of compression of the nucleus is given by $(p_{\text{nucl}} - p_0)\,dV$. It should be equal to the energy gain, $\sigma\,dS$, resulting from surface shrinkage, where σ is the ESE of the gas–solution interface. Hence, we find that

$$p_{\text{nucl}} - p_0 = \frac{\sigma dS}{dV} = \frac{2\sigma}{r_{\text{nucl}}} \tag{14.27}$$

(the *Laplace equation*, 1806). This equation is valid for any curved phase boundary, also concave ones (for which $p_{\text{nucl}} < p_0$ and the radius of curvature is conventionally regarded as negative). Parameter $p_c \equiv p_{\text{nucl}} - p_0$ is called the *capillary pressure* of this curved surface.

We know from thermodynamics that when the pressure changes at constant temperature, we have

$$\left(\frac{d\mu_j}{dp}\right)_T = V_j. \tag{14.28}$$

We shall integrate this equation between limits given by the pressures p_{nucl} and p_0:

$$\Delta\mu_{\text{nucl}} \equiv \mu_{\text{nucl}} - \mu_0. \tag{14.29}$$

Using Eq. (14.27), we finally find that

$$\Delta\mu_{\text{nucl}} = \frac{2\sigma V_{\text{nucl}}}{r_{\text{nucl}}} \tag{14.30}$$

[the *Thomson (Kelvin) equation*, 1870].

Two conditions must be fulfilled for spontaneous nucleation: (1) the chemical potential of the primary product should be no less than μ_{nucl}, and (2) conditions enabling the "encounter" of N_{nucl} particles of the primary product should exist.

The first condition implies that the concentration, c^{nucl}_{prim}, of the primary products in the nucleation zone should be higher than the equilibrium concentration c^{0}_{prim}. Allowing for Eq. (3.13), we can define the required degree of supersaturation by the relation

$$\Delta\mu_{nucl} = RT \ln \frac{c^{nucl}_{prim}}{c^{0}_{prim}}. \tag{14.31}$$

It follows from Eqs. (14.30) and (14.31) that the required degree of supersaturation will be higher the smaller the size of the nuclei.

When this supersaturation exists, the nucleation rate will be proportional to the probability p_{nucl} of formation of a favorable configuration of particles of the primary product. According to the Boltzmann law, this probability is determined by the work w_{nucl} of formation of a single nucleus:

$$p_{nucl} = B \exp\left(-\frac{w_{nucl}}{kT}\right), \tag{14.32}$$

where B is a normalizing factor and k is the Boltzmann constant.

Detailed calculations show that the work of formation of a single nucleus in a supersaturated solution w_{nucl} is determined by the expression

$$w_{nucl} = \frac{4\pi}{3}\sigma r^2 \tag{14.33}$$

The smaller the nucleus (or higher the degree of supersaturation), the smaller will be work w_{nucl} and the larger will be the probability of nucleation.

The calculation above is valid for a spherical nucleus forming in bulk solution or on an electrode surface completely wetted by the liquid electrolyte, where the wetting angle $\alpha \approx 0$ (Fig. 14.8*a*). The work of nucleation decreases markedly when wetting is incomplete (Fig. 14.8*b*), since the electrode–electrolyte contact area is smaller. The work also decreases when asperities, microcracks, and the like are present on the surface. Thus, Eq. (14.33) states merely the highest possible value of work w_{nucl}.

In an electrochemical system, gas supersaturation of the solution layer next to the electrode will produce a shift of equilibrium potential (as in diffusional concentration polarization). In the cathodic evolution of hydrogen, the shift is in the negative direction, in the anodic evolution of chlorine it is in the positive direction. When this step is rate determining and other causes of polarization do not exist, the value of electrode polarization will be related to solution supersaturation by

$$\pm\Delta E = \frac{\Delta\mu_{nucl}}{nF} = \frac{RT}{nF} \ln \frac{c^{nucl}_{j}}{c^{0}_{j}}. \tag{14.34}$$

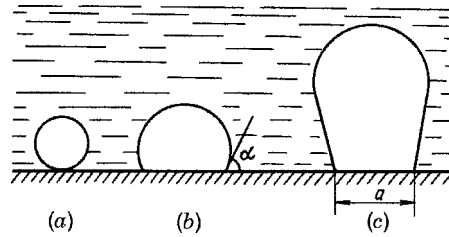

FIGURE 14.8 Gas-bubble nuclei on an electrode with (*a*) complete and (*b*) incomplete wetting of the surface by the liquid, and (*c*) a gas bubble at the moment of tearing away.

With Eq. (14.32) for the reaction rate and Eq. (14.34) for polarization, we obtain the following general form of the polarization equation:

$$i = A \exp\left[-\frac{\gamma}{(\Delta E)^2}\right] \tag{14.35}$$

where A and γ are constants. Thus, when plotted as i vs. $(\Delta E)^{-2}$, the experimental data should fall onto a straight line. Such a function is actually observed in a number of cases.

Nucleus Growth After nucleation the degree of supersaturation of the solution in the immediate vicinity of the nucleus has fallen, and other nuclei can form only some distance away from the first nucleus. It follows that nucleus growth will occur (at least initially) not by the fusion of neighboring nuclei but by the direct addition of primary-product particles. For noncrystalline nuclei (bubbles or drops) no difficulties other than diffusional transport of particles to the nucleus are present at this stage. It is merely necessary that the chemical potential of these particles (or degree of supersaturation) not be inferior to the chemical potential in the nucleus itself, at the size attained. The requirements as to the needed degree of solution supersaturation diminish as the nucleus grows larger.

Another question that arises is the limiting size of the gas bubbles. As the bubble volume V_b increases, the buoyancy force $V_b g \Delta\rho$ of the bubble increases (g is the acceleration of gravity and $\Delta\rho$ is the density difference between the liquid and the gas). The bubble will tear away from the electrode surface as soon as this buoyancy force becomes larger than the force f_{ret} retaining the bubbles.

The retaining force depends on the "neck" perimeter πa along which the bubble is anchored on the surface (Fig. 14.8*c*) and on the wetting angle α; it can be formulated as $\pi a \sigma \sin \alpha$. It follows when the surface is readily wetted (α is small) that the retaining force, and hence the volume of the bubble tearing away, is considerably smaller than when the surface is poorly wetted. Figure 14.9 shows the relation between the wetting angle and the final bubble volume, which was calculated and confirmed experimentally in 1933 by B. Kabanov and A. Frumkin.

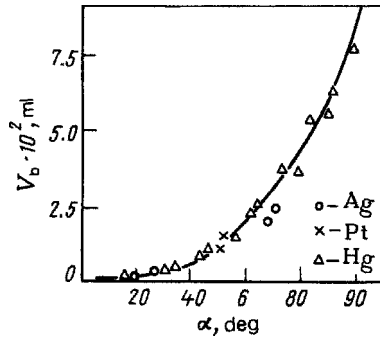

FIGURE 14.9 Volumes of the departing gas bubbles as a function of wetting angle (the solid line is the calculated function). (From Kabanov and Frumkin, 1933).

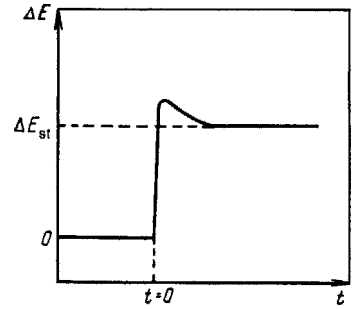

FIGURE 14.10 Polarization–time relation during the formation of a new phase.

The electrode's wetting angle depends on potential; it is largest at the PZC when $\sigma^{(S,L)}$ is largest, and decreases with increasing distance from this point. This effect is the origin of a characteristic feature of hydrogen and oxygen evolution at nickel electrodes in the electrolysis close to the PZC of nickel; hence, the oxygen bubbles are quite large. The potential of hydrogen evolution is far from the PZC, and the gas is evolved in the form of very fine bubbles forming a "milky cloud." This phenomenon provides the basis for technical degreasing of metal surfaces by strong cathodic or anodic polarization. The wetting of the surface by the aqueous solution increases with increasing distance from the PZC, the force with which oil droplets stick to the surface decreases, and they are carried away.

When a gas bubble has torn away, usually the small nucleus of a new bubble is left behind in its place. Therefore, in gas evolution an appreciable supersaturation is needed only for creating an initial set of nuclei, and subsequent processes require less supersaturation. Hence, in a galvanostatic transient the electrode's polarization will initially be higher but will then fall to a lower, steady-state value (Fig. 14.10). Such a time dependence of polarization is typical for many processes involving formation of a new phase.

14.5.3 Crystal-Phase Formation (Metal Deposition)

Initial Stage Mercury electrodes can be used to study the kinetics of the initial step of cathodic metal ion discharge without complications due to subsequent steps. Here, the primary reaction product, metal atoms, do not form nuclei or crystallites but continue to exist as an amalgam or solution in mercury. We must remember, however, that even the kinetics of the initial step depends on the electrode material; hence, the laws found for mercury cannot be used for other metals.

Experience shows that in the deposition of a number of metals (mercury, silver, lead, cadmium, and others), the rate of the initial reaction is high, and the associated polarization is low (not over 20 mV). For other metals (particularly of the iron group), high values of polarization are found. The strong inhibition of cathodic metal deposition that is found in the presence of a number of organic substances (and which was described in Section 14.3) is also observed at mercury electrodes (i.e., it can be also associated with the initial step of the process).

Nucleation The formation of solid crystalline nuclei on a foreign substrate is basically subject to the same laws as the formation of noncrystalline nuclei. Specific features found in the case of crystalline nuclei are (1) considerably higher ESE values; (2) a faceted rather than spherical shape; and (3) anisotropic properties (i.e., different ESE values σ_i for different crystal faces i).

For any ideal crystal, a point can be found for which the distances h_i from these faces obey the relation

$$\frac{\sigma_1}{h_1} = \frac{\sigma_2}{h_2} = \cdots = \frac{\sigma_i}{h_i} = \text{const.} \tag{14.36}$$

Hence, condition (14.34) for crystalline nuclei can be written as

$$\Delta\mu_{\text{nucl}} = \frac{2\sigma_l V_{\text{nucl}}}{h_i}. \tag{14.37}$$

In metal deposition, the primary products form adsorbates on the electrode surface rather than a supersaturated solution. Their excess chemical potential $\Delta\mu_{\text{nucl}}$ is directly related to polarization and given by $nF\,\Delta E$. The total excess surface energy $U_{\text{nucl}} = \Sigma\, S_i\sigma_i$. Otherwise, all the results described above remain valid.

Nucleus Growth The basic difference between reactions producing a new crystalline phase and reactions producing a gas or liquid phase is the step of nucleus growth. Difficulties exist in the incorporation of primary reaction products into the lattice.

In metal deposition the nuclei practically grow by direct discharge of metal ions on them. Initially, elevated current densities are observed at the nuclei (which have a small area). Under these conditions concentration polarization can exist, owing to slow metal ion supply.

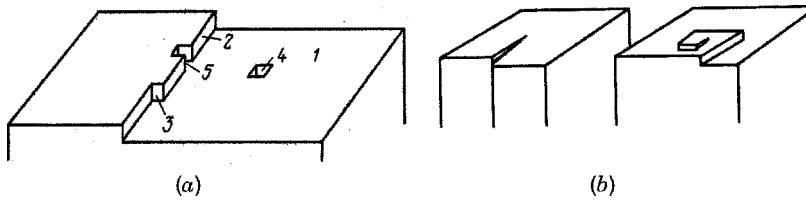

FIGURE 14.11 (*a*) Structure of a growing crystal face; (*b*) face growing on a lattice with a screw dislocation.

The structure of growing crystal faces is inhomogeneous (Fig. 14.11*a*). In addition to the lattice planes (1), it features steps (2) of a growing new two-dimensional metal layer (of atomic thickness), as well as kinks (3) formed by the one-dimensional row of metal atoms growing along the step. Lattice plane holes (4) and edge vacancies (5) can develop when uniform nucleus growth is disrupted.

Metal ions are most readily discharged at the lattice plane (in positions 1). Discharge is hindered near steps 2 and kinks 3, since hydrated metal ions have difficulty approaching the discharge site. On the other hand, the metal atoms are most readily built into the lattice in positions 3, where they interact with a larger number of neighbors than in positions 1. Hence, nucleus growth is associated with surface diffusion of adatoms (completely discharged) or adions (partly discharged) from positions of type 1 to positions of type 3, where they are added to the lattice. In this way, the rows along individual layer steps and the growing layers themselves are completed in succession.

After complete formation of each successive monolayer of atoms, the next layer should start to form. This requires two-dimensional nucleation by the union of several adatoms in a position 1. Like three-dimensional nucleation, two-dimensional nucleation requires some excess energy (i.e., elevated electrode polarization). Introducing the concept of excess linear energy ρ of the one-dimensional face (of length L) of the nucleus, we can derive an expression for the work of formation of such a nucleus (analogous to that used in Section 14.2.2). When the step of two-dimensional nucleation is rate determining, the polarization equation becomes, instead of (14.39),

$$i = A \exp\left(-\frac{\gamma}{|\Delta E|}\right). \tag{14.38}$$

When the growing crystal surface is nonideal and has defects, face growth can continue even without periodic two-dimensional nucleation. A crystal having the common *screw dislocations* in its lattice (Fig. 14.11*b*) can serve as an example. A V-shaped step along which the atoms after discharge can be built into the lattice is formed on the surface of such a crystallite. The growing step circles the face on top of the crystallite continuously and does not vanish as the face grows. Therefore, this spiral growth is a continuous process obviating intermediate two-dimensional

nucleation. There are cases where in the presence of screw dislocations the growing faces are not monatomic but have appreciable thickness. For this reason, spiral growth of crystallite faces can be followed visually (Kaishev et al., 1950).

Polarization equations of the type (14.35) or (14.38) contain the mean values of true current density. However, the rate-determining step is more often concentrated at just a few segments of the electrode; the true working area changes continuously and an exact determination of this area is practically impossible. This gives rise to difficulties in an interpretation of polarization data.

REFERENCES

Arrhenius, S., *Z. Phys. Chem.*, **4**, 226 (1889).

Brønsted, J., *Z. Elektrochem.*, **20**, 201 (1918).

Eyring, H., S. Glasstone, and K. J. Laidler, *The Theory of Rate Processes*, McGraw-Hill, New York, 1941.

Frumkin, A., *Z. Phys. Chem.*, **160A**, 116 (1932).

Frumkin, A., *Z. Phys. Chem.*, **164A**, 121 (1933).

Horiuti, J., and M. Polanyi, *Acta Physicochim. URSS*, **2**, 505 (1935).

Kabanov, B., and A. Frumkin, *Zh. Fiz. Khim.*, **4**, 539 (1933).

Kaishev, R., A. Sheludko, and R. Bliznakov, *Commun. Bulg. Acad. Sci.*, **1**, 137 (1950).

Kristalik, L., *Electrochim. Acta*, **13**, 1045 (1968).

Temkin, M., *Zh. Fiz. Khim.*, **22**, 1081 (1948).

15

Reactions at Nonconsumable Electrodes

In the present chapter we want to look at certain electrochemical redox reactions occurring at inert electrodes not involved in the reactions stoichiometrically. The reactions to be considered are the change of charge of ions in an electrolyte solution, the evolution and ionization of hydrogen, oxygen, and chlorine, the oxidation and reduction of organic compounds, and the like. The rates of these reactions, often also their direction, depend on the catalytic properties of the electrode employed (discussed in greater detail in Chapter 28). It is for this reason that these reactions are sometimes called *electrocatalytic*. For each of the examples, we point out its practical value at present and in the future and provide certain kinetic and mechanistic details. Some catalytic features are also discussed.

15.1 SIMPLE ELECTROCHEMICAL REACTIONS

Conditionally, an electrochemical reaction will be called *simple* when the following conditions hold (at least as an approximation):

1. The electron transfer step is the only reaction step, which means that other parallel or consecutive steps are absent.
2. Neither the starting material nor the reaction product, nor any intermediates, are adsorbed on the electrode.
3. During the reaction, chemical bonds are not broken, new chemical bonds are not formed, and the geometry of the reacting species remains unchanged.

Electrochemical reactions only involving a change of charge of simple or complex ions but not any change in inner geometry are commonly called *outer-sphere electron transfer reactions*. For some time, the reduction and oxidation of simple and

Fundamentals of Electrochemistry, Second Edition, By V. S. Bagotsky

complex iron ions involving a change in valency of the iron had been regarded as an example of such simple reactions:

$$Fe^{3+} + e^- \rightleftharpoons Fe^{2+}, \tag{15.1}$$

$$[Fe(CN)_6]^{3-} + e^- \rightleftharpoons [Fe(CN)_6]^{4-}. \tag{15.2}$$

Later, closer examination revealed that these reactions are attended by a marked change in the geometry of the hydrated ions.

Historically, the reduction of persulfate ions has also been assumed to be a simple reaction:

$$S_2O_8^{2-} + 2e^- \rightarrow 2SO_4^{2-}. \tag{15.3}$$

It involves rupture of an O–O bond, and two electrons per reacting ion take part in it, so it also does not meet the criteria above. The reaction is simple insofar as on many metals, the persulfate and sulfate ions are weakly adsorbed.

Simple electrochemical oxidation–reduction reactions do not by themselves have any important applications. However, results of great value for the theory of electrochemical kinetics and electrocatalysis have been obtained when these reactions were studied experimentally in greater detail. Thus, in the instance of persulfate ion reduction, it has been possible to quantitatively elucidate the influence of electric double-layer structure on electrode kinetics. In this reaction, double-layer effects (ψ'-effects) become particularly clearly evident, since divalent ions are involved. The rate of this reaction also depends on the metal selected for the electrode; this effect could (at least in part) be explained in terms of the influence exerted by the metal on the value of the ψ'-potential to be used in the kinetic equation (14.16) governing this reaction. In fact, the ψ'-potential seen at a given value of electrode potential in a solution of given composition depends on the metal's zero-charge potential E_{zc}. Metals differ greatly in their zero-charge potentials. With a knowledge of E_{zc}, and using the theory of electric double-layer structure, values of the ψ'-potential can be calculated rather accurately. On this basis, important refinements can be introduced into kinetic equations of the type of Eq. (15.16), and the reaction rates that would be observed in the absence of double-layer effects can be calculated. Figure 15.1 shows such "corrected" polarization curves for the cathodic reduction of persulfate ions at mercury and at a number of metals similar to mercury. It can be seen from the figure that for most metals, these curves are rather close (Frumkin et al., 1975). It follows that in the particular case of this reaction, the influence of the metal is due primarily to double-layer effects, the phenomenon observed being kinetic rather than strictly catalytic.

Yet the view that the rates of electron transfer in simple reactions are principally independent of the electrode metal (which for some time had been current in the electrochemical literature) cannot be maintained in this strict form. Many experimental data relating to the exchange current densities of reactions involving simple cations (such as Fe^{2+} and Fe^{3+}) provide evidence that the electrode metal does exert a rather strong influence on the reaction rates.

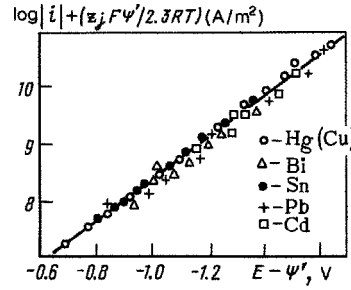

FIGURE 15.1 Polarization curves for the reduction of $S_2O_8^{2-}$ ions in 5×10^{-4} *M* $Na_2S_2O_8$ + 0.009 *M* NaF solution at different metals.

15.2 HYDROGEN EVOLUTION AND IONIZATION

The equations of these reactions in aqueous solutions are

$$2H^+ + 2e^- \rightleftharpoons H_2; \tag{15.4a}$$

$$2H_2O + 2e^- \rightleftharpoons H_2 + 2OH^-. \tag{15.4b}$$

Cathodic hydrogen evolution is one of the most common electrochemical reactions. It is the principal reaction in electrolytic hydrogen production, the auxiliary reaction in the production of many substances forming at the anode, such as chlorine, and a side reaction in many cathodic processes, particularly in electrohydrometallurgy. It is of considerable importance in the corrosion of metals. Its special characteristic is the fact that it can proceed in any aqueous solution; particular reactants need not be added. The reverse reaction, which is the anodic ionization of molecular hydrogen, is utilized in batteries and fuel cells.

The equilibrium potential of the hydrogen electrode is established at electrodes of platinized platinum and other finely divided platinum group metals in both acidic and alkaline solutions. In the latter, it is also established at electrodes of finely divided nickel. All these electrodes are sensitive to contamination; they will lose their activity even at low concentrations of an adsorbing impurity, so that their open-circuit potential (OCP) no longer corresponds to the equilibrium potential of the hydrogen reaction. At other metals the hydrogen potential is not established because of the low exchange current densities of the hydrogen reaction on them and also because of interference from spontaneous dissolution found for many metals (particularly, iron) in the region of the equilibrium hydrogen potential.

Most metals (other than the alkali and alkaline-earth metals) are corrosion resistant when cathodically polarized to the potentials of hydrogen evolution, so that this reaction can be realized at many of them. It has thus been the subject of innumerable studies, and became the fundamental model in the development of current kinetic concepts for electrochemical reactions. Many of the principles

presented in Chapters 6, 13, and 14 have been established, precisely in studies of this reaction.

In the past, elevated voltages in electrolysis cells (a cell overvoltage) had been attributed mainly to polarization of the hydrogen evolution reaction. Hence the term *hydrogen overvoltage* became common for this kind of polarization.

The range of current densities encountered in cathodic hydrogen evolution is extremely wide. Corrosion of metals may become important at rates of hydrogen evolution on the order of 10^{-5} to 10^{-4} mA/cm^2, whereas in industrial electrolyzers, where this reaction occurs at the cathode, the current densities attain values of 10^3 mA/cm^2 (10^4 A/m^2) and more.

In alkaline solutions the equilibrium potential of the hydrogen reaction and the true potentials of hydrogen evolution (which include polarization) are moved to rather more negative values. Hence, the reaction is difficult to study; at many electrodes, discharge of the solution cations and incorporation of the resulting metal atoms into the lattice of the electrode material (see Section 16.5) are possible in addition to hydrogen evolution. Owing to the energy of alloy formation, these additional processes will occur at potentials more positive than the equilibrium potential of the particular metal, and the contribution of metal ion discharge to the total current recorded during cathodic polarization may be large. At intermediate values of pH, buffered solutions are used to avoid marked changes in solution acidity caused by the consumption of hydroxonium ions or formation of hydroxyl ions.

Figure 15.2 shows polarization curves for hydrogen evolution at electrodes of different metals in acidic electrolyte solutions. The results of polarization measurements are highly sensitive to the experimental conditions, in particular to the degree of solution and electrode surface purification; for this reason, marked differences exist among the data reported by different workers. The curves shown still provide the correct picture of the common features.

It can be seen from Fig. 15.2 that in semilogarithmic plots of ΔE vs. $\log i$, the polarization characteristics are linear [i.e., obey the Tafel equation (6.3)]. Slopes b' practically coincide for most metals and have values of 0.11 to 0.13 V. However, the absolute values of polarization recorded for a given current density (CD) vary within

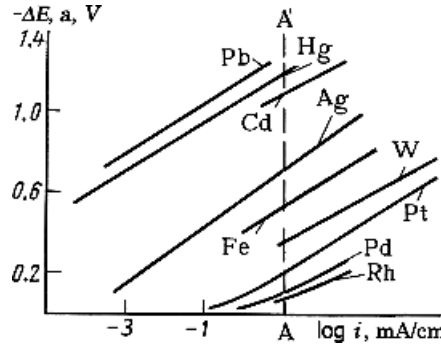

FIGURE 15.2 Polarization curves for hydrogen evolution with various metals in acidic solutions.

wide limits. The values of the exchange CD (intersections of the extrapolated polarization curves with the horizontal axis) and of constant a in the Tafel equation differ accordingly. Traditionally, the current densities are stated in mA/cm^2 (rather than A/m^2) when this equation is used; hence, the values of constant a reported in the literature refer to a current density of 1 mA/cm^2 (intersections with the line AA′).

The highest values of polarization are observed for the *s*- and *p*-metals: lead, mercury, and certain others ("metals with high hydrogen overvoltage"), the lowest are observed for transition metals (*d*-metals), and particularly for the platinum group metals ("metals with low hydrogen overvoltage"). The constants a for lead and rhodium differ by 1.25 V, according to the data of Fig. 15.2. When allowing for the slopes of the polarization curves, this corresponds to a change in reaction rate at any given value of potential by a factor of about 10^{11}; the exchange CD varies between 10^{-15} mA/cm^2 for lead and 3×10^{-4} mA/cm^2 for rhodium. Such a strong variation in reaction rate between different metal electrodes is particularly typical for cathodic hydrogen evolution.

In aqueous solutions, approximately one atom of deuterium, D, is present for every 7000 atoms of the ordinary hydrogen isotope (protium, H). In the evolution of "heavy" hydrogen, HD, the polarization is approximately 0.1 V higher than in the evolution of ordinary hydrogen, H_2. Hence during electrolysis the gas will be richer in protium, and the residual solution will be richer in deuterium. The relative degree of enrichment is called the *separation factor* (S) of the hydrogen isotopes,

$$S = \frac{(D/H)^{\mathrm{L}}}{(D/H)^{\mathrm{G}}} \tag{15.5}$$

(here H and D are the corresponding atom fractions of protium and deuterium). The values of S depend on the material and surface state of the electrode, the solution composition, and other factors, and at 75°C vary between 3 and 4 for mercury and platinized platinum, and 7 and 8 for iron and graphite (i.e., are unrelated to the overall value of electrode polarization). Measured values of S are somewhat reduced by isotope exchange between the gas and the liquid:

$$H_2^{(G)} + HDO^{(L)} \longleftrightarrow HD^{(G)} + H_2O^{(L)}, \tag{15.6}$$

which interferes with the isotope separation and is catalytically accelerated to a different extent by different metal surfaces. The higher values of S found at lower temperatures and higher current densities can be explained in terms of a lower influence of this reaction.

Unlike the cathodic reaction, anodic oxidation (ionization) of molecular hydrogen can be studied for only a few electrode materials, which include the platinum group metals, tungsten carbide, and in alkaline solutions nickel. Other metals either are not sufficiently stable in the appropriate range of potentials or prove to be inactive toward this reaction. For the materials mentioned, it can be realized only over a relatively narrow range of potentials. Adsorbed or phase oxide layers interfering with the reaction form on the surface at positive potentials. Hence, as the polarization is raised, the anodic current will first increase, then decrease (i.e., the electrode becomes passive; see Fig. 16.3 in Chapter 16). In the case of nickel and tungsten

carbide, these changes may prove to be irreversible; the oxide layer cannot be reduced completely after a return to more negative potentials, and the activity remains low.

15.2.1 Mechanism of the Hydrogen Evolution Reaction

Cathodic hydrogen evolution is a complex two-electron reaction occurring through several consecutive, simpler intermediate steps. Each of these steps is sometimes referred to with the name of the scientist who had suggested that it was rate determining for the overall reaction; the steps are:

A. The *discharge* (Volmer) *step*,

$$H_3O^+ + e^- \rightarrow H_{ads} + H_2O \tag{15.7}$$

B. The *recombination* (Tafel) *step*,

$$2H_{ads} \rightarrow H_2 \tag{15.8}$$

C. The *electrochemical desorption* (Heyrovský) *step*,

$$H_3O^+ + H_{ads} + e^- \rightarrow H_2 + H_2O \tag{15.9}$$

These three steps can combine in different ways to three possible reaction pathways, I, II, and III. We shall represent them as a table analogous to that in Section 13.1:

Step k	l_k	μ_k(I)	μ_k(II)	μ_k(III)
A	1	2	1	
B	0	1		−1
C	1		1	2

The minus sign in the table signifies that in cathodic hydrogen evolution following the third pathway, step B follows Eq. (15.8) from right to left.

It is important not only to establish the true reaction pathway followed under different experimental conditions, but also to decide which of the two consecutive steps is rate determining in a given pathway. It had been thought in the past that cathodic hydrogen evolution follows pathway I, constituting the sequence of a discharge and a recombination step. In 1905, Julius Tafel put forward the opinion that the recombination step is rate determining while the discharge step is in equilibrium (the *recombination theory of hydrogen overvoltage*). The physical basis of this theory is the fact that the recombination of two atoms will not occur instantaneously (in every collision) but with some finite, low rate. This is due to the considerable energy liberated in the union of the two atoms; this energy is concentrated in the resulting molecule and causes it to redissociate into atoms. At different catalysts, particularly at metals, recombination is accelerated by the elimination of part of the excess energy by the catalyst surface. A strong argument in favor of the recombination theory

were the parallels existing between the catalytic activities of the various metals in the surface recombination of adsorbed hydrogen atoms in the gas phase and their activities in cathodic hydrogen evolution. The rates of both reactions increase in the order Pb < Zn < Ag < Fe < Pt.

Slow recombination of hydrogen atoms has the effect that the surface concentration (degree of surface coverage) of the hydrogen atoms under cathodic current, $\theta_{H,i}$, is higher than that at zero current, $\theta_{H,0}$. According to recombination theory, polarization is due precisely to these changes, because step A is in equilibrium. Assuming that the activity of an adsorbed hydrogen atom is proportional to its surface concentration, we have

$$\Delta E = \frac{RT}{F} \ln \frac{\theta_{H,i}}{\theta_{H,0}}. \tag{15.10}$$

On a homogeneous surface, the rate of the atom recombination step will be proportional to the square of the atom surface concentrations:

$$v_B = k_B \theta_{H,i}^2. \tag{15.11}$$

In a reaction following the first pathway, this rate will be proportional to the total current i: $i = 2Fv_B$ (regardless of which step is the slow step). Combining the last two equations, we obtain

$$\Delta E = \text{const} + \frac{RT}{2F} \ln i. \tag{15.12}$$

Thus, the recombination theory provided the first theoretical interpretation of the linear relation between polarization and the logarithm of current density that had been established experimentally. It is true, though, that the preexponential factor in Eq. (15.12) [$2.303(RT/2FI) \approx 0.03$ V] is four times smaller than the experimental values of slope b'; but it has been shown in later work that factors closer to the experimental values can be obtained when an inhomogeneous surface is assumed.

A basic defect of these ideas is their failure to provide an explanation of the substantial effects of solution composition, in particular the pH value, on the rate of the electrochemical reaction. Since hydrogen ions are not involved in the recombination step, the rate of this step according to Eq. (15.12) should not depend on solution pH. Yet in many cases the rate of hydrogen evolution at constant potential is proportional to the hydrogen ion concentration in solution.

The idea that the discharge of different ions could be slow was suggested as early as the end of the nineteenth century. The slowness was attributed to the appreciable energy needed to break up the complexes (including those with solvent molecules) formed by the ions in solution. According to current concepts, another contribution to the activation energy arises from the need for reorganization of the solvent molecules close to the ions undergoing discharge.

In 1924, John Alfred Valentine Butler derived an equation for the equilibrium potential of an electrode using the equations for the finite rate of anodic and cathodic steps.

Max Volmer (1885–1965).

In 1930, Max Volmer and Tibor Erdey-Grúz used the concept of a slow discharge step for cathodic hydrogen evolution (*slow discharge theory*). According to these ideas, the potential dependence of electrochemical reaction rate constants is described by Eq. (6.5). Since hydrogen ions are involved in the slow step A, the reaction rate will be proportional to their concentration. Thus, the overall kinetic equation can be written as

$$i = i_A = Fv_A = Fk_A c_{H^+} \exp\left(-\frac{\beta FE}{RT}\right). \tag{15.13}$$

This equation explains the experimental reaction rates, both as a function of potential (under the plausible assumption that $\beta \approx 0.5$) and as a function of solution pH.

The idea that the adsorbed hydrogen atoms that have been produced by discharge can be eliminated from the electrode surface by recombination is faced with difficulties no matter which of the steps is the slow step. The degree of surface coverage, $\theta_{H,i}$, by adsorbed atoms can increase only up to a limiting value of unity. According to Eq. (15.11), at this point the limiting recombination rate is attained, and thus the limiting rate of the overall reaction, which cannot be faster than any of its consecutive steps. However, for hydrogen evolution such a limiting current is not observed experimentally (in the absence of concentration polarization with respect to H_3O^+ ions). Another difficulty are the improbably high values obtained for constant k_B in Eq. (15.11) in the case of metals where the values of $\theta_{H,i}$ are known to be low (e.g., mercury). These difficulties can be avoided when it is assumed that the reaction follows pathway II: that the adsorbed hydrogen atoms are eliminated from the surface via an electrochemical desorption step. This step was first suggested by Jaroslav Heyrovský in 1925. For electrodes with homogeneous surfaces, the rate of this step can be described as

$$i = i_C = Fv_C = Fk_C\, c_{H^+} \theta_{H,i} \exp\left(-\frac{\beta_C F}{RT}\right). \tag{15.14}$$

The steady-state coverage, $\theta_{H,i}$, of the surface by hydrogen atoms can be found from the balance of their rates of formation and elimination. Discharge of the ions occurs only at sites free of adsorbed hydrogen. Hence, the reaction rate will be proportional to the fraction of free surface when considerable amounts of hydrogen are present on the surface, and it can in brief be written as $Fh_A c_{H^+}(1-\theta_{H,I})$. The rate of electrochemical desorption can be written, similarly, as $Fh_C c_{H^+} c_{H^+} \theta_{H,i}$. In the steady state these two rates will be identical, which implies that

$$\theta_{H,i} = \frac{h_A}{h_A + h_C}; \tag{15.15}$$

that is the degree of coverage always remains below unity, and the overall current is not limited by the attainment of complete surface coverage.

For a reaction following the second pathway, the total current is given as the sum of currents of the two steps: $i = i_A + i_C = 2i_A = 2i_C$. Hence,

$$i = 2Fh_C c_{H^+} \theta_{H,i} = \frac{2Fh_A h_C c_{H^+}}{h_A + h_C}. \tag{15.16}$$

The rates of the individual steps of cathodic hydrogen evolution at different metals are a complex function of bond energy W_{M-H} of the hydrogen adsorbed at the metal surface. For the discharge step, the rate first increases with increasing bond energy because of decreasing activation energy, then it goes through a maximum, and finally, it decreases again, owing to increasing hydrogen adsorption (i.e., a decreasing fraction of free surface). A similar situation is found for the recombination and the electrochemical desorption step: The reaction first is accelerated with increasing bond energy, owing to increasing surface concentration, but then it becomes slower, owing to increasing activation energy of desorption.

A detailed analysis of these effects shows that in most cases the reaction follows the second pathway. For metals with low and intermediate bond energies (the *s*- and *p*-metals and some transition metals), slow discharge followed by electrochemical desorption is more likely. For the transition metals with high bond energy (nickel, tungsten, tantalum, etc.), slow electrochemical desorption is more likely. A reaction following the first pathway with a slow recombination step evidently is observed only for activated electrodes of platinum metals at low values of polarization. Often, conditions exist when different steps have comparable rate constants (i.e., when there is no clear-cut rate-determining step). No unambiguous evidence is available so far that the reaction may also follow the third pathway.

15.2.2 Influence of Solution Composition

Hydrogen can be evolved not only as a result of the discharge of hydroxonium ions, H_3O^+, but also by discharge of other proton donors, HA, that may be present in the solution, including the water molecules themselves:

$$2HA + 2e^- \rightarrow H_2 + 2A^-, \tag{15.17}$$

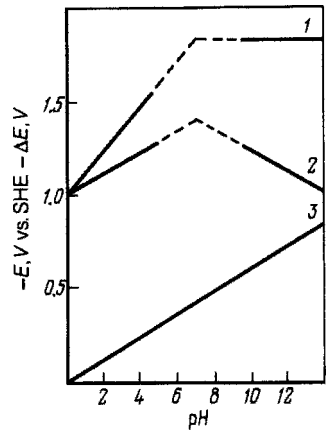

FIGURE 15.3 pH dependence of potential (1) and polarization (2) in cathodic hydrogen evolution at a mercury electrode (10 mA/cm^2), and the pH dependence of equilibrium potential of the hydrogen electrode (3).

where HA = H_3O^+, H_2O, NH_4^+, RSH, and so on. It may then be asked what the relative contributions of reactions involving different proton donors are. As a general rule, in acidic solutions where the concentration of H_3O^+ ions is high, it will be precisely these ions that provide the main contribution to the overall current; but in alkaline solutions where their concentration is very low, hydrogen is evolved primarily by discharge of water molecules. In hydroxonium ion discharge, the reaction rate at a given potential E, according to Eqs. (15.13) and (15.14), will be proportional to the concentration of these ions, to a first approximation. It follows from these equations that $(\partial E/\partial \log c_{H^+})_i = 2.303(RT/\beta F)$. The electrode potential shifts by about 0.12 V in the negative direction when the pH is raised by a unit, since $\beta \approx 0.5$ (Fig. 15.3, curve 1). In alkaline solutions where water molecules are discharged, the reaction rate at a given potential (or the potential at a given rate) is independent of solution pH. Since the equilibrium potential of the hydrogen electrode moves 0.06 V in the negative direction when the pH is raised by a unit (curve 3), polarization under these conditions will decrease. A plot of polarization against pH for constant current goes through a maximum (curve 2). In acidic solutions the slope of the curve is approximately 0.06 V; in alkaline solutions it is −0.06 V. Other proton donors can display their influence mainly in neutral solutions, where the polarization values for the discharge of H_3O^+ ions and water molecules are highest.

The composition of the electrolyte solution influences the rate of hydrogen evolution not only in a direct way, which is through the concentrations of species undergoing discharge, but also in an indirect way, through its effect on electric double-layer structure, in particular through the value of the ψ'-potential. The general equation (15.16) that describes this effect becomes for the reaction considered here (slow discharge in acidic solutions),

$$i = Fk_A c_{H^+} \exp\left[-\frac{(1-\beta)F\psi'}{RT}\right] \exp\left(-\frac{\beta FE}{RT}\right). \tag{15.18}$$

The ψ'-potential is negative for most metals in the region of cathodic hydrogen evolution. It depends both on the total electrolyte concentration and on specifically adsorbing, surface-active ions present in the solution. Since the value of the ψ'-potential is close to that of the ψ_2-potential, Eq. (10.8) can be used to describe the concentration dependence.

Consider a few particular cases. The relation between polarization and solution pH at constant current that is reported in Fig. 15.3 refers to the case where there is no marked change in total solution concentration when the pH is varied (e.g., at high concentrations of a foreign or buffer electrolyte). When the measurements are made in pure acid solutions not containing a foreign electrolyte, the absolute values of the ψ'-potential will decrease with increasing acid concentration (i.e., this potential assumes less negative values). Putting function (10.8) into Eq. (15.18), we obtain

$$i = Fk'_{\mathrm{A}}(c_{\mathrm{H}^+})^{\beta} \exp\left(-\frac{\beta FE}{RT}\right). \tag{15.19}$$

It follows from this equation that in the case being considered, the reaction rate is proportional to a fractional power of hydrogen ion concentration. The value of $(\partial E/\partial \log c_{\mathrm{H}^+})_i = 2.303RT/F$; that is, the potential shifts by 0.06 rather than 0.12 V in the negative direction when the solution pH is raised by a unit, while the value of polarization is independent of solution pH. When an excess of foreign electrolyte is added to the dilute solution of a pure acid, the reaction rate will decrease since the ψ'-potential shifts in the positive direction. The influence of surface-active ions (e.g., I^- or $[NH_4]^+$) on hydrogen evolution that arises through changes in the ψ'-potential was described in Section 14.3.2 (see Fig. 14.6).

15.2.3 Ways of Influencing the Hydrogen Evolution Reaction

In industrial electrolyzers where hydrogen evolution occurs at the cathodes (as the principal or auxiliary reaction), any polarization of this reaction will raise the working voltage (*overvoltage*), and thus the electrical energy consumption; hence, it is a fundamental problem to reduce polarization to the largest possible extent. When hydrogen evolution is an undesirable side reaction (as, e.g., in metal deposition in electrohydrometallurgy), the problem is, to the contrary, that of raising the polarization of this reaction. This is even more important in corrosion processes attended by hydrogen evolution.

For lower values of polarization in hydrogen evolution, one must first select the proper electrode materials. Metals and alloys of the iron group are most suitable under this aspect in alkaline solutions: iron, steel, binary and ternary alloys with nickel and cobalt. In certain cases, these materials can be used without noticeable corrosion, even in neutral and weakly acidic solutions, since during hydrogen evolution the solution next to the cathode surface becomes alkaline. In acidic solutions carbon or graphite cathodes are used most often. Electrodes containing platinum group metals are used when it is necessary to lower the working voltage of the electrolyzers to the largest possible extent.

It is of great value in efforts to reduce polarization to raise the true working surface area by using strongly roughened or even porous electrodes instead of smooth

electrodes. Such electrodes find ever-increasing use in industry. Higher values of polarization in hydrogen evolution are attained mainly by the addition of different surfactants, both neutral and cationic, to the electrolyte. But other methods are used as well. For instance, in batteries the zinc electrodes are often amalgamated in order to reduce their corrosion (at amalgams, like at mercury, the rate of hydrogen evolution is low). For environmental reasons, though, the use of mercury in batteries should be minimized.

15.3 REACTIONS INVOLVING OXYGEN

The equations of the principal reaction in aqueous solutions are

$$O_2 + 4H^+ + 4e^- \rightleftharpoons 2H_2O, \tag{15.20a}$$

$$O_2 + 2H_2O + 4e^- \rightleftharpoons 4OH^-. \tag{15.20b}$$

Anodic oxygen evolution is the principal reaction in electrolytic oxygen production, the auxiliary reaction in the production of many substances forming at the cathode, as for instance in electrohydrometallurgy, and a side reaction in a number of anodic processes, particularly in the production of chlorine and other oxidizing agents. Like hydrogen evolution, this reaction occurs in aqueous solutions without the addition of special reactants. The reverse reaction, which is the *cathodic reduction of oxygen* (also called the *oxygen ionization reaction*), is used in metal–air batteries and fuel cells. It is of considerable importance in the corrosion of metals.

Other reactions involving oxygen are those reaction steps in oxygen reduction which are of importance in their own right, such as the formation of hydrogen peroxide as a relatively stable intermediate:

$$O_2 + 2H^+ + 2e^- \rightleftharpoons H_2O_2, \tag{15.21}$$

and its further cathodic reduction to water:

$$H_2O_2 + 2H^+ + 2e^- \rightarrow 2H_2O, \tag{15.22}$$

as well as its electrochemical oxidation [the reverse of reaction (15.21)]. The reverse of reaction (15.22), the anodic direct oxidation of water to hydrogen peroxide, has not yet been achieved.

The standard electrode potential E_A^0 of reaction (15.20) calculated thermodynamically is 1.229 V (SHE) at 25°C. For reactions (15.21) and (15.22), these values are 0.682 and 1.776 V, respectively. The equilibrium potentials of all these reactions have the same pH dependence as the potential of the reversible hydrogen electrode; therefore, on the scale of potentials E_r (against the RHE), these equilibrium potentials are independent of pH. This picture is disturbed for reactions (15.21) and (15.22) in alkaline solutions because of the dissociation $H_2O_2 \rightleftharpoons H^+ + HO_2^-$ (Fig. 15.4).

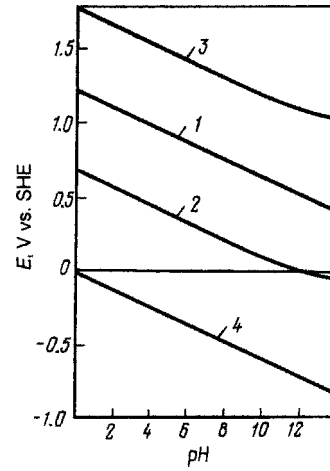

FIGURE 15.4 pH dependence of equilibrium potentials of various reactions: (1) reaction (15.20); (2) reaction (15.21); (3) reaction (15.22); (4) reaction (15.4).

The relative values of the potentials given above indicate that hydrogen peroxide is thermodynamically unstable and may decompose spontaneously via the reaction

$$2H_2O_2 \rightarrow 2H_2O + O_2. \tag{15.23}$$

Ordinarily, this is a slow reaction, and hydrogen peroxide is relatively stable, but the reaction is very strongly catalytically accelerated by various solid materials as well as by iron ions, and so on.

The oxygen reactions occur at potentials where most metal surfaces are covered by adsorbed or phase oxide layers. This is particularly true for oxygen evolution, which occurs at potentials of 1.5 to 2.2 V (RHE). At these potentials many metals either dissolve or are completely oxidized. In acidic solutions, oxygen evolution can be realized at electrodes of the platinum group metals, the lead dioxide, and the oxides of certain other metals. In alkaline solutions, electrodes of iron group metals can also be used (at these potentials, their surfaces are practically completely oxidized).

For oxygen reduction, one can use electrodes made of carbon materials, and when the solutions are alkaline, one can also use electrodes of silver and nickel, apart from those made of platinum metals.

At almost all electrodes, reaction (15.20) occurs with appreciable polarization in both the cathodic and anodic directions; the exchange CD of this reaction is very low: 10^{-10} to 10^{-6} mA/cm^2. For this reason the equilibrium potential of this reaction is not established at the electrodes. The OCP measured in oxygen is between 0.85 and 1.1 V (RHE); that is, it is 0.15 to 0.4 V more negative than the equilibrium potential.

The equilibrium potential of reaction (15.21) is relatively readily established at mercury and graphite electrodes in alkaline solutions containing hydrogen peroxide.

15.3.1 Anodic Oxygen Evolution

The kinetics and mechanism of the oxygen evolution reaction, like those of hydrogen evolution, have been the subject of innumerable studies going back to the beginning of the twentieth century. However, progress has been modest. This is to be explained by the complexity of the reaction itself and by the possibility of simultaneous anodic reactions: the formation and growth of oxide layers, dissolution of the metal, and the oxidation of solution components. The experimental data obtained by different workers do not always coincide; there are effects of pretreatment of the electrode surface, time-dependent changes in the state of this surface, the impurities present in the solution, and other factors. An interpretation of the experimental data is further complicated by the fact that the cathodic reaction, as a rule, follows a pathway [e.g., that involving intermediate hydrogen peroxide formation via reaction (15.21)], which is not the same as that of the anodic reaction; hence, it is not correct to compare the kinetic parameters of these reactions.

The polarization curves for the oxygen evolution reaction are more complex than those for hydrogen evolution. Usually, several Tafel sections with different slopes are present. At intermediate CD their slope b' is very close to 0.12 V, but at low CD it sometimes falls to 0.06 V. At high CD higher slopes are found; at potentials above 2.2 V (RHE) new phenomena and processes are possible, which are considered in Section 15.6.

The polarization that is seen in oxygen evolution will of course depend on the nature of the electrode. It is interesting to note that in alkaline solutions much higher values of polarization are found at platinum or PbO_2 electrodes than at superficially oxidized iron group metals. To a first approximation, the polarization at a given CD is independent of solution pH; this implies that the coefficient $-(\partial E/\partial \mathrm{pH})_i = 0.06$ V, like the analogous coefficient for the equilibrium potential. The reaction is also highly sensitive to the concentration of a number of solution components, particularly anions. Figure 15.5 shows an example: polarization curves recorded in perchloric acid solutions having different concentrations.

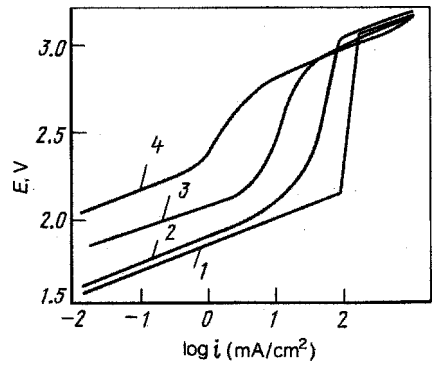

FIGURE 15.5 Polarization curves for anodic oxygen evolution at a platinum electrode in perchloric acid solutions with various concentrations: (1) 1.34; (2) 3: (3) 5; (4) 9.8 *M*.

The complexities of oxygen evolution, which is a four-electron reaction, are due to the fact that it is a multistep reaction and that oxygen adsorbed on the electrode is involved in it. As early as 1905 it was suggested by Fritz Förster that oxygen is evolved as a result of decomposition of higher oxides forming as unstable intermediates. A large number of pathways have subsequently been suggested for this reaction. It is assumed in almost all of them that the first step is the formation of additional adsorbed oxygen-containing species of the type OH_{ads} or O_{ads} by discharge of water molecules or OH^- ions:

$$2H_2O \xleftrightarrow{-H^+,-e^-} OH_{ads} \xleftrightarrow{-H^+,-e^-} O_{ads}. \tag{15.24}$$

These species are adsorbed not only on the bare metal surface but also on surface sections already oxidized. They can undergo further reaction in a variety of steps, both purely chemical ones and steps of the electrochemical desorption type:

$$2O_{ads} \rightleftharpoons O_2, \tag{15.25}$$

$$O_{ads} + H_2O \rightleftharpoons O_2 + 2H^+ + 2e^-, \tag{15.26}$$

$$2[O_{ads} + MO_x \rightleftharpoons MO_{x+1}] \rightleftharpoons O_2 + 2MO_x \tag{15.27}$$

(M is the electrode material), as well as many others, including the analogous reactions involving OH^-.

This great variety of pathways makes it difficult to decide which of the steps is the rate-determining step. It is most likely that at intermediate current densities the overall reaction rate is determined by the special kinetic features of step (15.24) producing the oxygen-containing species. The slopes of $b' \approx 0.12\,V$ observed experimentally are readily explained with the aid of this concept. Under different conditions, one of the steps in which these species react further may be the slow step, or several of the consecutive steps may occur with similar kinetic parameters.

15.3.2 Cathodic Oxygen Reduction

Systematic studies of cathodic oxygen reduction, unlike those of its anodic evolution, were only started in the 1950s when required for the realization of fuel cells. The large polarization of this reaction is one of the major reasons that the efficiency of the fuel cells developed so far is not very high.

Two major pathways exist for this reaction, one bypassing hydrogen peroxide (first pathway) and the other involving intermediate peroxide formation via reaction (15.21) (second pathway). The peroxide formed is either electrochemically reduced to water via reaction (15.22) or decomposed catalytically on the electrode surface via reaction (15.23), in which case half of the oxygen consumed to form it reemerges [in both cases the overall reaction corresponds to Eq. (15.20)].

The basic difference between the two pathways resides in the fate of the O–O bond in the original oxygen molecule, which in the first pathway is broken in the initial reaction step. The resulting oxygen atoms are adsorbed on the electrode and then are reduced electrochemically:

$$O_2 \rightleftharpoons 2\,[O_{ads} \xleftrightarrow{+2H^+,+2e^-} H_2O] \tag{15.28}$$

(it cannot be ruled out that bond breaking occurs during addition of the first electron and/or proton) This pathway corresponds to the one followed in anodic oxygen evolution, but since the two reactions occur at different potentials, the nature and number of oxygen species on the surface may differ.

In the reaction following the second pathway, the O–O bond is not broken while the first two electrons are added; it is preserved in the H_2O_2 produced as an intermediate, and breaks in a later step, when the hydrogen peroxide is reduced or catalytically decomposed. An analog for this pathway does not exist in anodic oxygen evolution.

The second pathway is seen distinctly at mercury and graphite electrodes. These electrodes are quite inactive in the catalytic decomposition of H_2O_2. Moreover, at them the potential where the peroxide is reduced further is more negative than the potential where it is formed from oxygen. Hence, within a certain range of not too negative potentials, the reaction can occur in such a way that the hydrogen peroxide formed accumulates in the solution.

At other electrodes the peroxide immediately undergoes further conversion, and practically none accumulates in the solution. In this case its intermediate formation can be detected and examined quantitatively with a rotating ring–disk electrode; at high rates of rotation of the electrode, the intermediate produced is rapidly carried away from the disk surface before it can react further and can be ascertained at the ring electrode. According to these studies, intermediate H_2O_2 formation is not observed at a number of active metals, particularly the platinum group metals (i.e., the reaction apparently follows the first pathway). In other cases the reaction is found to occur in parallel following both of the pathways, while their relative importance depends on the experimental conditions, such as solution composition and electrode surface treatment. Solution impurities as a rule promote peroxide formation.

At mercury and graphite electrodes the kinetics of reactions (15.21) and (15.22) can be studied separately (in different regions of potential). It follows from the experimental data (Fig. 15.6) that in acidic solutions the slope $b' \approx 0.12$ V. The reaction rate is proportional to the oxygen partial pressure (its solution concentration). At a given current density the electrode potential is independent of solution pH; because of the shift of equilibrium potential, the electrode's polarization decreases by 0.06 V when the pH is raised by a unit. These data indicate that the rate-determining step is addition of the first electron to the oxygen molecule:

$$O_2 + e^- \rightleftharpoons O_2^-. \tag{15.29}$$

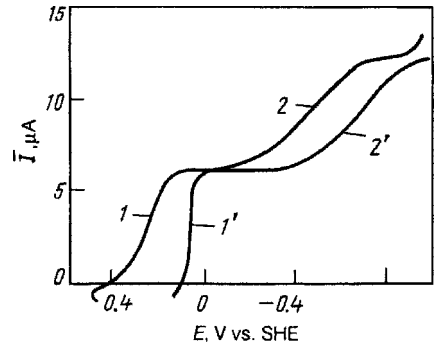

FIGURE 15.6 Polarization curves for reactions (15.21) (1,1′) and (15.22) (2,2′) at the dropping mercury electrode in acidic (1,2) and alkaline (1′,2′) solutions.

The resulting unstable molecular ion O_2^- rapidly adds another electron and protons to yield hydrogen peroxide. In alkaline solutions the same pathway is followed, but owing to the much lower polarization, the reaction becomes practically reversible ($b' = 0.03$ V); its rate then is determined by oxygen transport to the surface, and polarization is of the concentration type (Bagotsky and Yablokova, 1953).

Polarization is much higher for the electrochemical reduction of hydrogen peroxide. The slope has the unusually high value of about 0.3 V. At a given current density the electrode potential in this reaction is again independent of solution pH. These and certain other data indicate that addition of the first electron to the peroxide molecule and simultaneous peroxide decomposition is the rate-determining step:

$$H_2O_2 + e^- \rightarrow OH_{ads} + OH^-. \tag{15.30}$$

At the platinum electrode the individual steps of the four-electron reaction cannot be studied separately. Slope b' has its usual value of about 0.12 V, but in contrast to what is seen at the mercury electrode, the polarization is practically independent of solution pH (i.e., the potential at a given current density shifts by 0.06 V in the negative direction when the pH is raised by a unit). It follows that the reaction rate depends on hydrogen ion concentration. The step in which an electron and a proton are transferred while the O–O bond is broken is probably the rate-determining step.

15.4 REACTIONS INVOLVING CHLORINE AND OTHER HALOGENS

The principal reaction involving chlorine is

$$Cl_2 + 2e^- \rightleftharpoons 2Cl^-. \tag{15.31}$$

The standard electrode potential of this reaction is 1.358 V vs. SHE; the equilibrium potential is independent of solution pH.

Anodic chlorine evolution by electrolysis of concentrated chloride solutions is used for the large-scale industrial production of chlorine. The cathodic reaction, which is the ionization of molecular chlorine, is used in certain types of batteries.

Because of the considerable corrosivity of chlorine toward most metals, anodic chlorine evolution can only be realized for a few electrode materials. In industry, graphite had been used primarily for this purposes in the past. Some oxide materials, manganese dioxide for instance, are stable as well. At present the titanium–ruthenium oxide anodes (DSA; see Chapter 28) are commonly used.

The mechanism of anodic chlorine evolution has been studied by many scientists. In many respects this reaction is reminiscent of hydrogen evolution. The analogous pathways are possible. The most probable one is the second pathway, in which the adsorbed chlorine atoms produced are eliminated by electrochemical desorption, but sometimes the first pathway is also possible. As a rule the first step, which is discharge of the chloride ion, is the slow step.

One of the most important problems in chlorine production is that of reducing the rate of anodic oxygen evolution that occurs as a parallel reaction and is responsible not only for a waste of electric power but also for contamination of the product. Figure 15.7 shows the relative positions of the polarization curves for anodic chlorine and oxygen evolution. Oxygen evolution starts earlier, since its equilibrium potential is more negative, but because of a higher polarizability in the oxygen reaction, at intermediate and high current densities, chlorine evolution is predominant.

Higher current yields of chlorine can be obtained when raising the chloride concentration, which shifts the equilibrium potential of the chlorine electrode to more negative values and reduces the effect of concentration polarization. In practice, NaCl solutions having a concentration of about 5.3 *M* are used in electrolysis. To raise the current yields, it is very important to maintain the optimum value of pH, which as a rule is between 2 and 3. In diaphragm cells, the catholyte becomes strongly alkaline, owing to hydrogen evolution. This produces a risk of OH^- ion diffusion through the diaphragm into the anode compartment, and thus of an increase

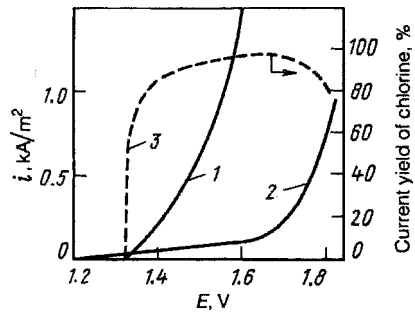

FIGURE 15.7 Polarization curves for anodic chlorine (1) and oxygen (2) evolution at a graphite electrode, and the current yields of chlorine as a function of potential (3).

in anolyte pH, which will accelerate the oxygen evolution reaction and lower the current yields of chlorine. To counteract this effect, the alkali being formed is drained from the cathode compartment continuously, and the chloride solution is introduced into the anode compartment. The (convective) filtration or solution flow through the diaphragm toward the cathode, which develops under these conditions, prevents a back diffusion of OH^- ions.

There are further side reactions occurring in chlorine evolution. Molecular chlorine reacts with aqueous solutions to hypochlorous acid, HClO:

$$Cl_2 + H_2O \rightleftharpoons HClO + HCl. \tag{15.32}$$

The concentration of the hypochlorous acid forming in acidic and weakly acidic solutions is low, but in alkaline solutions the equilibrium is shifted to the right, in the direction of hypochlorite formation. Since at the cathode of chlorine cells two OH^- ions are produced for each Cl_2 molecule, this alkali will shift the equilibrium (15.29) completely to the right when electrolysis is conducted in a common solution (without a diaphragm, i.e., in an undivided cell), and no gaseous chlorine will be evolved. One can thus obtain dilute sodium or other hypochlorite solutions. At higher concentrations the ClO^- ions start to undergo anodic oxidation to chlorate ions, ClO_3^-:

$$ClO^- + 2H_2O \rightleftharpoons ClO_3^- + 4H^+ + 4e^-. \tag{15.33}$$

Chlorates also form by dismutation of the hypochlorite ions in the bulk solution:

$$3ClO^- \rightleftharpoons ClO_3 + 2Cl^-. \tag{15.34}$$

Current world chlorate production (about 700 kilotons per year) is based entirely on an electrochemical method where reactions (15.21) to (15.34) occur simultanously in undivided cells. A small amount of bichromate ions are added to the solution to reduce chlorate losses by rereduction at the cathode; these form a thin protective layer at the cathode which passivates the reduction of chlorate and hypochlorite ions.

Perchlorates are also produced electrochemically. The oxidation of chlorate to perchlorate ions occurs at a higher positive potential (above 2.0 V vs. SHE) than chloride ion oxidation. The current yield of perchlorate is lower when chloride ions are present in the solution; hence, in perchlorate production concentrated pure chlorate solutions free of chlorides are used. Materials stable in this potential range are used as the anodes; primarily, these include smooth platinum, platinum on titanium, and lead dioxide.

Methods have been developed for perchloric acid synthesis which involve the electrolysis of solutions containing hydrogen chloride or molecular chlorine. These processes occur at high anode potentials (2.8 to 3.0 V vs. SHE), when oxygen is evolved at the anode in parallel with perchloric acid formation. The current yields of perchloric acid will increase considerably when the reaction is conducted at low temperatures (e.g., -20°C).

Electrolytic fluorine production from molten eutectics of anhydrous hydrogen fluoride and potassium fluoride, with the composition KF·HF ($t_f = 239$°C) or KF·2HF ($t_f = 82$°C), is of great practical importance. The equation for anodic fluorine generation is the analog of reaction (15.31) from right to left. This reaction, which has been known for about 100 years, was developed commercially in the 1950s when fluorine began to be widely used for the fluorination of organic compounds and production of fluoropolymers. At present the total fluorine production is several tens of kilotons per year. Anodes of steel, copper, or of magnesium alloys are used for electrolysis. In the presence of fluorine, these metals quickly form a thin superficial fluoride layer protecting them against further corrosion in the highly aggressive medium. At the graphite cathodes, hydrogen is evolved. Hydrogen fluoride is added continuously to the melt to maintain the original HF/KF ratio. The cell voltage is rather high (8 to 12 V) because of the considerable ohmic losses and of high values of polarization of the electrodes. Often, difficulties arise in the production because of poor wetting of the anodes by the melt and the development of anode effects (see Section 8.3).

Unlike chlorine and fluorine, the free bromine and iodine are produced by chemical methods (reaction of chlorine with bromide or iodide solutions). Electrochemical methods are used to produce the salts of their oxygen-containing acids, the bromates and iodates, from the corresponding bromide and iodide solutions. These reactions are analogous to those in chlorate production [Eqs. (15.31) to (15.34)] and involve the intermediate formation of hypobromites and hypoiodites.

15.5 REACTIONS INVOLVING ORGANIC SUBSTANCES

Like inorganic substances, organic substances can be anodically oxidized and/or cathodically reduced. Such reactions are widely used for the synthesis of various organic compounds (electroorganic synthesis). Moreover, they are of importance for the qualitative and quantitative analysis of organic substances in solutions, as for instance in polarography (see Lund and Baizer, 1991).

Reactions involving organic substances have some special features. Many of these substances are poorly soluble in aqueous solutions. Sometimes their solubilities can be raised by adding to the solution the salts of aromatic sulfonic acids with cations of the type $[NH_4]^+$ or alkali metal ions. These salts have a salting-in effect on poorly soluble organic substances. In many cases solutions in mixed or nonaqueous solvents (e.g., methanol) are used. Suspensions of the organic substances in aqueous solutions are also useful for electrosynthesis.

The solutions of many organic substances in water or other solvents are not by themselves electrically conducting. Hence, substances providing conductivity as well as pH control are added to these solutions. Many electrochemical reactions involving organic substances are invertible. Their efficiency depends strongly on the quality of the separators or diaphragms used to prevent the reaction products from reaching the auxiliary electrode.

Electrochemical reactors are inferior to chemical reactors in their productivity. Hence, electrosynthesis is used when chemical ways to synthesize a given substance

are impractical or inefficient. It is an important advantage of electrosynthesis that special reactants (oxidizing or reducing agents) which would be hard to reextract from the products need not be added to the system. Moreover, the conditions under which electrosynthesis proceeds (the potential, current, etc.) are readily monitored and adjusted. By now a large number of electrochemical reactions involving organic substances have been investigated, but so far few of them are commercially exploited.

Reactions involving organic compounds are highly diverse. Still, two basic types of mechanism can be distinguished: the electron–radical and the chemical mechanism. In the former, there is direct electron transfer between the electrode and an organic species yielding primarily the valence-unsaturated radicals $Q^{\cdot}H$ or the radical ions $Q^{\dot{-}}$ or QH_2^+ (here and in the following, stable valence-saturated organic compounds will be written as Q and QH_2, RH and RR′, etc.):

$$Q \xleftarrow{+e^-} Q^{\dot{-}} \xleftarrow{+H^+} Q^{\cdot}H \xleftarrow{+H^+} QH_2^+ \xleftarrow{+e^-} QH_2. \tag{15.35}$$

Most often, these radicals are unstable and can exist only while adsorbed on the electrode, although in the case of polycyclic aromatic compounds (e.g., the derivatives of anthracene), they are more stable and can exist even in the solution. The radicals formed first can undergo a variety of chemical or electrochemical reactions. This reaction type is the analog of hydrogen evolution, where electron transfer as the first step produces an adsorbed hydrogen atom, which is also a radical-type product.

The chemical mechanism rests on the effect of intervening redox systems (see Section 13.6). Here intermediate reactants such as H_{ads} species on a cathode surface, OH_{ads} species on an anode surface, or reducing and oxidizing agents in the solution layer next to the electrode are first produced electrochemically from solution components. The further interaction of these reactants with the organic substance is purely chemical in character, for example, following a reaction

$$Q + 2H_{ads} \rightleftharpoons QH_2. \tag{15.36}$$

Electrochemical equilibria between the oxidized and reduced forms of an organic substance are observed in only a few cases. The best known instance is the equilibrium between quinone and hydroquinone (or their derivatives):

$$C_6H_4O_2 + 2H^+ + 2e^- \rightleftharpoons \mathbf{C}_6H_4(OH)_2. \tag{15.37}$$

The equilibrium potential of this reaction is readily established at platinum electrodes; it is highly reproducible.

15.5.1 Reduction Reactions

For the cathodic reduction of organic substances, electrodes of two types are used: the platinum and the mercury type. Those of the first type (platinum metals, and in alkaline solutions nickel) exhibit low polarization in hydrogen evolution; their potential can be pushed in the negative direction no further than to -0.3 V (RHE). Hydrogen readily adsorbs on these electrodes, which is favorable for reduction

reactions following the chemical mechanism. Under the effect of certain impurities (poisons), they readily lose their activity. At electrodes of the mercury type (mercury itself, also lead, tin, cadmium, and others), much more negative potentials (up to -1.2 V vs. RHE, for instance) can be realized, since hydrogen evolution is slow. Here hydrogen adsorption is slight, hence reactions at electrodes of this type follow predominantly the electron–radical mechanism.

Unsaturated organic substances having double or triple bonds can be reduced (hydrogenated) only at electrodes of the platinum type (i.e., via the chemical mechanism). This process occurs with ease, but the electrochemical method of hydrogenation is still economically inferior to the common methods of catalytic hydrogenation of unsaturated compounds. If the compound in addition to a double bond has a functional group, its reduction owing to bond polarization is possible even at mercury-type metals (i.e., following an electron–radical mechanism). An example is the reduction of maleic to succinic acid:

$$\mathrm{COOHCH{=}CHCOOH} + 2\mathrm{H^+} + 2e^- \rightarrow \mathrm{COOHCH_2CH_2COOH}, \quad (15.38)$$

which will occur via both the electron–radical and the chemical mechanism.

At electrodes of the mercury type, electron–radical reactions can also be carried out when there is a deficit of proton donors in the solution. Then the radicals $\mathrm{Q^{\cdot}H}$ formed initially, instead of adding a second electron and second proton, will couple to a dimeric product:

$$2\mathrm{Q^{\cdot}H} \rightarrow \mathrm{HQQH}. \quad (15.39)$$

Reactions of this type are called *electrochemical hydrodimerization*. They are of great value for the synthesis of various bifunctional compounds. A reaction that has found wide commercial use is the hydrodimerization of acrylonitrile to adiponitrile (the dinitrile of adipic acid):

$$2\mathrm{CH_2{=}CHCN} + 2\mathrm{H^+} + 2e^- \rightarrow \mathrm{NC(CH_2)_4CN}. \quad (15.40)$$

Adiponitrile is readily hydrogenated catalytically to hexamethylenediamine, which is an important starting material for the production of nylons and other plastics. The electrochemical production of adiponitrile was started in the United States in 1965; at present its volume is about 200 kilotons per year. The reaction occurs at lead or cadmium cathodes with current densities of up to 200 mA/cm^2 in phosphate buffer solutions of pH 8.5 to 9. Salts of tetrabutylammonium $[\mathrm{N(C_4H_9)_4}]^+$ are added to the solution; this cation is specifically adsorbed on the cathode and displaces water molecules from the first solution layer at the surface. Therefore, the concentration of proton donors is drastically reduced in the reaction zone, and the reaction follows the scheme of (15.36) rather than that of (15.35), which would yield propionitrile.

Another group of reactions is that involving the reduction of different functional groups. A classical example is the reduction of nitrobenzene (and the analogous nitro

compounds), which had been studied by Fritz Haber at the end of the nineteenth century. This is possible at both electrodes of the platinum type and electrodes of the mercury type. The main reaction sequence is

$$\underset{\text{nitrobenzene}}{C_6H_5NO_2} \rightarrow \underset{\text{nitrosobenzene}}{C_6H_5NO} \rightarrow \underset{\text{phenylhydroxylamine}}{C_6H_5NHOH} \rightarrow \underset{\text{aniline}}{C_6H_5NH_2}. \quad (15.41)$$

By appropriate selection of the electrode potential and other conditions, one can control the reaction so that it will yield any one of these products. As a result of auxiliary chemical reactions, nitrosobenzene can be converted to azobenzene $C_6H_5N{=}NC_6H_5$ and azoxybenzene $C_6H_5N(=O)–NC_6H_5$, and the latter can be converted to hydrazobenzene $C_6H_5–NH–NH–C_6H_5$; phenylhydroxylamine can be converted to *p*-aminophenol $H_2NC_6H_4OH$ by internal rearrangement.

Another example of the reduction of functional groups is that of aromatic ketones. At the mercury electrode, a radical-type intermediate is formed as the primary product:

$$RR'C{=}O + H^+ + e^- \rightarrow RR'C^{\cdot}–OH. \quad (15.42)$$

Depending on the electrode potential, this radical either adds a second electron and a second proton to yield the corresponding secondary alcohol (A), or it dimerizes to the pinacol (B), a dihydric ditertiary alcohol:

$$RR'CH–OH \underset{(A)}{\xleftarrow{+H^+,+e^-}} RR'C^{\cdot}–OH \xrightarrow[(B)]{} 5RR'COHCOHRR'. \quad (15.43)$$

15.5.2 Reactions of Partial Oxidation

Reactions of partial electrochemical oxidation are of considerable interest in the electrosynthesis of various organic compounds. Thus, at gold electrodes in acidic solutions, olefins can be oxidized to aldehydes, acids, oxides, and other compounds. A good deal of work was invested in the oxidation of aromatic compounds (benzene, anthracene, etc.) to the corresponding quinones. To this end, various mediating redox systems (e.g., the Ce^{4+}/Ce^{3+} system) are employed (see Section 13.6).

A reaction of practical importance is the oxidation of a carbohydrate aldehyde group to a carboxyl group. This is the basis for a process converting glucose to calcium gluconate, a substance of pharmaceutical interest. The oxidation reaction occurs at graphite electrodes in the presence of the Br_2/Br^- redox system. Calcium salt is added to the solution to prevent further oxidation of free gluconic acid.

Common reactions are the anodic substitution of hydrogen atoms in organic compounds by halide or other functional groups:

$$RH + X^- \rightarrow RX + H^+ + 2e^-, \quad (15.44)$$

where X^- is the nucleophile: a halide ion, CN^-, OH^-, RO^-, $RCOO^-$, or others. These reactions are conducted chiefly with aromatic compounds; in the case of

aliphatic compounds, nonelectrochemical methods of substitution, as a rule, are more convenient.

As in reduction reactions, two possible mechanisms exist for substitution reactions: (1) electron–radical, involving the intermediate formation of radicals and their reaction with nucleophiles X^-:

$$RH \xrightarrow{-e^-,\,-H^+} R^{\cdot} \xrightarrow{-e^-,\,+X^-} RX, \tag{15.45}$$

and (2) chemical, involving the prior discharge of species X^-:

$$2X^- \xrightarrow{-2e^-} X_2 \xrightarrow{+RH} RX + HX. \tag{15.46}$$

In certain cases several hydrogen atoms can be replaced in the original organic compound.

Of great practical value is the thorough fluorination of hydrocarbons and other organic compounds, which can be used to produce valuable perfluorinated substances: for example,

$$C_2H_6 + 12F^- \rightarrow C_2F_6 + 6HF + 12e^-. \tag{15.47}$$

These reactions will occur at graphite, nickel, or platinum electrodes in solutions of sodium or potassium fluoride in anhydrous liquid hydrogen fluoride. They have rather complicated mechanisms (the example shown involves 12 electrons!). In many cases the starting materials are broken down to simpler ones, while in aromatic compounds, benzene rings may be opened. As a result, mixtures of different reaction products having different chain lengths and different degrees of fluorination are obtained. The reaction mechanism of thorough fluorination has not been established in a definite way.

Another group of reactions involving anodic oxidation is the anodic dimerization occurring at high anodic potentials. These reactions are considered in Section 15.6.

15.5.3 Complete Electrochemical Oxidation of Methanol

The complete electrochemical oxidation of methanol to carbon dioxide,

$$CH_3OH + H_2O \rightarrow CO_2 + 6H^+ + 6e^-, \tag{15.48}$$

has been a focus of attention in research over a number of recent decades, for two reasons: (1) it is a very convenient model reaction for many electrocatalytic phenomena (for further details, see Chapter 28), and (2) it is the current-producing reaction in a rather promising type of fuel cell, methanol–air (see Chapter 20).

The special kinetic and mechanistic features of this reaction began to be studied at platinum electrodes in the early 1960s. In recent years a number of groups in different countries published a large amount of research work concerning this reaction (see, e.g., Bagotsky et al., 1977; Parsons and Van der Noot, 1988; Iwasita and

Vielstich, 1990; Kauranen et al., 1996; Léger, 2001). As a result, it can now be said that the reaction mechanism has been established quite reliably, yet certain specific questions still elicit diverging views.

The main reaction product is carbon dioxide, but under certain conditions, other oxidation products are observed for short periods of time, such as formaldehyde, formic acid, and others. The oxidation of methanol to CO_2 yields six electrons, so that the specific capacity of methanol is close to 0.84 Ah/g.

The reaction goes through several consecutive steps. In a first step, the methanol molecule becomes dehydrogenated while adsorbing on platinum:

$$CH_3OH \longrightarrow \equiv C - OH_{ads} + 3H_{ads} \tag{15.49}$$

which gives rise to chemisorbed species, $\equiv$C–OH_{ads} and H_{ads}.

In the next step, species $\equiv$C–OH_{ads} are oxidized through chemical interaction with oxygen species OH_{ads} that are adsorbed on neighboring surface sites of the platinum electrode:

$$\equiv C\text{–}OH_{ads} + 3OH_{ads} \rightarrow CO_2 + 2H_2O. \tag{15.50}$$

The current-producing steps (those producing electrons) are the ionization of adsorbed hydrogen atoms and the anodic formation of new OH_{ads} species from water molecules:

$$3H_{ads} \rightarrow 3H^+ + 3e^-, \tag{15.51}$$

$$3H_2O \rightarrow 3OH_{ads} + 3H^+ + 3e^-. \tag{15.52}$$

Under certain conditions (e.g., during times at open circuit when the anodic formation of OH_{ads} is not possible), the $\equiv$C–OH_{ads} are transformed to $=CO_{ads}$, which are difficult to oxidize and may further inhibit methanol oxidation at the surface. It is for this reason that in studies of the adsorbed species by infrared spectroscopy, often predominantly the $=CO_{ads}$ rather than the $\equiv$C–OH_{ads} are observed.

The thermodynamic standard potential of the methanol electrode has a value of + 0.02 V (RHE); that is, it is quite close to the hydrogen electrode potential. The steady-state potential of a platinum electrode in aqueous methanol solutions is about + 0.3 V (RHE).

When a preactivated platinum electrode maintained at a constant potential in the range 0.3 to 0.8 V (RHE) by means of a potentiostat is brought into contact with a methanol solution, a large nonsteady current arises, which decreases rather rapidly and finally reaches a small steady-state value. The nonsteady current is connected with an increased number of chemisorbed organic particles. Thus, it can be concluded that this nonsteady current is due to the ionization of atomic hydrogen reaction (15.51), formed by the dehydrogenization process (15.49) during methanol adsorption. The steady-state current is due to the oxidation of the chemisorbed particles according to reactions (15.50) and (15.52).

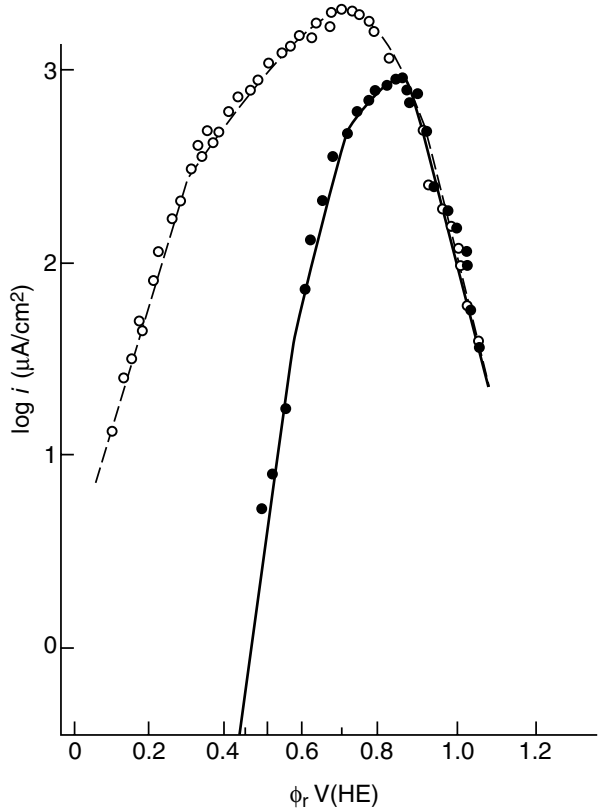

FIGURE 15.8 Dependence of the values of the maximal nonsteady current (1) and the steady-state current (2) on potential at a smooth platinum electrode in 1 *M* CH_3OH + 0.5 *M* H_2SO_4 solution.

Plots of current density vs. potential are shown in Fig. 15.8, both for the steady-state currents (rate of oxidation of the chemisorbed species) and for the transient anodic currents (rate of adsorption of species $\equiv C–OH_{ads}$ and simultaneous ionization of the resulting atomic hydrogen). Both curves go through a maximum in the region 0.6 to 0.65 V. At potentials more negative than 0.7 V (RHE) the rate of formation of chemisorbed species by adsorption is much higher than that of their further oxidation (i.e., the oxidation step is rate limiting). As a result, the degree of coverage of the surface by organic species increases. This retards further adsorption of these species (the descending part of curve 1 in Fig. 15.8). At potentials more positive than 0.7 V, the oxidation rate increases (because of the more positive value of potential and because of an increase in surface concentration of species OH_{ads}), and hence the rates of adsorption and oxidation become equal. Here the adsorption becomes rate limiting and there is no further accumulation of chemisorbed species.

Depending on current density, the working potential of steady-state methanol oxidation varies within the range 0.35 to 0.65 V (RHE). Therefore, the working voltage of a methanol–oxygen fuel cell will have values between 0.4 and 0.7 V.

15.5.4 Reactions Involving Organometallic Compounds

It had been shown in the preceding sections that the initial step in a number of cathodic and anodic reactions yields organic radicals, which then undergo further oxidation, reduction, or dimerization. In some cases reactions of another type are possible: reaction of the radical with the electrode metal, yielding organometallic compounds which are then taken up by the solution. Such reactions can be used in the synthesis of these compounds.

The best known example is the electrosynthesis of tetraethyllead (TEL) $Pb(C_2H_5)_4$, which has been in wide use as an antiknock additive of gasoline, and still is in a number of countries. This substance is readily produced by reaction of ethyl radicals with the lead electrode:

$$Pb + 4C_2\dot{H}_5 \rightarrow Pb(C_2H_5)_4. \tag{15.53}$$

Ethyl radicals can be produced in various ways: for instance, by cathodic reduction of ethyl bromide:

$$C_2H_5Br + e^- = C_2\dot{H}_5 + Br^-. \tag{15.54}$$

The reaction proceeds in a solution of $[N(C_2H_5)_4]Br$ in acetonitrile at lead cathodes. The current yield is about 70%.

Anodic processes can also be used for tetraethyllead electrosynthesis. Here solutions of organometallic compounds are used; the overall reaction is replacement of the metal in these compounds by another metal, lead. One such process uses a melt of the compound $NaAl(C_2H_5)_4$, from which radicals $C_2\dot{H}_5$ are produced anodically. The process is highly efficient, but it is not easy to isolate the TEL produced from the melt. More convenient is a commercial process involving the anodic oxidation of the Grignard reagent C_2H_5MgCl:

$$C_2H_5MgCl \rightarrow C_2\dot{H}_5 + Mg^{2+} + Cl^- + e^-. \tag{15.55}$$

The reaction occurs at lead anodes; at the cathode metallic magnesium is produced. An ether solution of the Grignard reagent is used to which ethyl chloride is added. The latter reacts with the magnesium that is formed, to regenerate part of the Grignard reagent consumed. The overall reaction in the electrolyzer follows the equation

$$3C_2H_5MgCl + 2C_2H_5Cl + Pb \rightarrow Pb(C_2H_4) + 2MgCl_2. \tag{15.56}$$

15.6 REACTIONS AT HIGH ANODIC POTENTIALS

A number of anodic reactions will proceed at platinum and some other electrodes at potentials between about 2.2 and 3.5 V vs. RHE, which is called the *region of high anodic potentials* (HAPs). According to the usual laws of electrochemical kinetics, rather vigorous oxygen evolution could be expected in this region in aqueous solutions, and decomposition (oxidation) of the solvent with evolution of the corresponding products in nonaqueous solutions. But under certain conditions these reactions are suppressed, and others proceed instead. The main reason for these effects are changes in the electrode's surface state.

It was shown in Section 10.5.4 that as the potential of a platinum electrode is moved from 0.75 to 2.2 V, the amount of oxygen adsorbed on it will increase up to a limiting value corresponding to degrees of surface coverage of 2 to 2.2. The properties of the "oxidized" platinum surface differ from those of "nonoxidized" surfaces. For instance, the surface potential changes upon oxidation, which in turn produces a change in surface charge density and in the PZC. The adsorption properties also change. There is a drastic increase in anion adsorption from the solution due to chemical (specific) interaction forces. It had been shown in Section 10.5.5 that at potentials more positive than 0.8 V, the organic substance is desorbed from the platinum surface because of its displacement by adsorbing oxygen (which can be used, in particular, to clean the surface from organic contaminants). However, at higher positive potentials, in the region that starts at about 1.6 to 1.7 V, adsorption of organic substances increases again, although now it occurs on the oxidized surface.

The enhanced adsorption of anions and other substances that occurs at increasingly positive potentials causes a gradual displacement of water (or other solvent) molecules from the electrolyte layer next to the electrode. This leads to a markedly slower increase in the rate of oxygen evolution from water molecules and facilitates a further change of potential in the positive direction. As a result, conditions arise that are favorable for reactions involving the adsorbed species themselves (Fig. 15.9). In particular, adsorbed anions are discharged forming adsorbed radicals:

$$A^{-}_{ads} \rightleftharpoons A^{\cdot}_{ads} + e^{-}, \tag{15.57}$$

which subsequently dimerize by recombination:

$$2A^{\cdot}_{ads} \rightleftharpoons AA, \tag{15.58}$$

or via an electrochemical desorption step:

$$A^{\cdot}_{ads} + A^{-}_{ads} \rightleftharpoons AA + e^{-} \tag{15.59}$$

(anodic dimerization).

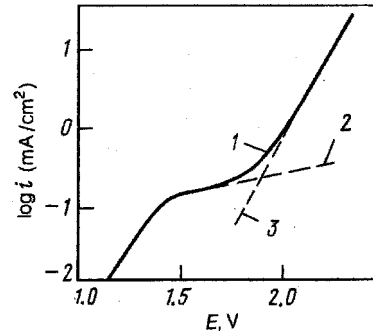

FIGURE 15.9 Anodic polarization curves recorded at a platinum electrode in the region of high anodic potentials in the presence of acetate ions: (1) total current; (2) partial current of oxygen evolution; (3) partial current of oxidation of adsorbed species.

In surface layers still containing a certain amount of water, reaction (15.24) may occur in parallel, yielding OH_{ads} groups, so that two different radical-type intermediates can react:

$$A^{\cdot}_{ads} + O^{\cdot}H^{-}_{ads} \rightleftharpoons AOH + e^{-}. \tag{15.60}$$

In concentrated sulfuric acid solutions at HAP, the adsorbed HSO_4^- ions are converted, according to reaction (15.57), to $HS^{\cdot}O_4$ radicals which dimerize, forming peroxydisulfuric (persulfuric) acid $H_2S_2O_8$. This acid is the intermediate for one of the commercialized methods of hydrogen peroxide production. The first efforts toward the electrosynthesis of peroxydisulfuric acid go back to 1878; commercial production started in 1908. The standard electrode potential of the overall reaction

$$2HSO_4^- \rightleftharpoons S_2O_8^{2-} + 2H^+ + 2e^- \tag{15.61}$$

is 2.10 V. The process occurs in 5.5 to 6.5 M H_2SO_4 solution at smooth platinum electrodes using current densities of 5 to 10 kA/m^2 and anode potentials of 3.0 to 3.2 V. The current yield of the product is 70 to 75%. Parallel reactions are oxygen evolution, and by a reaction of the type (15.60), the formation of peroxymonosulfuric acid H_2SO_5. Higher current yields can be achieved at a high current density and therefore high polarization of the oxygen evolution reaction. The region of HAP is not attained and peroxydisulfuric acid is not formed at platinized platinum, where the true current density and polarization are much lower. Sometimes, the process is conducted in ammonium sulfate solution and not in sulfuric acid, and a solution of ammonium peroxydisulfate is formed.

Many other peroxy compounds can analogously be produced in the region of HAP: for instance, sodium perborate $Na_2(BO_3)_2$ (from sodium metaborate $NaBO_2$) and peroxycarbonates. These compounds are used as stable oxidizing and bleaching agents.

Peculiar reactions occur during the oxidation of organic acid anions. In 1843, M. Faraday found that a hydrocarbon is evolved during the electrolysis of acetate solutions. These reactions were studied in 1849 by Hermann Kolbe, who showed that the acetate ions during electrolysis condense with the evolution of CO_2: that is, the reaction (in modern notation)

$$2CH_3COO^- \rightarrow C_2H_6 + 2CO_2 + 2e^- \tag{15.62}$$

(the *Kolbe reaction*) occurs. Other aliphatic acids, including substituted ones, react in an analogous way. The overall reaction can be written as

$$2[RCOO^- \xrightarrow{-e^-} RCOO^{\cdot} \xrightarrow{-CO_2} R^{\cdot}] \longrightarrow RR. \tag{15.63}$$

Thus, the $RCOO^{\cdot}$ radicals produced initially are unstable, and before (or while) undergoing dimerization, split up into simpler radicals and CO_2 molecules.

The anions of substituted acids will not always react according to this scheme. Some of them, particularly the α-substituted acids, form unsaturated compounds. More complex reactions also occur when dicarboxylate ions $^-COOCRCOO^-$ are used. When one of the carboxyl groups in the dicarboxylic acid is esterified, the Kolbe reaction proceeds without difficulty:

$$2R'OOCRCOO^- \rightarrow R'OOCRCOOR' + 2CO_2 + 2e^-. \tag{15.64}$$

Such reactions usually are called *Brown–Walker reactions.* They are of practical importance for the synthesis of higher carboxylic acids.

In Russia in the 1960s, an industrial production of sebacic acid, $HCOOC(CH_2)_4COOH$ (an important intermediate for different plastics), was started which involves the anodic condensation of monomethyl adipate $CH_3OOC(CH_2)_4COO^-$. Dimethyl sebacate is obtained via the scheme of (15.58), and then hydrolyzed in autoclaves to the final product. Methanol is used as a solvent to lower the rates of side reactions. The reaction occurs with current yields attaining 75% and with chemical yields (degrees of utilization of the original adipate) of 82 to 84% (Vassiliev et al., 1982). Upon introduction of this process it was no longer necessary to use castor oil, an expensive raw material that was needed to produce sebacic acid by the chemical process.

When several types of radicals are present on the electrode surface, they can interact in different ways. One of these reactions is that between organic radicals $R^{\cdot}$ with OH_{ads} groups, yielding alcohols ROH according to the scheme of (15.60). Reactions of this type or, in the more general case, reactions yielding ethers by interaction of radicals $R^{\cdot}$ with groups produced by decomposition of other solvents (e.g., $CH_3O^{\cdot}$), are known as *Hofer–Moest reactions*. In electrosynthesis these reactions are often undesirable, since they lower the yields of the product wanted.

Reactions involving a crossed anodic condensation are of practical interest when they combine organic radicals of different type. In solutions containing anions $RCOO^-$ and $R'COO^-$, condensation products of the type RR' are formed together with the standard products RR and $R'R'$ by the reactions described.

Unsaturated organic compounds that are present in the solution while these reactions proceed will also become adsorbed on the electrode and may act as acceptors for the radicals, yielding addition products:

$$2RCOO^- + C_2H_4 \rightarrow RH_2CCH_2R + 2CO_2 + 2e^- \tag{15.65}$$

(additive dimerization reactions). When dienes with two conjugated double bonds are used, the condensation products are unsaturated; for instance, with butadiene,

$$RCOO^- + H_2C{=}CHCH{=}CH_2 \rightarrow RH_2CCH_2R{=}CHCH_2R + 2CO_2 + 2e^-. \tag{15.66}$$

In solutions containing more than one compound of the RCOOH type, asymmetric products of the crossed addition of different radicals may form together with the standard additive dimers.

15.7 REACTION OF CARBON DIOXIDE REDUCTION

Electrochemical reduction of carbon dioxide has found no extensive application so far, yet it is of great interest for scientists in the fields of theoretical and applied electrochemistry. To a certain extent, it is analogous to the photochemical carbon dioxide reduction, but it involves no chlorophyll and yields simpler products. In recent years some books and reviews on this topic have been published (e.g., Taniguchi, 1989; Sullivan et al., 1993; Bagotsky and Osetrova, 1995).

From the applied point of view, this reaction can be used to solve some important issues: (1) production of organic subproducts (e.g., methanol, carbon monoxide, oxalic acid), which can be used for synthesizing many valuable organic substances; (2) manufacture of synthetic fuels or energy-storage media; and (3) removal and utilization of carbon dioxide in life-support systems for closed environments of spacecraft or submarines.

Electrochemical reduction of carbon dioxide is usually conducted in aqueous or nonaqueous electrolyte solutions at cathodes made of various materials. As a result, various organic substances can form. The most common reactions are as follows:

$$CO_2 + H^+ + 2e^- \rightarrow HCOO^-, \tag{15.67}$$

$$CO_2 + 2H^+ + 2e^- \rightarrow CO + H_2O, \tag{15.68}$$

$$CO_2 + 6H^+ + 6e^- \rightarrow CH_3OH + 2H_2O, \tag{15.69}$$

$$CO_2 + 8H^+ + 8e^- \rightarrow CH_4 + 2H_2O, \tag{15.70}$$

$$2CO_2 + 2e^- \rightarrow (COO^-)_2. \tag{15.71}$$

The standard redox potential E_r^0 for these reactions in solutions at pH 7 (when referred to the potential of the hydrogen electrode in the same solution) varies from -0.218 V for reaction (15.71) to $+0.170$ V (for reaction (15.70) (i.e., to a rough approximation are close to zero).

The reaction products often compromise a mixture of various substances. Moreover, the reduction of carbon dioxide in aqueous solutions in the cathodic potential region is always accompanied by hydrogen evolution. Hence, an important criterion that describes the reaction selectivity is the faradaic yield η_k for each individual kth organic reaction product.

To diminish the influence of the concurrent hydrogen evolution, CO_2 reduction is usually performed under conditions when the rate of hydrogen evolution is small. This can be achieved, for example, in neutral solutions with good buffer properties (pH interval from 5 to 8). Often, 0.1 to 1 *M* $KHCO_3$ solutions with pH about 8 are used. Because of the low solubility of CO_2 in water (0.036 *M* at 20°C) and many nonaqueous solutions, continuous bubbling of CO_2 through the solution is needed.

Faradaic yields and the composition of reaction products are influenced mainly by the nature of the cathode material. Metallic electrodes used in aqueous solutions can be classified into four groups according to the nature of the principal reaction product:

Group I (Hg, Pb, Sn, In, Pd)	$HCOO^-$ is formed
Group II (Au, Ag, Zn)	CO is formed
Group III (Cu, Ru, Mo)	CH_4, C_2H_6, CH_3OH, etc. are formed
Group IV (Pt, Ni, Fe, Al, etc.)	CO_2 does not reduce

This classification is rather arbitrary, since different reaction products may form at the same electrode, depending on the reaction conditions. Nonmetallic substances such as oxides, semiconductors, and organic N_4 complexes are used as electrode materials as well.

The reaction selectivity and faradaic yields are sensitive to the reaction conditions (e.g., the electrode potential, the solution composition, the presence of accidental impurities). This is the reason for discrepancies between the data on the composition of the reaction products reported by various authors.

Faradaic yields often decline during electrolysis and sometimes even drop to zero. This precludes accumulating high concentrations of the reaction products. As a rule, such an effect is caused be the reaction products entering the anodic region of the cell and their oxidation back to CO_2. The process can be inhibited by using appropriate separators. A decline in the faradaic yield may also result from a gradual deactivation (poisening) of the electrode.

From a practical standpoint, formic acid or its salts are the least valuable reaction products. The energy content of formic acid upon its reverse oxidation to CO_2 is insignificant, and its separation from the solutions is a labor-consuming process. At present, maximum effort goes into the search for conditions that would ensure purposeful (with high faradaic yields) synthesis of methanol, hydrocarbons, oxalic acid, and other valuable products.

On mercury electrodes, high faradaic yields (up to 100%) for the formation of formic acid or formate ions can easily be achieved. The reaction proceeds with a significant polarization at potentials E_r ranging from -1.0 to -1.5 V. Electrodes prepared from amalgams of alkali metals behave like the mercury electrode. With amalgams, high cathodic potentials necessary for the CO_2 reduction can be achieved even in the absence of external polarization. In such a case, the cathodic process is balanced by the anodic dissolution of the alkali metal. In reactors with amalgams, no auxiliary anode for polarization of the working electrode is needed and therefore there is no danger of reoxidation of the reaction product. With the use of sodium amalgams, the formation of sodium formate solutions with concentrations up to 340 g/L were reported with reaction rates (calculated by the amount of dissolved sodium) corresponding to current densities up to 115 mA/cm^2. On other group I metals the faradaic yield of formate formation is also high (on lead up to 85%). In some cases on metals of group I, formation of minor quantities of carbon monoxide CO was observed.

The faradaic yield of CO formation on group II metals strongly depends on the value of the electrode potential. On silver and gold at definite potentials, yields up to 90 to 100% can be achieved. On zinc also, high yields (80%) were reported.

Formates and carbon monoxide are products of a shallow reduction of carbon dioxide (two electrons per one CO_2 molecule). In the last few years, much attention has been paid the problem of obtaining products of deeper reduction (e.g., methanol or methane) which may be used as fuels in engines or in fuel cells.

Ruthenium is a known active catalyst for the hydrogenation of carbon monoxide to hydrocarbons (the *Fischer–Tropsch synthesis*). It was shown that on ruthenized electrodes, methane can form in the electroreduction of carbon dioxide as well. At temperatures of 45 to 80°C in acidified solutions of Na_2SO_4 (pH 3 to 4), faradaic yields for methane formation up to 40% were reported. On a molybdenium electrode in a similar solution, a yield of 50% for methanol formation was observed, but the yield dropped sharply during electrolysis, due to progressive poisoning of the electrode.

Of great interest and importance are studies on carbon dioxide reduction on copper electrodes, performed primarily by Japanese scientists. Under certain conditions, formation of methane and ethylene with high faradaic yields (up to 90%) was observed. The efficiency and selectivity of this reaction depends very much on the purity and the state of the surface of the copper electrode. For this reason, many of the published results are contradictory.

In aprotic nonaqueous electrolyte solutions, due to the absence of hydrogen ions and other proton donors, during electroreduction of carbon dioxide the main reaction products turn out to be carbon monoxide and/or oxalate ions $(COO^-)_2$. On metals of group I, oxalate is mainly formed with a yield of 60 to 80%, whereas with group II metals the main reaction product (with a similar high yield) is carbon monoxide. In the presence of appreciable amounts of water acting as proton donor, the composition of the reaction products changes dramatically, and large amounts of formate are formed. In some cases in the presence of traces of water, the formation of more complex organic reaction products [i.e., glyoxylic acid (HCO–COOH), tartaric acid $(CHOHCOOH)_2$, and malic acid (HOOC–CH_2–CHOH–COOH)] was observed.

The mechanism of carbon dioxide reduction in aqueous and nonaqueous solutions was investigated by several authors. It is now generally accepted that the reduction of carbon dioxide to formate ions is a multistep reaction with the intermediate formation of free radicals $CO_2^{\cdot-}$ and $HCO_2^{\cdot}$ either in the solution or adsorbed on the electrode:

$$CO_2 + e^- \rightarrow CO_2^{\cdot-}, \tag{15.72}$$

$$CO_2^{\cdot-} + BH \rightarrow HCO_2^{\cdot} + B^-, \tag{15.73}$$

$$HCO_2^{\cdot} + e^- \rightarrow HCO_2^-, \tag{15.74}$$

where BH is a proton donor, say, water molecule. In the region of more positive potentials, the rate-determining step is the transfer of the second electron, whereas at more negative potentials, the transfer of the first electrode is the limiting step. In aprotic nonaqueous solutions, protonation of the radicals $CO_2^{\cdot-}$ through reaction (15.73) is impossible. Further transformation of these radicals may proceed via two pathways, (1) dimerizations with the immediate formation of oxalate ions:

$$2CO_2^{\cdot-} \rightarrow (COOH^-)_2, \tag{15.75}$$

or (2) interaction with a CO_2 molecule with the formation of another dimeric radical anion $(COO)_2^{\cdot-}$, with the subsequent transfer to it of a second electron:

$$CO_2^{\cdot-} + CO_2 \rightarrow (COO)_2^{\cdot-} \xrightarrow{+e^-} (COO^-)_2. \tag{15.76}$$

The intermediate formation of both types of radicals was shown by spectroscopic methods.

For synthetic fuels or energy-storage media to be produced electrochemically, it is necessary that the carbon dioxide reduction be conducted at potentials only slightly (not more than by 0.2 V) more negative than the corresponding equilibrium potential. To do this requires extensive research aiming at refining the catalysts and the conditions for this process.

Summing up, it can be said that the reaction of the electrochemical reduction of carbon dioxide will be the subject of painstaking research for a long time to come. In the future this reaction is very likely to play an important role in the electrochemical industry.

15.8 REACTION OF NITROGEN REDUCTION

From a fundamental point of view, it would be very interesting to find a way to achieve an electrochemical reduction of another very "inert" compound—the reduction of molecular nitrogen to ammonia—a reaction that is analogous to the well-known large-scale industrial process of ammonia production. Some papers on

this topic can be found in the literature. It seems that under certain conditions (nonaqueous solutions, high nitrogen pressures, use of illuminated semiconductor electrodes, etc.) some appreciable faradaic yields of ammonia can be obtained.

REFERENCES

Bagotsky, V., and I. Yablokova, *Zh. Fiz. Khim*., **27**, 1663 (1953).

Bagotsky, V., Yu. Vassiliev, and O. Khazova, *J. Electroanal. Chem.*, **81**, 229 (1977).

Butler, J. A. V., *Trans. Faraday Soc*., **19**, 729 (1924).

Erdey-Gruz, T., and M. Volmer, *Z. Phys. Chem*., **150A**, S203 (1930).

Förster, F., *Elektrochemie wässriger Lösungen*, Barth, Leipzig, 1905.

Frumkin, A., N. Nikolaeva-Fedorovich, N. Berezina, and Kh. E. Keis, *J. Electroanal. Chem*., **58**, 189 (1975).

Haber, F., *Z. Angew. Chem.*, **13**, 433 (1900).

Heyrovský, J., *Recl. Trav. Chim. Pays-Bas*, **44**, 499 (1925).

Kolbe, H., *Ann. Chem*., **69**, 257 (1849).

Tafel, J., *Z. Phys. Chem*., **50**, 641 (1905).

Vassiliev, Yu., E. Kovsman, and G. Freidlin, *Electrochim. Acta*, **27**, 953 (1982).

MONOGRAPHS AND REVIEWS

Bagotsky, V. S., and N. Osetrova, Electrochemical reduction of carbon dioxide, *Russ. J. Electrochem.*, **31**, 409 (1995).

Iwasita, T., and W. Vielstich, Progress in the study of methanol oxidation by in situ, ex situ and on-line methods, in *Advances in Electrochemical Science and Engineering*, R. Alkire et al., Eds., Vol. 1, Wiley, New York, 1990, p. 127.

Kauranen, P., E. Skou, and J. Munk, Kinetics of methanol oxidation on carbon-supported Pt and Pt + Ru catalysts, *J. Electroanal. Chem.*, **404**, 1 (1996).

Kinoshita, Kim, *Electrochemical Oxygen Technology*, Wiley, New York, 1992.

Léger, J.-M., Mechanistic apects of methanol oxidation on platinum based electrocatalysts, *J. Appl. Electrochem*., **31**, 767 (2001).

Lund, H., and M. M. Baizer, *Organic Electrochemistry: An Introduction and Guide*, Marcel Dekker, New York, 1991.

Parsons, R., and T. Van der Noot, The oxidation of small organic molecules: a survey of recent fuel cell related research, *J. Electroanal. Chem*., **257**, 9 (1988).

Sullivan, B. P., K. Krist, and H. E. Guard, Eds., *Electrochemical and Electrocatalytic Reactions of Carbon Dioxide*, Elsevier, Amsterdam, 1993.

Taniguchi, I., Electrochemical and photoelectrochemical reduction of carbon dioxide, in *Modern Aspects of Electrochemistry*, J. Bockris et al., Eds., Vol. 20, Kluwer, New York, 1989, p. 327.

16
Reactions Involving Metals

16.1 REACTING METAL ELECTRODES

Electrochemical systems with reacting metal electrodes are widely used in batteries, electrometallurgy, electroplating, and other areas. Corrosion of metals is a typical example of processes occurring at reacting metal electrodes.

At most metals that are in contact with an electrolyte containing their own ions, the equilibrium potential of the metal's discharge and ionization reaction,

$$M \rightleftharpoons M^{z+} + ze^- \tag{16.1}$$

or in the case of electrodes of the second kind, that of a reaction of the type

$$M + zA^- \rightleftharpoons MA_z + ze^-, \tag{16.2}$$

is relatively readily established (A^- is an anion; e.g., OH^-, Cl^-, $\frac{1}{2}SO_4^{2-}$).

When the metal is in contact with an electrolyte solution not containing its ions, its equilibrium potential theoretically will be shifted strongly in the negative direction. However, before long a certain number of ions will accumulate close to the metal surface as a result of spontaneous dissolution of the metal. We may assume, provisionally, that the equilibrium potential of such an electrode corresponds to a concentration of ions of this metal of about 10^{-6} *M*. In the case of electrodes of the second kind, the solution is practically always saturated with metal ions, and their potential corresponds to the given anion concentration [an equation of the type (3.35)]. When required, a metal's equilibrium potential can be altered by addition of complexing agents to the solution (see Eq. (3.37)].

Some metals are thermodynamically unstable in aqueous solutions because their equilibrium potential is more negative than the potential of the reversible hydrogen electrode in the same solution. At such electrodes, anodic metal dissolution and cathodic hydrogen evolution can occur as coupled reactions, and their open-circuit potential (OCP) will be more positive than the equilibrium potential (see Section 13.7).

Fundamentals of Electrochemistry, Second Edition, By V. S. Bagotsky

According to their exchange current, densities i^0 (or standard rate constants k^0) and polarization in reactions involving their dissolution or deposition in solutions of simple salts (sulfates, chlorides, etc.), the metals can be provisionally divided into two groups: that of metals with high polarizability (low exchange current density), which includes chromium, manganese and the metals of the iron and platinum group, and that of metals with low polarizability (high exchange current density), which includes the others. In the second group, constants k^0 have values on the order of 10^{-2} to 1 cm/s and exchange current densities i^0 between 100 and 10^4 mA/cm^2. Up to current densities (CDs) of 100 mA/cm^2, these metals exhibit an activation polarization of no more than 20 mV. Metals of the first group have values of k^0 and i^0, which are two to four orders of magnitude lower, and polarization here can attain several tenths of a volt.

The reactions occurring at reacting metal electrodes are associated with structural changes: lattice destruction or formation of the metal and, in certain cases, of other solid reaction components (oxides, salts, etc.). One should know the metal's original bulk and surface structure in order to analyze the influence of these structural changes.

Solid metals obtained upon solidification of the molten metal exhibit grain structure. They consist of fine crystallites randomly oriented in space. The size of the individual crystallites (grains) is between 10^{-7} m (fine-grained structure) and 10^{-3} m (coarse-grained structure). The crystal structure of the individual grains as a rule is not ideal. It contains various types of defects: vacant sites, interstitial atoms or ions, and dislocations (lattice shearing or bending). Microcracks sometimes evolve in the zones between crystallites.

The metal surface is polycrystalline and has a rather complex profile. Because of different crystallite orientations at the surface, different crystal faces are exposed, such as smooth low-index faces and "stepped" high-index faces. Surface texture where a particular kind of face is predominant can develop in individual cases. Microcracks and various lattice defects (dislocations, etc.) will also emerge at the surface.

Thus, the individual atoms (ions) at a metal surface exist under different geometric and hence, energy conditions. Yet the surface particles as a rule retain a certain mobility. Because of their surface diffusion, the original surface structure may change to a more stable state. When the surface is in contact with an electrolyte solution, this process is accelerated, owing to the continued exchange occurring via the solution, such as the dissolution of particles from the most active sites and their redeposition at other sites.

During mechanical working of the metal, both the bulk and surface structures are altered. Cutting, abrading, polishing, and other treatments deform the surface layer and increase the number of defects in it. Under sufficient force a surface "milling" producing an almost amorphous surface layer up to 100 nm thick will occur. Beneath this layer the lattice distortion extends to depths attaining tenths of a millimeter (work hardening of the surface). A crystalline surface state can be restored by careful annealing or electrochemical polishing (Section 16.6).

It would be of great value for studies of different electrochemical phenomena if measurements could be made not at polycrystalline surfaces but at particular

faces of sufficiently large single crystals of a given metal. It is a rather difficult task, unfortunately, to produce "pure" faces and work with them. In contact with solutions, segments or steps of other faces can appear on such a face, owing to the exchange that occurs. Up to now, therefore, reliable data as to the electrochemical properties of individual faces or how they differ from those of polycrystalline surfaces are scarce.

Electrochemical processes involving metals, such as metal ion discharge and metal atom ionization, can be studied without the complications of structural changes when electrodes of the molten metal (at elevated temperatures and in nonaqueous electrolytes) or of the metal's liquid amalgam are used instead of the solid metal.

16.2 ANODIC METAL DISSOLUTION

Various electrochemical reactions are possible during anodic polarization of a metal electrode in aqueous solutions:

1. Anodic dissolution (oxidation) of the metal with the formation of soluble [reaction (16.1)] or insoluble [reaction (16.2)] products
2. The formation of adsorbed and phase oxide or salt layers (films) on the surface
3. The anodic oxidation of solution components (e.g., organic impurities)
4. Anodic oxygen evolution (also anodic chlorine evolution, in solutions containing chlorides)

Each of these reactions occurs in its own typical potential range. Several reactions may occur in parallel. The oxidation of solution components and the evolution of oxygen and chlorine are discussed in Chapter 15, the formation of surface layers in Section 16.3. In the present section we discuss anodic metal dissolution.

The shape of polarization curves for metals with low polarizability depends primarily on concentration polarization. In the case of highly polarizable metals, where activation polarization can be measured sufficiently accurately, the polarization curve can usually be described by an equation of the type (6.3) (i.e., by a Tafel equation). For metals forming polyvalent ions, slope b' in this equation often has values between 30 and 60 mV.

Anodic dissolution reactions of metals typically have rates that depend strongly on solution composition, particularly on the anion type and concentration (Kolotyrkin, 1959). The rates increase upon addition of surface-active anions. It follows that the first step in anodic metal dissolution reactions is that of adsorption of an anion and chemical bond formation with a metal atom. This bonding facilitates subsequent steps in which the metal atom (ion) is torn from the lattice and solvated. The adsorption step may be associated with simultaneous surface migration of the dissolving atom to a more favorable position (e.g., from position 3 to position 1 in Fig. 14.11*a*), where the formation of adsorption and solvation bonds is facilitated.

In iron dissolution in alkaline solutions, the rate is proportional to OH^- ion concentration, to a first approximation. The first step of this reaction is usually described as

$$Fe + OH^- \rightleftharpoons Fe(OH)^-_{ads}. \tag{16.3}$$

This step is followed by steps involving electron transfer and the addition of further hydroxyl ions, which continues until the final reaction products are formed:

$$Fe(OH)^-_{ads} \xrightarrow{-e^-} Fe(OH)_{ads} \underset{-e^-}{\overset{+OH^-}{\longrightarrow}} Fe(OH)_2 \left[\underset{-H_2O}{\overset{+OH^-}{\longrightarrow}} HFeO^-_2 \right]. \tag{16.4}$$

Structural surface inhomogeneity influences the anodic dissolution process in the case of metals with appreciable activation polarization. As a rule, segments with perturbed structure dissolve more rapidly than ordered segments. In a number of cases this causes crystallites to break away from the electrode surface and form metal sludge.

In the case of metals of variable valency forming ions of different charge, peculiar effects are possible. The thermodynamic potential for the reaction $Cu^+ \rightleftharpoons Cu + e^-$ (0.521 V) is more positive than that for the reaction $Cu^{2+} \rightleftharpoons Cu^+ + e^-$ (0.153 V). For this reason the ions Cu^+ formed during anodic polarization in the first of these reactions will at once be furher oxidized to Cu^{2+}. Therefore, ions Cu^+ as the reaction intermediate are thermodynamically unstable at all values of potential. When an aqueous solution is prepared from a salt of univalent copper, the spontaneous disproportionation (dismutation reaction $2Cu^+ \rightarrow Cu + Cu^{2+}$ is possible. When the copper electrode is polarized anodically and the potential is moving in the positive direction, the relative amount of Cu^+ ions formed primarily increases. In the solution, the additional ions will undergo dismutation and yield Cu^{2+} ions as well as fine copper powder which deposits at the bottom of the cell in the form of sludge. Thus, formation of a Cu^{2+} ion via Cu^+ consumes two copper atoms, one of them ending up in the sludge; that is, the current yield of copper dissolution (the relation between copper lost and charge consumed) has doubled.

A similar situation is found for certain metals not forming stable ions of variable valency. In anodic magnesium dissolution, Mg^+ ions are formed first. They do not undergo dismutation like the Cu^+ ions, but as a strong reducing agent react with water according to

$$2Mg^+ + 2H_2O \rightarrow 2Mg^{2+} + H_2 + 2OH^-. \tag{16.5}$$

In this case, one magnesium atom is consumed for the formation of one Mg^{2+} ion, but the current yield of magnesium again has doubled, because every other magnesium atom is spent not for electron generation but for hydrogen evolution.

When the potential of the magnesium electrode is made more positive, the rate of Mg^+ ion formation increases, and with it that of reaction (16.5). Therefore, the rate of hydrogen evolution increases instead of falling off, with increasing anodic polarization of the magnesium (see Section 13.7). This phenomenon has become known as the *negative difference effect.*

The phenomena occurring during the anodic dissolution of binary alloys of metals M and N (where M is the more electronegative metal) depend on the alloy type. In the case of heterogeneous alloys, the two components dissolve independently, each following its own behavior. At potentials intermediate between the equilibrium potentials of the two metals, metal M may dissolve selectively. When its concentration in the alloy is low, a pure surface of metal N may develop after some time. When its concentration is high, however, particles of metal N will lose their connection with the base, shed, and form sludge. In the case of homogeneous alloys, both metals will dissolve at potentials intermediate between the equilibrium potentials of the alloy and of metal N. However, the N^{z+} ions formed can undergo discharge and redeposit, now as the pure metal rather than as an alloy. Usually, metal sludge is also formed under these conditions.

16.3 SURFACE-LAYER FORMATION

In the anodic polarization of metals, surface layers of adsorbed oxygen are almost always formed by reactions of the type of (10.18) occurring in parallel with anodic dissolution, and sometimes, phase layers (films) of the metal's oxides or salts are also formed. Oxygen-containing layers often simply are produced upon contact of the metal with the solution (without anodic polarization) or with air (the air-oxidized surface state).

The first step of oxide-layer formation is oxygen adsorption (chemisorption). In the case of platinum, the process stops at this stage, and depending on the conditions, an incomplete or complete monolayer of adsorbed oxygen is present on the platinum surface. In the case of other metals, layer formation continues. When its thickness δ has attained two to three atomic diameters, the layer is converted to an individual surface phase that is crystalline (more seldom, amorphous) and has properties analogous to those of the corresponding bulk oxides.

The surface-phase layers will differ in character depending on the structures of metal and oxide. On certain metals (zinc, cadmium, magnesium, etc.), loose, highly porous layers are formed which can attain appreciable thicknesses. On other metals (aluminum, bismuth, titanium, etc.), compact layers with low or zero porosity are formed which are no thicker than 1 μm. In a number of cases (e.g., on iron), compact films are formed which have a distorted lattice, owing to the influence of substrate metal structure and of the effect of chemical surface forces. The physicochemical and thermodynamic parameters of such films differ from those of ordinary bulk oxides. Because of the internal stresses in the distorted lattice, such films are stable only when their thickness is insignificant (e.g., up to 3 to 5 nm).

As a rule, different types of oxide film will form simultaneously on metal electrodes: for instance, porous phase layers on top of adsorbed layers. Often, aging processes occur in the oxide layers, which produce time-dependent changes in the properties or even transitions between different forms.

Sufficiently strong cathodic polarization will reduce the oxide layers on many metals, but in certain cases (on titanium, tantalum, etc.) the oxide film cannot be

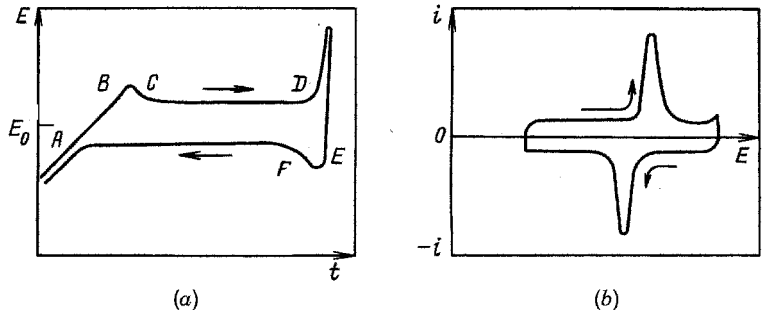

FIGURE 16.1 Charging curves recorded when an adsorbed layer of oxygen adatoms or a phase oxide layer are formed: (*a*) galvanostatic; (*b*) potentiostatic.

removed by electrochemical means. A bare, nonoxidized metal surface can be obtained by thermal reduction under hydrogen or by mechanical stripping of a metal surface layer in a medium (gas or solution) carefully freed of oxygen.

The anodic formation and cathodic reduction of an oxide layer can be studied by recording charging curves when other reactions (anodic metal dissolution or oxygen evolution, cathodic hydrogen evolution) do not occur at the surface. The anodic and cathodic scans of a galvanostatic charging curve are shown schematically in Fig. 16.1*a*. In the initial segment *AB* of the anodic curve, an adsorbed layer of oxygen atoms is formed; this segment is analogous to the oxygen region of the anodic charging curve for platinum (see Fig. 10.9). A phase oxide layer starts to form and grow when a certain potential has been reached. Initially, one usually sees an overshoot of the potential in the positive direction (segment *BC*), which is due to difficulties in the nucleation of the new phase. After that, the potential as a rule remains almost unchanged; owing to polarization, it is somewhat more positive than the equilibrium potential of this phase. At the end of layer growth (point *D*), the potential shifts briskly to a more positive value where another reaction starts (e.g., oxygen evolution). In the cathodic scan, following an initial overshooth of the potential in the negative direction (segment *EF*), the oxide layer is reduced, again at a practically constant value of potential, but this time somewhat more negative than the equilibrium potential. In a potentiodynamic charging curve, narrow high current peaks are recorded in the regions where the oxide layer is formed and reduced (Fig. 16.1*b*).

Charging curves of a different type are recorded at certain metals: Instead of the horizontal sections in the galvanostatic curves, sloping segments arise, the hysteresis between the anodic and cathodic segments is larger, and the current peaks in potentiodynamic curves are more diffuse.

During anodic polarization, oxide layers may form even in solutions where they are soluble, particularly so in acidic solutions. In this case, the layers have a stationary thickness that depends on the equilibrium between the rates of electrochemical

formation and chemical dissolution of the layer. Such layers vanish within a certain time after interruption of the current.

Oxide layers thinner than 0.4 μm are inaccessible to direct observation. Their thickness can be determined ellipsometrically; this method utilizes changes in optical polarization that occur during the reflection of plane-polarized light by the surface. The amount of oxygen contained in the layer can be determined from the length of the horizontal section in the cathodic galvanostatic charging curve. However, all these methods yield only average values, since possible unevenness of the layer is disregarded.

Many types of oxide layers have a certain, not very high electrical conductivity of up to 10^{-6} to 10^{-5} S/cm. Conduction may be cationic (by M^{z+} ions) or anionic (by O^{2-} or OH^- ions), or of the mixed ionic and electronic type. Often, charge transport occurs by a semiconductor hole-type mechanism, hence, oxides with ionic and ionic-hole conduction are distinguished (in the same sense as *p*-type and *n*-type conduction in the case of semiconductors, but here with anions or cations instead of the electrons, and the corresponding ionic vacancies instead of the electron holes). Electronic conduction is found for the oxide layers on iron group metals and on chromium.

The behavior of metal electrodes with an oxidized surface depends on the properties of the oxide layers. Even a relatively small amount of chemisorbed oxygen will drastically alter the EDL structure and influence the adsorption of other substances. During current flow, porous layers will screen a significant fraction of the surface and interfere with reactant transport to and product transport away from the surface. Moreover, the ohmic voltage drop increases, owing to the higher current density in pores. All these factors interfere with the electrochemical reactions, particularly with further increase in layer thickness.

In the case of electrodes with purely ionically conducting layers which are completely or almost completely nonporous, an electrochemical reaction is possible only at the inner surface of the layer (at the metal boundary). When conduction is cationic, an anodic current will cause metal ionization [and a cathodic current will cause metal ion discharge] at this boundary according to Eq. (16.1). Ions M^{z+} will migrate to (enter from) the layer's outer surface (the electrolyte boundary), where the reaction with the solution occurs; for example,

$$2M^{z+} + zH_2O \rightleftharpoons M_2O_{z+} + 2zH^+. \tag{16.6}$$

When conduction is anionic, the O^{2-} ions produced (consumed) at the outer surface in the reaction

$$H_2O \rightleftharpoons (O^{2-})_{\text{lattice}} + 2H^+ \tag{16.7}$$

will migrate to (have migrated out from) the layer's inner surface, where they undergo the electrochemical reaction (have formed in the reaction)

$$2M + zO^{2-} \rightleftharpoons M_2O_z + 2_z e^-. \tag{16.8}$$

The electrochemical overall reaction at the electrode can be written as

$$2M + zH_2O \rightleftharpoons M_2O_z + 2zH^+ + 2ze^- \tag{16.9}$$

[i.e., the layer increases (decreases) in thickness during current flow].

When the layer has electronic in addition to ionic conductivity, the electrochemical reaction will be partly or completely pushed out to its outer surface. In addition, other electrochemical reactions involving the solution components, particularly anodic oxygen evolution, can occur on top of the layer.

In many cases the electrochemical reaction rates at such electrodes are governed by migration of the carriers through the layer. Their migration rates are proportional to the potential gradient, $\Delta\psi/\delta$, inside the layer [i.e., at a given electrode potential (given value of $\Delta\psi$), they are inversely proportional to layer thickness: $i = \text{const}/\delta$]. When other reactions are absent, layer growth is proportional to current density: $d\delta/dt = \text{const}\ i$. Hence, $\delta(d\delta/dt) = \text{const}$, and after integration we have

$$\delta^2 = \text{const}\ t \tag{16.10}$$

(i.e., layer thickness increases with the square root of time during electrochemical oxide formation).

In very thin (nanometer) films, where the potential gradient may exceed 10^8 V/m, another mechanism of ion migration is observed, which involves periodic jumps of ions between equilibrium positions. In this case, the rate of migration is not proportional to the potential gradient but obeys the exponential law

$$i = k \exp\left(\frac{\gamma\Delta\psi}{\delta}\right), \tag{16.11}$$

with the corresponding change in the laws of film growth.

Nonporous layers that are practically nonconducting and completely insulate the electrode surface from the electrolyte solution will form during anodic polarization on certain metals (aluminum, titanium, etc.). Even when a high external voltage (e.g., 100 V) is applied, no anodic current will pass through the electrode. Such layers are employed in the production of electrolyte capacitors which are distinguished by high values of capacitance, since the layers are so thin.

In individual cases, anodic polarization of metals in electrolyte solutions will produce surface layers (adsorbed or phase) which instead of oxygen, contain the solution anions. Thus, anodic polarization of silver in chloride-containing solutions yields a surface layer of silver chloride, while the anodic polarization of lead in sulfuric acid solution yields a lead sulfate layer. Layers of sulfides, phosphates, and other salts can be formed in the same way. In many respects the properties of such salt layers are analogous to those of the oxide layers.

Oxide and salt layers on metal electrodes are of great practical value. Electrodes with thick phase layers are used in batteries, and various types of thin layers will produce passivation of metals.

16.4 PASSIVATION OF ELECTRODES

Passivation of an electrode with respect to a certain electrochemical reaction is the term used for the strong hindrance experienced under certain conditions by a reaction which under other conditions (in the electrode's active state) will occur without hindrance at this electrode. *Passivation of metals* implies the hindrance frequently observed with respect to anodic metal dissolution.

16.4.1 Passivation of Metals

Passivation of metals is very important in applied electrochemistry. It sharply retards the spontaneous dissolution of a number of metals when these are in contact with electrolyte solutions (i.e., raises their corrosion resistance). The passivation of metal anodes also interferes with the normal function of batteries and electrolyzers. Passivation of metals is displayed most distinctly when during anodic polarization the potential is gradually made more positive. Figure 16.2*a* shows a typical anodic polarization curve recorded potentiodynamically with a slow linear potential scan. Segment *AB* corresponds to the region of ordinary anodic dissolution of nonpassivated (active) metal; the rate of the anodic reaction increases as the potential is made more positive. In segment *BC*, when potential E_{pass} and a certain critical current density i_{cr} have been reached, the reaction rate will decrease drastically to a new value, i_{pass}, when the potential is made more positive. Thus, for iron in 0.5 *M* H_2SO_4 solution at 25°C, the value of i_{cr} is about 250 mA/cm^2, whereas that of i_{pass} is about 0.007 mA/cm^2 (i.e., the current has decreased by four to five orders of magnitude). The value of i_{pass} remains almost constant within the wide range of potentials of section *CD*, which is the region of passivity of the metal. It is only when the potential is made much more positive (point *D*) that the current rises again, which is due to renewed acceleration of anodic metal dissolution or (and) to the start of oxygen evolution. In the former case, region *DE* is called the *region of transpassivation of the metal*; usually, metal oxidation products of higher valency than in the active dissolution region *AB* are formed here.

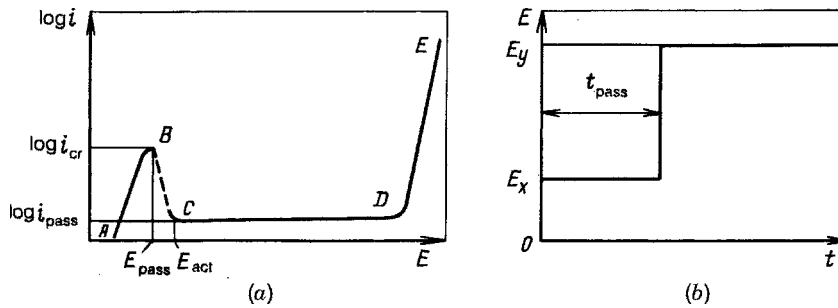

FIGURE 16.2 (*a*) Potentiodynamic log *i* vs. *E* curve; (*b*) galvanostatic *E vs. t* curve for anodic metal dissolution and passivation.

When the polarization curve is recorded in the opposite (cathodic) direction, the electrode will regain its active state at a certain potential E_{act}. The activation potential E_{act} is sometimes called the *Flade potential* (Flade, 1911). The potentials of activation and passivation as a rule are slightly different.

The limits of transition region *BC* are not very distinct and depend on the experimental conditions. At high potential scan rates (short duration of the experiment), passivation will start later (i.e., potential E_{pass} will be somewhat more positive, and for a short time the currents may be higher than i_{cr}).

Passivation looks different when observed under galvanostatic conditions (Fig. 16.2*b*). The passive state will be attained after a certain time t_{pass} when an anodic current i_x which is higher than i_{cr} is applied to an active electrode. As the current is fixed by external conditions, the electrode potential at this point undergoes a discontinuous change from E_x to E_y, where transpassive dissolution of the metal or oxygen evolution starts. The passivation time t_{pass} will be shorter the higher the value of i_x. Often, these parameters are interrelated as

$$(i_x - i_{cr})t_{pass}^{1/n} = \text{const}, \tag{16.12}$$

where constant n has values between 1 and 2.

Under the effect of oxidizing agents, a metal may become passivated even when not anodically polarized by an external power source. In this case, passivation is evident from the drastic decrease in the rate of spontaneous dissolution of the metal in the solution. The best known example is that of iron passivation in concentrated nitric acid, which had been described by M. V. Lomonosov as early as 1750. Passivation of the metal comes about under the effect of the oxidizing agent's positive redox potential.

For a number of metals the oxidizing action of air oxygen is sufficient to produce the passive state. In their air-oxidized state, metals such as tantalum, titanium, and chromium are very stable in aqueous solutions.

The character of the passivation phenomena that can be observed at a given metal strongly depends on the composition of the electrolyte solution, particularly on solution pH and the anions present. The passivating tendency as a rule increases with increasing pH, but sometimes it decreases again in concentrated alkali solutions. A number of anions, particularly the halide ions Cl^- and Br^-, are strong activators.

In the process of passivation, metals usually are found only in one of the two extreme states, active or passive. The transition between these states occurs suddenly and discontinuously. The intermediate state in region *BC* can only be realized with special experimental precautions. It is in this sense that passivation differs from the inhibition of electrochemical reactions observed during adsorption of a number of surface-active substances, where the degree of inhibition varies smoothly with the concentration of added material.

Practically all metals can be passivated. Even lithium, which is a highly active alkali metal, can be passivated in concentrated LiOH solution; this is the reason for its greatly reduced rate of reaction with water.

16.4.2 Various Types of Electrode Passivation

When metals become passivated their anodic dissolution rates are reduced, but the rates of other reactions will not necessarily be different. For instance, a platinum electrode is completely passivated with respect to its own anodic dissolution, but many electrochemical reactions involving dissolved and gaseous substances occur at it with great ease and speed over a wide range of potentials. Under certain conditions, though, other reactions also become passivated at this electrode. For instance, the ionization of molecular hydrogen [reaction (1.32) from right to left] is very fast at potentials of up to 0.2 to 0.3 V vs. RHE, but at more positive potentials this reaction begins to be hindered, and around 1.0 V its rate is greatly reduced (Fig. 16.3).

In the middle of the nineteenth century, Grenet primary batteries were very popular. In these batteries a negative zinc electrode was in contact with the acidic solution of a strong oxidizing agent such as a mixture of sulfuric and chromic acid. Here, the zinc is relatively stable; its rate of reaction with the solution is low. However, under anodic polarization, zinc dissolution proceeds in the normal way, without any important hindrance. Here we have an example where the zinc electrode is passivated not with respect to anodic metal dissolution but with respect to the cathodic reactions coupled with it: the reduction of chromic acid and the evolution of hydrogen at zinc. For this reason the current of spontaneous zinc dissolution is low. Since the exchange CD of the former reaction is much higher than that of the other two reactions, the electrode's OCP will practically coincide with the equilibrium potential of zinc discharge and ionization. A similar situation is found in primary batteries with lithium electrodes that have been developed recently, where the lithium electrode is in contact with an electrolyte prepared with thionyl chloride $SOCl_2$, another strong oxidizing agent (see Section 19.6.4).

Peculiar effects are seen during the passivation of magnesium and aluminum in aqueous solutions. In acidic solutions, vigorous spontaneous dissolution is observed for magnesium, while in alkaline solutions a compact oxide layer that passivates it completely is formed on its surface. In neutral and weakly alkaline solutions (roughly between pH 6 and 11), a "semipassive" state is attained in which hydrogen evolution, and thus spontaneous magnesium corrosion, is strongly hindered, whereas anodic magnesium dissolution is less difficult. As a result of such passivation, the steady-state

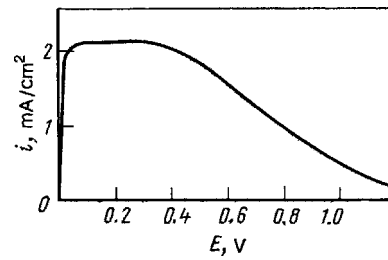

FIGURE 16.3 Polarization curve for the ionization of molecular hydrogen at a rotating platinum electrode ($f = 16\ s^{-1}$) in 0.5 M H_2SO_4 solution.

OCP of magnesium is 0.6 to 1.1 V more positive than the thermodynamic value. The negative difference effect that is seen in anodic magnesium dissolution (see Section 16.2) can, in part, be attributed to partial mechanical disintegration of the passivating layer during magnesium dissolution.

The behavior of aluminum in neutral and weakly alkaline solutions resembles the behavior of magnesium, but the negative difference effect is much less pronounced at aluminum. The steady-state potential of aluminum is approximately 1 V more positive than the thermodynamic value. Yet unlike magnesium, aluminum will not passivate in strongly alkaline solutions, but undergoes fast dissolution to soluble aluminates.

16.4.3 Origins and Mechanisms of Passivation

The suggestion that the passive state of metals is due to oxide layers present on their surface had been put forward as early as 1836 by M. Faraday. In some form or other, this concept has survived up to the present. The passive state is in fact brought about by factors (anodic polarization, the action of oxidizing agents) that promote the formation of a variety of layers on the surface. Often, passivation of metals has been attributed to a mechanical blocking of part of the surface by a chemically inert insulating layer. This mechanism is readily explained with the example of passivation of a lead electrode in sulfuric acid solution under galvanostatic anodic polarization (the process that occurs at the negative electrode of lead–acid batteries during discharge). A rather compact, porous layer of lead sulfate is formed on the electrode surface by the reaction

$$\mathrm{Pb} + \mathrm{HSO_4^-} \rightleftharpoons \mathrm{PbSO_4} + \mathrm{H^+} + 2e^- . \tag{16.13}$$

After an initial overshoot, a constant potential E_1 is attained at the electrode (Fig. 16.4); this is governed by the kinetics of lead sulfate crystallization. After some time, the potential begins to shift in the positive direction, slowly at first but then rapidly. This

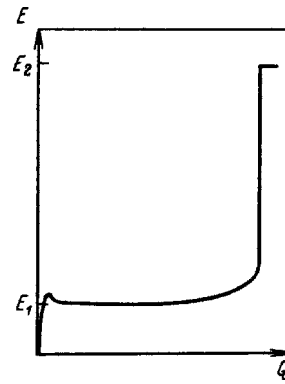

FIGURE 16.4 Galvanostatic E vs. i curve for the anodic polarization of lead in 5 M H_2SO_4.

shift is due to the increase in true current density occurring in the pores of the layer when the total pore cross section decreases in the growing layer. The result is an increase in polarization of the electrode; the ohmic potential drop also increases in the pores. When galvanostatic polarization is continued, the potential moves to a value E_2, where a new electrochemical reaction, the formation of lead dioxide, $PbSO_4$, begins. The oxidation of lead to lead sulfate ceases completely, even though an abundant supply of metallic lead remains. Passivation starts when the thickness of the lead sulfate layer is about 1 μm.

In corrosion studies of iron, the passivation of iron in acidic, neutral, and alkaline solutions has been a topic of great interest. On passive iron one always finds a thin oxide film (3 to 5 nm) which in its structure and properties differs from known iron oxides (see Section 16.3). This film is nonporous and isolates the metal surface from the solution. It has marked electronic conductivity; during anodic polarization film growth continues because of the migration of iron ions and electrons in the film. However, in acidic solutions the film dissolves continuously from outside with a certain constant rate. A stationary situation is attained in which the rate of anodic oxidation of the passive metal, i_{pass} (the rate of film growth), is equal to the rate of film dissolution. The slight potential dependence of i_{pass}, or constant rate of migration of the ions in the film, implies that the potential gradient $\Delta\psi/\delta$ in the film is practically constant. It follows that film thickness δ should increase when the potential is made more positive ($\Delta\psi$ increases). The rate of film dissolution at constant potential decreases with increasing solution pH; there is a corresponding decrease in the value of i_{pass} and an increase in steady-state film thickness. All these conclusions concerning film thickness are confirmed by the results of measurements.

In the concepts described, passivation is attributed to the formation of phase layers that mechanically screen the electrode surface and isolate it from the solution, but the changes in surface properties of the metal have been disregarded. Boris V. Ershler showed in 1942 that the passivation of metallic platinum in hydrochloric acid solutions was due to minute amounts of adsorbed oxygen atoms present on the platinum surface. At a given potential, the rate of anodic platinum dissolution decreases with increasing oxygen coverage, θ_O, of the electrode surface according to an exponential law:

$$i = k \exp(-\gamma\theta_O). \tag{16.14}$$

The coefficient γ has a high value, of about 12. This implies that an increase in θ_O by 0.06 (i.e., an increase in the number of sites taken up by oxygen, which amounts to 6% of the total number of sites) produces a 50% drop in reaction rate.

When an adsorbed oxygen layer appears on the surface of platinum, an important restructuring of the electric double layer occurs; the metal's surface potential $\chi^{(Pt)}$ increases, owing to the polar character of the Pt–O bonds, and the interfacial potential Φ and potential ψ_0 of the ionic EDL part decrease accordingly. The rate of anodic metal dissolution depends precisely on potential ψ_0 and hence is strongly reduced by the EDL rearrangement caused by adsorption. Therefore, in the case of platinum the passivating effect of the adsorbed oxygen layer is due not to a protective

mechanical action but to more subtle effects: the redistributions of charges and potential drops in the surface layer.

Similar effects may exist at other metals. For instance, when the surface of an iron electrode is thermally reduced in hydrogen and then anodically polarized at a current density of 0.01 mA/cm^2 in 0.1 *M* NaOH solution, passivation sets in after 1 to 2 min (i.e., after a charge flow of about 100 mC/cm^2). This amount of charge is much smaller than that required for formation of even a thin phase film. Since prior to the experiment, oxygen had been stripped from the surface, passivation can only be due to the adsorbed layer formed as a result of polarization.

Passivation phenomena on the whole are highly multifarious and complex. One must distinguish between the primal onset of the passive state and the secondary phenomena that arise when passivation has already occurred (i.e., as a result of passivation). It has been demonstrated for many systems by now that passivation is caused by adsorbed layers, and that the phase layers are formed when passivation has already been initiated. In other cases, passivation may be produced by the formation of thin phase layers on the electrode surface. Relatively thick porous layers can form both before and after the start of passivation. Their effects, as a rule, amount to an increase in true current density and to higher concentration gradients in the solution layer next to the electrode. Therefore, they do not themselves passivate the electrode but are conducive to the onset of a passive state having different origins.

16.5 CATHODIC METAL DEPOSITION

Cathodic deposition (electrocrystallization) of metals is the basic process in electrometallurgy and electroplating.

Two types of metal deposition are distinguished: that on the same metal and that on a substrate (matrix) consisting of another metal. In the latter case a number of special features can arise.

Underpotential Deposition of Metal Atoms Because of the energy of interaction between a foreign substrate and the adsorbed metal atoms formed by discharge, cathodic discharge of a limited amount of metal ions producing adatoms is possible at potentials more positive than the equilibrium potential of the particular system, and also more positive than the potential of steady metal deposition.

Incorporation of Metal In certain cases, metal atoms, after their discharge, can penetrate into the substrate metal, forming alloys or intermetallic compounds in the surface layer and down to a certain depth. This effect has been known for a long time in the discharge of metals at liquid mercury, where liquid or solid amalgams are formed. In 1968 B. Kabanov showed that an analogous effect is present in metal ion discharge at many solid metals.

Epitaxy In many cases, the structure of the deposit will duplicate that of the substrate when the crystallographic parameters of the metal being deposited are not

overly different from those of the substrate metal (not by more than 15%). The influence of substrate structure can extend to several thousand atomic layers of the metal being deposited (which is equivalent to a deposit thickness of up to 1 μm). Epitaxy is pronounced in deposits of copper, silver, and zinc.

An important problem in metal deposition is the quality of adhesion of the deposit to the substrate (both foreign and native). In electroplating, one of the major requirements is high strength and reliability of adhesion. In electrohydrometallurgy and electroforming, metals are often deposited on a foreign matrix, and then separated from it; here, to the contrary, poor adhesion is required. The quality of adhesion—apart from other possible factors—depends on the structure and cleanliness of the substrate surface. Hence, prior to the start of deposition the substrate is carefully conditioned both by mechanical (grinding, polishing) and chemical (etching, degreasing) means.

After formation of a primary deposit layer on foreign substrates, further layer growth will follow the laws of metal deposition on the metal itself. But when the current is interrupted even briefly, the surface of the metal already deposited will become passivated, and when the current is turned back on, difficulties will again arise in the formation of first nuclei, exactly as at the start of deposition on a foreign substrate (see Section 14.5.3). This passivation is caused by the adsorption of organic additives or contaminants from the solution. Careful prepurification of the solution can prolong the delay with which this passivation will develop.

16.5.1 Polarization in Metal Deposition

In the steady state, polarization in the case of poorly polarizable metals arises primarily from limitations in the rate of reactant supply (concentration polarization) and from phenomena associated with crystallite growth. In the case of highly polarizable metals, an appreciable activation polarization that is associated with the step of metal ion discharge is found, and the contribution due to growth of the new phase is slight against this background. Experience shows that for such metals the values of polarization in electrocrystallization are similar to those in metal ion discharge at the mercury electrode (where a new phase is not formed).

Polarization in metal deposition is highly sensitive to solution composition. When present in the solution, a number of complexing agents and surfactants will strongly enhance it. In electroplating, it is very common that metals are deposited from solutions of their complex salts (e.g., cyanide complexes). In such solutions, the metal exists in the form of different complex anions, of the type $\mathrm{MCN})_k^{(k-z_+)}$ with different values of k, which are in mutual equilibrium. The surface concentration of the anions will be lower than the bulk solution concentration, since cathodic metal deposition most often occurs at potentials where the surface charge and the ψ'-potential have negative values. This effect is more pronounced the higher the anion's charge. One can assume, therefore, that only species having a low negative charge $(k - z_+)Q^0$ will be discharged, even when their relative concentration is low.

The strong polarization observed in the discharge of these ions can have a number of reasons: a slow chemical step replenishing the supply of reacting species by

the dissociation of complexes with higher values of k, slow ligand desorption from the surface after discharge of the ions, and so on. Sometimes a drop in current is observed after crossing of the PZC; this is an effect of electrostatic repulsion of the anions from the negatively charged surface (see Section 14.5).

The influence of surfactants on polarization can also have a number of reasons: their effect on EDL structure (change in ψ'-potential) when an adsorbed oxygen layer appears on the surface of platinum or the formation of layers fairly strongly adsorbed on the electrode and hindering passage of the reacting species.

In almost all cases, typical peak values of enhanced polarization due to nucleation of the new phase are seen at the initial stage of the process.

16.5.2 Parallel Reactions

For many metal–solution systems, the equilibrium electrode potential is more negative than the equilibrium potential of the reversible hydrogen electrode in the same solution. However, even if it is not, polarization during cathodic metal deposition may push the electrode potential to a value more negative than that of the RHE. Then cathodic hydrogen evolution will occur in parallel with metal ion discharge (as long as the polarization of hydrogen evolution at the metal is not very high). A typical example is the cathodic deposition of zinc from acidic zinc sulfate solution, which is attended by copious hydrogen evolution. Under these conditions the current yields of metal deposition depend on many factors: the current density, solution composition, and so on.

Parallel hydrogen evolution can have two effects.

1. In contrast to metal ion discharge, hydrogen evolution according to reaction (15.4) causes a pH increase of the solution layer next to the cathode. At a certain value of pH in this layer, hydroxides or basic salts of the metal start to precipitate, which affects the mechanism of further metal deposition and also the structure and properties of the deposit produced.
2. In simultaneous hydrogen ion discharge, the resulting adsorbed hydrogen atoms are incorporated into the growing metal deposit. This alters the mechanical properties of the metal; hydrogen embrittlement occurs. This effect is pronounced in the iron group metals, but is less distinct in copper and zinc. It is not observed in cadmium or lead deposition.

When ions of different metals, M^{z+} and N^{z+}, are present together in the solution, simultaneous discharge of the ions and alloy formation between the two metals is possible. To this end the electrode potential must be more negative than that of the more electronegative metal, M. When the concentration of ions N^{z+} of the more electropositive metal is low, the electrode potential will shift to the said value as a result of concentration polarization. However, when the concentration of these ions is high, the equilibrium potentials of the two metals are highly different, and metal N is poorly polarizable, discharge of the more electronegative ions will be hindered. In this case the equilibrium potentials of the two metals can be moved closer together

by suitably selected complexing agents. The electrolytic formation of metallic alloys is practiced in a number of technical fields.

The refining (purification) of metals rests on the separate dissolution and cathodic redeposition of different metals. In the anodic dissolution of the original metal sample, other more electronegative metals present as impurities dissolve together with the base metal. More electropositive impurity metals will not dissolve, but sediment as a sludge that can then be separated from the solution. During the ensuing cathodic deposition of base metal from the solution obtained, the electronegative impurity metals will not deposit at the potential selected but remain in solution. In this way a rather complete separation of the base metal from other metals, both more electropositive and more electronegative, is attained. Highly pure metals can be obtained by prior fractional metal deposition at mercury and subsequent fractional redissolution from of the resulting amalgam.

16.5.3 Structure of the Metal Deposits

In cathodic metal deposition as practiced in electrohydrometallurgy and electroplating, the main effort is toward producing compact deposits having low porosity. In other requirements that should be met by the deposits, these two areas of electrochemical technology are different. It is the principal task of electrohydrometallurgy to produce metal of a certain purity. However, in electroplating, mechanical strength, hardness, freedom from internal stresses, and certain optical properties of the films are required. Hence, in electroplating a large research effort is made to learn about the different factors influencing the structure of metallic coatings.

The structure of metallic deposits is determined primarily by the size, shape (faceting), type of arrangement, and mutual orientation of the crystallites. Two factors may influence the orientation and spatial alignment of the microcrystals in electrocrystallization: the field direction (or direction of the electric current) and the nature of the substrate. The deposits are said to have *texture* when the crystallites are highly oriented in certain directions. Epitaxy implies that the lattice is altered under the influence of the substrate.

Different ways of the structural classification of deposits exist. In one system, the following structures are distinguished arbitrarily: (1) fine-crystalline deposits lacking orientation, (2) coarse-crystalline deposits poorly oriented, (3) compact textured deposits oriented in field direction (prismatic deposits), and (4) isolated crystals with a predominant orientation in the field direction (friable deposits, dendrites). The structure of metal deposits depends on a large number of factors: solution composition, the impurities present in the solution, the current density, surface pretreatment, and so on.

A very general rule can be formulated: In metal deposition, higher activation polarization will favor the formation of fine-crystalline, compact deposits. Friable, coarse-crystalline deposits are formed in the deposition of poorly polarizable metals in solutions of simple salts, but relatively compact, fine-crystalline deposits are formed in the deposition of metals having high polarizability. A strong increase in polarization, and hence the formation of fine-crystalline deposits, will result when

various complexing agents or surfactants are added to salt solutions of poorly polarizable metals.

This situation is rather easy to explain. If the primary step of metal ion discharge is hindered, the appreciable electrode polarization associated with it will compensate for the energetic difficulties of formation of new metal nuclei and lead to the formation of more nuclei. Here, the overall charge is distributed over a large number of nuclei, and any individual nucleus will not undergo much further growth.

The formation of new nuclei and of a fine-crystalline deposit will also be promoted when a high concentration of the metal ions undergoing discharge is maintained in the solution layer next to the electrode. Therefore, concentration polarization will have effects opposite those of activation polarization. Rather highly concentrated electrolyte solutions, vigorous stirring, and other means are employed to reduce concentration polarization. Sometimes, special electrolysis modes are employed for the same purposes: currents that are intermittent, reversed (i.e., with periodic inverted, anodic pulses), or asymmetric (an ac component superimposed on the dc).

Higher current densities and the associated increase in polarization also favor the formation of compact, fine-crystalline deposits. At very high CD approaching the limiting diffusion current, the opposite effect is often seen: Owing to depletion of reacting ions in the solution layer next to the electrode, nonuniform crystal growth starts (i.e., an enhanced growth of projecting points of the deposit in the direction of the incoming flux of ions to be discharged). Then friable, spongy deposits, sometimes even distinct dendrites (branched or acicular treelike crystals), are formed. Electrolysis at currents close to the limiting CD is often used to produce metal powder, which spontaneously separates from the substrate. At high CD the coating quality may also deteriorate because of simultaneous hydrogen evolution and because of the metal hydroxides and basic salts that are formed under these conditions, owing to the attendant increase in solution pH.

Surfactants have very diverse effects on electrolytic metal deposition. Most often they raise the polarization of the electrode drastically, and hence cause formation of fine-crystalline deposits. The surfactant effects depend strongly on the relative rates of new surface formation and adsorption of the surfactant on this surface, since in electrochemical deposition new sections of metal surface form and grow continuously. There are cases when the surfactants will adsorb on slowly growing faces (e.g., the lateral face of whiskers) but do not manage to become adsorbed on the rapidly growing front face (tip). This leads to an enhanced growth of dendritic crystals. In other cases, to the contrary, surfactants contribute to leveling of the surface profile and to the elimination of macroscopic roughness on the surface (brighteners).

It follows from the above that electrolyte solutions having a complex composition must be used to obtain high-quality metal coatings. As a rule, these solutions contain the following components: (1) salt of the metal being deposited, (2) a complexing agent, (3) base electrolyte (neutral salt, to increase the conductivity), (4) buffer agents to help to maintain the optimum value of solution pH, (5) additives to reduce anode passivation, (6) surfactants, and others.

16.6 ELECTROCHEMICAL METAL TREATMENTS

Different electrochemical surface treatments have found extensive use for the purposes of providing metal parts with particular properties, appearance, and shape. This includes the application of superficial oxide or salt films (see Section 16.3), metal films (Section 16.5), and a number of methods that exploit the selective anodic dissolution of different segments of the metal surface. We examine briefly a few examples of the latter type.

Electrolytic etching (pickling) of metals (primarily, ferrous) is used to rid the surface of the relatively thick oxide layers (scale, rust, etc.) prior to the application of various coatings. The treatment time is shorter, and fewer chemicals are needed than in chemical etching. Etching can be anodic or cathodic. In anodic etching the dissolving metal and the evolving oxygen bubbles lift the oxides from the surface mechanically. The reaction is fast; hence, there is a danger of excessive etching. Cathodic etching is based on a partial electrochemical reduction of the oxides and on their mechanical removal from the surface by hydrogen bubbles. It is usually attended by hydrogenation of the metal. In both cases, electrolytes on the basis of sulfuric (more rarely, hydrochloric) acid are used; the current densities are between 50 and 500 mA/cm^2, the anodic etching times are between 1 and 5 min, and the cathodic etching times are between 10 and 15 min. Etching of parts having complex profiles will be nonuniform, owing to the low throwing power of the bath.

Electrochemical polishing (electropolishing) of metals is used to level and smoothen microroughness (of up to 1 μm) on metal surfaces so that these will become mirrorsmooth and more corrosion resistant, and exhibit less friction. This process will not affect the macroscopic surface roughness; hence, sometimes a prior mechanical surface conditioning is required. Electropolishing is based on the selective anodic dissolution of raised points. Unlike mechanical polishing, it will not produce any deformation of the metal's surface layer. Moreover, it is far less laborious and can be used for parts complex in shape. Electropolishing is used, for example, for the surface treatment of various steels, aluminum and silver, and nickel and copper coatings.

Electropolishing is performed in concentrated mixtures of acids (sulfuric, phosphoric, chromic, etc.). Often, organic acids and glycerol are added. It is somewhat inconvenient that almost all metals and alloys require their own solution composition. For electropolishing, intermediate and high current densities are used, between about 0.1 and 500 mA/cm^2. Depending on current density, the process requires between 30 s and 20 to 30 min. Usually, a metal layer 2 to 5 μm thick is removed under these conditions.

Different views exist as to the reasons for selective dissolution of the asperities. According to older concepts, convection of the liquid is hindered in the solution layers filling recesses; hence, reaction products will accumulate there and raise the concentration and viscosity in these layers. Both factors tend to lower a metal's anodic dissolution rate relative to that at raised points. According to other concepts, a surface condition close to passive arises during electropolishing. In this case, the conditions for passivation of the metal at raised points differ from those in recesses.

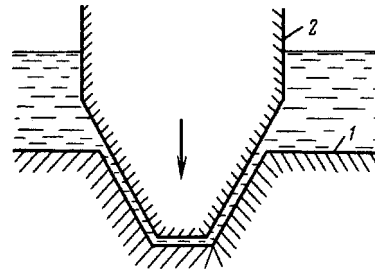

FIGURE 16.5 Electrochemical machining of metals: (1) workpiece (anode); (2) tool (cathode).

Formation of a continuous passivating layer is difficult at raised points; the degree of passivation is lower, and dissolution will be faster. The overall phenomenon of electrochemical polishing is highly complex, and a variety of factors contribute to the effect of surface leveling.

The electrochemical machining (ECM) *of metals* rests on the selective local anodic dissolution of metal. It is used to give metal parts the required shape and size, to drill holes, create hollows, cut shaped slots, and fashion parts of a complex pattern (e.g., the blades of gas turbines). It is an advantage of this method that it can also be used for hard metals (high-alloy steels and other alloys, metals in the quenched state, etc.).

Selective local dissolution of metals is attained under conditions set up so that a system's throwing power is very low. In particular, very small distances (0.05 to 0.2 mm) are maintained between the cathode and the anode section to be removed. The cathode's configuration is the reverse (negative) of a part's desired shape (Fig. 16.5). The projecting part of the cathode (tool) is brought to a working distance from the workpiece. As anode sections are machined away, the cathode is advanced continuously in the direction of the anode so that the original distance is maintained; thus, continuously new sections of the anode surface are engaged in the process.

Electrochemical machining is performed in concentrated solutions of salts: alkali chlorides, sulfates, or nitrates. Very high current densities are used: hundreds or thousands of kA/m^2 when referring to the surface area of the anodic working sections. At a current density of 10^4 mA/cm^2, the rate of iron dissolution is about 0.15 mm/min. This should also be the rate of advance of the cathode in the direction of the anode. High rates of solution flow through the working gap are used to eliminate the reaction products and heat evolved (e.g., flow rates of 10^4 cm/s).

The ECM accuracy depends on the extent to which that current flow spreads beyond the sections being machined can be avoided. To reduce this spread, conditions are selected under which neighboring sections not to be machined are passivated. Under optimum conditions, parts can be machined to tolerances of 0.1 mm.

REFERENCES

Ershler, B., *Dokl. Akad. Nauk USSR*, **37**, 258, 262 (1942).

Faraday, M., *Philos. Mag.*, **IX**, 53 (1836).

Flade, F., *Z. Fig. Khim.*, **76**, 513 (1911).

Kabanov, B., *Electrochim. Acta*, **13**, 19 (1968).

Kolotyrkin, Ya., *Dokl. Akad. Nauk SSSR*, **29**, 295 (1955); *Proc. 9th Meeting CITCE*, Paris, 1957, London, 1959, p. 406.

Lomonosov, M., dissertation (1750); cited from *Collected Works* [in Russian], Academy of Sciences, Moscow, 1950, Vol. 1, p. 349.

MONOGRAPHS

Budevski, E., G. Staikov, and W. J. Lorenz, *Electrochemical Phase Formation and Growth*, Wiley-VCH, Chichester, West Sussex, England.

Paunovic, M., and M. Schlesinger, *Fundamentals of Electrochemical Deposition*, Wiley, New York, 1991.

PART III
Applied Aspects of Electrochemistry

17
Industrial Electrolytic Processes

At all stages of the development of electrochemistry, an intimate connection existed between the development of theoretical concepts and the discovery of solutions for a practical application of electrochemical processes and phenomena. Theoretical investigations have been stimulated by the practical use of various electrochemical phenomena and processes, and the theoretical concepts that were developed have in turn contributed significantly to the development of applied electrochemistry.

Today, applied electrochemistry is of great value for the economy. Electrolytic processes are used to manufacture a number of valuable materials. Electrochemical power sources (batteries) are used widely in many technical fields. Almost each large plant has its own metal plating workshop. Various electrochemical and other methods are used to protect metals against corrosion, an electrochemical phenomenon causing huge economic losses. It will suffice to mention that the world's electrochemical industries (e.g., chlor-alkaline electrolysis, aluminum electrolysis) consume about 10% of all electrical energy generated today.

The various aspects of applied electrochemistry have been discussed in detail in numerous textbooks and monographs, both general and specialized. In the present chapter we provide only a brief outline characterizing the main areas of industrial electrolytic processes together with their economic and scientific value.

17.1 CHLOR–ALKALI ELECTROLYSIS

Among electrolytic processes used to produce materials, we customarily distinguish those in which electrodes are reacting: that is, where the metal or other electrode material is involved in the reaction (Chapter 16) from those with nonconsumable electrodes (Chapter 15). A very important industrial process with nonconsumable electrodes is the electrolysis of sodium chloride solution (brine) producing chlorine at the anode and sodium hydroxide NaOH (caustic soda) in the catholyte via the overall reaction

$$2Cl^- + 2H_2O \rightarrow Cl_2 + H_2 + 2OH^-. \qquad (17.1)$$

Fundamentals of Electrochemistry, Second Edition, By V. S. Bagotsky

The third reaction product, hydrogen, is usually not utilized in chlor–alkali electrolysis. Current annual world production of chlorine by electrolysis is over 30 that of alkali is 35 megatons, and it increases by 2 to 3% per year. This industry consumes about 100 billion kilowatthours of electrical energy per year.

Three processes exist for chlor–alkali electrolysis: (1) the mercury-cell process, (2) the diaphragm-cell process, and (3) the membrane-cell process. The first two were developed in the 1880s, the third in the 1960s. They have in common that chlorine is evolved at the anode electrolytically by discharge of chloride ions. In the mercury-cell process, a mercury cathode is used at which, owing to the strong polarization of hydrogen evolution, sodium ions are discharged and sodium amalgam is formed. When the amalgam has attained a certain concentration, it is pumped to another cell and decomposed with water:

$$2\mathrm{Na(Hg)} + 2\mathrm{H_2O} \rightarrow 2\mathrm{NaOH} + \mathrm{H_2} + \mathrm{(Hg)}. \qquad (17.2)$$

This yields a solution of highly pure alkali (free of chloride ions), which can be used in the manufacture of synthetic fibers. The mercury, which has been stripped of sodium, is returned to the electrolyzer. The cost of chlorine is higher in the mercury-cell than in the diaphragm-cell process. In addition, the mercury-cell process is ecologically dangerous, owing to the possible escape of mercury into the environment; hence, it has increasingly been discontinued in all countries.

In the diaphragm-cell process, a solid cathode (iron) is used where hydrogen is evolved [reaction (15.4)]. Porous asbestos diaphragms are used to prevent mixing of the catholyte and anolyte, but owing to the finite permeability of these diaphragms, the alkaline solution that is produced near the cathode still contains important levels of chloride ions as an impurity.

In the membrane-cell process, highly selective ion-exchange membranes of Du Pont's Nafion type are used which allow only the sodium ions to pass. Thus, in the anode compartment an alkali solution of high purity is produced. The introduction of Nafion-type membranes in chlor–alkali electrolyzers led to a significant improvement in their efficiency. Today, most new chlor–alkali installations use the membrane technology. Unfortunately, the cost of Nafion-type membranes is still very high.

For a long time synthetic graphite has been used as the anode material. However, the stability of graphite anodes is not very high; they undergo gradual surface oxidation and erosion and thus become thinner. Hence, the gap between the electrodes, and with it the ohmic voltage drop in the electrolyte, increase during operation. The graphite anodes have a service life of 6 to 24 months. The development of new electrode materials on the basis of RuO_2 and TiO_2 mixed oxides at the end of the 1950s was a significant advance. The titanium–ruthenium oxide anodes exhibit low polarization for chlorine evolution. Moreover, their chemical stability is high, so that sometimes they are also described as low-wear or "dimensionally stable" anodes (DSA).

The theoretical OCV of cells consisting of a hydrogen electrode (in alkaline solution) and a chlorine electrode is 2.17 V. Practical cell voltages of most modern

electrolyzers are 3.3 to 3.8 V at a current density of 1 kA/m^2. With current yields of 95% for the anodic process, this corresponds to an energy consumption of 2600 to 3000 kWh per ton of chlorine.

When chlor–alkali electrolysis is conducted in an undivided cell with mild-steel cathode, the chlorine generated anodically will react with the alkali produced cathodically, and a solution of sodium hypochlorite NaClO is formed. Hypochlorite ions are readily oxidized at the anode to chlorate ions; this is the basis for electrolytic chlorate production. Perchlorates can also be obtained electrochemically.

17.2 WATER ELECTROLYSIS

Electrolytic hydrogen production [by reaction (15.4)] is economically inferior to the large-scale chemical process based on the steam reforming of natural gas (methane). However, it is employed successfully in those cases when modest quantities of hydrogen are needed locally or when highly pure hydrogen is required. An appreciable increase in electrolytic hydrogen production is expected in the future as natural gas resources diminish and the production of cheap electrical power in nuclear power plants increases. Water electrolyzers use alkaline electrolyte solution, which has the major advantage that iron resists corrosion [i.e., the electrodes and structural parts can be made from iron (steel)]. The theoretical OCV of the hydrogen–oxygen cell at 25°C is 1.229 V. Electrolysis is conducted with a cell voltage of 1.8 to 2.1 V at current densities of 2 to 4 kA/m^2. Improved designs where the working voltage is 1.6 to 1.7 V have been developed recently. The electrical energy consumption is 3.5 to 5 kWh per cubic meter of hydrogen.

A process involving water electrolysis is the production of heavy water. During cathodic polarization the relative rates of deuterium discharge and evolution are lower than those of the normal hydrogen isotope. Hence, during electrolysis the solution is enriched in heavy water. When the process is performed repeatedly, water with a D_2O content of up to 99.7% can be produced. Electrochemical methods are also used widely in the manufacture of a variety of other inorganic and organic substances.

17.3 ELECTROMETALLURGY

In the electrolyic production of metals, both aqueous solutions (electrohydrometallurgy) and melts are used. Solutions involving nonaqueous solvents have also found uses in recent years. We distinguish electroextraction, which is the primary production of a metal from the materials obtained when processing and leaching the original ores, and electrorefining, which is the purification of metals by their anodic dissolution and subsequent cathodic redeposition. Zinc, cadmium, and manganese are the most important metals obtained by electroextraction from aqueous solutions; this route is also used to produce copper from poor oxide ores. Electrolysis in melts is used to produce aluminum and a number of the alkali and alkaline-earth metals

(lithium, sodium, magnesium, calcium, and others) which cannot be produced from aqueous solutions because they are unstable in water. Refining is widely used for the production of more highly pure copper, gold, nickel, lead, and other metals.

Electrolytic aluminum production is the most important process in both volume and significance. World production is about 15 megatons per year, consuming about 240 billion kilowatthours of electrical energy. Aluminum oxide (alumina), Al_2O_3, is subjected to electrolysis at a temperature of 950°C; to this end it is dissolved in molten cryolite Na_3AlF_6, with which it forms a eutectic melting at about 940°C. Carbon anodes that are anodically oxidized to CO_2 in the process are employed. The overall electrolysis reaction can be written as

$$2Al_2O_3 + 3C \rightarrow 4Al + 3CO_2. \tag{17.3}$$

The aluminum produced has a higher density than the melt and collects at the bottom of the cell. The anodes are replaced as they are consumed. The theoretical OCV for reaction (17.3) is about 1.2 V, and the theoretical consumption of electrical energy (assuming a 100% current yield) is 3.6 kWh/kg. However, the actual cell voltage is 4.2 to 4.5 V, and the current yields are 85 to 90%, which implies a practical energy consumption of 14 to 16 kWh/kg. The rather high voltage is required because the side reaction of aluminum with CO_2 must be suppressed; this is achieved with a large gap between the electrodes (30 to 50 mm), which in turn implies ohmic voltage drops of more than 2 V in the electrolyte. The heat produced as a result of these internal voltage losses serves to maintain the required working temperature of the cell. About 20% of the cost of aluminum metal is due to electrical energy consumption, and 45% is due to the production of sufficiently pure alumina as a starting material.

17.4 ELECTROPLATING

The electrolytic application of thin metal coatings to other metals evolved during the middle of the last century. Today, it is one of the highest-volume chemical technologies; literally every metal-working plant has its own plating section.

Among the coatings we distinguish functional types from those applied for protection and ornament. The latter have the chief purpose of protecting a base metal against corrosive and erosive attack by the medium surrounding it and of giving its surface a particular appearance, such as luster, color, and so on. Often, coatings of nickel, chromium, and zinc are used here. Functional coatings are used for a variety of purposes: to produce reflecting surfaces, conducting paths (in printed circuits), magnetic layers, surfaces with specific friction parameters (sliding bearings), and others. Metal deposition is also used to join parts (electrochemical welding or brazing) and to restore the surfaces of worn parts.

During recent decades, demands regarding the quality and properties of metal coatings have increased sharply. This is due, on one hand, to advances in microelectronics, and on the other hand, to increasing uses of metal parts in corrosive environments.

MONOGRAPHS

Landau, U., E. Yeager, and D. Kortan, Eds., *Electrochemistry in Industry: New Directions*, Plenum Press, New York, 1982.

Lapicque, E., and A. Strock, *Electrochemical Engineering and Energy Storage*, Plenum Press, New York, 1994.

Pletcher, D., *Industrial Electrochemistry*, Chapman & Hall, London, 1982.

18
Electrochemical Reactors

18.1 DESIGN PRINCIPLES

Electrochemical reactors (cells, tanks) are used for the practical realization of electrolysis or the electrochemical generation of electrical energy. In developing such reactors one must take into account the purpose of the reactor as well as the special features of the reactions employed in it. Most common is the classical reactor type with plane-parallel electrodes in which positive and negative electrodes alternate and all electrodes having the same polarity are connected in parallel. Reactors in which the electrodes are concentric cylinders and convection of the liquid electrolyte can be realized by rotation of one of the electrodes are less common. In batteries, occasionally the electrodes are in the form of two long ribbons with a separator in between which are wound up as a double spiral.

The maximum values of electric power and unit output of electrochemical cells vary within wide limits. The total current load admitted by individual electrolyzers for the electrochemical production of various materials in plant or pilot installations (their capacity) is between 10 A and 200 kA, while the current loads that can be sustained by different types of battery (their current ratings) are between 10^{-5} A and 20 kA. Corresponding differences exist in the linear dimensions of the electrodes (between 5 mm and 3 m) as well as in the overall mass and size of the reactors.

In practice, groups (batteries) comprising a certain number of cells connected in series, and sometimes also in parallel, are generally used instead of single cells. The number of cells in series is determining for the voltage. Large electrolysis plants commonly contain as many as 100 or more individual electrolysis cells, and power is supplied from rectifying equipment producing voltages of up to 400 V. Electrochemical power sources are often built in the form of batteries composed of individual primary or secondary cells so as to yield battery voltages of 9, 12, or 24 V and more. For a series combination of the individual cells to groups, the positive lead from each cell is linked with an intercell bus to the negative lead of the following cell.

Another version of cell or group arrangement is that using *bipolar electrodes* (Fig. 18.1*a*). Here, combined electrodes are used: One side of the electrode functions

Fundamentals of Electrochemistry, Second Edition, By V. S. Bagotsky

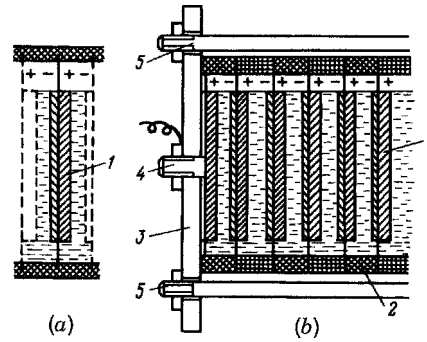

FIGURE 18.1 (*a*) Bipolar electrode; (*b*) filter-press reactor: (1) bipolar electrode; (2) gaskets; (3) end plate; (4) positive current collector; (5) tie bolts.

as the positive electrode of one cell; the other side functions as the negative electrode of the next cell. The bipolar electrodes alternate with electrolyte compartments, and both must be sealed carefully along the periphery to prevent outflow of electrolyte and to provide a reliable separation of the electrolyte in neighboring compartments by the electrode plates. The separating plates also function as cell walls and intercell connectors (i.e., the current between neighboring cells merely crosses a thin wall having negligible resistance). This implies considerable savings in the size and mass of the reactor.

Several possibilities exist for the assembly of reactors with bipolar electrodes. In the sections of a filter-press design (Fig. 18.1*b*), the blocks of electrodes and separators forming electrolyte compartments are tightened with the aid of end plates and tie bolts. Sealing is realized with the aid of gaskets, which are compressed during tightening of the assembly. After sealing, the compartments are filled with electrolyte by means of special narrow channels in the gaskets or electrode edges, which also enables circulation of the electrolyte. In batteries one often finds a modular design where individual cells or groups of cells are sealed by a plastic linen.

Interelectrode Gap The relative electrolyte volume available per unit surface area of the electrodes is determined by the distance (gap) between the electrodes. This distance is between fractions of a millimeter and some 10 cm. The ohmic losses in the electrolyte increase with the distance between the electrodes. On the other hand, when the electrolyte volume is too small, the reactant concentrations will change rapidly. Often, the electrolyte volume in a reactor is increased by providing space for the electrolyte not only between the electrodes but also above or below the block of electrodes. Sometimes the electrolyte is pumped around in an external circuit, including an additional electrolyte vessel.

Separators Separators made of insulating material are almost always arranged between electrodes of different polarity. They have a variety of functions, ranging from a mechanical separation of the electrodes and prevention of accidental contact to the strictest separation of anolyte and catholyte (the electrolyte volumes at the

anode and cathode) that is possible without upsetting the ionic conduction. Separators influence reactor efficiency decisively (for more details, see Section 18.2).

Supply and Withdrawal of Reaction Components In the continued operation of a reactor with reacting solid electrodes (as in electrohydrometallurgy), provisions must be made for periodic replacement of the electrodes. Reactants dissolved in the electrolyte are replenished and dissolved products withdrawn by appropriate adjustments of electrolyte composition, which may be continuous (e.g., when an external loop is operated) or batchwise. Gas-diffusion electrodes are used for the supply of gaseous reactants (Section 18.4). When gas is evolved in the reaction (as in water electrolysis) there is the danger of gas accumulation in the electrolyte (i.e., of large volumes of gas bubbles remaining in the space between the electrodes and producing a strong increase in electrolyte resistance). Various devices are used to prevent this, in particular the *gas lift*, which is the natural vertical rise of the liquid electrolyte, caused by an ascending flow of the gas-filled (less dense) layer of electrolyte close to the electrode surface; the loop is completed by a descending flow of the liquid from which the gas bubbles have been separated. Copious gas evolution during the electrolysis of liquid solutions is associated with another problem, which is the loss of electrolyte in the form of mist consisting of very small droplets. Therefore, special spray separators are installed from which the liquid carried off with the gas is returned to the cell.

Scale Factor Large-volume reactors have a number of specific features. When the electrodes are of considerable height and the total current is large, ohmic losses will occur within the electrodes, leading to a nonuniform current-density distribution (Section 18.3). Special feeders of relatively large cross section are used to reduce the ohmic losses in electrodes. Nonuniformity of the current distribution can be made even worse when stratification of the electrolyte solution occurs (i.e., when electrolyte layers of lower density that are depleted by the reaction will gather in the upper part of the reactor, and denser layers will accumulate in the lower part).

With increasing reactor size, the withdrawal of the heat evolved during the reaction becomes more difficult. This gives rise to a nonuniform temperature distribution within the reactor and thus a differentiation of conditions for the electrochemical reaction in different reactor parts. In a number of cases the thermal conditions can be improved through cooled electrodes.

Selection of Corrosion-Resistant Materials The concentrated solutions of acids, alkalies, or salts, salt melts, and the like used as electrolytes in reactors as a rule are highly corrosive, particularly so at elevated temperatures. Hence, the design materials, both metallic and nonmetallic, should have a sufficiently high corrosion and chemical resistance. Low-alloy steels are a universal structural material for reactors with alkaline solutions, whereas for reactors with acidic solutions, high-alloy steels and other expensive materials must be used. Polymers, including highly stable fluoropolymers such as PTFE, become more and more common as structural materials for reactors. Corrosion problems are of particular importance, of course, when materials for nonconsumable electrodes (and especially anodes) are selected, which must be sufficiently stable and at the same time catalytically active.

Mass- and Volume-Related Figures of Merit All electrochemical reactors should be sufficiently compact in their design. For batteries that are used in mobile applications, the figures of prime importance are the mass or volume of the device per unit of stored energy, which are given in kg/kWh or dm^3/kWh, or in the corresponding reciprocals representing the energy densities by mass or volume. For electrolyzers permanently installed in special rooms, the chief parameter is the productivity (e.g., the current load) per unit of floor space, since this is the parameter that determines the volume of the building required.

The productivity of modern electrolyzers per unit volume or unit of floor space as a rule is lower than that of chemical reactors with a similar purpose. This is due to the fact that in an electrochemical reactor the reactions occur only at the electrode surfaces, while in a chemical reactor they can occur in practically the full volume. Therefore, recent efforts go in a direction of designing new, more efficient electrochemical reactors.

With solid (and particularly polymeric) electrolytes which at the same time function as separators, one can appreciably reduce the distance between the electrodes and hence increase the electrode area per unit of reactor volume. Very compact equipment for water electrolysis which has no liquid electrolyte has been designed.

An appreciable increase in working area of the electrodes can be attained with porous electrodes (Section 18.4). Such electrodes are widely used in batteries, and in recent years they are also found in electrolyzers. Attempts are made to use particulate electrodes which consist of a rather thick bed of particulate electrode material into which the auxiliary electrode is immersed together with a separator. Other efforts concern *fluidized-bed reactors*, where a finely divided electrode material is distributed over the full electrolyte volume by an ascending liquid or gas flow and collides continuously with special current collector electrodes (Section 18.5).

Economic Performance Figures The economics of electrochemical reactors depends on many factors. The *current yields* are a figure of particular significance. When expensive reactants are used (e.g., in the electrosynthesis of a number of organic substances), the *chemical yield* is another significant parameter; this is the ratio between the amount of product actually obtained and that which, according to the reaction equation, can theoretically be obtained from a given amount of reactant consumed. The analogous parameter for batteries is the degree of reactant utilization (the ratio between the capacity available on discharge and that theoretically calculated for the amount of active materials present in the battery).

18.2 SEPARATORS

18.2.1 Purpose and Types

The major functions of separators in electrochemical reactors are (1) the mechanical separation of electrodes of different polarity and prevention of their contact (e.g., during vibrations) and of electronic conduction (short-circuiting) between

them; (2) the prevention of dendrite growth and of the formation of metallic "bridges" between the electrodes during metal electrocrystallization; (3) the restriction of mixing of the anolyte and catholyte and prevention of transfer of solutes and colloidal or suspended particles between the electrodes (such separators are also known as diaphragms); and (4) containment of the active material at the electrodes and preventing it from crumbling and shedding. While serving in all these functions, the separator should not pose any significant resistance to ionic current flow in the electrolyte, and it should not interfere with the transport of substances that are involved in the electrode reactions or with the free access of electrolyte to all electrode segments. In some cases a separator also functions as a matrix material for the electrolyte (i.e., by capillary forces retains the electrolyte close to the electrode surface).

Plastic or ebonite rods, plastic cords 2 to 3 mm thick, separator sheets consisting of thin grids of perforated or corrugated PVC, polymer-fiber or fiberglass cloth, and other materials are used for a geometric separation of electrodes. Such separators contain large pores or holes (between 0.1 and 5 mm). They cause little screening of the electrodes, but they also completely lack any capacity for electrolyte retention. Another group are the porous separators (diaphragms), which have pore radii between 20 nm and 100 μm. Sometimes these separators are divided arbitrarily into porous (with mean pore radii larger than 5 μm) and microporous (with smaller pore radii); they are used in electrolyzers and batteries. A special group of separators are *swollen membranes*, polymeric materials that interact with the aqueous or nonaqueous solutions. Upon entry of solvent molecules into the polymer structure, the distance between individual macromolecules increases (the membrane swells), and migration of the solution ions in the membrane becomes possible. The pores in such membranes are not larger than 2 nm.

In porous separators the pore radii are large compared to the size of molecules. Hence, interaction between the electrolyte and the pore walls has practically no qualitative effects on the ionic current through the separator; the transport numbers of the individual ions have the same values in the pores as in the bulk electrolyte. In swollen membranes the specific interaction between individual ions and macromolecules is very pronounced. Hence, these membranes often exhibit selectivity in the sense that different ions are affected differently in their migration. As a result, the transport numbers of the ions in the membrane differ from those in the electrolyte outside the membrane. In the limiting case, certain types of ion are arrested completely, and the membrane is called *permselective* (see Chapter 5).

Chemically inert and sufficiently stable materials are used to make the separators (e.g., the microfibrous chrysotile asbestos). Papermaking technology is used to prepare sheets (asbestos cardboard). Sometimes a mass containing asbestos fibers is applied to wire-gauze electrodes. More recently, asbestos substitutes have been introduced because of health risks in the asbestos industry. In batteries, porous diaphragms made of various synthetic resins (e.g., PVC) are used. Cellophane (hydrated cellulose), polyethylene radiation-grafted with polyacrylic acid, and various types of ion-exchange resins are examples of materials for swelling membranes. Recently, a new kind of chemically and thermally highly stable ion-exchange

membrane based on perfluorinated sulfonic acid cation-exchange resins (of the Nafion type) has found successful use in chlor–alkali electrolysis and other applications.

18.2.2 Chief Parameters

Influence on Electrolyte Conductivity In porous separators the ionic current passes through the liquid electrolyte present in the separator pores. Therefore, the electrolyte's resistance in the pores has to be calculated for known values of porosity of the separator and of conductivity, σ, of the free liquid electrolyte. Such a calculation is highly complex in the general case. Consider the very simple model where a separator of thickness d has cylindrical pores of radius r which are parallel and completely electrolyte-filled (Fig. 18.2). Let l be the pore length and N the number of pores (all calculations refer to the unit surface area of the separator). The ratio $\beta = l/d$ (where $\beta \equiv \cos\alpha \geq 1$) characterizes the tilt of the pores and is called the *tortuosity factor* of the pores. The total pore volume is given by $N\pi r^2 l$, the porosity by

$$\xi = \frac{N\pi r^2 l}{d} = N\pi r^2 \beta. \tag{18.1}$$

The electrolyte resistance in the pores is given by

$$R_p = \frac{l}{N\sigma\pi r^2}. \tag{18.2}$$

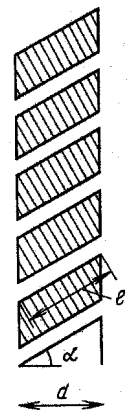

FIGURE 18.2 Separator model with cylindrical pores.

The ratio between R_p and the resistance, $R_E = d/\sigma$, of an electrolyte layer of the same thickness,

$$\varepsilon = \frac{R_p}{R_E} = \frac{\beta}{N\pi r^2}, \tag{18.3}$$

is the *attenuation factor of conduction* or *coefficient of resistance rise* (sometimes called the *relative resistance*). By definition, $\varepsilon \geq 1$. Comparing Eqs. (18.1) and (18.3), we can see that

$$\varepsilon = \frac{\beta^2}{\xi}. \tag{18.4}$$

The coefficient ε increases with increasing tortuosity and decreasing porosity. It is independent of pore radius when the values of these parameters are constant; the decrease in radius r that occurs while the total porosity is kept unchanged will be compensated for by an increase in the number of pores, N.

The coefficient ε is independent of electrolyte conductivity. A quantity useful for practical calculations is the electrolyte's effective conductivity in the separator, which is related to ε as

$$\varepsilon_{\text{eff}} = \frac{\sigma}{\varepsilon}. \tag{18.5}$$

Using this quantity, one can abandon specific models of separator pore structure and calculate the overall resistance from the separator's overall geometry.

Real porous separators differ from the model above. It was found experimentally that in real porous systems the relation

$$\varepsilon \sim \xi^{-m} \tag{18.6}$$

holds (*Archie's law*), where m has values between 1.8 and 3.5 instead of $m = 1$ for the model above.

The coefficient ε should be low for separators in electrochemical reactors. It has values between 1.1 and 1.6 for simple separators, but for porous diaphragms and swollen membranes it has values between 2 and 10. The total porosity should be at least 50%, and the separator's pore space should be impregnated completely and sufficiently rapidly with the liquid electrolyte.

Diffusion Through Separators Like current flow, the diffusion of dissolved components through separators will be delayed by decreasing porosity and increasing tortuosity. The attenuation factor of diffusion, ε_D ($= D/D_{\text{eff}}$), usually coincides with that of conduction.

Filtration of Liquids Depending on the specific electrochemical reactor type, the filtration rate of a liquid electrolyte through the separator should be either high (to secure a convective supply of substances) or very low (to prevent mixing of the anolyte and catholyte). The filtration rate that is attained under the effect of an external force Δp depends on porosity. For a separator model with cylindrical pores, the volume filtration rate can be calculated by *Poiseuille's law:*

$$\frac{dV}{dt} = \frac{N\pi r^4}{8l\eta}\Delta p = \frac{\xi r^2}{8l\eta\beta}\Delta p, \tag{18.7}$$

where η is the liquid's viscosity.

It can be seen here that in contrast to conduction, liquid flow depends not only on the porosity and tortuosity but also on pore size. When other parameters remain unchanged, a decrease in pore radius by a factor of 10 causes a decrease in liquid flow rate by a factor of 100.

18.3 MACROKINETICS OF ELECTROCHEMICAL PROCESSES (SYSTEMS WITH DISTRIBUTED PARAMETERS)

Electrochemical macrokinetics deals with the combined effects of polarization characteristics and of ohmic and diffusion factors on the current distribution and overall rate of electrochemical reactions in systems with distributed parameters. The term *macrokinetics* is used (mainly in Russian scientific publications) to distinguish these effects conveniently from effects arising at the molecular level.

During electric current flow in a cell, the current is not always distributed uniformly over the full working area of the electrodes (i.e., the current densities are different at different surface segments). A nonuniform current distribution may arise for two reasons: differences in potential between different segments of the electrode surface (owing to differences in ohmic resistance between these segments and the auxiliary electrode or current collector) or differences in electrolyte composition (owing to differences in the diffusion conditions). In these cases it can also be said that different segments of the electrode are not equally accessible. Systems where such effects appear are called *systems with distributed parameters*. In electroplating, cells where the current distribution is uniform (nonuniform) are said to have good (poor) *throwing power*.

Consider a cell with one positive and two negative electrodes where the latter are at different distances, l_1 and l_2, from the former (Fig. 18.3). We shall assume for the sake of simplicity that polarization of the electrodes is proportional to current density [i.e., $\Delta E = \rho i$ (ρ is the combined polarization resistance of the positive and negative electrodes)]. The voltages of the two halves of the cell, which are in parallel, are identical; hence, the sum of ohmic losses and polarization in the two halves should also be identical. The ohmic losses in the electrolyte are given by li/σ. Thus,

$$\rho i_1 + \frac{l_1 i_1}{\sigma} = \rho i_2 + \frac{l_2 i_2}{\rho}$$

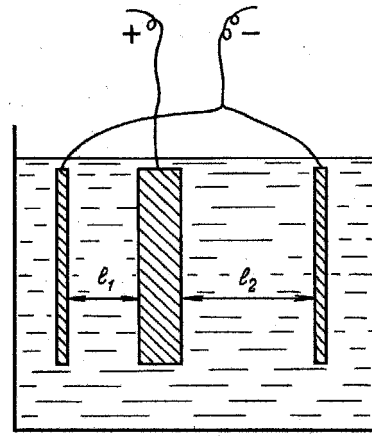

FIGURE 18.3 Electrochemical cell with dissimilar distances between electrodes.

or

$$\frac{i_1}{i_2} = \frac{\rho\sigma + l_2}{\rho\sigma + l_1} \tag{18.8}$$

(i.e., the current densities are not the same for the two electrodes).

The current density distribution will be least uniform ($i_1/i_2 = l_2/l_1$) when polarization resistance and/or conductivity are low and $\rho\sigma \ll l$. Uniformity increases with increasing $\rho\sigma$, and the current density in the two halves becomes the same when $\rho\sigma \ll l$. Thus, the throwing power depends on the parameter $\rho\sigma$; the higher this parameter, the more uniform will be the current distribution. At high values of polarization, ρ must be replaced by dE/di, and the value of this derivative is no longer a constant but decreases with increasing current density. Accordingly, the throwing power becomes poorer with increasing current density.

Consider as an example the current distribution in a cell with tall electrodes, where ohmic voltage losses arise in the current collector (Fig. 18.4*a*). Let b be the width, d the thickness, and h the height of the current collector, and ρ the conductivity of the current-collector material. We shall assume that the electrode is working on both sides (i.e., its working area is given by $S = 2bh$) and that current collection at the upper edge is uniform over the full width of the current collector (its cross section is bd). The current density at height x will be designated as i_x. The total current in the current collector at this level, I_x, will evidently be given by

$$I_x = 2b \int_0^x i_x \, dx. \tag{18.9}$$

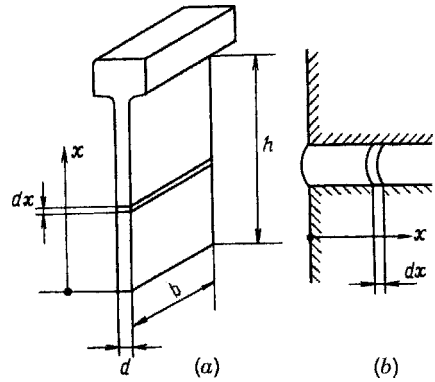

FIGURE 18.4 Concerning the derivation of equations for nonuniform current distribution: (*a*) in a flat electrode; (*b*) in a cylindrical pore.

The ohmic potential drop along the section from x to $x + dx$ is given by

$$d\varphi_{\text{ohm}} \frac{dx}{\sigma b d} I_x = \frac{2dx}{\sigma d} \int_0^x i_x \, dx, \tag{18.10}$$

and the total potential drop in the current collector from height x to the upper edge of the electrode (at $x = h$), where the external lead is fastened, is given by

$$\varphi_{\text{ohm},x} = \frac{2}{\sigma d} \int_x^h dx \int_0^x i_x \, dx. \tag{18.11}$$

In this example the current density distribution is nonuniform in the vertical, since at all heights x the sums of ohmic potential drops and polarization of the two electrodes must be identical. In the top parts of the electrodes, where the ohmic losses are minor, the current density will be highest, and it decreases toward the bottom. The current distribution will be more uniform the higher the polarization.

The most general form of a differential equation for the distribution of potential and current density in a system with ohmic losses is obtained when Eq. (18.10) is differentiated. Let s_V ($= 2/d$) be the working surface area referred to unit volume (of the current collector). Considering that $dE = d\varphi_{\text{ohm}}$, owing to the constancy of the sums of ohmic losses and polarization (which includes the appropriate signs), we find that

$$\frac{d^2E}{dx^2} = \frac{s_V}{\sigma} i_x. \tag{18.12}$$

For a cylindrical pore (Fig. 18.4*b*), consider the case where concentration gradients arise in the solution but ohmic potential drops can be neglected. With Π as the

pore's perimeter, A as the pore's cross section, and S_p as the pore's surface area, it is evident that $s_V \equiv S_p/V = \Pi/A$. In a solution layer at distance x from the pore mouth, the concentration gradient of component j will be related to the current I_x crossing this layer as

$$I_x = n\,FAD_j\left(\frac{dc_j}{dx}\right)_x. \tag{18.13}$$

The total current in layer x [by analogy with (18.9)] is given by

$$I_x = \Pi \int_0^x i_x\,dx. \tag{18.14}$$

Differentiating Eqs. (18.13) and (18.14), we find the general form of the differential equation in systems with concentration changes:

$$\frac{d^2c_j}{dx^2} = \frac{s_V}{nFD_j}\,i_x. \tag{18.15}$$

For a solution of differential equations (18.12) and (18.15) and for a quantitative calculation of the current distribution, we must know how the current density depends on polarization at constant reactant concentrations or on reactant concentrations at constant polarization. We must also formulate the boundary conditions. Examples of such calculations are reported below.

18.4 POROUS ELECTRODES

In industrial electrochemical cells (electrolyzers, batteries, fuel cells, and many others), porous metallic or nonmetallic electrodes are often used instead of compact nonporous electrodes. Porous electrodes have large true areas, S_p, of the inner surface compared to their external geometric surface area S [i.e., large values of the formal roughness factors $\gamma \equiv S_p/S$ (parameters γ and s_V are related as $\gamma = s_V d$)]. Using porous electrodes, one can realize large currents at relatively low values of polarization.

In porous liquid-phase electrodes, all pores are filled with liquid electrolyte (solution or melt). When part of the pores are gas filled, the electrodes are called *gas–liquid*. When the electrode is nonconsumable and chemically inert, its pore structure will remain unchanged during operation (or change very slowly on account of secondary aging processes). The structure of an electrode that reacts changes continuously.

In the pores of the electrodes, practically no natural convection of the liquid takes place. Reactants dissolved in the liquid can be supplied in two ways from the external surface to the internal reaction zones (and reaction products transported away in the opposite direction): (1) by diffusion in the motionless liquid (*diffusion electrode*),

and (2) with a liquid flow passing the porous electrode under the stimulus of an external force (*flow-through electrode*). In some cases, porous electrodes are working on one side only, the front that is turned toward the auxiliary electrode; the other side (the back) is used for reactant supply. When the reactant is a gas, it is usually supplied to the reaction zone from the back of the electrode. Electrodes of this type are called *gas-diffusion electrodes*.

18.4.1 Liquid-Diffusion Electrodes

Let the net (overall) current density of the porous electrode be i. Under conditions of uniform work of the full internal surface area, the value of i would be γ times larger than the current density i_0 of a smooth electrode, working at the same value of polarization and in an electrolyte having the same composition. This case is rare in practice, and it is more common to find that i is smaller than its maximum value $i_{\max} = \gamma i$. The ratio between these parameters,

$$h = \frac{i}{i_{\max}} = \frac{i}{\gamma i_0} \qquad (h \leq 1), \tag{18.16}$$

is called the *efficiency factor* of the porous electrode.

Porous electrodes are systems with distributed parameters, and any loss of efficiency is due to the fact that different points within the electrode are not equally accessible to the electrode reaction. Concentration gradients and ohmic potential drops are possible in the electrolyte present in the pores. Hence, the local current density, $i_{S,x}$ (referred to the unit of true surface area), is different at different depths x of the porous electrode. It is largest close to the outer surface ($x = 0$) and falls with increasing depth inside the electrode.

Mathematical calculations of the current-density distribution in a direction normal to the electrode are rather difficult; hence, to discuss the major qualitative trends, we shall limit ourselves to reviewing the simplest cases. Consider the processes occurring in a porous electrode of thickness d operated unilaterally. The current density generated at depth x per unit volume will be designated as i_{Vx}, and it is obvious that $i_{Vx} = s_V i_{S,x}$.

We discuss the particular case where only ohmic potential drops are present; concentration gradients are absent. The current-density distribution normal to the surface can be found by integrating the differential equation (18.12) with the boundary conditions

$$(\Delta E)_{x=0} = (\Delta E)_0; \qquad \left(\frac{dE}{dx}\right)_{x=d} = 0. \tag{18.17}$$

The first condition implies that the electrode's polarization as a whole (which is measured at its front face where $x = 0$) is given and has the value $(\Delta E)_0$. According to the second condition, a potential gradient does not exist close to the rear face, since here the total current flowing in the direction of the front face is low.

For a solution of Eq. (18.12), we must also know the dependence of current density on polarization. First we consider the simpler case of low values of polarization when the linear function (6.6) with ρ as the kinetic parameter is valid. Solving the differential equation for these conditions, we arrive at the following expression for the distribution of local current densities in the electrode in a direction normal to the surface:

$$i_{S,x} = \frac{i_0 \cosh[(d-x)/L_{\text{ohm}}]}{\cosh(d/L_{\text{ohm}})}, \tag{18.18}$$

where

$$L_{\text{ohm}} \equiv \sqrt{\frac{\rho\sigma_{\text{eff}}}{s_V}}; \qquad i_0 = \frac{(\Delta E)_0}{\rho}. \tag{18.19}$$

Curves showing the current densities as functions of x are presented for two values of electrode thickness in Fig. 18.5. The parameter L_{ohm} has the dimensions of length; it is called the *characteristic length* of the ohmic process. It corresponds approximately to the depth x at which the local current density has fallen by a factor of e (approximately 2.72). Therefore, this parameter can be used as a convenient characteristic of attenuation of the process inside the electrode.

The net current density can be computed by integrating the volume current density $i_{V,x}$ over electrode thickness:

$$i = s_V \int_0^d i_{S,x}\, dx = i_0\, L_{\text{ohm}}\, s_V \tanh\frac{d}{L_{\text{ohm}}}. \tag{18.20}$$

Substituting Eq. (18.20) into (18.16), we find that

$$h = \tanh\frac{d}{L_{\text{ohm}}}. \tag{18.21}$$

It can be seen here that for $d < L_{\text{ohm}}$ (a "thin" electrode) $h \to 1$, the electrode will work uniformly throughout, and the current depends only on electrochemical reaction

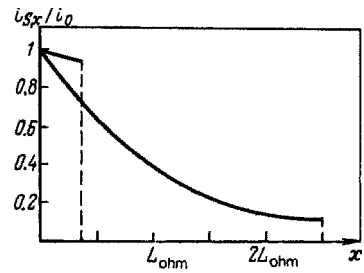

FIGURE 18.5 Current density distribution inside a porous electrode [according to Eq. (18.18)] for two values of electrode thickness: $d_1 = 0.33L_{\text{ohm}}$ and $d_2 = 2.5L_{\text{ohm}}$.

kinetics (*internal kinetic control* of electrode operation). However, for $d > L_{\text{ohm}}$ (a "thick" electrode), h decreases (*internal ohmic control* of electrode operation). Owing to the ohmic potential drops, layers of the electrode deeper than 2 to 3 L_{ohm} contribute practically nothing to the total current. At very low values of L_{ohm} (which are comparable with the dimensions of the structural elements in the electrode), the process is fully "pushed out" to the outer surface, and the inner segments of the electrodes are almost inoperative.

According to Eq. (18.18), the relative current density distribution, $i_{S,x}/i_0$, in a direction normal to the electrode surface is independent of the absolute values of current density. However, as the current density rises to values where polarization starts to depart from the linear function (6.6), the situation is perturbed and factors L_{ohm} and h start to decrease.

Figure 18.6 shows polarization curves for a smooth electrode and for a porous electrode with the roughness factor $\gamma = 100$. A system that at low currents works under internal kinetic control (i.e., with $h = 1$) was selected as the example. In this current range (segment AB in curve 2) the distance between the curves is constant and equal to the logarithm of the roughness factor. As the current increases, h begins to decrease, owing to increasing influence of the ohmic factors, and the curves begin to merge. The region of internal ohmic control is situated between points B and C. It is typical that in this region the slope of the polarization curve is double that found for a smooth electrode. As the current is raised further, the process is pushed out to the outer surface, and the porous electrode loses its advantages (*external kinetic control*, segment *CD*; *external diffusion control*, segment *DE*).

When only taking into account the concentration polarization in the pores (disregarding ohmic potential gradients), we must use an equation of the type (18.15). Solving this equation for a first-order reaction $i_{S,x} = nFh_m c_{j,x}$ leads to equations exactly like (18.18) for the distribution of the process inside the electrode, and like (18.20) for the total current. The rate of attenuation depends on the characteristic length of the diffusion process:

$$L_{\text{diff}} = \sqrt{\frac{nFD_{\text{eff}}}{s_V h_m}}. \tag{18.22}$$

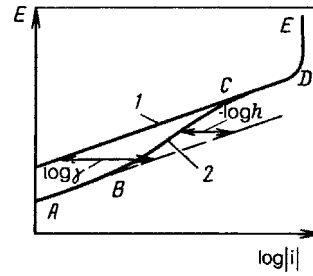

FIGURE 18.6 Schematic of the polarization curves for smooth (1) and porous (2) electrodes.

Unlike the earlier case, L_{diff} here decreases with increasing current not only at large but also at small values of polarization, since h_m depends on polarization. For $d > L_{\text{diff}}$ (particularly when polarization is significant), the electrode will work under internal diffusion control.

18.4.2 Gas-Diffusion Electrodes

The solubilities of most gases in solutions are low; hence, for reactions involving gaseous reactants (particularly for the reactions in fuel cells and other power sources), gas-diffusion electrodes are usually employed, which contact the electrolyte with their front face and the gas space with the other (rear) face (Fig. 18.7). The pore space of such electrodes is partly liquid filled, partly gas filled. The electrochemical reactions occur mainly beneath thin electrolyte films forming at the pore walls close to the places where gas and liquid pores meet: near the *three-phase boundaries*. These zones offer optimum conditions for the simultaneous access of gas (through the film) and dissolved reaction components (along the film). These zones must be made as large as possible to achieve high electrode efficiencies; this can be attained at certain volume proportions between gas and liquid pores. In addition, these zones should be distributed sufficiently uniformly throughout the electrode.

Most electrode materials are hydrophilic and readily wetted by aqueous solutions. Two methods are used to create and maintain an optimum gas/solution ratio in the electrode. The first method employs a certain excess gas pressure in the gas space. This causes the liquid to be displaced from the wider pores; in finer pores the liquid continues to be retained by capillary forces. The second method employs partial wetproofing of the electrode by the introduction of hydrophobic materials (e.g., fine PTFE particles). Then the electrolyte will penetrate only those pores in the hydrophilic electrode material where the concentration of hydrophobic particles is low.

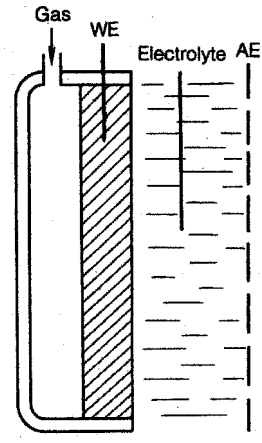

FIGURE 18.7 Schematic of a gas-diffusion electrode.

The macrokinetics of processes in gas-diffusion electrodes is analogous to that in liquid-phase electrodes. In calculations, one must take into account, however, that the electric current and the solute species will be carried only through that part of pore space which is electrolyte filled, whereas gas supply is accomplished primarily not by diffusion through the liquid but by flow in the gas channels.

18.5 THREE-DIMENSIONAL ELECTRODES

Certain three-dimensional electrodes, also known as *slurry* or *fluidized-bed electrodes*, are sometimes used as well in order to have a strongly enhanced working surface area. Electrodes of this type consist of fine particles of the electrode material (metal, oxide, carbon, or other) kept in suspension in the electrolyte solution by intense mixing or gas bubbling. A certain potential difference is applied to the system between an inert feeder electrode and an auxiliary electrode that are immersed into the suspension. By charge transfer, the particles of electrode material constantly hitting the feeder electrode acquire its potential (fully or at least in part), so that a desired electrochemical reaction may occur at their surface. In this reaction, the particles lose their charge but reacquire it in subsequent encounters with the feeder electrode.

Reactors containing electrodes of this kind are used when reactants are present in the solution in an extremely low concentration, and their rate of diffusion to a quiescent electrode (even a porous one) would be too low. An acceleration of the reaction at three-dimensional electrodes is attained owing to shorter diffusional transport distances to the closest particles in suspension and also owing to strong turbulence in the system.

Electrodes of this type can, for instance, be used to extract traces of certain metals from seawater or to perform reactions with gases having very low solubility in a given medium. They can also be used to reduce electrochemically or to oxidize particles of materials having very low conductivity. Their efficiency depends on many factors, including the time of contact of the particles with the feeder electrode and the quality of this contact (low resistance to charge transfer during the encounters).

MONOGRAPH

Fahidy, T. Z., *Principles of Electrochemical Reactor Analysis*, Elsevier, Amsterdam, 1985.

19

Batteries (Electrochemical Power Sources)

An *electrochemical power source* (EPS) is a device that converts the energy of a chemical reaction occurring in it directly electrochemically to electrical energy. An EPS comprises one or several single galvanic cells. In each such cell a comparatively low voltage is generated, typically 0.5 to 4 V for different classes of cells. Where higher voltages are required, the necessary number of cells are connected in series to form a galvanic battery. Colloquially, the term *battery* is often used as well to denote single galvanic cells. This usage is retained in this book.

By their principles of functioning, batteries can be classified as follows:

1. *Primary (single-discharge) batteries.* A primary battery contains a finite quantity of the reactants participating in the reaction; once this quantity is consumed (on completion of discharge), a primary battery cannot be used again ("throwaway batteries").

2. *Storage (multiple-cycle) batteries* (also called *secondary* or *rechargeable batteries*). On the completion of discharge, a storage battery can be recharged by forcing an electric current through it in the opposite direction; this will regenerate the original reactants from the reaction (or discharge) products. Therefore, electric energy supplied by an external power source (such as the grid) is stored in this battery in the form of chemical energy. During the discharge phase this energy is delivered to a consumer independent of the grid. Good rechargeable batteries or cells will sustain a large number of such charge–discharge cycles (hundreds or even thousands).

3. *Fuel cells*. In the fuel-cell mode of operation, reactants are fed into the cell (or battery) continuously while reaction products are removed continuously. Hence, fuel cells (the more appropriate term, *fuel battery*, is not commonly used) can deliver current continuously for a considerable length of time that depends primarily on external reactant storage.

Fundamentals of Electrochemistry, Second Edition, By V. S. Bagotsky

The classification into primary and storage batteries is not rigorous since under certain conditions (in the laboratory) a primary battery may be recharged, whereas storage batteries are sometimes discarded after a single use.

19.1 CHEMICAL CURRENT-PRODUCING REACTIONS IN BATTERIES

Reactions in batteries are chemical reactions between an oxidizer and a reducer. In reactions of this type, the reducer being oxidized releases electrons while the oxidizer being reduced accepts electrons. An example of such a redox reaction is the reaction between silver oxide (the oxidizer) and metallic zinc (the reducer):

$$Ag_2O + Zn \rightarrow 2Ag + ZnO, \tag{19.1}$$

in which electrons are transferred from zinc atoms of metallic zinc to silver ions in the crystal lattice of silver oxide. When reaction (19.1) is allowed to proceed in a jar in which silver oxide is thoroughly mixed with fine zinc powder, no electrical energy is produced despite all the electron transfers at grain boundaries. This is because these transfers occur randomly in space and the reaction energy is liberated as heat, which can raise the temperature of the reaction mixture to dangerous levels. The same reaction does occur in batteries, but in an ordered manner in two partial reactions separated in space and accompanied by electric current flow (Fig. 19.1).

In the simple normal case a battery (cell) consists of two electrodes made of different materials immersed in an electrolyte. The electrodes are conducting metal

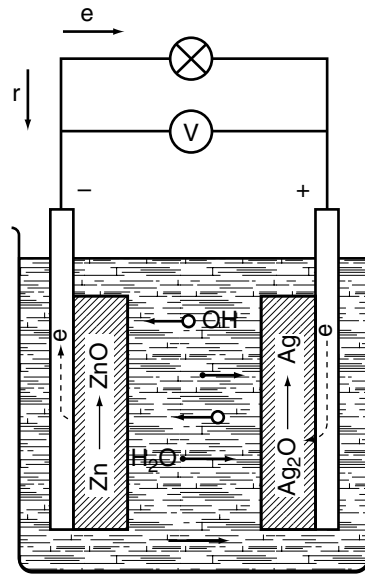

FIGURE 19.1 Schematic of processes in a zinc–silver oxide battery during discharge.

plates or grids covered by reactants (the active materials); the oxidizer is present on one electrode, the reducer on the other. In silver–zinc cells the electrodes are metal grids, one covered with silver oxide and the other with zinc. An aqueous solution of KOH serves as the electrolyte. Schematically, this system can be written as

$$\mathrm{Zn}\,|\,\mathrm{KOH},\, aq\,|\,\mathrm{Ag_2O}. \tag{19.2}$$

When the electrodes above are placed into the common electrolyte making electrolytic contact between them, an OCV develops between them (here $\mathscr{E} = 1.6$ V), zinc being the negative electrode.

When they are additionally connected by an electronically conducting external circuit, the OCV causes electrons to flow through it from the negative to the positive electrode. This is equivalent to an electric current I. This current is the result of reactions occurring at the surfaces of the electrodes immersed into the electrolyte: zinc being oxidized at the negative electrode,

$$\mathrm{Zn} + 2\mathrm{OH}^- \rightarrow \mathrm{ZnO} + \mathrm{H_2O} + 2e^-, \tag{19.3}$$

and silver oxide being reduced at the positive electrode,

$$\mathrm{Ag_2O} + \mathrm{H_2O} + 2e^- \rightarrow 2\mathrm{Ag} + 2\mathrm{OH}^-. \tag{19.4}$$

These electrode reactions sustain a continuous flow of electrons in the external circuit. The OH^- ions produced by reaction (19.4) in the vicinity of the positive electrode are transported through the electrolyte toward the negative electrode to replace OH^- ions consumed in reaction (19.3). The electric circuit as a whole is thus closed. Apart from the OCV, the current depends on the cell's internal resistance and on the ohmic resistance present in the external circuit. Current flow will stop as soon as at least one of the reactants is consumed.

Thus, in contrast to what occurred in the jar, in an EPS the overall chemical reaction occurs in the form of two spatially separated partial electrochemical reactions. Electric current is generated because the random transfer of electrons is replaced by a spatially ordered overall process.

The silver–zinc cell is a storage battery: After discharge, it can be recharged by forcing through it an electric current in the reverse direction. In this process the two electrode reactions (19.3) and (19.4) as well as the overall reaction (19.2) go from right to left electrons flowing in the sense of arrow r in Fig. 19.1.

19.2 PERFORMANCE OF BATTERIES

19.2.1 Electrical characteristics

OCV and Discharge Voltage The OCV, $\mathscr{E}_0$, of a galvanic cell depends on the electrochemical system selected for it and is somewhat affected by the electrolyte

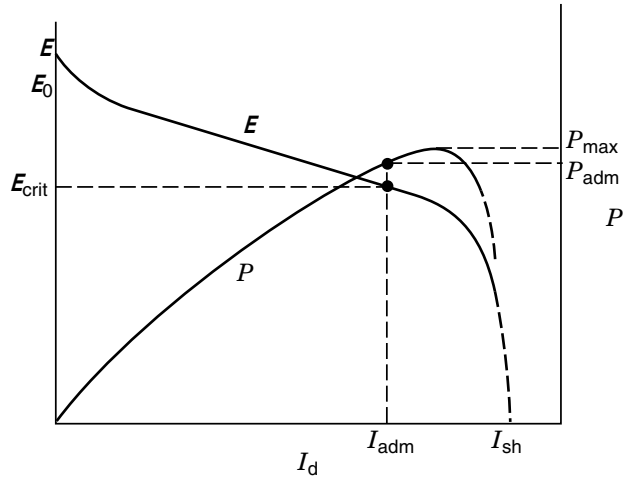

FIGURE 19.2 Typical current–voltage curve and dependence of discharge power on load current.

concentration, degree of discharge of the cell, temperature, and other factors. Once these parameters have been fixed, the OCV is a fairly reproducible quantity. Because of electrode polarization and ohmic voltage drops, the discharge voltage of a cell, $\mathscr{E}_d$, is lower than the OCV and depends on the value of the discharge current, I_d. A typical current–voltage curve is plotted in Fig. 19.2. The discharge voltage depends strongly on structural and technological features of the cell, on temperature, and on numerous other factors. The spread in values of the discharge voltage is greater than that of OCV values.

The functional dependence of the discharge voltage, $\mathscr{E}_d$, on discharge current I_d is sometimes represented by a simplified linear equation,

$$\mathscr{E}_d = \mathscr{E}_0 - I_d R_{\text{app}}, \tag{19.5}$$

where it is assumed that the apparent internal resistance, R_{app}, is constant. This is a rather crude approximation, especially when the current–voltage curve actually is S-shaped. The formal parameter, R_{app}, includes not only the internal ohmic resistance of the cell, but also terms arising from polarization of the electrodes. I_{sh} in Fig. 19.2 denotes the current at $R_{\text{app}} \to 0$ (short circuit).

Discharge Curves While a cell undergoes discharge, a gradual decrease of the voltage is normally observed. Typical plots of $\mathscr{E}_d$ vs. the time of discharge, τ, or the amount of electric charge, Q_d, delivered are reported in Fig. 19.3. The degree of voltage falloff differs between cell types, varying from 5 to 10% of the initial level, $(\mathscr{E}_d)_{\text{init}}$, in some systems to 50% in other systems. This decrease in voltage may be caused by higher polarization of the electrodes arising from an altered ratio of reactants and reaction products at the electrodes and/or by increased ohmic resistance. The terminal decrease of voltage at the end of discharge may be steep or gradual. For this

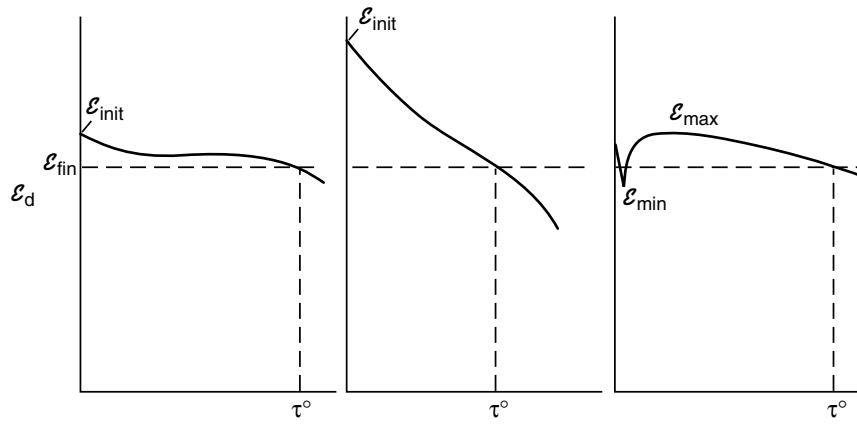

FIGURE 19.3 Typical discharge curves for various battery types.

reason it is recommended to terminate discharge at a certain cutoff voltage, $(\mathscr{E}_d)_{fin}$, even though the reactants are not yet completely consumed.

For energy estimates it is convenient to use the parameter of mean discharge voltage under given discharge conditions, $\overline{\mathscr{E}}_d$, which is defined as the mean integral or mean arithmetic value of discharge voltage over a given discharge period τ.

Discharge Current and Discharge Power The discharge current of a battery depends on the external circuit resistance, R_{ext}, and is given by Ohm's law as $I_d = \mathscr{E}_d/R_{ext}$ or, when using the simplified expression (19.5), as

$$I_d = \frac{\mathscr{E}_0}{R_{app} + R_{ext}}. \tag{19.6}$$

The power delivered by a cell during discharge is found as $P = \mathscr{E}_d I_d$ or, with Eqs. (19.5) and (19.6), as

$$P = \frac{\mathscr{E}_0^2 R_{ext}}{(R_{app} + R_{ext})^2}. \tag{19.7}$$

Neither the discharge current nor the power output are sole characteristics of a cell, since both are determined by the external resistance, R_{ext}, selected by the user. However, the maximum admissible discharge current, I_{adm}, and associated maximum admissible power, P_{adm}, constitute important characteristics of all cell types. These performance characteristics place a critical lower bound, $\mathscr{E}_{crit}$, on cell voltage; certain considerations (such as overheating) make it undesirable to operate at discharge currents above I_{adm} or cell voltages below $\mathscr{E}_{crit}$. To a certain extent the choice of values for I_{adm} and $\mathscr{E}_{crit}$ is arbitrary. Thus, in short-duration (pulse) discharge, significantly higher currents can be sustained than in long-term discharge (see Fig. 19.2).

Cell Capacity and Stored Energy The electric charge, Q_d, that has passed through the external circuit over a discharge period τ is given by $Q_d = \int_0^\tau I_d\,dt$ or, for $I_d =$ const, simply by $Q_d = I_d\tau$. In the literature on batteries, this charge is expressed in ampere-hours (Ah). The total charge that can be delivered by the battery during a full discharge is called its *ampere-hour capacity*, C. As a rule, this parameter is stated in the battery specifications for defined discharge modes (in terms of discharge currents and temperatures).

Electrical Characteristics of Storage Batteries While a storage battery undergoes recharging, the charge voltage, $\mathscr{E}_{ch}$, will be higher the higher the charge current, I_{ch}. The charge voltage will also increase with time as the amount of charge stored increases. A battery is charged, either to a certain final charge voltage, $(\mathscr{E}_{ch})_{fin}$, or to the point where the cell has accepted an amount of charge defined as its charge capacity. The mean discharge voltage is always lower than the mean charge voltage.

The discharge Ah capacity of an ideal storage cell is equal to its charge Ah capacity. Charging, however, is frequently accompanied by side reactions. For instance, in aqueous solutions, hydrogen and/or oxygen often start to be generated before charging is completed. For this reason the Ah efficiency of capacity (or current) utilization, $\mu_Q = Q_d/Q_{ch}$, often is less than unity.

Comparative Characteristics Often, the electric and other characteristics of batteries differing in size, design, or electrochemical system need to be compared. The easiest way is by using normalized (reduced) parameters. Thus, current density serves as a measure of the relative reaction rate. Therefore, plots of voltage vs. current density provide a useful characterization of a battery, reflecting its specific properties independent of its size.

Widely used parameters are the specific energy or power per unit mass ($w = W/M$, in Wh/kg, or $p = P/M$, in W/kg). In each battery type the specific energy is a falling function of specific power. Plots of w vs. p (Ragone, 1968) yield a clear illustration of the electrical performance parameters of given types of batteries and are very convenient for their comparison (see Fig. 19.4).

19.2.2 Operational Characteristics

Battery characteristics depend strongly on the operating temperature. As a rule, both the discharge voltage and the reactant utilization coefficient are lower at lower temperatures. On the other hand, increased temperatures are conducive to side reactions (such as corrosion processes) and thus reduce battery efficiency. Therefore, each battery type is designed for a specific temperature range within which its characteristics will be within the prescribed limits.

Another group of important battery characteristics are the lifetime parameters. For primary batteries and charged storage batteries, a factor of paramount importance is the rate of self-discharge. Self-discharge may be the result of processes occurring at one of the electrodes (e.g., corrosion of zinc in batteries with zinc anodes or the decomposition of higher metal oxides in batteries with oxide cathodes), or it

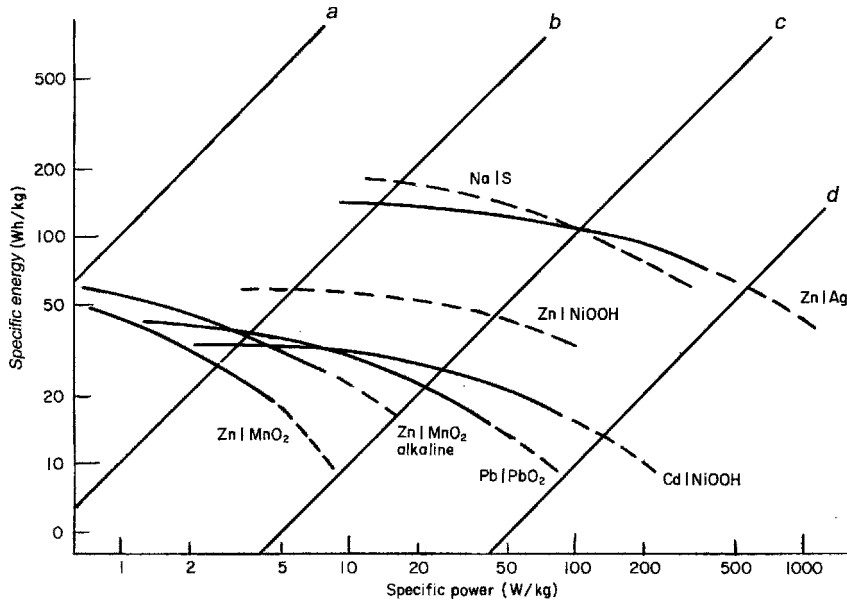

FIGURE 19.4 Dependence of the specific energy w with respect to mass on the specific discharge power p for various heavy drain batteries; the straight lines correspond to different times of full discharge τ_d: $\tau_d = 100$ h (*a*); 10 h (*b*); 1 h (*c*); 6 min (*d*).

may be the result of processes taking place in the battery as a whole (internal short circuits due to growth of metallic dendrites between the electrodes or to a "shuttle action" of impurities in the electrolyte which are oxidized at the positive electrode and reduced at the negative electrode, or external short circuits due to insufficient insulation between the electrodes).

The rate of self-discharge determines *shelf life* (the maximum admissible interval between manufacturing and utilization in discharge) and *service life* (including the time of discharge) of primary batteries. The service life of storage batteries usually is understood as being the charge–discharge cycles.

The last group of parameters relates to handling of the batteries. These include the mechanical strength (e.g., with respect to vibrations and shock accompanying transportation), maintenance, and "foolproofness" (a term introduced by Thomas A. Edison in 1911 as one of the characteristics of storage batteries).

19.3 ELECTROCHEMICAL SYSTEMS

The numerous existing battery types vary in their size, structural features, and nature of the chemical reactions. They vary accordingly in their performance and parameters. This variety reflects the diverse conditions under which cells operate, each field of application imposing its specific requirements.

All batteries are based on a specific electrochemical system: a specific set of oxidizer, reducer, and electrolyte. Conditionally, an electrochemical system is written as

$$\text{oxidizer} \,|\, \text{electrolyte} \,|\, \text{reducer}. \tag{19.8}$$

Often, the oxides of certain metals are used as the oxidizer. In the names of systems and batteries, though, often only the metal is stated, so that the example reported above is called a silver–zinc, rather than silver oxide–zinc battery (or system).

Batteries are known for about 100 electrochemical systems. Today, many of them are of mere historical interest. Commercially, batteries of less than two dozens of systems are currently produced. The largest production volumes are found in just three systems: (1) primary zinc–manganese batteries (today with an alkaline electrolyte, in the past with a salt electrolyte), (2) rechargeable lead–acid batteries, and (3) rechargeable alkaline (nickel–cadmium and nickel–iron) batteries. Batteries of these systems have been manufactured for more than a century, and until today have been widely used. Two more types gained increasing importance during the second half of the twentieth century: nickel–hydride storage batteries and a variety of lithium batteries. Other battery systems are of relatively limited use, mainly to supply power needs in military devices.

In subsequent sections we provide brief information on batteries of various electrochemical systems. The major electrochemical features of each type will be pointed out. The relative discharge characteristics of batteries of the various systems are shown in Fig. 19.4 as a Ragone plot of w vs. p. For specific details of design and manufacturing technology, as well as for more details on performance and characterization, battery books and monographs should be consulted.

19.4 PRIMARY BATTERIES

19.4.1 Leclanché (Zinc–Carbon) Batteries

$$\text{MnO}_2 \,|\, \text{NH}_4\text{Cl}, \, aq \,|\, \text{Zn} \tag{19.9}$$

For over 100 years, primary zinc–manganese dioxide (or zinc–carbon) batteries have been produced and used as the major primary battery. Their popularity is due to a favorable combination of properties: They are relatively cheap, have satisfactory electrical parameters and a convenient storage life, and offer convenient utilization. Their major disadvantage is a strong voltage decrease during progressive discharge; depending on the load, the final voltage is just 50 to 70% of the initial value. Zinc–carbon batteries are manufactured as leakproof "dry" batteries having the electrolyte soaked up by a matrix. Mostly small sizes with capacities of up to 4 Ah are produced.

The first zinc–carbon cell made in 1876 by the French engineer G.-L. Leclanché was a glass jar containing an aqueous solution of ammonium chloride into which were immersed an amalgamated zinc rod (the negative electrode) and a porous

earthenware pot packed with a mixture of manganese dioxide and powdered coke and containing a carbon-rod current collector at the center (positive electrode). Quite soon a zinc can serving simultaneously as the anode and cell container replaced the zinc rod.

The discharge reaction at the positive electrode,

$$MnO_2 + H_2O + 2e^- \rightarrow MnOOH + 2OH^-, \qquad (19.10)$$

can be regarded as a process of cathodic intercalation of hydrogen atoms into the lattice of MnO_2. This causes the electrolyte near the cathode to become alkaline, and as a result, ammonium ions decompose, forming free ammonia.

The anodic oxidation of zinc in salt solutions produces Zn^{2+} ions, and in practice is accompanied by various secondary reactions, resulting in the formation of barely soluble complex compounds. Zinc ions diffuse to zones with higher pH, where, after hydrolysis, they precipitate as oxychlorides $ZnCl_2 \cdot xZn(OH)_2$ or hydroxide $Zn(OH)_2$. Crystals of $Zn(NH_3)_2Cl_2$ formed by interaction with free ammonia also precipitate. These products all shield the active materials of both electrodes, increase the internal resistance and the pH gradient, and produce deterioration of the cell parameters. The zinc ions can also react with the product of discharge of the positive electrode to hetaerolite $ZnO \cdot Mn_2O_3$, forming a new solid phase.

Thus, the electrode processes occurring in zinc–carbon batteries with salt electrolytes are complicated, and their thermodynamic analysis is difficult. In a rough approximation disregarding secondary processes, the current-producing reaction can be described as

$$Zn + 2MnO_2 + 2H_2O \rightarrow Zn(OH)_2 + 2MnOOH. \qquad (19.11)$$

Often, the equation

$$Zn + 2MnO_2 + 2NH_4Cl \rightarrow Zn(NH_3)_2Cl_2 + 2MnOOH \qquad (19.12)$$

is used, but it also fails to supply an exhaustive description of the process inasmuch as the actual Ah capacity of a battery can be higher than that corresponding to the amount of ammonium chloride in reaction (19.12).

Depending on the composition of the active materials and on the manganese dioxide type employed, the OCV of freshly manufactured zinc–carbon cells with salt electrolyte varies between 1.55 and 1.85 V. It decreases during discharge and formation of the variable-composition mass. Upon prolonged storage of undischarged batteries, their OCV also decreases.

From the 1960s onward, alkaline zinc–manganese dioxide batteries started to be produced. They have appreciably better electrical performance parameters (see Section 19.4.3) but do not differ from Leclanché batteries in their operating features, are produced in identical sizes, and can be used interchangeably with them. Thus, a gradual changeover occurred and phaseout of the older system is now almost complete.

19.4.2 Zinc Electrode in Alkaline Solutions

Metallic zinc was used as a material for the negative electrode in the earliest electrical cell, Volta's pile, and is still employed in a variety of batteries, including batteries with alkaline electrolytes.

The operation of zinc anodes in alkaline solutions (mainly 20 to 40% KOH) involves specific features. In the anodic dissolution of zinc,

$$Zn + 4OH^- \rightarrow ZnO_2^{2-} + 2H_2O + 2e^-, \tag{19.13}$$

the consumption of alkali is high, since two OH^- ions are needed for each electron liberated, and zincate ions are formed as a soluble product (called the *primary process* in zinc electrode dissolution). The solubility of zincate ions in alkaline solutions having the concentration above is 1 to 2 mol/L. When saturation has been reached, zinc hydroxide starts to sediment on the zinc surface and the primary process practically stops. Here the capacity of the zinc electrode is limited by the available volume of alkali solution rather than by the amount of zinc; about 10 mL of the solution is needed for each ampere-hour. When the current density is very low, the zinc electrode continues to function in the saturated zincate solution, its dissolution now producing insoluble zinc oxide (the *secondary process*):

$$Zn + 2OH^- \rightarrow ZnO + H_2O + 2e^-. \tag{19.14}$$

Since under these conditions, discharge of the cell as a rule results in the production of one OH^- ion for each electron at the positive electrode [Eq. (19.4)], the secondary process overall occurs without the consumption of alkali, and a solution volume of 1 to 2 mL/Ah is practically sufficient for operation of the cell.

Thus, there are two possible modes of utilizing zinc anodes in alkaline solutions. In the first and older mode, only the primary process is used, with monolithic zinc anodes and a large volume of electrolyte. In the second mode, the secondary process is employed, with powdered zinc anodes at which the true current densities are much lower than at smooth electrodes.

19.4.3 Alkaline Manganese Dioxide Batteries

$$MnO_2 \,|\, 27\text{–}40\%\ \text{KOH},\ aq \,|\, Zn \tag{19.15}$$

Compared with the Leclanché batteries, alkaline manganese dioxide batteries offer better performance at high discharge currents and lower temperatures and a better shelf life. They are more expensive than Leclanché batteries, but their cost per unit of energy is competitive and resources of raw materials are sufficient for mass production of these batteries.

Rather than natural ores as in Leclanché batteries, electrolytic manganese dioxide (EMD), which is produced by anodic oxidation of Mn^{2+} ions at graphite electrodes in solutions of manganese salts, is used as the active material for the positive

electrode. Owing to a higher conductivity of the alkaline solution and lack of precipitation of solid $Zn(NH_3)_2Cl_2$, a smaller volume of electrolyte solution than in Leclanché batteries is needed in the pores of the active mass. Hence, alkaline cells contain more MnO_2 than do Leclanché batteries of the same size, and their capacity at low current drains is 50% higher. At high current drains where Leclanché batteries have a much lower capacity, alkaline batteries then have a capacity that is higher by a factor of 3 to 6.

19.5 STORAGE BATTERIES

19.5.1 Lead–Acid Batteries

$$PbO_2 \,|\, 30\text{–}40\%\ H_2SO_4,\ aq \,|\, Pb \tag{19.16}$$

Lead batteries are the storage batteries most widely used at present. This is readily explained by their low price, high reliability, and good performance. Their cycle life is a few hundred charge–discharge cycles, and for some cell types, even more than 1000 cycles.

The first working lead cell, manufactured in 1859 by a French scientist, Gaston Planté, consisted of two lead plates separated by a strip of cloth, coiled, and inserted into a jar with sulfuric acid. A surface layer of lead dioxide was produced by electrochemical reactions in the first charge cycle. Later developments led to electrodes made by pasting a mass of lead oxides and sulfuric oxide into grids of lead–antimony alloy.

Current-Producing Reactions In the charged lead battery, the negative electrode contains sponge lead and the positive electrode contains lead dioxide, PbO_2. The current-producing reactions during charge (ch) and discharge (disch) are described by the following equations:

$$(+) \qquad PbO_2 + 3H^+ + HSO_4^- + 2e^- \underset{\text{ch}}{\overset{\text{disch}}{\rightleftharpoons}} PbSO_4 + 2H_2O; \tag{19.17}$$

$$(-) \qquad Pb + HSO_4^- \underset{\text{ch}}{\overset{\text{disch}}{\rightleftharpoons}} PbSO_4 + H^+ + 2e^-; \tag{19.18}$$

$$\text{(cell)} \qquad PbO_2 + Pb + 2HSO_4^- \underset{\text{ch}}{\overset{\text{disch}}{\rightleftharpoons}} 2PbSO_4 + 2H_2O. \tag{19.19}$$

(At the concentrations used in the batteries, sulfuric acid is practically dissociated into H^+ and HSO_4^- ions.) Thus, discharge of the battery consumes sulfuric acid and produces barely soluble lead sulfate on both electrodes. This reaction mechanism was suggested as early as 1881 by Gladstone and Tribe in their theory of *double sulfatation*. The concentration of sulfuric acid drops from 30–40% (depending on battery type) in a charged lead–acid battery to 12–24% at the end of discharge.

Passivation During discharge the active materials are not fully utilized: At low current drains the degree of utilization is 40 to 60%. At high drains it drops to 5 to 10%,

which is due to concentration polarization (i.e., a sharp decrease to almost zero in sulfuric acid concentration in the pores of the positive electrode). At small drains, a premature drop in discharge voltage is caused by passivation of the electrodes coming about by shielding of the active materials (both lead and lead dioxide) by formation of a dense, fine-grained layer of lead sulfate.

Special additives such as barium sulfate, potassium lignosulfonate, and tanning agents are introduced into the active material to reduce passivation of the negative electrodes. The organic additives are adsorbed at the surface of lead and lead sulfate, where they hinder the formation of new nuclei of lead sulfate and promote the growth of larger crystal grains and formation of looser layers. At the same time these additives prevent the sintering of the spongy lead during cycling and storage (hence the term *expander* used for them).

19.5.2 Alkaline Nickel–Cadmium (Iron) Storage Batteries

$$\mathrm{NiOOH}\,|\,20\text{–}22\%\ \mathrm{KOH},\ aq\,|\,\mathrm{Cd} \tag{19.20}$$

Ni–Cd storage batteries have a long cycle life (a few thousand charge–discharge cycles), are compact in size, and are easy to operate. The first patent for a Ni–Cd battery was granted in 1901 to a Swedish engineer, Waldemar Jungner. Pocket-type positive electrodes were used in the first alkaline storage batteries. In 1928, first experiments were made with a new electrode type based on sintered porous nickel ("sintered electrodes"). In the early 1930s the development of sealed alkaline batteries was reported (an important point in view of unpleasant and potentially hazardous leakage of alkali from a battery). Both battery types were developed further after World War II, and by about 1950, mass production of these new battery types was begun.

Electrochemical Processes The charged positive electrodes of these batteries contain NiOOH, an oxide hydroxide of trivalent nickel, and the negative electrodes contain metallic cadmium or iron (M). As a rule, KOH solution serves as the electrolyte. The main current-producing reactions on the electrodes and in the cell in general can be written as

$$(+)\qquad 2\mathrm{NiOOH} + 2\mathrm{H_2O} + 2e^- \underset{\text{ch}}{\overset{\text{disch}}{\rightleftharpoons}} 2\mathrm{Ni(OH)_2} + 2\mathrm{OH^-}; \tag{19.21}$$

$$(-)\qquad \mathrm{M} + 2\mathrm{OH^-} \underset{\text{ch}}{\overset{\text{disch}}{\rightleftharpoons}} \mathrm{M(OH)_2} + 2e^-; \tag{19.22}$$

$$(\text{cell})\qquad 2\mathrm{NiOOH} + 2\mathrm{H_2O} + \mathrm{M} \underset{\text{ch}}{\overset{\text{disch}}{\rightleftharpoons}} 2\mathrm{Ni(OH)_2} + 2\mathrm{M(OH)_2}. \tag{19.23}$$

The processes taking place on the positive electrode actually are more complicated. Several modifications of nickel oxides exist which in particular differ in their degrees of hydration, so the equations above do not correctly describe the water balance in the reaction. The hydroxide of divalent nickel is formed as β-$\mathrm{Ni(OH)_2}$ and

has a lamellar structure with disordered crystal lattice. This disorder has a beneficial effect on the electrochemical activity. Charging typically produces an oxide hydroxide of trivalent nickel in the form β-NiOOH. However, at high alkali concentrations or high charge currents, γ-NiOOH that has a large specific volume may form. The resulting swelling leads to a deterioration of contact and deformation of the electrode.

The conductivity of pure $Ni(OH)_2$ is very low but increases markedly even at slight degrees of oxidation. After discharge, the battery's active mass contains a residual 20 to 40% of nonreduced NiOOH, and thus remains sufficiently highly conductive. Upon charging, higher nickel oxides of the type of $NiO_x \cdot yH_2O$ (where x varies between 1.6 and 1.8) as well as NiOOH are formed. The higher oxides are unstable and liberate excess oxygen spontaneously by decomposition. Owing to the temporary existence of higher oxides upon charging, the OCV of freshly charged batteries is higher and amounts to 1.45 to 1.7 V. As these oxides decompose, it decreases gradually to a steady-state value of 1.30 to 1.34 V.

Sintered Electrodes In these electrodes the active materials are present in pores of a sintered nickel support plate. This plate is manufactured by sintering of highly disperse nickel powder produced by thermal decomposition of nickel pentacarbonyl $Ni(CO)_5$. The plates are filled by impregnating them in alternation with concentrated solutions of salts of the corresponding metals (Ni or Cd) and with an alkali solution serving to precipitate insoluble oxides or hydroxides.

Sealed Batteries During charging of the batteries, hydrogen and/or oxygen may evolve at the electrodes. Complete sealing will be admissible only when pressure buildup by evolved gases is avoided. For sealed Ni–Cd batteries, this problem was solved by an appropriate balance of reactants in the battery. This must be such that during charging, reduced nickel is exhausted and anodic oxygen evolution will start at the positive electrode, long before cathodic hydrogen evolution would start at the negative electrode. To this end an excess of the nonreduced cadmium oxide, CdO, is provided in the negative electrode, and battery design is such that oxygen evolved at the positive electrode easily reaches the surface of the negative electrode and reacts with the metallic cadmium formed during charging. The oxygen thus is caught in a closed cycle of anodic evolution and cathodic reaction and cannot accumulate.

Nickel–Iron Storage Batteries The first alkaline nickel–iron storage batteries were proposed in 1901 by Thomas Alva Edison. They have design features and properties similar to those of nickel–cadmium batteries, although some of their parameters are different. The main difference resides in the potential of the negative electrodes: The equilibrium potential of the cadmium electrode is 20 mV more positive, and the equilibrium potential of the iron electrode is 50 mV more negative than the equilibrium hydrogen potential in the same solution. This difference is small but very significant, inasmuch as the iron electrode can corrode with concomitant hydrogen evolution, leading to an appreciable self-discharge of the battery. For cadmium this process is thermodynamically unfeasible; hence, cadmium is corrosion resistant

and the self-discharge of nickel–cadmium batteries is very low. Nickel–iron batteries are very rugged, much cheaper than nickel–cadmium batteries, and are used primarily in industrial transport applications.

Nickel–Hydride Storage Batteries An important advance in alkaline nickel storage batteries has been the introduction of metal hydrides as the active material in the negative electrode. As early as about 1950 it was evident that certain metal alloys could reversibly take up considerable quantities of hydrogen into their crystal lattice (i.e., form metal hydrides). The equilibrium potential of such alloys after hydrogen uptake in a solution is close to that of the hydrogen electrode, and upon anodic polarization, the hydrides yield electrical charge equivalent to the amount of absorbed hydrogen.

Nowadays, such hydride electrodes are used widely to make alkaline storage batteries which in their design are similar to Ni–Cd batteries but exhibit a considerably higher capacity than these. These two types of storage battery are interchangeable, since the potential of the hydride electrode is similar to that of the cadmium electrode. The metal alloys used to prepare the hydride electrodes are multicomponent alloys, usually with a high content of rare-earth elements. These cadmium-free batteries are regarded as environmentally preferable.

19.5.3 Silver–Zinc Batteries

Attempts to develop a rechargeable battery with zinc negative electrodes were made repeatedly as early as the 1890s. The first successful silver–zinc battery was developed in 1941 by a French scientist, H. André, whose cell design had two essentially new features: the use of a swelling cellophane-type material for separators and a strictly limited volume of electrolyte solution, so that the zinc electrode operated only via the secondary process. Despite their high cost, these batteries immediately attracted great attention, owing to their excellent performance, with specific energies as high as 130 Wh/kg or 300 Wh/dm^3 (three to four times more than for other storage batteries), and their slight load dependence.

Rechargeable zinc electrodes have two major problems. During charging of the battery and electrolytic zinc deposition [reaction (19.3) from right to left], zinc crystallizes in the form of thin, branching crystals (dendrites) which grow into the solution and reach the opposite electrode rapidly, leading to an internal short circuit and breakdown of the battery. During cycling of the battery a gradual migration of active materials of the zinc electrode can be observed (shape change of the electrode). There are many possible causes for such a migration (nonuniform current distribution over the electrode surface, gravitational forces, etc.). Using a swelling separator and operating with only the secondary zinc process, it was possible to mitigate the consequences of these adverse effects, but so far their causes are not well understood, and no means are known to prevent them completely. For these reasons the cycle life of silver–zinc storage batteries is rather limited; depending on the cycling mode, it amounts to no more then 30 to 100 cycles.

19.6 LITHIUM BATTERIES

Long ago it was already a very tempting idea to use lithium or other alkali metals as a negative electrode in batteries. These metals have a markedly more negative thermodynamic value of electrode potential than other metals, hence would be expected to lead to much higher open-circuit and discharge voltages and, as a result of these higher voltages, to higher specific energies of the corresponding batteries. Because of their high chemical activity and of their violent interaction with water and other protonic solvents, however, the alkali metals are difficult to use in batteries, and all attempts to design batteries with alkali metals and aqueous electrolyte solutions proved futile. But starting in the 1960s, another avenue was opened up when batteries containing lithium and aprotic electrolyte solutions were introduced and broadly developed.

19.6.1 Throwaway Cells with Electrolyte Solutions Prepared from Aprotic Organic Solvents

The solvents used in one type of throwaway cells are propylene carbonate (PC), tetrahydrofuran (THF), dimethylformamide (DMF), γ-butyrolactone (BL), and other aprotic solvents (see Section 8.2). Certain lithium salts, such as the perchlorate, $LiClO_4$, and the tetrachloroaluminate, $LiAlCl_4$, have a rather high solubility in these solvents. The resulting solutions have a conductivity that is high enough for them to be used in batteries. The cathode materials used in these batteries are manganese dioxide, MnO_2, fluorinated carbon, CF_x, iron sulfide, FeS_2, and quite a few other inorganic compounds. During discharge, metallic lithium dissolves anodically while its ions undergo intercalation into the cathodes, for instance,

$$MnO_2 + xLi^+ + xe^- \rightarrow Li_xMnO_2 \tag{19.24}$$

Batteries of this type have rather high specific energies (up to 600 Wh/kg), their reliability is satisfactory, and they can be stored for a long time without marked self-discharge. A certain disadvantage is the relatively low value of the highest admissible discharge current density (this is not over 2 to 3 mA/cm^2), which is due to the slowness of lithium ion intercalation into the cathode materials.

19.6.2 Lithium–Thionyl Chloride Throwaway Batteries

In batteries of this type, solutions of lithium salts in thionyl chloride, $SOCl_2$, are used as the electrolyte. Exceptionally, this strongly oxidizing solvent also serves as the active material for the cathodic reaction. Thus, during discharge thionyl chloride is electrochemically reduced at a cathode made of carbon materials:

$$2SOCl_2 + 4Li^+ + 4e^- \rightarrow SO_2 + S + 4LiCl. \tag{19.25}$$

In contrast to lithium ion intercalation into solid inorganic compounds, this reaction is fast, and the corresponding batteries sustain high dicharge current densities (up to 50 mA/cm^2).

These batteries are used mainly for specialized technical equipment where power sources of small size but high power are needed. During early production years, cases of rather violent spontaneous explosion were observed, so that domestic uses were ruled out. The specific energy can be as high as 1000 Wh/kg, which is the highest value among known types of electrochemical power sources.

19.6.3 Rechargeable Lithium Batteries

Because of their high specific energies in terms of volume and of mass, throwaway lithium batteries have become remarkably popular during the last decade as power sources for small instruments in both the mass consumer sector (watches, digital cameras, mobile phones, calculators, etc.) and in specialized equipment. Multimillion production figures exist in a number of countries. Still, the production volume of throwaway lithium batteries is only a small fraction of the total production volume of all throwaway batteries. The major limiting factor for a wider use of lithium batteries is their high cost, which arises from the need for carefully purified chemicals and from the relatively high labor cost.

For these reasons the design of rechargeable lithium batteries that can be reused is of great interest. The major obstacle here is the poor reversibility of the lithium electrode. During battery charging, spongy lithium is deposited from the solution. For various reasons, including rapid oxidation, this deposit rapidly loses contact with the bulk of the lithium electrode. Hence, with every discharge–charge cycle of such a battery, the amount of lithium participating in the electrode reaction decreases, and the battery's discharge capacity drops off.

The design of *lithium ion batteries* has been a great achievement toward overcoming this defect. In these rechargeable batteries, a carbon matrix material is used instead of lithium as the negative electrode which, during charging, takes up lithium ions by cathodic intercalation:

$$x\mathrm{Li}^+ + \mathrm{C}_n + xe^- \underset{\text{disch}}{\overset{\text{ch}}{\rightleftharpoons}} \mathrm{Li}_x\mathrm{C}_n. \tag{19.26}$$

(Often, the assumption is made that $n = 6$; i.e., calculations are referred to the graphite ring C_6 as a unit in the carbon matrix material.)

The intercalate $\mathrm{Li}_x\mathrm{C}_6$ has a sufficiently negative electrode potential; at values of x close to unity, it is a mere 0.5 V more positive than the potential of metallic lithium, which implies that the activity of lithium in the intercalate is rather high and close to that of metallic lithium. During discharge, the lithium ions undergo anodic deintercalation, which continues until the supply of lithium ions intercalated during charging is exhausted. An important advantage of the lithium ion electrode is the lack of formation of loose, spongy lithium during charging. For this reason, such electrodes will sustain long-term cycling (more than 1000 cycles without an important loss of performance).

Materials for the positive electrode are selected among those which, unlike carbon, will intercalate lithium ions during anodic polarization (i.e., during discharge) while retaining a sufficiently highly positive value of potential. During charging of these electrodes, lithium ions undergo deintercalation. The first materials suggested for these purposes were titanium disulfide, TiS_2, and various vanadium oxides with working potentials around 3 V (relative to the potential of a metallic lithium electrode). Subsequently, materials with even more positive values of potential (up to 4 V) were found: for instance, partially lithiated oxides of nickel, cobalt, and manganese; Li_yNiO_2, Li_yCoO_2, and $Li_yMn_2O_4$. Cycling of such an electrode involves a reaction of the type

$$Li_yNiO_2 + xLi^+ + xe^- \underset{\text{disch}}{\overset{\text{ch}}{\rightleftharpoons}} Li_{y+x}NiO_2. \tag{19.27}$$

In summary, cycling of a lithium ion battery is attended by lithium ions passing through the electrolyte from the negative to the positive electrode on charge, and in the opposite direction on discharge. For this reason the term *rocking-chair batteries* was coined for batteries of this type.

19.6.4 Scientific Problems in the Field of Lithium Batteries

Apart from the work toward practical lithium batteries, two new areas of theoretical electrochemistry research were initiated in this context. The first is the mechanism of passivation of highly active metals (such as lithium) in solutions involving organic solvents and strong inorganic oxidizers (such as thionyl chloride). The creation of lithium power sources has only been possible because of the specific character of lithium passivation. The second area is the thermodynamics, mechanism, and kinetics of electrochemical incorporation (intercalation and deintercalation) of various ions into matrix structures of various solid compounds. In most lithium power sources, such processes occur at the positive electrode, but in some of them they occur at the negative electrode as well.

Problems in these two areas are under investigation in a number of research groups around the globe. The second area is addressed in Chapter 25 and the first area is described below.

Lithium Electrode Passivation Thermodynamically speaking, lithium–electrolyte systems are not in equilibrium, and theoretically, it should be possible for the solvent to be reduced by reacting with lithium (even more so when liquid oxidizers such as thionyl chloride are used as the solvent). Yet under certain high-purity conditions (particularly in the complete absence of traces of water or other protonic substances), the rate of this interaction and hence, in a battery, the rate of self-discharge are negligibly low. In an experiment, a commercial lithium–copper oxide cell had lost less than 2% of its capacity after 16 years of storage. Such data for low-capacity losses correlate with data obtained by microcalorimetry which indicate that the amount of heat liberated by lithium corrosion and cell self-discharge is exceedingly small. It follows that production conditions satisfying the basic requirements of high

purity of the solvents and other chemicals (and the maximum level of residual water traces) can be realized in practice.

The corrosion resistance of lithium electrodes in contact with aprotic organic solvents is due to a particular protective film forming on the electrode surface when it first comes in contact with the solvent, preventing further interaction of the metal with the solvent. This film thus leads to a certain passivation of lithium, which, however, has the special feature of being effective only while no current passes through the external circuit. The passive film does not prevent any of the current flow associated with the basic current-generating electrode reaction. The film contains insoluble lithium compounds (oxide, chloride) and products of solvent degradation. Its detailed chemical composition and physicochemical properties depend on the composition of the electrolyte solution and on the various impurity levels in this solution.

The low corrosion rate of lithium notwithstanding, certain unresolved practical problems persist in this area. This is true in particular for the behavior of lithium cells following interruptions of the discharge process. It was seen that immediately after termination of a discharge episode, the corrosion rate is considerably higher than prior to discharge. Impedance measurements have shown that the resistance of the protective film on the lithium surface when measured after a discharge episode is considerably lower than that of the original film. This question is highly relevant for the practical use of lithium batteries, where, as a rule, intermittent discharge modes are prevalent.

REFERENCES

André, H., *Bull. Soc. Fr. Electr*., Ser. 60, 1132 (1941).

Edison, Thomas A., Reversible galvanic battery, U.S. patent 678,722, 1901.

Gladston, J. H., and A. Tribe, *Nature*, **25**, 221, 461 (1881).

Jungner, W., Swedish patent 1556722, January 1901.

Leclanché, G.-L., *Compt. Rend.*, **83**, 54 (1876).

Planté, G., *Compt. Rend.*, **49**, 402 (1859); **50**, 640 (1860).

Ragone, D. V., *Proc. Society of Automotive Engineers Conference on Review of Battery Systems for Electrically Powered Vehicles*, SAE, Warrendale, PA, 1968.

REVIEWS

Bagotzky, V. S., and A. M. Skundin, *Chemical Power Sources*, Academic Press, London, 1980.

Besenhard, J. O., Ed., *Handbook of Battery Materials*, Wiley-VCH, Chichester, West Sussex, England, 1999.

Skundin, A. M., O. N. Efimov, and O. V. Yarmolenko, The state-of-the-art and prospects for the development of rechargeable lithium batteries, *Russ. Chem. Rev*., **71**, 329 (2002).

Vincent, C. A., and B. Scrosati, *Modern Batteries: An Introduction to Electrochemical Power Sources*, Edward Arnold, London, 1997.

20
Fuel Cells

20.1 INTRODUCTION

The initial aim of work on fuel cells had been that of realizing an idea that originally had been propounded by Wilhelm Ostwald as early as 1894, of converting the chemical energy of natural fuels directly electrochemically to electrical energy. (In his paper, he wrote: "In the future power production will be connected with electrochemistry.") This conversion would circumvent the intermediate generation of thermal energy, so that its efficiency would not be subject to the restrictions (Carnot cycle) of the second law of thermodynamics. It could thus be higher than that in thermal engines producing electrical energy by traditional ways.

Ostwald's idea, based on thermodynamics, ignored the kinetic aspects, and early experimental work on fuel cells revealed the large difficulties inherent in a direct electrochemical oxidation of a natural fuel such as coal (Baur and Tobler, 1933). Cells using hydrogen as a fuel proved to be an easier task, but despite the early discoveries by William R. Grove in 1839, it was only in the early 1940s that practical, operative fuel cells of this type could be set up in the laboratory (Spiridonov, 1941; Davtyan, 1947). In 1947, Oganes K. Davtyan published the first monograph on the problem of fuel cells,

A relatively large hydrogen–oxygen fuel battery was designed by Francis Bacon in England in 1960. In the cells of this battery a concentrated alkaline electrolyte was used. The working temperature was 200 to 240°C, the gas pressure, 2 to 4 MPa. The electrical power was about 5 kW. After this demonstration of a working fuel cell battery by Bacon, research into fuel cells gained strong momentum worldwide.

At this time, the original aim of creating devices for more efficient production of grid power was supplemented by the further aim of creating autonomous power sources that would operate under conditions where grid power was unavailable, such as in certain means of transport, in mobile devices, and in remote areas. The term *fuel cell* now began to lose its original meaning of an electrochemical power source converting natural fuel and acquired the new meaning of an electrochemical power source which, in contrast to ordinary batteries, would work continuously as long as the reactants [i.e., a reducer ("fuel") and an oxidizer] were supplied.

Fundamentals of Electrochemistry, Second Edition, By V. S. Bagotsky

In most cases, fuel cells are operated with air oxygen as the oxidizer. Pure oxygen can be used when no air is available, as in submarines or spaceships. The reducer most often is hydrogen, either pure or technical grade, that is produced by steam conversion or gasification reactions of natural gas, petroleum products, and/or other liquid organic compounds.

Major types of hydrogen–oxygen fuel cells broadly developed since about 1960 are the following:

1. *Alkaline fuel cells* (AFCs). The electrolyte is 40 to 70% KOH, the working temperatures are 60 to 240°C. Such systems were used in the spacecraft of the *Apollo* program and in the U.S. space shuttle.
2. *Medium-temperature phosphoric acid fuel cells* (PAFCs). The electrolyte is 85 to 95% phosphoric acid; the working temperatures are 180 to 200°C. Such systems were used to build numerous autonomous power plants with an output of up to about 250 kW, and even some with an output of up to 4 MW, in the United States, Japan, and other countries.
3. *High-temperature molten-carbonate fuel cells* (MCFCs). The electrolyte is a molten mixture of carbonates of sodium, potassium, and lithium; the working temperature is about 650°C. Experimental plants with a power of up to 0.5 MW have been built with such systems in the United States and Japan.
4. *High-temperature solid-oxide fuel cells* (SOFCs). The working electrolyte is a solid electrolyte based on zirconium dioxide doped with oxides of yttrium and other metals; the working temperatures are 800 to 1000°C. Experimental plants with a power of up to 100 kW have been built with such systems in the United States and Japan.
5. *Membrane-type fuel cells*. The electrolyte is a polymeric ion-exchange membrane; the working temperatures are 60 to 100°C. Such systems were first used in *Gemini* spaceships. These fuel cells subsequently saw a rather broad development and are known as (solid) polymer electrolyte or proton-exchange membrane fuel cells (PEMFCs).

From about 1990, renewed interest and activity in the design of improved fuel cells has been evident, essentially for the following two reasons:

1. Following the environmental degradation caused by rising motor vehicle populations in a number of agglomerations, authorities started to insist by legislation that a certain percentage of "zero-emission" vehicles be introduced (e.g., in California). For this reason, almost all large automakers in the world have now begun to develop versions of electric vehicles and fuel-cell-based power plants for these vehicles.
2. Longer uninterrupted operation of a number of smaller electronic devices (mobile phones, portable PCs, etc.) will require the ordinary batteries driving them to be replaced by power sources of higher capacity.

The greatest advances were made in the field of membrane-based fuel cells. Current models drastically differ from the first prototypes of the 1960s in their design and performance parameters. Work was started as well on fuel cells of a new type known as direct methanol fuel cells (DMFCs), where methanol as a convenient liquid fuel replaces hydrogen, which is inconvenient because of the difficulties inherent in its handling, storage, and transport. Methanol is regarded as a promising fuel for future automobiles.

20.2 DESIGN PRINCIPLES OF FUEL CELLS

Fuel-cell-based power plants (or *electrochemical generators*, the rather appropriate Russian term) have several constituent parts: (1) the fuel cell battery or stack itself; (2) vessels for the reactants (hydrogen or methanol; oxygen when needed); (3) special devices controlling the supply of reactants and withdrawal of the reaction products according to their consumption and formation in the electrochemical reactions; (4) devices for temperature and, where applicable, moisture control in the stack; and (5) devices for power conditioning (current, voltage).

In hydrogen–oxygen fuel cells, gas-diffusion electrodes are used. In Bacon's battery, they were of a hydrophilic type and worked with a certain excess gas pressure (see Section 18.4.2). Almost all later models of hydrogen–oxygen fuel cells used hydrophobized gas-diffusion electrodes consisting of a porous hydrophobic diffusion layer and a catalytically active layer. The diffusion layer is usually made of carbon black (acetylene or other) and some 35% (by mass) of PTFE applied to a conducting substrate (most often, thin graphitized cloth). Its porosity is as high as 45 to 60%, which is particularly important when air rather than pure oxygen is supplied as the oxidizer and nitrogen must diffuse back out.

In the design of membrane-type fuel cell stacks (batteries), membrane–electrode assemblies (MEAs) are used, which consist of a sheet of membrane and of the two electrodes (positive and negative) pressed onto it from either side.

Fuel cells as a rule are stacked according to a filter-press design. A certain number of membrane–electrode assemblies are combined in series to a block having the desired working voltage. Bipolar plates that secure electrical contact between the individual elements and separate the gas and electrolyte compartments of neighboring elements are arranged between the diffusion layer of the positive electrode in one element and the diffusion layer of the negative electrode in its neighbor element. It follows that these plates must be impermeable to gases and liquids and have a good electronic conductivity. In early models, these plates were titanium, gold-plated to lower the contact resistance. Today, graphite plates are used. For their additional function in gas transport, they have channels about 0.2 mm deep which serve to distribute the gases to the entire surface area of the diffusion layers of each electrode. Such patterned plates are rather expensive unless pressed from conductive plastic material.

20.3 PROTON-EXCHANGE MEMBRANE FUEL CELLS

20.3.1 Major Development Stages

The first version of a membrane fuel cell stack having a power of 1 kW was built in the early 1960s by General Electric Co. for the *Gemini* spacecraft. A sulfonated polystyrene ion-exchange membrane was used as an electrolyte in these cells. The electrodes contained about 4 mg/cm^2 of platinum catalyst. Because of the membrane's considerable ohmic resistance, the current density was less than 100 mA/cm^2, while the voltage of an individual element was 0.6 to 0.7 V, so the specific power was not over 50 mW/cm^2. Owing to insufficient chemical resistance of these membranes, the overall service life of the stack was less than 2000 h.

Following a period of slack, decisive improvements were made after 1990 in the area of PEMFCs. Modern models now achieve specific powers of over 600 to 800 mW/cm^2 while using less than 0.4 mg/cm^2 of platinum catalysts and offering a service life of several tens of thousands of hours. These advances were basically attained by the combination of two factors: (1) using new proton-exchange membranes of the Nafion type, and (2) developing ways toward much more efficient utilization of the platinum catalysts in the electrodes.

20.3.2 Membranes

Starting in the early 1970s, Du Pont began commercialization of their new Nafion ion-exchange membranes. They consist of a perfluorinated sulfonic acid polymer having a compact hydrophobic backbone of $-(CF_2)_n-$ groups invested with a certain number of hydrophilic groups terminating in $-SO_3H$. The perfluorinated backbone provided a chemical stability many times higher than that of other membranes known up to that time, so that the lifetime of fuel cells incorporating such a membrane could be improved by two to three orders of magnitude. Upon proper wetting of the membrane, the sulfonic acid groups dissociate and secure a relatively high protonic conductivity, about 0.1 S/cm at 80°C, which is three to four times more than that of older membranes. The complex production process and, accordingly, the relatively high price are certain disadvantages of the Nafion membranes.

The usual working temperature of fuel cells with Nafion-type membranes is 80 to 90°C. Under these conditions, moisture must be supplied to keep the membranes wet, which usually is attained by passing the reactant gases through water that is somewhat warmer (by 5 to 10°C) than the cell's working temperature, thus saturating them with water vapor.

20.3.2 Platinum Catalysts

In the first membrane-type fuel cells, the dispersed platinum catalyst was pure metal because of its large consumption. Smaller consumption and a much more efficient utilization of the platinum catalyst were attained by depositing the metal on a highly disperse carbon carrier. The best results were attained by using Vulcan XC-72 furnace

black, possibly because of its sulfur impurities, which lead to special surface properties.

The platinum concentrations in the platinized carbon blacks are reported to be between 10 and 40% (by mass), sometimes even higher. At low concentrations the specific surface area of the platinum on carbon is as high as 100 m^2/g, whereas unsupported disperse platinum has surface areas not higher than 10 to 15 m^2/g. However, at low platinum concentrations, thicker catalyst layers must be applied, which makes reactant transport to reaction sites more difficult. The degree of dispersion and catalytic activity of the platinum depend not only on its concentration on the carrier but also on the chemical or electrochemical method used to deposit it.

A considerable decrease in platinum consumption without performance loss was attained when a certain amount (30 to 40% by mass) of the proton-conducting polymer was introduced into the catalytically active layer of the electrode. To this end a mixture of platinized carbon black and a solution of (low-equivalent-weight "ionomeric") Nafion is homogenized by ultrasonic treatment, applied to the diffusion layer, and freed of its solvent by exposure to a temperature of about 100°C. The part of the catalyst's surface area that is in contact with the electrolyte (which in the case of solid electrolytes is always quite small) increases considerably, due to the ionomer present in the active layer.

A further improvement in the catalyst–membrane contact is attained by hot-pressing the hydrogen and oxygen electrode with their catalytically active layers against the membrane (during 1 to 5 min at a temperature of 130 to 155°C and a pressure of 15 to 70 kg/cm^2). This operation produces single membrane–electrode assemblies (MEAs) 0.7 to 1.2 mm thick (Gottesfeld and Zawodzinski, 1997).

20.3.4 Poisoning of Platinum by CO Impurities in the Hydrogen

In most cases, fuel cells are operated not on pure (electrolytic) hydrogen but on technical hydrogen produced by converting liquid fuels such as methanol or petroleum products. Even after an initial purification, technical hydrogen always contains carbon monoxide (CO) and a number of other substances as trace impurities. Even low levels of CO in hydrogen (less than 10 ppm) give rise to marked polarization of the hydrogen electrode. This polarization is caused by strong specific adsorption of CO, leading to poisoning of the platinum catalyst. The fraction of platinum surface that remains free for adsorption and subsequent electrochemical oxidation of hydrogen decreases sharply upon CO adsorption.

A few possibilities exist to fight this phenomenon:

1. When raising the working temperature of the fuel cell to, for instance, 120 to 130°C instead of the usual 80 to 90°C, one shifts the adsorption equilibrium between hydrogen and CO in favor of hydrogen, which implies a higher maximum admissible concentration of CO in hydrogen. This is evident from the phosphoric acid fuel cells working at 180 to 200°C, where despite the use of platinum catalysts, CO concentrations in the hydrogen of up to 100 ppm can be admitted. However, at working

temperatures of over 100°C, the membranes in PEMFCs will dry out, and their resistance rises drastically.

2. A more reliable and promising possibility of fighting poisoning of the platinum catalysts by CO is catalyst modification by alloying. It could be shown in particular that platinum–ruthenium catalysts are much less sensitive to poisoning by traces of CO in the hydrogen than pure platinum. Possibly this is due to a much lower adsorption energy of CO because of a different crystal structure or electronic state of the alloy.

At present, anodes containing platinum–ruthenium catalyst (with about 50 atom % of Ru) are used in most membrane fuel cells designed for the use of technical hydrogen.

All these developments have helped to lower the content of platinum metals to 0.05 mg/cm^2 at the hydrogen electrode and to 0.1 mg/cm^2 at the oxygen electrode while preserving performance. The power density of hydrogen–oxygen fuel cells with the new membrane–electrode assemblies is assumed to be 500 to 700 mW/cm^2 when working with pure oxygen and a value three to four times less when working with air at ambient pressure. Today, PEMFCs and power plants based on such systems are built by a number of companies in America and Europe.

20.4 DIRECT METHANOL FUEL CELLS

20.4.1 Major Development Stages

Methanol is a very promising type of fuel for fuel cells. Its handling, storage, and transport are much less dangerous and much more convenient than those of hydrogen gas. These advantages are particularly important when designing small low-power fuel cells for supplying electronic devices such as portable PCs and mobile phones. Methanol is quite active electrochemically, in contrast to petroleum products and other potential organic fuels. Its specific energy comes close to that of gasoline. For this reason it is discussed as a potential fuel in fuel cells powering electric cars.

Two possibilities exist in the use of methanol for fuel cells: (1) its prior catalytic or oxidative conversion to technical hydrogen, and (2) its direct anodic oxidation at the fuel cell electrodes. The first possibility implies a need for additional bulky equipment for methanol conversion and subsequent purification of the technical hydrogen produced. The more attractive second possibility implies certain difficulties arising from the relatively slow anodic oxidation of methanol, even at highly active platinum electrodes, but is pursued vigorously at present by the design of direct methanol fuel cells.

The direct anodic oxidation of methanol became much more attractive after it was shown that platinum–ruthenium alloys are catalytically much more active in this reaction than pure platinum (pure ruthenium is totally inactive in this reaction).

Very early during research into the anodic oxidation of methanol in the 1960s, it was repeatedly attempted to build experimental models of methanol–oxygen or methanol–air fuel cells. Most of these studies were conducted in sulfuric acid solutions

containing methanol; hence the same electrolyte was used for the first fuel cells. Owing to the slow rate of methanol oxidation at platinum, large amounts of platinum catalyst had to be used. For this reason, interest vaned, and for three decades little was published in the scientific and technical literature on methanol fuel cells.

The situation changed drastically in the mid-1990s in view of the considerable advances made in the development of membrane hydrogen–oxygen (air) fuel cells, which could be put to good use for other types of fuel cells. At present, most work in methanol fuel cells utilizes the design and technical principles known from the membrane fuel cells. Both fuel-cell types use Pt–Ru catalyst at the anode and pure platinum catalyst at the cathode. The membranes are of the same type.

The major difference between the two fuel-cell types resides in reactant supply. For methanol fuel cells, methanol supply can be either as vapor (after evaporation in a special evaporator) or as solute in the aqueous solution (in concentrations between 2 and 5 mol/L). The second variant has the advantage that there is no need to moisten the reactant gases to keep the perfluorinated membrane in working condition at the working temperatures of 60 to 100°C. It is necessary, on the other hand, to remove excess water. Water will diffuse through the membrane to the side of the cathode and must be removed from there by forced air (or oxygen) convection. When water removal is insufficient, a risk of flooding and ensuing loss of operability of the cathode arises.

20.4.2 Methanol Permeation Through the Membrane

A basic problem in the operation of direct methanol fuel cells is the gradual permeation of methanol to the side of the oxygen electrode by diffusion through the membrane. This process, termed *methanol crossover*, has two undesirable effects: (1) unproductive losses of methanol, and (2) setting up of a mixed potential at the oxygen electrode (i.e., a negative potential shift of this electrode, and hence a drop in working voltage of the cell). At the cathode, methanol that has arrived by diffusion is oxidized directly to CO_2 at the platinum catalyst without generating current. For this reason, the maximum concentration of methonol used when supplying it in aqueous solution is about 2 mol/L, even though the cell parameters improve when higher concentrations are used.

20.4.3 Development Prospects

The development of highly efficient methanol fuel cells depends on a number of scientific aspects: (1) the development of more highly active catalysts for methanol oxidation at temperatures not over 60 to 70°C (desirable in cells without ruthenium, which is in short supply); (2) the development of selective catalysts for the oxygen electrode (i.e., of catalysts insensitive to the presence of methanol); and (3) the development of new membrane materials having a lower methanol permeability.

Another tempting task is that of replacing toxic methanol with less toxic materials, such as ethanol, glycol, and similar chemicals, which would necessitate the development of new catalyst variants able to oxidize these substances efficiently.

REFERENCES

Bacon, F. T., *Ind. Eng. Chem*., **52**, 301 (1960).

Baur, E., J. Tobler, *Z. Elektrochem*., **39**, 168 (1933).

Grove, W., *Philos. Mag.*, **14**, 447 (1839).

Ostwald, W., *Z. Elektrochem*., **1**, 122 (1894).

Spiridonov, P., *Nauka Zhizn* [in Russian], **6**, 22 (1941).

MONOGRAPHS AND REVIEWS

Acres, G. J. K., Recent advances in fuel cell technology and its application, *J. Power Sources*, **100**, 60 (2001).

Cacciola, G., V. Antonucci, and S. Freni, Technology updates and new strategies on fuel cells, *J. Power Sources*, **100**, 67 (2001).

Costamagna, P., and S. Srinivasan, Quantum jumps in the PEMFC science and technology from the 1960s to the year 2000: I. Fundamental scientific aspects; II. Engineering, technology development and application aspects, *J. Power Sources*, **102**, 242, 253 (2001).

Davtyan, O. K., *The Problem of Direct Conversion of the Chemical Energy of Fuels into Electrical Energy* [in Russian], Publishing House of the USSR Academy of Sciences, Moscow, 1947.

Gottesfeld, S., and T. A. Zawodzinski, Direct methanol oxidation fuel cells: from a 20th century electrochemist's dream to a 21st century emerging technology, in *Electrochemical Science and Engineering*, R. C. Alkire et al., Eds., Vol. 5, Wiley, New York, 1988.

Kordesch, K., and G. Simader, *Fuel Cells and Their Application,* VCH, Weinheim, Germany, 1996.

McNicol, B. D., D. A. J. Rand, K. R. Williams, Fuel cells for road transportation purposes—yes or no? *J. Power Sources*, **100**, 47 (2001).

Perry, M. L., and T. F. Fuller, Historical perspective of fuel cell technology in the 20th Century, *J. Electrochem. Soc*., **149**, 59 (2002).

Vielstich, W., Ed., *Handbook of Fuel Cells*, Vol. 1, Wiley-VCH, Weinheim, Germany, 2002.

21
Some Electrochemical Devices

21.1 ELECTROCHEMICAL CAPACITORS AND SUPERCAPACITORS

Electrostatic capacitors are widely used as reactive elements in ac circuits and electronic devices for the temporary storage of electric charge (and electrical energy) and its subsequent delivery in the form of brief, high-power electrical pulses. Interest has arisen more recently in building various new types of capacitors based on electrochemical systems and having higher energy storage capacity. We dwell briefly on the basic properties of ideal electrostatic capacitors in order to provide a clearer understanding of the special features of various types of capacitors and of their differences relative to other types of electrochemical devices for electrical energy storage.

21.1.1 Ideal Electrostatic Capacitor

An ideal (classical) electrostatic capacitor consists of two plane-parallel metal plates having surface areas S and a mutual distance δ, the gap being filled with air or a dielectric layer (the latter variety often is called a *film capacitor*). When a capacitor is charged (by applying an electrostatic potential difference $\Delta\psi$ between the two plates), electrical charges $+Q$ (an electron deficit) and $-Q$ (an electron excess), which are equal in magnitude but opposite in sign, will accumulate on the plates. The values of Q are proportional to the potential difference:

$$Q = C\,\Delta\psi. \tag{21.1}$$

The electrostatic capacity, C, of the capacitor (in farads) is given by

$$C = \frac{S\varepsilon\varepsilon_0}{\delta}, \tag{21.2}$$

where $\varepsilon_0 = 8.85 \times 10^{-12}$ F/m is the permittivity of free space (vacuum), and ε is the relative permittivity of the dielectric between the plates.

Fundamentals of Electrochemistry, Second Edition, By V. S. Bagotsky

An important parameter of all capacitors, apart from their electrostatic capacity, is the maximum potential difference, $(\Delta\psi)_{max}$, between the plates which can be admitted before relation (21.1) is upset (e.g., because of electric breakdown).

Placing an additional amount of charge dQ on a partly charged capacitor requires doing work against electrostatic repulsion forces: $dW = \Delta\psi\ dQ$. The total electric energy accumulated in a capacitor with charge Q is given [with Eq. (21.1)] by

$$W_e = \int_0^Q \Delta\psi\ dQ = \int_0^Q Q\ \frac{dQ}{C} = \frac{Q^2}{C} = C(\Delta\psi)^2, \tag{21.3}$$

which means that the energy accumulated is proportional to the square of the potential difference.

During discharge of the capacitor, its voltage falls linearly with the amount of charge removed. Usually, discharge is not allowed to occur all the way to zero voltage but only to a given final voltage, $(\Delta\psi)_{fin}$, so that the amount of electrical energy given off is smaller as well.

Large energies cannot be accumulated, owing to the limitations concerning the largest admissible values of $\Delta\psi$. In their specific energy storage capacity, capacitors are much inferior to other devices for the accumulation and storage of electrical energy. Thus, a capacitor of 10 μF is needed to accumulate at a potential difference of 100 V and an energy of 1 mJ. For technical reasons, the gap between the plates of a film capacitor cannot be reduced below a few tens of micrometers. It follows from Eq. (21.2) that at this distance of separation, the surface area of the plates of a 10 μF capacitor would have to be on the order of 10 m^2, which gives a volume ($V = S\delta$) of the capacitor on the order of 1 dm^3, corresponding to a specific energy of about 10^{-3} J/kg. We point out for comparison that batteries (where charge is not merely accumulated but is generated continuously by a faradaic electrochemical reaction) have specific energies of tens of Wh/kg, corresponding to several thousand J/kg (see Chapter 19).

However, electrostatic film capacitors have an important special feature representing an advantage over batteries and other energy storage devices: The rate of delivery of the electrical charges (i.e., the value of the discharge current) depends only on the properties of the external circuit; it is not limited by internal factors. In an ideal film capacitor, the discharge current does not encounter any internal ohmic resistance, nor is there any polarization of the electrodes (plates) during current flow. In expressions such as (19.5) and (19.7) for the discharge current and discharge power of batteries, the formal value of parameter R_{app} is zero for an ideal film capacitor. The values of discharge current and discharge power depend only on the resistance R_{ext} and other properties of the external circuit and can become as large as desired. Hence, electrostatic film capacitors have no substitutes when brief but very powerful electrical energy pulses are needed (such as for the photoflash in modern cameras).

Ideal film capacitors have another important special feature (i.e., their operation is not linked to chemical reactions); hence, phenomena of aging and degradation of the active masses are absent. For this reason such a capacitor will sustain an unlimited number (many millions) of charge–discharge cycles.

The basic defect of film capacitors is their low value of specific electrostatic capacity. Therefore, such capacitors are practically useful only in the pico- and nanofarad range. For this reason, valiant attempts have been made in recent years to increase the specific capacity of capacitors per unit of mass, volume, and plate (electrode) surface area.

21.1.2 Electrolytic Capacitors

Historically, the first capacitors using an electrochemical system were the electrolytic capacitors. Built like film capacitors, they have electrodes made of aluminum foil on which by electrochemical oxidation a thin film of aluminum oxide (i.e., 10 to 100 nm thick) is grown to serve as the dielectric. Solutions are used as the electrolyte which aid self-repair of the oxide film on aluminum after accidental damage. Such electrolytes are solutions of salts of a number of organic acids (trifluoroacetic, salicylic, and some others). Because of the small thickness of the oxide layer, electrolytic capacitors have a markedly higher capacity than film capacitors. They can thus be used in the microfarad range.

Electrolytic capacitors have the defect that their parameters depend on temperature and that considerable leakage currents appear during storage of charged capacitors. A marked decrease in the leakage currents as well as an increase in specific capacity can be attained when instead of aluminum foil, electrodes of thin (and stronger) tantalum foil are used. Recent developments are in electrolytic capacitors using foils and the oxides of niobium and tantalum, which have a high dielectric permittivity but cost much less than tantalum oxide.

21.1.3 Double-Layer Capacitors

It had already been pointed out (Chapter 10) that because of the small distance of separation between the charges on the metal surface and the counterions of the solution pressed against the metal surface, the electric double layer forming on metal electrodes in contact with electrolyte solutions has a capacity measuring tens of microfarad per square centimeter of true surface area of the electrode, which is a value incomparably higher than that which can be attained with film or electrolytic capacitors. The question inevitably comes to mind as to whether high-value capacitors could be built using such double layers.

Work in this area has been conducted in many laboratories since the early 1980s. The electrodes to be used in such a double-layer capacitor should be ideally polarizable (i.e., all charges supplied should be expended), exclusively for the change of charge density in the double layer [not for any electrochemical (faradaic) reactions]. Ideal polarizability can be found in certain metal electrodes in contact with elelctrolyte solutions free of substances that could become involved in electrochemical reactions, and extends over a certain interval of electrode potentials. Beyond these limits ideal polarizability is lost, owing to the onset of reactions involving the solvent or other solution components.

A classical example of ideally polarizable electrodes is mercury in an inert electrolyte solution of the KCl or K_2SO_4 type. Using mercury electrodes to build a capacitor is inconvenient, of course. Electrodes made of carbon materials have an ideal polarizability close to that of mercury. These materials have the further advantage that they are readily fashioned into electrodes having a high true surface area per unit of geometric surface area (i.e., a high value of the formal roughness factor). In this case, one gains an appreciable increase in double-layer capacity, owing to the increase in size of the electrode–electrolyte interface.

In recent years, many types of double-layer capacitors have been built with porous or extremely rough carbon electrodes. Activated carbon or materials produced by carbonization and partial activation of textile cloth can be used for these purposes. At carbon materials, the specific capacity is on the order of $10\,\mu F/cm^2$ of true surface area in the region of ideal polarizability. Activated carbons have specific surface areas attaining thousands of m^2/g. The double-layer capacity can thus attain several tens of farads per gram of electrode material at the surfaces of such carbons.

The working potential window at the electrodes of double-layer capacitors made of carbon spans approximately from -0.5 to $+1.0\,V$ (RHE). At more positive potentials, irreversible anodic oxidation of the carbon material to CO_2, and with it a deterioration of the electrode properties, starts. At more negative potentials, hydrogen evolution might start. Thus, the maximum voltage, $(\Delta\psi)_{max}$, to be applied to a capacitor assembled from two carbon double-layer electrodes is about 1 to 1.5 V. Somewhat higher values of the maximum voltage, up to 2 to 3 V, can be attained when using electrolyte solutions in nonaqueous solvents, although at the expense of higher internal resistance.

It follows from these data that the (theoretical) specific capacity of the active materials of such a double-layer capacitor may attain 100 F/g. This is many orders of magnitude above the values characterizing other capacitor types (film and electrolytic). For this reason such capacitors have also become known as *super-* or *ultracapacitors*.

The operation of a double-layer capacitor is tied to a displacement of electrolyte ions. In a fully charged capacitor, anions accumulate as counterions in the solution layer next to the positively charged electrode while the concentration of the cations decreases. At the negative electrode, the opposite situation is seen. During discharge, the ionic concentrations level out to the bulk solution values by migration and diffusion.

21.1.4 Pseudocapacitors

Another type of supercapacitor has been developed in which instead of ideally polarizable electrodes, electrodes consisting of disperse platinum metals are used at which thin oxide films are formed by anodic polarization. Film formation is a faradaic process which in certain cases, such as the further partial oxidation and reduction of these layers, occurs under conditions close to reversibility.

Such processes are referred to as *pseudofaradaic*, and the capacity that corresponds to the surface processes is referred to as *pseudocapacity*. Capacitors built according to this principle are known as *pseudocapacitors*.

Detailed studies have been performed on pseudocapacitors with layers of hydrated ruthenium oxide, $RuO_2 \cdot H_2O$. Protons relatively readily undergo intercalation and deintercalation in this material:

$$HRuO_2 + xH^+ + xe^- \rightleftharpoons H_{1+x}RuO_2. \tag{21.4}$$

During cathodic polarization (discharge of the positive electrode, charging of the negative electrode), the reaction occurs from left to right; during anodic polarization it occurs from right to left. Thus, during charging, protons pass through the solution from the positive to the negative electrode; during discharge, they go in the opposite direction. The high reversibilility of this system is due to the high mobility of protons in hydrated ruthenium oxide. Often, pseudocapacitors exhibit the ordinary changes in the amounts of charge in the electric double layer in addition to the pseudofaradaic reaction.

The total capacity of a ruthenium oxide electrode [the usual double-layer capacity plus the pseudocapacity of reaction (21.4)] is rather high (i.e., several hundred F/g), even more than at the electrodes of carbon double-layer capacitors. The maximum working voltage of ruthenium oxide pseudocapacitors is about 1.4 V.

A wider application of ruthenium oxide capacitors is hindered by the high cost of ruthenium oxide. Attempts have been reported, therefore, to substitute ruthenium oxide with other, cheaper materials capable of intercalation and deintercalation of hydrogen and/or other ions. Promising results with pseudocapacities of about 100 F/g have been obtained with the mixed oxides of ruthenium and vanadium and also with mixed oxides on the basis of manganese oxide.

Great scientific and practical interest has been aroused by pseudocapacitors built with electronically conducting polymers (see Chapter 26). Such capacitors most often contain two symmetric electrodes consisting of a polymer that is capable of the electrochemical intercalation of both anions (*p*-doping) and cations (*n*-doping): for instance, a polyacetylene or polythiophene derivative. The electrodes are undoped when the capacitor is discharged. Charging is attended by *n*-doping of the negative and *p*-doping of the positive electrode. The charged (doped) electrodes have a high electronic conductivity and hence can be discharged with relatively high currents. The specific capacity of polymer electrodes undergoing doping is 40 to 60 F/g.

The supercapacitors described in the literature have an overall specific capacity of about 1 to 5 F/g (i.e., when allowing for the weight of the two electrodes, the leads, the electrolytes, and all peripheral components). In them, electric energy can be accumulated with a density of 1 to 5 Wh/kg (which is one to two orders of magnitude less than in batteries).

21.1.5 Impedance of Supercapacitors

It was seen above that different types of electrochemical supercapacitors exhibit specific capacities many orders of magnitude higher than the film and electrolytic capacitors known before. It must be added at once, however, that the behavior of supercapacitors differs appreciably from that of ideal film capacitors. In contrast to

film capacitors, supercapacitors have a noticeable and sometimes rather high internal resistance (impedance).

This resistance is caused by many factors. With the aim of having a maximum specific surface area and thus maximum specific capacity, highly disperse materials are used in the electrodes of all types of supercapacitors. The pores of these materials are filled with electrolyte through which current flows when the capacitor is operated. The resistance of the electrolyte in the branched system of fine and ultrafine pores is high, causing considerable ohmic losses. In highly disperse systems, ohmic voltage losses also develop between the individual grains of electrode material. Another factor is hindered diffusion and migration of ions in the system of fine pores, but these processes are necessary for the formation and decay of the counterion layers in the solution next to the electrode when there is a change in the amount of charge in the electrode. In the case of supercapacitors, losses due to the limited rate of the faradaic reaction itself (e.g., because of slow diffusion of protons into the solid phase of ruthenium oxide) are superimposed on these phenomena.

The influence of all these factors increases with the current density in the capacitors. During charging with very low currents, their influence is insignificant, so that the capacitors readily and without losses are charged to almost their full capacity. However, the main purpose of these capacitors is high-current discharge, which is attended by appreciable voltage losses and, as a result, a drastically lower value of the capacity that can be realized in practice when discharge is terminated at a given final voltage.

Thus, unlike ideal film capacitors, the supercapacitors do not admit discharge with arbitrarily high currents. Realistic discharge currents are restricted to values following from equations of the type (19.5) with real values of parameter R_{app}. Literature values for this parameter are highly divergent for the various types of superconductors. It evidently is inversely proportional to the surface area of the electrodes and thus to the electrostatic capacity C; that is, $R_{app} = \gamma/C$. The value of coefficient γ depends on the current and varies between 10^{-2} and $10^{2}\ \Omega \cdot \mathrm{F}$. Over brief time intervals, supercapacitors can be operated with specific powers attaining several kW/kg (i.e., an order of magnitude more than the most powerful batteries). At high discharge currents, the specific energy storage capacity of supercapacitors decreases by several orders of magnitude, for the reasons stated above.

According to the goal set by the U.S. Department of Energy, the final aim in the development of supercapacitors is that of attaining a specific power of about 1.5 kW/kg while preserving an energy storage capacity of about 20 kWh/kg.

As in batteries, and for the same reasons, a certain self-discharge may occur in charged supercapacitors. Undoubted advantages of supercapacitors over storage batteries are the longer cycle life (many thousands of charge–discharge cycles), the wider interval of working temperatures (from -50 to $+60$°C) and the lack of gas evolution during operation, hence the feasibility of sealed designs.

The practical value of supercapacitors has been proven over a certain intermediate range of currents. At lower currents ordinary batteries which have a higher

specific energy reserve are more appropriate. At high currents, losses during supercapacitor discharge may prove to be excessive.

An instance of the successful use of a supercapacitor is its parallel branching with a lead–acid battery in starters of internal combustion engines. Often, particularly in cold weather, the power of the storage battery is not high enough for rapid starting of the engine. A considerable acceleration of the starting operation is attained when supercapacitors are used in parallel with the battery.

21.2 ELECTROCHEMICAL TRANSDUCERS

Starting in the 1950s, electrochemical principles have been employed in the development of new technical means for the acquisition, measurement, storage, transformation, and transfer of various types of information. By now many electrochemical devices have been developed for such purposes and are used to build automated systems for the control of production processes, for the automation of geophysical observations and measurements, and for many other purposes. This field, intermediate between electrochemistry, informatics, and electronics, is also known as *chemotronics*.

Electrochemical information transducers can be grouped according to their functions:

1. Devices for converting nonelectrical effects and signals to electrical signals. This group includes numerous sensors for measuring and controlling the temperature, pressure, linear accelerations, vibrations, various mechanical and acoustic parameters, flow rates and the consumption of liquids, and similar parameters.
2. Devices for converting one type of electrical signal to others. This group includes various integration and storage devices, timing relays, remote-controlled resistors, modulators for electric-current parameters, and so on.
3. Devices for converting electrical signals to other, nonelectrical signals and effects. This group includes electroosmotic micropumps, different types of balancing devices, color indicators, and so on.

These various types of information transducers differ in their operating mechanism and in the operating principles underlying their functioning. Widely used are those transducers that rely on measuring limiting diffusion currents. Transducers of this type could be called *concentration sensors* or *liquid-phase sensors*; some of them are known as *solions*. These are electrochemical cells with "inert" electrodes that are identical in their nature. However, the working surface area of one of the electrodes (the indicator electrode) is tens of times smaller than that of the other electrode. Both electrodes are immersed into a solution containing a reversible redox system—for instance, I_2/I^- or $Fe(CN)_6^{3-}/Fe(CN)_6^{4-}$—where the concentration of

one of the components (e.g., the oxidized one) is many times smaller than that of the other component. A small voltage on the order of 0.2 to 0.3 V is applied to the cell, the polarity being such that at the indicator electrode the component being present in lower concentration would react (the oxidizer would be reduced, for instance). Under these conditions, a stable steady-state value of the limiting diffusion current will be established in due time in the cell, this value being determined by the laws of diffusion to the indicator electrode (see Chapter 4). The cell design is such that an external effect (linear acceleration, vibration, pressure change, temperature change, etc.) will give rise to motion of the liquid close to the indicator electrode. To this end the indicator electrode usually is placed into a narrow channel or gap. The liquid flow produced leads to an increase in size of the limiting diffusion current, which is readily recorded by electrical measuring devices.

In electrochemical transducers of the second type, most often phase transitions occurring during electrochemical reactions and obeying the laws of Faraday are employed. Gas coulometers designed to measure the amount of charge that has passed the circuit (e.g., as an integral of current over time) rely on determining the volume of gas (usually of hydrogen) evolved at a suitable indicator electrode, whereas mercury coulometers rely on determining the volume of liquid mercury deposited cathodically. The less convenient weighing of the amount of a solid metal deposited cathodically is used more rarely.

It is well to remember that in the past, the unit of electrical current—the *international ampere*—was defined as the strength of an invariant current which, when sent through a silver nitrate solution, would deposit 1.111800 mg silver at the cathode. Today, another definition of the ampere as an SI unit is valid.

In discrete counters that should provide a signal when a certain amount of electric charge has passed the circuit, a change in potential of an indicator electrode which is due to a phase change is employed. For instance, a silver electrode immersed into a chloride solution can be covered anodically by a thin layer of AgCl when passing a given amount of charge. Subsequently, this electrode is made the cathode in a measuring circuit. A sudden change in electrode potential will occur after complete reduction of the AgCl layer and exposure of the naked Ag surface.

Thin metal films (e.g., copper films) on insulating materials are employed in remote-controlled resistors. The electrical resistance of such a film can be regulated in both directions, by cathodic growth of the film or by anodic dissolution of the film, leading to a decrease in film thickness.

Information transducers based on electrokinetic phenomena can be used to convert various mechanical and acoustic effects to electrical signals and, vice versa, to convert electrical signals to mechanical effects. The forced flow of an electrolyte solution through a porous membrane made of insulating material gives rise to *streaming potentials*, which are indicative of the external forces that have induced this flow. If, on the other hand, an electrical potential difference is applied to an electrolyte solution from different sides of a membrane dividing this solution, electroosmotic liquid flow through the membrane will be induced. This effect is basic to electrokinetic microdosing devices for liquids that are widely used for medical purposes. The electrochemical information transducers often differ from their electronic

analogs by higher sensitivities in the low-frequency range, and differ from their mechanical analogs by lower energy requirements and smaller size.

MONOGRAPH

Conway, B. E., *Electrochemical Supercapacitors: Fundamentals and Technological Applications*, Kluwer Academic, Dordrecht, The Netherlands, 1999.

22
Corrosion of Metals

Corrosion (from Latin *corrodere*, "gnaw to pieces") of metals is the spontaneous chemical (oxidative) destruction of metals under the effect of their environment. Most often it follows an electrochemical mechanism, where anodic dissolution (oxidation) of the metal and cathodic reduction of an oxidizing agent occur as coupled reactions. Sometimes a chemical mechanism is observed.

Corrosion (rusting) of metals is causing huge losses to the economy. This process affects the metal structures of buildings and bridges, the equipment of chemical and metallurgical plants, river and sea vessels, underground pipelines, and other structures. In the United States, for instance, corrosion-related losses approach a figure of $100 billion per year, which is almost 5% of the gross national product. Direct losses attributable to corrosion include expenditures for the replacement of individual parts, units, entire lines or plants, and for various preventive and protective tasks (such as the application of coatings for corrosion protection). Indirect losses arise when corroded equipment leads to defective products that must be rejected; they also arise during downtime required for preventive maintenance or repair of equipment. About 30% of all steel and cast iron are lost because of corrosion. Part of this metal can be reprocessed as scrap, but about 10% is irrevocably lost.

The significance of corrosion protection has risen sharply in recent years for a number of reasons: (1) because of efforts to reduce the metal content of parts (e.g., by using thinner metallic support structures); (2) with the use of new types of equipment and processes involving expensive equipment operated under extreme conditions, such as nuclear reactors and jet and rocket engines; and (3) in connection with the development of products having extremely thin metal films, such as printed circuit boards and integrated circuits.

Corrosion science has now developed into an independent branch of electrochemistry that has intimate connections with other fields of science, particularly physical metallurgy. Its chief concerns are the origin and mechanisms of the various forms of corrosive attack and the development of efficient ways to fight corrosion.

Fundamentals of Electrochemistry, Second Edition, By V. S. Bagotsky

22.1 VARIOUS TYPES OF CORROSION

Corrosion phenomena can be classified according to the type of corroding medium acting on the metal. Corrosion in nonelectrolytic media is distinguished from that in electrolytic media. The former include dry hot gases, organic liquids (e.g., gasoline), and molten metals. Electrolytic media are most diverse, and include ambient air (with moisture and other components), water (seawater, tap water) and aqueous solutions (acids, alkalies, salt solutions), moist soil (for underground pipelines, piles, etc.), melts, and nonaqueous electrolyte solutions.

Corrosion phenomena can also be classified according to the visible aspects of corrosive attack (Fig. 22.1). This may be general (continuous), affecting all of the exposed surface of a metallic object, or localized. General corrosion can be uniform and nonuniform. Depending on the width and depth of the segments affected by localized corrosion, we may speak of spot, pit (large or small), or subsurface corrosion. Often, intercrystalline corrosion is encountered, which propagates in the zones between individual metal crystallites. Cracks develop between or in individual crystals in the case of stress corrosion cracking.

Certain types of corrosion are selective. Thus, corrosion cracking is observed primarily in the case of alloys and only when these are in contact with particular media. Corrosion is often enhanced by various extraneous effects. Stress corrosion cracking can occur under appreciable mechanical loads or internal stresses; corrosion fatigue develops under prolonged cyclic mechanical loads (i.e., loads alternating in sign).

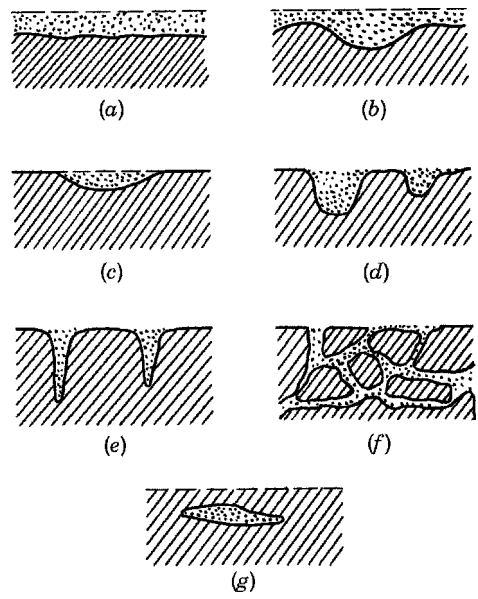

FIGURE 22.1 Aspects of metallic corrosion: (*a*) uniform general; (*b*) nonuniform general; (*c*) localized (spots); (*d*) large pits; (*e*) small pits; (*f*) intercrystalline; (*g*) subsurface.

Other factors are fretting and cavitation in a liquid (impact of the liquid). Corrosion can also occur due to electric currents (stray currents in soils).

Almost all metals are subject to corrosion, an exception being the noble metals (the platinum metals, gold, silver) which under ordinary conditions do not corrode. Corrosion of iron is the most prominent problem since parts and structures consisting of iron and steels are used so widely.

Different parameters are used to characterize the corrosion rate: the loss of mass by the metal sample within a certain length of time (per unit area), the decrease in sample thickness, the equivalent electric current density, and so on. For most metals undergoing uniform general corrosion, these parameters in order of magnitude can be interrelated (while allowing for atomic masses and densities) as $1\ \text{g/m}^2\cdot\text{yr} \approx 10^{-4}\ \text{mm/yr} \approx 10^{-4}\ \text{A/m}^2$.

22.2 MECHANISMS OF CORROSION PROCESSES

The analysis of corrosion processes comprises examining the special features in a given metal's anodic dissolution, establishing the nature of the cathodic reaction (which is coupled with metal dissolution), and defining in greater detail the loci of the anodic and cathodic partial reaction. In corrosion, the equilibrium potential of reduction of the oxidizing agent is always more positive than that of dissolution of the metal (at the given solution composition). The main cathodic reactions in metal corrosion are hydrogen evolution and the reduction of dissolved oxygen. It is only in special cases when the corresponding reactants are available that chlorine, nitric acid, or other oxidizing agents will be reduced. Hydrogen evolution occurs at much more negative potentials than oxygen reduction. Hence, corrosion coupled with hydrogen evolution can be observed only for metals having sufficiently negative equilibrium potentials—the alkali and alkaline-earth metals, aluminum, magnesium, zinc, iron, and so on—and is encountered predominantly in acidic and alkaline media. Oxygen-depolarized corrosion occurs in contact with air, most often in neutral solutions (atmospheric corrosion, waterline corrosion in seawater, etc.).

In Section 13.7 we noted that the rate of corrosion (spontaneous dissolution) of metals depends on the shape and position of both the anodic polarization curve for metal dissolution and the corresponding cathodic curve and is determined by the point of intersection of these curves. The anodic curves 1 and 2 in Fig. 22.2*a* are for metals with a more negative and more positive potential, respectively. For the former, the state of the system corresponds to point *A*; the corrosion current is high, owing to the high rate of hydrogen evolution. For the latter, the potential is in a region where no hydrogen is evolved. Oxygen reduction is the only possible cathodic reaction. Because of the limited solubility of oxygen in water, this reaction occurs with concentration polarization (limiting current density i_l), which imposes a limit on the overall rate of the process: diffusion-controlled corrosion (point *B*). Oxygen-depolarized corrosion occurs mainly when the liquid film on the metal is thin, so that oxygen access to the electrode is sufficiently fast. In solutions, the rate of oxygen-depolarized corrosion depends on stirring intensity.

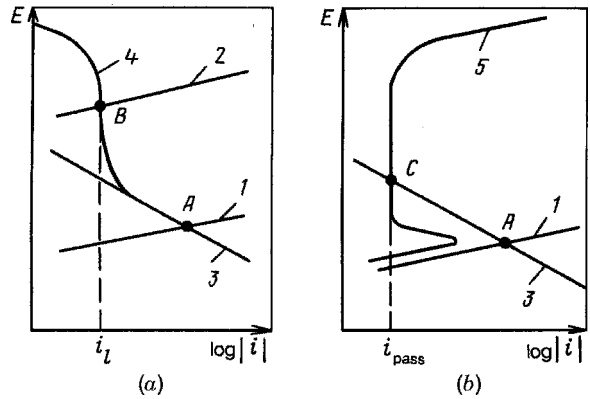

FIGURE 22.2 Schematic polarization curves for spontaneous dissolution: (*a*) of active metals; (*b*) of passivated metals. (1,2) Anodic curves for active metals; (3) cathodic curve for hydrogen evolution; (4) cathodic curve for air–oxygen reduction; (5) anodic curve of the passivated metal.

Passivation of the metal and the associated sharp decline of its anodic dissolution rate have a strong effect on corrosion rates (curve 5 and the point of intersection *C* in Fig. 22.2*b*). Passivation is encountered more often under the effect of oxidizing agents (e.g., in the presence of oxygen).

When the metal surface is homogeneous, the anodic and cathodic partial reaction will be distributed uniformly over all surface segments; at different times both the anodic and the cathodic reaction will occur at each segment. The surface of a metal's liquid amalgam can be cited as an example of an ideally homogeneous surface. Rather good homogeneity is found as well on annealed surfaces of highly pure solid metals.

A nonuniform distribution of the reactions may arise when the metal's surface is inhomogeneous, particularly when it contains inclusions of other metals. In many cases (e.g., zinc with iron inclusions), the polarization of hydrogen evolution is much lower at the inclusions than at the base metal; hence, hydrogen evolution at the inclusions will be faster (Fig. 22.3). Accordingly, the rate of the coupled anodic reaction (dissolution of the base metal) will also be faster. The electrode's OCP will become more positive under these conditions. At such surfaces, the cathodic reaction is concentrated at the inclusions, while the anodic reaction occurs at the base metal. This mechanism is reminiscent of the operation of shorted galvanic couples with spatially separated reactions: Metal dissolves from one electrode; hydrogen evolves at the other. Hence, such inclusions have been named *local cells* or *microcells*.

The idea that metal corrosion could be due to local-cell action was put forward in 1830 by Auguste Arthur de la Rive, and became very popular. An extreme view derived from this idea is the assertion that perfectly pure metals lacking all foreign inclusions will not corrode. However, it does not correspond to reality. It was established long ago

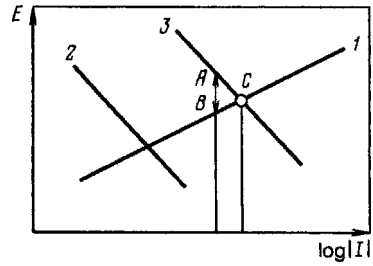

FIGURE 22.3 Polarization curves: (1) anodic polarization of bare base metal; (2) cathodic polarization of bare base metal; (3) cathodic polarization in the presence of foreign inclusion.

that even superpure metals with homogeneous surfaces are subject to corrosion, which is sometimes rather intense, because of coupled reactions occurring without spatial separation. Thus, local cells constitute an accelerating factor but are not the cause of metal corrosion.

The surface of the base metal is anodically polarized under the effect of local cells. For a graphical analysis of the phenomena, one must construct the polarization curves for the partial currents at the base metal as well as the overall anodic I_a vs. E curve reflecting the effective rate of dissolution of this metal under anodic polarization. The rate of the cathodic process, I_c, at the inclusions is described by the corresponding cathodic polarization curve (since the surface areas of anodic and cathodic segments differ substantially, currents rather than current densities must be employed here). At open circuit the two rates are identical.

A current (the local cell's short-circuit current) flows between anodic and cathodic surface segments. When the solution's ohmic resistance, R, between these segments is low, the resulting ohmic voltage drop can be neglected and the assumption made that the potentials are identical at the two types of surface segment. In this case, the current, I_s, of spontaneous dissolution and also the electrode's potential will correspond to the point of intersection of the curves for I_a and I_c (point C in Fig. 22.3). However, in general, the ohmic voltage drop I_sR in the solution cannot be neglected, and the current of spontaneous dissolution of the metal will have a value such that the corresponding potential difference, $E_a - E_c$, between the anodic and cathodic segments will be I_sR (section AB).

Calculations of resistance R are associated with certain difficulties. For disk-shaped inclusions spaced far apart and having radii r_0, the resistance between the edge and center of a disk can be written, under certain assumptions, as

$$R = \frac{2r_0}{\pi\sigma} \tag{22.1}$$

(σ is solution conductivity). In solutions where $\sigma \approx 10^{-3}$ S/m and with inclusions having a radius $r_0 \approx 1$ μm, the resistance is about 1 mΩ; it will have no effect even when the current at the cathodic segment is high, and the metal surface can be

regarded as equipotential. For inclusions of large size or solutions with lower conductivities, the ohmic voltage drop as a rule must be taken into account.

The effects of impurities are less important for oxygen-depolarized than for hydrogen-depolarized corrosion, since the values of polarization for oxygen reduction found at different metals differ less strongly than those for hydrogen evolution.

When corrosion occurs under local-cell action, it may happen that the impurity concentration at the metal surface increases with advancing dissolution of the base metal; hence, the corrosion rate will increase.

In solutions of nonelectrolytes (e.g., of iodine in chloroform), metals are oxidized in a direct chemical reaction with the oxidizing agent. It has been shown recently that even in electrolyte solutions, metals may corrode by the chemical mechanism, which leads to kinetic laws differing from those described in Section 13.7 for coupled electrochemical reactions. In electrolyte solutions, the chemical mechanism can be visualized as the intimate local coupling of the two electrochemical process steps (i.e., these steps will occur simultaneously at the same surface site). This has an important effect on the energy requirements of the elementary reaction act. An isolated elementary act is attended by a change in charge of the particle in solution and, hence, by appreciable solvent reorganization, but when the anodic and cathodic act are intimately linked (e.g., when a hydrogen ion in the solution is replaced by a metal ion) the required degree of reorganization is much smaller. In this case the principle of independent electrochemical reactions (see Section 13.7) is no longer valid. The chemical mechanism is of some importance in the corrosion of Fe, Cr, and Mn, particularly at elevated temperatures.

22.3 CORROSION PROTECTION

Electrochemical and nonelectrochemical ways to protect metals against corrosion can be distinguished. The nonelectrochemical ways include dense protective films that isolate the metal against effects of the medium and may be paint, polymer, bitumen, enamel, and the like. It is a general shortcoming of these coatings that when they are damaged mechanically, they lose their protective action, and local corrosion activity arises.

Electrochemical methods of protection rest on different precepts: (1) electroplating of the corroding metal with a thin protective layer of a more corrosion-resistant metal, (2) electrochemical oxidation of the surface or application of other types of surface layer, (3) control of polarization characteristics of the corroding metal (the position and shape of its polarization curves), and (4) control of potential of the corroding metal.

The polarization characteristic of a corroding metal can be controlled by various additives to the solution, called *corrosion inhibitors*, which adsorb on the metal and lower the rates of the cathodic and/or anodic reaction. Inhibitors are used primarily for acidic electrolyte solutions, sometimes also for neutral solutions. Various organic compounds with –OH, –SH, $–NH_2$, –COOH, and so on, as the functional groups are used as inhibitors. The effects of an organic inhibitor, tetradecylpiperidinium

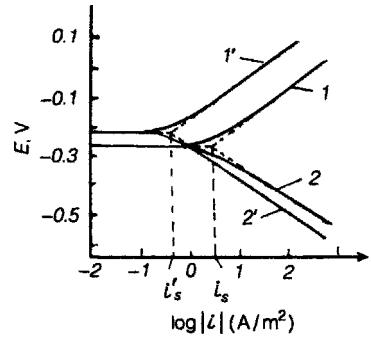

FIGURE 22.4 Anodic (1,1′) and cathodic (2,2′) polarization curves for an iron electrode in pure 1 *M* HCl (1,2) and in 1 *M* HCl with 5×10^{-5} *M* $C_{14}H_{29}Br$ (1′,2′).

bromide, on the polarization curves of hydrogen evolution and metal dissolution are shown in Fig. 22.4. This inhibitor markedly lowers the rate of both the anodic and cathodic processes. However, since the effect on the anodic process is slightly stronger, the metal's OCP moves in the positive direction. The current of spontaneous dissolution decreases by about one order of magnitude when the inhibitor is present.

A condition for inhibitor action is its adsorption on the metal at the open-circuit potential. Neutral inhibitor molecules will not adsorb when this potential is far from the metal's point of zero charge (see Section 10.4.2). In this case, inhibitors forming ions are used: cations (e.g., from amino compounds) or anions (from compounds with sulfo groups), depending on the sign of surface charge. Inhibitor action is often enhanced greatly when mixtures of several substances are used.

When the metal is polarized cathodically, its spontaneous dissolution rate will decrease. The potential of a base metal can be made more negative when this metal is linked electrically to another, more electronegative metal which is present in the same electrolyte medium. This produces a macroscopic galvanic couple where the base metal is cathodically polarized under the effect of the second metal. The latter, called *protector*, is anodically polarized and gradually consumed by anodic dissolution. This type of metal protection is called *cathodic protection*. An example is galvanized iron, where zinc is functioning as a protective film and simultaneously, when the film has been damaged, as cathodic protector.

Sometimes anodic protection is used, in which case the metal's potential is made more positive. The rate of spontaneous dissolution will strongly decrease, rather than increase, when the metal's passivation potential is attained under these conditions. To make the potential more positive, one must only accelerate a coupled cathodic reaction, which can be done by adding to the solution oxidizing agents readily undergoing cathodic reduction (e.g., chromate ions). The rate of cathodic hydrogen evolution can also be accelerated when minute amounts of platinum metals, which have a strong catalytic effect, are incorporated into the metal's surface layer (Tomashov, 1955).

The best known way of lowering the corrosion of iron is by its alloying with chromium, nickel, and other metals. The corrosion resistance of the corresponding stainless steels is due to the fact that chromium is readily passivated. This is a quality that is found even in alloys with relatively low chromium contents. Hence, stainless steels are practically always strongly passivated, and their spontaneous dissolution rates are very low.

REFERENCES

de la Rive, A. A., *Ann. Phys. (Poggendorff's)*, **19**, 221 (1830).

Tomashev, N. D., *Usp. Khim*. [in Russian], **24**, 453 (1955).

MONOGRAPHS

Kaesche, H., *Die Korrosion der Metalle*, Aufl. 2, Springer-Verlag, Berlin, 1978; English translation: *Metallic Corrosion*, NACE, Houston, TX, 1987.

Marcus, P., and J. Oudar, Eds., *Corrosion Mechanisms in Theory and Practice*, Marcel Dekker, New York, 1995.

23

Electrochemical Methods of Analysis

Electrochemical phenomena and processes are useful for the quantitative and qualitative chemical analysis of various substances and media, including liquids, gases, and solids. The high accuracy of the electrochemical methods of analysis derives from the fact that they are based on highly exact laws (e.g., those of Faraday).

The methods of electrochemical analysis are instrumental. It is very convenient that electrical signals are used for the perturbation: current, potential, and so on, and that the result (the response) again is obtained as an electrical signal. This is the basis for the high speed and accuracy of the readings, for the extensive possibilities of automated recording of the results, as well as for automation of the entire analysis. Electrochemical methods of analysis are distinguished by their high sensitivity, selectivity (the possibility of analyzing certain substances in the presence of others), speed of the measurements, and other advantages. In many cases extremely small volumes, less than 1 mL, of the test solution will suffice for electrochemical analysis.

The following are the major groups of electrochemical methods for chemical analysis:

1. *Conductometry*, which measures the electrical conductivity of the electrolyte solution being examined
2. *Coulometry*, which measures the amount of charge Q consumed for the complete conversion (oxidation or reduction) of the substance being examined
3. *Voltammetry*, which determines the steady-state or transient polarization characteristics of electrodes in reactions involving the substance being examined
4. *Potentiometry*, which measures the open-circuit equilibrium potential of an indicator electrode, for which the substance being examined is potential determining

Electrochemical methods are of importance in their own right for direct chemical analyses; but in addition, in a number of cases, they are ancillary to other methods of analysis (e.g., the titration of solutions).

Fundamentals of Electrochemistry, Second Edition, By V. S. Bagotsky

23.1 CONDUCTOMETRY

Conductometry is a nonselective method of analysis; all types of mobile ion present in the solution (or other medium being examined) contribute to conductivity, and the contributions of the individual types cannot be distinguished in the values measured. Hence, conductometry is primarily useful when determining the concentrations in binary electrolyte solutions (e.g., for determining the solubilities of poorly soluble compounds). In the case of multicomponent systems, conductometry is used when the qualitative composition of the solution is known and invariant, as, for example, in the continuous or batch analysis of solutions in process streams. Conductometry can also be used to monitor the rinsing of deposits and materials. Straightforward conductometry is important in determining the total ion content (degree of mineralization) of natural waters and in the quality control of water after purification or distillation.

Conductometric titration rests on the marked changes that occur near the titration endpoint in the relation between conductivity and the amount of titrant added (an extreme or inflection point). It is used in particular for the titration of acids with base (and vice versa) in colored and turbid solutions or solutions containing reducing and oxidizing agents (i.e., in those cases where the usual color change of acid–base indicators cannot be seen).

Conductometric analysis is performed in both concentrated and dilute solutions. The accuracy depends on the system; in binary solutions it is as high as 0.1%, but in multicomponent systems it is much lower.

23.2 COULOMETRY

Coulometry can be regarded as an analog of titration where the substance being examined is quantitatively converted to a reaction product not by the addition of titrant, but by a certain amount of electric charge Q. As in titration, the endpoint must be determined. To determine the endpoint during current flow, one combines coulometry with another of the electrochemical methods described, and accordingly is concerned with conductometric, potentiometric, or amperometric coulometry.

In coulometry, one must define exactly the amount of charge that was consumed at the electrode up to the moment when the endpoint signal appeared. In galvanostatic experiments (at constant current), the charge is defined as the product of current and the exactly measured time. However, in experiments with currents changing continuously in time, it is more convenient to use special coulometers, which are counters for the quantity of charge passed. Electrochemical coulometers are based on the laws of Faraday; with them the volume of gas or mercury liberated, which is proportional to charge, is measured. Electromechanical coulometers are also available.

For coulometric analysis, the substance being examined must react in 100% current yields [i.e., other (secondary) reactions must be entirely absent]. In efforts to avoid side reactions, coulometry most often is performed potentiostatically (amperometrically) (i.e., the electrode potential is kept constant during the experiment), and the current consumed at the electrode is measured. The current is highest at the start of the

experiment; it decreases as the substance being examined is consumed. The coulometric endpoint is that where the current has become zero.

The drop in current that occurs in coulometric experiments may arise not only from the decrease in bulk concentration of the substance being analyzed, but also from a decrease in its surface concentration caused by the development of concentration gradients (see Section 11.2.1). Low values of current density and strong solution stirring are used to avoid the interference of such effects. Thin-layer cells where the electrodes are very close together (tens of micrometers) and the parameter ratio S/V is high, are often used to shorten the experiments.

The galvanostatic version of coulometric analysis is used more rarely even though the determination of charge Q is greatly facilitated by constancy of the current. Here, the endpoint is determined from the typical potential rise associated with the changeover to a different reaction. The shape of the potential–time curve is the same as that of the curve for transient concentration polarization under galvanostatic conditions (see Fig. 12.10), although in the present case the potential change should occur when the bulk concentration drops to zero, not when merely the surface concentration drops to zero.

23.3 AMPEROMETRY

In many cases the concentration of a substance can be determined by measuring its steady-state limiting diffusion current. This method can be used when the concentration of the substance being examined is not very low, and other substances able to react in the working potential range are not present in the solution.

An example of amperometric methods used for analytical purposes is the sensor proposed in 1953 by Leland C. Clark, Jr. for determining the concentration of dissolved molecular oxygen in aqueous solutions (chiefly biological fluids). A schematic of the sensor is shown in Fig. 23.1. A cylindrical cap (1) houses the platinum or other indicator electrode (2), the cylindrical auxiliary electrode (3), and an electrolyte (e.g., KCl) solution (4). The internal solution is separated by the polymer

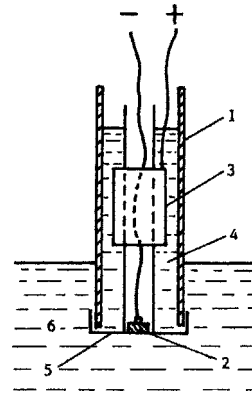

FIGURE 23.1 Schematic of a Clark oxygen sensor.

membrane (5) from the external test solution (6). The oxygen contained in the test solution diffuses through the membrane into the internal solution and is reduced at the cathodically polarized indicator electrode. The reduction current is determined by the rate of oxygen diffusion through the membrane, which in turn depends (through Fick's law) on the concentration of dissolved oxygen in the test solution.

Another example of an amperometric method is the method of polarography, which was widely used for analytical purposes some decades ago and which is described in detail in the following section.

23.4 POLAROGRAPHY

23.4.1 Dropping Mercury Electrode

In polarography a dropping mercury electrode (DME) is used. A DME setup is shown in Fig. 23.2. Under the pressure of a mercury column of height h, mercury flows with the constant-volume flow rate w from a glass capillary K. The drop forming at the capillary tip grows, and it tears away when at a time t_{dr} after the start of formation it has attained a certain mass. After its detachment a new drop starts to form and grow, and the cycle is repeated. The growing drop, while suspended, is used as the cathode for reduction of various substances (since mercury readily undergoes anodic dissolution, it cannot be used as an "inert" anode). Usually, a potentiostatic circuit is used (i.e., during the drop's life its potential E is kept constant). The flow rate w can be varied by changes in mercury column height. The drop time t_{dr} is sometimes controlled with an electrically actuated hammer which taps the capillary when needed (before natural drop detachment under the pull of gravity). A typical value of the drop's radius at the time of detachment is about 0.5 mm, and its surface area about 3 mm^2.

Charge for formation of an EDL corresponding to the set potential E must constantly be supplied to the DME because of the continuous renewal and growth of the surface. The charge, Q_{dl}, present on each side of the EDL depends on the potential

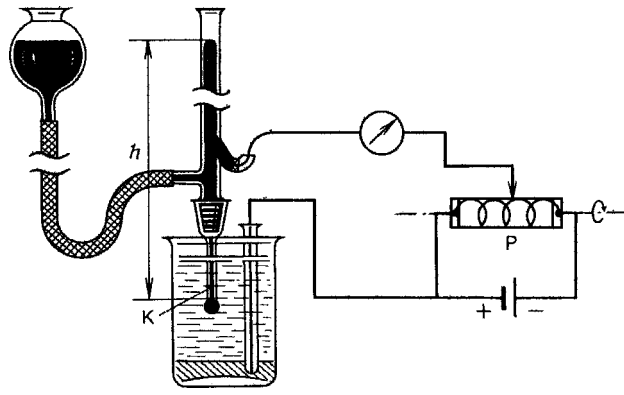

FIGURE 23.2 Dropping mercury electrode.

difference $\Delta\psi$ between the two layers of charge. Depending on the sign of $\Delta\psi$, the charging current I_{ch} can be positive or negative. It is readily measured in solutions where no electrochemical reactions take place and hence no faradaic current is recorded. When an electrochemical reaction takes place, the faradaic current I_f can be found from the difference between the measured current I_{meas} and the charging current: $I_f = I_{meas} - I_{ch}$.

The conditions of DME operation are transient since the drop surface grows and moves, diffusion is transient, and a nonfaradaic current is present. The current passing through the electrode will increase from a minimum value at drop birth to a maximum value at the time of drop detachment. However, after detachment of each drop the processes are repeated exactly (i.e., all parameters when averaged over drop life will be time invariant). For this reason the DME is often employed as a quasisteady electrode and the value of the averaged (during the drop's lifetime) current $\bar{I}$ is used. Usually, sluggish instruments are used to record the current; these only sense the averaged current (or display only minor current fluctuations).

The problem of convective diffusion toward the growing drop was solved in 1934 by Dionýz Ilkovič under certain simplifying assumptions. For reversible reactions (in the absence of activation polarization), the averaged current at the DME can be represented as

$$\bar{I} = 3.572nFD^{1/2}w^{2/3}t_{dr}^{1/6}\,\Delta c_j \tag{23.1}$$

(the *Ilkovič equation*). The DME has the advantage of continuous renewal (i.e., impurities will not accumulate on its surface or in its volume), so that the measurements have high reproducibility.

23.4.2 Classsical Polarographic Technique

The first version of a polarographic technique was put forward in 1922 by the Czech scientist Jaroslav Heyrovský. Classsical polarography is the measurement of quasisteady-state polarization curves with linear potential scans applied to the DME sufficiently slowly (υ between 1 and 20 mV/s), so that within the lifetime, t_{dr}, of an individual drop, the potential would not change by more than 3 to 5 mV. With special instruments (polarographs), one can record the resulting I vs. E curves (polarograms) automatically.

In the classical version one uses a two-electrode cell with DME and a mercury AE (the pool) at the bottom of the cell (see Fig. 23.2). The latter, which has a large surface area, is practically not polarized. The current at the DME is low and causes no marked ohmic potential drop in the solution and no marked polarization of the AE. Hence, to change the DME potential, it will suffice to vary the external voltage $\mathscr{E}_{ext}$ applied to the cell. During the measurements, I vs. $\mathscr{E}$ rather than I vs. E curves are recorded.

For polarization one uses a very simple galvanostatic arrangement with low resistance in the external circuit (Fig. 23.2). The voltage of the power source is controlled and varied with the aid of a low-resistance potentiometric device P. Usually, this device is a wire wound in 10 to 20 turns around a drum, which is rotated. The brush

in the center does not rotate but can move along a guide in a direction parallel to the drum axis. When the drum is rotated, the brush slides along the wire; thus, a smooth variation of voltage $\mathscr{E}_{ext}$ is obtained. A linear voltage scan rate is obtained through slow, uniform drum rotation.

During the measurements the DME potential is moved in a negative direction relative to the AE potential (otherwise, the mercury drop would start to dissolve anodically), a cathodic current flows, and cathodic reactions (metal ion discharge or the reduction of other compounds) take place.

The discharge of metal ions at mercury and formation of the corresponding amalgams are reversible in most cases. The equilibrium potential of an amalgam electrode is determined by an equation of the type (3.29). Concentration polarization arises as soon as a cathodic current flows; metal accumulates in the surface layer of the mercury forming amalgams, while the concentration of the corresponding metal ions in the solution layer at the surface decreases. The shape of the polarization curve is determined by Eq. (6.28) (the amalgam bulk concentration is zero); it is that of a typical wave, the *polarographic wave* (see Fig. 6.5, curve 3).

Figure 23.3 shows a polarogram recorded in an aqueous solution of $1 \times 10^{-3}\,M$ $PbCl_2 + 5 \times 10^{-4}\,M$ $CdCl_2 + 1\,M$ KCl (curve 1) as well as a curve (2) for the charging current recorded in the base electrolyte, $1\,M$ KCl. The polarographic curve obtained after subtracting the charging current (curve 3) corresponds to the faradaic reaction current. In practice, the curve for the faradaic current is constructed not by measuring a charging curve in the base electrolyte in each case but by assuming that this curve is the linear continuation of the initial section *AB* in the polarogram.

The first wave (segment *BCD*) corresponds to lead ion discharge with lead amalgam formation. The current of cadmium ion discharge is superimposed on the limiting current of this reaction in the region of the second wave (segment *DEF*). Discharge of the base-electrolyte ions (alkali metal or hydrogen ions) starts at even more negative potentials (to the right of point *F*).

Characteristic parameters of each wave are the value of the half-wave potential $E_{1/2}$, which is defined by Eq. (6.26), and the wave "height" [the value of the limiting diffusion current, $I_{d,ox}$, determined by the Ilkovič equation (23.1) for $c_{S,j} = 0$]. The

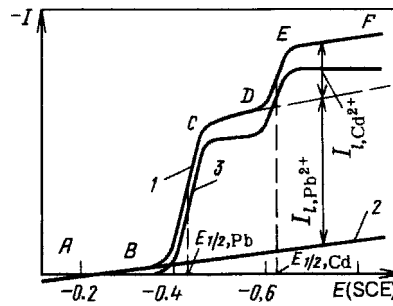

FIGURE 23.3 Polarogram measured in $1 \times 10^{-3}\,M$ $PbCl_2 + 5 \times 10^{-4}\,M$ $CdCl_2 + 1\,M$ KCl solution.

value of $E_{1/2}$ depends on the nature of the ions undergoing discharge and can be used to identify them. From the value of the limiting current, we can determine the concentration of the reactant ions in the solution.

Polarograms are sometimes distorted by *polarographic maxima*, where the current in individual segments of the I vs. E curves is much higher (several times) than the limiting diffusion current. A number of reasons exist for the development of these maxima.

13.4.3 Possibilities and Disadvantages of the Polarographic Method

The polarographic method can be used to analyze a large group of solutes qualitatively and quantitatively (even when they are present simultaneously) that can be reduced within the working potential range of the DME. It is an advantage of the method that solutions with low concentrations of the test substances can be analyzed, approximately down to (1 to 5) $\times 10^{-5}\,M$. The volume of the solution sample needed for analysis can be as small as 1 mL or less. Hence, one can detect less than 0.01 mg of the substance being examined. The error limits of analysis are $\pm 2\%$ when appropriate conditions are maintained.

Because of these advantages, polarography became very popular immediately after its inception in 1922. For the development of this method, Heyrovský was awarded a Nobel prize in 1959. Over the period from 1922 to 1960, several tens of thousands of papers concerned with the use and improvement of polarography were published. However, interest in this method declined markedly in the 1960s, due primarily to a drastic increase in the requirements to be met by methods of chemical analysis. With the production of new superpure materials and increasing awareness for ecological problems, it became necessary to develop much more sensitive methods of analysis able to detect the different impurities down to a level of $10^{-8}\,M$.

The major defects of classical polarography are as follows: (1) it is not possible to increase the sensitivity drastically, owing to interference from DME charging currents;

Jaroslav Heyrovský (1870–1967; Nobel prize, 1959).

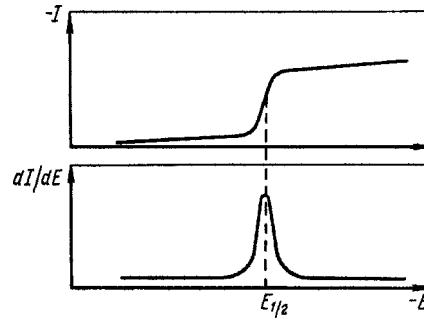

FIGURE 23.4 Polarographic curves plotted as I vs. E and as dI/dE vs. E.

(2) the measuring time is long (between 3 and 10 min for a single solution sample); and (3) substances that can be oxidized but not reduced cannot be analyzed by the method.

Numerous attempts have been made to overcome some of the defects listed. Electrical circuits for an automatic compensation of charging currents and a direct recording of the faradaic current are available in modern polarographs to reduce the influence of the charging currents. However, the accuracy of such compensation is limited, particularly at low reactant concentrations.

The sensitivity and selectivity can be raised when recording as a function of potential not the current but its derivative with respect to potential. In this case a curve with maximum is obtained (Fig. 23.4) instead of the polarographic wave. The potential of the maximum corresponds to the half-wave potential in an ordinary polarographic curve, and the height of the maximum is proportional to the concentration of the substance being examined. A signal proportional to the derivative can be formed in polarographs with the aid of relatively simple electric circuitry.

Along with their advantages, dropping mercury electrodes have disadvantages. In particular, they cannot be used at potentials more positive than the equilibrium potential of mercury in a given solution; hence, they are unsuitable for most anodic reactions. Also, work with DME is inconvenient (e.g., in the field), and it is for this reason that solid electrodes are often used for polarographic measurements. Conditions must then be set up that will provide a quantitative control of diffusion of the substance in solution so that the concentration can be calculated from the limiting current. This is possible in two cases: with microelectrodes [where a steady state is established quite rapidly; see Eq. (11.26)] and with rotating-disk electrodes. These electrodes are suitable for measurements both in the classical polarographic mode and in various new modes. It must be pointed out that today the term *polarography* is reserved for DME measurements; measurements involving other types of electrodes are called *voltammetric*.

23.5 TRANSIENT VOLTAMMETRIC TECHNIQUES

In the transient voltammetric methods, one measures the characteristic parameters on transient polarization curves after some potential or current perturbation has been

applied to the electrode. Many versions of transient methods of voltammetric analysis using single or repetitive potential or current signals with different shapes and amplitude have been described. These versions have been developed with the basic aim of raising the method's sensitivity by increasing the ratio between the levels of useful signal (the faradaic current) and background (charging current, etc.). Under transient diffusion conditions the faradaic currents are much higher than in the steady state (see Chapter 11). Charging currents arise for two reasons: (1) a change of potential and associated change in EDL charge density, and (2) a continuous increase in electrode area. In classical polarography only the second of these reasons is of practical importance; at solid electrodes only the first reason is important.

In transient measurements one must record rapidly changing currents or potentials. In the past, cathode-ray oscilloscopes have been used for this purpose (at present, improved recording devices or computers are used as well), hence the term *oscillographic polarography* (or *oscillographic voltammetry*). This term is unfortunate since it reflects only the device used to record the results, rather than the essential features of the method used for the measurements.

23.5.1 Impressed-AC Method

This method was proposed in 1941 by Jaroslav Heyrovský under the name *oscillographic polarography*. Here, an adjustable sinusoidal alternating current is applied galvanodynamically to the electrode; its strength (amplitude) is selected so that the electrode potential is scanned through the full potential range required. In a solution not containing reacting substances (Fig. 23.5, curves 1), the potential–time relation is also sinusoidal (Fig. 23.5*a*). When a reacting substance is present (curves 2), steps or arrests appear in the E vs. t curve at the potential where the corresponding reaction starts. The lengths of the arrests correspond to the transition time t_{lim}, after which the surface concentration of the reacting species has fallen to zero [see Section 11.2, Eq. (7.9)]. The higher the reactant concentration, the longer the step will be. The changes in the curves can be seen more distinctly when plotting dE/dt against t (Fig. 23.5*b*). When the curve is plotted as dE/dt against E (the corresponding transformation is accomplished in the oscilloscope itself), closed curves are obtained which, when a reactant is not present, are elllipses (Fig. 23.5*c*). When a reactant is present, typical dents appear in the upper and lower halves of the ellipse. The position of the dents relative to the axis of potentials is characteristic for the nature of the reactant; their height is characteristic for its concentration. When several reactants are present in the solution, several pairs of dents develop in the curve. This method allows very rapid measurements to be made, but in its sensitivity and selectivity, it is inferior to other transient voltammetric techniques.

23.5.2 Method of Consecutive Potentiostatic Pulses

In this method, which was proposed in 1957 by Geoffrey C. Barker, a series of potentiostatic pulses of increasing amplitude (Fig. 23.6*a*) are applied to the electrode. Between pulses the electrode is at a potential where there is no reaction; during

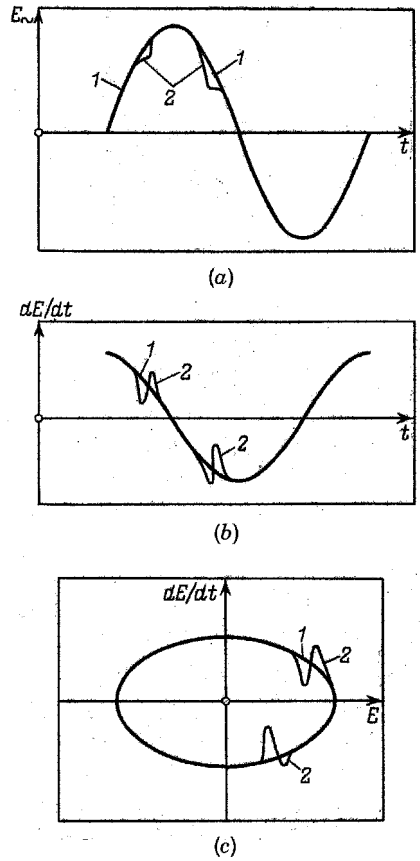

FIGURE 23.5 Curves obtained when impressing an alternating current on the electrode and plotted in different sets of coordinates: (1) base–electrolyte solution; (2) solution with reactant.

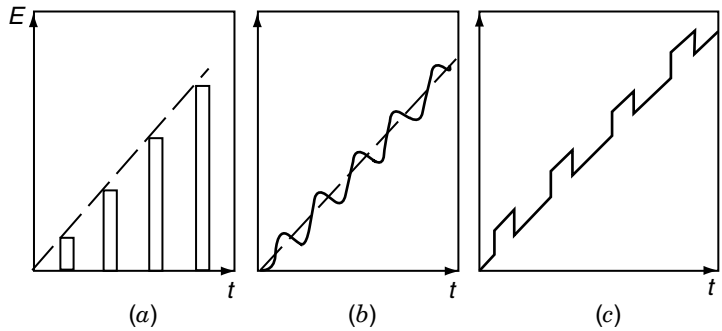

FIGURE 23.6 (*a*) Sequence of potentiostatic pulses of increasing amplitude; (*b*) linear potential scan with superimposed sinusoidal signals; (*c*) linear potential with superimposed rectangular signals.

this time the concentration changes caused by a prior pulse will level off. The typical length of an individual pulse is 40 to 60 ms, that of the interval between the pulses is 1 s. By this time the transient current due to the change of the EDL charge has practically fallen to zero, and the current being measured is basically faradaic. The diffusion conditions are transient because of the short duration of the pulses, and the current is many times higher than the steady-state current. This is a situation favorable for the determination of small amounts of impurities.

The method of potentiostatic pulses is sometimes combined with the DME (called *pulse polarography*). In this case the pulse frequency should match the drop frequency, where each pulse is used at a definite time in the drop life. In Barker's method, large pulse amplitudes are used. Other versions of the potentiostatic pulse technique are square-wave and staircase voltammetry; here small-amplitude pulses are used.

23.5.3 Linear Potential Scan Voltammetry

Voltammograms with characteristic current maxima are obtained (see Fig. 12.9) when linear potential scans (LPS) which are not particularly slow are applied to an electrode. The potentials at which a maximum occurs depend on the nature of the reactant, while the associated current depends on its concentration. When several reactants are present in the solution, several maxima will appear in a curve.

According to Eq. (12.8), the faradaic current is proportional to the square root of scan rate v. According to Eq. (12.13), however, the charging current is proportional to the scan rate. Thus, the ratio I_f/I_{ch} decreases with increasing v, and the measuring sensitivity falls. For this reason, relatively low scan rates, 20 to 50 mV/s, are used in measurements at solid electrodes.

Under optimum conditions LPS voltammetry is an order of magnitude more sensitive than polarography (i.e., the detection limit is about $10^{-6}M$). As in classical polarography, somewhat higher sensitivity and selectivity can be attained when using a differential version (i.e., when recording, as a function of potential, not the current but its derivative with respect to potential).

23.5.4 AC Voltammetry

This term combines a group of methods where periodic alternating potential signals of sinusoidal (Fig. 23.6*b*), rectangular (Fig. 23.6*c*), or other form are superimposed on a slow LPS. The signal amplitude is low, usually 10 to 20 mV. The total current through the electrode is not measured, only its alternating component. Plots of this component against the dc potential (without its periodic excursions) pass through a maximum. As in other cases, the position of the maximum is characteristic for the nature of the reactant, and the height of the maximum is characteristic for its concentration.

Rather high charging currents cross the electrode when a variable potential component is applied. Therefore, to reduce the influence of these currents in the case of rectangular pulses, the measurements are made at a specific time after the potential change, when the charging current has decreased drastically. In the case of sinusoidal superimposed currents, one uses another device based on the fact that the

alternating charging current (or capacitive current) and the alternating faradaic current have different phase shifts relative to the applied alternating voltage. The capacitive current component has a phase lead of 90° relative to the voltage; for the faradaic current this lead is 45° or less, depending on the character of the reaction (see Section 12.5). Hence, one can use phase-sensitive instruments to measure the ac only in a particular phase. For instance, when measuring the current with a phase shift of 90° relative to voltage, the capacitive current will not appear at all, since at this point it goes through zero, yet a significant fraction of the faradaic current can still be measured at that time. When used in combination with the DME, this method has been called *vector polarography*.

The methods of ac voltammetry are widely used for kinetic studies of different electrochemical reactions. The sensitivity for analytical purposes is about $10^{-7}M$. It can be raised by about an order of magnitude when versions are used in which the ac signal is recorded not at the fundamental frequency of the ac voltage, but at its second harmonic, or when still more complicated effects are used.

23.6 POTENTIOMETRY

Potentiometry is suitable for the analysis of substances for which electrochemical equilibrium is established at a suitable indicator electrode at zero current. According to the Nernst equation (3.31), the potential of such an electrode depends on the activities of the potential-determining substances (i.e., this method determines activities rather than concentrations).

As an example, consider the potentiometric determination of concentration $c_N^{(x)}$ of ions N^{z+} in a solution E_x which is to be accomplished with the aid of an electrode of metal N. Using a simple cell with the reference electrode M_R/E_R,

$$M_R \,|\, E_R \,\vdots\, E_x \,|\, N, \tag{23.2}$$

we find that the measured value of potential is distorted by the diffusion potential φ_d present between solutions E_R and E_x, which in most cases cannot be calculated exactly. For activity determinations we must also know the standard potential E^0 of the electrode used. To change over from activities to concentrations, the activity coefficients of the electrolyte must be known as a function of concentration.

The problem can be simplified when the peculiar concentration cell

$$M_R \,|\, E_R \,|\, E_1 \,|\, N \,|\, E_x \,\vdots\, E_R \,|\, M_R \tag{23.3}$$

is used. The test solution is on the right-hand side of the cell, and solution E_1 with the exactly known concentration $c_N^{(1)}$ of ions N^{z+} (the standard solution) is on the left-hand side of the cell. When a standard solution is used which has an ionic strength close to that of the test solution, the activity coefficients in the two solutions can be assumed to be approximately the same. If, in addition, the two solutions differ but slightly in their ionic compositions, the difference in diffusion potentials, $\Delta\varphi_d$,

between the left- and right-hand parts of the cell can be neglected. Under these conditions the voltage of cell (23.3) assumes the form

$$\mathscr{E}_{(x)} = \frac{RT}{z_+F} \ln \frac{c_N^{(x)}}{c_N^{(1)}}, \tag{23.4}$$

offering the possibility to calculate concentrations $c_N^{(x)}$ directly from measured OCV values $\mathscr{E}_{(x)}$. The concentrations of anions can be measured analogously when electrodes of the second kind are used.

It is a special feature of potentiometry that the response signal depends not on the parameter (activity or concentration) that is measured but on its logarithm. On one hand, this implies poorer accuracy and sensitivity of the measurements; for instance, an error of 0.2 mV committed in determining the potential or OCV produces an error in the concentration value found of 0.8% for $z_j = 1$, 1.6% for $z_j = 2$, and 2.4% for $z_j = 3$. On the other hand, however, the accuracy does not depend on the absolute value of the concentration being measured. This is an important difference relative to methods of analysis where the limiting current or current of a maximum is determined, and where the relative error often increases drastically with decreasing concentration and decreasing faradaic current. Hence, potentiometry can be used over a much wider range of concentrations than the voltammetric methods: from concentrated solutions down to solutions with a concentration of 10^{-5} to $10^{-7}\,M$ of the ion being determined, or down to even lower concentrations when ionic equilibria exist (see Section 3.5.4). Thus, the solution pH can be determined over the pH range -2 to 15. When dealing with wide concentration ranges of different ions, it is convenient to use the concentration exponent $\mathrm{pJ} = -\log c_j$, which is the analog of parameter pH for the hydrogen ions.

An important condition for potentiometry is high selectivity; the electrode's potential should respond only to the substance being examined, not to other components in the solution. This condition greatly restricts the possibilities of the version of potentiometry described here when metal electrodes are used as the indicator electrodes. The solution should be free of ions of more electropositive metals and of the components of other redox systems (in particular, dissolved air). Only corrosion-resistant materials can be used as electrodes. It is not possible at all with this method to determine alkali or alkaline-earth metal ions in aqueous solutions.

23.6.1 Ion-Selective Electrodes

Considerable progress was made in overcoming the difficulties pointed out above, when highly selective membranes started to be used in potentiometry instead of the metallic indicator electrodes. The first work involving thin glass membranes goes back to the beginning of the twentieth century (Max Cremer and Fritz Haber). Work involving a variety of new membrane types was started in the 1960s; these studies expanded the potential applications of potentiometry dramatically.

Consider the same example, of determining the concentration of ions N^{z+}, but now while using a membrane having ideal permselectivity (i.e., a membrane that is

permeable only for ions N^{z+} but completely impermeable for all other ions present in the system). Let this membrane be designated as $\mu\{N^{z+}\}$. We use the cell

$$M_R \,|\, E_R \,|\, E_1 \,|\, \mu\{N^{z+}\} \,|\, E_x \,|\, E_i \,|\, M_i, \tag{23.5}$$

which is the analog of cell (23.2). At the interfaces between the two solutions and the membrane, equilibria are established for ions N^{z+}, and certain potential differences develop between the phases (see Sections 5.3 and 5.4). According to Eq. (5.5), for the left-hand side this potential difference can be written as

$$\varphi_G = \text{const} + \frac{RT}{z_+F} \ln \frac{a_N^{(x)}}{a_N^{(1)}}; \tag{23.6}$$

the expression for the right-hand interface is analogous (and contains the same value of the constant). Hence, we have for the full cell's OCV (under the assumptions made above),

$$\mathscr{E}_{(x)} = \frac{RT}{z_+F} \ln \frac{c_N^{(x)}}{c_N^{(1)}} \tag{23.7}$$

[i.e., exactly the same OCV value is obtained as in the case of cell (23.2)].

Thus, the behavior of the selective membrane $\mu\{N^{z+}\}$ is completely equivalent to that of an electrode of metal N. Hence, membranes of this type are called ion-selective electrodes, and in the particular case discussed, the membrane is called an *N^{z+}-selective electrode*. Sometimes the term is extended to the entire left half of cell (23.5), which in addition to the membrane contains the standard solution and the reference electrode.

The conclusion above is valid for ideally selective membranes. Real membranes in most cases have limited selectivity. A quantitative criterion of membrane selectivity for an ion N^{z+} to be measured, relative to another ion M^{z+}, is the selectivity coefficient $\sigma_{M/N}$. The lower this coefficient, the higher the selectivity will be for ions N^{z+} relative to ions M^{z+}. An electrolyte system with an imperfectly selective membrane can be described by the scheme (5.16). We assume, for the sake of simplicity, that ions N^{z+} and M^{z+} have the same charge. Then the membrane potential is determined by Eq. (5.17), and the equation for the full cell's OCV becomes

$$\mathscr{E}_{(x)} = \frac{RT}{z_+F} \ln \frac{c_N^{(x)} + \sigma_{M/N} c_M^{(x)}}{c_N^{(1)}} + \varphi_d. \tag{23.8}$$

A diffusion potential φ_d can develop in the membrane since in the case being considered, it contains two types of mobile ion. However, this potential is small.

It can be seen from Eq. (23.8) that as long as concentration $c_M^{(x)}$ is much lower than $\sigma_{M/N}^{(x)} c_N$, the ions M^{z+} will have no influence on the readings of the N^{z+}-selective electrode. If, for instance, $\sigma_{M/N} \approx 10^{-6}$, this conclusion holds up to concentrations of ion

M^{z+}, which are four to five orders of magnitude higher than those of ions N^{z+}. The influence of the foreign ion must be taken into account, but at still less favorable concentration ratios.

Equation (23.8) had been derived in 1937 by Boris P. Nikol'skij for glass electrodes used to determine the hydrogen ion concentration when the sodium ions contained in the glass membrane are the foreign ions. Various cell designs exist for potentiometry with ion-selective electrodes. The design most often used is shown schematically in Fig. 23.7. A membrane (1) covers the lower part of a cylindrical cell. The cell contains the standard (internal) solution (2) and the reference electrode (3). The membrane is in contact with the test (external) solution (4), which contains a second reference electrode (5). The cell can be miniaturized as a capillary for analyses in extremely small solution volumes [e.g., the fluid inside an individual (physiological) cell].

It is the major task of practical ion-selective potentiometry to develop sufficiently selective and stable membranes. Different membranes are presently used: solid and liquid, organic and inorganic, homogeneous and heterogeneous. An example of homogeneous solid membranes is a membrane that consists of a thin layer of single-crystal lanthanum fluoride, LaF_3, which has unipolar fluoride ion conduction. This membrane can be used for the potentiometric determination of F^- ions in solutions at concentrations between approximately 10^{-6} and 1 *M*. The selectivity of this membrane is such that measurements can be made with a 1000-fold excess of most other types of ion. Fluoride-selective electrodes are used widely for the analysis of noxious fluorides in the air or in industrial fumes (following their prior absorption by aqueous solution). The sensitivity of the method is so high that as little as 0.1 $\mu g/m^3$ can be detected.

In heterogeneous solid membranes, the active (selective) material is mixed in the form of a powder with a suitable binder (e.g., silicone rubber) and cast in the form of thin membranes. In this case, the difficulties associated with single-crystal fabrication are avoided, and better stability is obtained than in membranes compressed from polycrystalline powder.

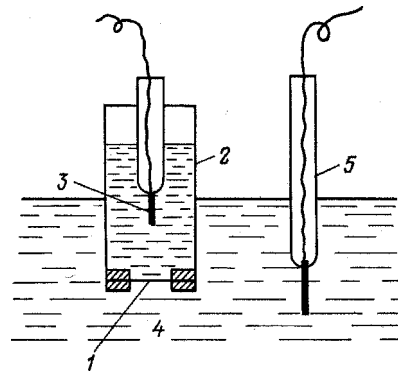

FIGURE 23.7 Schematic of a cell with ion-selective electrode.

Unfortunately, solid materials with high ionic selectivity are rare. Many organic and inorganic ion exchangers are poorly selective with respect to different ions of like charge. For this reason, liquid membranes have become very popular. They consist of an interlayer of liquid that is immiscible with aqueous solutions (or test solutions in other solvents), and displays selectivity with respect to an individual ion or group of ions. Immiscibility of the working fluid with water is attained when aliphatic compounds with long hydrocarbon chains or aromatic compounds are used. Selectivity is attained through the specific chemical interaction between functional groups of these compounds or other, added substances and the given sort of ion.

By now a large number of ion-selective substances are known. They are used for the potentiometric concentration determination of practically all kinds of cations and anions. Numerous publications and monographs of the last two decades are concerned with ion-selective electrodes.

23.6.2 Glass Electrode

Glass electrodes were the first ion-selective electrodes to become known. For more than 60 years, they have been widely used for pH determinations in solutions, both in industry and in scientific research, particularly in biology and medicine. The conductivity of glass at room temperature is very low. It arises from the slight mobility of sodium ions in the glass. Special types of glass are used for glass electrodes to lower their resistance. In addition, they are made as thin as possible. Usually, the electrodes are blown from glass tubing in the form of bulbs having a wall thickness of about 0.1 mm.

In its usual form, glass does not contain hydrogen ions. However, during the leaching of glass in aqueous solutions its surface layer is altered to a certain depth; water molecules enter, and hydration processes and some swelling occur. Part of the sodium ions in the surface layer are leached out and are replaced by hydrogen ions from the solution. Equilibrium is established between the hydrogen ions in the surface layer and those in solution; hence, an equilibrium potential difference between the phases arises. The special feature of this surface layer is its exceptionally high selectivity toward hydrogen ions (relative to sodium ions or other cations). For different types of glass, the selectivity coefficients for hydrogen ions relative to other ions are between 10^{-9} and 10^{-14}. For this reason, the two sides of the membrane act as good hydrogen electrodes. In contrast to other types of ion-selective membranes, the current between the two surface layers is transported across the central part of the glass membrane by different ions, the sodium ions.

Figure 23.8 shows the readings of a glass electrode [the measured values of $E_{(x)}$ of a cell of the type (23.5)] as a function of solution pH. In the range from acidic to neutral solutions, this curve perfectly obeys Eq. (23.7) (i.e., the potential varies linearly by 0.06 V per unit of pH). However, in alkaline solutions the curve departs from this function ("alkali error of the glass electrode"); in strongly alkaline solutions the readings of the electrode are practically independent of solution pH. This is due to violation of the selectivity conditions. At a pH value of 10 and a sodium ion

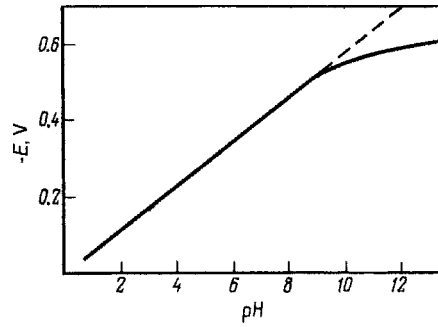

FIGURE 23.8 Potential of a glass electrode as a function of solution pH.

concentration in the solution of 0.1 *M*, the concentration ratio of sodium and hydrogen ions is 10^9. Under these conditions the electrode's potential is appreciably codetermined by the sodium ions. At still higher pH values, the membrane functions entirely as a sodium electrode.

REFERENCES

Barker, G. C., *Anal. Chim. Acta*, **18**, 118 (1958).

Clark, L. C., and G. Saches, *Ann. N.Y. Acad. Sci*., **148**, 133 (1968).

Cremer, M., *Z. Biol*., **47**, 562 (1906).

Haber, F., and Z. Klemensiewicz, *Z. Phys. Chem*., **67**, 385 (1909).

Heyrovský, J., *Chem. Listy*, **16**, 256 (1922); *Philos. Mag.*, **47**, 303 (1923).

Ilkovič, D., *Collect. Trav. Chim. CSR*, **6**, 498 (1934).

Nikol'skij, B. P., *Zh. Fiz. Khim*., **10**, 495 (1937).

MONOGRAPHS

Bond, A. M., *Modern Polarographic Methods in Analytical Chemistry*, Marcel Dekker, New York, 1980.

Galus, Z., *Fundamentals of Electrochemical Analysis*, Ellis Horwood, Chichester, West Sussex, England, 1976.

Lakshminarayanaiah, N., *Membrane Electrodes*, Academic Press, New York, 1976.

Nürnberg, H. W., Ed., *Electroanalytical Chemistry,* Vol. 10 of *Advances in Analytical Chemistry and Instrumentation*, Wiley, London, 1975.

Vassos, B. N., and G. W. Ewing, *Electroanalytical Chemistry*, Wiley, New York, 1983.

24

Electrochemistry and the Environment

ALEXANDER SKUNDIN (*Sections 24.1 to 24.4*)

A. N. Frumkin Institute of Physical Chemistry and Electrochemistry, Russian Academy of Sciences, Moscow, Russia

ALVIN J. SALKIND (*Section 24.5*)

Bioengineering Division, University of Medicine and Dentistry of New Jersey, Piscataway, New Jersey

24.1 CHEMICAL AND ELECTROCHEMICAL PROCESSES

On the whole, electrochemical processes in the winning of various metals and other substances are more acceptable ecologically (although not always economically) than commercial chemical or metallurgical processes used for winning the same substances. As a rule, they proceed at a lower temperature and generate a considerably smaller amount of side products. Most of the side products that are generated (hydrogen, oxygen) are ecologically harmless. The target products of the electrochemical industries as a rule are sufficiently pure and need no additional purification (which sometimes also leads to ecologically harmful discharges). As an example, consider the electrolytic production of pure hydrogen compares with its much cheaper production by the reforming of hydrocarbons, during which the hydrogen itself as well as the environment are contaminated by CO and other harmful foreign substances.

In a thorough ecological comparison of electrochemical with other manufacturing methods, of course, the pollution of air and water by the additional generation of electric power must also be taken into account. Fortunately, the largest electrochemical industries, such as aluminum production, as a rule are concentrated around ecologically clean hydropower plants.

Improvements in the electrochemical processes will allow further reduction of their harmful ecological effects. These include a reduction in energy requirements

Fundamentals of Electrochemistry, Second Edition, By V. S. Bagotsky

through the use of improved electrocatalysts and membranes, or in a number of industries, by substituting cathodic air–oxygen reduction for cathodic hydrogen evolution. These also include the elimination of harmful components in a number of electrochemical industries and in products such as mercury in chlor–alkali electrolysis plants and in certain batteries, cyanides in electroplating, and chromates in other electrolytic processes. In the near future, the largest contribution that electrochemistry could make to overall protection of the atmosphere is the design of sufficiently efficient fuel cells to replace internal combustion engines in automobiles.

24.2 MONITORING THE ENVIRONMENT

Almost every method of electrochemical instrumental analysis, including those mentioned in Chapter 23, has been used to monitor contamination in the environment (in both air and water), including conductometric, potentiometric, and amperometric devices and devices for adsorption measurement.

24.2.1 Electrochemical Instruments for the Analysis of Gaseous Media

Potentiometric instruments are used most often when analyzing harmful contaminants in the air at production sites or in cities. Electrodes, whose potential is, as a rule, a linear function of the logarithm of concentration of the substance to be determined (by Nernst's law), are the sensing elements in such instruments. Most potentiometric sensors are highly selective.

When analyzing hot gases for their hydrogen sulfide content, for instance, a solid electrolyte sensor consisting of the galvanic cell

$$\mathrm{C}\,|\,\mathrm{Me}\,|\,\mathrm{MeS}\,|\,\text{solid electrolyte}\,|\,\text{gas being analyzed}\,|\,\mathrm{Ar, C} \qquad (24.1)$$

is used. A ceramic that is a sulfide ion conductor consisting of binary sulfides of an alkaline-earth metal (Ca, Ba) and a lanthanide (Nd, Sm, Y) is used here as the solid electrolyte; MeS is calcium or barium sulfide. The cell's OCV measured with an electronic voltmeter varies linearly with the logarithm of hydrogen sulfide concentration.

A similar device with Nasicon solid electrolyte $Na_3Sc(PO_4)_3$ is used when analyzing the concentration of nitrogen oxides in air. The electrochemical system in this sensor can be formulated as

$$\mathrm{Ni}_x\mathrm{O}_y\,|\,\text{Nasicon}\,|\,\text{gas being analyzed}\,|\,\mathrm{PbO_2} \qquad (24.2)$$

The sensor's function rests on the property of lead dioxide to sorb nitrogen oxides (NO_x), forming lead nitrate. In this case the lead nitrate concentration is proportional to the nitrogen oxide concentration in the air. The sorption of the nitrogen oxides is a reversible process: The PbO_2 is regenerated completely within a few minutes when exposed to clean air (free of nitrogen oxides).

An instrument for determining the concentration of carbon monoxide in air may serve as an example of an amperometric gas analyzer. In this case, a three-electrode cell with a gelled aqueous sulfuric acid solution or with a solid polymer electrolyte is used. In this cell, a given constant value of potential that corresponds to the limiting diffusion current of CO oxidation is maintained at the working electrode with a potentiostat. Over the range of CO concentrations from about 5 to 200 mg/m^3, the limiting current is proportional to the CO concentration in the gas being analyzed. All three electrodes are porous, hydrophobized gas-diffusion electrodes (see Section 18.4.2). The active layer in the electrodes consists of highly disperse platinum catalyst mixed with fluoropolymer powder. It is a decided defect of this sensor that the current of hydrogen oxidation adds to that of CO oxidation when hydrogen is present as well. It could be shown that a distinct selectivity arises when mixed platinum—rhodium catalysts are used; at equal-volume concentrations of CO and hydrogen, the current of CO oxidation then exceeds that of hydrogen oxidation by a factor of 25 to 30.

24.2.2 Electrochemical Instruments for the Analysis of Aqueous Media

The simplest estimate of the overall salinity of water (its ionic impurity content) is obtained by measuring its conductivity. Such measurements can be useful, for instance, when checking the purity of rinsing waters from the plating and metal-finishing industries. A quantitative estimate of the degree of contamination is possible via conductometry when the qualitative composition of the ionic contaminants is known and does not change.

The most reliable electrochemical method for the qualitative and quantitative determination of nonferrous metal ions is voltammetry. In practical ecological surveys, both classical polarography at the dropping mercury electrode by which concentrations of reducible substances not under $10^{-5}\,M$ can be determined, and numerous related methods having a sensitivity about two orders of magnitude higher (square-wave, pulse, oscillographic polarography), are widely used. Polarographic studies at microelectrodes and inverse polarography became popular more recently. In inverse polarography, the metal to be analyzed is deposited cathodically on an electrode during a certain length of time, even from highly dilute solutions, and is then dissolved anodically by a brief anodic pulse.

Among potentiometric methods of analysis that are important for ecological applications, the one most widely used is that of pH measurements with an indicator electrode whose potential is a function of the hydrogen ion concentration. More recently, ion-selective electrodes reversible to other cations such as those of heavy metals have become available.

An example of the amperometric analysis of water is the use of Clark electrodes for determining the concentration of dissolved oxygen. (Clark electrodes are most popular for oxygen determinations in biological fluids.) In a Clark electrode, the indicator electrode is separated from the test fluid by a polymer membrane that is permeable to oxygen. A potential at which the limiting current of oxygen reduction is set up is maintained at the indicator electrode. This current is proportional to the concentration of oxygen dissolved in the water being analyzed.

A universal electrochemical instrument for estimating water purity on the basis of adsorption measurements was developed at the Moscow Institute of Electrochemistry. The indicator electrode in this potentiostatic instrument consists of platinum. During cathodic polarization in clean solution (e.g., of sulfuric acid), a monolayer of hydrogen is adsorbed on the platinum surface. Organic substances and most ions will also adsorb on platinum from solutions containing them. By their adsorption, these contaminants will displace adsorbed hydrogen. The amount of contaminants adsorbed can thus be determined by measuring the difference between the amounts of hydrogen adsorbed from the clean solution and from the solution being analyzed.

It is not possible with this instrument to exactly determine the chemical nature of the contaminants, but certain qualitative conclusions are possible. Since the adsorption of substances depends on potential, either the organic contaminants or certain heavy-metal ions will become adsorbed on platinum when selecting appropriate working potentials. From the readiness of the adsorbed organic contaminants to undergo oxidation upon anodic polarization, it is also possible to distinguish categories of contaminants that are easy or difficult to oxidize, or take up an intermediate position. The former include low-molecular-weight alcohols, aldehydes, and acids, the latter include phenols, aromatic acids, and many surfactants; aromatic and alicyclic compounds are difficult to oxidize. The adsorption method has a very high sensitivity, on the order of 0.01 mg/L for total organic carbon and of 0.001 mg/L for heavy-metal ions.

24.3 PURIFICATION PROCEDURES (ELIMINATION OF POLLUTANTS)

The scale of practical uses of the electrochemical methods available for purifying effluents and render them harmless is rather small at present and does not correspond to the possibilities of electrochemistry. Diverse electrochemical technologies exist for effluent purification. In many plating and metal-finishing industries, rinsing waters containing nonferrous metal ions are electrolyzed while depositing the corresponding metals at the cathode. In solutions highly dilute in heavy metals, unfortunately, the current yields of the useful reactions are small. In addition, rinsing waters in these industries may have insufficient conductivity, so that the power consumption for purification is rather high. Some increase in efficiency could be attained with three-dimensional electrodes (see Section 18.5).

Two variants of purification by sorption must also be counted among the electrochemical methods. In the first variant, the sorbent is obtained electrochemically. Here effluents containing both organic and inorganic contaminants, heavy-metal salts in particular, are subjected to electrolysis with steel or aluminum anodes. During electrolysis these anodes dissolve while hydrogen is evolved at the (steel) cathode. The layer next to the cathode, and subsequently all the water in the gap between the electrodes, becomes so alkaline that the dissolved iron and aluminum ions will form highly porous hydroxides (alumogels and the corresponding iron gels) with a very highly developed surface area which in time will coagulate together

with the contaminants that have adsorbed on them, and thus are readily eliminated from the effluent. This purification method is also known as *electrocoagulation*.

The resulting sludge can be used to manufacture building materials, road cover materials, and the like. Adsorptive purification is able to liberate the water from contaminants that cause its bad smell and taste. It is highly effective for the removal of xenobiota and of traces of petroleum products. In some cases it can even decolorize the water.

In the second variant (*electrosorptive purification*, properly speaking), a material with high electronic conductivity, usually activated carbon or another carbon material, is used as the adsorbent. The adsorption of most substances depends on the charge of the adsorbent surface. The electrostatic adsorption of ions of a given sign increases when the adsorbent surface is oppositely charged, whereas the adsorption of most organic substances is greatest on uncharged adsorbent surfaces. In electrosorptive purification, the adsorbent is polarized from an external source (with the aid of an auxiliary electrode) in such a way that its potential (or charge) will be most favorable for the adsorption of particular contaminants. The adsorbent is readily regenerated afterward by changing the potential to values where the contaminants become desorbed.

The purification of water by electroflotation is of interest, too. In ordinary flotation, a gas (as a rule, air) is passed through the water to be purified. Its bubbles, while rising, carry along the surface-active contaminants as well as colloidal or other substances suspended in the water. The finer the gas bubbles, the more efficient the flotation. In electroflotation, the gases (hydrogen and oxygen) are obtained by electrolysis with the aid of electrodes arranged at the bottom of the electroflotation vessel. The size of the gas bubbles produced depends on solution pH and electrode charge (see Section 14.5.2). Under certain conditions of electrolysis, one can obtain rather finer bubbles than from the compressed air, so that in the final analysis, electroflotation is economically quite acceptable, even though the energy requirements for gas production by electrolysis are much higher than those for the production of compressed air.

An efficient method for degreasing and purifying effluents containing organic contaminants is the complete electrochemical oxidation of these substances to carbon dioxide and water, as well as to nitrogen when nitrogen-containing substances are present. The anodic oxidation of many organic substances is easy, but some are difficult to oxidize. For the complete oxidation of an organic substance to carbon dioxide and water, a rather large amount of energy is consumed. In the case of hydrocarbons, for instance, 11.5 Ah per gram of the material is consumed for oxidation. With an average voltage in the electrolyzer of 2.5 V and a contaminant concentration of merely 100 ppm, the energy consumption will be 3 kWh per cubic meter of the water being treated.

Attempts to build electrochemical systems for oxidative purification of effluents have met a number of problems:

1. Many effluents have low conductivity values.

2. Many substances are oxidized only at rather high anodic potentials, which narrows the available selection of corrosion-resistant anode materials. An alternative to platinum metals are certain metals with an oxide coating (PbO_2, MnO_2, SnO_2) which

are used in traditional methods of electrochemical purification by oxidative destruction. At corrosion-resistant metals such as titanium and tantalum, the activity with respect to anodic oxidation reactions of organic substances is too low. An important increase in electrocatalytic activity can be attained by promoting (activating) the surfaces of these refractory metals with minute amounts of platinum metals or platinum metal oxides (electrodes of the DSA type; see Section 28.7). Most recently, electrodes made of synthetic, boron-doped diamond have begun to find applications on an industrial scale. These electrodes are plates of a carrier material onto which a thin layer of synthetic diamond measuring a few micrometers in thickness has been applied by CVD (chemical vapor deposition). These electrodes have an exceptionally high corrosion resistance. They are ecologically more acceptable than the widely used lead dioxide electrodes.

3. The anodic oxidation of organic substances is a complex multistep process. The question as to the depth of oxidation required (and sufficient) has to be answered in each case. Where intermediate oxidation products pose no ecological risk, one can stop at incomplete oxidation. However, in the anodic oxidation of many aromatic substances, the corresponding quinones are formed in the first step, and these are more harmful than the original substances. Upon more profound oxidation, the benzene rings are broken and aliphatic substances are formed that are almost as harmless as carbon dioxide.

4. In anodic processes conducted at high potentials, radical-type intermediates often are formed that lead to a polymerization (resin formation) of the organic substances and to passivation of the anodes.

An alternative to the direct anodic oxidation of organic contaminants are the methods of indirect oxidation with the aid of oxidizers formed electrochemically in situ. These oxidizers (or mediators) can be obtained in both anodic and cathodic processes. Anodic agents are the salts of hypochloric acid (hypochlorites), the permanganates, the persulfates, and even ozone.

Indirect oxidation with hydrogen peroxide obtained by cathodic reduction of air oxygen is of great interest. At porous gas-diffusion electrodes made of sufficiently cheap carbon materials, hydrogen peroxide can be produced at high rates (with current densities of up to 200 mA/cm^2). With aqueous peroxide solutions, one can oxidize many contaminants (phenols, quinones, aniline, chloramines, salicylic acid, benzoic acid, etc.) to carbon dioxide. The formation of carcinogenic organic chlorine compounds which often is seen when treating effluents oxidatively with chlorine is not possible here.

Among electrochemical methods of water purification, one can also list the various electromembrane technologies, electrodialysis in particular. The simplest electrodialyzer consists of three compartments separated by semipermeable membranes (usually, cation- and anion-exchange membranes). The water to be purified is supplied to the central (desalination) compartment. In the outer (concentration) compartments, electrodes are set up between which a certain potential difference is applied. Under the effect of the electric field, ions pass through the membranes so that the concentration of ionic contaminants in the central compartment decreases.

24.4 MEDICAL APPLICATIONS OF ELECTROCHEMISTRY

In medicine and electrochemistry, one can find many points of common concern. Electrochemistry as a science started with medical experiments by the Italian physiologist Luigi Galvani. Many processes in living organisms (such as cell division and fusion, nerve pulse propagation, etc.) occur via electrochemical mechanisms. For this reason, electrochemistry is able to model a number of processes occurring in living organisms, which in turn has led to progress in fundamental medical science.

In medical practice, methods and instruments relying on electrochemical principles are widely used in diagnosing various diseases. The most important ones are electrocardiography, where the transmembrane potential of the muscle cells during contraction of the heart muscle is measured, and electroencephalography, where impulses from nerve cells of the brain are measured. They also include the numerous instruments used to analyze biological fluids by electrochemical methods (see also Section 30.3).

In addition, electrochemical methods and instruments based on electrochemical phenomena may find direct uses in healing various diseases. The most significant example of a direct healing method relying on an electrochemical phenomenon is defibrillation, a technique used in reanimation where contraction of the heart muscle is provoked by an electrical pulse.

Electrochemical healing methods also include the electrodialytic introduction of drugs through the skin of a patient. With these methods a precise dosage of the drug and its highly accurate topical introduction are possible. In this way one can, for instance, arrange for a system of insulin supply according to a fixed program or according to signals from an electrochemical sensor for glucose in blood.

A very important but as yet unresolved medical problem is the realization of an artificial heart. Modern technologies can be used to implant into the human body miniature pumps capable of pumping the required amount of blood at the required rate, but it is very difficult to secure an appropriate electric power supply to these pumps. An implantation of ordinary electrochemical batteries is not feasible, since an overly large battery would be required to secure uninterrupted function of the pumps for several years. The assurance of long-term sterile conditions at the site of introduction of the leads is a problem that would have to be solved when setting up the power source outside the body. The most readily acceptable approach would be an implanted fuel cell using blood glucose as the fuel and oxygen bound to red blood cells as the oxidizer. The anodic oxidation of glucose has been a subject of numerous studies, but unfortunately, so far neither electrodes nor conditions have been found that would sustain a sufficiently selective and rapid electrochemical oxidation of glucose.

24.4.1 Electrochemical Detoxification of the Organism

More recently, an indirect method of electrochemical detoxification of organisms has been put into practice. It is based on a model of the detoxifying function of the liver. A normal liver produces cytochrome P450, which assures the hydroxylation

and oxidation of all types of toxins arriving in an organism. In indirect electrochemical detoxification, a solution is introduced that contains sodium hypochlorite (NaClO), which, like enzyme systems, is an oxygen carrier. The NaClO solution can be introduced intravenously or used in open-cavity surgery. It is obtained by electrolysis of isotonic physiological solution (0.89% NaCl solution). Having performed its oxidative function, this NaClO is converted to NaCl in exactly the concentration found in healthy organisms.

Another indirect electrochemical healing method involves the artificial kidney machine, with electrochemical regeneration of the dialysis solution. The common kidney machine is a dialyzer in which blood of the patient (who suffers from kidney insufficiency) and a dialysis solution are pumped around in two different loops, and carbamide (urea), creatinine, and other metabolites are transferred by dialysis into the dialysis solution. For complete extraction of the metabolites, each hemodialysis session requires almost 200 L of this solution to be pumped through, so hemodialysis can only be performed in a hospital setting. In machines equipped with electrochemical regeneration, the dialysis solution is run in a closed loop, including an electrolyzer in which the carbamide is oxidized to nitrogen and carbon dioxide. The solution volume needed in this loop is rather small, so that portable kidney machines could become a reality.

In Section 24.3, use of electrosorption for effluent purification was mentioned. The same principle of an electrochemically controlled hemosorption (sorptive blood purification) is used in modern toxicology to extract toxins from blood. By appropriate potential control of the carbon sorbent, particular toxins can be removed selectively without traumatizing the blood, that is, without removing essential blood components such as the thrombocytes.

24.4.2 Electrochemical Life-Supporting Systems

Electrochemical applications in the field of medicine also touch on the vital activities performed in isolated environments. Water electrolysis has long been used to produce oxygen for breathing in submarines. Various regenerative systems that were developed for manned spacecraft are of great interest. In such systems, the atmosphere must be freed from carbon dioxide and condensates containing the exhaled matter from the astronauts, and water must be regenerated from urine. The system of water regeneration includes purification of urine, toilet, and personal-hygiene effluents as well as of the condensate of atmospheric moisture. The condensate of atmospheric moisture and the urine are purified most effectively by electrocatalytic oxidation of urea and other organic contaminants of low molecular weight. Reverse osmosis with a final anodic after-purification is used to purify the toilet and personal-hygiene effluents.

Cathodic reduction is the most promising approach to the removal of carbon dioxide from a closed atmosphere. Methods developed so far provide for electrode materials, electrolytes, and electrolysis conditions where CO_2 can be reduced to liquid organic products of low molecular weight such as formic acid. More complex systems are required to regenerate foodstuffs from the rejects of human vital activities during

prolonged space flights. An important task before electrochemistry in this connection is the synthesis of glucose by electrochemical reduction of CO_2.

24.5 ELECTROCHEMICAL ASPECTS OF BONE REMODELING AND FRACTURE REPAIR

The remodeling and biofeedback of bones have always been of substantial interest to the scientific community from both the research and clinical points of view. The main goals have been primarily: (1) to determine the real feedback mechanism of bones, and (2) to utilize the nature of the feedback system of bone tissue to accelerate the healing process in fractures and other nonunions by creating a similar environment artificially at the fracture sites. Bone tissue has a number of physiological functions that make it a unique connecting tissue and a special electrodic surface. The mechanical function of bone involves not only structural support of the muscular system and load transfer, but also repair and remodeling. Mechanical deformation and the biopotentials associated with deformation have been shown to be associated with the repair and remodeling process.

Bone is a porous tissue composite material containing a fluid phase, a calcified bone mineral, hydroxyapatite (HA), and organic components (mainly, collagen type). The variety of cellular and noncellular components consist of approximately 69% organic and 22% inorganic material and 9% water. The principal constituents of bone tissue are calcium (Ca^{2+}), phosphate (PO_4^{3-}), and hydroxyl (OH^-) ions and calcium carbonate. There are smaller quantities of sodium, magnesium, and fluoride. The major compound, HA, has the formula $Ca_{10}(PO_4)_6(OH)_2$ in its unit cell. The porosity of bone includes membrane-lined capillary blood vessels, which function to transport nutrients and ions in bone, canaliculi, and the lacunae occupied in vivo by bone cells (osteoblasts), and the *micropores present in the matrix.*

The capacity of hard tissue such as bone to generate potentials in response to mechanical stress has been known from the beginning of the nineteenth century. A piezoelectric theory to account for the electric potential observed in dry bone on deformation was proposed by Fukada and Yasuda in 1957 and subsequently explored by many others in the 1950s and 1960s as well as by Friedenberg et al. in 1971.

In the case of wet bone, the origin of electric biopotentials generated through cantilever bending is less clear. Although there is some piezoelectric effect, most of the signal is believed to originate from streaming potential electrokinetics, as discussed in the review by Guzelsu and Salkind in 1991. The surface of bone matrix is negatively charged under physiological conditions and repels the particles carrying the same electrical charge. This leads to a potential difference between the bone surface and the bulk of the fluid. The magnitude of the potential depends on many parameters, including chemical composition, pH, and temperature. This potential counteracts the tendency of bone to dissolve. It has been shown that when bones bend, the convex surface develops a positive surface potential, and the concave surface, a negative potential Fig. 24.1. Thus, the deposition of calcium material is enhanced on the concave side. The opposite effects occur on the convex side. This remodeling tends to straighten misaligned bone.

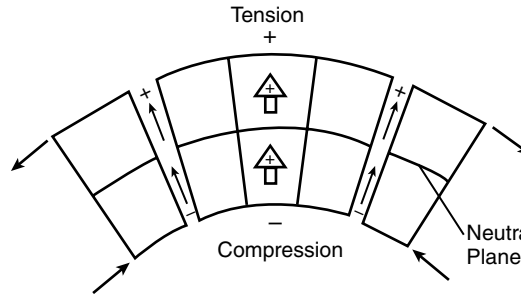

FIGURE 24.1 Surface potentials generated by bending of bone.

Under an electric field, charged bone particles move through the suspending fluid due to electrostatic forces. As a unit, parts of the attracted opposite-charge-carrying entities close to the surface also move with the bone particle. The surface of this unit is called the *surface of shear*, and the potential at this surface with respect to the solution is the *electrokinetic* or *zeta potential* (see Chapter 31). Zeta potentials can be calculated from streaming potential experiments on porous plugs by measuring the generated streaming potential. Measuring the zeta potential is a very useful experimental determination for examining the repair process and the efficacy of devices.

When a fracture occurs in the normal repair process, the blood clots that form on the broken ends are the beginning of the healing process. The fracture site surface becomes somewhat more negative and the exchange current is tipped in the direction of deposition. The cells of the intact endosteum and the periosteum undergo rapid mitosis, and the daughter cells migrate to the fracture site. An external callus, an enlarged collar of cartilage and bone, forms and encircles the bone at the level of the fracture to immobilize the site. This temporary bone (callus) is replaced with real bone later in the process. Unlike skin, broken bones heal without scar formation. However, immobilized muscles weaken and wither and often require rehabilitation and strengthening exercises.

However, there are a significant number of cases, sometimes estimated as 19% of fractures, where repair does not occur in a reasonable amount of time. The problems are associated primarily with severe injury, infection, arthritis, or biochemical abnormalities. A very common cause, known as the *compartment syndrome*, is related to severe swelling pressure on the blood vessels that limits blood access to the muscles. In many of these cases, electrical stimulation has been shown to be effective in accelerating repair.

The electrical stimulation of bone has gone through several approaches. The first and oldest method was invasive and required surgical intervention to place an osteogenesis device or a lead wire electrode at the fracture site to provide a small dc voltage. However, infection often occurred because of the skin penetration. The second approach was mainly noninvasive and involved several methods of coupling an electromagnetic field to body tissues. These are through-the-intact-skin inductive (mainly, low frequencies) or capacitive (mainly, high frequencies) coupling.

There were numerous experiments trial over a 25-year period starting around 1960 with implanted electrodes to stimulate bone formation (osteogenesis). Chemical trials were launched in 1970 as reported by Friedenberg et al. (1971) and reviewed by Salkind et al. (1986). Many studies reported that the application of small currents stimulated osteogenesis at the negative electrode. Various metals and configurations were tested and produced for commercial sale. An early investigator reported that fracture healing was influenced favorably only when the cathode was placed directly at the fracture site. With stainless steel cathodes, currents of less than 5 μA were ineffective, whereas those in the range 5 to 20 μA produced progressingly increased bone formation. Higher currents produced cellular necrosis. It was later recognized that current density, not current, is the important factor. Clinical trials were launched in 1970. Information from a device manufacturer, Teletronics Ltd., about their Osteotim device indicated a bipolar lead construction with a constant current of 20 μA delivered to the fracture site (this company ceased operation in 1996).

Subsequent investigation resulted in a technique of inducing the required negative potential at the fracture site by electromagnetic coupling through intact skin. This were reported by Basset et al. in 1974 and were reviewed by Basset in 1889. The main noninvasive technique in use is that of pulsed electromagnetic fields (PEMFs).

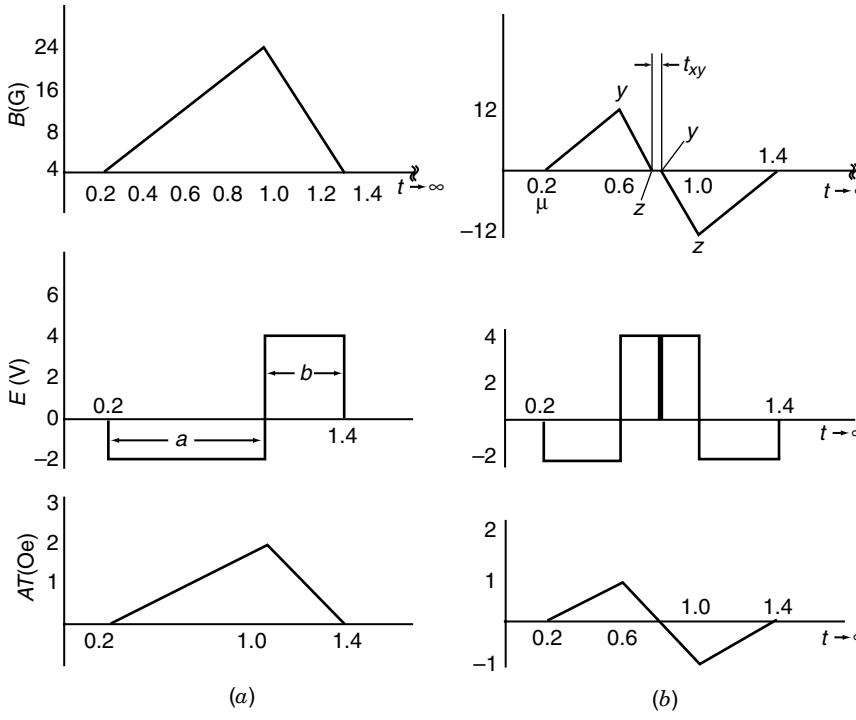

FIGURE 24. 2 PEMF energy profile: (*a*) prior format; (*b*) new format.

This technique is medically attractive as well as economical and has achieved commercial success. Initially, the devices were very heavy and required so much electrical power that they were not portable. Later work (Guzelsu et al., 1994) provided a more effective pulse characteristic that was also energy saving, which led to battery-powered portable devices. Figure 24.2 indicates the earlier and later PEMF characteristics.

The U.S. Food and Drug Administration approved several electrical bone growth stimulators, primarily for fractures at the middle of long bones, such as a tibia (shinbone) that has not healed in at least nine months. Also, the mechanisms of healing may not be understood completely; manufacturers' studies have shown that the device did, in fact, affect cellular processes.

REFERENCES

Basset, C. A., R. J. Pawluk, and A. A. Pilla, *Ann. N.Y. Acad. Sci.*, **238**, 242 (1974).

Friedenberg, Z. B., M. C. Harlow, and C. T. Harlow, *J. Trauma*, **11**, 883 (1971).

Fukada, F., and I. Yasuda, *J. Phys. Soc. Jpn.*, **12**, 1158 (1957).

Guzelsu, N., A. J. Salkind, X. Shen, U. Patel, S. Thaler, and R. Berg, Effect of electromagnetic stimulation with different waveforms on cultured fibroplasts, *Bioelectromagnetics*, **15**, 115 (1994).

REVIEWS

Basset, C. A., Therapeutic use of pulsed electromagnetic fields (PEMFs), critical reviews, *Biomed. Eng.*, **17**, 451 (1989).

Guzelsu, N., and A. J. Salkind, Electrochemical aspects of bone remodeling, in *Electrochemistry in Transition*, J. Murphy, Ed., Plenum Press, New York, 1991.

Salkind, A. J., A. Spotnitz, B. Derkovitz, B. Owens, K. Stokes, and M. Bilitch, Electrically driven implantable prostheses, in B. Owens, Ed., *Implantable Biomedical Devices*, Plenum Press, New York, 1986.

MONOGRAPHS

Rajeshwar, K., and J. G. Ibanez, *Environmental Electrochemistry*: *Fundamentals and Application in Pollution Abatement*, Academic Press, San Diego, CA, 1997.

Scott, K., *Electrochemical Processes for Clean Technology*, Royal Society of Chemistry, Cambridge, 1995.

Sequeira, C. A. C., Ed., *Environmentally Oriented Electrochemistry*, Elsevier, Amsterdam, 1994.

Itogi Nauyki i Tekhniki, Seriya Elektrokhimiya [*Frontiers in Science and Technology*, *Electrochemistry*, in Russian], Vol. 31, *Electrochemistry and Medicine*, VINITI Publishers, Moscow, 1990.

PART IV
Selected Topics in Electrochemistry

25

Solid-State Electrochemistry

ULRICH STIMMING and HENGYONG TU (*Part A*)
Technische Universität, München, Germany

PART A SOLID ELECTROLYTES

25.1 DEFECTS IN SOLIDS

25.1.1 Crystal Defects and Nonstoichiometry

Crystalline solids are built up of regular arrangements of atoms in three dimensions; these arrangements can be represented by a repeat unit or motif called a *unit cell*. A unit cell is defined as the smallest repeating unit that shows the full symmetry of the crystal structure. A perfect crystal may be defined as one in which all the atoms are at rest on their correct lattice positions in the crystal structure. Such a perfect crystal can be obtained, hypothetically, only at absolute zero. At all real temperatures, crystalline solids generally depart from perfect order and contain several types of defects, which are responsible for many important solid-state phenomena, such as diffusion, electrical conduction, electrochemical reactions, and so on. Various schemes have been proposed for the classification of defects. Here the size and shape of the defect are used as a basis for classification.

Lattice Vacancies and Interstitials Defects such as lattice vacancies and interstitials fall into two main categories: intrinsic defects, which are present in pure crystal at thermodynamic equilibrium, and extrinsic defects, which are created when a foreign atom is inserted into the lattice.

Intrinsic Defects The simplest crystalline defects involve single or pairs of atoms or ions and are therefore known as *point defects*. Two main types of point defect have been identified: Schottky defects and Frenkel defects. A *Schottky defect* consists of a pair of vacant sites: a cation vacancy and an anion vacancy. A Schottky defect is

Fundamentals of Electrochemistry, Second Edition, By V. S. Bagotsky

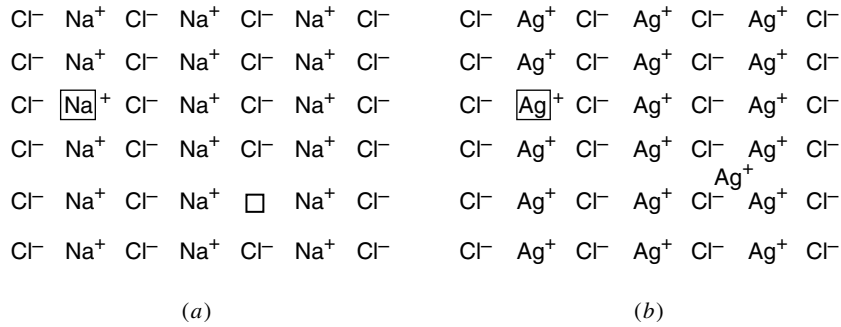

FIGURE 25.1 Schematic representations of (*a*) a Schottky defect in NaCl and (*b*) a Frenkel defect in AgCl. (From Gelings and Bouwmeester, 1997, Fig. 3.36, with permission from CRC Press LLC via CCC.)

the principal point defect in an alkali halide type of structure and is shown for NaCl in Fig. 25.1*a*. There are equal numbers of anion and cation vacancies, in order to preserve local electroneutrality as much as possible, both inside the crystal and at the crystal surface. The presence of defects, even in small concentrations, often influence greatly the properties of materials. For instance, point defects such as Schottky defects are responsible for the optical and electrical properties of NaCl. A *Frenkel defect* usually occurs on only one sublattice of a crystal and consists of an atom or ion moving into an interstitial position, thereby creating a vacancy. Silver chloride with the alkali halide–type structure has predominantly this defect with silver as the interstitial atom (Fig. 25.1*b*). The formation of anion Frenkel defects usually occurs in compounds with the fluorite structure, such as CaF_2 and ZrO_2. In this case, an ion, F^- or O^{2-}, occupies the interstitial site.

Extrinsic Defects Extrinsic defects occur when an impurity atom or ion is incorporated into the lattice either by substitution onto the normal lattice site or by insertion into interstitial positions. Where the impurity is aliovalent with the host sublattice, a compensating charge must be found within the lattice to pre-serve electroneutality. For example, inclusion of Ca^{2+} in the NaCl crystal lattice results in the creation of an equal number of cation vacancies. These defects therefore alter the composition of the solid. In many systems the concentration of the dopant ion can vary enormously and can be used to tailor specific properties. These systems are termed *solid solutions* and are discussed in more detail in Section 25.1.2.

Nonstoichiometric Compounds Intrinsic defects are stoichiometric defects (i.e., they do not involve any change in overall composition). Defects can also be nonstoichiometric. In the case of extrinsic defects where the host crystal is doped with aliovalent impurities, the solid so formed is a nonstoichiometric compound because the ratio of the atomic components is no longer the simple integer. There is also

another mechanism whereby an ionic crystal can become nonstoichiometric. If the crystal contains an element with a variable valency, a change in the number of ions of that element can be compensated by changes in ion charge; this maintains the electroneutrality but alters the stoichiometry. For example, nonstoichiometry of the acceptor-doped $Ln_{1-x}A_xBO_3$ (Ln, rare-earth element; A, alkaline-earth element; B, transition-metal element) has been investigated by a number of investigators. In general, substitution of divalent alkaline-earth ions on the A site increases the concentration of oxygen vacancies. Temperature and oxygen partial pressure determine whether charge compensation occurs by increased valency of the transition metal ion at the B site or by the formation of ionized oxygen vacancies. Nonstoichiometric compounds are of wide use in the field of solid-state electrochemistry because their properties can be modified by changing the proportions of the atomic constituents.

Defect Clusters Detailed studies reveal that the apparently simple point defects such as vacancies and interstitials are often, in fact, more complex. Instead of single atom defects, larger defect clusters tend to form. Vacancies in ionic crystals are effectively charged: anion vacancies possessing an overall positive charge and cation vacancies an overall negative charge. Thus, these vacancies of opposite charge can attract each other to form clusters. The smallest cluster would be either an anion vacancy/cation vacancy pair or an aliovalent impurity–cation vacancy pair. Although these clusters show overall electroneutrality, they are dipolar and can attract other pairs to form larger clusters. Solid electrolytes are generally massively defective compounds with high ionic conductivities (see Section 25.2), and it is believed that defect clustering is very significant in these systems.

Dislocations Dislocations are stoichiometric line defects. A dislocation marks the boundary between the slipped and unslipped parts of crystal. The simplest type of dislocation is an edge dislocation, involving an extra layer of atoms in a crystal (Fig. 25.2). The atoms in the layers above and below the half-plane distort beyond its edge and are no longer planar. The direction of the edge of the half-plane into the crystal is know as the *line of dislocation*. Another form of dislocation, known as a *screw dislocation*, occurs when an extra step is formed at the surface of a crystal, causing a mismatch that extends spirally through the crystal.

Grain Boundaries The descriptions of crystalline solids so far have been restricted to single crystals. However, most materials are polycrystalline, although made up of a single chemical phase. In these materials, the individual crystallites or grains in the crystals have different orientations. When two grains of different orientation meet, the region between the grains is called a *grain boundary*. Thus grain boundaries are interface defects. Depending on the misorientation between the adjoining grains, different types of grain boundaries can be formed. In real application, the importance of grain boundaries in controlling the properties and behavior of polycrystalline materials has been well recognized.

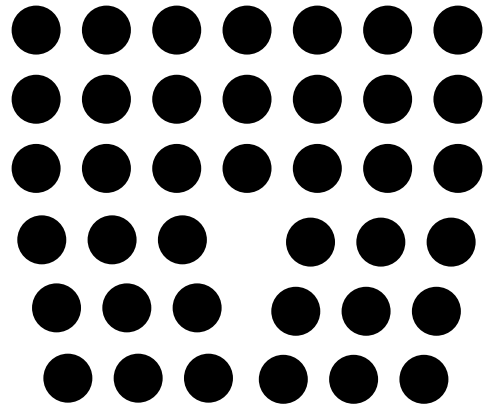

FIGURE 25.2 Schematic two-dimensional representation of atom positions around an edge dislocation. (From Gelings and Bouwmeester, 1997, Fig. 3.38, with permission from CRC Press LLC via CCC.)

TABLE 25.1 Kröger–Vink Notation for Point Defects in Crystals

Type of Defect	Symbol	Remarks
Vacant M site	V''_M	Divalent ions are chosen as an example, with MX as the compound formula
Vacant X site	V_x^{++}	M^{2+}, X^{2-}: cation and anion
Ion on lattice site	M_M^x, X_X^x	^{x}: uncharged
L on M site	L'_M	L^+ dopant ion
N on M site	N_M^-	N^{3+} dopant ion
Free electron	e'	
Free (electron) hole	h^*	
Interstitial M ion	M_i^{++}	$^+$: effective positive charge
Interstitial X ion	X''_j	$'$: effective negative charge

Notation for Point Defects in Crystals The charges of defects and of the regular lattice particles are only important with respect to the neutral, unperturbed (ideal) lattice. In the following discussion, the charges of all point defects are defined relative to the neutral lattice. Thus, only the effective charge is considered, being indicated by a dot ($\cdot$) for a positive excess charge and by a prime ($'$) for a negative excess charge. The notation for defects most often used was introduced by Kröger and Vink and is given in Table 25.1. Only fully ionized defects are indicated in the table.

25.1.2 Solid Solutions

Solid solutions are very common in crystalline solids. A *solid solution* may be defined as a single crystalline phase with variable composition. In general, these

solids maintain a basic structural framework throughout the solid solution range. The extent of solid solution formation is very dependent on the chemical system and can vary from fractions of a percent to 100%. The effects of solid solution formation can be to introduce or enhance physical properties, such as mechanical strength, conductivity, and ferromagnetism. A particularly interested effect in solid-state electrochemistry is the enhancement of ionic and ionic/electronic conductivity in solids. In ionic systems, solid solutions may be formed not only in two basic types (substitutional or interstitial), but also in a considerable variety of more complex mechanisms, starting with these two basic types. Let us deal with these in some detail.

Substitutional Solid Solutions Substitutional solid solutions involve direct substitution of ions or atoms by different but isovalent ions or neutral atoms, respectively. An example of a substitutional solid solution is the series of oxides formed on reacting Al_2O_3 and Cr_2O_3 together at high temperatures. Both of these end-member phases have the corundum crystal structure and the solid solution may be formulated as $(Al_{2-x}Cr_x)O_3$; $0 \leq x \leq 2$. Thus, when the structure is considered as a whole and the occupancy of all the sites is averaged out, it is useful to think of each site as being occupied by an "average cation" whose properties, atomic number, size, and so on, are intermediate between those of Al^{3+} and Cr^{3+}. Substitutional solid solution mechanisms are employed widely in alloy formation (e.g., in brass, copper, and zinc, atoms replace each other over a wide range of composition, with a general formula $Cu_{1-x}Zn_x$).

For a range of simple substitutional solid solutions to form, certain requirements must be met. First, the ions that replace each other must be isovalent. If this were not the case, other structural changes (e.g., vacancies or interstitials) would be required to maintain electroneutrality. Second, the ions that replace each other must be fairly similar in size. From a review of the experimental results on metal alloy formation, it has been suggested that 15% size difference can be tolerated for the formation of a substantial range of substitutional solid solutions. For solid solutions in nonmetallic systems, the limiting difference in size appears to be somewhat larger than 15%, although it is very difficult to quantify this. To a certain extent, this is because it is difficult to quantify the sizes of the ions themselves, but also because solid solution formation is very temperature dependent.

In considering whether or not solid solutions form, an important factor is the crystal structure of the two end members. In systems that exhibit complete ranges of solid solution, it is clearly essential that the two end members be isostructural. The reverse is, however, not necessarily true. For example, LiF and CaO both have the rock salt structure but they do not form solid solutions. Although complete ranges of solid solutions form in favorable cases, as for example between Al_2O_3 and Cr_2O_3, it is far more common to have incomplete ranges of solid solutions. In such cases it is no longer necessary that the end members be isostructural. For example, Mg_2SiO_4 and Zn_2SiO_4 have quite different structure. Mg_2SiO_4 adopts the olivine structure, with octahedral Mg and tetrahedral Si, while Zn_2SiO_4 has tetrahedral coordination for both Zn and Si. Therefore, limited solid solutions are obtainable: $Mg_{2-x}Zn_xSiO_4$, $0 \leq x \leq 0.2$; $Zn_{2-x}Mg_xSiO_4$, $0 \leq x \leq 0.3$.

Interstitial Solid Solutions Interstitial solid solutions involve occupation of a site by introduced ions or atoms, which is normally empty in the crystal structure, and no ions or atoms are left out. Many metals form interstitial solid solutions in which small atoms (e.g., hydrogen, carbon, boron, nitrogen) enter empty interstitial sites within the host structure of the metal. Palladium metal is well known for its ability to absorb an enormous volume of hydrogen gas, and the product hydride is an interstitial solid solution of formula PdH_x, $0 \leq x \leq 0.7$, in which hydrogen atoms occupy interstitial sites within the face-centered cubic palladium metal structure. Hydrogen reacts at elevated temperatures with many transition metals and their alloys to form hydrides. Many of these compounds (MH_n) show large deviations from ideal stoichiometry ($n = 1, 2, 3$) and can exist as multiphase systems. The lattice structure is that of a typical metal with hydrogen atoms on the interstitial sites; and for this reason they are also called *interstitial hydrides*. Metal hydrides are very effective at storing large amounts of hydrogen in a safe and compact way; thus, they have promising applications in hydrogen storage for fuel cells. Another technologically important interstitial solid solution is that of carbon in the octahedral sites of face-centered cubic γ-Fe. This solid solution is the starting point for the manufacture of steel.

Interstitial/vacancy Solid Solutions In ionic solids where substitution is made by an aliovalent ion, electroneutrality is maintained either by the formation of vacancies or by the introduction of interstitials.

Cation Vacancies If the cation of the host structure has a lower charge than the cation that is replacing it, cation vacancies may be introduced for the preservation of electroneutrality. Alternatively, the substitution of an anion by one of lower charge may also achieve this in certain systems. For example, NaCl is able to dissolve a small amount of $CaCl_2$, and the mechanism of solid-solution formation involves the replacement of two Na^+ ions by one Ca^{2+} ion, leaving one vacancy on the Na^+ sublattice, $Na_{1-2x}Ca_{x}Cl$ (where x denotes a vacancy).

Cation Interstitials The mechanism is to create interstitial cations wherein a cation of lower charge substitutes for one of higher charge. This is a common substitution mechanism and occurs provided that the host structure has suitable-sized interstitial sites to accommodate the extra cations. The Lisicon system is a solid solution between Li_2ZnGeO_4 and Li_4GeO_4. Solid solution members have the general formula $Li_{2+2x}Zn_{1-x}GeO_4$. Solid solution involves the replacement of Zn^{2+} cations by two Li^+ ions, one of which substitutes directly onto the Zn tetrahedron, while the other enters interstitial octahedral sites, resulting in high Li^+ ion conductivity for this material.

Anion Vacancies If the cation of the host structure has a higher charge than the replacing cation, electroneutrality may be maintained by introducing vacancies into the anion sublattice. The best-known examples of anion vacancies occur in the stabilized zirconia, such as calcium- or yttrium-stabilized zirconia. The high-temperature

cubic zirconia phase with the fluorite structure is stabilized by substitution of Zr^{4+} by either Ca^{2+} or Y^{3+}, thus introducing anion vacancies (i.e., $Zr_{1-x}Ca_xO_{2-x}$ or $Zr_{1-x}Y_xO_{2-x/2}$). These materials show high oxide ion conductivity at temperatures around 1000°C and have been used as solid electrolytes (see Section 25.2).

Anion Interstitials The other mechanism by which a cation of higher charge may substitute for one of lower charge creates interstitial anions. This mechanism appears to be favored by the fluorite structure in certain cases. For example, calcium fluoride can dissolve small amounts of yttrium fluoride. The total number of cations remains constant with Ca^{2+}, Y^{3+} ions disordered over the calcium sites. To retain electroneutrality, fluoride interstitials are created to give the solid solution formula $Ca_{1-x}Y_xF_{2+x}$.

Double Substitution In such processes, two substitutions take place simultaneously. For example, in perovskite oxides, La^{3+} may be replaced by Sr^{2+} at the same time as Co^{3+} is replaced by Fe^{3+} to give solid solutions $La_{1-x}Sr_xCo_{1-y}Fe_yO_{3-\delta}$. These materials exhibit mixed ionic and electronic conduction at high temperatures and have been used in a number of applications, including solid oxide fuel cells and oxygen separation.

Change in Unit Cell Parameters of Solid Solutions: Vegard's Law The formation of solid solutions usually results in change in unit cell parameters of the end members. According to Vegard's law, unit cell parameters should change linearly with composition. However, Vegard's law is a generalization that applies to solid solutions formed by random substitution or distribution of ions. It assumes implicitly that the changes in unit cell parameters with composition are governed purely by the relative sizes of the atoms or ions that replace each other in a simple substitutional mechanism. In practice, many systems show significant variation from linearity. For example, complete solid solution can form in the Al_2O_3–Cr_2O_3 system with the hexagonal corundum structure. However, a positive deviation from Vegard's law is found in the unit cell parameters. This has been explained in terms of the solid-solution–forming regions of alumina-rich and chrome-rich microdomains.

25.2 SOLID ION CONDUCTORS

Solid electrolytes are a class of materials exhibiting high ionic conductivity, like liquid electrolytes, although they are in the solid state. Unlike liquid electrolytes, solid electrolytes usually have a rigid framework structure and there is one mobile ionic species. Such materials have been known for several decades. For example, Nernst (1899) demonstrated that the electrical conduction through ZrO_2–Y_2O_3 at elevated temperatures was due mainly to mobile oxygen ions. Ionic conductors have always provided a fascinating interdisciplinary field of study ever since their discovery by Faraday at the Royal Institution in London over 200 years ago. Solid electrolytes presently find wide applications in energy storage by new types of high-performance

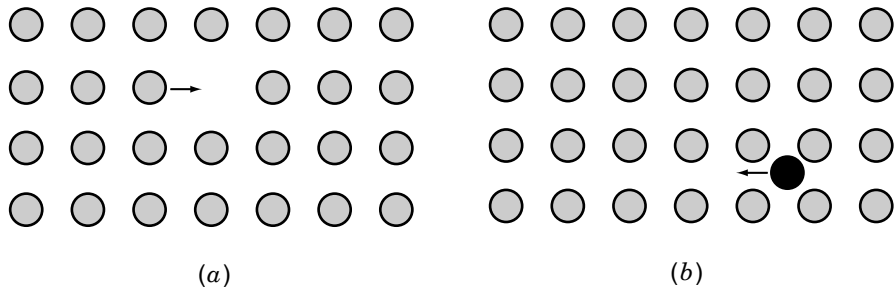

FIGURE 25.3 Schematic representation of ionic motion by (*a*) a vacancy mechanism and (*b*) an interstitial mechanism. (From Smart and Moore, 1996, Fig. 5.4, with permission from Routledge/Taylor & Francis Group.)

batteries, efficient energy conversion by fuel cells, generation of hydrogen fuel by electrolysis, chemical sensors, solar cells, electrochromic windows or displays, and many others. These applications will have a tremendous impact on many aspects of our life, environment, and economy.

25.2.1 Ionic Conductivity in Solids

Point defects in solids make it possible for ions to move through the structure. Ionic conductivity represents ion transport under the influence of an external electric field. The movement of ions through a lattice can be explained by two possible mechanisms. Figure 25.3 shows their schematic representation. The first, called the *vacancy mechanism*, represents an ion that hops or jumps from its normal position on the lattice to a neighboring equivalent but vacant site or the movement of a vacancy in the opposite direction. The second one is an interstitial mechanism where an interstitial ion jumps or hops to an adjacent equivalent site. These simple pictures of movement in an ionic lattice, known as the *hopping model*, ignore more complicated cooperative motions.

Ionic conductivity, σ, is defined as

$$\sigma = nze\mu, \tag{25.1}$$

where n is the number of charge carriers per unit volume, ze is their charge (expressed as a multiple of the charge on an electron, $e = 1.602189 \times 10^{-19}$ C), and μ is their mobility, which is a measure of the drift velocity in a constant electric field. In the case of crystals where the ionic conductivity is carried by the vacancy or interstitial mechanism, n, the concentration of charge carriers, will be closely related to the concentration of defects in the crystal. As ion jumps from one site to the other, there is clearly going to be an energy barrier to this happening. In general, the ion movement is expected to follow the lowest energy path available; a schematic diagram of the energy changes involved in such a pathway is shown in Fig. 25.4.

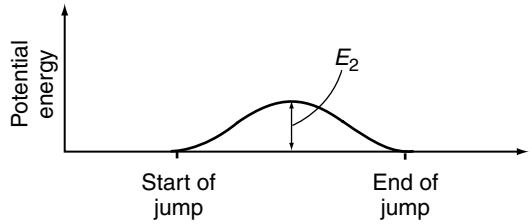

FIGURE 25.4 Schematic representation of the change in energy during motion of an ion along the lowest energy path. (From Smart and Moore, 1996, Fig. 5.6, with permission from Routledge/Taylor & Francis Group.)

Notice that the energy of the ion is the same at the beginning and the end of the jump; the energy required to make the jump, E_a, is known as the *activation energy* for the jump. This means that the temperature dependence of the mobility of the ions can be expressed by an Arrhenius equation:

$$\mu \propto \exp\left(-\frac{E_a}{kT}\right) \tag{25.2}$$

or

$$\mu = \mu_0 \exp\left(-\frac{E_a}{kT}\right), \tag{25.3}$$

where μ_0 is a proportionality constant known as a *preexponential factor*. μ_0 depends on the attempt frequency (the number of times per second that the ion attempts the move), the distance moved by the ion, and the size of the external field. If the external field is small (up to about 300 V/cm), a temperature dependence of $1/T$ is introduced into the preexponential factor. If we combine all this information in Eq. (25.1), we arrive at an expression for the variation of ionic conductivity with temperature that has the form

$$\sigma = \frac{\sigma_0}{T} \exp\left(-\frac{E_a}{kT}\right). \tag{25.4}$$

The term σ_0 now contains n and ze as well as the information on attempt frequency and jump distance. This expression accounts for the fact that ionic conductivity increases with temperature.

25.2.2 Oxide Ion Conductors

In oxide ion conductors, current flow occurs by the movement of oxide ions through the crystal lattice. This movement is a result of thermally activated hopping of the

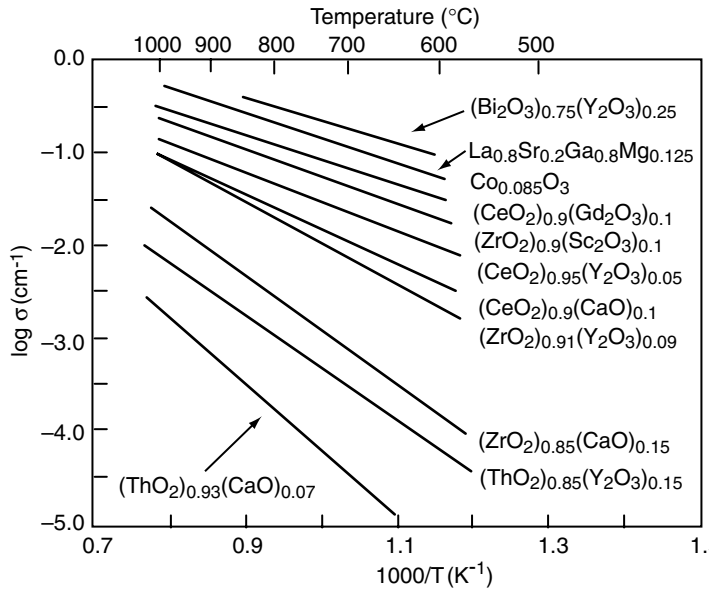

FIGURE 25.5 Arrhenius plots of some oxide ion conductors. (Courtesy of Prof. Tatsumi Ishihara, Kyushu University, Japan.)

oxide ions, moving from crystal lattice site to crystal lattice site, with a superimposed drift in the direction of the electric field. The ionic conductivity is consequently strongly temperature dependent. Figure 25.5 shows the Arrhenius plots of some promising oxide ion conductors.

Pure ZrO_2 has three polymorphs as a function of temperature: a monoclinic form ($< 1100°C$), a tetragonal form with a distorted fluorite structure ($< 2400°C$), and a cubic form at higher temperature. A cubic fluorite-type solid solution can be structurally stable up to its melting point by substitution of the host cation with either a rare earth or an alkaline earth, and is thus called *stabilized zirconia*. In these solid solutions the substitution of Zr^{4+} with aliovalent cations such as Ca^{2+} or Y^{3+} has the effect of introducing oxygen vacancies to maintain overall electroneutrality. These oxygen vacancies supply the equivalent sites, allowing the oxygen ions to migrate, resulting in high ionic conductivity. As is evident from Fig. 25.5, some stabilized ziconia show very high conductivities at temperatures above 800°C. Increasing the dopant concentration will lead to the introduction of more vacancies into the lattice and should result in higher conductivity. Unfortunately, this correlation applies only at low concentrations of dopant, and it is found that at higher concentrations the ionic conductivity is limited. Such behavior is shown in Fig. 25.6 for a number of ZrO_2-based systems. As shown, the isothermal conductivity does increase as the level of substitution increases; however, a maximum is observed at relatively low additions of the dopant because of the interactions of the substitutional cation with the charge-compensating oxygen vacancy that it introduces.

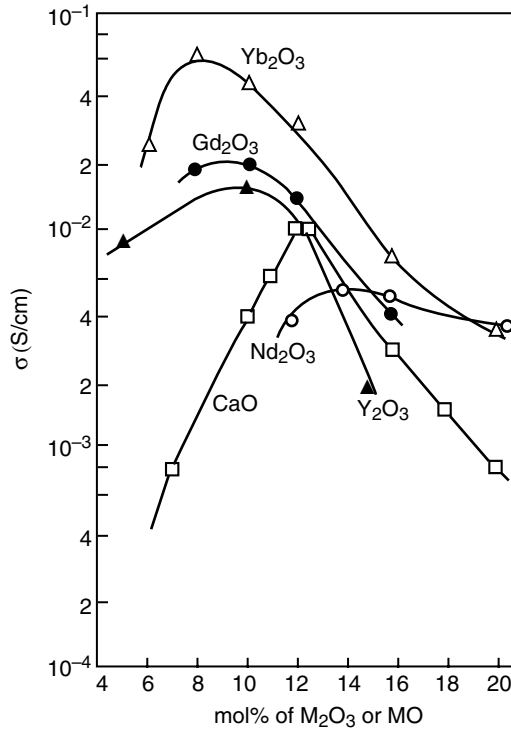

FIGURE 25.6 Composition dependence of conductivity (800°C) of solid solution in the ZrO_2–M_2O_3 (or –MO) system. (From Gelings and Bouwmeester, 1997, Fig. 6.2, with permission from CRC Press LLC via CCC.)

Pure ceria (CeO_{2-x}) exists in the fluorite structure over a wide temperature and oxygen partial pressure range ($x \approx 0.3$). For small values of x, ceria is a mixed conductor, but the electronic (n-type) conductivity dominates with increasing degree of nonstoichiometry. Ceria-based solid solutions, $Ce_{1-x}Ln_xO_{2-\delta}$, show a higher ionic conductivity than stabilized ZrO_2 (particularly at lower temperatures). Among various ceria-based phases, the highest level of ionic conductivity is characteristic of the solid solutions $Ce_{1-x}Ln_xO_{2-\delta}$, where Ln = Gd or Sm, $x = 0.10$ to 0.20, as shown in Fig. 25.5 for Gd. The ionic conductivity regime is narrow in ceria-based solid solutions and is a function of the dopant concentration. These materials easily develop n-type electronic conduction in low oxygen partial pressures and at high temperatures, due to the partial reduction of Ce^{4+} to Ce^{3+}. Therefore, ceria-based solid solutions have limited application in a low-oxygen concentration environment and at high temperatures, despite their high ionic conductivity compared with stabilized zirconia.

Bismuth sesquioxide, Bi_2O_3, exhibits a high oxide ion conductivity at high temperature without doping of aliovalent cations. The oxide transforms from the monoclinic

α-form to the cubic δ-form at 729°C, which is accompanied by a jump of conductivity from $\sim 10^{-3}$ to ~1 S/cm. The δ-phase has a fluorite-type structure with a complicated disorder in the oxygen sublattice. The stabilization of the highly conductive δ-Bi_2O_3 phase can be achieved by the substitution of bismuth with rare-earth dopants (such as Y, Dy, or Er) and their combinations with higher-valency cations such as W or Nb. As shown in Fig. 25.5, $(Bi_2O_3)_{0.75}(Y_2O_3)_{0.25}$ exhibits the highest conductivity among the various types of oxide ion conductors. Unfortunately, Bi_2O_3-based materials show thermodynamic instability in reducing atmospheres just like the CeO_2-based oxide ion conductors. Hence, the applicability of these oxides in electrochemical cells is considerably limited.

Perovskite-type ABO_3 phases derived from lanthanum gallate, $LaGaO_3$, possess a higher ionic conductivity than stabilized zirconia and are thus promising materials for electrochemical cells operating in the intermediate temperature range (650 to 800°C). Compared with CeO_2-based electrolytes, the electrolytic domain of doped $LaGaO_3$ extends to substantially lower oxygen chemical potentials. High oxide ion conductivity in $LaGaO_3$ can be achieved by substituting lanthanum with alkaline-earth elements and/or incorporating divalent metal cations, such as Mg^{2+}, into the gallium sublattice in order to increase the oxygen vacancy concentration. The optimized materials of general stoichiometry $La_{1-x}Sr_xGa_{1-y}Mg_yO_{3-\delta}$ (LSGM) are actively developed. For the LSGM series, the maximum ionic transport is achieved at $x = 0.10$ to 0.20 and $y = 0.15$ to 0.20; further acceptor-type doping leads to progressive vacancy association processes. Further development of the LSGM compositions has proven interesting, with a small amount of Co introduced onto the B-site found to improve performance without introducing electronic conductivity, as shown in Fig. 25.5.

Oxide ion conductors have found widespread applications in our modern society. The devices based on oxide ion conductors include oxygen sensors, solid oxide fuel cells (SOFCs), and oxygen pump.

25.2.3 Fluoride Ion Conductors

Several solid electrolytes exist that exhibit high fluoride ion conductivities; they are predominantly of fluorite- or tysonite-type structures. Figure 25.7 shows conductivities of some fluoride ion conductors. Calcium fluoride, CaF_2, is fluorite itself. F^- can conduct through its vacancies generated by partial replacement of Ca^{2+} sites with a monovalent cation such as Na^+. CaF_2 incorporated with 1 mol % NaF exhibits a conductivity of 10^{-3} S/cm at 400°C. It is noted from the Fig. 25.7 that even pure CaF_2 exhibits considerable conductivity. β-PbF_2, with the same fluorite-type structure, exhibits conductivity as large as 1 S/cm at 400°C, and 10^{-6} S/cm even at room temperature. A variety of mixed fluorides with fluorite-type or related structures have been derived. Of these, $PbSnF_4$ is the best F^- conductor to date in a relatively low temperature region. In contrast with structurally equivalent oxides, CaF_2 and PbF_2 can form fluorite-type solid solutions with fluorides of higher valent cations such as BiF_3. Such solid solutions are expressed, for example, by $Pb_{1-x}Bi_xF_{2+x}$, in which the excess F^- occupies the interstitial sites. These solid solutions are good F^- conductors (Fig. 25.7). LaF_3 has the tysonite-type structure and exhibits a conductivity

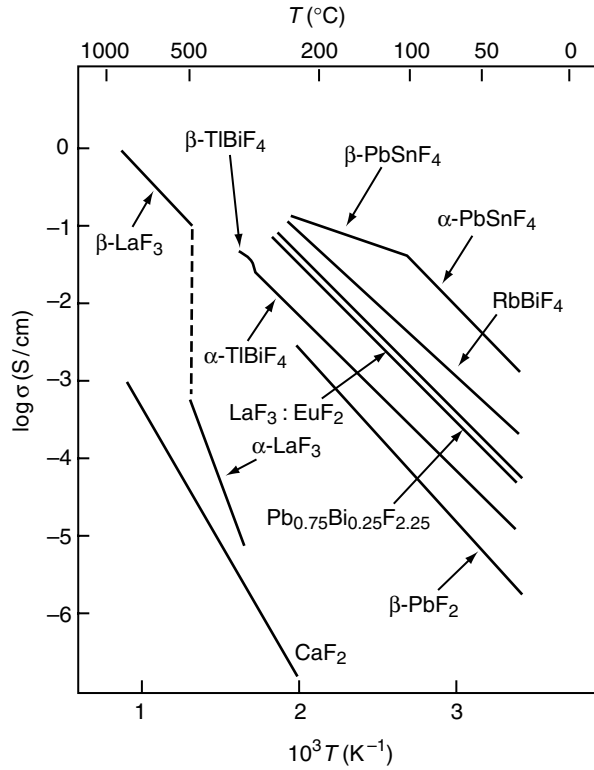

FIGURE 25.7 Conductivity of some fluoride ion conductors as a function of $1/T$. (From Gelings and Bouwmeester, 1997, Fig. 6.3, with permission from CRC Press LLC via CCC.)

of 3×10^{-6} S/cm even at room temperature. Tysonite-type solid solutions are formed with divalent metal fluorides such as BaF_2 or EuF_2. $La_{1-x}Eu_xF_{3-x}$, for example, has anion vacancies. The conductivity of these phase is higher than that of pure LaF_3. Uses of the fluoride ion conductors include their incorporation into solid-state batteries with high power density and oxygen sensors.

25.2.4 Silver and Copper Ion Conductors

Most AgX and CuX compounds have a crystallographic transition point in the temperature region of several hundred degrees Celsius at which a drastic change in conductivity is observed. For example, conductivity of AgI is increased by three orders of magnitude when it is transformed from wurzite-type β-phase to the cubic α-form at 147°C (Fig. 25.8). The silver ion conductivity after the transformation is ~1 S/cm, which is almost the same as that of the molten phase (m.p. 552°C) and even comparable to an H_2SO_4 solution. Cuprous iodide, CuI, undergoes a similar transition at 430°C and turns into a very good Cu^+ conductor. The ionic conduction of α-AgI (or

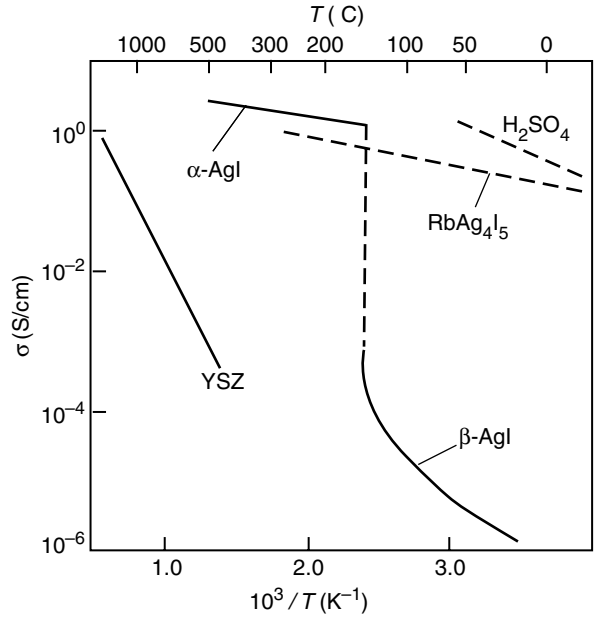

FIGURE 25.8 Temperature dependence of conductivity for typical silver ion conductors, AgI and $RbAg_4I_5$, compared with those for YSZ and an aqueous solution of H_2SO_4. (From Gelings and Bouwmeester, 1997, Fig. 6.5, with permission from CRC Press LLC via CCC.)

CuI) is not due to point defects but to partial occupation of crystallographic sites. The defective structure is sometimes called *structural disorder* to distinguish it from point defects. There are a large number of vacant sites for the cations to move into. Thus, ionic conductivity is enabled without use of aliovalent dopants. A common feature of both compounds is that they are composed of extremely polarizable ions. This means that the electron cloud surrounding the ions is easily distorted. This makes the passage of a cation past an anion easier. Due to their high ionic conductivity, silver and copper ion conductors can be used as solid electrolytes in solid-state batteries.

25.2.5 Sodium Ion Conductors

The β-alumina family, a series of compounds in the Na_2O–Al_2O_3 system, is one of the most important groups of solid electrolytes. The principal members are the β- and β″-phases, the ideal compositions of which are $Na_2O \cdot 11Al_2O_3$ ($NaAl_{11}O_{17}$) and $Na_2O \cdot 5.33Al_2O_3$, although they are usually nonstoichiometric. Conductivity of a typical single crystal of β-Al_2O_3 is as high as ~0.01 S/cm at 25°C along the conduction plane (perpendicular to the *c*-axis). Ionic conduction in β (or β″)-Al_2O_3 is anisotropic because of the two-dimensional nature of the structure and several orders of magnitude lower along the *c*-axis. The β″-phase exhibits a conductivity one order

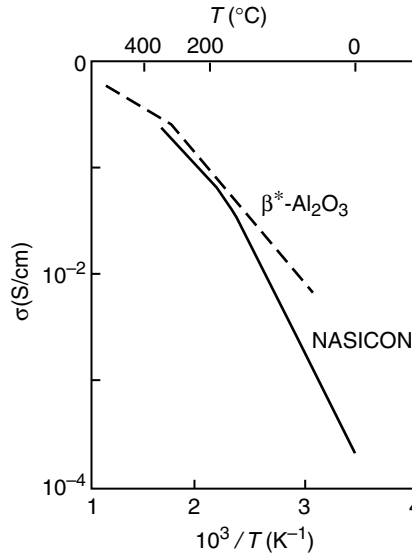

FIGURE 25.9 Conductivity of NASICON and sintered β″-alumina as a function of 1/*T*. (From Gelings and Bouwmeester, 1997, Fig. 6.8, with permission from CRC Press LLC via CCC.)

of magnitude higher than that of the β-phase. Sintered polycrystalline β″-phase, often used for Na–S batteries, shows poorer conductivity at room temperature, but its conductivity reaches a level high enough for practical use at high temperature (~300°C), as shown in Fig. 25.9. The Nasicon (Na superionic conductor) family is another series of good sodium ion conductors with a conductivity comparable to that of β-alumina. The Nasicon is a solid solution in the $NaZr_2(PO_4)_3$–$Na_4Zr_2(SiO_4)_3$ system and can be represented by $Na_{1+x}Zr_2P_{3-x}Si_xO_{12}$. The maximum conductivity is obtained at $x = 2$, at which composition the activation energy for ionic conduction shows a minimum. Its conductivity is 2×10^{-2} S/cm at 300°C (Fig. 25.9). In contrast to β-alumina, Nasicon is a three-dimensional conductor. Significant conduction of Na^+ takes place due to partial occupation of possible sites in the structure. Although Nasicon shows excellent conductivity, there is the problem that these materials are unstable towards liquid sodium.

25.2.6 Lithium Ion Conductors

Lithium ion conductors are of technological importance for applications as solid electrolytes for all-solid-state lithium batteries with high energy density and may solve the safety problems of the rechargeable lithium ion batteries using nonaqueous liquid electrolytes. Lithium ion conduction has been investigated in a variety of solid materials. Among the lithium halides, lithium iodide exhibits the highest conductivity of $\sim 10^{-7}$ S/cm at room temperature. Doping LiI with aliovalent impurities such as CaI_2 increases its conductivity for the same reason as described before,

the conductivity of LiI—1 mol %, CaI_2 being $\sim 10^{-5}$ S/cm at 25°C. Another Li^+ conductor binary compound is Li_3N. Its crystal structure is built up of Li_2N layers in hexagonal arrangement stacked along the *c*-axis with the rest of Li in between. Intralayer migration of the latter Li^+ (Li_2) is responsible for ionic conduction. Thus, its single crystal shows highly anisotropic conductivity, i.e., 1.2×10^{-3} S/cm at 25°C along the layers, while it is about two orders of magnitude lower along the *c*-axis. The conductivity of polycrystalline samples is typically 7×10^{-4} S/cm at room temperature. Oxide lithium ion conductors such as Li_4SiO_4 and Li_4GeO_4 have moderately good Li^+ conductivity, $\sim 10^{-4}$ S/cm at 300 to 400°C, and versatile host structures for doping. They are built of isolated SiO_4 and GeO_4 tetrahedra and Li^+ ions are distributed through a network of face-sharing polyhedral sites. Substitutions by Al, Zn, and Al have all led to improvement in conductivity of several orders of magnitude, especially at lower temperatures (~25 to 300°C). The best conductor at medium temperatures that has been found so far is $Li_{14}ZnGe_4O_{16}$, for which $\sigma = 10^{-1}$ S/cm at 300°C. It has been named Lisicon. The highest room-temperature conductivity occurs in $Li_{3.5}V_{0.5}Ge_{0.5}O_4$ for which $\sigma = 5 \times 10^{-5}$ S/cm.

25.2.7 Proton Conductors

The proton, the atomic nucleus of hydrogen, has an extremely small ionic radius compared with that of ordinary ions. Thus, it is unlikely that protonic conduction occurs as a result of the proton jumping from one crystallographic site to another. A large number of entirely different classes of materials conduct protons in their structures, which include ion-exchange membrane materials, solid-state inorganic acids, derivatives of β-aluminas and perovskite-type oxides. The ion-exchange membrane materials (e.g., Nafion) are dealt with in detail in Chapter 26. Figure 25.10 shows the conductivity of some proton conductors. $H_3[PMo_{12}O_{40}] \cdot nH_2O$ ($n \sim 29$), one of the solid-state inorganic acids, shows a remarkably high conductivity (~0.1 S/cm) at room temperature. As shown in Fig. 25.10, the conductivity of $H_3[PMo_{12}O_{40}] \cdot nH_2O$ ($n \sim 29$) depends very slightly on temperature. At higher temperature or under dry conditions, its conductivity is drastically reduced because of the loss of water. β- or β″-Al_2O_3 exhibits proton conductivity when its Na^+ ions are ion-exchanged with H_3O^+ and/or NH_4^+. Of these compounds, $(NH_4^+)(H_3O^+)_{2/3}Mg_{2/3}Al_{31/3}O_{17}$, derived from β″-phase, has the highest conductivity, 10^{-4} S/cm at 25°C. Gallium analogs of β- or β″-alumina are ion exchanged more smoothly, and NH_4-β-gallates thus formed show higher conductivity than their alumina counterparts (Fig. 25.10). High proton conductivity of perovskite-type oxides based on $SrCeO_3$ was discovered in 1981. In these oxides, trivalent cations (Y^{3+}, Yb^{3+}, Nd^{3+}, etc.) are partially substituted for cerium. Typical dopant concentration is around 5%. These materials are normally *p*-type semiconductors in air at high temperature. However, they rapidly develop proton conductivity at high temperature (800 to 1000°C) in the presence of a hydrogen-containing atmosphere (pure H_2 or H_2/H_2O) because positive holes are consumed according to

$$H_2(g) + 2h^+ = 2H^+ \tag{25.5}$$

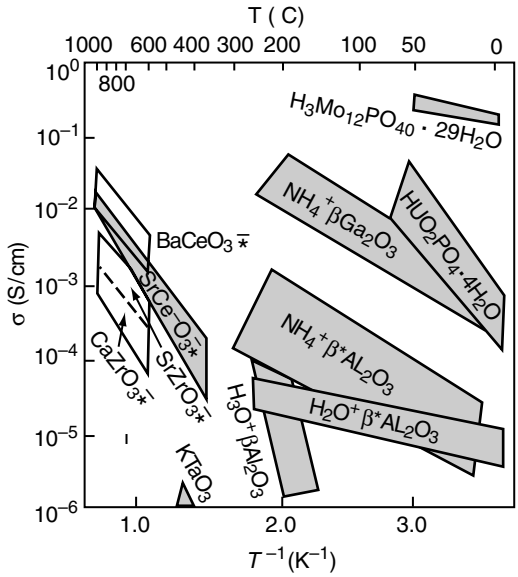

FIGURE 25.10 Conductivity of some proton conductors as a function of $1/T$. The overlapping area between $BaCeO_3$ and $SrCeO_3$ indicates solid solutions based on these compounds. (From Gelings and Bouwmeester, 1997, Fig. 6.17, with permission from CRC Press LLC via CCC.)

or

$$H_2O(g) + 2h^+ = 2H^+ + \tfrac{1}{2}O_2 \tag{25.6}$$

and H^+ ions are introduced into their crystal lattice at the same time. The proton conductivity of $SrCe_{1-x}Yb_xO_{3-\delta}$ ($x = 0.05$) in H_2 at 800°C is about 0.02 S/cm. The growing importance of cleaner energy and other application fields in our modern society increases the need for solid proton conductors with high conductivity for fuel cells, electrolyzers, sensors, hydrogen pumps, electrochemical reactors, and electrochromic devices.

25.2.8 Glassy Ion Conductors

While crystalline solids exhibit high ionic conductivity in various systems of materials, as described above, it has been found that glasses can support high ionic conductivity. The first breakthrough was the accidental discovery that highly conducting glass phases are formed in the $AgI–Ag_2SeO_4$ system. The unusual glasses are purely Ag^+ ion conductors and exhibit conductivity around 10^{-2} S/cm at ambient temperature. Glasses show some advantages over crystalline solid, which include isotropic conduction, absence of grain boundaries, ease of fabrication into complex shape, wide compositional flexibility, and high ionic coupled with low electronic conductivity. Various glassy solid F^- conductors have been developed. A glass in

the ZrF_4–BaF_4 system, the first example of such conductors, exhibits a conductivity of $\approx 10^{-6}$ at 200°C. Extensive studies have been performed with this system. According to the results, there are basically two types of fluorine ions: a bridging fluorine (forming a bonding Zr–F–Zr) and a nonbridging fluorine (Zr–F–Ba). The positional exchange takes place much easier between the latter fluorine ions. It is therefore believed that F^- can migrate in the glassy structure through channels connecting positions of the nonbridging fluorine. Other glass phases based on AgI also show a high Ag^+ conduction at room temperature. For example, a glass with the composition $3AgI \cdot Ag_2MoO_4$ exhibits a conductivity of 0.02 S/cm at 25°C. Although details of the mechanism are not completely understood, the glassy structure itself is held responsible for the high conductivity because most of these compounds show a decrease in conductivity by three orders of magnitude when crystallized at elevated temperature. Oxide and sulfide glasses are investigated extensively as Li^+ conductors. Simple binary glasses in the Li_2O–SiO_2 and Li_2O–Bi_2O_3 systems show a conductivity of $\approx 10^{-6}$ S/cm at room temperature, while the phosphate system is somewhat less conductive at the same Li_2O content. Binary sulfide glasses in the system Li_2S–B_2S_3 or Li_2S–SiS_2, for example, show a higher conductivity than their oxide counterparts because S^{2-} is larger and more polarizable. The former exhibits a conductivity as high as 10^{-4} S/cm at room temperature.

25.3 SOLID MIXED IONIC–ELECTRONIC CONDUCTORS

Solid mixed ionic–electronic conductors (MIECs) exhibit both ionic and electronic (electron–hole) conductivity. Naturally, in any material there are in principle nonzero electronic and ionic conductivities (σ_{el}, σ_i). It is customary to limit the use of the term MIEC to those materials in which σ_i and σ_{el} do not differ by more than two orders of magnitude. It is also customary to use the term MIEC if σ_i and σ_{el} are not too low (σ_i, $\sigma_{el} \geq 10^{-5}$ S/cm). Obviously, there are no strict rules. There are processes where the minority carriers play an important role despite the fact that σ_i/σ_{el} exceeds those limits and σ_i, $\sigma_{el} < 10^{-5}$ S/cm. In MIECs, ion transport normally occurs via interstitial sites or by hopping into a vacant site or a more complex combination based on interstitial and vacant sites, and electronic (electron/hole) conductivity occurs via delocalized states in the conduction/valence band or via localized states by a thermally assisted hopping mechanism. With respect to their properties, MIECs have found wide applications in solid oxide fuel cells, batteries, smart windows, selective membranes, sensors, catalysis, and so on.

25.3.1 Metallic Mixed Conductors

Some MIECs exhibit metallic properties. These materials can have different concentration of the mobile ionic species, compared with that of electrons and holes. Silver chalcogenides, $Ag_{2+\delta}X$ (X = S, Se, or Te) is an example of a metallic MIEC that conduct electrons and silver ions. These materials are good electronic conductors (close to metallic) and show interesting electronic behavior as a function of temperature as

well as of composition. They transform to a high-symmetry phase (≈137°C) where the Ag^+ ions are randomly distributed, giving rise to ionic conductivity. For example, in the high-temperature phase, $Ag_{2+\delta}Se$ shows the metallic behavior of electronic conductivity for high values of δ. With a decrease in δ, the electronic conductivity shows evidence for a phase transition. The magnitude of change in electronic conductivity at the phase transition is also determined by stoichiometry. However, the ionic conductivity of the high-temperature phase is essentially independent of δ.

25.3.2 Mixed-Conducting Oxides

Acceptor-doped perovskite oxides with the generic formula $La_{1-x}A_xCo_{1-y}B_yO_{3-\delta}$ (A = Sr, Ba, Ca and B = Fe, Cu, Ni) exhibit mixed ionic–electronic conductivity. In the system of $La_{1-x}Sr_xCo_{1-y}Fe_yO_{3-\delta}$, the perovskites with higher Sr and Co contents have higher oxygen anion defects, because Sr on the A-site lattice of perovskite acts as an acceptor, enhancing the formation of oxygen vacancies. In addition, Co ions on the B-site appear to have a smaller binding energy for oxygen than do Fe ions. The ionic conductivity at 800°C in air can be one or two orders of magnitude higher than that of stabilized zirconia. For example, compositions with high Sr and Co contents showed ionic conductivity on the order of 0.1 to 1.0 S/cm. The electronic conductivity of compositions in this series can be extremely high, typically in the range 10^2 to 10^3 S/cm, because of a large difference in the mobilities, with $\mu_e \gg \mu_i$. In general, the perovskite $La_{1-x}A_xCo_{1-y}B_yO_{3-\delta}$ exhibits complex dependence of mixed ionic–electronic conductivity on composition, temperatures, and oxygen partial pressure. In the investigation of amorphous or glassy materials for possible solid electrolytes, some were found to be MIECs. $(40 - x)Fe_2O_3$–xNa_2O–$60P_2O_5$ is a glassy MIEC conducting Na^+ and electrons. The ionic conductivity for $x = 35$ is $\sim 10^{-10}$ S/cm at 25°C and 10^{-7} S/cm at 150°C. The electrons propagate by hopping between localized states. The sum of concentrations of mobile ions and conduction electrons varies slowly with x compared to the variation in ion and electron concentrations.

25.3.3 *pn*-Junctions in Mixed Conductors

MIECs may be made nonuniform to the extent that they become *n*-type on one side and *p*-type on the other side, thus forming *pn* or *pin* (*i* = intrinsic) junctions. ZrO_2 + 10 mol % Y_2O_3 subject to an oxygen partial pressure, P_{O_2}, gradient at elevated temperatures becomes *p*-type near the high P_{O_2} ($P_{O_2} \sim 1$ atm) side and *n*-type near the low P_{O_2} ($P_{O_2} < 10^{-20}$ atm) side. In MIECs, *p* and *n* regions can be formed under applied voltage. The electric field either pushes mobile ions to one side, as in Li-doped Si, or Li exhibits a nonnegligible mobility in Si. One uses a *p*-type Si with uniformly doped fixed acceptors to prepare the *pn*-junction. Li is diffused into one side of the solid to form an excess donor region. The application of a voltage for a limited time in the reverse bias direction forces Li' to move into the *p* region, forming an intrinsic region between the *p* and *n* regions.

25.4 ELECTROCHEMICAL REACTIONS AT INTERFACES WITH SOLID ELECTROLYTES

In this section we treat some electrochemical reactions at interfaces with solid electrolytes that have been chosen for both their technological relevance and their scientific relevance. The understanding of the pecularities of these reactions is needed for the technological development of fuel cells and other devices. Investigation of hydrogen or oxygen evolution reactions in some systems is very important to understand deeply complex electrocatalytic reactions, on the one hand, and to develop promising electrocatalysts, on the other.

25.4.1 Investigations in a Wide Temperature Range

The polyhydrates $HClO_4 \cdot 5.5H_2O$ and $DClO_4 \cdot 5.5D_2O$ are acid compounds, which solidify in a type-1 clathrate structure (space group Pm3n, lattice constant 12 Å) consisting of a host lattice, formed by the water molecules, and anionic guest species. The water molecules have tetragonal short-range coordination, which creates smaller pentagonal and larger hexagonal cages in which the anions are located. The protons are part of the water structure and are delocalized over the crystalline network; thus, the polyhydrates are ionic solids with the protons being the mobile species in the crystal. Because of this ability, these polyhydrates are a suitable system for investigating the electrochemical behavior of proton conductors in the liquid and in the solid state (i.e., in a wide temperature range, usually not accessible in electrochemistry).

Hydrogen Reaction The hydrogen evolution reaction was investigated at the interface $Ag/HClO_4 \cdot 5.5H_2O$ between 140 and 228 K. Analogous measurements were also performed in $DClO_4 \cdot 5.5D_2O$. A linear relationship between current density and potential is observed at any temperature for both hydrogen and deuterium evolution reactions. A comparison of the current density of the hydrogen and deuterium evolution at the same temperature and overpotential shows that the isotope effect is large: At 203 K and -0.5 V, the current density of the hydrogen evolution is about one order of magnitude higher than the current density of the deuterium evolution. The isotope effect becomes larger with decreasing temperature: At 173 K and -0.75 V, the current density of hydrogen evolution is 50 times higher than for deuterium evolution. From the slope of the current–potential curves in semilogarithmic plots, the charge transfer coefficient $n\alpha$ was determined as a function of temperature. The value of $n\alpha$ depends on temperature and on the isotope. For $HClO_4 \cdot 5.5H_2O$, $n\alpha$ decreases with temperature from 0.4 at 220 K to 0.15 at 140 K. For $DClO_4 \cdot 5.5D_2O$, $n\alpha$ varies from 0.29 at 220 K to 0.15 at 160 K and 0.05 at 140 K.

Oxygen Reaction An understanding of the anodic evolution of oxygen on metal or metal oxide electrodes is one of the most challenging problems in the field of electrocatalysis. RuO_2 has been identified as one of the most active electrocatalyts. The kinetics of this reaction on RuO_2 and Pt electrodes in an $HClO_4 \cdot 5.5H_2O$ electrolyte was investigated as a function of temperature, ranging from 186 to 297 K for RuO_2

and from 195 to 298 K for Pt, respectively. The current–potential relationship in the form of Tafel plots and charge-transfer coefficients shows different behavior with temperature. At higher current densities, a small deviation of the Tafel slope toward higher values appears for the RuO_2 system. This deviation increases significantly in the frozen state and cannot be attributed to an ohmic drop, which was estimated to be less than 1 mV. For the Pt system in the potential range explored, straight lines were obtained at each temperature. The charge-transfer coefficients show a temperature dependence for RuO_2 in contrast to platinum, which remains fairly constant in the temperature range investigated ($n\alpha = 0.42$ at 298 K). For RuO_2, $n\alpha$ decreases from ca. 1 at 298 K to 0.4 at 186 K, with a change in slope close to the melting point of the electrolyte. Arrhenius plots (log i vs. $1/T$) show clear differences between the kinetic current in the liquid and in the frozen state in both systems. The exponential current density decay in the liquid state is changed at the freezing point of the electrolyte. After freezing, current densities are higher than in the liquid electrolyte. Then, after passing through a maximum, the current density decays again with decreasing temperature. In both the liquid and the frozen states of electrolytes, the activation energy for RuO_2, contrary to expectation, increases as the overpotential increases. The variation of the activation energy is 0.56 and 0.59 eV/V for the liquid and frozen state, respectively. The preexponential factor in the same electrode potential range, in the liquid state varies by about six orders of magnitude and in the frozen state by about five orders of magnitude. The remarkable result is that both activation energy and preexponential factor increase with increasing overpotential. The fact that the preexponential factor for RuO_2 is strongly potential-dependent supports the picture of a surface complex whose concentration is potential dependent. The evaluation of activation energies and frequency factors indicates that the entropy turnover of the reaction plays a significant role for the higher catalytic activity of RuO_2 in comparison to platinum. These results indicate that the evolution of oxygen on RuO_2 and Pt proceeds in a strikingly different way.

25.4.2 Reactions in Solid Electrolyte Fuel Cells

Hydrogen Oxidation Solid oxide fuel cells (SOFCs) promise to provide a highly efficient and environmentally product. Porous Ni/YSZ cermet (YSZ: yttria-stabilized zirconia) is currently the most common anode material for SOFC applications because of its low cost. It is also chemically stable in reducing atmospheres at high temperatures, and its thermal expansion coefficient is close to that of YSZ electrolyte. More important, the intrinsic charge-transfer resistance that is associated with the electrocatalytic activity at the Ni/YSZ boundary is low. More than 30% by volume of continuous porosity is required to facilitate the transport of reactant and product gases. Nickel serves as an excellent reforming catalyst and electrocatalyst for electrochemical oxidation of hydrogen. It also provides predominant electronic conductivity for anode. The YSZ constitutes a framework for the dispersion of Ni particles and acts as an inhibitor for the coarsening of Ni powders during both consolidation and operation. Activation polarization is related to the charge-transfer processes and

depends on the area of electrode/electrolyte/gas triple-phase boundaries (TPB). It was found that the performances of Ni/YSZ cermet is strongly dependent on the processing. Therefore, knowledge of reaction mechanisms and rate-determining steps would indeed be useful to optimize all processing variables.

The hydrogen oxidation at the interface produces water according to the reaction

$$H_2 + O_O^{\times} = H_2O + V_O^{\cdot\cdot} + 2e^- . \tag{25.7}$$

The kinetics of H_2 oxidation has been investigated on a Ni/YSZ cermet using impedance spectroscopy at zero dc polarization. The hydrogen reaction appears to be very complex. The electrode response appears as two semicircles. The one in the high-frequency range is assumed to arise partly from the transfer of ions across the TPB and partly from the resistance inside the electrode particles. The semicircle observed at low frequencies is attributed to a chemical reaction resistance. The following reaction mechanism is suggested:

$$H_2 \rightleftharpoons 2H_{ad,Ni}; \tag{25.8}$$

$$2(H_{ad,Ni} \rightleftharpoons H_{ad,Ni}^{+} + e^-). \tag{25.9}$$

Diffusion of $H_{ad,\,Ni}$ to the Ni/YSZ boundary is followed by proton transfer:

$$2(H_{ad,Ni}^{+} + O_{YSZ}^{2-} \rightleftharpoons OH_{YSZ}^{-}); \tag{25.10}$$

$$2OH_{YSZ}^{-} \rightleftharpoons H_2O + O_{YSZ}^{2-}. \tag{25.11}$$

Oxygen Reduction The overall reaction for the oxygen reduction at a SOFC cathode can be written as

$$O_2 + 2V_o^{\cdot\cdot} + 4e^- = 2O_o^{x}. \tag{25.12}$$

This reaction is made up of a series of bulk and surface processes. One or several of these processes can be rate-determining steps. The polarization process on oxide electrodes is markedly dependent on the electrode material, due to the fact that different oxide materials show different catalytic activity for oxygen reduction. For example, the activity of four doped perovskite electrodes studied at 800°C can be ranked as follows: $LaCoO_3 > LaMnO_3 > LaFeO_3 > LaCrO_3$. At 800°C, the proposed rate-determining step is the charge-transfer reaction for strontium-doped $LaCoO_3$ electrode in contact with YSZ electrolyte, the dissociation of absorbed oxygen molecules for strontium-doped $LaFeO_3$ and $LaMnO_3$, and oxygen diffusion on the electrode surface for strontium-doped $LaCrO_3$. For $LaCoO_3$ and $LaMnO_3$ electrodes with doped CeO_2 electrolyte, the rate-determining step is the charge-transfer reaction at low temperatures but switches to the dissociative adsorption of oxygen at higher temperatures up to 800°C.

To date, the three-phase boundary area is considered as the electrochemical reactive site for oxygen reduction on oxide electrodes. An example is the increase observed in oxygen reaction kinetics of strontium-doped $LaMnO_3$ electrode with increasing triple-phase boundary length. The reactive area for the oxygen reduction is often not limited to the triple point but can spread along the electrode surface, and the spreading of the reaction zone is related to defect chemistry of the cathode material. The concentration of oxygen adsorption sites is related directly to the concentration of defects in the electrode. The electrocatalytic activity of doped $LaMnO_3$ is greatly enhanced under high cathodic polarization. Under those conditions, the electrode material is partly reduced, resulting in a marked increase in the oxygen concentration inside the electrode. The oxygen reaction takes place not only at the three-phase boundary but also on the electrode surface according to the following equations:

$$\tfrac{1}{2}O_2 + V^{\cdot\cdot}_{o(\text{manganite})} + 2e^- = O^{x}_{o(\text{manganite})}; \tag{25.13}$$

$$O^{x}_{o(\text{manganite})} + V^{\cdot\cdot}_{o(\text{electrolyte})} = O^{x}_{o(\text{electrolyte})} + V^{\cdot\cdot}_{o(\text{manganite})}. \tag{25.14}$$

Thus, the enhanced activity of the electrode can be attributed to the presence of both electrons and oxygen vacancies (mixed electronic and ionic conduction) in the electrode material.

PART B SOLID-STATE REACTIONS

In addition to metals, other substances that are solids and have at least some electronic conductivity can be used as reacting electrodes. During reaction, such a solid is converted to the solid phase of another substance (this is called a *solid-state reaction*), or soluble reaction products are formed. Reactions involving nonmetallic solids occur primarily in batteries, where various oxides (MnO_2, PbO_2, NiOOH, Ag_2O, and others) and insoluble salts ($PbSO_4$, AgCl, and others) are widely used as electrode materials. These compounds are converted in an electrochemical reaction to the metal or to compounds of the metal in a different oxidation state.

Nonmetal electrodes are most often fabricated by pressing or rolling of the solid in the form of fine powder. For mechanical integrity of the electrodes, binders are added to the active mass. For higher electronic conductivity of the electrode and a better current distribution, conducting fillers are added (carbon black, graphite, metal powders). Electrodes of this type are porous and have a relatively high specific surface area. The porosity facilitates access of dissolved reactants (H^+ or OH^- ions and others) to the inner electrode layers.

25.5 HETEROGENEOUS SOLID-STATE REACTIONS

Solid-state reactions between two phases of constant composition are called *heterogeneous solid-state reactions*. The mechanism of heterogeneous solid-state reactions

is not a simple one. In the reaction the lattice of one substance is destroyed and that of another substance is freshly formed. Two types of solid-state reactions are distinguished.

25.5.1 Reactions Via the Solution Phase

In the case of substances having at least some solubility (e.g., 10^{-6} mol/L), the reaction often follows a scheme involving dissolved species:

$$\mathrm{A} \rightleftharpoons \mathrm{A_{sol}} \pm ne^- \rightleftharpoons \mathrm{B_{sol}} \rightleftharpoons \mathrm{B}. \tag{25.15}$$

This mechanism is followed in particular in the reactions of lead sulfate in the electrodes of lead–acid storage batteries. At the negative electrode,

$$\mathrm{PbSO_4} + 2\mathrm{H^+} + 2e^- \rightleftharpoons \mathrm{Pb} + \mathrm{H_2SO_4}. \tag{25.16}$$

At the positive electrode,

$$\mathrm{PbSO_4} + 2\mathrm{H_2O} \rightleftharpoons \mathrm{PbO_2} + \mathrm{H_2SO_4} + 2\mathrm{H^+} + 2\,e^- \tag{25.17}$$

(during charging of the battery from left to right, during discharge from right to left). In these reactions, due to a slight solubility of lead sulfate in sulfuric acid, the ions Pb^{2+} in the solution are deposited as metallic lead on one electrode and oxidized to PbO_2 at the other electrode.

Reactions of this type can also occur when the conductivity of one of the phases is very low or practically zero. In these reactions, the sites of reactant lattice destruction and product lattice formation are spatially separated. During the reaction, dissolved species diffuse from the dissolution sites to sites where they undergo further reaction and form the nuclei of the new phase. The length of the diffusion pathway in the solution depends on the degrees of dispersion of the original reactant and resulting product, and most often is between 10^{-5} and 10^{-3} m.

25.5.2 Topochemical Reactions

In topochemical reactions all steps, including that of nucleation of the new phase, occur exclusively at the interface between two solid phases, one being the reactant and the other the product. As the reaction proceeds, this interface gradually advances in the direction of the reactant. In electrochemical systems, topochemical reactions are possible only when the reactant or product is porous enough to enable access of reacting species from the solution to each reaction site. The number of examples electrochemical reactions known to follow a truly topochemical mechanism is very limited. One of these examples are the reactions occurring at the silver (positive) electrode of silver–zinc storage batteries (with alkaline electrolyte):

$$\mathrm{Ag} + 2\mathrm{H_2O} + 2e^- \rightleftharpoons \mathrm{AgO} + 2\mathrm{OH^-} \tag{25.18}$$

and

$$AgO + 2H_2O + 2e^- \rightleftharpoons AgO_2 + 2OH^-. \tag{25.19}$$

In heterogeneous solid-state reactions where the composition of both solid reactants does not change, the electrode's equilibrium potential depends only on the nature of the two phases, not on their relative amounts. Hence, during the reaction the potential does not change. It also remains constant when the current is interrupted after partial reduction or oxidation.

25.6 ELECTROCHEMICAL INTERCALATION

Electrochemical *intercalation* is a process of incorporation of foreign species (ions, atoms, or compounds) into the bulk (into the crystal lattice) of solid electrodes ("hosts") during their polarization. *Deintercalation* is the reverse process, removal of these species. As a result of the intercalation process, a new solid intercalation compound is formed with properties different from those of the host material. The intercalating species (intercalates) arrive either from the electrolyte or are formed in situ as result of an electrochemical reaction. In contrast to the heterogeneous solid-state process, the composition and properties of the intercalation compound change gradually during the process. For this reason, the unfortunate expression *homogeneous solid-state processes* is sometimes used.

Historically, the first known example of electrochemical intercalation is the incorporation into the palladium crystal lattice of hydrogen atoms formed from hydrogen ions during cathodic polarization of this metal. The incorporation of hydrogen atoms can be regarded as the incorporation of protons with simultaneous incorporation of electrons arriving from the external circuit. After incorporation into the surface layer, the hydrogen atoms begin to move by diffusion into the bulk of the metal. During a subsequent anodic polarization the hydrogen atoms are removed from the metals and enter the solution in the form of hydrated (solvated) ions. An analogous phenomen is observed at other metals: for instance, at iron and titanium, and is the reason for the *hydrogen brittleness* of these metals after the cathodic deposition of other metals on their surface.

Another example for reactions with the insertion of protons is the cathodic reduction of manganese dioxide, which occurs during discharge of the positive electrodes in zinc–manganese dioxide batteries. This reaction can be formulated as

$$MnO_2 + xH^+ + xe^- \rightarrow MnOOH_x. \tag{25.20}$$

During the reaction, protons which have been produced from water molecules or from the hydroxonium (H_3O^+) ions of the solution are inserted into the manganese dioxide lattice. At the same time, an equivalent number of Mn^{4+} ions of the lattice are reduced to Mn^{3+} ions by the electrons arriving through the external circuit. Hence, the overall balance of positive and negative charges in the lattice remains unchanged.

Even the lattice structure of manganese dioxide, up to a certain limit, will remain unchanged during proton insertion, although there may be some minor increase in the lattice parameters. Thus, the reaction product, Mn(III) oxide, accumulates without forming a new phase; the homogeneity of the original reactant phase is preserved. Hence, reactions of this type are also known as *homogeneous solid-state reactions*. The degree of reduction in a phase of varying composition can be described by the ratio x between the number of Mn^{3+} ions and the total number of manganese ions in the lattice or, what amounts to the same thing, the ratio between the number of protons and the total number of manganese ions.

When the solid-state reaction is homogeneous and a phase of varying composition is formed, there will be a smooth change in equilibrium potential as the degree of oxidation changes. Hence, the discharge curves of batteries in which homogeneous solid-state reactions take place (e.g., the reduction of manganese dioxide, curve 1 in Fig. 25.11) exhibit a gradually decreasing discharge voltage, whereas those of batteries in which a heterogeneous process takes place (e.g., the reduction of silver oxide, curve 2) exhibit a discharge voltage which is constant for a long time.

A typical feature in homogeneous solid-state reactions is the slow diffusion of the species inserted in the host lattice. In any individual grain, therefore, a nonequilibrium concentration distribution of these species is found during the reaction; the concentration changes are more rapid at the surface than inside the grain. This gives rise to hysteresis effects. Thus, when a manganese dioxide electrode is partly discharged at a high current density and the current is then interrupted, the potential will be rather negative directly after the interruption. Then diffusional leveling of the concentration within the grains sets in, and the potential shifts in the positive direction until it reaches the equilibrium value for the actual oxidation state. This is the reason

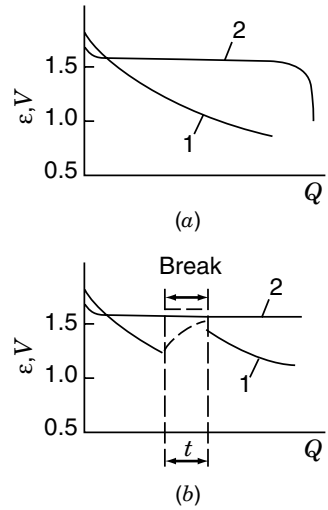

FIGURE 25.11 Discharge curves of batteries with oxides as the positive electrode: (*a*) continuous discharge; (*b*) interrupted discharge; (1) MnO_2, (2) Ag_2O.

Boris N. Kabanov (1904–1988).

for the "recovery" of zinc–manganese dioxide cells during breaks in discharge (Fig. 25.10*b*); in silver–zinc cells, such an effect is not observed.

Protons are not the sole species that can be incorporated into the lattices of different host materials. At the beginning of the 1960s, Boris N. Kabanov showed that during cathodic polarization of different metals in alkaline solutions, intercalation of atoms of the corresponding alkali metal is possible. As a result of such an electrochemical intercalation, either homogeneous alloys are formed (solid solutions) or heterogeneous polyphase systems, or even intermetallic compounds, are formed.

In the 1980s it was shown that during cathodic polarization of some solid compounds (oxides, halcogenids) in aprotic solvents containing dissolved lithium salts, an incorporation of lithium atoms is possible. On titanium dioxide this reaction can be written as

$$TiS_2 + xLi^+ + xe^- \rightleftharpoons TiS_2Li_x. \tag{25.21}$$

This reaction is invertible—during anodic polarization, lithium is removed from the host lattice. Intercalation and deintercalation processes occur in the potential range + 1.5 to 2.5 V vs. the equilibrium potential of metallic lithium in the same solution [the higher the value of x, the higher will be the value of the (positive) potential]. Thus, the intercalation compound TiS_2Li_x can be used as a positive electrode together with metallic lithium as a negative electrode for the production of batteries (primary as well as secondary) with a voltage of about 2 V. The development and broad application of various highly efficient lithium batteries (see Chapter 19) led to an increased interest in investigations of lithium intercalation into various host materials. Up to now a great many such investigations were published.

The properties of lithium intercalation compounds depend in a decisive manner on the nature of the host material. If oxides of metals with varying valency are used instead of TiS_2, the potential of the electrode (consequently also, the battery voltage) will increase to 3 V. Even higher values (up to 4 V) are obtained when as host material

partially lithiated oxide of nickel, cobalt, or manganese [Li_xMeO_2 (Me = Co, Ni, Mn)] with a layered spinel-type structure is used. Under certain conditions these compounds can be cycled (alternating intercalation and deintercalation) for a long time without appreciable deterioration.

Intercalation compounds of lithium and other species into the layered structure of graphite, synthesized by chemical methods, have been known for a long time. In the mid-1980s, the possibility of a reversible lithium intercalation from aprotic solutions containing lithium salts into certain carbonaceous materials was discovered:

$$C_6 + xLi^+ + xe^- \rightleftharpoons C_6Li_x \tag{25.22}$$

(in the case of carbonaceous materials containing fragments of graphite rings C_6, the value of x is commonly related to one C_6 ring). The first publications showed the possibility of cycling these compounds some thousands of times. The cycling depth (maximum value of x) corresponds to a specific capacity of this compound up to 350 mAh/g.

The intercalation compounds of lithium with graphite are very different in their behavior from intercalation compounds with oxides or halcogenides. Intercalation processes in the former compounds occur in the potential region from 0 to −0.4 V vs. the potential of the lithium electrode. Thus, the thermodynamic activity of lithium in these compounds is close to that for metallic lithium. For this reason, lithium intercalation compounds of graphite can be used as negative electrodes in batteries rather than the difficultly of handling metallic lithium, which is difficult to handle.

At the end of the 1990s in Japan, large-scale production of rechargeable lithium ion batteries was initiated. These contained lithium compounds intercalated into oxide materials (positive electrodes) as well as into graphitic materials (negative electrode). The development of these batteries initiated a further increase in investigations of the properties of different intercalation compounds and of the mechanism of intercalation and deintercalation processes.

The depth of intercalation and the activity of the intercalation compound (i.e., the equilibrium potential of the electrode) depend in a decisive manner on the nature of the carbonaceous material: on its crystallographic structure and the degree of graphitization. Many investigations show that the best results can be achieved with amorphous structures containing a mesophase: nuclei of graphite cryctallites. Such materials are coke, pyrographite, and materials produced by pyrolysis (carbonization) of polymers at temperatures of approximately 2000 to 2500°C. During intercalation of lithium in well-organized graphite structures, the formation of compounds of the type LiC_{n6} (with values $x = 1$ and $n = 1, 2, 3, \ldots$) can be observed. On the curve of the potential dependence of Li_xC_6 on the intercalation degree x, some horizontal segments can be observed that correspond to the formation of LiC_6, LiC_{12}, LiC_{18}, and so on. At the same time during intercalation of lithium into amorphous structures and mesophases, this curve has a smooth shape, corresponding to a homogeneous structure. All mentioned phenomena depend to a great degree on the composition of the electrolyte, especially on the nature of the solvent.

At present, intercalation compounds are used widely in various electrochemical devices (batteries, fuel cells, electrochromic devices, etc.). At the same time, many fundamental problems in this field do not yet have an explanation (e.g., the influence of ion solvation, the influence of defects in the host structure and/or in the host stoichiometry on the kinetic and thermodynamic properties of intercalation compounds). Optimization of the host stoichiometry of high-voltage intercalation compounds into oxide host materials is of prime importance for their practical application. Intercalation processes into organic polymer host materials are discussed in Chapter 26.

REFERENCES

Alonso-Vante, N., H. Colell, U. Stimming, and H. Tributsch, *J. Phys. Chem*., **97**, 7381 (1993).

Cappadonia, M., S. Krause, and U. Stimming, *Electrochim. Acta*, **42**, 841 (1997).

Ishihara, T., T. Shibayama, S. Ishikawa, et al., *J. Eur. Ceram. Soc*., **24**, 1329 (2004).

Kabanov, B. N., *Electrochim. Acta*, **13**, 19 (1968).

Nernst, W., *Z. Electrochem*., **6**, 41 (1899).

MONOGRAPHS AND REVIEWS

Gelings, P. J., and H. J. M. Bouwmeester, Eds., *The CRC Handbook of Solid State Electrochemistry*, CRC Press, Boca Raton, FL, 1997.

Julien, Ch., J. P. Pereira-Ramos, and A. Momchilov, *New Trends in Intercalation Compounds for Energy Storage*, Kluwer, New York, 2002.

Kudo, T. and K. Fueki, Eds., *Solid State Ionics,* VCH, Weinheim, Germany, 1990.

Minh, N. Q., and T. Takahashi, *Science and Technology of Ceramic Fuel Cells*, Elsevier, Amsterdam, 1995.

Rao, C. N. R., and J. Gopalakrishnan, Eds., *New Directions in Solid State Chemistry*, Cambridge University Press, Cambridge, 1986.

Rickert, H., Ed., *Electrochemistry of Solids*, Springer-Verlag, New York, 1982.

Smart, L., and E. Moore, Eds., *Solid State Chemistry: An Introduction*, 2nd ed., Chapman & Hall, London, 1996.

West, A. R., Ed., *Basic Solid State Chemistry*, 2nd ed., Wiley, Chichester, West Sussex, England, 1999.

26
Conductive Polymers

KLAUS MÜLLER
Retired from the Battelle Institute, Carouge, Switzerland

26.1 ACTIVE POLYMERS

It has been a long way from early synthetic polymers created as artificial substitutes (*Kunststoffe*) for scarcening metal resources, to modern materials tailormade to fill specific functions through particular properties and processing characteristics in many areas of application. Ever since they were first prepared, surprising new or improved properties have been discovered or engineered.

Today, *active polymers* are known that exhibit technically interesting reactions to applied physical actions (e.g., electric fields, chemical concentrations, pressure, light) that can be employed in devices of various types; for example:

- *Ferroelectrics*: Poly(vynidilene fluoride) undergoes electrostriction when subjected to high ac fields, thus can be made into actuators; applied pressure produces a piezoelectric response useful in sensors.
- *Dielectrics*: In certain high-dielectric-constant elastomers, bending or stretching can be induced by strong electric fields (ESSPs, elecrostatically stricted polymers).
- *Viscoelastics*: Certain silicone elastomers undergo changes in shear modulus under the influence of electric fields, which might be useful in active mechanical damping applications.
- *Polymer gels*: In response to pH changes in their environment, materials derived from poly(acrylonitrile) will swell or shrink in a slow analogy to muscle action, thought to have robotic applications.
- *Polymer–metal composites*: Cationic mobility activated electrically in membranes of the Nafion (DuPont) and Flemion (Asahi Glass) type leads to a bending response, again mimicking muscle action.

Fundamentals of Electrochemistry, Second Edition, By V. S. Bagotsky

In this chapter we focus on two electrochemically relevant, active polymer types: ionically conductive polymers and electronically conductive polymers, and discuss new developments emerging in their context.

26.2 POLYMERS WITH IONIC FUNCTIONS

Polymer molecules with just one or a few ionic groups, in most cases terminal and anionic, are called *macroions*. They are encountered primarily in *living polymers*, polymer molecules present in a polymerizing reaction system that will grow as long as monomers (e.g., esters or nitriles of methacrylic acid) continue to be supplied. The ionic charge of the macroion always transfers to the last monomer added, keeping the macroion ready for the next such addition.

Polymers with a sizable number of ionic groups and a relatively nonpolar backbone are known as *ionomers*. The term was first used for copolymers of ethylene with carboxylated monomers (such as methacrylic acid) present as salts, and cross-linked thermoreversibly by divalent metal ions. Such polymers are useful as transparent packaging and coating materials. Their fluorinated forms have been made into very interesting ion-exchange membranes (considered further below).

Polymers with a very high number of ionic groups in or at the polymer chain which are water soluble in their dissociated form are known as *polyelectrolytes*. Polymers with a very high number of ionic groups having their polyion made insoluble by chemical cross-linking or three-dimensional polymerization constitute the technically important group of *ion exchangers*.

26.2.1 Polyelectrolytes

Synthetic examples include the poly(meth)acrylates used as flocculating agents for water purification. Biological examples are the proteins, nucleic acids, and pectins. Chemically modified biopolymers of this class are carboxymethyl cellulose and the lignin sulfonates. Polyelectrolytes with cationic and anionic substituents in the same macromolecule are called *polyampholytes*.

Solutions of polyelectrolytes contain polyions and the free (individual) counterions. The dissociation of a polyacid or its salt yields polyanions, and that of a polybase or its salt yields polycations, in addition to the simple counterions. The polyampholytes are amphoteric; their dissociation yields polyions that have anionic and cationic functions in the same ion and often are called *zwitterions* (as in the case of amino acids having H_3N^+ and COO^- groups in the same molecule). Such an amphoter will behave as a base toward a stronger acid and as an acid toward a stronger base; its solution properties (particularly its effective charge) will be pH dependent, and an isoelectric point (pH value) exists where anionic and cationic dissociation is balanced so that the polyion's charges add up to zero net charge (and solubility is minimal).

Inorganic polyelectrolytes exist, too; polyphosphates, –O–P(=O)(–OH)–, are the most common (soluble) ones.

In solutions, the counterions of polyelectrolytes are H_3O^+ (for the polyacids) and OH^- (for the polybases), cations such as K^+ and Na^+, or anions such as Cl^- (for the polysalts). The addition of polyvalent counterions (such as Ca^{2+}, Mg^{2+}, Cu^{2+}, Al^{3+}) produces ionic cross-linking interfering with solubility: The polyelectrolyte precipitates and may be redissolved upon addition of a strong acid (such as HCl). This can be regarded as a special case of ion exchange.

In the dissolved state, dissolved macromolecules tend to coil up, but the macroions of polyelectrolytes stretch out, owing to repulsive forces between their charged groups, and violent mechanical action may actually break their chains. The accumulation of like charges closely spaced along the macromolecular chain leads to a certain rigidity of the macroion, owing to the repulsive forces. This causes the solution to have a higher viscosity than expected for a soluble uncharged macromolecule and gives rise to some other specific rheological features (shear flow involving chain stretching). Also, the repulsive interactions imply that polyelectrolytes do not exhibit a single dissociation constant for like groups: the polyion's charge, which increases with increasing dissociation at higher dilutions, interferes with further dissociation (i.e., the "dissociation constant" decreases with increasing degree of dissociation).

By definition, in a solution all ions belong to the same phase, even though counterions may cluster more or less diffusely around the macroions. When significant amounts of a simple 1 : 1 electrolyte (such as KCl) are added to a polyelectrolyte solution, dissociation of the polyelectrolyte macromolecule is repressed; in an extreme case the polyelectrolyte may be "salted out." An undissociated polyacid may be precipitated by generous addition of a simple acid such as HCl.

Proteins that are polyampholytes, upon addition of electrolyte, first undergo some "salting in" up to a certain ionic strength, since electrostatic interactions between ions are shielded by the additional simple ions of both sign. Adding more salt will then cause salting out as the added ions compete for water that would otherwise solvate the protein.

26.2.2 Ion Exchangers

Ion exchangers are polymer electrolytes prepared a priori as insoluble solids (salts, acids, bases; hydrated, possibly gel-like). Their polymer backbone is three-dimensional. Many are polyvinyl compounds (substituted polyethylenes) having the general formula $[–CH_2–CXH–]_n$, where different substituents X lead to rather different products:

$X = CH_2–SO_3^-$	Sulfonic acid: strong acids
$X = COO^-$	Carboxylic acid: weak acids
$X = CH_2–NH(C_2H_5)_2^+$	Tertiary amine: weak bases
$X = CH_2–N(CH_3)_3^+$	Quaternary amine: strong bases
$X = CH_2–N(CH_2–COO^-)_2$	Aminediacetic acid: complex formers

Instead of or in addition to CH_2, a phenylene group may be built in, as in the simple sulfonic acid cation exchanger shown schematically, *in just two dimensions*, in Fig. 26.1.

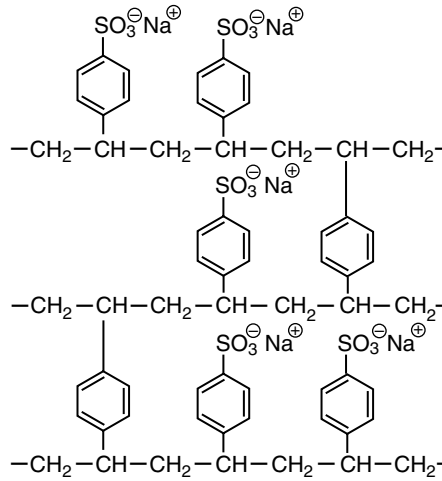

FIGURE 26.1 Cation exchanger (sodium salt form): two-dimensional scheme.

Such materials can be synthesized from appropriate starting materials; the sulfonate resin shown in Fig. 26.1, for instance, by sulfonation of styrene–divinylbenzene copolymers. Other simple resins are of the phenol–formaldehyde condensation type. The anionic groups can be sulfonate, carboxylate, or phenolic hydroxyl; the cationic groups can be tertiary or quaternary amino groups. Chelating groups serving to form complexes with particular heavy-metal ions are valuable for their selectivity. Aluminosilicates such as zeolites and bentonites are cation exchanges of mineral (inorganic) origin. Humic acids are an example of natural organic ion exchangers.

It is relevant to note that the number of charged sites on all these materials corresponds to a volume concentration equivalent to as much as a 5 or 6 M salt solution.

These products, although insoluble, take up water, swell, and dissociate. The polyions remain locked in place. The technical products ordinarily come in the shape of grains, sheets, coatings, or hollow tubes. The counterions can migrate between sites in the grains, etc., and are free to migrate out into the bathing solution and undergo replacement by ions from this solution.

This counterion exchange is an equilibrium process leading to distributions such as those described in Sections 5.3 and 5.4. The water content of the ion exchanger will depend on the bathing solution and on the kinds of ions present. *Coions* (simple solution ions having the same sign as the macroion) together with their own counterions will also enter the ion-exchanger material.

For chemical and electrostatic reasons, some ions are bound more strongly than others. Polyvalent cations are much more strongly bound than univalent cations; the same holds for anions. Thus, when a solution containing Ca^{2+} ions (hard water) is passed through a cation exchanger which is present in its Na^+ or H^+ form, the Ca^{2+} ions are held back in it and the Na^+ or H^+ ions leave instead. Similarly, an anion exchanger in the OH^- form will retain Cl^- or SO_4^{2-} ions from the solution. By a cation and anion exchanger in series, the former in the H^+ and the latter in the OH^-

form, water passing through will undergo desalting. This is the principle of preparation of deionized water.

Since ion exchange is an equilibrium process, it can be understood that the deionization or desalting will only go to a certain limit. Also, by its composition and stoichiometry, any ion exchanger has a certain finite capacity. When this is exhausted, regeneration must be performed, usually with strong acid, to regenerate a cation exchanger, and with strong alkali, to regenerate an anion exchanger. Such exchangers commonly exist as filled columns, some in parallel and some in series. The entire desalting and regeneration process can be automated by sensors and valves.

Complete deionization of hard water often is not necessary: the Ca^{2+} and Mg^{2+} ions may more simply be replaced by Na^+ ions, and an exhausted cation exchanger can then be regenerated with concentrated NaCl solution.

Another important application is the recovery of metal values from such sources as galvanic effluents or certain leachates. Conversely, as an analogy to regeneration, an ion exchanger loaded with mineral cations can serve as a depot fertilizer in hydrocultures.

Often, ion exchangers are made into membranes (flat sheets, rolled sheets, capillaries, hollow fibers) separating different solutions. On the one hand, this can serve to make the ion-exchange processes continuous; on the other hand, further technological opportunities arise (discussed in Section 26.2.3).

Ion-exchanger columns can be used for ionic separation. This application rests on selectivity series that depend on ionic charge, ionic radius, and other factors. A cationic series is given by $Li^+ < H^+ < Na^+ < Cs^+ < Mg^{2+} < Ca^{2+} < Al^{3+} < Ce^{4+}$; an anion series, by $F^- < Cl^- < Br^- < NO_3^- < HSO_4^{2-} < I^-$; written in terms of rising binding strength. This can be used for analyses (ion-exchange chromatography).

26.2.3 Ion-Exchange Membranes

Ion exchangers made in sheet form (or in the form of tubes, capillaries, or hoses) add a number of dimensions to ion exchange. When such a sheet is placed between solutions:

- Ion-exchange processes can be driven by concentration gradients or by an electric field applied across the membrane (electrodialysis), the ions not merely being exchanged but actually passing across.
- Such processes can be conducted continuously (whereas an ion-exchange column is always operated discontinuously).
- Synthetic applications are possible, such as the regeneration of acid and alkali from waste salt.

When the sheet is placed between directly adjacent electrodes, it acts as an electrolyte (often, the sole electrolyte between the electrodes):

- Power can be generated when supplying suitable reactants to the electrodes (fuel-cell operation).

- Power can be stored when the two electrodes accept opposite charge (certain rechargeable batteries and capacitors).
- Chemicals (hydrogen, oxygen, chlorine, caustic soda) can be generated by power supplied to the electrodes (electrolysis).

All these processes make use of the fact that an ion-exchange membrane is *permselective* (selectively permeable) to ions of one sign only, which means that the anions and cations are made to cross different membranes or that only one type is involved in the process taking place. The density of ionic sites in the membrane must be high enough for ionic conduction to occur by a relay-type migration from site to site roughly following the electric field.

In *electrodialysis*, where an electric field is applied by electrodes across (pairs of) different membranes sitting in receiving solutions and enclosing a feed solution to be purified, contaminating cations migrate across the cation exchange membrane(s) toward the solution surrounding the negative electrode, and contaminating anions migrate across the anion-exchange membrane(s) toward the solution surrounding the positive electrode. The enclosed solution thus becomes purified. This principle (Fig. 26.2) can be used for seawater desalination, to turn brackish water into drinking water, or to reduce water hardness (see Chapter 24).

It is easy to see that the process could be conducted regeneratively: for instance, with spent acid (sodium sulfate as a feed solution). Sulfuric acid could be generated

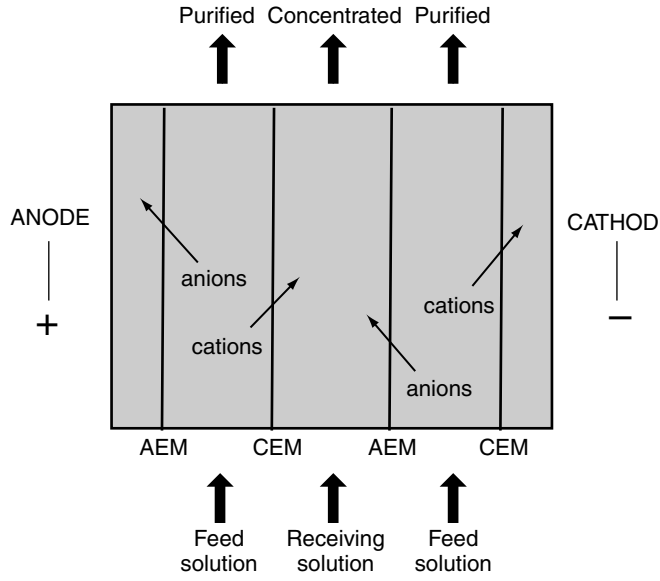

FIGURE 26.2 Electrodialysis: purifying a feed solution. An alternation of anion-exchange membranes and cation-exchange membranes is placed between electrodes in a receiving solution outside the last membranes. Only a central section is shown.

in the compartment around the positive electrode and sodium hydroxide in the compartment around the negative electrode, if water was electrolyzed in these receiving compartments (oxygen evolution at the positive electrode leaving behind protons to make sulfuric acid with the sulfate ions, hydrogen evolution at the negative electrode leaving behind hydroxyl ions to make caustic soda from the sodium ions arriving through the respective membrane).

Much more simply, the same result can be attained with *bipolar membranes*, membranes consisting of an anion- and cation-permeable (an anion- and cation-exchange) membrane laminated together. At such a membrane, when mounted between electrodes so that the cation-exchange layer faces the anode, water is split into H^+ and OH^- ions so that the acidic and alkaline solutions required for regeneration as above are produced at the respective surfaces of the bipolar membrane. When such membranes are suitably integrated into the sequence of membranes in the electrodialysis unit above, gas evolution at the electrodes is not needed; the acid–base pair is produced with about half the power.

This is not to say, however, that these processes always are economically feasible, since electric power could still be overly expensive; witness the scarcity of drinking water in many coastal regions.

Fuel cells (hydrogen–oxygen, hydrogen–air, methanol–air) and *industrial electrolysis* (water, chlor–alkali) using ion-exchange membranes are the most demanding applications for the membranes. In these applications, the membranes have often been designated as *SPE*, which can be read as *solid polymer electrolyte* or *solid proton exchange*. Here:

- The membranes should be very thin, to lower the IR drop (at the high currents used in technical cells, every millivolt counts), yet mechanically strong, to withstand shear, tear, and pressure.
- The membranes should be stable in contact with aggressive chemicals.
- Reactive radicals may be generated at the electrodes in contact with the membranes, attacking the membranes.
- In the membrane–electrode assembly (MEA: a membrane squeezed in between two electrodes), mechanical forces are applied.
- The operating temperatures are fairly high, again to lower the IR drop and to accelerate the electrode reactions, yet the membrane must remain highly hydrated, and uniformly so, to avoid hot spots.
- The membranes must fill separating functions (gases, methanol, water) and sealing functions (at the cell periphery) in addition to their ionic permselectivity.

Membranes in chlor–alkali electrolysis require highly pure brine feed; the water used in membrane water electrolyzers must also be rather pure.

Du Pont's Nafion membranes have been the first truly successful membranes in these applications. They are made of a perfluorinated and sulfonated polyalkylene ionomer ($-CF_2-$ or $>CF-$ throughout). Such a composition leads to

hydrophilic and hydrophobic regions. At 80°C, the protonic conductivity is about 0.1 S/cm. Thicknesses around 0.1 mm are feasible. Thin Teflon gauze is a useful reinforcement for such membranes. In these membranes, quality requirements and synthetic difficulties are such that high prices have been maintained even though Dow and Asahi came out with analogous products. For a rather long time now, hopes have been nourished that radiation-grafted membranes filling the same functions could be cheaper (for a review and progress in the field, see Gubler et al., 2005).

Typical chemical structures of ion-exchange membranes for technical applications are shown in Fig. 26.3. Judging superficially, they may look somehow similar, but structural details do lead to important differences in behavior and performance. Membrane fuel cells are discussed in detail in Chapter 20.

In the field of chlor–alkali electrolyzers, Japan has been the leader in replacing mercury cell technology with membrane cell technology. Only now is overdue replacement under way in the United States and Europe. The Aciplex membrane and zero-gap cell technology of Asahi Kasei Chemicals (Tokyo), for instance, are employed for plants with annual production figures in the 100-kiloton range. New membranes have also been announced by Asahi Glass (Tokyo) and PolyFuel (Mountain View, California), for example.

In battery applications, new lithium ion batteries called *lithium ion polymer batteries* (or more simply but misleadingly, *lithium polymer batteries*) work with a full matrix of ionically conducting polymer, this polymer being present inside the porous electrodes and as a separator between the electrodes. They are offered in attractive flat shapes for mobile applications (mobile phones, notebooks).

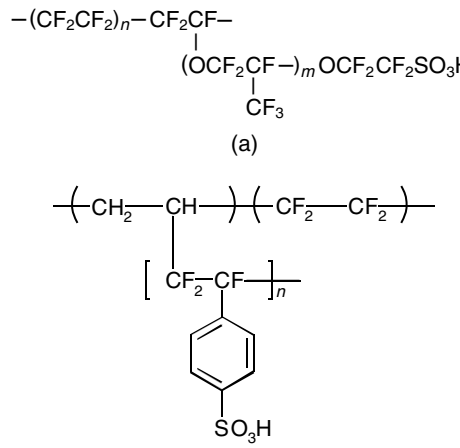

FIGURE 26.3 Chemical structure of (*a*) Du Pont's Nafion membrane material (after Hopfinger and Mauritz, 1981, with permission from Springer sbm); (*b*) CEC (Japan)'s Raymion membrane (as reported by Gubler et al., 2005, with permission from Wiley-VCH).

26.3 POLYMERS WITH ELECTRONIC FUNCTIONS

26.3.1 Conventional Approaches

Two older ideas of how to make organic polymers conductive are obvious:

1. Mixing enough conducting particles (such as soot, carbon fibers, steel fibers, aluminum fibers) into the polymer to provide a reasonably continuous filler network. In this approach, polymer-specific processability and corrosion resistance are retained, while applications such as flat heating elements (made of plastic sheet) or electromagnetic shielding (made of thin coatings) are available. Certain electrochemical cell components have been machined from such materials.
2. Providing an ion exchanger with a sufficient number of redox groups so that conduction can occur by a relay-type redox-change mechanism. Examples are hydroquinone-derived redox polymers and polyvinyl polymers with a tetrathiafulvalene, ferrocene, or carbazole group, which have been found useful for research and analytical applications.

26.3.2 Intrinsically Conductive Organic Polymers

"For the discovery and development of conductive polymers," the 2000 Nobel Prize in Chemistry went to Alan J. Heeger, Alan G. MacDiarmid, and Hideki Shirakawa. By that time, a large community of chemists, physicists, and engineers worldwide was engaged in the development, improvement, and applications of *intrinsically conductive polymers*, also called (testifying to their popularity) electronically conducting polymers, electrically conductive plastics, electronic polymers, synthetic metals, organic conductors, conductive polymers, and plastic metals. The simplest ones are illustrated in Fig. 26.4.

Synthesis Basically, two methods are available, which both start (evidently) from suitable monomers: (1) chemical synthesis, followed by doping, and (2) electrochemical synthesis directly in a doped state.

The original, "serendipitous discovery" (Heeger, 2000; MacDiarmid, 2000; Shirakawa, 2000) occurred in the 1970s along route (1). Acetylene HC≡CH accidentally polymerized with more than the usual amount of Ziegler–Natta catalyst yielded a lustrous, silvery but insulating polymer film which, when for curiosity exposed to iodine vapor, became metallically conducting. Polymerization had produced $[–CH=CH–]_x$, a polyene called polyacetylene according to its genesis, consisting of a carbon chain with alternating single and double bonds, by chemical intuition forming an extended π-electron system (with a *cis* or *trans* configuration of the single bonds around CH=CH). It was found that the *trans* configuration is more stable; *cis* changes irreversibly into it upon heating.

Despite the name, the material is consistently represented as $(CH)_x$ in most places, a formula that should definitely be replaced by $(C_2H_2)_x$ not only to reflect correctly the name and genesis from acetylene monomer but also to facilitate comparison with

Structure	MW Monomer Unit	Conductivity (S/cm) of the Oxidized Polymer
	26 (13)	3–1000
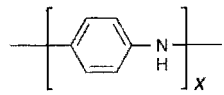	91	0.01–5
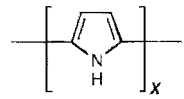	65	0.3–100
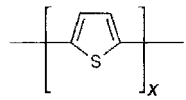	82	2–150
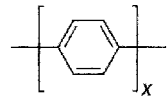	76	10–500

FIGURE 26.4 Simple conductive organic polymers. From top to bottom: polyacetylene, polyaniline, polypyrrole, polythiophene, and polybenzene (poly-*p*-phenylene). (Adapted from Novák et al., 1997, with permission of the American Chemical Society.)

other poly(monomer)s and allow for the representation of alternating bonds and configuration.

Historically, the first conductive polymer was prepared along route (2) but at the time not recognized: Letheby in 1862 (!) subjected aniline to anodic oxidation in sulfuric acid.

Subsequent to the discovery of conducting polyacetylene, scores of monomers, for the most part aromatic and often heterocyclic, substituted or not, have been anodically oxidized to yield polymers with alternating single–double bond systems. In certain cases, addition of an oxidizing agent to the dissolved monomer produces analogous results. While "textbook" examples are shown in Fig. 26.4, a generous listing of electrochemically interesting polymers can be found in Novák et al. (1997) in tables providing indications as to preparation, structure, and properties.

An example for chemical preparation that can be carried out within seconds in a beaker is this: *Dissolve pyrrole in dilute sulfuric acid. Add ferric chloride as an aqueous solution and watch the black polypyrrole precipitate.* The oxidizing Fe^{3+} ions are reduced to Fe^{2+}, imparting one +-charge and donating their now excessive Cl^- ion as dopant ion to the polymer.

For an electrochemical preparation, *dissolve pyrrole (to concentrations of 0.1 to 0.5 M) in propylene carbonate containing traces of water and 0.2 M lithium salt*

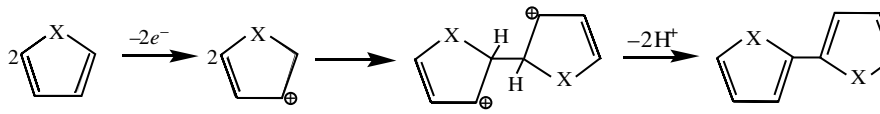

FIGURE 26.5 Initial polymerization step (dimerization) (examples: X = NH, pyrrole; X = S, thiophene).

(such as trifluoroborate, hexafluorophosphate, perchlorate, trifluoromethanesulfonate), electrolyze the solution galvano- or potentiostatically between a lithium sheet as the cathode and a conductive substrate (graphite, platinum, gold, steel, indium–tin oxide) as the anode (the voltage might be 3.7 to 4.5 V vs. the lithium cathode); passing a charge equivalent to 2.3 electrons per monomer molecule, you obtain a doped, conducting polypyrrole film on the anode. The same procedure could be followed to make polythiophene from thiophene.

Two electrons per monomer molecule go for chemical polymerization (abstraction of two hydrogen atoms from two chain-linking sites; for the first step, dimerization with one hydrogen abstracted per molecule; see Fig. 26.5):

$$x\mathrm{Py} - 2xe^- \rightarrow \mathrm{Py}_x + 2x\mathrm{H}^+. \tag{26.1}$$

The remaining 0.3 electron goes for charge production in the polymer, attended by entry of an equivalent of electrolyte anions as dopant:

$$\mathrm{Py}_x - 0.3xe^- + 0.3x\mathrm{LiC1O_4} \rightarrow [\mathrm{Py}_x^{0.3x+} + 0.3x\,\mathrm{C1O_4^-}] + 0.3x\mathrm{Li}^+. \tag{26.2}$$

Contrary to naive expectation, an extended π-electron system such as that in the original silvery polyacetylene film does not imply perfect bond conjugation or perfectly like bonds, or conduction along the chain: It only implies a degree of charge-density delocalization. Such a material has the electronic structure of a semiconductor.

The oxidation and/or reduction reactions yield polymeric systems having an extended π-electron system along the chain. Doping to the conducting state, in the instance of polyacetylene by exposure to iodine vapor (*p*-doping, oxidizing),

$$(\mathrm{C_2H_2})_x + 3xy\mathrm{I_2} \rightarrow [(\mathrm{C_2H_2^{2y+}})_x + 2xy\mathrm{I_3^-}] \qquad (y \leq 0.1), \tag{26.3}$$

or sodium naphthalide (*n*-doping, reducing),

$$(\mathrm{C_2H_2})_x + 2xy\mathrm{NaNph} \rightarrow [(\mathrm{C_2H_2^{2y-}})_x + 2xy\mathrm{Na}^+] + 2xy\mathrm{Nph} \qquad (y \leq 0.1), \tag{26.4}$$

causes these molecules to exist as charge-transfer complexes (indicated by square brackets in the equations above) between delocalized ionic centers at the chain and vicinal counterions. In terms of band theory, doping produces midgap states supporting

conduction. Simplifying, in the example above, the I_2 molecules are thought to abstract electrons from the polyacetylene chain forming I_3^- ions as counterions and making the abstraction sites radical cations called *polarons*. These counterions are relatively immobile. When very many are present in the doped material, the polarons will become mobile in the field of closely spaced counterions. Thus, at doping levels sufficiently high, commonly of an order of magnitude of 10% relative to the monomer units in the polymer, the polymer then becomes conductive.

However, another obstacle to high bulk conductivity of such a polymer exists. In view of the finite length and vast number of constitutive polymer chains, bulk conduction requires electrons to jump between chains (or polarons to transfer between chains in the opposite direction). It is obvious, then, that local order, crystallinity, and good contact between the different crystal domains in the polymer are further prerequisites for conduction.

In the case of polyaniline (see Fig. 26.4), the situation is more complicated, since polymerization occurs across the basic nitrogen atom, the electron state of which depends on pH. Thus, doping is possible not only by oxidation but also by a pH change; conduction of the material rises by 9 to 10 orders of magnitude between pH 5 and 1 ($\sim$1 *M* aqueous HCl).

As in the case of ordinary polymers, copolymerization of two or more different monomers to a conductive polymer is possible, although evidently more stringent compatibility requirements exist in view of the conjugate bonding desired.

While chemists have advanced the range of available polymers, and electrochemists have electropolymerized countless monomers, doping and undoping them electrochemically during and after synthesis to learn about behaviors suitable for polymer batteries, physicists have developed conduction models that have advanced the understanding of conductivity in the polymers and, beyond that, of the physics of molecular materials in general, together creating the basis for exciting new applications. Much has been learned from the spectroscopic signals of *n*- or *p*-doped states.

Structure The polymers are produced as powders or as films on the electrodes. Most conductive polymers have a fibrous structure, each fiber consisting of hundreds of strands of polymer molecules. Techniques exist to control fiber preparation so as to obtain nanofibers expected to be particularly useful as catalyst substrates and in electronic applications (MacDiarmid, 2000).

On a molecular level, the monomers link up as straight as possible (1,4 or 2,5 in typical aromatic molecules), although some 1,2 or 2,3 bonding may also occur (and lead to inferior properties). As in ordinary chemistry, substituents have a directive effect.

Conduction in the raw doped polymer can be improved by devices such as compression and stretching and judicious after-synthesis dopant ion exchange. Matrix-guided electropolymerization also yields superior products.

Properties Only general remarks can be made here in view of the vast multitude of conductive polymers that have been prepared.

Polyacetylene in the doped state is sensitive to air and moisture. Other polymers (e.g., those of pyrrole, thiophene, and benzene) are stable in air and/or toward humidity in their doped and undoped states. Generally, when stored in the doped state, the polymers lose "doping level" by mechanisms not fully understood; in most cases the loss is reversible.

Some of the polymers can be processed like ordinary polymers even in the doped state, which is one of their virtues. Like ordinary polymers, blending of different polymers (e.g., a conducting polymer and an ordinary polymer) is possible. The mutual compatibility of the two polymers can be improved by choosing in the conductive polymer a tenside-type dopant ion that has a tail having affinity to the nonconductive polymer.

The most interesting properties are exhibited by thin films, where rapid changes in doping level, conductivity, and optical transmission can be obtained. Thicker films exhibit vastly slower kinetics, which is due to slow counterion transport and, to some extent, to slow conformation changes.

The limit of dopability generally amounts to fractions (0.1 to 0.3) of a charge per monomer unit. A few of the polymers admit both *p*- and *n*-doping. On principle, doping is a rather highly reversible process. The associated conductivity change can be as large as 10^{10} orders of magnitude, the best conductivities being at least as high as 500 S/cm.

Within certain limits, the counterions serving as dopant ions can be exchanged, as in an ion exchanger. This is a useful action when synthesis is easier with one type of ion and charge storage is easier with another type of ion.

Transient doping can be attained by light; photodoping results in simultaneous *p*- and *n*-doping, observable photoconduction, and photocurrents that can lead to polymer solar cells. Conversely, simultaneous charge injection from two electrodes yields states which during their recombination emit light; that is, the conductive polymer then constitutes a light-emitting diode. This electroluminescence can occur in different colors and is bright enough to consider lighting applications. Also, doping changes the passive optical properties (spectrum of light transmission: electrochromism). (Heeger, 2000).

Instabilities of doped conductive polymers are largely an environmental problem: Some polymers when *p*-doped to the limit have oxidation potentials high enough to attack the most inert solvents. Most will attack water even at much lower doping levels.

Environmentally stable polymers exist. Thus, polyanilines are used as corrosion-inhibiting coatings and can be made into electrochromic windows. Polyaniline as well as polypyrrole and polythiophene are useful as antistatic and antimagnetic shielding devices. Polypyrrole is useful as a microwave-absorbing material and as a host for physiologically and analytically interesting dopant species, released by ion-exchange mechanisms in time and/or on demand.

Polymer Batteries The discovery that doping of polyacetylene produced a highly conducting material was followed swiftly by the realization that this material was a rechargeable battery material which, optimistically, might lead to lightweight

high-capacity plastic batteries. Since both *n*- and *p*-doped $(C_2H_2)_x$ material could be made, all-plastic batteries were predicted.

Polyacetylene proved quite incapable of working in a realistic battery context, and MacDiarmid did not mention this application in his Nobel lecture of October, 8 2000. However, other materials have proven their worth, and prototype batteries made with polypyrrole and polyaniline as cathodes (positives), and metal or lithiated carbon materials as anodes (negatives), have been demonstrated in due course by the Japanese and German industry, for instance. Novák et al. (1997) have reviewed the field in detail.

Many configurations of a polymer battery are possible. Figure 26.6*a* shows just one, that which has been most popular in research, as a cell undergoing discharge. The metal dissolves, as in a zinc–manganese dioxide cell, sending metal ions M^+ into the electrolyte and electrons through the external circuit to do work in the load. On arrival in the doped polymer, they neutralize charges (polarons) in the doped polymer, liberating the associated dopant anions, which pass into the electrolyte, joining the metal ions from the anode to form salt for which the electrolyte is reservoir. Basically, the process is reversible, certainly with the polymer and less certainly with many metal anodes. Zinc (in aqueous systems) and certain lithium alloys and lithium hosts (in aprotic nonaqueous systems) have given anodes of satisfactory rechargeability.

Suitable polymer anodes have not been found; instead, in the search for improved lithium hosts, lithium-inserting carbon materials have been developed and batteries produced, usually with a metal oxide or sulfide anode (hence they are not considered further here).

Concentrating on polymer cathodes, materials have been engineered that exhibit:

- A charge density (capacity) of > 200 Ah/kg
- A voltage difference with respect to a lithium counterelectrode of > 2 V

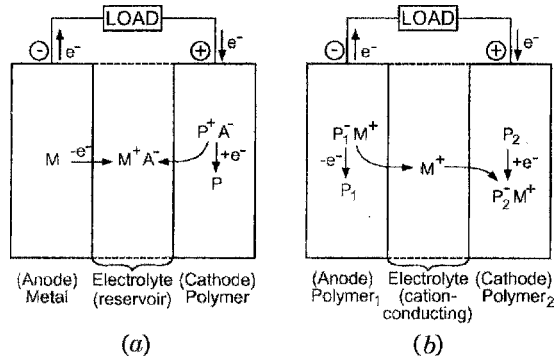

FIGURE 26.6 (*a*) *p*-doped conductive polymer in battery cell configuration; (*b*) *n*-doped polymers in supercapacitor configuration. Both the metal M and conductive polymer P generally have a conductive support. (Adapted from Novák et al., 1997, with permission of the American Chemical Society.)

- Coulombic efficiencies close to 100%
- Cycle lives of >500 cycles
- Self-discharge of $<1\%$ per day
- Shelf lives of >1 year

A point meriting attention is the voltage difference above. Doped polymers are rather electropositive (up to more than 4 V vs. a lithium electrode in the same solution), so much so that charging may have to be limited in order not to exceed the stability limits of the electrolyte (typically, propylene carbonate or acetonitrile as aprotic nonaqueous solvents).

During discharge of a cell as shown in Fig. 26.6*a*, the voltage falls continuously, so that a calibrated discharge curve can serve as an indicator of the state of (remaining) charge. As discharge progresses beyond a certain point, the polymer's conductivity becomes the limiting factor (although before this will happen, the discharge voltage of the battery cell will have decreased to a level unsatisfactory for most applications). A sloping discharge voltage curve generally is considered a disadvantage, which must be compensated electronically or accepted by a flexible user.

As to anodes, in most of the research work a generously dimensioned sheet of lithium metal has been used. Such an electrode is rather irreversible, but this is not noticed when a large excess of lithium is employed. Li–Al alloys and carbon materials inserting lithium cathodically during recharging can be used as anodes in nonaqueous solutions. Zinc has been used in polymer batteries with aqueous electrolyte (on the basis of polyaniline).

Despite all efforts, and despite the obvious potential offered by doped conductive polymers as a battery cathode, no decisive breakthrough to a cheap, highly rechargeable (half)-plastic battery has been achieved so far. Now, judging, by analogy, from the long odyssey of fuel cell development (Grove, 1839; Ostwald, 1894; the *Apollo* moon mission in 1969; yet work to develop cheap fuel-cell-powered cars is an ongoing effort in 2004), this definitely should not preclude future breakthroughs.

In fact, the polymer systems already work as *supercapacitors* (Conway, 1999), which constitute alternative charge-storage devices highly interesting for supplementary peak power supply and for excess (braking) power absorption in battery-driven cars, for instance. In this case the configuration is a sandwich such as that shown in Fig. 26.6*b*, of two electronically conductive polymer sheets with an ionically conducting electrolyte in between, and potentially—when the electrodes are porous—without any free electrolyte, which is a great advantage for the design of bipolar stacks of very high (transient) energy density. In this existing application, polyanilines, polypyrroles (Ingram et al., 2004), and polythiophenes are preferred. Thus, a polyaniline system with $LiPF_6$ electrolyte was reported to yield capacities on the order of 100 F/g, a system with poly(methylthiophene) capacities as high as 240 F/g.

New Frontiers The Nobel prize award of 2000 was a good occasion to fathom the most interesting current developments (Heeger, 2000; MacDiarmid, 2000; Shirakawa,

2000). It was said that the strongest current efforts relate to conjugated polymers in their undoped, *semiconductive* state. As already pointed out, some such materials exhibit electroluminescence, glowing when a voltage is applied across. Luminescent plastics would make attractive light displays in mobile phones and information boards, and possibly, if the speed were high enough, a flat television screen could be developed from luminescent plastic. As a reverse, the absorption of light (photodoping) could be made to produce solar power. Here the flexibility and large area of plastic sheets is an advantage, the challenge then being an appropriate current collector. Heeger (2000) reported his work on optical-quality thin films of metallic polymers which are transparent and can be used as antistatic coatings and electrodes in liquid-crystal displays.

Electrochromism has already been mentioned: Thin layers of certain conductive polymers have light absorption that depends on the state of charge (doping), so that light absorption (the degree and color) can be controlled electrically. Thin films of a substituted polythiophene in a field-effect transistor (FET) configuration have shown field-dependent conduction changes. This could be the basis for minute switches. MacDiarmid (2000) elaborated on nanoelectronics applications, for which a new high-voltage electrospinning process could produce electronic junctions and devices with at least one dimension in the 100-nm range. Nanofibers were produced from a polystyrene solution in tetrahydrofuran and from a polyaniline solution in sulfuric acid. Such fibers would be useful as substrates for electronically active materials and also as substrates for catalysts. Also, line patterns of conducting polymers produced by a new electrochemical lithography procedure offer the promise to develop, on the low end, low-cost (disposable) plastic or paper electronic devices needed to mark and control mass merchandise, and on the high end, high-resolution addressing matrices for a liquid-crystal display.

All this, in summary, would amount to additional sections on conductive polymers and to a future chapter on semiconductive polymers, currently representing an encouraging outlook for a journey begun in serendipity.

REFERENCES

Grove, W., *Philos. Mag.*, **14**, 447 (1839).

Heeger, A. J., Semiconducting and metallic polymers: the fourth generation of polymeric materials, Nobel lecture, December 8, 2000.

Ingram, M. D., H. Staesche, and K. S. Ryder, "Activated" polypyrrole electrodes for high-power supercapacitor applications, *Solid State Ionics*, **169**, 51 (2004).

Letheby, H., *J. Chem. Soc.*, **15**, 161 (1862).

MacDiarmid, A. G., "Synthetic metals": a novel role for organic polymers, Nobel lecture, December 8, 2000.

Ostwald, W., *Z. Elektrochem.*, **1**, 122 (1894).

Shirakawa, H., The discovery of polyacetylene film: the dawning of an era of conducting polymers, Nobel lecture, December 8, 2000.

REVIEWS AND MONOGRAPHS

Conway, B. E., *Electrochemical Supercapacitors: Scientific Fundamentals and Technological Applications*, Kluwer/Plenum, New York, 1999.

Gray, F. M., *Solid Polymer Electrolytes: Fundamentals and Technological Applications*, Wiley, New York, 1991.

Gray, F. M., *Polymer Electrolytes*, Royal Society of Chemistry, Cambridge, 1997.

Gubler, L., S. A. Gürsel, and G. G. Scherer, Radiation-grafted membranes for polymer electrolyte fuel cells, *Journal Fuel Cells*, August 2005.

Hopfinger, A. J., and K. A. Mauritz, Theory of the structure of ionomeric membranes, in *Comprehensive Treatise of Electrochemistry*, Vol. 2, *Electrochemical Processing*, J. O'M. Bockris, B. E. Conway, E. Yeager, and R. E. White, Eds., Plenum Press, New York, 1981, p. 521.

Inzelt, G., M. Pineri, J. W. Schultze, and M. A. Vorotyntsev, Electron and proton conducting polymers: recent developments and prospects, *Electrochim. Acta*, **45**, 2403 (2000).

Lyons, M. E. G., *Electroactive Polymer Electrochemistry*, Part 2, *Methods and Applications*, Kluwer, New York, 1996.

Novák, P., K. Müller, K. S. V. Santhanam, and O. Haas, Electrochemically active polymers for rechargeable batteries, *Chem. Rev*., **97**, 207 (1997).

27

Physical Methods for Investigation of Electrode Surfaces

JAMES McBREEN
Brookhaven National Laboratory, Upton, New York

Abbreviations frequently used in the literature on application of physical methods for investigation of the electrode surface:

AES	Auger electron spectroscopy
AFM	atomic force microscopy
EMIRS	electrochemically modulated infrared reflectance spectroscopy
EQCM	electrochemical quartz crystal microbalance
EXAFS	extended X-ray absorption fine structure
FTIR	Fourier transform infrared spectroscopy
GIXS	glancing incident X-ray scattering
HREELS	high-resolution electron energy loss spectroscopy
IRRAS	infrared reflection–absorption spectroscopy
IRS	infrared spectroscopy
LEED	low-energy electron diffraction
NMR	nuclear magnetic resonance
RRS	resonance Raman spectroscopy
SERS	surface-enhanced Raman spectroscopy
SFG	sum-frequency generation
SHG	second harmonic generation
SNIFTIRS	subtractively normalized interfacial Fourier transform infrared spectroscopy
STM	scanning tunneling spectroscopy
SXRD	X-ray diffraction
XANES	X-ray absorption near edge structure

Fundamentals of Electrochemistry, Second Edition, By V. S. Bagotsky

XAS	X-ray absorption spectroscopy
XPS	X-ray photoelectron spectroscopy
XRD	X-ray diffraction

27.1 TOPICS OF INVESTIGATION

Until the advent of modern physical methods for surface studies and computer control of experiments, our knowledge of electrode processes was derived mostly from electrochemical measurements (Chapter 12). By clever use of these measurements, together with electrocapillary studies, it was possible to derive considerable information on processes in the inner Helmholtz plane. Other important tools were the use of radioactive isotopes to study adsorption processes and the derivation of mechanisms for hydrogen evolution from isotope separation factors. Early on, extensive use was made of optical microscopy and X-ray diffraction (XRD) in the study of electrocrystallization of metals. In the past 30 years enormous progress has been made in the development and application of new physical methods for study of electrode processes at the molecular and atomic level.

Ideally, it should be possible to use the physical methods for time-resolved in situ measurements. The use of these methods requires the existence of a well-developed theoretical basis for each method.

In studying an electrode process there are many things we would like to know. These can be classified according to the locus of the processes that can occur in going from the electrode bulk to the electrode surface, across the Helmholtz layer, and into the bulk of the electrolyte.

27.1.1 Electrode Bulk Processes

In most electrode reactions no changes occur in the electrode bulk. However, there are a number of technologically important reactions that involve intercalation reactions, such as the ingress of hydrogen into metals and alloys and the ingress of lithium ions into carbon, metals, alloys, metal oxides, and chalcogenides. Other examples are $Ni(OH)_2$ and conductive polymer electrodes. These reactions are of importance in metal hydride and lithium ion batteries and supercapacitors. The intercalation reactions often involve phase changes that can be studied by in situ XRD. Deintercalation of Li from $LiNiO_2$ results in a valence change of Ni from Ni(III) to Ni(IV). In situ X-ray absorption spectroscopy (XAS) can be used to determine the valence change. Because of its element-specific nature, XAS is very useful in the study of the chemical and structural environment of dilute dopant atoms in oxides such as $LiNiO_2$. Ex situ nuclear magnetic resonance (NMR) studies can be used to elucidate the various locations of Li ions in these oxides.

In the case of $Ni(OH)_2$ and conductive polymer electrodes, solvent and anions intercalate into the electrode at anodic potentials. Electrochemical quartz crystal microbalance (EQCM) is a useful technique for monitoring the ingress and egress of solvent and anions in these materials.

27.1.2 Surfaces of Metal Single Crystals

Until the advent of low-energy electron diffraction (LEED) it was assumed that the atoms on single-crystal surfaces had the same periodicity as the bulk. Quite often, to minimize the free energy, the equilibrium position of surface atoms can be different from that given by the lattice periodicity of the bulk. Often, the interatomic spacing between the top atomic layers differs from that deeper in the bulk, without any noticeable change in lateral symmetry. This is known as *surface relaxation*. A typical effect is a 5 to 10% contraction between the first and second layers and a smaller but measurable expansion between the second and third and the third and fourth layers. In a few cases, particularly with precious metals, the surfaces are reconstructed, and the lateral symmetry of the surface often differs from that of the bulk. This is called *surface reconstruction*. At positive potentials, upon the adsorption of oxides or anions, the surface structure reverts to that of the bulk. This is referred to as *lifting* the reconstruction. X-ray reflectivity is a very powerful technique for studying surface relaxation since it gives structural information in the surface normal direction. Surface X-ray diffraction (SXRD) and scanning tunneling spectroscopy (STM) can be used to study surface reconstruction since both techniques probe the in-plane structure of the surface layer. A major advantage is that it is possible to do in situ measurements with X-ray reflectivity, SXRD and STM.

27.1.3 Adsorption of Monolayers

Adsorbed monolayers, whether they are hydrogen, oxygen, carbon monoxide, anions, or cations, have always been of interest to electrochemists. The first in situ physical methods used to study monolayers were reflectance spectroscopy and ellipsometry. In the mid-1970s, several groups developed ex situ techniques to use the conventional high-vacuum methods of surface science that were developed about a decade earlier. The ex situ techniques included LEED, X-ray photoelectron spectroscopy (XPS), and Auger spectroscopy. In the 1980s, several new in situ techniques were developed: ECQM, SXRD, X-ray reflectivity, various proximal probe techniques such as STM and atomic force spectroscopy (AFM), XAS, Fourier transform infrared (FTIR) spectroscopy, and surface-enhanced Raman spectroscopy (SERS). Other techniques are second harmonic generation (SHG) and sum-frequency generation (SFG).

27.1.4 Surface Topography and Morphology

STM, X-ray reflectivity, and AFM are excellent in situ techniques for studying surface topography and morphology. Scanning electron microscopy is a useful ex situ technique.

27.1.5 Electrocrystallization

STM, SXRD, and X-ray reflectivity are excellent techniques for in situ studies of metal and alloy deposition. XRD is also useful for determining the crystal orientation of deposits.

27.1.6 Anodic Films

A wide variety of in situ techniques are available for the study of anodic films. These include reflectance, ellipsometry, X-ray reflectivity, and SXRD. X-ray reflectivity can be used to study thick surface layers up to 1000 Å. The reflectance technique has been used to study oxide growth on metals, and it yields information on oxide thickness, roughness, and stoichiometry. It the only technique that can give information on buried metal–oxide interfaces. It is also possible to get information on duplex or multiple-layer oxide films or oxide films consisting of layers with different porosity. Films with thicknesses of anywhere from 10 to 1000 Å can be studied. XAS can be used to study the chemistry of dilute components such as Cr in passive oxide films.

27.2 X-RAY METHODS

27.2.1 X-Ray Diffraction

In electrochemistry the two most common uses of XRD are the study of the bulk structure of battery materials and the two-dimensional structure of surface layers on single-crystal electrodes. In both cases XRD can yield valuable structural data. This includes determination of the crystal phases and grain sizes and interplanar spacings of bulk materials. In the case of monolayers on single-crystal surfaces, SXRD can yield information on surface reconstruction, the two-dimensional phase behavior of adsorbed monolayers, and the orientational relationship between surface layers and the bulk. Given good data, interpretation of the experimental data is relatively straightforward. Because the signal and probe are hard X-rays it is possible to do in situ measurements. However, XRD is not useful for the study of amorphous or poorly ordered materials because the diffracted signals from these materials are very weak. In cases where the material is a mixture of ordered and amorphous materials, XRD preferentially probes the regions of the materials with a high degree of structural order. Details on bulk XRD can be found in textbooks (Cullity, 1978; Barrett and Massalski, 1980) and there are several excellent reviews of SXRD (Toney and Melroy, 1991; Robinson and Tweet, 1992; Nagy and You, 2002).

The basic principles of XRD are best described by the Bragg treatment of X-ray scattering by single crystals. Figure 27.1 shows that X-ray scattering can be represented as a reflection by successive planes of atoms in a crystal, where the spacing between the planes is d. The angle between the planes and the direction of the beam is θ. Ray R_1 is specularly reflected by the first plane to yield R_1'. Ray R_2 is reflected from the second plane to yield ray R_2'. The reflected beams make an angle 2θ with the direction of the incident beams. The extra path length traversed by the second ray is $2x$. If the rays R_1' and R_2' are to reinforce one another, they must have the same phase. This condition is met if $2x = n\lambda$, where n is an integer and λ is the X-ray wavelength. From trigonometry, $x = d \sin \theta$. So the condition for constructive interference becomes

$$2d \sin \theta = n\lambda, \qquad n = 1, 2, 3, \ldots . \tag{27.1}$$

This is the Bragg condition, or *Bragg's law*, the fundamental law of X-ray crystallography.

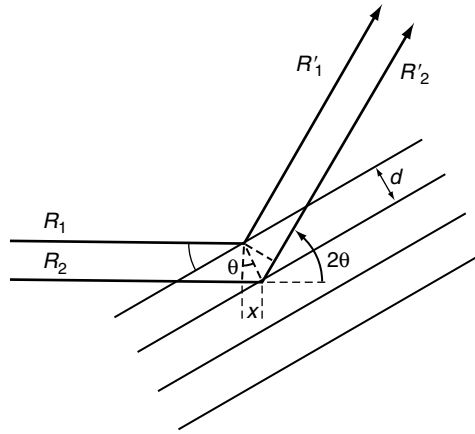

FIGURE 27.1 X-ray reflection from a set of planes.

27.2.2 Bulk XRD of Battery Materials

XRD on battery materials can be classified as powder diffraction, a technique developed by Peter Debye and Paul Scherrer. In powder diffraction the material consists of microscopic crystals oriented at random in all directions. If one passes a monochromatic beam of X-rays through a flat thin powder electrode, a fraction of the particles will be oriented to satisfy the Bragg relation for a given set of planes. Another group will be oriented so that the Bragg relationship is satisfied for another set of planes, and so on. In this method, cones of reflected and transmitted radiation are produced (Fig. 27.2). X-ray diffraction patterns can be recorded by intercepting a

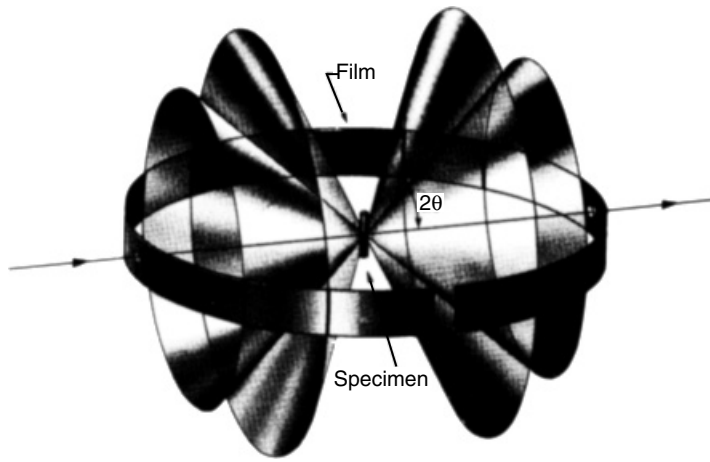

FIGURE 27.2 Debye–Scherrer powder method. Cones of reflected and transmitted radiation are produced. In this example the pattern is recorded with photographic film. Alternatively, the patterns can be recorded with a rotating detector on a goniometer, a position-sensitive detector, or an image plate detector.

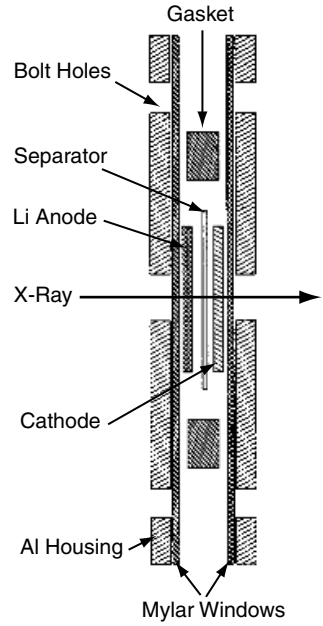

FIGURE 27.3 Spectroelectrochemical cell for in situ XRD on battery electrode materials.

small arc of these cones with a rotating detector on a goniometer. Alternatively, a complete set of rings can be recorded on an image plate detector. These data can be processed to yield X-ray diffraction patterns. With conventional X-ray tubes, the reflected signals are recorded. With synchrotron X-rays, the measurements are usually done in the transmission mode.

Figure 27.3 shows a typical spectroelectrochemical cell for in situ XRD on battery electrode materials. The interior of the cell has a construction similar to a coin cell. It consists of a thin Al_2O_3-coated $LiCoO_2$ cathode on an aluminum foil current collector, a lithium foil anode, a microporous polypropylene separator, and a nonaqueous electrolyte (1 *M* $LiPF_6$ in a 1 : 1 ethylene carbonate/dimethylcarbonate solvent). The cell had Mylar windows, an aluminum housing, and was hermetically sealed in a glove box.

In situ XRD spectra were collected on beam line X18A at the National Synchrotron Light Source (NSLS) located at Brookhaven National Laboratory (BNL). The X-ray wavelength (λ) was 1.195 Å. The step size of the 2θ scan was 0.02° in the regions with Bragg reflections and 0.05° in the regions without reflections. The XRD spectra were collected in the transmission mode (Liu et al., 2004).

Figure 27.4 shows a charge curve for the cell when it was charged over a period of 12 hours from 3.0 to 5.2 V. During the charge, 16 XRD scans were collected continuously. The time at which each spectrum was acquired is shown in Fig. 27.4. The time for each scan was about 45 min. The corresponding spectra are shown in Fig. 27.5. Four hexagonal phases, H1, H2, O1a, and O1, were observed and their Bragg peaks were indexed in Fig. 27.5. The phase transition from H1 to H2 started in scan 4 and

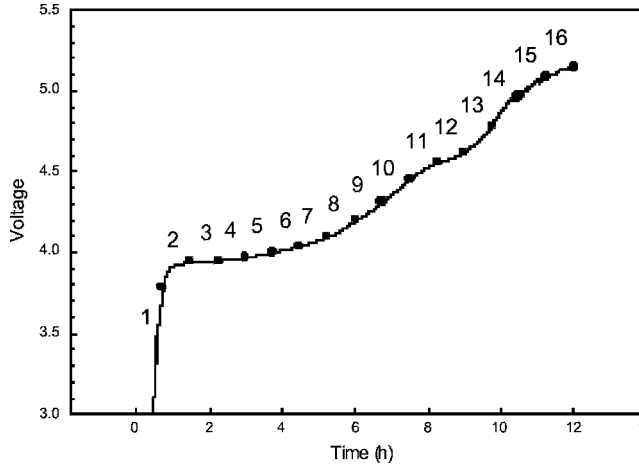

FIGURE 27.4 First charge curve of an Al_2O_3-coated $LiCoO_2$/Li cell from 3 to 5.2 V at a 12-h rate. (From Liu et al., 2004, with permission from The Electrochemical Society.)

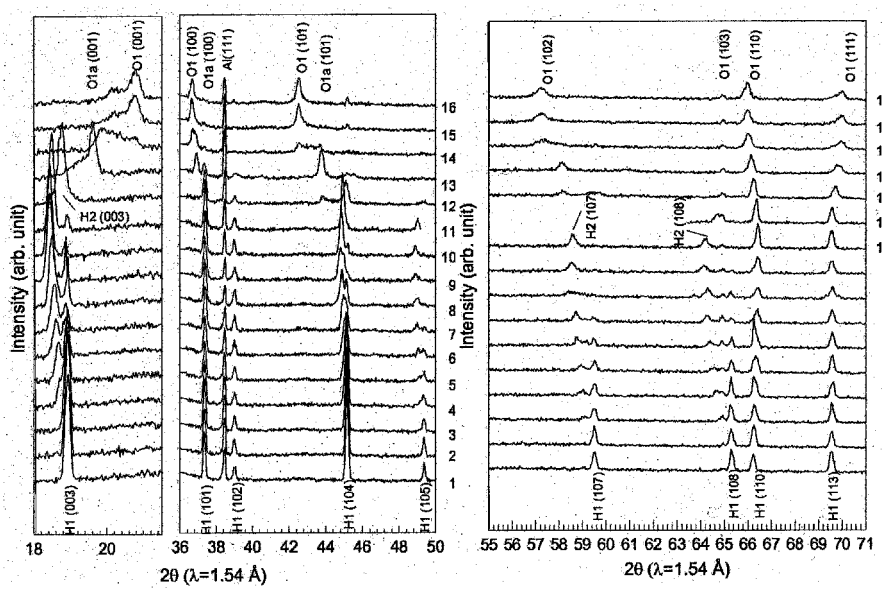

FIGURE 27.5 In situ XRD patterns of an Al_2O_3-coated $LiCoO_2$ cathode during the first charge from 3 to 5.2 V at the 12-h rate. The three panels from left to right show spectra in (003), the (101) to (105), and (107) to (113) regions, respectively. (From Liu et al., 2004, with permission from The Electrochemical Society.)

was completed on scan 11. In this phase transition there is an expansion along the *c*-axis and a contraction along the *a*-axis. At higher states of charge there is a major contraction along the *c*-axis with the formation of the O1a and O1 phases. These results show the wealth of structural information that can be obtained with in situ XRD.

27.2.3 Surface X-Ray Diffraction

Surfaces, adsorbed layers, and passive films consist of a small number of diffracting atoms (-10^{15} to 10^{16}), so SXRD requires intense synchrotron X-ray sources of high brightness, capable of delivering a large photon flux into a small spatial and angular region. The brightness of synchrotron X-ray sources can be six to eight orders of magnitude higher than that of X-ray tubes.

X-rays obey the same rules of geometric and physical optics as visible light, and the laws of reflection and refraction hold. Reflection and refraction are described by Snell's law and the Fresnel equations, which are covered in textbooks on optics (Jenkins and White, 1957; Born and Wolf, 1970). The only difference between light and X-rays is in the index of refraction and the absorption coefficient. An important consequence of this is that for light, air has a smaller index of refraction than most dense media, whereas for X-rays, the refractive index of most materials is smaller than that of air. Because of this, total reflection of X-rays can occur at a small critical angle. This effect can be used to enhance the contribution of the surface to the signal and decrease penetration into the bulk. This is why the glancing incident X-ray scattering (GIXS) approach is used in surface diffraction experiments. In surface diffraction experiments, the X-rays enter the cell at a very low angle ($\leq 0.8°$). Provisions have to be made in cell design to minimize the path length of the X-rays in the electrolyte at such low angles. Kondo et al. (2002) have developed an advanced spectroelectrochemical cell (Fig. 27.6). The black closed part (A) in the figure is a single-crystal Au disk (diameter 10 mm, thickness 5 mm). The body of the cell (H) and the sample holder (J) were made of poly(chlorotrifluoroethylene). The cell has an inlet (F) and an outlet (G) for electrolyte. The cell has a Pt counter electrode (B) and an Ag/AgCl reference electrode (C). The end of the electrolyte dome was sealed with 6-μm Mylar film, which served as an X-ray window. The holder part can move up and down along the direction normal to the electrode surface with precise control by a micrometer (I). The cell has an outer chamber (K) made of Mylar film which was flushed with N_2 to prevent oxygen ingress through the X-ray window. In one orientation, electrochemical measurements could be done in meniscus mode, and in another orientation, SXRD measurements could be done in the GIXS mode. In this mode the electrolyte is only a thin layer ($\sim$20 μm) between the Mylar window and the electrode. When electrochemistry is performed, such as the deposition of an adsorbed monolayer, the single crystal is moved away from the Mylar window. The potential is fixed and the electrode is moved up to the Mylar window. The thin electrolyte film is adequate for maintaining control of electrode potential in the absence of any significant faradaic process. In this type of experiment the scattering from the remaining electrolyte is of the same order as that from an adsorbed monolayer.

The electrochemical cell is mounted in a four-circle diffractometer. This has four concentric motions, three of which, called ω, φ, and χ, move the sample and one that moves the detector by an angle 2θ. Further details on surface diffraction are found in the reviews on XRD cited above. Figure 27.7 shows a typical surface X-ray diffraction experiment. In the glancing angle geometry, the X-ray beam impinges onto the surface at an angle ϕ and is detected at a combination of an in-plane grazing

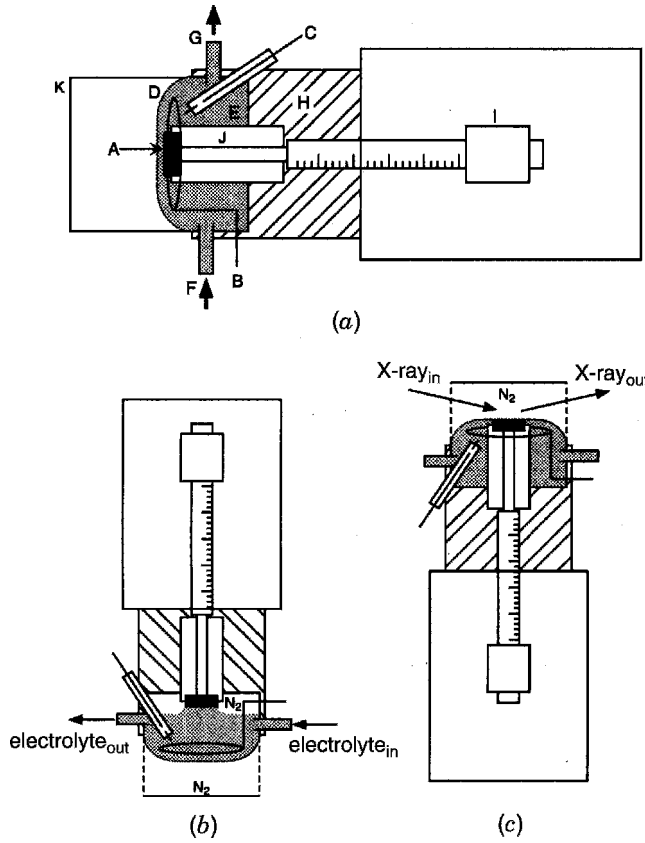

FIGURE 27.6 (*a*) Schematic side view of a spectroelectrochemical cell designed for in situ SXS measurements. (A) Single-crystal disk electrode, (B) Pt counter electrode, (C) Ag/AgCl reference electrode, (D) Mylar window, (E) electrolyte solution, (F) inlet for electrolyte solution, (G) outlet for electrolyte solution, (H) cell body, (I) micrometer, (J) electrode holder, (K) outer chamber. (*b*) Cell configuration for electrochemical measurement. (*c*) Cell configuration for SXRD measurement. (From Kondo et al., 2002, with permission from Elsevier.)

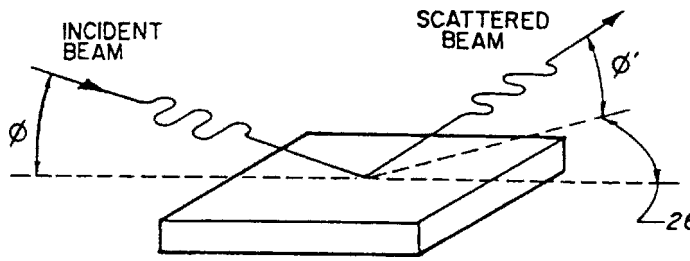

FIGURE 27.7 Grazing incidence X-ray scattering geometry. The X-rays are incident on the sample at an angle ϕ and are detected at a combination of two angles 2θ and $2\phi'$.

angle (2θ) and a second grazing angle ϕ'. The incident and exit angles are controlled by the sample tilt angle χ. Corrections for background are made by doing an ω-scan in the same way as for bulk crystallography. The background measured nearby is subtracted. The contribution of the surface layer to the signal is enhanced by keeping the angle of incidence below the critical angle (~0.5°). The low angle of incidence permits the beam to sample a large number of scatters. Thus, the combination of the intense beam from the synchrotron and the grazing incidence geometry makes surface diffraction experiments possible. The data are analyzed in a manner similar to that used for bulk diffraction.

27.2.4 X-Ray Reflectivity

Specular reflectivity is obtained by recording the reflectivity in the plane of incidence of the X-rays. It gives structural information in the surface normal direction. Figure 27.8 shows reflectivity data for a Au(100) surface (Gibbs et al., 1988). The reflectivity data are fitted to a model that sums up the interference caused by X-ray scattering among the surface layers. This can be done using continuum models based on the Fresnel equations or on discrete models that include surface roughness, the surface density, and the deviation of the top layer spacing from the bulk spacing. Details are given in several publications (Gibbs et al., 1988; Ocko et al., 1991). In a specular reflectivity experiment the incident beam strikes the surface at an angle θ and the intensity is recorded in the plane of incidence at an angle 2θ. Data are collected as a

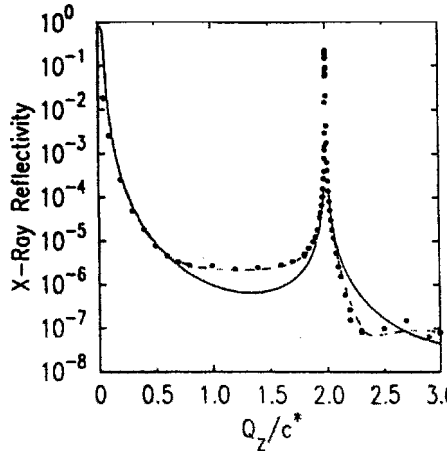

FIGURE 27.8 Specular reflectivity for a clean Au(100) surface in vacuum at 310 K (···). The solid line is calculated for an ideally terminated lattice. The dashed line is a fit to the data with a reconstructed surface with a 25% increase in the surface density combined with a surface relaxation that increases the space between the top and next layers by 19%. In addition, the data indicate that the top layer is buckled or corrugated with a buckling amplitude of 20%. (From Gibbs et al., 1988, with permission from the American Physical Society.)

function of θ. The diffuse background scattering is determined from measurements slightly off the specular direction. After subtraction of the background, the data are normalized by the incidence intensity. To determine electrode morphology it is necessary to perform rocking scans, where the detector angle 2θ is fixed and the incidence angle θ is varied. This yields information on off-specular scattering that is related to the electrode roughness (Sinha et al., 1988). So a combination of measurements of SXRD and X-ray reflectivity can provide information on atomic roughness, surface relaxations, surface reconstructions, location of adsorbed atoms, and the density distribution of an electrolyte above an electrode. A convenient technique for following electrochemical reactions is to fix the sample at an anti-Bragg position, the reflectivity minimum of the curve in Fig. 27.8, and step or scan the electrode potential. This is useful for the study of surface reconstruction kinetics or the growth of surface layers.

A special notation is used to describe surface reconstructions and surface overlayers and is described in books on surface crystallography (Clarke, 1985). The lattice vectors $\mathbf{a}'$ and $\mathbf{b}'$ of an overlayer are described in terms of the substrate lattice vectors **a** and **b**. If the lengths $|\mathbf{a}'| = m|\mathbf{a}|$ and $|\mathbf{b}'| = n|\mathbf{b}|$, the overlayer is described as $m \times n$. Thus, a commensurate layer in register with the underlying atoms is described as 1×1. The notation gives the dimension of the two-dimensional unit cell in terms of the dimensions of an ideally truncated surface unit cell.

The combination of SXRD and X-ray reflectivity is a very powerful technique for the study of adlayers on single-crystal surfaces. An interesting example is the work of Wang et al. (1998) on the adsorption of Tl and Br on Au(111) from 1 m*M* TlBr in 0.1 *M* $HClO_4$.

Electrochemical, SXRD, and X-ray reflectance measurements showed that Tl–Br coadsorption occurs over a wide potential region with distinct structural phases occurring at different potentials. These phases and the cyclic voltammogran are shown in Fig. 27.9. At potentials positive to peak A, bromide forms a close-packed, rotated hexagonal layer similar to that formed in the absence of Tl^+ in solution. At potentials negative to peak E, thallium forms a close-packed, rotated-hexagonal layer similar to that formed in the absence of Br^- in solution. Between peaks A and B, no ordered phase is formed. At intermediate potentials, between peaks B and E, three superlattice structures which do not exist and the absence of either Tl or Br^- are observed. From an analysis of in-plane fractional-order diffraction intensities and specular reflectivity, two bromides per Tl are found in the 3–$(\sqrt{13} \times \sqrt{13})$ phase with one Br within and the other above the Tl adlayer. At more negative potentials, the 2TlBr–$(3 \times \sqrt{3})$ phase is identified. The ratio of the partial charges on Tl and Br is likely to be the most important factor in determining the stoichiometry and adlattice symmetry. The registry of the adsorbates in the 2TlBr–$(3 \times \sqrt{3})$ phase and the lateral displacements of the top layer of Au atoms were determined from analysis of the X-ray reflectivity. This adlayer-induced subsurface relaxation results in more uniform spacings between Tl and the three neighboring gold atoms as well as an increase in the Br–Au separation. This phenomenon of surface response to an over layer is similar to those observed from semiconductor or surfaces, and demonstrates an active role of the substrate atomic structure in the formation of surface compounds on metal electrode surfaces.

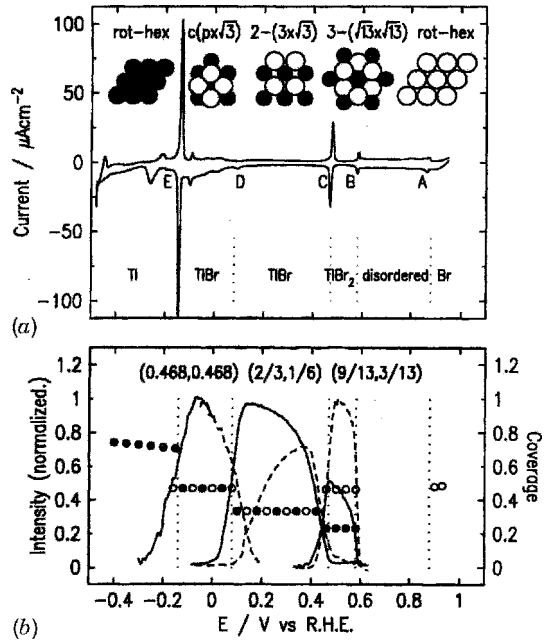

FIGURE 27.9 (*a*) Voltammetry curve for the UPD of Tl on Au(111) in 0.1 *M* $HClO_4$ containing 1 m*M* TlBr. Sweep rate 20 mV/s. The in-plane and surface normal structural models are deduced from the surface X-ray diffraction measurements and X-ray reflectance. The empty circles are Br and the filled circles are Tl. (*b*) Potential-dependent diffraction intensities at the indicated positions for the three coadsorbed phases. (From Wang et al., 1998, with permission from Elsevier.)

Specular reflectivity can also be used to study thick surface layers up to 1000 Å. Since the specular reflectivity of X-rays from a surface depends on the variation of the index of refraction along the normal to the surface, the method can be used to probe the normal electron density profile. The reflectance technique has been used to study oxide growth on metals (You et al., 1992), and it yields information on oxide thickness, roughness, and stoichiometry. It the only technique that can give information on the buried metal–oxide interfaces. It is also possible to get information on duplex or multiple-layer oxide films or oxide films consisting of layers with different porosity. Films with thicknesses from 10 to 1000 Å can be studied. Thus, the technique can be used to study surface layers all the way from monolayers to thick oxide films. The information derived from reflectivity studies accrues from the fact that whenever the index of refraction changes within a sample, part of the incident wave is reflected and part is transmitted. Interference between the beams reflected at different interfaces leads to an oscillatory pattern in the reflectivity as a function of incident angle. The effect is analogous to the optical interference fringes form oil films on water. Figure 27.10 shows reflectivity results for an electrochemically grown oxide film on a 2000-Å Ta film on a soda–lime glass slide (Wiesler et al., 1991). For a single oxide layer on a metal, the frequency of the oscillations is proportional to the

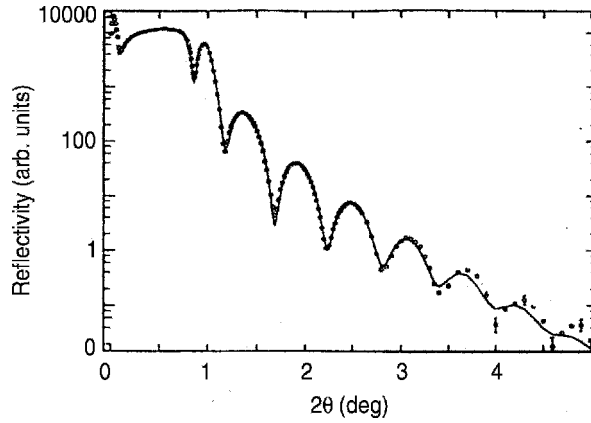

FIGURE 27.10 X-ray reflectivity data for an oxide film grown on a 2000-Å Ta film that was sputtered onto a soda glass slide. The oxide films were grown by ramping the potential, in 0.05 *M* H_2SO_4, at 0.1 V/s to 6.0 V SCE. The data indicate the growth of Ta_2O_3 with an anodizing ratio of 20.0 ± 1.0 Å/V. (From Wiesler et al., 1991, with permission from The Electrochemical Society.)

oxide layer thickness and the amplitude depends on surface roughness. The roughness also determines the attenuation of the reflectivity at higher scattering angles. The oscillations can be interpreted to determine the electron density profile with depth below the surface. The models also account for the widths of the interfaces and can elucidate effects due to interface intermixing, interdiffusion, or roughness. Models for multiple layers have been developed. The amplitude of the beam reflected at each interface is proportional to the change in electron density at that interface. This is directly related to changes in the refractive index profile in the z direction. Structural information is extracted by comparing the experimental data with that derived from a model. Details of various theoretical treatments of X-ray reflectivity are beyond the scope of this review; the reader is referred to the review paper by Nagy and You (2002) and references therein.

27.2.5 X-Ray Absorption Spectroscopy

The application of X-ray absorption spectroscopy (XAS) to structural determinations is a relatively new technique. The technique has been reviewed by Abruña (1991). XAS is simply accurate determination of the X-ray absorption coefficient of a material as a function of photon energy in an energy range that is below and above the absorption edge of one of the elements in the material. Absorption measurements are usually done at a K or L_3 edge, as absorption at the L_3 edge is much higher than at the other L edges. The K edge is due to absorption by a $1s$ core state and the L_3 edge to absorption by a $2p_{3/2}$ core state. Measurements at the K edge are most suitable for elements of low atomic number (low Z) and for first-row transition metal elements. In the case of platinum, the K edge is at 78.4 keV, where the synchrotron photon flux is too low, whereas the L_3 edge for platinum is at 11.5 keV, which is close

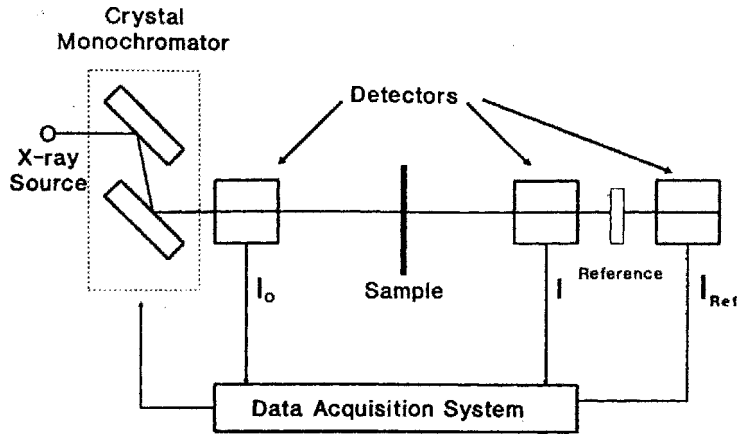

FIGURE 27.11 Experimental setup for a transmission XAS experiment.

to the energy maximum for the photon flux from conventional synchrotron sources. The simplest method for XAS is a transmission XAS experiment. Figure 27.11 is a schematic representation of the experimental configuration. It consists of an X-ray source, a double-crystal monochromator, a thin sample of the material, ionization chamber detectors for monitoring the beam intensity before and after it passes through the material, and a data acquisition system. The data acquisition system is used for several purposes. This includes stepping the monochromator to pass the desired photon energies, alignment of the sample in the beam, and monitoring the signals from the detectors. Usually, three detectors are used with a reference sample such as a metal foil in front of the third detector. The time for obtaining a full spectrum is typically 20 minutes and is limited primarily by the dead time needed for rotation of the crystals in the monochromator.

During an XAS experiment, core electrons are excited. This produces empty states called *core holes*. These can relax by having electrons from outer shells drop into the core holes. This produces fluorescent X-rays that have a somewhat lower energy than the incident X-rays. The fluorescent signal is proportional to the absorption. Detection of this signal is a useful method for measuring absorption by dilute systems such as under potential deposited (UPD) monolayers.

X-ray absorption spectroscopy (XAS) is an ideal method for in situ studies of electrochemical systems because both the probe and signal are penetrating X-rays. The great advantage is that XAS is element specific, and this permits investigation of the chemical environment of a constituent element in a composite material. It also permits studies of dilute systems. Since XAS probes only short-range order, it can provide structural information on amorphous materials, liquids, gases, adsorbed monolayers, as well as hydrated ions and complexes in solution. Because of this, XAS is finding application in an enormous variety of electrochemical systems. Examples are in situ electrode studies of UPD layers, passive films on iron, Cr species in passive films, carbon-supported fuel cell catalysts, redox polymer electrodes, battery electrode materials, and additives in battery electrodes.

An important characteristic of synchrotron X-rays is that they are 100% polarized in the plane of the synchrotron ring. This has important implications in XAS studies of UPD layers on single crystals. XAS measurements on UPD layers are done in a cell similar to that used for SXRD. The incident X-rays enter and exit the cell at a glancing angle. Measurements are made in the fluorescence mode using multi-element solid-state detectors. By doing measurements with the crystal surface parallel or perpendicular to the plane of polarization, it is possible to get information on the in-plane structure of the UPD layer and on the interactions of the UPD atoms with both the substrate atoms and the electrolyte. At third-generation light sources, complete spectra can be obtained in about 45 minutes.

Figure 27.12 shows two in situ Cu XAS spectra for a Cu UPD layer on Pt at 0.2 V (SCE) in 0.5 M H_2SO_4 + 10^{-4} M $CuSO_4$, recorded in both parallel and perpendicular polarizations. These data were obtained at the European Synchrotron Research Facility (ESRF) in Grenoble, France (Soldo et al., 2002). The signal-to-noise level is excellent because it is a third-generation facility.

XAS spectra consist of two parts, the near-edge part that extends about 50 eV around the edge at 8979 eV and the small oscillations that extend up to 1000 eV above the edge. Normalized spectra, close to the edge, for the two polarizations and for a Cu foil, are shown in Fig. 27.13. This is referred to as an *X-ray absorption near-edge structure* (XANES). The fine structure in the XANES region can be explained in terms of transition of the ejected photoelectron to unoccupied states in the vicinity of the Fermi level and to the long mean free path of the low-energy photoelectron, which results in multiple scattering around the excited atom. The shape of the edge

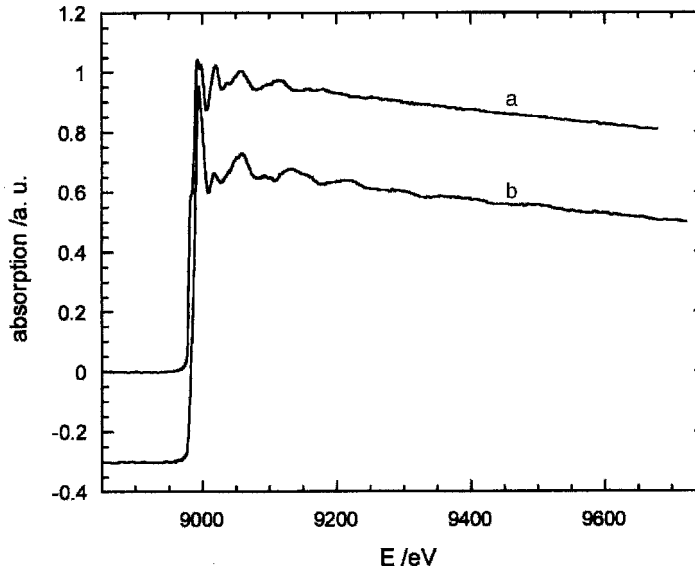

FIGURE 27.12 In situ X-ray absorption spectra for a Cu full layer obtained in sulfate solution at 0.2 V (SCE): parallel (a) and perpendicular (b) polarizations. (From Soldo et al., 2002, with permission from Elsevier.)

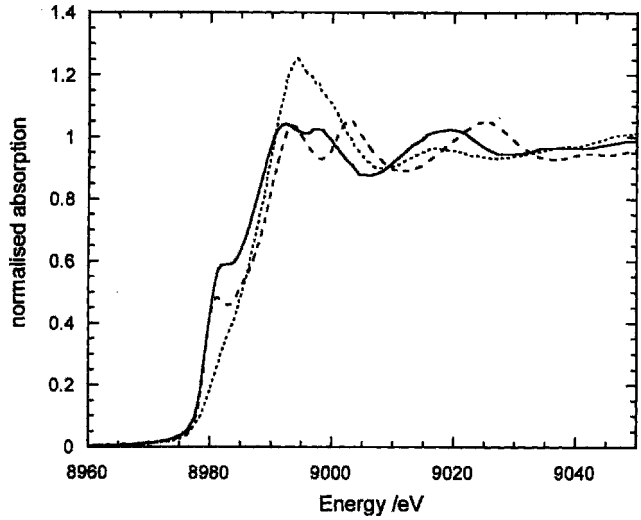

FIGURE 27.13 Cu K edge XANES spectra for a Cu full layer in sulfate solution at 0.2 V (SCE) in parallel (solid line) and perpendicular (dotted line) polarizations and for metallic copper (dashed line). (From Soldo et al., 2002, with permission from Elsevier.)

yields information on both the type and symmetry of the ligands around the excited atom. The XANES gives chemical information, such as coordination symmetry and oxidation state. At higher oxidation states the edge is shifted to higher energies.

The XANES features for the two polarizations are quite different. For the parallel polarization, the features are similar to those of metallic Cu. The spectrum for the perpendicular polarization has the features of copper oxide.

The small oscillations from 9000 to 9700 eV are referred to as the *extended X-ray absorption fine structure* (EXAFS). In the EXAFS region the process can be explained by simple backscattering, and the theory has been worked out in detail (Koningsberger and Prins, 1988). A small fraction of the outgoing photoelectron wave, associated with the excited electron, is backscattered by surrounding atoms. The EXAFS is a final-state interference effect whereby, depending on energy (E), the backscattered wave interferes constructively or destructively with the outgoing wave. The EXAFS spectrum is the superimposition of contributions from different coordination shells to the backscattering process. EXAFS gives information on coordination numbers and bond distances. The EXAFS is separated from the XAS spectrum by first subtracting the pre-edge background and then separating the EXAFS from the low-frequency oscillations of the background by use of a cubic spline function. Figure 27.14 shows the EXAFS for the Cu monolayer in the two polarizations. The Fourier transform of the EXAFS yields the radial structure function, which is shown in Fig. 27.15. This gives peaks in r-space that represent coordination shells. The r distance is somewhat shorter than the real bond distance because of a phase shift due to the backscattering process. The Fourier transform for the perpendicular polarization has a broad peak at 1.6 Å, suggesting the presence

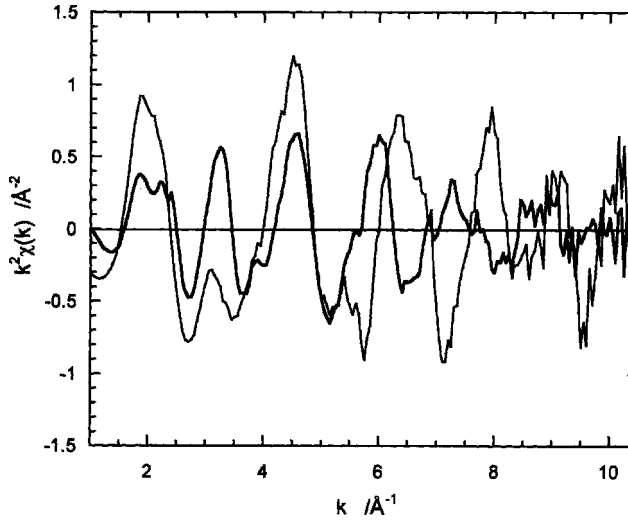

FIGURE 27.14 k^2 weighted EXAFS signals for a Cu monolayer in sulfate solution: parallel (thick solid line) and perpendicular (thin solid line) polarizations. (From Soldo et al., 2002, with permission from Elsevier.)

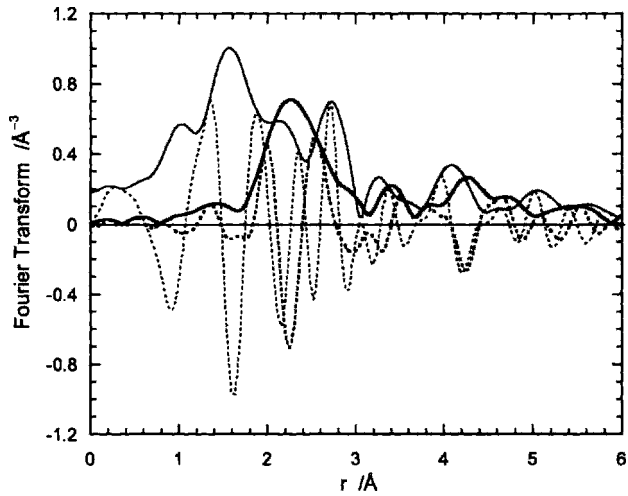

FIGURE 27.15 Fourier transform signals (transform magnitude: solid line; imaginary part: dashed line) for a UPD Cu monolayer on Pt(111) in sulfate solution: parallel (thick line) and perpendicular (thin line) polarizations. (From Soldo et al., 2002, with permission from Elsevier.)

of a Cu–O bond where oxygen atoms are bonded to Cu perpendicular to the crystal surface. The humps at about 2.2 and 2.7 Å suggest Cu–Pt bonds. The Fourier transform for the parallel polarization is consistent with the presence of Cu–Cu and/or Cu–Pt bonds.

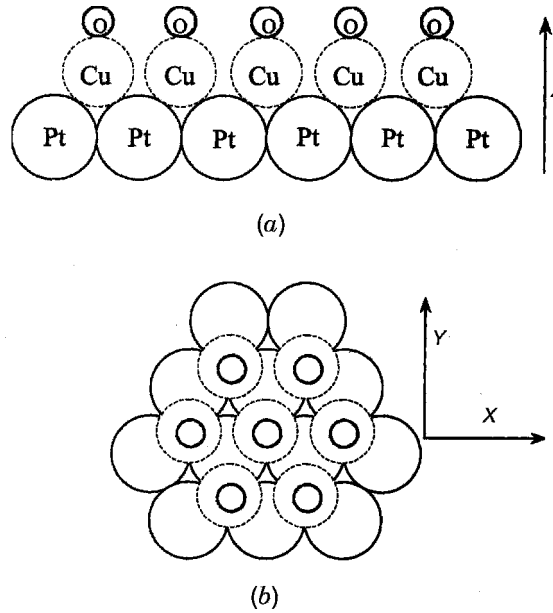

FIGURE 27.16 Cu full layer in sulfate solution (structural model used for FEFF6 calculations): (*a*) side view; (*b*) top view. Thin solid line; platinum atoms; dashed line; copper atoms; thick solid line; oxygen atoms. (From Soldo et al., 2002, with permission from Elsevier.)

Final determination of the structure was made by proposing a structural model with Cu sitting in threefold hollow sites and O atoms on atop sites with respect to the Cu atoms (Fig. 27.16). A program, FEFFIT, was used to analyze the data (Stern et al., 1995). This calculates the phase and amplitude parameters for the various backscatters. The EXAFS for the parallel polarization could be fitted six Cu–Cu interactions at a bond distance of 2.67 Å and three Cu–Pt interactions at 2.6 Å. For the perpendicular polarization, the data could be fitted one Cu–O interaction at 1.96 Å and three Cu–Pt interactions at 2.6 Å. The Cu–Pt bond length is shorter than the sum of the metallic radii of Cu and Pt, which is 2.66 Å. This indicates a Cu oxidation state different from zero, which agrees with the XANES results.

The advantages of XAS are that it is element specific, can be used in situ, and yields both chemical and structural information. Also, the theory is very well developed. The main disadvantage is the need to use a synchrotron facility.

27.3 SCANNING PROBE METHODS

27.3.1 Scanning Tunneling Microscopy

The scanning tunneling microscope (STM) was invented by Binnig and Rohrer in 1982. This quickly led to the award of a Nobel prize in 1986. Initially, STM proved

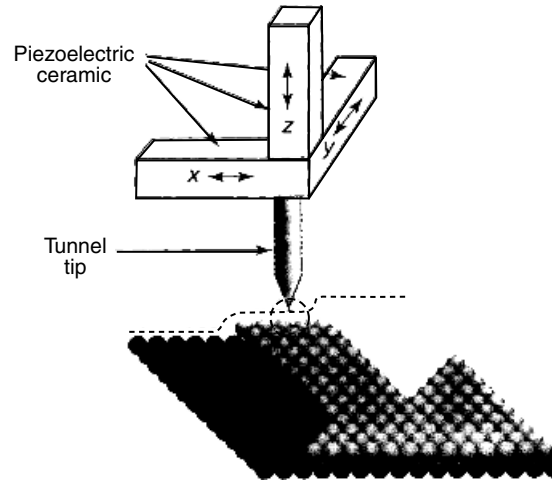

FIGURE 27.17 Schematic of a scanning tunneling microscope.

to be a high-resolution technique for looking at metallic surfaces in vacuum. In 1986 it was demonstrated that the STM could operate with the metal electrodes covered with electrolyte (Sonnenfeld and Hansma, 1986). The technique is particularly powerful in studies of well-defined single-crystal surfaces, where it can provide atomic resolution in an electrochemical environment [see the reviews of Sonnenfeld et al. (1990) and Itya (1999)]. The STM led to the development of several other scanning probe techniques, such as atomic force microscopy (AFM). AFM can be used to probe the surfaces of insulators.

Figure 27.17 is a schematic of a scanning tunneling microscope. The technique is based on the measurement of a tunneling current that flows between the electrode and a sharp metal tip. Tips are usually fabricated by electrochemical etching of Pt–Ir or tungsten wires. The tip is mounted on a piezoelectric (piezo) *xyz* scanner that controls the movement of the tip. The tip is brought sufficiently close (-5 to 20 Å) to the surface for an electron tunneling current to flow between the tip and the surface. Electron tunneling occurs when the electron cloud beyond the tip overlaps with the electron cloud above the electrode surface. When overlap occurs, electrons tunnel between the tip and the electrode. The current is typically 0.1 to 10 nA, and the voltage applied is 2 mV to 2 V. In an STM experiment the tip is scanned across the surface by applying voltages to the x and y piezos. As the tip is scanned laterally, a feedback system applies voltages to the z piezo to keep the tunneling current, I, constant. An alternative, less common method is to keep the height of the tip constant. A single scan, in the constant-current mode, is a plot of the voltage applied to the z piezo vs. the voltage applied to the x piezo. The movements produced in the piezos are typically 10 to 40 Å/V. A critical aspect in the design of the STM is providing a method to get the tip close to the surface within range of the z-piezo travel. The results can be presented as a topographic plot. Recently, the trend is to plot gray-scale

or color images in which the height, z, is displayed as a shade of gray or different colors. This type of plotting facilitates the determination of the symmetry of an ordered array.

In in situ STM experiments the tip is immersed in the cell electrolyte. Electrochemical reactions can occur on all the exposed metal surface of the tip. It is important to suppress these electrochemical currents to values that are considerably less than the tunneling current. This is done by sheathing all but a few micrometers at the end of the tip, with an insulating layer of glass or polymer (Bach et al., 1993).

The great advantage of STM is the ability to do in situ structural studies on electrode surfaces. However, STM does not yield chemical information. STM-derived structural information is confined to a very small area on the electrode, typically $1000\,\text{Å} \times 1000\,\text{Å}$, so meaningful correlations between the structural data and electrochemical data can be done only on single-crystal surfaces. The close proximity of the tip to the electrode surface can distort kinetic data acquired by an STM.

Brankovic et al. (2001) used STM to study Pt and Au deposits on Ru(0001) surfaces. They demonstrated a monolayer-to-multilayer spontaneous deposition of Pt from H_2PtCl_6 on an UHV-prepared Ru(0001) surface without applying an external potential. The coverage and morphology of the Pt deposit depend on the concentration of platinum ions and the time of immersion. They also found that spontaneous deposition of Pt on Ru(0001) can be modified by coadsorption of Sb ions as illustrated in Fig. 27.18A, which shows a scanning tunneling microscopy (STM) image of a weakly ordered superlattice of nanoclusters obtained from a solution containing Pt and Sb ions. It is very surprising that clusters $\sim 30\,\text{Å}$ in diameter, with a monoatomic thickness and a 20-Å cluster separation, spontaneously form a hexagonal lattice with weak long-range order on the Ru(0001) surface. The insert displays a magnified section of the image, showing a hexagonal symmetry for the nanoparticles. Figure 27.18B displays a fractal, single-crystal multilayer deposit of Au on

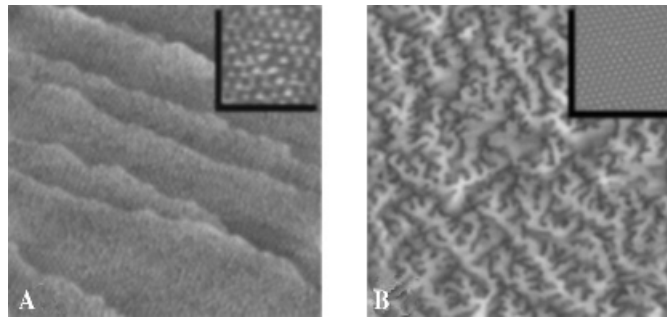

FIGURE 27.18 (A) Weakly ordered Pt nanoclusters deposited spontaneously on a Ru(0001) surface from a solution containing $10^{-3}\,M$ $PtCl_6^{2-} + 10^{-4}\,M$ $Sb^{3+} + 0.1\,M$ H_2SO_4. Image recorded at open-circuit potential; image size: $1000\,\text{Å} \times 1000\,\text{Å}$, insert: $200 \times 200\,\text{Å}$. (B) Fractal growth of Au on Ru(0001) from $0.1\,M$ $H_2SO_4 + 5 \times 10^{-6}\,M$ $AuCl_3$; E = 0.6 V. Image size: $3000\,\text{Å} \times 3000\,\text{Å}$, insert $53\,\text{Å} \times 53\,\text{Å}$. (From Brankovic et al., 2001, with permission from Elsevier.)

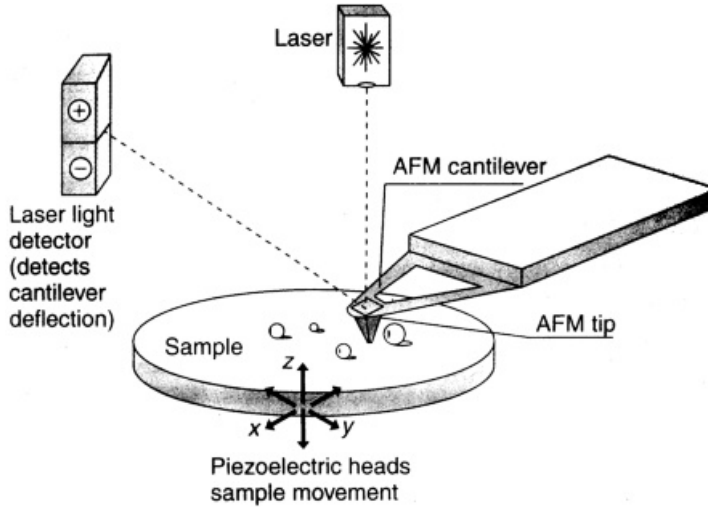

FIGURE 27.19 Schematic of the AFM.

Ru(0001) obtained by a conventional electrodeposition process from $AuCl_3$ solutions. The insert shows an atomically resolved image of a $\sqrt{3} \times \sqrt{3}$ Cl adlayer that forms on the ordered Au(111) terraces at 0.6 V. This fractal growth is similar to the growth observed in vacuum at the metal–gas interface.

27.3.2 Atomic Force Microscopy

The principle of AFM is illustrated in Fig. 27.19. The technique makes use of van der Waals forces between the tip and the surface. Since no electric current is involved, the technique can be used to characterize nonconducting surfaces. The tip is made of Si, SiO_2, or Si_3N_4, all of which can be micromachined. The tip is attached to a cantilever that bends under the force acting between the tip and sample surface. The cantilever deflection is optically detected by a laser beam reflected off the back of the cantilever into a position-sensitive detector. Imaging is usually done in the contact mode, where the beam deflection is maintained at a constant value by moving the z piezo up and down, and by recording the z piezo voltage as a function of the x and y positions.

27.4 ELECTROCHEMICAL QUARTZ CRYSTAL MICROBALANCE

The electrochemical quartz crystal microbalance (EQCM) is a very useful technique for detecting small mass changes at the electrode surface that accompany electrochemical processes. In 1880, Jacques and Pierre Curie discovered that when stress was applied to some crystals, such as quartz, it resulted in an electrical potential across the

crystal whose magnitude was proportional to the applied stress. This behavior is known as the *piezoelectric effect*. The discovery was reviewed by Cady in 1946. Later the Curies discovered that the application of a potential across the crystal resulted in a corresponding mechanical strain. This effect, called the *converse piezoelectric effect*, is the operational basis of EQCM. The piezoelectric effect occurs only in materials that are acentric: that is, materials that crystallize into noncentrosymmetric space groups. This results in dipole effects that are the source of the piezoelectric effect. There are several excellent reviews of EQCM (Buttry, 1991; Ward, 1995, Hepel, 1999).

The core of an EQCM is a sliver (~300 μm thick and 1.3 to 2. 6 cm in diameter) of quartz that is sliced from a quartz rod at an angle of approximately 35°15′ with respect to the crystallographic *x*-axis. This is referred to as the *AT cut*. The electric field is applied using two electrodes that are vapor deposited on opposite faces of the quartz disk. The electrodes are arranged so that only the circular parts at the center are in register. Figure 27.20*a* shows top and edge views of the crystal with vapor-deposited electrodes. The disk is mounted at the bottom of a tubular Teflon cell with O-rings. Alternatively, it can be mounted in a glass pipe joint attached to the bottom of a glass cell. In operation, one electrode is exposed to the air and the other is in contact with the electrolyte.

If an electric field of the proper frequency is applied across the quartz crystal, the crystal will oscillate in a mechanically resonant mode. These conditions correspond to the creation of a standing acoustic shear wave that has a node midpoint between the two faces of the crystal and two antinodes at both faces of the disk. This is depicted schematically in Fig. 27.20*b*. In an EQCM experiment the crystals are operated at the fundamental resonant frequency that is a function of the thickness of the crystal. A crystal with a thickness of 330 μm has a resonant frequency of 5 MHz. Crystals with these characteristics are commercially available. In an EQCM experiment, an alternating electric field of 5 MHz is applied to excite the quartz crystal into

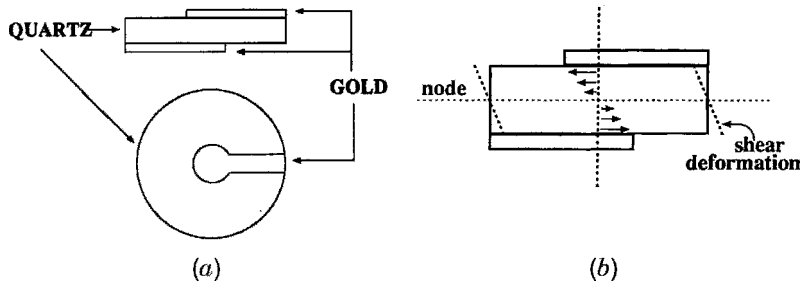

FIGURE 27.20 (*a*) Top and edge views of quartz crystal with keyhole-shaped vapor-deposited gold electrodes. (*b*) Edge view of the quartz crystal, showing the node of the acoustic wave passing through the center of the disk. Also shown is the deformation of the crystal caused by the shear motion. The thickness and motions are not drawn to scale. The arrows indicate relative magnitudes of shear deformation within the crystal. (From Buttry, 1991, with permission from Wiley-VCH.)

resonant oscillation. The shear motion is confined to the area where the electrodes are in register. A Wenking type of potentiostat, wherein the working electrode is at hard ground, is used to control the electrochemistry. The parameters measured are the usual electrochemical parameters, such as current, potential, and charge along with the oscillation frequency of the quartz disk.

Any mass changes that occur on the working electrode are reflected in changes in the frequency. The quantitative relationship is given by the *Sauerbrey equation*:

$$\Delta f = -\frac{f_0^2 m}{N\rho} = -\frac{2f_0^2 m}{n(\rho\mu)^{1/2}} \tag{27.2}$$

where Δf is the frequency change induced by the gain or loss of mass; f_0 is is the resonant frequency in hertz of the quartz crystal microbalance (QCM) prior to the addition or removal of mass; m is the mass per unit area of the deposit in g/cm^2; N is the frequency constant of the quartz crystal ($N = 0.167 \times 10^6$ Hz·cm for a 5-MHz AT-cut quartz); n is the harmonic number of the oscillation; ρ is the density of quartz ($\rho = 2.468$ g/cm^3); and μ is the shear modulus of quartz ($\mu = 2.947 \times 10^{11}$ g/cm·s^2). The negative sign indicates that the addition of mass decreases the resident frequency, and vice versa. The equation can be written simply as

$$\Delta f = -C_f m, \tag{27.3}$$

where C_f is a constant. For a 5-MHz crystal, C_f is 56.6 Hz·cm^2/μg. This simple linear relationship is true only if there is less than a 2% change in the resonant frequency due to the mass change.

Since the frequency can be measured within an accuracy of 1 Hz, a 5-MHz EQCM can detect 10 ng/cm^2. This corresponds to 10% of a monolayer of Pb atoms. Much higher sensitivity can be achieved with thinner quartz crystals operated at higher frequencies, as the sensitivity increases with f_0^2.

The advantages of EQCM are that it is an in situ method. ECQM has excellent sensitivity for detecting mass changes. EQCM has been used to study UPD processes and can detect the presence or lack of coadsorption of anions during UPD. It is also useful in the study of corrosion processes. In the case of $Ni(OH)_2$ and conductive polymer electrodes, solvent and anions can intercalate into the electrode at anodic potentials. The electrochemical quartz crystal microbalance (ECQM) is a useful technique for monitoring the ingress and egress of solvent and ions in these materials. A major advantage of EQCM is that the total cost of the equipment is only $10,000.

The major disadvantage of EQCM is that it does not yield chemical information. It is important to couple EQCM with other techniques, such as cyclic voltammetry and spectroscopic measurements. Then ECQM becomes a very powerful technique.

Arai et al. (1997) used EQCM to study iodide absorption on polycrystalline gold in 1 *M* $NaClO_4$ containing different concentrations of NaI. Figure 27.21 shows dynamic frequency change-potential Δf–E curves for 0.1 *M* $NaClO_4$ containing different concentrations of NaI. The frequency at potentials more positive than −0.8 V was less than that found without NaI. The frequency increased with

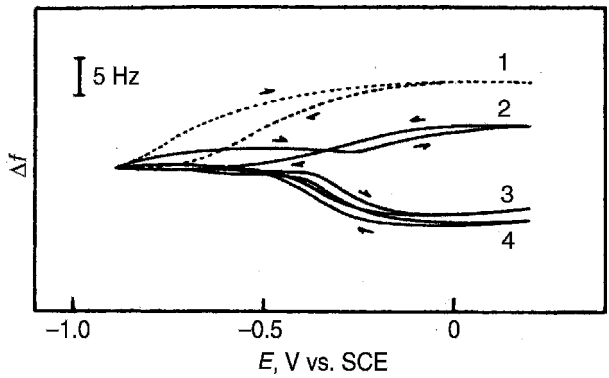

FIGURE 27.21 Frequency change–potential curves for 0.1 M $NaClO_4$ containing NaI. Concentration: (1) 0 M, (2) 5.0×10^{-6} M, (3) 5.0×10^{-5} M, (4) 1.0×10^{-4} M. Scan rate: 0.1 V/s. (From Arai et al., 1997, with permission from Elsevier.)

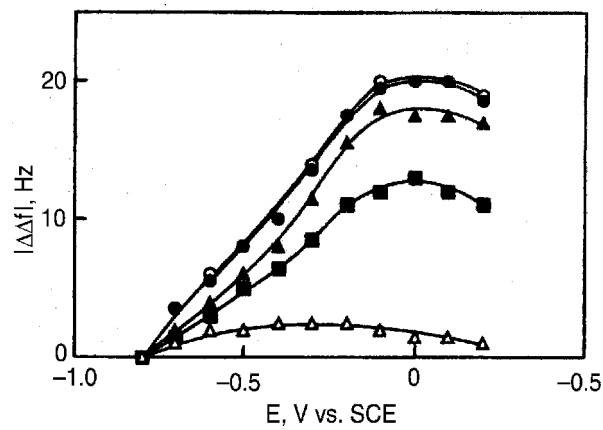

FIGURE 27.22 Potential dependence of frequency change for Au electrode in 0.1 M $HClO_4$ containing NaI. Concentration: ○, 1.0×10^{-4} M; ●, 5.0×10^{-5} M; ▲, 1.0×10^{-5} M; ■, 5.0×10^{-6} M; △, 1.0×10^{-6} M. (From Arai et al., 1997, with permission from Elsevier.)

NaI concentration, up to 1×10^{-4} M. They also obtained steady-state data using a potential step method. The applied potential was initially set at −0.9 V, where no iodide absorption occurs. The electrode was stepped to various positive potentials and Δf(ad) was recorded until equilibrium values were obtained. Similar measurements were done in an electrolyte without NaI, and Δf(no–ad) was recorded as a reference. The net change in frequency was determined as $|\Delta\Delta f| = \Delta f(\text{ad}) - \Delta f(\text{no–ad})$. Figure 27.22 shows $|\Delta\Delta f|$ vs. E plots for various NaI concentrations. Analysis of the data showed that iodide adsorption occurred in accordance with the Temkin isotherm.

27.5 OPTICAL SPECTROSCOPY

27.5.1 Polarized Light

Two optical spectroscopies, reflectance and ellipsometry, use monochromatic polarized light. The description of a monochromatic light wave includes the obvious parameters, such as frequency, phase, propagation direction, and amplitude. The description also needs to include the orientation of the electric and magnetic vectors in space. Since these two parameters are orthogonal, it is only necessary to consider the electric vector. If the electric vector, along a wave in space, lies in a plane, the light is called *linearly polarized*. The best explanation of the optics of these techniques was given in 1973 by R. H. Muller. A brief summary is presented here. Figure 27.23 shows the sinusoidal electric field distribution along the propagation direction z at a fixed instant in time. The plane that contains the electric vectors is called the *plane of polarization*. In a linearly polarized beam, all the light rays have the same angle for the plane of the electric field oscillation.

In a reflectance or ellipsometry experiment, measurements are always referred to the physical plane of incidence, as defined in Fig. 27.24. If the polarization is parallel to this plane of incidence, the parameters related to it are denoted by the subscript p. For polarization perpendicular to the plane, the subscript s is used. When a linearly polarized beam is reflected, one often finds that the parallel and perpendicular components undergo changes in amplitude and phase. Thus, two beams that are in

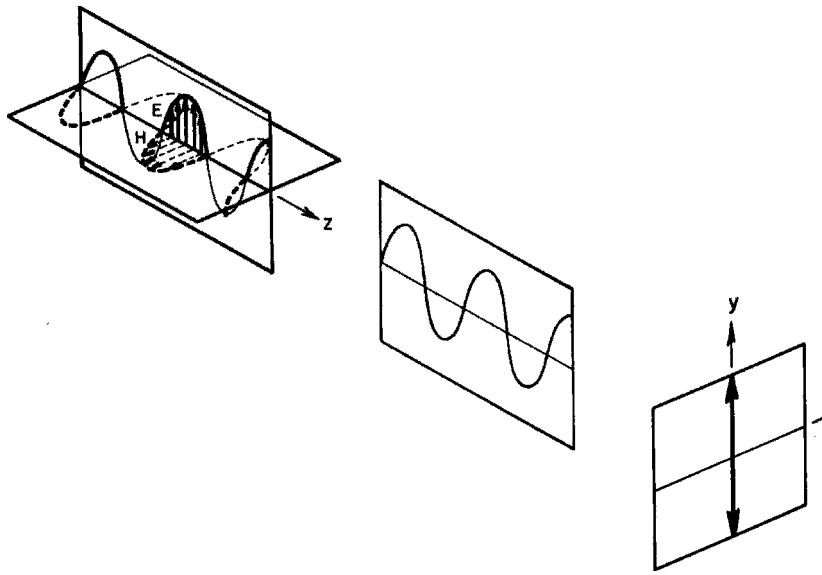

FIGURE 27.23 Electric (**E**) and magnetic (**H**) vectors in a linearly polarized light wave. The plane of polarization contains the electric field vectors in space. At a fixed location, the tip of the electric vector traces a straight line as a function of time. (From Muller, 1973, with permission from Wiley-VCH.)

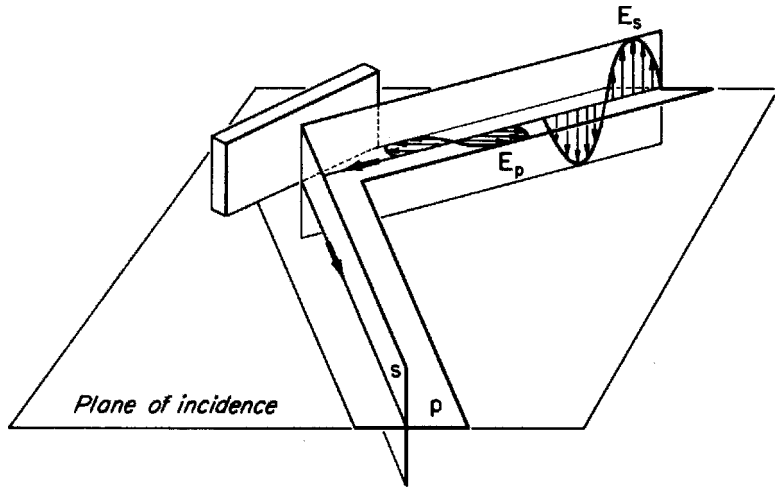

FIGURE 27.24 Reflection of polarized light. The plane of incidence is defined by the incident and reflected beam. The *s* and *p* components are indicated for the incident light, with the electric vector normal and parallel, respectively, to the plane of incidence. (From Muller, 1973, with permission from Wiley-VCH.)

phase upon striking the surface will be out of phase upon reflection. Figure 27.25 shows graphically what happens. The resulting electric field vector for the ray pair traces out a spiral as it propagates. The projection of the spiral on an intersecting plane is an ellipse; hence the light is elliptically polarized. The shape of the ellipse is determined by the relative amplitudes and phase differences of the two beams.

27.5.2 Reflectance Spectroscopy

Reflectance measurements involve measurements of the intensity of light reflected from a flat specular surface of an electrode in a spectroelectrochemical cell. The incident light is polarized either parallel (*p*) or perpendicular (*s*) to the plane of incidence, as shown in Fig. 27.24. A detector monitors the intensity of the reflected beam. The light is monochromatic, but the spectrometers usually can be tuned over large wavelength ranges. There are excellent reviews of reflectance by McIntyre (1973) and Plieth et al. (1992).

The reflectance, R, is defined as the ratio of the reflected light intensity to the intensity of the incident beam. Usually, one determines the change in reflectance, ΔR, induced by some parameter, such as the electrode potential. Experimentally, one measures only the intensity of the reflected beam, I_R. So if the incident intensity remains constant, the reflected beam gives $\Delta R/R = \Delta I_R/I_R$. Experimental results are presented as plots of $\Delta R/R$ vs. the parameter of interest, such as the frequency of the incident light or electrode potential. Modulation schemes, wherein the beam is chopped or the potential is modulated, are used to enhance the signal-to-noise ratio.

Arai et al. (1997) also used reflectance to study iodide absorption on gold. Figure 27.26 shows reflectance data for a gold electrode in various electrolytes.

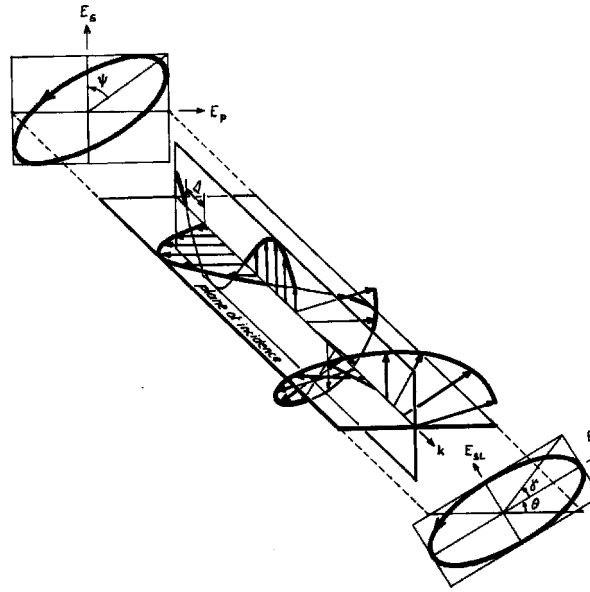

FIGURE 27.25 Elliptic polarization resulting from the superposition of two linear components of different phase and amplitude. (From Muller, 1973, with permission from Wiley-VCH.)

A cyclic voltammogram in 0.1 *M* $NaClO_4$ is also shown. There is an inflection in the reflectance curves in the vicinity of −0.2 to 0.4 V. The exact potential is dependent on the anion. The effect may be due to surface reconstruction. Figure 27.27 shows cyclic voltammograms and dynamic reflectivity change–potential curves in 0.1 *M* $NaClO_4$ containing various concentrations of NaI. The data agree with the EQCM data in that the onset of iodide absorption occurs at −0.8 V. They also did steady-state measurements using a potential-step method identical to that used in the EQCM studies. The net change in reflectivity is given as $|\Delta R/R_0| = R/R_0(\text{ad}) - R/R_0(\text{no–ad})$. $|\Delta R/R_0|$ vs. E plots are shown in Fig. 27.28. There was good agreement between the EQCM and the reflectance data.

27.5.3 Ellipsometry

As discussed above, the reflection of linearly polarized light from a surface generally produces elliptically polarized light, because the parallel and perpendicular components are reflected with different efficiencies and different phase shifts. These changes in intensity and phase angle can be analyzed to characterize the reflecting system. This approach is called *ellipsometry*.

In ellipsometry two parameters are determined. These are Δ, the phase angle between the leading and trailing components in Fig. 27.24, and the ratio of the electric field amplitudes E_p and E_s, which defines the second parameter, ψ. $|E_p|/|E_s| = \tan \psi$. Δ and ψ may be recorded as functions of other experimental variables, such as potential and time.

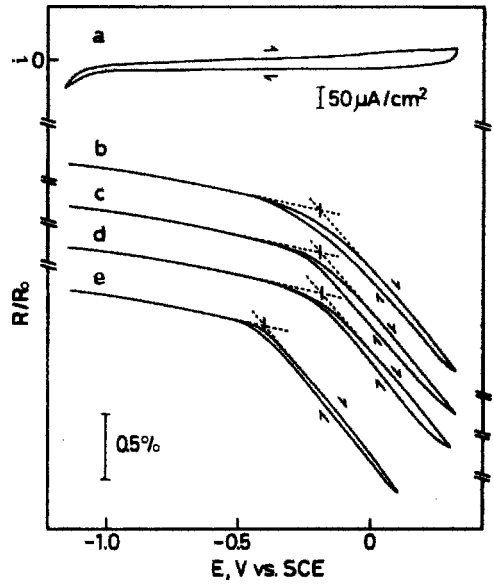

FIGURE 27.26 Cyclic voltammogram obtained on Au electrode in 0.1 *M* $NaClO_4$ (a) and reflectivity change–potential curves for 0.1 *M* $NaClO_4$ (b), 0.1 *M* $LiClO_4$ (c), 0.1 *M* $NaNO_3$ (d), and 0.1 *M* NaOH (e). Scan rate: 0.1 V/s. (From Arai et al., 1997, with permission from Elsevier.)

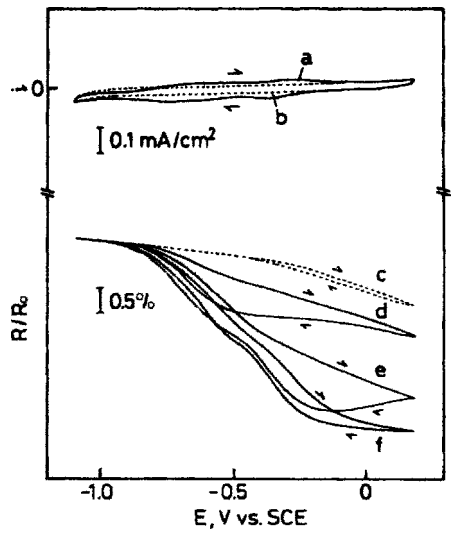

FIGURE 27.27 Cyclic voltammograms (a) and (b) and reflectivity change–potential curves (c) to (f) for 0.1 *M* $NaC1O_4$ containing NaI. Concentration: (b) and (c) 0 *M*, (d) 5.0×10^{-6} *M*, (e) 5.0×10^{-5} *M*, (a) and (f) 1.0×10^{-4} m*M*. Scan rate: 0.1 V/s. (From Arai et al., 1997, with permission from Elsevier.)

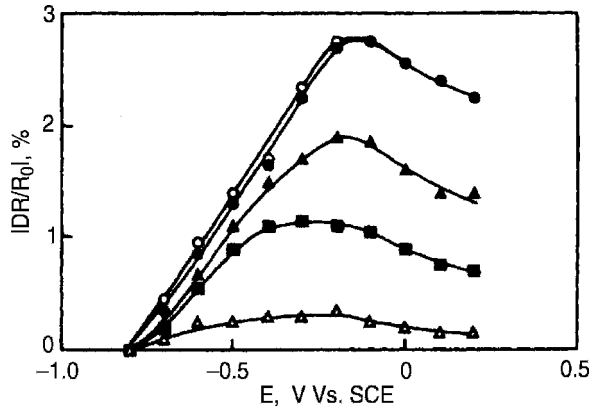

FIGURE 27.28 Potential dependence of reflectivity change for Au electrode in 0.1 M $HClO_4$ containing NaI. Concentration: ○, $1.0 \times 10^{-4} M$; ●, $5.0 \times 10^{-5} M$; ▲, $1.0 \times 10^{-5} M$; ■, $5.0 \times 10^{-6} M$; △, $1.0 \times 10^{-6} M$. (From Arai et al., 1997, with permission from Elsevier.)

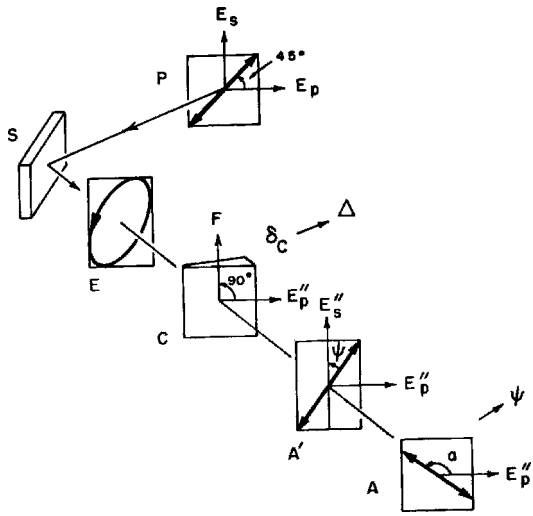

FIGURE 27.29 Arrangement of the components and states of polarization in an ellipsometer with linear polarization incident on the specimen. (From Muller, 1973, with permission from Wiley-VCH.)

The best way to describe ellipsometry is by the simple arrangement of Muller (1973) that is shown in Fig. 27.29. Light that is polarized at 45° with respect to the plane of incidence (P) impinges on the surface of an electrode (S). For this light, $E_p = E_s$, and $\Delta = 0$. The reflected light is elliptically polarized because of changes in the phase and amplitude of the p and s components. The reflected beam passes through an optical component called a compensator (C), which is adjusted to restore the original

condition $\Delta = 0$. The position of the compensator required for the restoration is a measure of the value of Δ induced by the reflection. The resulting linearly polarized beam is passed through a second polarizer, which is an analyzer (A) that is rotated until its axis of transmission is orthogonal to the plane of polarization of the incoming light. This is referred to as the *condition of extinction*. The angular position of the analyzer is a measure of ψ. Complete extinction can only be achieved by proper adjustment of both the compensator and the analyzer. This type of operation, which was common up until 30 years ago, is called *null-point detection*. This was superseded by rotating element ellipsometry, where either the polarizer or the analyzer is rotated and the other element is fixed. This results in a sinusoidal output that can be analyzed to derive Δ and ψ.

Ellipsometry is used to study film growth on electrode surfaces. It is possible to study films at the partial monolayer level and all the way up to coverage of thicknesses of thousands of angstroms while doing electrochemical measurements. To get useful data it is important to determine Δ and ψ for the bare electrode surface and the surface with a film. These data are processed to derive the film thickness, d, and the refractive index, $\check{n}$, which consists of a real (n) and imaginary part (k), $\check{n} = n - ik$. So ellipsometry gives information on the thickness and refractive index of surface films.

Spectroscopic ellipsometry and polarization modulation ellipsometry are two important developments. In spectroscopic ellipsometry, determinations of Δ and ψ are made over a large wavelength range, from the near ultraviolet to the near infrared. This greatly reduces the ambiguity in interpretation of data. Polarization modulation ellipsometry employs modulation of the state of polarization at high frequency (50 kHz) by applying a strain wave to a fused quartz crystal placed in the path of the incident beam. This type of ellipsometer has no moving parts. This reduces noise and increases the rate of data acquisition. Recent advances in ellipsometry have been reviewed by Gottesfeld et al. (1995) and Christensen and Hamnett (2000).

De Souza et al. (1997) used spectroscopic ellipsometry to study the oxidation of nickel in 1 *M* NaOH. Bare nickel electrodes were prepared by a series of mechanical polishing followed by etching in dilute HCl. The electrode was then transferred to the spectroelectrochemical cell and was cathodically polarized at -1.0 V vs. Hg/HgO for 5 minutes. The electrode potential was then swept to -0.9 V. Ellipsometry data were recorded at several potentials during the first anodic and cathodic sweep. Figure 27.30 shows a voltammogram for Ni in 1.0 *M* NaOH. The potentials at which data were recorded are shown. Optical data were obtained for various standard materials, such as NiO, α -$Ni(OH)_2$, β-$Ni(OH)_2$, β-NiOOH, and γ-NiOOH.

Figure 27.31 shows plots of Δ and ψ as a function of wavelength. Physical film models were used to fit the data. Porous films and surface roughness were modeled using the Bruggeman effective medium approximation. The interpretation of spectroscopic ellipsometer measurements by use of different optical models showed the formation of the following films during the first voltammetric cycle, starting from freshly polished and etched nickel electrodes:

1. In the first anodic peak (-0.9 to -0.4 V), a compact film of β-$Ni(OH)_2$ is formed.
2. The layer in the second anodic peak ($+0.4$ to $+0.6$ V) contains a mixture of $Ni(OH)_2$ and NiOOH with an overlayer of NiOOH.

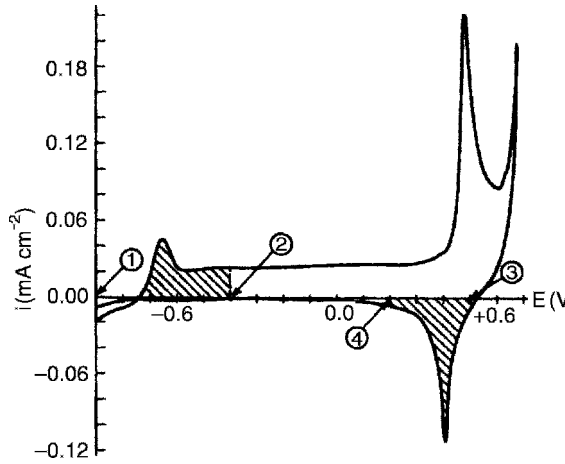

FIGURE 27.30 Voltammogram of Ni in 1.0 *M* NaOH solution; scan rate 10 mV/s. Pretreatment: polishing, immersion in dilute HCl solution and cathodic reduction at −1.1 V vs. Hg/HgO in 1.0 *M* NaOH, for 10 min. Potentials where the ellipsometer spectra were obtained are indicated by arrows: (1) −0.9 V, (2) −0.4 V, (3) +0.5 V, and (4) +0.2 V. (From de Souza et al., 1997, with permission from Elsevier.)

3. In the cathodic peak (+0.5 to +0.2 V), the β-NiOOH in the overlayer was reduced completely, and that embedded in the $Ni(OH)_2$ was partially reduced to $Ni(OH)_2$.
4. NiOOH is still found at very cathodic potentials (−0.9 V), along with some electrode roughness. A potentiostatic hold at this potential shows that $Ni(OH)_2$ is very slowly reduced to Ni, with a concomitant decrease in electrode roughness.

The advantages of ellipsometry are that it is an in situ technique that can be used to study film growth on electrodes. The main disadvantage is that it does not provide chemical information.

27.5.4 Raman Spectroscopy

When light interacts with matter, most of the light either goes through the sample or is elastically scattered, without change in photon energy. This is called the *Raleigh effect*. However, a small fraction of the photons exchange energy with the sample and are inelastically scattered, with a change in energy reflecting the loss and gain of energy. This is the Raman effect, and it yields information about the sample from the changes in energy in the scattered photons. The various aspects of Raman spectroscopy have been reviewed (Pettinger, 1992).

If an incident photon excites a molecule to a higher virtual state and is reemitted without loss in energy, the result is Raleigh scattering. Reemission to a final state other than the original state results in Raman scattering. The Raman effect produces discrete energy differences relative to the energy of the incident light. These differences

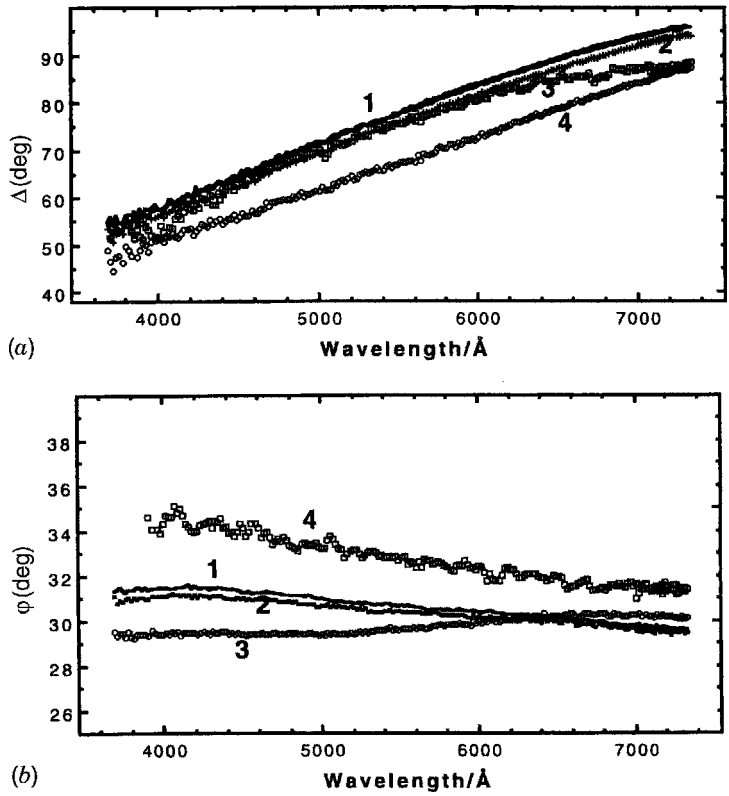

FIGURE 27.31 Ellipsometer spectra of a bare Ni electrode substrate (previously immersed in dilute HCl solution and reduced cathodically at $E = -1.1$ V) in 1.0 M NaOH solution and for electrodes at three selected potentials (indicated on the voltammogram in Fig. 27.30). (*a*) Experimental Δ values; (*b*) experimental ψ values; (1) substrate, (2) $E = -0.4$ V, (3) $E = +0.5$ V, and (4) $E = +0.2$ V (in cathodic scan direction). (From de Souza et al., 1997, with permission from Elsevier.)

correspond to quanta of the normal vibrational modes of the molecule. So a Raman spectrum consists of a strong line (the exciting line) of the same frequency as the incident illumination together with weaker lines on either side shifted from the strong line by frequencies ranging from a few to about 3500 wave numbers. In practice, only the Stokes lines are studied. These are Raman emissions at lower energy than the excitation energy. The frequency shifts, which are the differences between the frequencies of the Raman lines and the exciting line, are independent of the frequency of the exciting line. So excitation and detection can be done in the visible region. This is convenient for doing in situ studies. Raman spectroscopy provides molecular vibration information.

The probability of Raman scattering is quite small. This normally requires the use of intense laser sources and concentrated samples. A high-resolution double or triple monochromator is used to separate the Raman lines from the intense Raleigh line.

In most work on electrochemical systems, use is made of two effects that greatly enhance the Raman signals. One is resonance Raman spectroscopy (RRS), wherein the excitation wavelength corresponds to an electronic transition in an adsorbed molecule on an electrode surface. The other effect is surface-enhanced Raman spectroscopy (SERS), which occurs on certain surfaces, such as electrochemically roughened silver and gold. This effect, discovered by Fleischmann et al. (1974), yields enhancements of 10^5 to 10^6. The vast majority of publications on Raman studies of electrochemical systems use SERS. The limitations of SERS are that it occurs on only a few metals and the mechanism of the enhancement is not understood. There is speculation that only a small part of the surface is involved in the effect. There is a very good review of SERS (Pemberton, 1991).

Savinova et al. (2000) used SERS to study the interface between Ag(111) and alkaline electrolyte. Figure 27.32 shows a cyclic voltammogram for Ag(111) in 1 m*M* NaOH + 0.5 m*M* NaF. The voltammogram has asymmetric anodic and cathodic peaks between the hydrogen evolution region and the region of Ag_2O formation. Figure 27.33 shows SERS of Ag(111) in 0.5 *M* NaF + 1 m*M* NaOH. The spectra exhibit two main potential dependent bands ν_1 at 540 to 560 cm^{-1} and ν_2 at 803 to 819 cm^{-1} in the potential range from −0.9 to 0.3 V. There is considerable hysteresis in the bands in going from the anodic to the cathodic scans. These bands are attributed to the formation of a number of potential-dependent adsorbates above the point of zero charge (E_{pzc}) of the Ag electrode. These are OH groups (OH_{ads}) and oxidelike species (O_{ads}). Adsorbed hydroxide species are indicated by the presence of Raman bands at 540 to 560 cm^{-1} and at 803 to 819 cm^{-1}, attributed to Ag–OH stretching and AgO–H

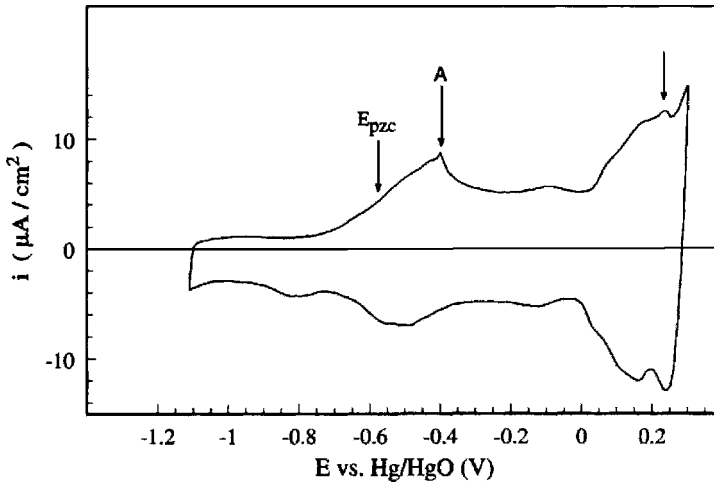

FIGURE 27.32 Cyclic voltammogram of the Ag(111) electrode in 1 m*M* NaOH + 0.5 mM NaF (pH 11). Sweep rate is 0.05 V/s. The arrows indicate the positions of the voltammetric peaks and the point of zero charge (PZC) of the Ag(111) in neutral NaF electrolyte. (From Savinova et al., 2000, with permission from Elsevier.)

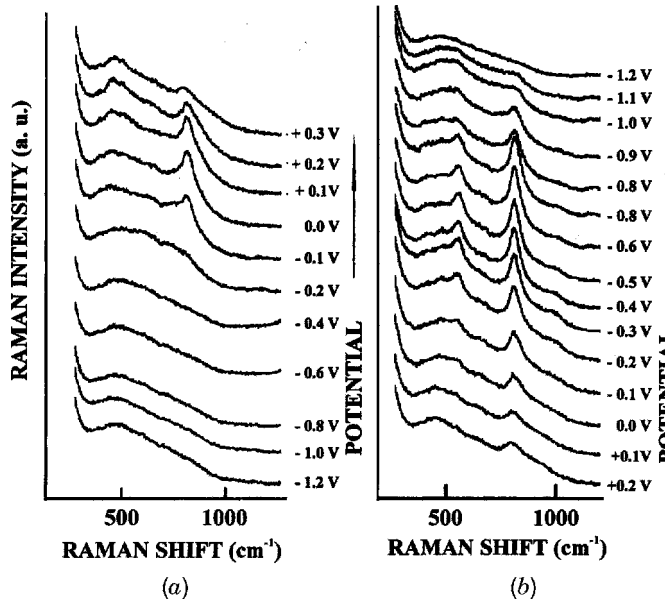

FIGURE 27.33 Evolution of the Raman spectra of the Ag(111) electrode in 1 m*M* NaOH + 0.5 *M* NaF (pH 11) in H_2O upon scanning the potential in the (*a*) positive and (*b*) negative direction. (From Savinova et al., 2000, with permission from Elsevier.)

bending vibrations, respectively. A strong isotope shift of the Raman bands toward lower frequencies is observed in D_2O solutions, proving their assignment.

27.5.5 Second Harmonic Generation

In a second harmonic generation (SHG) experiment, the output of a pulsed laser is focused on the surface under study and the intensity of light generated at the interface at twice the incident frequency is measured. This effect occurs in noncentrosymmetric crystals. It also occurs at an electrochemical interface because the symmetry is broken at the interface. For this reason SHG has remarkable surface and interface specificity. Powerful pulsed lasers such as Nd : YAG are used to generate intense electric fields at the surface at minimum average incident powers so as to maximize signal without damaging the surface. Thus, SHG is a surface-specific and nondestructive probe. Furthermore, because it can be used to probe any interface accessible to light, it can be used to study electrochemical reactions in situ. An important feature of the technique is that the probe light and optical signal that are generated at the surface of interest are easily transmitted through the electrolyte. There are reviews by Richmond (1991) and Corn (1992).

In a typical experiment, linearly polarized pulsed laser light of frequency ω strikes the electrode surface at an angle θ from the surface normal. The harmonic light of frequency 2ω generated at or near the angle of specular reflection is analyzed

for polarization following rejection of the fundamental beam by filters and a monochromator. The photon yield of the SHG signal is very low, typically on the order of 10^{-12}%, hence the need for powerful lasers.

Because the second harmonic response is sensitive to the polarizability of the interface, it is sensitive to the adsorption and desorption of surface species and is capable of quantifying surface species concentrations. Furthermore, SHG can be used to quantify surface order and determine surface symmetry by measuring the anisotropic polarization dependence of the second harmonic response. SHG can also be used to determine important molecular-level and electrochemical quantities such as molecular orientation and surface charge density.

SHG has been used to study electrode surface symmetry and order using an approach known as SH rotational anisotropy. A single-crystal electrode is rotated about its surface normal and the modulation of the SH intensity is measured as the angle (φ) between the plane of incidence and a given crystal axis or direction. Figure 27.34 shows in situ SHG results for an Au(111) electrode in 0.1 *M* $NaClO_4$ + 0.002 *M* NaBr, using a *p*-polarized beam. The results indicate the presence of two distinct onefold

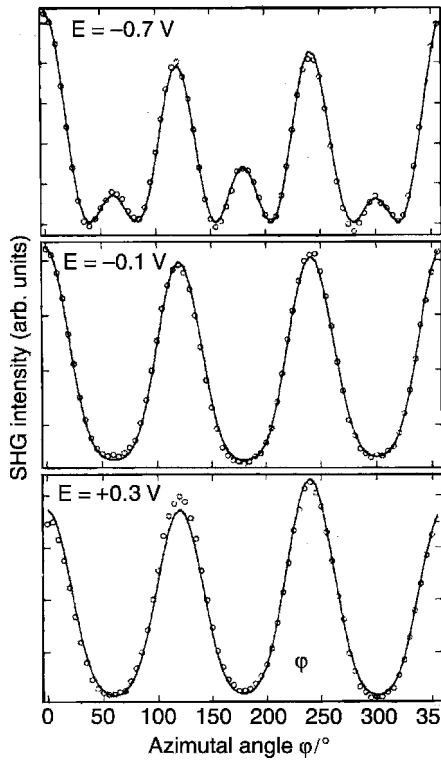

FIGURE 27.34 SHG-intensity recorded on Au(111) under *p*-polarisation vs. azimuthal angle φ for three electrode potentials $E = -0.7$ V, -0.1 V, and $+0.3$ V. Electrolyte was 1 *M* $NaClO_4$ + 0.002 *M* NaBr. (From Pettinger et al., 1995, with permission from Elsevier.)

axial symmetries in different potential ranges. At negative potentials the surface has the well-known Au(111)-($\sqrt{3}$ H 23) reconstruction. This reconstruction is lifted on the adsorption of oxide, hydroxide, or anions, such as sulfate or bromide. The results indicate a possible second reconstruction at positive potentials (Pettinger et al., 1995).

The advantages of SHG are that it uses visible light and that the experimental setup is relatively simple. Limitations of SHG are the lack of a good theory on the microscopic level and its inability to identify adsorbed species.

27.5.6 Sum-Frequency Generation

Surface sum-frequency generation (SFG) is a nonlinear, vibrational spectroscopic technique sensitive only to the interface region between two phases. The technique involves combining a fixed visible laser beam at frequency ω_{vis}, and a tunable infrared laser beam, ω_{IR}, on the surface of the electrode generating a third beam, ω_{SF}, where $\omega_{vis} + \omega_{IR} = \omega_{SF}$. As the infrared frequency is scanned and comes into vibrational resonance with molecules on the surface, an increase in the sum frequency signal, ω_{SF}, is detected. The intensity of a peak in an SFG spectrum is proportional to the square of the number of molecules on the surface. The signal is also affected by the orientation of the molecules. SFG detects only polar-oriented molecules at the interface. SFG combines the benefits of SHG with spectroscopic sensitivity to molecular adsorbates and thus provides a nondestructive, surface-specific probe of molecular vibrations of adsorbed species. SFG is typically sensitive to coverages as low as 5% of a monolayer.

A thin-layer cell for SFG measurements is shown in Fig. 27.35 (Baldelli et al., 1999). The IR and visible beams impinge on the sample surface at different angles.

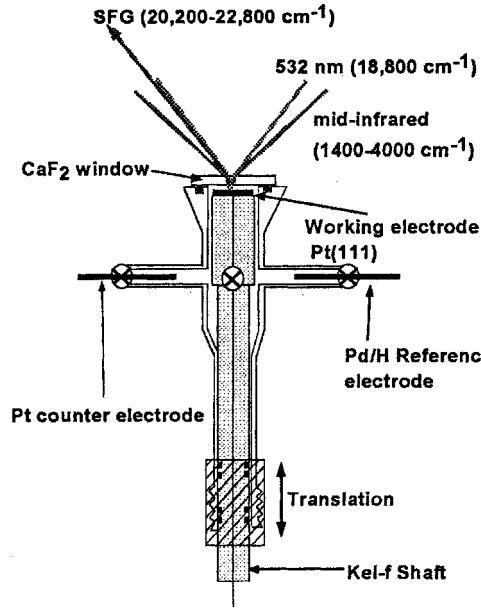

FIGURE 27.35 Electrochemical cell for SFG experiments. (From Baldelli et al., 1999, with permission from the American Chemical Society.)

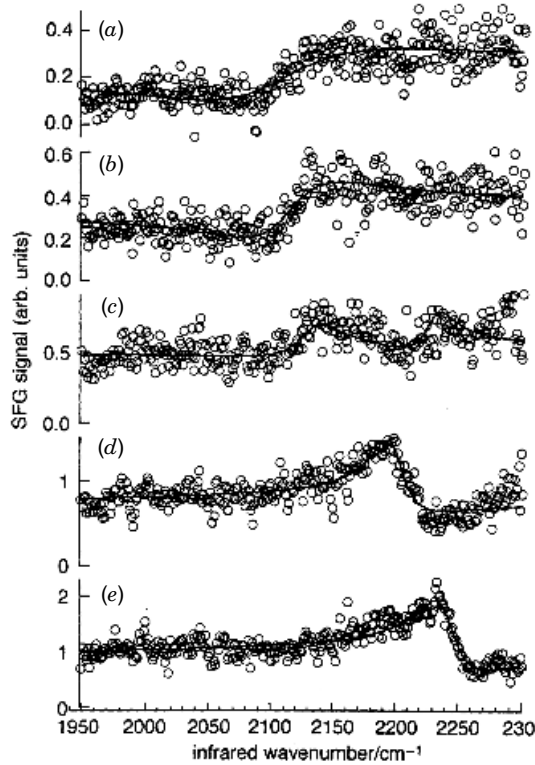

FIGURE 27.36 SFG spectra of Ag in 0.01 *M* KOCN + 0.1 *M* $NaClO_4$ at an electrode potential of (*a*) −0.4, (*b*) −0.2, (*c*) 0, (*d*) +0.2, (*e*) +0.4 V vs. SCE. (From Bowmaker et al., 1998, with permission from the Royal Society of Chemistry.)

The respective angles are typically 45° and 33° or 65° and 55°. IR-transparent CaF_2 or ZnSe windows are used.

Bowmaker et al. (1998) have used SFG to study the adsorption of cyanate ions on polycrystalline silver. Results are shown in Fig. 27.36. The SFG spectra show two bands, one in the region 2100 to 2130 cm^{-1} in the potential range from −0.6 to 0 V vs. SCE, and another in the region 2200 to 2240 cm^{-1} in the potential range 0 to 0.4 V. These bands are assigned to the asymmetric stretching mode of OCN^- ions bound to the Ag surface. The lower wave number band is assigned to cyanate N-bonded to a bridging surface site, whereas the higher wave number band is assigned to cyanate in a terminal N-bonding mode.

27.6 INFRARED SPECTROSCOPY

Infrared spectroscopy (IRS) is a very powerful technique for the study of adsorbates on electrode surfaces. The two major obstacles to applying in situ IRS are strong absorption of infrared (IR) light by the electrolyte and the difficulty of detecting

small absorbances from the adsorbed layer over the very large absorbance of the electrolyte. These problems have been solved by the use of ultrathin-layer cells and the application of optical or electrochemical modulation techniques coupled with phase-sensitive detection. The thin-layer cells are similar to those used in SFG measurements. These cells also function in the external reflection mode. IR-transparent CaF_2 or ZnSe windows are used. The electrolyte layer thickness is typically -0.5 to $2.0\,\mu m$. There is a review of IRS at the solid solution interface by Nichols (1992).

In the early work of Bewick and Robinson (1975), a simple monochromator system was used. This is called a *dispersive spectrometer*. In the experiment the electrode potential was modulated between two potentials, one where the adsorbed species was present and the other where it was absent. Because of the thin electrolyte layer, the modulation frequency is limited to a few hertz. This technique is referred to as *electrochemically modulated infrared reflectance spectroscopy* (EMIRS). The main problem with this technique is that data acquisition time is long. So it is possible for changes to occur on the electrode surface.

A significant advance was the application of the Fourier transform technique to enhance the signal. The optical arrangement of a Fourier transform infrared (FTIR) spectrometer is shown in Fig. 27.37 (Habib and Bockris, 1984). A beam of light from an IR source is directed to a beamsplitter, where part of the beam is transmitted to a

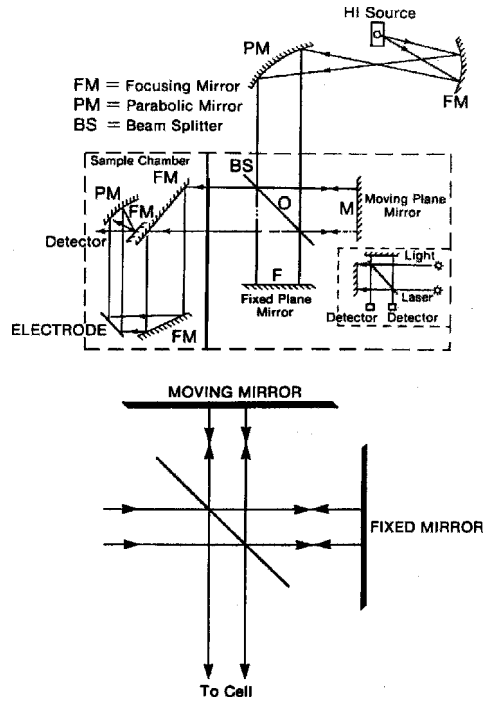

FIGURE 27.37 Optical arrangement of an FTIR spectrophotometer. (From Habib and Bockris, 1984, with permission from Elsevier.)

fixed mirror and a part reflected to a movable mirror. The beams are reflected back from the mirrors to the beamsplitter, where they undergo interference. This interference is a function of the wavelength of the radiation and the distances (δ) traveled by the light reflected by the two mirrors. The resulting intensity as a function of δ is called an *interferogram*. The intensity as a function of wave number can be derived by Fourier transformation of the interferogram. This yields a conventional IR spectrum. Since modern FTIR spectrometers can record interferograms in milliseconds, many interferograms can be collected and signal averaged. In this type of experiment, IR spectra are obtained at two potentials, one at which the adsorbate is present, the other where it is not. To get the final data, the two sets of spectra are subtracted. The technique is referred to as *subtractively normalized interfacial Fourier transform infrared spectroscopy* (SNIFTIRS).

Another technique, *polarization-modulated infrared reflection-absorption spectroscopy* (IRRAS), takes advantage of the fact that light polarized parallel to the plane of incidence at the metal surface is absorbed much more strongly by the adsorbate molecules than that polarized perpendicular to the plane. Modulating between the two polarizations with a photoelastic modulator (PEM) results in the intensities of the parallel and perpendicular components of the radiation, I_p and I_s, being detected alternately. Since only *p*-polarized light is surface sensitive, the modulation between the two polarizations yields an ac signal due to the adsorbed species at the electrode surface. This accrues from the fact that I_p and I_s are attenuated equally, by randomly oriented gas- or liquid-phase molecules, throughout the optical path, except close to the electrode surface. A PEM can be incorporated into either a dispersive or a FTIR spectrometer. In both cases a double modulation scheme is used to produce both the sum $(I_p + I_s)$ and the difference $(I_p - I_s)$ of these two intensities. The ratio $(I_p - I_s)/(I_p + I_s)$ is the infrared spectrum only of the species close to the surface. In contrast to EMIRS and SNIFTIRS, the IRRAS spectrum appears as a normal infrared spectrum and can be obtained at a single potential. In this way it is possible to record the spectra of species on the surface of the electrode and to ascertain their variation with potential and concentration.

In situ infrared spectroscopy allows one to obtain structure-specific information at the electrode–solution interface. It is particularly useful in the study of electrocatalytic reactions, molecular adsorption, and the adsorption of ions at metal surfaces.

Conventional IR and SFG experiments are confined to studies in the mid-infrared region. This is adequate for determining internal vibration modes for adsorbed molecules and intermediates. The vibrations of absorbates with surface metal atoms are expected to occur in the far-infrared, below 400 cm^{-1}. Because of the strong absorption of far-IR radiation by water, it is impossible to do experiments with conventional sources such as a globar. However, small synchrotron rings, such as the UV ring at the National Synchrotron Light Source (NSLS) at Brookhaven National Laboratory (BNL), can generate intense radiation in the far-IR region. This permits detection of metal–adsorbate interactions.

Bowmaker et al. (1998) have also used IR from a synchrotron source in the SNIFTIRS mode to study cyanate adsorption on silver. The spectra are shown in Fig. 27.38. The far-IR spectrum shows a broad band at about 360 cm^{-1} at electrode

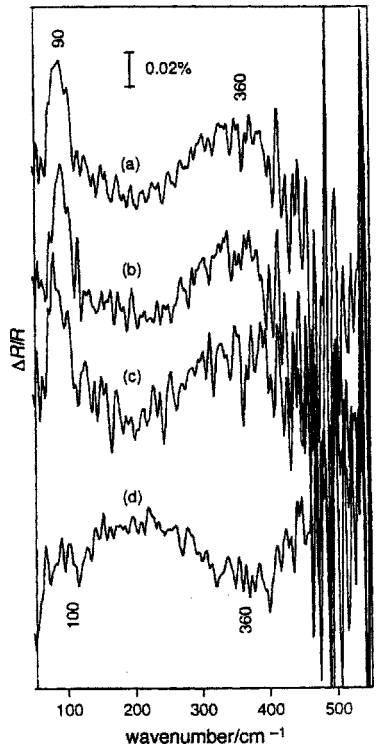

FIGURE 27.38 Relative reflectance of an Ag electrode in 0.01 KOCN + 0.1 *M* $NaClO_4$ in the SNIFTIRS mode at −1.0 V relative to +0.35 V (vs. SCE). (*a*) average of 10 ratioed spectra, (*b*) average of first five spectra, (*c*) average of last five spectra, (*d*) as for (*a*), but at 0.35 V relative to −1.0 V. (From Bowmaker et al., 1998, with permission from the Royal Society of Chemistry.)

potentials above 0 V. This is assigned to the ν(AgN) mode of terminally bound cyanate. The far-IR spectrum also shows a sharper band at 90 cm^{-1} that may be due to a bending mode of cyanate. Measurements were also made on a Cu electrode. The results were similar except that the bands were at 400 cm^{-1} and 160 cm^{-1}. This indicates that the bonding is dependent on the nature of the metal electrode.

27.7 ELECTROCHEMICAL NMR

Electrochemical nuclear magnetic resonance (NMR) is a relatively new technique that has recently been reviewed (Babu et al., 2003). NMR has low sensitivity, and a typical high-field NMR instrument needs 10^{18} to 10^{19} NMR active atoms (e.g., ^{13}C spins), to collect good data in a reasonable time period. Since 1 cm^2 of a single-crystal metal contains about 10^{15} atoms, at least 1 m^2 of surface area is needed to meet the NMR sensitivity requirement. This can be met by working with carbon-supported platinum

fuel cell catalysts. These catalysts have a platinum loading of about 15% and the particles are about 25 Å in diameter. About 45% of the Pt atoms are surface atoms. Because of this, one can get surface information on the Pt by doing ^{195}Pt NMR. By combining ^{195}Pt NMR with ^{13}C NMR, it is possible to get valuable information on the Pt surface and the adsorption CO and methanol oxidation intermediates on Pt.

27.8 EX SITU METHODS

The commercial availability of reliable ultrahigh-vacuum (UHV) technology in the late 1960s was crucial to the development of several surface analysis techniques. Initially, these techniques were used largely in semiconductor research. In many of these techniques, either the probe or the signal, or both, are electrons. This requires the absence of electrolyte and the introduction of the electrode into a UHV system. So in early work the electrode had to be removed from the cell, rinsed, and dried prior to introduction into the UHV system. Later, several groups devised elaborate schemes whereby clean single-crystal surfaces could be prepared and characterized in UHV and transferred back and forth between an electrochemical cell and the UHV, using a system of interlocks and manipulators. A schematic of such a system is shown in Fig. 27.39 (Hubbard et al., 1995). This eliminates the problem of exposure of the electrode to air. In such an apparatus it is possible to characterize the electrode

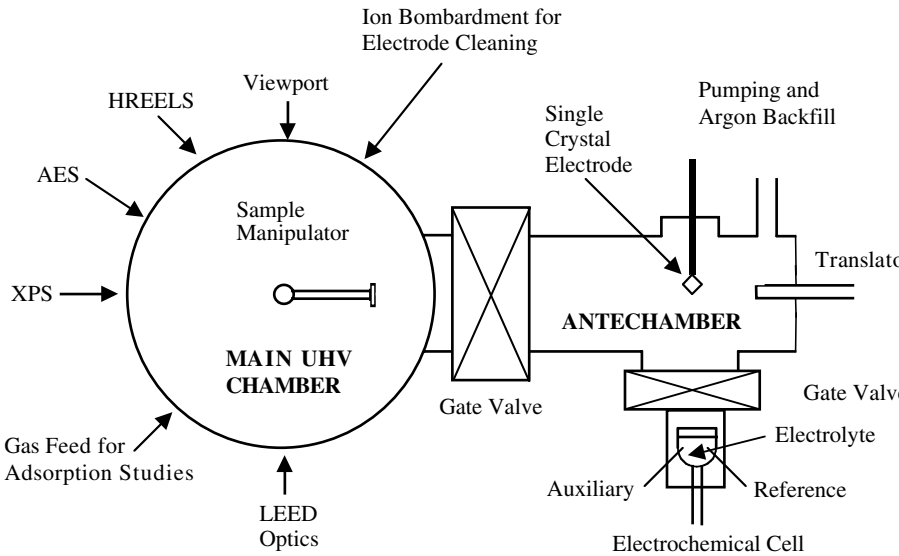

FIGURE 27.39 Schematic diagram of a surface electrochemistry apparatus, showing UHV system, transfer manipulators, and interlocks.

surface before and after doing electrochemistry. For instance, the long-range order of the electrode surface and adsorbed layers can be determined by low-energy electron diffraction (LEED); the elemental composition can be measured by Auger electron spectroscopy (AES) and by X-ray photoelectron spectroscopy (XPS); the vibrational spectrum of the adsorbate can be determined by high-resolution electron energy loss spectroscopy (HREELS). There are excellent reviews of this work (Hubbard et al., 1995; Soriaga et al., 1996).

The surface sensitivity of most electron probe techniques is due to the fact that the penetration depth of electrons into metals falls to a minimum of 4 to 20 Å when their kinetic energy is between 10 and 500 eV. It is also convenient that electrons at these energies have de Broglie wavelengths on the order of angstroms. With a monochromatic beam, it is possible to do LEED.

27.8.1 Low-Energy Electron Diffraction

Low-energy electron diffraction (LEED) differs from XRD and neutron diffraction in that the electrons cannot penetrate into the bulk more than a few angstroms. So the information comes from the top one or two layers at the surface. Figure 27.40 is a schematic of a typical LEED apparatus. The LEED optics consists of an electron gun and a hemispherical phosphor-coated screen. Grids are used to filter inelastically scattered electrons, and the elastically diffracted electrons are accelerated toward the screen. The results are an array of spots on the screen that can be photographed through the bell jar window. The location of the diffracted beams defines the reciprocal lattice of the real surface. The real-space unit cell can be generated from the reciprocal lattice using well-known relationships. Visual observation of the photographs can often yield point-group symmetries of the atoms on the surface.

LEED is a very specific tool for examination of the geometric pattern of atoms on a surface. In electrochemistry, it has been used to study surface reconstruction.

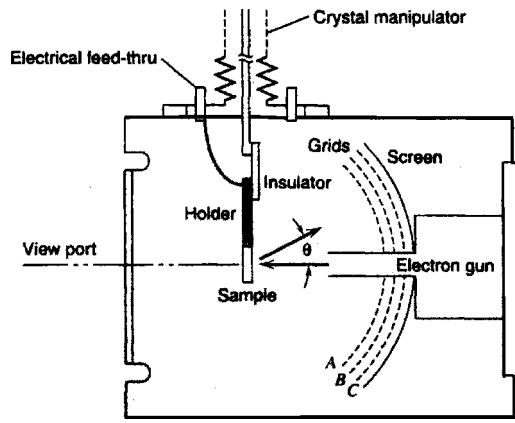

FIGURE 27.40 Schematic diagram of a LEED apparatus.

LEED has also been used to study the adsorption of halide ions, cyanide and thiocyanate ions, and organic molecules on single-crystal metal surfaces.

27.8.2 Auger Electron Spectroscopy

Auger electron spectroscopy (AES) is used for elemental analysis on surfaces. The Auger process is illustrated in Fig. 27.41. In an Auger experiment a beam of electrons, with energies between 2 and 10 keV, are directed at the sample surface. The impinging electrons eject a core K level electron. In the subsequent relaxation process, an electron from an upper L_1 level falls in to the vacant core level, and the released energy ejects an electron in a different L_3 level to the vacuum. This is the Auger electron. An electron analyzer such as a cylindrical mirror analyzer (CMA), in conjunction with a channel electron multiplier detector, is used to determine the energy of the Auger electrons. The energy of the Auger electrons is dependent on the binding energies of the K, L_1, and L_3 levels that are involved but not on the energy of the incident electrons. The Auger electron is designated as KL_1L_3 and its characteristic energy is given by

$$E_{KL_1L_3} = E_K - E_{L_1} - e\phi_{sp}, \tag{27.4}$$

where e is the electronic charge and ϕ_{sp} is the spectrometer work function. $E_{KL_1L_3}$ is characteristic of a given atom that endows AES with its element specificity. Even though the incident electrons have high energies, AES is surface sensitive because of the limited escape depth of the lower-energy Auger electrons. This escape depth is about 20 Å. The Auger process involves three electrons and is not applicable for analysis of H or He.

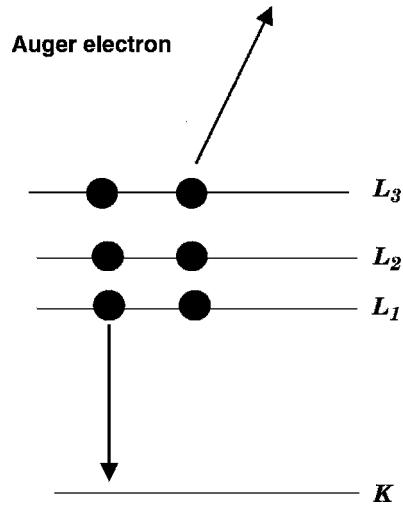

FIGURE 27.41 Electronic diagram of the Auger emission process.

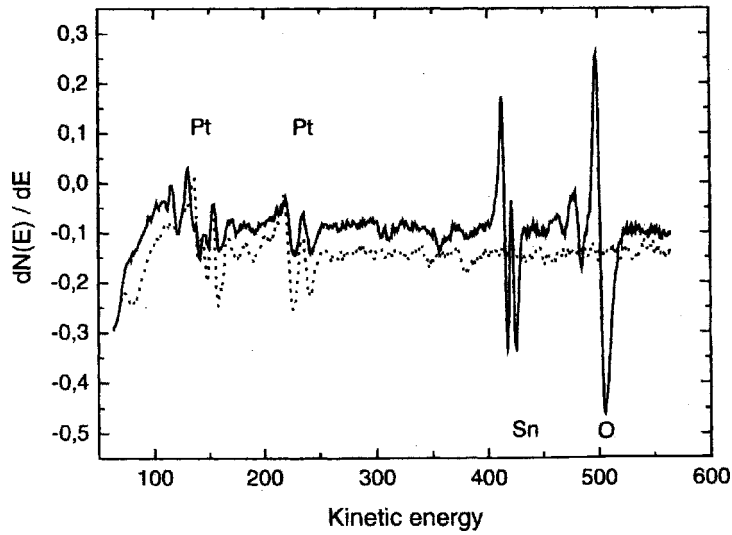

FIGURE 27.42 AES spectrum of Pt(111) before (dashed line) and after UPD Sn deposition (solid line). (From Tillmann et al., 2003, with permission from Elsevier.)

The Auger peaks are superimposed on a large background of other scattered electrons. A CMA can filter these spurious electrons and allow the Auger electrons to reach the detector. The results are usually plotted as a derivative spectrum.

Figure 27.42 is a derivative AES spectrum of Pt(111) before and after UPD Sn deposition (Tillmann et al., 2003). These experiments were done in a UHV transfer system. The results indicate a very clean surface. The oxygen is probably associated with the adsorbed Sn.

AES is a useful element-specific technique for quantitative determination of the elemental composition of a surface. Although some chemical information is available in principle, the technique is used largely for elemental analysis. Electron beam damage can decompose organic adsorbates and cause damage, particularly on insulating surfaces. In some cases, the beam can reduce metal oxides.

27.8.3 X-Ray Photoelectron Spectroscopy

X-ray photoelectron spectroscopy (XPS) is based on the photoelectric effect. When a sample is irradiated with monochromatic X-rays, such as the K_α lines of Mg (1253.6 eV) or Al (1486.6 eV), core-level electrons from the inner shells of atoms in the sample will be ejected from the sample to the surrounding vacuum. The kinetic energy, E_K, of the emitted photoelectron is given by

$$E_K = h\nu - E_B - e\phi_{sp}, \tag{27.5}$$

where $h\nu$ is the energy of the incident X-ray photon, E_B is the binding energy of the core electron, and $e\phi_{sp}$ is the spectrometer work function.

Electron energies are analyzed using a concentric hemisphere analyzer in conjunction with a channel electron multiplier. Even though X-rays can penetrate to a few thousand angstroms, the emitted electrons have low energies and their escape depth is ~20 Å. Depth profiling, to lower depths, can be done by varying the angle between the surface and the X-rays.

XPS also yields chemical information directly. For instance, if an element in a sample exists in different valence states, the XPS peak may broaden and show a shoulder. It is possible to deconvolute the peaks and determine valence states and the relative amount of each state in the sample. It is important to do this type of work by comparison of E_B values of standard reference compounds.

The binding energy, E_B, increases with atomic number Z, and this decreases the electron yield from the Auger process, so AES is most sensitive to elements with $Z < 45$. XPS provides higher sensitivity for heavier elements.

XPS is very useful for the study of surface layers and corrosion films. In the case of corrosion films and oxides it is important to do depth profiling by coupling XPS with ion milling of the surface. Another important aspect of XPS is that the incident X-rays cause negligible damage to the surface.

Tillmann et al. (2003) also used XPS to study UPD Sn on Pt(111). Figure 27.43 shows an overview spectrum after Sn deposition. An expanded view of the left-hand side is shown in the inset. The Sn 3*d* peak appears as a doublet. This splitting is due to a quantum effect called *spin–orbit coupling*.

In addition to SERS, Savinova et al. (2000) used XPS for ex situ studies of the interface between Ag(111) and alkaline electrolyte. Figure 27.44 shows XPS data for

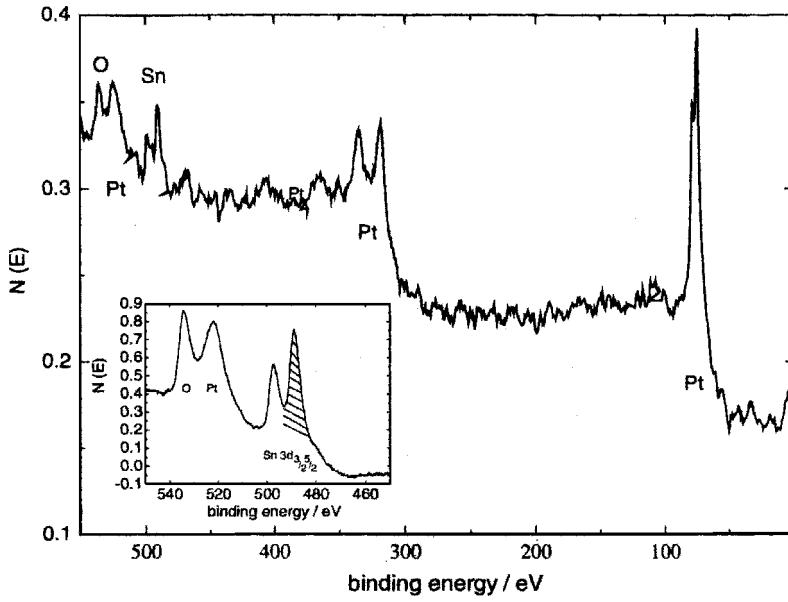

FIGURE 27.43 XPS spectrum of Pt(111) after UPD Sn deposition. (From Tillmann et al., 2003, with permission from Elsevier.)

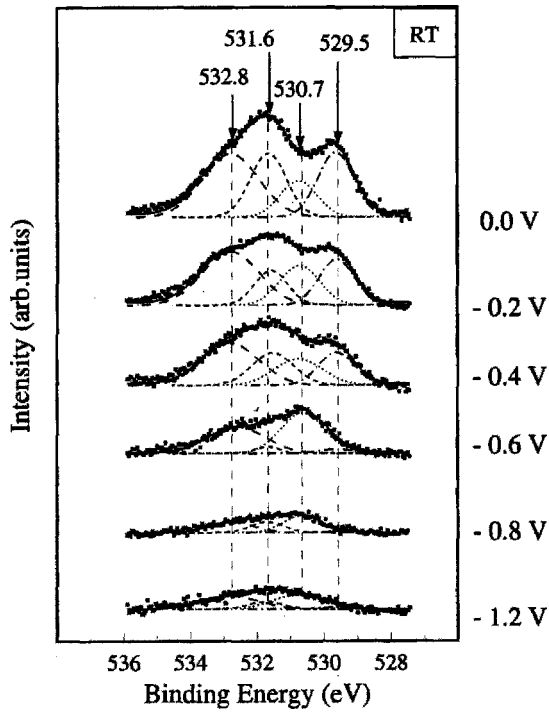

FIGURE 27.44 XPS data for Ag(111) that was emersed from electrolyte at specified potentials. (From Savinova et al., 2000, with permission from Elsevier.)

Ag(111) that was emersed from 1 m*M* NaOH + 0.5 m*M* NaF at specified potentials. The data were deconvoluted into a number of peaks. Above −0.8 V vs. Hg/HgO, the data indicate the presence of a number of adsorbed oxygen species. They coupled the XPS with thermal desorption in an effort to identify the species. The peaks at 529.6 eV and 531.6 eV could be assigned to adsorbed oxygen and OH species, respectively.

27.8.4 High-Resolution Electron Energy Loss Spectroscopy

High-resolution electron energy loss spectroscopy (HREELS) is a very useful technique for studying the vibrational modes of molecules adsorbed on surfaces. When electrons impinge on a surface, almost all of them are inelastically scattered at energies that are lower than the primary energy of the impinging electrons E_p. Electron energy losses can occur for several reasons, such as core-level ionization, valence-level excitations, and vibrational excitations. The energy losses due vibrational excitation are very small since these losses range up to 5000 cm^{-1}. This is equivalent to 600 meV. Hence, the loss peaks due to vibrational interactions lie close to the elastic peak and can only be observed if the electron energy loss measurements are done

at high resolution in the meV range. The excitation electron beam is made monochromatic to within 2 to 5 meV by use of an electrostatic analyzer. The scattered beam is at lower energy because of vibrational excitation of sample surface species. So a plot of these energy losses as a function of differences in energy between the excitation and scattered beams yields a spectrum similar to an IR spectrum. To detect a vibration, it must have a dipole moment component that is perpendicular to the surface. IRRAS has a similar requirement.

HREELS is an extremely sensitive surface technique. CO can be detected at coverages as low as 0.0001 monolayer and H at coverages of 0.01 monolayer. The energies accessible to HREELS range from 100 to 5000 cm^{-1}. So it is possible to get the equivalent of spectra from the far-infrared to the visible region, using HREELS. Because of the low energy of the impinging electrons, the beam penetration of the surface is less than 10 Å. The low energies avoid problems of decomposition of absorbed organic molecules by the beam.

Kim et al. (1996) used in situ STM and ex situ HREELS to study adsorption of benzene on Pd(111). Figure 27.45 shows HREEL spectra for Pd(111) after emersion at (A) 0.5 V and (B) 0.2 V RHE. Except for the peak at 1717 cm^{-1} (h) which is due

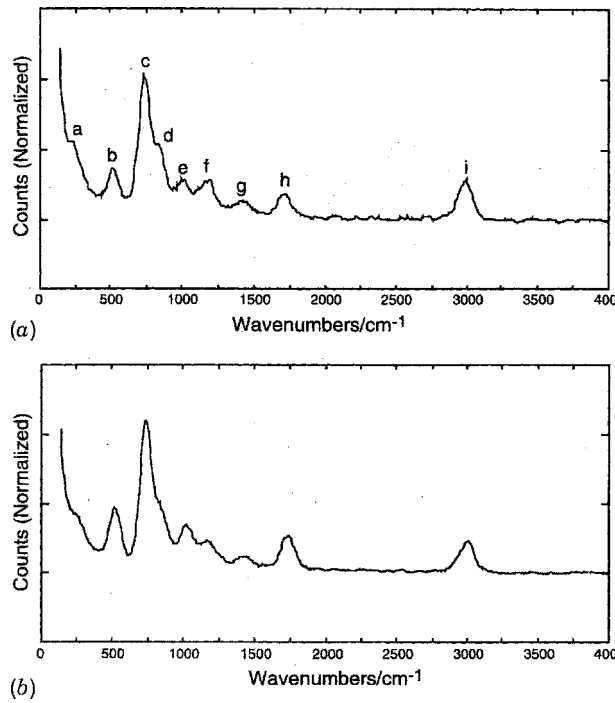

FIGURE 27.45 HREELS spectra for Pd(111) after emersion from 100 m*M* CF_3COOH + 1 m*M* benzene electrolyte at (*a*) 0.5 V and (*b*) 0.2 V RHE. The peak intensities were normalized with respect to the elastic peak. (From Kim et al., 2003, with permission from Elsevier.)

to CO, all the other peaks could be attributed to the chemisorbed benzene. The peaks at (a) 265 cm^{-1} and (b) 515 cm^{-1}, are due to Pd–C chemical bonds. Peaks (c) and (d) are out-of-plane C–H bends. Peaks (e) and (i) are in-plane stretches, and peaks (f) and (g) are in-plane C–H bends. By invoking the selection rule that if a vibration is detected by HREELS, it must have a dipole moment component that is perpendicular to the surface they were able to conclude that the benzene did not lie flat on the electrode surface but was slightly tilted. This was in agreement with their STM results.

27.8.5 Soft X-Ray X-Ray Absorption Spectroscopy

Soft X-ray X-ray absorption spectroscopy (soft X-ray XAS) is an ex situ technique that uses soft X-rays with energies in the range 150 to 1200 eV, to do XAS. This energy range covers the K edges of B, C, N, O, and F and the $L_{2,3}$ edges of the first-row transition metal elements. Soft X-ray XAS has some degree of surface specificity. In an XAS experiment, tunable X-rays impinge on a sample. When the X-ray reaches a specific energy, such as the K edge of oxygen (532 eV), 1*s* electrons are ejected. The resulting core hole can relax in two ways. One is by having an electron drop from higher levels into the core hole, which results in the emission of fluorescent X-rays. The other mode of relaxation is the ejection of Auger electrons. A schematic diagram of the process is given in Fig. 27.46. Both the fluorescent X-rays and the Auger electron signals are proportional to the X-ray absorption. So both signals can be processed to yield XAS spectra. The fluorescent X-rays in this energy range have an escape depth of about 3000 Å, whereas the Auger electrons have an escape depth of only 50 Å. So the fluorescent X-ray signal gives information about

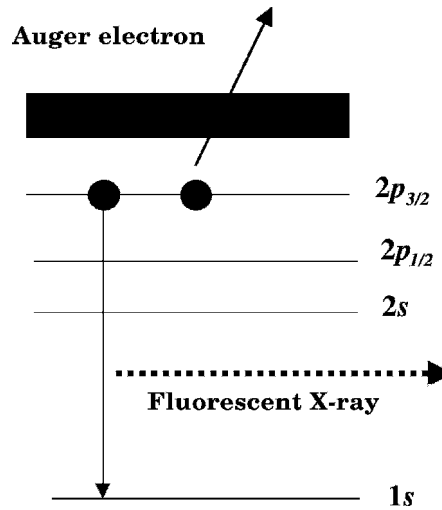

FIGURE 27.46 Soft X-ray XAS. The black band represents states in the vicinity of the Fermi level.

the bulk, and the Auger signal yields information on the region close to the surface. By doing fluorescence and electron yield measurements simultaneously, one can get both surface and bulk information in the same experiment.

Soft X-ray absorption measurements are done at low-energy synchrotron X-ray facilities such as the UV ring at NSLS or the Advanced Photon Source (APS) at Lawrence Berkeley National Laboratory (LBNL). The beam size is typically 1 mm in diameter. The electron yield data are usually obtained in the total electron yield (EY) mode, measuring the current from a channel electron multiplier (Channeltron). Sometimes a voltage bias is applied to increase surface sensitivity. This is referred to as the *partial electron yield* (PEY) *mode*. Fluorescence yield (FY) data are recorded using a windowless energy dispersive Si (Li) detector. The experiments are conducted in vacuum at a pressure of $\sim 2 \times 10^{-7}$ torr.

$LiNi_{0.5}Mn_{0.5}O_2$ is a promising cathode material for lithium ion batteries. Ni and Mn K edge XAS has been used to determine the oxidation state of Ni and Mn in the as-prepared material and to follow changes in oxidation state when the material is cycled in a spectroelectrochemical cell (Yoon et al., 2002). The results indicated that the as-prepared material contained Ni(II) and Mn(IV). During charging, lithium is removed from the oxide and Ni(II) converts to Ni(IV). Mn remains as Mn(IV). Soft X-ray Ni and Mn $L_{2,3}$ edge XAS, in both the PEY and FY modes, was used to study any differences between the surface and bulk in charged electrodes (Yoon et al., 2004). Figure 27.47 shows a set of normalized Ni $L_{2,3}$ edge XAS spectra of $L_{1-x}Ni_{0.5}Mn_{0.5}O_2$

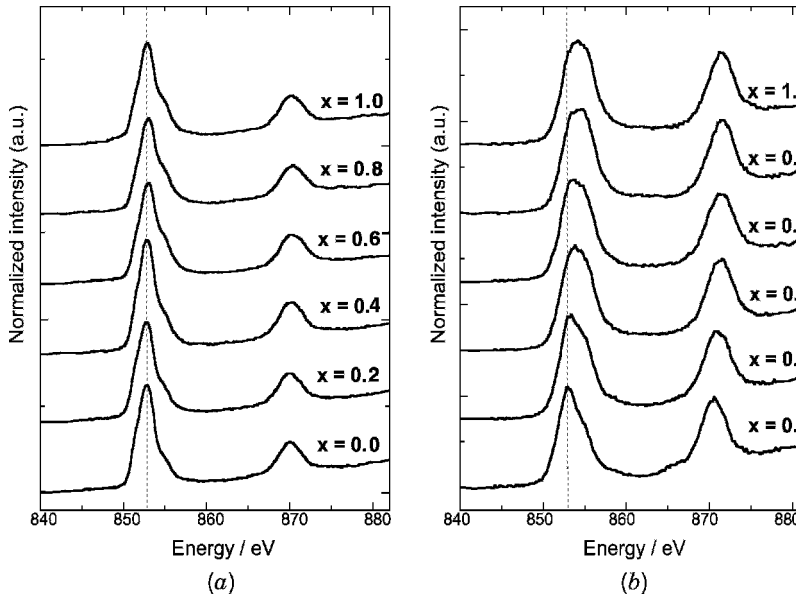

FIGURE 27.47 Normalized Ni $L_{2,3}$ edge XAS spectra of $L_{1-x}Ni_{0.5}Mn_{0.5}O_2$ cathodes at different x values using the (*a*) PEY and (*b*) FY methods. (From Yoon et al., 2004, with permission from The Electrochemical Society.)

cathodes at different x values using the PEY and FY methods. There are two peaks in the spectra, one at 853 eV (L_3 edge) and the other at 870 eV (L_2 edge). In the PEY mode the L_3 edge position remains constant, indicating that the Ni on the surface of the $LiNi_{0.5}Mn_{0.5}O_2$ particles remains in the divalent Ni(II) state. In the FY mode there is a continuous shift in the L_3 edge position, consistent with the conversion of Ni(II) to Ni(IV) in the bulk. For some reason the surface composition of higher-valent [$>$ Ni(II)] nickel oxides are often different than the bulk. In any case, one has to be careful in drawing conclusions about bulk properties from data obtained by electron signal methods such as AES, XPS, and soft X-ray XAS in only the EY mode. Most publications on soft X-ray XAS only present data obtained in the EY mode.

Soft X-ray XAS is a useful method for studying surface films and the chemical environment of dilute components in alloys, oxides, and corrosion films.

27.9 THE FUTURE OF PHYSICAL METHODS IN ELECTROCHEMISTRY

X-Ray Methods The availability of third-generation synchrotron X-ray sources and the development of advanced detectors will permit time-resolved XRD and XAS measurements. The intense sources will make it possible to do nonresonant inelastic X-ray scattering (NRIXS) measurements. The technique, which requires intense sources, is analogous to Raman spectroscopy in that hard X-rays are used to probe light elements in materials in much the same way as visible light is used in Raman spectroscopy to examine materials that are not transparent in the ultraviolet or infrared. XAS data on light elements can be extracted from the data. The technique permits the investigation of the chemical environment of light elements such as Li and O using hard X-rays as the probe. The hard X-rays can penetrate electrolyte.

Scanning Probe Methods The main problem with scanning probe methods is the lack of chemical information. Methods have to be devised to get chemical information simultaneously with the images.

Electrochemical Quartz Crystal Microbalance Future advances will require the coupling of EQCM with spectroscopic techniques that yield chemical information. EQCM has been coupled with ellipsometry (Gottesfeld et al., 1995). However, ellipsometry does not yield chemical information.

Optical Methods Reflectance and ellipsometry suffer from lack of a theory at the molecular level. The same is true for SERS and SHG. The main advances will be in the use of far-IR spectroscopy and SFG. SFG measurements performed with femtosecond lasers open up new possibilities for time-resolved adsorbate studies.

Ex Situ *Methods* XPS and HREELS will continue to be very useful ex situ methods for the study of electrode surfaces. Soft X-ray XAS in both the EY and FY modes should find wider application.

REFERENCES

Arai, K., F. Kusu, K. Ohe, and K. Takamura, *Electrochim. Acta*, **42**, 2493 (1997).

Bach, C. E., R. J. Nichols, W. Beckmann, H. Meyer, A. Schulte, J. O. Besenhard, and P. D. Jannakoudakis, *J. Electrochem. Soc.*, **140**, 1281 (1993).

Baldelli, S., N. Markovic, P. Ross, Y.-R. Shen, and G. Somorjai, *J. Phys. Chem*., **B103**, 8920 (1999).

Bewick, A., and J. Robinson, *J. Electroanal. Chem.*, **60**, 163 (1975).

Binnig, G., H. Rohrer, C. Gerber, and E. Wiebel, *Phys. Rev. Lett*., **49**, 57 (1982).

Bowmaker, G. A., J.-M. Leger, A. Le Rille, C. A. Melendres, and A. Tadjeddine, *J. Chem. Soc. Faraday Trans.*, **94**, 1309 (1998).

Brankovic, S., J. McBreen, and R. R. Adžić, *J. Electroanal. Chem*., **503**, 99 (2001).

Curie, J., and P. Curie, *Bull. Soc. Min. Fr.*, **3**, 90 (1880).

De Souza, L. M. M., F. P. Kong, F. R. McLarnon, and R. H. Muller, *Electrochim. Acta*, **42**, 1253 (1997).

Fleischmann, M., P. J. Hendra, and A. J. McQuillan, *Chem. Phys. Lett*., **26**, 163 (1974).

Gibbs, D., B. M. Ocko, D. M. Zehner, and S. G. H. Mocherie, *Phys. Rev.*, **B38**, 7303 (1988).

Habib, M. A., and J. O'M. Bockris, *J. Electroanal. Chem*., **180**, 287 (1984).

Kim, Y.-G., J. E. Soto, X. Chen, Y.-S. Park, and M. P. Soriaga, *J. Electroanal. Chem.*, **554–555**, 167 (2003).

Kondo, T., K. Tamura, M. Takahashi, J. Mizuki, and K. Uosaki, *Electrochim. Acta*, **47**, 3075 (2002).

Liu, L., L. Chen, X. Huang, X.-Q. Yang, W.-S. Yoon, H. S. Lee, and J. McBreen, *J. Electrochem. Soc*., **151**, A1344 (2004).

Ocko, B. M., D. Gibbs, K. G. Huang, D. M. Zehner, and S. G. H. Mocherie, *Phys. Rev.*, **B44**, 6429 (1991).

Pettinger, B., J. Lipkowski, and S. Mirwald, *Electrochim. Acta*, **40**, 133 (1995).

Savinova, E. R., D. Zemlyanov, B. Pettinger, A. Scheybal, R. Schögl, and K. Doblhofer, *Electrochim. Acta*, **46**, 175 (2000).

Sinha, S. K., E. B. Sirota, S. Garoff, and H. B. Stanley, *Phys. Rev*., **B38**, 2297 (1988).

Soldo, Y., E. Sibert, G. Tourillon, J. L. Hazemann, J. P. Levy, D. Aberdam, R. Faure, and R. Durand, *Electrochim. Acta*, **47**, 3081 (2002).

Sonnenfeld, R., and P. K. Hansma, *Science*, **232**, 211 (1986).

Stern, E. A., M. Newville, B. Ravel, Y. Yacoby, and D. Haskel, *Physica*, B **208–209**, 117 (1995).

Tillmann, S., G. Samjeské, K. A. Friedrich, and H. Baltruschat, *Electrochim. Acta*, **49**, 73 (2003).

Wang, J. X., I. K. Robinson, and R. R. Adžić, *Surf. Sci*., **412–413**, 374 (1998).

Yoon, W.-S., M. Balasubramanian, X.-Q. Yang, Z. Fu, D. A. Fischer, and J. McBreen, *Electrochem. Solid-State Lett.*, **5**, A263 (2002).

Yoon, W.-S., Y. Paik, X.-Q. Yang, M. Balasubramanian, J. McBreen, and C. P. Grey, *J. Electrochem. Soc.*, **151**, A246 (2004).

You, H., C. A. Melandres, Z. Nagy, V. A. Maroni, W. Yun, and R. M. Yoncoo, *Phys. Rev.*, **B45**, 11288 (1992).

MONOGRAPHS AND REVIEWS

Abruña, H. D., X-ray absorption spectroscopy in the study of electrochemical systems, in *Electrochemical Interfaces*, H. D. Abruña, Ed. VCH, Weinheim, Germany, 1991, p. 1.

Babu, P. K., E. Oldfield, and A. Wieckowski, Nanoparticle surfaces studied by electrochemical NMR, in *Modern Aspects of Electrochemistry*, J. O'M. Bockris, Ed., Vol. 36, Kluwer, New York, 2003, p. 1.

Barrett, C. S., and T. B. Massalski, *The Structure of Metals*, 3rd ed., McGraw-Hill, New York, 1980.

Born, M., and W. Wolf, *Principles of Optics*, Pergamon Press, Oxford, 1970.

Buttry, D. A., The quartz crystal microbalance as an in situ tool in electrochemistry, in H. D. Abruña, Ed., *Electrochemical Interfaces*, VCH, Weinheim, Germany, 1991, p. 529.

Cady, W. G., *Piezoelectricity*, McGraw-Hill, New York, 1946.

Christensen, P., and A. Hamnett, In-situ techniques in electrochemistry: ellipsometry and FTIR, *Electrochim. Acta*, **45**, 2443 (2000).

Clarke, L. J., *Surface Crystallography*, Wiley, New York, 1985.

Corn, R. M., In situ second harmonic generation studies of molecular orientation at electrode surfaces, in *Adsorption of Molecules at Metal Electrodes*, J. Lipkowski and P. N. Ross, Eds., VCH, New York, 1992, p. 391.

Cullity, B. D., *Elements of X-ray Diffraction*, 2nd ed., Addison-Wesley, Reading, MA, 1978.

Gottesfeld, S., Y.-T. Kim, and A. Redondo, Recent applications of ellipsometry and spectroellipsometry in electrochemical systems, in *Physical Electrochemistry*, I. Rubenstein, Ed., Marcel Dekker, New York, 1995, p. 393.

Hepel, M., Electrode–solution interface studied with electrochemical quartz crystal nanobalance, in *Interfacial Electrochemistry*, A. J. Wieckowski, Ed., Marcel Dekker, New York, 1999, p. 599.

Hubbard, A. T., E. Y. Cao, and D. A. Stern, Analysis of surface layers on well-defined electrode surfaces, in *Physical Electrochemistry*, I. Rubenstein, Ed., Marcel Dekker, New York, 1995, p. 469.

Itaya, K., Atomic-scale aspects of anodic dissolution of metals: studies by in situ scanning tunneling microscopy, in *Interfacial Electrochemistry*, A. J. Wieckowski, Ed., Marcel Dekker, New York, 1999, p. 187.

Jenkins, F. A., and H. E. White, *Fundamentals of Optics*, McGraw-Hill, New York, 1957.

Koningsberger, D. C., and R. Prins, *X-Ray Absorption: Principles, Applications, Techniques of EXAFS, SEXAFS, and XANES*, Wiley, New York, 1988.

McIntyre, J. D. E., Specular reflection spectroscopy of the electrode–solution interface, in *Advances in Electrochemistry*, *1*, Vol. 9, 1973, p. 61.

Muller, R. H., Principles of ellipsometry, in *Advances in Electrochemistry*, *1*, Vol. 9, 1973, p. 167.

Nagy, Z., and H. You, Applications of surface X-ray scattering to electrochemistry problems, *Electrochim. Acta*, **47**, 3037 (2002).

Nichols, R. J., IR spectroscopy of molecules at the solid–solution interface, in *Adsorption of Molecules at Metal Electrodes*, J. Lipkowski and P. N. Ross, Eds., VCH, New York, 1992, p. 347.

Pemberton, J. E., Surface enhanced Raman scattering, in *Electrochemical Interfaces*, H. D. Abruña, Ed., VCH, Weinheim, Germany, 1991, p. 193.

Pettinger, B., In situ Raman spectroscopy at metal electrodes, in *Adsorption of Molecules at Metal Electrodes*, J. Lipkowski and P. N. Ross, Eds., VCH, New York, 1992, p. 285.

Pleith, W., W. Kozlowski, and T. Twomey, Reflectance spectroscopy and ellipsometry of organic monolayers, in *Adsorption of Molecules at Metal Electrodes*, J. Lipkowski and P. N. Ross, Eds., VCH, New York, 1992, p. 285.

Richmond, G. L., Investigations of electrochemical interfaces by nonlinear optical methods, in *Electrochemical Interfaces*, H. D. Abruña, Ed., VCH, Weinheim, Germany, 1991, p. 265.

Robinson, I. K., and D. J. Tweet, Surface X-ray diffraction, *Rep. Prog. Phys.*, **55**, 599 (1992).

Sonnenfeld, R., J. Schnier, and P. K. Hansma, Scanning tunneling microscopy: a natural for electrochemistry, in *Modern Aspects of Electrochemistry*, J. O'M. Bockris et al., Eds., Vol. 21, Kluwer, New York, 1990, p. 1.

Soriaga, M. P., D. A. Harrington, J. L. Stickney, and A. Wiekowski, Ultrahigh-vacuum surface analytical methods in electrochemical studies of single-crystal surfaces, in *Modern Aspects of Electrochemistry*, J. O'M. Bockris et al., Eds., Vol. 28, Kluwer, New York, 1996, p. 1.

Toney, M. F., and O. R. Melroy, Surface X-ray scattering, in *Electrochemical Interfaces*, H. D. Abruña, Ed., VCH, Weinheim, Germany, 1991, p. 55.

Ward, M. D., Principles and applications of the electrochemical quartz crystal microbalance, in *Physical Electrochemistry*, I. Rubenstein, Ed., Marcel Dekker, New York, 1995, p. 293.

Wiesler, D. G., M. F. Toney, C. S. McMillan, and W. H. Smyrl, in *The Applications of Surface Analysis Methods to Environmental/Materials Interactions*, D. R. Baer, C. R. Clayton, and G. D. Davis, Eds., Electrochemical Society, Pennington, N.J., 1991, p. 440.

28
Electrocatalysis

28.1 INTRODUCTION

28.1.1 The Field of Electrocatalysis

The science of electrocatalysis provides the connection between the rates of electrochemical reactions and the bulk and surface properties of the electrodes on which these reactions proceed.

In electrocatalysis, the major subject are redox reactions occurring on "inert," nonconsumable electrodes and involving substances dissolved in the electrolyte while there is no stoichiometric involvement of the electrode material. Electrocatalytic processes and phenomena are basically studied in aqueous solutions at temperatures not exceeding 120 to 150°C. Yet electrocatalytic problems sometimes emerge as well in high-temperature systems at interfaces with solid or molten electrolytes.

In redox reactions, the electrode is not "inert" in the full meaning of the term. It serves not only to feed current through the electrolyte but also acts as a catalyst (as a "catalytic electrode") determining the rates and special features of electrochemical reactions occurring at its surface.

The degree to which an electrode will influence the reaction rates is different for different electrochemical reactions. In complex electrochemical reactions having parallel pathways, such as a reaction involving organic substances, the electrode material might selectively influence the rates of certain individual steps and thus influence the selectivity of the reaction (i.e., the overall direction of the reaction and the relative yields of primary and secondary reaction products).

Historically, electrocatalytic science developed from investigations into cathodic hydrogen evolution, a reaction that can be realized at many metals. It was found in a number of studies toward the end of the nineteenth century that at a given potential, the rate of this reaction differs by several orders of magnitude between metals. In one of the first theories of hydrogen evolution, the *recombination theory of hydrogen overvoltage*, the rate of this reaction was linked directly to the rate of the catalytic

Fundamentals of Electrochemistry, Second Edition, By V. S. Bagotsky

(nonelectrochemical) step of recombination of hydrogen atoms to hydrogen molecules on the electrode surface.

The term *electrocatalysis* was first used by Nikolai Kobozev in 1936, when little work was done as yet in electrocatalysis as we understand it today. Research in electrocatalysis was strongly stimulated in the early 1960s by efforts toward the development of various kinds of fuel cells. Studies were initiated on the various factors influencing the rates, not only of hydrogen evolution but also of other reactions, particularly cathodic oxygen reduction and the complete oxidation of simple organic substances ("fuels") to carbon dioxide. The term *electrocatalysis* began to be used in a universal fashion following publications of Thomas Grubb in which he showed that the electrochemical oxidation of hydrocarbons (methane, ethane, ethylene, etc.) is possible at platinum metal electrodes at temperatures below 150°C, in contrast to gas-phase oxidations, which at the same catalysts would proceed with perceptible rates only at temperatures above 250°C.

In 1965, synergistic (nonadditive) catalytic effects were discovered in electrochemical reactions. It was shown in particular that the electrochemical oxidation of methanol on a combined platinum–ruthenium catalyst will occur with rates two to three orders of magnitude higher than at pure platinum even though pure ruthenium is catalytically altogether inactive.

Appreciable interest was stirred by the sucessful use of nonmetallic catalysts such as oxides and organic metal complexes in electrochemical reactions. From 1968 on, work on the development of electrocatalysts on the basis of the mixed oxides of titanium and ruthenium led to the fabrication of active, low-wear electrodes for anodic chlorine evolution which under the designation "dimensionally stable anodes" (DSA) became a workhorse of the chlorine industry.

All these achievements were of great practical as well as theoretical importance and brought electrocatalysis into being as a separate branch of science.

28.1.2 Special Features of Electrocatalysis

Electrocatalytic reactions have much in common with ordinary (chemical) heterogeneous catalytic reactions, but electrocatalysis has certain characteristic special features:

1. The rate of an electrochemical reaction depends, not only on given system parameters (composition of the catalyst and electrolyte, temperature, state of the catalytic electrode surface) but also on electrode potential. The latter parameter has no analog in heterogeneous catalytic gas-phase reactions. Thus, in a given system, the potential can be varied by a few tenths of a volt, while as a result, the reaction rate will change by several orders of magnitude.
2. In electrochemical reactions, the catalyst surface is in contact not only with the reacting species but also with other species (i.e., the solvent molecules and the electrolyte ions), which in turn influence the properties of the surface and give rise to special reaction features.

3. In electrochemical systems, not only the reactant species but also electrons must be supplied to and/or withdrawn from the catalyst particles, since the electrons are directly involved in all electrochemical reactions.

28.1.3 Electrocatalysis and Electrochemical Kinetics

It is the basic task of electrochemical kinetics to establish the functional relations between the rate of an electrochemical reaction at a given electrode and the various external control parameters: the electrode potential, the reactant concentrations, the temperature, and so on. From an analysis of these relations, certain conclusions are drawn as to the reaction mechanism prevailing at a given electrode (the reaction pathway and the nature of the slow step).

In electrocatalysis, in contrast to electrochemical kinetics, the rate of an electrochemical reaction is examined at constant external control parameters so as to reveal the influence of the catalytic electrode (its nature, its surface state) on the rate constants in the kinetic equations.

Electrocatalytic effects cannot be studied in depth without a detailed knowledge of the kinetics and mechanism of the electrochemical reaction being examined. In fact, diverse effects can be exerted on the reaction:

1. An influence on the reaction pathway (i.e., on the nature and sequence of intermediate reaction steps)
2. An influence on the nature of the slow step (i.e., replacing a given slow step by a faster one)
3. A direct acceleration of the slow step and thus of the reaction as a whole

28.2 ELECTROCATALYSIS AND ADSORPTION EFFECTS

Like other heterogeneous chemical reactions, electrochemical reactions are always multistep reactions. Some intermediate steps may involve the adsorption or chemisorption of reactants, intermediates, or products. Adsorption processes as a rule have decisive influence on the rates of electrochemical processes.

To illustrate the influence exerted by the energy of adsorption of an intermediate on the rate of an electrocatalytic reaction, consider a very simple two-step reaction of the type $A \rightarrow X \rightarrow B$ where X, the intermediate, is reversibly adsorbed on the electrode (with a degree of surface coverage θ_X). For the sake of simplicity, the electrode surface will be assumed to be homogeneous (i.e., conditions of Langmuir adsorption hold), while the system lacks adsorbed species other than X. The rate, v_{ads}, of the adsorption step (the first step) is then proportional to the bulk concentration of the starting material, c_A, and to the free surface part $(1 - \theta_X)$ (the part not taken up by species X), while the rate of further transformation of intermediate X, v_{des}, which is tied to its desorption, will be proportional to the surface fraction, θ_X, taken up by it:

$$v_{ads} = k_{ads} c_A (1 - \theta_X) \quad \text{and} \quad v_{des} = k_{des} \theta_X. \tag{28.1}$$

In the steady state, the rates of adsorption and desorption are equal to each other and to the overall rate of this reaction: $v_r = v_{ads} = v_{des}$. For the steady-state value of surface coverage, this gives

$$\theta_X = \frac{k_{ads} c_A}{k_{ads} c_A + k_{des}}, \tag{28.2}$$

while the steady-state reaction rate (rate of formation of B), v_r, can be written as

$$v_r = \frac{k_{des} k_{ads} c_A}{k_{ads} c_A + k_{des}}. \tag{28.3}$$

The rate constants of the adsorption and desorption step, k_{ads} and k_{des}, depend on the energy, W, of bonding of the adsorbed species to the electrode surface. Higher bond energies imply that adsorption is facilitated and k_{ads} increases while k_{des} decreases. These functions can be formulated as

$$k_{ads} = B \exp\left(\frac{\gamma W}{RT}\right) \quad \text{and} \quad k_{des} = B' \exp\left(\frac{-\gamma W}{RT}\right). \tag{28.4}$$

One can see when putting these expressions into Eq. (28.3) that at low values of W when k_{ads} is small (and the overall reaction rate is limited by the first step), v_r increases with increasing W. At larger values of W, v_r increases more slowly and attains a maximum, then starts to decrease. At this point the overall reaction rate is then limited by the second step.

Thus, a plot of reaction rate against adsorption energy of the intermediate species is bell or volcano-shaped and has a distinct maximum. This bell-shaped relation between the rate of a catalytic chemical reaction and the adsorption energy of an intermediate was described first by Aleksei Balandin in the 1930s and is usually associated with his name. This basic relation is preserved in more complex situations when the simplifying assumptions made above no longer hold.

The reaction rate will be influenced not only by the surface concentration of reacting species but also by other factors, which may include the orientation of these species on the surface and their bonding to neighboring species. This implies that an analysis of electrocatalytic phenomena must include a full consideration of all features of adsorption.

28.3 METAL ELECTRODES: INFLUENCE OF THE NATURE OF THE METAL

28.3.1 Groups of Metals

Metal electrodes are the electrodes most commonly used on the cathodic side when conducting electrochemical reactions, in both the laboratory and in industry. On the

anodic side, their usefulness is restricted to the range of potentials where the metal undergoes neither dissolution nor oxidation. At more positive potentials a metal electrode may become covered by a thick oxide layer and will then essentially behave like an oxide electrode.

The catalytic activity of metals is correlated significantly with their position in the periodic table of the elements, since it depends on the electronic structure of the metal atoms. High catalytic activity is found in the transition metals or *d-metals*, metals consisting of atoms with unfilled *d*-electron shells. They include the metals of subgroups IVB to VIIIB in the periodic table, prominently the metals of the platinum and iron group but also such metals as vanadium, molybdenum, and manganese. The catalytic activity of *sp*-metals (i.e., nontransition metals from subgroups IB, IIB, IIIA, and IVA, including "mercury-like" metals such as cadmium, lead, and tin) is much lower, but since they exhibit high hydrogen overvoltage (and thus a low rate of hydrogen evolution), they are useful as cathode materials giving high yields in the electroreduction of organic substances (Tafel, 1898).

It must be pointed out that such a distinction between active transition metals and inactive nontransition metals is conditional and ambiguous. Thus, the degree of activity also depends on the nature of the electrochemical reaction. As an example, mercury, which ordinarily is regarded as a material lacking catalytic activity, is a highly active electrode catalyst for the reduction of oxygen to hydrogen peroxide [Eq. (15.21)]. It is more active than pyrolytic graphite, and possibly even more active than platinum (reliable data for this reaction at platinum are lacking).

Platinum and other metals of the platinum group are the most universal catalysts for many electrochemical reactions. They are stable over a wide range of potentials in most solutions, including strongly acidic and strongly alkaline solutions. Their activity as a rule is high in a variety of reactions.

Despite their high cost, they are used in industrial electrolyses, fuel cells, and many electrochemical devices. The large investments associated with platinum electrocatalysts usually are paid back by appreciably higher efficiencies.

Platinum is particularly convenient, too, for scientific studies of electrocatalytic phenomena, since its surface state (e.g., its degree of oxidation) is readily controlled and reproducible. It is easy to prepare in different degrees of dispersion.

In alkaline solutions, nickel electrodes are quite common, particularly when conducting cathodic reactions (hydrogen generation, the reduction of certain organic materials). They resist corrosion under these conditions. With certain precautions (taking care not to exceed the limits of potential), nickel electrodes in alkaline solutions are useful, too, for certain anodic reactions such as the oxidation of hydrogen and methanol.

Silver and gold, which are corrosion resistant in many solutions, are rather efficient catalysts for the cathodic reduction of oxygen and certain other reactions. Some *sp*-metals (mercury, tin, zinc) exhibit interesting catalytic properties for the cathodic reduction of CO_2. Copper might be a very interesting material for a number of electrochemical reactions, but so far has not been examined thoroughly.

28.3.2 Correlation Between Catalytic Activity of Metals and Their Bulk Properties

The scientific literature abounds in attempted correlations between the catalytic activities, A_{cat}, of a series of catalytic electrode metals and some set of bulk properties, X_{cat}, of these metals. Such correlations would help in understanding the essence of catalytic action and will enable a conscious selection of the most efficient catalysts for given electrochemical reactions.

Most of these studies, mainly in the period 1955 to 1970, have been concerned with cathodic hydrogen evolution. Different parameters characterizing the bulk properties of each metal have been adduced, including physical parameters such as electron work function, electrical conductivity, hardness, compressibility, temperature of evaporation, and heat of evaporation, and chemical parameters such as the affinity to hydrogen or oxygen.

Many of the parameters above are by themselves interrelated. Thus, the heat of sublimation characterizing the chemical bond strength in the crystal lattice correlates with the temperature of fusion and with the compressibility of a metal. Therefore, finding a correlation with a new parameter does not necessarily imply the gain of new, independent information concerning the nature of catalytic action.

For this reason, few of all these attempts to find a correlation have produced unambiguous results of scientific value. Often, this has been due to an unfortunate selection of numerical values for the parameters characterizing the catalytic activity, A_{cat}, and physicochemical property, X_{cat}, of the catalyst. Large differences exist between the numerical values determined or selected by different workers and different laboratories. On the experimental side, many factors, such as sample history, sample preparation, and measuring procedure, influence the results. A point of importance often underestimated is the degree of purity of the metal sample used in the tests, since slight traces of an alloying component or impurity often have a strong effect on the parameters of a metal. These critical points notwithstanding, a number of interesting results have been obtained in these attempts at establishing correlations.

28.3.3 Criteria for Catalytic Activity

Selecting a rigorous and convenient quantitative parameter characterizing the catalytic activity, A_{cat}, is of prime importance when studying electrocatalytic phenomena and processes. The parameter usually selected is the current density, i (in A/cm^2), at a specified value of electrode potential, E. The current density is referred to the electrode's true working surface area [which can be measured by the Brunauer–Emmett–Teller (BET) or other methods]. Closely related to this "true" current density is another parameter, known as the *turnover number* γ (in s^{-1}), and indicating the number of elementary reaction acts performed or number of electrons transferred in unit time per surface atom (or catalytic surface site) of the catalyst.

Difficulties can arise when comparing the catalytic activities of different electrodes where slopes b of the plots of current (or logarithm of current) against potential are different. The schematic plots of log i vs. ΔE shown in Fig. 28.1 refer to the

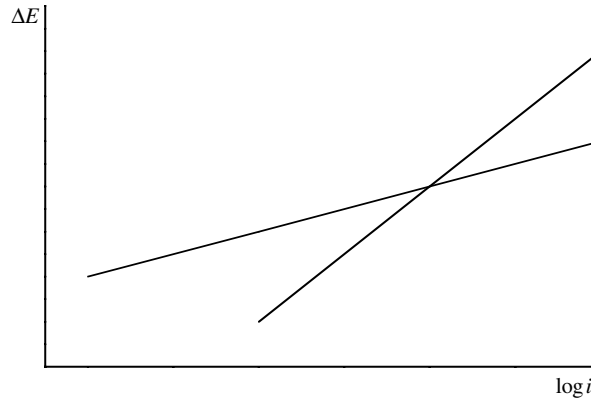

FIGURE 28.1 Relative reaction rates for a reaction with different Tafel slopes at two different electrodes.

same reaction occurring at two different catalytic electrodes and have different slopes b. It is evident that different regions of potential are associated with different relative reaction rates, to the extent that in one region the first, and in the other region the second, electrode is more active. In such a case, the catalytic activity becomes a relative concept tied to the potential, E_{comp}, at which comparison is made. The selection of appropriate potentials E_{comp} is a fundamental question, since many factors influencing the reaction rate depend on this potential.

Often, it will be found that currents for a given reaction cannot be measured at all metals at the same value of potential. At some metals the currents would be too low for a reliable, sufficiently accurate determination; at others they might be too high for a satisfactory experimental realization. A comparison will then be possible only after an extrapolation of data obtained in a different region of potentials, to the value of E_{comp} selected for comparison. This extrapolation may not be sufficiently reliable where the Tafel section of the polarization curve is too short or indistinct.

Often, the equilibrium potential of a given reaction is selected as E_{comp}, which implies that exchange current densities i^0 usually obtained by extrapolating the experimental log i vs. ΔE curves to $\Delta E = 0$ are compared.

28.3.4 Correlation with the Electron Work Function

The values of electron work function λ^0 (see Section 9.2.1) have been adduced most often when correlating electrocatalytic activities of given metals. They are situated between 3 and 5 eV. Two points were considered when selecting the electron work function as the parameter of comparison: (1) it characterizes the energy of the electrons as basic, independent components of all electrochemical reactions, and (2) it is closely related to many other parameters of metals.

It has sometimes been suggested that the rate of cathodic reactions (in which electrons are transferred from the metal to a reacting species) should be higher the lower

the work function (i.e., the easier it is to extract electrons from the metal), and vice versa, the rate of anodic reactions in which electrons are transferred in the opposite direction should be lower the lower the work function. Kinetic equations explicitly containing λ^0 have even been formulated.

It is readily shown, however, that such primitive conclusions generally are not valid. In fact, the energetic situation relevant for an electrochemical reaction depends not on the work associated with transferring an electron into vacuum (the work function), but rather, transferring the electron to that point in the electrolyte solution where the reacting species is located. A substantial difference exists between the work functions into vacuum (λ^0) and into a solution (λ^E). It had been shown in Section 9.2.2 that the work functions into solutions when compared between different metals, all at one and the same electrode potential (e.g., E_{comp}), have identical values. In other words, the electron work function into solutions is independent of the metal; it has the same value for all metals at any given electrode potential. Thus, the work of extracting an electron from the metal into vacuum, λ^0, is irrelevant for the energetic situation of electrochemical reactions; it should not influence their rates directly, and it should not appear explicitly in the kinetic equations.

It was demonstrated, however, in 1947 by John O'M. Bockris that between the exchange current densities of the hydrogen reaction at different metals and the values of the electron work function (into vacuum), a definite correlation does exist. Many workers have confirmed this correlation. An example of this correlation is shown as a plot of log i^0 vs. λ^0 in Fig. 28.2.

Two distinct linear and parallel relations are seen: one (to the left) for metals for which the surface charge, $Q_{S,M}$, is positive, and another (to the right) for metals for

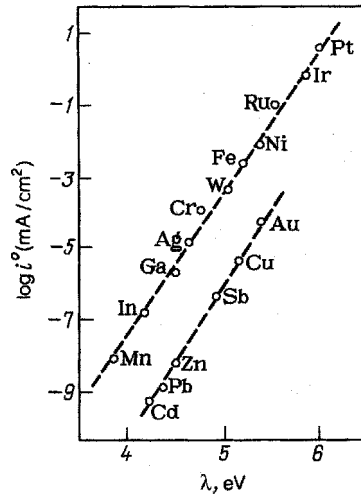

FIGURE 28.2 Relation between the exchange current densities of hydrogen evolution and ionization at different metals and the electron work functions.

which $Q_{S,M}$ is negative. The 0.4-eV difference between the two straight lines is due to a different orientation of the water molecules on positively and negatively charged surfaces.

The figure shows that the increase in exchange current density by 10 orders of magnitude (from mercury and cadmium to platinum) is attended by (not caused by) an increase in work function from 4 eV to 5 eV. This relationship only extends to metals having a work function in this limited range of values of λ^0. It was shown later that if lanthanides (*f*-metals) are included for which the work function has values between 3 and 3.5 eV and for which the exchange current densities are lower than at many *sp*-metals, a plot of log i^0 vs. λ^0 is bell shaped and goes through a maximum approximately at $\lambda^0 = 4$ eV. A detailed analysis of the correlation between the catalytic activities of many metals and their work function values can be found in papers by Sergio Trasatti (1977).

28.3.5 Correlation with the Bond Energy of Intermediates

Adsorbed atomic hydrogen is the intermediate species in cathodic hydrogen evolution. It was shown in 1935 by Juro Horiuti and Michael Polanyi that the bond energy, $W_{M\text{-}H}$, of hydrogen atoms with the metal surface is the chief parameter determining the energy of activation in the step of proton discharge. Roger Parsons and Heinz Gerischer pointed out in 1958 that a "bell-shaped" relation similar to that described in Section 28.2 should exist between the rate of cathodic hydrogen evolution and the values of $W_{M\text{-}H}$.

The lack of accurate data for the bond energies of atomic hydrogen on many metals so far does not allow reliable relationships to be formulated between the exchange current densities of hydrogen evolution and this bond energy. At the transition metals, this bond energy is determined from the heat evolved upon the adsorption of hydrogen gas. The values thus determined are between 200 and 300 kJ/mol (higher values are found at metals taking hydrogen up into their bulk, such as titanium).

For *sp*-metals, bond energies cannot be measured in this way, since the heat evolved during hydrogen adsorption is very small. Therefore, in 1965, Lev Krishtalik suggested to find the hydrogen-bond energies at *sp*-metals by measuring the activation energy of hydrogen evolution in the region of barrierless discharge (where the activation energy coincides with the bond energy). In this way a value of 160 to 170 kJ/mol was found for silver and a value of 120 kJ/mol for cadmium.

One of the many published correlations between the logarithms of exchange current density of the hydrogen reaction at different metals and the values of hydrogen-bond energy on the same metals is reported in Fig. 28.3. Considering all the points mentioned, one can certainly conclude that a certain bell shape does exist in this plot, but it would not be justified to draw any quantitative conclusions going beyond this assertion (Petrii and Tsirlina, 1994).

Summarizing the discussion above, we can only say that all the relations observed experimentally between the parameters of catalytic activity of metals and parameters of their physicochemical bulk properties are secondary. The primary factor influencing the catalytic activity of all metals and most of their physicochemical parameters are

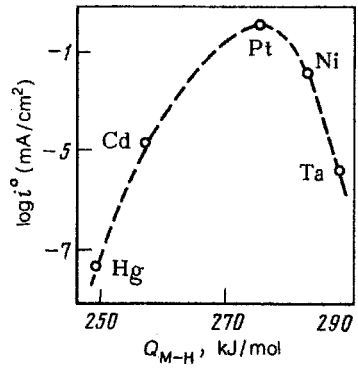

FIGURE 28.3 Plot of the exchange current densities of hydrogen evolution and ionization at different metals against the bond energy between the metal and atomic hydrogen.

the special features of electron structure of their atoms, which in turn are related to their atomic number (i.e., their position in the periodic table).

A very important criterion for electron structure is the *percent d-character*, which characterizes the number of unpaired electrons in the *d*-orbitals of the individual metal atom. Because of the vacancies existing in these orbitals, metals will interact with electron-donating species forming electron pairs. It is this interaction that determines the special features of adsorption of these species and, as a consequence, the catalytic activity of a given metal.

28.4 METAL ELECTRODES: INFLUENCE OF SURFACE STATE AND STRUCTURE

The catalytic activity of an electrode is determined not only by the nature of the electrode metal (its bulk properties) but also by the composition and structure of the surface on which the electrochemical reaction takes place. These parameters, in turn, depend on factors such as the method of electrode preparation, the methods of surface pretreatment, conditions of storage, and others, all having little effect on the bulk properties.

When studying the influence of the various surface factors, the following points generally are difficult to control: (1) Preparation of a surface having given properties, (2) the unambiguous qualitative and quantitative identification of structural surface parameters, and (3) conservation of a given structure when considering the changes that might occur not only during preparation and pretreatment but also during the measurements themselves.

The major factors that characterize the structure and state of catalyst surfaces and may influence their activity are the crystallographic orientation of the surface and of its individual segments, the presence of structural defects of different kinds or of

points (*active sites*) with special properties, and the presence of accidental or consciously added traces of foreign matter.

28.4.1 Influence of Crystallographic Surface Structure

Approximately up to the mid-1960s, electrochemical measurements were made at polycrystalline electrodes, either smooth sheets of metal or metal deposits on a suitable conducting substrate. The surface structure of these electrodes was disordered and in most cases unknown in detail. The interest then shifted to electrodes having a more highly ordered and controlled surface structure, particularly to individual single-crystal faces of metals. The first single-crystal electrodes studied (Piontelli et al., 1961) were of zinc, cadmium, gold, lead, and other *sp*-metals. In those first efforts, difficulties still existed with imperfections of the single-crystal surfaces, with methods to unambiguously identify the crystal orientation and cleanness of a given face and secure absence of fragments of foreign faces.

The early technology used to prepare single-crystal electrodes was very laborious. Relatively large single crystals were grown by slow crystallization of a molten metal and subsequent cutting of these crystals at angles rigorously controlled relative to the crystallographic axes.

The methods of X-ray diffraction usually were used to determine the orientation of crystal faces. Low-energy electron diffraction (LEED) gives more accurate results. However, such measurements provide an exact characterization only of the initial surface state of the electrodes. It is more difficult to determine the surface state after the electrochemical studies, and even more so during these studies.

Many studies at single-crystal electrodes of *sp*-metals were directed at the special features of double-layer structure and the potential of zero charge at the various single-crystal faces. It was shown that rather large differences could exist between the potentials of zero charge of different faces (see Table 10.1).

The platinum-group metals that are of particular interest with respect to electrocatalytic phenomena have high melting points, and growing good single crystals proved to be quite difficult. In 1980, Jean Clavilier suggested a different way of preparing single-crystal electrodes. The end of a polycrystalline wire of the metal is fused in the flame of a burner and is then allowed to cool down slowly in a hydrogen atmosphere. The small spherical electrodes thus obtained have an almost perfect single-crystalline structure. This method was found to be feasible for platinum-metal electrodes. Because of its simplicity, this method is now widely used.

With the introduction of this method and with further improvements in classical ways of growing single crystals, the studies on individual single-crystal faces expanded rapidly. Many hundred papers relating to such electrodes have been published since the 1970s.

It was quickly seen from studies on platinum single crystals that voltammograms for hydrogen adsorption and desorption differ somewhat among the different faces and between the single-crystal faces and polycrystalline platinum. Despite these differences, though, they have common traits as well. The areas under these curves,

which represent the total amount of adsorbed hydrogen, are almost identical for all faces and correspond to one hydrogen atom per surface atom of platinum.

Further studies showed that more basic differences in the behavior of the individual faces of platinum single crystals are possible in the adsorption of other substances. For instance, data for the (100) face of platinum indicate that CO is adsorbed predominantly in a bridged position involving simultaneous bonding to two platinum surface atoms, while on the (110) face CO is adsorbed in a linear (standing) orientation involving bonding to a single surface atom.

Many data concerning the influence of face structure on the rate of electrocatalytic reactions appear contradictory. They demonstrate that such an influence does exist, but as a rule, all these effects are highly specific, and the rules found for a given reaction differ from those holding for another reaction.

For a given reaction conducted at different metals, according to the literature, the order of decreasing catalytic activity of the faces will not be the same; for instance, for cathodic hydrogen evolution at gold the order is $(110) > (100) > (111)$, at tungsten it is $(111) > (110) > (100)$. Moreover, for a given reaction at a given metal, this order may depend on the composition of the electrolyte solution and on the experimental conditions. Thus, for cathodic oxygen reduction at platinum single crystals, the order is $(111) > (110) > (100)$ in alkaline solution, $(110) > (111) > (100)$ in perchloric acid solution, and because of the interfering influence of anion adsorption, $(110) > (100) > (111)$ in sulfuric acid solution.

The differences between faces usually are small. The reaction rates observed at the different faces as a rule are of the same order of magnitude and differ by no more than a factor of 3 to 5. Significant catalytic effects where one of the faces is tens of times more (or less) active than the other single-crystal faces of the same metal are rare. One of the few examples is the reduction of CO_2 on platinum which occurs with the formation of a strongly bound chemisorbed product (called *reduced* CO_2). At the (111) face, this reaction is many times slower than at the other faces [some workers even believe that it does not occur at all at the (111) face].

It is very difficult in view of the vast amount of experimental data to draw general conclusions that would hold for different, let alone all electrocatalytic systems. The crystallographic orientation of the surface undoubtedly has some specific influence on adsorption processes and on the electrochemical reaction rates, but this influence is rather small. It can merely be asserted that the presence of a particular surface orientation is not the decisive factor for high catalytic activity of a given electrode surface.

The question arises in view of this conclusion: whether surface crystallinity (or any regular surface structure) is needed at all for catalytic action. An answer to this question can be obtained by studies on electrodes having an amorphous surface (i.e., a surface bare of any structural regularity). There has been some interest in studies of this kind in recent years. An ideal electrode having an amorphous surface is mercury (or any other electrode consisting of a liquid or molten metal). Cathodic hydrogen evolution is very slow at mercury, but this is not significant per se, since at a solid lead electrode having a crystalline surface, it is even slower. On the other hand, the two-electron reduction of molecular oxygen to hydrogen peroxide in alkaline

solution is much faster at mercury electrodes than at many metal electrodes having a crystalline surface. Thus, at least for this reaction, the presence of crystal structure is not indispensable for high catalytic activity.

It is of interest from this point of view to compare results obtained at a given metal in the liquid and solid form. Such studies are possible at gallium electrodes (with a melting point of about 30°C). Experiments have shown that at solid gallium at +28°C, cathodic hydrogen evolution is about two to four times faster than at liquid gallium at +32°C (Pris et al., 1966). Thus, in this example an effect of crystallinity can be seen, but is quite insignificant. Unfortunately, hardly any data from analogous measurements at other metals (e.g., involving high-temperature electrocatalytic reactions) are available.

Recently, data for the behavior of solid metal electrodes having an amorphous surface structure have become available. Such electrodes can be prepared in different ways. From certain alloys of metals with nonmetals (e.g., $Fe_{60}Co_{20}Si_{10}B_{10}$), amorphous electrodes can be prepared by fast quenching or by vacuum evaporation and condensation on a cooled substrate. Single-component amorphous metals can be obained by implantation of the proper ions or by implantation of inert-gas ions. It must be pointed out, however, that solid amorphous structures are highly unstable and readily undergo recrystallization. Some positive or negative effects are sometimes seen when studying such electrodes, but despite the numerous experimental data that exist, it is once more impossible to draw any convincing and unambiguous conclusions as to any special catalytic features that might exist.

28.4.2 The Problem of Active Sites

As early as 1925, Hugh S. Taylor suggested that in heterogeneous catalytic reactions, not the entire catalyst surface is involved but the reaction occurs predominantly at certain special points or segments of the surface that he named *active sites*. Since that time, the presence of special points or segments with higher catalytic activity has been asserted not only for heterogeneous chemical reactions but also for electrochemical reactions.

These special points have been associated with special topographical features of the catalyst surface: for instance, a specific position of surface atoms at edges, vertices, or steps in the crystal lattice on the catalyst surface rather than the more abundant positions on the crystal faces. A higher coordination of individual surface atoms may also be important; sometimes the *B5 sites*, where adsorbed species are surrounded by five surface atoms, are regarded as particularly active. On high-index faces of crystallites, the numerous lattice steps present there could be the special points. Special activity is often attributed to lattice defects such as dislocations, kinks, vacancies, stacking faults, and intergrain boundaries emerging at the crystal surface.

There is no doubt that all the special sites listed above might have adsorptive and other properties differing from those of "normal" surface atoms. For this reason the rate of an electrochemical reaction could be higher or lower at such sites. The sign and magnitude of the overall effect depends on the relative numbers of special points and "normal" surface atoms.

On metal electrodes having coarse-crystalline structure, the number of special crystal sites (vertices, edges) is small relative to the total number of all surface atoms, so that their (positive or negative) contribution to the overall rate must be quite small. At highly disperse, fine-crystalline deposits, however, the situation is different. Here special effects are really observed; they are considered in more detail in Section 28.5.4.

At smooth metal electrodes that have been subjected to annealing, the number of different crystallographic defects (dislocations, kinks, etc.) emerging at the surface is between 10^9 and $10^{13}\,cm^{-2}$. This number is small relative to the total number of surface atoms (which is on the order of $10^{15}\,cm^{-2}$). In the literature, attempts have been described to determine the catalytic activity of electrodes having an artificially boosted number of surface defects. These experiments gave no unambiguous results; in some cases some increase, in other cases some decrease in activity was observed.

In conclusion, therefore, at least for metal catalysts it will not be justified to identify crystallographic defects emerging at the electrode surface with the active sites responsible for the catalytic activity of the electrode as a whole.

28.4.3 Influence of Surface Impurities

Almost always, foreign species not involved in a given electrochemical reaction are present on the surface of catalytic electrodes. In some cases these species can have a strong or even decisive effect on reaction rate. They may arrive by chance, or they can be consciously introduced into the electrocatalytic system to accelerate (promoters) or retard (inhibitors) a particular electrochemical reaction relative to others.

Accidental surface impurities can have most diverse origins. On the surfaces of smooth metal electrodes obtained by metallurgical methods, one almost always finds carbon species produced by thermal destruction of organic material that had somehow arrived on the surface. Often, impurities arrive on an electrode surface when it comes into contact with an insufficiently purified electrolyte.

On the surface of metal electrodes, one also finds almost always some kind or other of adsorbed oxygen or phase oxide layer produced by interaction with the surrounding air (air-oxidized electrodes). The adsorption of foreign matter on an electrode surface as a rule leads to a lower catalytic activity. In some cases this effect may be very pronounced. For instance, the adsorption of mercury ions, arsenic compounds, or carbon monoxide on platinum electrodes leads to a strong decrease (and sometimes total suppression) of their catalytic activity toward many reactions. These substances then are spoken of as catalyst poisons. The reasons for retardation of a reaction by such poisons most often reside in an adsorptive displacement of the reaction components from the electrode surface by adsorption of the foreign species.

In some cases, adsorbed foreign species may give rise to acceleration of a reaction. In the literature, a few cases have been described where strong "catalytic effects" were observed on catalytically inactive electrodes when small amounts of platinum species that had by accident arrived in the electrolyte solution became adsorbed on their surface.

Methods exist to remove undesired impurities from the surface, but it is preferable in electrocatalytic experiments to reduce chances that such impurities reach the

surface, by selecting the appropriate experimental conditions. At platinum electrodes, good results of surface purification are attained by multistep anodic and cathodic activation. In a pure sulfuric acid solution, the electrode is first held for a few minutes at a potential of about 1.2 V (RHE). At this potential most organic substances are oxidized and desorbed from the electrode surface. For the reduction of adsorbed oxygen, the electrode is then held at a potential somewhat more negative than 0 V (RHE). Finally, excess adsorbed hydrogen is removed by holding the electrode at a potential of about 0.3 V (RHE).

A radical approach serving to remove all impurities from the electrode surface is that of slicing away a thin layer of metal right during the measurements (i.e., without withdrawing the electrode from the solution or breaking its polarizing circuit). Sometimes, bombardment of the surface with an ion beam is used for a similarly radical surface purification.

28.5 HIGHLY DISPERSE METAL CATALYSTS

For higher efficiency in catalytic action and smaller quantitative needs, the catalysts often are used in a highly disperse state. An important practical criterion for such catalysts is the specific reaction rate [i.e., the reaction rate per unit mass of the catalyst (A/g)].

Most often, these disperse metal catalysts are supported by an electronically conducting substrate or carrier that should provide for uniform supply or withdrawal of electrons (current) to or from all catalyst crystallites. The substrate should also serve to stabilize the disperse state of the catalyst and retard any spontaneous coarsening of the catalyst crystallites. Two situations are to be distinguished: (1) the disperse metal catalyst is applied to a substrate consisting of the same metal, and (2) it is applied to a chemically different substrate (a foreign substrate). Platinized platinum is a typical example of the former situation.

28.5.1 Methods for Preparing Electrodes with Disperse Catalysts

Different ways exist to prepare electrodes with highly disperse metal catalysts and lead to the corresponding electrode varieties.

Formation of the Electrode from Highly Disperse Metal Powders The first step in making such an electrode is the preparation of the catalyst itself in a highly disperse (powdered) state. Metal powders can be made by thermal decomposition of oxides and certain other compounds of the given metal: for instance, of platinum dioxide, PtO_2 (the method of Roger Adams) or gaseous nickel pentacarbonyl, $Ni(CO)_5$. Metal powders can be precipitated from the corresponding metal salt solutions when a suitable reducing agent is present. Highly disperse metal powders (e.g., of nickel) can be obtained from their alloys with aluminum by a method suggested in 1925 by Murray Raney. When such an alloy is treated with a hot alkaline solution, the aluminum is leached out, leaving a fine skeleton of the base metal called *skeleton* or *Raney nickel*.

These highly disperse metal powders are very active chemically, and hence unstable; they readily aggregate to coarser particles, and readily oxidize when in contact with air. Their stability rises significantly when they have been applied to a suitable substrate.

The second step is the preparation of mechanically strong, conveniently manipulated electrodes from the powder. To this end the powders are pressed or rolled or applied as a paste to a conducting substrate. Special binders as well as a simultaneous or subsequent thermal treatment can be used to enhance the strength. Conductive fillers can be added to the electrode to provide enhanced conductivity.

Direct Chemical or Electrochemical Deposition of the Disperse Catalyst This method of direct deposition from a solution of its salt on a suitable conducting substrate is simpler and more practical than the preparation of electrodes from the finished powders. It has the merit of being able to provide better contact between the catalyst and substrate, and multicomponent metal catalysts can be deposited from a solution containing a mixture of salts of several metals.

Combined Method In this method the catalyst (e.g., platinum) is first applied to carbon black (or other highly disperse first substrate), and the platinized carbon black is then applied to a heavier second substrate providing for the required rigidity and strength of the electrode. In the first fuel cells developed in the 1960s and 1970s, the disperse platinum catalyst was used as such, which led to high platinum loadings. With carbon black as a first substrate, platinum catalyst loadings in the electrodes of hydrogen–oxygen fuel cells could be reduced from 4–6 mg/cm^2 to tenths of mg/cm^2 without loss (or even with a gain) in performance (Gottesfeld and Zawodzinski, 1997).

Incorporation into a Polymer Layer In recent years a new electrode type is investigated which represents a layer of conducting polymer (such as polyaniline) into which a metal catalyst is incorporated by chemical or electrochemical deposition. In some cases the specific catalytic activity of the platinum crystallites incorporated into the polymer layer was found to be higher than that of ordinary dispersed platinum, probably because of special structural features of the platinum crystallites produced within the polymer matrix. A variant of this approach is that of incorporating the disperse catalyst directly into the surface layer of a solid polymer electrolyte.

28.5.2 Crystallite Size and Specific Surface Area

As a rule, the dispersed catalysts are polydisperse (i.e., contain crystallites and/or crystalline aggregates of different sizes and shapes). For particles of irregular shape, the concept of (linear) size is indefinite. For such a particle, the diameter d of a sphere of the same volume or number of metal atoms may serve as a measure of particle size.

The specific surface area of an ideal, monodisperse catalyst per unit of its mass is related to its diameter d as $S = 6/\rho d$, where ρ is the density. In the case of platinum,

a particle diameter of 5 nm corresponds to a specific surface area of 56 m^2/g. With a particle size of 2.2 nm, the largest specific surface area, of 127 m^2/g, attainable with platinum is reached. At this crystallite diameter all platinum atoms of a particle are surface atoms (i.e., the particle contains no "inert" bulk atoms). The specific surface area of disperse catalysts can be measured quite accurately by low-temperature nitrogen or helium adsorption (the BET method) or, in the case of platinum, in terms of the amount of charge consumed for the electrochemical adsorption or desorption of a monolayer of hydrogen atoms (see Section 10.5.2).

28.5.3 Macrokinetic Limitations in Electrodes with Disperse Catalyst

Experience has shown that the specific or "intrinsic" catalytic activity of electrodes with disperse metal catalysts when referred to the true working surface area often remains below that of smooth (compact) electrodes consisting of the same metal. Of course, owing to the large increase in total working surface area, the overall reaction rate is larger, but as a rule it is not larger by the expected factor of γ.

One of the main reasons for a lower specific activity resides in the fact that electrodes with disperse catalysts have a porous structure. In the electrolyte filling the pores, ohmic potential gradients develop; and because of slow diffusion, concentration gradients of the reacting species also develop. In the disperse catalysts, additional ohmic losses will occur at the points of contact between the individual crystallites and at their points of contact with the substrate. These effects produce a nonuniform current distribution over the inner surface area of the electrode and a lower overall reaction rate.

Another factor producing an apparent decrease in the activity of disperse catalysts is steric hindrance. In reactions involving relatively large molecules, not all of the inner surface area of the catalyst may by accessible for these molecules, so that the true working surface area is smaller than that measured by BET or hydrogen adsorption.

Apart from these macrokinetic limitations, two more effects exist that may influence the overall electrochemical characteristics of an electrode with disperse catalyst in the positive or negative direction: (1) an influence of the crystallite size itself on the intrinsic catalytic activity (Section 28.5.4) and (2) an influence of the catalyst substrate (Section 28.5.5). These two effects have great importance for the practical use of disperse catalysts and for the theoretical analysis of electrocatalytic effects.

28.5.4 Influence of Catalyst Crystallite Size

It was found in studies of methanol oxidation (Khazova, 1967) that the specific rate of this reaction at platinized platinum (per unit area of the catalyst's true working surface area) was one to two orders of magnitude smaller than at smooth platinum. This difference in rates was seen at all values of potential (Fig. 28.4), including those more negative than 0.5 V, where methanol adsorption on platinum is the rate-limiting step. This slow rate of the adsorption and reaction of methanol at platinized platinum is not the result of the foregoing macrokinetic factors. In fact, adsorption on platinized

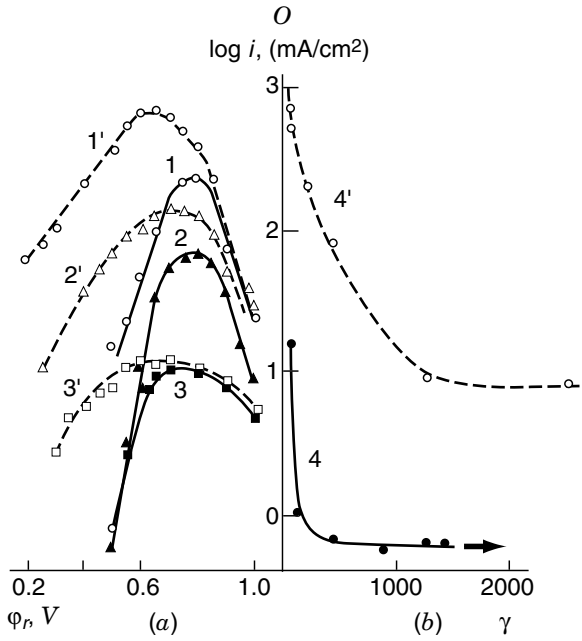

FIGURE 28.4 (*a*) Dependence on potential of the rates of methanol adsorption (1′–4′) and oxidation (1–4) on smooth platinum $\gamma \sim 3$ (1–1′) and on platinized platinum with a roughness factor $\gamma = 400$ (2–2′) and $\gamma = 1200$ (3–3′) from a solution of 1 *M* CH_3OH = 0.5 *M* H_2SO_4; (*b*) dependence of this rate on the roughness factor γ of platinum at the potential $E_r = 0.5$ V (RHE). (From Khazova et al., 1967.)

platinum is slow upon admission of the very first quantities of methanol, when concentration gradients cannot have developed as yet and when, owing to the small currents, potential gradients will practically not exist in the catalyst pores.

Similar size effects have been observed in some other electrochemical systems, but by far not in all of them. At platinized platinum, the rate of hydrogen ionization and evolution is approximately an order of magnitude lower than at smooth platinum. Yet in the literature, examples can be found where such a size effect is absent or where it is in the opposite direction. In cathodic oxygen reduction at platinum and at silver, there is little difference in the reaction rates between smooth and disperse electrodes. In methanol oxidation at nickel electrodes in alkaline solution, the reaction rate increases markedly with increasing degree of dispersion of the nickel powders. Such size effects have been reported in many papers and were the subject of reviews (Kinoshita, 1982; Mukerjee, 1990).

For the size effects, several possible reasons are discussed:

1. Special topographic features of the surfaces of small crystallites. The smaller the size of a crystallite, the larger will be the relative fraction of "special"

sites (edges, vertices) on its surface. This becomes particularly important with crystallites measuring less than 10 nm, where the number of "normal" sites becomes small compared to that of "special" sites having a catalytic activity that can be larger or smaller.

2. Reactions involving large (e.g., organic) molecules require a certain coordination between several closely spaced surface sites. The smaller the crystallite, the smaller will be the probability of finding segments offering a favorable coordination.
3. Differences in the parameters of the electron gas between fine crystallites and the compact metal or large crystals.
4. According to EXAFS experiments, the number of oxygen atoms relative to metal atoms in the air-oxidized state is much higher in fine crystallites than in large crystals, so that their behavior approaches that of oxides.

28.5.5 Influence of the Catalyst Substrate

Experimental observations exist according to which a foreign substrate may influence the catalytic properties of the microcrystalline metal supported by it, and the supported metal conversely may influence the catalytic properties of the substrate.

A quantitative investigation of the influence exerted by a substrate on the properties of disperse catalysts is hampered by the distorting effects of many other factors, particularly the macrokinetic limitations and the size effects mentioned in Section 28.5.4.

It was found in the 1960s that disperse platinum catalyst supported by certain oxides will in a number of cases be more active than a similar catalyst supported by carbon black or other carbon carrier. At platinum deposits on a mixed carrier of WO_3 and carbon black, hydrogen oxidation is markedly accelerated in acidic solutions (Hobbs and Tseung, 1966). This could be due to a partial spillover of hydrogen from platinum to the oxide and formation of a tungsten bronze, H_xWO_3 ($0 < x < 1$), which according to certain data has fair catalytic properties.

It was seen when studying mixed systems Pt–WO_3/C and Pt–TiO_2/C that with increasing percentage of oxide in the substrate mix the working surface area of the platinum crystallites increases, and the catalytic activity for methanol oxidation increases accordingly. With a support of molybdenum oxide on carbon black, the activity of supported platinum catalyst for methanol oxidation comes close to that of the mixed platinum–ruthenium catalyst.

28.6 BINARY AND MULTICOMPONENT METAL CATALYSTS

The search for new, more highly active and less expensive materials for catalytic electrodes and the attempts at reducing the loading of expensive platinum catalysts has led to numerous studies in the area of binary and multicomponent metal systems. These included various metal alloys as well as mixed microdeposits containing several

metals. A peculiar binary system are electrodes with adatoms on their surface, isolated foreign metal atoms adsorbed on the surface of a given metal.

28.6.1 Metal Alloys

Electrodes of metal alloys can be made, either metallurgically (from melts of the individual alloy components) or by the joint chemical or electrochemical deposition of several metals from combined solutions of their salts. More detailed studies have been performed with metallurgical alloys of metals of the platinum group with metals of group IB of the periodic table. Alloys Pt–Au are homogeneous up to 19 atom % of Pt or 5 atom % of Au, and otherwise constitute heterogeneous mixtures of two phases, one platinum-rich (α_1) and one gold-rich (α_2). Hydrogen ionization proceeds only at the platinum-rich phase; it does not proceed at pure gold or at the gold-rich phase. However, at pure gold, even small α_1-phase impurities produce an appreciable increase in the current of hydrogen ionization.

Metallurgical palladium–ruthenium alloys are of interest insofar as at a component ratio of 40% Ru and 60% Pd, hydrogen is adsorbed as on pure Pd, and oxygen is adsorbed as on pure Ru. The overvoltage for hydrogen evolution at this alloy is just as low as it is at Pd, that for oxygen evolution is as low as it is at Ru.

Considerable efforts were expended in studies of binary and multicomponent metal electrodes obtained by the joint chemical or electrochemical deposition from solutions. At such electrodes, the effects arising from alloy composition are superimposed on the size effects arising from the disperse state of the catalyst. In the studies of disperse binary systems, the phase composition has often remained unknown. Depending on the method of preparation, one might obtain samples that have a phase composition corresponding to the equilibrium phase diagram, or metastable samples sometimes undergoing restructuring during their storage and use (catalyst aging). For all these reasons the results obtained for the behavior of codeposited multicomponent metal catalysts sometimes differ from those for analogous catalysts obtained by metallurgical methods.

A general problem existing with all multicomponent catalysts is the fact that their catalytic activity depends not on the component ratio in the bulk of the electrode but on that in the surface layer, which owing to the preferential dissolution of certain components, may vary in time or as a result of certain electrode pretreatments. The same holds for the phase composition of the surface layer, which may well be different from that in the bulk alloy. It is for this reason that numerous attempts at correlating the catalytic activities of alloys and other binary systems with their bulk properties proved futile.

In the late 1960s it was discovered (Entina, 1968; Binder et al., 1972) that a strong synergy effect exists in the platinum–ruthenium system. Alloys of these two metals are two to three orders of magnitude more active catalytically for the anodic oxidation of methanol than pure platinum, whereas pure ruthenium is altogether inactive for this reaction. Prolonged exploitation of such anodes is attended by a gradual decrease in catalytic activity of the alloys because of slow anodic dissolution of ruthenium from the surface layer. A similar situation is seen for platinum–tin alloys, which

are highly active toward methanol oxidation, too, but are even less stable in time, owing to tin dissolution from the surface layer.

The Pt–Ru catalysts have another important property. In contrast to pure platinum, they are almost insensitive to poisoning by carbon monoxide CO. They can be used, therefore, in the hydrogen electrodes of hydrogen–oxygen fuel cells operated with technical hydrogen containing marked amounts of CO.

The synergistic effect seen in Pt–Ru alloys has aroused great interest, since it opened perspectives for their use in efficient methanol fuel cells. Many studies were performed to elucidate the origins of this effect. Some workers believe that it is due to changes in the electron structure of platinum upon alloy formation with ruthenium. A popular interpretation is the *bifunctional mechanism*, according to which the organic species are preferentially chemisorbed on platinum sites while the ruthenium sites facilitate the adsorption of the OH_{ads} species needed for oxidation of the organic species.

At joint electrolytic deposits of platinum with chromium, nickel, or cobalt, the polarization of an oygen electrode at intermediate current densities is about 50 to 80 mV lower than at pure platinum. This is a much smaller effect than that of Pt–Ru alloys described above, yet it is of great practical value inasmuch as high polarization of oxygen electrodes leads to considerable energy losses in a number of electrochemical industries. Here the effect was explained in terms of changes in the distance between neighboring Pt atoms in the alloy as well as with changes in the electron structure of Pt when alloyed with ruthenium.

28.6.2 Adatoms

Very peculiar catalytic effects have been detected on metal electrodes with surfaces modified by adatoms (Watanabe and Motoo, 1975). Adatoms is the name given to submonolayer amounts of atoms of a foreign metal adsorbed on the surface of a given metal (see Kokkinidis, 1986). Adatoms are formed by specific adsorption and partial charge transfer when the metal electrode is immersed into a solution of salt of a foreign metal. They can also be formed by electrochemical deposition of the foreign metal at a potential somewhat more positive than the equilibrium potential of this foreign metal [i.e., at a potential where phase layers of the foreign metal cannot yet be deposited (*underpotential deposition*)]. Because of this partial charge transfer, the adatoms have an effective charge intermediate between that (zero) of a neutral atom and that of the foreign metal ion in the solution; hence, one could also use the term *adions*. The intermediate charge value depends on the potential of the electrode; it will be smaller (less positive) the more negative the potential. At sufficiently positive potentials, the adatoms will be oxidized and become desorbed from the surface as normal ions.

Adatoms produce a strong change in catalytic properties of the metal on which they are adsorbed. These catalytic effects are highly specific. They depend both on the nature of the metal and on the nature of the adatoms; they also depend on the nature of the electrochemical reaction. For instance, tin adatoms on platinum strongly (by more than two orders of magnitude) enhance the rate of anodic methanol oxidation,

while tin adatoms on palladium rather strongly depress the rate of this reaction. Lead adatoms on platinum inhibit methanol oxidation. Lead adatoms on platinum and palladium strongly enhance the rate of formic acid oxidation.

In view of their highly diverse catalytic effects, adatoms have been the subject of numerous scientific studies. The catalytic activity of the adatoms may have various sources:

- The creation of additional sites with an enhanced adsorption of active forms of the oxygen-containing species OH_{ads} involved in the slow oxidation step of the organic species chemisorbed on the platinum surface (bifunctional mechanism of catalytic action);
- A decrease in the surface concentration of strongly chemisorbed C=O species blocking the surface (and thus retarding the reaction); or
- Changes in electron structure of the surface owing to strong interaction of the valence orbitals of the adsorbed species with the electron gas of the base metal.

Despite the fact that in many cases, metal electrodes with adatoms are catalytically highly active, they have found rather limited practical use in electrochemical devices. This is due to the low stability of these electrodes: The adatoms readily undergo oxidation and desorption from the surface, whereupon the catalytic activity is no longer boosted. In some cases, attempts have been made to extend the existence of the active condition by adding the corresponding ions to the working electrolyte of the electrochemical device so as to secure permanent renewal of the adatom layer.

28.7 NONMETALLIC CATALYSTS

In electrochemical systems, many restrictions exist in the use of metal catalysts. Most metals other than the expensive noble metals are unstable at anodic potentials and cannot be used for anodic processes. The catalytic activity and selectivity of metal catalysts basically are determined by their chemical nature and are rarely open to adjustments.

To the contrary, multicomponent nonmetallic systems such as mixed oxides often provide the possibility for a smooth or discontinuous variation of electrophysical parameters, and thus for some adjustment of their catalytic properties. In a number of cases, one can do without expensive platinum catalysts, instead using nonmetallic catalysts. Serious research into the properties of nonmetallic catalytic electrodes was initiated in the 1960s in connection with broader efforts to realize various kinds of fuel cells.

28.7.1 Carbon Materials

Among the carbon materials, different types of graphite have long been used in a number of technical electrochemical processes (e.g., as anodes in electrochemical

chlorine production, as anodes and cathodes in electrometallurgical processes in solutions and in melts). They have acceptable values of electronic conductivity and a high chemical stability in alkaline and acidic solutions.

We distinguish natural carbon materials and artificial materials obtained by carbonizing certain organic materials. The various kinds of carbon are distinguished by a wide variety of structures and chemical compositions of the surfaces and thus of electrophysical and surface properties. Graphite has a distinct crystal structure and high electronic (metal-like) conductivity. Highly oriented pyrolytic graphite (HOPG) obtained by high-temperature decomposition of organic compounds (at temperatures of up to 3500°C) has a high degree of preferential crystallographic orientation (i.e., is an analog of metal single crystals) and hence is widely used in laboratory research.

Other types of carbon (amorphous or "transitional" forms with turbostratic structure) consist of fragments of graphitelike regions cross-linked to a three-dimensional polymer by carbon chains. Unlike graphite, the transitional forms are organic semiconductors with electrical properties determined by delocalized π-electrons.

In electrocatalysis, the activated carbons, glassy carbon, and carbon black are the transitional forms used. Carbon black is the product of incomplete combustion or decomposition of organic compounds. The shape of its particles is close to spherical. They contain several carbon atom lattice fragments arranged without order. Various types of carbon black serve as substrates for metal catalysts, the properties of the carbon blacks themselves having a strong effect on the catalytic activity of the combined catalysts thus obtained.

Glassy carbon is obtained by specifically controlled thermal decomposition of certain carbonaceous materials. Because of its almost ideally smooth, glasslike surface, it is the favorite material for laboratory studies demanding an exact knowledge of the true surface area. The electrochemical and other properties of glassy carbon depend on the temperature at which it was produced.

Depending on the nature of the material and on the conditions of its preparation and pretreatment, different oxygen compounds in the form of quinone groups C=O, phenol groups C–OH, carboxyl groups C–COOH, and other groups are to be found on the surface. These oxygen-containing groups can act as active sites in electrocatalytic reactions. They also influence the potential distribution in the surface layer and thus the kinetics of the electrochemical reactions. The concentration of surface groups is particularly high in the activated carbons obtained by thermal surface treatment of carbon materials in different gas atmospheres. These carbons have very large specific surface areas (up to 1000 m^2/g), are catalytically active for cathodic oxygen reduction, and hence are widely used as catalysts for oxygen electrodes in metal–air batteries and fuel cells.

Great promise exists in the use of graphitic carbons in the electrochemical synthesis of hydrogen peroxide [reaction (15.21)] and in the electrochemical reduction of carbon dioxide to various organic products. Considering the diversity in structures and surface forms of carbonaceous materials, it is difficult to formulate generalizations as to the influence of their chemical and electron structure on the kinetics and mechanism of electrochemical reactions occurring at carbon electrodes.

A distinct answer has been found, however, with respect to the influence of crystallographic orientation of pyrolytic graphite on the rates of various reactions. It could be shown that the rate of cathodic oxygen reduction at the basal plane of graphite is much lower than at surfaces with edge orientation (Morcos and Yeager, 1970). To the contrary, the rates of simple redox reactions hardly depend on face orientation.

The high activity toward oxygen reactions exhibited by the edge structures of pyrolytic graphite having a large number of broken carbon bonds can be explained in terms of a large number of quinone groups present on these surfaces and favoring the adsorption of the reacting oxygen molecules.

28.7.2 Oxides

Oxides of various metals are a broad class of electrode materials useful in many electrochemical processes (Trasatti, 1980–1981). The surfaces of practically all metals (both base and noble) become covered by layers of chemisorbed oxygen upon anodic polarization. The composition and properties of these layers depend on potential, on the electrolyte, and on the electrolysis conditions. They are often rather thick and have a distinct phase character, so that the metal electrode is converted to a typical oxide electrode. One can also make electrodes directly from oxides deposited in some way or other on various conducting substrates.

The oxides often are nonstoichiometric (with an excess or deficit of oxygen). Many oxides are semiconducting, and their conductivity can be altered by adding various electron donors or acceptors. Relative to metals, the applications of oxide catalysts in electrochemistry are somewhat limited. Cathodic reactions might induce a partial or complete reduction of an oxide. For this reason, oxide catalysts are used predominantly (although not exclusively) for anodic reactions. In acidic solutions, many base-metal oxides are unstable and dissolve. Their main area of use, therefore, is in alkaline or neutral solutions.

We distinguish electrodes consisting of simple oxides, from those consisting of complex oxide systems. The latter include cations of different metals or cations of a given metal in different valence states. An example for the latter type is cobalt cobaltite Co_3O_4 (a spinel structure) containing Co^{2+} and Co^{3+} ions.

Simple Oxides of Base Metals Electrodes of lead dioxide, PbO_2, which in contrast to other base-metal oxides are stable in sulfuric acid are an example for a simple oxide system. In a number of cases, this electrode serves as the anode in the electrosynthesis of organic compounds in acid media.

Nickel oxide anodes are another example for a relatively simple oxide electrocatalyst used rather widely in the oxidation of organic substances (alcohols, amines, etc.) in alkaline solutions at relatively low anodic potentials (about $+0.6$ V RHE). These processes, which occur at an oxidized nickel surface, are rather highly selective. As an example, we mention the industrial oxidation of diacetone-L-sorbose to the corresponding acid in vitamin C synthesis. This reaction occurs at nickel oxide electrodes with chemical yields close to 100%.

It was seen when analyzing the kinetic data for alcohol oxidation reactions that the catalytic action of nickel oxide is due to a mediator mechanism. Higher oxide forms interact with the adsorbed organic species and oxidize them. In the following step the higher oxide forms are regenerated by electrochemical oxidation of lower oxide forms.

Tin dioxide, SnO_2, is of great scientific interest as an electrode material. It is an *n*-type semiconductor whose conductivity is low but can readily be raised by doping. In undoped semiconductors of this type, blocking of the anodic current owing to a small concentration of minority carriers (holes in the valence band) should be expected. Therefore, the catalytic activity toward anodic chlorine evolution from chloride solutions is low. Upon illumination of the SnO_2 electrode, additional holes are generated, their concentration rises, and at the same time the rate of anodic chlorine evolution increases substantially. The same effect can be attained when doping the SnO_2 with antimony. When fluorine is used as a dopant, the conductivity rises as well but catalytic activity fails to appear. This example shows that the catalytic activity of this semiconductor is not merely due to sufficient conductivity. With antimony as a dopant, evidently not only an increase in conductivity but also some changes in the state of tin oxide are induced which give rise to catalytic activity.

Complex Base-Metal Oxides Complex oxide systems include the mixed oxides of some metals which have perovskite or spinel structure. Both the perovskites and the spinels exhibit catalytic activity toward cathodic oxygen reduction, but important differences exist in the behavior of these systems.

An example for a compound of the perovskite type is $LaNiO_3$. In other compounds of the perovskite type, nickel may be replaced by cobalt or iron, and lanthanum in part by alkaline-earth metals, an example being $La_{0.8}Sr_{0.2}CoO_3$. The activity of perovskites toward cathodic oxygen reduction is low at room temperature but rises drastically with increasing temperature (particularly so above 150°C). In certain cases the activity rises so much that the equilibrium potential of the oxygen electrode is established.

A similar relation between catalytic activity and temperature is seen in another complex oxide system, lithiated nickel oxide obtained when incorporating lithium hydroxide into the semiconducting lattice of nickel oxide. The temperature dependence of catalytic activity found for these materials is explained in terms of temperature-dependent changes in their magnetic properties. Above the Néel temperature, conditions become favorable for adsorption of the paramagnetic oxygen molecule in a flat (lying) position in which the simultaneous transfer of two electrons from two adsorption sites on the catalyst surface to the two ends of the oxygen molecule is possible, which leads to dissociation of the molecule.

Cobaltites with spinel structure have compositions MCo_2O_4, where M is a metal forming divalent cations, such as zinc, cadmium, magnesium, nickel, manganese, and divalent cobalt. In contrast to the perovskites, the cobaltites have a rather high catalytic activity already at room temperature. Experiments show that the activity increases with increasing spinel structure content (i.e., increasing number of Co^{3+} ions) of the catalyst surface. The trivalent cobalt ions promote the withdrawal of

electron pairs from adsorbed oxygen molecules, thus making them more reactive. However, the nature of the divalent ions has an important influence on the rate and mechanism of the oxygen reduction reaction.

In a number of studies a correlation was seen between the amount of nonstoichiometric oxygen in the spinel and the spinel's activity. It appears that excess oxygen consolidates the spinel's defect structure with a large number of active sites. Strong anodic polarization leads to ordering of this structure and thus to a decrease in catalytic activity.

It is interesting to note that cobalt cobaltite, Co_3O_4, is a good catalyst, too, for anodic chlorine evolution. In this case, too, a correlation is observed between the reaction rate and the spinel's defect concentration (amount of nonstoichiometric oxygen).

Oxides of Platinum Metals Anodes of platinum (and more rarely of other platinum metals) are used in the laboratory for studies of oxygen and chlorine evolution and in industry for the synthesis of peroxo compounds (such as persulfuric acid, $H_2S_2O_8$) and organic additive dimerization products (such as sebacic acid; see Section 15.6). The selectivity of the catalyst is important for all these reactions. It governs the fraction of the current consumed for chlorine evolution relative to that consumed in oxygen evolution as a possible parallel reaction; it also governs the current yields and chemical yields in synthetic electrochemical reactions.

During the anodic polarization of platinum to potentials of about 3.0 V (RHE), one or several layers (but no more than three) of chemisorbed oxygen are formed, which sometimes are called the α-oxide of platinum. The limiting thickness of these layers is about 1.3 nm. They can be studied both by electrochemical methods and by ellipsometry. At more positive potentials phase-oxide surface layers, the β-oxides are formed. The quantitative composition and structure of these layers and the exact limits of potential for their formation depend on many factors: composition of the electrolyte solution, time of polarization, surface history, and often remain unknown.

The character of the oxide layers influences the kinetics and mechanism of the electrochemical reactions occurring on the platinum anode surface. The relation between the rate of oxygen evolution and oxide layer thickness is complex. In the region where the α-oxides exist, the reaction rate decreases with increasing oxide layer thickness. In the region where the β-oxides exist, the reaction rate depends little on oxide layer thickness or, according to some data, increases with increasing oxide layer thickness.

It is interesting to note that according to photoelectrochemical measurements, the α-oxide of platinum exhibits a photoeffect that is typical for *n*-type semiconductors, while for the β-type oxide the sign of the photoeffect is opposite, and typical for a *p*-type semiconductor. This is an indication for important differences in the properties of these two types of oxide layer.

The current yields of persulfate ion synthesis (for which oxygen evolution is a competing reaction) also strongly depend on the character of the oxide layer. These yields are high (about 70%) at oxide layers having a compact structure and marked electronic conductivity. They are perceptibly lower at the partly hydrated, thicker layers having higher ionic conductivity.

Titanium–Ruthenium Oxide Nodes One of the most important achievements of applied electrocatalysis was formulated in 1968 by Henry Beer when he suggested replacing the graphite anodes used in chlorine production by titanium anodes coated with a layer of the mixed dioxides of titanium and ruthenium. These titanium–ruthenium oxide anodes gained wide acceptance and revolutionized electrolytic chlorine production. While exhibiting a very high catalytic activity and selectivity toward anodic chlorine evolution, these anodes lack the major defect of graphite electrodes, which are gradually eroded and become thinner. For this reason, the new anodes were termed DSA (dimensionally stable anodes).

Titanium dioxide is a catalytically inactive but rather corrosion-resistant material. Ruthenium dioxide is one of the few oxides having metal-like conductivity. It is catalytically quite active toward oygen and chlorine evolution. However, its chemical stability is limited, and it dissolves anodically at potentials of 1.50 to 1.55 V (RHE) with appreciable rates. A layer of mixed titanium and ruthenium dioxides containing 1–2 mg/cm^2 of the precious metal has entirely unique properties in terms of its activity and selectivity toward chlorine evolution and in terms of its stability. With a working current density in chlorine evolution of 20 to 50 mA/cm^2, the service life of such anodes is several years (up to eight years).

The layer of titanium and ruthenium oxides usually is applied to a titanium substrate pyrolytically, by thermal decomposition (at a temperature of about 450°C) of an aqueous or alcoholic solution of the chlorides or of complex compounds of titanium and ruthenium. The optimum layer composition corresponds to 25 to 30 atom % of ruthenium. The layer contains some quantity of chlorine; its composition can be written as $Ru_{0.25}Ti_{0.75}O_{(2-x)}Cl_x$. At this deposition temperature and Ru–Ti ratio, the layer is a poorly ordered solid solution of the dioxides of ruthenium and titanium. Chlorine is completely eliminated from the layer when this is formed at higher temperatures (up to 800°C), and the solid solution decomposes into two independent phases of titanium dioxide and ruthenium dioxide no longer exhibiting the unique catalytic properties.

28.7.3 Metal Complexes with Organic Ligands

The idea of using organic metal complexes as catalysts for electrochemical reactions (Jasinski, 1964) can be traced back to the biocatalysts in which such complexes often are the catalytically active sites and which are distinguished by a high catalytic activity. This area has seen a strong development starting in the 1960s.

For electrocatalysis, compounds of the porphyrin series are of major interest: monomeric and polymeric phthalocyanines, tetraphenylporphyrins, tetraazaporphyrins, tetraazaannulenes, and other N_4 *complexes*. The structures of some of these complexes are shown in Fig. 28.5.

These compounds contain a developed system of conjugated double bonds imparting distinct semiconductor properties on them. Metal ions of variable valency can serve as the central ion M: cobalt, nickel, iron, manganese, copper, and so on. In such systems, electron transitions can occur in the conjugated system of the ligands and in the electronic system of the central metal ion. These transitions are the basis for their catalytic activity toward various reactions.

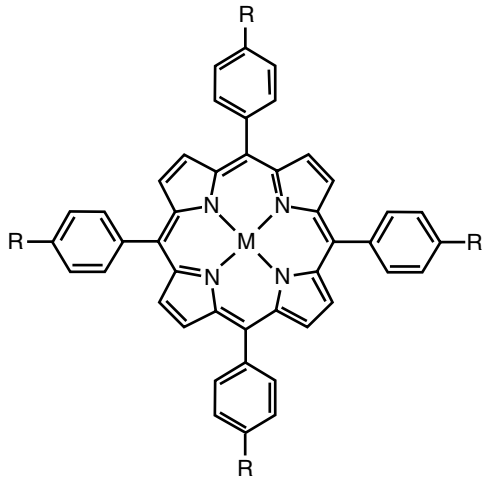

Tetra(R-phenyl)porphyrin

R = H, OCH_3(TPP, TMeOPP)
M = Co, Fe (MTPP, MTMeOpp)

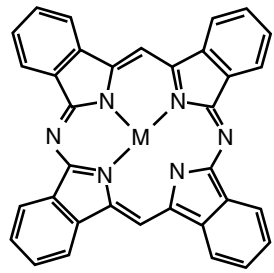

Phthalocyanine (Pc)
(tetrabenzotetraazaporphyrin)

M = Co, (Fe MPc)

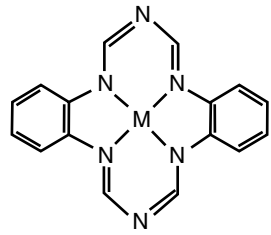

Dibenzotetraazaannulene (TAA)

M = Co, (CoTAA)

FIGURE 28.5 Structure of N_4 complexes.

At the N_4 complexes, cathodic oxygen reduction has been studied in the greatest detail. These systems are of great practical value inasmuch as these complexes are practically the only nonplatinum catalysts that can be used for oxygen reduction in acidic solutions.

The catalytic activity of the N_4 complexes depends both on the nature of the central metal ion and on the nature of the ligand and all substituents. It was found that the metal ion is the active site where the electrocatalytic process is accomplished. During its adsorption, an oxygen molecule forms a stable complex (adduct) with the

metalloporphyrin. The higher electron density close to the central ion which is brought about by the system of conjugated bonds facilitates electron transfer to the oxygen molecule and serves to accelerate its reduction.

The N_4 complexes are rather stable in acidic solutions. However, sometimes the stability is not high enough, particularly so at higher temperatures. It was quite unexpected, therefore, to find that after pyrolysis at temperatures of 600 to 800°C the catalytic activity of these compounds not only failed to decrease but in some cases even increased. The major result of pyrolysis is a drastic increase in catalyst stability. Tests have been reported where after pyrolysis such catalysts have worked for 4000 to 8000 h without activity loss. The reasons for the conservation of high activity after pyrolysis are not entirely clear. The activity evidently is associated with the central ion that has attained a "favorable" environment of pyrolysis products.

28.7.4 Bioelectrocatalysis

Enzymes are highly active catalysts in many biological processes. A very important feature in the catalytic action of enzymes is their high selectivity. Any enzyme that is active toward a particular reaction involving a particular substrate is entirely inactive toward other reactions and toward other substrates. (Note that in biochemistry, a substrate is the substance undergoing reaction under the catalytic effect of the enzyme.)

The enzymes are protein molecules having globular structure, as a rule. The molecular masses of the different enzymes have values between ten thousands and hundred thousands. The enzyme's active site, which, as a rule, consists of a nonproteinic organic compound containing metal ions of variable valency (iron, copper, molybdenum, etc.) is linked to the protein globule by covalent or hydrogen bonds. The catalytic action of the enzymes is due to electron transfer from these ions to the substrate. The protein part of the enzyme secures a suitable disposition of the substrate relative to the active site and is responsible for the high selectivity of catalytic action.

Enzyme catalysis in the 1970s became a subject of interest to electrochemists since the enzymes, unlike most other metal and nonmetal electrocatalysts, have a number of important special features:

1. They display their activity not in concentrated alkaline and/or acidic solutions but in dilute neutral solutions.
2. They display their activity, not at elevated temperatures (e.g., 40 to 80°C) but close to room temperature.
3. They have an exceedingly high specific activity per active site; the turnover number γ is as high as 10^6 to $10^8\ s^{-1}$ in certain enzyme reactions, while at ordinary electrocatalysts having a number of reaction sites on the order of $10^{17}\ cm^{-2}$, γ has a value of about $1\ s^{-1}$ at a current density of $10\ mA/cm^2$. Thus, the specific catalytic activity of the active sites of enzymes is many orders of magnitude higher than that of all other known catalysts for electrochemical (and also chemical) processes.

All these considerations have served as a basis for attempts at using various enzymes in electrochemical reactions. This field of research became known as *bioelectrocatalysis*.

In biological systems, the enzymes are homogeneous catalysts. For their use in heterogeneous electrochemical reactions, they must be immobilized on a carrier suitable for fashioning an electrode. This is most often achieved by adsorption of the enzyme on a carbon material (carbon black, graphite, etc.). This immobilization usually leads to some decrease in activity of the enzymes, but on the other hand, raises their stability.

As an example of the accelerating effect of an enzyme on an electrochemical reaction, consider the influence exerted by laccase immobilized on carbon black, on the cathodic reduction of oxygen to hydrogen peroxide in phosphate–acetate buffer solutions at pH values between 3 and 6 (where the enzyme retains its activity). In this system, a potential close to the equilibrium potential of the oxygen/hydrogen peroxide couple is actually established. The exchange current density of this reaction in the presence of laccase corresponds to a turnover number of $\gamma = 10^{-6}\ s^{-1}$, while at a platinum electrode without the enzyme it is given by $\gamma = 10^{-8}\ s^{-1}$ (it must be pointed out that for free (nonimmobilized) laccase in solution, the specific catalytic activity is still 30 times higher than after its immobilization on carbon black).

Mediators can be used in certain cases when the enzyme does not interact with a substrate directly. Thus, in the presence of dehydrogenase immobilized on carbon black, cathodic hydrogen evolution can be realized only when adding methylviologen to the solution. The enzyme reduces methylviologen, while the reduced form of this mediator in turn reduces protons to gaseous hydrogen in the solution layer next to the electrode.

The high specific activity of enzymes and the theoretical possibility of using them to conduct electrochemical reactions are topics of great scientific interest. However, it is difficult to envisage prospects for a practical use of enzymes for an acceleration and intensification of industrial electrode processes. The difficulty resides in the fact that enzymes are rather large molecules, and on the surface of an enzyme electrode, fewer active sites are available than on other electrodes. Per unit surface area, therefore, the effect expected from the use of enzymes is somewhat reduced.

Another area exists, however, where the use of enzyme electrodes offers great promise. Owing to their high selectivity and their capability of reacting only in the presence of specific substrates, they can be used as sensors for the presence of particular, biologically active substances in a solution, and in certain cases for determining the concentration of these substances.

28.8 STABILITY OF ELECTROCATALYSTS

The activity of catalysts for electrochemical reactions (like that of catalysts for chemical reactions in general) as a rule falls off with time. The degree and rate of this decline depend on a large number of factors: the catalyst type, its method of preparation, its working conditions (composition of the electrolyte solution, temperature,

current density, working potential, length of the time of use) as well as the conditions of storage prior to initiating the work. The main reason for a drop in activity are various side reactions occurring, both while the catalyst is stored in an idle condition and while it works under current flow:

1. Corrosion (spontaneous dissolution) of the catalytically active material, and hence a decrease in the quantity present. Experience shows that contrary to widespread belief, marked corrosion occurs even with the platinum metals. For smooth platinum in sulfuric acid solutions at potentials of 0.9 to 1.0 V (RHE), the steady rate of self-dissolution corresponds to a current density of about 10^{-9} A/cm^2. Also, because of enhanced dissolution of ruthenium from the surface layer of platinum–ruthenium catalysts, their exceptional properties are gradually lost, and they are converted to ordinary, less active platinum catalysts.

2. Spontaneous recrystallization of the catalyst leading to a decrease of its specific surface area (sintering of catalysts), and possibly also to a change in chemical and/or phase composition of the surface layer. The recrystallization of disperse catalysts that occurs as a result of surface diffusion of its atoms or of the permanent dissolution and redeposition of its surface atoms is caused by the general tendency of materials to attain a lower surface area and lower excess surface energy. The rate of this process is higher the higher the degree of dispersion of a catalyst.

3. The adsorption and accumulation of various impurities from the electrolyte or surrounding atmosphere on the catalyst surface. The rate of accumulation of impurities on the catalyst surface depends on its activity for adsorption, which often is parallel to its catalytic activity.

28.9 OTHER ASPECTS OF ELECTROCATALYSIS

Together with its central aspect, of studying the activity of catalysts in electrochemical reactions as a function of the nature and state of the catalyst, the term *electrocatalysis* is sometimes used as well to describe other areas of interest:

1. The kinetics and mechanism of individual electrochemical steps in catalytic processes occurring in the liquid phase, such as the hydrogenation of organic compounds by hydrogen in alkaline solutions at a three-dimensional catalyst of suspended metallic nickel powder. This reaction proceeds via an electrochemical mechanism: Hydrogen is ionized at the nickel particles, while the electrons being liberated sustain the coupled step of reduction of the organic substance. Often, few differences exist with respect to the mechanism and other features between electrochemical processes and catalytic processes in the liquid phase, and similar techniques are used to study them.

2. The use of electrochemical techniques when examining the properties of various catalysts and studying general catalytic problems. Thus, in 1936 Alexander Frumkin and co-workers ascertained a linear section in the electrochemical charging

curve of the platinum electrode over the potential range from 0 to 0.3 V (RHE). On the basis of these measurements, Mikhail Temkin formulated his idea of a logarithmic adsorption isotherm (the *Temkin isotherm*) as well as his theory of processes on energetically inhomogeneous surfaces. This work was a starting point for the use of electrochemical techniques in studies of various catalytic phenomena which proved to be very convenient and productive.

3. Influencing the activity of catalysts for heterogeneous chemical reactions by electrochemical means. In 1973, Dmitri Sokol'skij showed that by applying a certain potential to a catalyst one can influence the rates of liquid-phase hydrogenation reactions of organic compounds. In the 1990s it was shown by Costas Vayenas et al. that a similar influence can be exerted in the case of gas-phase reactions. Thus, in the oxidation of ethylene with oxygen at 370°C at a platinum catalyst supported on a solid electrolyte, it was shown that the potential of the catalyst shifts by 0.5 V in the positive direction and the reaction rate at the same time rises by a factor of 26 when a current of 1 μA is applied to anodically polarize the catalyst with the aid of an auxiliary electrode. The turnover number of the catalytic reaction is 74,000 times larger than that due to current flow. This effect appears to be due to a change in adsorption energy of the reaction components on the polarized catalyst. Work in this area of catalysis became known as *nonfaradaic electrochemical modification of catalytic activity* (NEMCA).

28.10 DISCUSSION

A period of high research activity in electrocatalysis began after it had been shown in 1963 that fundamentally, an electrochemical oxidation of hydrocarbon fuel can be realized at temperatures below 150°C. This work produced a number of important advances. They include the discovery of synergistic effects in platinum–ruthenium catalysts used for the electrochemical oxidation of methanol.

Of considerable interest was the demonstration that metalloporphyrins and the like can be used as nonmetallic catalysts in electrochemical reactions, nourishing hopes that in the future, expensive platinum catalysts could be replaced. Starting in 1968, dimensionally stable electrodes with a catalyst prepared from the mixed oxides of titanium and ruthenium found widespread use in the chlorine industry.

Each of these advances (together with many other results) can be regarded as an important discovery in the field of electrocatalysis having great theoretical and practical significance. Yet, after these first achievements, a period of disenchantment and pessimism began in the 1970s and 1980s. This was due to the fact that in the attempts at an industrial realization of a number of the foregoing achievements, considerable difficulties were encountered. Despite the demonstration that the low-temperature oxidation of hydrocarbons fundamentally is possible, it was found that the rates that could be realized in practice were so low, and the loadings of platinum catalysts needed were so high, that at present this reaction was without realistic prospects. Also, even though in fuel cells catalysts without platinum can be used, most of the versions offered still used platinum-based catalysts.

The only achievement that saw wide industrial acceptance were the anodes with titanium–ruthenium catalyst.

Some pessimism in assessing the situation in the field of electrocatalysis may also derive from the fact that one of the final aims of work in this field, setting up a full theory of electrocatalysis at a quantum-mechanical level while accounting for all interactions of the reacting species with each other and with the catalyst surface, is still very far from being realized. So far we do not even have a semiempirical—if sufficiently general—theory with which we could predict the catalytic activity of various catalysts.

At present, most workers hold a more realistic view of the promises and difficulties of work in electrocatalysis. Starting in the 1980s, new lines of research into the state of catalyst surfaces and into the adsorption of reactants and foreign species on these surfaces have been developed. Techniques have been developed that can be used for studies at the atomic and molecular level. These techniques include the tunneling microscope, versions of Fourier transform infrared spectroscopy and of photoelectron spectroscopy, differential electrochemical mass spectroscopy, and others. The broad application of these techniques has considerably improved our understanding of the mechanism of catalytic effects in electrochemical reactions.

Work in electrocatalysis is conducted in many university and government laboratories and in industrial establishments. The total volume of the work going on is rather large, but many efforts contain an element of fortuity. Exploratory studies often run ahead of systematic studies and generalizations. Difficulties exist when comparing experimental results obtained by different authors. Inconsistent opinions often are expressed when discussing the results.

Progress in the theory of electrocatalytic phenomena depends on the information content of experiments, on the breadth of capture of each phenomenon examined. A great deal of attention in electrocatalysis is still reserved for studies of catalysts based on metals of the platinum group. This is due not only to the high catalytic activity of these metals but also to the fact that owing to a number of specific properties of these catalysts, the corresponding electrochemical studies have an exceptionally high information content and admit generalizations that are also significant for other catalyst types.

Important close-range problems that must be solved in applied electrocatalysis include the task of drastically increasing the activity of catalysts for oxygen electrodes (both for oxygen evolution and for oxygen reduction), of increasing the activity of catalysts for methanol oxidation, and for developing catalysts for the deliberate synthesis of a number of organic substances by electrochemical reduction of carbon dioxide.

It may be possible to achieve an adequate solution of these problems by developing catalysts with surface properties that have been tailored deliberately so as to provide a favorable catalytic action on all intermediate steps that need it. Such catalysts should be polyfunctional and exhibit a certain degree of chemical and structural surface microheterogeneity. Electrochemical nanoelectrochemistry (see Chapter 36) may be a possible approach for synthesizing such surfaces. For a detailed investigation and control of these catalytic surfaces, the tools available among the experimental physical methods (see Chapter 27) will be useful.

REFERENCES

Balandin, A., *Z. Phys. Chem*., **2B**, 289 (1929).

Beer, H., Belgian patent 710.551 (1968).

Binder, H., A. Koehling, and G. Sandstede, in *From Electrocatalysis to Fuel Cells*, G. Sandstede, Ed., Seattle, WA, 1972, p. 43.

Bockris, J. O'M., *Trans. Faraday Soc*., **43**, 417 (1947).

Clavilier, J., *J. Electroanal. Chem*., **107**, 205 (1980).

Entina, V., *Elektrokhimiya*, **4**, 111 (1968).

Frumkin, A., and A. Shlygin, *Izv. Akad. Nauk USSR Ser. Khim*., **1936**, 773 (1936).

Gerischer, H., *Bull. Soc. Chim. Belg.*, **57**, 596 (1958).

Grubb, W., *Nature*, **198**, 883 (1963).

Grubb, W., and L. Niedrach, *J. Electrochem. Soc*., **110**, 1086 (1963).

Hobbs, B. S., and A. C. C. Tseung, *Nature*, **222**, 556 (1966).

Horiuti, J., and M. Polanyi, *Acta Physicochim. URSS*, **2**, 505 (1940); *J. Mol. Catal. Chem*., **199**, 185 (2003).

Jasinski, K., *Nature*, **201**, 1212 (1964).

Khazova, O., Yu. Vassiliev, and V. Bagotsky, *Elektrokhimiya*, **3**, 1020 (1967).

Kobozev, N., and V. Monblanova, *Zh. Phys. Khim*., **7**, 645 (1936).

Krishtalik, L., *Usp. Khim*., **34**, 1831 (1965).

Morcos, J., and E. Yeager, *Electrochim. Acta*, **15**, 953 (1970).

Motoo, S., Electrocatalysis by ad-atoms, *Proc. Electrochemical Society*, PV 84-12, 1994, p. 331.

Mukerjee, S., *J. Appl. Electrochem*., **20**, 537 (1990).

Parsons, R., *Trans. Faraday Soc*., **54**, 1053 (1958).

Petrii, O., and G. Tsirlina, *Electrochim. Acta*, **39**, 1739 (1994).

Piontelli, R., G. Poli, and G. Stravalle, in *Transactions of the Symposium on Electrode Processes*, E.Yeager, Ed., Wiley, New York, 1961, p. 67.

Pris, E., K. Sabot, S. Raicheva, and I. Bagotskaya, *Elektrokhimiya*, **2**, 1209 (1961).

Raney, M., *Ind. Eng. Chem*., **32**, 1190 (1940); U.S. Patents 1,563,587, 1,628,190, and 1,915,473 (1925).

Tafel, J., *Liebigs Ann. Chem*., **301**, 285 (1898); *Z. Elektrochem*., **12**, 112 (1906).

Taylor, H. S., *Proc. R. Soc. London*, **108**, 105 (1925).

Trasatti, S., *J. Electroanal. Chem*., **39**, 163 (1972).

Vayenas, C. G., et al., *Nature*, **343**, 625 (1990).

Watanabe, M., and S. Motoo, *J. Electroanal. Chem*., **60**, 267 (1975).

MONOGRAPHS AND REVIEWS

Frumkin, A. N., B. B. Damaskin, and O. A. Petrij, Charge transfer in chemisorption processes, *Z. Phys. Chem. (Leipzig)*, **256**, 728 (1975).

Gottesfeld, S., and T. A. Zawodzinski, Direct methanol oxidation fuel cells: from a 20th century electrochemists' dream to a 21st century emerging technology, in *Electrochemical Science and Engineering*, R. C. Alkire et al., Eds., Vol. 5, Wiley, New York, 1997, p. 195.

Kinoshita, K., Small-particle effects and structural considerations for electrocatalysis, in *Modern Aspects of Electrochemistry*, J. O'M. Bockris, Eds., Vol. 14, Kluwer, New York, 1982, p. 557.

Kinoshita, K., *Carbon: Electrochemical and Physicochemical Properties*, Wiley, New York, 1988.

Kokkinidis, K., Underpotential deposition and electrocatalysis, *J. Electroanal. Chem*., **201**, 217 (1986).

Lipkowski, J., and Ph. N. Ross, Eds., *Adsorption of Molecules at Metal Electrodes*, Wiley, New York, 1993.

Lipkowski, J., and Ph. N. Ross, Eds., *Electrocatalysis*, Wiley, New York, 1998.

Petrij, O. A., and G. A. Tsirlina, Size effects in electrochemistry, *Russ. Chem. Rev*., **70**, 285 (2001).

Sokol'skij, D. V., and G. D. Zakumbaeva, *Adsorption and Catalysis of 8th Group Metals* [in Russian], Nauka Publishers, Alma-Ata, Kazakhstan, 1973.

Tarasevich, M. R., and V. A. Bogdanovskaya, Bioelectrocatalysis: enzymes as catalysts for electrochemical reactions, in *Topics in Bioelectrochemistry*, G. Milazzo, Ed., Vol. 5, Wiley, New York, 1983.

Trasatti, S., The work function in electrochemistry, in *Electrochemistry and Electrochemical Engineering*, H. Gerischer and Ch.W. Tobias, Eds., Vol. 10, Wiley, New York, 1977, p. 213.

Trasatti, S., Ed., *Electrodes of Conductive Metal Oxides*, Elsevier, Amsterdam, Part A, 1980, Part B, 1981.

Vayenas, C. G., et al., in *Modern Aspects of Electrochemistry*, J. O'M. Bockris et al., Eds., Vol. 29, Kluwer, New York, 1996, p. 57.

29

Photoelectrochemistry

The effects of luminous (or other electromagnetic) radiation on the properties of electrodes and on electrochemical reactions are the subject of photoelectrochemistry. Luminous radiation (light) can produce changes in the open-circuit potentials and in the polarization characteristics of electrodes; at constant potential, the current may change (anodic or cathodic photocurrents appear), whereas at constant current, the electrode potential may change (photopotentials appear). It is an important special feature that electrochemical reactions may become possible which at the same potentials in the dark are thermodynamically prohibited (i.e., associated with an increase in Gibbs energy); under illumination, such reactions are possible because of the energy supplied from outside.

The first observations of photoelectrochemical phenomena were made in 1839 by Antoine Becquerel (1788–1879). He used symmetric galvanic cells consisting of two identical metal electrodes in a dilute acid. When illuminating one of the electrodes he observed current flow in the closed electric circuit.

Studies of photoelectrochemical phenomena are of great theoretical value. With light as an additional energy factor, in particular, studies of the elementary act of electrochemical reactions are expedited. Photoelectrochemical phenomena are of great practical value as well. One of the most important research activities nowadays is development of electrochemical devices for a direct conversion of luminous (solar) into electrical energy and photoelectrochemical production of hydrogen.

For photoelectrochemical measurements, light in the visible and near-ultraviolet part of the spectrum is most commonly used. The incident radiation is characterized by the energy of the photons (light quanta), which is given by $h\nu$ (where h is the Planck constant and ν is the frequency of the light wave), and by the light intensity or photon flux striking the object. For visible light the photon energies are between 1.63 eV (for the red limit, with a wavelength of $\lambda = 760$ nm) and 3.1 eV (for the violet limit, with $\lambda = 400$ nm). The energies are higher in the ultraviolet (e.g., 6.2 eV at $\lambda = 200$ nm). Electrochemical systems are less strongly influenced by photons having lower energies (in the infrared part of the spectrum). The usual light sources for laboratory work are mercury or xenon lamps, which are used in combination with

Fundamentals of Electrochemistry, Second Edition, By V. S. Bagotsky

monochromators as filters for light of a particular frequency. The cell walls (or special windows in the walls) should be transparent to the light used.

Laser illumination, which allows for significantly higher photon flux, has become widespread lately. An undesirable side effect of high intensities is heating of the solution layer next to the electrode. This effect can be reduced when intermittent (pulsed) light is used. Light pulses offer the additional possibility to examine after effects of the illumination: the relaxation processes that occur when the system returns to its original condition.

The first step in a photoelectrochemical reaction is photon absorption (capture) by the substrate and the change in electron energy (*photoexcitation*) occurring in the substrate as a result of photon absorption. This step is followed by other chemical or electrochemical reaction steps involving the activated substrate.

We distinguish two basic types of photoelectrochemical reaction:

1. Photoexcitation of the electrode (of the electrons in its surface layer) and subsequent reaction of ordinary, nonactivated reactants at the electrode (Section 29.3)
2. Photoexcitation of reactant particles in the solution and their subsequent reaction at a nonactivated electrode (Section 29.4)

Electron photoemission from an electrode into an electrolyte solution, which yields solvated (hydrated) electrons, can be regarded as a particular case of reactions with photoexcitation of the electrode (Section 29.2).

It will be necessary to provide quantitative criteria for studies of photoelectrochemical phenomena. These phenomena are a function of photon energy and appear only at energies above a particular *threshold energy* $h\nu_{thr}$ (or below a particular threshold wavelength, λ_{thr}, of the light). The threshold energy is an important characteristic of any given phenomenon.

For phenomena involving electrons crossing the phase boundary (photocurrents, electron photoemission), the *quantum yield* γ of the reaction is a criterion frequently employed. It is defined as the ratio between the number of electrons, N_e, that have crossed and the number of photons, N_{ph}, that had reached the reaction zone (or, in another definition, the number of photons actually absorbed by the substrate): $\gamma = N_e/N_{ph}$.

29.1 ENERGY LEVELS OF ELECTRONS

29.1.1 Electrochemical Potential of Electrons in Metals and Semiconductors

The Fermi energy, W_F, is reckoned from the energy of the valence-band bottom (zero-point energy) and gives the kinetic energy of the electrons at the highest occupied level of this band. This energy is equal to the chemical potential of the electrons.

The points of reference thus defined for the different metals (i.e., their valence-band bottoms) are all different and exist in different phases, so that it is difficult to

compare the electron energies in these metals. It will be advantageous to always choose a point of reference that is present in the same phase. Our choice is a point m in vacuum just outside the conductor (the concept of "just outside the conductor" had been explained in Section 9.1). When the metal as a whole is uncharged (i.e., when there is no external field and the outer potential $\psi_{ex}^{(M)}$ is zero), a point in vacuum infinitely far from the metal surface can also be used as the point of reference, since the work required to transfer a charge from the point $x \to \infty$ to point m is zero.

The Fermi level (for which the symbol U_F is used to distinguish it from the Fermi energy) is the level of total energy of the energy-richest electrons relative to this new point of reference and is given by the work that must be expended in transferring an electron from vacuum (from point m) to the highest occupied level of the valence band in the metal. In this transfer, work must be expended to overcome both electrostatic and chemical forces. The concept of Fermi level U_F coincides completely with that of the electrochemical potential of electrons in the metal, $\overline{\mu}_e^{(M)}$ (relative to the given point of reference).

In electron emission from a metal into vacuum, primarily electrons from the highest occupied level are extracted. Therefore, the work function $\lambda^{(M)}$ involved in this act, under the assumptions made, is equal to the Fermi level or electrochemical potential of electrons in the metal, but with an inverted sign [compare with Eq. (9.2)]:

$$\lambda^{(M)} = -\overline{\mu}_e^{(M)} = -U_F^{(M)}. \tag{29.1}$$

In the present chapter, all values of μ_j, $\overline{\mu}_j$, λ, W_F, and U_F refer to a single electron (or single species) and are stated in electron volts, as in Section 9.1. We recall that the values of work functions are always positive; hence, the values of $\overline{\mu}_e^{(M)}$ and $U_F^{(M)}$ are always negative (electron transfer from vacuum into a metal is associated not with an expenditure but with a gain of energy).

Consider the case of a junction between two different metals α and β. Generally, they will have different values of the Fermi energy and work function. Between the two metals, a certain Volta potential $\varphi_V^{(\beta,\alpha)}$ will be set up. This implies that the outer potentials $\psi_{ex}^{(M)}$ at points a and b, which are just outside the two metals, are different. However, it will be preferable to count the Fermi levels or electrochemical potentials from a common point of reference. This can be either point a or point b. Since these two points are located in the same phase, the potential difference between them (the Volta potential) can be measured. Hence, values counted from one of the points of reference are readily converted to the other point of reference when required.

Unlike the values of $\overline{\mu}_e$, values of electron work function $\lambda^{(M)}$ always refer to the work of electron transfer from the metal to "its own" point of reference. Hence, in this case, the relation established between these two parameters by Eq. (29.1) is disturbed. The condition for electronic equilibrium between two phases is that of equal electrochemical potentials $\overline{\mu}_e$ of the electrons in them [Eq. (2.5)]. In Fig. 29.1 the energies of the valence-band bottoms (or negative values of the Fermi energies) are plotted downward relative to this common level, in the direction of decreasing energies, while the values of the electron work functions are plotted upward. The difference in energy levels of the valence-band bottoms (i.e., the difference in chemical potentials of the

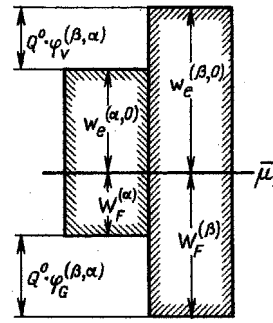

FIGURE 29.1 Energy levels of the electrons in two metals α and β which are in contact.

electrons in the two metals) according to Eq. (2.6) corresponds to the work $Q^0\varphi_G^{(\beta,\alpha)}$ associated with overcoming the Galvani potential. On the other hand, the work function difference according to Eq. (9.8) corresponds to the work $Q^0\varphi_V^{(\beta,\alpha)}$ associated with overcoming the Volta potential between the two metals.

29.1.2 Electrochemical Potential of the Electrons in Solutions

Electrolyte solutions ordinarily do not contain free electrons. The concept of *electrochemical potential of the electrons in solution*, $\bar{\mu}_e^{(E)}$, can still be used for those among the bound electrons that will participate in redox reactions in the solution. Consider the equilibrium $Ox + ne^- \rightleftharpoons Red$ in the solution. In equilibrium, the total change in Gibbs energy in the reaction is zero; hence the condition for equilibrium can be formulated as

$$\bar{\mu}_e^{(E)} = \frac{1}{n}\,[\bar{\mu}_{red}^{(E)} - \bar{\mu}_{ox}^{(E)}]. \tag{29.2}$$

The electrochemical potential of the electron depends on the redox properties of the system; the higher the value of $\bar{\mu}_{Ox}^{(E)}$ (or the stronger the oxidizing agent and the higher its electron affinity), the higher will be the energy gain in electron transfer from the point of reference to species Ox [i.e., the lower (or more negative) will be the value of $\bar{\mu}_{Ox}^{(E)}$]. In the reaction considered, the species Ox and Red differ by n unit charges; therefore, the expression for electrochemical potential of the electrons in solution can also be written [when allowing for Eq. (3.8)] as

$$\bar{\mu}_e^{(E)} = \frac{1}{n}\,[\mu_{red}^{(E)} - \mu_{ox}^{(E)}] - Q^0\psi^{(E)}. \tag{29.3}$$

When the solution in this redox system is in contact with a nonconsumable metal electrode (e.g., a platinum electrode), the equilibrium set up also implies equal electrochemical potentials, $\bar{\mu}_e^{(M)}$ and $\bar{\mu}_e^{(E)}$, of the electrons in the metal and electrolyte.

According to Eq. (3.21) and taking into account that the electrode potential differs by a constant term from the metal–solution Galvani potential, we thus have an expression for the equilibrium potential of this electrode and, at the same time, for the equilibrium potential, E_{redox}, of this redox system:

$$Q^0 E_{\text{redox}} = \frac{1}{n} [\overline{\mu}^{(\text{E})}_{\text{red}} - \overline{\mu}^{(\text{E})}_{\text{ox}}] + \text{const.} \tag{29.4}$$

It follows from the last two equations that between the values of $\overline{\mu}^{(\text{E})}_e$ and the redox potential, the relation

$$\overline{\mu}^{(\text{E})}_e = A - Q^0 E_{\text{redox}} \tag{29.5}$$

exists (i.e., the more positive the redox potential E_{redox}, the more negative will be the value of $\overline{\mu}^{(\text{E})}_e$, and vice versa). Constant A in this equation (which is the value of $\overline{\mu}^{(\text{E})}_e$ for $E_{\text{redox}} = 0$) depends only on the reference electrode against which potential E_{redox} has been measured, not on the nature (metal or semiconductor) of the electrode which is in contact and equilibrium with the electrolyte solution.

When the electrochemical potential of the electrons in the metal is counted from the point of reference just outside the metal, then at the electrode potential $E = 0\,\text{V}$ it should also be equal to the value of A. At other potentials it will be determined by an equation analogous to Eq. (29.5):

$$\overline{\mu}^{(\text{M})}_e = A - Q^0 E. \tag{29.6}$$

It is important to notice that this relation between the values of $\overline{\mu}^{(\text{M})}_e$ and E is preserved even when the electrode is not in equilibrium with the solution: $\overline{\mu}^{(\text{M})}_e \neq \overline{\mu}^{(\text{M})}_e$, in particular when it is ideally polarizable.

Constant A in Eqs. (29.5) and (29.6) is about $-4.4\,\text{eV}$ when the standard hydrogen electrode is used as the reference electrode. This value has been determined from experimental values for the electron work function of mercury in vacuum, $\lambda^{(\text{Hg})}$, which is 4.48 eV, and for the Volta potential, $\varphi^{(\text{M,E})}_{\text{V}}$, between the solution and a mercury electrode polarized to $E = 0\,\text{V}$ (SHE), which is $-0.07\,\text{V}$ (the work of electron transfer is $-0.07\,\text{eV}$). The sum of these two values, according to Eq. (9.8), corresponds to the solution's electron work function at this potential (i.e., to the value of constant A with an inverted sign).

Thus, an unambiguous correlation exists between the values of electrode potential (electrochemical scale) and the Fermi levels or values of electrochemical potential of the electrons defined as indicated (physical scale); see the symbols at the vertical axes in Fig. 29.2.

The value of $\overline{\mu}^{(\text{M})}_e$ defined by Eq. (29.6) is sometimes called the *absolute electrode potential measured against vacuum*. We must remember here that we are concerned with electrochemical potentials stated in electron volts rather than with electrostatic potentials stated in volts. Hence, this absolute potential, which can be determined

experimentally, is unrelated to the problem of determining absolute values of the Galvani potential that had been discussed in Section 9.4.2. Using absolute (electrochemical) potentials, we can state the EMF of a galvanic cell as the difference between two parameters,

$$\mathscr{E} = \frac{1}{Q^0}\,[\overline{\mu}_e^{(M_2)} - \overline{\mu}_e^{(M_1)}], \tag{29.7}$$

each referring to just one of the electrodes; in Section 2.4.1 the same had been achieved, analogously, with the aid of electrode potentials. Thus, *absolute potentials* in a certain sense are equivalent to *electrode potentials* but differ from them insofar as they are not tied to any particular reference electrode.

29.1.3 Electron Transitions Between Electrode and Solution

The elementary act of an electrochemical redox reaction is the transition of an electron from the electrode to the electrolyte or conversely. Such transitions obey the *Franck–Condon principle*, which says that the electron transition probability is highest when the energies of the electron in the initial and final states are identical.

It follows from the Franck–Condon principle that in electrochemical redox reactions at metal electrodes, practically only the electrons residing at the highest occupied level of the metal's valence band are involved (i.e., the electrons at the Fermi level). At semiconductor electrodes, the electrons from the bottom of the conduction band or holes from the top of the valence band are involved in the reactions. Under equilibrium conditions, the electrochemical potential of these carriers is equal to the electrochemical potential of the electrons in the solution. Hence, mutual exchange of electrons (an exchange current) is realized between levels having the same energies.

When a net current flows and the electrode's polarization is ΔE, its Fermi level is shifted by $-Q^0\,\Delta E$ relative to level $\overline{\mu}_e^{(E)}$, down in the case of anodic polarization, and up in the case of cathodic polarization. The higher the electrode's catalytic activity toward a given reaction, the lower will be the polarization at a given current density, and the smaller will be the shift.

29.2 ELECTRON PHOTOEMISSION INTO SOLUTIONS

Events of electron photoemission from a metal into an aqueous solution had first been documented in 1966 by Geoffrey C. Barker and Arthur W. Gardner on the basis of indirect experimental evidence. The formation of solvated electrons in nonaqueous solutions (e.g., following the dissolution of metallic sodium in liquid ammonia) had long been known, but it was only in the beginning of the 1950s that their existence in aqueous solutions was first thought possible. It is probably for this reason that even nowadays in aqueous solutions we more often find the term *solvated* than *hydrated electrons*.

When photons are absorbed in a metal, the ensemble of electrons are excited and some of the electrons are promoted to higher energy levels. The excited state is preserved in the metal for only a short time, and the system returns rapidly to its original state. When the photon energy $h\nu$ is higher than the metal's electron work function, $\lambda^{(M,E)}$, in the solution at a given potential, individual excited electrons can be emitted into the solution. Usually, the quantum yields of this process are low (e.g., around 10^{-4}) and depend on the depth of the layer in which the photons are absorbed.

Photoemission produces "dry" (nonsolvated) electrons leaving the metal surface with a high initial velocity. An excess photon energy of 0.05 eV is enough to impart a velocity of about 10^5 m/s to the electron. In the first layers of solution, the electrons are strongly decelerated and *thermalized* (i.e., their kinetic energy is reduced to values typical for thermal motion at the given temperature). During thermalization processes "dry" electrons, which are initially emitted into the conduction band of the solvent, reach the bottom edge of the conduction band and then go through two (or more) localized states in the bandgap. Several picoseconds after photon adsorption, the electrons end up in a localized "solvated' state at distances of 1 to 5 nm from the electrode surface. The electron's hydration energy in aqueous solutions is about 1.5 to 1.6 eV.

The further fate of the solvated electrons depends on solution composition. When the solution contains no substances with which the solvated electrons could react quickly, they diffuse back and are recaptured by the electrode, since the electrochemical potential of electrons in the metal is markedly lower than that of solvated electrons in the solution. A steady state is attained after about 1 ns); at this time the rate of oxidation has become equal to the rate of emission, and the original, transient photoemission current (the electric current in the galvanic cell in which the illuminated electrode is the cathode) has fallen to zero. Also, in the case when solvated electrons react in the solution yielding oxidizable species (e.g., $Zn^{2+} + e_S^- \rightarrow Zn^+$), steady-state current is zero since the photoemitted charge is recaptured by oxidation of the intermediate species ($Zn^+ - e_M^- \rightarrow Zn^{2+}$).

Steady photoemission currents can be realized when acceptors (scavengers) for the solvated electrons are present in the solution. A good scavenger should be nonelectroactive at the potential of interest, should react quickly with solvated electrons, and the reaction products should be either nonelectroactive or reducible. A reaction with acceptors implies that the current of reoxidation of the solvated electrons becomes lower, and thus a steady photoemission current appears. The acceptors most often used are nitrous oxide, N_2O, and hydroxonium ions, H_3O^+. In the former case, $OH^{\cdot}$ radical is produced in the scavenging process, which undergoes further reduction on the electrode, thus doubling the photocurrent:

$$N_2O + e_S^- \rightarrow N_2O^{\cdot -}; \tag{29.8a}$$

$$N_2O^{\cdot -} + H_2O \rightarrow N_2 + OH^- + OH^{\cdot}; \tag{29.8b}$$

$$OH^{\cdot} + e_M^- \rightarrow OH^-. \tag{29.8c}$$

Water molecules do not react with the solvated electrons in the time scale of charge recapture, and hence do not function as acceptors.

An important feature of the photoemission current is its unusual dependence on the acceptor concentration. It follows from theory and is confirmed by experiments that at low concentrations, the current is proportional to the square root of acceptor concentration: $I_{ph} \sim c_{acc}^{1/2}$. At high concentrations, when practically all electrons that have been emitted react with the acceptor, the photoemission current no longer depends on the acceptor concentration.

The basic law of electron photoemission in solutions which links the photoemission current with the light's frequency and with electrode potential is described by Eq. (9.6) (the *law of five halves*). This equation must be defined somewhat more closely. As in the case of electrochemical reactions (see Section 14.2), not the full electrode potential E as shown in Eq. (9.6) is affecting the metal's electron work function in the solution but only a part $(E - \psi')$ of this potential which is associated with the potential difference between the electrode and a point in the solution just outside the electrode. Hence the basic law of electron photoemission into solutions should more correctly be written as

$$I_{ph} = C[h\nu - \lambda^{(E)}]^{5/2} = C[h\nu - B - Q^0(E - \psi')]^{5/2}. \tag{29.9}$$

Here C is a constant that depends on light intensity and on the experimental conditions. Constant B [cf. Eq. (9.5)] depends on the reference electrode.

Photoemission phenomena are of great value for a number of areas in electrochemistry. In particular, they can be used to study the kinetics and mechanism of electrochemical processes involving free radicals as intermediates. Photoemission measurements can be also used to study electric double-layer structure at electrode surfaces. For instance by measuring the photoemission current in dilute solution and under identical conditions in concentrated solutions (where we know that $\psi' = 0$), we can find the value of ψ' in the dilute solution by simple calculations using Eq. (29.9).

At electrode potentials more negative than approximately -2.8 V (SHE), free solvated electrons appear in the solution as a result of (dark) emission from the metal. At this potential the electrochemical potential of the electrons according to Eq. (29.6) is about -1.6 eV, which is at once the energy of electron hydration in electron transfer from vacuum into an aqueous phase.

29.3 PHOTOEXCITATION OF SEMICONDUCTOR ELECTRODES

29.3.1 Behavior of Illuminated Semiconductor Electrodes

Semiconductor electrodes exhibit electron photoemission into the solution, like metal electrodes, but in addition they exhibit further photoelectrochemical effects due to excitation of the electrode under illumination. The first observations in this area were made toward the middle of the twentieth century. At the end of the 1940s,

Vladimir I. Veselovsky studied the photoelectrochemical behavior of metals covered with oxide layers having semiconductor properties. In 1955, Walter H. Brattain and Charles G. B. Garrett published a paper in which they established the connection between the photoelectrochemical properties of single-crystal semiconductors and their electronic structure.

The behavior of a semiconductor depends on its own nature and also on that of the phase in contact with it. We shall examine *n*-type semiconductors as an example, which are often used and which contain electron-donating impurities. These impurities produce a strong decrease in work function. This implies that the electrochemical potential, $\overline{\mu}_e^{(S)}$, of the electrons in them [the superscript$^{(S)}$ stands for the semiconductor] is rather high (just slightly negative). When contact is made with an electrolyte, the original value of $\overline{\mu}_e^{(S)}$ in the semiconductor, as a rule, is higher than that of the redox system in the solution. For this reason, a partial transition of electrons into the solution starts to take place, the semiconductor becomes positively charged, its potential moves in the positive direction, and the values of $\overline{\mu}$ come closer together (in the case of semiconductors, complete electronic equilibrium with the solution is often not established, i.e., some difference between the $\overline{\mu}_e$ values remains).

The excess positive charge appearing in the semiconductor's surface layer (which constitutes a depletion of electrons in this layer) leads to an upward bending of the band edges (see Fig. 29.2). As the semiconductor's potential is moved in the positive direction, the Fermi level, in accordance with Eq. (29.6), moves in the negative direction. The edges of valence and conduction bands in the bulk semiconductor move together with it. The energies of the band edges at the surface itself (i.e., the degree of band bending) depend on the repartition of the total potential change ΔE between the surface and interfacial potential. Figure 29.2 shows schematically the positions of the band edges and Fermi level for two values of electrode

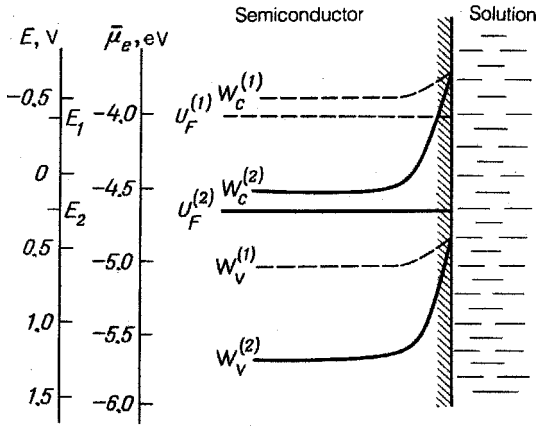

FIGURE 29.2 Energy bands in an *n*-type semiconductor in contact with an electrolyte solution for two values, E_1 and E_2, of electrode potential ($E_2 > E_1$).

potential $E_2 > E_1$ in the case where only the surface potential changes while the interfacial potential remains practically constant (the band edges are "pinned to the surface").

When semiconductors are irradiated with photons of high energy, electron photoemission is possible, as in the case of metals. When the photon energy is lower than the electron work function in the solution, under given conditions, but is still higher than the semiconductor's bandgap W_g,

$$\lambda^{(S,E)} > h\nu > W_g, \tag{29.10}$$

interband electron transitions can occur from the valence band to the conduction band above. The result of such a transition is the formation of a pair of free carriers, an electron in the conduction band and a positive hole in the valence band. This is an event equivalent to the electron transitions to higher energy levels in the valence band that occur in metals.

The difference between metals and semiconductors becomes apparent when the further fate of these excited charges is considered. In metals an excited electron will very quickly (within a time on the order of 10^{-14} s) return to its original level, and the photon's original energy is converted to thermal energy. Photoexcitation has no other consequences.

In semiconductors, which have a bandgap, recombination of the excited carriers—return of the electrons from the conduction band to vacancies in the valence band—is greatly delayed, and the lifetime of the excited state is much longer than in metals. Moreover, in *n*-type semiconductors with band edges bent upward, excess electrons in the conduction band will be driven away from the surface into the semiconductor by the electrostatic field, while positive holes in the valence band will be pushed against the solution boundary (Fig. 29.3). The electrons and holes in the pairs produced are thus separated in space. This leads to an additional stabilization of the excited state, to the creation of some steady concentration of excess electrons in the conduction band inside the semiconductor, and to the creation of excess holes in the valence band at the semiconductor–solution interface.

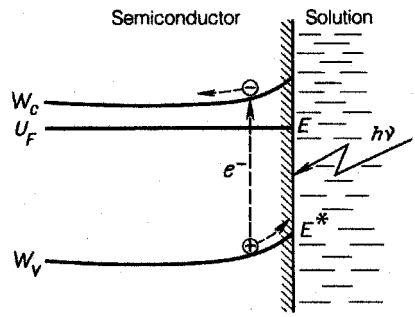

FIGURE 29.3 Charge separation during photoexcitation of a semiconductor electrode.

These two groups of excited carriers are not in equilibrium with each other. Each of them corresponds to a particular value of electrochemical potential; we shall call these values $\overline{\mu}_e^{(S)*}$ and $\overline{\mu}_h^{(S)*}$. Often, these levels are called the *quasi-Fermi levels* of excited electrons and holes. The quasilevel of the electrons is located between the (dark) Fermi level and the bottom of the conduction band, and the quasilevel of the holes is located between the Fermi level and the top of the valence band. The higher the relative concentration of excited carriers, the closer to the corresponding band will be the quasilevel. In *n*-type semiconductors, where the concentration of electrons in the conduction band is high even without illumination, the quasilevel of the excited electrons is just slightly above the Fermi level, while the quasilevel of the excited holes, $\overline{\mu}_h^{(S)*}$, is located considerably lower than the Fermi level.

Because of the excess holes with an energy lower than the Fermi level that are present at the *n*-type semiconductor surface in contact with the solution, electron transitions from the solution to the semiconductor electrode are facilitated ("egress of holes from the electrode to the reacting species"), and anodic photocurrents arise. Such currents do not arise merely from an acceleration of reactions which, at the particular potential, will also occur in the dark. According to Eq. (29.6), the electrochemical potential, $\overline{\mu}_h^{(S)*}$, corresponds to a more positive value of electrode potential (E^*) than that which actually exists (E). Hence, anodic reactions can occur at the electrode even with redox systems having an equilibrium potential more positive than E (between E and E^*) (i.e., reactions that are prohibited in the dark).

When the illuminated electrode is not potentiostated, the space charge in its surface layer will decrease under the effect of the holes accumulating at the surface itself; the degree of band bending will also decrease, and the electrode potential will move in the negative direction. It can be shown that the maximum value of this potential shift is equal to the original (dark) value of the semiconductor's surface potential in contact with the solution (i.e., to the original value of band bending).

The electrons produced in the conduction band as a result of illumination can participate in cathodic reactions. However, since in *n*-type semiconductors the quasi-Fermi level is just slightly above the Fermi level, the excited electrons participating in a cathodic reaction will almost not increase the energy effect of the reaction. Their concentration close to the actual surface is low; hence, it will be advantageous to link the *n*-type semiconductor electrode to another electrode which is metallic, and not illuminated, and to allow the cathodic reaction to occur at this electrode. It is necessary, then, that the auxiliary metal electrode have good catalytic activity toward the cathodic reaction.

Analogous effects are seen at *p*-type semiconductors at which cathodic reactions are accelerated when the electrode is illuminated. For heightened effects, one can combine in a single cell an *n*- and a *p*-type semiconductor and allow the anodic reaction to occur at the former and the cathodic reaction to occur at the latter.

29.3.2 Devices Based on the Photoexcitation of Semiconductor Electrodes

The phenomena listed can be used for the design of practical devices in which luminous (solar) energy is converted directly to electrical or chemical energy. The

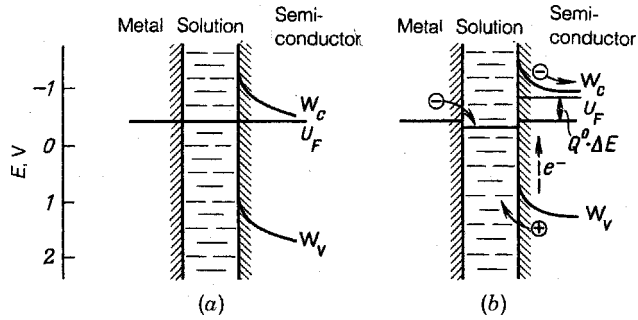

FIGURE 29.4 Energy diagrams for a cell with CdS photoanode in an alkaline solution containing ions S^{2-} and S_2^{2-}: (*a*) in the dark; (*b*) under illumination.

devices for the production of electrical energy are galvanic cells in which the anodic reaction occurring at an illuminated electrode is fully compensated by the reverse (cathodic) reaction occurring at a dark electrode (i.e., there is no overall current-producing reaction, and no overall chemical change whatever occurs in the system). Cells of this type, where the electrodes are operated under different conditions but where the same electrode reaction occurs in different directions at the two electrodes, are called *regenerative*.

Figure 29.4 shows an example, the energy diagram of a cell where *n*-type cadmium sulfide CdS is used as a photoanode, a metal that is corrosion resistant and catalytically active is used as the (dark) cathode, and an alkaline solution with S^{2-} and S_2^{2-} ions between which the redox equilibrium $S_2^{2-} + 2e^- \rightleftharpoons 2S^{2-}$ exists is used as the electrolyte. In this system, equilibrium is practically established, not only at the metal–solution interface but also at the semiconductor–solution interface. Hence, in the dark, the electrochemical potentials of the electrons in all three phases are identical.

The band edges are flattened when the anode is illuminated, the Fermi level rises, and the electrode potential shifts in the negative direction. As a result, a potential difference ΔE_{ph} which amounts to about 0.6 to 0.8 V develops between the semiconductor and metal electrode. When the external circuit is closed over some load R, the electrons produced by illumination in the conduction band of the semiconductor electrode will flow through the external circuit to the metal electrode, where they are consumed in the cathodic reaction. Holes from the valence band of the semiconductor electrode at the same time are directly absorbed by the anodic reaction. Therefore, a steady electrical current arises in the system, and the energy of this current can be utilized in the external circuit. In such devices, the solar-to-electrical energy conversion efficiency is as high as 5 to 10%. Unfortunately, their operating life is restricted by the low corrosion resistance of semiconductor electrodes.

Devices for the production of chemical energy differ from the ones described, in that different electrode reactions now occur at the cathode and anode. As the result of overall current-producing and current-consuming reactions, energy-rich products

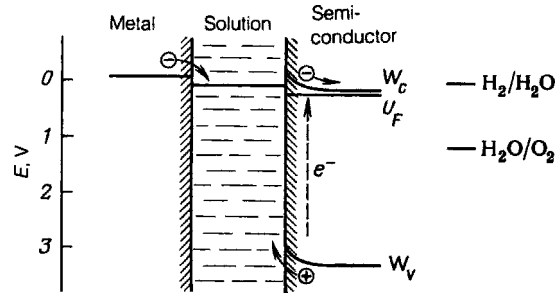

FIGURE 29.5 Energy diagram for water photoelectrolysis with a TiO_2 anode.

are generated (*photoelectrolysis*); their chemical energy can be utilized. Of greatest interest is the photoelectrolytic production of hydrogen. The first cells of this type were built in 1972 by Akira Fujishima and Kenichi Honda in Japan. Their photoanode was titanium dioxide, TiO_2 (an *n*-type semiconductor); their cathode was platinized platinum. A porous separator was used in the cell to keep the anodic and cathodic reaction products apart.

The energy diagram of a cell of this type is shown schematically in Fig. 29.5. In a semiconductor having a sufficiently wide bandgap (e.g., in strontium titanate, $SrTiO_3$, we have $W_g = 3.2\,\text{eV}$), the quasilevel $\overline{\mu}_h^{(S)*}$ of the holes is located appreciably below $\overline{\mu}_e^{(E)}$ for the water–oxygen redox system, while the quasilevel $\overline{\mu}_e^{(S)*}$ of the electrons is located appreciably above $\overline{\mu}_e^{(E)}$ for the water-hydrogen redox system. Hence, under illumination and with the external circuit closed, anodic oxygen evolution will readily occur at such an electrode (the electrode is readily polarized, and thus high current densities are possible), and cathodic hydrogen evolution consuming the electrons that have been generated in the semiconductor's conduction band and have traveled to the platinum electrode will occur at this electrode.

According to Eq. (29.10), only light of the ultraviolet part of the spectrum can be absorbed when the bandgaps are so wide, and such devices are not suitable for solar energy conversion. Titanium dioxide has a slightly narrower bandgap (about 3 eV). However, in this material the quasilevel of the electrons is slightly below $\overline{\mu}_e^{(E)}$ for the water–hydrogen redox system, so that hydrogen evolution is no longer possible. Other materials having lower values of W_g may have an even larger difference between these levels. This difficulty can be overcome when a power source of low voltage (e.g., 0.4 to 0.6 V) that will shift the potential of the platinum electrode in the negative direction is included in the external circuit. Using this device, one can electrolytically produce hydrogen and oxygen with cell voltages about four times lower than by electrolysis in the dark (the theoretical voltage for water electrolysis is 1.23 V; see Section 15.3).

The overall energy conversion efficiency (the ratio between the chemical energy of hydrogen and the solar energy striking the electrode, corrected for the energy consumed to sustain the additional voltage mentioned) is about 6%. Even in this case, problems concerning stability of the semiconductor electrode arise. Numerous

studies aiming at finding more efficient and more stable semiconductor systems are still going on at the present time.

29.4 PHOTOEXCITATION OF REACTING SPECIES

The absorption of visible light of a particular frequency by atoms or molecules of a solute is perceived by our eyes as the color of this substance. Hence, only colored substances—natural or synthetic dyes—are excited by visible light. Under ultraviolet light, substances not absorbing in the visible part of the spectrum can also be excited.

Upon excitation of the molecule, one or several electrons are lifted to a higher energy level. When the lifetime of the photoexcited state of molecules j is sufficiently long (i.e., longer than the time required for electronic transitions between particles), this state can be described in terms of a new value $\overline{\mu}_j^{(E)^*}$ of the electrochemical potential, which is higher than the value $\overline{\mu}_j^{(E)}$ of nonexcited particles.

Often, the primary photoexcited species are unstable and are converted (e.g., by chemical reaction with other solution components) to more stable secondary species, which, as a rule, still have an electrochemical potential higher than the original, unexcited species. Sometimes an entire chain of such conversions may be involved.

An excited particle that is to become involved in the electrochemical reaction must be sufficiently close to the electrode surface to diffuse to the surface within the lifetime of its excited state. It is better yet when it is present on the surface as an adsorbate. Sometimes, dyes are applied to the surface which are not themselves involved in any electrochemical reaction but which when excited react with the solution to produce a soluble secondary substance that will react (sensitization of the electrode surface).

In the case of species involved in a redox reaction, any change in their electrochemical potential upon photoexcitation will also cause a change in electrochemical potential $\overline{\mu}_e^{(E)}$ of the electrons in the solution. When the excited species is an oxidizing agent, the value of $\overline{\mu}_e^{(E)}$ according to Eq. (29.2) will decrease; but when it is a reducing agent, the value of $\overline{\mu}_e^{(E)}$ will increase. A corresponding change will also occur in the redox potential of a reaction involving photoexcited species. This change can be ascertained by measuring the open-circuit potential of a metallic indicator electrode in the solution containing the photoexcited species (when the excited species are sufficiently stable, the indicator electrode may even by outside the illuminated region).

A change in thermodynamic properties of the excited species has several consequences. For instance, cathodic reduction of an excited oxidizing agent is possible at less negative potentials than that of a nonexcited one. In particular, in polarographic measurements at the dropping mercury electrode this leads to a shift of half-wave potential in the positive direction (*photopolarography*; Berg, 1965). In electrochemical reactions, the apparent kinetic parameters may change.

When, in a symmetric galvanic cell suitably assembled, the region of the solution close to one of the electrodes is illuminated, a potential difference between the

electrodes will develop owing to photoexcitation of dissolved species. An electric current is recorded in the system when the circuit is closed; the reaction of the photoexcited species at the first electrode (e.g., the cathodic reduction of an excited oxidizing agent) will be compensated by the reverse reaction at the second electrode. Thus, a cell of this type is regenerative, and its luminous energy is converted to electrical energy.

The classical example of such a device is a cell where thionine dye is used. Thionine is the oxidizing agent in the reaction: $T + e^- + H^+ \rightleftharpoons TH$. Thionine itself is hard to reduce electrochemically. Therefore, the mediating redox system Fe^{3+}/Fe^{2+} is used, which functions as an electron shuttle. The excited form of thionine, T^*, produced under illumination is readily reduced by divalent iron ions:

$$T^* + Fe^{2+} + H^+ \rightleftharpoons TH + Fe^{3+}. \tag{29.11}$$

The thionine reduction product TH is anodically reoxidized to thionine, while the Fe^{3+} ions are cathodically rereduced to Fe^{2+} ions. Thus, the chemical composition of the system will not change during current flow. The potential difference between the electrodes that can be used to extract electrical energy is 0.2 to 0.4 V under current flow. The conversion factor of luminous to electrical energy is very low in such cells, about 0.1%. This is due to the numerous side reactions, which drastically lower the overall efficiency. Moreover, the stability of such systems is not high. Therefore, the chances for a practical use are not evident so far.

REFERENCES

Barker, C., and A. Gardner, *J. Electrochem. Soc.*, **113**, 1182 (1966).

Becquerel, A., *C. R. Acad. Sci.*, **6**, 145 (1839).

Berg, H., Photopolarography, in *Modern Aspects of Polarography*, T. Kambara, Ed., Plenum Press, New York, 1966.

Brattain, W. H., and C. G. B. Garrett, *Bell Syst. Tech. J.*, **34**, 129 (1955).

Fujishima, A., and K. Honda, *Nature*, **238**, 37 (1972).

Veselovsky, V., *Zh. Fiz. Khim.*, **20**, 1493 (1946).

MONOGRAPH

Pleskov, Yu. V., *Solar Energy Conversion: A Photoelectrochemical Approach*, Springer-Verlag, Berlin, 1990.

30
Bioelectrochemistry

Many of the physical and chemical processes and phenomena that are basic to the vital function of all biological systems are electrochemical in nature. It is the primary task of bioelectrochemistry to reveal the mechanisms and basic electrochemical features of such biological processes.

Electrochemistry and bioelectrochemistry have the same sources: They have emerged as sciences from the famous experiments of the Italian physiologist and anatomist Luigi Aloisio Galvani. In 1786, when experimenting with prepared frog legs, he discovered when he touched the muscle tissue with two pieces of metal that were dissimilar but in mutual contact, a contraction of the muscles which was analogous to that provoked by the discharge of a Leyden jar. Recognizing the metals as conductors but not as a source of electricity, he ascribed the effect to a special "animal electricity." The Italian physicist Alessandro Volta in 1794 offered a different interpretation for the effect when he pointed out that the origin of this *galvanic effect* is the contact between the two dissimilar metals and their contact with the muscle tissue. A dispute developed between Galvani and Volta that ended with a temporary victory of Volta. It was in fact discovered that when dissimilar metals are in contact with each other and with an ionic conductor, potential differences arise in the circuit which more specifically will give rise to muscle contraction. This was the starting point for the concepts of electrode potentials, which are a highly important component of modern electrochemistry. On the other hand, a number of observations were made in the first half of the nineteenth century from which it was concluded that potential gradients exist even in living tissue. In fact, even Galvani, when repeating his experiments with identical metal pieces, had obtained the same effect as before; but his contemporaries had paid no attention to these studies. Thus, Galvani's ideas were also vindicated, and it is from these ideas that bioelectrochemistry started.

Bioelectrochemistry is a science at the junction of many other sciences: electrochemistry, biophysics, biochemistry, electrophysiology, and others. The biological systems are extremely diverse in their constitution and detailed mechanism of functioning; each system has its own specific morphological and physiological features. In contrast to electrophysiology, bioelectrochemistry is concerned only with the

Fundamentals of Electrochemistry, Second Edition, By V. S. Bagotsky

Luigi Galvani (1737–1798).

general and basic laws of the electrochemical processes occurring in biological entities, and disregards the particular features of specific systems. For this reason, bioelectrochemical studies often are conducted not on natural objects but on synthetic model systems (e.g., artifical membranes).

From an electrochemical viewpoint, biological systems are highly branched circuits consisting of ionic conductors: of aqueous electrolyte solutions and highly selective membranes. These circuits lack metallic conductors, but it has been found relatively recently that they contain sections that behave like electronic conductors (i.e., sections in which electrons can be transferred over macroscopic distances, owing to a peculiar relay-type mechanism).

In the present chapter a brief outline of two major lines of modern bioelectrochemistry is given: studies of transmission of the nervous impulse (Section 30.1) and

Alessandro Volta (1745–1827).

studies of the bioenergetic processes within cells (Section 30.2). Both are related to the mechanism of cell membrane function and to membrane structure. In Section 30.3 a number of points are discussed which are somewhat outside bioelectrochemistry but which are relevant for the use of electrochemical methods in biological and medical problems.

30.1 TRANSMISSION OF THE NERVOUS IMPULSE

30.1.1 Functions and Structure of Cell Membranes

Cells are the working units of all biological systems. All basic vital functions occur in cells: the reproduction of genetic information, chemical metabolism and biosynthesis, the bioenergetic accumulation and transformation of the different kinds of energy, and so on. The nerve cells of multicellular organisms transmit the information from various receptors (the organs of sight, hearing, etc.) and internal controlling organs in the central nervous system and brain to the executive organs (muscle, endocrine, or other system) for analysis of this information and for the transmission of response instructions. The nerve cells of the peripheral nervous system have long, thin (dendritic) processes, the axons, which provide possibilities for a direct transmission of needed information over long distances. Muscle cells, too, have the shape of long, thin fibers through which information and commands can be transmitted.

In their vital functions the cells are in constant interaction with their surroundings. Various chemical substances enter the cell, and others leave it; energy effects are also possible (the inflow of photons). Cells are surrounded by thin membranes (surface or plasma membranes) which enclose them and jointly with them regulate all types of exchange and interaction with the surroundings. These membranes are 7 to 15 nm thick. Inside the cells again different types of intracellular membrane are found which have an extremely strongly extended surface area (folds, numerous bulges, etc.). These membranes surround a nucleus and are the constituents of different cell organelles: the mitochondria, the chloroplasts, and so on. Intracellular membranes are 5 to 9 nm thick.

Both the intracellular and the plasma membranes are actively involved in the cell's vital functions. In the surface membranes of axons, processes of information transfer in the form of electrical signals (*nerve impulses*) take place. Bioenergy conversion processes occur at the intracellular membranes of the mitochondria and chloroplasts.

The intracellular and plasma membranes have a complex structure. The main components of a membrane are lipids (or phospholipids) and different proteins. Lipids are fatlike substances representing the esters of one di- or trivalent alcohol and two aliphatic fatty acid molecules (with 14 to 24 carbon atoms). In phospholipids, phosphoric acid residues, –O–PO(O^-)–O–, are located close to the ester links, –CO–O–. The lipid or phospholipid molecules have the form of a compact polar *head* (the ester and phosphate groups) and two parallel, long nonpolar *tails* (the hydrocarbon chains of the fatty acids). The polar head is hydrophilic and readily interacts with water; the hydrocarbon tails to the

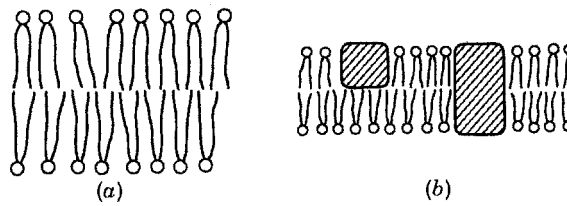

FIGURE 30.1 Lipid bilayer membrane (*a*) and the location of protein molecules in it (*b*).

Cell membranes consist of two layers of oriented lipid molecules (*lipid bilayer membranes*). The molecules of these two layers have their hydrocarbon tails toward each other, while the hydrophilic heads are outside (Fig. 30.1*a*). The mean distance between lipid heads is 5 to 6 nm. Various protein molecules having a size commensurate with layer thickness "float" in the lipid layer. Part of the protein molecules are located on the surface of the lipid layer; others thread through the layer (Fig. 30.1*b*). Thus, the membrane as a whole is heterogeneous and has a mosaic structure.

30.1.2 Electrochemical Properties of Cell Membranes

All biological systems contain aqueous electrolyte solutions. These solutions consist of strong electrolytes (inorganic salts) as well as various organic substances with acidic or basic functional groups which usually behave as weak electrolytes. The solutions are often gel-like in their consistency because of the polyelectrolytes, proteins, and other macromolecules contained in them. The pH values of biological solutions as a rule are between 6.7 and 7.6.

An outer cell membrane separates the intracellular solution or cytoplasm from the extracellular solution. These two solutions differ in their compositions. The extracellular fluid contains primarily Na^+ and Cl^- ions (0.1 to 0.5 M) as well as minor amounts of K^+, Ca^{2+}, and Mg^{2+} ions, while the cytoplasm has a high concentration of K^+ ions (0.1 to 0.5 M) and low concentrations of Na^+ and Cl^- ions. Principal anions in the cytoplasm are the relatively large anions of different organic acids, including polyanions. As an example we report the major inorganic ions contained in the extra- and intracellular solutions of frog muscle (in mM):

	Na^+	K^+	Cl^-
Outside the cell	120	2.5	120
Inside the cell	9.2	140	3.5

The specific resistance of the extracellular fluid is 2 to 200 Ω·cm. The ionic mobilities and specific resistance in the cytoplasm are of the same order of magnitude as those in the extracellular fluid, despite the gel-like consistency commonly associated with the cytoplasm.

The membranes also have a certain, though small ionic conductivity. The electrical resistance of membranes when referred to unit surface area is 10^2 to 10^3 $\Omega \cdot cm^2$, which when allowing for the small membrane thickness (about 10 nm) corresponds to the rather high value of specific (volume) resistance of 10^8 to 10^9 $\Omega \cdot cm$.

This high resistance is due to the difficult transfer of hydrated ions through the hydrophobic part of the lipid layer (the permeability of the membrane for nonhydrated organic substances is two to three orders of magnitude higher than that for ions). The transfer can be accomplished in two ways: via special ionic channels formed by the protein molecules, or by ionophores. The latter are large, mobile organic molecules wrapping the ions to be transferred from all sides with a "fur coat" of hydrophobic groups. Such complexes form on one side of the membrane, pass through the lipid layer, and decompose on the other side. A distinguishing feature of all these versions of transport is their high selectivity. Hence, the formal values of the mobilities and transport numbers of different ions in the membrane may be highly different.

A very important property of the membranes are the membrane potentials that are established. For biological membranes, the membrane potential is defined as the potential in the fluid within the cell relative to that in the fluid outside the cell: $\varphi_m = \psi^{(i)} - \psi^{(e)}$. Nowadays techniques are available for direct measurements of membrane potentials in various cells; they use microelectrodes or microprobes in the form of Luggin glass capillaries highly drawn out (with diameters of less than 1 μm) which can be inserted into the cell and into the extracellular fluid.

In the cell's nonexcited state (see Section 30.1.3), the membrane potential, φ_m, is always negative (i.e., the cytoplasm is negatively charged relative to the extracellular solution). For different cell types the values of φ_m vary between -50 and -100 mV; for frog muscle the value is -90 mV.

Two questions arise in connection with the ionic permeability present in membranes: How can the ionic concentration gradients between the two sides of the membrane be preserved despite leakage of ions, and how is the membrane potential related to these gradients? These questions have been explored in extended studies still continuing.

One of the founders of experimental neurophysiology, the German Julius Bernstein, in 1902 advanced the concept that biological membranes are permeable only to K^+ ions, not to any other ions. As a result, a Donnan equilibrium is set up (Section 5.4.1) and a certain membrane potential develops the value of which is determined, according to Eq. (5.15), by the K^+ ion concentrations in both solutions. These concentrations in turn depend on the concentrations of other, nonpermeating ions, particularly on the concentration of organic anions in the cytoplasm. The potential gradient that develops compensates the effect of the concentration gradient (the electrochemical potentials, $\overline{\mu}_{K^+}$, of the potassium ions in the two solutions become identical), and hence the concentrations of these ions will not become equal. For frog muscle, a value of -103 mV is calculated for the membrane potential from Eq. (5.15), which is close to, though a little more negative than, the experimental value.

In the 1940s a number of phenomena were discovered which do not fit these ideas. It was shown in particular that biological membranes are permeable, not only

to K^+ ions but also to Na^+ and Cl^- ions. It is true that these membranes have different permeabilities for different ions. The permeability (the fluxes of ions crossing the membrane under the effect of identical "driving forces," i.e., identical concentration and potential gradients) can be measured with the aid of tracer atoms. Such measurements have shown that the permeability for Na^+ ions is about 75 times lower than that for the K^+ ions. Despite this difference, the total flux of Na^+ ions from the external solution into the cytoplasm (along the potential gradient) is substantially the same as that of K^+ ions in the opposite direction (against the potential gradient). The large organic ions present in the cytoplasm practically do not cross the membrane.

Membrane permeability for the Cl^- ions is not in contrast to the conclusion that a simple membrane equilibrium such as that described in Section 5.4.1 is established at the membrane. In fact, the membrane potential calculated for the example above with Eq. (5.26) from the Cl^- ion concentration ratio is exactly -90 mV (i.e., the Cl^- ions in the two solutions are in equilibrium, and there is no unidirectional flux of these ions).

Another situation is found for the Na^+ ions. When the membrane is permeable to these ions, even if only to a minor extent, they will be driven from the external to the internal solution, not only by diffusion but when the membrane potential is negative, also under the effect of the potential gradient. In the end, the unidirectional flux of these ions should lead to a concentration inside that is substantially higher than that outside. The theoretical value calculated from Eq. (5.15) for the membrane potential of the Na^+ ions is $+66$ mV. Therefore, permeability for Na^+ ions should lead to a less negative value of the membrane potential, and this in turn should lead to a larger flux of potassium ions out of the cytoplasm and to a lower concentration difference of these ions. All these conclusions are at variance with experience.

Thus, the ideas above do not suffice for an interpretation of all experimental results. These ideas include the assumption that the ions move in the membrane only under the effect of concentration and potential gradients (diffusion and migration), and that transport of one sort of ions is independent of the transport of other sorts of ions. This transport of ions under the effect of external forces has been named *passive ionic transport*.

In the attempt to overcome the contradictions, the assumption must be made that aside from passive transport in the cell, an active transport of Na^+ ions from the cytoplasm to the external solution is accomplished by the action of peculiar molecular *pumps*.

The possibility of active transport of substances across membranes had first been pointed out in the middle of the nineteenth century by the physiologist Emil Heinrich du Bois-Reymond, a German of Swiss descent. The ability to accomplish active transport of ions and uncharged molecules in the direction of increasing electrochemical potentials is one of the most important features of cell membrane function. The law of independent ionic migration as a rule is violated in active transport.

The ionic composition of the cell is maintained by operation of the sodium–potassium pump, which pumps ions from more dilute to more concentrated solutions: the Na^+ ions from the cytoplasm to the solution outside, and the K^+ in the opposite

direction. We shall not discuss the details of the molecular operating mechanisms of this pump (of which many particulars are still not clear), but only point out certain features of its action. The transport of the Na^+ and K^+ ions is coupled; the ions are pumped, strictly in a 2 : 3 ratio. It follows that transport is the result of a cyclic process; in one half-period the Na^+ ions are transferred in one direction, and in the other half-period the K^+ ions are transferred in the opposite direction.

Active transport against the action of external forces requires the expenditure of a certain energy. This energy is 0.1 to 0.2 eV for transport of each Na^+ ion in the direction indicated (for the example reported above, 90 meV for overcoming the potential gradient and 66 meV for overcoming the concentration gradient, which is a total of 156 meV). For the K^+ ions the transport energy is much lower (10 to 20 meV), since here the potential gradient aids in overcoming the concentration gradient.

The energy needed to transport ions across the membrane is obtained by the cell in chemical reactions occurring in it: that is, the oxidation of organic substances with oxygen (for more details, see Section 30.2). Every second about 10^{11} to 10^{12} ions are transported across 1 m^2 of membrane area. This process requires 20 to 30% of all energy generated by the cell. It has been calculated that the total power of the ionic pumps in the cells of the brain is about 1 watt.

The setting up of a membrane potential φ_m is associated with the formation of an electric double layer which has most of its charges close to the (outer and inner) membrane surfaces, within the range of the lipid heads. A temporary change in charge density in the EDL (e.g., by supply of charge from outside) will produce a change in membrane potential. By operation of the ion pumps and ionic redistribution, the original state of the membrane is reestablished quite rapidly when the external action has ceased. The membrane's specific electrical capacitance can be determined by direct measurements. It is about 1 $\mu F/cm^2$. According to the electrostatic capacitor relation, this is exactly the capacitance of a layer 5 nm thick where the relative permittivity ε is about 6.

Allowing for all these data, one can describe the electrochemical properties of a cell membrane with the electrical equivalent circuit shown in Fig. 30.2. Here the capacitor C_m simulates the membrane's capacitance. Between its plates the potential difference φ_m is established, which is in fact the membrane potential. To the left of the capacitor the branches mediating passive transport (leakage) are shown, and to the right the branches mediating active transport. Each of the branches of passive transport includes a power source E_j and a resistance R_j. The power source simulates the work of transfer due to the concentration gradient of the corresponding ion j. The voltage E_j of this source, which is the theoretical value of the membrane potential, is calculated from Eq. (5.15). Resistance R_j is the resistance to ionic transport. It is inversely proportional to the ionic mobilities in the membrane or the membrane's permeability for ions. The resistances for K^+ and Na^+ ions are about 10^2 to 10^3 $\Omega \cdot cm^2$; for the Na^+ ions the value is almost two orders of magnitude higher, as had been pointed out above. The resistances for the K^+ and Na^+ ions in the active transport branches, R_j, differ from the corresponding values, R_j, in the passive transport branches, since the transport mechanisms in these branches are different. The ion

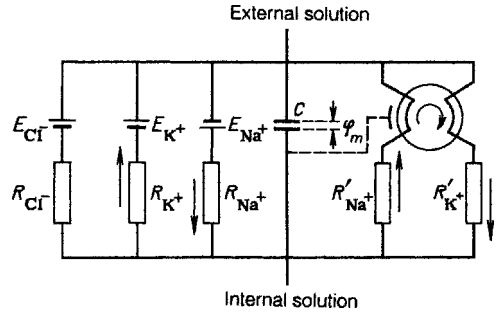

FIGURE 30.2 Electrical equivalent circuit of a cell membrane.

pump accomplishing coupled transport of the Na^+ and K^+ ions against the electrochemical potential gradients is shown in the right-hand part of the circuit. It has a feedback (shown as a dashed line in the circuit) which regulates its work depending on the value of φ_m, and maintains the required values of the concentration gradients and membrane potential.

It can be seen from this equivalent circuit that the actual value of membrane potential φ_m should be intermediate between the extreme values of the theoretical membrane potentials E_j for the different ions [i.e., between -103 mV for the K^+ ions and $+66$ mV for Na^+ ions, which is confirmed by experiments ($\varphi_m = -90$ mV)].

30.1.3 Excitation of Cell Membranes

Another important property of the outer membranes of nerve and muscle cells is their susceptibility to excitation under the effect of electric action. Excitation can be brought about, for example, by an external electric current pulse. Pulses can be applied to the membrane with the aid of two microelectrodes, one residing in the extracellular fluid and the other introduced through the membrane into the cytoplasm.

When a current pulse is applied, part of the charges introduced will be consumed for changing the charge density in the EDL (i.e., for changing the membrane potential). The potential change will depend on the value of current and length of the pulse. When the current (flow of positive charges) is out of the cell, the membrane potential will move in the positive direction (its negative value will decrease), which is called *membrane depolarization*. When the current is in the opposite direction, the negative value of φ_m will increase, which is called *membrane hyperpolarization*.

Ordinarily, when the current pulse is over, the excess charges will be drained through the passive transport channels, and by operation of the sodium–potassium pumps the original values of membrane potential and of the concentration gradients will be reestablished. However, when in the case of depolarization the negative value of φ_m has dropped below a certain threshold value, which is about -50 mV, the picture changes drastically: Excitation of the membrane occurs. When the current is turned off, the membrane potential not only fails to be restored but continues to

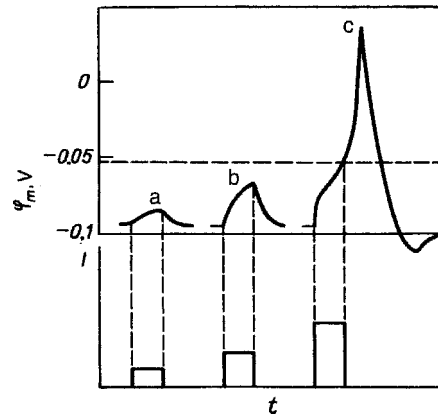

FIGURE 30.3 Changes in membrane potential φ_m of a cell membrane occurring upon application of depolarizing current pulses of different amplitude I: (a,b) below threshold; (c) excitation of the membrane during an above-threshold pulse.

change in the positive direction. It goes through zero, attains values of 30 to 50 mV (membrane polarity reversal), and only after this excursion returns rather quickly to the original value (Fig. 30.3). This spontaneous surge or burst of potential has been called the *action potential* or *spike*.

The burst lasts a few milliseconds. The character of the excitation (the amplitude and duration of the action potential) is independent of the original current pulse parameters; the only condition that must be met to produce this process is attainment of the threshold potential. A higher intensity and/or longer duration of the original pulse only accelerates attainment of the threshold potential but does not alter the shape of the action potential. Following its return to the original state, the membrane can be excited again only after a certain time (a few milliseconds), during which it is in the refractory (nonexcitable) state.

It has been shown by extremely delicate experiments (including the use of tracer atoms) that membrane excitation occurs because of changes in permeability for the ions. The ionic permeability (or the resistance R_j to the ion flux during passive transport which is inversely proportional to it) is not constant but depends on potential. When the threshold potential is attained, the permeability for Na^+ ions and hence the flux of these ions from the extracellular fluid into the cytoplasm increase drastically. This decrease in R_{Na^+} produces an additional shift of the membrane potential in the positive direction, which in turn causes a further increase in permeability and Na^+ ion flux, and so on (i.e., the process is self-accelerating). The membrane potential shifts until it comes close to the theoretical value for the Na^+ ions (+66 mV). In this state the permeability for Na^+ ions is two to three orders of magnitude higher than the original value. With a certain time delay (of about 1 to 2 ms) the permeability for K^+ ions and their flux out of the cell also start to increase. This produces an opposite change of membrane potential (i.e., a shift in the negative direction). At the same

time there is a drastic drop in permeability for Na^+ ions and, a little later, for the K^+ ions. In the end the system returns to its original state.

Thus, in biological membranes (in contrast to the ordinary membranes described in Sections 5.4 and 26.2) we encounter a new phenomenon, the ability to regulate the ionic permeability by changes in membrane potential. The reasons for this effect are not completely clear. It may occur because of both changes in the properties and geometry of the ionic channels and a partial blocking of these channels by other ions (*gating* of the channels) and changes in the conditions for ionic transport by ionophores.

30.1.4 Propagation of the Excitation

The idea that signals are transmitted along the nerve channels as an electric current had arisen as early as the middle of the nineteenth century. Yet even the first measurements performed by H. Helmholtz showed that the transmission speed is about 10 m/s (i.e., much slower than electric current flow in conductors). It is known today that the propagation of nerve impulses along the axons of nerve cells (which in humans are as long as 1.5 m) is associated with an excitation of the axon's outer membrane.

Each nervous impulse is a group of consecutive action potential bursts. It had been pointed out above that these bursts are identical in shape. The information to be transmitted by the impulse is encoded in terms of the number of individual bursts in a group and of the intervals between bursts.

The membrane of a nerve cell at first is excited in a narrow zone close to the point of signal input. The associated local changes in membrane potential and polarity give rise to potential gradients along the membrane as well as to a longitudinal electric current, in both the cytoplasm (in the direction from the excited to neighboring segments) and in the external solution (in the opposite direction). The current leaves the cytoplasm along a closed contour through a neighboring membrane section (Fig. 30.4) and depolarizes it (i.e., produces a change in membrane potential in the positive direction). Owing to the ohmic potential drop and also because of dissipation of the current in the extracellular solution, the amplitude of the induced potential change is lower than that of the original change (i.e., the signal is attenuated during transmission). Neighboring sections become excited as long as the threshold potential is attained, will in turn relay the signal to the following section, and so on. Hence, the excitation propagates along the membrane surface over large distances without attenuation.

The longitudinal depolarizing effect propagates from an excited section in both directions. But owing to their refractory state, sections that had just been excited previously will not be reexcited, so the impulses continue in only one direction. The energy needed for transmission of the undamped impulse is taken from the energy expended to maintain concentration gradients (i.e., in the last analysis, from the energy that is generated by the cell for ion pump operation).

The speed of impulse propagation is determined by the time required for edl charging in neighboring membrane sections and depends on EDL capacitance and

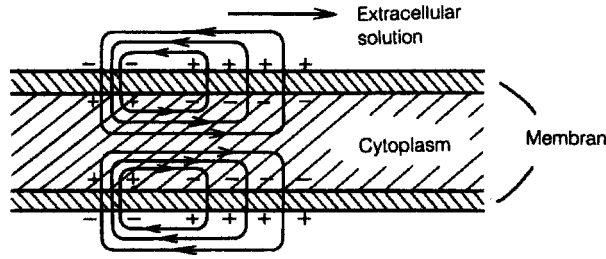

FIGURE 30.4 Nerve impulse propagation by longitudinal currents in the extracellular solution and in the cytoplasm.

on the amplitude of the longitudinal current. The current, in turn, depends on the resistance of the extracellular solution and cytoplasm between neighboring sections, at a given potential gradient. The cross section of the cytoplasm is very small, so that its resistance (which is inversely proportional to cross section) provides the main contribution. The propagation speed is 20 to 30 m/s in squid axon, which has a relatively large cross section (about 1 mm^2). Much lower velocities are found for the usual axons with smaller cross sections.

The axons of the more complex nervous system of vertebrates have a special structure securing higher transmission speed. They are surrounded by a rather compact sheath of secondary cells (the myelin sheath) which completely insulates the membrane from the extracellular solution. It is only at certain points found at intervals of 1 to 2 mm that this sheath has gaps, the nodes of Ranvier, which are 1 to 2 μm wide, and where the membrane is in contact with the electrolyte. The insulated axon sections have a low capacitance; hence, the longitudinal currents basically are used for the charging of more distant bare sections. The impulse thus jumps, as it were, along the nodes of Ranvier. The speed of impulse transmission in a myelinated axon is two to three orders of magnitude higher than that in a nonmyelinated axon having the same cross section.

Nerve impulse propagation along axons can be simulated by a rather simple electrochemical device (the model of Lillie, 1936). In this device an iron wire is immersed into concentrated nitric acid. Here the iron acquires a rather positive potential and becomes completely passivated. If the wire is activated at some point (e.g., by mechanical disruption of the passive film), the potential at this point immediately becomes more negative. Longitudinal currents have the effect that the passivating layer of a neighboring section begins to be reduced while the original section repassivates. The activation zone propagates at a certain constant speed all along the wire. In a more complex version of this model, a large number of iron electrodes are fused at certain intervals into glass tubing. The inside of the tubing is filled with a salt solution, the outside is in contact with concentrated nitric acid. When one of the electrodes is activated, the activation spreads in jumps to the next, and then to the following electrode, exactly as in myelinated axons. In 1963, the British scientists Alan L. Hodgkin, Andrew F. Huxley, and Sir John Eccles were awarded the Nobel

Prize in Medicine for their work on the excitation of cell membranes and of nerve impulse propagation.

30.2 BIOENERGETICS

30.2.1 Oxidizing Reactions in Cells

The energy requirements of the cells of living organisms are met by energy set free by chemical reactions involving the oxidation of organic nutrients by air oxygen. These reactions can conditionally be written as

$$(CH_2O) + O_2 \rightarrow CO_2 + H_2O, \tag{30.1}$$

where (CH_2O), a carbohydrate fragment, stands for typical nutrients. The thermodynamic parameters of reaction (30.1) are $-\Delta H = 503$ kJ/mol and $-\Delta G = 470$ kJ/mol. In biological systems, oxidation reactions occur isothermally (*cold combustion*) and instead of yielding thermal energy (which would involve an enthalpy decrease) they immediately produce other forms of Gibbs energy: the energy of chemical bonds in reaction intermediates or the energy of electric fields. Such reactions, which produce Gibbs energy, are called *exergonic* (as distinguished from exothermal). Analogous reactions proceed in fuel cells operated with organic reducing agents (fuels).

The pathway of the metabolic process converting the original nutrients, which are of rather complex composition, to the simple end products of CO_2 and H_2O is long and complicated and consists of a large number of intermediate steps. Many of them are associated with electron and proton (or hydrogen-atom) transfer from the reduced species of one redox system to the oxidized species of another redox system. These steps as a rule occur, not homogeneously (in the cytoplasm or intercellular solution) but at the surfaces of special protein molecules, the enzymes, which are built into the intracellular membranes. Enzymes function as specific catalysts for given steps.

Considering the many steps involved in the overall reaction, we may ask about the chemistry (stoichiometry) and energetics of each intermediate step. Through the work of numerous biochemists, the chemistry of most steps has now been determined and the enzymes revealed which catalyze each of these steps.

The energetics of each intermediate step can be characterized by the Gibbs energies of the corresponding redox systems or the equilibrium potentials of a nonconsumable electrode in contact with these systems [which are related to the Gibbs energies through Eq. (3.24)]. Using the scale of the reversible hydrogen electrode in the same solution, i.e., in a solution having a pH of about 7, we find a value of 1.22 V for the electrode potential of air oxygen with a partial pressure of 0.2 atm and a value of 0.0 V for hydrogen; for major nutrients, the values are between -0.1 and $+0.1$ V (on the scale of the standard hydrogen electrode, all potentials given in the present section would be 0.41 V more negative).

In each oxidation step of the metabolic process the system's oxidation state becomes a little higher, and the electrode potential accordingly moves in the positive direction. On its way to complete oxidation (i.e., during a potential change of about 1.2 V), the system passes through several tens of intermediate steps; hence, the energy change in each step is small and corresponds to an increase in electrode potential by 10 to 20 mV. Thus, each individual redox reaction occurs with very similar electrode potentials (Gibbs energies) of the redox systems involved in this reaction. The high rates of these reactions which are found at extremely low driving forces are the amazing special feature of biological systems, and attest to the extreme efficiency of enzyme catalysis.

The high catalytic activity of enzymes has a number of sources. Every enzyme has a particular active site configured so as to secure intimate contact with the substrate molecule (a strictly defined mutual orientation in space, a coordination of the electronic states, etc.). This results in the formation of highly reactive substrate–enzyme complexes. The influence of the individual enzymes also rests on the fact that they act as electron shuttles between adjacent redox systems. In biological systems one often sees multienzyme systems for chains of consecutive steps. These systems are usually built into the membranes, which secures geometric proximity of any two neighboring active sites and transfer of the product of one step to the enzyme catalyzing the next step.

The first steps of the metabolic process are the purely chemical enzymatic breakdown of the original nutrients into simpler, low-molecular-weight compounds. This breakdown occurs first in the digestive tract and then in the cells. The basic oxidation steps occur at the membranes of the cell mitochondria (the higher the energy demand of a cell, the more mitochondria will be contained in it, which may be tens of thousands). Hydrogen atoms are split off from the low-molecular-weight organic compounds under the effect of the enzyme dehydrogenase. These atoms are transferred to molecules of the organic compound NAD (nicotinamide-adenine dinucleotide), which functions as a hydrogen acceptor and by this reduction process yields the compound $NADH_2$. The Gibbs reaction energy in the NAD/$NADH_2$ system corresponds to an electrode potential of about 0.08 V. The further oxidation (dehydrogenation) of $NADH_2$ then occurs purely electrochemically. The electrons and protons are transmitted through a multienzyme system called the *electron transfer chain*. The last step is electron and proton transfer from the enzyme cytochrome oxidase to an oxygen molecule existing as a hemoglobin complex. This oxygen reduction step is entirely analogous to electrochemical oxygen reduction without the intermediate formation of hydrogen peroxide (see Section 15.3.2).

A remarkable feature of the bioenergetic oxidation reactions of nutrients in cells is the fact that they are always coupled to another reaction, that of synthesis of the energy-rich chemical substance adenosine triphosphate (ATP) from adenosine diphosphate (ADP) and phosphate (oxidative phosphorylation; Engelgardt and Ljubimova, 1939):

$$A\text{–}PO_3^-\text{–}OH + H_2PO_4^- \rightleftharpoons A\text{–}PO_3^-\text{–}PO_3^-\text{–}PO_3^-\text{–}OH + H_2O \qquad (30.2a)$$

(here A is the complicated heterocyclic compound adenosine) or, in an abbreviated form,

$$\mathrm{ADP} + \mathrm{P} \rightleftharpoons \mathrm{ATP} + \mathrm{H_2O}. \qquad (30.2b)$$

The phosphorylation reaction is also localized in the cell mitochondria. The enzyme ATP synthetase present in the mitochondrial membranes is involved in this reaction. The back reaction, which is the hydrolysis of ATP to ADP, occurs at other points of the cell and involves another enzyme, ATPase. The concentrations of the main reaction components, ADP and ATP, in cytoplasm are about 1 m*M*.

The synthesis of ATP is endergonic, and associated with an increase in Gibbs energy by about 30.7 kJ/mol. This energy is stored in the ATP molecule as the chemical bond energy between the third (outermost) phosphate group and the remainder of the molecule. These energy-rich chemical bonds are called macroergic. This energy is released in the back reaction (i.e., ATP hydrolysis to ADP).

In the oxidation of organic nutrients in the cell, on an average about 6 mol of ATP is synthesized for each mole of oxygen consumed. Therefore, the mean efficiency of conversion of the chemical energy in the oxidation of organic substances (470 kJ/mol) to the energy of ATP molecules is about 40%.

The ATP molecule is a universal energy carrier in the cell, and it is the principal one. It will sustain all reactions and processes requiring Gibbs energy: active ion transport (ion pump operation), biosynthesis of proteins and other substances, muscle contraction, and so on. It is also employed for temporary energy storage in the cell.

The coupling mechanism of the phosphorylation of ADP molecules and of electron transfer through the membrane during the oxidation of organic substances is not entirely clear, and different viewpoints have been expressed in this respect. According to the chemiosmotic theory of Peter Mitchell (1961), concentration (or electrochemical-potential) gradients of the hydrogen ions develop in the oxidation of organic substances between the two sides of the mitochondrial membrane. As a result, a membrane potential of about 0.2 V is established while the solution on the outside is negatively charged. The electric field in the membrane acts as the driving force of the phosphorylation reaction. Subsequently, the existence of a membrane potential has been demonstrated experimentally for the mitochondrial membranes. Thus, even here we have to do with an electrochemical mechanism through which the chemical energy of the oxidation reaction is converted, first to the energy of an electrical field, then to the chemical energy of ATP molecules.

30.2.2 Photosynthesis

Photosynthesis is the reverse of reaction (30.1): the formation of carbohydrates and oxygen from water and carbon dioxide with solar energy. Photosynthesis occurs in the chloroplasts contained in the cells of green plants. The chloroplasts hold two types of photosynthetic systems, which are called PSI and PSII. These systems

operate in synchronization. Each system (containing one reaction site) holds about 200 molecules of chlorophyll (abbreviated Chl) and a set of different enzymes. Several different forms of chlorophyll molecules exist.

Chlorophyll absorbs photons having a wavelength of about 680 nm and an energy of about 1.8 eV. The primary act of the photosynthetic reaction is excitation of the chlorophyll molecules during photon absorption:

$$\mathrm{Chl} + h\nu \rightarrow \mathrm{Chl}^{*}. \tag{30.3}$$

This raises the electrochemical potential, $\overline{\mu}_j$, of these molecules and alters the formal value of electrode potential in redox reactions involving the chlorophyll (see Section 29.4).

In a system containing other redox systems (e.g., the systems $\mathrm{A} + e^{-} \rightleftharpoons \mathrm{A}^{-}$ and $\mathrm{D} \rightleftharpoons \mathrm{D}^{+} + e^{-}$, which in the dark are in equilibrium with chlorophyll), redox reactions of the type of

$$\mathrm{Chl}^{*} + \mathrm{D} \rightarrow \mathrm{Chl}^{-} + \mathrm{D}^{+} \tag{30.4a}$$

and

$$\mathrm{Chl}^{-} + \mathrm{A} \rightarrow \mathrm{Chl} + \mathrm{A}^{-} \tag{30.4b}$$

are possible after excitation of the chlorophyll. These reactions result in a unidirectional electron transfer from donors D to acceptors A, which is associated with an increase in electrochemical potential of these bound electrons and transfer of the oxidizing functions to species D^{+}.

Photosynthesis occurs consecutively, first in PSII and then in PSI (Fig. 30.5). The excited chlorophyll in PSII is a strong oxidizing agent and has a redox potential of about 1.4 V. It can set free molecular oxygen by oxidation of water molecules. According to Eq. (15.20), four electrons are needed for the formation of one oxygen molecule [i.e., four chlorophyll molecules (each adding one electron upon excitation) and four photons]. Hence, the reaction proceeds through intermediate enzyme redox systems of the type $\mathrm{D}^{+}/\mathrm{D}$, permitting a temporary "accumulation" of electrons. These intermediate systems are not fully known.

The reducing agent A^{-} produced in the coupled reaction has a potential of about 0.3 V (i.e., is relatively weak and unable to reduce the CO_2 molecules to CH_2O groups). The latter process requires participation of a further photochemical system PSI involving another variety of chlorophyll molecules. In it the reducing agent A^{-} is oxidized in an analogous way via the intermediate redox systems $\mathrm{Y}^{+}/\mathrm{Y}$ and $\mathrm{Z}/\mathrm{Z}^{-}$, and a strong new reducing agent Z^{-} is formed which has a redox potential of about -0.2 V. The photochemical reactions as such terminate with the formation of $NADPH_2$ (the reduced form of NAD phosphate; the redox potential is about 0 V). Further steps of CO_2 reduction and carbohydrate formation then occur as enzymatic reactions in the dark.

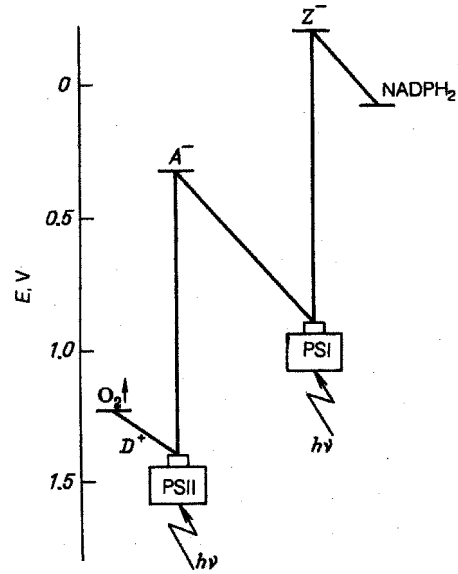

FIGURE 30.5 Schematic representation of the energy levels in photosynthesis.

In the photosynthesis reactions occurring in each of these two consecutive stages, four photons are involved per molecule of oxygen evolved. In the redox steps immediately following excitation of the chlorophyll, the electrochemical potential of electrons in the reducing agents being formed increases by about 1.1 eV at each stage (i.e., by a total of 2.2 eV). It then decreases during later redox steps, owing to inevitable energy losses. This decrease is particularly marked in the transition from PSII to PSI (see Fig. 30.5).

The individual steps of the multistep chemical reduction of CO_2 with the aid of $NADPH_2$ require an energy supply. This supply is secured by participation of ATP molecules in these steps. The chloroplasts of plants contain few mitochondria. Hence, the ATP molecules are formed in plants not by oxidative phosphorylation of ADP but by a phosphorylation reaction coupled with the individual steps of the photosynthesis reaction, particularly with the steps in the transition from PSII to PSI. The mechanism of ATP synthesis evidently is similar to the electrochemical mechanism involved in their formation by oxidative phosphorylation; owing to concentration gradients of the hydrogen ions between the two sides of internal chloroplast membranes, a certain membrane potential develops on account of which the ATP can be synthesized from ADP. Three molecules of ATP are involved in the reaction per molecule of CO_2.

In photosynthesis, the reaction involves eight photons for each oxygen molecule, each with an energy of about 1.8 eV (175 kJ/mol). Hence the efficiency of

solar-to-chemical energy conversion in photosynthetic systems with chlorophyll is about 40%.

30.3 ELECTROCHEMICAL METHODS IN BIOLOGY AND MEDICINE

30.3.1 Biological Macropotentials

In nerve impulse propagation, potential gradients develop in the extracellular solution, and ionic fluxes and electric currents appear in a direction along the membrane surface. The electrical fields of billions of synchronized cells add up, and in a strongly attenuated form can be measured at the outside of the living organism as biological *macropotentials*. For an analysis of individual cell functions, this external potential is not of great interest, but sometimes it will characterize the function of the body or of entire individual body organs.

Biological macropotentials are used widely in medicine for diagnostic purposes: electrocardiograms to characterize heart action, electroencephalograms to characterize brain function, and electromyograms to characterize muscle activity. Inert (absolutely polarizable) metal electrodes are applied to different points of the body surface in order to do such measurements, and potential differences are determined between any two of these electrodes as functions of time (e.g., during contraction of the heart muscle). The potential differences that can be measured at the body surface are very small; in cardiograms they are tenths of a millivolt, and in encephalograms they are hundredths of a millivolt. Hence sensitive measuring devices with electronic amplifiers are used for such analyses.

Cases are known where the external potentials attain high values. Even in antiquity, incomprehensible features of certain fishes were noted. Around 1800 it became clear that these features are associated with electric phenomena, and they were attributed to so-called "animal electricity." It was in 1832, finally, that Faraday could show that the various types of electricity, including the animal variety, are identical in nature. Studies of the "electric" fishes performed in the first half of the nineteenth century had a notable effect on the development of bioelectrochemistry.

The electricity-producing system of electric fishes is built as follows. A large number of flat cells (about 0.1 mm thick) are stacked like the flat unit cells connected in series in a battery. Each cell has two membranes facing each other. The membrane potentials of the two membranes compensate for each other. In a state of rest, no electrostatic potential difference can be noticed between the two sides of any cell or, consequently, between the ends of the stack. The ends of nerve cells come up to one of the membranes of each cell. When a nervous impulse is applied from outside, this membrane is excited, its membrane potential changes, and its permeability for ions also changes. Thus, the electrical symmetry of the cell is perturbed and a potential difference of about 0.1 V develops between the two sides. Since nervous impulses are applied simultaneously to one of the membranes in each cell, these small potential differences add up, and an appreciable voltage arises between the ends of the stack.

In the electric organ of fishes, a number of such stacks are connected in parallel and in series. The total voltage attains 500 V in the electric eel. A current pulse of about 0.5 A develops when this voltage appears across an external circuit (in fresh water or seawater). For the electric ray, these numbers are 60 V and 50 A, respectively. The length of such an electric pulse is comparable with the time of cell membrane excitation (i.e., 1 to 2 ms, which is quite sufficient to defeat a designated victim). Some species of fish use pulses repeated at certain intervals.

30.3.2 Electrochemical Sensors

The chemical composition of biological objects is extremely complex. They contain the macromolecules of proteins, lipids, and many other substances in addition to low-molecular-weight organic and inorganic compounds. Different external effects can produce both quantitative and qualitative composition changes; some substances disappear and/or others appear. Some substances that are essential for the functioning of the cells or of the entire organism are present in very small concentrations, $10^{-5}M$ and less.

The qualitative and quantitative analysis of such media is usually performed in vitro (i.e., on samples withdrawn from the biological organism). After the sampling, different methods of chemical analysis can be used, including the electrochemical methods described in Chapter 23. However, this method has the important defect that the samples withdrawn no longer interact with the remainder of the organism, which can affect their composition. Hence great effort has been expended recently in developing in vivo methods of analysis (i.e., performing analysis directly in the living organism). The only methods of analysis that are suitable here are electrochemical methods using different microelectrodes and microsensors introduced into the organism. It is an important special feature of electrochemical methods that they allow continuous, long-term measurements to be made which could encompass different phases of vital activity of the biological object examined.

Almost all of the methods described in Chapter 23 can be used for in vivo analyses, both voltammetric and potentiometric ones. The former are used primarily in the analysis of organic substances, which, within certain ranges of potential, can be either oxidized or reduced. Another popular method is the amperometric determination of oxygen in different biological media with the Clark electrode (Section 23.3).

Thin wires made of platinum metals or carbon fibers are used as the microelectrodes, which are introduced or implanted into the test medium. It must be verified that the electrodes are compatible with the medium (e.g., that there is no clotting effect during contact with blood). Problems often arise due to the adsorption of substances that are foreign to a given reaction (e.g., of proteins when determining the concentration of low-molecular-weight organic substances). In a number of cases, membranes can be used (e.g., membranes glued to the electrode) that will hold back the foreign macromolecules but allow the substances to be examined to penetrate to the electrode surface.

The concentrations of hydrogen ions (solution pH) and of a number of other inorganic ions: Na^+, K^+, Ca^{2+}, Cl^-, PO_4^{3-}, and so on, are determined potentiometrically.

Glass electrodes are used for the analysis of hydrogen ions; various other types of ion-selective electrodes are used for the other ions. Electrodes with ion-selective solvent membranes have become very popular. These electrodes are made in the form of thin glass capillaries (about 1 μm in diameter), which in the lower part contain a small volume of a liquid that is immiscible with water; the remainder of the capillary is filled with electrolyte solution (e.g., 3 *M* KCl).

In both voltammetry and potentiometry, usually only one electrode (the working electrode) is introduced or implanted into the living organism. The auxiliary or reference electrode is positioned at the most convenient point: for instance, at the outside of the organism. Since the working electrodes are extremely small, the currents in the measuring circuit are also small, sometimes hundredths of a microampere only. In certain cases (e.g., when thin capillaries are used), a high resistance arises in the measuring circuit, which could be hundreds or thousands of megohms. Under such conditions one must use very sensitive measuring instruments. Sometimes it may be necessary to provide for protection against extraneous electrostatic interference (with a *Faraday cage*).

30.3.3 Influence of Electric Currents on the Organism

If as a result of electrochemical processes, electrostatic potential gradients and electric currents can arise in different sections of a cell or whole organism, then conversely, currents or potential gradients applied from outside will produce certain changes in the cells and organisms. It is natural that these changes will depend on the electric field or current parameters.

In the limit, an *electroshock*, possibly with lethal results, can develop when a strong current acts on the organism. Weak effects are often utilized for medicinal purposes. Methods are known where an electrical stimulation is applied to individual points of the body surface which will have effects on different organs. Such a stimulation is used in particular against pain (electroanaesthetization, electronarcosis), for influencing the psychic state (induce feelings of comfort or discomfort), for the "refreshing" of memory, and so on. It is quite possible that the analogous effects of the well-known method of acupuncture rest on local electric pulses which develop under the effect of inserted needles and then spread over the body.

Often, an electrical stimulation of cardiac activity is used in medical practice. Under normal conditions the electrical impulses needed for the uninterrupted rhythmic contraction of heart muscles are generated by a special organ, the sinoatrial node. External electrical pulses can be used when this organ's function is disturbed. *Pacemakers* contain batteries with voltages of 3 to 5 V and a special electronic device generating electrical pulses with the required periodicity. The entire device is built into a titanium capsule (with a volume of about 50 mL) which is implanted in a convenient place of the body. The capsule also serves as the auxiliary electrode. The platinum or platinum–iridium working electrode is inserted through the vein directly into the muscle of the right ventricle of the heart. A current pulse of about 30 μA is quite sufficient for excitation of the cell membranes in this muscle and subsequent transmission of the impulse over the entire muscle system of the heart. The

energy stored in the primary battery secures uninterrupted function of the pacemaker for 5 to 10 years. Starting in about 1970, research efforts were intensified concerning the use of electrical current for faster union of fractured bones (see Section 24.5).

In recent years work was started in which this sort of phenomena are studied at the cell level, particularly the electrical breakdown of cell membranes and the fusion of neighboring cells under the influence of electric fields. These studies are of great value, in particular, for the further development of cell engineering and gene technology.

30.3.4 Use of Electrokinetic Methods

It will be shown in Section 31.3 that electrophoresis can be used for the qualitative and quantitative analysis of proteins, enzymes, and other naturally occurring macromolecular substances. The electrophoretic mobility of macromolecules in electric fields depends on their total charge, which differs between different molecules. For the analysis one uses zone electrophoresis (electrochromatography). The method works essentially as follows. The original mixture of macromolecules is introduced at a particular point into a horizontal glass tube filled with dilute electrolyte solution. When an electric field is applied along the tube, the various molecules, owing to their different transport rates, will become spatially separated and after a certain time will have gathered in different segments of the tube. The concentration of each individual fraction can be determined by optical techniques. Thickeners or various other devices that immobilize the solution [e.g., a strip of filter paper to soak up the solution (paper electrochromatography)] are used in practice against the remixing caused by convection in the liquid solution. This method is often used in clinical practice to diagnose various illnesses from changes in composition of the protein molecules.

The same principle is used for the preparative separation of mixtures of biological materials, the extraction of different individual components from these mixtures, and their purification. In this case one uses an electrophoretic method with continued introduction of individual portions of the mixture and withdrawal of portions of pure fractions. There have been reports that such processes were accomplished in spacecraft where, since gravitational forces are absent, the liquid solutions can be used without the danger of natural convection.

Electroosmosis is used in medicine for introducing into the body continuously or periodically liquid medications in rigorously defined quantities.

REFERENCES

Bernstein, J., *Pflügers Arch. Gesamte Philos*., **92**, 521 (1902).

du Bois-Reymond, E., *Ann. Phys. Chem*., **58**, 1 (1843).

Engelgardt, W. A., and M. N. Ljubimova, *Nature*, **144**, 668 (1939).

Faraday, M., Papers presented to the Royal Society, October 24, 1831 and January 12, 1932.

Galvani, L., *Boloniensi Scientarum e Artum Institut at que Academia Commentarii*, Vol. 7, Bologna, Italy, 1791, 55 pp.

Helmholtz, H., *Arch. Anat. Physiol. Wiss. Med*., **71**, 199 (1852).
Hodgkin, A. L., and A. F. Huxley, *Nature*, **144**, 710 (1939).
Lillie, R. S., *Biol. Rev*., **11**, 181 (1936).
Mitchell, P., *Naturwissenschafter*, **8**, 191 (1961).
Volta, A., *Philos. Trans*., **2**, 430 (1800).

MONOGRAPH

Blank, M., and G. Milazzo, *Bioelectrochemistry*, Plenum Press, New York, 1991.

31

Electrokinetic Processes

Electric double layers are formed in heterogeneous electrochemical systems at interfaces between the electrolyte solution and other conducting or nonconducting phases; this implies that charges of opposite sign accumulate at the surfaces of the adjacent phases. When an electric field is present in the solution phase which acts along such an interface, forces arise that produce (when this is possible) a relative motion of the phases in opposite directions. The associated phenomena historically came to be known as *electrokinetic phenomena* or *electrokinetic processes*. These terms are not very fortunate, since a similar term, *electrochemical kinetics*, commonly has a different meaning (see Part II).

Four different electrokinetic processes are known. Two of them, *electroosmosis* and *electrophoresis*, were described in 1809 by Ferdinand Friedrich Reuss, a professor at the University of Moscow. The schematic of a cell appropriate for realizing and studying electroosmosis is shown in Fig. 31.1*a*. An electrolyte solution in a U-shaped cell is divided in two parts by a porous diaphragm. Auxiliary electrodes are placed in each of the half-cells to set up an electric field in the solution. Under the influence of this field, the solution starts to flow through the diaphragm in the direction of one of the electrodes. The flow continues until a hydrostatic pressure differential (height of liquid column) has been built up between the two cell parts which is such as to compensate the electroosmotic force.

Electrophoresis can be observed in solutions containing suspended matter (solid particles, liquid drops, gas bubbles) in a highly disperse state (Fig. 31.2*a*). Under the influence of an electric field, these particles start to be displaced in the direction of one of the electrodes. Often, this movement is toward the negative electrode or cathode; hence, electrophoresis has occasionally been called *cataphoresis*.

In 1861, Georg Hermann Quincke described a phenomenon that is the converse of electroosmosis: When an electrolyte solution is forced through a porous diaphragm by means of an external hydrostatic pressure P (Fig. 31.1*b*), a potential difference called the *streaming potential* arises between indicator electrodes placed on different sides of the diaphragm. Exactly in the same sense, in 1880, Friedrich Ernst Dorn described a phenomenon that is the converse of electrophoresis: During

Fundamentals of Electrochemistry, Second Edition, By V. S. Bagotsky

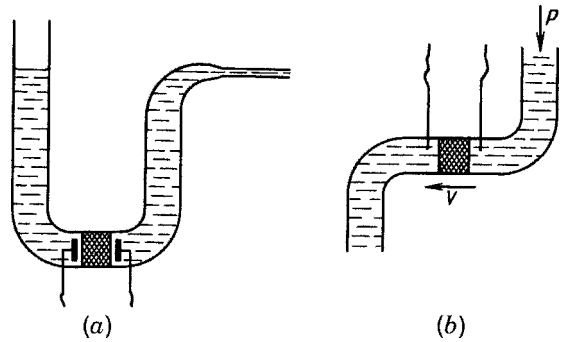

FIGURE 31.1 Schematic design of cells for studying electroosmosis (*a*) and streaming potentials (*b*); the velocity of electroosmotic transport can be measured in terms of the rate of displacement of the meniscus in the capillary tube (in the right-hand part of the cell).

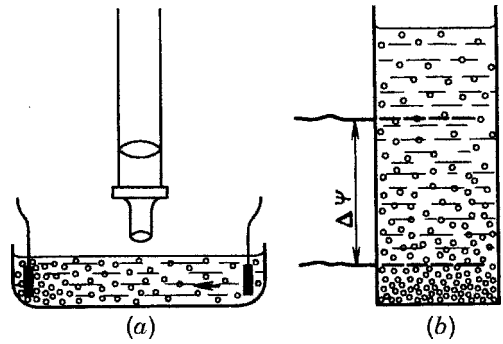

FIGURE 31.2 Schematic design of cells for studying electrophoresis (*a*) and sedimentation potentials (*b*).

the sedimentation or floating up of suspended particles under the force of gravity (or, e.g., the centrifugal force in a centrifuge), a potential difference called the *sedimentation potential* arises between indicator electrodes set up in the top and bottom parts of the solution (Fig. 31.2*b*).

All four processes have the same origin, since they are all based on the phenomenon of slip of the liquid along the surface of the other phase when a tangential electric field is present, or conversely, on the phenomenon that an electric field will arise during slip of the liquid.

The electrokinetic processes can actually be observed only when one of the phases is highly disperse (i.e., with electrolyte in the fine capillaries of a porous solid in the cases of electroosmosis and streaming potentials), with finely divided particles in the cases of electrophoresis and sedimentation potentials (we are concerned here with degrees of dispersion where the particles retain the properties of an individual phase, not of particles molecularly dispersed, such as individual molecules or ions). These processes are of great importance in particular for colloidal systems.

Theoretically, electrokinetic processes should also occur in nondisperse systems, but then additional factors arise (vortex formation in the liquid, settling of the particles, etc.) which produce a strong distortion. Hence, electrokinetic processes can be regarded as one of the aspects of the electrochemistry of disperse heterogeneous systems.

Electrokinetic processes only develop in dilute electrolyte solutions. The second phase can be conducting or nonconducting. Processes involving insulators are of great importance, since they provide the only way of studying the structure and electrical properties of the surface layer of these materials when they are in contact with the solution. Hence, electrokinetic processes can also be discussed as one of the aspects of insulator electrochemistry.

Auxiliary electrodes are placed into the solution to set up the electric field that is needed to produce electrophoresis or electroosmosis. Under these conditions an electric current passes through the solution and the external circuit; its value depends on the applied voltage and on solution conductivity. The lower this conductivity, the higher will be the electric field strength **E** (or ohmic voltage drop) in the solution that can be realized at a given value of current.

It is important to point out that electrokinetic transport processes have no direct connection with the electrochemical reactions occurring at the auxiliary electrodes during current flow, nor to current flow in the solution (even though as a rule the transport is proportional to current; see below). In electrophoresis, the finely divided particles move in the direction of one of the electrodes, and when adhesion is sufficiently strong, can deposit on it, forming relatively thick layers. Transport of these particles and their subsequent deposition on the electrode do not obey the laws of Faraday [Eq. (1.34)], in contrast to the migration and electrochemical deposition of metal ions. Apparent transport numbers are usually much larger than unity (they can be as high as tens of thousands). Solvent transport during electroosmosis is also much greater than that in the solvation sheaths of ions migrating in the electric field.

Transport processes of this type are called *nonfaradaic transport*. The nonfaradaic transport considered here is a steady-state process, in contrast to nonfaradaic currents mentioned previously that were due, for example, to charging of the electric double layer. Electrokinetic processes are of great practical significance, as discussed in Section 31.3.

31.1 ELECTROKINETIC POTENTIAL

31.1.1 Metal–Solution Interface

The electrokinetic processes have electrostatic origins; they are linked to the charges present on both sides of the slip plane close to the phase boundary. The charge and potential distribution in the surface layer can be described by the relations and laws outlined in Chapter 10.

Consider in more detail the phenomena occurring at the interface between the solution and a small metallic particle involved in electrophoresis. Upon contact with the electrolyte solution, the metal acquires a certain value of electrode potential E,

which may be the equilibrium value (with respect to ions of the same metal in the solution or to any redox system) or a nonequilibrium value. In accordance with this potential, there will exist a certain Galvani potential φ_G, and depending on the composition of the electrolyte solution (and particularly on any surface-active ions that may be present) a certain value of the interfacial potential Φ and certain type of ionic double-layer structure, particularly of its diffuse part.

As the particle moves relative to the electrolyte solution, the layer of water molecules that is directly adjacent to the particle surface is strongly bound and will be pulled along. The thickness of this bound layer is approximately one or two diameters of a water molecule. We shall write x_k for the x-coordinate of this layer's outer boundary, which is the slip plane. The electrostatic potential at this plane relative to the potential in the bulk solution is designated by the Greek letter ζ and called the *zeta potential* or *electrokinetic potential* of the interface discussed. This potential is a very important parameter characterizing the electrokinetic processes in this system.

It follows from the definition cited that the size of the zeta potential depends on the structure of the diffuse part of the ionic EDL. At the outer limit of the Helmholtz layer (at $x = x_2$) the potential is ψ_2, in the notation adopted in Chapter 10. Beyond this point the potential asymptotically approaches zero with increasing distance from the surface. The slip plane in all likelihood is somewhat farther away from the electrode than the outer Helmholtz layer. Hence, the value of ζ agrees in sign with the value of ψ_2 but is somewhat lower in absolute value.

When a tangential electric field is present, all charges that exist in the surface layers of the particles from the surface out to the slip plane will be pulled along by the particles, that is, the charges $Q_S^{(M)}$ on the surface of the metal itself and the charges $Q_S^{(E)}$ of opposite sign in the solution in the region between x_1 or x_2 and x_k (here and in the following, Q_S will always be the symbol for surface charge density). The effective charge, $(Q_S^{(M)})_k$, of the moving particle [for which we can write $(Q_S^{(M)})_k = Q_S^{(M)} - Q_S^{(E)}$] is compensated by charge of opposite sign in more distant regions of the diffuse EDL part.

All factors influencing the potentials of the inner or outer Helmholtz plane will also influence the zeta potential. For instance, when, owing to the adsorption of surface-active anions, a positively charged metal surface will, at constant value of electrode potential, be converted to a negatively charged surface (see Fig. 10.3, curve 2), the zeta potential will also become negative. The zeta potential is zero around the point of zero charge, where an ionic edl is absent.

It also follows from what was said that a zeta potential will be displayed only in dilute electrolyte solutions. This potential is very small in concentrated solutions where the diffuse edl part has collapsed against the metal surface. This is the explanation why electrokinetic processes develop only in dilute electrolyte solutions.

31.1.2 Insulator–Solution Interface

Insulators lack free charges (mobile electrons or ions). At interfaces with electrolyte solutions, steady-state electrochemical reactions involving charge transfer across the interface cannot occur. It would seem, for this reason, that there is no basis at this interface for the development of interfacial potentials.

Experience shows, however, that this is not so. A number of processes exist that will lead to charge accumulation in the surface layers of insulators. In the interaction with aqueous solutions, a dissociation of acidic or basic functional groups existing on the insulator surface may occur, also a hydrolysis of saltlike groups. These processes can be reinforced by partial interaction between the surface layer and the solvent and by swelling of this layer. Polar or charged surface groups may also arise upon rupture of chemical bonds directly at the surfaces of individual crystallites. An important source of electric charges at solid surfaces is the specific adsorption of solution ions.

The charges present on the insulator surface in contact with the solution give rise to an accumulation of ions of opposite sign in the solution layer next to the surface, and thus formation of an electric double layer. Since straightforward electrochemical measurements are not possible at insulator surfaces, the only way in which this EDL can be characterized quantitatively is by measuring the values of the zeta potential in electrokinetic experiments (see Section 31.2).

Experiments show that in highly dilute electrolyte solutions (with concentrations between 10^{-5} and $10^{-7}\,M$), the zeta potentials at insulators can be as high as ± 0.2 V. Often (but not always) the zeta potentials of solid insulators are negative. In the past this fact has been linked to *A. Coehn's rule*, according to which the insulator with the lower permittivity ε during triboelectrification with another insulator will charge up negatively. However, the rule cannot be applied to conductors (the electrolyte solution). The negative surface charge of many insulators such as silicates (glasses) is due to the dissociation of acidic surface groups. Proton-accepting surfaces (metal oxides or hydroxides) will charge up positively. Experience shows that the specific adsorption of solution ions is very important for the charging of insulators. For instance, when colloidal silver iodide is prepared from solutions of potassium iodide and silver nitrate, the AgI particles will charge up negatively, owing to anion adsorption when an excess of KI is present (relative to the stoichiometric requirement for AgI precipitation), but when an excess of $AgNO_3$ is present, they will charge up positively, owing to cation adsorption.

The absolute value of the zeta potential decreases with increasing solution concentration. Sometimes the concentration dependence is nonmonotonic. Solutions containing polyvalent ions with charge opposite in sign to that of the surface have a particularly strong effect. Figure 31.3 shows plots of zeta potentials for a negatively charged glass surface against the concentrations of salt solutions having cations of different charge. We see that as the cation charge increases, the concentration required to depress the absolute value of ζ to a certain level decreases drastically. Charge reversal of the surface is observed at higher concentrations in the case of tri- and tetravalent cations. All these observations are in perfect agreement with the theories of EDL structure (Chapter 10).

31.1.3 Electrochemical Properties of Colloidal Solutions

A solution is called *colloidal* when it contains particles between approximately 5 and 200 nm (i.e., outside the limits where ordinary optical measurements are possible).

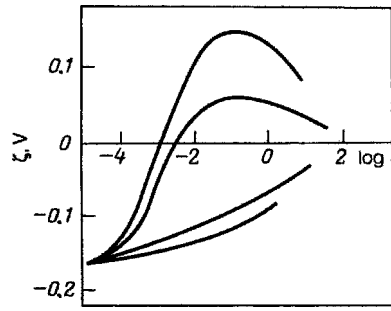

FIGURE 31.3 Zeta potentials of a glass surface as functions of the concentrations of salt solutions with the cations (from bottom to top): K^+, Ca^{2+}, Al^{3+}, Th^{4+}.

The colloidal particles can be crystalline or constitute an amorphous agglomeration of individual molecules. The definition also includes nonaggregated large macromolecules such as proteins. An arbitrary distinction is made between hydrophobic colloids (sols) and hydrophilic colloids (gels), which depends on the degree and type of interaction with the aqueous solvent.

Hydrophobic colloidal particles move readily in the liquid phase under the effect of thermal motion of the solvent molelcules (in this case the motion is called *Brownian*) or under the effect of an external electric field. The surfaces of such particles as a rule are charged (for the same reasons for which the surfaces of larger metal and insulator particles in contact with a solution are charged). As a result, an EDL is formed and a certain value of the zeta potential developed.

A very important property of colloidal solutions is linked to this EDL: their stability against coagulation (coalescence of the particles and their precipitation as a separate phase). From the fact that they have a zeta potential, it can be concluded that the moving colloidal particles have some effective charge, $(Q_S)_k$. Because of this charge, electrostatic repulsion forces develop between the individual particles and prevent a close approach and coagulation of the particles moving about in the solution. The fact that the particles are charged and have a certain zeta potential also influences the rheological properties (viscosity) of the colloidal solutions.

As at other interfaces, the effective surface charge of colloidal particles depends on the total concentration and composition of the solution, particularly on polyvalent or surface-active ions that may be present. When the zeta potential is reduced below a certain critical (absolute) value, which is approximately 25 to 30 mV, the colloidal solution becomes unstable.

31.2 BASIC EQUATIONS OF ELECTROKINETIC PROCESSES

The basic equations of electrokinetic processes establish the connection between zeta-potential values and the parameters of the electrokinetic processes: the velocity

of relative motion of the phases or the potential difference established in the solution as a result of such motion. These equations are used predominantly for calculating the zeta potentials of the various interfaces from parameters of the electrokinetic processes which have been found experimentally. The equations are used less often for the inverse problem, for calculating the velocity of motion from known values of the zeta potential.

The equations of the electrokinetic processes were derived in 1903 by the Polish physicist Maryan Ritter von Smoluchowski on the basis of ideas concerning the function of EDL in these processes that had been developed by H. Helmholtz in 1879. These equations are often called the *Helmholtz–Smoluchowski equations*.

Electroosmosis Consider the electroosmotic motion of a solution in a porous solid consisting of insulating material. We shall assume for the sake of simplicity that the pores are cylindrical and have a radius r. When an electric field having the field strength $\mathbf{E}$ is applied, the liquid will start to move under the influence of the electric force acting on the excess charges $(Q_S)_k$ present in a thin layer between the slip plane x_k and the outer limit of the EDL in the diffuse EDL part. We shall write δ_0 for the thickness of this layer (of slipping charges).

The charge density $(Q_S)_k$, the zeta potential, and the thickness δ_0 are interrelated by the plate-capacitor relation

$$(Q_S)_k = \frac{\varepsilon_0 \varepsilon \zeta}{\delta_0}. \tag{31.1}$$

The electrical force acting on charge $(Q_S)_k$ is

$$f_e = \mathbf{E}(Q_S)_k = \frac{\varepsilon_0 \varepsilon \mathbf{E} \zeta}{\delta_0}. \tag{31.2}$$

The linear velocity of the liquid developing under the effect of this force is zero directly at the solid surface, and increases to some maximum value v at the distance $x = \delta_0$ from the surface. Solution regions farther out lack the excess charges that could come under the effect of the external electric field; hence, there is no further increase in liquid velocity (Fig. 31.4). When the layer (δ_0) is much thinner than the capillary radius, $\delta_0 \ll r$, the assumption can be made that the bulk of the solution moves with a uniform velocity v.

The velocity v of liquid motion can be found from the condition that the electric force should be compensated by the viscous friction force f_{fr}. The latter is proportional to the velocity gradient in the layer of slipping charges:

$$f_{fr} = \frac{\eta v}{\delta_0} \tag{31.3}$$

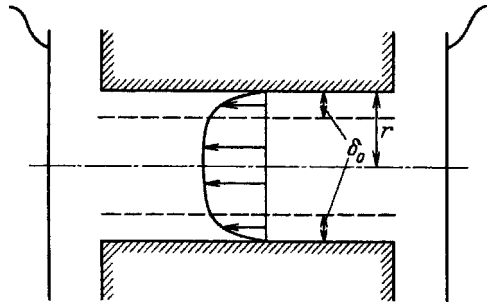

FIGURE 31.4 Velocity distribution in the electroosmotic solution flow in a cylindrical pipe (pore).

(η is the viscosity; for aqueous solutions $\eta \approx 1 \times 10^{-3}$ Pa·s). Equating the two forces, we find the desired equation linking the velocity of liquid motion and the zeta potential:

$$v = \frac{\varepsilon_0 \varepsilon \mathbf{E} \zeta}{\eta}. \tag{31.4}$$

At an electric field strength in the solution of, for example, 100 V/m and a zeta potential of 0.05 V, the velocity of liquid motion will be 3.5×10^{-6} m/s, which is on the same order of magnitude as the velocities of the ions in solutions.

The electric field also gives rise to a migration current density $E\sigma$ [see Eq. (1.4)]. Hence, in Eq. (31.4) we can replace the parameter of field strength **E** by current density, which is more readily measured:

$$v = \frac{\varepsilon_0 \varepsilon \mathbf{E} \zeta}{\eta \sigma} i. \tag{31.5}$$

Sometimes, not the linear but the volume velocity *dV/dt* of the liquid is used:

$$\frac{dV}{dt} = vS = \frac{\varepsilon_0 \varepsilon \mathbf{E} \zeta}{\eta \sigma} I \tag{31.6}$$

(S is the total solution cross section in the porous solid).

A number of special features follow from the equations reported. The linear velocity of electroosmotic transport of the liquid is independent of the geometric parameters of the porous diaphragm (the size and number of pores, the thickness, etc.), and the space velocity depends only on S. At given values of the current, the transport rate increases with decreasing solution conductivity (increasing field strength).

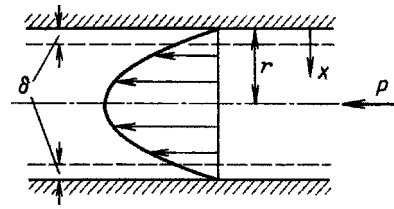

FIGURE 31.5 Velocity distribution in the motion of a solution in a cylindrical pipe (pore) under the effect of the external force P.

Streaming Potential When the solution is forced through the porous solid under the effect of an external pressure P, the character of liquid motion in the cylindrical pores will be different from that in electroosmotic transport. Since the external pressure acts uniformly on the full pore cross section, the velocity of the liquid will be highest in the center of the pore, and it will gradually decrease with decreasing distance from the pore walls (Fig. 31.5). The velocity distribution across the pore is quantitatively described by the Poiseuille equation,

$$v_x = \frac{P[r^2 - (r - x)^2]}{4\eta l}, \tag{31.7}$$

where x is the distance from the pore wall (which has a maximum value of $x = r$) and l is pore length.

At the distance $x = \delta_0$ the expression for velocity can be written as

$$v_0 = \frac{Pr\delta_0}{2\eta l} \tag{31.8}$$

(where it is taken into account that $\delta_0 \ll r$).

During motion of the solution, excess charges are transported which are present in the slip layer. This flux of charges is equivalent to the electrical current in the solution. Taking into account that the perimeter of the slip layer is close to $2\pi r$, we find for the current

$$I = 2\pi r(Q_S)_k v_0 = \frac{\varepsilon_0 \varepsilon \pi r^2 \zeta}{l\eta} P. \tag{31.9}$$

Current flow in a pore of length l and total cross section S produces an ohmic potential drop in the solution, which is the streaming potential:

$$\varphi_{str} = IR = \frac{Il}{\pi r^2 \sigma} = \frac{\varepsilon_0 \varepsilon \zeta}{\eta \sigma} P. \tag{31.10}$$

Like the velocity of electroosmosis, the value of the streaming potential is independent of geometric parameters of the porous solid through which the liquid is forced.

Electrophoresis The physical situation of relative motions of a solution and another (insulating) phase during electrophoresis is exactly the same as in electroosmosis. Hence, the linear velocity of a cylindrical particle (which is the equivalent of a cylindrical pore) is given by the value following from Eq. (31.4). With particles of different shape, this velocity can be written as

$$v = \gamma \frac{\varepsilon_0 \varepsilon \mathbf{E} \zeta}{\eta}, \tag{31.11}$$

where γ is a coefficient allowing for particle shape. For spherical particles $\gamma = \frac{2}{3}$.

Sedimentation Potential The equation for the sedimentation potential is the analog of Eq. (31.10). As in the case of electrophoresis, one can allow for the shape of sedimenting particles by using the coefficient γ. The hydrostatic pressure P is replaced by the "pressure" of the column of sedimenting (or floating) particles, which evidently is given by $g\mathrm{M}[1 - (\rho_0/\rho)]$, where g is the acceleration of gravity (or other force), M is the mass of particles in a column measuring 1 m^2 in cross section, and ρ_0 and ρ are the densities of the solvent and suspended matter.

Interrelations Between the Electrokinetic Processes Equation (31.4) for electroosmosis and Eq. (31.10) for the streaming potential, as well as the analogous equations for the other two electrokinetic processes, yield the relation

$$\frac{v}{\mathbf{E}\gamma} = \frac{\varphi_{\mathrm{str}} \sigma}{P}. \tag{31.12}$$

This equation is valid regardless of solution properties (the values of ε and η), surface properties (the value of ζ), and the size of the disperse-phase elements. All parameters of this equation can be determined by independent measurements. The validity of Eq. (31.12) was demonstrated by such measurements. This result is an additional argument for the claim that all four of the electrokinetic processes actually obey the same laws and have the same physical origin.

Range of Application of the Equations Deduced The equations reported above are not entirely rigorous. A number of assumptions and approximations have been made when deducing them, and hence the range of application of the equations is somewhat restricted. Motion of the solution has always been regarded as laminar. It was assumed that the second phase is an insulator, and hence will not distort the electrical field existing in the solution. It was assumed that an enhanced surface conductivity is not found close to the interface (this could, for instance, be caused by the higher concentration of

ions in the EDL) and that the values of dielectric constant and viscosity of the solution in the layer next to the surface are the same as those in the bulk solution. The assumption was used, finally, that the characteristic size of the disperse phase (e.g., pore radius r) is larger than the thickness δ_0 of the layer of slipping charges.

Departures of the electrokinetic behavior of real systems from that described by the equations reported occurs most often because of breakdown of two of the assumptions above: because of marked surface conductivity (particularly in dilute solutions, where the bulk conductivity is low) and because of a small characteristic size of the disperse-phase elements (e.g., breakdown of the condition of $\delta_0 \ll r$ in extremely fine-porous diaphragms). A number of more complicated equations allowing for these factors have been proposed.

31.3 PRACTICAL USE OF ELECTROKINETIC PROCESSES

Electrokinetic processes are widely used in different fields of science and technology. We had already mentioned the use of electrokinetic processes for research into the electric properties of surface layers of insulating materials. Such measurements are used, in particular, when studying the surface properties of polymeric materials, their behavior in different media, and their interactions with other materials (e.g., with adsorbing surface-active substances). The results of this research are used in textile, cellulose and paper, and other industries.

An important technique for the qualitative and quantitative analysis of different macromolecular materials is based on the electrophoretic separation of particles having different transport velocities (e.g., because they have different zeta potentials). This technique is used for the analysis of proteins, polysaccharides, and other naturally occurring substances whose molecular size approaches that of colloidal particles (for more details, see Section 30.3.4). It is an advantage of the electrophoretic method that mild experimental conditions can be used—dilute solutions with pH values around 7, room temperature, and so on—which are not destructive to the biological macromolecules.

In manufacturing, electrophoresis is used to apply coatings of different inorganic or organic materials to conducting substrates. The best known example is the protective coating of metal parts (e.g., car bodies) with primers or paint. Another example is the application of mixed coatings of barium and strontium compounds on tungsten wire used in cathode-ray tubes. Both aqueous electrolyte solutions and solutions on the basis of different organic or mixed solvents are used in these applications. The particles in the suspensions are between 1 and 50 μm. Voltages between several tens and several hundreds of volts are used to set up the electrical fields. Typical current densities in the (poorly conducting) solutions are 1 to 5 mA/cm^2. The electrophoretic application of a paint coat of 20 μm takes about 5 min (for comparison: electrolytic plating of a copper layer of the same thickness with a current density of 5 mA/cm^2 would require more than 3 h). The electrophoretic coatings obtained are very uniform, and the throwing power of the baths is high (i.e., one can coat parts of complex shape).

Electroosmosis is used to remove liquid (moisture) from different porous solids (e.g., in drying soil for building purposes, which improves the bond between the foundations and the soil). A combination of electrophoresis and electroosmosis is sometimes used to dry peat or clay. In this way, the water content of peat can be reduced from 90% to 55–60%. Unfortunately, the energy required for a further reduction of the water content is very high.

REFERENCES

Dorn, F. E., *Wied. Ann*., **9**, 513; **10**, 46 (1880).

Quincke, G. H., *Ann. Phys. (Poggendorff's)*, **113**, 513 (1861).

Reuss, F. F., *Mem. Soc. Nat. Moscow*, **2**, 327 (1809).

Smoluchowski, M., *Ann. Phys*., **21**, 756 (1906); *Bull. Acad. Sci. Cracovie*, p. 182 (1903).

32

Interfaces Between Two Immiscible Electrolyte Solutions

ZDENĚK SAMEC

J. Heyrovský Institute of Physical Chemistry, Academy of Sciences of the Czech Republic, Prague, Czech Republic

An interface between two immiscible electrolyte solutions (ITIES) is formed between two liquid solvents of a low mutual miscibility (typically, $<1\%$ by weight), each containing an electrolyte. One of these solvents is usually water and the other one is a polar organic solvent of a moderate or high relative dielectric constant (permittivity). The latter requirement is a condition for at least partial dissociation of dissolved electrolyte(s) into ions, which thus can ensure the electric conductivity of the liquid phase. A list of the solvents commonly used in electrochemical measurements at ITIES is given in Table 32.1.

A typical interface of this type would be

$$R^+X^-(w)\,|\,R^+X^-(o), \tag{32.1}$$

where R^+X^- represents a binary electrolyte (e.g., tetra-*n*-butylammonium chloride) in a partition equilibrium between phases (w) and (o). This is an extraction system of practical significance in separation science or in organic synthesis using the phase-transfer catalysis (PTC). ITIES with a common ion (e.g., the cation R^+) rather than with a common electrolyte is of interest as a model for the ion-selective electrode,

$$R^+A^-(w)\,|\,R^+X^-(o). \tag{32.2}$$

Here A^- and X^- represent a highly hydrophilic and hydrophobic anion, respectively, equilibrium concentrations of which in the other phase are practically zero. Typical examples are chloride and tetrakis (4-chlorophenyl)borate anions, respectively.

Fundamentals of Electrochemistry, Second Edition, By V. S. Bagotsky

TABLE 32.1 Polar Organic Solvents Exhibiting Low Miscibility with Water and Their Relative Dielectric Constants ε and Densities ρ at 298 K

Solvent	ε	ρ (g/cm^3)
Aliphatic		
1,2-Dichloroethane	10.36	1.2458
1,6-Dichlorohexane	8.6[a]	1.0677
2-Octanone	9.51[b]	0.820
Aromatic		
Nitrobenzene	34.82	1.1984
o-Nitrophenyl octyl ether	24.20	1.0410[b]
Benzonitrile	25.90[b]	1.0093

[a]308 K.
[b]293 K.

Ion partition equilibria at ITIES were first studied by Walther Nernst in 1892. Nernst derived the fundamental relationship linking the equilibrium difference of the inner (or Galvani) potentials, $\varphi_G^{(w,o)} = \varphi_G^{(w)} - \varphi_G^{(\sigma)}$, to the ratio of ion concentrations in the aqueous and organic phases. Later, in 1953, F. M. Karpfen and J. E. B. Randles introduced the related concept of the distribution potential, which is the Nernst potential difference established at ITIES due to the equilibrium partition of electrolyte(s). Present understanding of the structure of an ITIES stems in part from the theoretical model of two adjoining space-charge regions (diffuse double layer), which was proposed in 1939 by F. J. W. Verwey and K. F. Niessen following the classical work by G. Gouy and D. L. Chapman. Modern experimental studies of polarization phenomena at ITIES have been initiated by Gavach et al. (1968), who were the first to employ a four-electrode methodology for this purpose, and by Koryta et al. (1977), who defined the conditions under which an ITIES can behave as an ideally polarized electrode.

32.1 EQUILIBRIUM GALVANI POTENTIAL DIFFERENCE

32.1.1 Charge-Transfer Processes at ITIES

There are in principle two types of charge-transfer processes at ITIES, a single ion and a single electron transfer reaction. The first one can be described as the transfer of an ion $X_i^{z_i}$ with charge number z_i:

$$X_i^{z_i}(w) \rightleftharpoons X_i^{z_i}(o). \tag{32.3}$$

The second one is an electron transfer between a redox system Ox_1/Red_1 in phase (w) and a redox system Ox_2/Red_2 in phase (o), which can be described as, e.g.

$$Ox_1^{z_{o1}}(w) + Red_2^{z_{R2}}(\sigma) \rightleftharpoons Red_1^{z_{R1}}(w) + Ox_2^{z_{o2}}(\sigma). \tag{32.4}$$

Each of the heterogeneous charge-transfer reactions (32.3) and (32.4) can be coupled to a homogeneous chemical reaction. Often, an ion association or complex formation occurs, for example, transfer of the K^+ cation facilitated by the formation of the complex with valinomycine (Val) in the potassium-selective electrode,

$$K^+(w) + Val(o) \rightleftharpoons KVal^+(o). \tag{32.5}$$

At a constant temperature T and pressure p, the condition of ion transfer equilibrium (32.3) is given by the equality of the electrochemical potentials in both phases. This condition yields the Nernst equation for the equilibrium Galvani potential difference,

$$\varphi_G^{(w,\sigma)} = \varphi_{G0i}^{(w,\sigma)} + \frac{RT}{Z_i F} \ln \frac{a_i(\sigma)}{a_i(w)}, \tag{32.6}$$

where $\varphi_{G0i}^{(w\sigma)} = \Delta G_{tr,i}^{o,w\to\sigma}/z_i F$ is the standard ion transfer potential, and $\Delta G_{tr,i}^{o,w\to\sigma}$ is the standard Gibbs energy of ion transfer from phase (w) to phase (o). This parameter is actually the difference in the standard Gibbs energy of ion solvation in the two phases. Ions with a large positive or large negative value of $\Delta G_{tr,i}^{o,w\to\sigma}$ are denoted as *hydrophilic* and *hydrophobic ions*, respectively. Transfer of a single ion $X_i^{z_i}$ is scarcely the only charge-transfer reaction occurring at ITIES, and generally, we have to do with multi-ion partition systems. Thus, in the extraction system described above, the electroneutrality condition requires that both cation R^+ and anion X^- be involved in the partition equilibrium. Hung (1980) has developed a general method for calculation of the corresponding equilibrium potential difference (i.e., distribution potential). The treatment is based on the electroneutrality condition for N ionic species in each phase,

$$\sum_{i=1}^{N} z_i c_i(w,o) = 0, \tag{32.7}$$

and the mass conservation law,

$$c_i(w) + r c_i(o) = c_i^0(w) + r c_i^0(o), \tag{32.8}$$

where $r = V(o)/V(w)$ is the ratio of the volume of phase (o) to that of phase (w), and $c_i(s)$ and $c_i^0(s)$ are the equilibrium and initial concentrations of the ion i ($i = 1, 2, \ldots, N$), respectively. Then a substitution from Eqs. (32.6) and (32.8) into Eq. (32.7) gives

$$\sum_{i=1}^{N} \frac{z_i[c_i^0(w) + c_i^0(\sigma)]}{1 + r \exp[z_i F(\varphi_G^{(w,\sigma)} - \varphi_{G0i}^{(w,\sigma)})/RT]} = 0, \tag{32.9}$$

where the formal ion transfer potentials $\varphi_{G0i}^{(w,\sigma)1}$ comprise the logarithmic term with the ratio of the ion activity coefficients. An analytical solution of Eq. (32.9) can be

obtained only in some specific cases. The simplest one is represented by the partition of a single binary electrolyte R^+X^-. In this case, the distribution potential depends neither on the volume ratio r nor explicitly on the electrolyte concentration and is given by the formal ion transfer of the cation, $\varphi_{G0+}^{(w,\sigma)}$, and the anion, $\varphi_{G0-}^{(w,\sigma)}$:

$$\varphi_G^{(w,\sigma)} = \tfrac{1}{2}[\varphi_{G0+}^{(w,\sigma)} + \varphi_{G0-}^{(w,\sigma)}] \tag{32.10}$$

The numeric solution of Eq. (32.9) for the interface $R^+A^- \mid R^+X^-$ with the common cation R^+ is shown in Fig. 32.1. The expected Nernstian response of 59 mV per decade is observed only in a limited range of the ratio of concentrations of electrolytes R^+A^- and R^+X^-. When this ratio is too low or too high, the equilibrium potential approaches the distribution potential of the electrolyte that is present in excess.

A similar thermodynamic procedure is applicable to the electron transfer reaction, Eq. (32.4). By using the equilibrium condition, which expresses the equality of the sum of the electrochemical potentials of reactants and products, an expression for the equivalent Nernst potential difference can be derived:

$$\varphi_G^{(w,o)} = \varphi_{G0el}^{(w,\sigma)} + \frac{RT}{F} \ln \frac{a_{Ox,2}^{(o)}\, a_{Red,1}^{(w)}}{a_{Red,2}^{(o)}\, a_{Ox,1}^{(w)}}. \tag{32.11}$$

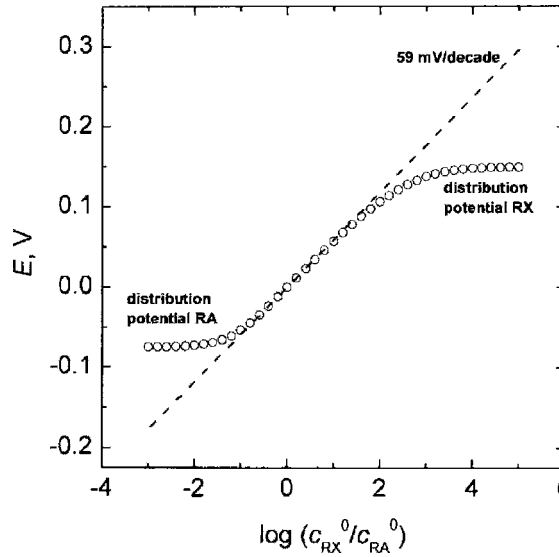

FIGURE 32.1 Equilibrium potential difference $E = \varphi_G^{(w,o)}$ for the interface $R^+A^- \,|\, R^+X^-$ with the common cation R^+ as a function of the ratio of the initial concentrations of electrolytes R^+A^- and R^+X^-, as calculated using Eq. (32.9) for the phase volume ratio $r = V(o)/V(w) = 0.001$, and the standard ion transfer potentials $\varphi_{G0R+}^{(w,o)} = 0$, $\varphi_{G0A-}^{(w,o)} = -0.15$ V, $\varphi_{G0X-}^{(w,o)} = 0.3$ V. The dashed line corresponds to the ideal Nernstian behavior.

The standard Galvani potential difference $\varphi^{(w,0)}_{G,0el}$ can be related to the standard electrode potentials $E^0_{ox1/red1}(w)$ and $E^0_{ox2/red2}(o)$ on the hydrogen scale in water or organic solvent, respectively,

$$\varphi^{(w,\sigma)}_{G0el} = E^0_{ox2/red2}(\sigma) - E^0_{ox1/red1}(w) + \varphi^{(w,\sigma)}_{G0H+} \tag{32.12}$$

where $\varphi^{(w,\sigma)}_{GOH+}$ is the standard Galvani potential difference for hydrogen ion transfer (Samec, 1979).

32.1.2 Scale of Galvani Potential Differences

A relative scale of the standard Gibbs energies of ion transfer or the standard ion transfer potentials can be established based on partition and solubility measurements. The partition equilibrium of the electrolyte R^+X^- can be characterized by a measurable parameter, the partition coefficient P_{RX}:

$$P_{RX} = \exp\left(-\frac{\Delta G^{0,w\to o}_{RX}}{2RT}\right) = \frac{a^{(o)}_{\pm}}{a^{(w)}_{\pm}} = \frac{\gamma^{(o)}_{\pm} c^{(o)}_{RX}}{\gamma^{(w)}_{\pm} c^{(w)}_{RX}}, \tag{32.13}$$

where $\Delta G^{0,w\to o}_{RX} = \Delta G^{0,w\to o}_{tr,R^+} + \Delta G^{0,w\to o}_{tr,X^-}$ is the standard Gibbs energy of electrolyte transfer, $a_{\pm}$ and $\gamma_{\pm}$ represent the mean activity and the mean activity coefficient of the electrolyte, respectively, and c_{RX} is the electrolyte concentration. The difference between the standard Gibbs energies of transfer of two ions can be obtained from the ratio of the partition coefficients of their salts with the same counterion.

Analogously, solubility measurements yield the mean activity $a^{(s)}_{\pm}$ of electrolyte (s = w, o), and the corresponding standard Gibbs energy $\Delta G^{0(s)}_{RX}$ of solution (in the molar scale),

$$\Delta G^{0(s)}_{RX} = -2RT \ln a^{(s)}_{\pm}. \tag{32.14}$$

The standard Gibbs energy of electrolyte transfer is then obtained as the difference $\Delta G^{0,w\to o}_{RX} = \Delta G^{0(o)}_{RX} - \Delta G^{0(w)}_{RX}$. To establish the absolute scale of the standard Gibbs energies of ion transfer or ion transfer potentials, an extrathermodynamic hypothesis must be introduced. For example, for the salt tetraphenylarsonium tetraphenylborate ($TPAs^+TPB^-$) it is assumed that the standard Gibbs energies of transfer of its ions are equal,

$$\Delta G^{0,w\to o}_{TPAsTPB} = 2\Delta G^{0,w\to o}_{tr,TPAs^+} = 2\Delta G^{0,w\to o}_{tr,TPB^-}. \tag{32.15}$$

This assumption allows evaluation of $\Delta G^{0,w\to o}_{tr,TPAs^+}$ and $\Delta G^{0,w\to o}_{tr,TPB^-}$ from the partition or solubility measurements of TPAsTPB. Standard Gibbs energies of transfer of other ions are then obtained from the partition or solubility measurements of their salts with $TPAs^+$ or TPB^-. Data inferred from partition and solubility measurements can differ, because in the former case an equilibrium partition of both solvents takes

TABLE 32.2 Standard Gibbs Energy of Transfer and Standard Ion Transfer Potentials for Ion Transfer Between Water and Nitrobenzene Derived from Partition Measurements

Ion	$\Delta G_{\mathrm{tr,i}}^{0,\mathrm{w}\to\mathrm{o}}$ (kJ/mol)	$\varphi_{\mathrm{G0i}}^{(\mathrm{w,o})}$ (mV)
Li^+	38.2	396
TMA^+	3.4	35
TBA^+	−23.9	−248
$TPAs^+$	−35.9	−373
Cl^-	29.7	−308
TPB^-	35.9	373

place (i.e., the two solvents are mutually saturated). Selected values of $\Delta G_{\mathrm{tr,i}}^{0,\mathrm{w}\to\mathrm{o}}$ or $\varphi_{\mathrm{G0i}}^{(\mathrm{w,o})}$ for ion transfer between water and nitrobenzene obtained from the partition measurements are given in Table 32.2.

32.2 IDEALLY POLARIZABLE ITIES

According to Eq. (32.10), the distribution potential corresponding to the equilibrium partition of the electrolyte RX is independent of the electrolyte concentration. On the other hand, when more than two ions are involved in the partition equilibrium, there always exists a thermodynamic relationship between the potential difference $\varphi_{\mathrm{G}}^{(\mathrm{w,o})}$ and the concentrations of ions present. More specifically, let us consider an ITIES with a different electrolyte in each phase,

$$\mathrm{R^+X^-(w)}\,\big|\,\mathrm{S^+Y^-}(\sigma). \tag{32.16}$$

Koryta et al. (1977) have shown that the distribution potential for such an ITIES fulfills the inequality $\varphi_{\mathrm{G0S+}}^{(\mathrm{w,o})}$, $\varphi_{\mathrm{G0X-}}^{(\mathrm{w,o})} \ll \varphi_{\mathrm{G}}^{(\mathrm{w,o})} \ll \varphi_{\mathrm{G0R+}}^{(\mathrm{w,o})}$, $\varphi_{\mathrm{G0Y-}}^{(\mathrm{w,o})}$, provided that RX consists of highly hydrophilic ions and SY consists of highly hydrophobic ions. Although the distribution potential for such a system can be calculated with high accuracy, the potential can hardly be established in practice, because the activity ratios for all ions are either too low or too high: $a_{\mathrm{S+}}^{(\mathrm{o})}/a_{\mathrm{S+}}^{(\mathrm{w})} \gg 1$, $a_{\mathrm{Y-}}^{(\mathrm{o})}/a_{\mathrm{Y-}}^{(\mathrm{w})} \gg 1$, $a_{\mathrm{R+}}^{(\mathrm{o})}/a_{\mathrm{R+}}^{(\mathrm{w})} \ll 1$, and $a_{\mathrm{X-}}^{(\mathrm{o})}/a_{\mathrm{X-}}^{(\mathrm{w})} \ll 1$. In this case, the potential difference $\varphi_{\mathrm{G}}^{(\mathrm{w,o})}$ can be controlled by externally supplied charge, because only a small portion of this charge is required to shift the ion partition equilibria. The ITIES then behaves as an ideally polarizable electrode.

32.3 POLARIZATION MEASUREMENTS

A well-defined polarization of an ITIES can be accomplished by means of a four-electrode system with two couples of current-supplying (counter) and potential-measuring (reference) electrodes, which are connected to phases (w) and (o) in the

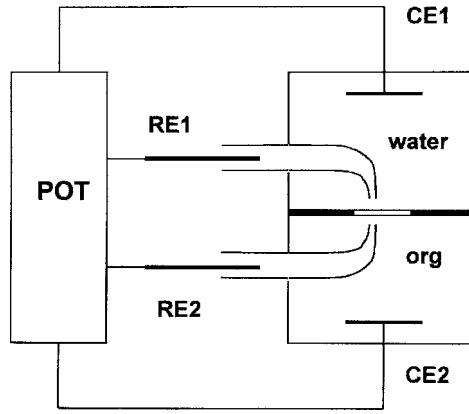

FIGURE 32.2 Scheme of a four-electrode system for polarization measurements at an ITIES comprising a potentiostat (POT), two reference electrodes connected to the cell by means of Luggin capillaries (RE1, RE2), and two counter electrodes (CE1, CE2). The planar ITIES is formed at the edge of a round hole in a glass barrier between the spaces for the aqueous (water) and the organic (org) phases.

cell (Fig. 32.2) (Samec et al., 1979). Reference electrodes are usually connected by means of Luggin capillaries, the tips of which are typically about 1 mm from the boundary. Under some conditions (e.g., low electrical current or large-area reference electrodes), three- or two-electrode configurations are possible, where one or two reference electrodes, respectively, comprise the function of both the reference and counter electrodes. Polarization measurements have performed been usually at planar ITIES, which is most suitable for ensuring the same potential difference over the entire interface. A spherical boundary is encountered in various assemblies with a pendant electrolyte drop or dropping (ascending) electrolyte electrode. Micro-sized ITIES (or μITIES) can be realized by supporting ITIES at the tip of a micropipette or on the microhole drilled in a polymer film. The potential difference or the electric current across an ITIES is controlled by means of a potentiostat or galvanostat, respectively. When the current flows through an ITIES, there is always a potential difference between the tips of the Luggin capillaries and the ITIES due to the solution resistance R, the ohmic potential drop IR, which has to be subtracted from the applied voltage E_{cell},

$$E_{\text{cell}} = \varphi_{\text{G}}^{(\text{w,o})} + IR - E_{\text{ref}}. \tag{32.17}$$

The ohmic potential drop can be compensated by means of positive feedback of the potentiostat or by algebraic subtraction under potentiostatic or galvanostatic conditions, respectively.

32.4 STRUCTURE OF ITIES

According to the model proposed by Verwey and Niessen (1939), an electric double layer is formed at an ITIES, which consists of two ionic space charge regions. As a whole the electric double layer is electrically neutral, so for the excess charge density $Q_S^{(w)}$ in the part of the double layer in the aqueous phase, and for the part in the organic phase, $Q_S^{(o)}$,

$$Q_S^{(w)} + Q_S^{(o)} = 0. \tag{32.18}$$

Assuming that the two space-charge regions are separated by a layer of solvent molecules (inner layer or mixed solvent layer), the Galvani potential difference $\varphi_G^{(w,o)}$ can be expressed as the sum of three contributions:

$$\varphi_G^{(w,o)} = \varphi_{in}^{(w,o)} + \varphi_2^{(o)} - \varphi_2^{(w)}, \tag{32.19}$$

where $\varphi_{in}^{(w,o)}$, $\varphi_2^{(o)}$, and $\varphi_2^{(w)}$ are the potential differences across the inner layer and the space-charge regions in the organic and the aqueous phases, respectively. Distribution of both the ions and the electric potential in the space-charge region can be obtained by solving the Poisson–Boltzmann equation assuming that the ions can be represented by point charges, as in the model of Gouy and Chapman (see Fig. 32.3):

$$Q_S^{(w)} = -(8\varepsilon^{(w)}RTc^{(w)})^{1/2} \sinh \frac{F\varphi_2^{(w)}}{2RT}, \tag{32.20}$$

$$Q_S^{(o)} = -(8\varepsilon^{(o)}RTc^{(o)})^{1/2} \sinh \frac{F\varphi_2^{(o)}}{2RT}, \tag{32.21}$$

where $\varepsilon^{(w)}$ and $\varepsilon^{(o)}$ are the dielectric constants of phases (w) and (o), respectively, and $c^{(w)}$ or $c^{(o)}$ are the electrolyte concentrations in phases (w) and (o), respectively. The chemical composition of the electrolytes is not important, and Eqs. (32.20) and (32.21) apply to both the extraction system with the electrolyte RX in partition equilibrium and to immiscible solvents each containing a different electrolyte. Molecular dynamics simulations of an ITIES suggest that the interface is molecularly sharp but rough. The interfacial roughness can be described as the protrusion of water molecules, hydrogen-bonded to each other, into the organic solvent, or as thermally populated capillary waves on the sharp interface.

Thermodynamic analysis of the ideally polarizable ITIES in the absence of the ion association yields the electrocapillary equation (for $T,p = \text{const}$) (Kakiuchi and Senda, 1983)

$$-d\gamma = Q_S^{(w)}\, dE_{o+}^{(w,o)} + \Gamma_{R+}^{(w,o)}\, d\mu_{RX} + \Gamma_{Y-}^{(w,o)}\, d\mu, \tag{32.22}$$

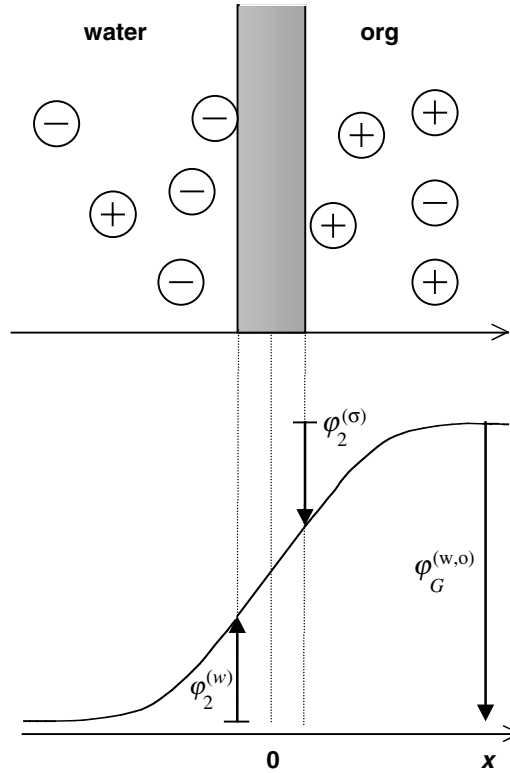

FIGURE 32.3 Modified Verwey–Niessen model of an ITIES with an inner layer (shaded area) separating two space-charge regions.

where γ is the interfacial tension, the $\Gamma_j^{(w,o)}$ are relative surface excess concentrations, and $E_{o+}^{(w,o)}$ is the potential difference of the cell:

$$\mathrm{RE}\|\mathrm{S^+X^-(w')}|\mathrm{S^+Y^-(\sigma')}|\mathrm{S^+Y^-(\sigma)}|\mathrm{R^+X^-(w)}\|\mathrm{RE} \tag{32.23}$$

with the aqueous RE being reversible to anion X^- and the organic RE being reversible to cation S^+. The surface charge density $Q_S^{(w)}$ is given by

$$Q_S^{(w)} = -\left(\frac{\partial\gamma}{\partial E_{o+}^{w-}}\right)_{T,p,\mu} = F(\Gamma_{R+}^{(w,o)} - \Gamma_{X-}^{(w,o)}) = -F(\Gamma_{S+}^{(w,o)} - \Gamma_{Y-}^{(w,o)}) \tag{32.24}$$

A related quantity is the differential capacity C,

$$C = \left(\frac{dQ_S^{(w)}}{dE_{o+}^{w-}}\right)_{T,p,\mu}. \tag{32.25}$$

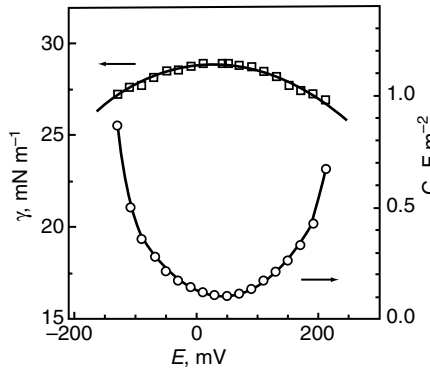

FIGURE 32.4 Potential dependence of the interfacial tension γ and the capacity C for the interface between solutions of 5 mM tetrabutylammonium tetraphenylborate in 1,2-dichloroethane and 100 mM LiCl in water. The potential scale E represents the Galvani potential difference $\varphi_G^{(w,o)}$ relative to the standard ion transfer potential for tetraethylammonium ion, $\varphi_{G0TEA+}^{(w,o)} \approx 0.02$ V.

Suitable electrolytes for the aqueous phase (w) comprise, for example, LiCl, HCl, $MgCl_2$, $MgSO_4$, while suitable electrolytes for the organic phase (o) comprise salts of, for example, tetrabutylammonium, tetraphenylarsonium, or bis(triphenylphosphoranylidene)ammonium cations with tetraphenylborate, tertrakis(4-chlorophenyl)borate, or tetrakis[3,5-bis(trifluoromethyl)phenyl]borate anion.

Interfacial and capacity measurements represent two fundamental experimental approaches to study the structure of the polarized ITIES. Interfacial tension has been measured by classical methods, including drop weight/drop time, maximum bubble pressure, or pendant-drop method. Capacity data are usually obtained by means of impedance spectroscopy. Typical electrocapillary and capacity curves are shown in Fig. 32.4. In the absence of specific ion adsorption, the positions of the electrocapillary maximum (potential of zero charge) and capacity minimum usually coincide and are close to zero on the scale of the Galvani potential differences $\varphi_G^{(w,o)}$. Experimental approaches to dynamics of ITIES rely on X-ray or quasielastic light-scattering measurements and neutron reflection methodology. Structural information can be inferred by using nonlinear optical methods such as second harmonic generation (SHG) or vibrational sum frequency spectroscopy (VSFS).

32.5 CHARGE-TRANSFER RATE

An electric current flowing through an ITIES splits into nonfaradaic (charging or capacity) and faradic current contributions. The latter contribution comprises the effects of both the transport of reactants to or from the interface, and the interfacial charge transfer, the rate of which is a function of the interfacial potential difference. By applying a transient electrochemical technique, these two effects can be resolved

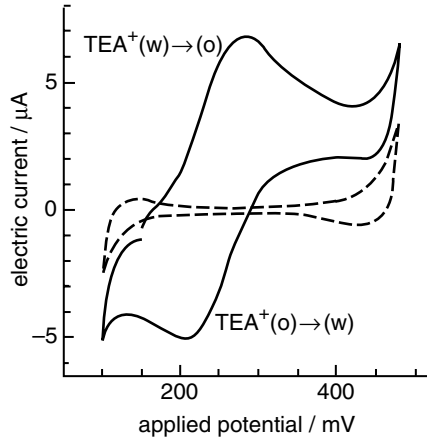

FIGURE 32.5 Cyclic voltammogram for the interface between solutions of 5 m*M* tetrabutylammonium tetraphenylborate in 1,2-dichloroethane and 5 m*M* NaCl in water in the absence (dashed line) and the presence (solid line) of 0.5 m*M* tetraethylammonium in the aqueous phase. Sweep rate 10 mV/s, interfacial area 0.02 cm^2.

and the charge-transfer rate can be evaluated. In contrast to the bulk ion transport, the transfer of an ion across ITIES, as described by Eq. (32.3), is accompanied by a significant change in the ion solvation shell. A dynamic role in this process is played by thermally excited capillary waves. However, re-solvation is relatively fast, and the apparent first-order rate constant of ion transfer is rather high (>0.1 cm/s). The overall reversibility of a typical ion transfer reaction is demonstrated in Fig. 32.5, which shows the cyclic voltammogram of an ITIES in the presence and absence of a semihydrophobic ion (tetraethylammonium cation). Such voltammograms show the same characteristics as those measured at electrodes (e.g., the peak potential difference is $59/z$ mV and the peak current is proportional to the square root of the sweep rate). The peak potential is closely related to the standard ion transfer potential $\varphi_{G0j}^{(w,o)}$.

The mechanism of electron transfer across an ITIES is similar to that of a homogeneous electron transfer in solutions. The main difference is that the reactants are separated by a liquid–liquid boundary, and as a result, the Gibbs energy of electron transfer across ITIES is a function of the Galvani potential difference $\varphi_G^{(w,o)}$. The limiting factor for both types of reactions is the energy of reorganization of the solvent and the inner sphere of reactants leading to the formation of an activated complex, which is followed by a tunnel transition of electron from the donor to the acceptor electron energy level. A fundamental theory of both ion and electron transfer at ITIES was developed by Rudolph Marcus in 1990.

Irradiation of an ITIES by visible or UV light can give rise to a photocurrent, which is associated with the transfer of an ion or electron in its excited state. Alternatively, the photocurrent can be due to transfer of an ionic product of the photochemical reaction occurring in the solution bulk. Polarization measurements of the photoinduced charge transfer thus extend the range of experimental approaches to

photochemical processes, allowing to investigate their mechanism as well as to study the specific effects of the electrical field on these processes.

32.6 APPLICATIONS

Apart from the study of physicochemical aspects such as ion solvation, and biomimetic aspects such as photosynthesis or carrier-mediated ion transfer (Volkov et al., 1996, 1998), there are several areas of potential applications of electrochemical IBTILE measurements comprising electroanalysis, lipophilicity assessment of drugs, phase transfer catalysis, electro-assisted extraction, and electrocatalysis.

Studies of the polarized IBTILE provide a fundamental knowledge that makes it possible to explain phenomena occurring at the membranes of ion-selective electrodes. In addition, the rates of ion transfer and assisted ion transfer reactions are proportional to concentrations, which is a basis of an amperometric ion-selective (sensitive) electrode.

Drugs are administrated mostly in their hydrophilic (usually protonated) forms. Their pharmacokinetics depends on several factors, including drug lipophilicity. It has commonly been accepted that the species crossing the biological membrane to reach the target site must be electrically neutral. Hence, drug lipophilicity has been evaluated by measuring the partition coefficient of the neutral drug form in a two-phase liquid system. From the electrochemical point of view, this approach is unsatisfactory, because the transfer of even highly lipophilic ions across the liquid and bilayer lipid membranes is possible. A more convenient approach that considers the partition of both the neutral and ionic drug forms, as well as acid–base equilibrium in both phases, has been proposed, which is based on the construction of an ion partition diagram of the solute, in analogy with Pourbaix's pH–potential diagrams, used widely in the electrochemistry of corrosion (Reymond et al., 1996).

Phase transfer catalysis (PTC) has been utilized in organic synthesis to perform reactions in organic solvents when some of reactants are present in the aqueous phase (e.g., the substitution reaction involving alkylchlorides RCl),

$$\mathrm{RCl(o) + NaCN(w) \rightarrow RCN(o) + NaCl(w).} \tag{32.26}$$

The rate of this reaction is negligible until a tetraalkylammonium chloride [e.g., tetrabutylammonium chloride (TBACl) is added as a catalyst. It has usually been considered that the role of the catalyst is to transfer the reactant physically, as the ion pair TBA^+CN^-, from the aqueous to the organic phase, where the homogeneous chemical reaction can occur. Although this is possible in organic media of low dielectric permittivity, a different mechanism is more likely when the organic electrolytes can dissociate into ions. Essentially, the salt added undergoes a partition leading to a distribution potential, which drives the ion (e.g., CN^-) or the electron to the target substance.

Two-phase liquid systems or liquid membranes have found applications in various separation technologies. Liquid membranes have an advantage over traditional

solvent extraction in that the volume of the organic phase can be decreased considerably and hence the costs associated with expensive solvents and ligands reduced. Electro-assisted extraction by the application of a potential difference across a polarizable liquid membrane appears to be a potential alternative.

Electron transfer processes leading to a product adsorbed in the interfacial region σ are of practical interest. These processes include the deposition of a metal such as Cu or Pd at ITIES, the preparation of colloidal metal particles with catalytic properties for homogeneous organic reactions, or electropolymerization.

REFERENCES

Gavach, C., T. Mlodnicka, and J. Guastalla, *C.R. Acad. Sci.*, **C266**, 1196 (1968).

Hung, L. Q., *J. Electroanal. Chem.*, **115**, 159 (1980).

Kakiuchi, T., and M. Senda, *Bull. Chem. Soc. Jpn*., **56**, 2912 (1983).

Karpfen, F. M., and J. E. B. Randles, *Trans. Faraday Soc.*, **49**, 823 (1953).

Koryta, J., M. Březina, and P. Vaný́sek, *J. Electroanal. Chem.*, **75**, 211 (1977).

Marcus, R. A., *J. Phys. Chem.*, **94**, 1050 (1990); *J. Chem. Phys.*, **113**, 1618 (2000).

Nernst, W., *Z. Phys. Chem.*, **9**, 137 (1892).

Reymond, F., G. Steyaert, P.-A. Carrupt, B. Testa, and H. Girault, *J. Am. Chem. Soc.*, **118**, 11951 (1996).

Samec, Z., *J. Electroanal. Chem.*, **99**, 197 (1979).

Samec, Z., V. Mareček, and J. Weber, *J. Electroanal. Chem.*, **100**, 841 (1979).

Verwey, E. J. W., and K. F. Niessen, *Philos. Mag.*, **28**, 435 (1939).

REVIEWS AND MONOGRAPHS

Girault, H. H., and D. J. Schiffrin, in *Electroanalytical Chemistry*, Vol. 15, A. J. Bard, Ed., Marcel Dekker, New York, 1989, p. 1.

Volkov, A. G., and D. W. Deamer, Eds., *Liquid–Liquid Interfaces: Theory and Methods*, CRC Press, Boca Raton, FL, 1996.

Volkov, A. G., D. W. Deamer, D. L. Tanelian, and V. S. Markin, Eds., *Liquid Interfaces in Chemistry and Biology*, Wiley, New York, 1998.

33

Various Electrochemical Phenomena

YURIJ TOLMACHEV *(Section 33.1)*

Kent State University, Kent, Ohio

LEONID KANEVSKY *(Section 33.2)*

A. N. Frumkin Institute of Physical Chemistry and Electrochemistry, Russian Academy of Sciences, Moscow, Russia

33.1 ELECTROCHROMISM

Like chemical reactions, electrochemical reactions are often accompanied by a change in color. For example, colorless WO_3 can be reduced either chemically or electrochemically to form intensely colored compounds known as tungsten bronzes:

$$WO_3 + xe^- + xH^+ \rightarrow H_xWO_3, \tag{33.1.1}$$

where $x = 0.1$ (gray), 0.2 to 0.4 (blue), 0.6 (purple), 0.7 (brick red), and 0.8 to 1.0 (golden bronze). Another example is the oxidation of ferrocyanide to ferricyanide:

$$\underset{\text{(pale)}}{[Fe^{II}(CN)_6)^{4-}} - e^- \rightarrow \underset{\text{(yellow)}}{[Fe^{III}(CN)_6]^{3-}}. \tag{33.1.2}$$

In general, the term *electrochromism* is used to describe the change in light absorption as a result of an electrochemical reaction. Recent interest in electrochromism stems from its potential applications in numerous devices, such as flat screen displays, antidazzle mirrors, "smart" windows, and others.

Figure 33.1*a* illustrates the idea of the smart window. In this device a layer of electrochromic material and a layer of a transparent ion-conducting electrolyte are sandwiched between two optically transparent electrodes (OTEs). Indium-doped tin oxide on glass is used most commonly as the OTE. This material has very low

Fundamentals of Electrochemistry, Second Edition, By V. S. Bagotsky

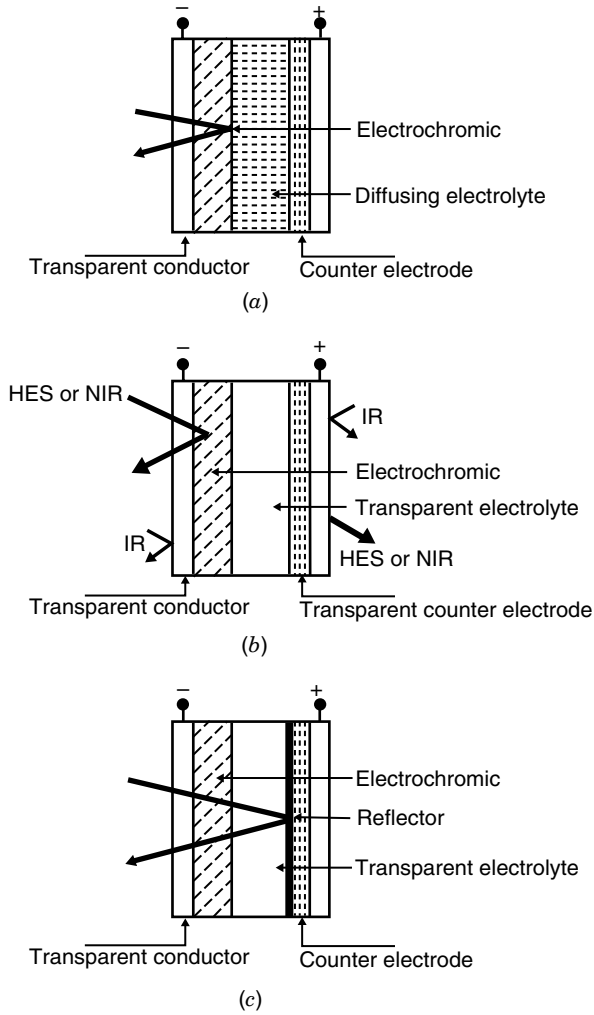

FIGURE 33.1 Schematic illustration of (*a*) a "smart" window or transmission display; (*b*) a front-illumination display; (*c*) an antidazzle mirror. (From Bohnke, 1992, with permission of Cambridge University Press.)

absorbance in the visible and near-infrared range, good electrical conductivity as a highly doped semiconductor, and reasonable chemical stability. In the bleached state, the window has high transmission for high-energy solar radiation (HER) and near-infrared radiation (NIR). In the colored state the window does not transmit (but rather, reflects or adsorbs) HER and NIR. Such windows are used in automobiles: On cloudy days or at dusk, one prefers to drive with untinted windows, but on sunny days, with colored (tinted) windows.

Figure 33.1*b* illustrates the principle of a front-illuminated display. In this case, the light goes through an OTE, then through an electrochromic layer. The electrolyte

behind the electrochromic layer is filled with a white diffuse scattering material (most often, TiO_2 powder). When viewed from the front, the cell appears white in the bleached state, due to the color of the diffuse scattering filler in the electrolyte. In the colored state, some of the incident and scattered light is adsorbed by the electrochromic material, and the cell appears in the color complementary to the color of the electrochromic material in transmission. Since the light does not penetrate the diffuse scattering layer, the counter electrode does not have to be transparent in this device.

As shown in Fig. 33.1*b*, such variable transmission devices can also be used as pixels in back-illuminated flat screen displays. Different materials can be used to produce pixels of different colors, similar to cathode-ray tubes (CRTs) or liquid-crystal displays (LCDs). Also, some electrochromic materials can develop different colors depending on the applied potential (i.e., capable of *polyelectrochromism*). Electrochromic displays have several interesting advantages over CRTs and LCDs. First, unlike CRT and LCD, electrochromic materials do not require constant application of voltage to maintain the colored state. Once the required charge passes and the required potential is established, power to the electrochromic cell can be disconnected, and the color can persist at the open-circuit potential (i.e., electrochromic material shows a memory effect). Another advantage related to the fact that the color intensity of individual pixels can gradually be controlled by adjusting the injected charge. This allows tonal gradation at the pixel level. In contrast, tonal gradation in LCD relies on stippling with pixels, which causes deterioration of spatial resolution.

Figure 33.1*c* shows the principle of a variable reflectance mirror. In this device, the electrochromic layer is placed in front of a mirror, which can also be used as the working electrode. In the bleached state, the reflectance of this mirror is high, but in the colored state, some of the incident and reflected light is absorbed by the electrochromic layer, and the reflectance is lower. Such devices are used as antidazzle rear-view mirrors in automobiles. In some commercial products, a photoelement is used to monitor the light incident on the mirror. If there is a car behind you with its front lights on, the photoelement detects it and sends a signal to a power supply to switch the mirror into the colored state. Once the dazzling source is gone, the mirror is switched back into the bleached state.

A large number of materials show electrochromic properties; however, only a few of them are interesting for practical applications since for this purpose, additional requirements must be fulfilled: (1) as discussed above, for most applications the materials need to have a colorless (bleached) state; (2) the electrochromic transformations should occur without parasitic reactions, such as gas evolution or material degradation; (3) to be considered practical, the electrochromic materials should survive at least 10^5 coloring–bleaching cycles; (4) the rate of electrochromic transformation needs to be sufficiently fast (1 s for most applications); and (5) due to problems with leaking and diffusion in liquids, it is preferable to have insoluble solid electrochromic materials.

Presented below are several electrochromic materials that showed significant promise for practical devices.

Metal Oxides Tungsten trioxide, undoubtedly the most widely studied electrochromic material, is used in several types of commercial electrochromic devices.

Upon reduction, WO_3 forms mixed-valence ($W_x^{V}W_{1-x}W^{VI}$) tungsten bronzes, H_xWO_3, which have different colors depending on the degree of reduction, x [see Eq. (33.1)]. Due to parasitic reaction, such as hydrogen evolution, and decreased reversibility, the use of WO_3 in electrochromic devices is limited to $0 \leq x \leq 0.3$ (i.e., between the untinted and blue states). Equation (33.1) shows that the coloration reaction is accompanied by an injection of electrons and counterions (H^+ in this case). Usually, it is the ion intercalation/deintercalation, not the electron transport, that limits the rate of electrochromic transformation. Of course, this rate depends on the thickness of the film, its structure, and the type of intercalated ion. In the case of WO_3, only H^+ and Li^+ ions have the possibility of an reversible intercalation.

Several other oxide materials, such as MoO_3, Nb_2O_5, and TiO_2, also show coloration in the reduced state. On the other hand, some other oxides acquire color in the oxidized state. Some examples are:

$$\underset{\text{(colorless)}}{Ir(OH)_3} \rightarrow \underset{\text{(blue)}}{IrO_2 \cdot H_2O} + H^+ + e^-; \tag{33.1.3}$$

$$\underset{\text{(colorless)}}{Ni(OH)_2} + OH^- \rightarrow \underset{\text{(black)}}{NiOOH} + H_2O + e^-. \tag{33.1.4}$$

If an anodically colored electrochromic material (e.g., IrO_2) is used as one electrode in the device in Fig. 33.1*b* and a cathodically colored (e.g., WO_3) is used as the other electrode, a much larger change in transmission per charge supplied can be seen compared to the case when only one electrode is electrochromic. Also, the use of an intercalation material as the counter electrode may be advantageous for the device shown in Fig. 33.1*a*, as it can minimize undesired reactions on the counter electrode.

Oxide materials in the colored state are usually mixed-valence compounds with a variable range of composition. The color usually arises from low-energy intraband electronic transitions.

Other Inorganic Compounds Prussian Blue represents another type of inorganic mixed valence electrochromic materials. This material is known in three states:

$$\underset{\text{(Prussian White)}}{[Fe^{II}Fe^{II}(CN)_6]^{2-}} \overset{-e^-}{\underset{+e^-}{\rightleftarrows}} \underset{\text{(Prussian Blue)}}{[Fe^{III}Fe^{II}(CN)_6]^-} \overset{-e^-}{\underset{+e^-}{\rightleftarrows}} \underset{\text{(Prussian Brown)}}{[Fe^{III}Fe^{III}(CN)_6]}. \tag{33.1.5}$$

K^+ is generally used as the reversibly intercalating ion since it leads to insoluble compounds for all the forms. In the mixed-valence Prussian Blue compound, Fe^{3+} is in the high-spin state and coordinated octahedrally with the N ends of the cyanides, whereas Fe^{3+} is low-spin and octahedrally coordinated with the C ends of the

cyanides. The intense blue color is due to intraband *d*-electron transitions. Prussian White is formed at potentials more negative than 0.1 V vs. SCE, Prussian Blue exists between 0.1 and 0.6 V, and Prussian Brown is formed at potentials more positive than 0.8 V. Between 0.6 and 0.8 V, an intermediate green color is formed. Thus, Prussian Blue can form four different colored states (i.e., shows polyectrochromism). Yet in most applications only white–blue transition is used because of problems with the stability of Prussian Brown. Numerous other mixed hexacyanometallates, including those of Ru, Os, Pd, V, Ni, Co, Cu, and In, also show electrochromic behavior.

Molecular Metal Complexes Compounds of this type do not form delocalized electronic bands in the solid state, and their color is due to *intramolecular* electronic transitions. Many complexes of transition metals with organic ligands belong to this class. $Fe^{2+/3+}$ complexes with phenanthroline (red/colorless) and $Ru^{2+/3+}$ with 2,2′-bipyridine (orange/colorless), and their analogs received most attention. As most of such compounds are soluble in water, special procedures have been developed for immobilization of the complexes on electrodes. Such procedures include impregnation of the complexes into polymer films or modification of the ligand followed by polymerization of the monomer complex.

Ru^{3+} 2,2′-bipyridine complexes can form a large number of colored compounds upon successive reduction, with the formal Ru oxidation state from $+2$ to -4. In the case of highly reduced complexes, proper representation of the electrochromic reaction is actually the reduction of the ligand, not that of the metal center.

Similar behavior (i.e., an electrochromic reduction–oxidation of the ligand) is observed with phtalocyanine and related macrocyclic complexes. Such complexes are insoluble in most solvents and can readily be immobilized on the electrode. Lutetium(III) (bis)phtalocyanine attracted particular attention. The metal ion in this complex is much larger than the size of the ring cavity, and rather than going inside the ring, it is sandwiched between two phtalocyanine ligands. As prepared, lutetium(III) (bis)phtalocyanine has a green color. An one-electron oxidation leads to a yellow compound, a two-electron oxidation—to red. It can also be reduced stepwise to light blue, blue, and violet forms.

Organic Molecules It can be seen from our earlier discussion that the presence of a transition metal ion is not always required for an electrochromic effect. Indeed, many organic molecules can yield colored products as a result of reversible reduction or oxidation. 4,4′-Bipyridinium salts are the best known example of such compounds. These compounds can be prepared, stored, and purchased in colorless dicationic form ($bipm^{2+}$). One electron reduction of the dication leads to the intensely colored radical cation ($bipm^{+\cdot}$). Such radical cations exist in equilibrium with their dimers ($bipm_2^{2+}$). In the case of methyl viologen, the radical cation is blue and the dimer is red. By varying the substient group in the molecule, different colors can be obtained.

Since most bipirydinum salts are soluble in water and other solvents, numerous methods have been developed for immobilization of these electrochromic molecules

on electrodes. $bipm^{2+}$ and $bipm^{+\cdot}$ can be retained in the polymers electrostatically, covering the electrodes, provided that the polymers contain anionic groups (such as Nafion). Also, if the R-group in the molecule has a polymerizable functionality (such as vinyl or pyrrole), insoluble electrochromic polymers can be prepared. Another approach is to introduce a terminal siloxane group such as $–Si(OCH_3)$ into the R-group. Upon acid-catalyzed hydrolysis of the siloxane groups, the molecules can be attached to an OTE or polymerize, forming Si–O–Sn and Si–O–Si linkages, respectively.

Electrolytes for Electrochromic Devices Liquids are generally used as electrolytes in electrochemical research, but they are not well suited for practical devices (such as electrochromic displays, fuel cells, etc.) because of problems with evaporation and leakage. For this reason, solid electrolytes with single-ion conductivity are commonly used (e.g., Nafion membranes with proton conductivity. In contrast to fuel cells in electrochromic devices, current densities are much lower, so for the latter application, a high conductivity value is not a necessary requirement for the electrolyte.

33.2 ELECTROCHEMICAL NOISE

Electrochemical noise is the name given to spontaneous fluctuations of parameters in an electrochemical system. Different types of such noise are encountered: (1) fluctuations of an electrode's potential at zero external current; (2) fluctuations of electrode potential when the system is galvanostatically controlled (a current of constant density passes through the electrode), (3) fluctuations around a theoretical zero value of the current flowing between two perfectly identical electrodes, (4) fluctuations of the imposed current when the system is potentiostatically controlled, and (5) fluctuations of the potential difference ΔE between unlike electrodes, and similar phenomena.

Basically, fluctuations of two types are involved: (1) microfluctuations of current or potential having as their immediate cause the thermal motion of the particles contained in the electrochemical system, where the energy of the noise is close to the mean energy of thermal motion, kT; and (2) macrofluctuations, where the total energy of the noise is greatly in excess of that of thermal motions. Noise involving microfluctuations is often called *equilibrium noise*; that involving macrofluctuations is called *nonequilibrium noise*.

Noise is characterized by the time dependence of noise amplitude A. The measured value of A (the instantaneous value of potential or current) depends to some extent on the time resolution of the measuring device (its frequency bandwidth Δf). Since noise always is a signal of alternating sign, its intensity is characterized in terms of the mean square of amplitude, A^2, over the frequency range Δf, and is called (somewhat unfortunately) *noise power*. The Fourier transform of the experimental time dependence of noise intensity leads to the frequency dependence of noise intensity. In the literature these curves became known as *PSD* (power spectral density) *plots*.

An important early paper on fluctuation processes is that of Harry Nyquist (1928), who suggested an equation linking the mean-square amplitude of thermal noise in an electrical circuit to the resistance R of the noise EMF (or current) generator:

$$A^2 = 4kTR\,\Delta f, \tag{33.2.1}$$

where k is the Boltzmann constant and T the absolute temperature. Noise in electrochemical systems was discovered long ago. Indications can be found as early as Vetter's well-known 1961 monograph. Concentrated studies of electrochemical noise were initiated in the 1970s.

In their first paper on noise, Tyagai and Luk'yanchikova (1967) considered a very simple redox reaction of the type of $O + ze^- = R^{z-}$. According to these authors, when the reaction rate is limited by a slow-discharge step, the mean-square amplitude of the noise is given by

$$A^2 = \frac{2kT}{e}\left(\frac{\Delta f}{i^0 S}\right)^{1/2}. \tag{33.2.2}$$

When it is limited by slow diffusion of the reactants, the mean-square amplitude is

$$A^2 = \left(\frac{4}{\pi}\right)^{1/4}\left[\frac{\Delta f}{Sf^{1/2}}(c_O D_O^{1/2} + c_R D_R^{1/2})\right]. \tag{33.2.3}$$

According to these equations, in kinetically controlled reactions the mean-square amplitude is about 10^{-9} V, while in reactions occurring under diffusion control it is almost an order of magnitude smaller. Thus, the size of electrochemical (thermal) equilibrium fluctuations is extremely small.

This implies that powerful equipment must be used for noise measurements and that experiments are difficult. It will be necessary in particular to use electrodes with a very small surface area (e.g., microelectrodes), to have a minimum ohmic series resistance in the measuring circuit, and to work with extremely low concentrations of the electroactive components in the test system. For these reasons, studies and the analysis of thermal noise in electrochemical systems are basically of academic interest. Barker (1969) concluded that "although little is to be gained from studies of noise in equilibrium systems with thermal agitation and finite size of charge transfer events, experiments far from equilibrium may cast some light on the mechanism of charge transfer. Noise measurements are most likely to prove informative when charge transfer is catalyzed by a minor component of the interface."

The mean-square amplitude of nonequilibrium noise, quite in contrast to that of equilibrium thermal noise, may reach rather high values: for instance, hundreds of millivolts during anodic polarization of semiconductors (Parkhutik and Timashev, 2000).

One of the major reasons for the development of nonequilibrium noise in electrochemical systems is the inhomogeneity (micro- or macro-heterogeneity) of electrode surfaces. For this reason, the analysis of electrochemical noise proved

very helpful in studies of different corrosion processes occurring on fully or partly passivated metal surfaces.

It was learned that pitting-type metal and semiconductor corrosion is attended by the generation of noise seen in the form of dynamic irregularities in the changes of the anodic potential and current density. Thus, electrochemical noise studies were applied to the corrosion and passivation of metals and to their activation by external chemical (activating additives in the electrolyte) or electrochemical (anodic or cathodic polarization) agents.

Uniform and pitting-type corrosion of various materials (carbon steels, stainless steels, aluminum, etc.) could be characterized in terms of noise properties of the systems: fluctuation amplitudes in the time domain and spectral power (frequency dependence of power) of the fluctuations. Under-film corrosion of metals having protective nonmetallic coatings could also be characterized. Thus, corrosion research was enriched by a new and sufficiently correct method of looking at various aspects of the action of corrosive media on metals.

Basically, experimental studies of metals by electrochemical noise measurements involve detection of the fluctuations of potential and current between two metal samples that are identical in their size and surface preparation. As a rule, one works with two or three smooth parallel plates having surface areas of 0.1 to 1 cm^2. Porous objects cannot be used for such studies, since their branched structure may give rise to highly indefinite, irreproducible noise effects. Precision instruments are used to measure currents and potential differences with errors not exceeding fractions of a nanoampere or microvolt. Discrete readings can be recorded using computers; special programs for the acquisition and initial processing of the experimental results are available.

Figure 33.2 shows results obtained by studies of electrochemical noise for the corrosion behavior of carbon steel A516–70 in carbonate solutions with and without NaCl as an activator (Cheng et al., 2000). It can be seen that in ordinary carbonate solution the fluctuations of potential of a test electrode and the fluctuations of current flowing between a pair of identical electrodes are small. Added NaCl causes a drastic increase in intensity of the electrochemical noise. The PDS plots (Fig. 33.3) differ accordingly.

The following criteria are usually applied when analyzing these power spectra: the magnitude of power, the frequency at which the power begins to fall off, and the slope of the descending part of the plot. From such an analysis one can sufficiently well identify the various types of corrosive attack (uniform, crevice, pitting).

The concepts and basic approach used in studies of electrical fluctuations in corrosion processes proved to be very successful as well in mechanistic studies of electrode reactions taking place at materials covered by passivating films. A typical example is the electrochemical dissolution of silicon. From an analysis of the noise characteristics of this process, it has been possible to identify many features as well as the conductivity of the nanostructures of porous silicon being formed on the original silicon surface.

Electrochemical noise studies have also been beneficial in lithium battery research. The lithium electrode sitting in the aprotic electrolyte is covered by a passivating film

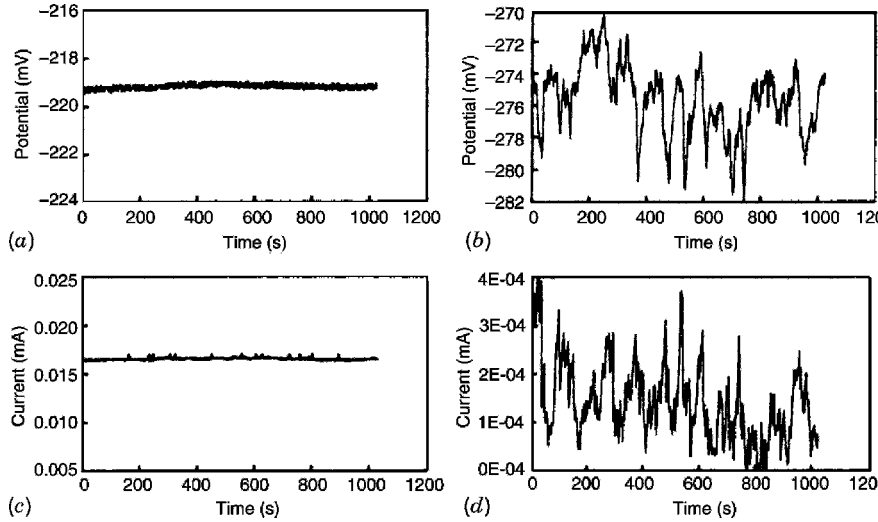

FIGURE 33.2 Potential (*a*, *b*) and current (*c*, *d*) fluctuations of A526-70 carbon steel in 0.5 *M* $NaHCO_3$ solution (*a*, *c*) and (after 1 h of immersion) in 0.5 *M* $NaHCO_3$ + 0.5 *M* Cl^- solution (*b*, *d*). (From Cheng et al., 2000, with permission of the *Bulletin of Electrochemistry*.)

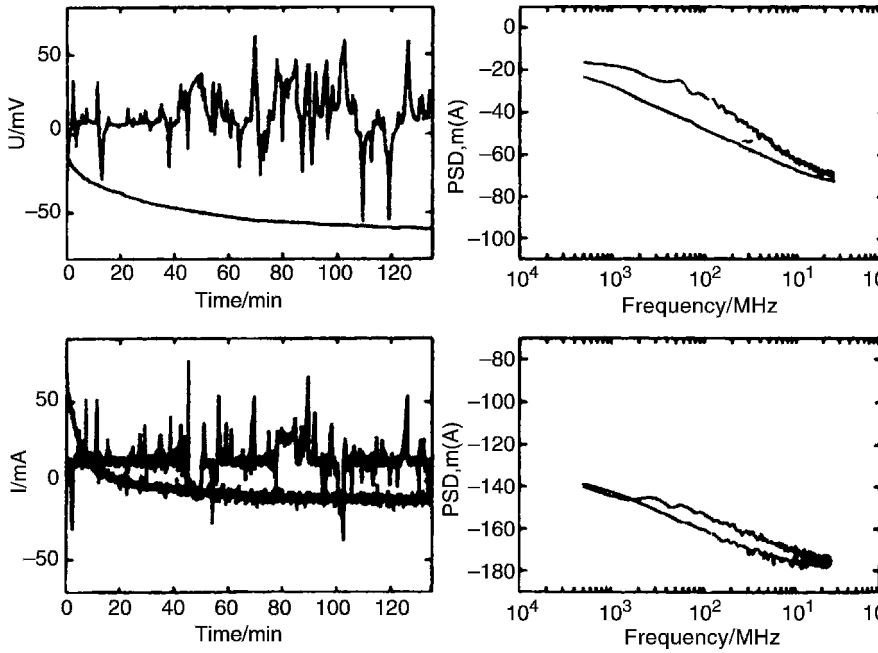

FIGURE 33.3 Potential PSD plots (a) and current PSD plots (b) for A526-70 carbon steel at different immersion times in 0.5 *M* $NaHCO_3$ + 0.5 *M* Cl^- solution. (From Cheng et al., 2000, with permission of the *Bulletin of Electrochemistry*.)

that consists of products formed when Li reacts with its environment, and can undergo changes. In their steady state, the Li electrodes have a low, time-invariant level of potential fluctuations indicative for a stable passive film on the Li surface.

A polarization of the electrode with currents corresponding to normal loads applied when cycling rechargeable Li batteries leads to a change in the state of the Li surface. This can be seen from an important change in amplitude of the electrochemical noise pointing to activation of the working electrode and destruction of its passivating surface film. It was found when analyzing the noise properties of polarized Li electrodes that the intensity and character of the fluctuations depend strongly on electrolyte composition: that is, the solvent and lithium salt.

The dynamics of electrochemical noise genererated by polarized Li electrodes in aprotic electrolytes can be explained as follows. During anodic polarization, the lithium dissolves vigorously beneath its passivating film, leading to cracking of this film and exposure of an active Li surface. The size of the activated-surface portion increases, and with it the surface heterogeneity, which is attended by increasing noise intensity. In parallel, passivation of the clean lithium surface takes place. Where this additional passivation is fast, the surface heterogeneity, and with it the noise intensity, remain low. Where repassivation is slow, the surface heterogeneity and the noise level increase.

During cathodic polarization, Li is deposited on the metal surface beneath the passivating film. The growing deposits may cause perforation of this film by Li crystals and the formation of a new active Li surface. This raises the heterogeneity of the Li surface and with it the intensity of electrochemical noise.

33.3 ELECTROCHEMICAL PROPERTIES OF HIGH-TEMPERATURE SUPERCONDUCTORS

It had been discovered toward the end of the nineteenth century that for certain inorganic multicomponent materials the critical temperature, T_{cr}, below which the material becomes superconducting can be as high as 150 to 250 K (i.e., it reaches virtually ambient temperatures), quite in contrast to superconductors known earlier, which would become superconducting only when the system was cooled down to temperatures close to 0 K. These materials thus were termed *high-temperature superconductors* (HTSCs). This phenomenon of high-temperature superconductivity is of exceptional interest inasmuch as it represents a marked step toward the practical use of superconductivity in electrical plants and grids, including all the technical and economic possibilities thus opening up.

Among the high-temperature superconductors one finds various cuprates (i.e., ternary oxides of copper and barium) having a layered structure of the perovskite type, as well as more complicated oxides on the basis of copper oxide which also include oxides of yttrium, calcium, strontium, bismuth, thallium, and/or other metals. Today, all these oxide systems are studied closely by a variety of specialists, including physicists, chemists, physical chemists, and theoreticians attempting to elucidate the essence of this phenomenon. Studies of electrochemical aspects contribute markedly to progress in HTSCs.

The HTSCs usually are relatively bulky samples prepared by technologies used to make ceramic parts. It is important, therefore, to develop methods that will yield HTSCs in the form of thin films supported on various carriers. One of the possibilities for making such films is by electrochemical synthesis of HTSCs, a method much simpler than ceramic technology and not requiring high temperatures. It has been shown that during anodic and cathodic cycling of a copper electrode in an aqueous solution containing the other cations needed, a thin oxide film which in its composition corresponds to HTSC is formed on the electrode surface. Another possibility is the electrochemical deposition of metal alloys from a solution containing all the components needed, followed by controlled thermal oxidation of these alloys.

The transition to the state of superconductivity depends not only on temperature but also on the state of the HTSC. Slight changes in stoichiometry and phase composition and in other materials parameters may cause loss of the ability to display superconductivity. The valence state of the copper and oxygen ions in the crystal lattice is very important, too. In compounds of the type $YBa_2Cu_3O_7$, the formal charge of the anions is one elementary charge higher than that of the cations. This indicates that a certain number of Cu^{3+} ions may exist at sites of Cu^{2+} ions, and/or a certain number of O^- ions may exist at sites of O^{2-} ions. Knowing the exact valence state of these ions is extremely important for a theoretical explanation of superconductivity in these materials.

For all these reasons, the stability of the superconducting state and ways to control it are questions of prime importance. Many studies have addressed the degradation of the properties of HTSC under the influence of a variety of factors. They included more particularly the corrosion resistance of HTSC materials exposed to aqueous and nonaqueous electrolyte solutions as well as to water vapor and the vapors of other solvents. It was seen that the corrosion resistance depends strongly both on the nature (chemical composition, structure, etc.) of the HTSC materials themselves and on the nature of the aggressive medium.

In some cases the stability of HTSC materials in contact with electrolytes is quite satisfactory, so they can be used for electrochemical measurements. Such measurements are made for various reasons. A number of workers have used cyclic voltammograms to characterize the state of HTSC materials. A constant shape of these curves over a certain length of time was evidence for conservation of the superconducting state during this time interval.

HTSCs can also be used as consumable and as nonconsumable electrodes. When an electrode is *ideally consumable* and parasitic reactions typically occurring at nonconsumable electrodes (oxidation or reduction of the solvent and other components) can be excluded, the valence state of its ions will change upon polarization of this electrode; upon anodic polarization the charge of the cations will increase and that of oxygen will decrease. The opposite is true during cathodic polarization. These electrochemical effects can then be used for two purposes: a quantitative determination of the valence state of the ions in the crystal lattice and a deliberate, controlled alteration of this valence state, both highly interesting for a thorough characterization of the materials.

It must be kept in mind, however, that the electrochemical polarization of a HTSC material often is attended by secondary effects. Apart from raising the cationic charge, anodic polarization often produces partial degradation of the material due to dissolution of certain cations. During cathodic polarization it is very difficult to prevent a reduction of the solvent or of solutes. In such cases the electrode ceases to be ideally consumable, and quantitative measurements aiming at determining or changing the valence state of the ions become meaningless.

Many papers have been published regarding HTSCs used as inert, nonconsumable electrodes for kinetic and mechanistic studies of various electrode reactions occurring at them. Most of these studies were performed at room temperature when the materials were not in their state of superconductivity. Unfortunately, to date a given reaction has rarely been studied at similar temperatures just above and below T_{cr}, that is, at temperatures where the same material is once in its normal state and once in its superconducting state. The electronic structure of materials differs sharply between these two states, and quantitative studies under these conditions might provide valuable information as to the mechanism of the elementary act of charge transfer from the electrode to a reacting species, and vice versa.

33.4 ELECTROCHEMICAL "COLD FUSION"

In March 1989, Martin Fleischmann and Stanley Pons reported their discovery of cold nuclear fusion. They announced that during electrolysis of a solution of lithium hydroxide in heavy water (D_2O) with a cathode made of massive palladium, nuclear transformations of deuterium at room temperature can be recorded. This announcement, which promised humankind a new and readily available energy source, was seized upon immediately by the mass media in many countries. Over the following years, research was undertaken worldwide on an unprecedented scale in an effort to verify this finding.

Initially, cold fusion was investigated exclusively with just the aim of verifying the very possibility that such an unusual process could occur. Two fusion reactions of deuterium nuclei ^{2}D were regarded as being most likely:

$$^2\mathrm{D} + {}^2\mathrm{D} \rightarrow {}^3\mathrm{He} + n + 3.26\,\mathrm{MeV}; \tag{33.4.1}$$

$$^2\mathrm{D} + {}^2\mathrm{D} \rightarrow {}^3\mathrm{T} + \mathrm{P} + 3.26\,\mathrm{MeV}. \tag{33.4.2}$$

Reaction (33.4.1) yields the helium isotope ^{3}He and a neutron n; reaction (33.4.2) yields tritium ^{3}T and light hydrogen (a proton) P, in both cases with the liberation of a huge amount of energy.

In the experimental verification, therefore, it was attempted to find the following phenomena:

1. An anomalous liberation of heat
2. The generation o631f neutrons

3. The formation of the isotope ^{3}He, which would be revealed by a departure from the natural ratio of isotopes ^{3}He and ^{4}He
4. The formation of tritium
5. The formation of high-energy protons

When considering the needs for experimental equipment and skills, only large nuclear research centers that have both radiochemical laboratories and research facilities in the areas of high-energy and elementary-particle physics could have been able reliably to conduct a full program of measurements. However, even outside such centers and before realizing the full complexity of the tasks, scientists started forming interdisciplinary groups. Often, the groups centered around electrochemists having the task to organize the electrolysis process.

When judging by communications available in the open literature, none of effects 1 through 5 could so far be observed repeatedly and reproducibly under rigorously controlled conditions. Provisionally, all instances of published experimental confirmation can be placed into two groups: (1) the observation of sporadic sufficiently pronounced manifestations, and (2) the observation of more invariant but very weak effects (as a rule, at the level of background noise, particularly in the detection of neutrons and tritium). However, there were far fewer confirmations than infirmations (i.e., work in which the "successful" experiments could be carefully reproduced or the method used to determine the products was analyzed and shown to be in error). Such work has been of exceptional value in the area of advancing the methods and techniques used in experimental studies.

More particularly, a serious breakthrough was achieved in the methods of electrochemical calorimetry. Initial conclusions as to anomalous heat evolution during the electrolysis of solutions prepared with heavy water were caused by an incorrect formulation of control experiments in light water. In fact, none of the communications confirming anomalous heat evolution have been free of procedural errors, so that one cannot even discuss a sporadic observation of this effect. In contrast to all other experimental manifestations, heat evolution is indicative of any possible nuclear transformation, which implies that in its absence, neither reaction (33.4.1) nor reaction (33.4.2) can be suggested to occur.

Another result of the cold-fusion epopee that was positive for electrochemistry are the advances in the experimental investigation and interpretation of isotope effects in electrochemical kinetics. Additional studies of isotope effects were conducted in the protium–deuterium–tritium system, which had received a great deal of attention previously; now these effects have become an even more powerful tool for work directed at determining the mechanisms of electrode reactions, including work at the molecular level. Strong procedural advances have been possible not only in electrochemistry but also in the other areas.

In parallel with the detailed checking of evidence for cold fusion, the range of hypotheses as to the nature of the phenomenon was at first extended very strongly at different levels. It must be pointed out at once that most of these hypotheses did not contain any specifically electrochemical element, except that from the very

beginning, electrolysis was regarded merely as the method used to hydrogenate the palladium:

$$D_2O + e^- \rightarrow OD^- + [D_{ads}(Pd) \rightarrow PdD_x] \tag{33.4.3}$$

and/or evolve gas:

$$D_2O + e^- \rightarrow D_{ads}(Pd) + OH^- + \tfrac{1}{2}D_2. \tag{33.4.4}$$

At an early stage, *solid-state hypotheses* were prevalent (i.e., suppositions concerning various mechanisms of the nuclear reaction in the palladium hydride phase PdD_x). This had to do with a number of earlier observations of neutron generation during the cracking of "heavy ice" (solid D_2O) and lithium hydride, which had not received equally wide publicity. However, these hypotheses become physically realistic only for deuterium-containing solid phases having dielectric properties. There the separation of charge occurring at the edges of developing cracks may indeed give rise to exceptionally strong electric fields having energies close to those of nuclear transformations. It is rather difficult to suggest that palladium hydrides could be a dielectric, since the conductivitiy of PdH_x phases (at least for $x < 1$) has been measured repeatedly and was found to be close to metallic. It remains to suggest that the conductivity falls strongly when more concentrated hydrides are formed. Reliable results concerning this possibility are not yet available in the scientific literature.

Somewhat later it was hypothesized that mechanochemical and sonochemical phenomena induced by gas-bubble transformations could be of decisive importance. Several serious scientific groups have up to now looked at this problem. The mechanism being tested by them is not able, of course, to satisfy the power levels claimed in nuclear reactions, but it is of high scientific interest. It has already been found that it is not at all compulsory to generate the gas electrolytically in order to utilize the energy of the bubbles, and that the gas itself need not at all contain deuterium. One of the model reactants used in current investigations in this area, more particularly, is deuterated acetone C_3D_6O.

A number of attempts have been made to accomplish nuclear transformations of heavier elements while making use of similar electrode–solution systems. Undoubtedly, most of these attempts belong in the area of science fiction. To some extent, this casts a shadow on all those who have participated in cold-fusion experiments.

Lines of research exist, moreover, which are related genetically to cold fusion (insofar as they started both prior to and after the Fleischmann–Pons report) but are well above any accusations of science fiction. Apart from the research cited above into processes that are mechanically or sonically induced, we can here add the *warm fusion* occurring during ion implantation (i.e., under appreciably milder conditions than "genuine" thermonuclear fusion).

Electrochemistry was at the source of the cold-fusion "boom," but then at first sight seemed to stand aside. However, as a matter of fact, the central point in the experiments concerning electrolysis at palladium has been a phenomenon which now is investigated more vigorously and persistently: electrochemical intercalation.

Palladium hydride is a unique model system for fundamental studies of electrochemical intercalation. It is precisely in work on cold fusion that a balanced materials science approach based on the concepts of crystal chemistry, crystallography, and solid-state chemistry was developed in order to characterize the intercalation products. Very striking examples were obtained in attempts to understand the nature of the sporadic manifestations of nuclear reactions, true or imaginary. In the case of palladium, the effects of intercalation on the state of grain boundaries, the orientation of the crystals, reversible and irreversible deformations of the lattice, and the like have been demonstrated.

Thus, despite the highly negative assessment of cold fusion as such, the competent science community cannot negate the existence of many positive consequences that have arisen from this epopee.

REFERENCES

Barker, G. C., *J. Electroanal. Chem.*, **21**, 127 (1969).

Bohnke, O., Applications of proton conductors in electrochromic devices, in *Proton Conductors: Solids, Membranes and Gels—Materials and Devices*, P. Colomban, Ed., Cambridge University Press, New York, 1992.

Cheng, Y. F., M. Wilmott, and J. L. Luo, *Bull. Electrochem.*, **16**, 487 (2000).

Fleischman, M., and S. Pons, *J. Electroanal. Chem.*, **261**, 301 (1989).

Mastragostino, M., in *Applications of Electroactive Polymers*, B. Scrosati, Ed., Chapman & Hall, London, pp. 223–249.

Monk, P. M. S., R. J. Mortimer, and D. R. Rosseinsky. *Electrochromism: Fundamentals and Applications*, VCH, Weinheim, Germany, 1995.

Nyquist, H., *Phys. Rev*., **32**, 110 (1928).

Parkhutik, V. P., and S. F. Timashev, *Russ. J. Electrochem.,* **36**, 1221 (2000).

Scrosati, B., Ed., *Applications of Electroactive Polymers*, Chapman & Hall, London, pp. 250–282.

Tyagai, V. A., and N. B. Luk'yanchikova, *Sov. Electrochem.*, **3**, 273 (1967).

Vetter, K. J., *Elektrochemische Kinetik*, Springer-Verlag, Berlin, 1961.

34

Main Concepts of Elementary Reaction Act Theory

ALEXANDER KUZNETSOV

A. N. Frumkin Institute of Physical Chemistry and Electrochemistry, Russian Academy of Sciences, Moscow, Russia

Experimental studies of electrode kinetics resulted in the formulation of the basic empirical relationship, the *Volmer–Butler* equation, (6.10) or (6.13), describing the dependence of the electric current on the electrode potential. This equation involves the potential E, the rate constants, and the concentrations.

Equation (6.13), in fact, reflects the physical nature of the electrode process, consisting of the *anode* (the first term) and *cathode* (the second term) reactions. At *equilibrium potential*, $E = E_0$, the rates of both reactions are equal and the net current is zero, although both anode and cathode currents are nonzero and are equal to the *exchange current* i^0. With the variation of the electrode potential, the rate of one of these reactions increases, whereas that of the other decreases. At sufficiently large electrode polarization (i.e., deviation of the electrode potential from E_0), one of these processes dominates (depending on the sign of $E - E_0$) and the dependence of the net current on the potential is approximately exponential (*Tafel equation*).

Important parameters involved in the Volmer–Butler equation are the transfer coefficients α and β. They are closely related to the *Brönsted relation* [Eq. (14.5)] and can be rationalized in terms of the slopes of the potential energy surfaces [Eq. (14.9)]. Due to the latter, the transfer coefficients α and β are also called *symmetry factors* since they are related to the symmetry of the transitional configuration with respect to the initial and final configurations.

In general, the potential dependence of the current is determined by both the potential dependence of the concentrations of the reacting particles near the electrode surface and the potential dependence of the reaction rate constant itself (i.e., the *probability of the elementary reaction act per unit time*, W).

Fundamentals of Electrochemistry, Second Edition, By V. S. Bagotsky

The concentrations of the reactants and reaction products are determined in general by the solution of the transport diffusion–migration equations. If the ionic distribution is not disturbed by the electrochemical reaction, the problem simplifies and the concentrations can be found through equilibrium statistical mechanics. The main task of the microscopic theory of electrochemical reactions is the description of the mechanism of the *elementary reaction act* and calculation of the corresponding transition probabilities.

As follows from the *Brönsted relationship*, the symmetry factors for the cathode and anode processes are related to each other [see Eq. (6.17*a*)]:

$$\alpha + \beta = 1. \tag{34.1}$$

Equation (6.13) then results in the following relationship between the cathode and anode currents[†]:

$$i_a = i_c \exp\left(\frac{e\eta}{k_B T}\right) \tag{34.2}$$

Thus, it is sufficient to discuss in detail the microscopic mechanism of only one: say, cathode reaction.

The elementary electrochemical reactions differ by the degree of their complexity. The simplest class of reactions is represented by the *outer-sphere electron transfer reactions*. An example of this type is the electron transfer reactions of complex ions. The electron transfer here does not result in a change of the composition of the reactants. Even a change in the intramolecular structure (*inner-sphere reorganization*) may be neglected in many cases. The only result of the electron transfer is then the change in the outer-sphere *solvation* of the reactants. The microscopic mechanism of this type of reaction is very close to that for the outer-sphere electron transfer in the bulk solution. Therefore, the latter is worth considering first.

34.1 OUTER-SPHERE ELECTRON TRANSFER REACTIONS IN THE BULK SOLUTION

Let us consider the electron transfer between two rigid metal ions located some distance x from each other in the bulk of the solution. It is assumed that the inner-sphere reorganization of the donor D and acceptor A does not take place. The experiments show that the rate constants of these reactions differ by many orders of magnitude and the processes have an activated character even for identical ions D and A. The questions to be answered are: Why does the electron exchange between identical ions in the solution require activation? What is the reaction coordinate?

[†] In this chapter we use notations generally accepted in theoretical physics instead of those used in other chapters of this book: the Boltzmann constant k_B instead of the gas constant R, the elementary electrical charge e (in Chapter 1 denoted Q^0) instead of the Faraday constant F (obviously, $k_B T/e \equiv RT/F$). Electrode polarization (overvoltage) ΔE is denoted η. For all reactions we assume that $n = 1$.

How does the transition probability depend on the properties of the solvent and the reactants?

The microscopic mechanism of these reactions is closely related to interaction of the reactants with the medium. When the medium is polar (e.g., water), this interaction is primarily of electrostatic nature. The ionic cores of the donor and acceptor located at fixed spatial points in the medium produce an average equilibrium polarization of the medium, which remains unchanged in the course of the reaction and does not affect the process of electron transfer itself. The presence of the transferable electron in the donor induces additional polarization of the solvent around the donor that is, however, different from polarization in the final state where the electron is located in the acceptor.

It is important to distinguish various components of the solvent polarization which play different roles in the process of electron transfer. Most generally, the *total polarization* of the solvent (i.e., the dipole moment per unit volume) $\mathbf{P}_t(r)$ at a spatial point of the solvent r may consist of four components:

$$\mathbf{P}_t(r) = \mathbf{P}_f(r) + \mathbf{P}_v(r) + \mathbf{P}_{or}(r) + \mathbf{P}_{tr}(r), \tag{34.3}$$

where $\mathbf{P}_f(r)$ is due to the polarization of the electron shells, $\mathbf{P}_v(r)$ is due to intramolecular vibrations, and $\mathbf{P}_{or}(r)$ and $\mathbf{P}_{tr}(r)$ are due to the orientational and translational motions of the solvent molecules as a whole.

One of the most important characteristics of these components is the time of their response to varying electric fields. The electronic polarization has the shortest time $\tau_f \leq 10^{-15}\,\mathrm{s}^{-1}$. All other components are related with the nuclei motion and are characterized by longer times, from $\tau_v \sim 10^{-14}\,\mathrm{s}^{-1}$ to τ_{or}, $\tau_{tr} \geq 10^{-11}\,\mathrm{s}^{-1}$. Another important characteristics is the contribution of the components into $\mathbf{P}_t(r)$ that is characterized by the value of the *dielectric constant* at corresponding frequencies of the external electric field. For most solvents the *high-frequency dielectric constant* $\varepsilon_\infty \sim 2$. The dielectric constants corresponding to lower frequencies vary from one solvent to another in a broad interval. For water as the most important solvent, the high value of *low-frequency dielectric constant* $\varepsilon_0 = 78$ is attributed primarily to a large permanent dipole moment of the water molecule changing its orientation under the influence of the electric field. The values $\varepsilon_* \sim 4$ to 5 in the intermediate frequency range may be related to intramolecular motions.

The electron taking part in the redox reaction under consideration occupies the high-energy molecular orbitals of the reactants, and its motion is much slower than the motion of the electrons in the solvent molecules. Thus, the electric field produced by this moving electron in the medium varies with the characteristic time τ_{ext}, which is much longer than τ_f:

$$\tau_{ext} > \tau_f. \tag{34.4}$$

Therefore, the electronic polarization induced by the transferable electron in the medium can follow any *instant position* of the electron without delay. This means that at any position of the transferable electron between the donor and acceptor, the electronic polarization of the medium induced by this electron is practically the same, and therefore the energy of the interaction of the electron with this polarization is

also the same (flat potential). Such potential does not produce any force and hence does not affect the dynamics of the electron transfer.

This component of solvent polarization is called *fast* or *inertialess polarization*, $\mathbf{P}_{\text{fast}}$, since it follows in an inertialess way the motion of the electron. It involves, however, only part of the electronic polarization:

$$\mathbf{P}_{\text{fast}} = \mathbf{P}'_e. \tag{34.5}$$

The time τ_{ext} is, however, shorter than other characteristic times:

$$\tau_{\text{ext}} < \tau_v, \tau_{\text{or}}, \tau_{\text{tr}}. \tag{34.6}$$

Therefore, the other types of polarization do not change their configuration when the electron changes its spatial position. This polarization is called *slow or inertial polarization*, $\mathbf{P}_{\text{slow}}$ ($= \mathbf{P}$; the subscript "slow" is omitted below). It reacts only to the average position of the transferable electron (in the donor or in the acceptor). The inertial polarization includes all other components and *part of the electronic polarization*:

$$\mathbf{P} = \mathbf{P}_{\text{e}} + \mathbf{P}_v + \mathbf{P}_{\text{or}} + \mathbf{P}_{\text{tr}}. \tag{34.7}$$

Inclusion of part of the electronic polarization into the inertial polarization is due to strong interaction between the nuclei and electrons of the medium. The (slow) change in the nuclei positions inevitably produces polarization of the electron shells of the solvent molecules. Therefore, the latter also contribute to the slow polarization.

When one places an electron into the donor molecule, the equilibrium fast polarization, which is purely electronic forms first. Being independent of the electron position, it is unimportant for the dynamics of electron transfer. Afterward the average slow polarization $\mathbf{P}_{0i}$ arises that corresponds to the initial (i) charge distribution (the electron in the donor). The interaction of the electron with this polarization stabilizes the electron state in the donor (with respect to that in the isolated donor molecule) (i.e., its energy level is lowered) (Fig. 34.1). At the same time, a given configuration of slow, inertial polarization destabilizes the electron state (vacant) in the acceptor (Fig. 34.1). Therefore, even for identical reactants, the electron energy levels in the donor and acceptor are different at the initial equilibrium value of slow polarization.

Electron transfer from D to A at this configuration would require the energy $\delta \mathsf{E} = \varepsilon_{\text{A}}^i - \varepsilon_{\text{D}}^i$ (Fig. 34.1). Thus, in the absence of an external energy source (e.g., light), electron transfer at this configuration is impossible. However, the thermal motion in the medium produces fluctuations of the inertial polarization around its initial equilibrium value, $\mathbf{P}_{0i}$. This in its turn results in the variation of the position of the electron energy levels ε_{D} and ε_{A}. In the process of variation of the inertial polarization, the energy levels ε_{D} and ε_{A} may pass through a configuration where they are at resonance, $\varepsilon_{\text{D}}(\mathbf{P}^*) = \varepsilon_{\text{A}}(\mathbf{P}^*)$. At this configuration electron transfer from D to A may occur with some probability κ_e. The requirement of matching of the electron energy levels is called the *Franck–Condon principle.*

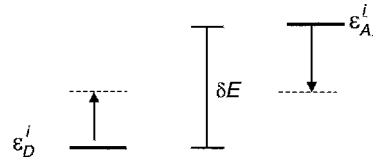

FIGURE 34.1 Electron energy diagram. Electron energies in the donor ε_D^i and acceptor ε_A^i at the initial equilibrium value of the solvent polarization $\mathbf{P}_{0i}$ are different: $\varepsilon_A^i - \varepsilon_D^i = \delta E$. The fluctuations of the solvent polarization bring them to a resonance position where the electron transfer can occur.

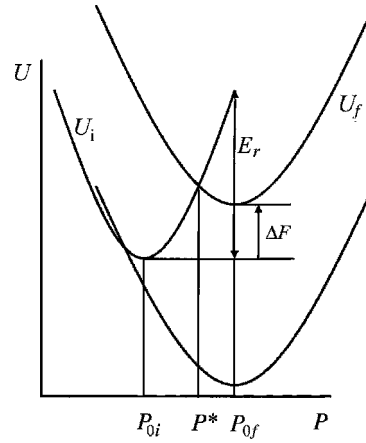

FIGURE 34.2 One-dimensional scheme of the free-energy surfaces of the initial and final states. Medium polarization plays the role of the reactive modes. Matching of the electron energy levels $\varepsilon_D = \varepsilon_A$ corresponds to crossing of the free-energy surfaces $U_i(\mathbf{P}^*) = U_f(\mathbf{P}^*)$. Electron transfer corresponds to the transition from U_i to U_f at the transitional configuration P*. ΔF is the free-energy of the transition. The lower free-energy surface of the final state corresponds to the inverted region.

In the classic, high-temperature limit, the probability of the fluctuation of the inertial polarization in the condensed medium to a value **P** is determined by the value of the *Gibbs free energy* of the system at a given **P** [i.e., $U_i(\mathbf{P})$]. This quantity is the *free-energy surface* of the initial state determining the dynamics of the inertial polarization **P**. It has a minimum value at $\mathbf{P} = \mathbf{P}_{0i}$ and increases when **P** deviates from $\mathbf{P}_{0i}$. A similar quantity for the final state $U_f(\mathbf{P})$ describes the fluctuations of the polarization when the electron is located in A. It has a minimum value at the equilibrium polarization $\mathbf{P} = \mathbf{P}_{0f}$ corresponding to the final charge distribution (the electron in A) (Fig. 34.2).

Matching of the electron energy levels occurs at the crossing of the free-energy surfaces:

$$U_i(\mathbf{P}) = U_f(\mathbf{P}). \tag{34.8}$$

The *transitional configuration* **P*** corresponds to the point of minimum free energy on the crossing above. It is the *saddle point* on crossing free-energy surfaces. The variation of **P** from $\mathbf{P}_{0i}$ brings the system to the transitional configuration **P***. This is the activation process since it is related to an increase of the free energy. If at **P** = **P*** the electron transfer from D to A took place, **P** relaxes to $\mathbf{P}_{0f}$ with the lowering of the free energy, thus completing the reaction. Therefore, the inertial polarization creates the *Franck–Condon barrier* for the transition and plays the role of *reactive modes* (i.e., degrees of freedom, the motion along which brings the system from the initial equilibrium configuration to the final one). The electron transfer corresponds to the transition from the initial free-energy surface, U_i, to the final one, U_f, at their crossing. In fact, there is a large set of reactive modes, since the polarization $\mathbf{P}(\mathbf{r})$ is a *field* rather then a single quantity. The values of the polarization at various spatial points **r** represent such reactive variables. The free-energy surfaces are thus *multidimensional* and the transition from the initial state to the final one can follow various trajectories in this space. However, usually only trajectories close to an optimum one give a considerable contribution to the *transition probability*. Thus, one may discuss the transition in terms of the *reaction coordinate* q_r that corresponds to the optimum trajectory passing through the saddle point.

The *activation free energy* is equal to

$$F_a = U_i(\mathbf{P}^*) - U_i(\mathbf{P}_{0i}). \tag{34.9}$$

It was calculated by Rudolph A. Marcus (1956) in the form

$$F_a = \frac{[E_s(x) + \Delta F(x)]^2}{4E_s(x)}, \tag{34.10}$$

where ΔF is the *free energy of the reaction* for a given interreactant distance x, and E_s(x) is called the *solvent reorganization energy*, that is, the reorganization free energy of the inertial polarization

$$E_s(x) = \frac{c}{8\pi}\int d^3r[\mathbf{D}_i(\mathbf{r}) - \mathbf{D}_f(\mathbf{r})]^2; \qquad c = \frac{1}{\varepsilon_\infty} - \frac{1}{\varepsilon_0}, \tag{34.11}$$

where $\mathbf{D}_i(\mathbf{r})$ and $\mathbf{D}_f(\mathbf{r})$ are the electric inductions created by the transferable electron located in the donor D and acceptor A, respectively. The integral is calculated over the volume of the solvent.

Equation (34.10) describes the dependence of the activation free energy on the free energy of transition ΔF for electron transfer between two discrete energy levels (one in the donor, ε_D, and one in the acceptor, ε_A). The quantity ΔF involves the difference of these electron energies, the solvation free energies of the reaction products, w_p^s, and the initial reactants, w_r^s, and the works required to bring the reaction products, w_p, and the reactants, w_r, from infinity to a given interreactant distance 34.

A simple quadratic form of Eq. (34.10) is due to an identical parabolic form of the free-energy surfaces U_i and U_f. Since the dependence of the activation free energy on ΔF is nonlinear, the *symmetry factor* α may be introduced by a differential relationship,

$$\alpha = \frac{dF_a}{d\Delta F} = \frac{1}{2}\left(1 + \frac{\Delta F}{E_s}\right). \tag{34.12}$$

It depends on ΔF. For free-energy surfaces of identical shape, α characterizes the symmetry of the transitional configuration. For symmetric reactions $\Delta F = 0$ and $\alpha = \frac{1}{2}$. The transitional configuration **P*** is located here in the middle between the initial and final configurations (Fig. 34.2). When $\Delta F \to -E_s$, α tends to zero. The activation free energy also tends to zero according to Eq. (34.10), and one has the *activationless transition*. The transitional configuration coincides here with the initial equilibrium configuration. When $\Delta F = E_s$, the symmetry factor $\alpha = 1$ and the activation free energy is equal to the free energy of the transition ΔF. One then has the *barrierless transition*, and the transitional configuration coincides with the final equilibrium configuration. The region of ΔF values in the neighborhood of $\Delta F = 0$ is called the *normal region*.

An equation of the type Eq. (34.9) (with q_k instead of **P**) is valid for any shape of the free-energy surfaces as functions of the coordinates of any reactive modes q_k provided that the motion along q_k is classical. If the motion along some coordinates Q is quantum mechanical, these modes should be excluded from the free-energy surfaces. The transition along these modes has a tunnel character.

34.2 ADIABATIC AND NONADIABATIC REACTIONS

The matching of the electron energy levels is the necessary condition for electron transfer. However, in general, the passage through the transitional configuration does not necessarily result in electron transfer. The probability of electron transfer during the passage through the transitional configuration is determined by its quantum-mechanical behavior. Thus, despite the classical character of motion along the solvent polarization modes, the problem as a whole is quantum mechanical in nature. Fully quantum-mechanical calculations were first performed by Rezo R. Dogonadze and Venjamin G. Levich (1959) for *nonadiabatic reactions* (see below). When the motion along the reactive modes is purely classical, a combined semiclassical approach may be used based on *Landau–Zener theory*. It shows that the probability P_{LZ} of the change in electron state from that in the donor to that in the acceptor during the passage of the transitional configuration depends on the relationship between the characteristic time τ_e required for the resonance electron exchange between the donor and acceptor and the time τ_n during which nearly resonance configuration exists. If

$$\tau_e \ll \tau_n, \tag{34.13}$$

the electron has time for the exchange between D and A, and the *Landau–Zener probability* P_{LZ} is equal to unity. This is the case for *adiabatic reaction*. In the opposite limit,

$$\tau_e \gg \tau_n, \tag{34.14}$$

the time of the existence of the transitional configuration is small and the probability for a change of electron state is also small. It may be estimated as the ratio

$$P_{LZ} = \frac{\tau_n}{\tau_e} \ll 1 \tag{34.15}$$

and the reaction is called *nonadiabatic* (or diabatic). The time τ_e is equal to

$$\tau_e = \frac{\hbar}{V}, \tag{34.16}$$

where $2\pi\hbar = h$ is the Planck constant and V_{if} is the *electron resonance integral*,

$$V_{if} = \int d^3x \, \varphi_D V \varphi_A. \tag{34.17}$$

It is determined by the overlap of the electron wave functions of the donor, φ_{D}, and acceptor, φ_{A}, and by the interaction V of the electron with the acceptor.

The time during which nearly resonance configuration (within the energy interval on the order of V_{if}) exists is

$$\tau_n \approx \frac{V_{if}}{\hbar v |\partial U_i/\partial q_r - \partial U_f/\partial q_r|} = \frac{V_{if}}{\hbar v |U_i' - U_f'|}, \tag{34.18}$$

where v is the thermal velocity of the motion along the reaction coordinate q_r and $U_i' - U_f'$ is the difference in the slopes of the free-energy surface profiles along the reaction coordinate q_r.

Thus, the *Landau–Zener parameter* $2\pi\gamma_{\mathrm{LZ}}$ determining adiabatic or nonadiabatic character of transitions is [see Eqs. (34.15), (34.16), and (34.18)]

$$2\pi\gamma_{\mathrm{LZ}} = 2\pi \frac{V_{if}^2}{\hbar v |U_i' - U_f'|}. \tag{34.19}$$

At a small value of this parameter, the system can perform multiple passages through the transitional configuration before the electron transfer occurs. The exact expression for the transition probability taking into account these multiple passages has the form

$$P_\Sigma = \frac{1 - e^{-2\pi\gamma_{\mathrm{LZ}}}}{} \tag{34.20}$$

It gives 1 and $4\pi\gamma_{LZ}$ in the limit of large and small values of the Landau–Zener parameter, respectively.

The expression for the transition probability per unit time W taking into account the process of activation has the form

$$W = \frac{\omega}{2\pi}\kappa_e e^{-F_a/k_B T}, \tag{34.21}$$

where ω is the *effective frequency* of the polarization fluctuations in the initial potential well U_i and κ_e is the *electron transmission coefficient*, which for adiabatic reactions is equal to 1 and for nonadiabatic reactions is

$$\kappa_e = \frac{2\pi}{\omega}\frac{1}{\hbar}V_{if}^2\sqrt{\frac{\pi}{k_B T E_s}}. \tag{34.22}$$

The change in the inner-sphere structure of the reacting partners usually leads to a decrease in the transition probability. If the intramolecular degrees of freedom behave classically, their reorganization results in an increase in the activation barrier. In the simplest case where the intramolecular vibrations are described as harmonic oscillators with unchanged frequencies, this leads to an increase in the reorganization energy:

$$E_r^t = E_s + E_r^{\text{inner}}. \tag{34.23}$$

In the case where they represent quantum vibrational modes, this leads to the appearance of a small tunnel factor in the transmission coefficient κ_e.

An interesting prediction of the theory is the existence of the *inverted region* for nonadiabatic reactions. It is characterized by abnormal behavior of the transition probability W and is located at the values of the free energy of the transition $-\Delta F > E_r$ (Fig. 34.2). In the normal region where $|\Delta F| < E_r$, the transition probability W increases with an increase in the quantity $-\Delta F$ due to a decrease of the activation barrier F_a [see Eq. (34.10)]. As shown in Fig. 34.2, in the inverted region, F_a increases with an increase in $-\Delta F$, resulting in a decrease of W. The symmetry factor α is negative in the inverted region [see Eq. (34.12)]. Such behavior was observed for a series of electron transfer reactions in the bulk solutions. The general physical mechanism described in Sections 34.2 and 34.3 is equally applicable to electrochemical charge-transfer reactions.

34.3 ELECTROCHEMICAL ELECTRON TRANSFER

Let us consider a cathode electron transfer process at metal electrode. The role of the electron donor is played here by the metal electrode. The specific feature of this donor consists of the fact that its electron energy spectrum is practically continuous

with the *Fermi level* ε_F lying in the conduction band. The electrons occupy practically all energy levels almost up to the Fermi level ε_F, whereas the levels above ε_F are practically empty. The probability of the occupation of various energy levels is described by the *Fermi distribution function*,

$$f(\varepsilon) = \left[1 + \exp\left(\frac{\varepsilon - \varepsilon_F}{k_B T}\right)\right]^{-1}. \tag{34.24}$$

It varies rather sharply with the electron energy, whereas the *density of electron states* $\rho(\varepsilon)$ is almost constant in the energy interval of interest.

In view of very small spacing of the energy levels, one may not restrict oneself by consideration of the electron transfer from only one electron state in the metal, and all energy spectra should be taken into account. However, the entire process is composed of transitions with the participation of individual energy levels ε. Therefore, the electron transfer from an energy level ε to the reactant located a distance x from the electrode surface in the solution is considered first (Fig. 34.3).

The physical picture of the transition is the same as for electron transfer in the bulk solution. At the initial equilibrium polarization $\mathbf{P}_{0i}$ the positions of the energy levels ε and ε_A do not coincide and fluctuation of the polarization is required to bring them into the resonance position where electron transfer from the electrode to the acceptor is possible. The following points should be taken into account, which are specific for electrode processes:

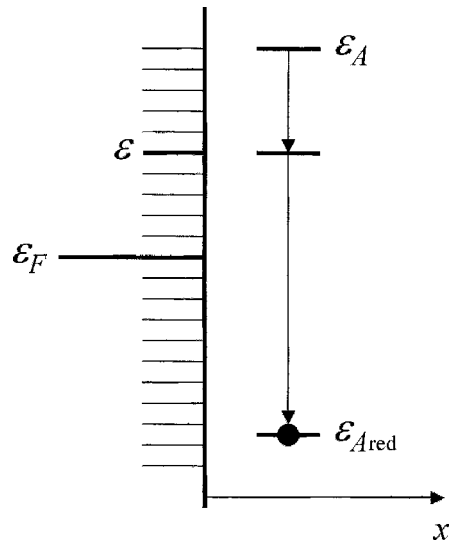

FIGURE 34.3 Electron energy diagram. A fluctuation of the solvent polarization brings the energy levels ε_A and ε to the resonance position. After the electron transfer, the occupied energy level ε_A relaxes to its equilibrium position for the reduced form ε_{Ared}.

1. The position of energy level ε_A is subjected to fluctuations, whereas that of level ε is independent of solvent polarization.
2. The electron is delocalized in the metal. Therefore, the resonance integral $V_{if}(\varepsilon)$ for a given electron state ε is always small, due to the small overlap of the electron wavefunctions of the metal and the ion, and the transitions from the individual energy levels are nonadiabatic.
3. The occupation of energy level ε depends on its position with respect to the Fermi level and should be taken into account in calculation of the transition probability. The number of electrons within a given energy interval $d\varepsilon$ is equal to $\rho(\varepsilon)f(\varepsilon)\,d\varepsilon$.
4. The reorganization energy E_s of the slow polarization is, roughly speaking, almost one-half of that for the bulk solution.
5. The electron energy in the metal and the acceptor depends on the distribution of the electric potential at the interface.

The expression for the transition probability per unit time W (with due account of the points above) is formally the same as in Eqs. (34.21), (34.22), and (34.10). The free energy of the transition ΔF is equal to

$$\Delta F(\varepsilon, E) = \varepsilon_A - e\psi_1 + w_p^s - \varepsilon + eE - w_r^s, \tag{34.25}$$

where ψ_1 is the potential at the site of the reactant localization and all quantities except ε and E depend on the distance x, and w_p^s and w_r^s are the solvation free energies of the ion A in the reduced and oxidized forms.

Since the electron transitions, in principle, are possible from any energy level in the metal, one has to perform the summation of small probabilities over all energy levels (i.e., to integrate over ε). This results in the following general expression for the cathode current i_c:

$$i_c = e\int dx\, c_{\mathrm{ox}}(x)\int d\varepsilon\, \rho(\varepsilon) f(\varepsilon)\frac{\omega}{2\pi}\kappa_e e^{-F_a(\varepsilon,E)/k_\mathrm{B}T}, \tag{34.26}$$

where integration over x means that the electron transfer may take place at different distances between A and the electrode surface, although with different probabilities. The electron transmission coefficient κ_e decreases exponentially with the increase in x due to decreasing overlap of the electron wavefunctions. Therefore, in fact, only a small interval Δx of distances near the electrode surface gives a considerable contribution to the integral over x, resulting in an approximate formula

$$i_c \approx e c_{\mathrm{ox}}\Delta x\,\rho\frac{\omega}{2\pi}\kappa_e\int d\varepsilon f(\varepsilon) e^{-(E_s+\Delta F)^2/4E_s k_\mathrm{B}T}, \tag{34.27}$$

where a weak dependence of ρ and κ_e on ε was neglected.

The properties of the electrode are involved in ρ and κ_e in Eq. (34.27). The current is thus explicitly proportional to the density of electron states in the metal and the overlap of the electron wavefunctions involved in κ_e.

The surface concentration $c_{\mathrm{Ox}}\Delta x$ in general depends on the electrode potential, and this can affect significantly the form of the $i(E)$ curves. In some situations this dependence can be eliminated and the potential dependence of the probability of the elementary reaction act can be studied (called *corrected Tafel plots*). This is, for example, in the presence of excess concentration of supporting electrolyte when the ψ_1 potential is very small and the surface concentration is practically independent of E. However, the current is then rather high and the measurements in a broad potential range are impossible due to diffusion limitations. One of the possibilities to overcome this difficulty consists of the attachment of the reactants to a spacer film adsorbed at the electrode surface. The measurements in a broad potential range give dependences of the type shown in Fig. 34.4.

The current increases first exponentially and then levels off. The same dependence follows from Eq. (34.27). At not large deviations of the electrode potential from the equilibrium potential (i.e., at not large overpotentials, $\eta_c = E_0 - E$), the approximate form of Eq. (34.27) is as follows:

$$i_c \approx i_0 \exp\left[\frac{e\eta_c}{2k_{\mathrm{B}}T} - \frac{(e\eta_c)^2}{4E_s k_{\mathrm{B}}T}\right]. \tag{34.28}$$

An important exact result follows from Eq. (34.27) for the *observable symmetry factor* α_{obs}, defined as

$$\alpha_{\mathrm{obs}} = -\frac{d\ln i_c}{d(e\eta/k_{\mathrm{B}}T)}. \tag{34.29}$$

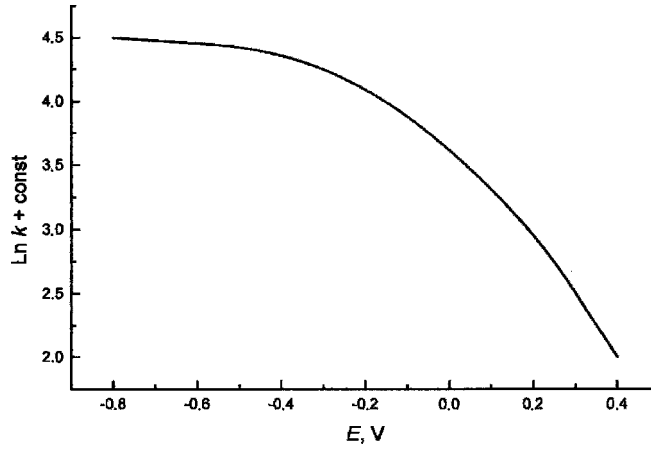

FIGURE 34.4 Dependence of electrochemical rate constant on the electrode potential for outer-sphere electron transfer. An exponential increase in the normal region changes for the plateau in the activationless region.

The observable symmetry factor is equal to the average value of the *partial symmetry factor* $\alpha(\varepsilon)$, defined by Eq. (34.12) for the transition from the energy level ε:

$$\alpha_{obs} = \langle \alpha(\varepsilon) \rangle. \tag{34.30}$$

The weight of each $\alpha(\varepsilon)$ in the average value is proportional to the relative contribution of the partial cathode current for a given ε, $i_c(\varepsilon)$, to the total cathode current i_c. Using the fact that the free energy of the transition $\Delta F(\varepsilon,E)$ depends only on the difference $\varepsilon - eE$, one can rewrite Eq. (34.30) in an equivalent form:

$$\alpha_{obs} = \langle \alpha(\varepsilon) \rangle = \langle 1 - f(\varepsilon) \rangle. \tag{34.31}$$

Usually, a narrow energy interval near some energy level ε^* gives the major contribution to the average in Eq. (34.31). Therefore, it may finally be written as

$$\alpha_{obs} \approx 1 - f(\varepsilon^*). \tag{34.32}$$

Equation (34.32) is remarkable in the relation that it shows that (1) the observable symmetry factor is determined by occupation of the electron energy level in the metal, giving the major contribution to the current, and (2) that the observable symmetry factor does not leave the interval of values between 0 and 1. The latter means that one cannot observe the inverted region in a traditional electrochemical experiment. Equation (34.32) shows that in the *normal region* (where α_{obs} is close to $\frac{1}{2}$) the energy levels near the Fermi level provide the main contribution to the current, whereas in the activationless ($\alpha_{obs} \approx 0$) and barrierless ($\alpha_{obs} \approx 1$) regions, the energy levels below and above the Fermi level, respectively, play the major role.

The physical mechanism described allows one to answer two basic questions: (1) Why does the electrochemical process usually require activation? and (2) Why is there no inverted region in the current–overpotential dependence?

The first question is related to the fact that in view of the continuous nature of the metal electron energy spectrum, the electron energy level in the acceptor ε_A always matches some energy level ε in the metal as well as at the initial equilibrium value of the slow polarization $\mathbf{P}_{0i}$. The answer to this question lies in the fact that the energy level ε_A is usually located far above the Fermi level at $\mathbf{P} = \mathbf{P}_{0i}$ and matches the metal energy levels, which are practically empty. Activation is therefore required to bring this level to the region around the Fermi level where the transitions are much more probable. The absence of the inverted region can be understood from Fig. 34.5, where the free-energy surfaces corresponding to various electron states are shown.

When the overpotential is small, the free-energy surface $U_{i\varepsilon_F}$ corresponding to the Fermi energy ε_F gives the major contribution to the total transition probability. With an increase in the overpotential, the free-energy surface of the final state U_f shifts down with respect to $U_{i\varepsilon_F}$, resulting in a decrease in the activation free energy until zero (curve $U^f_{a.l.}$ in Fig. 34.5). Further increase in the overpotential brings this pair of free-energy surfaces, $U_{i\varepsilon_F}$ and U_f, into a position corresponding to the inverted

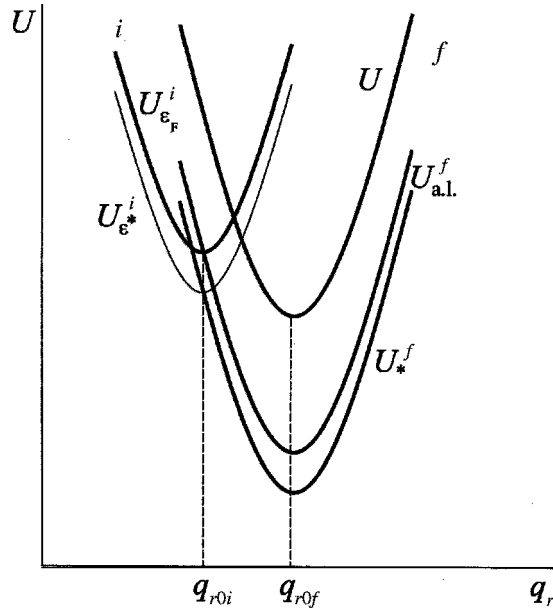

FIGURE 34.5 Scheme explaining the absence of the inverted region in the electrochemical processes. The position of the free-energy surfaces $U^i_{\varepsilon_F}$ and U^f_* corresponds to the inverted region. However, the major contribution to the current is due to the transition from $U^i_{\varepsilon_*}$ to U^f_*, which are in activationless configuration.

region (curve U^f_* in Fig. 34.5). However, now the probability of transition from ε_F is smaller than that for an energy $\varepsilon_* < \varepsilon_F$, which is in an activationless position (curve $U^i_{\varepsilon_*}$ in Fig. 34.5). Thus further increase in the overpotential brings into play the lower electron energy levels of the metal, retaining the activationless character of the transition.

34.4 ELECTROCHEMICAL ADIABATICITY PARAMETER. MEDIUM DYNAMICS VS. STATIC DISTRIBUTION

It was noted in Section 34.2 that the Landau–Zener probability of electron transition at a matching of ε_A and a given energy level ε in the metal is small. However, in the process of polarization fluctuations (i.e., in the process of motion along the reaction coordinate q_r), the energy level ε_A may match sequentially many energy levels in the metal. This increases overall Landau–Zener probability (i.e., the electron transmission coefficient), but at the expense of an increase in the activation free energy. In the normal overpotential region, an energy interval on the order of $\Delta\varepsilon \sim k_B T$ near the Fermi level gives the major contribution. Thus, the *effective Landau–Zener parameter for electrochemical reactions* is $2\pi\gamma_{LZ}\rho k_B T$ since the

quantity $\rho k_B T$ represents the number of electron states in a given energy interval $k_B T$. If

$$2\pi\gamma_{LZ}\rho k_B T \ll 1, \tag{34.33}$$

the reaction as a whole is nonadiabatic. This means that when the system passes a set of transitional configurations in the neighborhood of the Fermi level, the electron transition is unlikely and in most cases the system returns to the initial equilibrium configuration along the initial free-energy surface $U_{i\varepsilon_F}$. Thus, it approaches many times the transitional configuration before the electron transition really occurs.

Therefore, one may then speak about an average (in time) *statistical distribution* of the electron energies in the acceptor $\Phi_i(\varepsilon_A)$ due to the polarization fluctuations. Each position of ε_A corresponds to some value(s) of the slow polarization **P**. This static picture is based on one of the formulations involved in the Franck–Condon principle and stating that the electron transfer occurs at constant (in time) values of the nuclei coordinates. The idea on the static distribution of the electron energy levels was developed for electrochemical reactions by Heinz Gerischer (1960) and is sometimes used for a description of the electron transfer processes. It gives correct values of the activation free energy for nonadiabatic reactions, but in a more general aspect it is misleading since it ignores the dynamics of the medium. The latter is of crucial importance for the electron transfer in condensed media: (1) The motion of molecular environment brings the system to the transitional configuration; (2) the dynamics of the medium determines the time of existence of the transitional configuration and hence the electron transmission coefficient; and (3) the motion of the medium molecules toward the final equilibrium configuration destroys the resonance of the energy levels and makes the transition irreversible in quantum-mechanical meaning.

The first two points were discussed in detail in Section 34.1. The third one is also of great importance. This can be seen from the following discussion. Let us consider a certain static polarization value at which the level ε_A is located just above the Fermi level. Due to the interaction with the metal and the acceptor, the electron will oscillate quantum mechanically between them and one may speak of an average occupation $<n_A>$ of the acceptor electron state in the long-time limit. However, the existence of some electron density in the acceptor does not allow one to state that the reaction took place. If one takes the acceptor away from the electrode surface to the bulk solution at this fixed polarization value, the electron occupation of the acceptor orbital $<n_A> \to 0$ (i.e., no reaction took place).

Only if one takes into account the solvent dynamics, the situation changes. The electron transfer from the metal to the acceptor results in the transition from the initial free energy surface to the final surface and subsequent relaxation of the solvent polarization to the final equilibrium value P_{0f}. This brings the energy level ε_A (now occupied) to its equilibrium position ε_{Ared} far below the Fermi level, where it remains occupied independent of the position of the acceptor with respect to the electrode surface.

34.5 ADIABATIC ELECTROCHEMICAL ELECTRON TRANSFER REACTIONS

The smallness of the electron transmission coefficient for the transition from individual energy levels does not mean that all electrochemical electron transfer reactions should be nonadiabatic. If the inequality opposite to Eq. (34.33) is fulfilled,

$$2\pi\gamma_{LZ}\rho k_B T \gg 1, \tag{34.34}$$

the reaction is adiabatic.

The physical picture of the transition is different here from that for nonadiabatic reaction. Equation (34.34) shows that the probability of electron transfer becomes equal to 1 when the acceptor energy level ε_A passes a small energy interval $\Delta\varepsilon \sim 1/(2\pi\gamma_{LZ}\rho)$ ($\ll k_B T$) near the Fermi level. However, unlike the nonadiabatic case, backward transfer of the electron from the acceptor to the metal occurs with probability 1 after further passage of the energy interval $\sim\Delta\varepsilon$. Therefore, multiple electron transitions occur in the process of motion along the reaction coordinate in the neighborhood of the Fermi level (Fig. 34.6). When the energy level ε_A approaches the final equilibrium position, the backward transitions become unlikely, since all the states in the metal are occupied. Thus, the electron remains in the acceptor.

In terms of free-energy surfaces, multiple electron transitions correspond to multiple transitions between various free-energy surfaces of the initial and final states, and the system in fact moves along some effective potential profile. Multiple electron transitions allow one to speak about an average occupation $<n_A(q_r)>$ of the

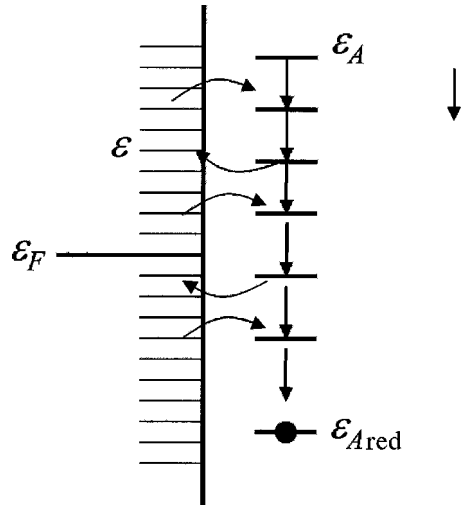

FIGURE 34.6 Scheme of multiple electron transitions in adiabatic electrochemical reactions.

acceptor energy level ε_A which depends on the reaction coordinate q_r. This quantity is determined by the ratio of the probabilities of forward and backward electron transitions and varies smoothly from zero at $q_r = q_{r0i}$ to 1 at $q_r = q_{r0f}$. The interaction of this electron density with solvent polarization creates an effective potential profile along the reaction coordinate $U(q_r)$ with two minima (at the initial and final equilibrium configurations q_{r0i} and q_{r0f}) and a maximum at the transitional configuration (q_r^*). This picture allows one to use theoretical approaches and computer simulations for the transitions in one-dimensional double-well potential. The idea on the use of the average partial occupation of the donor and acceptor for the energy levels at the transitional configuration for the calculation of the activation free energy was first formulated by Noel S. Hush (1958).

The height of the potential barrier is lower than that for nonadiabatic reactions and depends on the interaction between the acceptor and the metal. However, at not too large values of the effective electrochemical Landau–Zener parameter $2\pi\gamma_{LZ}\rho k_B T$, the difference in the activation barriers is insignificant. Taking into account the fact that the effective electron transmission coefficient is 1 here, one concludes that the rate of the adiabatic outer-sphere electron transfer reaction is practically independent of the electronic properties of the metal electrode.

Approximate calculation of the integral over ε in Eq. (34.27) shows that the *effective electron transmission coefficient* for nonadiabatic reactions is equal to

$$\kappa_{\text{eff}}^{\text{nonad}} = \pi\kappa_e\rho k_B T, \tag{34.35}$$

whereas at large $2\pi\gamma_{LZ}\rho k_B T$ values, it is 1 (adiabatic reactions). The analytical calculations at the intermediate values of $2\pi\gamma_{LZ}\rho k_B T$ are difficult. However, computer simulations allow one to obtain the curve shown in Fig. 34.7, which may serve as an interpolation between the nonadiabatic and adiabatic limits.

34.6 ELECTRIC DOUBLE-LAYER EFFECTS ON THE ELEMENTARY ACT OF ELECTRON TRANSFER

In the crudest approximation, the effect of the electrical double layer on electron transfer is taken into account by introduction of the electrostatic energy $-e\psi_1$ of the electron in the acceptor into the free energy of the transition ΔF [Frumkin correction; see Eq. (34.25)], so that corrected Tafel plots are obtained in the coordinates $\ln i_c$ vs. $e(E - \psi_1)$. Here ψ_1 is the average electric potential at the site of location of the acceptor ion. It depends on the concentration of supporting electrolyte and is small at large concentrations. Such approach implies in fact that the reacting ion represents a probe ion (i.e., it does not disturb the electric field distribution).

A more sophisticated approach takes into account the fact that the presence of the reacting ion at a given point in the solution distorts the distribution of other ions of the electrolyte and thereby distorts the potential distribution. This phenomenon is called the effect of the *micropotential*. The average ψ_1 potential is then replaced by another average potential, ψ_{micro}, calculated in the presence of the reacting ion at a given point.

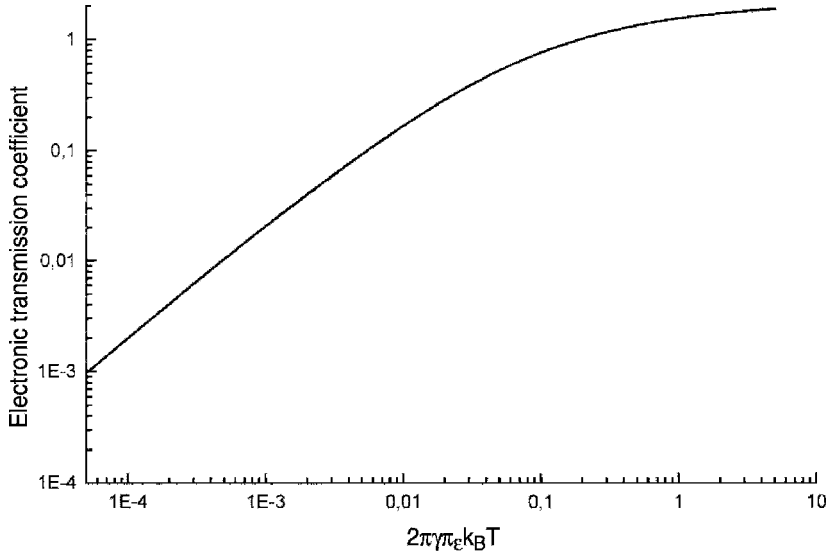

FIGURE 34.7 Dependence of the effective electron transmission coefficient on the electrochemical Landau–Zener parameter.

A more rigorous approach should take into account the fact that the micropotential in the initial (oxidized acceptor ion) and final (reduced acceptor) states are different, due to different forms of the ionic atmosphere around the reacting ion. Thus, a *reorganization of the ionic atmosphere* occurs in the course of the electron transfer. Therefore, the degrees of freedom describing the ionic atmosphere must be considered as reactive modes along with the degrees of freedom describing the solvent polarization.

Hence, the activation free energy should involve the difference in the free energies at the transitional configuration and initial equilibrium configuration, $F^* - F^i$, which is due to interaction of the charges with the ionic atmosphere. The quantity F^i is calculated as the equilibrium free energy F_z for the charge ze interacting with the ions of the electrolyte and the external field created by the metal electrode where z is the valence number of the acceptor in the oxidized form. The quantity F^* may also be calculated as the equilibrium free energy $F_{z-\alpha}$ for the ion with an effective charge $e(z-\alpha)$, where α is the symmetry factor. The difference $F_{z-\alpha} - F_z$ depends on the electrode potential. In general, this dependence may be rather complicated. At small ψ_1 values, it is described approximately as

$$F_{z-\alpha} - F_z \approx -\alpha e \psi_1 + F^0_{z-\alpha} - F^0_z, \tag{34.36}$$

where $F^0_{z-\alpha} - F^0_z$ is the difference in the free energies of the ionic atmosphere at zero electrode potential. This approximation, in fact, reduces the potential dependence to

the Frumkin correction. The final expression for the activation free energy can again be transformed to a quadratic form similar to Eq. (34.10), with $E_s + E_r^{\text{i.at.}}$ for E_s, where $E_r^{\text{i.at.}}$ is the reorganization energy of the ionic atmosphere.

34.7 BOND-BREAKING ELECTRON TRANSFER

The electron transfer from the electrode to a molecule in the solution can produce a considerable reorganization of the intramolecular structure, up to breaking of a chemical bond. The reactions where the electron transfer and the breaking of the chemical bond occur in one elementary act without the formation of metastable intermediates are called *dissociative electron transfer*. The physical mechanism of these reactions is basically similar to that for simple outer-sphere electron transfer reactions. The main difference consists of two points: (1) the coordinate r along the chemical bond to be broken should be considered as the reactive mode, along with the slow polarization of the solvent; and (2) the harmonic approximation is insufficient for a description of the motion along the coordinate r. Since the breaking of the chemical bond is related with large-amplitude vibrations, the shape of the potential energy for the initial molecule, $U^{\text{ox}}(r)$, can deviate considerably from a parabolic form. As for the potential energy for the reduced form, $U^{\text{red}}(r)$, it has no minimum at all and represents a decreasing potential reflecting a decay character of the final state (Fig. 34.8).

The free-energy surfaces of the initial and final states, $U_i(\mathbf{P},r)$ and $U_f(\mathbf{P},r)$, then involve two contributions: the parabolic free energy as a function of the slow polarization, $U_i^s(\mathbf{P})$ and $U_f^s(\mathbf{P})$, and nonparabolic molecular potential $U^{\text{ox}}(r)$ and $U^{\text{red}}(r)$:

$$\begin{aligned} U_i(\mathbf{P},r) &= U_i^s(\mathbf{P}) + U^{\text{ox}}(r), \\ U_f(\mathbf{P},r) &= U_f^s(\mathbf{P}) + U^{\text{red}}(r). \end{aligned} \tag{34.37}$$

The activation free energy may therefore be represented as a sum of two contributions:

$$F_a(\Delta F) = F_s(\Delta F_s) + F_m(\Delta F_m), \tag{34.38}$$

where $F_s(\Delta F_s)$ and $F_m(\Delta F_m)$ are the activation barriers along the solvent polarization modes and the molecular degree of freedom, respectively. Importantly, the values of $F_s(\Delta F_s)$ and $F_m(\Delta F_m)$ depend on the partial free energies of transitions, ΔF_s and ΔF_m, along respective degrees of freedom (Fig. 34.8).

The optimum values of ΔF_s and ΔF_m must be chosen such as to minimize the total activation free energy in Eq. (34.38) with the constraint

$$\Delta F_s + \Delta F_m = \Delta F. \tag{34.39}$$

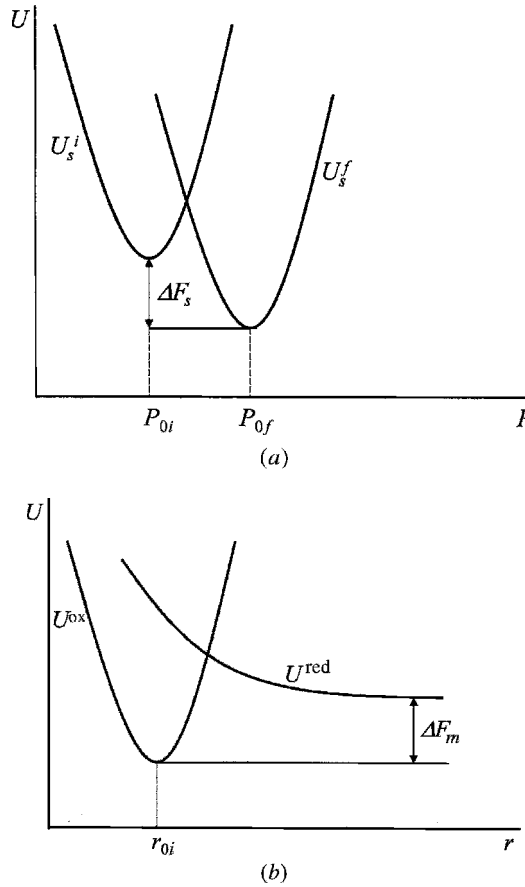

FIGURE 34.8 Free-energy surfaces for the dissociative electron transfer reaction: (*a*) for the solvent polarization; (*b*) along the coordinate *r* of the molecular chemical bond. U^{ox} corresponds to stable molecule in oxidized form. U^{red} is the decay potential for the reduced form. ΔF_s and ΔF_m are the partial free energies of the transition determining mutual arrangement of the two sets of the free-energy surfaces.

In the model where the potentials $U^{ox}(r)/U^{red}(r)$ are described by Morse/exponential functions, this general procedure results in a simple quadratic form for the activation free energy with the total reorganization energy

$$E_r^t = E_s + D, \tag{34.40}$$

where D is the dissociation energy of the chemical bond.

In general, the molecular parameters involved in the potentials $U^{ox}(r)$ and $U^{red}(r)$ are different, and the dependence of F_a on ΔF has no such simple form. However, simple algorithms exist which allow numerical calculations of this dependence for

arbitrary forms of molecular potentials. Similar to ordinary outer-sphere electron transfer, the free energy of the transition ΔF depends on the electrode potential and electron energy ε [see Eq. (34.25)].

34.8 REORGANIZATION ENERGY OF THE MEDIUM AND THE FREQUENCY FACTOR

One of the important physical parameters involved in the final equations for the electric current is the reorganization energy of the medium [see Eq. (34.10)]. In general, it consists of the outer-sphere reorganization energy of the solvent polarization E_s, the intramolecular reorganization energy of the reactants E_r^{inner}, and the reorganization energy of the ionic atmosphere $E_r^{\text{i.at.}}$. For many reactions, E_s gives the main contribution to the total reorganization energy.

The reorganization energy of the slow polarization for the reactions at metal electrodes can be calculated with the use of Eqs. (34.11). For a spherical model of the reacting ion, it is equal approximately to

$$E_s = \frac{ce^2}{2}\left(\frac{1}{a} - \frac{1}{2x}\right), \tag{34.41}$$

where a is the ionic radius and x is the distance between the reactant and electrode surface. This result is obtained with neglect of an inhomogeneity introduced by the reacting ion. More generally, E_s may be calculated as the difference of two solvation free energies:

$$E_s = F_e^0 - F_e^\infty, \tag{34.42}$$

where F_e^0 is the outer-sphere electrostatic solvation free energy of the single-charged reacting ion in the medium characterized by static (low-frequency) dielectric constant ε_0, and F_e^∞ is the same for the medium characterized by high-frequency dielectric constant ε_∞. This procedure is also valid for the inhomogeneous media (e.g., for electron transfer at the interface of two immiscible liquids or at the semiconductor–electrolyte interface).

An important physical quantity determining the transition probability for the adiabatic reactions is the preexponential *frequency* [see eq. (34.21) with κ_e replaced by 1]. This quantity can be calculated using the relationship

$$\frac{\hbar\omega}{k_B T} = \frac{Z_\#}{Z_i}, \tag{34.43}$$

where $Z_\#$ and Z_i are the *vibrational partition functions* of the transition state and the initial state. It is of importance that the transition state represents here the set of configurations in the neighborhood of the saddle point on the lower adiabatic free-energy surface along all vibrational degrees of freedom except one coordinate

(reaction coordinate). The potential profile along the latter is characterized by an imaginary frequency describing the potential barrier, whereas the free energy along all other coordinates represents a multidimensional potential well.

For simple outer-sphere electron transfer reactions, the effective frequency ω is determined by the properties of the slow polarization of the medium. For a liquid like water, where the temporal relaxation of the slow polarization as a response to the external field is single exponential, the effective frequency is equal to

$$\omega \approx \frac{1}{\tau_L}\sqrt{\frac{E_s}{V_{if}}}, \tag{34.44}$$

where τ_L is the longitudinal relaxation time for the solvent polarization. Since the relaxation time is related in general with the viscosity of the liquid, the dependence of the preexponential factor in the reaction-rate constant on the viscosity may serve as an indication of the adiabatic character of the transition. For reactions accompanied by a change in the intramolecular structure, the effective frequency involves the contribution of the intramolecular frequencies. The preexponential factor for nonadiabatic reactions is independent of the effective frequency since the electron transmission coefficient is inversely proportional to this frequency.

34.9 ELECTROCHEMICAL PROTON TRANSFER

Hydrogen evolution at metal electrodes is one of the most important electrochemical processes. The mechanisms of the overall reaction depend on the nature of the electrode and solution. However, all of them involve the transfer of proton from a donor molecule in the solution to the adsorbed state on the electrode surface as the first step. The mechanism of the elementary act of proton transfer from the hydroxonium ion to the adsorbed state on the metal surface is discussed in this section.

An important observation on the proton behavior in chemical compounds is that it is a quantum particle. In particular, the frequency of its valence vibrations in molecules such as hydroxonium ion is on the order of $\Omega \sim 10^{14}\ \mathrm{s}^{-1}$ [i.e., the energy of corresponding vibrational quantum $\hbar\Omega\,(\approx 0.3\,\mathrm{eV})$ is much higher than the thermal energy $k_\mathrm{B}T\,(\sim 0.025\,\mathrm{eV})$].

The second important point is common for all charge-transfer reactions. The proton is a charged particle, and as such, interacts strongly with solvent polarization. The first model taking into account both these points was proposed by Dogonadze et al. (1967).

At least three components of the system change their state in the case of proton transfer reaction: (1) electrons of the water molecule and the electrode providing the chemical bonding of the proton with a water molecule and the metal surface, (2) the proton itself, and (3) medium polarization. The characteristic times τ_e, τ_p, and τ_s for

all three components are quite different. The electrons are the fastest moving, whereas the proton moves faster than solvent polarization but slower than the electrons:

$$\tau_e \gg \tau_p \gg \tau_s. \tag{34.45}$$

Therefore, electrons adjust their state to any instant position of the proton and solvent polarization in both the initial (hydroxonium ion) and final (adsorbed hydrogen atom) states. The proton in the hydroxonium ion "sees" an average electron cloud but "feels" any instant configuration of solvent polarization.

In view of a large vibrational energy quantum, the proton in the hydroxonium ion and the adsorbed hydrogen atom occupies mainly its ground initial χ_{0i} and final χ_{0f} vibrational states. The proton energy E_{pi}^0 depends on the solvent polarization $\mathbf{P}$, and at some value $\mathbf{P}^*$ matches the energy E_{pf}^0 of the final state. At this configuration, tunnel transition of the proton from the hydroxonium ion to the metal surface is possible with some probability P_{LZ}, similar to that for electron transfer [see Eq. (34.20)]. However, the Landau–Zener parameter now (in the case of totally nonadiabatic reactions) involves the electron–proton resonance integral

$$V_{ep} \approx V_{if} \int dr_p \chi_{pi}^0(r_p) \chi_{pf}^0(r_p) \tag{34.46}$$

rather than the purely electron resonance integral V_{if}. Here χ_{pi}^0 and χ_{pf}^0 are the proton wave functions of the ground initial and final states.

Thus, overcoming the activation barrier is performed here by fluctuation of the solvent polarization to the transitional configuration $\mathbf{P}^*$, whereas electron–proton transmission coefficient is determined by the overlap of the electron–proton wavefunctions of the initial and final states.

As noted in Section 34.2, the proton coordinate (such as that of a quantum particle) should be eliminated from the free-energy surfaces used for calculation of the activation free energy. The characteristics of the proton are reflected in the energies at the points of minimum of these free-energy surfaces, which involve the energies of the initial, E_{pi}^0, and final, E_{pf}^0, ground proton vibrational states, respectively. This is denoted by the superscript 0 in the free-energy surfaces $U_i^0(\mathbf{P})$ and $U_f^0(\mathbf{P})$.

The proton remains in its ground state even at the transitional configuration $\mathbf{P}^*$ (i.e., no classical stretching of the length of the proton chemical bond in H_3O^+ takes place at this transition). Of course, the spacing of the proton vibrational energy levels is smaller than that for the electrons. Therefore, the contribution of the transitions with the participation of excited vibrational proton states in general may not be ignored entirely. They correspond to the transitions between different free-energy surfaces $U_i^m(\mathbf{P})$ and $U_f^n(\mathbf{P})$, which differ from $U_i^0(\mathbf{P})$ and $U_f^0(\mathbf{P})$ by the energies at the points of minimum, which include the proton excitation energies, $E_{pi}^m - E_{pi}^0$ and $E_{pf}^n - E_{pf}^0$, for the mth and nth vibrational states. Usually, the role of the contribution of the excited states increases toward the activationless and barrierless regions. In the normal region the transitions between the ground states dominate and the current–overpotential dependence is described by a simple exponential form similar

to Eq. (34.28) for electron transfer. It would follow the nonlinear Tafel plot for large overpotentials in the absence of the excited vibrational states. However, the contribution of the latter results in a broader overpotential range with approximately constant observable symmetry factor $\alpha_{obs} \approx \frac{1}{2}$.

Acknowledgments

This chapter was written when the author was at the University of Ulm (Germany) as a research award winner of the Alexander Humboldt Foundation.

REFERENCES

Dogonadze, R. R., and V. G. Levich, *Dokl. Akad. Nauk SSSR*, **124** (1959).

Dogonadze, R. R., A. M. Kuznetsov, and V. G. Levich, *Elektrokhimiya*, **3**, 739 (1967).

Gerischer, H., *Z. Phys. Chem*., N.F., **26**, 223, 325 (1960).

Hush, N. S., *J. Chem. Phys*., **28**, 962 (1958).

Marcus, R. A., *J. Phys. Chem*., **24**, 966, 979 (1956).

REVIEWS AND MONOGRAPHS

Hanggi, P., P. Talkner, and M. Borkovec, *Rev. Mod. Phys*., **62**, 251 (1990).

Kuznetsov, A. M., *Charge Transfer in Physics, Chemistry and Biology*, Gordon & Breach, Reading, Berkshire, England, 1995.

Kuznetsov, A. M., *Charge Transfer in Chemical Reaction Kinetics*, Presses Polytechniques et Universitaires Romandes, Lausanne, Switzerland, 1997.

Kuznetsov, A. M., *Stochastic and Dynamic Views of Chemical Reaction Kinetics in Solutions*, Presses Polytechniques et Universitaires Romandes, Lausanne, Switzerland, 1999.

Kuznetsov, A. M., and J. Ulstrup, *Electron Transfer in Chemistry and Biology*, Wiley, Chichester, West Sussex, England, 1999.

Schmickler, W., *Interfacial Electrochemistry*, Oxford University Press, New York, 1996.

35

Computer Simulation in Electrochemistry

EZEQUIEL LEIVA
National University, Córdoba, Argentina

35.1 INTRODUCTION

The first two questions that the reader may ask is *why* and *when* computer simulations may be useful in general as well as in the particular case of electrochemistry. However, before attempting to give an answer to these questions, we must also address the question of *what* computers simulations are, or at least what we mean when we speak of computer simulations. The term *computer simulation* is used with a rather broad meaning ranging from the numerical resolution of phenomenological equations up to calculation of the time evolution of a quantum-mechanical system, described by first-principles calculations. A good example of the first case would be the problem of the numerical solution of the diffusion equations in connection with electron transfer reactions, as addressed in Chapter 4. This is not the type of problem we address here, but rather, we shall concentrate on problems where the *atomistic* nature of matter is considered, or at least when some modeling is required at a level were the molecular sizes become relevant. This type of simulation is closely related to the emerging field of nanotechnology, where processes must be modeled at the molecular scale, and structuring at the nanometer scale becomes relevant. In this respect we approach the *why* formulated above.

In many macroscopic systems, the massive behavior is a convoluted answer to many microscopic features of the system. For example, the catalysis of the electrooxidation of an organic molecule may be generated by some local arrangement of atoms on a catalyst, defined at the atomic level. If some hypotheses are available to explain the enhancement of the reaction, this can be checked by inserting these hypotheses in the model. In a first approximation, a qualitative explanation is often sought. If this is

Fundamentals of Electrochemistry, Second Edition, By V. S. Bagotsky

satisfactory, the next step will be to introduce parameters in the model that may also be changed in the experimental system. A further comparison between the experiment and the theoretical results will then deliver information on the parameters governing the reaction, which may be changed to optimize the reaction. A more sophisticated attempt would be to calculate the parameters from first-principles calculations, introducing them directly into the simulation. Although this will be the final goal of theoreticians in the future, it happens very often that electrochemical systems are in many cases still too complicated for such an attempt to succeed.

Another possible use of atomistic simulations would be the possibility of checking the simplest phenomenological approaches, that is, to validate an alternative description of the system based in a simpler mathematical description.

Turning to the question of *when*, it is important for a careful consideration of the physical problem to avoid energy and resource wasting. For example, although it would be quite useless to employ a detailed atomistic model to consider particle diffusion at relatively large scales, this description may be indispensable when studying the creation of atomic clusters on the surface of an electrode. Thus, before starting with the computational study of a given electrochemical phenomenon, the key parameters driving the response of the system should be identified as well as the relevant space and time scales of the problem.

Depending on whether or not stochastic features are introduced in the simulation procedure, simulation methods are sometimes classified as *stochastic* or *deterministic*. Although the second term is usually applied to methods related to the numerical solution of Newton's equations, the first term is applied to a wide variety of simulation methods.

In this chapter we address first the electrochemical application of the more familiar method of molecular (or atom) dynamics, and later turn to consider Monte Carlo methods, in each case giving a short introduction that should motivate the reader to pursue reading more specific works. Although the present research field is relatively new, the investigations are already too extensive to review in detail in a single chapter. For this reason, we discuss here the more extended research branches in the field and present a few representative examples. The application of simulations applied to nanostructuring problems is discussed in Chapter 36; liquid–liquid interfaces have been addressed by I. Benjamin (1997).

35.2 MOLECULAR (ATOM) DYNAMICS

The main idea behind classical molecular (or atom) dynamics (MD) is fairly simple. To illustrate this for the relatively simple case of an ensemble of atoms, let us consider a system of N particles, each having mass m_i with Cartesian coordinates $\{\mathbf{r}_i\}$. The motion of this system of particles can be described by solving a set of equations of the type

$$m_i \frac{d^2\mathbf{r}_i}{dt^2} = \mathbf{f}_i, \tag{35.1}$$

given by Newton's second law, where $\mathbf{f}_i$ is the force exerted on particle i, which can be calculated from the potential energy of the system $U(\{\mathbf{r}_i\})$ according to

$$\mathbf{f}_i = -\nabla_i U(\{\mathbf{r}_i\}) = -\frac{\partial U(\{\mathbf{r}_i\})}{\partial x_i}\,\hat{i} - \frac{\partial U(\{\mathbf{r}_i\})}{\partial y_i}\,\hat{j} - \frac{\partial U(\{\mathbf{r}_i\})}{\partial z_i}\,\hat{k}, \tag{35.2}$$

where (x_i, y_i, z_i) are the coordinates of particle i. Thus, once the interactions between the particles are given through $U(\{\mathbf{r}_i\})$, integration of the set of equations (35.1) allows prediction of the behavior of the system at all times, provided that some boundary conditions are given. The usual physical situation is one where the positions and velocities are known at a certain time t_0, and the evolution of the system for $t > t_0$ is sought, so that $6N$ boundary conditions are delivered by the initial positions and velocities of the particles. Once the trajectory of the system has been obtained [i.e., the set $\{\mathbf{r}_i(t)\}$ for all t], the properties of the system can be calculated using this information and eventually the set of momenta of the particles $\{\mathbf{p}_i(t)\}$. Since even for very simple forms of $U(\{\mathbf{r}_i\})$, integration of Eq. (35.1) cannot be performed analytically for more than two particles, approximate methods are required. We illustrate one of the methods here to give a concrete example. From the Taylor expansion of the position of particle i, the following equation can be obtained:

$$\mathbf{r}_i(t + \Delta t) = 2\mathbf{r}_i(t) - \mathbf{r}_i(t - \Delta t) + \left(\frac{d^2\mathbf{r}_i}{dt^2}\right)_t \Delta t^2 + \cdots. \tag{35.3}$$

Thus, positions of the particles at the time $t + \Delta t$ can be computed from the positions at times t and $t - \Delta t$, and the second derivative, $(d^2\mathbf{r}_i/dt^2)_t$, that corresponds to the acceleration. The latter can be computed via Eqs. (35.1) and (35.2). Equation (35.3) is known as the *Verlet algorithm*. A number of methods are discussed in specific textbooks (e.g., Allen and Tildesley, 1992), and the choice must be taken by making a balance between accuracy and cost in execution speed.

The main handicap of MD is the knowledge of the function $U(\{\mathbf{r}_i\})$. There are some systems where reliable approximations to the true $U(\{\mathbf{r}_i\})$ are available. This is, for example, the case of ionic oxides. $U(\{\mathbf{r}_i\})$ is in such a case made of coulombic (pairwise) interactions and short-range terms. A second example is a closed-shell molecular system. In this case the interaction potentials are separated into intraatomic and interatomic parts. A third type of physical system for which suitable approaches to $U(\{\mathbf{r}_i\})$ exist are the transition metals and their alloys. To this class of models belong the *glue model* and the *embedded atom method*. Systems where chemical bonds of molecules are broken or created are much more difficult to describe, since the only way to get a proper description of a reaction all the way between reactant and products would be to solve the quantum-mechanical problem at each step of the reaction.

35.2.1 Metal–Water and Ionic Solution–Metal Interphases

Metal–water and solution–metal interfaces is of primary importance since many electrochemical processes occur there that are relevant for electrocatalysis, corrosion,

and electrochemical phase growth. The difficulties found in attempting to get a function $U(\{\mathbf{r}_i\})$ that describes the water–water, water–ion, ion–ion, water–metal, ion–metal, and metal–metal interactions properly have been discussed extensively in reviews (cf. the list below). Many water properties seem to be reproduced reasonably well with pairwise water–water potentials that involve short-range potentials with embedded charges. Depending on whether or not deformation of the molecule is allowed in the model, the terms *rigid* and *flexible* water have been coined. Some more evolved water models, denoted *polarizable models*, allow modification of the internal charge distribution in response to the electric field generated by the environment. Long-range coulombic interactions require special handling within the periodic boundary conditions usually employed.

The treatment of water–metal interactions deserves even more research. This is so because when a water molecule approaches a metal surface, two types of interactions can be envisaged. One of them is due to the polarization of the metal due to the partial charges that occur on the water molecule, and the other is due to overlap of the electronic clouds of the water molecules with the electronic cloud of the metal, called *chemical interactions*. For a water–Pt system, the latter predominate over the former, amounting to 90% of the total energy.

To represent two metal–water interphases simultaneously, a slab of water molecules is usually located between two walls, which may be made of mobile atoms or may present a corrugation representing a metal single-crystal surface. An electric field between the two metal slabs may be applied so as to simulate the effect of a surface charge density Q_S. Two relevant properties that can be obtained from simulations are the oxygen and hydrogen density averaged on the direction parallel to the surface of the electrode. These are shown in Fig. 35.1 for a simulation of water close to a Pt(100) surface. In the case of the oxygen density, three peaks are clearly distinguishable, while in the case of hydrogen density, a feature appears in the intermediate region between the first and second oxygen peaks. The coincidence between the oxygen and hydrogen peaks indicates that most of the water molecules are lying

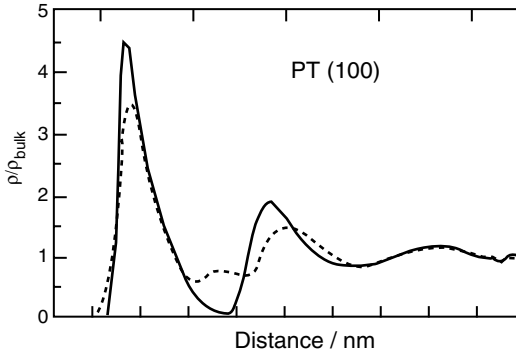

FIGURE 35.1 Oxygen (solid line) and hydrogen (dashed line) density profiles from a simulation of water close to a Pt(100)–water interphase. (From Berkowitz et al., 1999, with permission from CRC Press LLC via CCC.)

flat on the corrugated surface. However, the densities in Fig. 35.1 correspond to an average, and a more detailed analysis shows that the water layer closer to the surface should actually be divided into two sublayers, one made of water molecules laying flat on the surface and other layer consisting of "flip-up" and "flip-down" molecules.

Molecular dynamics simulations have also been used to study the effect of the presence of surface defects and the distribution of ions at the electrochemical double layer. The classical approach described previously has been challenged in recent times through the use of models that involve the calculation of both atomic and the electronic structures of the interface, as made by J. W. Halley et al. (1998).

35.2.2 Electron Transfer Reactions

Since the pioneering work of Rudolph A. Marcus (1956) and Noel S. Hush (1958) and through subsequent very different theoretical approaches, it has been shown that even when no bonds are created or broken during an electron transfer reaction (ETR), reorganization of the solvation shell around ions should deliver an important contribution to the activation free energy. Depending on the strength of the interaction between the electrode and the reacting species, reactions are usually classified into diabatic and adiabatic. The term *diabatic* is employed to describe a reaction where the interaction of the reactants with the electrode is weak. The second term, *adiabatic*, is used to describe a strong interaction. The situation in both cases is illustrated in Fig. 35.2, where the free energy A of the system metal–redox couple system is represented as a function of a reaction coordinate that can be imagined as one of the solvent vibrational modes.

The left (solid) parabolic curve represents the oxidized state, the right one, the reduced state. Let us assume that the system is initially at the oxidized state (left curve). When the interaction metal–reaction species is small, the electronic coupling between is small and the system may oscillate many times on the left parabolic curve (ox) before it is transferred to the curve on the right (red). On the other hand, if the interaction is strong, the free energy should no longer be represented by the two solid curves in the intermediate region of the reaction coordinate, but rather, by the dashed

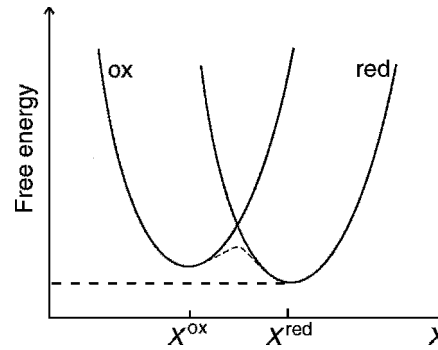

FIGURE 35.2 Scheme of diabatic (solid line) and adiabatic (dashed line) free-energy curves for a simple electrochemical redox reaction Ox → Red.

line. In this case, the system should go through the dashed line from the oxidized state to the reduced state.

The theories mentioned above construct these reaction coordinate curves on the basis of some assumption for the interaction between the particles of the system, then making some approximation to get them, as, for example, to assume harmonic behavior of all the oscillatory freedom degrees, assumption of no recrossings through the free-energy maximum once the system has gone through, and so on. On the other hand, computer simulations allow the construction of free-energy curves from knowledge of the interactions alone, and some of the approximations of the theories may be checked. However, free-energy calculations are more involved than the energy calculations mentioned above, and they require further considerations.

The activation free-energy function for reactants (r) and products (p), Δg_r and Δg_p, can be calculated from the probabilities $P_r(x)$ and $P_p(x)$ of finding the reactants and products with the reaction coordinate x. A suitable choice for x is the difference in potential energy between reactant and product, $\varepsilon_p - \varepsilon_r = \Delta\varepsilon$ when the heavy particles have the same set of coordinates, and the probabilities $P_i(x)$ (i = r, p) are constructed by observing with which frequency the system is found in a given value of x. Thus, in a molecular dynamics run consisting of N_r simulation steps for the reactant (say, the ox state on the left side of Fig. 35.2), $P_r(x)$ would be calculated from the number of times $n_r(x)$ the condition $x = \Delta\varepsilon$ is found to occur.

As explained didactically by King and Warshel (1990), a histogram for $n_r(x)$ can be constructed in which the number of times the condition $x = \Delta\varepsilon$ occurs is collected for all x, and the functions $P_r(x)$ and $P_p(x)$ can be obtained. A technique called *umbrella sampling* is used for this purpose. Figure 35.3 shows curves for Δg_r

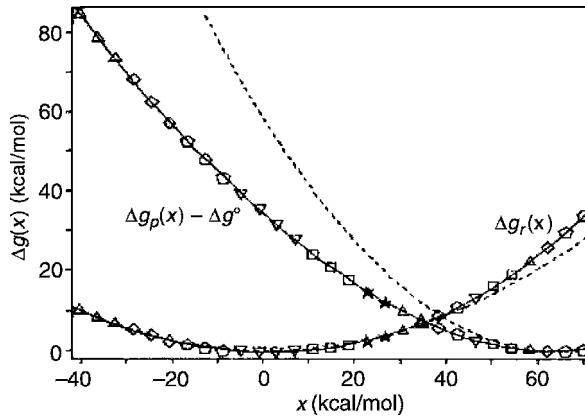

FIGURE 35.3 Free-energy functions for reactant Δg_r (ΔE) and product Δg_p (ΔE) of an electron transfer reaction as calculated using umbrella sampling within a simple dipolar diatomic solvent. ΔG^0 is the reaction free energy. Solid lines are polynomial fittings to the simulated points. Dashed lines are parabolic extrapolations from the minimum of the curves. (From King and Warshel, 1990, with permission from the American Institute of Physics.)

and Δg_p calculated by using this method within a simple dipolar diatomic solvent, where the interactions are of Lennard–Jones type plus a coulombic contribution. Note the good overlap between the curves of reactant and product. Umbrella sampling methods have been widely employed to study ETR under different approaches, in some of them introducing the quantum-mechanical aspects of the problem.

35.2.3 Electrochemical Ion-Transfer Reactions

The field of electrochemical ion transfer reactions (EITRs) is relatively recent compared with that of electron transfer reactions, and the application of molecular dynamics simulations to study this phenomenon dates from the 1990s. The simulations may shed light on various aspects of the EITR. One of the key questions on this problem is if EITR can be interpreted in the same grounds as those employed to understand electron transfer reactions (ETRs). For example, let us consider the electrochemical oxidation reaction of iodine:

$$I^-_{sol} \rightarrow I_{sol} + e^-_{met}. \tag{35.4}$$

This reaction involves the approach of the I^- ion to the surface of the electrode, with a concomitant change in its own solvation status and that of the electrode. Straightforward application of the theory of ETR (e.g., Marcus's theory) would lead to a picture where the system is at the red state (right-hand curve in Fig. 35.2), until a solvent fluctuation brings it to the intersection point of the curve, where electron transfer from the iodide to the electrode takes place. The actual problem, however, is more complicated, since as the simulations show, the approach of the reduced species to the surface of the electrode may play an important role, so that the curves in Fig. 35.2 show just a part of the problem. It is enlightening to consider the work of Pecina et al. (1995), who have employed molecular dynamics simulations to study reaction (35.4), where 304 rigid water molecules were located between two parallel platinum surfaces, the iodine–water and iodide–metal interactions were based on results of ab initio calculations, and the iodine interactions were approached by those of I^- without the charge. An important quantity to understand in development of the reaction is the mean force $f_s(z)$ exerted by the solvent on the solute as a function of distance z from the metal surface. This is shown in Fig. 35.4. Different regions may be distinguished in the curves for iodine and iodide, depending on the approach to the metal surface. At distances larger than 6.5 Å, bulk conditions predominate and the solvent forces disappear for both ion and atom. In the range between 6.5 and 3.5 Å, the particles experiment a strong repulsive mean force due to water displacement from the surface and progressive loss of the solvation shell. At relatively short distances from the surface, there are no water molecules between the solutes and the metal surface, and the mean force remains constant. A similar model has been employed by Schmickler (1983) to investigate the transmission coefficient of ion transfer reactions.

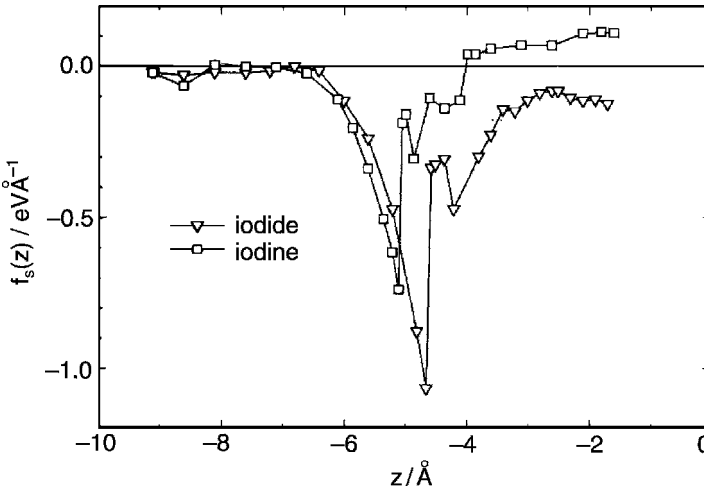

FIGURE 35.4 Mean solvent force for iodide and iodide as a function of the distance between solute and electrode, in the absence of an external field. $z = 0$ corresponds to the top layer of metal atoms. (From Pecina et al., 1995, with permission from Elsevier.)

35.3 MONTE CARLO METHODS

35.3.1 Some Basic Ideas on Random Variables and Markov Chains

The term *Monte Carlo* is often used to describe a wide variety of numerical techniques that are applied to solve mathematical problems by means of the simulation of *random variables*. The intuitive concept of a *random variable* ξ is a simple one: It is a variable that may take a given value of a set, but we do not know in advance which value it will take in a concrete case. The simplest example at hand is that of flipping a coin. We know that we will get head or tail, but we do not know which of these two cases will result in the next toss. Experience shows that if the coin is a fair one and we flip it many times, we obtain an average of approximately half heads and half tails. So we say that the *probability* p to obtain a given side of the coin is $\frac{1}{2}$.

A random variable is defined in terms of the values it may take and the related probabilities. In the example we consider, we may write

$$\xi = \text{side of the coin} \rightarrow \begin{Bmatrix} \text{head} & \text{tail} \\ p_{\text{head}} = \frac{1}{2} & p_{\text{tail}} = \frac{1}{2} \end{Bmatrix}, \tag{35.5}$$

where we wrote in the upper part of array *the value taken by the random variable* and the corresponding *probability* in the lower part. A longer but essentially display would result for a random variable associated with the numbers coming out of a roulette game (with $P = 1/37$), so we come closer to the name associated with the present numerical techniques (Monte Carlo is the name of a city most famous for its casinos). In some cases, the random variable ξ may take any value in the interval $[a, b]$. If this is the case, ξ is termed a *continuous* random variable.

A *Markov chain* is a sequence of trials that samples a random variable ξ and satisfies two conditions, namely that the outcome of each trial belongs to a finite set of outcomes $\{\xi_1, \xi_2, \ldots, \xi_N\}$, and that the outcome of each trial depends only on the outcome of the trial that immediately precedes it. Two states ξ_i and ξ_j are assumed to be linked by a transition probability $\Pi_{i\to j}$, which is the probability of obtaining the state j at the time $t+1$ given that the system is at state i at time t.

In statistical mechanics the properties of a system in equilibrium are calculated from the partition function, which depending on the choice for the ensemble considered involves a sum over different states of the system. In the very popular canonical ensemble, that implies a constant number of particles N, volume V, and temperature T conditions, the quasiclassical partition function Q is

$$Q = \frac{V^N}{N!\,\Lambda^{3N}} \int \frac{\exp[-U(\mathbf{r})/k_\mathrm{B}T]}{V^N}\, d\mathbf{r}, \tag{35.6}$$

where $U(\mathbf{r})$ is the potential energy function of the system, k_B is Boltzmann's constant, and $\Lambda = (h^2/2\pi m k_\mathrm{B}T)^{1/2}$. When a given property Y depends only on the coordinates $\mathbf{r}$, calculation of its average value, $\langle Y\rangle$, involves "just" an integration over the configuration space of the system:

$$\langle Y\rangle = \frac{1}{Q}\,\frac{V^N}{N!\,\Lambda^{3N}} \int Y(\mathbf{r})\,\frac{\exp[-U(\mathbf{r})/k_\mathrm{B}T]}{V^N}\, d\mathbf{r} = \int Y(\mathbf{r}) p(\mathbf{r})\, d\mathbf{r}, \tag{35.7}$$

where $p(\mathbf{r})$ is the probability of finding the system in the configuration $\mathbf{r}$. The configuration integral in Eq. (35.7) is a formidable task, even for very simple interatomic potentials, and it is in this respect that Monte Carlo methods come to aid. However, application of the Monte Carlo method is not a straightforward integration to get Q but a somehow more sophisticated way to get the average $\langle Y\rangle$ without the need to calculate Q. The idea is that one is able to get a succession of configurations, each having a weight proportional to the probability p of their occurrence:

$$p = p(\mathbf{r}) = \frac{\exp[-U(\mathbf{r})/k_\mathrm{B}T]}{\int \exp[-U(\mathbf{r})/k_\mathrm{B}T]}\, d\mathbf{r}. \tag{35.8}$$

If this is possible, the quantity $\langle Y\rangle$ can be calculated by taking an average of the value of $Y(\mathbf{r})$ over the configurations generated. Such a succession of states is achieved by generating a Markov chain of states. To do this, let us think of the configuration of the system $\{\mathbf{r}\}$ as a random variable, where the probabilities for the occurrence of all the individual configurational states of the system can be stored in a vector $\mathbf{p}$. The transition probability Π_{ij} between states $\{\mathbf{r}\}_i$ and $\{\mathbf{r}\}_j$ must be calculated by a suitable algorithm [e.g., that due to Metropolis (see Allen and Tildesley, 1992)].

$$\Pi_{ij} = \frac{1}{N_i} \min\left\{1, \exp\left(\frac{U_{N,j} - U_{N,i}}{k_\mathrm{B}T}\right)\right\}; \qquad \Pi_{ii} = 1 - \sum_{j\neq i} \Pi_{ij}, \tag{35.9}$$

where the function min $\{\cdot\}$ selects the minimal value between 1 and exp $[(U_{N,j} - U_{N,i})/k_B T]$. An initial configuration must be chosen, and from it a chain of new configurations are generated where the transitions probabilities between them are given by Eq. (35.9). In each step of the simulation, the transition probability Π_{ij} is calculated and compared with a random number η, generated with a uniform probability between 0 and 1. If $\eta < \Pi_{ij}$, the new configuration is accepted; otherwise, it is rejected. In the case of the NVT ensemble under consideration, where the particles may take virtually any position in space, the different configurations are generated by small displacements of the particles in the simulation box. The energy changes associated with these displacements are those introduced in Eq. (35.9) to calculate the Π_{ij}. On the other hand, it can be assumed that the particles in the system may take only definite positions in space; these are the *lattice models*. To differentiate the latter, the former simulations are called *off-lattice simulations*. Other ensembles exist, where the simulations can be performed, such as the *NPT* (constant N, pressure P, and T) and μVT (constant chemical potential μ, V, and T) ensembles. The latter, denoted the *grand canonical ensemble*, is particularly useful in electrochemistry, since control of the electrostatic potential difference involves control of the chemical potential of some of the species present at the electrochemical interphase.

The Monte Carlo method as described so far is useful to evaluate equilibrium properties but says nothing about the time evolution of the system. However, it is in some cases possible to construct a Monte Carlo algorithm that allows the simulated system to evolve like a physical system. This is the case when the dynamics can be described as thermally activated processes, such as adsorption, desorption, and diffusion. Since these processes are particularly well defined in the case of lattice models, these are particularly well suited for this approach. The foundations of dynamical Monte Carlo (DMC) or kinetic Monte Carlo (KMC) simulations have been discussed by Fichthorn and Weinberg (1991) in terms of the theory of Poisson processes. The main idea is that the rate of each process that may eventually occur on the surface can be described by an equation of the Arrhenius type:

$$k_f = A e^{-E^{\neq}/k_B T}, \tag{35.10}$$

where k_f is the experimental rate constant for the forward reaction and A is called the *frequency factor*. The theoretical basis for the evaluation of parameters in Eq. (35.10) is given by the *transition-state theory*, also called *activated-complex, absolute-reaction-rate theory*. Once all the processes that may occur at a certain step of the simulation have been identified, each is assigned a rate v_i. The probability of a process to occur can thus be represented on a straight line by a segment proportional to its rate. If the sum of all the segments is normalized to unit length, the occurrence of a process can be selected by generating a random number between 0 and 1 and choosing the process corresponding to the segment on which the random number has been found to fall. The elapsed time Δt until the accepted change has an exponential distribution.

35.3.2 Brownian Dynamics

We mentioned above that MD simulations can describe the behavior of systems made of a few thousands of atoms for times on the order of nanoseconds, and this is so because detailed prediction of atomic behavior requires very short integration steps in the numerical procedure. Whereas in some systems the minor details of the trajectory of the particles of the system are important, as, for example, if we are studying the generation mechanism of a cluster on a surface through a mechanical procedure, in other cases some degrees of freedom of the system just provide a background in which the relevant motion occurs. A good example of this is a front of ions diffusing in a solution to join a growing nanostructure, where the long-time trajectory of the ions is important, but their short-time jumps are irrelevant, as well as the motion of the solvent in which they are diffusing. In the latter case, the Brownian dynamics methods are of use, where the deterministic Newton's equations (35.1) are replaced by a set of equations such as

$$m_i \frac{d^2\mathbf{r}_i}{dt^2} = \mathbf{f}_i - \xi m_i \frac{d\mathbf{r}_i}{dt} + \mathbf{g}_i, \tag{35.11}$$

where $\mathbf{f}_i$ is derived from a potential as in Eq. (35.2), ξ is a friction coefficient that may be different for different types of particles, and $\mathbf{g}_i$ is a random force on the particle i that is taken to be independent of the $\mathbf{g}$'s on other particles. These equations of motion can be integrated numerically as in the deterministic case, with the additional feature that two random variables related to position and velocity occur that must be sampled from a Gaussian distribution.

35.3.3 Off-Lattice Models

In contrast to the lattice models discussed below, off-lattice models allow the chemical species under consideration to occupy in principle any position in space, so that important information concerning the relaxation and space distribution of the constituents of the system can be obtained. We discuss next some applications of these models to electrochemical problems.

Electrochemical Double Layer In the absence of specific adsorption, the reciprocal of the capacitance C of the electrochemical double layer can be written as

$$\frac{1}{C} = \frac{1}{C_{\text{ion}}} + \frac{1}{C_m} + \frac{1}{C_{\text{dip}}}. \tag{35.12}$$

The term $1/C_{\text{ion}}$ corresponds to the rearrangement of free charge due to the charging of the interface and can be estimated from a suitable theory (e.g., Gouy–Chapman). The term $1/C_m$ is due to a contribution from electronic rearrangement at the surface of the metal. It occurs because the center of mass of the charge induced on the metal lies in front of the ideal metal edge. Finally, the term $1/C_{\text{dip}}$ is a contribution from the

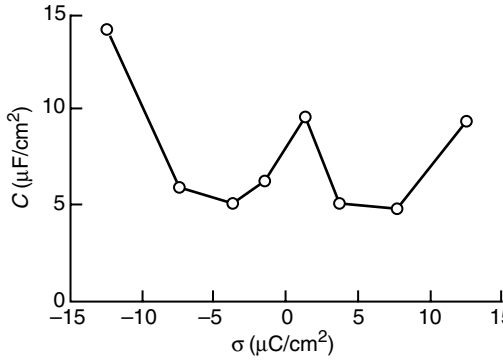

FIGURE 35.5 Solvent contribution to the capacitance of the electrochemical double layer as obtained from a Monte Carlo simulation. (From Aloisi et al., 1989, with permission from the American Institute of Physics.)

rearrangement of the solvent molecules due to charging of the system. Aloisi et al. (1989) have performed off-lattice MC simulations with the purpose of calculating $1/C_{\text{dip}}$, enclosing 128 rigid water molecules in a rectangular cell with periodic boundary conditions in the x and y directions, while the two walls perpendicular to the z direction, which were 30 Å apart, carried opposite charges of the same magnitude. The results for capacitance as a function of the surface charge density are given in Fig. 35.5. A maximum is observed at small positive charges, which was attributed to the breaking of hydrogen bonds. This maximum resembles that obtained for some experimental systems by subtracting from the experimental data the $4\pi/\varepsilon\kappa$ contribution to the reciprocal capacitance, by performing the *Parson–Zobel plots*. MC simulations have also been employed to study the distribution of ions in the diffuse double layer that make the contribution to the capacitance C_{ion} defined above. In this case, the ions are considered to be charged hard spheres embedded in a dielectric continuum representing the solvent.

Stability and Generation of Metallic Nanostructures The Monte Carlo methods described in this section are complementary to the atom dynamics simulations and were found very useful in understanding the reasons for the unusual stability of clusters generated by electrochemical nanostructuring. Although this application is discussed in Chapter 36, we give here a summary of the main ideas. Small agglomerates of metals atoms may be generated with a designed geometry on a metal surface through interaction of the tip of a scanning tunneling microscope with the surface. Whereas the creation of these clusters can be studied by molecular dynamics methods, which employs a constant number of particles in the simulation, evolution of the sizes and composition of these clusters through exchange of matter with the solution requires a different approach. In fact, matter exchange corresponds to the grand canonical condition, where the system has fixed the volume, the temperature, and the chemical potential but not the number of particles, so that a grand ganonical Monte Carlo (GCMC) simulation, with fixed μ, V, and T, appears as a suitable alternative.

Furthermore, fixing the chemical potential of some of the atoms of the system corresponds to the electrochemical situation of potentiostatic control, since the chemical potential of the atoms μ_M can be written as

$$\mu_M = \overline{\mu}_{M^{+z}} + z\overline{\mu}_e, \tag{35.13}$$

where $\overline{\mu}_{M^{+z}}$ is the electrochemical potential of the ion cores M^{+z} and $\overline{\mu}_e$ is the electrochemical potential of electrons. In the experimental system, $\overline{\mu}_{M^{+z}}$ is fixed by the concentration of ions in the bulk of the solution, and $\overline{\mu}_e$ is varied through the potentiostatic control, with the concomitant change of μ_M. In this way, by changing μ_M in a GCMC simulation, the growth or dissolution of nanoclusters upon electrode polarization can be studied. It must be pointed out that these simulations only deliver information on equilibrium properties. The study of dynamic properties would require kinetic MC simulations like those mentioned below.

35.3.4 Lattice Models

The main idea of a lattice model is to assume that atomic or molecular entities constituting the system occupy well-defined lattice sites in space. This method is sometimes employed in simulations with the grand canonical ensemble for the simulation of surface electrochemical proceses. The Hamiltonians H of the lattice gas for one and two adsorbed species from which the transition probabilities Π_{ij} can be calculated have been discussed by Brown et al. (1999). We discuss in some detail MC lattice model simulations applied to the electrochemical double layer and electrochemical formation and growth two-dimensional phases not addressed in the latter review. MC lattice models have also been applied recently to the study the electroxidation of CO on metals and alloys (Koper et al., 1999), but for reasons of space we do not discuss this topic here.

Electrochemical Double Layer Although the use of lattice models (LMs) to study the electrochemical double layer has been superseded by MD dynamics and off-lattice MC simulations, LM played an important role in early development of new theories for the electrochemical double layer. After the work of the schools of Frumkin and Parsons, there was a consensus that the solvent molecules in the outer Helmholtz plane could be modeled as an ensemble of dipoles which could take up two or more orientations. These were usually considered to be point dipoles, arranged in a regular planar lattice between two perfectly conducting parallel metal plates separated by a distance d. The problem of accounting properly for interactions of the dipoles with each other were addressed by Schmickler (1983), who compared several approximations, arriving at the conclusion that the mean-field approximation and the Bethe approximation were not satisfactory for strongly polar solvent in the case of dipoles with a finite number of orientations in space. This study was followed by Monte Carlo studies. The simulations were performed in a regular hexagonal lattice, taking a rhombic simulation shell with periodic boundary conditions, and employed three different dipole models.

Among MC lattice models of the double layer, it is also worth mentioning the work of Nazmutdinov et al. (1988), who used a lattice model involving two monolayers of water molecules on the surface of an electrode, forming a hexagonal close-packed array. The interaction of each water molecule in contact with the metal surface (assumed to be Hg) was taken from quantum-mechanical calculations. Information was obtained concerning the relative numbers of molecules with different numbers of hydrogen bonds, and it was concluded that the hypothesis of an icelike state of water in a monolayer on Hg is rather unlikely.

Formation and Growth of Low-Dimensionality Phases at the Electrochemical Iinterphase Among metal electrodeposition processes, much effort has been devoted to study of the underpotential deposition (UPD) phenomenon, which implies the deposition of a metal M on the surface of an electrode or substrate S of different nature at potentials more positive than those predicted from the Nernst equation. GCMC simulations of lattice models, where the chemical potential μ is one of the parameters fixed in the simulations, can be used to study the UPD of the metal M on a substrate S and draw general trends. This was the methodology applied by Giménez and Leiva (2003) to study the formation and growth of low-dimensionality phases on surfaces with defects. To emulate (100) surfaces, the system was characterized by a square lattice of adsorption sites.

As a general rule, systems where the cohesive energy of M is lower than that of S yield the UPD. On the other hand, if the cohesive energy of M is higher than that of S, the UPD generally occurs. Simulations for these systems can be performed in the presence of substrate-type islands in order to emulate surface defects and study how these defects are decorated. Defects can be related to different dimensionalities of the deposit. Whereas a flat terrace is a two-dimensional deposit, monatomic steps and kink sites are one- and zero-dimensional deposits, respectively. Partial coverage degrees step and kink sites can be defined relative to the total number of step and kink sites available, respectively. The simulations allowed to classify the system into two types of behavior concerning the decoration of defects. On one side, UPD systems usually show a sequential decoration of defects and the islands remain stable, as illustrated in the upper part of Fig. 35.6 for deposition of Ag on a surface of Pt(100) with islands. In this case the partial isotherms shown that first kink sites are decorated, then steps, and finally, surface coverage is completed. On the other hand, in UPD systems there is no sequential filling of the defects and the islands disintegrate, as shown in the lower part of Fig. 35.6. These results show qualitative trends that in the experimental systems may be complicated by the presence of anion adsorption and kinetic effects, not accounted in the MC simulations.

Dynamics of Crystal Growth In the preceding section we illustrated the use of a lattice Monte Carlo method related to the study of equilibrium properties. The KMC and DMC method discussed above was applied to the study of dynamic electrochemical nucleation and growth phenomena, where two types of processes were considered: adsorption of an adatom on the surface and its diffusion in different environments.

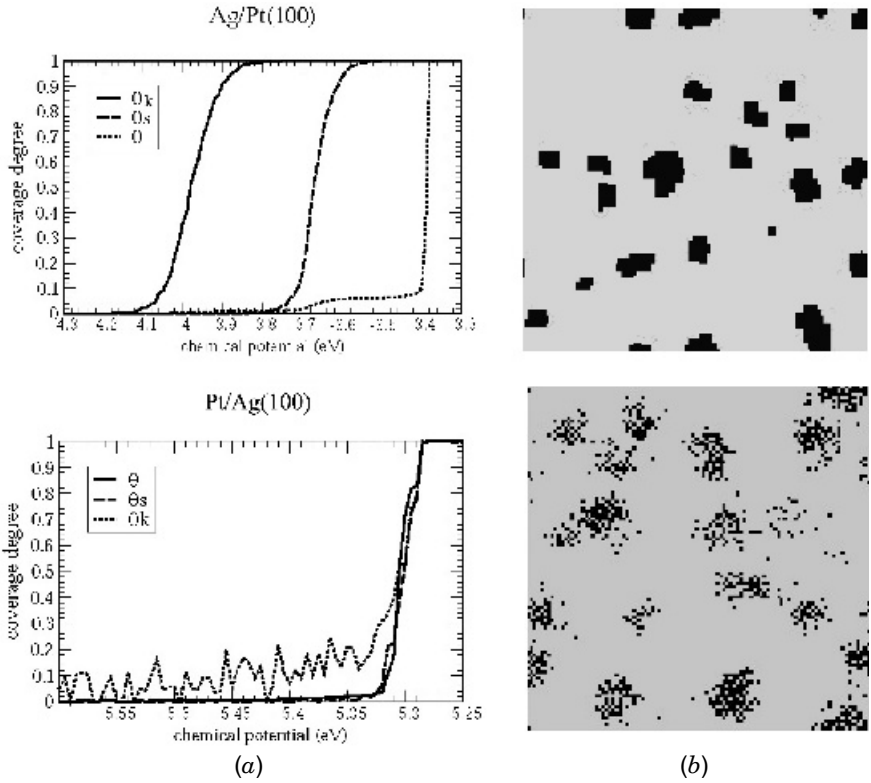

FIGURE 35.6 (*a*) Adsorption isotherms for the deposition of a metal of a foreign (100) substrate in the presence of surface defects. Coverage degree of the submonolayer (θ), step sites (θ_s), and kink sites (θ_k) as a function of chemical potential. (*b*) Final status upon completion of the monolayer. The upper figures correspond to the behavior of a typical UPD system, the lower to an OPD system. (From Giménez et al., 2003, with permission of the American Chemical Society.)

The main aim was to study a system involving electrochemical phase formation in a Frank–van der Merwe system emphasizing the role of metal–metal interactions. Thus, the embedded atom method potential was employed for a system that presents a negligible lattice misfit: Ag deposition on Au(111) and Au(100) surfaces were simulated using rectangular and hexagonal lattices, respectively. The activation barriers for Ag single-adatom diffusion were found markedly different on the Au(111) and Au(100) faces, the latter being considerably larger, due to the more open nature of the surface. This fact, combined with the various attempt frequencies, resulted in a diffusion coefficient on Au(111) that was seven orders of magnitudes larger than on Au(100) and originated strong differences in the morphologies of the deposits: In energetically rough surfaces, island formation should prevail, whereas in more smooth surfaces, the growth of the new phase should take place predominantly at steps. When

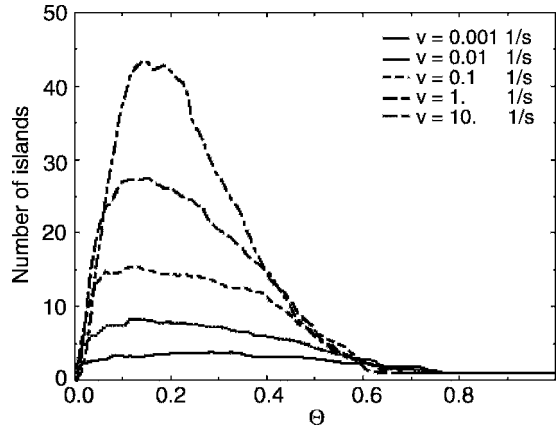

FIGURE 35.7 Results of a kinetic Monte Carlo simulation. Number of islands as a function of the coverage degree for various deposition rates v of Ag on Au(100). (From Giménez et al., 2002, with permission of The Electrochemical Society.)

an atom is electrodeposited on the surface, it will perform a random walk until it is oxidized until it meets a second diffusing atom or until it attaches to a growing island or step. As the deposition rate is accelerated, more atoms are found wandering on the surface at the same time, more encounters between diffusing atoms may occur, and thus more islands are generated. This is shown in Fig. 35.7, where the number of islands is presented as a function of the coverage degree for different deposition rates of Ag on Au(100). Larger deposition rates result in a larger number of islands at the same coverage. In the case of the lower deposition rates, a relatively wide region is found where the number of islands remains nearly constant, justifying the assumption made in instantaneous nucleation models.

Acknowledgments

Grants from CONICET, Secyt UNC, Agencia Córdoba Ciencia, Program BID 1201/ OC-AR PICT No. 06-12485 are acknowledged.

REFERENCES

Aloisi, G., M. L. Foresti, R. Guidelli, and P. Barnes, *J. Chem. Phys*., **91**, 5592 (1989).

Benjamin, I., *Annu. Rev. Phys. Chem.*, **48**, 407–451 (1997).

Fichthorn, K. A., and W. H. Weinberg, *J. Chem. Phys.*, **95**, 1090 (1991).

Giménez, M. C., and E. P. M. Leiva, *Langmuir*, **19**, 10538 (2003).

Giménez, M.C., M. G. Del Popolo, et al., *J. Electrochem. Soc*., **149**, E109 (2002).

Halley, J. W., A. Mazzolo, Y. Zhou, and D. Price, *J. Electroanal. Chem*., **450**, 273 (1998).

Hush, N. S., *J. Chem. Phys*., **28**, 962 (1958).

King, G., and A. Warshel, *J. Chem. Phys*., **93**, 8682 (1990).

Koper, M. T. M., J. J. Lukkien, et al., *J. Phys. Chem*., **B103**, 5522 (1999).

Marcus, R. A., *J Chem. Phys*., **24**, 979 (1956).

Nazmutdinov, R. R., A. M. Kuznetsov, and M. S. Shapnik, *Elektrokhimiya*, **24**, 138 (1988).

Pecina, O., W. Schmickler, and E. Spohr, *J. Electroanal. Chem*., **394**, 29 (1995).

Schmickler, W., *J. Electroanal. Chem*., **149**, 15 (1983).

REVIEWS AND MONOGRAPHS

Allen, M. P., and D. J. Tildesley, *Computer Simulation of Liquids*, Oxford Science Publications, Oxford, 1992.

Benjamin, I., Molecular dynamics simulations in interfacial electrochemistry, in *Modern Aspects of Electrochemistry*, J. O'M. Bockris et al., Eds., Vol. 31, Kluwer, New York, 1997, p. 115.

Berkowitz, M. L., C. Yeh, and E. Spohr, Chapter 3, in *Interfacial Electrochemistry*, A. Wieckowski, Ed., Marcel Dekker, New York, 1999.

Brown, G., P. A. Rikvold, S. J. Mitchell, and M. A. Novotny, Chapter 4, in *Interfacial Electrochemistry*, A. Wieckowski, Ed., Marcel Dekker, New York, 1999.

Guidelli, R., and W. Schmickler, *Electrochim. Acta*, **45**, 2317 (2000).

Schmickler, W., Chapter 6, in *Structure of Electrified Interfaces*, J. Lipkowski and P. N. Ross, Eds., Wiley-VCH, New York, 1993.

Spohr, E., Computer simulations of electrochemical interfaces, in *Advances in Electrochemical Science and Engineering*, R. C. Alkire and D. M. Kolb, Eds., Vol. 6, Wiley, New York, 1997.

36

Nanoelectrochemistry

EZEQUIEL LEIVA
National University, Córdoba, Argentina

36.1 INTRODUCTION

Nanoscale science is an emerging field where scientists are beginning to manipulate matter at the atomic and molecular scales in order to obtain materials and systems with novel and improved properties. One of the reasons for this is that the physical and chemical properties of nanostructures are often significantly different from the same material in bulk. This can be understood on geometrical grounds in the following example. Let us take a simple cubic arrangement of $10 \times 10 \times 10 = 1000$ atoms. Although this seems to be a relatively large number, it is found that nearly half of the atoms (488/1000) of this cluster belong to the surface. If some average property of the cluster is calculated (i.e., the binding energy), important deviations from the bulk are expected to occur, increasing dramatically with the decreasing size of the cluster. In fact, if the size of the edge of the cube in the previous example is divided by 2, the fraction of surface atoms increases to 0.78.

The term *electrochemical nanostructuring* can be used to mean different things. In some cases, this term is employed to refer to the generation at will of nanostructures (i.e., structures with sizes on the order of 10^{-9} m) on electrode surfaces, involving a given positioning with a certain precision. In other cases, the term *nanostructuring* is used to describe the generation of nanometric patterns with a more or less narrow size distribution and a periodic or random ordering on the surface, but without control on the spatial location of the nanostructures. In this chapter we refer to the first type of techniques. A general overview on the principles of electrochemical nanosystem technologies can be found in the review by Schultze and Bressel (2001).

Fundamentals of Electrochemistry, Second Edition, By V. S. Bagotsky

36.2 PROBE-INDUCED ELECTROCHEMICAL NANOSTRUCTURING OF METALLIC SURFACES

Electrochemical nanostructuring on solid surfaces has been undertaken using different types of techniques, which share a common instrument for their implementation—a scanning probe microscope (SPM), described in Chapter 27. The common feature of all SPM techniques is that a solid probe with a sharp tip (its size determines the locality of the signal measured) is physically scanned by means of piezoelectric translators over the surface of a sample, with a separation between the tip and the sample of the order of angstroms. A certain signal (current, force, etc) containing local information of the surface below the probe is recorded for every single image point of the surface. Basically, two operation modes are possible. In one of them, the *constant-height mode*, the vertical position of the probe (say, z) remains constant while it is rastered on the surface and the signal (current, force, etc) is measured for each position (x, y) on the surface. In the other mode, denoted the *constant signal mode*, the signal of the probe is kept constant through readjustment of the position of the vertical piezoelement. In this case the z coordinate is the output signal that defines the topography of the surface.

A typical example of a SPM device is the scanning tunneling microscope (STM). In this device a potential difference is applied between the metallic tip and the metal substrate and the tunneling current flowing between them is the signal measured. The exponential dependence of the tunneling current on the tip–surface distance makes this device very sensitive to the topology of the surface in the z direction. For this reason, in the origin of the SPM techniques, the most popular application was to get topological information, but soon an alternative application was developed (Eigler and Schweizer, 1990), consisting in the possibility of manipulation of matter at the atomic level. The manipulation of single atoms requires extreme conditions, such as ultrahigh vacuum and very low temperatures, approaching absolute zero, to avoid the influence of impurities and minimize thermal motion. However, nanostructures involving tens, hundreds, or thousands or atoms are fairly more stable, so experiments with this relatively large number of atoms can be performed at room temperature, and what is interesting for electrochemists, in the presence of an electrolyte solution.

Since the late 1980s, STM has been applied successfully to electrochemical systems, where the potentials of the tip and of the substrate can be controlled separately by means of a bipotentiostat, allowing great flexibility to study surfaces under a variety of polarization conditions. In the case of the electrochemical use of STM, a number of applications have appeared that allow for nanostructuring at the electrochemical interphase. Some of them are illustrated in Fig. 36.1. In the first, denoted *tip-induced local metal deposition* (TILMD), nanoclusters are generated on the surface of a substrate by transfer of matter from the tip of the STM (Fig. 36.1*a*). The material on the tip is renewed continuously by deposition from a solution containing ions of the metal to be deposited (Kolb et al., 1997). In the second method (Fig. 36.1*b*) defects are generated on a metal surface, and the holes generated in this way are later decorated through deposition of the foreign metal (Li et al., 1996; Xia et al., 1999). In the third

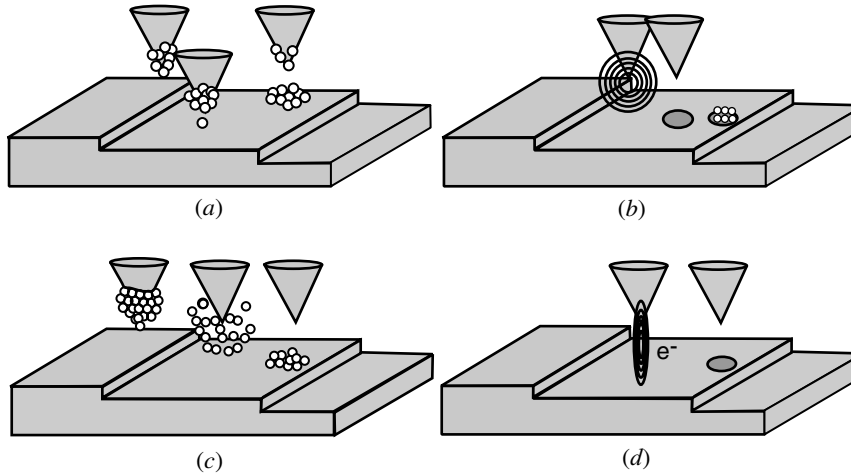

FIGURE 36.1 Schematic illustration of some electrochemical techniques employed for surface nanostructuring: (*a*) tip-induced local metal deposition; (*b*) defect nanostructuring; (*c*) localized electrochemical nucleation and growth; (*d*) electronic contact nanostructuring.

method (Fig. 36.1*c*) the tip of an STM is used as an electrochemical nanoelectrode to generate supersaturation conditions with respect to the bulk metal equilibrium potential, and nucleation and growth of a single clusters are achieved (Schindler et al., 2000, 2002). The fourth method (Fig. 36.1*d*) involves some significant electronic interaction between the tip and the substrate, leading to the occurrence of nanoholes on the surface. In the following sections we discuss each of these applications in detail, with a short discussion on the theoretical aspects of the problem, if this is available. A related SPM technique, scanning electrochemical microscopy (SECM), which can also be employed to generate nanostructures, is discussed at the end of the chapter.

36.3 DEFECT NANOSTRUCTURING

In this method the creation of defects is achieved by the application of ultrashort (10 ns) voltage pulses to the tip of an electrochemical STM arrangement. The electrochemical cell composed of the tip and the sample within a nanometer distance is small enough that the double layers may be polarized within nanoseconds. On applying positive pulses to the tip, the electrochemical oxidation reaction of the surface is driven far from equilibrium. This leads to local confinement of the reactions and to the formation of nanostructures. For every pulse applied, just one hole is created directly under the tip. This overcomes the restrictions of conventional electrochemistry (without the ultrashort pulses), where the formation of nanostructures is not possible. The holes generated in this way can then be filled with a metal such as Cu by

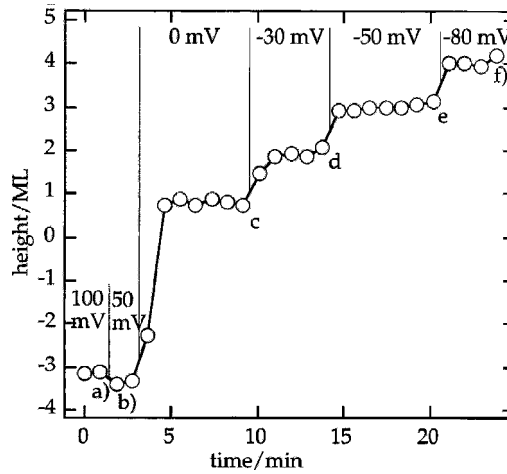

FIGURE 36.2 Height of the Cu nanostructure generated in a hole on a Au(111) surface as a function of time when a sequence of potential steps running in the negative direction are applied to the electrode. (From Xia et al., 1999, with permission from Elsevier.)

accurate potentiostatic control (Xia et al., 1999). Figure 36.2 shows the height of the nanostructure (in units of monolayer height) as a function of time, when a sequence of potential steps running in the positive direction are applied to the electrode. Some relevant findings of these experiments were:

1. It is possible to generate holes on the surface of the substrate through the application of very short negative voltage pulses to the STM tip. This procedure only succeeds using highly concentrated electrolytes.
2. If the potential applied to the substrate is controlled carefully, it is possible to confine the deposition of copper from the solution to the volume inside the hole. This is so because metal deposition on the Cu(1×1) structure outside the hole is disfavored with respect to metal deposition on the hole, where the lattice parameter of Cu should be close to that of the bulk metal.
3. As shown in Fig. 36.2, cluster growth above the surface level of the substrate is layer by layer. This is due to the lower binding energy of the atoms at the border of the hole. For each layer growing over the surface level, an extra free energy cost must be paid to generate this border. According to this fact, this effect should be stronger the smaller the hole, since the relative number of border atoms is larger.
4. The size of the deposit depends on the size of the hole and not on polarization time, denoting a certain balance between electrochemical energy and the surface energy of the cluster. This technique has been also employed to study the filling of Au cavities by Bi and Ag. In the latter work, the behavior of Bi is contrasted with that of Ag. While the holes are filled at underpotentials in the first

case, the Au holes are only filled by Ag during the layer-by-layer growth of Ag at overpotentials (Solomun and Kautek, 2001).

Monte Carlo simulations of this system have shown that by sweeping the chemical potential of Cu, a cluster is allowed to grow within the hole rising four atomic layers above the surface. As in the experiments, it is found that its lateral extension remains confined to the area defined by the borders of the original defect.

Another nanostructuring technique shares some common features with that described above and is shown in Fig. 36.3. A polymer-coated Pt ultramicroelectrode is used as the tip of a STM, and graphite is used as substrate. Ag atoms are deposited on the tip at underpotentials, so that approximately one atomic monolayer is deposited on the tip. After this, a first bias pulse is applied to the tip, causing the formation of a shallow pit. Then a second bias pulse with a smaller amplitude is applied to cause the desorption of silver from the tip. The silver ions desorbed diffuse and migrate across the tip–sample gap and deposit on the high coordination sites present

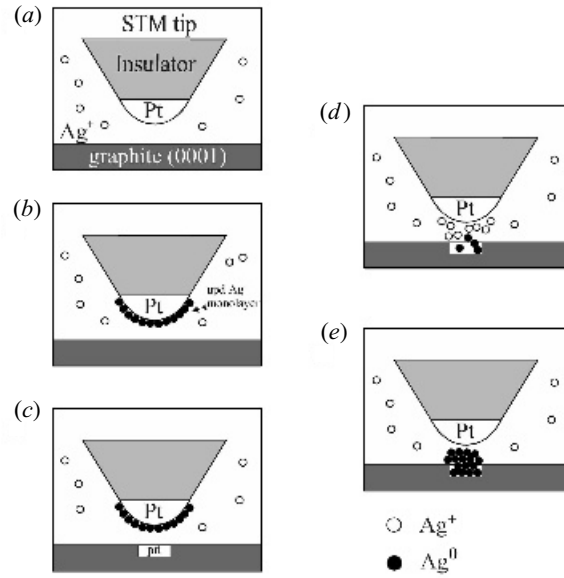

FIGURE 36.3 Schematic diagram illustrating the main features of the mechanism for STM–tip directed silver nanostructure deposition on graphite: (*a*) a freshly prepared polymer-coated platinum microelectrode is immersed in a dilute aqueous silver-plating solution, and a tunneling junction is established with a graphite basal plane surface; (*b*) silver is deposited at the underpotential on the Pt surface, resulting approximately in a silver atomic layer; (*c*) through application of a first bias pulse, a pit is formed on the surface of graphite; (*d*) Ag is desorbed from the tip through a second bias pulse; (*e*) a silver particle is formed on the pit by deposition of silver ions in its proximity. (From Li et al., 1996, with permission from the American Institute of Physics.)

at the edge of the pit. The final result is a silver particle having typical dimensions of 100 to 500 Å in diameter and 5 to 40 Å in height (Li et al., 1996). Besides the experiments, these authors developed a model for this process that was tested by means of Brownian dynamics (BD) simulations of the type described in Section 35.3.2. The main points addressed by these simulations were the relative role of adsorbed and dissolved Ag in supplying the silver required for the nanostructuring on the time scale of the experiment, the ion flux as a function of the tip–sample separation, and the importance of the electric field in promoting silver transport by migration for dissolved and adsorbed silver components.

36.4 TIP-INDUCED LOCAL METAL DEPOSITION

Figure 36.4*a* shows the scheme for the generation of nanonclusters in some detail. The initial state (I) corresponds to the STM tip located in front of the surface of the substrate on which the material is going to be deposited. The surface may be nacked, or covered by a metal monolayer. This is, for example, the case where a monolayer of a metal can be deposited at potentials more positive than the Nernst reversible potential (underpotential deposition). Stage II corresponds to the electrodeposition of metal on the tip. Stage III is the formation of a connective neck between the tip and the surface, and stage IV corresponds to the retraction of the tip. As the tip separates from the electrode, a cluster remains behind in many cases, which typically comprises 20 to 100 atoms and is a few monolayers high. As simple as it seems, experiments attempted by this technique are not always successful, depending very strongly on the nature of the materials involved. The method works well and reproducibly for several combinations of metals, in particular for copper and palladium clusters on Au(111) (Kolb et al., 1997; Engelmann et al., 1998). A typical arrangement of clusters obtained by means of this technique is shown in Fig. 36.4*b*. For other combinations, such as Cu on Ag(111) and Ni on Au(111), cluster formation is not observed (Kolb et al., 1998, 2000a).

Since the number of atoms involved is relatively small, this appears as an interesting problem to tackle by the atom dynamics (AD) techniques described in Chapter 35. Pioneering work in this area was done by Landman et al. (1990, 1993) for the interaction of a Au tip with a Ni surface, and vice versa. Applications to different electrochemical systems were developed by Del Pópolo et al. (2001, 2003). These studies were useful to an understanding of the way in which Cu and Pd clusters are generated on Au surfaces. The simulations were also helpful to show why in some cases the nanostructuring *is not* successful. This is, for example, the case when Cu nanostructuring on Ag is attempted. For this system, the experiments show only disperse two-dimensional structures. When a simulation is carried loading a tip with Cu and approaching it to a Ag(111) surface, surface damage or very small clusters are obtained on the surface. A systematic study with different metal couples shows that a necessary condition for nanostructuring is that the binding energies of the metals involved are similar.

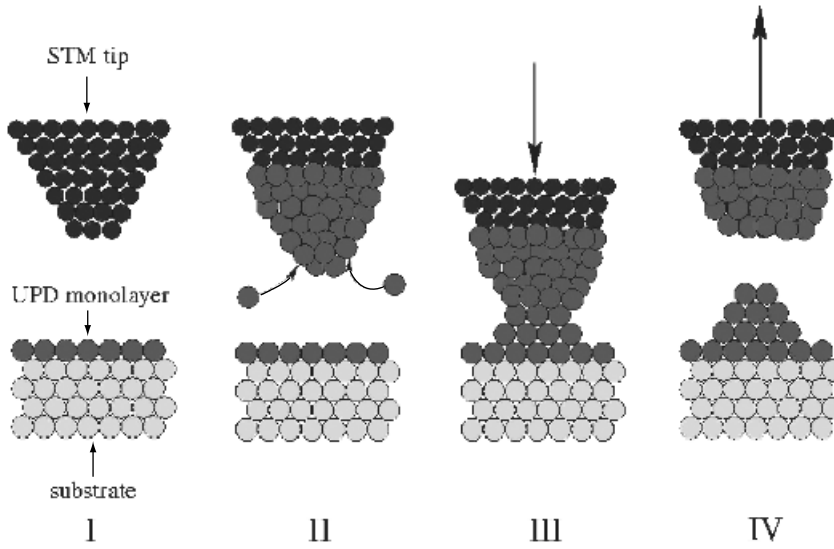

(*a*)

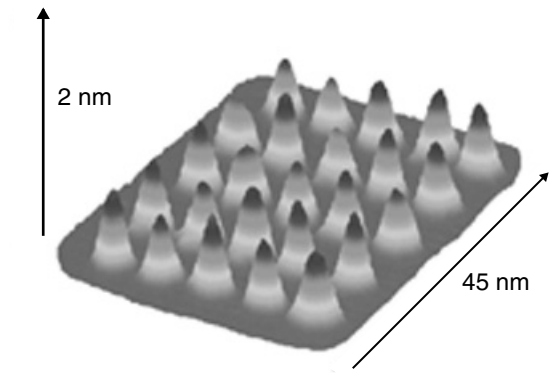

(*b*)

FIGURE 36.4 (*a*) Scheme of the various stages involved in tip-induced local metal deposition: (I) initial state of the STM tip and the substrate, with a monolayer deposited at underpotentials also shown; (II) metal deposition on the tip of the STM; (III) jump-to-contact; (IV) tip retraction; (*b*) arrangement of nanostructures resulting after a set of TILMD processes. (The dimensions of the arrows are not exact but are drawn to give an estimation of the size of the nanostructures.) (From Kolb et al., 2000b, with permission of Wiley-VCH.)

A remarkable feature of the clusters generated by the present procedure was their unusual stability. In fact, it was found that Cu nanoclusters generated on Au(111) surfaces presented the amazing property of remaining stable at potentials above the reversible dissolution potential for bulk Cu (Kolb et al., 2002).

This is not easy to understand, since on thermodynamic grounds clusters should be less stable than the bulk material. It is possible that clusters generated by electrochemical nanostructuring may undergo a certain degree of alloying with the material of the surface that could increase their stability. Indeed, Monte Carlo simulations show that if achievable, such alloying will improve the stability of the clusters toward dissolution.

An alternative type of tip-induced nanostructuring has recently been proposed. In this method, a single-crystal surface covered by an underpotential-deposited monolayer is scanned at a close tip–substrate distance in a certain surface area. This appears to lead to the incorporation of UPD atoms into the substrate lattice, yielding a localized alloy. This procedure works for Cu clusters on Pt(111), Pt(100), Au(111), and for some other systems, but a model for this type of nanostructuring has not been available until now. (Xiao et al., 2003).

36.5 LOCALIZED ELECTROCHEMICAL NUCLEATION AND GROWTH

As pointed out above, an STM tip can be used to nucleate and grow single clusters. In this type of experiment, cluster deposition on a STM tip is achieved when it is retracted about 10 to 20 nm from the substrate surface. Under these conditions, where the feedback loop is disabled, absence of mechanical contact between the tip and the substrate in ensured. Then a positive potential pulse is applied to the tip, the metal deposited on it is dissolved, and it diffuses toward the substrate surface, where a nucleus develops and grows to yield a cluster, typically 20 nm wide.

Experiments and simulations show that the characteristics of the nanostructures generated by this procedure are basically given by five parameters: the distance between the STM and the substrate, the quantity of material loaded on the tip, the maximum ion current density for the dissolution of the material on the tip, the potential of the substrate, and the diameter of the STM apex. The controlled variation of these five parameters allows tailoring of the diameter and height of the clusters.

Since the separation between the tip and the surface is such that their respective double layers do not overlap, the nanostructuring process can be described simply through the diffusion of the ions toward the surface. Thus, the concentration profiles of the diffusing ions define effective Nernst potential profiles that can be employed to predict the regions where the oversaturation conditions will contribute to metal nucleation and growth.

Model calculations are shown in Fig. 36.5, where the tip has been modeled as a hemisphere with a radius $a = 50\,\text{nm}$. During the few milliseconds after the

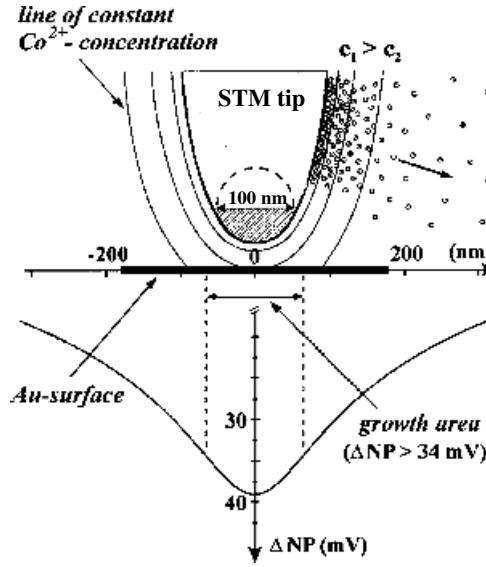

FIGURE 36.5 Model calculation employed to study the dependence of the cluster diameter on the distance between the STM and the substrate surface for localized electrochemical nucleation and growth. The lower part of the figure shows the profile of the Nernst potential for the Co^{2+}/Co potential as a function of the distance from the tip center. The lines indicate a constant Co^{2+} concentration. (From Schindler et al., 2000, with permission from the American Institute of Physics.)

application of the positive pulse to the tip, this hemisphere acts as a continuous M^+-ion-emitting surface with a constant M^+ emission rate. Thus, the diffusion equations can be solved with these boundary conditions, and the concentration profiles underneath the tip can be obtained. For distances between 5 and 40 nm, it is found that a constant M^+ concentration is established within 100 to 200 μs, yielding stationary currents during the emission time (2 to 3 ms). With these quasi-stationary concentration profiles, a Nernst potential profile can be constructed, as shown in the lower part of Fig. 36.5. It is found that for a 1 m*M* Co^{2+} solution, a local increase in the effective Nernstian potential on the order of 30 to 70 mV can be achieved. This is enough to generate localized nucleation on a Au substrate region right below the tip, avoiding delocalized nucleation on the rest of the substrate surface.

This technique also appears as a very promising one, since there is no restriction concerning the nature of the adsorbate and the substrate. In fact, Co has been deposited successfully on a Au(111) surface by this technique. This is not possible by means the TILMD technique described above, since due to the fact that the cohesive energy of Co is larger than that of Au (4.39 vs 3.93 eV), the interaction of a Co-loaded tip with a Au surface would lead to a hole on the substrate. Si(111)

surfaces have also been nanostructured successfully with Pb clusters using this technique (Schindler et al., 2002).

36.6 ELECTRONIC CONTACT NANOSTRUCTURING

We use the term *electronic contact nanostructuring* to describe two different types of nanostructuring techniques where the key role is played by the electronic contact between the tip and the substrate, yielding nanocativies on a surface. However, as we will see, the two alternatives seem to involve quite different physical processes.

In the first of these procedures a Cu electrode is immersed in a Cu^{+2}-containing solution, and the tip is positioned over the desired location, applying a potential positive of the Nernst potential for Cu/Cu^{+2} in that solution. On the other hand, the electrode potential is held at a slightly negative potential with respect to the Cu/Cu^{2+} couple (typically, –50 mV). After 3 minutes under these conditions, and although the polarization conditions of the sample are such that dissolution is not expected, the result is a hole about 100 nm wide and a few nanometers deep. Similarly, if instead of choosing a fixed position on the surface, a repetitive scan is run on a segment on the surface, grooves occur whose depth depends on negative polarization of the sample. After analyzing various hypotheses to explain this remarkable result, the authors arrived at the conclusion that the dissolution process occurs via direct electron transfer from the Cu/Cu^{2+} redox system to the tip. A rough estimation shows that only a minute fraction (about 10^{-5}) of the total tunneling current flowing between the surface and the TYP would be used for the dissolution process (Xie and Kolb, 2000).

The second procedure is different from the previous one in several aspects. First, the metallic substrate employed is Au, which does not show a remarkable dissolution under the experimental conditions chosen, so that no faradaic processes are involved at either the substrate or the tip. Second, the tip is polarized negatively with respect to the surface. Third, the potential bias between the tip and the substrate must be extremely small (e.g., – 2 mV); otherwise, no nanocavity formation is observed. Fourth, the potential of the substrate must be in a region where reconstruction of the Au(111) surface occurs. Thus, when the bias potential is stepped from a significant positive value (typically, 200 mV) to a small negative value and kept there for a period of several seconds, individual pits of about 40 nm result, with a depth of two to four atomic layers. According to the authors, this nanostructuring procedure is initiated by an important electronic (but not mechanical) contact between tip and substrate. As a consequence of this interaction, and stimulated by an enhanced local reconstruction of the surface, some Au atoms are mobilized from the Au surface to the tip, where they are adhered. When the tip is pulled out of the surface, a pit with a mound beside it is left on the surface. The formation of the connecting neck between the tip and surface is similar to the TILMD technique described above but with a different final result: a hole instead of a cluster on the surface (Chi et al., 2000).

36.7 NANOSTRUCTURING BY SCANNING ELECTROCHEMICAL MICROSCOPY

The scanning electrochemical microscope (SECM) is an SPM device where the probe is an ultramicroelectrode (UME) and the signal measured is a faradaic current from electrolysis of solution species. The main difference between the SECM and STM and related techniques is the chemical sensitivity of the probe and the use of a solution containing ions or molecules that are the active species responsible for the signal. (Bard et al., 1989; Enstrom et al., 1986). Although structuring with this type of technique is usually over the nanometer range, we discuss them because the possibility of handling different systems seems to be very good. Also, further developments will certainly extend the design sizes into the nanoscale.

A typical configuration of a SECM system is shown in Fig. 36.6. In this case the solution contains oxidized (Ox) species (denoted *mediators*) that are reduced on the active part of the microelectrode yielding the reduced (Red) species. The figure also shows a possible reaction of the Red species with the electrode, with the reaction rate k_{red}. If k_{red} is very large, the approach of the tip to the surface will result in an increase in the reduction reaction (current) on the tip because the regeneration of Ox on the tip will be more efficient in a smaller gap. On the other hand, if k_{red} is close to zero, the only effect of the tip approach to the surface will be the depletion of the Ox species in the gap upon reduction, whose diffusion from the bulk of the solution is now hindered by the probe. These two mechanisms, which result in the *positive* and *negative feedback operation modes*, can be used to map the reaction rate k_{red} on the surface.

A different operation mode can be employed in SECM if some species are only generated via a reaction on the substrate and they are electrochemically active for

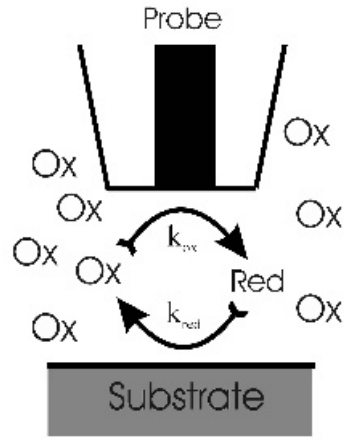

FIGURE 36.6 Typical configuration of a scanning electrochemical microscope. In this case the solution contains Ox species (mediators) that are reduced on the active part of the microelectrode, yielding the reduced Red species. A possible reaction of the Red species with the substrate, with the reaction rate k_{red} illustrated.

reaction on the tip. In this case, they can be detected by their electrochemical reaction on the tip, and surface activity for the generation can be mapped as before. This is the *generation–collection mode* of a SECM and has been employed to obtain chemical concentration maps of corrosion products and biological or polymeric materials.

The two previous applications show the potentiality of SECM for the nanostructuring of surfaces: The SECM probe can be employed as a microscopic source or sink of electrons and chemical reagents. With the tip positioned close to the substrate, these reagents perform modifications to surfaces on a micrometric or nanometric scale, turning the SECM into a versatile nanofabrication device. The local composition of the solution can be changed to provide the driving force for localized chemical reactions. For example, oxidizing species can be generated electrolytically to etch locally metal or semiconductor surfaces with fast etching rates, such as Cu and GaAs. When the materials have relatively slower etching rates and the diffusion of the etchant prevents localization of the etching patterns, more sophisticated approaches can be taken. In these cases, a scavenging reaction can be employed to keep the etchant confined within a very thin diffusion layer surrounding the tip. We discuss other specific examples in this section.

SECM has also been used to deposit a gold microstructure on *n*-Si(111) and indium oxide. In these experiments, Au is dissolved anodically from the ultramicro electrode under constant potential according to the reaction

$$\mathrm{Au} + 4\mathrm{Cl}^- \rightarrow \mathrm{AuCl}_4^- + 3e^-. \tag{36.1}$$

To deposit Au structures, a Au probe is approached to the surface until a positive feedback is observed. This is due to the regeneration of Cl^- species on the substrate while Au is deposited from AuCl_4^- according to the reverse reaction, leading to an increase in the local concentration of Cl^-. The microelectrode is then left at this position above the substrate for a certain time, after which it is withdrawn from the surface. The potential of the substrate, the electrolyte, and the pH were found to be the most significant parameters determining in determining the rate of Au electrodeposition and its structure (Amman and Mandler, 2001).

Metal deposition can also be achieved on nonconducting substrates. For example, metal ions included in an ion-exchanging polymer film can be reduced by species generated at a SECM tip. These metal ions are denominated *precursors*. Alternatively, a compound deposited on the surface can be used as precursor (e.g., AgCl). Then, some redoxactive species are reduced (to yield Red) on the tip, with a subsequent reaction of Red with the AgCl to yield metallic Ag. This procedure thus allows "developing" Ag lines on a AgCl-coated nonconducting sample (Hess et al., 1997).

Acknowledgments

Grants from CONICET, Secyt UNC, Agencia Córdoba Ciencia, Program BID 1201/OC-AR PICT No. 06-12485 are acknowledged.

REFERENCES

Amman, E., and D. Mandler, *J. Electrochem. Soc.*, **148**, C533 (2001).

Bard, A. J., F. R. F. Fam, J. Kwak, and O. Lev, *Anal. Chem.*, **61**, 132 (1989).

Chi, Q., J. Zhang, E. P. Friis, J. E. E. Andersen, J. Ulstrup, *Surf. Sci.*, **463**, L641 (2000).

Del Pópolo, M. G., E. P. M. Leiva, and W. Schmickler, *Angew. Chem.*, **113**, 4807 (2001).

Del Pópolo, M. G., E. P. M. Leiva, H. Kleine, J. Meier, U. Stimming, M. Mariscal, and W. Schmickler, *Appl. Phys. Lett.*, **81**, 2635 (2002); *Electrochim. Acta*, **48**, 1287 (2003).

Eigler, D. M., and E. K. Schweizer, *Nature*, **344**, 524 (1990).

Engelmann, G. E., J. C. Ziegler, and D. M. Kolb, *J. Electrochem. Soc.*, **145**, L33–L35 (1998).

Enstrom, R. C., M. Weber, D. J. Wunder, R. Burgess, and S. Winquist, *Anal. Chem.*, **58**, 844 (1986).

Hess, C., K. Borgwart, C. Ricken, D. G. Ebling, and J. Heinze, *Electrochim. Acta*, **42**, 3065 (1997).

Kolb, D. M., R. Ullmann, and T. Will, *Science*, **275**, 1097 (1997).

Kolb, D. M., R. Ullmann, and J. C. Ziegler, *Electrochim. Acta*, **3**, 2751 (1998).

Kolb, D. M., G. E. Engelmann, and J. C. Ziegler, *Solid State Ionics*, **131**, 69 (2000a).

Kolb, D. M., G. E. Engelmann, and J. C. Ziegler, *Angew. Chem. Int. Ed. Engl.*, **39**, 1123 (2000b).

Landman, U., W. D. Luedtke, N. A. Burnham, and R. J. Colton, *Science*, **248**, 454 (1990).

Li, W., G. S. Hsiao, D. Harris, R. M. Nyffenegger, J. A. Virtanen, and R. M. Penner, *J. Phys. Chem.*, **100**, 20103 (1996).

Schindler, W., D. Hoffmann, and J. Kirschner, *J. Appl. Phys.*, **87**, 7007 (2000).

Schindler, W., P. Hugelmann, M. Hugelmann, and F. X. Kärtner, *J. Electroanal. Chem.*, **522**, 49 (2002).

Solomun, T., and W. Kautek, *Electrochim. Acta*, **47**, 679 (2001).

Xia, X. H., R. Schuster, V. Kirchner, and G. Ertl, *J. Electroanal. Chem.*, **461**, 102 (1999).

Xiao, X., M. Nielinger, and H. Baltruschat, *Electrochim. Acta*, **48**, 3093 (2003).

Xie, Z., and D. M. Kolb, *J. Electroanal. Chem.*, **481**, 177 (2000).

REVIEWS AND MONOGRAPHS

Kaifer, A., and M. Gimez-Kaifer, *Supramolecular Electrochemistry*, Wiley-VCH, New York, 1999.

Landman, U., and W. D. Luedtke, Consequences of tip-sample interactions, in *Scanning Tunneling Microscopy III*, R. Wiesendanger and H. J. Güntherodt Eds., Springer-Verlag, Berlin, 1993.

Lorentz, W. J., and W. Plieth, Eds., *Electrochemical Nanotechnology*, Wiley-VCH, New York, 1996.

Schultze, J. W., *Electrochemistry in Molecular and Microscopic Dimensions*, Elsevier, Amsterdam, 2003.

Schultze, J. W., and A. Bressel, *Electrochim. Acta*, **47**, 3 (2001).

Staikov, G., W. J. Lorenz, and E. Budevski, Chapter 1 in *Imaging of Surfaces and Interfaces*, J. Lipkowski and P. N. Ross, Eds., Wiley, New York, 1999.

37
Development of Electrochemistry

This chapter is not a systematic account of the history of electrochemistry, nor does it give detailed descriptions of all the contributions made by numerous scientists who have worked in the field. The main objective of the chapter is to outline the most important milestones in the development of electrochemistry and to show the relationship between the development of electrochemistry and other sciences. At all stages of the development of electrochemistry, an intimate connection existed between the development of theoretical concepts and the discovery of methods for a practical application of electrochemical processes and phenomena.

37.1 FIRST ELECTROCHEMICAL POWER SOURCES

In 1791, the Italian physiologist Luigi Galvani (1737–1898) demonstrated in his remarkable experiments that muscle contraction similar to that produced by discharge of a Leyden jar will occur when two different metals touch the exposed nerve in a frog. This phenomenon was correctly interpreted in 1792 by the Italian physicist Alessandro Volta (1745–1827), who showed that this *galvanic effect* originates from the contact established between the two metals and from the contact between these metals and the muscle tissue. In March 1800, Volta reported a device designed on the basis of the same phenomenon, which could produce "inexhaustible electric charge." Now known as the *Volta pile*, this was the first example of a practical electrochemical device: an electrochemical power source (a *battery*).

The Volta pile was of extraordinary significance for developments both in the sciences of electricity and electrochemistry, since a new phenomenon, a continuous electric current, hitherto not known, could now be realized. Soon various properties and effects of the electric current were discovered, including many electrochemical processes. In May of 1800, William Nicholson and Sir Anthony Carlisle electrolyzed

Fundamentals of Electrochemistry, Second Edition, By V. S. Bagotsky

water producing hydrogen and oxygen[†]. In 1803, processes of metal electrodeposition were discovered. In 1807, Sir Humphry Davy first isolated alkali metals by electrolyzing salt melts. All these processes constituted stimuli in the development of first (1805) theoretical notions concerning the mechanism of charge transport in aqueous solutions (Theodor Freiherr von Grotthuss, 1785–1822). In 1814, the notion *electrochemistry* began to replace the older notion *galvanism.* In 1833–1834, Michael Faraday (1791–1867) performed numerous electrochemical experiments, introduced a new electrochemical terminology (electrode, cathode, cation, etc.), and established his famous laws of electrolysis.

During the next decades after the appearance of the Volta pile and of different other versions of batteries, fundamental laws of electrodynamics and electromagnetism were formulated based on experiments carried out with electric current supplied by batteries: Ampère's law of interaction between electrical currents (1820), Ohm's law of proportionality between current and voltage (1827), the laws of electromagnetic induction (Faraday, 1831), Joule's law of the thermal effect of electric current, and many others.

The appearance of electrochemical batteries provided an impetus in research into practical applications of electric current. The first prototype of electric telegraph appeared in 1804. In 1838, Jacobi experimented with a battery-driven motorboat on the Neva River not far from St. Petersburg. These achievements led to rapid development of the theory and practice of electrical engineering, and the seventh decade of that century saw the appearance of a revolutionary new power source: the electromagnetic generator (Werner von Siemens, 1866), which soon surpassed their predecessors in both electrical and economic parameters.

The development of a variety of batteries taking place during the second half of the nineteenth century led to basic work in electrochemical thermodynamics. In 1847–1851, Hermann von Helmholtz (1821–1894) and William Thomson (Lord Kelvin, 1824–1907) established a connection between the OCV of batteries and the thermal effect of the chemical reaction proceeding during discharge. Experimental discrepancies between the values of these two parameters were explained later (1874–1878) by a professor of mathematical physics at Yale University, Josiah Willard Gibbs (1839–1903), who took into account the reaction entropy and established the concept of free enthalpy (the *Gibbs energy*). The paper by Gibbs was published in a little known journal, *Transactions of the Connecticut Academy*, and remained unnoticed by most scientists. Subsequently, the ideas of Gibbs were again "discovered" by other scientists. For this reason, many laws and equations in thermodynamic have double names (e.g., the Gibbs–Helmholtz equation, the Gibbs–Duhem equation).

For an analysis of the OCV of batteries, the notion of *electrode potential* was of prime importance. In 1883, Friedrich Wilhelm Ostwald (1853–1932; Nobel prize, 1909) gave a clear description of this notion. At his suggestion, his student Walther Nernst (1864–1941; Nobel prize, 1920) investigated the thermodynamic equilibrium

[†]It must be noted that already a decade earlier the Dutchmen P. van Troostwijk and J.R. Deim [*J. Phys.* **2**, 130 (1790)] showed that during spark discharge a (short-time) process of water electrolysis is achieved. These results were known by Nicholson and Carlisle when (using the then new Volta pile) they reported on long-time water electrolysis, but in their publication these results were not mentioned [R. de Levie, *J. Electroanal. Chem*., **476**, 92 (1999)].

Friedrich Wilhelm Ostwald (1853–1932; Nobel prize, 1909) in 1886 gave in his textbook a description of the state-of-art of electrochemistry at the end of the nineteenth century.

conditions at electrode surfaces and in 1869 derived his famous equation linking the electrode potential with ion concentrations in the solution. From this point on, analysis of processes and phenomena at electrodes were based primarily on use of this Nernst equation, regardless of whether or not equilibrium conditions existed. This purely thermodynamic approach is sometimes called the *Nernst hiatus* (Bockris, 1970), because for a long time it inhibited the development of electrochemical kinetics. It must be noted that Nernst himself, in contrast to his teacher W. Ostwald, was interested in problems of the rate of electrochemical reactions. He assumed (1904) that the rate of such reactions is limited by the diffusion of reaction components toward the electrode surface and established an equation for the limiting diffusion current. Together with Ostwald he assumed that the step of charge-transfer proper proceeds with an infinitely high rate and does not limit the overall reaction rate.

In 1873, Gabriel Lippmann (1845–1921; Nobel prize, 1908) performed extensive experiments of the electrocapillary behavior of mercury and established his equation describing the potential dependence of the surface tension of mercury in solutions. In 1853, H. Helmholtz, analyzing electrokinetic phenomena, introduced the notion of a capacitor-like electric double layer on the surface of electrodes. These publications

marked the beginning of a large number of investigations of properties of the electrode–electrolyte interface.

Numerous measurements of the conductivity of aqueous solutions performed by the school of Friedrich Kohlrausch (1840–1910) and the investigations of Jacobus van't Hoff (1852–1911; Nobel prize, 1901) on the osmotic pressure of solutions led the young Swedish physicist Svante August Arrhenius (1859–1927; Nobel prize, 1903) to establish in 1884 in his thesis the main ideas of his famous theory of electrolytic dissociation of acids, alkalis, and salts in solutions. Despite the sceptitism of some chemists, this theory was generally accepted toward the end of the century.

In 1886, Wilhelm Ostwald published the first detailed textbook on electrochemistry (1150 pages). In this book he gave a description of the historical development of electrochemistry and of the state of art of this branch of science at the end of the nineteenth century.

In 1894, the German electrochemical society under the presidency of W. Ostwald was founded (later renamed the Bunsen Society for Applied Physical Chemistry), which began to publish a specialized journal, *Zeitschrift für Elektrochemie*. In 1902, the American Electrochemical Society was founded (from 1930, the Electrochemical Society, Inc.), which began to publish the *Transactions of the Electrochemical Society* and beginning in 1948, the *Journal of the Electrochemical Society*.

37.2 DEVELOPMENT OF A LARGE-SCALE ELECTROCHEMICAL INDUSTRY

After the development of electrodynamic generators, many large-scale electrolysis processes became possible. In 1888 the electrolytic production of aluminum was organized, and in 1883 the first patent for chlor–alkali electrolysis was issued. The considerable development of various electrolytic processes led to the appearance of the notions of current density and overvoltage. Julius Tafel (1862–1918), a specialist in organic chemistry working in Ostwald's laboratory and studying electrosynthesis of various organic compounds, became interested in problems of cathodic hydrogen evolution and in 1905 established his well-known equation linking overvoltage and current density. This equation marked the beginning of electrochemical kinetics. Many subsequent investigations in this field were devoted to an interpretation of the values of the constants in the Tafel equation.

Electrochemical kinetic studies performed during the first half of the twentieth century were intimately related to the advance in various electrochemical industries. The development of complex relectrochemical reactions (particularily reactions with organic compounds) made it necessary to study the mechanism of different reactions in greater detail. For a long time simplified ideas on reaction mechanisms prevailed. All cathodic reduction reactions (with inorganic or organic components) were regarded as an interaction of these components with hydrogen freshly formed at the cathode (*in statu nascendi*). By analogy, oxidation reactions were regarded as an interaction with oxygen at the anode. It was also generally assumed that the rate of electrochemical reactions was limited by intermediate chemical steps [e.g., in the case of cathodic hydrogen

evolution, by the rate of the reaction of recombination of two hydrogen atoms adsorbed at the electrode's surface with the formation of a hydrogen molecule (the *recombination theory of hydrogen overvoltage*)]. Following Ostwald's and Nernst's concepts, the rate of the electrochemical charge transfer itself was regarded as a very fast reaction not influencing the overall reaction rate. It was only in 1924 that John Alfred Valentine Butler (1899–1966) and then in 1930 that Max Volmer (1885–1965) and Tibor Erdey-Grúz (1902–1976) developed the concept of a finite rate of charge transfer and of the influence of the electrode potential on this rate (the *theory of slow discharge*).

The beginning of the twentieth century also marked a continuation of studies of the structure and properties of electrolyte solution and of the electrode–electrolyte interface. In 1907, Gilbert Newton Lewis (1875–1946) introduced the notion of thermodynamic activity, which proved to be extremally valuable for the description of properties of solutions of strong electrolytes. In 1923, Peter Debye (1884–1966; Nobel prize, 1936) and Erich Hückel (1896–1981) developed their theory of strong electrolyte solutions, which for the first time allowed calculation of a hitherto purely empiric parameter—the mean activity coefficients of ions in solutions.

In 1910, Georges Gouy (1854–1926) and independently, in 1913, David L. Chapman (1869–1958) introduced the notion of a diffuse electrical double layer at the surface of electrodes resulting from a thermal motion of ions and their electrostatic interactions with the surface.

Studies in the field of electrochemical kinetics were enhanced considerably with the development of the dropping mercury electrode introduced in 1923 by Jaroslav Heyrovský (1890–1967; Nobel prize, 1959). This electrode not only had an ideally renewable and reproducible surface but also allowed for the first time a quantitative assessment of diffusion processes near the electrode's surface and so an unambiguous distinction between the influence of diffusion and kinetic factors on the reaction rate. At this period a great number of electrochemical investigations were performed at the dropping mercury electrode or at stationary mercury electrodes, often at the expense of other types of electrodes (the "mercury boom" in electrochemistry).

In 1919, Alexander N. Frumkin (1895–1976) published in Odessa his thesis, "Electrocapillary Phenomena and Electrode Potentials," in which he gave a detailed analysis of the problem and an analysis of the notion of *potential of zero charge.* This parameter proved to be of extraordinary value for the explanation of various electrochemical phenomena. In 1928 he and Gorodetzkaya showed the possibility of linking the difference of the PZC of two metals with their volta potential and thus contributed to solving a basic problem in electrochemistry: the origin of the EMF of a galvanic cell. In 1928 he established the Frumkin adsorption isotherm. In the next decade he succeeded to link problems of electrochemical kinetics with phenomena in other fields of science. In 1932, he showed that the Brønsted coefficient used widely in homogeneous catalysis is a close analog to the transfer coefficient in electrochemical reactions. The next year he established the far-reaching influence of the structure of the DEL on electrode surfaces on the kinetics of electrochemical reactions (the *Frumkin effect*). In 1958, A. Frumkin organized within the Academy of Sciences of the USSR a specialized Institute of Electrochemistry (from 1978 the A. N. Frumkin Institute of Electrochemistry, and from 2004, after a merger with the

The name of Alexander Naumovich Frumkin (1895–1976) dominated electrochemistry for over fifty years of the twentieth century (Roger Parsons).

Institute of Physical Chemistry, the A. N. Frumkin Institute of Physical Chemistry and Electrochemistry of the Russian Academy of Sciences). In 1965 the first issue of *Elektrokhimiya* (the Russian journal of electrochemistry) was published. In 1952 the first monograph on electrochemical kinetics written by Frumkin and co-workers was published in Moscow.

At the same time in many other countries, several groups or schools of electrochemists emerged, dedicated primarily to problems of electrochemical kinetics: John O'M. Bockris and Ernest Yeager (1924–2002) in the United States; Brian E. Conway in Canada; Roger Parsons in the UK; Klaus Vetter (1916–1974), Heinz Gerischer (1919–1994), and Wolf Vielstich in Germany; Lucien Gierst in Belgium; Sergio Trasatti and Rolando Guidelli in Italy; and many others.

In 1949, J. Bockris, P. Van Rysselberghe, M. Pourbaix, and others founded the Comité International de Thermodynamique et Cinétique Electrochimique (CITCE), which was subsequently transformed into the International Society of Electrochemistry (ISE). At about the same time, the publication of two major English electrochemical journals was organized: *Electrochimica Acta* and the *Journal of Electroanalytical Chemistry*.

John O'M. Bockris in 1965 and Heinz Gerischer in 1988 analyzed problems of the further development of electrochemistry.

37.3 FUEL CELLS AND LITHIUM BATTERIES

After the first demonstration of a high-power oxygen–hydrogen fuel cell in 1960 and the discovery of the possibility of a direct electrochemical oxidation of various organic compounds (fuels), the interests of electrochemists in many countries shifted toward these problems. A huge number of investigations were initiated, which led to the emergence of two new areas of theoretical electrochemistry: *electrocatalysis* and the *theory of porous electrodes*. This period is marked by increased use of new physical methods for investigation of the surface of electrodes. Use of these methods led to a new understanding of the role of the surface's state and of adsorption phenomena on the rate and mechanism of various electrocatalytic reactions.

Another factor also contributed to the appearance of new concepts in electrochemistry in the second half of the twentieth century: The development and broad application of lithium batteries was a stimulus for numerous investigations of different types of *nonaqueous electrolytes* (in particular, of solid polymer electrolytes). These batteries also initiated investigations in the field of *electrochemical intercalation processes*.

Thus, it can be seen that at all stages of the development of electrochemistry, theoretical investigations have been stimulated by the practical use of various electrochemical phenomena and processes, and the theoretical concepts that were developed have in turn contributed significantly to the development of applied electrochemistry.

REFERENCES

Arrhenius, S., Über die Dissociation der in Wasser gelösten Stoffe, *Z. Phys. Chem.*, **1**, 631 (1887).

Bockris, J. O'M., Electrochemistry: the underdeveloped science, *J. Electroanal. Chem*., **9**, 408 (1965).

Butler, J. A. V., The kinetic interpretation of the Nernst theory of electromotive force, *Trans. Faraday Soc*., **19**, 729 (1924).

Chapman, D. L., Contribution to the theory of electrocapillarity, *Philos. Mag*., Ser. 6, **25**, 475 (1913).

Davy, H., On some chemical action of electricity, *Philos. Trans.,* p. 1 (1806); p. 99 (1807).

Debye, P., and E. Hückel, "Zur Theorie der Elektrolyte, 1: Gefrierpunktserniedrung und verwandte Erscheinungen; 2: Das Grenzgesetz für die elektrische Leitfähigkeit, *Phys*. Z., **24**, 185, 305 (1923).

Erdey-Gruz, T., and M. Volmer, Zur Theorie der Wasserstoffüberspannung, *Z. Phys. Chem*., **150A**, 203 (1930).

Faraday, M., *Experimental Researches in Chemistry and Physics*, R. Taylor & W. Francis, London, 1859.

Frumkin, A. N., Electrocapillary phenomena and electrode potentials [in Russian], dissertation, Commercial Publishers, Odessa, Ukraine, 1919.

Frumkin, A., Die Elektrokapillarkurve, *Ergeb. Exakten Naturwiss*., **7**, 235 (1928).

Frumkin, A., Bemerkung zur Theorie der Wasserstoffüberspannung, *Z. Phys. Chem*., **160A**, 116 (1932).

Frumkin, A., Wasserstoffüberspannung und Struktur der Doppelschicht, *Z. Phys. Chem*., **164A**, 121 (1933).

Frumkin, A., and A. Gorodetzkaya, *Z. Phys. Chem*., **136**, 215, 451 (1928).

Frumkin, A. N., V. S. Bagotsky, Z. A. Iofa, and B. N. Kabanov. *Kinetics of Electrode Reactions* [in Russian], Moscow University Publishers, Moscow, 1952.

Galvani, L., De viribus electricitatis artificialis in motu musculari commentaries, in *Boloniensi Scientarum e Artium Institut at que Academia Commentarii*, Vol. 7, Bologna, Italy, 1792.

Gerischer, H., Quo vadis, Elektrochemie, *Ber. Bunsenges. Phys. Chem*., **92**, 1436 (1988).

Gibbs, J. W., On the equilibrium of heterogeneous substances, *Trans. Conn. Acad. Arts Sci*., **3**, 108, 343 (1874–1878).

Gouy, G., Sur la constitution de la charge électrique à la surface d' un electrolyte, *Compt. Rend*., **149**, 654 (1910).

Grotthus, Th., Sur la decomposition de l'eau et de corps qu'elle tient en dissolution à l'aide de l'électricité galvanique, *Ann. Chim*., **58**, 54 (1805).

Heyrovský, J., *Chem. Listy*, **16**, 256 (1922); *Philos. Mag*., **47**, 303 (1923).

Kohlrausch, F., and L. Holborn, *Das Leitvermögen der Elektrolyte*, Teubner, Leipzig, 1898.

Lewis, G. N., Outlines of a new system of thermodynamic chemistry, *Proc. Am. Acad*., **43**, 259 (1907).

Lippmann, G., Beziehungen zwischen den Capillaren und elektrischen Erscheinungen, *Ann. Phys. (Poggendorff's)*, **29**, 546 (1873).

Nernst, W., Die elektromotorische Wirksamkeit der Ionen, *Z. Phys. Chem*., **4**, 129 (1869).

Nernst, W., Theorie der Reaktionsgeschwindigkeit in heterogenen Systemen, *Z. Phys. Chem*., **47**, 52 (1904).

Nicholson, W., and A. Carlisle, Experiments in galvanic electricity, *Philos. Mag*., **7**, 337 (1800).

Ostwald, W., *Lehrbuch der allgemeinen Chemie*, Engelmann, Leipzig, 1883.

Ostwald, W., *Elektrochemie: Ihre Geschichte und Lehre*, Veidt & Co., Leipzig, 1886.

Tafel, J., Über die Polarisation bei kathodischer Wasserstoffentwicklung, *Z. Phys. Chem*., **50**, 641 (1905).

van't Hoff, J. H., *Études de dynamique chimique*, Frederik, Müller, Amsterdam, 1884.

Volta, A., *Schriften über die tierische Elektrizität, Schreiben an den Herrn Abt Dr.Vasali, Professor der Physik an der Universität Turin*, Calve, Prague, Czechoslovakia, 1796.

Volta, A., On the electricity exited by the mere contact of conducting substances of different kind, letter to the Right Hon. Sir Joseph Banks, K.B.P.R.S., *Philos. Trans*., 1800, Vol. 2, plate XVII, p. 430 (1800).

von Helmholtz, H., *Über die Erhaltung der Kraft*, Reimer, Berlin, 1847.

APPENDIX A: Derivation of the Main Equation of Debye–Hückel Theory

The relation between the spatial distribution of the electrostatic potential $\psi(x)$ and the spatial distribution of charge density $Q_V(x)$ can be stated, generally, in terms of Poisson's differential equation,

$$\forall^2\psi = -\frac{Q_V(x)}{\varepsilon_0\varepsilon}, \tag{A.1}$$

where $\forall^2$ is the mathematical Laplace operator (in Cartesian coordinates, $(\forall^2 \equiv \partial^2/\partial x^2 + \partial^2/\partial y^2 + \partial^2/\partial z^2)$, $\varepsilon_0 = 8.85 \times 10^{-12}$ F/m is the permittivity of vacuum, and ε is the relative permittivity (dielectric constant) of the medium considered (for water and aqueous solutions, $\varepsilon = 78.5$).

For the problem of potential distribution around a point charge (here the central ion) it is convenient to use the spherical system of coordinates, where in this case all parameters depend only on the distance r from the central ion, regardless of the direction.

In this coordinate system Poisson's equation takes the form

$$\frac{1}{r^2}\frac{d(r^2(d\psi/dr))}{dr} = -\frac{Q_V}{\varepsilon_0\varepsilon}. \tag{A.2}$$

A second equation linking parameters ψ and Q_V is needed so that they may be calculated individually. To derive such an equation it was assumed that the concentration of ions c_j is determined by the Boltzmann distribution law,

$$c_j = c_j^0 \exp\left(-\frac{z_j F\psi_0}{RT}\right), \tag{A.3}$$

where c_j^0 is the concentration averaged over the entire volume and $w_{\text{pot}} = z_j F\psi_0$ is the potential energy at a given point.

Fundamentals of Electrochemistry, Second Edition, By V. S. Bagotsky

Space charge arises because the character of cation distribution differs from that of anion distribution (the signs of z_j are different). The volume charge density depends on the ion distribution,

$$Q_V(r) = F\Sigma z_j c_j(r) = F\Sigma z_j c_{V,j} \exp\left(-\frac{z_j F\psi_0(r)}{RT}\right), \tag{A.4}$$

where the summation extends over all ions, including $j = m$.

When combining Eqs. (A.1) and (A.4), we obtain a second-order nonlinear differential equation for $\psi_0(r)$ which is mathematically very difficult to solve. Therefore, in DH theory a simplified equation is used: The exponential terms of Eq. (A.4) are expanded into series and only the first two terms of each series are retained [$\exp(y) \approx 1 + y$]. When we include the condition of electroneutrality and use the ionic strength I_c we can write this equation as

$$Q_V(r) = F\Sigma z_j c_j^0\left(1 - \frac{z_j F\psi_0}{RT}\right) = -\frac{2F^2 I_c}{RT}\psi_0. \tag{A.5}$$

This simplification is admissible only for sufficiently small values of $z_j F\psi/RT$; for instance, it is correct within 10% for values of $\psi_0 < RT/2z_j F = 12.5/z_j$ mV. Although Eq. (A.5) is limited in its range of application because of this restriction, it is conditionally used as well at higher values of $|\psi_0|$.

Combining Eqs. (A.1) and (A.5), we find the basic differential equation of Debye–Hückel theory:

$$\frac{1}{r^2}\frac{d(r^2\, d\psi_0/dr)}{dr} = \kappa^2\psi_0, \tag{A.6}$$

where parameters independent of coordinates are gathered together in the constant κ (units: m^{-1}) defined by

$$\kappa \equiv F\left(\frac{2I_c}{RT\varepsilon_0\varepsilon}\right)^{1/2}. \tag{A.7}$$

This equation has the general solution

$$\psi_0(r) = \frac{C_1}{r}\exp(\kappa r) + \frac{C_2}{r}\exp(-\kappa r). \tag{A.8}$$

To find the values of the integration constants C_1 and C_2, we must formulate the boundary conditions. At large distances from the central ion, the value of ψ is zero, hence $C_1 = 0$. Equation (7.30) can be used as the second boundary condition. Substituting the value of ψ [the second term on the right-hand side of Eq. (A.8) into

the expression for Q_V [Eq. (A.5)] and integrating by parts from $r = 0$ to $r = \infty$, we find that

$$C_2 = \frac{z_m Q^0}{4\pi\varepsilon_0\varepsilon}. \tag{A.9}$$

Thus,

$$\psi_0(r) = \frac{z_m Q^0}{4\pi\varepsilon_0\varepsilon r} \exp(-\kappa r). \tag{A.10}$$

We can find the potential of the ionic atmosphere by subtracting from the overall value of potential $\psi(r)$ in accordance with Eq. (7.32) the value of potential of the central ion:

$$\psi_{\text{atm}}(r) = \frac{z_m Q^0}{4\pi\varepsilon_0\varepsilon r} [\exp(-\kappa r) - 1]. \tag{A.11}$$

This is Eq. (7.33), the main equation of the first version of Debye–Hückel theory.

APPENDIX B: Derivation of the Main Equation of Gouy–Chapman Theory

In the Gouy–Chapman theory the distribution of charges and potential for the diffuse EDL are calculated in a manner similar (but not identical) to that in the Debye–Hückel theory, except that now the *initial charge* is not a point charge but a plane (i.e., a charged surface), and the diffuse charge has a flat shape. It must be said that the Gouy–Chapman theory was created about 10 years earlier than Debye–Hückel theory and probably had a great influence on the development of the latter.

For the flat one-dimensional problem with the sole coordinate x, the Poisson equation can be written as

$$\frac{d^2\psi}{dx^2} = -\frac{Q_V(x)}{\varepsilon_0\varepsilon}. \tag{B.1}$$

The total excess charge, $Q_{S,\mathrm{E}}$, in the solution per unit surface area is determined by the expression

$$Q_{S,\mathrm{E}} = \int_0^\infty Q_V(x). \tag{B.2}$$

Integrating the Poisson equation over x and allowing for Eq. (B.2) as well as for the fact that in the interior of the solution, $(d\psi/dx)_{x\to\infty} = 0$, we find that

$$Q_{S,\mathrm{M}} = -Q_{S,\mathrm{E}} = -\varepsilon_0\varepsilon\left(\frac{d\psi}{dx}\right)_{x=0} \tag{B.3}$$

(the minus sign indicates that for $Q_{S,\mathrm{M}} > 0$, we should have $d\psi/dx < 0$).

The volume charge density depends on the ion distribution, which obeys the Boltzmann equation:

$$Q_V(x) = F\,\Sigma\, z_j c_j(x) = F\,\Sigma\, z_j c_{V,j} \exp\left(-\frac{z_j F\psi}{RT}\right). \tag{B.4}$$

Fundamentals of Electrochemistry, Second Edition, By V. S. Bagotsky

Substituting this expression into Eq. (B.1), we obtain the basic differential equation for the potential distribution:

$$\frac{d^2\psi}{dx^2} = -\frac{F}{\varepsilon_0\varepsilon}\,\Sigma\, z_j c_{V,j} \exp\left(-\frac{z_j F\psi}{RT}\right). \tag{B.5}$$

In this one-dimensional flat case the Laplace operator is simpler than in the case with spherical symmetry arising when deriving the Debye–Hückel limiting law. Therefore, the differential equation (B.5) can be solved without the simplification (of replacing the exponential factors by two terms of their series expansion) that would reduce its accuracy. We shall employ the mathematical identity

To solve this equation we employ the mathematical identity

$$\left(\frac{d\psi}{dx}\right)^2 \equiv 2\int (d^2 dx^2) d\psi, \tag{B.6}$$

which can readily be verified by differentiating both sides with respect to x.

We substitute into it Eq. (B.5) and integrate it over ψ from the current value of ψ to $\psi = 0$ (at $x \to \infty$). We determine the integration constant from the condition that for $\psi = 0$ we also have $d\psi/dx = 0$. As a result, we have

$$\left(\frac{d\psi}{dx}\right)^2 = \frac{2RT}{\varepsilon_0\varepsilon}\,\Sigma\, z_j c_{V,j}\left[\exp\left(-\frac{z_j F\psi}{RT}\right) - 1\right]. \tag{B.7}$$

As a simplification we shall consider the binary solution of a $z:z$ electrolyte. In this case

$$\begin{aligned}\left(\frac{d\psi}{dx}\right)^2 &= \frac{2RTc_V}{\varepsilon_0\varepsilon}\left[\exp\left(-\frac{zF\psi}{RT}\right) + \exp\left(\frac{zF\psi}{RT}\right) - 2\right] \\ &= \frac{2RTc_V}{\varepsilon_0\varepsilon}\left(2\sinh\frac{zF\psi}{RT}\right)^2.\end{aligned} \tag{B.8}$$

Parameters ψ and $d\psi/dx$ differ in sign; hence,

$$\frac{d\psi}{dx} = -2\left(\frac{2RTc_V}{\varepsilon_0\varepsilon}\right)^{1/2}\sinh\frac{zF\psi}{RT}. \tag{B.9}$$

When integrating this equation (which is readily accomplished for small and large values of $zF\psi/RT$ separately) we can find the distribution of potential $\psi(x)$ relative to distance x. At low values of ψ this distribution is exponential.

It is the major aim of diffuse EDL theory to establish the relation between the charge $Q_{S,M}$ and potential ψ_0 at point $x = 0$ (the total potential drop across this layer).

Substituting the value of the derivative $d\psi/dx$ for $x = 0$ into Eq. (B.3) we find for the surface charge

$$Q_{S,\mathrm{M}} = 2A \sinh \frac{zF\psi_0}{2RT}, \tag{B.10}$$

where $A \equiv \left(\frac{2RTc_{\mathrm{V}}}{\varepsilon_0 \varepsilon}\right)^{1/2}$, and for the differential capacity the main equation of the Gouy–Chapman theory [see Eq. (10.3)],

$$C \equiv \frac{dQ_{S,\mathrm{M}}}{d\psi_0} = 2A \cosh \frac{zF\psi_0}{2RT}, \tag{B.11}$$

General Bibliography

MONOGRAPHS AND CONTRIBUTED BOOKS

Abruña, A., Ed., *Electrochemical Interfaces*, VCH, New York, 1991.

Bockris, J. O'M., and S. U. M. Khan, *Surface Electrochemistry: A Molecular Level Approach*, Plenum Press, New York, 1993.

Bockris, J. O'M., and A. K. N. Reddy, *Modern Electrochemistry*, Plenum Press, New York, 1998.

Hamman, C. H., A. Hamnett, and W. Vielstich, *Electrochemistry*, Wiley-VCH, New York, 1998.

Koryta, J., J. Dvoř á k, and L. Kavan, *Principles of Electrochemistry*, Wiley, Chichester, West Sussex, England, 1993.

Lipkowski, J., Ed., *The Electrochemistry of Novel Materials*, Wiley-VCH, New York, 1994.

Lipkowski, J., Ed., *Surface of Electrified Interfaces*, Wiley-VCH, New York, 1993.

Lipkowski, J., and P. N. Ross, Eds., *Adsorption of Molecules at Metal Electrodes*, Wiley-VCH, New York, 1992.

Newman, J., and K. E. Thomas-Alyea, *Electrochemical Systems*, 3rd ed., Wiley, New York, 2004.

Rubinstein, I., Ed., *Physical Electrochemistry*, Marcel Dekker, New York, 1995.

Schmickler, W., *Interfacial Electrochemistry*, Oxford University Press, New York, 1996.

Wieckowski, A., Ed., *Interfacial Electrochemistry: Theory, Experiment and Applications*, Marcel Dekker, New York, 1999.

SERIALS

Bard, A. J., Ed., *Electroanalytical Chemistry*, Marcel Dekker, New York.

Bockris, J. O'M., B. E. Conway, et al., Eds., *Modern Aspects of Electrochemistry*, Vols. 1–3, Butterworth, London; Vols. 4 and up, Kluwer, New York.

Delahay, P., C. W. Tobias, H. Gerischer, et al., Eds., *Advances in Electrochemistry and Electrochemical Engineering*, Wiley-Interscience, New York; continued as R. C. Alkire, H. Gerischer, et al., Eds., *Advances in Electrochemical Science and Engineering*, Wiley, New York.

Fundamentals of Electrochemistry, Second Edition, By V. S. Bagotsky

Gileadi, E., et al., Eds., *Encyclopedia of Electrochemistry*, Vols. 1–9, Wiley-VCH, New York, 2001–2002.

PERIODICALS

Bulletin of Electrochemistry, Central Electrochemical Research Institute, Karaikudi, India.

Electrochemical and Solid State Letters, Electrochemical Society, Pennington, N.J.

Electrochemical Communications. Elsevier, Amsterdam.

Electrochimica Acta, Pergamon Press, Oxford.

Elektrokhimiya [in Russian], Nauka Publishers, Moscow; English translation: *Soviet Electrochemistry*, continued as *Russian Electrochemistry*, Consultants Bureau, New York.

Journal of Applied Electrochemistry, Chapman & Hall, London.

Journal of Electroanalytical Chemistry and Interfacial Electrochemistry, Elsevier Sequoia, Lausanne, Switzerland.

Journal of Power Sources, Elsevier Sequoia, Lausanne, Switzerland.

Journal of the Electrochemical Society, Electrochemical Society, Pennington, N.J.

Physical Chemistry Chemical Physics, A Journal of the European Chemistry Society (incorporates the *Faraday Transactions, Berichte der Bunsen Gesellschaft*).

Solid State Electrochemistry, Greifswald.

AUTHOR INDEX

The index lists only authors whose contributions are explicitly discussed in the text. Authors merely appearing in literature references are not included.

Fundamentals of Electrochemistry, Second Edition, By V. S. Bagotsky

SUBJECT INDEX

The index lists only those page numbers where a given term is used or explained for the first time, or where another aspect of the same term is discussed.

Fundamentals of Electrochemistry, Second Edition, By V. S. Bagotsky